

REAL GAS FLOWS WITH HIGH VELOCITIES

VLADIMIR LUNEV



CRC Press
Taylor & Francis Group

REAL GAS FLOWS WITH HIGH VELOCITIES

VLADIMIR LUNEV



CRC Press
Taylor & Francis Group
Boca Raton London New York

CRC Press is an imprint of the
Taylor & Francis Group, an **informa** business

CRC Press
Taylor & Francis Group
6000 Broken Sound Parkway NW, Suite 300
Boca Raton, FL 33487-2742

© 2009 by Taylor & Francis Group, LLC
CRC Press is an imprint of Taylor & Francis Group, an Informa business

No claim to original U.S. Government works
Printed in the United States of America on acid-free paper
10 9 8 7 6 5 4 3 2 1

International Standard Book Number-13: 978-1-4398-0465-0 (Hardcover)

This book contains information obtained from authentic and highly regarded sources. Reasonable efforts have been made to publish reliable data and information, but the author and publisher cannot assume responsibility for the validity of all materials or the consequences of their use. The authors and publishers have attempted to trace the copyright holders of all material reproduced in this publication and apologize to copyright holders if permission to publish in this form has not been obtained. If any copyright material has not been acknowledged please write and let us know so we may rectify in any future reprint.

Except as permitted under U.S. Copyright Law, no part of this book may be reprinted, reproduced, transmitted, or utilized in any form by any electronic, mechanical, or other means, now known or hereafter invented, including photocopying, microfilming, and recording, or in any information storage or retrieval system, without written permission from the publishers.

For permission to photocopy or use material electronically from this work, please access www.copyright.com (<http://www.copyright.com/>) or contact the Copyright Clearance Center, Inc. (CCC), 222 Rosewood Drive, Danvers, MA 01923, 978-750-8400. CCC is a not-for-profit organization that provides licenses and registration for a variety of users. For organizations that have been granted a photocopy license by the CCC, a separate system of payment has been arranged.

Trademark Notice: Product or corporate names may be trademarks or registered trademarks, and are used only for identification and explanation without intent to infringe.

Library of Congress Cataloging-in-Publication Data

Lunev, Vladimir.
Real gas flows with high velocities / author, Vladimir Lunev.
p. cm.
Translated from the Russian manuscript.
“A CRC title.”
Includes bibliographical references and index.
ISBN 978-1-4398-0465-0 (alk. paper)
1. Aerodynamics, Hypersonic. 2. Gas flow. I. Title.

TL571.5.L86213 2009
629.132'306--dc22

2008048879

Visit the Taylor & Francis Web site at
<http://www.taylorandfrancis.com>

and the CRC Press Web site at
<http://www.crcpress.com>

Contents

Abstract	ix
Preface	xi
Author	xv
1 Gas Dynamic Model and Equations of Gas Flows	1
1.1 Outline of the Gas Dynamic Model of Gas Flows	1
1.2 Postulates and Equations of Gas Dynamics: One-Dimensional Flow	7
1.2.1 The Momentum Conservation Law	8
1.2.2 The Energy Conservation Law	9
1.3 Equations of State	11
1.4 Some Knowledge of Molecular Kinetic Theory	18
1.5 Entropy and the Second Law of Thermodynamics	24
1.6 Speed of Sound	28
1.7 Integral Equations of Fluid and Gas Motion: Simple Examples	32
1.7.1 Mass Conservation Law	33
1.7.2 Momentum Conservation Law	33
1.7.3 Energy Equation	34
1.8 Some Questions of the Kinematics of Fluid Media:	
Differential Vector Operators	39
1.8.1 Particle Trajectories and Streamlines	40
1.8.2 Curl and Deformation Rate	41
1.8.3 Vector Divergence	44
1.8.4 Vector Divergence of a Vector Pair	46
1.9 Differential Equations of Gas Dynamics	46
1.9.1 Mass Conservation or Continuity Equation	46
1.9.2 Momentum Equation: Viscous Stress Field	47
1.9.3 Energy Equation	48
1.10 Rheological Model of Newtonian Fluids and Gases	51
1.11 Initial and Boundary Conditions	55
1.11.1 Boundary Conditions	56
1.11.2 Existence and Uniqueness of Solutions of Gas Dynamic Problems	58
1.12 Similarity and Modeling in Gas Dynamics	58
1.12.1 First Approach: Inviscid Perfect Gas	59
1.12.2 Second Approach: Similarity Theory	60
1.12.3 Real Gases	62
1.12.4 Unsteady Flows	63
1.12.5 Motion of Bodies in Heavy Fluids	64
1.12.6 Self-Similar Problems	64
1.13 Curvilinear Coordinate Systems: Euler Equations	65
1.13.1 Other Operators	65
1.13.2 Cylindrical System	67
1.13.3 Spherical Coordinates	68
1.13.4 Curvilinear Surface-Fitted Coordinate System for Plane and Axisymmetric Flows	69
1.13.5 General Case	70

1.14	Navier–Stokes Equations in Curvilinear Coordinates	72
1.15	Turbulent Flows	76
1.16	Viscous and Inviscid Flow Models	78
2	Inviscid Gas Dynamics: General Issues and Simple Solutions	81
2.1	Stream Function, Potential, and Vortex	81
2.1.1	Curl and Velocity Circulation	82
2.1.2	Velocity Potential	84
2.2	Integrals of Gas Dynamic Equations	85
2.2.1	Steady-State Adiabatic Flows	86
2.2.2	Potential Adiabatic Flows of Barotropic Gases	87
2.3	One-Dimensional Stationary Flows	90
2.3.1	General Equations and Role of the Mach Number	90
2.3.2	Laval Nozzle: Isentropic Flow	92
2.3.3	Thermal Nozzle	95
2.3.4	Variable Flow-Rate Nozzle	95
2.4	Linear Equations of Gas Dynamics	96
2.5	Sound Wave Propagation	99
2.6	Nonlinear Effects: Expansion Fans and Shock Waves	102
2.7	Steady-State Flow Past Thin Bodies: Similarity Law	105
2.7.1	Similarity Law	107
2.7.2	Unsteady Analogy	109
2.8	Thin Bodies in Supersonic Flow	110
2.8.1	Plane Flows	110
2.8.2	Axisymmetric Problems	113
2.9	Subsonic Flow Past Thin Bodies	117
2.10	Cylinder, Sphere, and Other Bodies in an Incompressible Flow	123
2.11	Stagnation Points and Singular Lines	129
2.11.1	Plane Rotational and Irrotational Flows	129
2.11.2	Axisymmetric Flow	130
2.11.3	Two Planes of Symmetry	131
2.11.4	Stagnation Point with a Positive Pressure Gradient	132
2.11.5	Wedge in Incompressible Flow	133
2.11.6	Singular Surfaces and Lines	134
2.12	Forces in Subsonic Flows	135
2.13	Aerodynamic Characteristics	140
2.14	Accelerated Motion of Bodies	143
3	Shock Waves	147
3.1	Introduction: Formulation of Problems	147
3.2	Shock Wave Structure in a Viscous Gas	149
3.3	Normal Shock Waves in Perfect Gases	151
3.4	Shock Waves in Normal Gases	156
3.5	Oblique Shocks	163
3.6	Losses across Shock Waves	170
3.7	Piston and Wedge Problems	173
3.7.1	Linear and Quadratic Approximations	174
3.7.2	Hypersonic Approximation of a Thin Shock Layer: Newton Formula	175

4 Theory of Characteristics	181
4.1 Formulation of the Problem	181
4.2 One-Dimensional Unsteady Flows	184
4.3 Steady-State Two-Dimensional Flows	191
4.4 Three-Dimensional Flows	196
4.5 Simple Waves	200
4.6 Properties of Expansion and Compression Waves	203
4.6.1 Expansion Waves	204
4.6.2 Compression Waves	206
4.7 Propagation of Disturbances in Nonuniform Media	208
4.7.1 Waves in Continuous Media	208
4.7.2 Short Wave in a Vortex Flow	209
4.7.3 Short Wave/Contact Discontinuity Interaction	211
4.7.4 Reflection of Disturbances from Sonic Lines	214
4.7.5 Flow behind the Point of the Flow Turn	214
4.8 Interaction of Sound and Shock Waves	215
4.9 Breakdown of an Arbitrary Discontinuity	219
4.9.1 Irregular Shock Interactions	225
4.10 Disturbances in Thin Layers	227
4.11 Shock Front Equation	231
4.12 Waves in Anomalous Media	235
5 Mixed (Subsonic–Supersonic) Flows	239
5.1 Formation of Mixed Flows	239
5.2 Transonic von Kàrmàn and Chaplygin Equations	242
5.3 Formulation of Gas Dynamic Problems	246
5.3.1 Supersonic Flows	247
5.3.2 Subsonic Flows	249
5.3.3 Transonic Flows	250
5.4 Supersonic Flow Past Blunt Bodies	250
5.5 Nozzle and Jet Flows	256
5.5.1 Supersonic Jets	257
5.5.2 Subsonic Jets	259
5.5.3 Interaction of Jets with Barriers	259
5.6 Subsonic Flow Past a Convex Corner	260
5.7 Interaction of Disturbances with a Subsonic Region	262
5.8 Existence of Steady-State Solutions	267
6 Self-Similar or Group Solutions	269
6.1 Basic Concepts	269
6.2 Cone in Incompressible Flow	271
6.3 Some Transonic Problems	273
6.4 Cone in Supersonic Flow	276
6.5 Conical Flows	280
6.6 Cone at Incidence	284
6.7 Thin Delta Wing in a Supersonic Flow	290
6.8 Strong Blast	294
6.9 Blast in Real Gases	301
6.10 Self-Similar Time-Dependent Dissipative Flows	303

7 Flows with Strong Shocks	313
7.1 Hypersonic Stabilization and Compressed Shock Layer	313
7.2 Busemann and Newton Formulas	319
7.3 Blunt Bodies: Similarity Law	327
7.4 Aerodynamic Characteristics	329
7.5 Limiting Solution: Free Layer	337
7.6 Piston Problem	342
7.7 Truncation Series Method for the Vicinity of a Stagnation Point	344
7.8 Constant-Density Flow in the Vicinity of the Axis of Symmetry of a Blunt Body	349
7.9 Variable-Density Flow along the Axis of Symmetry	354
7.10 Thin Three-Dimensional Shock Layers	357
7.11 Flow in the Vicinity of the Planes of Symmetry of a Conical Body	362
7.12 Jet Flowing Counter to a Hypersonic Flow	368
7.13 Degenerate Shock Layer Equations	371
8 Hypersonic Flow Past Thin Sharp Bodies	377
8.1 Distinctive Features of the Nonlinear Theory	377
8.2 Basic Equations: Time-Dependent Analogy	379
8.3 Analogy for the Integral Conservation Laws	383
8.4 Similarity Law	385
8.5 Flow around Thin Wings	388
8.6 Thin Bodies at High Incidence	390
8.7 Time-Dependent Flows: Curved Body Rule	394
9 Flows Past Thin, Slightly Blunted Bodies	401
9.1 General Pattern of the Flow Past Thin Blunt Bodies	401
9.2 Similarity Law and Blast Analogy	405
9.3 Role of the High-Entropy Layer in Real Gas Effects	410
9.4 Flow Past Blunt Cones	412
9.5 Bodies of Revolution at Incidence	421
9.6 Wings with Blunt Edges	429
9.7 Wings with Blunt Noses	434
9.8 Some Properties of the Three-Dimensional Vortex Layers on Blunt Bodies	437
9.9 Nonuniform Hypersonic Flow Past a Yawed Cylinder	442
10 Physicochemical Models of Relaxing Gases	445
10.1 Formulation of the Problem	445
10.2 Basic Postulates of the Relaxing Medium Model	446
10.3 Equations of State for Gas Mixtures	450
10.4 Relaxation Equations and Limiting Flow Regimes	454
10.5 Gas Composition and Basic Reactions	458
10.6 Entropy and Equilibrium Conditions	461
10.7 Equilibrium of the Internal Degrees of Freedom: Boltzmann Distribution	468
10.8 Equilibrium of Chemical Reactions and Composition of Gases	472
10.9 Reaction Rates	476
10.10 Relaxation of Complex Systems	479
10.11 Relaxation–Reaction Interaction	482

10.12 Relaxation of the Electron Temperature	487
10.13 Conclusion	489
11 Nonequilibrium Gas Flows	491
11.1 Equations of Nonequilibrium Gas Flows	491
11.2 Limiting Flow Regimes	493
11.2.1 Frozen Flow	494
11.2.2 Equilibrium Flows	494
11.2.3 Isentropicity of the Limiting Flows	496
11.2.4 Quasistationary Solutions	497
11.3 Limiting Speeds of Sound and Their Hierarchy	498
11.4 Speed of the Propagation of Disturbances in Nonequilibrium Gases	503
11.5 Shock Waves and Relaxation Zones	505
11.5.1 Hypersonic Shocks	508
11.5.2 Nonequilibrium Shock Waves	511
11.6 Short Waves and Weak Shocks in Nonequilibrium Gases	512
11.7 Near-Equilibrium Flows and Viscosity-Relaxation Analogy	516
11.8 General Theory of Stationary Waves in Relaxing Media	525
11.9 The Law of Binary Similarity	535
11.10 Nonequilibrium Flows Past Bodies	536
11.10.1 Flow Past Sharp Bodies with an Attached Shock	537
11.10.2 Thin Shock Layer in a Hypersonic Flow	538
11.10.3 Stagnation Point on a Blunt Body	539
11.10.4 Sphere and a Slender ($\theta = 10^\circ$) Spherically Blunted Cone	543
11.10.5 Bodies in a Nonequilibrium Supersonic Flow	545
11.11 Nozzle and Jet Flows: Hardening Effect	549
11.12 Thermal Rarefaction Waves	552
11.13 Sublimation Waves	557
12 Viscous Flows and Boundary Layers	563
12.1 Boundary Conditions and Equations of Motion for Dissipative Viscous Gas Flows	563
12.2 Some Exact Solutions of Navier-Stokes Equations	567
12.2.1 General Case $U_\delta = cx^m$	573
12.3 Parabolization of Incompressible Navier-Stokes Equations	574
12.4 Boundary Layer on a Flat Plate in an Incompressible Flow	579
12.5 Parabolization of the Compressible Navier-Stokes and Boundary Layer Equations	583
12.6 Boundary Layer in a Compressible Gas	589
12.6.1 Boundary Layer on a Flat Plate (in Particular, on a Wedge or a Cone in a Supersonic Flow)	592
12.6.2 Boundary Layer at the Blunt-Body Stagnation Point	595
12.7 Models and Properties of Turbulent Flows	597
12.8 Integral Relations and Approximate Methods: Boundary Layer on Blunt Bodies	602
12.9 Viscous-Inviscid Interaction: Basic Effects	612
12.9.1 Displacement Effect	612
12.9.2 Transverse Curvature Effect	613
12.9.3 End Effects	613
12.9.4 External Flow Nonuniformity Effect	614
12.9.5 Non-Thin (or Spread) Shock Effect	614

12.10 Boundary Layer in a Nonuniform Flow	616
12.11 Method of Mass-Average Parameters for the Boundary Layer in a Nonuniform Flow	621
12.12 Hypersonic Boundary Layer on Thin Sharp Bodies	625
12.13 Entropy Effect on Bluff and Thin Blunt Bodies	637
12.14 Flows in Viscous Continuous and Shock Layers	653
12.15 Problems of a Three-Dimensional Boundary Layer	669
12.15.1 Heat Transfer in a Divergent Flow	673
13 Viscous Flows of Multicomponent Gases	679
13.1 Physical and Chemical Models of Nonequilibrium Dissipative Gas Flows	679
13.2 Properties of Nonequilibrium Boundary Layers and Viscous Shock Layers	689
13.2.1 Frozen Boundary Layer	689
13.2.2 Equilibrium Boundary Layer	690
13.3 Transport Coefficients of Individual Components	699
13.3.1 Thermal Conductivities	699
13.3.2 Viscosity	699
13.3.3 Diffusivities	701
14 Elements of Radiating Gas Dynamics	703
14.1 Physics of Gas Radiation	703
14.2 Radiant Field in Radiating and Absorbing Jets	706
14.3 Flows of Intensely Radiating Gases	712
14.4 Flows of Nonequilibrium Radiating Gases	717
Bibliography	721
Index	727

Abstract

This book is devoted to real gas flows with regard for the physical and gas dynamic effects accompanying high-velocity flight in the air or other atmosphere and, in particular, the entry of bodies into the atmosphere of the Earth and other planets.

The chapters devoted to these particular problems are preceded by the presentation of the general theory of supersonic and, to some extent, subsonic flow, necessary for the comprehension of high-velocity gas dynamics in a united methodological aspect. In this respect, the monograph, which is mainly intended for senior and postgraduate students specializing in aerospace engineering, can be also useful for a wide circle of scientific researchers working at aviation institutes and in the aerospace industry.

In memory of academician Kh. A. Rakhmatullin, prominent scientist and remarkable man.

Preface

This book encompasses a wide range of fundamental gas dynamic problems stimulated mainly by the challenges that have arisen with high-velocity flight of vehicles in the air (or other) atmosphere. Here the term *high velocity* is synonymous with *high supersonic*, or *hypersonic*, that is, appreciably greater than the speed of sound, velocity.

However, hypersonic theory is only a branch of general gas dynamics and its isolated presentation is related to great difficulties owing to a need either to make numerous references to various handbooks (preferably, to a single handbook, which is not always possible) or to outline fragmentary elements of the general theory, which cannot, of course, be in competition with the systematic presentation of the subject. For this reason, apart from the chapters devoted to particular problems, the book also includes a general section, where the physical and mathematical foundations of gas dynamics are outlined. At the same time, this section incorporates some new elements, both methodological and concerning the essence of the problems.

The format of the book is particularly justified by the fact that previous monographs covering the same subject, which played a fundamental role in the formation of scientific views of several generations of scientists in gas dynamics, were written fairly long ago. This makes expedient the methodical revitalization and reassessment of their contents in the context of present-day gas dynamics, whose rapid development should be reflected in programs for training scientific researchers and in timely renewal of the corresponding handbooks. In this respect, the book reflects the concept of high-velocity gas dynamics developed in the second half of the twentieth century.

Thus, the book represents a manual of modern gas dynamics with emphasis placed on supersonic and, particularly, hypersonic flows. For this reason, many purely hydrodynamic divisions of the general theory of liquid and gas flows are omitted from the book, while subsonic flows are only touched upon in the context of their general properties that might manifest themselves in supersonic flow around bodies.

The book includes the topics of both inviscid and viscous gas dynamics; however, their presentations are highly nonuniform. Thus, while the presentation of inviscid gas dynamics constitutes almost an entire monograph, viscous flow theory is chiefly outlined as applied to hypersonic flight in the upper atmosphere. This is due to both the limitations on space and on the purely temporal and physical constraints of the author, which are understandable bearing in mind that the theme of viscous fluid and gas flow is, in truth, boundless.

From the methodical point of view, asymptotic analysis is typical of the hypersonic branch of general gas dynamic theory, that is, the study of certain limiting flow regimes (characterized by high flow velocity, limitingly thin bodies, limitingly strong shock waves, etc.) if, naturally, they adequately reflect the flow properties over the actual range of the flow conditions and body shapes. Precisely the onset of the manifestation of these asymptotic properties usually determines a rather conditional boundary between hypersonic and supersonic gas dynamics.

At high gas temperatures accompanying hypersonic atmospheric flight, various physical and chemical processes usually occur, such as dissociation, ionization, radiation; they are the reason behind the term *real gas*, which is used in this book devoted mainly to the flow of precisely this gas.

Taking real-gas properties into account often leads to exceptional gas dynamic effects; however, in most cases, these effects are, as it were, superimposed on the fundamental properties of flows, which makes it possible to use to study the common methods (particularly, of analytical and qualitative nature) developed for gases with the equation of state of the general form.

However, this book is not a manual on gas physics; therefore, the physical properties of gas mixtures and the high-temperature processes in them are described from the phenomenological standpoint, which is quite sufficient in order to give an idea of the origin, structure, and specific features of the additional equations encompassing the basic system of gas dynamic equations and to construct then the general gas dynamic theory of real-gas flows. Experience has shown that this approach is preferable for readers who proceed to these problems from the gas dynamic direction.

Apart from general theory, the book includes a set of particular problems. The difficulty of their choice is obvious; in this respect, the author was guided by both the significance and typicality of particular problems as determined in recent time and, to a certain extent, his own scientific interests, which lie mainly in the field of problems associated with flow around bodies. For this reason, problems of nozzle and jet flows are only briefly presented in the book.

Many previously unsolvable problems of gas dynamics became fairly simple with the development of computational mathematics and equipment. However, in the opinion of the author, the numerical methods are to this day inferior to the analytical methods when it comes to the creation of concepts and notions that could serve as the basis for understanding the essence of gas dynamic and other physical problems. In this connection, the author tried to avoid cumbersome approximate methods, however effective these were in the past, and he set himself the task to give the reader an idea of the general patterns and features of typical flows and the real gas effects on these flows, with reference to some simple, analytically treatable examples, similarity laws, and asymptotic analysis. For the same purpose, the results of exact numerical solutions and experimental data are used, though the topics of both computational and experimental gas dynamics are omitted from the book, since the specific features of these two branches do not make it possible to entwine them in the book without considerably enlarging it.

We note that at present the fundamental gas dynamic information is taken from either experiments or—to an increasing extent—from exact numerical calculations. However, experience has shown that in both cases some reliable ideas on the qualitative nature and the properties of flows are required*, the book focuses precisely on the description of these properties.

Finally, the author endeavored to use a concise style of writing, without going into the details of cumbersome algebra, particularly on topics of a special, not general nature. Giving an outline of the reasoning and presenting the final results is the optimal approach for the reader who wants to familiarize himself with the subject and presents no obstacles for a searching reader who wishes to deepen his knowledge of the subject.

On the whole, the book is intended for scientific researchers and engineers working in the aerospace industry and senior and postgraduate students of universities and technological institutes.

* An idea of “absolute” numerical algorithms that could solve an arbitrary problem without any *a priori* knowledge of the properties of its solutions is no more than a myth.

In conclusion, I would like to note that the book is the result of my 50 years of scientific work within the walls of the Central Institute of Machine Building (TsNIIMash), where I was for many years head of the Hypersonic Gas Dynamics Laboratory, and my 40 years of pedagogical activity at the Moscow Physico-Technical Institute. However, the book is not the fruit of only the author's efforts. Its creation was made possible thanks to the creative atmosphere, the exchange of ideas and information that always distinguished the Russian school of scientists in gas dynamics. Therefore, I express my gratitude to all my colleagues and collaborators, my teachers and pupils, as unintentional coauthors of this book.

I am particularly grateful to my pupils and colleagues V. I. Vlasov, A. B. Gorshkov, G. N. Zalogin, B. A. Zemlyanskii, and R. V. Kovalev, who rendered great help, both ideological and practical, during my work on the book.

For their toil in translation of the book from Russian into English, I wish to thank Dr. Ninel T. Pashchenko (Chapters 1–4) and Professor Michail G. Lebedev (Preface and Chapters 5–14), who also carried out the scientific and literary editing of the Russian manuscript and its translation as a whole.

I am sincerely grateful to my wife, Maya S. Luneva, for her literary and mathematical polishing of the text and for her patience of many years pending the completion of the work on this book.

Author

Vladimir V. Lunev, PhD graduated from Moscow University's Department of Mechanics and mathematics in 1954, and in 1956 earned a PhD in physics and mathematics and a DSc in 1966. Since 1962, Dr. Lunev has acted as head of the Laboratory of Hypersonic and Physical Gas Dynamics of the Central Scientific Research Institute of Machine Building in Korolev (TSNIImash). Also, since 1962 Dr. Lunev has served as an assistant professor, and since 1969 has been a full professor at the Moscow Institute of Physics and Technology, Department of Aero-Physics and Space Research. He is a wide-range specialist in the area of gas dynamics with particular specialization in hypersonic velocity motions of flying apparatus, especially all associated physical-chemical processes in real gases.

Dr. Lunev is a member of the Russian Academy of Natural Science, a member of the National Community of Russia, and is a recipient of the Lenin Prize (1966), the highest scientific award of the Soviet Union. He is an author of several books and more than 100 publications in journals. The Russian version of this volume was written in the best traditions of the Russian Fluid Mechanics School. For this book the author was awarded the Professor Zhukovsky Prize.

1

Gas Dynamic Model and Equations of Gas Flows

In this chapter we will formulate a gas flow model that will be termed gas dynamic; it is adequate to the typical regimes of the motion of vehicles of standard dimensions in moderately dense gas media, such as the atmospheres of Earth and some other planets, or the flow past the models of such vehicles in bench testing. Within the framework of this model, the equations governing the gas flows will be derived and some attendant theoretical problems will be elucidated.

The basic mechanical and physical laws governing gas dynamic processes are first formulated with reference to the simple example of the one-dimensional flow, which does not require, in particular, making recourse to complicated vector and tensor procedures; we next pass on to the derivation of the gas dynamic equations in the general form.

At the same time, some classical elements of the theory, such as kinematics, tensor analysis, and so on, are given only in a condensed form. Their detailed presentation can be found in the books by Kochin, Kibel, and Roze (1963), Loitsyanskii (1966), Rakhmatullin et al. (1970), Sedov (1972), Landau and Lifshitz (1959), and others.

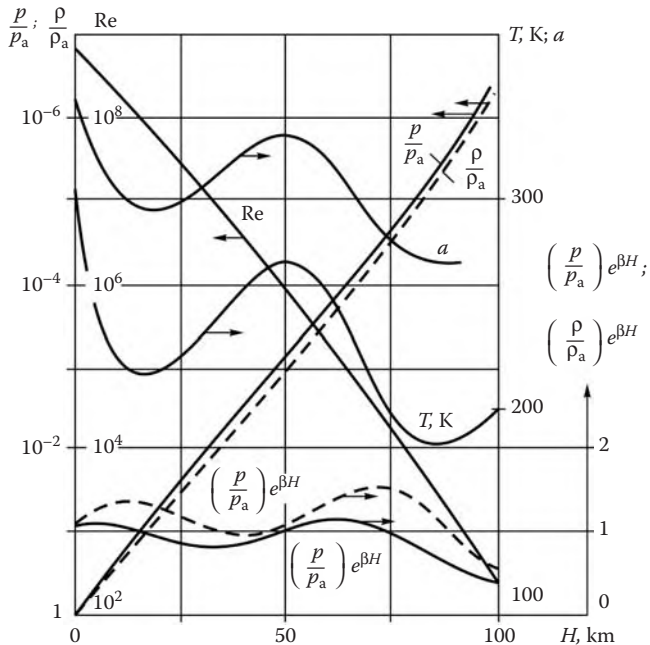
1.1 Outline of the Gas Dynamic Model of Gas Flows

Before presenting the general theory of gas flows we will describe the main *gas dynamic model* of a gas medium, common for a wide range of gas dynamic problems.

Generally, we will take the term *model of a medium* to mean a set of equations governing the processes under consideration, together with some additional conditions (boundary, initial, etc.), determining completely a particular process. The essence of the gas dynamic model will be explained in the following.

In constructing a gas dynamic model (as well as a model in any other branch of science) one should first take into consideration purposes and conditions of its application. The main purpose is to provide the engineering development of various vehicles intended for flights mainly in the Earth's atmosphere (or their reentry from different space orbits) (*external problems*), to study the flows in nozzles and ducts (*internal problems*), and so on. In external problems, which constitute the subject matter of this book, preconditions for the application of gas dynamic models are determined by the vehicle size L and the range of flight velocities U and ambient medium parameters, for instance, pressure p , density ρ , temperature T , and so on, which, in their turn, are dependent on the flight altitude H .

While the temperature in the terrestrial atmosphere varies fairly slightly, namely, on the range $T \approx 200\text{--}300\text{ K}$, the pressure and density can change by several orders of magnitude. This is illustrated in Figure 1.1, in which mean statistical parameters of gases in the Earth's atmosphere are presented (the parameters of the so-called "standard atmosphere"). Integrating the hydrostatic equation $dp = -\rho g dH$, where $g = 9.81\text{ m/s}^2$ is the gravity acceleration, together with the condition of the isothermal atmosphere $p/\rho = p_a/\rho_a$, we obtain

**FIGURE 1.1**

Parameter distributions in the Earth's atmosphere (a [m/s] is the speed of sound; Re corresponds to $L = 1$ m and $U = 7$ km/s).

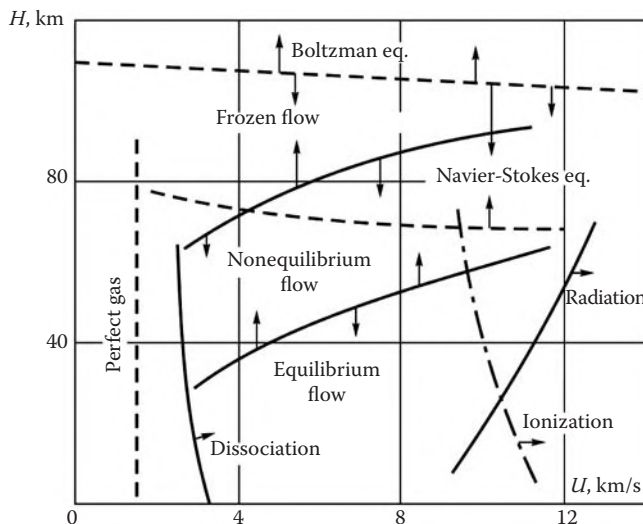
$$\begin{aligned} \frac{p}{p_a} = \frac{\rho}{\rho_a} = \frac{n}{n_a} = \frac{l_a}{l} = \exp(-\beta H), \quad \beta = \frac{g \rho_a}{p_a} = 0.14 \text{ km}^{-1} \\ p_a = 10^5 \text{ N/m}^2 = 1 \text{ atm}, \quad \rho_a = 1.29 \text{ kg/m}^3 \\ n_a = 2.5 \cdot 10^{19} \text{ cm}^{-3}, \quad l_a = 6 \cdot 10^{-6} \text{ cm} \end{aligned} \quad (1.1.1)$$

Here, the quantities n , l (numerical concentration and mean free path of molecules), p_a , and so on are divided by their values at sea level. As can be seen from Figure 1.1,* these formulas describe satisfactorily the density and pressure in the atmosphere for $\beta = 0.14 \text{ km}^{-1}$.

In sufficiently dense atmospheric layers ($H \leq 100$ km) the variation of the ratio ρ/ρ_a and other ratios can be as great as 10^6 -fold, thus influencing some particular features of physical and gas dynamic flow models. Generally speaking, these models vary depending on flight ranges, which are conditionally presented in Figure 1.2.

The vast majority of gas dynamic theories (except for those for low-density gases) are based on the fundamental model, or hypothesis, of a *continuous medium*, despite the corpuscular structure of gases, which allows sufficiently free motion of molecules and atoms throughout a volume filled by the particles. This model implies the possibility to pass from a collection of individual parameters of separate molecules to a set of average macroscopic

* In this and subsequent figures the arrows at curves indicate the scale with which the corresponding curve is associated

**FIGURE 1.2**

Approximate ranges of the influence of different physical processes on the flow past a sphere of 1 m radius in flight in the Earth's atmosphere.

parameters in describing the state and properties of a gas medium. This is possible thanks to high molecular concentration in the terrestrial atmosphere (this will be discussed in more detail in Section 1.4). For sufficiently rarefied gases (for example, for atmospheric layers at $H > 100\text{--}120$ km) such thermodynamic notions as pressure and temperature no longer exist in the conventional sense and the main characteristic of this low-density medium is the *function of molecular distribution* with respect to velocities, space, time, and so on. This flow model (which forms the basis of the *kinetic theory of gases*) can be considered the ultimate stage in constructing the hierarchy of continuum models in decreasing gas densities. The free-molecular flow region, where the gas can no longer be considered a continuous medium, is located on a lower density level (but on a higher one with respect to the flight altitude).

As the gas density increases (i.e., at flight altitudes $H \leq 90\text{--}100$ km), there is a wide range of applicability of a simpler macroscopic model. We will call it a *gas dynamic model of medium*, since the gas dynamics in the ordinary sense of this term deal precisely with the flow regimes pertaining to this range.

In this case the state and dynamics of a gas are completely described by a set of macroscopic parameters such as the gas velocity vector \mathbf{U} , the *basic thermodynamic parameters* p, ρ, T , and e , for instance, pressure, density, temperature, and specific (referred to unit gas mass) energy, and a set of *kinetic parameters* (λ_i) determining, in general case, the state and composition of mixtures of various i -th species. This model consists of the following main elements:

1. Finite (algebraic) relations between thermodynamic parameters called the *equations of state*. In particular, in the standard (room) conditions these are the Clapeyron equation of state $p = \tilde{R}\rho T$, where \tilde{R} is the gas constant for a given gas, and the caloric equation of state $e = c_v T$, where c_v is the constant specific heat at constant volume (density). These gases are referred to as *perfect*.

2. Relations between internal macroscopic forces (stresses) and a velocity field, or a *rheological* model of a medium (viscous fluids and gases in the case under consideration).
3. And, finally, a set of equations based on the fundamental laws of conservation of mass, momentum and energy.

Gas dynamics as a whole could be divided into two hierarchy stages ordered in increasing gas density. Generally, in addition to a normal force due to the hydrostatic pressure p , any area element in a gas is exposed to the action of viscous stresses. Moreover, heat fluxes due to heat conductivity and diffusion and diffusive fluxes of gas mixture components (in the case of multicomponent media) pass through the element. These effects are referred to as *dissipative*. Being taken into account, together with a real model of a viscous fluid, they lead to the *Navier–Stokes equations*, which can be considered as the highest stage of the gas dynamic model hierarchy.*

Strictly speaking, the main parameter determining the viscous flow structure is a dimensionless combination of parameters called the *Reynolds number*, $Re = \rho UL/\mu$, rather than the density. For gases, as well for fluids, the viscosity μ depends mainly on temperature; for this reason, the order of the magnitude of the Reynolds number in the atmospheric flight is mainly determined by density. The altitude dependence of Re for typical reentry conditions is plotted in Figure 1.1.

In high- Re flows the viscosity effect is concentrated only in narrow *boundary layers* (mainly in the vicinity of solid surfaces) whose thicknesses are of the order of $LRe^{-1/2}$; outside these layers, the flow is inviscid and is described by *Euler equations*.

This model gives rise to a wide and fundamental branch of gas dynamics, the theory of *inviscid* or, as they are frequently called, *ideal* fluids, and most of this book is devoted precisely to this subject.

Apart from the Reynolds number, we will note one more important parameter that makes it possible to determine qualitatively different physical and mathematical features of gas dynamic problems. This is the *Mach number*, $M = U/a$, a being the speed of sound in the gas. With respect to this parameter, all gas flows could be divided into *subsonic* ($M < 1$), *transonic* ($M \approx 1$), and *supersonic* ($M > 1$). The zero Mach number ($M = 0$) corresponds to the *incompressible fluid model*, while the $M \gg 1$ flows are called *hypersonic*.

The previous consideration was concerned with one aspect of the fundamentals of gas medium models. The other aspect is related to the variation of gas properties with increasing temperature, namely, to the accompanying physical-chemical processes.

Cold air is mainly a mixture of diatomic gases, oxygen (21% of the total number of air molecules) and nitrogen (78%), with a small amount of argon (about 1%). For relatively low temperatures, $T \leq 500 - 700$ K (i.e., as will be shown, for intermediate supersonic flight velocities with the Mach numbers $M \leq 3$) the air can be considered as a perfect diatomic gas. However, the air temperature increases appreciably with the flight velocity. The matter is that at the stagnation point (e.g., in a flow past a blunt body) the increase in the internal energy of gas particles is of the order of the kinetic energy of the relative motion of the gas, which is very high in hypersonic flight. Thus, at velocities $U = 8 - 10$ km/s a perfect gas acquires the temperature as high as $T \approx 3 \cdot 10^4 \div 6 \cdot 10^4$ K. Of course, the original, or *normal*, gas state can no longer exist at such temperatures.

* A good historical survey of the development of fluid and gas dynamics can be found in Loitsyanskii (1966).

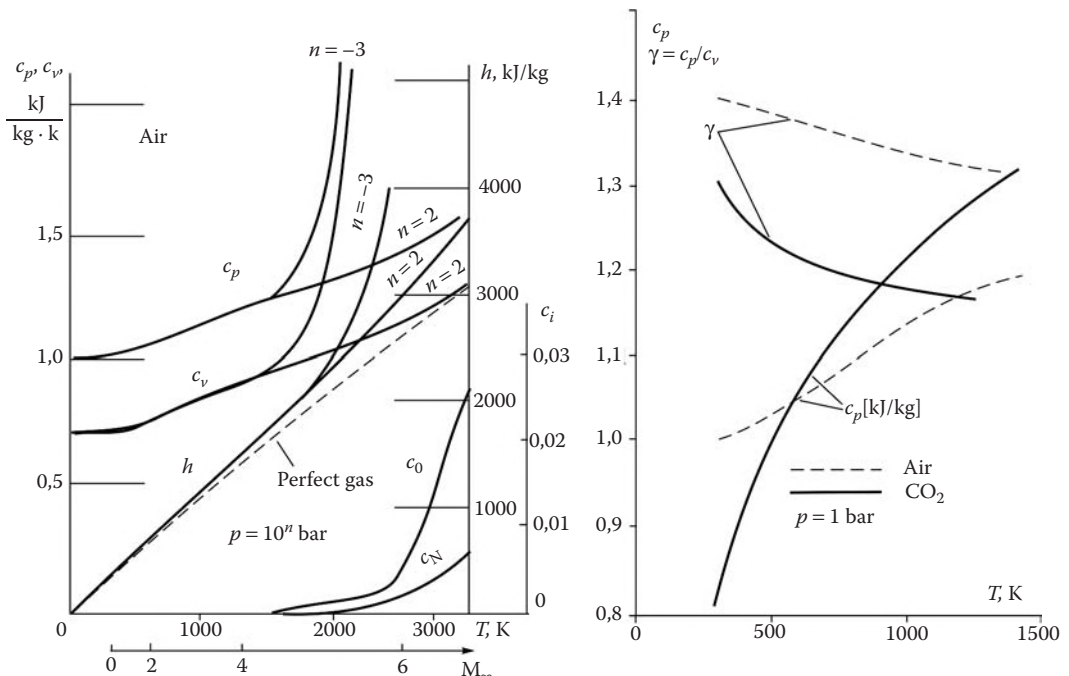


FIGURE 1.3
Specific heats, adiabatic exponents, and species concentrations for equilibrium air and carbon dioxide.

As the temperature increases, vibrational degrees of freedom of air molecules are first excited, which leads to an increase in specific heats (Figure 1.3). For $T > 2000 \text{ K}$ molecular oxygen begins to decompose (dissociate) into an atomic one, while for $T > 4000 \text{ K}$ nitrogen does the same. With further temperature increase, the *ionization* process begins, which gives rise to the formation of free electrons (Figure 1.4).

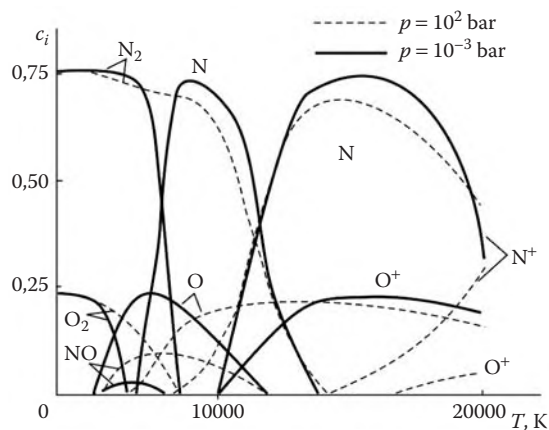


FIGURE 1.4
Dependence of the mass concentrations of molecules, atoms, and ions in equilibrium air.

An important fact is that these processes are energy intensive. A part of the kinetic energy of the flow incident on a blunt body, which is spent in physical and chemical processes at its stagnation point, is shown in Figure 1.5. Clearly, the energy of molecular vibrations is relatively small, while ionization and dissociation require up to 75% of the flow energy. These effects make many results of the perfect gas dynamics inapplicable.

The crucial role is played by the relation between the rates of physicochemical and gas dynamic processes. If reactions proceed much more rapidly than the thermodynamic state of the gas changes, then the gas can be considered to be in equilibrium at any point. Such flows are called the *equilibrium flows*. In the other limiting case, physicochemical processes have no time to start, since a gas particle rapidly leaves the flow region under consideration, so that the gas composition does not change. Such flows are termed *frozen*.

In both limiting cases it is sufficient to use only the main thermodynamic parameters (p, ρ, T, e) to describe the gas state, the parameters being related by finite equations (equations of state). In these cases, the mathematical and gas dynamic properties of equations governing the gas flows and the formulations of problems do not differ from those for a perfect gas.

A major part of the book is devoted to the theory of precisely these flows; we will call this theory *equilibrium gas dynamics*. In actual practice, its applicability range is rather wide, but from the theoretical point of view it is even wider, since the theoretical laws established by this theory are quite general and have a meaning even for a wide intermediate region of physically and chemically *nonequilibrium* flows.

The *nonequilibrium gas dynamics* differs from the equilibrium one by the presence of additional differential equations (in some cases, their number can be as high as several tens), which leads to the appearance of some new effects, both physical and mathematical.

Whether one or another type of the flow past a body is realized, depends on the flow conditions. Since the rates of physicochemical processes usually increase with the gas density, equilibrium flow regimes are typical for flights at relatively low altitudes (at $H \leq 30$ km for bodies of standard dimensions, $L \sim 1$ m), while frozen flows take place at very high altitudes (about $H \geq 80$ km). The boundary of essentially viscous flows is located slightly lower. The boundaries of the influence of physicochemical processes are strongly dependent on the flight velocity; they are also shown in Figure 1.2.

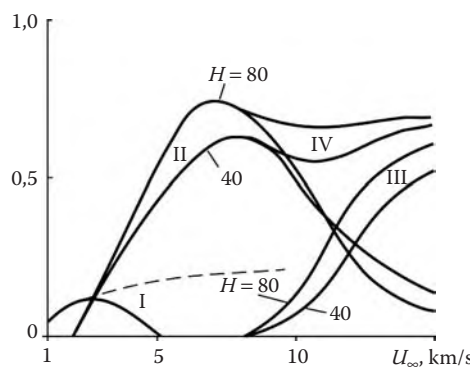


FIGURE 1.5

Ratio of the energies of vibration (I), dissociation (II), and ionization (III), as well as the sum of two last energies (IV), to the kinetic energy $1/2U_{\infty}^2$ of the translational movement of undisturbed gas for flight altitudes 40 and 80 km (dashed line is plotted for the vibrational energy in the absence of dissociation).

Before closing the general review of the models and properties of gas flows that will be studied in what follows, we will make an important remark on the methodology of constructing gas dynamic flow models.

There are two approaches to the construction of physical models of gas media. The first consists in using the appropriate physical laws and relations obtained by generalizing empirical data. This way (we will call it *phenomenological*) has a doubtless historical priority, does not require detailed knowledge of the fluid behavior at the molecular level, and is quite sufficient to construct axiomatics for the theoretical fluid and gas dynamics. Therefore, it provides the basis for all known handbooks on the theory and this book is not an exception.

The second, *molecular-kinetic*, approach is based on an analysis of the properties of a gas medium considered a large ensemble of colliding molecules whose random motions and collisions lead eventually to the macroscopic laws. The corresponding kinetic theory is based on the so-called *Boltzmann equation*, which is so general that both the Navier–Stokes and Euler equations can be mathematically obtained from the Boltzmann equation as its limiting forms.

This theory is beyond the scope of this book, but sometimes it will be used since it gives a possibility to widen our views on the origin of one or another of the basic results by applying very simple molecular-physical reasoning.

We note in conclusion that the applicability range of the gas medium and flow models thus formulated cannot be obtained within the framework of the model itself but is established by the totality of the corresponding studies, both theoretical and experimental, and, more generally, by the totality of experience gained by generations of researchers in the field of fluid and gas dynamics.

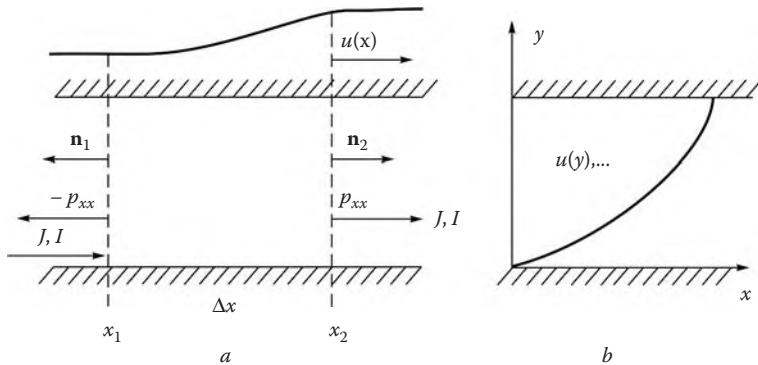
1.2 Postulates and Equations of Gas Dynamics: One-Dimensional Flow

These laws and equations will be first considered with reference to the example of a geometrically very simple one-dimensional real gas flow, that is, a flow in a rectilinear channel (tube) of an arbitrary cross-section (its area is set to be $\Sigma_0 = 1$), which does not vary along the longitudinal x axis. The wall influence is neglected, which makes it possible to consider the pressure p , the density ρ , the temperature T , the internal energy e , the longitudinal velocity u , and so on as the functions of x and t only.

Almost all laws of mechanics and physics are originally formulated for material bodies of fixed masses. Therefore, to define such a body we introduce a notion of a *fluid volume* $\Delta\Omega^*$ bounded by a *fluid surface* $\Delta\Sigma^*$ with no mass flux across any surface element. Thus, the surface under consideration consists of the same particles and moves together with the flow as if it were frozen in it.

A small fluid volume $\Delta\Omega^*$ bounded by a surface $\Delta\Sigma^*$ will play a role of an elementary fluid particle for which we will derive an equation of motion using three fundamental conservation laws for mass, momentum, and energy, the particular properties of a continuum medium being postulated as may be necessary.

The *mass conservation law* for a fluid particle can be written as $d(\rho\Delta\Omega^*)/dt = 0$. In an one-dimensional flow $\Delta\Omega^* = \Sigma_0\Delta x = \Delta x = x_2(t) - x_1(t)$, where $x_1(t)$ and $x_2(t)$ are the fluid boundaries of the volume $\Delta\Omega^*$ (Figure 1.6a). Using the relation

**FIGURE 1.6**

On the derivation of the equations of motion for gases.

$$\frac{d}{dt}(x_2 - x_1) = u_2 - u_1 = \frac{\partial u}{\partial x} \Delta x \quad \left(u_i = \frac{dx_i}{dt} \right) \quad (1.2.1)$$

we obtain the *mass conservation equation*, or the *continuity equation*

$$\frac{d\rho}{dt} = \frac{\partial\rho}{\partial t} + u \frac{\partial\rho}{\partial x} = -\rho \frac{\partial u}{\partial x} \quad (1.2.2)$$

Here, the operator d/dt is the total derivative describing the change of a parameter for a particular fluid particle. By differentiating the function $\rho(t, x)$ as a composite, or total, function of time, $\rho(t, x) = \rho[t, x(t)]$, we obtain Equation 1.2.2.

1.2.1 The Momentum Conservation Law

Let the stress $p_{xx}(x_2)$ act from the right on a section $x = \text{const}$ bounding the volume $\Delta\Omega^*$ at time t , the stress being equal to the force for $\Sigma_0 = 1$. The positive direction of this and the following vectors are taken to coincide with that of the x axis. The same force, however oppositely directed, for instance, $-p_{xx}(x_1)$, acts on the same area from the left; hence, the net force acting on the volume is $(\partial p_{xx}/\partial x)\Delta x$. The *momentum equation* is obtained by applying the Newton law to a fluid particle of the mass $\rho\Delta x$

$$\begin{aligned} \rho \frac{du}{dt} &= \frac{\partial p_{xx}}{\partial x} = -\frac{\partial p}{\partial x} + \frac{\partial \tau_{xx}}{\partial x} \\ p_{xx} &= -p + \tau_{xx} \end{aligned} \quad (1.2.3)$$

Here, the second equation involves the hypothesis (by no means formal) on the possibility of separating out the *hydrostatic*, or *thermodynamic*, pressure p from acting internal forces. The pressure force acts on a fluid particle along its inward normal from outside and is independent of the particle orientation. This pressure has the same meaning as that in a quiescent gas and enters in the same thermodynamic relations (to be given in what follows).

The term τ_{xx} is the *viscous stress*, the representation of which in terms of other parameters defines the *rheological model* of a medium. Here, we deal with *Newtonian fluids* only, for which all viscous stresses depend on the velocity field only through linear combinations of velocity derivatives that are absent in a gas at rest (the last statement is the general

property of fluids). In what follows, this model will be formulated in detail; here we give expressions for viscous stresses only for two simple types of the flow, namely, for the longitudinal one-dimensional flow and for a simple *shear flow* (Figure 1.6b) with a longitudinal velocity $u = u(y)$ dependent on the transverse coordinate only. In these cases

$$\tau_{xx} = \mu' \frac{\partial u}{\partial x}, \quad \tau_{xy} = \mu \frac{\partial u}{\partial y} \quad (1.2.4)$$

Here and in what follows, the first subscript of τ means the direction of an acting force, while the second one means that of the normal to an area element.

The second formula expresses the empirical *Newton friction law* (here μ is the conventional viscosity coefficient), while the first formula is a generalization of the second one. The relation between the coefficients μ and μ' may vary depending on the mutual orientation of the velocity vector and the area element, as well as on the flow type. Later we shall obtain that $\mu' = 4\mu/3$ for gases, while for incompressible fluids the relation $\mu' = 2\mu$ holds.

We note that Equation 1.2.3 does not involve mass, or body, forces; they will be taken into account in Section 1.7.

1.2.2 The Energy Conservation Law

Let us fit the coordinate system to a moving fluid volume $\Delta\Omega^*$ setting, for example, the origin at the volume midpoint. Then at volume deformation all relative velocities of its points are of the order of $\Delta u = (\partial u / \partial x)\Delta x$, while the kinetic energy of this relative motion is of the order of $(\Delta u)^2 \sim (\Delta x)^2$ and can be neglected. The gas in the volume can be considered to be at rest so that in this case the energy conservation law represents the first law of thermodynamics

$$\rho \Delta\Omega^* de + dA = dQ \quad (1.2.5)$$

Here, e is the *specific* (per unit mass) *internal energy* of the gas, dA is the work of external forces acting on the gas within the volume $\Delta\Omega^*$, and dQ is the external heat influx. Fluid boundaries of the volume, $x_i(t)$, move at velocities $\pm\Delta u/2$ in the opposite directions against external forces (p_{xx} on the right and $-p_{xx}$ on the left). Hence, in a time dt the work done on a deforming volume is as follows:

$$dA = -p_{xx}\Delta u dt = -p_{xx}d\Delta\Omega^* = pd\Delta\Omega^* - \tau_{xx} \frac{\partial u}{\partial x} \Delta\Omega^* dt \quad (1.2.6)$$

It is important that, in view of the smallness of Δu , the difference in force magnitudes can be neglected.

We will now consider the term dQ in Equation 1.2.5. First of all, it can be related with some external heat sources (e.g., radiation) with the mass intensity q . Moreover, heat or energy fluxes can pass through volume faces at their own specific (per unit area) intensities $J(x_1)$ on the left and $J(x_2)$ on the right, with the total contribution equal to $-(\partial J / \partial x)\Delta x$. Making the summation and taking into account that $d\Delta\Omega^* = \rho \Delta\Omega^* d\rho^{-1}$ we reduce Equation 1.2.5 to one of the two forms of the differential equation for energy

$$\begin{aligned} \frac{de}{dt} + p \frac{d\rho^{-1}}{dt} &= \frac{dh}{dt} - \frac{1}{\rho} \frac{dp}{dt} = q_{\text{eff}}, \quad h = e + \frac{p}{\rho} \\ q_{\text{eff}} &= q + \frac{\mu'}{\rho} \left(\frac{\partial u}{\partial x} \right)^2 - \frac{1}{\rho} \frac{\partial J}{\partial x} \end{aligned} \quad (1.2.7)$$

Here, h is the *specific enthalpy* of the gas that is often used instead of the energy e . The term q_{eff} has the meaning of the *effective heat influx*, the left-hand side of the equation having the conventional form of the first law of thermodynamics for an inviscid gas.

The three gas dynamic equations thus obtained are quite general from the physical point of view. Their form depends neither on a particular gas nor on internal processes in the gas. This is due, in particular, to the fact that the internal energy was defined in such a fashion that it includes the energies of all physicochemical processes, both equilibrium and nonequilibrium, occurring in gases. This approach is generally accepted in physical gas dynamics (including this book), but it is not the only possible approach. Thus, in combustion theory e may often mean the translational energy of molecules, the chemical heat sources being included in q .

Finally, for the sake of completeness we will give an *equation of chemical kinetics* for species i of a gas having the *mass concentration* $c_i = \rho_i/\rho$ and *partial density* ρ_i . By analogy with the previous equation, the mass conservation law can be reduced to the form:

$$\rho \frac{dc_i}{dt} = \rho \Lambda_i - \frac{\partial I_i}{\partial x} \quad (1.2.8)$$

Here, the equality $d(\rho_i \Delta \Omega^*) = \rho \Delta \Omega^* dc_i$ is taken into account.

The chemical source of species i is denoted by Λ_i , while I_i is the specific intensity of its mass flux through fluid volume boundaries due to diffusion processes. In accordance with the definition of fluid surface, the sum of all these fluxes is zero: $\sum_{i=1}^n I_i = 0$. The number of these equations must be equal to the number of the species and can be as high as a few dozen in gas dynamics.

We will now specify the fluxes J and I_i . Separating out the term J_T , which is due only to heat conduction, in the first flux and restricting ourselves to binary gas mixtures (e.g., those consisting, say, of atoms and molecules with concentrations of c_1 and $c_2 = 1 - c_1$) for the second flux, we can determine these fluxes from the empirical *Fourier's* heat conduction and *Fick's* diffusion laws as follows:

$$J_T = -\lambda \frac{\partial T}{\partial x}, \quad I_1 = -\rho D_{12} \frac{\partial c_1}{\partial x} \quad (1.2.9)$$

Here, λ and D_{12} are *thermal conductivity* and *binary diffusion*, respectively. However, in the general case, the energy is also transferred by diffusion of components having different energies. For example, if h_1 and h_2 are the enthalpies of these components, the total energy flux is

$$J = -\lambda \frac{\partial T}{\partial x} - \rho D_{12}(h_1 - h_2) \frac{\partial c_1}{\partial x} \quad (1.2.10)$$

This expression can be simplified for $c_1 = c_1(T)$ (e.g., in the case of isobaric equilibrium processes, as will be shown in the following). In this case we have

$$J = -\lambda_{\text{eff}} \frac{\partial T}{\partial x}, \quad \lambda_{\text{eff}} = \lambda + \rho D_{12}(h_1 - h_2) \frac{dc_1}{dT} \quad (1.2.11)$$

Here, λ_{eff} is the *effective thermal conductivity* of the gas.

Thus, the system of the Navier–Stokes equations for one-dimensional flows has been derived. Letting the *transport coefficients* μ , μ' , λ , and D_{12} , or the derivatives of u and so on, in the *dissipative* terms of these equations tend to zero, we obtain as a result the Euler equations governing inviscid gas flows.

In any case, the system of four equations (all equations of the form of 1.2.8 are considered as a single equation) for six unknown functions u , p , ρ , T , e , and c_i is as yet unclosed. Additional relations closing the system are the equations of state to be discussed, together with the transport coefficients, in Section 1.3.

1.3 Equations of State

Here, equations of state for gases are postulated for gases in a physically and chemically equilibrium state, that is, the state in which a mechanically and adiabatically insulated system can reside indefinitely. Therefore, the results of the equilibrium gas dynamics are applicable only to equilibrium, or *reversible*, processes formed by a sequence of states that replace one another infinitely slowly, that is, to fairly slow (in this sense) flows.

It is known from thermodynamics that in this case it is sufficient to specify only two thermodynamic parameters, say p and T , in order to determine the state of a gas (or any other medium). Thus, the equilibrium is based on a *two-parameter gas model* with equations of state of the type

$$\rho = \rho(p, T), \quad e = e(p, T), \quad h = h(p, T) \quad (1.3.1)$$

Eliminating the temperature from these relations, we obtain the equations of state in the form $\rho = \rho(p, e)$ or $\rho = \rho(p, h)$, which is sufficient, at least, for inviscid equations in which temperature does not enter at all.

The simplest two-parameter gas is a perfect gas with *Clapeyron's equation of state*

$$p = nkT = nm \frac{N_0 k}{N_0 m} = \frac{R}{\bar{M}} \rho T \quad (1.3.2)$$

Here, $R = kN_0 = 8.314 \text{ J/(mole} \cdot \text{K)}$, $k = 1.38 \cdot 10^{-23} \text{ J/K}$, $N_0 = 6.02 \cdot 10^{23} \text{ 1/mole}$, $\bar{M} = mN_0 \text{ g/mole}$, m is the molar mass, R is the universal gas constant, N_0 is the Avogadro number, that is, the number of molecules in a gas mole, \bar{M} is the molar gas mass in grams per mole, k is the Boltzmann constant, and n is the *number concentration*, or the number of molecules in a unit volume equal to 1 m^3 in the SI system in which the values of R and k are given. However, in physics the molecular concentration is usually referred to 1 cm^3 , as has been done above, in Section 1.1.

Moreover, for a perfect gas there exists the *caloric equation of state*

$$e = c_v T, \quad h = c_p T, \quad (c_p/c_v = \gamma) \quad (1.3.3)$$

which is valid in this form only when the specific heats at constant pressure c_p and volume c_v are constant. For standard, or atmospheric, conditions, air is a perfect gas with the following parameters

$$\begin{aligned} c_p &= 0.24 \text{ kcal/(kg} \cdot \text{K)} = 1 \text{ J/(kg} \cdot \text{K)} = 1000 \text{ m}^2/(\text{s}^2 \cdot \text{K}) \\ c_v &= 0.17 \text{ kcal/(kg} \cdot \text{K)} = 0.715 \text{ J/(kg} \cdot \text{K)} = 715 \text{ m}^2/(\text{s}^2 \cdot \text{K}) \\ \bar{M} &= 28.9, \quad \gamma = 1.405 \end{aligned}$$

In the general case, the relations of the type 1.3.1 are valid for a wide class of liquid media including superdense gases (the so-called Van der Waals gases) or liquid metals at superhigh pressures, and so on. Therefore, the theory outlined in the book, especially for inviscid media, is usually of a general nature, though we bear in mind primarily applications concerned with flights in the Earth's atmosphere.

The validity of relations 1.3.1 is usually restricted by the condition of gas equilibrium. The substantiation and the range of reliability for such a model can be obtained only within the framework of thermodynamics of nonequilibrium processes, the theory of which will be outlined in the subsequent chapters, where the two-parameter equilibrium

gas model will be rigorously substantiated. However, in general terms, its origin can be clarified here.

We will consider mixtures of *moderately dense gases* whose molecules interact only during relatively short time intervals of collision.* This gas model appears to be valid over the entire practical range of conditions concerned with atmospheric flights, since the gas density behind the shock wave ahead of a moving body cannot exceed (as will be seen later) 10–20-fold undisturbed density, which is not sufficient to abandon the model accepted.[†]

In the mixtures under consideration the characteristics of individual species are, as it were, independent of those for other components. In particular, for each species i of the mixture the Clapeyron equations in the form $\bar{M}_i p_i = R \rho_i T$ are valid, together with certain dependences of energies e_i on the temperature and the state of internal degrees of freedom. The total pressure and energy are determined in accordance with the addition *Dalton law*

$$\begin{aligned} p &= \sum_i p_i = \frac{R}{\bar{M}} \rho T, & \frac{1}{\bar{M}} &= \sum_i \frac{c_i}{\bar{M}_i}, & e &= \sum_i c_i e_i \\ h &= e + \frac{p}{\rho} = \sum_i h_i c_i, & h_i &= e_i + \frac{p_i}{\rho_i}, & c_i &= \frac{\rho_i}{\rho} \end{aligned} \quad (1.3.4)$$

Here, c_i is the *mass concentration* of species i .

In these equations no assumption is made on chemical equilibrium of the gas mixture, so that they may be used for describing nonequilibrium flows as well. Even from general physical considerations, the statement that an equilibrium gas state with given pressure, temperature, and element composition is associated with quite definite parameters $\bar{M} = \bar{M}(p, T)$ and $h = h(p, T)$, looks plausible and leads to dependences of the form 1.3.1.

We call the quantity \bar{M} the mean *molar mass of a gas mixture* (or simply the molar mass). It was precisely in this fashion that the value $\bar{M} = 28.9$ for air in standard conditions was obtained.

Equilibrium dependences $\bar{M}(p, T)$ and $h(p, T)$ are presented[‡] in Figure 1.7 for air on pressure and temperature ranges typical of aerodynamics. Clearly, at high temperatures the air enthalpy is essentially greater than that of a perfect gas. As the temperature (and, hence, atom concentration) increases, the molar mass decreases. The fact that its value $\bar{M} \approx 10$ is lower than the molar mass of atomic air, $\bar{M} \approx 14$, can be explained by the presence of the electron gas, which, though having a negligible concentration, influences the number of particles. We note the weak, “logarithmic,” dependence of \bar{M} and h on the pressure.

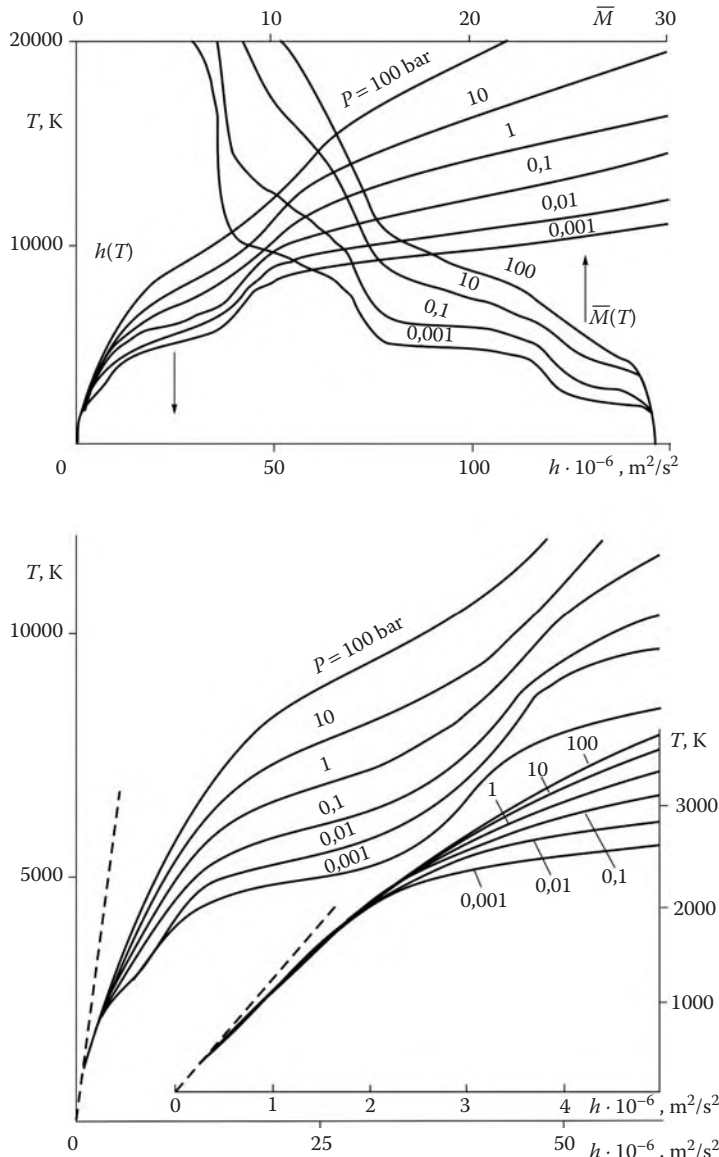
We will note some properties of the equations of state for equilibrium gases. Relations 1.3.1 make it possible to introduce the notions of total specific heat capacities at constant volume (density) and pressure, as follows:

$$c_v = \left(\frac{\partial e}{\partial T} \right)_p = \left(\frac{\partial h}{\partial T} \right)_p - \frac{1}{\rho} \left(\frac{\partial p}{\partial T} \right)_p, \quad c_p = \left(\frac{\partial h}{\partial T} \right)_p \quad (1.3.5)$$

* In physics these gases are called *ideal*, but here this term is kept for inviscid gases, as accepted in gas dynamics.

[†] In plenum chambers of some gas dynamic setups the gas density can exceed the standard density by a factor of a hundred and more. In this case one should take into account the so-called *Van der Waals effects* of molecular interaction.

[‡] These and subsequent curves are plotted in accordance with tables computed by Predvoditelev et al. (1959) for $T < 20,000$ K and Kuznetsov (1965) for $T \geq 20,000$ K.

**FIGURE 1.7**

Temperature dependence of the enthalpy and the molecular weight for equilibrium air. Dashes relate to a perfect gas.

These heat capacities include the effect of the heat spent for physicochemical conversions in the gas and, as can be seen from the form of the curve $h(T, p)$ in Figure 1.7, vary monotonically, the range of their variation for equilibrium air being sufficiently large. For relatively low temperatures they are presented in Figure 1.3.

From physical considerations it follows that for all gases $c_p > c_v$. In fact, heating at constant pressure is accompanied by gas expansion and, hence, a part of the heat is spent for the expansion work, as distinct from heating at constant volume.

Substituting the composite function $h = h[T, p(\rho, T)]$ in the formula 1.3.5 we obtain the relation

$$c_p - c_v = \left(\frac{\partial p}{\partial T} \right)_\rho \left[\frac{1}{\rho} - \left(\frac{\partial h}{\partial p} \right)_T \right] \quad (1.3.6)$$

It will be shown later that in a gas with a constant \bar{M} the enthalpy or internal energy and, hence, the heat capacities may depend on the temperature only. Then

$$c_p - c_v = \frac{R}{\bar{M}}, \quad \frac{p}{\rho h} = \frac{\gamma - 1}{\gamma} \quad (1.3.7)$$

Here, the latter formula is valid only for perfect gases and is obtained in view of Equation 1.3.3.

To emphasize the distinction between this equation of state and that for a perfect gas we rewrite Equation 1.3.4 in terms of Equation 1.3.7 with the following result

$$\begin{aligned} \frac{p}{\rho h} &= \frac{RT}{\bar{M}h} = \frac{\gamma - 1}{\gamma} \frac{1}{Z} = \frac{\gamma_* - 1}{\gamma_*} \\ \gamma_* &= \frac{h}{e}, \quad Z(p, T) = \frac{h\bar{M}}{M_0 c_{p0} T} \\ \gamma_* &= \gamma_*(p, T) = \frac{\gamma Z}{\gamma Z - \gamma + 1} \end{aligned} \quad (1.3.8)$$

Here, c_{p0} , \bar{M}_0 , and γ are the specific heat, the molar mass, and the adiabatic exponent for a gas in an initial state, for example, for air in standard conditions. The function Z can be considered a measure of the gas imperfection. For air (as shown in Figure 1.8 for the range of temperatures as high as hundreds of thousands of degrees) it varies within relatively close limits, $Z = 1 - 3.5$.

The function γ_* is the effective adiabatic exponent, which, for the present, is termed so by analogy. The curves for air and carbon dioxide CO_2 are presented in Figure 1.9. Clearly,

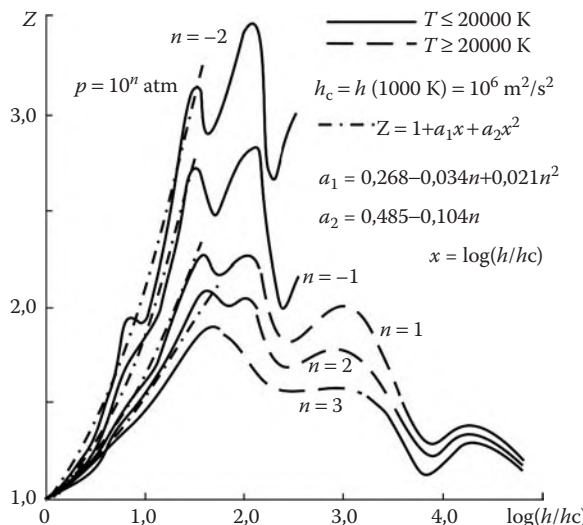


FIGURE 1.8

Dependence of the function Z on the enthalpy for air at constant pressure.

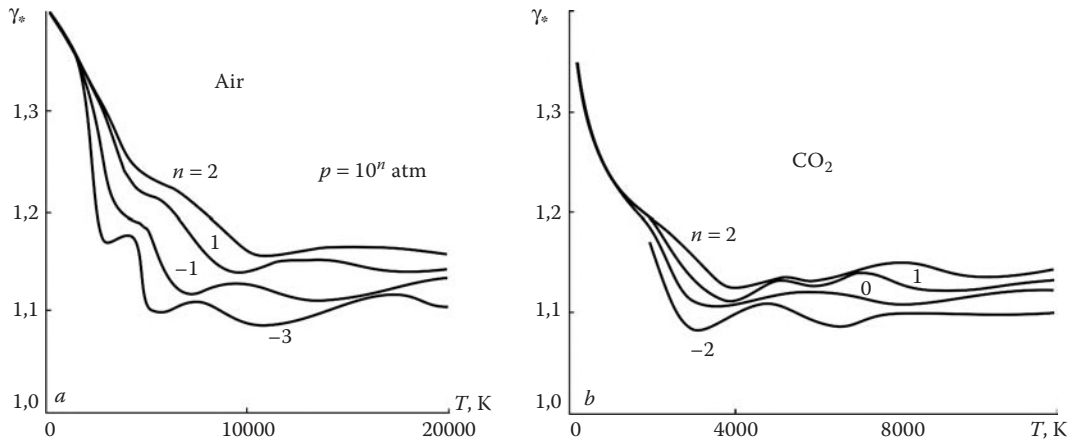


FIGURE 1.9
Effective adiabatic exponent $\gamma_*(T)$ for air and carbon dioxide.

for these gases at high temperatures the exponent γ_* is close to unity and is considerably smaller than its value for a cold gas.

In carbon dioxide (CO_2) vibrational degrees of freedom are excited very early; therefore, the deviation of its behavior from that of a perfect gas starts at lower temperatures than for air.

As distinct from a perfect gas, the effective adiabatic exponent is not usually equal to the specific heat ratio, $\gamma_* \neq \gamma_c = c_p/c_v$. The functions γ_* and γ_c are compared in Figure 1.10.

As follows from Figures 1.8 to 1.10, the quantities Z , γ_* , and other are, in general, weakly varying functions of the temperature and, especially, of the pressure (the pressure dependence is practically logarithmic). Therefore, the required values of γ_* can be obtained from the figures by interpolation. Moreover, on a limited interval of the p and T variation one can consider γ_* to be constant, thus modeling a real gas by a perfect gas with an appropriate adiabatic exponent. It is convenient to represent the equation of state in the form 1.3.8; then such a gas (with a slightly varying γ_*) is termed *quasiperfect*.

Finally, we will mention transport coefficients. For usual gases under standard conditions they depend on the temperature only. At comparatively low temperatures viscosity is determined from the *Sutherland law*

$$\mu = \mu_a \frac{T_0 + T_a}{T_0 + T} \left(\frac{T}{T_a} \right)^{3/2}, \quad \mu_a = 1.72 \cdot 10^{-5} \text{ kg/m} \cdot \text{s}$$

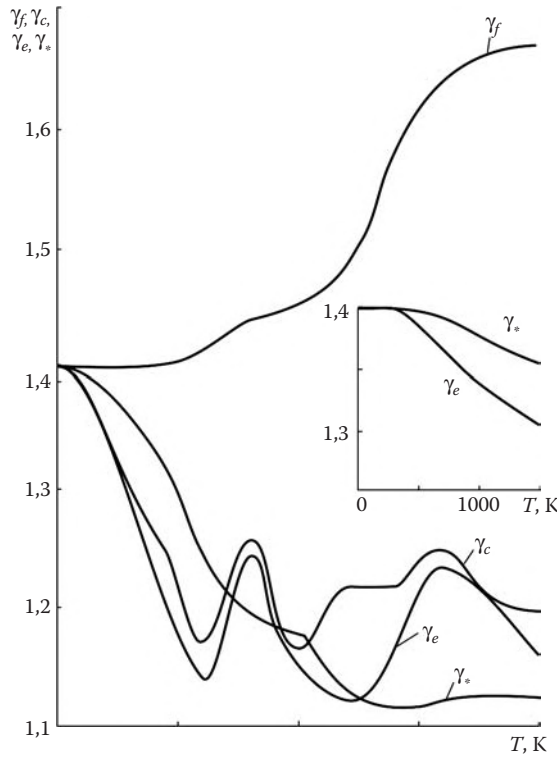
$$T_0 = 110 \text{ K}, \quad T_a = 273 \text{ K} \quad (1.3.9)$$

Here, the quantities T_0 and μ_a are given for air for which this formula is valid up to temperatures $T \leq 2500$ K. The curve $\mu(T)$ determined by the previous equation is quite satisfactorily approximated by the dependence (dashes in Figure 1.11a).

$$\mu = \mu_*(T/T_*)^{0.7}, \quad T_* = 200 \text{ K}$$

$$\mu_* = 1.3 \cdot 10^{-5} \text{ kg/(m} \cdot \text{s)} \quad (1.3.10)$$

The curves $\mu(T, p)$ for high-temperature equilibrium air are plotted in Figure 1.11b and can be approximated, up to their peak points, either by a linear temperature dependence

**FIGURE 1.10**

Temperature dependence of different adiabatic exponents for air at $p = 1 \text{ atm}$; $\gamma_* = h/e$, $\gamma_e = a^2 \rho/p$, $\gamma_c = c_p/c_v$, and $\gamma_f = c_p^{(0)}/c_v^{(0)}$.

or by a formula similar to 1.3.10

$$\frac{\rho\mu}{p} = C \left(\frac{h}{h_0} \right)^{-n}, \quad n = 0.3, \quad h_0 = 10^6 \text{ J/kg}$$

$$C = 1.45 \cdot 10^{-10} (\text{kg} \cdot \text{s})/\text{m}^3$$

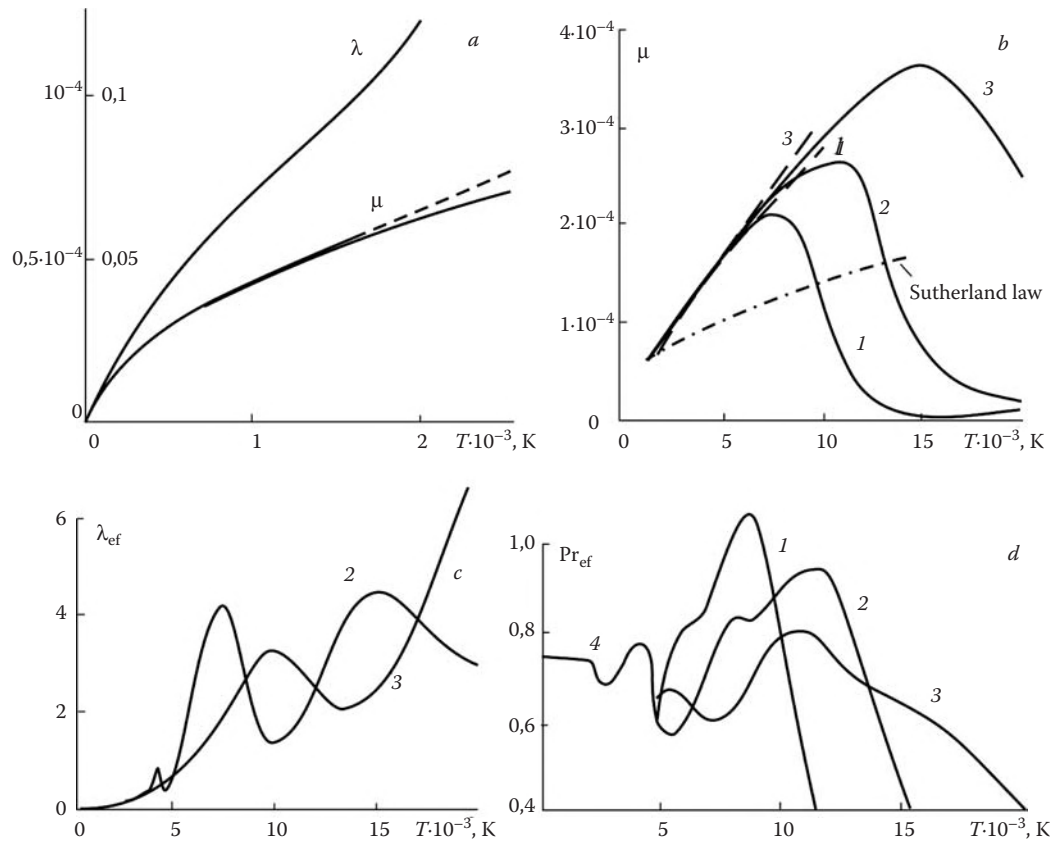
$$T_0 = 1000 \text{ K} \leq T \leq 7500 \text{ K} \quad (1.3.11)$$

This formula (Murzinov, 1966; dashes in Figure 1.11b) coincides with 1.3.10 at moderate temperatures; does not include the temperature, and can be preferred for equilibrium flows, for which the upper limit of applicability, $T = 7500 \text{ K}$, is quite sufficient for the majority of reentry problems.

It is convenient to use the dimensionless *Prandtl* (*Pr*), *Schmidt* (*Sc*), and *Lewis* (*Le*) numbers instead of the thermal conductivity and diffusion coefficients

$$Pr = \frac{\mu c_p}{\lambda}, \quad Sc = \frac{\mu}{\rho D}, \quad Le = \frac{\rho D c_p}{\lambda} \quad (1.3.12)$$

These quantities are usually near-constant at temperatures, at which there is no noticeable physicochemical gas conversions. For gases they are of the order of and even close to unity; thus, for air $Pr = 0.7 - 0.73$ at $200 \text{ K} \leq T \leq 2500 \text{ K}$ (Figure 1.11d).

**FIGURE 1.11**

Transport coefficients for equilibrium air; curves 1 to 4 relate to $p = 10^{-2}, 1, 10^2$, and 10^{-1} bar, respectively; $[\lambda] = \text{Wt}/(\text{m}^2 \cdot \text{K})$ and $[\mu] = \text{kg}/(\text{m} \cdot \text{s})$.

However, the situation essentially changes as temperature increases and gas composition starts to change due to chemical reactions. It can be seen from Figure 1.4 how complicated are the pressure and temperature dependences of the air component concentrations. This is the reason why the function μ is appreciably nonmonotonic. To an even greater extent this is true for thermal conductivity of high-temperature gases. The point is that the energy transfer in multicomponent mixtures is effected (and often solely) by diffusion of the components, so that in many important problems the energy flux 1.2.10 can be presented in the form $J = -\lambda_{\text{eff}}(\partial T / \partial x)$, where λ_{eff} is the effective thermal conductivity. The coefficients μ and λ_{eff} , as well as the effective Prandtl number Pr_{eff} , are presented in Figure 1.11b, c, and d. We note that Pr_{eff} is distinguished by essentially nonmonotonic behavior (Vasilevskii, Sokolova, and Tirsikii, 1986, curves 1 to 3; and Hansen, 1959, curve 4).

We will now touch on the behavior of fluids; it is customary to assume that these are incompressible, at least, within the framework of hydrodynamic problems. Thus, when water is compressed under a pressure of 1 atm, the relative variation of its volume is as low as $5 \cdot 10^{-5}$. However, even this low compressibility can be crucial, for example, in the process of blast wave propagation. As distinct from gases, the viscosity of fluids decreases as the temperature increases, following approximately the $\mu \sim e^{\theta/T}$ law. For melt quartz

the value of θ is as high as 60,000 K, while for water $\theta \approx 1800$ K. At the same time, the temperature dependence of the thermal conductivity of fluids is weaker than that of gases. Due to elevated viscosity, the Prandtl numbers for fluids are fairly large (they can amount to several tens and even hundreds) and depend strongly on the temperature.

In conclusion, we will make several comments on the definition of the internal energy. In the conservation laws written down in Section 1.2, the gas energy includes the energies of the formation of all the species, the values of which depend on certain reference values. We assumed these gases to be perfect under standard conditions, in spite of the inapplicability of this model for superlow temperatures and, which is the most important, the liquefaction of gases even at the temperatures of the order of several tens of absolute degrees.* These equations are not meant for the application under conditions close to this limit. At the same time, the constant term in the expression for the internal energy could be ignored in the conservation law in view of its additive nature. Therefore, in the equations of the equilibrium state of gases, as adopted previously, the reference values of their internal energies are determined precisely by the conditions of their perfectness under standard conditions. The energies of the formation of oxygen and nitrogen molecules in the air are taken to be zero, while the reference values of the energies of other components, which are formed in the air mixture as temperature increases, are determined with allowance for the thermal effects in the reactions of their formation. Thus, the energy of atom formation at molecular dissociation is often included in their energy, this addition being often quite large.

However, other situations can occur, in which this approach is not preferred. Thus, in evaporation of a solid (or liquid) body, the vaporization heat could be included in the energy of vapors. However, the vapors are more often considered as an independent gas (e.g., a perfect gas), irrespective of its origin, with the corresponding correction introduced in the energy equation. A similar situation occurs in combustion of condensed media or metastable, though nonequilibrium, gas mixtures (e.g., those of hydrogen and oxygen, methane and oxygen, etc.); in this case, the gaseous combustion products can exist separately, as individual gases. In this situation, as distinct from the gas dynamics of reacting gas mixtures, the internal energies of both original gases and final gaseous products are often written irrespective of the mode of their origin or combination, while the energy of their mutual conversion is assigned to external heat sources. However, a single reference energy can be introduced in this case too and the process of the mutual conversion of different substances can be considered adiabatic (strictly speaking, this process is precisely of this type). We will specify these questions in the process of the solution of particular problems.

1.4 Some Knowledge of Molecular Kinetic Theory

The knowledge of molecular kinetic theory will be used to substantiate (though on an intuitive level) the gas dynamic model of a gas medium discussed previously. A reader preferring to remain on the phenomenological point of view and to consider the model

* At 1 atm oxygen is liquefied at $T = 90.3$ K, nitrogen at 77.5 K, and so on. The liquefaction of air in supersonic aerodynamic setups occurs owing to inadequate heating of working gases (air). However, the change in the flow features in this case makes the interpretation of measurements so difficult that these test regimes are considered inapplicable.

as given from the Heaven can skip this section without damage to the study of the main contents of the book, at least, up to the chapters devoted to nonequilibrium gas flows.

To be adequate, a continuum model requires, at least, two conditions to be satisfied:

1. The number of molecules in a characteristic domain (volume) Ω of the flow under consideration must be large.
2. The mean free time must be relatively small, $\tau \ll t_0$ (where t_0 is the scale time for physical or gas dynamic processes under consideration) in order for an average gas state to follow the variation of local conditions. This requires, at least, a relative smallness of the mean free path, $l \ll L$ (L is the characteristic size of the region Ω).

The first of these conditions is less crucial than the second one. For instance, at an altitude of $H = 90$ km, which is, in general, limiting for the theories outlined in the book, there are more than 10^{10} molecules in the volume of 1 mm^3 , but the mean free path is $l \approx 2 \text{ cm}$. This quantity is small compared with the body size $L = 1 \text{ m}$ but, generally speaking, is not so small if its differential ΔL (used in deriving differential equations of motion) is considered as the length scale.

However, it turns out (see Chapter 10) that only a few molecular collisions are required in order for a chaotic state of the molecular ensemble to be established. This suggests that the continuum model is appropriate even for flow regions of the order of a few mean free paths, naturally, with the subsequent determination (either experimental or theoretical) of the real range of applicability of the model.

The ratio $Kn = l/L$ is called the *Knudsen number*; precisely this ratio determines the extent to which a real process is approximated by one or another continuum model.

We will now apply the concepts of molecular kinetic theory in order to determine the macroscopic parameters of the continuum model. We consider a small volume $\Delta\Omega$ and define, for example, an instantaneous density and a mean mass velocity of the ensemble of molecules of masses m_k , their number per unit volume being n

$$\rho = \frac{1}{\Delta\Omega} \sum_k m_k = nm, \quad \mathbf{U} = \frac{1}{\rho\Delta\Omega} \sum_k m_k \mathbf{W}_k = \langle \mathbf{W}_k \rangle \quad (1.4.1)$$

Here, \mathbf{W}_k is the absolute velocity of the chaotic molecular motion and summation is performed over all the molecules in the volume. The second equalities relate to molecules of the same sort and the angular brackets stand for the averaging over a given ensemble of molecules.

Formally, these quantities can be defined for any gas density; however, they describe adequately the macroscopic gas state only for high molecular concentration, which excludes the influence of various fluctuations on these parameters.

Moreover, the definition of the macroscopic gas parameters by summing over all individual molecules is an impracticable, though formally correct, procedure. For this reason, the *macroscopic* characteristic of a continuous medium used in molecular kinetic theory is the *function of molecular distribution* with respect to the coordinates x, y, z and the velocity projections W_x, W_y, W_z . This function denoted by f determines the number of molecules dn in a small volume $\Delta\Omega$ having velocities on the intervals $(W_x, W_x + dW_x)$, and so on:

$$dn = nf(x, y, z, W_x, W_y, W_z) d\Omega dW^3 \\ d\Omega = dx dy dz, \quad dW^3 = dW_x dW_y dW_z \quad (1.4.2)$$

The function f is governed by the previously mentioned Boltzmann equation.* The gas velocity in the volume $\Delta\Omega$ (for molecules of the same sort) is defined in terms of the distribution function as follows:

$$\begin{aligned}\mathbf{U} &= \int \mathbf{W}f dW^3 = \langle \mathbf{W} \rangle, & U_n &= \int W_n f dW^3 \\ U_n &= \mathbf{U} \cdot \mathbf{N}, & W_n &= \mathbf{U} \cdot \mathbf{n}\end{aligned}\quad (1.4.3)$$

Here, U_n is the velocity of the fluid surface propagation directed along the surface normal \mathbf{n} (introduced in Section 1.2).

We will now define the mean kinetic energy of the relative, or thermal, motion of molecules with relative velocities $\mathbf{V} = \mathbf{W} - \mathbf{U}$

$$\begin{aligned}\frac{1}{2}kT_x &= \frac{1}{2}m \int V_x^2 f dW^3 = \frac{1}{2}m \langle V_x^2 \rangle \\ T &= \frac{1}{3}(T_x + T_y + T_z) = \frac{m}{3k} \langle V^2 \rangle, & V^2 &= V_x^2 + V_y^2 + V_z^2\end{aligned}\quad (1.4.4)$$

The quantity T is called the temperature (arguments in favor of this term will be given in what follows).

Finally, we will define the internal stresses in a gas acting normally on a (unit) area $d\Sigma_x$, the normal being directed along the x axis. In order to exclude the average flow with the velocity \mathbf{U} , we consider this area a *movable fluid area* crossed by molecules at the normal relative velocity V_x . Molecules with $V_x > 0$ can be considered as “emanated” and those with $V_x < 0$ as “absorbed” by the surface; therefore, the total momentum transferred by molecules per unit time is equal to the unknown stress \mathbf{p}_x . Since $nmV_x f dV_x$ is an element of the molecular flow, we obtain the following equality

$$\mathbf{p}_x = -nm \int V_x \mathbf{V} f dW^3, \quad \mathbf{V} = \mathbf{i}V_x + \mathbf{j}V_y + \mathbf{k}V_z \quad (1.4.5)$$

where $\mathbf{i}, \mathbf{j}, \mathbf{k}$ are the unit coordinate vectors. Substituting V_x for \mathbf{V} yields p_{xx} , that is, the projection of the stress \mathbf{p}_x onto the x axis expressed in terms of the same integral as T_x in 1.4.4. Summation gives the fundamental invariant of viscous gas mechanics

$$p = -\frac{1}{3}(p_{xx} + p_{yy} + p_{zz}) = nkT \quad (1.4.6)$$

Generally, the sign in 1.4.5 and 1.4.6 can be arbitrarily chosen; here it corresponds to the definition of p_{xx} in Section 1.2, as accepted in mechanics.

The stress components p_{xx} and others are not necessarily mutually equal, but, luckily enough, one third of their sum is independent of the coordinate system orientation and, moreover, when taken with the opposite sign, satisfies the Clapeyron equation of state 1.3.2 with the temperature defined in terms of the mean molecular kinetic energy (i.e., irreproachably from the physical point of view).

We emphasize that, as mentioned in Section 1.3, these results are applicable only for *moderately dense* gases for which the duration of molecular interactions is considerably shorter

* See, for example, the books of Chapman and Cowling (1952), Huang (1963), Bond, Watson, and Welch (1965), and Kogan (1969).

than their mean free time. If σ is the so-called molecular *collision cross-section* determining their conventional size, then moderately dense gases can be defined as satisfying the condition $l \gg \sigma$. In this case, the attraction between molecules has no effect on the internal pressure in the gas, so that Equation 1.4.6 can be written for each individual component (the additivity Dalton's law being valid for them).

Molecular kinetic equilibrium is a special situation for a gas medium. In the absence of external forces this state is isotropic, so that all the previously considered quantities pertaining to different directions must be independent of them (i.e., the equalities $T_x = T$, $p_{xx} = -p$, and so on must hold). In this case, the corresponding distribution function can be reduced to the well-known *Maxwellian distribution function* which is represented in the form necessary for what follows

$$\frac{dn_\varepsilon}{n} = f_0(\varepsilon) = \frac{2}{\sqrt{\pi}} \left(\frac{\varepsilon}{kT} \right)^{1/2} e^{-\varepsilon/kT} d\frac{\varepsilon}{kT}, \quad \varepsilon = \frac{mV^2}{2} \quad (1.4.7)$$

Here, $dn_\varepsilon = dn_V$ is the number of molecules having the kinetic energy of the random motion on the range $(\varepsilon, \varepsilon + d\varepsilon)$ and the velocity on the range $(V, V + dV)$. In its original form this function involves an arbitrary constant expressed in terms of the total kinetic energy of thermal molecular motion which, in accordance with the definition of temperature in 1.4.4, is equal to $(1/2)m(V^2) = 3/2kT$ per molecule.

Moreover, in an isotropic gas state, all the mean velocity components in each direction s are equal, that is, $1/2m(V_s^2) = 1/2kT$. These equations hold for all the species of a gas mixture having the same value of T . Therefore, in accordance with the definition of the temperature as a measure of the relative heating of a substance, as accepted in thermodynamics, precisely this quantity is agreed upon to represent the equilibrium gas temperature, since there is no more obvious measure of the gas heating than the kinetic energy of the random motion of its molecules. The same formula is used in physics to define the absolute temperature, while a moderately dense, or perfect, gas itself plays the role of a standard thermometer, by reference of which one could in principle calibrate any other thermometer, if the two thermometers are in mutual equilibrium.

The result thus formulated represents the classical *principle of the energy equipartition*, in accordance with which in an equilibrium gas mixture the energy of gaseous species i per each of three independent translational degrees of freedom is the same and equal to $kT/2$.

On the basis of these principles, we will determine the caloric equation of gas state. The energy of translational degrees of freedom is equal to $3kT/2$ per molecule or $3RT/2$ per one mole of a gas. However, in the general case this is not the total energy of a gas. For two-atom, or binary, molecules, each of two vibrational degrees of freedom has the energy equal to $kT/2$, or RT per one mole. Thus, the following relations hold for monatomic and diatomic gases, respectively

$$\begin{aligned} e = c_v T &= \frac{3}{2} \frac{RT}{M}, & h = c_p T &= \frac{5}{2} \frac{RT}{M}, & \gamma &= \frac{c_p}{c_v} = \frac{5}{3} \\ e &= \frac{5}{2} \frac{RT}{M}, & h &= \frac{7}{2} \frac{RT}{M}, & \gamma &= \frac{7}{5} \end{aligned} \quad (1.4.8)$$

Moreover, the gas energy includes the energies of vibrations, electron levels, formation, and so on, which, usually, do not satisfy the equipartition principle even at equilibrium. We put aside (up to Chapter 10) the discussion of these topics because the general form of the equilibrium equations 1.3.1 makes allowance for all these processes.

It is appropriate to make an important remark on the equilibrium of a gas medium as a thermodynamic system. One can distinguish two stages of equilibrium. Typical of the first

one, namely, *molecular kinetic equilibrium* is the Maxwellian distribution that is attained as a result of only a few collisions. We bear in mind precisely this form of partial equilibrium when classifying equilibrium and nonequilibrium in this section and, in general, in kinetic theory. The underlying hypothesis of gas dynamics in general and of this book in particular is that of a possibility to achieve equilibrium or a state close to equilibrium.

However, the total gas equilibrium (in particular, for *physicochemical processes* in high-temperature gases) does not follow from this hypothesis, due, usually, to a long time necessary to achieve steady states in such processes. Thus, even nonequilibrium physicochemical processes occur as if on the background of the kinetic equilibrium. These are the processes that one should bear in mind when classifying equilibrium and nonequilibrium flows.

We will now consider gas flows with a weak spatial nonuniformity. It is known (Section 1.2) that stresses in a nonuniform flow incorporate both hydrostatic pressure and viscous stresses, the latter being dependent on area orientations. Obviously, such stresses cannot be derived from Equation 1.4.5 using the Maxwellian distribution for which there are no anisotropic stresses.

Further, we will take a small volume and, using the distribution function, evaluate the stresses acting on the boundary of this volume, as well as the mass, momentum, and energy fluxes across the boundary. The integration over all particles leads to some differential (since the volume is small) equations for the macroscopic characteristics of the flow. Naturally, the equations depend on the form of the distribution function chosen. Kinetic theory gives some fundamental results following from the Boltzmann equation:

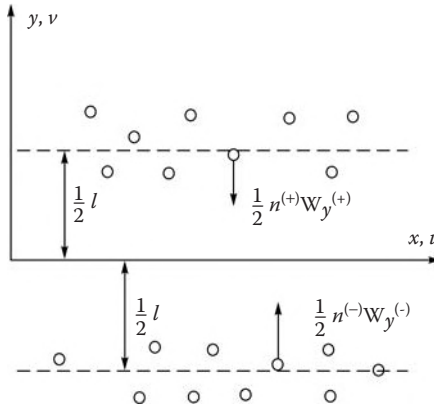
1. If the Maxwellian equilibrium distribution function is used, the inviscid Euler equations are obtained.
2. Putting $f = f_0 + f_1$, where f_1 is the correction term of the order of $l/L \ll 1$, one obtains the Navier–Stokes equations and the theory gives expressions for the transport coefficients.*

Thus, from the kinetic-theory point of view, the Navier–Stokes equations correspond to a slightly nonequilibrium gas state close to an equilibrium state.

It is natural to pose the question on equations of state and the meaning of the temperature definition 1.4.4 in the absence of equilibrium. The answer is that precisely this quantity, proportional to the gas energy, enters in both the Clapeyron Equation 1.4.6 and the caloric Equation 1.4.8 (with reservations concerning the rotational energy). As shown, these equations close the general system of gas dynamic equations.

In conclusion, we will discuss (though on an elementary level) the structure of dissipative terms obtained from the kinetic theory. We consider a *fluid area* moving at a mean velocity U , with an x axis aligned with the area and an y axis normal to it. As a rough approximation for the distribution function 1.4.5, we will choose two parallel sections $\Delta y_{\pm} = \pm l/2$ (Figure 1.12) and assume that molecules leaving one section at a mean velocity W_y are held up in the other section (and vice versa), thus transferring the specific mass flux $mn^{(+)}W_y^{(+)}/2$ from above and that $mn^{(-)}W_y^{(-)}/2$ from below, together with their momenta, energies, and so on. In the linear approximation, we let $W_y^{(\pm)} = V_s \pm \Delta W_y$, where V_s is the mean isotropic component of the thermal velocity of the particles, independent of the

* The equations of the next approximation are also known. However, the fact that they are poorly validated and difficult to survey does not allow one to use them for obtaining any significant results.

**FIGURE 1.12**

On the derivation of the formula for viscous stresses.

direction and close to the Maxwellian velocity V_{s0} . From the definition of the fluid area it follows that $n^{(+)}W_y^{(+)} = n^{(-)}W_y^{(-)}$.

In a very simple case of a shear flow (Figure 1.6b), when the velocity is directed along the x axis and is equal to $\pm\Delta u/2$ at the previously mentioned sections, the corresponding momenta transferred from above and below are equal to $nmV_s\Delta u/4$, correct to quadratic terms, that is, for $n^{(\pm)} = n$ and $W_y^{(\pm)} = V_s$. This is equivalent to a shear stress acting on the upper side of the area

$$\begin{aligned} p_{xy} = \tau_{xy} &= \frac{1}{2}nmV_s\Delta u = \mu \frac{\partial u}{\partial y}, \quad \Delta u = l \frac{\partial u}{\partial y}, \\ \mu &= \frac{1}{2}nmlV_s \sim \frac{\sqrt{mkT}}{\sigma^2} \end{aligned} \quad (1.4.9)$$

Here, μ is precisely the viscosity coefficient. The latter estimate for it follows from the conditions $V_s \sim (kT/m)^{1/2}$ and $nl\sigma^2 \sim 1$.

Let now the mean gas velocity be aligned with the y axis and equal to $\pm\Delta v/2$ in the sections $\Delta y_{\pm} = \pm l/2$. Then in our approximation, with account of the direction of the velocities in Figure 1.12, we have $W_y^{(\pm)} = V_s - \Delta v/2$, where $\Delta v = l(\partial v/\partial y)$, and, in accordance with 1.4.5, the total stress on the upper side of the area $y = 0$ is as follows:

$$p_{yy} = -mn \left(V_s - \frac{1}{2}\Delta v \right)^2 = -p_* + 2\mu \frac{\partial v}{\partial y}, \quad p_* = nmV_s^2 \quad (1.4.10)$$

Here, as in Equation 1.4.9, the terms of the order of $(\Delta v)^2$ are omitted. The quantity p_* , which has not been as yet determined, is independent of area element orientation; at the same time, it is related with the pressure p entering in the equation of state 1.4.6 by the formula

$$p_* = p + \frac{2}{3}\mu \operatorname{div} \vec{U}, \quad \operatorname{div} \vec{U} = \frac{\partial u}{\partial x} + \frac{\partial v}{\partial y} + \frac{\partial w}{\partial z} \quad (1.4.11)$$

where u , v , and w are the velocity projections in a Cartesian coordinate system (x, y, z) . We shall demonstrate in Section 1.8 that the *velocity divergence* operator $\operatorname{div} \vec{U}$ introduced previously is actually independent of the choice of a coordinate system. In Section 1.10 the

same result will be obtained using a phenomenological approach for arbitrary media, both liquid and gaseous.

Analogously, by substituting $c\Delta T$ for Δu in the derivation of formula 1.4.9 we can obtain formula 1.2.9 for the heat flux J_T with the thermal conductivity coefficient $\lambda = nmlcV_s/2$, where c is a coefficient having the same dimensionality (and order) as the gas heat capacity. A similar estimate $D \sim lV_s/2$ can be also obtained for the diffusivity coefficient by letting $n^{(+)} \neq n^{(-)}$ (see Chapter 13 for details).

However, the plausibility of all these formulas may be regarded as only qualitative. In particular, in Section 1.3 another formula for viscosity, namely, $\mu \sim T^{0.7}$, was presented.

1.5 Entropy and the Second Law of Thermodynamics

The system of equations obtained earlier for equilibrium processes with allowance for the equation of state 1.3.1 is closed. However, a complete theory of gas dynamics cannot be constructed without the second law of thermodynamics and the concept of entropy. Since these concepts are discussed in detail in courses on thermodynamics and statistical physics, we restrict ourselves to a brief outline of some basic results.

There exists a function of state, the entropy s , which for a closed thermodynamic system, for example, a gas volume of a fixed (in what follows, unit) mass without mass exchange with the ambient medium, in the reversible equilibrium process is governed by the law

$$Tds = de + dA = de + pd\frac{1}{\rho} = dh - \frac{1}{\rho}dp = dQ = qdt \quad (1.5.1)$$

Here, dQ is the heat influx and dA is the work performed by the system on the ambient medium. The other than first equalities are written down for inviscid gases, for which $dA = pd\rho^{-1}$.

A process is called reversible if it is formed by an infinitely slow sequence of equilibrium states, the same in the direct and reverse proceeding of the process.

The work performed by a system passing from state 1 to state 2 depends on the passage path; therefore, dA is not a total differential in the mathematical meaning and the integral of dA along a closed contour in some phase plane (e.g., in the (p, ρ^{-1}) -plane) is not equal to zero in the general case. However, the entropy is a function of state; therefore, $ds = dQ/T$ is a total differential, the quantity T^{-1} thus being an integrating factor of the differential relation 1.5.1.

For irreversible (say, sudden or sufficiently rapid) transition from point 1 to point 2 the following inequality holds

$$\Delta s = s_2 - s_1 \geq \int_1^2 \frac{dQ}{T} \quad (1.5.2)$$

Here the equality sign relates to reversible processes only. Therefore, *in a closed, adiabatically isolated system the entropy in equilibrium processes remains constant, while in irreversible processes it grows*. Thus, the greatest permissible value of the entropy corresponds to an equilibrium state.

The entropy is an additive function in the sense that if separate parts of an isolated system are not initially in equilibrium and begin to interact, then the entropy increment of the

system is equal to the sum of the entropy variations of its separate parts and grows when the system tends to equilibrium.

This statement can be supported by a model example of differently heated bodies with so slow heat exchange that their temperatures T_1 and T_2 are almost constant throughout the corresponding volumes, though they vary in time. Then, as the heat $dQ > 0$ is transferred from one body to the other (let $T_2 > T_1$), their entropies vary in an equilibrium fashion, $T_1 ds_1 = dQ$ and $T_2 ds_2 = -dQ$, while the entropy of the system as a whole grows irreversibly

$$ds = ds_1 + ds_2 = \left(\frac{1}{T_1} - \frac{1}{T_2} \right) dQ > 0 \quad (1.5.3)$$

This example is a particular case of the general approach to the extension of the applicability of equilibrium thermodynamics to real processes associated with the possibility of splitting a nonequilibrium (as a whole) system into a set of *locally equilibrium* subsystems with their own local values of the temperatures and other relevant parameters. Therefore, one can apply the laws of equilibrium thermodynamics to such subsystems describing their interaction and their states by means of apparently reversible (for each of them) processes (i.e., by means of *differential equations*).

For a gas flow, the role of these subsystems is played by elementary gas particles for which relations 1.5.1 or equations of Sections 1.2 and 1.3 are written. In fact, the irreversibility of all dissipative flows with a strong influence of viscosity and heat conduction is evident. For instance, an initially nonuniform flow in a tube with a hypothetical slip on the walls becomes uniform at the end section due to the action of viscosity. Reversing the motion (i.e., reversing the velocity direction), we cannot bring the uniform flow to the initial state, but in this case an entropy increment can be described by the differential Equation 1.5.1 with $dQ = q_{\text{eff}} dt$, where q_{eff} is the heat due to both heat conduction and mechanical energy dissipation; in accordance with Equation 1.2.7, it is always positive. In this sense, the process for each particle is reversible.

The second, very important example refers to nonequilibrium flows. In this case, the gas entropy grows due to irreversibility or a prescribed direction of reactions. For an entropy increment a special equation of the type $Tds = \Phi dt \geq dQ$ can be obtained, where Φ is a function of state.

However, this situation holds only in continuous flows. When flow parameters become discontinuous (e.g., in shock waves), a jumplike transition from one state to the other cannot be described by differential relations. The entropy increment, though satisfying condition 1.5.2, can be determined as a result of an imaginary reversible process relating both states.

The previously formulated statement on the irreversibility (in general) of real processes and the entropy growth in these processes should be explained, since unbounded flows past bodies correspond to an unbounded thermodynamic system. For this reason we will restrict the problem to a particular statement leading to further generalizations:

In a steady-state adiabatic flow of a real gas with uniform initial and final distributions of flow parameters, the net entropy increment when passing from an initial state to a final one is always positive.

Although the statement is evident from the very essence of the second law of thermodynamics, we will illustrate it by a particular example of the one-dimensional equilibrium viscous flow considered in Section 1.2. Combining Equations 1.5.1, 1.2.7 (with $q = 0$), and

1.2.11, letting $\rho u = \text{const}$ in a steady-state flow, using vanishing derivatives as $x \rightarrow \pm\infty$, and integrating within these limits yields the following expression for the entropy increment

$$\Delta s = s(+\infty) - s(-\infty) = \frac{1}{\rho u} \int_{-\infty}^{+\infty} \frac{1}{T} \left[\mu' \left(\frac{\partial u}{\partial x} \right)^2 + \frac{\lambda_{\text{eff}}}{T} \left(\frac{\partial T}{\partial x} \right)^2 \right] dx > 0 \quad (1.5.4)$$

which proves the statement.

Consider now some particular cases. Since the entropy and enthalpy are functions of state, the equation following from Equation 1.5.1

$$T \frac{\partial s}{\partial l} = \frac{\partial h}{\partial l} - \frac{1}{\rho} \frac{\partial p}{\partial l} = \frac{\partial e}{\partial l} + p \frac{\partial \rho^{-1}}{\partial l} \quad (1.5.5)$$

holds along any l direction in an equilibrium flow.

If continuous flows are reversible and adiabatic ($q_{\text{eff}} = 0$), they are *isentropic* as well, that is, the entropy of each particle is constant (sometimes only flows in which the entropy is constant throughout the entire flow are called isentropic; such *homogeneously isentropic* cases will be especially mentioned). In this case, $Tds = dQ = 0$ and the following *adiabatic equation* is valid

$$T \frac{dh}{dt} - \frac{1}{\rho} \frac{dp}{dt} = \frac{de}{dt} + p \frac{d\rho^{-1}}{dt} \quad (1.5.6)$$

In theory, it is often convenient to use the entropy and the pressure as the basic independent thermodynamic variables, instead of (p, T) , (p, h) , and so on. In this case, the dependence $h = h(p, s)$ is a full-bodied equation of state, which determines the other basic variables

$$\frac{1}{\rho} = \left(\frac{\partial h}{\partial p} \right)_s, \quad T = \left(\frac{\partial h}{\partial s} \right)_p \quad (1.5.7)$$

This follows immediately from Equation 1.5.1. Integrating 1.5.1 for a perfect gas and taking the Clapeyron equation into account we obtain the formula

$$s - s_0 = c_p \ln \frac{T}{T_0} - \frac{R}{M} \ln \frac{p}{p_0} \quad (1.5.8)$$

Here, s_0 , p_0 , and T_0 are certain constant parameters from the range of applicability of this formula (see Section 10.3 for details). Obviously, the formula cannot be extended to the range of superlow temperatures. In terms of Equation 1.3.7, the formula can be rewritten as follows:

$$h = c_p T = \Theta(s) p^{\frac{\gamma-1}{\gamma}}, \quad \rho = \frac{\gamma}{\gamma-1} \Theta^{-1} p^{\frac{1}{\gamma}}, \\ \Theta(s) = e^{\frac{s-s_0}{c_p}} \quad (1.5.9)$$

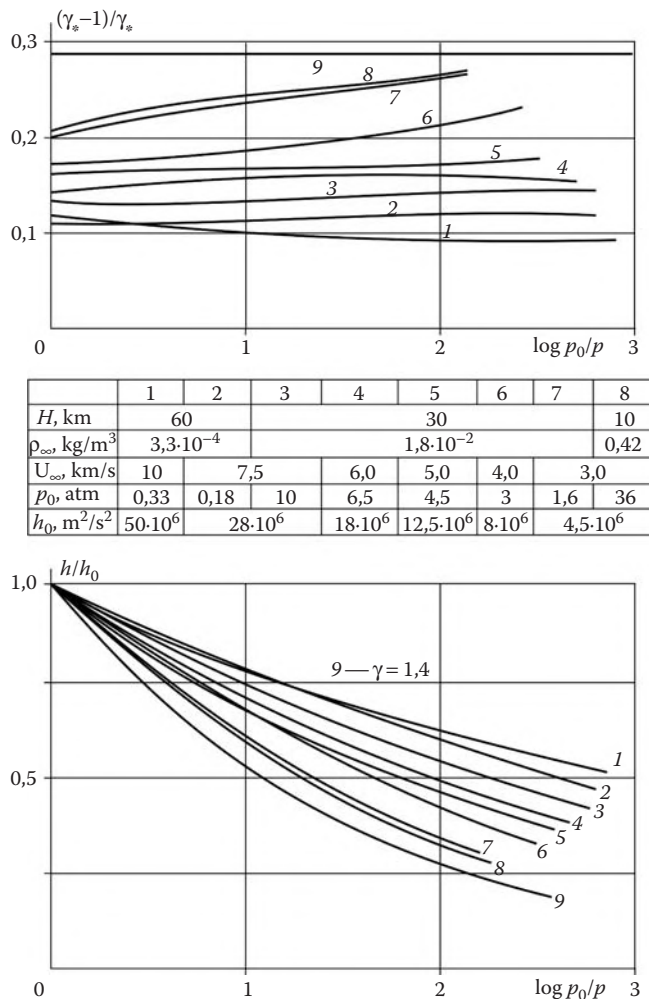
This dependence is called the *adiabat* or the *isentrope*. For real gases over a wide parameter range the exponent γ can be replaced by an effective exponent γ_* (see formula 1.3.8). Usually, the difference $\gamma_* - 1$ is small, so that the enthalpy (and, hence, γ_*) changes

only weakly along an isentrope (Figure 1.13), which justifies the name given to the quantity γ_* .

In conclusion, equating the mixed derivatives with respect to p and T in the differential ds in formula 1.5.1 and using the equation of state 1.3.4 we obtain the fundamental thermodynamic Gibbs equation

$$\rho \left(\frac{\partial h}{\partial p} \right)_T = \frac{T}{\bar{M}} \left(\frac{\partial \bar{M}}{\partial T} \right)_p \quad (1.5.10)$$

From this relation it follows, in particular, that in a gas with a constant molecular mass the enthalpy cannot be dependent on pressure.

**FIGURE 1.13**

Pressure dependence of h and γ_* at constant entropy for different values of p_0 and h_0 at the stagnation point on a blunt body and the atmospheric flight conditions presented in the figure.

1.6 Speed of Sound

The speed of sound is one of the fundamental notions of gas dynamics, a crucial role being played by the relation between the speed of sound and the gas velocity. The well-known fundamental difference between subsonic and supersonic flows is usually illustrated with reference to the following simple example. Let a mass point O moving at a velocity U in a gas at rest begin to generate at $t = 0$ sound signals (Figure 1.14). Clearly, the front of the initial disturbance is the sphere of radius at . At a subsonic flow velocity ($U < a$), disturbances overtake the sound source and fill the entire space as $t \rightarrow \infty$. The situation is different when $U > a$ and one can be easily convinced that all disturbances are localized inside the *Mach cone* with a moving vertex $x = Ut$ at the source and the cone half-angle, or the *Mach angle*, α^* determined by the formulas

$$\sin \alpha^* = \frac{a}{U} = \frac{1}{M}, \quad \tan \alpha^* = (M^2 - 1)^{-1/2} \quad (1.6.1)$$

A particular situation takes place when the source moves at transonic or sonic velocity and the disturbance front is almost plane (we can easily conjure up the situation looking at Figure 1.14a and b, and imagining that M tends to unity in the two figures).

This example is sufficient to attract attention to the subject, especially as the speed of sound itself is not directly involved in the original equations derived in Section 1.2. We will begin with the definition of the velocity of the propagation of sound (or acoustic) waves, that is, small perturbations of pressure (and other quantities) traveling throughout a gas, in contrast, for example, to entropy perturbations “frozen” in gas particles and propagating along their trajectories. Let a front of pressure disturbances propagate at a velocity D along the x axis throughout a quiescent gas (Figure 1.15). The pressure and density ahead of the front and behind it are p_1, ρ_1 , and p_2, ρ_2 , respectively.

The front may have a finite but constant thickness δ with continuous internal distributions of parameters in accordance with some stationary law in the front-fitted coordinate system, $x' = x - Dt$. Then the conservation laws on either side of the front are independent

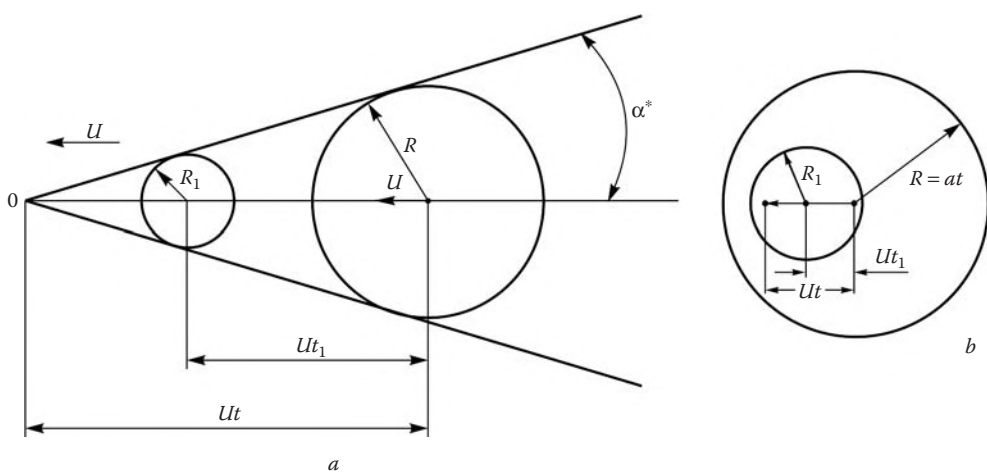
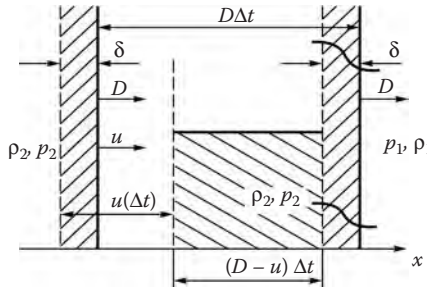


FIGURE 1.14

Propagation of disturbances at supersonic (a) and subsonic (b) velocities of the source.

**FIGURE 1.15**

On the definition of the speed of sound.

of the front thickness, provided that there are no viscous stresses on the external boundary of the front (see Section 1.7 for details).

We will consider a gas volume confined initially by two subsequent positions of the front spaced $\Delta x = D\Delta t$ apart and an arbitrary unit-area cylindrical surface coaxial with the x axis. The mass of the volume is $\rho_1 D\Delta t$. Due to the pressure difference $\Delta p = p_2 - p_1$, the gas behind the front acquires a velocity u ; therefore, after the gas has left the front, the volume of the gas mass decreases down to $(D - u)\Delta t$ for $u > 0$ (for $u < 0$ the volume increases).

Applying the mass, momentum, and energy conservation laws to this volume we obtain the relation between the parameters ahead of and behind the front

$$\begin{aligned} \rho_2(D - u) &= \rho_1 D, \quad p_2 - p_1 = \rho_1 D u, \\ \rho_1 D \left(e_2 - e_1 + \frac{1}{2} u^2 \right) &= p_2 u \end{aligned} \quad (1.6.2)$$

Eliminating the velocity u from these equations gives the relations between the thermodynamic parameters of the gas on either side of the front and the front velocity

$$\frac{\Delta p}{\Delta \rho} = \frac{p_2 - p_1}{\rho_2 - \rho_1} = \frac{\rho_1}{\rho_2} D^2, \quad e_2 - e_1 = \frac{1}{2} \left(\frac{1}{\rho_1} - \frac{1}{\rho_2} \right) (p_1 + p_2) \quad (1.6.3)$$

These formulas are valid for a front of an arbitrary intensity. To define the speed of sound let us pass to the limit

$$a^2 = \lim D^2 = \lim \frac{\Delta p}{\Delta \rho} = \frac{\partial p}{\partial \rho}, \quad \Delta p, \Delta \rho \rightarrow 0 \quad (1.6.4)$$

Here, we have intentionally omitted a subscript of the derivative, since the process to which this derivative relates is yet to be established.

Relation 1.6.2 have been written for the motion of the front along the positive direction of the x axis. In the general case, taking $D > 0$ we obtain

$$p_2 - p_1 = \pm \rho_1 D u \rightarrow \pm \rho_1 a u \quad (1.6.5)$$

Here, the upper and lower signs relate to disturbances traveling from left to right (as in Figure 1.15) and from right to left, respectively. Equation 1.6.3 is invariant with respect to the propagation direction.

Let us now discuss possible definitions of the derivative $\partial p/\partial\rho$ and, hence, the speed of sound. To do this, we represent the two-parameter equation of state $\rho = \rho(p, s) = \rho(p, T)$ in the form of expansions

$$\Delta\rho = \left(\frac{\partial\rho}{\partial p}\right)_s \Delta p + \left(\frac{\partial\rho}{\partial s}\right)_p \Delta s = \left(\frac{\partial\rho}{\partial p}\right)_T \Delta p + \left(\frac{\partial\rho}{\partial T}\right)_p \Delta T \quad (1.6.6)$$

In particular, Newton considered the process of compression-expansion in sound waves to be isothermal. The corresponding *isothermal speed of sound* is $a_T = (\partial p/\partial\rho)^{1/2}$, or $a_T^2 = p/\rho$ for a perfect gas, which is lower than the experimental value.*

This is quite natural, since the assumption that the process is isothermal means that there is an intensive temperature equalization. At the same time, by neglecting the effect of energy radiation in a gas (which is small for $T \leq 10,000$ K) and assuming that dissipation affects only the internal structure of the disturbance front, we can consider the transition through the front to be adiabatic with the adiabat equation $\Delta e = -p\Delta(1/\rho)$, which follows from Equation 1.6.3. Moreover, it will be shown later that the entropy increase caused by dissipation inside the front region, as predicted by relation 1.5.4, is so small that the front can be also considered to be isentropic (we put aside specific problems concerned, e.g., with the decay of high-frequency acoustic oscillations in which the entropy increase can be important). Putting $\Delta s = 0$ in expansions 1.6.6 we obtain the *adiabatic* or *isentropic* speed of sound a_e

$$\frac{1}{a_e^2} = \left(\frac{\partial\rho}{\partial p}\right)_s \quad (1.6.7)$$

We will now explain how the speed of sound enters in the equations of motion. We can imagine a flow field with an instantaneous distribution of parameters. Then we can determine spatial and time derivatives (using equations of Section 1.2) and find (if only formally) the solution at the next moment of time in terms of the increments $\Delta\rho = (\partial\rho/\partial t)\Delta t$ and so on. The derivative $\partial p/\partial t$ does not enter in those equations, so that the increment Δp can be determined only from the equation of state 1.6.6 as follows

$$\begin{aligned} \frac{d\rho}{dt} - \frac{1}{a_e^2} \frac{dp}{dt} &= \rho Q_e \\ Q_e &= \frac{1}{\rho} \left(\frac{\partial\rho}{\partial s}\right)_p \frac{ds}{dt} = \left(\frac{\partial\rho}{\partial s}\right)_p \frac{q}{\rho T} = \left(\frac{\partial\rho}{\partial h}\right)_p \frac{q}{\rho} \end{aligned} \quad (1.6.8)$$

Here, the right-hand side Q_e is a function of state and external heat sources only and for $q = 0$ it vanishes totally. The same result could be derived using the second relation 1.6.6, which would involve the derivative dT/dt , together with the isothermal speed of sound. Eliminating this derivative by means of Equation 1.5.1 leads again to 1.6.8, though in a more complicated fashion.

From this moment on, the disturbance propagation velocity must be a result of the solution of gas dynamic problems and, as will be seen later, it is equal to a_e .

* Newton explained the discrepancy by the presence of suspended solid particles and water vapor in the atmosphere. It is interesting to cite the comment of the well-known scientist in the field of aerodynamics von Kármán (1947) in this connection: "It is interesting to see that even such a genius could succumb to the temptation of explaining an essential discrepancy between theory and experiment by wishful thinking."

For a perfect gas one can obtain a sequence of formulas (see 1.3.2, 1.5.9, and 1.4.4)

$$\begin{aligned} a^2 = a_e^2 &= \gamma \frac{RT}{M} = \gamma \frac{p}{\rho} = (\gamma - 1)h = \\ (\gamma - 1)\Theta(s)p^{(\gamma-1)/\gamma} &= \frac{\gamma}{3}\langle V^2 \rangle \quad \left(\Theta = \exp\left(\frac{s - s_0}{c_p}\right) \right) \end{aligned} \quad (1.6.9)$$

Here, $\langle V^2 \rangle$ is the square of the root-mean-square velocity of random molecular motion (cf. Section 1.4), which is of the order of the speed of sound. Clearly, the speed of sound at constant entropy increases with pressure, this circumstance determining a number of fundamental properties of equilibrium gas flows. In the general case, such a statement cannot be made on the basis of the existing thermodynamic laws, but for all known gases the condition $(\partial a_e^2 / \partial p)_s > 0$ holds without exceptions.

Generally speaking, the basic properties of gas dynamic processes, such as generation and propagation of disturbances and, in particular, shock waves, are determined (as will be seen in what follows) by the second isentropic derivative of the specific volume ρ^{-1} with respect to the pressure rather than by the derivative $(\partial a_e^2 / \partial p)_s$. More particularly, the fundamental postulate of gas dynamics is represented by the following condition

$$\begin{aligned} \left(\frac{\partial^2 \rho^{-1}}{\partial p^2} \right)_s &= - \left[\frac{\partial \rho^{-2} a_e^{-2}}{\partial p} \right]_s \frac{2A}{\rho^3 a_e^4} > 0 \\ A &= 1 + \frac{\rho}{2} \left(\frac{\partial a_e^2}{\partial p} \right)_s = \frac{\gamma + 1}{2} \end{aligned} \quad (1.6.10)$$

This condition is weaker than the previous one and holds for all known gases. The latter expression for A is written for a perfect gas.

Finally, by analogy with the case of a perfect gas, the speed of sound can be represented in the general case as follows

$$a_e^2 = \gamma_e \frac{p}{\rho}, \quad \gamma_e = \gamma_e(p, T) = \gamma_e(p, h) \quad (1.6.11)$$

The *equilibrium speed-of-sound coefficient* γ_e for air is also presented in Figure 1.10. Clearly, in the general case $\gamma_e \neq \gamma_* \neq \gamma_c$ (see Section 1.3). The relationships between these quantities can be obtained by substituting the equation of state 1.3.8 into one of the differential equations, 1.6.6

$$\frac{1}{\gamma_e} = \frac{1}{\gamma_*} - \left[p \frac{\partial \ln\left(\frac{\gamma_*-1}{\gamma_*}\right)}{\partial p} + \frac{\gamma_*-1}{\gamma_*} h \frac{\partial \ln\left(\frac{\gamma_*-1}{\gamma_*}\right)}{\partial h} \right] \quad (1.6.12)$$

Since γ_* depends on its arguments only weakly, the difference between γ_e and γ_* is small and for estimations on a bounded range of p and T the real gas can be replaced by an effective perfect gas letting $\gamma_e = \gamma_*$ (but not vice versa in view of the smallness of the difference $(\gamma_* - 1)$) which enters, for example, in the adiabatic Equation 1.5.9.

We will derive one more general expression for the speed of sound for the most commonly encountered forms of the equation of state specified as dependences on p and T (e.g., in the form of tables). To do this, we use, in addition to Equation 1.6.6, the adiabatic, or isentropic, equation written in the form:

$$dh = c_p dT + \left(\frac{\partial h}{\partial p} \right)_T dp = \frac{dp}{\rho}, \quad c_p = \left(\frac{\partial h}{\partial T} \right)_p \quad (1.6.13)$$

Thence, in view of Equation 1.3.6, we obtain the derivative

$$\left(\frac{\partial T}{\partial p}\right)_s = \frac{1}{c_p} \left[\frac{1}{\rho} - \left(\frac{\partial h}{\partial p}\right)_T \right] = \frac{c_p - c_v}{c_p} \left(\frac{\partial T}{\partial p}\right)_\rho \quad (1.6.14)$$

In terms of this relation we can rewrite 1.6.6 to the form:

$$\left(\frac{\partial \rho}{\partial p}\right)_s = \left(\frac{\partial \rho}{\partial p}\right)_T \cdot \left[1 + \left(\frac{\partial \rho}{\partial T}\right)_p \left(\frac{\partial p}{\partial \rho}\right)_T \left(\frac{\partial T}{\partial p}\right)_\rho \frac{c_p - c_v}{c_p} \right] \quad (1.6.15)$$

The product of the derivatives in the brackets is equal to -1 ; one can convince himself that this is correct by differentiating the composite function $\rho = \rho[T, p(T, \rho)]$. Hence, we have

$$a_e^2 = \left(\frac{\partial p}{\partial \rho}\right)_s = \frac{c_p}{c_v} a_T^2, \quad a_T^2 = \left(\frac{\partial p}{\partial \rho}\right)_T \quad (1.6.16)$$

Since $c_p > c_v$, the isentropic speed of sound is always greater than the isothermal one.

In conclusion, we will touch on the question of the possibility of the propagation of disturbances at an isothermal speed. To do this, we will consider a somewhat hypothetical example of a finite-thickness sound front in which there is an intensive heat exchange between a gas and an undisturbed medium in accordance with the law $q = \alpha(T_1 - T)$ (due to radiation, influence of cold channel walls, etc.), which only specifies the form of Equation 1.6.8. However, for very large values of the heat exchange coefficient, that is, in the $\alpha \rightarrow \infty$ limit, a reasonable (from the physical point of view) solution is $T_1 \rightarrow T$. Therefore, it is tempting to set immediately $\Delta T = 0$ in 1.6.6 and to replace 1.6.8 by the equation $a_T^2 \frac{dp}{dt} = \frac{dp}{dt}$ with the isothermal speed of sound. On the other hand, there appears to be little doubt about the validity of Equation 1.6.8 for any small but finite difference $T_1 - T$. All these questions, important for nonequilibrium processes, will be elucidated in Section 11.4.

1.7 Integral Equations of Fluid and Gas Motion: Simple Examples

The integral equations of motion follow immediately from the mass, momentum, and energy conservation laws. We will use these laws in their general form without addressing ourselves, if only possible, to the specific properties of the media under consideration.

The conservation laws are applied to a *moving* (in the general case) control volume Ω bounded by a control surface Σ across which the gas flows at a normal velocity U_n . If \mathbf{n} is the outward normal to an area element (see Figure 1.16 a and b) and \mathbf{U}_Σ is the gas velocity in a coordinate system fitted to the area $d\Sigma$, then the scalar product is $\mathbf{n} \cdot \mathbf{U}_\Sigma = -U_n$. Thus, there is convective mass transfer across the area $d\Sigma$ during a small time interval dt , the mass $\rho U_n d\Sigma dt$ flowing into the volume (for $U_n > 0$) or out of it (for $U_n < 0$) and carrying with it momentum, energy, and components of one or another substance.

For two-dimensional flows, whose parameters are independent of the coordinate z orthogonal to the drawing plane, the control volume Ω is confined within a unit-width plane layer between two planes $z = \text{const}$. The actions, which the volume Ω experiences from the two planes, compensate each other.

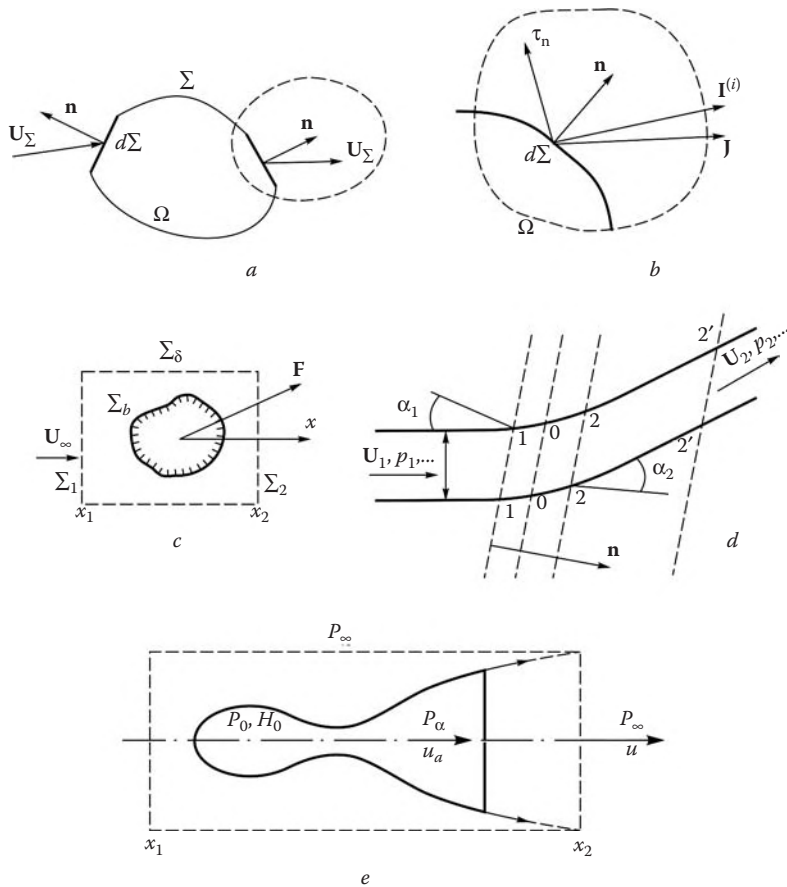


FIGURE 1.16
On the derivation of the integral conservation laws and the equations of motion.

1.7.1 Mass Conservation Law

In the absence of internal mass sources, the mass of the gas in the volume Ω changes only due to the mass flow across the surface Σ . Hence,

$$\frac{\partial}{\partial t} \left(\int_{\Omega} \rho d\Omega \right) = \int_{\Sigma} \rho U_n d\Sigma \quad (1.7.1)$$

Naturally, in this case there are no internal mass sources and diffusive mass flows across the boundary; however, if a similar equation (a counterpart of Equation 1.2.8) would be written for the partial density ρ_i , then its right-hand side would involve these terms in the form of surfaces and volume integrals.

1.7.2 Momentum Conservation Law

If a volume Ω has a fixed mass and is bounded by a fluid surface, then, according to Newton's law, its total acceleration is a sum (integral) of all external surface forces \mathbf{p}_n acting on it and certain distributed mass forces which $\rho \mathbf{g}$. However, in the general case the mass of the

control volume is variable and, therefore, one should also take into account the momentum of the gas flowing through the volume. To do this, it is sufficient to represent this portion of the gas as an individual body and to take into account the fact that the total momentum is a vector sum of individual terms.

The momentum of a unit volume is $\rho\mathbf{U}$, while the momentum equal to $\rho U_n \mathbf{U} d\Sigma dt$ is carried across an area $d\Sigma$ in a time dt , so that we obtain the following integral equation for momentum conservation in the volume Ω

$$\frac{\partial}{\partial t} \left(\int_{\Omega} (\rho \mathbf{U} d\Omega) \right) = \int_{\Sigma} (\rho U_n \mathbf{U} + \mathbf{p}_n) d\Sigma + \int_{\Omega} \rho \mathbf{g} d\Omega$$

$$\mathbf{p}_n = -\mathbf{n} p + \vec{\tau}_n \quad (1.7.2)$$

As in Section 1.2, here p is the pressure and $\vec{\tau}_n$ is the viscous stress.

1.7.3 Energy Equation

No additional principal assumptions are required to derive the energy equation. At each surface element in a time dt , an external force performs a work $\mathbf{p}_n \cdot \mathbf{U} d\Sigma dt$ on a gas confined in a volume Ω . Moreover, the energy $\rho U_n E d\Sigma dt$ is carried through this area, where E is the total gas energy (internal and kinetic) per unit mass. There are also dissipative energy fluxes \mathbf{J} due to heat conduction and possible diffusion of molecules of various kinds with various energies. If the normal components of these vectors are positive, $J_n > 0$, then the energy leaves the volume and vice versa. Taking into account external heat sources q we obtain the following energy conservation equation in the integral form:

$$\frac{\partial}{\partial t} \int_{\Omega} \rho E d\Omega = \int_{\Sigma} (\rho U_n E + \mathbf{p}_n \cdot \mathbf{U} - J_n) d\Sigma + \int_{\Omega} \rho (\mathbf{g} \cdot \mathbf{U} + q) d\Omega$$

$$E = e + \frac{1}{2} U^2, \quad J_n = \mathbf{n} \cdot \mathbf{J} \quad (1.7.3)$$

It is convenient to write the system obtained in a generalized vectorial form

$$L_{\chi} = \frac{\partial}{\partial t} \int_{\Omega} \chi d\Omega - \int_{\Sigma} U_n \chi d\Sigma = \int_{\Sigma} P_{\chi} d\Sigma + \int_{\Omega} Q_{\chi} d\Omega \quad (1.7.4)$$

Here, L_{χ} signifies the operator on the left-hand side of the equation, while the generalized vectors of the unknown function χ and the surface force P_{χ} have the form:

$$\chi = [\rho, \quad \rho \mathbf{U}, \quad \rho E]^T, \quad P_{\chi} = [0, \quad \mathbf{p}_n, \quad \mathbf{p}_n \cdot \mathbf{U} - J_n]^T$$

$$Q_{\chi} = [0, \quad \rho \mathbf{g}, \quad \rho q + \rho (\mathbf{g} \cdot \mathbf{U})]^T \quad (1.7.5)$$

where the subscript T denotes transposition of the matrices.

Substituting any element of these columns into 1.7.4 we obtain one of the previous equations.

Two points related with the equations obtained should be explained. The first one is associated with a body with a surface $d\Sigma_b$ surrounded by an external control surface Σ ($\Sigma = \Sigma_1 + \Sigma_2 + \Sigma_{\delta}$ in Figure 1.16c). In this case the control volume Ω is confined by the surfaces Σ and Σ_b and the surface integrals in 1.7.4 should be taken over the entire surface

$\Sigma' = \Sigma + \Sigma_b$. However, the integrals over the surface Σ_b can be separated out to emphasize the integral action of the body on the flow. Then the momentum equation takes the form:

$$L_U = \frac{\partial}{\partial t} \int_{\Omega} \rho \mathbf{U} d\Omega - \int_{\Sigma} \rho U_n \mathbf{U} d\Sigma = \int_{\Sigma} \mathbf{p}_n d\Sigma - \mathbf{F}, \quad \mathbf{F} = \int_{\Sigma_b} \mathbf{p}_n d\Sigma \quad (1.7.6)$$

Here and in what follows the terms with $\rho \mathbf{g}$ are omitted; their role in gas dynamics will be discussed at the end of the section.

In the previous equations the vector \mathbf{F} represents the force acting on the body. In determining this force we have chosen the outward direction of the surface normal \mathbf{n} on Σ_b . Therefore, here \mathbf{p}_n is the stress acting on the body surface from the fluid. In a two-dimensional flow, in accordance with the reservations made at the beginning of this section, the force \mathbf{F} relates to a unit-width body (e.g., a wing). In the general case, a control volume can contain only a part of the body surface with the intersection of the planes Σ and Σ_b . In this case, the integration over the surface Σ should be performed only outside the domain occupied by the body, while the force \mathbf{F} relates only to the part of the body submerged in the domain Ω .

We note also that the condition $U_n = 0$ imposed on the surface and used in Equation 1.7.6 is justified only in the absence of gas injection through the surface. Otherwise, the momentum of the injected gas would affect the total momentum of the gas volume Ω . In other equations, the corresponding integrals over the surface Σ_b characterize the mass fluxes of gas components, their energy fluxes, and so on; they may arise due to surface diffusion, heat conduction, or gas injection.

The second point is concerned with the fact that the total local gas velocity \mathbf{U} entering explicitly in Equation 1.7.4 is dependent (in contrast to the normal velocity U_n across the area $d\Sigma$) on the choice of a coordinate system. The question arises how the equations change when passing from one coordinate system to another. We will show that *the equations do not change their form for any inertial (but only inertial) coordinate transformation in which velocities are transformed in accordance with the law*

$$\mathbf{U} = \mathbf{U}_0 + \mathbf{U}', \quad \mathbf{U}_0 = \text{const} \quad (1.7.7)$$

Here, \mathbf{U}' is the gas velocity in the new coordinate system and \mathbf{U}_0 is the velocity of the new coordinate system with respect to the old one. This result is evident for continuity Equation 1.7.1 since the total velocity does not enter in this equation at all. Consider now Equation 1.7.2. To emphasize how important inertial condition is 1.7.7 we will take into account the time dependence of the function \mathbf{U}_0 (letting $\mathbf{U}_0 = \mathbf{U}_0(t)$) rather than its space dependence (excluding, e.g., relative rotation of these coordinate systems). Obviously, the forces \mathbf{p}_n are invariant about any coordinate transformation; therefore, we may consider only the transformation of the operator $L_U(\mathbf{U})$

$$\begin{aligned} L_U(\mathbf{U}) &= \frac{\partial}{\partial t} \left(\int_{\Omega} \rho \mathbf{U} d\Omega \right) - \int_{\Sigma} \rho U_n \mathbf{U} d\Sigma = \\ &= L_U(\mathbf{U}') + \mathbf{U}_0 L_{\rho} + M \frac{d\mathbf{U}_0}{dt}, \quad M = \int_{\Omega} \rho d\Omega \end{aligned} \quad (1.7.8)$$

Here, the operator $L_U(\mathbf{U}')$ is obtained from the operator $L_U(\mathbf{U})$ by substituting \mathbf{U}' for \mathbf{U} , while the operator L_{ρ} is the left-hand side of the continuity equation in the form 1.7.4,

which is equal to zero. The last term is the acceleration of the gas volume Ω as a solid of mass M , which leads to the appearance of inertial forces in the momentum equation for a noninertial transformation of coordinates. However, for the constant velocity \mathbf{U}_0 this term also vanishes and $L_U(\mathbf{U}) = L_U(\mathbf{U}')$, that is, the momentum equation conserves its form.

It is easy to show that for the velocity \mathbf{U}_0 depending on coordinates, expression 1.7.7 becomes too cumbersome. In what follows we will transform the energy Equation 1.7.3 only for a constant velocity \mathbf{U}_0 . We will group together the \mathbf{U} -dependent terms on the left-hand side of the equation in a single operator. Then, in view of the equality

$$U^2 = \mathbf{U} \cdot \mathbf{U} = U_0^2 + 2 \cdot \mathbf{U}_0 \cdot \mathbf{U}' + (U')^2 \quad (1.7.9)$$

we obtain

$$\begin{aligned} \bar{L}_E(\mathbf{U}) &= \frac{1}{2} \frac{\partial}{\partial t} \left(\int_{\Omega} \rho \mathbf{U} \cdot \mathbf{U} d\Omega \right) - \int_{\Sigma} \left(\frac{1}{2} \rho U_n \mathbf{U} \cdot \mathbf{U} + \mathbf{p}_n \cdot \mathbf{U} \right) d\Sigma \\ &= \bar{L}_E(\mathbf{U}') + \frac{1}{2} U_0^2 L_\rho + \mathbf{U}_0 \left[L_U(\mathbf{U}') - \int_{\Sigma} \mathbf{p}_n d\Sigma \right] = \bar{L}_E(\mathbf{U}') \end{aligned} \quad (1.7.10)$$

Here, the operator \bar{L}_E is wider than L_E in 1.7.4. It is taken into account that $L_\rho = 0$ and the vanishing of the expression in the last brackets in the new coordinate system by virtue of Equation 1.7.2. Thus, the statement has been proved. (The terms ρg and J_n in Equation 1.7.3 omitted in the derivation have obviously no effect on this result.)

In the general case, it is difficult to use the integral equations thus derived for solving particular problems; however, sometimes they make it possible to obtain complete results. As an example generalizing the results of Section 1.6, we shall obtain expressions relating the states on either side of a steady oblique front of perturbations propagating through a moving uniform gas. Since the relations are invariant in any inertial coordinate system, consider the system fitted to the moving front. This frozen pattern is shown in Figure 1.16d. Here, all the parameters are constant in planes 1-1 and so on, parallel to the front, and vary only along the normal \mathbf{n} to the front. All streamlines, or particle trajectories, 1-0-2, can be brought into coincidence by translation along the front. There is no transfer of any quantity across the streamlines (as across smooth, thermally insulated channel walls); any internal sources are also absent.

We will confine the control volume by the planes 1-1 and 2-2 and two streamlines 1-0-2. Let v_n be the normal flow velocity across the front, \mathbf{n} the unit normal to the front aligned with the flow, J the magnitude of the vector \mathbf{J} , which in this case is directed along the normal, and $\vec{\tau}$ the viscous friction vector acting on the planes in the direction of the normal \mathbf{n} . Evidently, $v_{n1} = D$ is the normal velocity of the front propagation through the gas (Section 1.6). Then we have

$$\begin{aligned} -\mathbf{n}_1 = \mathbf{n}_2 = \mathbf{n}, \quad U_{n1} = v_{n1}, \quad U_{n2} = -v_{n2} \\ \vec{\tau}_{n1} = -\vec{\tau}_1, \quad \vec{\tau}_{n2} = \vec{\tau}_2, \quad J_{n1} = -J_1, \quad J_{n2} = J_2 \end{aligned} \quad (1.7.11)$$

Applying Equation 1.7.4 we obtain relations between the flow parameters at the end sections of the volume.

$$\begin{aligned} \rho_2 v_{n2} &= \rho_1 v_{n1} = m, & v_n &= \mathbf{n} \cdot \mathbf{U} \\ \rho_2 v_{n2} \mathbf{U}_2 + p_2 \mathbf{n} - \vec{\tau}_2 &= \rho_1 v_{n1} \mathbf{U}_1 + p_1 \mathbf{n} - \vec{\tau}_1 \\ \rho_2 v_{n2} E_2 + p_2 v_{n2} - \vec{\tau}_2 \mathbf{U}_2 + J_2 &= \\ \rho_2 v_{n2} H_2 - \vec{\tau}_2 \mathbf{U}_2 + J_2 &= \\ \rho_1 v_{n1} H_1 - \vec{\tau}_1 \mathbf{U}_1 + J_1 + mq_m & \\ H = E + \frac{p}{\rho} &= h + \frac{U^2}{2}, & h = e + \frac{p}{\rho} \end{aligned} \quad (1.7.12)$$

Here, H is the *total enthalpy* of gas, which plays an important role in gas dynamics. The quantity q_m is the total heat influx to the volume between the control surfaces referred to the mass flow rate m through the surfaces.

These equations always have a trivial solution, in which a front is absent ($p_2 = p_1$, $\tau = 0$, $J = 0$, and so on). In what follows we shall show that they have one more important solution corresponding to the *shock wave* that represents one of the fundamental phenomena in gas dynamics.

Now we will obtain an expression for the force \mathbf{F} acting on a body in an inviscid steady flow in terms of the flow parameters on the control volume boundary (Figure 1.16c). We decompose the force \mathbf{F} into two components, \mathbf{X} directed along the x axis, which is aligned to the freestream velocity \mathbf{U}_∞ , and \mathbf{Y} orthogonal to it. We denote the gas velocity projection onto the x axis as u and the orthogonal velocity component as \mathbf{U}_N . Then, projecting Equation 1.7.6 with $\partial/\partial t = 0$ onto the x axis, we obtain the scalar equation

$$X = - \int_{\Sigma_b} p n_x d\Sigma = \int_{\Sigma} (\rho U_n u - p n_x) d\Sigma \quad (1.7.13)$$

The expression for \mathbf{Y} remains vectorial (here, \mathbf{n}_N is the projection of the normal \mathbf{n} onto an $x = \text{const}$ plane)

$$\mathbf{Y} = - \int_{\Sigma_b} p \mathbf{n}_N d\Sigma = \int_{\Sigma} (\rho U_n \mathbf{U}_N - p \mathbf{n}_N) d\Sigma \quad (1.7.14)$$

As distinct from the outer control surface Σ , the normal to the body surface Σ_b is directed in the fluid volume.

The disadvantage of these relations is formal unboundedness of each term when a control volume is expanding; hence, it is necessary to define a finite force in terms of a difference of unbounded quantities. In order to avoid this, we multiply Equation 1.7.1 with $\partial/\partial t = 0$ by U_∞ , subtract the result from Equation 1.7.13, and introduce the freestream pressure p_∞ under the integral sign in the previous expressions (the integral of p_∞ over a closed surface is equal to zero). Thus we obtain

$$X = \int_{\Sigma} [\rho U_n (u - U_\infty) - n_x (p - p_\infty)] d\Sigma \quad (1.7.15)$$

$$\mathbf{Y} = \int_{\Sigma} [\rho U_n \mathbf{U}_N - (p - p_\infty) \mathbf{n}_N] d\Sigma \quad (1.7.16)$$

From general physical considerations there is good reason to believe that the quantities $u - U_\infty$, $p - p_\infty$, and U_N decay far from the body. This circumstance, which should be proved for each particular problem, ensures the convergence of the integrals when the control surface expands without bounds.

The transversal vector force \mathbf{Y} can be decomposed in some transverse axes, for example, the axes y and z with the unit vectors \mathbf{j} and \mathbf{k} , as follows

$$\mathbf{Y} = \mathbf{j} Y_y + \mathbf{k} Y_z \quad (1.7.17)$$

where Y_y and Y_z are the components of the force \mathbf{Y} .

As an illustration, we will choose a control volume in the form of a circular cylinder coaxial with the x axis. The volume is bounded by endfaces Σ_1 and Σ_2 and by a lateral surface Σ_δ (Figure 1.16c); we denote the radial, or normal, gas velocity on Σ_δ as $v_r = -U_{n\delta}$. On the endfaces we have $U_{n1} = u_1$, $n_{x1} = -1$, $U_{n2} = -u_2$, $n_{x2} = 1$, and $n_{x\delta} = 0$. In this case

$$\begin{aligned} X = & - \int_{\Sigma_2} [\rho u(U_\infty - u) - (p - p_\infty)] d\Sigma + \\ & \int_{\Sigma_1} [\rho u(U_\infty - u) - (p - p_\infty)] d\Sigma + \int_{\Sigma_\delta} \rho v_r(U_\infty - u) d\Sigma \end{aligned} \quad (1.7.18)$$

$$\begin{aligned} \mathbf{Y} = & \int_{\Sigma_1} \rho u \mathbf{U}_N d\Sigma - \int_{\Sigma_2} \rho u \mathbf{U}_N d\Sigma - \\ & \int_{\Sigma_\delta} [\rho v_r \mathbf{U}_N + (p - p_\infty) \mathbf{n}_N] d\Sigma \end{aligned} \quad (1.7.19)$$

The mass conservation law for this control volume has the form:

$$\int_{\Sigma} \rho U_n d\Sigma = \int_{\Sigma_1} \rho u d\Sigma - \int_{\Sigma_2} \rho u d\Sigma - \int_{\Sigma_\delta} \rho v_r d\Sigma = 0 \quad (1.7.20)$$

If the flow on the lateral surface Σ_δ is undisturbed ($v_r = 0$, $U_N = 0$, $p = p_\infty$, and $u = U_\infty$), then in Equations 1.7.18 to 1.7.20 all the integrals over Σ_δ are zero; if, moreover, the flow is undisturbed on the entry surface Σ_1 , then the first terms in 1.7.18 and 1.7.19 also vanish. This situation is frequent in supersonic flows. Reservations are required only in the case in which the control volume encloses only a part of the body (e.g., the forward part cut off by a plane Σ_2 with the section area s_b). Then, as noted previously, the integration in the section Σ_2 should be carried out over the area $\Sigma_2 - s_b$, while formulas 1.7.15 and 1.7.18 for X must include the term $p_\infty s_b$ on their right-hand sides. Thus, for the undisturbed flow on Σ_1 and Σ_δ instead 1.7.18 we obtain

$$X = \int_{\Sigma_2 - s_b} [\rho u(U_\infty - u) - (p - p_\infty)] d\Sigma + p_\infty s_b \quad (1.7.21)$$

Finally, we will touch on the question of the thrust T of a rocket engine. In Figure 1.16e we have plotted a jet issuing from the engine nozzle into an ambient medium (i.e., a gas at

rest). Obviously, in this case $U_\infty = 0$, while $u = 0$ everywhere, except for the section Σ_2 . Then from 1.7.18 it follows that

$$T = \int_{\Sigma_2} [\rho u^2 + (p - p_\infty)] d\Sigma \rightarrow \int_{\Sigma_2} u dG \quad (1.7.22)$$

The latter formula is valid for a distant section, where the jet pressure is equal to the surrounding one ($p = p_\infty$). Here, $dG = \rho u d\Sigma$ is a gas flow rate element. For the farthest section, the jet flow rate exceeds the initial one G_0 due to viscous *ejection* of the surrounding gas, so that Equation 1.7.22 gives a conservation law for a viscous jet.

But even if the viscosity influence is neglected, it follows from Equation 1.7.22 that, everything else being equal, the engine thrust increases with the jet velocity; in particular, it increases when the angles θ of the local velocity U to the nozzle axis decrease, since $u = U \cos \theta$.

Let us emphasize some important features of the integral equations.

First, they reflect only general conservation laws for a continuous medium and are independent of other particular properties of the medium.

Second, the continuity and all the more the differentiability of functions with respect to space are not used in deriving the equations; therefore, they hold at any number of gas dynamic discontinuities inside a gas volume or on its boundaries.

In conclusion, we will make some remarks on the role and a possible nature of body, or mass, forces, which, in the general case, enter in the momentum and energy equations (the terms $\rho \mathbf{g}$ and $\rho \mathbf{g} \cdot \mathbf{U}$). The most conventional of these forces is gravity with the acceleration \mathbf{g} . However, for gases and often even for fluids the role played by gravity is essential only for low-velocity motions (this will be shown in Section 1.12). At the same time, the gravity force plays a considerable, if not crucial, part in the generation of natural convection in nonisothermal gas and fluid media.

Other body forces can also exist. Thus, electromagnetic forces act on a plasma in motion (a medium containing free electrons and ions). Furthermore, in describing multiphase flows (e.g., those of a dusty gas) each phase is considered as a separate continuous medium, while the force interaction of the phases is replaced by an appropriate body force for each phase (Rakhmatullin, 1965). These problems are beyond the scope of this book; for this reason, in what follows we will not make allowance for body forces without mentioning especially this circumstance (including the gravity force, if otherwise is not stated).

1.8 Some Questions of the Kinematics of Fluid Media: Differential Vector Operators

Before proceeding to the derivation of the equations in the differential form, we will consider some important questions of fluid medium kinematics. They are important, since the kinematics describes geometrical flow patterns, while differential vector operators (velocity divergence, etc.) make it possible to write down the equations of motion in a compact, reference frame-invariant form.

1.8.1 Particle Trajectories and Streamlines

A fluid particle trajectory can be specified in the form of the time dependence of its coordinates. For example, in rectangular Cartesian coordinates we have

$$\begin{aligned} x &= x^*(t), & y &= y^*(t), & z &= z^*(t), \\ u &= \frac{dx^*}{dt}, & v &= \frac{dy^*}{dt}, & w &= \frac{dz^*}{dt} \end{aligned} \quad (1.8.1)$$

Here u , v , and w are the projections of the instant velocity \mathbf{U} onto the corresponding coordinate axes. These relations determine the velocity field in space and time. The envelope of the vectors $\mathbf{U}(t, x, y, z)$, or the line tangent to these vectors at each point, is called an instant streamline (Figure 1.17a). It is determined by a set of slope coefficients

$$\frac{dy}{dx} = \frac{v}{u}, \quad \frac{dz}{dx} = \frac{w}{u}, \quad \frac{dz}{dy} = \frac{w}{v} \quad (1.8.2)$$

Streamlines intersecting an arbitrary generator AB form a *stream surface*. If the generator is closed, such a surface forms a *stream tube* (Figure 1.17b).

In unsteady flows a streamline, generally speaking, does not coincide with a particle trajectory (dotted line in Figure 1.17a), but in steady-state flows both lines coincide and streamlines, stream surfaces, and tubes give a graphical representation of the flow. In an arbitrary curvilinear coordinate system x_i , $i = 1, 2, 3$, particle trajectories can also be specified by dependences $x_i = x_i^*(t)$, but in this case the corresponding velocity components u_i are, generally speaking, not equal to dx_i^*/dt : $u_i \neq dx_i^*/dt$ (see Section 1.13).

Particle trajectories can also be determined by their initial coordinates x_0^* , y_0^* , and z_0^* for $t = t_0$, which are used sometimes as independent *Lagrangian* variables, as distinguished from the original *Eulerian* coordinates x , y , and z .

The concept of the particle trajectory is associated with that of the *total*, or *substantive*, derivative of an arbitrary parameter χ (referred to as a fixed gas particle) with respect to time. This derivative is denoted by $\frac{d\chi}{dt}$, as distinct from partial derivatives with respect to time and space. Putting $\chi(t, x_i) = \chi[t, x_i^*(t)]$ yields

$$\frac{d\chi}{dt} = \frac{\partial \chi}{\partial t} + \sum_i \frac{\partial \chi}{\partial x_i} \frac{dx_i^*}{dt} = \frac{\partial \chi}{\partial t} + u \frac{\partial \chi}{\partial x} + v \frac{\partial \chi}{\partial y} + w \frac{\partial \chi}{\partial z} = \frac{\partial \chi}{\partial t} + (\mathbf{U} \cdot \vec{\nabla}) \chi \quad (1.8.3)$$

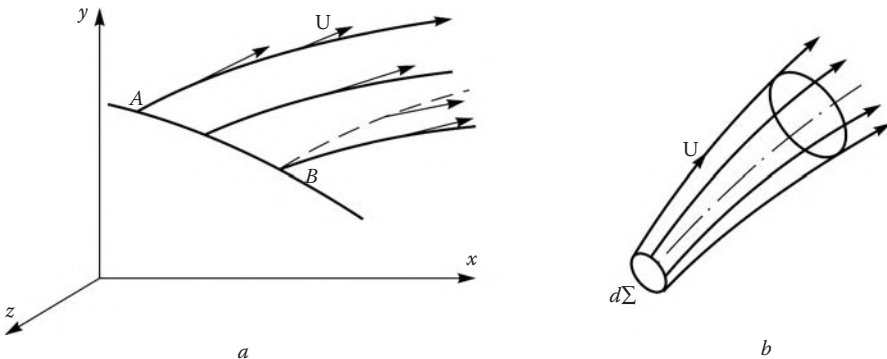


FIGURE 1.17
Streamlines, stream surfaces, and stream tubes.

The latter formulas are written in Cartesian coordinates. Here the differential *Hamilton operator* is used

$$\vec{\nabla} = \mathbf{i} \frac{\partial}{\partial x} + \mathbf{j} \frac{\partial}{\partial y} + \mathbf{k} \frac{\partial}{\partial z} \quad (1.8.4)$$

1.8.2 Curl and Deformation Rate

These concepts characterize a change in orientation (revolution) and shape of the initial volume of a fixed fluid particle. As an example, we have qualitatively shown in Figure 1.18 the evolution of the initial shape of a particle in plane shear motion (Figure 1.18a) and two forms of rotational motions around a center: $U(r) = c/r$ (Figure 1.18b) and $U = \omega r$ (Figure 1.18c). In the first two cases particles are deformed (in the second case with an apparent rotation), while in the third case they are not deformed at all and rotate, as in a solid, around some point with the same angular velocity ω .

However, this superficial impression is not sufficient to characterize, even qualitatively, the flow kinematics. Consider a local structure of the velocity field in a particle relative to a certain point (the pole O) moving at a translational velocity \mathbf{U}_0 . The appropriate expansion can be represented as a sum of two terms (the *first Helmholtz theorem*).

$$\mathbf{U}' = \mathbf{U} - \mathbf{U}'_0 = \frac{\partial \mathbf{U}}{\partial x} x' + \frac{\partial \mathbf{U}}{\partial y} y' + \frac{\partial \mathbf{U}}{\partial z} z' = \mathbf{U}'_\omega + \mathbf{U}'_\varepsilon, \quad \mathbf{r}' = \mathbf{i}x' + \mathbf{j}y' + \mathbf{k}z' \quad (1.8.5)$$

Here, \mathbf{r}' is the radius-vector of an arbitrary point relative to the pole.

It appears that these terms (i.e., the *rotational* \mathbf{U}'_ω and *deformation* \mathbf{U}'_ε ones, or, in projections, $u' = u'_\omega + u'_\varepsilon$, etc.) play qualitatively different roles in the flow classification.

Quite naturally, the rotational velocity component (if it exists) must have the same form as in the case of a solid body, whose angular velocity is $\vec{\omega}/2$ (i.e., it is determined by the vector product)

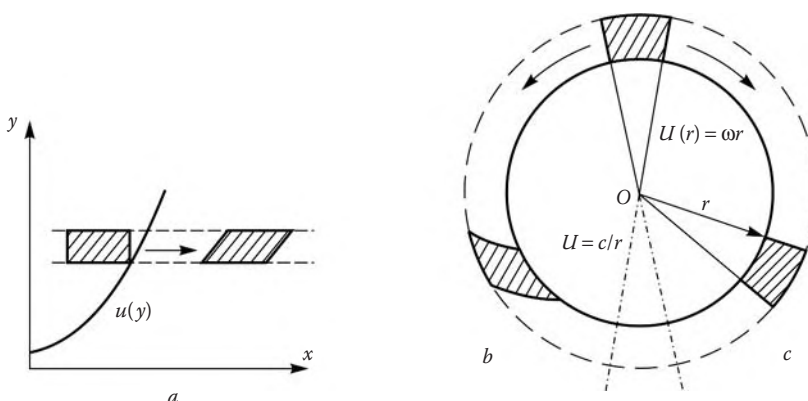


FIGURE 1.18
Shear and rotation flows.

$$\begin{aligned}\mathbf{U}'_\omega &= \frac{1}{2} \boldsymbol{\omega} \times \mathbf{r}' = \frac{1}{2} \begin{vmatrix} \mathbf{i} & \mathbf{j} & \mathbf{k} \\ \omega_x & \omega_y & \omega_z \\ x' & y' & z' \end{vmatrix} = \mathbf{i}u'_\omega + \mathbf{j}v'_\omega + \mathbf{k}w'_\omega \\ u'_\omega &= \frac{1}{2}\omega_y z' - \frac{1}{2}\omega_z y', \quad v'_\omega = -\frac{1}{2}\omega_x z' + \frac{1}{2}\omega_z x' \\ w'_\omega &= \frac{1}{2}\omega_x y' - \frac{1}{2}\omega_y x'\end{aligned}\tag{1.8.6}$$

To obtain expressions for ω_x , and so on, one should write the expansions of type 1.8.5 for the velocity components u'_ω , and so on, and try to separate out a structure of type 1.8.6. This turns out to be possible and results in the following relations

$$\omega_x = \frac{\partial w}{\partial y} - \frac{\partial v}{\partial z}, \quad \omega_y = \frac{\partial u}{\partial z} - \frac{\partial w}{\partial x}, \quad \omega_z = \frac{\partial v}{\partial x} - \frac{\partial u}{\partial y}\tag{1.8.7}$$

These terms are the components of a differential vector operator, namely, the *velocity rotor, or curl*.

$$\vec{\omega} = \text{curl } \mathbf{U} = \vec{\nabla} \times \mathbf{U} = \begin{vmatrix} \mathbf{i} & \mathbf{j} & \mathbf{k} \\ \frac{\partial}{\partial x} & \frac{\partial}{\partial y} & \frac{\partial}{\partial z} \\ u & v & w \end{vmatrix}\tag{1.8.8}$$

The velocity curl is an important kinematic characteristic of fluid motion. A vorticity field, as any other vector field, has *vorticity lines, tubes, and surfaces ("vorticity sheets")*. To have an idea of their possible shapes, one should replace \mathbf{U} by $\vec{\omega}$ in Figure 1.17.

The other terms of expansions 1.8.5 are also grouped in a symmetrical fashion to form the strain components of the velocity field

$$\begin{aligned}u'_\varepsilon &= \varepsilon_{xx}x' + \varepsilon_{xy}y' + \varepsilon_{xz}z' \\ v'_\varepsilon &= \varepsilon_{yx}x' + \varepsilon_{yy}y' + \varepsilon_{yz}z' \\ w'_\varepsilon &= \varepsilon_{zx}x' + \varepsilon_{zy}y' + \varepsilon_{zz}z' \\ \varepsilon_{xx} &= \frac{\partial u}{\partial x}, \quad \varepsilon_{yy} = \frac{\partial v}{\partial y}, \quad \varepsilon_{zz} = \frac{\partial w}{\partial z} \\ \varepsilon_{xy} = \varepsilon_{yx} &= \frac{1}{2} \left(\frac{\partial u}{\partial y} + \frac{\partial v}{\partial x} \right), \quad \varepsilon_{xz} = \varepsilon_{zx} = \frac{1}{2} \left(\frac{\partial u}{\partial z} + \frac{\partial w}{\partial x} \right) \\ \varepsilon_{yz} = \varepsilon_{zy} &= \frac{1}{2} \left(\frac{\partial v}{\partial z} + \frac{\partial w}{\partial y} \right)\end{aligned}\tag{1.8.9}$$

Here, the quantities ε_{ik} are the *strain rates*. Formulas 1.8.9 can be written in the following compact form:

$$\begin{aligned}U'_\varepsilon &= E_\varepsilon \mathbf{r}', \quad E_\varepsilon = \| \varepsilon_{ik} \| \\ \varepsilon_{ik} &= \frac{1}{2} \left(\frac{\partial u_k}{\partial x_i} + \frac{\partial u_i}{\partial x_k} \right), \quad i, k = 1, 2, 3\end{aligned}\tag{1.8.10}$$

Here, $x_1 = x$, $x_2 = y$, and $x_3 = z$, u_i are the velocity components, and E_ε is the *strain rate matrix, or tensor*. However, in spite of its general form, the formula for ε_{ik} is valid only in a Cartesian coordinate system (see Section 1.14). We will emphasize that the strain rates are symmetric: $\varepsilon_{ik} = \varepsilon_{ki}$.

Strain rates are of a fundamental importance in constructing rheological models of viscous fluid. Their names are justified by the fact that for $\varepsilon_{ik} = 0$ a fluid volume is “solidified” and is not deformed.

The quantities ε_{ik} , $i \neq k$, correspond to the *shear deformation*, a typical example of which is shown in Figure 1.18a, where $\varepsilon_{xy} = \varepsilon_{yx} = \frac{\partial u}{\partial y}$. An initial rectangle is transformed to a parallelogram of the same area (i.e., shear deformations are accompanied by changes in the particle shape). For example, it can be easily shown that the quantity $(\Delta u / \Delta y) \Delta t$ represents an angle α at which the y axis (frozen in a fluid) is turned in a time Δt (Figure 1.19c). Therefore, $2\varepsilon_{xy}$ is the rate of the variation of the angle between orthogonal fluid lines initially coinciding with the x and y axes.

On the contrary, the quantities ε_{ii} characterize a *linear strain rate* (i.e., a relative rate of the variation of the fluid segment lengths, the segments being located on coordinate axes). Formula 1.2.1, in particular, demonstrates this fact. We note that the last definitions of ε_{ik} are invariant with respect to revolution and any changes in the coordinate system and are related to intrinsic characteristics of velocity fields only.

Finally, a *volume strain rate* or *velocity divergence* is defined as the relative rate of the variation of a small fluid volume $\Delta\Omega^*$ (cf. Section 1.2)

$$\operatorname{div} \mathbf{U} = \lim_{\Delta\Omega^* \rightarrow 0} \frac{1}{\Delta\Omega^*} \frac{d\Delta\Omega^*}{dt} \quad (1.8.11)$$

Let us write down this formula in a Cartesian coordinate system for a fluid volume $\Delta\Omega^*$ initially coinciding with the coordinate parallelepiped $\Delta\Omega = \Delta x \Delta y \Delta z$ (Figure 1.19a). If this volume is convected by the flow at a velocity \mathbf{U} , then its fluid ribs become equal to $\Delta x'$, and so on, in a time Δt (Figure 1.19c). For small Δt the distortions of the segments and angles between them are so small that a new volume keeps an almost rectangular form and becomes equal to $\Delta\Omega^* = \Delta x' \Delta y' \Delta z'$. Then taking the logarithm and differentiating the expression and using Equation 1.2.1 for the rate of the variation the segment length we can easily obtain the relative rate of the volume variation (in linear approximation)

$$\operatorname{div} \mathbf{U} = \frac{\partial u}{\partial x} + \frac{\partial v}{\partial y} + \frac{\partial w}{\partial z} = \vec{\nabla} \cdot \mathbf{U} = \varepsilon_{xx} + \varepsilon_{yy} + \varepsilon_{zz} \quad (1.8.12)$$

Thence there follows an important result that *a sum of normal strain rates is invariant with respect to coordinate revolution*.

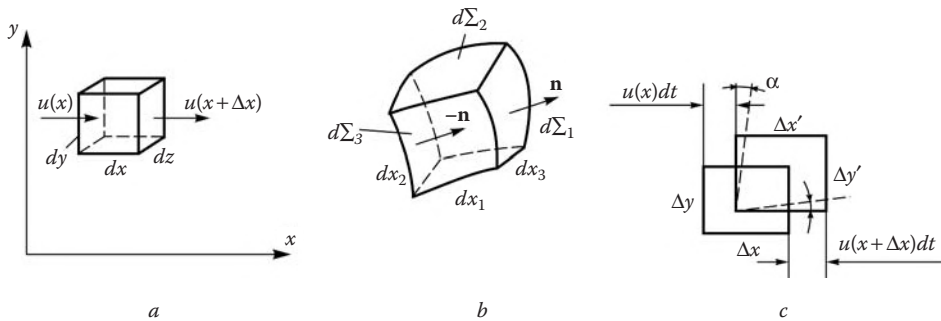


FIGURE 1.19
Elementary coordinate volumes.

We note also that the comparison of this result with 1.8.3 shows that, at least, scalar products with the vector $\vec{\nabla}$ are noncommutative (here $\vec{\nabla} \cdot \mathbf{U} \neq \mathbf{U} \cdot \vec{\nabla}$, as distinct from the situation with standard vectors).

Finally, let us analyze examples shown in Figure 1.18 on the basis of the results obtained. Let the z axis be directed normal to the figure plane (x, y plane), where $r = (x^2 + y^2)^{1/2}$. After some algebra, we can obtain the following result. The shear flow (a) exhibits not only deformation, $\varepsilon_{xy} = \varepsilon_{yx} = \frac{\partial u}{\partial y}$, but also rotation, $\omega_z = -\frac{\partial u}{\partial y}$, $\omega_x = \omega_y = 0$, which, on first sight, is somewhat unexpected. The rotational motion (b) turns out to be irrotational (i.e., $\omega = 0$), though it is precisely this flow that is borne in mind in everyday life when speaking of curls. However, actually this flow is possible only in an inviscid fluid as only it contains a concentrated curl at a singular point O . This will be discussed in Chapter 2. Only the flow pattern (c) is purely rotational and vertical, $\omega_z = 2\omega$, without exhibiting any deformations (all $\varepsilon_{km} = 0$).

1.8.3 Vector Divergence

In the general case we define this operator as follows:

$$\operatorname{div} \mathbf{A} = \lim_{\Delta\Omega, \Delta\Sigma \rightarrow 0} \left(\frac{1}{\Delta\Omega} \int_{\Delta\Sigma} A_n d\Sigma \right), \quad A_n = \mathbf{A} \cdot \mathbf{n} \quad (1.8.13)$$

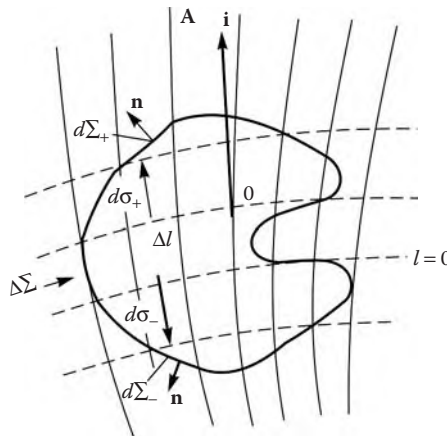
Here, \mathbf{n} is an outward normal to the area element $d\Sigma$, while A_n is the flux of the vector \mathbf{A} across this area. Such integrals over small volumes $d\Omega$ bounded by small surfaces $d\Sigma$ (shown, e.g., in Figure 1.19a and b) will be considered in Section 1.9 in deriving differential equations of motion.

The equivalence of this definition of velocity to that given in Equation 1.8.11 for $\mathbf{A} = \mathbf{U}$ can be proved as follows. Consider a fluid volume $\Delta\Omega^*$ bounded by a surface $\Delta\Sigma^*$ coinciding initially with the volume $\Delta\Omega$. Then the velocity U_n of a gas flowing across $\Delta\Sigma$ is equal to the normal velocity of the translation of the fluid surface $\Delta\Sigma^*$ and, hence, the right-hand side of 1.8.13 represents the relative rate of the variation of the fluid volume. In particular, formula 1.8.12 is valid for any vector \mathbf{A} with projections A_x, A_y, A_z , instead of u, v, w .

To make this general definition of divergence more universal and, in particular, independent of a volume shape, we will relate it to a local structure of the vector field. To do this, we fill an arbitrary small volume $\Delta\Omega$ by a bundle of vector lines tangent everywhere to \mathbf{A} . This is shown conditionally in Figure 1.20 for the section of the volume by a longitudinal plane. The extreme lines divide the surface $\Delta\Sigma$ in two parts, the upper one $\Delta\Sigma_+$ and the lower one $\Delta\Sigma_-$. In a simple case (the left part of the figure) each vector tube cuts out of them the areas $\Delta\Sigma_+$ and $\Delta\Sigma_-$, while in a more complicated case (the right part of the figure) the number of areas is greater and even. We will consider the first case; in the general case the reasoning is similar for each pair of appropriate areas. Since $\mathbf{A} \cdot \mathbf{n} = A \cos(\mathbf{A} \cdot \mathbf{n})$, the equality $A_n d\Sigma = A d\sigma$ holds, where $d\sigma$ is an orthogonal section of a vector tube. Thus, introducing a length l measured along the tube we replace the integral of $A_n d\Sigma$ over the surface $\Delta\Sigma$ by an integral over $\Delta\Sigma_-$ of the difference

$$(Ad\sigma)_+ - (Ad\sigma)_- = \frac{\partial(Ad\sigma)}{\partial l} \Delta l = \left(\frac{\partial A}{\partial l} + \frac{A}{R_{\text{eff}}} \right) d\sigma \Delta l, \quad \frac{1}{R_{\text{eff}}} = \frac{1}{d\sigma} \frac{d(d\sigma)}{dl} \quad (1.8.14)$$

over the surface $\Delta\Sigma_-$. Here, Δl is the vector tube length inside the volume and R_{eff} is the length of an effective vector tube (formed by a rectilinear continuation of vector lines up to

**FIGURE 1.20**

On the derivation of differential vectorial operators.

a region of their intersection). The sign of R_{eff} depends on whether the tube is divergent or convergent along a chosen l direction. If a vector field is formed by a divergent rectilinear bundle originating from a pole, then $R_{\text{eff}} = 2R$ at a distance R in a spherical bundle and $R_{\text{eff}} = R$ in a plane one.

The parameters A , $\partial A / \partial l$, and R_{eff} can be considered constant within a small volume and can be factored out from the integral. Since the integral of $d\sigma \Delta l$ over $\Delta\Sigma_-$ is equal to $\Delta\Omega$ we obtain

$$\operatorname{div} \mathbf{A} = \frac{\partial A}{\partial l} + \frac{A}{R_{\text{eff}}} \quad (1.8.15)$$

Thus, the divergence of a vector is dependent on local characteristics of a vector field and independent of the shape of the elementary volume in integral 1.8.13. Obviously, $\operatorname{div} \mathbf{A} = 0$ for $\mathbf{A} = \mathbf{A}_0 = \text{const}$. This means that an integral of the normal \mathbf{n} to the surface (over which the integral is taken) multiplied scalarly by any constant vector is equal to zero or, which is the same, the original integral of \mathbf{n} is equal to zero as well.

In conclusion we note that multiplying 1.8.13 by $\Delta\Omega$ and integrating over a large volume Ω we can easily prove that *the integral of the divergence of a vector over a volume is equal to the vector flux across a surface confining the volume*, since the contributions of all inner boundaries of volumes $\Delta\Omega$ are mutually compensated. This is the well-known *Gauss theorem*.

Gradient of a scalar function is a vector satisfying the relations

$$\operatorname{grad} \chi = \mathbf{l} \frac{\partial \chi}{\partial l}, \quad \mathbf{l}_1 \cdot \operatorname{grad} \chi = \frac{\partial \chi}{\partial l_1} \quad (1.8.16)$$

where \mathbf{l} is a normal to an isosurface $\chi = \text{const}$ in the direction of increasing χ , while \mathbf{l}_1 and l_1 are an arbitrary unit vector and its length; we note that the second formula 1.8.16 follows from the first one. In a Cartesian coordinate system we have

$$\operatorname{grad} \chi = \mathbf{i} \frac{\partial \chi}{\partial x} + \mathbf{j} \frac{\partial \chi}{\partial y} + \mathbf{k} \frac{\partial \chi}{\partial z} = \vec{\nabla} \chi \quad (1.8.17)$$

This vector can be obtained by replacing the vector \mathbf{A} in integral 1.8.13 by the scalar function χ . Really, letting $\mathbf{A} = \chi \mathbf{l}_1$ in 1.8.15, where \mathbf{l}_1 is an arbitrary constant vector, on the

basis of what was proved previously, we obtain again relations 1.8.16

$$\mathbf{l}_1 \operatorname{grad} \chi = \mathbf{l}_1 \frac{1}{\Delta \Omega} \int_{\Delta \Sigma} \chi \mathbf{n} d\Sigma = \frac{\partial \chi}{\partial l_1}, \quad \Delta \Sigma, \Delta \Omega \rightarrow 0 \quad (1.8.18)$$

These integrals enter also in the equations of Section 1.7; for $\chi = p$ they determine a force acting on a unit volume $\Delta \Omega$ in an inviscid gas.

1.8.4 Vector Divergence of a Vector Pair

We will attribute this name to a more sophisticated operator, which is formed by an integral of the product $(\mathbf{A} \cdot \mathbf{n}) \cdot \mathbf{B} = A_n \mathbf{B}$

$$\operatorname{div} (\mathbf{A} \cdot \mathbf{B}) = \frac{1}{\Delta \Omega} \int_{\Delta \Sigma} A_n \mathbf{B} d\Sigma = \frac{\partial(A \mathbf{B})}{\partial l} + \frac{A \mathbf{B}}{R_{\text{eff}}}, \quad \Delta \Omega, \Delta \Sigma \rightarrow 0 \quad (1.8.19)$$

The proof of the latter equality is obvious, since the replacement of the scalar A by the product $A \mathbf{B}$ in 1.8.14 and 1.8.15 does not change the procedure. By analogy with 1.8.12, the formula for this operator in Cartesian coordinates can be written as follows:

$$\operatorname{div} (\mathbf{A} \cdot \mathbf{B}) = \frac{\partial(A_x \mathbf{B})}{\partial x} + \frac{\partial(A_y \mathbf{B})}{\partial y} + \frac{\partial(A_z \mathbf{B})}{\partial z} \quad (1.8.20)$$

This operator will also be required in deriving the differential equations of motion.

1.9 Differential Equations of Gas Dynamics

The generality of the equations obtained in Section 1.7 is their important advantage; however, the most complete description of flow patterns and local flow properties can be obtained only on the basis of equations written in the differential form. Using these equations assumes the existence of continuous derivatives (of required orders) of flow parameters, which does not, however, exclude the possible use of these equations in analyzing solutions with isolated singular points (lines) in the vicinity of which derivatives may increase without bounds.

There are two main ways of deriving these equations. The first one is based on the application of the integral equations from Section 1.7 to a small volume $\Delta \Omega$ bounded by a surface $\Delta \Sigma$ consisting of fixed fragments of the coordinate surfaces. This method has its own advantages and will be applied at the end of the section. However, we will first apply the conservation laws (as in Section 1.2) to a moving fluid particle $\Delta \Omega^*$ of a fixed mass $\rho \Delta \Omega^*$.

1.9.1 Mass Conservation or Continuity Equation

The mass of an elementary fluid volume remains constant, that is, $d(\rho \Delta \Omega^*)/dt = 0$, which, together with 1.8.11, leads to the equation

$$\frac{d\rho}{dt} + \rho \operatorname{div} \mathbf{U} = 0 \quad (1.9.1)$$

The vector divergence operator was considered in the previous section. In addition, let us give one more argument of a purely physical nature in favor of the universal character of its definition: by virtue of this equation, the velocity divergence is expressed in terms of the total derivative of the gas density. These physical considerations can be referred to other operators to be used.

1.9.2 Momentum Equation: Viscous Stress Field

According to Newton's law the acceleration $d\mathbf{U}/dt$ of a particle of the mass $\rho \Delta \Omega^*$ is induced by a force due, in absence of body forces, to surface stresses \mathbf{p}_n acting on the outside of the surface $\Delta \Sigma$. Therefore, using 1.7.2 we arrive at the following equation

$$\rho \frac{d\mathbf{U}}{dt} = \text{Div } P = \frac{1}{\Delta \Omega} \int_{\Delta \Sigma} \mathbf{p}_n d\Delta \Sigma = -\text{grad } p + \text{Div } P_\tau, \quad \mathbf{p}_n = -\mathbf{n}p + \boldsymbol{\tau}_n$$

$$\Delta \Omega, \Delta \Sigma \rightarrow 0 \quad (1.9.2)$$

By analogy with 1.8.13, we will call the operator introduced the *divergence of the tensor P* of total internal stresses, the term being explained in what follows. In the second equality the hydrostatic part of the pressure is separated out and the definition, 1.8.18, for its gradient is used.

The divergence of the *viscous stress tensor* P_τ is obtained by replacing \mathbf{p}_n by $\boldsymbol{\tau}_n$. Clearly, the operator $\text{Div } P$ for inviscid flows is degenerated into a simple vector introduced in Section 1.8, namely, the pressure gradient, $\text{grad } p$, directed along the normal to isolines $p = \text{const}$.

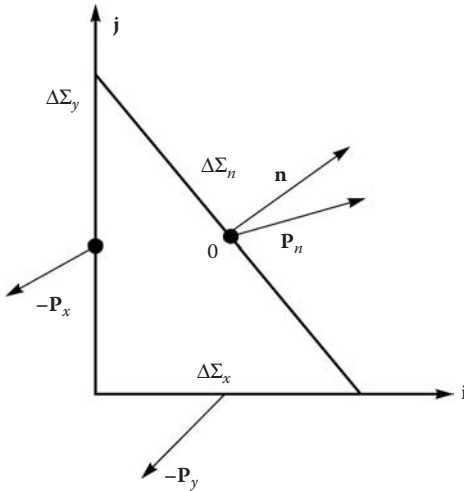
From this equation, together with physical considerations, it follows that the tensor divergence is a vector independent of both a coordinate system chosen and a coordinate volume shape. It should be only expressed in terms of the viscous stress field. The difficulties in this way are due to the fact that the vector \mathbf{p}_n is dependent not only on a coordinate system, but also on the area orientation, that is, a continual set of these vectors corresponds to each point of the space.

However, we will show that only three vectors of this set corresponding to noncoinciding normals can be independent. Consider a tetrahedron with faces $\Delta \Sigma_x$, $\Delta \Sigma_y$, and $\Delta \Sigma_z$ normal to the corresponding coordinate axes, and the base $\Delta \Sigma_n$ with the normal \mathbf{n} . Their traces are schematically shown in Figure 1.21. From positive directions of the coordinate axes the stresses \mathbf{p}_x , \mathbf{p}_y , and \mathbf{p}_z act on these areas (as in Section 1.2), changing signs on back sides of areas.

Let us apply 1.9.2 to the volume assuming that the gas acceleration is bounded, which is a normal situation in a flow. Let us represent the stresses inside the tetrahedron in the form of expansions $\mathbf{p}_x = \mathbf{p}_{x0} + \Delta \mathbf{p}_x$, and so on. Substituting them into the integral on the left-hand side we can see that the integral is formally of the order of $\mathbf{p}_0 \Delta \Sigma / \Delta \Omega \rightarrow \infty$ as $\Delta \Sigma \rightarrow 0$, where $\Delta \Sigma$ is the total area of the tetrahedron surface. Thence it follows that the stresses on the tetrahedron face must, in the main approximation, compensate each other, which leads to the following fundamental equation

$$\mathbf{p}_n = n_x \mathbf{p}_x + n_y \mathbf{p}_y + n_z \mathbf{p}_z, \quad n_x = \frac{\Delta \Sigma_x}{\Delta \Sigma_n}, \quad \dots \quad (1.9.3)$$

Here, n_x , n_y , and n_z are the direction cosines of the normal \mathbf{n} expressed in terms of tetrahedron face area ratios. The forces acting on a gas particle are determined by the subsequent terms of the expansion for which ratios $\Delta p_x \Delta \Sigma / \Delta \Omega$ are finite. Besides, we note that all the differential operators from Section 1.8 applied to constant quantities are equal to zero.

**FIGURE 1.21**

On the derivation of the formula for stresses on an arbitrary area.

Thus, the viscous stress field is specified by the system of three linearly independent basic vectors \mathbf{p}_x , \mathbf{p}_y , and \mathbf{p}_z (or by any other equivalent system). However, since each of the basic vectors is, in its turn, specified by its three projections onto the coordinate axes, the viscous stress field is specified by nine scalar quantities forming the *stress tensor* \mathbf{P} . In order not to digress from the main aim of this section, namely, the derivation of the equations of motion, properties of these tensors will be outlined in what follows.

Since the vectors \mathbf{p}_x , and so on, are (as distinct from \mathbf{p}_n) functions of coordinates only, we can perform the operations introduced in the previous section. For example, the product $n_x \mathbf{p}_x = \mathbf{p}_x(\mathbf{n})$; therefore, for $\mathbf{A} = \mathbf{i}$ the corresponding term of the integral 1.9.2 of \mathbf{p}_n is equal to $\partial \mathbf{p}_x / \partial x$. Thus, we have

$$\text{Div } \mathbf{P} = \frac{\partial \mathbf{p}_x}{\partial x} + \frac{\partial \mathbf{p}_y}{\partial y} + \frac{\partial \mathbf{p}_z}{\partial z} \quad (1.9.4)$$

Since this formula is important, let us derive it once more by analyzing directly the forces acting on the coordinate parallelepiped (Figure 1.19a). The force $\mathbf{p}_x(x + \Delta x)\Delta\Sigma_x$, where $\Delta\Sigma_x = \Delta y \Delta z$, acts on its right face, while the force $\mathbf{p}_x(x)\Delta\Sigma_x$ acts on the left face. This results in $(\partial \mathbf{p}_x / \partial x)\Delta\Omega$. Summing over all the directions yields expression 1.9.4. Putting here $\mathbf{p}_x = -p\mathbf{i}$, and so on, and changing sign we obtain formula 1.8.17 for the pressure gradient. Similarly, evaluating the integral of \mathbf{p}_n over an elementary coordinate volume we can obtain the expression for $\text{Div } \mathbf{P}$ in an arbitrary coordinate system.

1.9.3 Energy Equation

In deriving this equation one should, generalizing the results of Section 1.2, evaluate for three-dimensional flows the terms dA and dQ which enter in the first law of thermodynamics (Equation 1.2.5) in a coordinate system fitted to the particle itself, the relative velocity of its points being equal to ΔU . Evidently, the left-hand side of Equation 1.2.7 does not change. One should evaluate only the effective rate of the heat influx, q_{eff} . To do this, we will use the integrals on the right-hand side of Equation 1.7.3.

In evaluating the term q_τ (entering in q_{eff}), which characterizes the heat flux per unit mass of a gas associated with mechanical energy dissipation, we take into account the fact that, due to a small relative velocity $\Delta \mathbf{U}$, it is possible to neglect the variation of $\vec{\tau}_n$ over the fluid volume $\Delta\Omega^*$ in the integral of the viscous force work $\vec{\tau}_n \Delta \mathbf{U}$ (see Section 1.2). In a Cartesian coordinate system the left and right fluid faces $\Delta\Sigma_x^* = \Delta y \Delta z$ of the elementary volume $\Delta\Omega^*$ (Figure 1.19a) move from its center in the opposite directions at velocities $\pm(1/2)(\partial \mathbf{U}/\partial x)\Delta x$ against viscous forces $\pm \vec{\tau}_x \Delta \Sigma_x^*$, equal in magnitude (see Section 1.2). In a time dt these forces produce the work $dA_x = [\vec{\tau}_x(\partial U/\partial x)]\Delta\Omega^* dt$ on the gas confined in the volume $\Delta\Omega^*$. Therefore, summing over all the directions, by analogy with 1.8.20 we obtain the formula for the heat influx per unit volume

$$\rho q_\tau = \frac{1}{\Delta\Omega^*} \int_{\Delta\Sigma^*} (\vec{\tau}_n)^0 \cdot \mathbf{U} d\Sigma = \vec{\tau}_x \cdot \frac{\partial \mathbf{U}}{\partial x} + \vec{\tau}_y \cdot \frac{\partial \mathbf{U}}{\partial y} + \vec{\tau}_z \cdot \frac{\partial \mathbf{U}}{\partial z} \quad (\Delta\Omega^*, \Delta\Sigma^* \rightarrow 0) \quad (1.9.5)$$

Here, $(\vec{\tau}_n)^0$ is a stress at any point inside the volume $\Delta\Omega^*$.

Finally, according to 1.7.3 and 1.8.13, the rate q_j of the energy flux due to convective and diffusive transfer is equal to the divergence of the vector $-\mathbf{J}$. Thus, in view of 1.2.7, the energy equation, or the first law of thermodynamics, takes the form:

$$\begin{aligned} \frac{de}{dt} + p \frac{d\rho^{-1}}{dt} &= \frac{dh}{dt} - \frac{1}{\rho} \frac{dp}{dt} = q_{\text{eff}} \\ q_{\text{eff}} &= q + q_\tau + \text{Div } \mathbf{J} \end{aligned} \quad (1.9.6)$$

The system of equations obtained is a system for original, or *simple variables*, that is, for U, p, ρ , and so on. We will now derive the equations of motion in another, *conservative form*, or in *conservative variables*; the meaning of this term will be explained later. These equations are derived by direct application of the integral conservation laws (Section 1.7) to a fixed elementary volume $\Delta\Omega$ (Figure 1.19a and b).

For a small volume the integrands in the volume integrals of Equations 1.7.4 can be considered constant, so that the first term of the integral is equal to $\partial \chi / \partial t \Delta\Omega$. As for the surface integrals, we will express these in terms of the divergences of the corresponding vectors or other operators.

In the integral law of mass conservation, 1.7.1, one should put $\chi = \rho$, which leads to the continuity equation

$$\frac{\partial \rho}{\partial t} + \text{div}(\rho \mathbf{U}) = 0 \quad (1.9.7)$$

For the momentum equation, 1.7.2, the quantity transferred through the volume $\Delta\Omega$ is the unit volume momentum $\chi = \rho \mathbf{U}$. The integral of $\rho \mathbf{U} U_n$ over a small surface $\Delta\Sigma$ is, in accordance with 1.8.19, equal to the vector-divergence of the pair of the vectors $\mathbf{A} = \rho \mathbf{U}$ and $\mathbf{B} = \mathbf{U}$, and since the same force 1.9.2 acts on the volume, the required equation has the form:

$$\frac{\partial \rho \mathbf{U}}{\partial t} + \text{div}(\rho \mathbf{U} \cdot \mathbf{U}) = \text{Div } P \quad (1.9.8)$$

The same equation in a Cartesian coordinate system can be obtained using formula 1.8.20 and 1.9.4.

Finally, in evaluating the integral of the external force work, $\mathbf{p}_n \cdot \mathbf{U}$, in the energy equation written in the conservative form we obtain the *divergence of a vector-tensor product*, which, written in terms of viscous stresses $\vec{\tau}_n$, has the form:

$$\operatorname{div}(P_\tau \cdot \mathbf{U}) = \frac{1}{\Delta\Omega} \int_{\Delta\Sigma} \vec{\tau}_n \cdot \mathbf{U} d\Sigma = \frac{\partial(\vec{\tau}_x \cdot \mathbf{U})}{\partial x} + \frac{\partial(\vec{\tau}_y \cdot \mathbf{U})}{\partial y} + \frac{\partial(\vec{\tau}_z \cdot \mathbf{U})}{\partial z} \\ \Delta\Sigma, \quad \Delta\Omega \rightarrow 0 \quad (1.9.9)$$

This integral differs from 1.9.5 only by the fact that the vectors $\vec{\tau}_x$ and others are under a derivative sign, since, in contrast to $\Delta\mathbf{U}$, the velocity \mathbf{U} is not small. Otherwise, the reasoning is similar, as is, in particular, the form of the expression in a Cartesian coordinate system. The contribution of the hydrostatic pressure work, $-p\mathbf{n} \cdot \mathbf{U} = -pU_n$, as well as the energy transfer $\rho E U_n$, leads, evidently, to divergence of the vector \mathbf{U} multiplied by scalars. Thus, the required equation can be written in the form:

$$\frac{\partial\rho E}{\partial t} + \operatorname{div}[(\rho E + p)\mathbf{U}] = \rho q - \operatorname{div}\mathbf{J} + \operatorname{div}(P_\tau \mathbf{U}) \\ E = e + \frac{1}{2}U^2 \quad (1.9.10)$$

The form of the equations obtained, which do not contain variable coefficients of derivatives, is termed *conservative* or *divergent*, since formal integration over any volume does lead to the situation in which the conservation laws are satisfied for the volume. For example, Equation 1.9.7 for the steady-state one-dimensional channel flow considered in Section 1.7, takes the form $\partial\rho u/\partial x = 0$. Integrating this equation over the interval (x_1, x_2) we obtain the first integral Equation 1.7.12, irrespective of the internal structure of the region. The same situation occurs for other equations; because of this, such form of the equations is convenient, for example, in developing the so-called conservative algorithms to solve numerically gas dynamic problems and, primarily, to calculate solutions (discontinuous in a rigorous formulation) using the discontinuity-capturing approach. Moreover, this method frequently appears to be the only possible tool in obtaining equations in arbitrary coordinate systems.

However, since the equations involve derivatives of complexes of required functions, or *conservative variables*, they are not so convenient in analyzing their fundamental mathematical properties and obtaining analytical and semianalytical solutions; therefore, in what follows we will use the equations for original, or simple, gas dynamic variables.

Thus, the gas dynamic equations have been derived in both their basic forms. The two forms are naturally equivalent and can be reduced one to the other by means of simple transformations, similar to those used in Section 1.7 for coordinate transformations.

All the equations obtained previously have a compact universal vector form, independent of a coordinate system.

The universal nature of all the equations obtained here and in Section 1.7 manifests itself in that only hypotheses on the medium continuity and dissipation were used to derive them. At the same time, we have not specified the rheological model of a medium, that is, relations between pressure and other parameter distributions. Such equations are termed *equations in stresses*. The previously mentioned relations will be obtained in a later stage; they lead (as in Section 1.2) to the *Navier–Stokes equations*, though for three-dimensional flows. However, for inviscid flows these equations, together with equations of state from Section 1.3, are closed. They are termed *Euler equations* though Euler himself never wrote the energy equation.

The equations obtained form a group of *basic gas dynamic equations*. They are independent of the nature of physicochemical conversions in a gas, the entire energy of these conversions being included in the internal energy e . This group of equations is related with a group of physicochemical equations (e.g., Equation 1.2.8) only by equations of state and the transfer vector \mathbf{J} .

In conclusion, we will write down the explicit scalar form of the equations of motion for an inviscid compressible gas in a Cartesian coordinate system (x, y, z) with velocity projections (u, v, w) . To do this, we will project the vector equations (Equation 1.9.2) onto these axes and let $\text{Div } P_\tau = 0$; we also put $q_{\text{eff}} = q$ in Equation 1.9.6. Then, in view of 1.8.17, the required equations take the form:

$$\begin{aligned}\frac{du}{dt} &= \frac{\partial u}{\partial t} + u \frac{\partial u}{\partial x} + v \frac{\partial u}{\partial y} + w \frac{\partial u}{\partial z} = -\frac{1}{\rho} \frac{\partial p}{\partial x} \\ \frac{dv}{dt} &= -\frac{1}{\rho} \frac{\partial p}{\partial y}, \quad \frac{dw}{dt} = -\frac{1}{\rho} \frac{\partial p}{\partial z} \\ \frac{dh}{dt} &= \frac{\partial h}{\partial t} + u \frac{\partial h}{\partial x} + v \frac{\partial h}{\partial y} + w \frac{\partial h}{\partial z} = \frac{1}{\rho} \frac{dp}{dt} + q\end{aligned}\tag{1.9.11}$$

1.10 Rheological Model of Newtonian Fluids and Gases

It was shown in Section 1.9 that a viscous stress field is completely determined by three basic vectors, namely, the stresses associated with three linearly independent normals. According to 1.9.3, for a Cartesian coordinate system the basic vectors are \mathbf{p}_x , \mathbf{p}_y , and \mathbf{p}_z .

Since each of these vectors is specified by its three projections onto the coordinate axes, the stress field is determined by nine scalar quantities as the *stress tensor matrix*

$$P = \begin{pmatrix} p_{xx} & p_{yx} & p_{zx} \\ p_{xy} & p_{yy} & p_{zy} \\ p_{xz} & p_{yz} & p_{zz} \end{pmatrix}\tag{1.10.1}$$

Each column of the matrix consists of the projections of the appropriate vectors (the first subscript) onto the coordinate axis (the second subscript).

If a normal is represented in the form of a column of direction cosines, then the stress on any area element can be expressed as a scalar product

$$\mathbf{p}_n = P\mathbf{n} = P \begin{pmatrix} n_x \\ n_y \\ n_z \end{pmatrix} = \begin{pmatrix} p_{nx} \\ p_{ny} \\ p_{nz} \end{pmatrix} = \begin{pmatrix} p_{xx}n_x + p_{yx}n_y + p_{zx}n_z \\ p_{xy}n_x + p_{yy}n_y + p_{zy}n_z \\ p_{xz}n_x + p_{yz}n_y + p_{zz}n_z \end{pmatrix}\tag{1.10.2}$$

Clearly, the rows of the matrix are the projections of the vector \mathbf{p}_n onto the coordinate axes.

We note that the form of this matrix is, quite naturally, dependent on a coordinate system, which, in the general case, is not necessarily the Cartesian one. However, the quantity \mathbf{p}_n is coordinate-invariant. This suggests that all these matrices describe the same stressed state of a medium, or its tensor. Hence, this tensor is a physical characteristic (or a parameter) of the medium, such as its density, velocity, and so on. The divergence of the viscous stress tensor 1.9.2 or those of the vector-tensor products 1.9.5 and 1.9.9 are also invariant relative to coordinate systems, as the stress \mathbf{p}_n .

Replacing components p_{xy} by τ_{xy} , and so on, we obtain the viscous stress tensor P_τ . Formally, the relation looks as follows

$$\mathbf{p}_n = -\mathbf{n}p + \vec{\tau}_n \quad \rightarrow \quad P = -pE + P_\tau \quad (1.10.3)$$

Here, E is the unit matrix of the same order.

The complete form of matrices 1.10.1 is rather cumbersome and often its shorthand form is used. To obtain it, we should replace coordinates (x, y, z) by, for example, x_i , $i = 1, 2, 3$ with the appropriate basic vectors \mathbf{l}_i . Then \mathbf{p}_i are basic stress-vectors, while p_{ik} are their projections onto the unit vectors \mathbf{l}_k , $(i, k = 1, 2, 3)$; this makes it possible to use the following form for writing the tensor matrix

$$P = \|p_{ik}\| \quad (1.10.4)$$

The stress tensor, or, more exactly, its matrix, is symmetric about the principal diagonal; hence, the equality $p_{ik} = p_{ki}$ holds, which is equivalent to the three following equalities

$$p_{xy} = p_{yx}, \quad p_{xz} = p_{zx}, \quad p_{yz} = p_{zy} \quad (1.10.5)$$

To prove this statement, we will consider a small volume V between the planes of the triangles spaced apart along the z axis, as shown in Figure 1.21. The stress distributions over small areas $\Delta\Sigma_x$, and so on, may be considered uniform; therefore, the centers of application of the forces $\mathbf{p}_x \Delta\Sigma_x$, and so on, coincide with the centers of gravity of these areas, or with the midpoints of the corresponding segments. Let us write down the moment of the forces about an axis passing normal to the plane of the figure through the center O of an area $\Delta\Sigma_n$. In this case, the moment of the force \mathbf{p}_n is equal to zero, together with the moments of the stress components p_{xx} and p_{yy} since they pass through the point O and the forces \mathbf{p}_z acting from both sides are offset. Neglecting, as before, the moments of the inertia forces of volume V we obtain the condition of its equilibrium in the form $p_{xy}\Delta\Sigma_x\Delta y = p_{yx}\Delta\Sigma_y\Delta x$, where Δx and Δy are the distances from the point O to the areas. From geometrical considerations it follows that $\Delta\Sigma_x/\Delta\Sigma_y = \Delta x/\Delta y$, which proves one of the conditions, 1.10.5. The other conditions are obtained by applying the same approach to other coordinate planes. Clearly, a symmetric tensor involves six independent components instead of nine in the general case. In the general case, the more general equality holds (proved, e.g., in the book of Loitsyanskii, 1966)

$$\mathbf{i} \times \mathbf{p}_x + \mathbf{j} \times \mathbf{p}_y + \mathbf{k} \times \mathbf{p}_z = 0 \quad (1.10.6)$$

Projecting this equation onto the basic vectors we can obtain Equation 1.10.5.

In the light of what was outlined previously, the strain rate field 1.8.10 is a tensor of the same type, the vector field of the relative strain rates being an invariant, which assigns a physical meaning to the matrix of the *strain rate tensor* E_ε with elements ε_{ik} . As in Equation 1.8.10, we have

$$\mathbf{U}'_\varepsilon = E_\varepsilon \mathbf{r}', \quad E_\varepsilon = \|\varepsilon_{ik}\| \quad (1.10.7)$$

It is a matter of direct verification (similar to that in 1.10.2) that this product gives the column of the strain rate field, $u'_\varepsilon, v'_\varepsilon, w'_\varepsilon$ (1.8.9).

As shown in Section 1.8, the matrix E_ε possesses an important property, namely, the sum of its diagonal elements is the velocity divergence and, hence, is invariant about a coordinate transformation. We will show that the stress tensor has the same property, which, generally speaking, follows from the general theory of diagonally-symmetric tensors. To do this, we introduce the *mean normal stress* at a given point

$$p = -\frac{1}{4\pi} \int_{4\pi} p_{nn} d\gamma \quad (1.10.8)$$

Here, γ is a solid angle filled with rotating normals. Since $p_{nn} = \mathbf{p}_n \cdot \mathbf{n}$, using 1.10.2 we can reduce integral 1.10.8 to a sum of integrals of $n_i n_k$ with coefficients p_{ik} independent of \mathbf{n} and γ . It can be easily shown that the integrals of products $n_i n_k$ with $i \neq k$ over γ vanish, while the integrals of n_i^2 are equal to $4\pi/3$. Then we have

$$p = -\frac{1}{3}(p_{xx} + p_{yy} + p_{zz}) \quad (1.10.9)$$

According to Section 1.4, the quantity p for gases is the static pressure entering in the equation of state. In other cases, the mean value 1.10.8 or 1.10.9 is referred to as pressure.

Since in deriving the last formula the orientation of a Cartesian coordinate system is rather accidental, the sum on the right-hand side is invariant about coordinate system rotations. For systems of general form formula 1.10.8 gives a possibility to express p in terms of other components of the stress tensor.

We are coming now to the main purpose of this section, namely, the formulation of the *rheological model* of Newtonian fluids (i.e., the relations between stress and velocity fields). At the beginning we will give some preliminary considerations.

Viscous stresses arise only in a nonuniform velocity field and, hence, must depend on velocity derivatives. Since there are no viscous stresses in an inviscid flow (or they are extremely small), it is quite natural to assume (when taking into account viscous effects) that in the first approximation stresses depend linearly on the velocity derivatives with respect to space.

However, not any flow nonuniformity induces viscous stresses; thus, they are absent in "quasisolids" locally rotating fluids, since in this case there is no mutual displacement of neighboring particles. In other words, according to 1.8.5 through 1.8.10, viscous stresses are absent if the strain rates are zero, $\varepsilon_{ik} = 0$, so that the next step is to assume that viscous stresses are linear functions of strain rates.

These considerations lead to the *generalized friction law* (that of Newton or Navier and Stokes): *the stress tensor P in an isotropic Newtonian fluid is a linear function of the strain rate tensor E_ε*

$$\begin{aligned} P &= -p_* E + 2\mu E_\varepsilon \\ p_{ii} &= -p_* + 2\mu\varepsilon_{ii} = -p + \tau_{ii}, \quad p_* = p + \frac{2}{3}\mu \operatorname{div} \mathbf{U} \\ p_{ik} &= \tau_{ik} = 2\mu\varepsilon_{ik}, \quad i \neq k \end{aligned} \quad (1.10.10)$$

The components ε_{ik} are determined by formulas 1.8.10. An isotropic component of the stress tensor p_* and the *bulk viscosity* $2\mu/3$ are so chosen as to satisfy condition 1.10.9. Quite naturally, it coincides with that obtained earlier (cf. Equation 1.4.10). This, in particular, determines the quantity $\mu' = \frac{4}{3}\mu$ in 1.2.4 for viscous one-dimensional flows, while in incompressible fluids $\operatorname{div} \mathbf{U} = 0$ and $\mu' = 2\mu$.

By virtue of isotropy of fluid properties and the hypothesis of the linearity of the relations between strain rates and stresses, the viscosity coefficient is independent of both coordinates and gas velocities. The dependence of μ on other thermodynamic parameters was discussed in Section 1.3.

We note that precisely fluid media with a linear relation between the strain rate and stress tensors are referred to as Newtonian. Among these are all gases and most liquids with a simple molecular composition. However, multimolecular fluids frequently possess more

complicated, "non-Newtonian" rheological properties and cannot be described within the framework of the theory outlined.

The generalized friction law postulated previously is, generally speaking, a rigorous result of kinetic theory; in particular, it was derived in Section 1.4 within the framework of a very simple, model version of this theory.

However, in the general case this law (obtained long before the appearance of kinetic theory) is an empirical law of nature, though in its general form it could hardly be obtained directly from experiments.

Heuristically, this law could be obtained by generalizing the original Newton's law of friction 1.2.4 which, in its turn, can be verified by simple experiments. These generalizations are based on speculative but plausible considerations, partially given previously and some additional ones using isotropy of the medium, symmetry of tensors and their transformations, and so on (instructive considerations of such a kind are given in the book by Kochin, Kibel, and Roze, 1963, which is recommended to the readers to develop an independent sight on the subject). These considerations are not discussed here, but evidently no data exist presently to doubt the reliability of the law within the range of its applicability (cf. Section 1.1).

We note that occasionally it is assumed that $p_* = p + (2\mu/3 - \mu^{(2)})\operatorname{div} \vec{U}$ in Equation 1.10.10; thus, the *second, or bulk, viscosity* is introduced. However, previously we took $\mu^{(2)}$ to be zero by virtue of condition 1.10.9, which not only introduces a certain parameter p called the pressure, but also, in view of the equation of state 1.4.6, relates this pressure with the temperature representing the mean kinetic energy of translational molecular motion. Since the second viscosity is sometimes related with near-equilibrium gas flows, we reserve the detailed discussion of this question for Section 11.7.

Substituting 1.10.10 into the differential Equations 1.9.2 to 1.9.4 we arrive at the Navier–Stokes equations which, in view of Equation 1.8.9, in a Cartesian coordinate system take the form:

$$\begin{aligned} \rho \frac{du}{dt} &= -\frac{\partial p}{\partial x} - \frac{2}{3} \frac{\partial}{\partial x} (\mu \operatorname{div} \mathbf{U}) + 2 \frac{\partial}{\partial x} \left(\mu \frac{\partial u}{\partial x} \right) + \\ &\quad \frac{\partial}{\partial y} \left[\mu \left(\frac{\partial u}{\partial y} + \frac{\partial v}{\partial x} \right) \right] + \frac{\partial}{\partial z} \left[\mu \left(\frac{\partial u}{\partial z} + \frac{\partial w}{\partial x} \right) \right] \\ \rho \frac{dv}{dt} &= -\frac{\partial p}{\partial y} - \frac{2}{3} \frac{\partial}{\partial y} (\mu \operatorname{div} \mathbf{U}) + \frac{\partial}{\partial x} \left[\mu \left(\frac{\partial u}{\partial y} + \frac{\partial v}{\partial x} \right) \right] + \\ &\quad 2 \frac{\partial}{\partial y} \left(\mu \frac{\partial v}{\partial y} \right) + \frac{\partial}{\partial z} \left[\mu \left(\frac{\partial v}{\partial z} + \frac{\partial w}{\partial y} \right) \right] \\ \rho \frac{dw}{dt} &= -\frac{\partial p}{\partial z} - \frac{2}{3} \frac{\partial}{\partial z} (\mu \operatorname{div} \mathbf{U}) + \frac{\partial}{\partial x} \left[\mu \left(\frac{\partial u}{\partial z} + \frac{\partial w}{\partial x} \right) \right] + \\ &\quad \frac{\partial}{\partial y} \left[\mu \left(\frac{\partial v}{\partial z} + \frac{\partial w}{\partial y} \right) \right] + 2 \frac{\partial}{\partial z} \left(\mu \frac{\partial w}{\partial z} \right) \end{aligned} \tag{1.10.11}$$

Obviously, these equations are too cumbersome; for this reason, in order to present their mathematical properties in a more illustrative form, we will also write down the Navier–Stokes equations for an incompressible fluid with constant viscosity μ ; in view of

the condition $\operatorname{div} \mathbf{U} = 0$, they are brought to the form:

$$\rho \frac{du}{dt} = -\frac{\partial p}{\partial x} = \mu \Delta u, \quad \rho \frac{dv}{dt} = -\frac{\partial p}{\partial y} = \mu \Delta v, \quad \rho \frac{dw}{dt} = -\frac{\partial p}{\partial z} = \mu \Delta w \quad (1.10.12)$$

Here, the symbol Δ signifies the *Laplace operator*, which plays an important role in gas dynamics

$$\Delta = \vec{\nabla} \cdot \vec{\nabla} = \frac{\partial^2}{\partial x^2} + \frac{\partial^2}{\partial y^2} + \frac{\partial^2}{\partial z^2} \quad (1.10.13)$$

Finally, to close the energy equations of the previous section, 1.9.6 or 1.9.10, we must define the heat transfer vector \mathbf{J} . As indicated in Section 1.2, this vector consists of two terms: thermal \mathbf{J}_T and diffusive \mathbf{J}_D . The latter, together with the vectors $\mathbf{I}^{(c)}$ of the diffusive transfer of the gas mixture species, has, in the general case, a fairly complicated structure and will be discussed in Chapter 12. As for the first term, in an isotropic medium it is as follows

$$\mathbf{J} = -\lambda \operatorname{grad} T \quad (1.10.14)$$

where λ is thermal conductivity (Section 1.3). In fact, let us draw isosurfaces $T = \text{const}$ with normals \mathbf{n} . The heat is transferred only along the normals \mathbf{n} and, in accordance with the Fourier law (Section 1.2), $J = -\lambda \partial T / \partial n$ which, in view of 1.8.16, leads to 1.10.14.

In view of formulas 1.10.10 and 1.9.5 or 1.9.9 the energy equations could be easily written down in a Cartesian coordinate system: however, we will not present them owing to their cumbersome form. We note that in what follows the Navier–Stokes equations will mainly be used in limiting, truncated forms, which will be given in the course of the presentation.

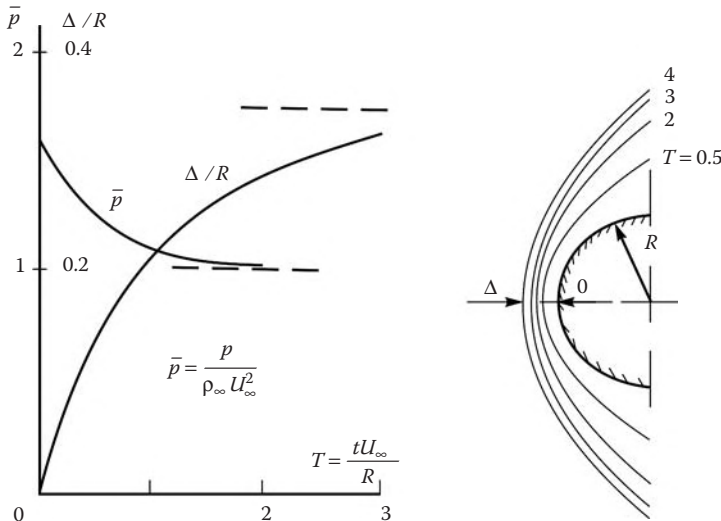
1.11 Initial and Boundary Conditions

To solve the previous equations of gas motion one should formulate some additional (initial and boundary) conditions. Their set should be sufficient for determining arbitrary functions in the general solution of the system of differential equations. The number and nature of these conditions depend mainly on the type and the number of equations and are determined for each class or type of problems separately. First of all, the spatial distributions of all unknown functions f should be specified at a time $t = t_0$

$$f(t_0, x, y, z) = f_0(x, y, z) \quad (1.11.1)$$

These are the *initial conditions* of the problem. Strictly speaking, all fluid flows are unsteady since they arise from rest. However, there exists also a wide and important class of steady-state flows. Their applicability to real processes is based on a rapid (as experiments show) decay of initial disturbances. Thus, if a body of size L acquires a constant velocity \mathbf{U}_∞ (in a coordinate system fitted to the body), then the flow in the vicinity of the body becomes steady-state in a time $t_1 \sim L/U_\infty$ (see an example in Figure 1.22). In this case reversing the motion leads to the problem of a steady-state flow past a fixed body at the freestream velocity \mathbf{U}_∞ . The same situation occurs in wind tunnels, where start-up effects also decay rapidly, so that the flow past a model in the tunnel can be considered steady.

An aircraft can move at a variable velocity (quite frequently this is the case) or a tunnel can be operated in an unsteady regime, but if a scale time t_2 of this unsteadiness is appreciably larger than the time t_1 for which the flow attains the steady state, then the flow can

**FIGURE 1.22**

Attainment of the steady-state pressure at the stagnation point O and the shape of the detached shock ahead of a sphere set in motion abruptly at a velocity $U_\infty = 2a_\infty$.

be considered *quasisteady* so that the stationary flow laws can be applied. This situation is typical in practice, but determination of t_1 and necessary ratios t_2/t_1 is possible only when analyzing particular problems.

1.11.1 Boundary Conditions

If a body moves in a uniform quiescent atmosphere, the upstream disturbances usually decay; therefore, reversing the motion we can formulate a natural boundary condition

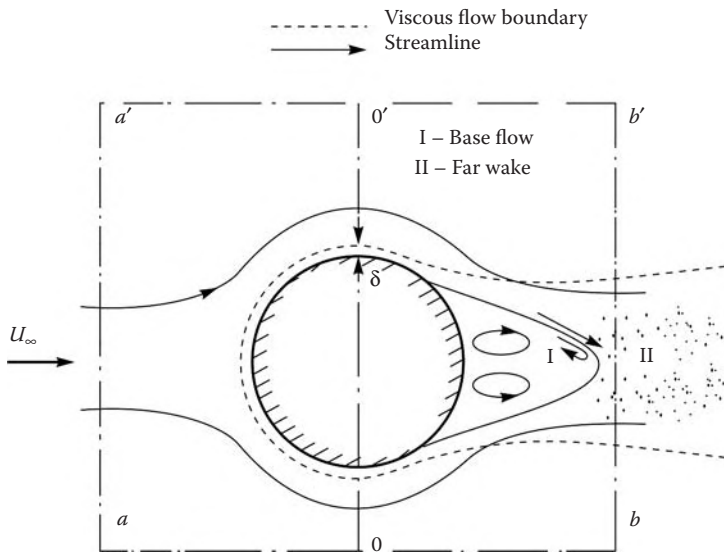
$$x \rightarrow -\infty \quad f \rightarrow f_\infty(y, z) \quad (1.11.2)$$

with the x -axis directed along the freestream velocity.

Actually, this condition has a meaning only if it is satisfied at a finite distance from the body. As follows from Section 1.6 (Figure 1.14), Figures 1.22 and 1.23 situations for supersonic and subsonic flows are different. In the first case, a domain of the disturbance propagation is bounded by a Mach cone or shock waves, while it is unbounded for subsonic flows. However, experience shows that disturbances induced by bodies immersed in a subsonic flow do not usually propagate upstream farther than a few (or even one) body diameters.

As for conditions far behind the body, it may seem that these are not necessary from the physical standpoint. Moreover, experiments show that the extent of a disturbed zone behind the body can be very large. This can be either a wake due to viscosity effects or a Mach cone behind a supersonic aircraft (Figures 1.14 and 1.23). Nevertheless, to make a solution of a certain idealized problem mathematically definite, one should frequently pose a condition of the total or partial decay of disturbances downstream of the body (e.g., in subsonic flows).

The situation with conditions on a body surface is simpler. Usually the body is considered solid and impermeable, so that the normal velocity of the displacement of its surface and a gas velocity must coincide.

**FIGURE 1.23**

Schematics of subsonic viscous flow past a body at high Reynolds numbers ($aa'b'b$ is a control surface on which boundary conditions are imposed).

Let a body surface be specified by the equation

$$F(t, x, y, z) = 0 \quad (1.11.3)$$

The components of its normal \mathbf{n} are as follows

$$\begin{aligned} n_x &= F_x \Delta^{-1}, & n_y &= F_y \Delta^{-1}, & n_z &= F_z \Delta^{-1} \\ \Delta^2 &= F_x^2 + F_y^2 + F_z^2 \end{aligned} \quad (1.11.4)$$

Differentiating Equation 1.11.3 with respect to time yields an equation to which the trajectories $x_*(t), y_*(t), z_*(t)$ of any point of the surface must satisfy. The equation can be written in the form that determines the normal velocity of the surface

$$D = n_x \dot{x}_* + n_y \dot{y}_* + n_z \dot{z}_* = -F_t \Delta^{-1}, \quad x_* = \frac{dx_*}{dt}, \quad \dots \quad (1.11.5)$$

At the same time, the gas velocity normal to the surface is

$$v_n = n_x u + n_y v + n_z w = \mathbf{n} \cdot \mathbf{U} \quad (1.11.6)$$

Thus, the impermeability condition on the surface takes the general form:

$$v_n = \mathbf{n} \cdot \mathbf{U} = D = -F_t \Delta^{-1} \quad (1.11.7)$$

We will now consider the tangent component of the gas velocity $v_l = \mathbf{U} \cdot \mathbf{l}$ on the body; here, $\mathbf{l}(l_x, l_y, l_z)$ is an arbitrary vector tangent to the surface. Since all fluids and gases are viscous, their interaction with the surface must have an effect on this velocity. Experiments,

together with kinetic theory, suggest the no-slip condition at the body surface for sufficiently dense gases

$$v_l = \mathbf{U}\mathbf{l} = l_x \dot{x}_* + l_y \dot{y}_* l_z \dot{z}_* \quad (1.11.8)$$

On a fixed body $v_l = 0$. An exception is provided by rarefied cases (at flight altitudes $H = 80 - 100$ km), for which the slip condition is imposed on the body surface (see Section 12.1).

However, in dense high-velocity flows, or, to be more specific, at high Reynolds numbers, $Re > 10^4$, the influence of viscosity is concentrated in a narrow (of the order of $LRe^{-1/2}$, see Section 1.16) wall region (except for the cases in which there are extended separation zones or wakes downstream of a body, as in Figure 1.23). Outside these boundary layers, the gas (or fluid) can be considered inviscid or frictionless: in these flows the quantity v_l could not be preassigned.

1.11.2 Existence and Uniqueness of Solutions of Gas Dynamic Problems

It is assumed that there exist solutions of reasonably posed physical problems for mathematically closed systems of equations and that they are unique. In the general case, the first statement cannot be mathematically proved; however, theoretical and experimental experience of gas dynamics shows its validity (probably, except for some cases concerned with physical singularities of the problems).

The second statement is more complicated, since it is concerned with possible nonuniqueness of the flow pattern for seemingly the same external conditions. In this case, some additional conditions, often being beyond the framework of the formulation of the problem, are needed for separating out the required solution (if possible at all).

The detailed formulation of typical gas dynamic problems appears to be possible only on the basis of a careful analysis of their physical and mathematical properties, which will be done in what follows.

1.12 Similarity and Modeling in Gas Dynamics

The similarity theory is one of the most effective methods to study physics and mechanics, effective in terms of intellectual efforts per some conventional unit of results. On the basis of physical intuition and simple logical considerations this theory often makes it possible to derive similarity laws, to predict specific, sometimes by no means evident, structure of solutions of certain problems, and to establish laws of evolution for processes described by these problems. The meaning and importance of the similarity laws for physics are that they make it possible to reduce a large variety of solutions to more narrow *groups of similarity* and thereby to facilitate their classification and determination of the control parameters. Moreover, they give a possibility to simulate one flow by another involved in a class of similar solutions.

There are two basic approaches to derive similarity laws:

1. Straightforward reduction of the equations and the initial and boundary conditions of a problem to a dimensionless form by referring all the involved quantities to typical scales of the problem.
2. Use of the similarity theory based only on the dimensional analysis of both governing and unknown parameters of the problem.

Since the subject under consideration is fairly important, we will outline both approaches.

1.12.1 First Approach: Inviscid Perfect Gas

Let a body shape with a typical scale length L be given together with the freestream parameters (with subscript “ ∞ ”)

$$f(x, y, z, t) = 0, \quad L, \quad \rho_\infty, \quad p_\infty, \quad h_\infty, \quad \mathbf{U}_\infty(u_\infty, v_\infty, w_\infty) \quad (1.12.1)$$

Here u , v , and w are the velocity components in a fixed Cartesian coordinate system (x, y, z) . An incident flow is assumed to be uniform and steady, but the flow as the whole can be unsteady due to a change in the body shape or its maneuver (oscillations, etc.).

Let us introduce dimensionless quantities

$$p' = \frac{p}{\rho_\infty U_\infty^2}, \quad \rho' = \frac{\rho}{\rho_\infty}, \quad h' = \frac{h}{U_\infty^2}, \quad \mathbf{U}' = \frac{\mathbf{U}}{U_\infty} \quad (1.12.2)$$

and

$$x' = \frac{x}{L}, \quad y' = \frac{y}{L}, \quad z = \frac{z}{L}, \quad t' = \frac{t U_\infty}{L} \quad (1.12.3)$$

Here, all the dimensional quantities are divided by typical scales of the gas dynamic problem. Obviously, the choice of the mode way of nondimensionalizing is rather arbitrary (e.g., one can choose p/p_∞ as the pressure scale) but the mode chosen here appears to be the most convenient one, especially in analyzing supersonic flow problems.

The aim is to bring the system of governing equations and initial and boundary conditions to a dimensionless form and to determine the dimensionless parameters or functions on which the solution of a problem depends. If these parameters, or, as they are termed, *similarity criteria*, coincide for different flows, then, due to the assumed uniqueness of the solution, the dependences of the dimensionless functions 1.12.2 on the dimensionless parameters 1.12.3 are also the same. Such flows are termed *similar*, while the fact of their existence is termed the *similarity law*. At the same time, dimensional quantities in similar flows (e.g., the pressure $p = p' \rho_\infty U_\infty^2$) are (or may be) quite different.

In new, dimensionless variables the equations of continuity, momentum and energy for inviscid gas 1.9.11 do not change their form and do not acquire any governing parameters. The equation of state for perfect gases $\gamma p' = (\gamma - 1)\rho' h'$ also does not change, which represents an advantage of the chosen system of dimensionless parameters.

Thus, a problem formulated in a dimensionless form depends on dimensionless conditions only

$$\begin{aligned} p'_\infty &= \frac{1}{\gamma M_\infty^2}, & h'_\infty &= \frac{1}{(\gamma - 1)M_\infty^2}, & \rho'_\infty &= 1 \\ \mathbf{l}_\infty &= \frac{\mathbf{U}_\infty}{U_\infty}, & \left(u'_\infty = \frac{u_\infty}{U_\infty}, \dots \right), & f(x', y', z', t') &= 0 \end{aligned} \quad (1.12.4)$$

Here, γ and M_∞ are the adiabatic exponent and the freestream Mach number, respectively, while \mathbf{l}_∞ is the unit vector in the velocity direction. The instant slopes of the vectors \mathbf{n} and \mathbf{l} at the same points of the body and, hence, boundary conditions 1.11.7 or 1.11.8 do not change. The coincidence of these conditions for different flows results in the flow similarity. Thence it follows, in particular, that the problem of inviscid flow past geometrically similar bodies oriented in the same fashion in the flow involves only two *similarity criteria*, γ and M_∞ .

This is the classical and the most known similarity law for inviscid perfect gas flows past bodies. Other similarity laws will be considered later after studying the similarity theory.

We also note that in a number of the so-called degenerate situations the similarity law admits a weakening of modeling conditions, namely, a decrease in the number of similarity criteria. An example is provided by an incompressible fluid flow, in which $\rho = \text{const}$, or, as will be shown in what follows, by the limiting case $M_\infty \rightarrow 0$. Here there is no need to use the equation of state for gases and the quantity $p'' = (p - p_\infty)/\rho_\infty U_\infty^2$ should be introduced instead of p' . It is easy to verify that in this form the problem does not involve the similarity criteria at all, that is, in similarity variables all geometrically similar incompressible fluid flows are identical.

1.12.2 Second Approach: Similarity Theory

The theory is based on the following postulates, which follow directly from general physical considerations or daily experience.*

- A. *All physical quantities can be divided, though not without a certain conventionality, into dimensional and dimensionless.* The first ones, such as length, velocity, and so on, are dependent on scales chosen for their measurement, while the second ones, such as ratios of triangle sides or of velocities (Mach numbers) are dimensionless.

Naturally, by choosing once and forever a system for measuring physical quantities (for example, SI) one can make these quantities dimensionless, which does not lead to any difficulties in daily engineering practice and even facilitates it. However, standard scales (like lengths: foot, meter, yard, etc.) are often chosen by an act of the will, the success of the theory under discussion thus being based on rejecting standard measurement scales in favor of specific ones, appropriate for each particular physical problem.

- B. *Dimensions of all physical quantities are subdivided into independent and dependent ones.*

In mechanics and even in thermodynamics, the dimensions of length L , time t , and mass M can be taken to constitute an independent system of quantities, while the dimensions of other quantities are expressed in terms of independent ones by means of formulas determining these quantities or reflecting the corresponding physical laws.

- C. *Relations between independent and dependent quantities always have the form of power monomials.* Generally speaking, this can be logically proved, but here one can be quite satisfied by recognizing the fact that physics does not know how to introduce new quantities in a way other than expressing them in terms of power monomials.

For example, the force \mathbf{F} is the product of the body mass m and the body acceleration \mathbf{a} . To obtain the work A one should scalarly multiply the force by the path \mathbf{S} ; thence it follows that their dimensions are $[F] = MLt^{-2}$ and $[A] = ML^2t^{-2}$.

There is an obvious consequence of this postulate. Let $f_k, k = 1, \dots, K$ be some parameters with independent dimensions that completely determine the dimensions of quantities f_n .

* There are many publications devoted to the subject, for example, monographs by Sedov (1959), Barenblatt (1982), and so on. Here we will outline only some basic statements necessary to understand further applications of the theory.

Then

$$f_n = \left(\prod_k f_k^{\alpha_{kn}} \right) \cdot \Pi_n \quad (1.12.5)$$

Here, α_{kn} are constant numbers and Π_n are the dimensionless coefficients that give the name of the following well-known Π -theorem of the similarity theory:

All the physical laws can be expressed in terms of functional relations between dimensionless quantities.

Briefly, the proof is reduced to the following. Let a quantity f_0 depend on other quantities f_k, f_n , no matter constant or variable, in accordance with a certain law. Let f_k have independent dimensions, while the dimensions of $f_n, n = K + 1, \dots, N$ are dependent and, hence, they can be represented in the form 1.12.5 (as well as f_0). Then we have

$$\begin{aligned} f_0 &= f_0(f_k, f_n) = \left(\prod_k f_k^{\alpha_{k0}} \right) \cdot \Pi_0 \\ \Pi_0 &= \Pi_0 \left[f_k, \left(\prod_k f_k^{\alpha_{kn}} \right) \cdot \Pi_n \right] \\ k &= 1, \dots, K, \quad n = K + 1, \dots, N \end{aligned} \quad (1.12.6)$$

Further, a crucial step is the choice of quantities f_k for a particular problem, rather than universal scales of any standard measurement system. Then, being referred to their own scales, all the $f_k = 1$ and original physical relations can be replaced by a functional relation between dimensionless quantities

$$\Pi_0 = \Pi_0(\Pi_{K+1}, \dots, \Pi_N) \quad (1.12.7)$$

This dependence gives the mathematical description of a certain similarity law, while variable or constant quantities Π_n are termed the *similarity variables* if they are related with independent variables of the problem (coordinates, time), or *similarity criteria* if they are related with external governing parameters of the problem.

At this point, one can finish the description of the general part of the similarity theory. One can make it a working tool of an analysis only by considering instructive examples, in particular, those that will be considered in the following.

We will derive once more the results obtained in the previous section using the similarity theory.

Consider, first, a perfect gas. The required solution of the problem of a steady-state flow past a given body must have the following form, for example, for pressure

$$p = p(x, y, z, h, \gamma, \rho_\infty, p_\infty, U_\infty) \quad (1.12.8)$$

Clearly, in this problem the dimensions of the parameters chosen to be scales should be independent and involve the dimensions of mass, length, and time. It is quite natural in gas dynamics to choose the body size L , the density ρ_∞ , and the velocity U_∞ as such scales, the quantities $\rho_\infty L^3$ and L/U_∞ playing the roles of a characteristic mass and a gas dynamic time scale of the problem, respectively. Then dividing each argument of 1.12.8 by the appropriate products of the scales we can see that, for example, the ratio $p' = p/(\rho_\infty U_\infty^2)$ depends only on those dimensionless parameters that can be formed of the arguments

$$p' = p'(x', y', z', t', M_\infty, \gamma, l_\infty) \quad (1.12.9)$$

Naturally, these quantities are the same as earlier, while the Mach number M_∞ appears here in nondimensionalizing p_∞ . Other functions (ρ' and so on) depend on the same parameters.

The above relations represent formally a similarity law, while the parameters γ and M_∞ are the similarity criteria for the same, dimensionless, shapes of body surfaces 1.12.4 (the latter goes without saying in this approach).

Clearly, a similarity law derived from the similarity theory is more brief and elegant, since it does not require the procedure of nondimensionalizing equations, boundary conditions, and so on. However, this advantage is, generally speaking, apparent, since in choosing governing parameters and, especially, in reducing their number one should bear in mind the general formulation of the problem, form of equations, boundary conditions, and so on.

The second example deals with a *viscous heat-conducting gas*. In this case, characteristic viscosity and thermal conductivity must be among the parameters in parentheses in 1.12.8; let these be μ_∞ and λ_∞ . The dimension of μ is $[\mu] = M/Lt$, but it is simpler to start with the formula for the friction $\tau \sim \mu \partial U / \partial y$. Since the dimension of friction coincides with that of $\rho_\infty U_\infty^2$, then $[\mu] = [\rho U L]$. Hence, an additional (to arguments of 1.12.9) similarity criterion is the already known Reynolds number $Re = \rho_\infty U_\infty L / \mu_\infty$.

Let us see how the Reynolds number appears in the dimensionless momentum equation. The dimensions of the convective and viscous terms in the equation are (see Equations 1.2.3 and 1.2.4) as follows:

$$\left[\rho u \frac{\partial u}{\partial x} \right] = \left[\rho_\infty \frac{U_\infty^2}{L} \right], \quad \left[\mu \frac{\partial^2 u}{\partial x^2} \right] = \left[\mu_\infty \frac{U_\infty}{L^2} \right] \quad (1.12.10)$$

Dividing the corresponding equations by $\rho_\infty U_\infty^2 / L$ yields dimensionless "inviscid" part of equations and the coefficient Re^{-1} of the viscous terms.

The temperature with the dimension $[T] = [h/c_p]$ enters in the energy equation for a heat-conducting gas; here c_p is the specific heat. Therefore, dividing the "heat conducting" term in, say, Equation 1.2.7 or 1.2.9 by the convective one we obtain

$$\frac{\partial \left(\lambda \frac{\partial T}{\partial x} \right)}{\partial x} : \rho u \frac{\partial h}{\partial x} = \frac{\lambda_\infty \rho_\infty U_\infty}{c_p L} = Pr Re, \quad Pr = \frac{c_p \mu}{\lambda} \quad (1.12.11)$$

Here, Pr is the Prandtl number introduced in Section 1.2. Since for gases $Pr \sim 1$, irrespective of flow conditions, the relative role of dissipative terms in the momentum and energy equations is the same and is characterized by the Reynolds number.

Thus, the complete set of the similarity criteria for a very simple case of a perfect gas looks as follows:

$$\gamma = \frac{c_p}{c_v}, \quad M_\infty = \frac{U_\infty}{a_\infty}, \quad Re = \frac{\rho_\infty U_\infty L}{\mu_\infty}, \quad Pr = \frac{\mu_\infty c_p}{\lambda_\infty} \quad (1.12.12)$$

These criteria are basic in gas dynamics. They also play the fundamental role for real gases with more general equations of state, although in the latter case the number of criteria can increase.

1.12.3 Real Gases

From the point of view of the previous considerations, real gas properties become apparent already in the Sutherland formula 1.3.9 for μ involving a characteristic temperature T_0

which does not vanish in the ratio $\mu' \equiv \frac{\mu}{\mu_\infty}$ in the dimensionless Navier–Stokes equations. Similarly to the equation of state for an imperfect gas in the form 1.3.8, here the effective adiabatic exponent γ_* (depending on p, T or p, h) enters in Equation 1.12.8 instead of γ . However, all these particularly thermodynamic parameters γ_*, μ , and others are introduced in gas dynamics from other branches of science having their own typical governing parameters. Being given, say, by resulting formulas or tables, they are dependent on dimensional, in a conventional meaning, temperature and pressure.

This seems to contradict the Π -theorem, which states that there exist only relations between dimensionless quantities. Formally this contradiction can be eliminated by introducing additional scales for pressure (p_c), temperature (T_c) or enthalpy ($h_c = c_p T_c$). Then, after the problem has been brought to a dimensionless form, it involves some additional dimensionless parameters: $p_c/(\rho_\infty U_\infty^2)$, h_c/U_∞^2 , and so on.

Moreover, these scales p_c, T_c are nothing more but usual units such as N/m^2 , Kelvin's degrees, and so on. Therefore, dimensionless flow fields are still dependent on dimensional flow parameters ρ_∞ and U_∞ , so that one can add these parameters to those in 1.12.12 as *dimensional similarity criteria* though violating scientific and aesthetic rigorousness of considerations.

Simpler particular situations can occur. Thus, for power-law temperature-viscosity dependence, $\mu \sim T^n$ (a particular case of approximation of 1.3.9), only a dimensionless ratio $\mu/\mu_\infty = (T/T_\infty)^n$ enters in the equations of motion. One can imagine a gas with such wonderful properties that the dependence $\gamma_*(h) = \gamma_*(h' U_\infty^2) = \gamma_*(h')$ is retained, however, we do not know such situations.

Degenerate or *limiting* cases in which one can eliminate a number of criteria or governing parameters will be considered in the corresponding sections of the book.

1.12.4 Unsteady Flows

The previous analysis does not deal with any specific properties of unsteady flows; for this reason it must be modified for the purpose of practical modeling. In particular, the typical time scale in gas dynamics, L/U_∞ , is not convenient for describing harmonic oscillations executed by a body in free ballistic flight about its center of gravity with a period t_0 . Therefore, instead of the dimensionless time $t' = tU_\infty/L$ one should introduce another time scale, $t'' = t/t_0$, to describe unsteady processes. Moreover, a length scale δ of unsteady processes, for example, a linear amplitude of the oscillations of the body nose or its center of gravity, can be a governing parameter. In this case, the body shapes are geometrically similar in time for the same dependences

$$f(x', y', z', t'', \delta/L) = 0 \quad (1.12.13)$$

However, the presence of two time and length scales leads to the appearance of additional similarity criteria in the form of ratios $Sh = L/(U_\infty t_0)$ and δ/L . The first criterion is the *Strouhal number* Sh , which enters directly in the equation of motion. We can assure ourselves by representing the solution in the form $u' = u'(t'', x', \dots)$ and substituting it in the dimensionless convective derivative

$$\frac{L}{U_\infty} \frac{du'}{dt} = Sh \frac{\partial u'}{\partial t''} + u' \frac{\partial u'}{\partial x'} + \dots \quad (1.12.14)$$

Here, the Strouhal number characterizes the unsteady effect on the general pattern of the flow past a body. Generally speaking, rigorously steady flows (and processes) do not exist;

they are limiting cases for unsteady processes as $Sh \rightarrow 0$. In this case, if a solution is time dependent this can be taken into account in a quasisteady approximation.

Nevertheless, sometimes it appears important for practice to know the terms of the solution of the order of Sh , no matter how small they may be. As will be shown in what follows, the damping of the oscillations of a body in free flight is to a large extent determined precisely by the unsteady component of the gas dynamic field.

1.12.5 Motion of Bodies in Heavy Fluids

In the foregoing we did not anywhere make allowance for the gravity acceleration \mathbf{g} effect on gas flows, restricting ourselves to a remark on its negligibility in Section 1.7. However, this acceleration is present everywhere, so that its effect should be evaluated in more detail.

For this purpose, we will consider a plane flow in an x, z plane with a z axis directed oppositely to the vector \mathbf{g} . Then the mass force of gravity, $\rho\mathbf{g}$, enters only in the projection of the momentum equation onto the z axis

$$u \frac{\partial u}{\partial x} + w \frac{\partial u}{\partial z} = -\rho g \quad (1.12.15)$$

Passing to variables 1.12.2 and 1.12.3, where L is the vertical dimension of a body, we obtain a term ρ'/Fr on the right-hand side, where $Fr = U_\infty^2/gL$ is the *Froude number* representing an additional similarity parameter and characterizing the effect of the gravity force (or any other external body force) on the flow. This effect depends on the quantities g , L , and U_∞ but not on the medium density. As can be seen, at $U_\infty > 100$ m/s and $L < 10$ m the term $Fr < 0.01$ can be omitted from the equations, as it has been done everywhere previously. Here, we are not dealing with, say, the start-up of a rocket, where at the initial moment all the aerodynamic forces, together with the *Archimedes buoyancy force*, may be completely neglected as compared with the engine thrust. The Archimedes force is, quite naturally, important in the flight of dirigibles and the floating of ships. However, in the motion of bodies in an unbounded medium with a constant density, $\rho' = 1$ (a dirigible in air or a submarine at a large depth), the last term in Equation 1.12.15 can be eliminated by making the substitution $p = p_{ef} - \rho g z$. Then, a given hydrodynamic problem for the parameters U and p_{ef} is reduced to an analogous problem for a weightless fluid.

However, this approach is unacceptable in the case of surface ships, the important role in their motion being played by heavy surface waves. These very interesting problems are, however, beyond the scope of this book.

1.12.6 Self-Similar Problems

Let a body surface be infinite in extent and formed by a bundle of rays originating from a single point, for example, the body vertex or nose. Such a *generalized cone* has no scalelength at all, so that we can form dimensionless parameters from arguments 1.12.9 only assuming that the solution depends on two variables, $p' = p'(\xi, \eta)$, where, for example, $\xi = y/x$ and $\eta = z/x$. Such flows are termed *conical*, while the problems that allow the reduction of dimensionality together with the reduction in the number of independent variables are termed *self-similar*. However, there remain many accompanying questions that could not be solved at this preliminary level. In particular, it appears that conical solutions occur only for supersonic but not subsonic flows. Actually, there are no infinitely long bodies; in a local supersonic flow all end disturbances are convected downstream and therefore the

flow past a conical body is independent of its length and is conical itself. This is the *self-similarity of the first kind*. On the contrary, a subsonic flow is always dependent on the end conditions, so that this flow cannot be conical. Nevertheless, as will be shown in Chapter 2, a simplified flow can exist in the vicinity of the body nose, in which the end effect is taken into account using only one parameter. This corresponds to the *self-similarity of the second kind* (Zeldovich and Raizer, 1967). In general, self-similar solutions permitting, as a rule, an analytical or semianalytical treatment, are of importance in studying flow properties and will be repeatedly used in the book.

1.13 Curvilinear Coordinate Systems: Euler Equations

The Cartesian coordinate system is very simple, but it is often more convenient to use other, curvilinear coordinate systems in which the flow description and the flow patterns appear to be even simpler and more illustrative. For this reason, we will derive the equations of motion in some orthogonal coordinate systems (in general in nonorthogonal coordinate systems, the equations are too cumbersome and will not be used in this book).

Curvilinear coordinates x_1, x_2, x_3 differ from the Cartesian coordinates by two principal features: first, the lengths dl_i and the areas $d\Sigma_i$ of the faces of a coordinate volume $d\Omega$ cut by the coordinate surfaces $x_i = \text{const}$ are variable (Figure 1.19b) and, second, the directions of the unit vectors \mathbf{l}_i of the coordinate lines x_i are variable as well. In an orthogonal coordinate system the length of the element dl_i of any spatial curve and the areas $d\Sigma_i$, as well as the volume $d\Omega$ itself, are determined as follows:

$$\begin{aligned} dl^2 &= dl_1^2 + dl_2^2 + dl_3^2, & dl_i &= H_i dx_i, \\ d\Sigma_1 &= H_2 H_3 dx_2 dx_3, & d\Sigma_2 &= H_1 H_3 dx_1 dx_3, \\ d\Sigma_3 &= H_1 H_2 dx_1 dx_2, & d\Omega &= H_1 H_2 H_3 dx_1 dx_2 dx_3 \end{aligned} \quad (1.13.1)$$

Here, H_i are the *Lamé coefficients* or *scale factors* that can be easily determined from geometrical considerations, for example, from Figure 1.24 for particular situations. We will write down the expression for the divergence of a vector \mathbf{A} in these coordinates using formula 1.8.13. Similarly to the case of Cartesian coordinates, it can be easily shown that along each direction x_i the flux of this vector is equal to $[\partial(A_i d\Sigma_i)/\partial x_i] dx_i$. Hence, summing over all directions yields

$$\text{div } \mathbf{A} = \frac{1}{H_1 H_2 H_3} \left(\frac{\partial A_1 H_2 H_3}{\partial x_1} + \frac{\partial A_2 H_1 H_3}{\partial x_2} + \frac{\partial A_3 H_1 H_2}{\partial x_3} \right) \quad (1.13.2)$$

For $\mathbf{A} = \mathbf{U}$ or $\mathbf{A} = \rho \mathbf{U}$ the formula obtained gives immediately the continuity equation in these coordinates in forms 1.9.1 or 1.9.7.

1.13.1 Other Operators

To write the general formula 1.8.3 for the total derivative one should let $dx_i^* = H_i^{-1} dl_i^*$, where dl_i^* is an element of a particle trajectory in space. Hence

$$\frac{d}{dt} = \frac{\partial}{\partial t} + \sum_i \frac{u_i}{H_i} \frac{\partial}{\partial x_i}, \quad i = 1, 2, 3 \quad (1.13.3)$$

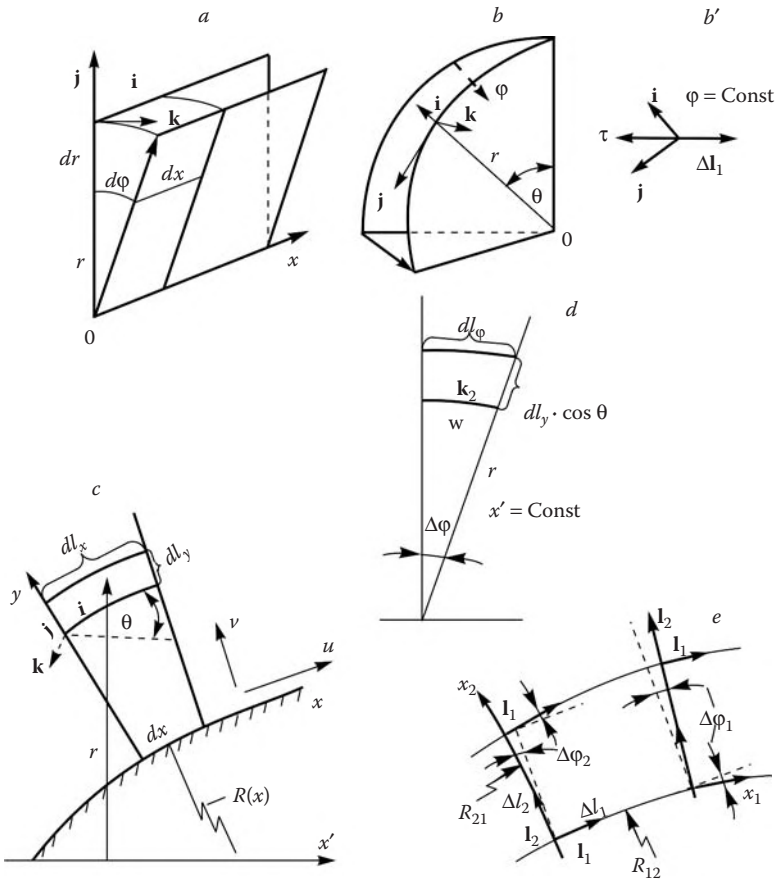


FIGURE 1.24
Systems of curvilinear coordinates.

To define the operator of the pressure gradient (or any other vector), it is sufficient to introduce the Cartesian coordinate system (l_1, l_2, l_3) tangent to the given system at each point (i.e., the system with the same unit vectors \mathbf{l}_i). For this system, formula 1.8.17 is valid, which can easily be brought to the form:

$$\text{grad } p = \vec{\nabla} p, \quad \vec{\nabla} = \sum_i \frac{\mathbf{l}_i}{H_i} \frac{\partial}{\partial x_i} \quad (1.13.4)$$

From methodical considerations the expression for the curl operator introduced in Section 1.8 will be presented in curvilinear coordinates at the end of Section 1.14.

Finally, in curvilinear coordinates the velocity vector \mathbf{U} and its total derivative have the form:

$$\mathbf{U} = \sum_i \mathbf{l}_i u_i, \quad \frac{d\mathbf{U}}{dt} = \sum_i \mathbf{l}_i \frac{du_i}{dt} + \sum_i u_i \frac{d\mathbf{l}_i}{dt} \quad (1.13.5)$$

The derivatives of the unit vectors \mathbf{l}_i along particle trajectories are expressed by the same formulas 1.13.3; in this case the partial derivatives $\partial \mathbf{l}_i / \partial x_i$ are nonzero, due to rotation of these vectors when moving along the coordinate lines, the scalar product being equal to zero, $\mathbf{l}_i (\partial \mathbf{l}_i / \partial x_j) = 0$.

Thus, in curvilinear coordinates the total derivative of the velocity involves (besides usual terms) additional terms proportional to velocities u_i , depending on the coordinate curvature. These additional terms are *inertial*.

These results are sufficient to derive inviscid equations in particular coordinate systems; the most frequently used systems will be given below.

1.13.2 Cylindrical System

In gas dynamics this system is used as frequently as the Cartesian one. It is shown in Figure 1.24a, and an analysis of this figure gives

$$\begin{aligned} x_1 &= x, \quad x_2 = r, \quad x_3 = \varphi, \quad \mathbf{l}_1 = \mathbf{i}, \quad \mathbf{l}_2 = \mathbf{j}, \quad \mathbf{l}_3 = \mathbf{k} \\ H_1 &= H_2 = 1, \quad H_3 = r, \quad u_1 = u, \quad u_2 = v, \quad u_3 = w \\ \frac{\partial \mathbf{l}_i}{\partial x} &= \frac{\partial \mathbf{l}_i}{\partial r} = 0, \quad \frac{\partial \mathbf{i}}{\partial \varphi} = 0, \quad \frac{\partial \mathbf{j}}{\partial \varphi} = \mathbf{k}, \quad \frac{\partial \mathbf{k}}{\partial \varphi} = -\mathbf{j} \end{aligned} \quad (1.13.6)$$

Clearly, the unit vectors do not change their directions when moving in a meridional plane, but \mathbf{j} and \mathbf{k} rotate with it.

Taking this into account we can bring the continuity equation to the form:

$$\frac{\partial \rho}{\partial t} = -\operatorname{div} \rho \mathbf{U} = -\frac{1}{r} \left(\frac{\partial \rho u r}{\partial x} + \frac{\partial \rho v r}{\partial r} + \frac{\partial \rho w}{\partial \varphi} \right) \quad (1.13.7)$$

Similarly, the total derivative is as follows:

$$\frac{d}{dt} = \frac{\partial}{\partial t} + u \frac{\partial}{\partial x} + v \frac{\partial}{\partial r} + \frac{w}{r} \frac{\partial}{\partial \varphi} \quad (1.13.8)$$

and the gradient operator is

$$\vec{\nabla} = \mathbf{i} \frac{\partial}{\partial x} + \mathbf{j} \frac{\partial}{\partial r} + \mathbf{k} \frac{1}{r} \frac{\partial}{\partial \varphi} \quad (1.13.9)$$

Substituting these expressions into Equation 1.9.2 we obtain its projections onto the basic coordinate vectors. Taking 1.13.8 into account they can be written in a compact form

$$\begin{aligned} \frac{du}{dt} &= -\frac{1}{\rho} \frac{\partial p}{\partial x} \\ \frac{dv}{dt} - \frac{w^2}{r} &= -\frac{1}{\rho} \frac{\partial p}{\partial r} \\ \frac{dw}{dt} + \frac{vw}{r} &= -\frac{1}{\rho r} \frac{\partial p}{\partial \varphi} \end{aligned} \quad (1.13.10)$$

The additional terms in the last two equations are *centrifugal* and *Coriolis* accelerations, respectively. To write the energy formula

$$\frac{dh}{dt} = \frac{1}{\rho} \frac{dp}{dt} + q \quad (1.13.11)$$

it is sufficient to use Equation 1.13.8.

For plane ($v = 0$) and axisymmetric ($v = 1$) flows, that is, independent of φ and having $w = 0$, the momentum equation (with y replaced by r) is the same, while the continuity equation can be written in a unified form:

$$\frac{\partial(\rho r^v)}{\partial t} + \frac{\partial(\rho u r^v)}{\partial x} + \frac{\partial(\rho v r^v)}{\partial r} = 0 \quad (1.13.12)$$

1.13.3 Spherical Coordinates

In this case, the position of a point is determined by a distance r from a center O , an inclination angle θ , and a meridional angle φ (Figure 1.24b). Hence

$$\begin{aligned} x_1 &= r, & x_2 &= \theta, & x_3 &= \varphi \\ \mathbf{l}_1 &= \mathbf{i}, & \mathbf{l}_2 &= \mathbf{j}, & \mathbf{l}_3 &= \mathbf{k} \\ u_1 &= v_r, & u_2 &= v_\theta, & u_3 &= v_\varphi \end{aligned} \quad (1.13.13)$$

An analysis of Figure 1.24b gives the following relations

$$\begin{aligned} H_1 &= H_r = 1, & H_2 &= H_\theta = r, & H_3 &= H_\varphi = r \sin \theta \\ \frac{\partial \mathbf{l}_i}{\partial r} &= 0, & \frac{\partial \mathbf{i}}{\partial \theta} &= \mathbf{j}, & \frac{\partial \mathbf{i}}{\partial \varphi} &= \mathbf{k} \sin \theta \\ \frac{\partial \mathbf{j}}{\partial \theta} &= -\mathbf{i}, & \frac{\partial \mathbf{j}}{\partial \varphi} &= \mathbf{k} \cos \theta, & \frac{\partial \mathbf{k}}{\partial \theta} &= 0 \\ \frac{\partial \mathbf{k}}{\partial \varphi} &= -\vec{\tau}, & \vec{\tau} &= \mathbf{i} \sin \theta + \mathbf{j} \cos \theta \end{aligned} \quad (1.13.14)$$

As follows from Figure 1.24b, the unit vectors \mathbf{i} and \mathbf{j} rotate with the radius-vector \mathbf{r} when the angle θ varies, whereas the vector \mathbf{k} does not vary its direction, so that the expressions for their derivatives with respect to θ are obvious. The derivatives with respect to φ can be easily obtained by introducing the unit vector $\vec{\tau}$ lying in the $\varphi = \text{const}$, $\theta = \pi/2$ planes (Figure 1.24b), this vector being collinear with the increments of all the vectors $\Delta \mathbf{l}_i$ when the meridional plane is turned by a small angle $\Delta \varphi$.

As a result, the following motion equations are obtained

$$\begin{aligned} \frac{dv_r}{dt} - \frac{v_\theta^2 + v_\varphi^2}{r} &= -\frac{1}{\rho} \frac{\partial p}{\partial r} \\ \frac{dv_\theta}{dt} + \frac{v_r v_\theta}{r} - \frac{\cot \theta}{r} v_\varphi^2 &= -\frac{1}{r \rho} \frac{\partial p}{\partial \theta} \\ \frac{dv_\varphi}{dt} + \frac{v_\theta v_\varphi \cot \theta + v_r v_\varphi}{r} &= -\frac{1}{\rho r \sin \theta} \frac{\partial p}{\partial \varphi} \\ \frac{\partial \rho}{\partial t} + \frac{1}{r^2} \frac{\partial(\rho v_r r^2)}{\partial r} + \frac{1}{r \sin \theta} \frac{\partial(\rho v_\theta \sin \theta)}{\partial \theta} + \frac{1}{r \sin \theta} \frac{\partial(\rho v_\varphi)}{\partial \varphi} &= 0 \\ \frac{d}{dt} = \frac{\partial}{\partial t} + v_r \frac{\partial}{\partial r} + \frac{v_\theta}{r} \frac{\partial}{\partial \theta} + \frac{v_\varphi}{r \sin \theta} \frac{\partial}{\partial \varphi} & \end{aligned} \quad (1.13.15)$$

For $v_\varphi = 0$ and $\partial/\partial\varphi = 0$ this system governs axisymmetric flows in a polar coordinate system r, θ , whose axis of symmetry is $\theta = 0$ and $\theta = \pi$. Similarly, putting $u = 0$ and $\partial/\partial x = 0$ in a cylindrical coordinate system, we arrive at the same polar system r, φ . Substituting φ , v , and w for θ , v_r , and v_θ in the latter system, we can assure ourselves that the momentum Equations 1.13.10 and 1.13.15 coincide in the two cases. The corresponding continuity Equations 1.13.7 and 1.13.15 can be written uniformly:

$$\frac{\partial \rho}{\partial t} + \frac{1}{r^{v+1}} \frac{\partial \rho v_r r^{v+1}}{\partial r} + \frac{1}{r (\sin \theta)^v} \frac{[\partial \rho v_\theta (\sin \theta)^v]}{\partial \theta} = 0 \quad (1.13.16)$$

Thence for $v = 1$ we obtain Equation 1.13.15 for axisymmetric flows, while for $v = 0$ we arrive at an equation for plane flows in polar coordinates.

1.13.4 Curvilinear Surface-Fitted Coordinate System for Plane and Axisymmetric Flows

This system is usually fitted to the surface of a reference body (a body in a gas flow); at the body surface one of the coordinates is assumed to be constant. The system is especially convenient in the case in which the disturbed region is concentrated in the vicinity of the body. We restrict ourselves to an orthogonal coordinate system x, y, φ constructed on plane ($v = 0$) and axisymmetric ($v = 1$) bodies. The x axis is aligned with the contour of the meridional cross-section of the body, while the y axis is normal to it ($y = 0$ on the surface); φ is the angle of the turn of the meridional plane about the axis of symmetry (Figure 1.24c and d). In this case we have

$$\begin{aligned} x_1 &= x, & H_x &= 1 + \frac{y}{R}, & x_2 &= y, & H_y &= 1 \\ x_3 &= \varphi, & H_\varphi &= r^v, & \mathbf{l}_1 &= \mathbf{i}, & \mathbf{l}_2 &= \mathbf{j}, & \mathbf{l}_3 &= \mathbf{k} \end{aligned} \quad (1.13.17)$$

Here, r is the distance from a point to the axis of symmetry and R is the radius of curvature of the body contour. In these coordinates, the total derivative and the gradient operator take the form:

$$\frac{df}{dt} = \frac{\partial f}{\partial t} + \frac{R}{R+y} u \frac{\partial f}{\partial x} + v \frac{\partial f}{\partial y} + \frac{w}{r} \frac{\partial f}{\partial \varphi} \quad (1.13.18)$$

$$\nabla p = \text{grad } p = \mathbf{i} \left(\frac{R}{R+y} \right) \frac{\partial p}{\partial x} + \mathbf{j} \frac{\partial p}{\partial y} + \frac{\mathbf{k}}{r} \frac{\partial p}{\partial \varphi} \quad (1.13.19)$$

For plane flows ($v = 0$) it should be let $w = 0$ and $\frac{\partial}{\partial \varphi} = 0$. To obtain the derivatives of the unit vectors, it should be taken into account, in addition to previous reasoning, that a displacement over a distance Δx along the x axis leads to rotation of the \mathbf{i} and \mathbf{j} vectors by the angle $\Delta x/R$, while the direction of the vector \mathbf{k} is unchanged. As for rotation of the coordinate trihedron about the axis of symmetry, it leads to the same derivatives \mathbf{l}_i as for the spherical coordinates. Thus we have

$$\begin{aligned} \frac{\partial \mathbf{i}}{\partial x} &= -\frac{\mathbf{j}}{R}, & \frac{\partial \mathbf{j}}{\partial x} &= \frac{\mathbf{i}}{R}, & \frac{\partial \mathbf{k}}{\partial x} &= 0, & \frac{\partial \mathbf{l}_i}{\partial y} &= 0 \\ \frac{\partial \mathbf{i}}{\partial \varphi} &= \mathbf{k} \sin \theta, & \frac{\partial \mathbf{j}}{\partial \varphi} &= \mathbf{k} \cos \theta \\ \frac{\partial \mathbf{k}}{\partial \varphi} &= -\mathbf{i} \sin \theta - \mathbf{j} \cos \theta \end{aligned} \quad (1.13.20)$$

Summing the results obtained, from the equation of motion 1.9.2 we get the following system of equations

$$\begin{aligned} \frac{du}{dt} + \frac{uv}{R+y} - \frac{w^2}{r} \sin \theta &= -\frac{R}{R+y} \frac{1}{\rho} \frac{\partial p}{\partial x} \\ \frac{dv}{dt} - \frac{u^2}{R+y} - \frac{w^2}{r} \cos \theta &= -\frac{1}{\rho} \frac{\partial p}{\partial y} \\ \frac{dw}{dt} + \frac{wv}{r} \cos \theta + \frac{uw}{r} \sin \theta &= -\frac{1}{r\rho} \frac{\partial p}{\partial \varphi} \\ \frac{\partial}{\partial t} \left(\rho r^v \frac{R+y}{R} \right) + \frac{\partial}{\partial x} (\rho u r^v) + \frac{\partial}{\partial y} \left(\rho v r^v \frac{R+y}{R} \right) \\ + \frac{1}{r} \frac{\partial}{\partial \varphi} \left(\rho w \frac{R+y}{R} \right) &= 0 \end{aligned} \quad (1.13.21)$$

As a very simple illustration we refer to the equations of a steady axisymmetric gas flow in a system of coordinates fitted to a cone with the semivertex angle θ . Actually, it is sufficient to put $w = 0$ and $R = \infty$ in the momentum Equation 1.13.21 in order for these to take the same form as in a conventional Cartesian system. At the same time, the continuity equation takes the form:

$$\begin{aligned} u \frac{\partial \rho}{\partial x} + v \frac{\partial \rho}{\partial y} + \rho \left(\frac{\partial u}{\partial x} + \frac{\partial v}{\partial y} \right) &= \rho Q_{\text{eff}} \\ Q_{\text{eff}} &= -\frac{v}{r} \left(u \frac{\partial r}{\partial x} + v \frac{\partial r}{\partial y} \right) = -\frac{v}{r} (u \sin \theta + v \cos \theta) \end{aligned} \quad (1.13.22)$$

For the plane flow ($v = 0$) we have the same equation as in Cartesian coordinates.

1.13.5 General Case

Actually, formulas 1.13.1 through 1.13.5 are quite general. However, the last formula contains the derivatives $\partial \mathbf{l}_i / \partial x_k$, which must be related with the scale factors determining a coordinate system. These relationships are derived in tensor calculus and for orthogonal systems have the form:

$$\begin{aligned} \frac{1}{H_i} \frac{\partial \mathbf{l}_i}{\partial x_i} &= -K_{i,i+1} \mathbf{l}_{i+1} - K_{i,i+2} \mathbf{l}_{i+2} \\ \frac{1}{H_k} \frac{\partial \mathbf{l}_i}{\partial x_k} &= K_{i,k} \quad (i \neq k), \quad K_{i,k} = R_{i,k}^{-1} = \frac{1}{H_i H_k} \frac{\partial H_i}{\partial x_k} \end{aligned} \quad (1.13.23)$$

Here, the numbering is cyclic, that is, at $i = 2$ we have $i+1 = 3$ but $i+2 = 1$. The notation $K_{i,k}$ denotes the projection of the normal curvature vector of a line x_i onto the plane containing the vectors \mathbf{l}_i and \mathbf{l}_k . In accordance with the *Dupin theorem*, the coordinate surfaces of a triorthogonal coordinate system intersect in the lines of their principal curvatures. We will explain the origin of these formulas by simple geometric considerations. In Figure 1.24e we have plotted an elementary coordinate cell with the sides $\Delta l_i = H_i \Delta x_i$ on an $x_3 = \text{const}$ surface. As the vector \mathbf{l}_1 displaces over a distance Δl_1 along the line $x_2 = \text{const}$, it turns by an angle $\Delta \varphi_1 = K_{12} \Delta l_1$, thus taking the increment $\Delta \mathbf{l}_1 = -\mathbf{l}_2 \Delta \varphi_1$. In the limit, we obtain the first term of the first formula (1.13.23). Similar reasoning for the $x_2 = \text{const}$ surface leads to the second term of this formula; considering the displacement of the vector \mathbf{l}_1 along the line $x_1 = \text{const}$ on the $x_3 = \text{const}$ surface we obtain the second formula 1.13.23. Formulas for K_{ik} are also obtained from an analysis of Figure 1.24e, for example

$$K_{12} = \lim \frac{\Delta \varphi_1}{\Delta l_1} = \lim \frac{(\Delta l_1)_{x_2+\Delta x_2} - (\Delta l_1)_{x_2}}{\Delta l_1 \Delta l_2} = \frac{1}{H_1 H_2} \frac{\partial H_1}{\partial x_2} \quad \Delta x_1, \Delta x_2 \rightarrow 0 \quad (1.13.24)$$

Together with Equations 1.13.3 and 1.13.5, these formulas make it possible to write the particle acceleration and the equation of motion projected onto the unit vectors \mathbf{l}_i

$$\begin{aligned} \frac{du_i}{dt} + u_i u_{i+1} K_{i,i+1} + u_i u_{i+2} K_{i,i+2} - \\ u_{i+1}^2 K_{i+1,i} - u_{i+2}^2 K_{i+2,i} &= -\frac{1}{\rho} \frac{1}{H_i} \frac{\partial p}{\partial x_i} \end{aligned} \quad (1.13.25)$$

The terms with $u_{i,k}$, $i \neq k$ are called the *Coriolis accelerations*, while those with u_i^2 are called the *centrifugal accelerations*. It can be easily verified that all the previous equations written for particular coordinate systems follow from Equation 1.13.25.

We note that in studying gas flows, especially three-dimensional ones, the so-called *adapted* coordinate systems are frequently used; these systems make allowance for flow properties in an optimal fashion. Thus, one of the coordinates can be directed along the primary direction of the velocity, and so on. Usually, these systems are fitted to the surface of a body in a gas flow, two coordinate lines, x_1 and x_3 , being taken on its surface, while the x_2 lines intersect it. The representation of the equations of motion in nonorthogonal systems of coordinates is the subject of Riemann geometry and tensor calculus and requires a very cumbersome mathematical apparatus. We do not use those systems in this book; for a detailed discussion of this subject the reader is referred to special literature.

Now we will write down *conservation-law equations* 1.9.7 through 1.9.10 in curvilinear coordinates. To do this with the scalar equations (those of continuity and energy), it is sufficient to use the divergence operator 1.13.2. However, making transformations in Equation 1.9.8 on the basis of the same operator and using expansion 1.13.5 we obtain

$$\begin{aligned} H_1 H_2 H_3 \operatorname{div} (\rho \mathbf{U} \cdot \mathbf{U}) &= \frac{\partial}{\partial x_1} (\rho H_2 H_3 u_1 \mathbf{U}) + \dots = \\ \mathbf{l}_1 \frac{\partial}{\partial x_1} (H_2 H_3 \rho u_1^2) + H_2 H_3 \rho u_1^2 \frac{\partial \mathbf{l}_1}{\partial x_1} &+ \dots \end{aligned} \quad (1.13.26)$$

Here, we have written only single terms of the groups of terms of the same type. Substituting expressions 1.13.23 for the derivatives $\partial \mathbf{l}_i / \partial x_k$ into this equation, we can then easily project it onto the unit vectors \mathbf{l}_i . However, owing to the appearance of free terms, the equations thus obtained are no longer conservative-law ones.

This regrettable circumstance can be passed over by expanding the vector $\mathbf{U} = u\mathbf{i} + v\mathbf{j} + w\mathbf{k}$ in the space-invariant unit vectors of a Cartesian coordinate system and projecting the momentum equation onto the same directions. In the fitted coordinate system (e.g., x, y in Figure 1.25a) the corresponding equations can be obtained directly from the conservation laws (Section 1.7) for an element of the coordinate volume (dashed in Figure 1.25a) using the Cartesian unit vectors and velocity components. However, it is simpler to apply the

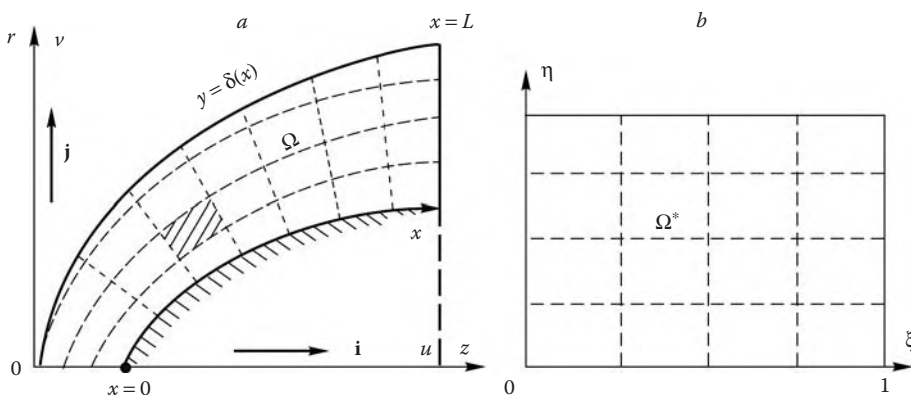


FIGURE 1.25
Transformation of the coordinate systems.

coordinate transformation directly to the equations written in the original Cartesian coordinates. We will elucidate the idea of this transformation with reference to the example of time-dependent two-dimensional equations written in the general conservation-law form

$$\frac{\partial \chi}{\partial t} + \frac{\partial F}{\partial z} + \frac{\partial G}{\partial r} = 0 \quad (1.13.27)$$

Here, r, z is the cylindrical or Cartesian coordinate system shown in Figure 1.25a, χ is an element of column 1.7.9, and the sum of two last terms is the sum of the divergence operators in any of Equations 1.9.7, 1.9.8, and 1.9.10. In order to rewrite Equation 1.13.27 first in the body-fitted curvilinear coordinates x, y (Figure 1.25a) and then in the normalized coordinate system ξ, η mapping the domain Ω in Figure 1.25a onto the domain Ω^* in Figure 1.25b, we introduce variables, which, for the sake of simplicity, are time-independent

$$\xi = f_1(y/\delta) = \xi(z, r), \quad \eta = f_2(x/L) = \eta(z, r), \quad f_i(1) = 1 \quad (1.13.28)$$

Omitting rather simple, though cumbersome, algebra, we will write down the final result of these transformations (see, e.g., Fletcher, 1988)

$$F_z + G_r = J(F_\xi^* + G_\eta^*) \quad (1.13.29)$$

Here and in what follows the subscripts refer to the differentiation with respect to the corresponding variables, J is the Jacobian of transformation 1.13.28, and F^* and G^* are the *generalized fluxes*

$$\begin{aligned} J &= \xi_z \eta_r - \xi_r \eta_z \\ JF^* &= \xi_z F + \xi_r G, \quad JG^* = \eta_z F + \eta_r G \end{aligned} \quad (1.13.30)$$

For a time-independent Jacobian J Equation 1.13.27 takes the completely conservation-law form

$$\frac{\partial \chi^*}{\partial t} + \frac{\partial F^*}{\partial \xi} + \frac{\partial G^*}{\partial \eta} = 0, \quad \chi^* = \frac{\chi}{J} \quad (1.13.31)$$

In the original Equation 1.13.27 the operators F and G may, if they allow for dissipative processes, include derivatives with respect to z and r , which can also be transformed to the new variables ξ and η ; this does not disturb the conservation-law nature of Equation 1.13.31. The main feature of these operators is that they can be expressed in terms of the Cartesian velocity components u and v and the fixed unit vectors \vec{i} and \vec{j} (see Figure 1.25a), which excludes the possibility of the appearance of non-conservation-law terms of the equations that enter in transformation 1.13.25 when projecting the vector momentum equation onto these directions.

1.14 Navier–Stokes Equations in Curvilinear Coordinates

In deriving the Navier–Stokes equations in curvilinear coordinates, two stages differing in their approaches should be separated out. These are the derivation of the equations for stresses and the derivation of the formulas for the strain rate tensor components ε_{ik} .

In view of the results obtained in Sections 1.9 and 1.13, the first question is solved fairly simply. In fact, the expression for the stress tensor divergence in the momentum equation

is almost the same as 1.13.2 if the components of the vector \mathbf{A}_i are replaced by the stresses p_i acting on the area elements $d\Sigma$, and so on. This follows from the fashion itself of the derivation of this operator in Section 1.9 by means of an integral over a small volume $d\Omega$. Thus, we have

$$\operatorname{Div} P = \frac{1}{H_1 H_2 H_3} \left[\frac{\partial(H_2 H_3 \mathbf{p}_1)}{\partial x_1} + \frac{\partial(H_1 H_3 \mathbf{p}_2)}{\partial x_2} + \frac{\partial(H_1 H_2 \mathbf{p}_3)}{\partial x_3} \right] \quad (1.14.1)$$

Then we must derive an expression for the dissipative heat flux q_τ in the energy Equation 1.9.6. This term, which is new compared with the Euler equations, is determined from formula 1.9.5. Generalizing the reasoning of that section the difference of the forces acting on opposite fluid faces $d\Sigma_i^*$ of a fluid volume $d\Omega^*$ could be neglected in view of the smallness of the relative velocities $\pm(1/2)\Delta U$ of these faces. Therefore, for determining the work performed by these forces, it is sufficient to introduce a local Cartesian system (l_1, l_2, l_3) in which the expressions for q_τ have the same form as earlier. Passing to the variables x_i and taking 1.13.1 into account we obtain

$$q_\tau = \frac{\vec{\tau}_1}{H_1} \frac{\partial \mathbf{U}}{\partial x_1} + \frac{\vec{\tau}_2}{H_2} \frac{\partial \mathbf{U}}{\partial x_2} + \frac{\vec{\tau}_3}{H_3} \frac{\partial \mathbf{U}}{\partial x_3} \quad (1.14.2)$$

Finally, the expression for the convective-diffusive heat flux $q_J = -\operatorname{div} \mathbf{J}$ is reduced to a combination of expressions 1.13.2 and 1.13.4 if, for example, $\mathbf{J} = \mathbf{J}_T = -\operatorname{grad} T$.

We are coming now to the derivation of rheological relations between stresses and strains in curvilinear coordinates. This analysis will be performed on the basis of purely geometric, though illustrative considerations, without invoking matrix transformations that are commonly accepted for these purposes.

On any area element in the space the relation between the vector \mathbf{p}_n and the strain tensor components depends only on the mutual orientation of this area and coordinate planes (e.g., formulas 1.9.3 and 1.10.2). Therefore, if at the center of this area O with the coordinates x_O one more Cartesian system of coordinates l'_i with the unit vectors \mathbf{l}'_i and the velocity projections u'_i onto these directions is introduced, then all the components p_{ik} are the same in the two coordinate systems provided the new system is tangent to the $x_i = \text{const}$ coordinate lines. The strain rates ε_{ik} are also the same, since they describe the extension and mutual rotation of the same fluid segments. Then, since expressions 1.8.10 for ε_{ik} in terms of the velocities u'_i and coordinates l'_i are known:

$$\varepsilon_{ik} = \frac{1}{2} \left(\frac{\partial u'_i}{\partial l'_k} + \frac{\partial u'_k}{\partial l'_i} \right) \quad (1.14.3)$$

Their new expressions in the original coordinates x_i can be obtained by the recalculation of the velocities and the derivatives in the vicinity of the point O . It should be taken into account that at the origin only the velocities $u'_i = u_i$ must coincide but not their derivatives with respect to their own coordinates.

If \mathbf{l}_i are the current unit vectors of the x_i coordinate lines, then in the vicinity of the point O the relation between the velocities u'_i and u_i and their derivatives is expressed by the following formulas (in this vicinity $dl'_i = dl_i = H_i dx_i$)

$$\begin{aligned} u'_k &= \sum_i u_i (\mathbf{l}'_k \cdot \mathbf{l}_i), \quad i, k, m = 1, 2, 3 \\ \frac{\partial u'_k}{\partial l'_m} &= \frac{\partial u'_k}{\partial l_m} = \frac{1}{H_m} \sum_i \left[\frac{\partial u_i}{\partial x_m} (\mathbf{l}'_k \cdot \mathbf{l}_i) - u_i \left(\mathbf{l}'_k \frac{\partial \mathbf{l}_i}{\partial x_m} \right) \right] \end{aligned} \quad (1.14.4)$$

The latter formula is simplified in the limit $\mathbf{l}'_i \rightarrow \mathbf{l}_i$, as the point O is approached, since the terms $(\cdot \mathbf{l}'_i)$ in this formula turn to zero or unity, so that ultimately we obtain

$$H_m \frac{\partial u'_k}{\partial l'_m} = \frac{\partial u_k}{\partial x_m} - \sum_i u_i \left(\mathbf{l}_k \frac{\partial \mathbf{l}_i}{\partial x_m} \right) \quad (1.14.5)$$

Thus, the problem of calculating the strain rates in curvilinear coordinates is reduced, as well as that for particle accelerations, to the calculation of the derivatives of vectors along coordinate lines.

Using these relations and expressions 1.13.23 for the derivatives of the unit vectors we will write down certain formulas for the same particular cases as in Section 1.13.

Thus, in a *cylindrical* coordinate system we have

$$\begin{aligned} \varepsilon_{xx} &= \frac{\partial u}{\partial x}, & \varepsilon_{rr} &= \frac{\partial v}{\partial r}, & \varepsilon_{\varphi\varphi} &= \frac{1}{r} \left(\frac{\partial w}{\partial \varphi} + v \right) \\ 2\varepsilon_{xr} = 2\varepsilon_{rx} &= \frac{\partial v}{\partial x} + \frac{\partial u}{\partial r}, & 2\varepsilon_{x\varphi} &= \frac{\partial w}{\partial x} + \frac{1}{r} \frac{\partial u}{\partial \varphi} \\ 2\varepsilon_{r\varphi} &= \frac{\partial w}{\partial r} + \frac{1}{r} \frac{\partial v}{\partial \varphi} - \frac{w}{r} \end{aligned} \quad (1.14.6)$$

In a *spherical* coordinate system

$$\begin{aligned} \varepsilon_{rr} &= \frac{\partial v_r}{\partial r}, & \varepsilon_{\theta\theta} &= \frac{1}{r} \left(\frac{\partial v_\theta}{\partial \theta} + v_r \right) \\ \varepsilon_{\varphi\varphi} &= \frac{1}{r} \left(\frac{1}{\sin \theta} \frac{\partial v_\varphi}{\partial \varphi} + v_r + v_\theta \cot \theta \right) \\ 2\varepsilon_{r\theta} &= \frac{1}{r} \frac{\partial v_r}{\partial \theta} + \frac{\partial v_\theta}{\partial r} - \frac{v_\theta}{r}, & 2\varepsilon_{r\varphi} &= \frac{\partial v_\varphi}{\partial r} + \frac{1}{r \sin \theta} \frac{\partial v_r}{\partial \varphi} - \frac{v_\varphi}{r} \\ 2\varepsilon_{\theta\varphi} &= \frac{1}{r} \left(\frac{1}{\sin \theta} \frac{\partial v_\theta}{\partial \varphi} + \frac{\partial v_\varphi}{\partial \theta} - v_\varphi \cot \theta \right) \end{aligned} \quad (1.14.7)$$

For plane flows it should be taken $r \rightarrow \infty$ and $w = 0$ in these formulas. In a *curvilinear* coordinate system fitted to an axisymmetric body we have

$$\begin{aligned} \varepsilon_{xx} &= \frac{R}{R+y} \left(\frac{\partial u}{\partial x} - \frac{v}{R} \right), & \varepsilon_{yy} &= \frac{\partial v}{\partial y} \\ \varepsilon_{\varphi\varphi} &= \frac{1}{r} \left(\frac{\partial w}{\partial \varphi} + u \sin \theta + v \cos \theta \right) \\ 2\varepsilon_{xy} &= \frac{\partial u}{\partial y} + \frac{R}{R+y} \frac{\partial v}{\partial x} - \frac{u}{R+y} \\ 2\varepsilon_{x\varphi} &= \frac{R}{R+y} \frac{\partial w}{\partial x} + \frac{1}{r} \left(\frac{\partial u}{\partial \varphi} - w \sin \theta \right) \\ 2\varepsilon_{y\varphi} &= \frac{1}{r} \left(\frac{\partial v}{\partial \varphi} - w \cos \theta \right) + \frac{\partial w}{\partial y} \end{aligned} \quad (1.14.8)$$

As for the expressions for ε_{ik} in the general orthogonal coordinate system, they could be written by applying the same algorithm to Equation 1.13.23.*

It can be seen that in changing from Cartesian to curvilinear coordinates nondifferential terms have appeared in some of the quantities ε_{ik} . This is partially due to a purely mathematical effect. Thus, in a translational motion of a gas as a solid body in the direction of any axis \mathbf{r} or in a rotational motion around this axis, the derivatives of the velocities u and w with respect to φ in a cylindrical coordinate system are nonzero, although all $\varepsilon_{ik} = 0$. At the same time, in a pure expansion of a gas with respect to the x axis, all $\varepsilon_{ik} = 0$, except for $\varepsilon_{\varphi\varphi}$ and ε_{rr} , since segments of fluid lines exhibit extension strains when expanding.

The sequence of equations obtained allows us to write down the complete set of Navier–Stokes equations for any particular case. We will only emphasize that in differentiating the stresses \mathbf{p}_i in formula 1.14.1 one should bear in mind that the unit vectors \mathbf{l}_i in the expansion $\mathbf{p}_i = \sum_k \mathbf{l}_k p_{ik}$, and so on, are variable, so that their derivatives with respect to x_i enter in the equation of motion, as they do due to the differentiation of the vector \vec{U} .

We shall explain this procedure with reference to a very simple example of the pure rotation of an incompressible fluid about an x axis; in this case the velocity has only one component $w = w(r)$. Then, in view of 1.14.6, we have

$$\begin{aligned} \mathbf{p}_2 &= \mathbf{p}_r = -\mathbf{j}p + \mathbf{k}p_{r\varphi}, & \mathbf{p}_3 &= \mathbf{p}_\varphi = \mathbf{j}p_{r\varphi} - \mathbf{k}p \\ p_{r\varphi} &= \mu\varepsilon_{r\varphi} = \mu \left(\frac{\partial w}{\partial r} - \frac{w}{r} \right) \end{aligned} \quad (1.14.9)$$

The other components of the strain rate and stress tensors are zero. Hence, by virtue of 1.13.6, we have

$$\text{Div } P = \frac{1}{r} \left(\frac{\partial r\mathbf{p}_r}{\partial r} + \frac{\partial \mathbf{p}_\varphi}{\partial \varphi} \right) = -\mathbf{j} \frac{\partial p}{\partial r} + \frac{1}{r} \mathbf{k} \left(\frac{\partial r p_{r\varphi}}{\partial r} + p_{r\varphi} \right) \quad (1.14.10)$$

Then taking 1.13.8 and 1.13.10 into account we can bring the Navier–Stokes equations to the form:

$$\frac{\partial w}{\partial t} = \nu \left(\frac{\partial^2 w}{\partial r^2} + \frac{1}{r} \frac{\partial w}{\partial r} - \frac{w}{r^2} \right) = \nu \frac{\partial}{\partial r} \left(\frac{\partial w}{\partial r} + \frac{w}{r} \right) = \nu \frac{\partial}{\partial r} \left(\frac{1}{r} \frac{\partial wr}{\partial r} \right) \quad (1.14.11)$$

In order to explain the meaning of the last formula, we will derive the components of the vortex $\vec{\omega}$ in a curvilinear coordinate system. Since their expressions in a local Cartesian coordinate system differ from 1.14.3 only by the sign between the terms, the algorithm of their derivation is the same as for ε_{ik} . We restrict ourselves to this example, for which we have

$$\omega_x = \omega = \frac{\partial w}{\partial r} + \frac{w}{r} = \frac{1}{r} \frac{\partial wr}{\partial r} \quad (1.14.12)$$

Then Equation 1.14.11 can be transformed to a somewhat specific form, frequently used in viscous hydrodynamics

$$\frac{\partial w}{\partial t} = \nu \frac{\partial \omega}{\partial r} \quad \text{or} \quad \frac{\partial \omega}{\partial t} = \frac{\nu}{r} \frac{\partial}{\partial r} \left(r \frac{\partial \omega}{\partial r} \right) \quad (1.14.13)$$

* We note that in Kochin et al. (1963) the general expressions for ε_{ik} were obtained by direct calculation of strains of fluid segments in a curvilinear coordinate system. In Sedov (1972) the same relations were derived using matrix and tensor transformations including other than orthogonal coordinate systems.

1.15 Turbulent Flows

The flow models considered in Section 1.14 were tacitly, or conventionally, assumed to be laminar (though it was not always necessary), that is, ordered and conserving the mutual position of the fluid (in the sense of Section 1.2) elementary, or small, as compared with the length scale L of the flow as a whole, particles with more or less smooth instantaneous spatial distributions (or “profiles”) of the mass-average flow parameters, dependent on neither the mode of choosing (“cutting”) these particles nor their dimensions. Moreover, the scale on which these profiles vary in time can be only the general gas dynamic time scale t_0 of the flow as a whole (for example, $t_0 \sim L/U$, U being the mean velocity of the flow). In these flows, the mass, momentum, and so on, exchange across fluid particle boundaries can take place on molecular level only.

However, under certain conditions, namely, for fairly high Reynolds numbers (e.g., at $Re > 10^3 - 10^6$, depending on the flow nature) laminar flows lose stability, so that the motion of elementary particles becomes chaotic, fluctuating, and always time dependent.

Experience shows that the dimensions of these fluctuating, or *turbulent* fluid particles can vary within wide limits; however, their mean size, or the turbulence scale l_t , is usually small compared with L , while the mean fluctuation time t_t is small compared with t_0 . Therefore, the instantaneous distributions of the mass-average parameters of turbulent particles is, first, dependent on their choice and, second, varies rapidly in time with the time scale t_t .

At the same time, the quantities l_t and t_t are much larger than typical distances and times of molecular interactions in liquids and gases; this means that the turbulent flow is a flow of a continuous medium, so that, according to present views, the detailed description of the turbulent flow structure is, in principle, quite possible within the framework of the Navier–Stokes equations.

However, actual solution of any practical problem on the basis of this model is as yet impossible owing to, first, extraordinary complexity (in view of the conditions $l_t \ll L$ and $t_t \ll t_0$) of these problems, which can be compared in this regard only with the problem of detailed description of chaotic molecular motion on microscopic level, and, second, the impossibility of specifying detailed initial and boundary conditions for these problems. Therefore, most of turbulence theories are based on the simplified, averaged *Reynolds turbulence model*, in accordance with which the chaotic motion of turbulent particles is, as it were, superimposed on the average, or main, flow whose parameters are averaged at each point over a time interval much larger than the fluctuation time scale, and, therefore, are independent of the latter. Precisely these average parameters are the main characteristics of turbulent flow, their spatial distributions being qualitatively similar to laminar ones, continuous, and, under certain conditions, even steady-state.

A possibility of this changeover from detailed to average description of the flow is based on the different orders of the length and time scales: $l_t \ll L$ and $t_t \ll t_0$; because of this, the exchange between separate fluid volumes Ω^* of the average flow, subject to the condition $L^3 \gg \Omega^* \gg l_t^3$, occurs due to the crossing of their boundaries by turbulent flows. This process is superficially similar to that of the intermolecular exchange described in Section 1.4 and can qualitatively be described using the same reasoning with separate molecules replaced by turbulent particles. This results in the same relations 1.10.10 between the *turbulent stress* and strain rate tensors, only with specific *turbulent viscosity* μ_t and *turbulent pressure* p_t substituted for molecular ones μ and p .

On the basis of this analogy, it is conventional to describe the turbulent flow model by the generalized laws 1.10.10

$$\begin{aligned} P^{(\Sigma)} &= P_\mu + P_t = -p_*^{(\Sigma)} E + 2\mu^{(\Sigma)} E_\varepsilon \\ \mu^{(\Sigma)} &= \mu + \mu_t, \quad p^{(\Sigma)} = p + p_t \\ p_*^{(\Sigma)} &= p^{(\Sigma)} + \frac{2}{3}\mu^{(\Sigma)} \operatorname{div} \mathbf{U} \end{aligned} \quad (1.15.1)$$

Here, P_μ and P_t are the molecular and turbulent stress tensors. Similarly, the law 1.10.11 for the total thermal flux takes the form:

$$\mathbf{J}^{(\Sigma)} = \mathbf{J}_\mu + \mathbf{J}_t = -\lambda^{(\Sigma)} \operatorname{grad} T, \quad \lambda^{(\Sigma)} = \lambda + \lambda_t \quad (1.15.2)$$

where λ_t is turbulent thermal conductivity. In these equations the strain rates ε_{ij} and the temperature gradient are determined in terms of the average velocities and temperature. However, as distinct from the molecular, purely thermodynamic parameters of a medium p , μ , and λ , the quantities p_t , μ_t , and λ_t are dependent on the flow structure; therefore, this model is in its essence mechanical or gas dynamic rather than rheological, in the exact meaning of this term. For the sake of brevity, we will term this turbulence model *pseudorheological*.

We note that the turbulent transport coefficients are usually much larger than the molecular ones, that is, $\mu_t \gg \mu$ and $\lambda_t \gg \lambda$; therefore, taking into account simultaneously molecular and turbulent transport processes, as has been done in the previous equations, is made rather for the sake of generality of the formulas and in order to be able to include, at least, purely formally, the transition from one regime to the other, than to reveal the nature of this process, since experimental verification of the postulated pseudorheological law 1.15.1 is rather poor precisely for the flow regimes in which $\mu_t \sim \mu$, $\lambda_t \sim \lambda$, and $p_t \sim p$.

The reason for generation of turbulence is dynamic instability of flows with large gradients of the flow parameters, which are usually due to the effect of viscosity (cf. Section 1.16). However, the turbulent stresses themselves are mainly caused by nonlinearity of the convective, that is, inviscid terms of the Euler equation. We will demonstrate this with respect to the example of two-dimensional incompressible Euler equations written in the conservation law form and the continuity equation

$$\begin{aligned} \frac{\partial u}{\partial t} + L(u) &= 0, \quad \frac{\partial v}{\partial t} + L(v) = 0 \\ L(f) &= \rho \frac{\partial uf}{\partial x} + \rho \frac{\partial vf}{\partial y} + \frac{\partial p}{\partial x}, \quad f = u, v \\ \frac{\partial u}{\partial x} + \frac{\partial v}{\partial y} &= 0 \end{aligned} \quad (1.15.3)$$

We represent the flow parameters φ as the sums of the mean steady-state quantities $\bar{\varphi}$ and the fluctuating time-dependent components φ'

$$\varphi = \bar{\varphi}(x, y) + \varphi'(t, x, y), \quad \varphi = u, v, p \quad (1.15.4)$$

Here, the bar means the averaging of a function over a time interval $\Delta t \gg t_t$, the mean of the fluctuating component being zero by definition.

Substituting these sums into Equation 1.15.3 and averaging we obtain the following equations

$$\begin{aligned} L(\bar{u}) &= -\frac{\partial \overline{\rho(u')^2}}{\partial x} - \frac{\partial \overline{\rho u' v'}}{\partial y} \\ L(\bar{v}) &= -\frac{\partial \overline{\rho u' v'}}{\partial x} - \frac{\partial \overline{\rho(v')^2}}{\partial y} \\ \frac{\partial \bar{u}}{\partial x} + \frac{\partial \bar{v}}{\partial y} &= 0 \end{aligned} \quad (1.15.5)$$

The operators $L(\bar{u})$ and $L(\bar{v})$ contain mean values only, while the terms obtained by averaging the products of velocity fluctuations represent the *turbulent stresses*

$$p_{xx} = -\overline{(\rho(u')^2)}, \quad p_{yy} = -\overline{(\rho(v')^2)}, \quad p_{xy} = p_{yx} = -\overline{(\rho u' v')} \quad (1.15.6)$$

The changeover from these relations to the pseudorheological model 1.15.1 is made using some additional hypotheses based, as noted previously, on the analogy with the molecular rheological model.

However, at this point the formulation of the turbulence model is not completed, since the functions μ_t and p_t of the model are as yet unknown. Their definition requires some additional hypotheses and reasoning; we shall revert to this question in Chapter 12.

1.16 Viscous and Inviscid Flow Models

Obviously, all fluids, that is, gases and liquids, possess some dissipative properties, such as viscosity, thermal conductivity, and diffusion; therefore, it might seem that the flows of these media can reliably be described only within the framework of the Navier–Stokes equations, either conventional or generalized. Nevertheless, the theory of inviscid flows in which dissipative effects in gases and liquids are neglected, while the Navier–Stokes equations are reduced to the Euler equations, turns out to be rather fruitful.

A possibility of this changeover from the more general viscous flow model to a particular or “simplified” inviscid model, can be substantiated, at least, on a preliminary level, by making recourse to the following reasoning. In Section 1.12 we have shown with reference to the example of one-dimensional flow that the relative role of the dissipative terms is determined by the Reynolds number $Re = \rho U_\infty L / \mu$ and is of the order Re^{-1} provided that the length scale L and the velocity U_∞ determine the orders of the derivatives of the flow parameters (cf. estimates 1.12.10 and 1.12.11).

We will now consider this question in more detail with reference to the Navier–Stokes equations for incompressible fluids (1.10.12). It is assumed that the derivatives entering in these equations are of the orders

$$\begin{aligned} \frac{\partial U_i}{\partial l_j} &\sim \frac{U_\infty}{L}, & \frac{\partial^2 U_i}{\partial l_j \partial l_k} &\sim \frac{U_\infty}{L^2} \\ U_i &= u, v, w; & l_j, l_k &= x, y, z \end{aligned} \quad (1.16.1)$$

The order of the derivatives of the pressure is determined from these equations in terms of the orders of the convective (the left side of the equations) and dissipative (the right side)

terms and, because of this, is not written here. In dimensionless variables 1.12.2 and 1.12.3, Equation 1.10.12 takes the form:

$$u' \frac{\partial u'}{\partial x'} + v' \frac{\partial u'}{\partial y'} = - \frac{\partial p'}{\partial x'} + \frac{1}{Re} \left(\frac{\partial^2 u'}{\partial x'^2} + \frac{\partial^2 u'}{\partial y'^2} \right) \quad (1.16.2)$$

Equation 1.10.12 is written down similarly.

In this equation all the derivatives are now of the order of unity or, using another terminology, of the *normal* order; therefore, the order of the dissipative terms in relation to that of the convective terms is Re^{-1} . In the problems of aerodynamics and, more generally, high-speed gas dynamics, the Reynolds number is rather large. Thus, in accordance with Figure 1.1, for a body with the dimension $L = 1$ m at $U_\infty = 7 \cdot 10^3$ m/s, we have $Re > 10^3$ already at flight altitudes $H < 90$ km, while under ground conditions the Reynolds number is $Re \sim 10^5$ even for $U_\infty \approx 1$ m/s. Thus, for $Re \gg 1$ the right-hand side of Equation 1.16.2 can be omitted with the result that this equation transforms into one of the Euler equations; it might seem that this substantiates the adequacy of the inviscid flow model.

However, this approach faces an obstacle of fundamental nature, which will be considered with reference to the example of the longitudinal (along the x axis, as in Figure 1.26) incompressible flow over a zero-thickness flat plate. In the inviscid formulation, the plate does not introduce any disturbances into the flow, since the constant solution $u' = 1, v' = 0$, and so on, satisfies both the Euler equations and the impermeability condition ($v' = 0$) on the plate surface. Contrariwise, the solution of this type cannot satisfy the no-slip condition $u' = v' = 0$, which is imposed on the plate surface in viscous fluid and gas flows. Therefore, in a vicinity of the plate surface there exists a region, or a *boundary layer*, of thickness δ , in which the velocity varies by a quantity of the order U_∞ and viscosity plays the crucial role. In this layer, the viscous terms on the right-hand side of Equation 1.16.1 must be of the same order as the convective terms on the left-hand side; this is possible only if the orders of the derivatives with respect to y are much larger than those of the derivatives with respect to x , which, as earlier, are determined by the plate length L .

In other words, we should put

$$\frac{\partial u}{\partial y} \sim \frac{U_\infty}{\delta} \gg \frac{\partial u}{\partial x} \sim \frac{U_\infty}{L}, \quad \frac{\partial^2 u}{\partial y^2} \sim \frac{U_\infty}{\delta^2} \gg \frac{\partial^2 u}{\partial x^2} \sim \frac{U_\infty}{L^2} \quad (1.16.3)$$

From the continuity equation for an incompressible fluid there follows:

$$\frac{\partial v}{\partial y} = - \frac{\partial u}{\partial x}, \quad v \sim \delta \frac{\partial u}{\partial x} \sim U_\infty \frac{\delta}{L} \quad (1.16.4)$$

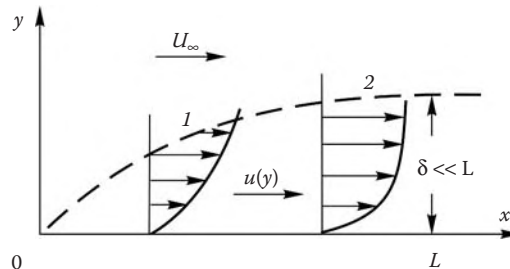


FIGURE 1.26
Flow in the laminar (1) and turbulent (2) boundary layers.

Then, equating the orders of the convective and viscous terms of the equations

$$u \frac{\partial u}{\partial x} + v \frac{\partial u}{\partial y} \sim \frac{U_\infty^2}{L} \sim v \frac{\partial^2 u}{\partial y^2} \sim v \frac{U_\infty}{\delta^2} \quad (1.16.5)$$

we obtain the following estimate for the boundary layer thickness

$$\delta \sim L Re^{-1/2} \quad (1.16.6)$$

A more accurate estimate for the laminar flat-plate boundary layer thickness ($\delta \approx 5L Re^{-1/2}$) will be derived in Chapter 12.

A similar reasoning could be made for a turbulent boundary layer, which is usually formed at the Reynolds numbers $Re \geq 10^5 - 10^6$, by substituting the turbulent viscosity μ_t for the molecular viscosity μ . However, the former turns out to be dependent on the thickness δ , which leads to an experimentally obtained relation $\delta/L \approx 0.38 Re^{-0.2}$, the ratio δ/L being fairly small in this case as well.

Thus, at high Reynolds numbers the relative boundary layer thickness is small, $\delta/L \ll 1$, which makes it possible to introduce a model for studying high-Re flows in which viscosity is taken into account as a *secondary* factor; in this model, the flows are described in the first stage within the framework of the inviscid theory with the impermeability condition imposed on solid surfaces; in the subsequent stage, the flow parameter distributions over the solid surface obtained in the first stage are used as the boundary conditions on the outer edge of the boundary layer.

This result, fundamental for gas and fluid mechanics, gave rise to a vast and very fruitful division of this theory, namely, theory of inviscid gas and fluid flows. The following 10 chapters of the book are devoted to precisely these flows. As for viscous flows, these will be touched on in Chapters 12 and 13, in which the model formulated previously will be substantiated more rigorously. It will be also shown that an exception from this model is furnished by separation flows (see, e.g., Figure 1.23), viscosity playing the crucial role in the development of these flows.

2

Inviscid Gas Dynamics: General Issues and Simple Solutions

In this chapter the general concepts and theorems of conventional inviscid gas dynamics are outlined for the case of a two-parameter gas. Basic properties of subsonic, transonic, and supersonic gas flows (as well as fundamental distinctions of the equations describing these types of flows) are illustrated with reference to typical problems regarding an analytical treatment. These are steady one-dimensional flows, flows past slender bodies (within the framework of the linear theory), and certain exact solutions of incompressible hydrodynamics. Incidentally, these problems are of their own value from the theoretical point of view and can be important in engineering.

A more detailed presentation of the issues discussed in this chapter, can be found in the books of Liepmann and Roshko (1957), von Mises (1958), Chernyi (1987), as well as in those cited in the introduction to Chapter 1.

2.1 Stream Function, Potential, and Vortex

The definition of streamlines (Equation 1.8.2) and stream surfaces in steady flows was given in Section 1.8. Specifying stream surfaces in the general form, $\Psi(x, y, z) = 0$, we can define normals \mathbf{n} to them from formulas 1.11.4. These normals are orthogonal to both the velocity \mathbf{U} and streamlines, which leads to the equation

$$u \frac{\partial \Psi}{\partial x} + v \frac{\partial \Psi}{\partial y} + w \frac{\partial \Psi}{\partial z} = 0 \quad (2.1.1)$$

Here, as earlier, x, y, z is a Cartesian coordinate system and u, v , and w are the velocity vector projections onto the axes. Obviously, a whole set of stream surfaces passing through various generators (AB in Figure 1.17a) can be drawn through any streamline.

We note that, in accordance with the terminology of partial differential equation theory, *streamlines are characteristics* of Equation 2.1.1 (see also Chapter 4).

For plane flows, which are independent of z and have $w = 0$, Equation 2.1.1 gives a streamline that is the intersection of a physical stream surface by the flow plane $z = 0$. In an axisymmetric flow, which is independent of the meridional angle φ and has the peripheral velocity $w = 0$ (Section 1.13) a stream tube coaxial with the axis of symmetry x is also defined by Equation 2.1.1 with $w = 0$ and y replaced by r . In this case a stream function ψ can be introduced as follows:

$$\frac{\partial \psi}{\partial x} = -C\rho vr^v, \quad \frac{\partial \psi}{\partial r} = C\rho ur^v \quad (2.1.2)$$

Here, $v = 1$ corresponds to axisymmetric flows, while $v = 0$ corresponds to plane ones, with r replaced by y . These relations automatically obey the steady ($\frac{\partial}{\partial t} = 0$) continuity Equation 1.3.12 on any solution and to Equation 2.1.1 with $w = 0$ and $y = r$, while the stream function ψ is constant on streamlines of two-dimensional flows.

The difference between the values of the stream function at two points of a flowfield determines the gas *flow rate* between them (between two concentric circles for $\nu = 1$). According to Figure 2.1 we have

$$(2\pi r)^\nu (\rho u \Delta y - \rho v \Delta x) = \frac{(2\pi)^\nu}{C} \Delta \psi \quad (2.1.3)$$

Putting $C = (2\pi)^\nu$ and integrating over a distance between two arbitrary points we obtain the required result.

In one-dimensional unsteady flows, which depend on t and r only, a counterpart of the stream function is the *mass function* $m(t, r) = \text{const}$ satisfying the continuity Equation 1.13.16 and subject to the conditions

$$\begin{aligned} \frac{\partial m}{\partial t} &= -C \rho v r^\nu, & \frac{\partial m}{\partial r} &= C \rho r^\nu \\ C &= (2\pi)^\nu \quad (\nu = 0 \text{ and } 1), & C &= 4\pi \quad (\nu = 2) \end{aligned} \quad (2.1.4)$$

The mass of the gas between points 1 and 2 is equal to Δm .

2.1.1 Curl and Velocity Circulation

The concept of the curl was introduced in Section 1.8 from purely kinematic considerations in a Cartesian coordinate system. Here, a more general definition of this operator will be given and some of its properties will be analyzed. For this purpose, we will first define the velocity circulation (and, in general, the circulation of any vector) as follows:

$$\Gamma_L = \int_L \mathbf{U} \cdot d\mathbf{L} \quad (2.1.5)$$

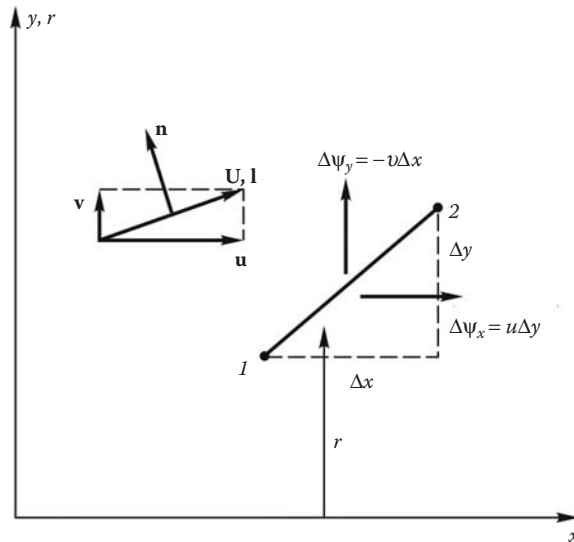


FIGURE 2.1

On the definition of the flow rate between two points in a flow.

Here, the integration is performed over a segment L of a curve with a vector differential $d\mathbf{L}$.

We will present two fundamental theorems of hydrodynamics.

Stokes theorem: *The circulation of a vector along a closed contour is equal to the flux of the curl of this vector through any surface Σ with the normal \mathbf{n} spanned on the contour*

$$\Gamma = \oint_L \mathbf{U} \cdot d\mathbf{L} = \int_{\Sigma} \omega_n d\Sigma, \quad \omega_n = \vec{\omega} \cdot \mathbf{n}, \quad \vec{\omega} = \operatorname{curl} \mathbf{U} \quad (2.1.6)$$

Since this theorem requires coordination of the directions of the vectors $d\mathbf{L}$ and \mathbf{n} , we, without considering the general case, will follow the right-hand rule for plane contours L and surfaces Σ , that is, go round the contour clockwise viewing along the normal \mathbf{n} directed usually (if otherwise not stated) along one of the coordinate axes. This is the general theorem of vector calculus rather than only hydrodynamics; here, it is presented without proof.

Tomson (Kelvin) theorem: *For a barotropic fluid, that is, a fluid with the equation of state $\rho = \rho(p)$, the circulation Γ^* along a closed fluid contour L^* is time-independent.*

To prove the theorem, we will calculate the time derivative $d\Gamma^*/dt$. Separating out a small fluid element $\Delta \vec{L}^* = \Delta \vec{r}^*$, where \vec{r}^* is the radius-vector (with an arbitrary pole) of the points of the curve L^* we obtain

$$\frac{d}{dt} \vec{U} \cdot \Delta \vec{L}^* = \Delta \vec{L}^* \frac{d\vec{U}}{dt} + \vec{U} \frac{d}{dt} \Delta \vec{r}^*$$

(For details see Loytsianskii, 1970).

At the same time, we have

$$\vec{U} \frac{d}{dt} \Delta \vec{r}^* = \vec{U} (\Delta \vec{U}) = \vec{U} \frac{\partial \vec{L}}{\partial L} \Delta L = \frac{1}{2} \frac{\partial U^2}{\partial L} \Delta L$$

Since the integral of $\partial U^2 / \partial L$ over a closed contour is zero, in view of 1.9.2 and 1.8.16 we obtain

$$\frac{d\Gamma^*}{dt} = \oint_{L^*} \frac{d\mathbf{U}}{dt} d\mathbf{L}^* = - \oint_{L^*} \frac{1}{\rho} \frac{dp}{dL} dL^* \quad (2.1.7)$$

In a barotropic fluid the quantity $\rho^{-1} dp$ is a total differential, so that in this case the integral on the right-hand side is zero; otherwise, the theorem does not hold.

It follows from these two theorems that if at any zero moment vortices are absent from any fluid volume of a barotropic gas flow, then the flow remains irrotational. Thus, if an incident flow is irrotational ($\omega = 0$), it is irrotational everywhere downstream.

Thus, *vortices in a gas flow can be generated by its nonbarotropic character*.

To make the point clear, let us express the vortex in steady two-dimensional (plane or axisymmetric) flows in terms of characteristic flow parameters. To do this, we shall use definition 1.8.7 and let $\partial/\partial t = 0$ in 1.9.11; thus we obtain the *Gromeka-Lamb equations*

$$\begin{aligned} \frac{1}{2} \frac{\partial U^2}{\partial x} - v\omega &= -\frac{1}{\rho} \frac{\partial p}{\partial x}, & \frac{1}{2} \frac{\partial U^2}{\partial r} + u\omega &= -\frac{1}{\rho} \frac{\partial p}{\partial r} \\ \omega &= \omega_z = \frac{\partial v}{\partial x} - \frac{\partial u}{\partial y} \end{aligned} \quad (2.1.8)$$

In accordance with 1.8.7, other components of the vortex are zero. Multiplying the equations by u and v , respectively, and subtracting one from the other we obtain equations involving derivatives with respect to normals \mathbf{n} to streamlines, their projections onto the x and r axes being $-v/U$ and u/U

$$U\omega = -\frac{1}{\rho} \frac{\partial p}{\partial n} - \frac{1}{2} \frac{\partial U^2}{\partial n} = -\frac{\partial H}{\partial n} + \frac{\partial h}{\partial n} - \frac{1}{\rho} \frac{\partial p}{\partial n}, \quad H = \frac{1}{2} U^2 + h \quad (2.1.9)$$

Here, H is the *total enthalpy* introduced in Section 1.7. Using Equation 1.5.5 for equilibrium two-parameter equation of state and passing to the stream function $d\psi = (2\pi r)^v \rho U dn$ we obtain the formula

$$\omega = (2\pi r)^v \rho \left(T \frac{\partial s}{\partial \psi} - \frac{\partial H}{\partial \psi} \right) \quad (2.1.10)$$

In what follows we shall demonstrate that, though in the majority of flows the enthalpy H is constant throughout the flow, the entropy is nonuniformly distributed in streamlines and $\omega \neq 0$ —more so in the case of nonequilibrium flows, for which relation 1.5.5 is not valid at all.

2.1.2 Velocity Potential

We are now coming to the class of *irrotational* flows with $\omega = 0$ including many subsonic or weakly perturbed supersonic flows, nozzle flows, and so on.

For irrotational flows a *velocity potential* $\Phi(t, x, y, z)$ can be introduced, such that

$$\mathbf{U} = \nabla \Phi = \text{grad} \Phi, \quad u = \frac{\partial \Phi}{\partial x}, \quad v = \frac{\partial \Phi}{\partial y}, \quad w = \frac{\partial \Phi}{\partial z} \quad (2.1.11)$$

It is easy to verify that the condition $\vec{\omega} = \text{curl} \mathbf{U} = 0$ is satisfied.

To conclude, we will present, as an example, the expressions for the potentials of simple incompressible flows ($\rho = \text{const}$) with axial ($v = 1$) and spherical ($v = 2$) symmetry. Introducing at each point a local Cartesian coordinate system (x, y, z) (instead of x, r, φ for $v = 1$ and r, θ, φ for $v = 2$; see Section 1.13 and Figure 1.24) we can bring expression 2.1.11 to the form:

$$v_r = \frac{\partial \Phi}{\partial r}, \quad v_\varphi = \frac{1}{r(\sin\theta)^{v-1}} \frac{\partial \Phi}{\partial \varphi}, \quad v_\theta = \frac{1}{r} \frac{\partial \Phi}{\partial \theta} \quad (2.1.12)$$

Let a source with a flow rate $G = c\rho v_r r^v$ be located at the origin $r = 0$; the source generates a flow with axial ($c = 2\pi$) or spherical ($c = 4\pi$) symmetry. In this case all the peripheral velocities and derivatives vanish, so that we can write the following formulas for the potential

$$\Phi = \frac{G}{2\pi\rho} \ln r \quad (v = 1); \quad \Phi = \frac{G}{4\pi\rho} \frac{1}{r} \quad (v = 2) \quad (2.1.13)$$

Consider a *vortex line* at the point $r = 0$. In the absence of vortices and for $r > 0$ the circulation along any contour enclosing the vortex line is constant on coaxial circles, $\Gamma = 2\pi v_\varphi r$, while the velocity $v_r = 0$ everywhere. The corresponding potential is $\Phi = (\Gamma/2\pi)\varphi$. The multivalence of this expression is not important, since only derivatives of the potential enter in the final expressions.

In conclusion, we will touch upon the question of the coordinate systems used in gas dynamics. Almost always conventional, that is, spatial coordinate systems are used. However, sometimes it is the *Lagrangian coordinates* (or variables) that turn out to be more

convenient; these are fitted to fixed fluid particles and are, therefore, constant along their trajectories. In this case, the independent variables in the general, time-dependent problem are the spatial coordinates (x_0, y_0, z_0) of these particles at the initial moment. In this formulation the spatial coordinates (x, y, z) are the functions of the Lagrangian coordinates and time. In stationary flows the role of time is played by the distance along the streamlines or, more generally, a streamwise x coordinate, while the Lagrangian variables are the coordinates (y_0, z_0) of these streamlines in a certain initial section $x = x_0$. In two-dimensional problems the stream function ψ and the mass function m introduced previously are usually used as Lagrangian variables. As for the equation for the r coordinate in the variables (x, ψ) or (t, m) , it is obtained by the reversion of the corresponding derivatives of ψ or m with respect to r 2.1.2 and 2.1.4.

2.2 Integrals of Gas Dynamic Equations

The differential equations of gas dynamics derived in Section 1.9 have an integral for the particular case of adiabatic equilibrium flows, namely, the constancy of the entropy, $s = \text{const}$, along particle trajectories (cf. Section 1.5). Moreover, in certain cases the equations have additional integrals, namely, the *Bernoulli integral* for adiabatic, though not necessarily equilibrium, steady flows and the *Lagrange integral* for time-dependent potential flows. In what follows we present the derivation of these relations, together with the anticipatory derivation of very useful equations of motion along and normal to streamlines.

We will represent the velocity vector in the form $\mathbf{U} = U\mathbf{l}$, where \mathbf{l} is the unit vector, and transform Equation 1.9.2 to the form:

$$\frac{d\mathbf{U}}{dt} = \mathbf{l} \frac{dU}{dt} + U \frac{d\mathbf{l}}{dt} = -\frac{1}{\rho} \text{grad} p \quad (2.2.1)$$

On the other hand, introducing at each point a local coordinate system with the $x = l$ axis aligned with the instantaneous direction of \mathbf{l} or \mathbf{U} , we obtain an expression for the substantive derivative 1.8.3

$$\frac{d}{dt} = \frac{\partial}{\partial t} + U \frac{\partial}{\partial l} \quad (2.2.2)$$

where dl is the arc differential of a particle trajectory.

Multiplying Equation 2.2.1 by \mathbf{l} scalarly and taking into account that an increment Δl of the unit vector \mathbf{l} is orthogonal to this vector we obtain the equation of motion projected onto the particle trajectory

$$\frac{dU}{dt} = \frac{\partial U}{\partial t} + U \frac{\partial U}{\partial l} = -\frac{1}{\rho} (\mathbf{l} \cdot \vec{\nabla} p) = -\frac{1}{\rho} \frac{\partial p}{\partial l} = -\frac{\partial h}{\partial l} + \frac{q}{U} \quad (2.2.3)$$

The last equality follows from the first law of thermodynamics.

The equation projected onto the normal to the trajectory is obtained by multiplying Equation 2.2.1 by an arbitrary vector \mathbf{n} normal to \mathbf{l}

$$\mathbf{n} \cdot \frac{d\mathbf{U}}{dt} = U \left(\mathbf{n} \cdot \frac{d\mathbf{l}}{dt} \right) = U \left(\mathbf{n} \cdot \frac{\partial \mathbf{l}}{\partial t} \right) + U^2 \left(\mathbf{n} \cdot \frac{\partial \mathbf{l}}{\partial l} \right) = -\frac{1}{\rho} \frac{\partial p}{\partial n} \quad (2.2.4)$$

Let \mathbf{n} be the principal normal to the trajectory in its osculating plane in which the vectors \mathbf{l} and $\partial\mathbf{l}/\partial t$ lie. Together with \mathbf{l} , the normal \mathbf{n} forms a right Cartesian coordinate system. Then $\partial\mathbf{l}/\partial t = -\mathbf{n}/R$, where R is the radius of curvature of the trajectory, positive for a convex (in the direction of \mathbf{n}) trajectory and negative for a concave one. In this case, the transverse pressure gradient is

$$\frac{\partial p}{\partial n} = -\rho U \left(\mathbf{n} \cdot \frac{\partial \mathbf{l}}{\partial t} \right) + \frac{\rho U^2}{R} \quad (2.2.5)$$

The second term on the right-hand side represents the contribution of centrifugal forces due to trajectory curvature, while the first one is the contribution of an unsteady component of the normal acceleration.

For steady-state flows the pressure derivative taken along the principal normal can be written as follows:

$$\frac{\partial p}{\partial n} = \frac{\rho U^2}{R} = -\rho U^2 \frac{\partial \theta}{\partial l} \quad (2.2.6)$$

Here, $\theta(l)$ is the slope of a streamline in the osculating plane.

Along the binormal \mathbf{b} to the trajectory (i.e., to the osculating plane) Equation 2.2.4 takes the form:

$$\frac{\partial p}{\partial b} = -\rho U \left(\mathbf{b} \cdot \frac{\partial \mathbf{l}}{\partial t} \right) \quad (2.2.7)$$

For steady-state flows the derivative in this direction is zero.

Equation 2.2.3 is used to obtain very important integrals of the equations of motion, which can be derived in two particular cases.

2.2.1 Steady-State Adiabatic Flows

It follows from 2.2.3 that for steady-state flows

$$\frac{dH}{dl} = \frac{q}{U}, \quad H = \frac{U^2}{2} + h \quad (2.2.8)$$

The total enthalpy H is termed the *stagnation enthalpy*, since $h = H$ for $U = 0$. For adiabatic flows the total enthalpy is constant along streamlines; thus, along streamlines the following *Bernoulli integral* holds

$$\frac{U^2}{2} + h = H = \frac{U_m^2}{2} = \text{const} \quad (2.2.9)$$

Here, U_m is the maximum velocity of gas expansion into a vacuum in the case in which $h \rightarrow 0$ simultaneously with $p \rightarrow 0$; this is always the case for equilibrium flows and often for some other flows; we shall meet with another situation in Section 11.11.

It is important to emphasize that in deriving integral 2.2.9 neither an equation of state nor additional information on gas properties was used, so that the equation is valid for adiabatic flows of any gas irrespective of the character (equilibrium or nonequilibrium) of physical-chemical processes occurring in the gas.

It follows from 2.2.3 that for flows with near-constant density the relation $(H - h)\rho = p_0 - p$ holds, so that instead of 2.2.9 we obtain

$$\frac{U^2}{2} + \frac{p}{\rho} = \frac{p_0}{\rho}, \quad \rho, p_0 = \text{const} \quad (2.2.10)$$

Along with H , the *stagnation pressure* p_0 is constant along streamlines. Historically, it is Equation 2.2.10 that was called the *Bernoulli equation*; afterwards this term was used for the more general integral 2.2.9.

Since in plane and axisymmetric flows a streamline is uniquely characterized by the stream function value on it, the dependences for H and p_0 can be written in the form $H = H(\psi)$ and $p_0 = p_0(\psi)$. For a uniform flow past a body the stagnation enthalpy is constant throughout the entire flow region and is continuous even across *shock waves* (see 1.7.12). In equilibrium adiabatic flows the entropy of a particle is conserved and therefore $s = s(\psi)$. Such flows are called *isentropic* or *uniformly isentropic* if the entropy is the same throughout the flow.

2.2.2 Potential Adiabatic Flows of Barotropic Gases

In this case $\mathbf{U} = \text{grad}\Phi$ and $U = \partial\Phi/\partial l$; therefore, integrating 2.2.3 with respect to l yields an integral that is called the *Lagrange integral*

$$\frac{\partial\Phi}{\partial t} + \frac{1}{2}U^2 + h = C(t) \quad (2.2.11)$$

The function $C(t)$ is determined by the flow parameters specified at a certain point of the flow. For bodies moving in a fluid, quiescent at infinity with the parameters h_∞ and so on, we have $C = h_\infty$. For steady flows the Lagrange integral transforms to the Bernoulli equation with $C = H$.

From the Bernoulli equation for perfect (or quasiperfect) gases, we can obtain some useful formulas relating the flow parameters along streamlines. In this case $(\gamma - 1)h = a^2$ and, hence,

$$H = h + \frac{1}{2}U^2 = \frac{a^2}{\gamma - 1} + \frac{1}{2}U^2 = \frac{1}{2}U_m^2 = \frac{a_0^2}{\gamma - 1} = \frac{1}{2}\frac{\gamma + 1}{\gamma - 1}a_*^2 \quad (2.2.12)$$

Here, a_0 is the speed of sound at the stagnation point ($U = 0$), while a_* is the *critical speed of sound*, that is the speed of sound at the sonic point at which $U = a$. Hence it follows

$$\frac{H}{h} = \frac{T_0}{T} = 1 + \frac{U^2}{2h} = 1 + \frac{\gamma - 1}{2}M^2, \quad M = \frac{U}{a} \quad (2.2.13)$$

Using 1.5.9 and 2.2.13 we obtain the formulas

$$\frac{p_0}{p} = \left(\frac{\rho_0}{\rho}\right)^\gamma = \left(\frac{T_0}{T}\right)^{\frac{\gamma}{\gamma-1}} = \left(1 + \frac{\gamma - 1}{2}M^2\right)^{\frac{\gamma}{\gamma-1}} \quad (2.2.14)$$

Here, p_0 and ρ_0 are the pressure and the density at the isentropic stagnation point. For small M formulas 2.2.14 take their limiting forms

$$\frac{p_0}{p} = 1 + \frac{1}{2}\gamma M^2, \quad \frac{\rho_0}{\rho} = 1 + \frac{1}{2}M^2 \quad (2.2.15)$$

All these curves are presented in Figure 2.2.

At high M the pressure decreases sharply, as

$$\frac{p}{p_0} = \left[(\gamma - 1)\frac{M^2}{2}\right]^{\gamma/(1-\gamma)} \quad (2.2.16)$$

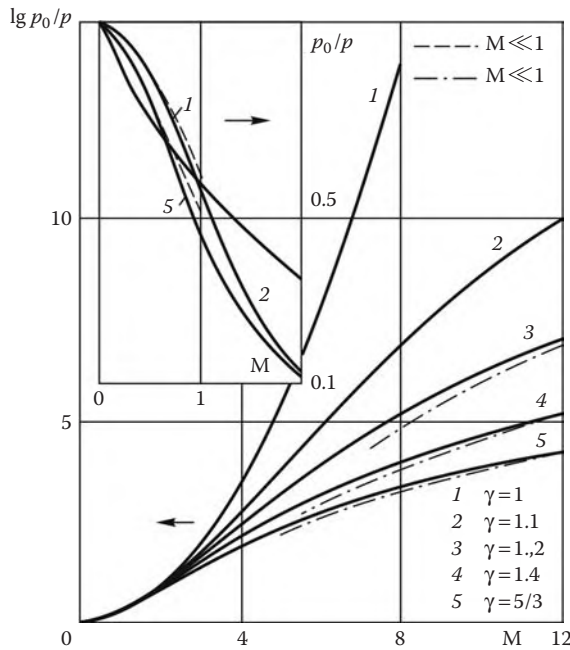


FIGURE 2.2
Mach number dependence of the pressure at a constant entropy.

At the sonic point ($M = 1$) the pressure p_* and the density ρ_* depend on γ only slightly; thus, for γ ranging from $5/3$ to 1 the pressure ratio p_*/p_0 varies from 0.487 to 0.605 (0.528 for $\gamma = 1.4$).

As $\gamma \rightarrow 1$, it follows from 2.2.14 that

$$\frac{p}{p_0} = \frac{\rho}{\rho_0} = e^{-M^2/2} \quad (2.2.17)$$

Formulas 2.2.12 to 2.2.16 can be generalized to the case of constant γ_* and γ_e introduced in Chapter 1 by Equations 1.3.8 and 1.6.11. Making the substitutions $\rho a^2 = \gamma_e p$ and $\gamma_e(\gamma_* - 1)h = \gamma_* a^2$ we reduce this generalization to the replacement of γ by γ_* , with the factor γ/γ_* appearing as a coefficient of M^2 .

In addition to other numerous applications, formulas 2.2.13 and 2.2.14 provide a basis for the gas dynamic diagnosis of flows in both bench and full-scale conditions. In fact, measuring pressures p_0 and p_∞ in the undisturbed flow we can easily determine the Mach number M_∞ , while measuring the stagnation temperature T_0 we can obtain T_∞ , a_∞ , and, hence, the flow velocity U_∞ . The pressure p_0 is measured at the forward stagnation point of a blunt body, for example, a long blunt-nosed cylinder (the Pitot probe), while the static pressure is measured on the body surface at a point where the pressure is equal to that in the undisturbed flow, for example, at the lateral surface of the probe at a distance of a few diameters from the nose (for subsonic velocities). However, for supersonic flows formula 2.2.14 is no longer applicable (the situation will be considered in Section 3.6).

We will consider some other properties of steady adiabatic flows. In a perfect gas the speed of sound in isentropic processes increases with the pressure as $a^2 \sim p^{(\gamma-1)/\gamma}$;

therefore, according to 2.2.12, one of the two inequalities

$$M < 1, \quad U < a_* < a; \quad M > 1, \quad U > a_* > a \quad (2.2.18)$$

always holds in steady flows. Moreover, these inequalities are valid for all gases for which the condition $(\partial a^2 / \partial p)_s > 0$ is satisfied (see Section 1.6), since a increases with the pressure, while U decreases by virtue of the relation $\rho U dU = -dp$.

For transonic flows ($U \approx a$) using the expansions

$$\frac{1}{2} \rho_* (U^2 - a_*^2) = p_* - p, \quad a^2 - a_*^2 = (p - p_*) \left(\frac{\partial a^2}{\partial p} \right)_s \quad (2.2.19)$$

we obtain the relation

$$\begin{aligned} 1 - M^2 &= 2A_* \frac{p - p_*}{\rho_* a_*^2} = 2A_* \left(1 - \frac{U}{a_*} \right) \\ A_* &= \left[1 + \frac{1}{2} \rho \left(\frac{\partial a^2}{\partial p} \right)_s \right]_{p=p_*} = \frac{\gamma + 1}{2} \end{aligned} \quad (2.2.20)$$

which will be useful in what follows. The latter equality is written for a perfect gas. According to Section 1.6, for all gases $A > 0$.

However, all these relations are valid only either along a streamline on which the entropy is constant or in the vicinity of a sonic line in a uniform isentropic flow. In the more general case of nonisentropic flow with different entropy values on different streamlines (but, naturally, with the same total enthalpy H) the generalization of these expansions in the vicinity of a sonic point with parameters p_* , s_* , and so on gives the following result

$$\begin{aligned} a_*^2 (M^2 - 1) &= U^2 - a^2 = 2(h_* - h) + (a_*^2 - a^2) = \\ &\quad - \frac{2}{\rho_*} A_* (p - p_*) - BT_* (s - s_*) \\ BT_* &= 2 \left(\frac{\partial h}{\partial s} \right)_p + \left(\frac{\partial a^2}{\partial s} \right)_p, \quad \left(\frac{\partial h}{\partial s} \right)_p = T \end{aligned} \quad (2.2.21)$$

For a perfect gas $a^2 = (\gamma - 1)h$ and $B = 3 + \gamma$. One more result can be obtained for a sonic point. Precisely at this point on a given streamline the *flow rate per unit area* ρu is maximum. This follows from the relation

$$d\rho u = \rho (1 - M^2) du \quad (2.2.22)$$

This question will be discussed in detail in the following section.

In conclusion, we will mention one more parameter used in gas dynamics, in particular, in one-dimensional flows. This is the *velocity coefficient* $\lambda = U/a_*$. According to 2.2.18, $\lambda \geq 1$ in supersonic and $\lambda \leq 1$ in subsonic flows, but it is bounded as $M \rightarrow \infty$. For a perfect gas

$$\lambda^2 = \frac{U^2}{a_*^2} = \frac{\gamma + 1}{\gamma - 1} \frac{U^2}{U_m^2} = \frac{\gamma + 1}{2} M^2 \left(1 + \frac{\gamma - 1}{2} M^2 \right)^{-1} \rightarrow \frac{\gamma + 1}{\gamma - 1} \quad \text{as } M \rightarrow \infty \quad (2.2.23)$$

2.3 One-Dimensional Stationary Flows

We will now consider steady-state flows in channels, so narrow (or, perhaps, so extended) and of so smooth shape, that the transverse nonuniformity of the channel flow parameters could be neglected and the variation along only the longitudinal coordinate, possibly, curvilinear, should be taken into account. This formulation of the problem is called *hydraulic* and is frequently used for describing flows in gas ducts of all kinds, such as jet engines, wind tunnels, and so on.

2.3.1 General Equations and Role of the Mach Number

The condition of the flow rate constancy across a channel can be written in the form:

$$\rho u \sigma = G = \text{const}, \quad u > 0 \quad (2.3.1)$$

Here, $\sigma(x)$ is the cross-sectional area, while ρ and u are the average density and velocity, respectively. Differentiating this equation and writing the equations of motion and energy along the channel axis we obtain the system of governing equations

$$\begin{aligned} \frac{1}{\rho} \frac{d\rho}{dx} + \frac{1}{u} \frac{du}{dx} &= -\frac{1}{\sigma} \frac{d\sigma}{dx}, & u \frac{du}{dx} &= -\frac{1}{\rho} \frac{dp}{dx}, \\ \frac{dh}{dx} - \frac{1}{\rho} \frac{dp}{dx} &= \frac{q}{u} = \frac{dH}{dx}, & H &= h + \frac{u^2}{2} \end{aligned} \quad (2.3.2)$$

Here, q is the heat transfer rate per unit mass. To close the system, we write the differential pressure-density relation 1.6.8, which is equivalent to the equation of state for equilibrium flows (for now we will assume the flow to be equilibrium)

$$\frac{d\rho}{dt} = u \frac{d\rho}{dx} = \frac{u}{a^2} \frac{dp}{dx} + \rho Q_e, \quad Q_e = \left(\frac{\partial \rho}{\partial h} \right)_p \frac{q}{\rho} \quad (2.3.3)$$

Here, the speed of sound is equal to the equilibrium one, $a = a_e$.

Combining these equations we obtain the basic equation in the form:

$$(1 - M^2) \frac{du}{dx} = Q_{\text{eff}} = -Q_e - \frac{u}{\sigma} \frac{d\sigma}{dx} \quad (2.3.4)$$

At the end of this section we shall consider some other effects, such as friction and mass transfer. However, they change only the form of the source term Q_{eff} . The equation makes it possible to draw certain quite general conclusions that will be later applied to particular flows.

The distinctive features of a solution of Equation 2.3.4 are determined by joint effect of the parameters M and Q_{eff} , in accordance with the inequalities

$$\begin{aligned} Q_{\text{eff}} > 0, \quad \frac{du}{dx} > 0, \quad M < 1; \quad \frac{du}{dx} < 0, \quad M > 1 \\ Q_{\text{eff}} < 0, \quad \frac{du}{dx} < 0, \quad M < 1; \quad \frac{du}{dx} > 0, \quad M > 1 \end{aligned} \quad (2.3.5)$$

For $Q_{\text{eff}} > 0$ the gas accelerates in a subsonic flow and decelerates in a supersonic flow, while for $Q_{\text{eff}} < 0$ the situation is the opposite.

The important property of these problems is a possibility for a *singular sonic point* to appear in a solution under the conditions

$$M \rightarrow 1, \quad \frac{du}{dx} \rightarrow \infty, \quad x \rightarrow x_*, \quad Q_{\text{eff}}^* = Q_{\text{ef}}(x_*) \neq 0 \quad (2.3.6)$$

Assuming then that the flow is adiabatic and isentropic in the vicinity of the sonic point, which will be substantiated later, and using Equation 2.2.20 for $U = u$ we obtain the solution in this vicinity

$$A_* \left(1 - \frac{u}{a_*}\right)^2 = \frac{Q_{\text{eff}}^*}{a_*} (x_* - x) \quad (2.3.7)$$

Thus, in the vicinity of the sonic point the velocity increment is of the order $a_* - u \sim (x_* - x)^{1/2}$, the total enthalpy and entropy increments being of higher order of smallness, $\Delta H, \Delta s \sim q(x_* - x)$, which justifies the assumptions made previously.

For $Q_{\text{ef}}^* \neq 0$ solution 2.3.7 exists only on one side of the section $x = x_*$ determined by the condition that the right-hand side is positive. In particular, in an accelerating subsonic nozzle ($M < 1, Q_{\text{eff}} > 0$) the solution of a seemingly natural problem with initial data of the type $x = x_b, u = u_b$ can be brought up only to a sonic point $x_* > x_b$ and cannot be continued through this point.

At the same time, gas outflow from a high-pressure container through a channel-mouthpiece (Figure 2.3) can always self-organize in such a way that the corresponding solution has no internal singularities.

This is provided by the displacement of the sonic section $x = x_*$ (if it exists) onto one of the channel ends (the entrance x_b or exit x_a as in Figure 2.3) by choosing specially the initial data of the problem, for instance, the gas flow rate through the mouthpiece. Moreover, the flow rate is not known beforehand and is determined by the flow along the entire channel length and, first of all, by the conditions in the end sections.

This fact takes implicitly into account the upstream influence of disturbances in a subsonic flow, though the sound propagation process itself is not involved in the formulation of the problem.

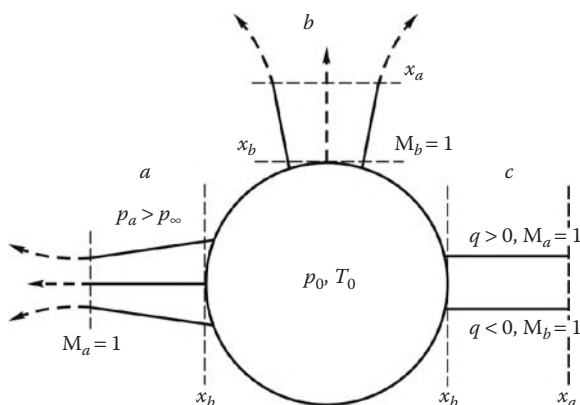


FIGURE 2.3
Gas outflow from a reservoir through nozzles.

Thus, the *regular solutions* (i.e., solutions with a finite derivative du/dx at a singular point) play a special role. It is evident that for this to be the case the conditions

$$M = 1, \quad Q_{\text{eff}}^* = 0, \quad x = x_* \quad (2.3.8)$$

must hold.

If Q_{eff} changes the sign at this point, a continuous transition through the sonic velocity is possible in such a nozzle, including the acceleration of the subsonic flow up to supersonic velocities.

In order for these conditions to be satisfied, the problem should be posed as follows: one should choose such an initial velocity $u_b(x_b)$ for which the sonic velocity is achieved either in a given section or at such a place where solution regularity can be ensured. Precisely this formulation of the problem is specific for the nozzle theory in general.

2.3.2 Laval Nozzle: Isentropic Flow

The convergent-divergent, or Laval, nozzle is a channel having a throat $O - O'$ (Figure 2.4a) called the *critical section*. For $q = 0$ we can express $a = a(u)$ using the Bernoulli integral and the equation of state. Then Equation 2.3.4 has the integral

$$\ln \bar{\sigma} = \int_{a_*}^u (M^2 - 1) \frac{du}{u}, \quad \bar{\sigma} = \frac{\sigma}{\sigma_*} \quad (2.3.9)$$

Here, σ_* is the sonic section area. By virtue of 2.2.18 we have $M > 1$ for $u > a_*$ and $M < 1$ for $u < a_*$; therefore, the integral on the right-hand side is always positive and, hence, the sonic section σ_* is minimal, that is, it coincides with the critical section. The same follows directly from Equation 2.3.4: for $M = 1$ we have $Q_e = 0$ and $d\sigma/dx = 0$, while the derivative

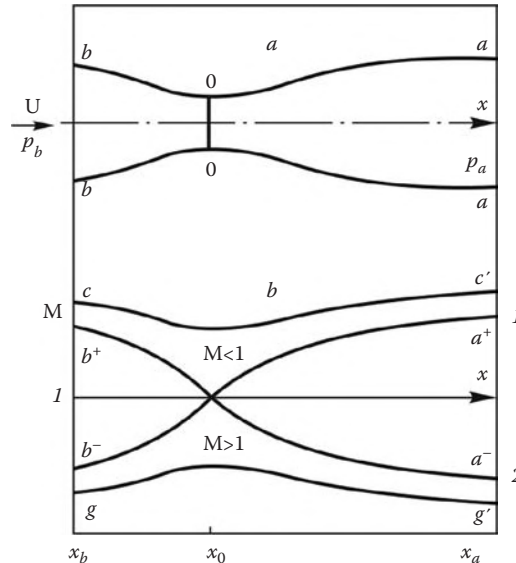


FIGURE 2.4

On the elementary theory of convergent-divergent nozzles.

du/dx is bounded. This result has an obvious physical meaning. Since, according to 2.2.22, the flow rate is maximum precisely at $M = 1$, the cross-sectional area of any streamtube is minimal at this point.

Thus, solution 2.3.9 has two branches, subsonic and supersonic, so that $u(\sigma)$ is a two-valued function with the branching point $\bar{\sigma} = M = 1$. For a perfect gas, by virtue of 2.2.23 integral, 2.3.9 is equal to

$$\bar{\sigma} = \frac{\sigma}{\sigma_*} = \frac{1}{M} \left[\frac{2}{\gamma + 1} \left(1 + \frac{\gamma - 1}{2} M^2 \right) \right]^{\frac{\gamma+1}{2(\gamma-1)}} \quad (2.3.10)$$

The two branches of the curve $\bar{\sigma}(M)$ are shown in Figure 2.5 for various γ . Subsonic branches are weakly dependent of γ , whereas the γ -dependence of the supersonic branches is considerable. In each nozzle section with a given ratio $\bar{\sigma}$ the flow with any of two Mach numbers ($M^- < 1$ and $M^+ > 1$) can be realized, provided the sonic velocity is achieved in the critical section. In this case any of four versions of the flow formed from curvilinear segments $b^\pm O$ and Oa^\pm in Figure 2.4b can theoretically be realized in a nozzle depending on the conditions imposed in the inlet and outlet sections.

However, for this solution two more flow regimes are possible, namely, completely subsonic (gg') and completely supersonic (cc') ones, the conditions $M \neq 1$ and $du/dx = 0$ being satisfied at the critical section.

The Mach numbers ranging from M_b^+ to M_b^- cannot be implemented at the inlet of a nozzle of given shape, since in this case the sonic speed, determined from the area ratio, is achieved already for $\sigma > \sigma_*$ and the flow in a narrowing channel is no longer possible.

Convergent-divergent nozzles are widely used in both aerodynamic facilities and rocket engines to accelerate flows from subsonic to supersonic velocities. For the reliable implementation of such flow regimes, the pressure p_a in the exit section must be no less than the surrounding one, $p_\infty \leq p_a$; otherwise, the elevated pressure can penetrate into the nozzle resulting in boundary layer separation and flow pattern distortion. For the same reason, other branches of the solution shown in Figure 2.4b and associated with flow deceleration, are hardly realizable.

Let us give a few examples. A narrowing head ("throat") at the outlet of a large reservoir with the stagnation pressure p_0 (Figure 2.3a) determines uniquely the flow rate of the gas

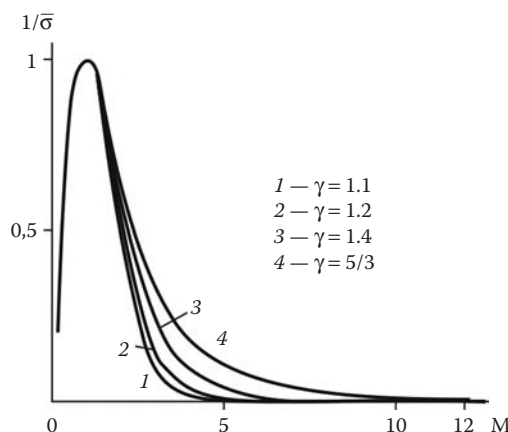


FIGURE 2.5

Mach number dependence of the cross-sectional area of convergent-divergent nozzles.

issuing from it if the ambient pressure does not exceed the sonic one, $p_\infty \leq p_*$. After leaving the nozzle the gas continues to expand and extreme streamlines can be considered the extensions of the nozzle walls with the sonic velocity at the end section.

Another example is furnished by the *spherical source* and its application to conical nozzles and jets expanding into vacuum. In a divergent head the sonic velocity is achieved at the head base, at least, for $p_a \geq p_\infty$. The flow in a conical nozzle can be simulated by a spherical source flow. In gas dynamics this problem has a solution only outside the sphere $x > x_*$ (with a source at the origin) at the surface of which the gas velocity is sonic (Figures 2.3b and 2.6).

Let $p_\infty \ll p_a$; in the limit the situation corresponds to the gas expansion into a vacuum. Then, starting from a certain section $x \geq x_m$, the gas velocity acquires its limiting value, so that the density in the nozzle decreases as $\rho/\rho_m \sim (x_m/x)^2$. This result could be applied to the expansion of high-altitude engine jets into a vacuum (Figure 2.6). In this case the density in each streamtube of the section σ follows the law $\rho \sim \rho_m \sigma_m / \sigma$, where ρ_m and σ_m are certain initial parameters, different, generally speaking, for each streamtube. The streamtubes are slightly curved. In fact, see Equation 2.2.6 for the streamtube curvature, $R^{-1} = -\partial\theta/\partial l$, where $l \sim x$ is the length along a streamline and θ is its inclination to the axis of symmetry. Then putting $\partial p/\partial n \sim p/x$ in an expanding jet we obtain ($p \sim \rho^\gamma$)

$$\frac{\partial\theta}{\partial x} \sim \frac{p}{x\rho U^2} \sim C_1 x^{-(2\gamma-1)}$$

$$\Delta\theta = C_2 x_m^{-2(\gamma-1)} \left[1 - \left(\frac{x_m}{x} \right)^{2(\gamma-1)} \right], \quad C_i = \text{const} \quad (2.3.11)$$

Here, $\Delta\theta$ characterizes the streamline curvature between the points x_m and x , which for $x_m/x \approx \text{const}$ decreases asymptotically with x_m , whereas for $x_m = \text{const}$ the parameter θ itself increases with x , though slowly. At the same time, we can let $\partial p/\partial n = 0$ near the axis of symmetry; then the streamlines form a bundle of diverging straight lines with a fictitious center in the vicinity of the nozzle exit. This is supported by the data presented in Figure 2.7.

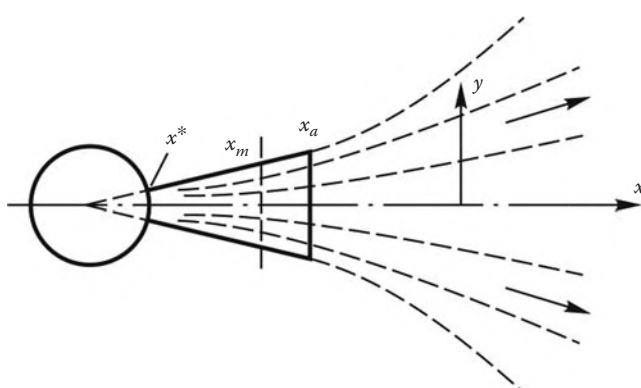


FIGURE 2.6
Jet outflow into a vacuum.

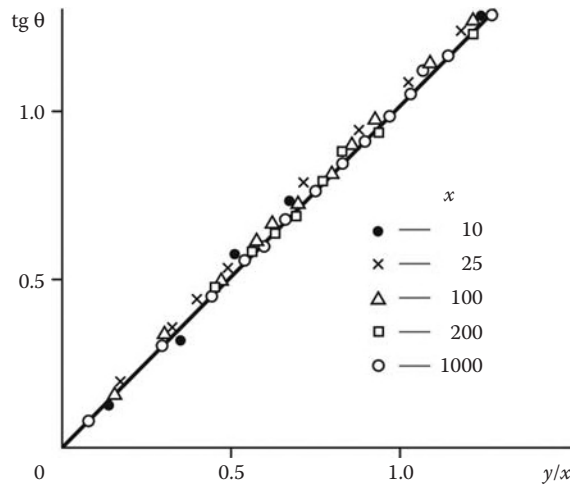


FIGURE 2.7
Slope of streamlines in the vicinity of the axis of symmetry of a jet.

2.3.3 Thermal Nozzle

This term is used for a channel in which the flow accelerates due to heat supply. These problems have an application to rocket engines. In this case, by virtue of 1.6.8 and 2.3.4 the following relations hold

$$Q_{\text{eff}} = -Q_e - \frac{u}{\sigma} \frac{d\sigma}{dx}, \quad Q_e = \left(\frac{\partial \rho}{\partial h} \right)_p \frac{q}{\rho} = -\frac{q}{h} \quad (2.3.12)$$

The latter equality is valid for a perfect gas. Thus, in a constant-area channel with heat supply the flow accelerates and “chokes” at $M = 1$. Further heat supply is impossible and the gas outflow from a reservoir through a heated head can be implemented only with a subsonic or sonic velocity in the outlet section $x = x_a$ (Figure 2.3c). A regular sonic point inside the head is possible only when q changes the sign with subsequent head cooling and further acceleration of the flow, already supersonic. As for an everywhere cooled head ($q < 0$), within it the sonic flow can occur only in the initial section $x = x_b$ with the subsequent flow acceleration.

In a heated convergent-divergent nozzle, the gas velocity in the critical section is subsonic and the sonic section is displaced to the divergent part of the nozzle. Other possible combinations are similarly considered. We note that in a thermal nozzle the flow acceleration and the Mach number increase are usually accompanied by an increase in the temperature and the speed of sound.

2.3.4 Variable Flow-Rate Nozzle

Let a gas be injected or sucked off through the channel walls along the channel length, so that the gas flow rate $G = G(x)$ in Equation 2.3.1 is variable. Then we have

$$\frac{1}{\rho} \frac{d\rho}{dx} + \frac{1}{u} \frac{du}{dx} = \frac{1}{G} \frac{dG}{dx} - \frac{1}{\sigma} \frac{d\sigma}{dx} \quad (2.3.13)$$

In the general case, the injected gas may have any velocity or enthalpy; in the hydraulic formulation this is equivalent to the distributed enthalpy or momentum influx. However,

in order to reveal purely flow-rate effects we will assume that the injected gas parameters are equal to the local parameters in the channel and the process is adiabatic. Then Equation 2.3.3 is valid and instead of 2.3.4 we have the equation

$$\frac{1}{u} (1 - M^2) \frac{du}{dx} = \frac{1}{G} \frac{dG}{dx} - \frac{1}{\sigma} \frac{d\sigma}{dx} = \frac{\sigma}{G} \frac{d}{dx} \frac{G}{\sigma} \quad (2.3.14)$$

which has the same solution as Equation 2.3.9

$$\ln \frac{G_* \sigma}{G \sigma_*} = \int_{a_*}^u (M^2 - 1) \frac{du}{u} \quad (2.3.15)$$

Further analysis does not differ from that performed previously. For example, in a constant-area channel a subsonic flow can be accelerated by gas injection only up to the sonic velocity, with the flow rate maximum G_* in the sonic section. For the subsequent gas acceleration gas suction is required.

In conclusion, we will pay attention to an intrinsic shortcoming of the hydraulic theory, essential for viscous problems. The average parameters, with which the theory deals (let us denote them by ρ_{eff} , u_{eff} , h_{eff}), must, generally speaking, satisfy the integral conservation laws for mass, momentum, and energy, as well as the equation of state

$$\begin{aligned} G &= \int_{\sigma} \rho u d\sigma = \rho_{\text{eff}} u_{\text{eff}} \sigma, & \int_{\sigma} \rho u^2 d\sigma &= G u_{\text{eff}} \\ \int_{\sigma} \rho u H d\sigma &= G H_{\text{eff}}, & H_{\text{eff}} &= h_{\text{eff}} + \frac{u_{\text{eff}}^2}{2}, & \rho_{\text{eff}} &= \rho(h_{\text{eff}}, p) \end{aligned} \quad (2.3.16)$$

Obviously, the three quantities, ρ_{eff} , u_{eff} , and h_{eff} , cannot simultaneously satisfy four relations for channel parameters given. However, one should reconcile oneself to this shortcoming for the sake of an elementary character of the theory obtained. Besides, this disagreement can be relatively small.

A detailed outline of the one-dimensional theory of channel flows is given—with many applications and generalizations to viscous flows—in the books of Abramovich (1953) and Chernyi (1987).

2.4 Linear Equations of Gas Dynamics

In Section 2.3 the consideration was reduced, though approximately, to the treatment of one-dimensional flows and the solution of ordinary differential equations. However, this case is probably exceptional in gas dynamics, and in what follows this partial differential equation will usually be considered.

In this section, only two-dimensional plane ($\nu = 0$) and axisymmetric ($\nu = 1$) problems are considered. This is not only a mathematical abstraction, though reflecting all the main properties of gas flows, but also a practically important subject of gas dynamics.

To begin with, we will note some mathematical properties of these equations. First of all, bearing in mind an important role of the speed of sound we will introduce it explicitly into the continuity Equation 1.9.1 by means of transformation 1.6.8

$$\frac{1}{\rho a^2} \frac{dp}{dt} + \operatorname{div} \mathbf{U} = -Q \quad (2.4.1)$$

We emphasize that in what follows, in accordance with Section 1.6, a , unless otherwise stated, is precisely the isentropic speed of sound $a = a_e = (\partial p / \partial \rho)^{1/2}$, while Q is considered to mean Q_e from Equation 1.6.8. For a perfect gas $a^2 = (\gamma p / \rho)^{1/2}$ and $Q_e = -q/h$.

In view of these relations and Equations 1.13.7 through 1.13.12, we obtain the following system for plane and axisymmetric flows

$$\begin{aligned} \frac{1}{\rho a^2} \frac{dp}{dt} + \frac{\partial u}{\partial x} + \frac{\partial v}{\partial r} &= Q_{\text{eff}} = -Q - v \frac{v}{r} \\ \frac{du}{dt} = -\frac{1}{\rho} \frac{\partial p}{\partial x}, \quad \frac{dv}{dt} = -\frac{1}{\rho} \frac{\partial p}{\partial r}, \quad \frac{dh}{dt} &= \frac{1}{\rho} \frac{dp}{dt} + q \\ \frac{d}{dt} &= \frac{\partial}{\partial t} + u \frac{\partial}{\partial x} + v \frac{\partial}{\partial r} \end{aligned} \quad (2.4.2)$$

Here, the term Q_{eff} (different from that of Section 2.3) takes into account both heat sources and the influence of axial symmetry.

The first three equations in 2.4.2 involve time and space derivatives of velocities and pressure only and in this sense they form the *first closed group of equations*. The last equation, or that of energy (cf. 1.13.11), involves derivatives of h taken only along streamlines. In what follows this *second group of equations* will be completed by making allowance for new physical processes. Moreover, in steady flows we can use Equation 2.2.8 for the total enthalpy H , thus excluding one of two momentum equations in 2.4.2.

Moreover, there exists a number of problems for which the two groups of equations are solved independently; these are the problems of the *linear small-perturbation theory*, which will be considered in subsequent sections.

We will now consider flows differing weakly from the uniform flow characterized by constant parameters U_0, p_0 , and so on. In this case setting

$$\begin{aligned} p &= p_0 + p_1, \quad \rho = \rho_0 + \rho_1, \quad u = U_0 + u_1, \quad v = v_1 \\ p_1, \rho_1, |u_1|, |v_1| &\ll p_0, \rho_0, U_0 \end{aligned} \quad (2.4.3)$$

in Equation 2.4.2 and omitting second-order terms (of the type of $u_1 \partial u_1 / \partial x$, etc.) we obtain a linear system of equations with constant coefficients

$$\begin{aligned} \frac{\partial u_1}{\partial t} + U_0 \frac{\partial u_1}{\partial x} &= -\frac{1}{\rho_0} \frac{\partial p_1}{\partial x}, \quad \frac{\partial v_1}{\partial t} + U_0 \frac{\partial v_1}{\partial x} = -\frac{1}{\rho_0} \frac{\partial p_1}{\partial r} \\ \frac{1}{\rho_0 a_0^2} \left(\frac{\partial p_1}{\partial t} + U_0 \frac{\partial p_1}{\partial x} \right) + \frac{\partial u_1}{\partial x} + \frac{\partial v_1}{\partial x} &= Q_{\text{eff}} \end{aligned} \quad (2.4.4)$$

The previous system is closed, which would not be the case if the continuity equation was taken in its original form 1.9.1 (with density derivatives retained), since it is independent of the energy conservation equation and the equation of state, which could be solved separately, for example, as follows

$$\begin{aligned} \frac{\partial h_1}{\partial t} + U_0 \frac{\partial h_1}{\partial x} &= \frac{1}{\rho_0} \frac{\partial p_1}{\partial t} + \frac{U_0}{\rho_0} \frac{\partial p_1}{\partial x} + q \\ \rho_1 = \left(\frac{\partial \rho}{\partial p} \right)_h p_1 + \left(\frac{\partial \rho}{\partial h} \right)_p h_1 & \end{aligned} \quad (2.4.5)$$

We will consider some properties of the system. Differentiating the first equation of 2.4.4 with respect to r and the second with respect to x and subtracting one from another we obtain the equation

$$\frac{\partial \omega}{\partial t} + U_0 \frac{\partial \omega}{\partial x} = 0, \quad \omega = \frac{\partial v_1}{\partial x} - \frac{\partial u_1}{\partial r} \quad (2.4.6)$$

This equation admits a family of solutions for the vortex ω ; these are arbitrary functions $\omega(x - U_0 t)$, that is, they have the form of vorticity waves convected by the flow. In a steady-state flow the vorticity has a constant transverse distribution and the general solution has the form:

$$\begin{aligned} u_1 &= u_{10}(r) + \frac{\partial \varphi_1}{\partial r}, & \varphi_1 &= \varphi_1(x, r) \\ v_1 &= \frac{\partial \varphi_1}{\partial r}, & \omega &= -\frac{du_{10}}{dr} \end{aligned} \quad (2.4.7)$$

Here, the first and second terms of u_1 are the *vortex* and *potential* components of the perturbed flow, the first being in this approximation a given function that does not influence Equation 2.4.4 and, hence, the pressure field.

For straightforward derivation of the equation for the perturbation potential we can eliminate pressure from 2.4.4 by cross-differentiation. We will perform this procedure for the nonlinear Equation 2.4.2 with $q = 0$. Setting $u = \partial \Phi / \partial x$ and $v = \partial \Phi / \partial y$ and eliminating the total derivative dp/dt from 2.4.1 by means of the Lagrange integral 2.2.11 we can obtain

$$\begin{aligned} \frac{1}{a^2} \frac{\partial^2 \Phi}{\partial t^2} + 2 \frac{u}{a^2} \frac{\partial^2 \Phi}{\partial t \partial x} + 2 \frac{v}{a_1} \frac{\partial^2 \Phi}{\partial t \partial r} = \\ \left(1 - \frac{u^2}{a^2}\right) \frac{\partial^2 \Phi}{\partial x^2} - 2 \frac{uv}{a^2} \frac{\partial^2 \Phi}{\partial x \partial r} + \\ \left(1 - \frac{v^2}{a^2}\right) \frac{\partial^2 \Phi}{\partial r^2} + \frac{v}{r} \frac{\partial \Phi}{\partial r} = 0 \end{aligned} \quad (2.4.8)$$

Here, the speed of sound is expressed, by virtue of the dependence $a = a(h)$ and the Lagrange integral, in terms of the first derivatives of Φ . Therefore, this equation is *quasilinear*, that is, linear with respect to higher-order derivatives, with the coefficients dependent (via a, u, v) on the first derivatives of Φ .

It is easy to linearize this equation, since for a uniform main flow all the derivatives of Φ are of the first order of smallness and one should simply set $u = U_0, v = 0$, and $a = a_0$ in the coefficients. This gives

$$\frac{1}{a_0^2} \frac{\partial^2 \Phi}{\partial t^2} + 2 \frac{U_0}{a_0^2} \frac{\partial^2 \Phi}{\partial t \partial x} = (1 - M^2) \frac{\partial^2 \Phi}{\partial x^2} + \frac{1}{r^v} \frac{\partial}{\partial r} \left(r^v \frac{\partial \Phi}{\partial r} \right) \quad (2.4.9)$$

Here, the local Mach number $M = U/a$ is for the moment retained. If perturbations are so small that $\Delta M^2 \ll 1 - M^2$, we can set $M^2 = M_0^2$ in this equation which completes the linearization. Otherwise, for $\Delta M^2 \sim 1 - M^2$ the linearization leads to qualitative errors and is unacceptable (throughout this chapter $M = M_0$).

Let us make a few remarks. Linearization can also be performed with respect to a variable flowfield, $U_0 = U_0(x, y)$ and so on, and, generally, in the case in which a problem has a small parameter ε . Then solution of the problem can be sought in a series-form of the type

$$f(X, \varepsilon) = f_0(X) + \varepsilon f_1(X) + \varepsilon^2 f_2(X) + \dots \quad (2.4.10)$$

This is a generalization of the expansion 2.4.3, where X is a set of independent variables. Substituting this solution in the equations and boundary conditions, expanding them in a power series in ε and equating the coefficients of the same powers of ε to zero, we obtain, usually but not always, a system of recurrent equations of which those for the *main approximation* are nonlinear (together with the original equations), while the equations for the subsequent terms f_i are linear, though with variable coefficients.

Frequently it is convenient to transfer boundary conditions for f specified on some line (surface) $X = X_s(\varepsilon)$ to the boundary $X_0 = X_s(0)$. Let a function f satisfy the boundary condition

$$f = f_s = f_{s0} + \varepsilon f_{s1}, \quad X = X_s = X_0 + \varepsilon X_1 \quad (2.4.11)$$

and is regular on the boundary. Equating the expansions

$$f(X_s) = f_0(X_s) + \varepsilon f_1(X_s) = f_0(X_0) + \varepsilon [X_1 f'_0(X_0) + f_1(X_0)] = f_{s0} + \varepsilon f_{s1} \quad (2.4.12)$$

we obtain the following boundary conditions

$$f_{s0} = f_0, \quad f_{s1} = f_1 + X_1 f'_0, \quad X = X_0 \quad (2.4.13)$$

In the case in which there are several variables x_i , the product $X_1 f'_0$ is equal to the sum of the products of x_i by the derivatives of f_0 with respect to x_i .

Let us indicate possible limitations for the linearization. Solutions of linear equations can have singularities at points or surfaces, where the functions themselves or their derivatives can increase without bounds. In this case the omitted nonlinear terms of the equation can exceed the retained ones, so that the linearization is no longer legitimate. As an example, we can indicate vicinities of the axis of symmetry in axisymmetric problems (see Sections 2.8 and 2.9).

Further, even the functions $f_0 \sim 1$ can have large derivatives, for example, $\partial f_0 / \partial X \sim \varepsilon^{-1}$, which makes the application of the linear theory completely impossible.

On the whole, linearization is justified only in the case in which the solutions for approximations f_0 and f_1 are considerably simpler than the solution of the original problem or allow one to reveal new properties intrinsic to the original nonlinear problem, especially if the required result itself is of the order of ε . This is the case of the flow past a thin body where forces acting on the body are of the same order as the relative body thickness, $\theta \sim \varepsilon$, or the case of an axisymmetric body at a small angle of attack α .

We note that the function $f_1(X) = [f(\varepsilon, X) - f_0(X)]/\varepsilon$ can be determined, for example, by numerical calculation of the original nonlinear problem for $\varepsilon = 0$ and for a certain $\varepsilon \neq 0$. In this case, the linear theory gives a simple method of representing the solution for small ε , which, in its turn, makes it possible to evaluate limiting (as $\varepsilon \rightarrow 0$) parameters important in aerodynamics.

2.5 Sound Wave Propagation

The propagation of small disturbances in a homogeneous medium is governed by a system of linear equations (Section 2.4). We will consider only plane adiabatic sound, or acoustic, waves propagating along the x axis (for example, in a constant-area tube). These problems with their simple and clear solutions give an idea of the salient features of both unsteady and, as we shall see subsequently, steady supersonic gas flows.

We obtain appropriate equations by equating the quantities U_0 , v , Q_{eff} , and v_1 in Equation 2.4.4 to zero

$$\frac{\partial u_1}{\partial t} = -\frac{1}{\rho_0} \frac{\partial p_1}{\partial x}, \quad \frac{\partial u_1}{\partial x} = -\frac{1}{\rho_0 a_0} \frac{\partial p_1}{\partial t} \quad (2.5.1)$$

Eliminating p_1 by cross-differentiation we obtain the equation for u_1

$$\frac{1}{a_0^2} \frac{\partial^2 u_1}{\partial t^2} = \frac{\partial^2 u_1}{\partial x^2} \quad (2.5.2)$$

This equation is termed the *wave equation*. It has the general solution (the *Dalembert solution*) involving two arbitrary functions

$$u_1 = f_1(x - a_0 t) + f_2(x + a_0 t) \quad (2.5.3)$$

Substituting this solution in any of the equations in 2.5.1 yields a formula for the pressure

$$p_1 = p - p_0 = \rho_0 a_0 [f_1(x - a_0 t) - f_2(x + a_0 t)] \quad (2.5.4)$$

Here it is taken into account that in a gas at rest $u = 0$ and $p = p_0$. An adiabatic sound wave is always isentropic. In fact, let the entropy $s = s(p, h)$; then

$$\Delta s = \left(\frac{\partial s}{\partial h} \right)_p \Delta h + \left(\frac{\partial s}{\partial p} \right)_h \Delta p = \frac{1}{T} \Delta h - \frac{1}{\rho T} d\rho = \frac{\Delta Q}{T} \quad (2.5.5)$$

Here, ΔQ corresponds to a possible heat release in the wave. If $\Delta Q = 0$, then $\Delta s = 0$, while $\Delta \rho = \rho_1 = p_1/a_0^2$ and $h_1 = p_1/\rho_0$.

The functions f_i have a clear physical meaning. If $f_2 = 0$, a perturbation wave propagates from left to right at the speed of sound conserving the given shape and vice versa, for $f_1 = 0$ it moves from right to left. Comparing solutions 2.5.3 and 2.5.4 we obtain the dependences

$$\begin{aligned} p_1 &= \Delta p = \rho_0 a_0 u_1, & u_1 &= f_1(x - a_0 t), & f_2 &= 0, \\ p_1 &= -\rho_0 a_0 u_1, & u_1 &= f_2(x + a_0 t), & f_1 &= 0 \end{aligned} \quad (2.5.6)$$

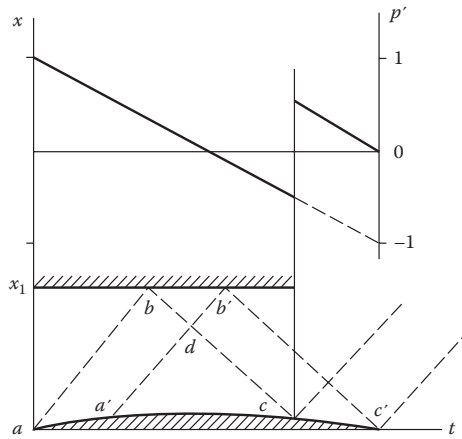
Naturally, these formulas coincide with 1.6.5 obtained directly from physical considerations, while the condition of the perturbation smallness takes the form $|\Delta p/p_0| = \gamma |u_1/a_0| \ll 1$, that is, the piston velocity u_0 generating the wave must be considerably smaller than the speed of sound, $u_0 \ll a_0$.

In the general theory of partial differential equations the lines $\eta_{\pm} = x \pm a_0 t = \text{const}$ are termed *characteristics*; they are trajectories along which perturbations propagate. The minus and plus signs relate to characteristics of the first and second families, respectively. If $f_i \neq 0$ only within the stripes $\eta_1 < \eta < \eta_2$, the lines η_i are termed (depending on the wave orientation) the *forward*, or *bow*, and *rear* wave fronts.

As an illustration we consider a simple example of gas motion in a channel generated by a piston that starts to move at $t = 0$ according to the law $x = x_0(t)$ at a velocity $u_0 = \dot{x}_0(t)$. The diagram is shown in Figure 2.8. Since initially the gas is at rest, $f_2 = 0$ and the function f_1 is determined from the condition on the piston. In this case $x_0 \sim u_0 t \ll a_0 t$ and, hence

$$f_1(\eta_-) = f_1(-a_0 t) = u_0(t) = u_0 \left(-\frac{\eta_-}{a_0} \right) \quad (2.5.7)$$

as $x \rightarrow 0$. Thus, on all the rays $\eta_- = \text{const}$ the solution is the same as at the point where the ray intersects the piston trajectory.

**FIGURE 2.8**

On the propagation of one-dimensional acoustic disturbances.

If the channel is bounded by an end wall $x = x_1$, then the previous solution is valid only to the left of the characteristic bc . On the wall $u = 0$ and $f_2 = -f_1$, which determines the solution in a reflected wave f_2 , which retains the incident wave shape, f_1 , thus being its specular reflection. In this case, $\Delta p = 2\rho a f_1$, that is, the *excessive pressure is doubled on reflection from the wall* (a particular case of the general result will be presented in Section 4.7). If the piston stops at a point a' , then the elevated pressure zone is, according to 2.5.6, represented by the triangle $bb'd$; further, the wave f_2 becomes again solitary. When it is reflected from the piston the situation in the strip cc' is repeated with the following propagation of the process along the tube without decaying, which is the property of linear equations only (as will be seen later).

If the reflected wave f_2 impinges the moving piston, then, on reflection, a local wave f_1 determined by 2.5.7 should be added to it in accordance with the superposition rule. This can be verified by satisfying directly the boundary conditions at the piston with the incident wave taken into account.

As an example, we have plotted in Figure 2.8 the quantity $p' = \Delta p / \rho a u_0$ for a piston moving according to the law $x = u_0 t(1 - t/t_0)$ (a parabolic arc in the plane $(t, x), t_0 = 1$) with the reflecting wall effect taken into account. Naturally, the pressure on the piston for $t > t_0$ cannot be determined without information on the piston motion.

These examples illustrate the following fundamental properties of the characteristics.

First, the characteristics confine regions of influence or dependence of the solution on initial and boundary conditions.

Second, the extension of the solution through a characteristic is not unique and depends on the extension of the corresponding boundary conditions.

Third, any characteristic may be a discontinuity line of the solution.

The third statement thus formulated relates only to linear problems. Discontinuities in a solution appear automatically in determining the functions f_i in 2.5.3 in the case of discontinuous boundary conditions. However, their substitution in Equation 2.5.2 is impossible, since the derivatives of u_1 do not exist at a discontinuity. To elucidate the situation let us replace the variables (t, x) by (η_+, η_-) , where $\eta_{\pm} = x \pm a_0 t$, and bring Equation 2.5.2 to the form:

$$\frac{\partial^2 u}{\partial \eta_+ \partial \eta_-} = 0 \quad (2.5.8)$$

Let us assume that the piston acquires a constant velocity u_0 not suddenly, but after a certain time τ , the transition function $u_0(t)$, $t \leq \tau$ being smooth. Then in the vicinity $-a\tau \leq \eta_- \leq 0$ the discontinuity is replaced by a continuous and smooth distribution of the function f_1 from $f_1 = 0$ to $f_1 = u_0$. This solution satisfies Equation 2.5.8 for any τ , since the equality $\partial f_1 / \partial \eta_+ = 0$ holds always. Therefore, letting $\tau \rightarrow 0$ we obtain a limiting discontinuous form of the solution satisfying the equation in this sense.

However, the question arises whether linearization of the original gas dynamic equations is legitimate on the background of discontinuous solutions, since quadratic terms of the type $u_1 \partial u_1 / \partial x \sim u_0^2 / a_0 \tau$ omitted in deriving Equation 2.4.4 cannot be considered to be small for small τ .

To avoid this difficulty we should construct solutions that are continuous and smooth in regions separated by discontinuity lines, on which conservation laws 1.6.5 must be satisfied. However, these conditions coincide with 2.5.6, that is, discontinuous solutions formally obtained from the general solution 2.5.3 satisfy these conditions automatically, which solves the problem.

2.6 Nonlinear Effects: Expansion Fans and Shock Waves

Formal ranges of applicability of the linear theory are determined by the condition $u \ll a$. However, even if this condition is satisfied, qualitative effects can arise that are not described by the theory. This could be properly explained only on the basis of the theory of nonlinear wave propagation. We will consider this subject in Chapter 4; however, the essence of these effects can be understood even now.

To do this, we will return to the piston problem treated in Section 2.5. Let a piston begin suddenly to move at a velocity $u_0 > 0$. Then compression and expansion waves propagate to the right and to the left, respectively, the equations for their forward fronts and pressures behind them being as follows

$$x = \pm a_0 t, \quad p_1 - p_0 = \pm \rho_0 a_0 u_1 \quad (2.6.1)$$

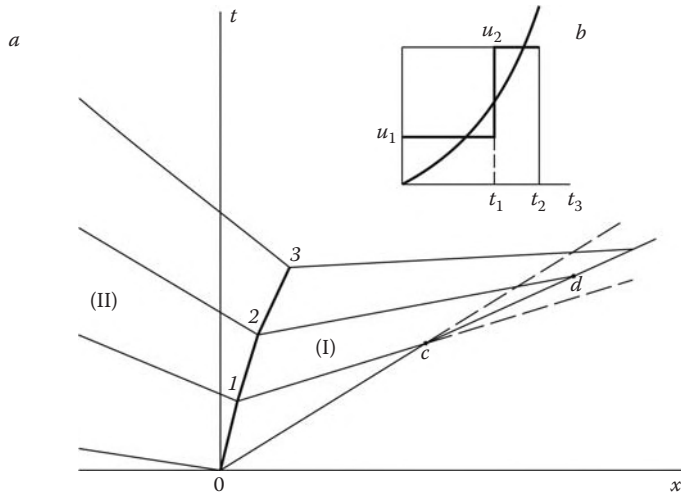
Here, the upper signs refer to the right wave, while the lower ones characterize the left wave. The diagram of the process is shown in Figure 2.9a.

Let at a moment $t = t_1$ the piston velocity change suddenly from u_1 to u_2 . Then new disturbances propagate from the point $t_1, x_1 = u_1 t_1$. As was assumed in Section 2.5, the disturbances propagate at a velocity a_0 due to a small difference between initial and disturbed flow parameters.

Let the piston move accelerating stepwise up to u_3, u_4, \dots, u_i at moments t_2, \dots, t_i and so on; we will consider this sequence u_i as an approximation to a certain real velocity variation (Figure 2.9b). Accumulation of disturbances can lead to a noticeable variation of the flow parameters ahead of the piston, which can no longer be described within the framework of the linear theory.

The point is that each subsequent $(i+1)$ -th perturbation propagates through a gas already possessing a translational velocity u_i and a speed of sound a_i . Then the absolute velocity of disturbances is $u_i \pm a_i$ and the corresponding characteristics satisfy the equations

$$x - x_i = (u_i \pm a_i)(t - t_i) \quad (2.6.2)$$

**FIGURE 2.9**

Nonlinear effects of disturbance propagation; 0-1-2-3 is the piston trajectory, I and II are the convergent and divergent characteristic bundles, and cd is the incipient shock wave.

The characteristics carry disturbances of a relative intensity

$$\Delta p_{i+1} = p_{i+1} - p_i = \pm \rho_i a_i (u_{i+1} - u_i) \quad (2.6.3)$$

We will now analyze the behavior and mutual locations of characteristics, for example, the forward characteristic and the next one. Accurate to the second-order terms, we can write

$$a_1 - a_0 = (p_1 - p_0) \left(\frac{\partial a}{\partial p} \right)_s \quad (2.6.4)$$

Then for the difference of the propagation velocities for the primary and secondary sonic waves we obtain, with 2.6.1 taken into account, the following formula

$$\Delta D = u_1 \pm (a_1 - a_0) = \pm A \frac{p_1 - p_0}{\rho_0 a_0} = u_1 A, \quad A = 1 + \frac{\rho}{2} \left(\frac{\partial a^2}{\partial p} \right)_s \quad (2.6.5)$$

We emphasize that, in accordance with the assumptions made in Section 1.6, the function A is always positive for all gases, so that the signs of ΔD and u_1 are the same. From the previous considerations there follows an important conclusion:

The secondary disturbance wave following a primary compression wave propagates more rapidly and, hence, overtakes the initial wave. Contrariwise, the secondary disturbance following an expansion wave propagates more slowly and lags behind more and more.

Thus, at subsequent accelerations of the piston a sequence of overtaking compression waves propagates to the right (they are shown in Figure 2.9 as convergent bundles (I) of first-family characteristics of), while a sequence of expansion waves lagging behind each other propagates to the left (a diverging fan of second-family characteristics (II), which form a fan wave).

We will consider in more detail the expansion wave and its particular case when $t_i, x_i \rightarrow 0$. This is a *centered wave* emanating from the origin and corresponding to a suddenly acquired finite velocity of the piston u_k (Figure 2.10a). The wave has a variable thickness δ and, therefore, it is, generally speaking, unsteady. However, a limitingly weak wave, whose forward and rear fronts are relatively close to the middle line $x = -D^*t$ can be replaced by a weak steady discontinuity front (in the sense of Section 2.5) for which relations 2.5.6 holds.

We will now consider the compression wave. Obviously, the solution described by formulas 2.6.2 and 2.6.3 is valid until characteristics intersect, which does occur by virtue of condition 2.6.5. We can easily determine the point (t_c, x_c) at which two first characteristics intersect, using the formulas given previously. The greater t_1 and the lower the perturbation velocity u_1 , the farther the characteristics intersect. In the limit, as $u_1 \rightarrow 0$, the intersection point goes to infinity and the linear theory (with constant-slope characteristics) becomes applicable everywhere. On the contrary, as $t_1 \rightarrow 0$, we obtain $t_c \rightarrow 0$, that is, the characteristics intersect immediately after the piston has started and the linear theory is everywhere inapplicable.

Evidently, the formal extension of characteristics (with their own values of the flow parameters) through the point of their intersection leads to a multivalued, physically meaningless solution in the region where the characteristics overlap.

Physically, it is obvious that the secondary disturbance wave having overtaken the primary one cannot coalesce with it. Experience and theory (see Chapter 4) have shown that in this case accumulation of disturbances on interaction of compression waves leads to the formation of a finite-strength discontinuity front, or a *shock wave* that propagates according to a nonlinear law at a velocity D (see Figure 2.10b).

We will give one more illustration of this effect. Let a wave with the pressure distribution shown in Figure 2.11 ($p(x)$ at $t = t_1$) travel along the x axis of a channel. Each part of its phase moves at its own velocity $a(p)$ with a maximum at point c . Therefore, taking account of the nonlinear character of the process results in wave deformation: the expansion stage ac extends in time (expansion fan), while the compression stage narrows to the point of "overturning," which means the shock wave formation.

Naturally, a discontinuity thus arising cannot be arbitrary, since a gas flow across it must satisfy certain conditions and, first of all, the mass, momentum, and energy conservation laws (Section 1.7). These conditions were partially derived in Section 1.6, where relations 1.6.2 and 1.6.3 characterize a discontinuity front of an arbitrary intensity, which propagates at a velocity D through a gas at rest. A special section will be devoted to shocks. Here we

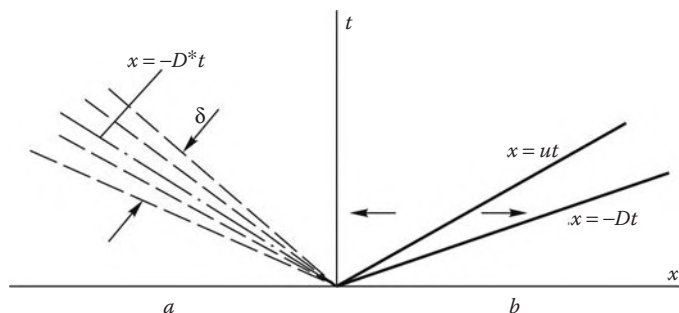


FIGURE 2.10
Centered expansion wave and shock wave.

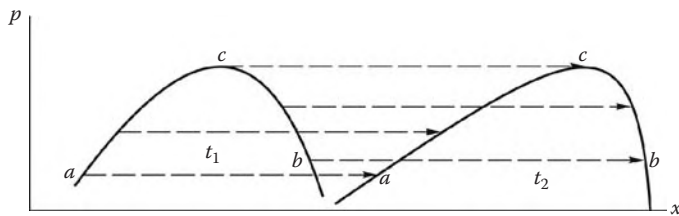


FIGURE 2.11
Nonlinear deformation of a wave.

can only note that the velocity of a finite-intensity shock is $D \geq a_0$ (i.e., it is always greater than the speed of sound).

2.7 Steady-State Flow Past Thin Bodies: Similarity Law

As shown in Section 1.6, disturbances induced by a mass point moving at a subsonic velocity in a gas at rest, $U < a$, leave the point behind and fill the entire space, as $t \rightarrow \infty$, while at $U > a$ all the disturbances are localized inside a *Mach cone* having a moving vertex and a semivertex angle α^* equal to the *Mach angle* determined by the formula

$$\sin \alpha^* = \frac{1}{M} = \frac{a}{U}, \quad \tan \alpha^* = (M^2 - 1)^{-1/2} \quad (2.7.1)$$

Obviously, this profound difference in the disturbance behavior must also take place in steady reversed flows.

We will consider a steady flow past a thin airfoil $r = r_b(x)$ on which the following conditions are imposed

$$\frac{v}{u} = \tan \theta = r'_b(x) \approx \theta \ll 1 \quad (2.7.2)$$

Here, u and v are the velocity components in a body-fitted coordinate system (x, r) (Figure 2.12).

In contrast to the problem of Section 2.5, in this case the system of linear equations obtained in Section 2.4 involves three unknown functions, p , u_1 , and v . Therefore, we use Equation 2.4.9 for the steady flow potential. Setting $\Phi = U_\infty x + \varphi$ and $M = M_\infty = U_\infty/a_\infty$ we can bring this equation to the form:

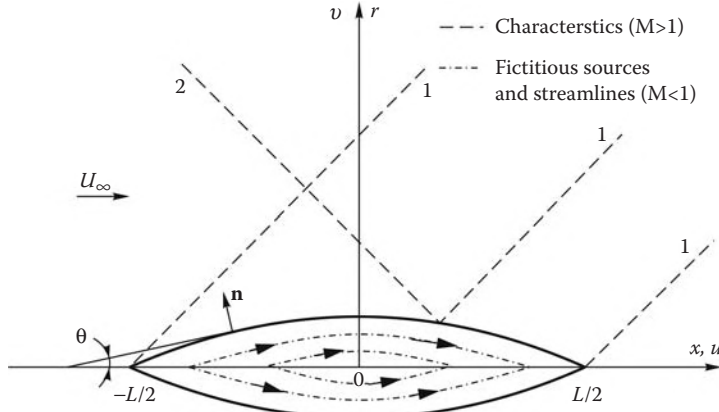
$$(M_\infty^2 - 1) \frac{\partial^2 \varphi}{\partial x^2} = \frac{\partial^2 \varphi}{\partial r^2} + \frac{v}{r} \frac{\partial \varphi}{\partial r} \quad (2.7.3)$$

Here and in what follows, for steady-state problems the subscript ∞ refers to the incident flow parameters. Obviously, in this case

$$u = U_\infty + u_1, \quad u_1 = \frac{\partial \varphi}{\partial x}, \quad v = \frac{\partial \varphi}{\partial r}, \quad u_1, v \ll U_\infty \quad (2.7.4)$$

Then the boundary condition in Equation 2.7.2 takes the form:

$$\frac{\partial \varphi}{\partial r} = v = U_\infty \theta(x) \quad (2.7.5)$$

**FIGURE 2.12**

On the problem of the flow around a thin airfoil.

Since for thin bodies the r axis coincides in the limit with the normal to the body \mathbf{n} , this condition is equivalent to specifying the outward derivative, $\frac{\partial \varphi}{\partial n}$, on a closed contour. This is the external *von Neumann condition* well-known in the theory of partial differential equations.

Finally, we close the system by determining the pressure, enthalpy, and density from the linearized form of the Bernoulli equation, the equation of state, and the adiabatic equation

$$\begin{aligned} h - h_\infty &= \frac{p - p_\infty}{\rho_\infty} = \frac{1}{2}(U_\infty^2 - u^2 - v^2) = -u_1 U_\infty = -U_\infty \frac{\partial \varphi}{\partial x} \\ \rho - \rho_\infty &= \frac{p - p_\infty}{a_\infty^2} \end{aligned} \quad (2.7.6)$$

In handbooks on mathematical physics, Equation 2.7.3 falls in the category of simplest and canonical. Its properties are essentially dependent on the sign of the coefficient $M_\infty^2 - 1$. Let us explain this for plane flows ($v = 0$).

For $M_\infty > 1$ this is a *hyperbolic equation* and can be reduced to the *wave equation* (Section 2.5) by substituting at for $(M_\infty^2 - 1)^{-1/2}x$. The most typical feature of this equation is localization of the influence of boundary and initial conditions (disturbances) on the solution in regions bounded by characteristics.

For $M_\infty < 1$ this is an *elliptic equation*, which can be reduced to the *Laplace equation*

$$\frac{\partial^2 \varphi}{\partial x^2} + \frac{\partial^2 \varphi}{\partial r_1^2} = 0, \quad r_1 = r \sqrt{1 - M_\infty^2} \quad (2.7.7)$$

This equation is appropriate for describing arbitrary disturbances in incompressible flows (as $M_\infty \rightarrow 0$); to convince oneself that this is true it is sufficient to make u/a and v/a tend to zero in Equation 2.4.8.

For given conditions on a closed curve, the solution of this equation (in contrast to the wave equation) is determined throughout the entire unbounded external region (or, for inner problems, in the entire region bounded by the contour).

This fundamental difference between the equations manifests itself in the salient features of supersonic and subsonic flows and influences the choice of the methods used to solve the corresponding problems.

We note that for $M_\infty = 1$ Equation 2.7.3 degenerates into an ordinary differential equation (for $v = 0$ it is $d^2\varphi/dr^2 = 0$) and, as will be shown later, is inadequate for describing flows with $M_\infty \approx 1$ (see Chapter 5).

We will now consider some properties of linearized problems.

2.7.1 Similarity Law

As shown in Section 1.12, inviscid flows past bodies are, in the general case, similar for geometrically similar bodies and the same M_∞ and γ . We will show below that within the framework of the linear theory for perturbations p_1, u_1, v , and so on, this similarity law can be reduced to the single similarity criterion $\theta_0\beta_{\pm}$, where θ_0 is a typical (maximum) slope of the body surface and

$$\beta_+ = \sqrt{M_\infty^2 - 1} \quad (M_\infty > 1), \quad \beta_- = \sqrt{1 - M_\infty^2} \quad (M_\infty < 1) \quad (2.7.8)$$

Solutions for the whole family of affinely similar bodies, $\tilde{r}_b = r_b/L\theta_0$, that is, bodies that differ only by the relative body thickness, L being the body scale length, are reduced to unified dependences. To make the proof of this statement more general, we will use system 2.4.4. Omitting the time derivatives and eliminating the derivative $\partial u_1/\partial x$ yields the equations

$$\begin{aligned} U_\infty \frac{\partial v}{\partial x} &= -\frac{1}{\rho} \frac{\partial \Delta p}{\partial r}, \quad \Delta p = p - p_\infty = p_1 \\ \frac{M_\infty^2 - 1}{\rho_\infty U_\infty} \frac{\partial \Delta p}{\partial x} + \frac{1}{r^v} \frac{\partial}{\partial r} (r^v v) &= 0 \end{aligned} \quad (2.7.9)$$

We will represent the solutions of the previous equations in the form of the following dependences:

$$\begin{aligned} K\tilde{p} &= \frac{\beta \Delta p}{\rho_\infty U_\infty^2 \theta_0} = p'(x', r'), \quad \frac{\beta \Delta u}{U_\infty \theta_0} = u'(x', r') \\ \Delta u &= u - U_\infty, \quad \frac{v}{U_\infty \theta_0} = v(x', r') \\ x' &= \frac{x}{L}, \quad r' = \beta \frac{r}{L}, \quad K = \theta_0 \beta \quad (\beta = \beta_+, \beta_-) \end{aligned} \quad (2.7.10)$$

Here, the *pressure coefficient* \bar{p} , the *normalized pressure coefficient* \tilde{p} , and the *ram pressure* $\rho_\infty U_\infty^2$ are introduced (see Section 1.12)

$$\bar{p} = \frac{\Delta p}{\rho_\infty U_\infty^2}, \quad \tilde{p} = \frac{\bar{p}}{\sin^2 \theta_0} \quad (2.7.11)$$

In these variables, Equation 2.7.9 takes a form that does not involve any governing parameters of the problem

$$\frac{\partial v'}{\partial x'} = -\frac{\partial p'}{\partial r'}, \quad \pm \frac{\partial p'}{\partial x'} + \frac{1}{(r')^v} \frac{\partial}{\partial r'} ((r')^v v') = 0 \quad (2.7.12)$$

The plus and minus signs in front of the first term of the latter equation relate to supersonic and subsonic flows, respectively.

Far ahead of the body, in the undisturbed flow region, the boundary conditions $\Delta p = v = 0$ are homogeneous.

The impermeability condition (2.7.5) on the body surface can be written as follows

$$v'_b = \theta'(x') = \frac{\theta}{\theta_0}, \quad r'_b = \beta \frac{r_b}{L} = K \tilde{r}_b(x'), \quad \tilde{r}_b = \frac{r_b}{\theta_0 L}, \quad \beta = (\beta_+, \beta_-) \quad (2.7.13)$$

Thence it follows that the solutions for affinely similar bodies, that is, with the same function $\tilde{r}_b(x')$, are the same for equal parameters $\theta_0 \beta_+$ or $\theta_0 \beta_-$ (each for its own flow regimes) in the sense that dependences 2.7.10 of dimensionless functions on dimensionless parameters are the same for the problems under comparison.

This is the general *similarity law for flows past thin bodies within the framework of the linear theory*, while the parameter $K_0 = \theta_0 \beta$ is the *similarity criterion*. Both functions, p' and \tilde{p} , also satisfy the similarity law.

The similarity law obtained provides a useful method of systematizing and recalculating flow parameters even beyond the framework of the linear theory that generated this law. Thus, the ratios of the exact pressure increments (Δp) on a wedge and a cone in supersonic flow to those (Δp_{lin}) obtained according to the linear theory, $\Delta p / \Delta p_{\text{lin}}$, plotted in Figure 2.13 against the parameter $K = \theta_c \sqrt{M_\infty^2 - 1}$ (see Section 2.8), form a single bundle of curves even for $\Delta p / \Delta p_{\text{lin}} \approx 2 \div 4$, that is, far beyond the range of the linear theory applicability. In Figure 2.14 the pressures on plane airfoils in the form of circular arcs and of $r = \theta_0 x(1 - x/L)^{1/2}$ curves, as well as for axisymmetric spindle-shaped, or *ogive* bodies with the same contours

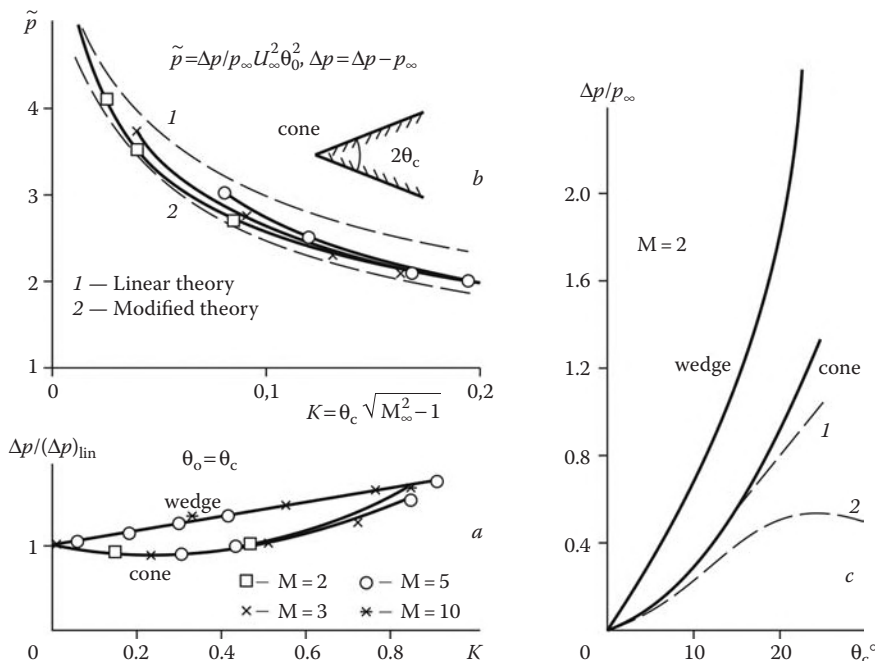
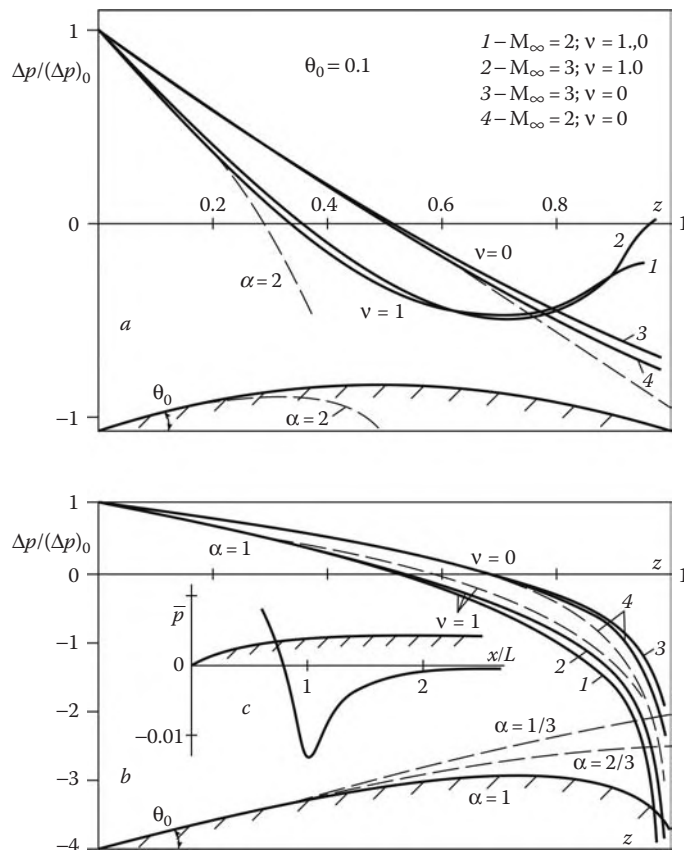


FIGURE 2.13

Pressure on thin wedges and cones.

**FIGURE 2.14**

Pressure on bodies of revolution and wing airfoils in a supersonic flow. Linear (dashed curves) and exact theories; $(\Delta p)_0$ is the pressure increment at the body nose.

of meridional sections, are presented. Clearly, similar curves for various K are almost indistinguishable (although for bodies of revolution, as distinct from plane bodies, the theoretical dependence of the solution on this parameter remains; see Section 2.8).

The universal nature of the solutions of form 2.7.10 means that the distribution of any fixed stage of a disturbance in the similarity variable plane (x', r') (e.g., $p'(r')$) is deformed in the physical variable plane, as $M_\infty \rightarrow 1$, displacing up and down from the body in accordance with an $r \sim r'/\beta$ law, so that the disturbed region forms in the limit a vertical strip. The disturbances themselves will be shown to grow as $p \sim \theta/\beta_{\pm}$ in the plane case and somewhat slower, as $p \sim \theta^2(-\ln K)$, in the axisymmetric case. In both cases this physically unfeasible result calls for the refinement of the thin body theory, which will be done in Section 5.2.

2.7.2 Unsteady Analogy

This term implies a mathematical similarity of problems for steady supersonic two-dimensional flows and unsteady one-dimensional flows induced by piston expansion in accordance with a $r = r_b(t)$ law or at a velocity $v_b = \dot{r}_b(t)$, the quantities U_0 and t_0 being the

expansion velocity and time scales, respectively. For the latter problem we introduce the dimensionless quantities as follows:

$$p'(t', r') = \frac{p - p_\infty}{\rho_\infty a_\infty U_0}, \quad v' = \frac{v}{U_0}, \quad t' = \frac{t}{t_0}, \quad r' = \frac{r}{a_\infty t_0} \quad (2.7.14)$$

In this case Equation 2.4.4 (with derivatives with respect to x omitted) describing unsteady piston expansion go over precisely to Equation 2.7.12 for supersonic flows, with the upper sign (plus) in the second equation and x' replaced by t' .

Similarly, the boundary conditions on the piston are

$$v'_b = \frac{v_b}{U_0}, \quad r'_b = \frac{r_b}{a_\infty t_0} = \frac{U_0}{a_\infty} \tilde{r}_b(t'), \quad \tilde{r}_b = \frac{r_b}{U_0 t_0} \quad (2.7.15)$$

Hence, the solutions of both problems, written in the dimensionless variables, are the same for the same values of the parameter $\beta_+ \theta_0 = U_0/a_\infty$ and the same functions $\tilde{r}_b(x')$ and $\tilde{r}_b(t')$.

So far, the quantity t_0 was arbitrary. Let now $t_0 = L/U_\infty$ be a gas dynamic time necessary for the body to pass a distance of its own length L . In this case, for dimensional quantities in similar steady and unsteady flows under comparison (subscripts s and n) the following recalculation formulas hold

$$\begin{aligned} L &= t_0 U_\infty, & U_0 &= a_\infty \beta_+ \theta_0, & x &= U_\infty t \\ r_s &= \frac{U_\infty}{a_\infty \beta_+} r_n, & \Delta p_s &= \frac{M_\infty^2}{\beta_+^2} \Delta p_n, & v_s &= \frac{M_\infty}{\beta_+} v_n \end{aligned} \quad (2.7.16)$$

The equivalence of both problems gives grounds to call the longitudinal coordinate x a "time" coordinate as well. In the general nonlinear case these problems are not equivalent but so mathematically similar, that more simple unsteady problems can advantageously be applied to resolve many questions of a fundamental nature even for steady problems.

All these results can be extended to three-dimensional flows; this can be easily verified by linearizing the original Equations 2.4.1 and 1.9.11 in Cartesian coordinates x, y, z under the assumption that two velocity components, v and $w \sim \theta_0 U_\infty$, are small. The parameter θ_0 can be either the relative body thickness (including the case of a near-planar wing of arbitrary shape) or its angle of attack α . The system of equations thus obtained differs from 2.4.4 by the substitution of y for r and $-\partial w/\partial z$ for Q_{eff} and by the presence of a linearized equation $\rho dw/dt = -\partial p/\partial z$, similar to the first two equations of system 2.4.4. The factor β_\pm of the derivative $\partial p/\partial x$ is still retained in the counterpart of the second equation of 2.7.9, which makes it possible to introduce the generalized similarity variables 2.7.10 with the additional parameters $w' = w/\theta_0 U_\infty$ and $z' = z\beta_\pm/L$. It turns out to be convenient to specify the body shape in a body-fitted coordinate system, which would not depend on the angle of attack. In this case, a parameter α/θ_0 is added to the similarity criteria, while the condition of the body shape similarity has, as earlier, the form $f'(x', y', z') = 0$.

2.8 Thin Bodies in Supersonic Flow

2.8.1 Plane Flows

We define a plane airfoil as a longitudinal section of a wing of infinite (or sufficiently large) span, when end effects can be neglected. Schematics of the flow around such an airfoil are

presented in Figure 2.12. Setting $r = y$ and $v = 0$ in 2.7.3 yields, by analogy with Section 2.5, the same Dalembert solution

$$\begin{aligned}\varphi &= f_1(\xi_-) + f_2(\xi_+), \quad \xi_{\pm} = x \pm \beta_+ y, \quad u - U_\infty = u_1 = \frac{\partial \varphi}{\partial x} = f'_1 + f'_2 \\ v &= \frac{\partial \varphi}{\partial y} = \beta_+(-f'_1 + f'_2), \quad \beta_+^2 = M_\infty^2 - 1 > 0\end{aligned}\quad (2.8.1)$$

The characteristics of the first and second families, ξ_- and ξ_+ , are plotted in Figure 2.12. In our problem $f_2 = 0$, so that all disturbances are concentrated to the right of the leading characteristic $x = \beta_+ y$ and are specified by a function f_1 determined from the boundary conditions 2.7.5. Therefore, we have

$$\begin{aligned}v &= -\beta_+ f'_1(x - \beta_+ y) = -\beta_+ f'_1(x) = U_\infty \theta(x) \\ f'_1(\xi_-) &= -U_\infty \theta(\xi_-) \beta_+^{-1} \\ \Delta p &= p_1 = p - p_\infty = -\rho_\infty U_\infty u_1 = \rho_\infty U_\infty^2 \beta_+^{-1} \theta(\xi_-)\end{aligned}\quad (2.8.2)$$

Here, the boundary conditions are swept from the body surface to the x axis, so that the shape of the surface affects the solution only via its slope $\theta(x)$. Referring all the coordinates to the airfoil length L and surface inclination angles to a characteristic slope θ_0 we can represent the solution in variables 2.7.10, with y replaced by r , as follows:

$$p' = v' = -u' = \theta'(x' - y') = \frac{\theta}{\theta_0} \quad (Ly' = y\beta_+) \quad (2.8.3)$$

On the airfoil surface the following relation takes place

$$\frac{\Delta p}{p_\infty} = B\theta(x), \quad B = \frac{\gamma M_\infty^2}{\sqrt{M_\infty^2 - 1}} \quad (2.8.4)$$

This formula is very popular in aerodynamics due to its simplicity; the range of its applicability, even for bodies with sharp narrowing of the rear, can be judged from the data presented in Figures 2.13 and 2.14.

This solution makes it possible to determine in retrospect the range of applicability of the linear theory resulting from the requirement $\Delta p \ll p_\infty$: not only θ_0 , but also $B\theta_0$ should be small. In limiting cases corresponding to hypersonic and transonic flows these conditions have the form:

$$\begin{aligned}B\theta &\sim M_\infty \theta \ll 1, \quad M_\infty \gg 1 \\ B\theta &\sim \theta(M_\infty^2 - 1)^{-1/2} \ll 1, \quad M_\infty - 1 \ll 1\end{aligned}\quad (2.8.5)$$

However, more thorough analysis to be done in Section 5.2 will lead to stronger conditions for the transonic velocity range. Moreover, we note that, in spite of the presence of formal estimates, the real limits of the linear theory applicability cannot be determined within the framework of the theory itself and require being checked using exact solutions.

We note one more interesting flow feature. From the relation

$$\frac{v}{u_1} = -(M_\infty^2 - 1)^{1/2} \quad (2.8.6)$$

it follows that in transonic flows the longitudinal velocity disturbances exceed considerably those of the transverse velocity, while in hypersonic flow the situation is the opposite.

For a thin airfoil of width h and length L the drag force X is as follows

$$X = h \int_{-L/2}^{L/2} \Delta p n_x dx = \frac{\rho_\infty U_\infty^2 h}{\sqrt{M_\infty^2 - 1}} \int_{-L/2}^{L/2} \theta^2 dx = \frac{1}{2} \rho_\infty U_\infty^2 L h c_x \quad (2.8.7)$$

Here, c_x is the dimensionless drag coefficient of the airfoil (or, more exactly, that of one of its sides, either upper or lower). According to the similarity law discussed previously, it is the *normalized drag coefficient*

$$\tilde{c}'_x = \frac{c_x \sqrt{M_\infty^2 - 1}}{\theta_0^2} \quad (2.8.8)$$

that is, the universal parameter for a given class of affinely similar profiles, rather than c_x itself.

The drag of a body induced by inviscid pressure distribution is termed the *wave drag*; the term will be explained in what follows. Clearly, the airfoil drag is quadratic in θ_0 , since both the pressure and the relative airfoil thickness δ/L are linear in θ_0 . We note that the drag coefficient is to some degree a conditional quantity, since it depends on the choice of the body scale length.* Here the chord length of a wing is chosen to be the scale, but instead of it the wing thickness can be chosen. For plane flows we take $h = 1$.

We will now consider a simple example of a flat plate at an angle of attack α . Pressures on the lower (+) and upper (-) sides of the plate are $\Delta p_\pm = \pm \rho_\infty U_\infty^2 \alpha / \beta_\pm$, so that the drag and lift coefficients of the plate are

$$c_x = \frac{2X}{\rho_\infty U_\infty^2 L} = \frac{4\alpha^2}{\sqrt{M_\infty^2 - 1}}, \quad c_y = \frac{2Y}{\rho_\infty U_\infty^2 L} = \frac{4\alpha}{\sqrt{M_\infty^2 - 1}} \quad (2.8.9)$$

Here, X is the drag and Y is the lift (normal to \mathbf{U}_∞).

In contrast to the drag, the lift depends linearly on α , since the projection of the surface normal onto the y axis is $n_y \approx 1$.

We will give one more solution for a parabola arc with a chord L and an edge slope θ . Let the origin be taken at the chord midpoint (Figure 2.12). Then we obtain

$$\begin{aligned} y_b &= \frac{1}{4} \theta_0 L (1 - 4x^2/L^2), & \theta &= -2x\theta_0/L \\ u' &= 2\xi'_- = -v', & -\frac{1}{2} < \xi'_- &= \xi_-/L < \frac{1}{2} \\ \xi_- &= x - \beta_+ y, & -\frac{1}{2}L &\leq x \leq \frac{1}{2}L \end{aligned} \quad (2.8.10)$$

In this case, the pressure distribution over the airfoil is linear (Figure 2.8) and $c'_x = 2/3$. If the angle of attack of an airfoil is α , the local pressure on it is equal (since the problem is linear) to the sum $\Delta p \sim \alpha + \theta$. Thus, the lift of the wing is equal to the sum of the lift of an airfoil at zero incidence (which is zero for a parabolic arc) and that of its chord considered as an isolated plate at an angle of attack α . However, now the wing drag is no longer additive since it is proportional to the square of the local angle of attack, $(\alpha + \theta)^2$.

* The coefficient 1/2 in formula 2.8.7 is also conditional; historically it is related to incompressible flows in the theory of which the ram pressure is, in accordance with the Bernoulli Equation 2.2.10, considered to mean the quantity $\rho_\infty U_\infty^2/2$ rather than $\rho_\infty U_\infty^2$, which would be more appropriate in supersonic gas dynamics.

We will make several remarks on nonlinear effects in supersonic flows past thin airfoils. The solution obtained previously propagates to infinity without being distorted. This peculiar feature is, however, a consequence of the fact that the flow model adopted is only approximate, and can be eliminated in a rigorous analysis by taking into account two points.

First, the finiteness of the real wing span should be taken into account, since disturbances induced by the central part of the wing (except for, probably, their wakes) are sooner or later offset by end effects. As for three-dimensional flows past finite bodies, all disturbances die out far from the body, as will be shown when considering flows past thin cones.

Second, nonlinear effects due to disturbance interactions (similar to those considered in Section 2.6) should be taken into account. The linear theory gives a finite increment, or a pressure discontinuity, on the leading and trailing characteristics; this, according to Section 2.6, corresponds to a weak shock, which, as will be shown in Chapter 4, dies out far from the body.

We note one more important effect: according to 2.8.8, the wing drag increases without bounds, as $M_\infty \rightarrow 1$. This is a result of the violation of linearization conditions 2.8.6, but, at the same time, this indicates that the drag really grows. This effect is termed the *sound barrier* and will be considered in Chapter 5.

2.8.2 Axisymmetric Problems

For the sake of simplicity, we will consider an acoustic problem of gas flow in front of an expanding piston, $r = r_b(t)$. For supersonic flows past bodies the results obtained in that problem could be recalculated using transformation 2.7.16. Just for a change, instead of the equation for the potential, we will use the original system 2.4.4, reduced to two last equations in which, moreover, u_1 , U_0 , and $\partial/\partial x$ are equated to zero.

Let at point ($t = 0, r = 0$) a piston begin to expand at a constant velocity $v_b = U_0$. The problem depends only on the set of parameters (U_0, a, t, r) ; therefore, in accordance with the similarity theory of Section 1.12, its solution is self-similar and depends on a single variable $\eta = r/at$ and the similarity criterion $K = U_0/a$. Let

$$\Delta p = \rho U_0^2 P(t, r), \quad v = \frac{U_0^2}{a} V(t, r) \quad (2.8.11)$$

Putting $P = P_0(\eta)$ and $V = V_0(\eta)$ we bring 2.4.4 to the form:

$$P'_0 = \eta V'_0, \quad \eta^2 P'_0 = (\eta V_0)', \quad \eta = r/at \quad (2.8.12)$$

The system has a solution

$$V_0 = \eta^{-1}(1 - \eta^2)^{1/2}, \quad P_0 = \frac{1}{2} \ln \frac{1 + \sqrt{1 - \eta^2}}{1 - \sqrt{1 - \eta^2}} \quad (2.8.13)$$

Thence, correct to the terms of the order η_0^2 , we obtain the flow parameters on the cone

$$V_0(\eta_0) = \frac{1}{\eta_0}, \quad P_0(\eta_0) = \ln \frac{2}{\eta_0} = \ln \frac{2a}{U_0}, \quad \eta_0 = U_0/a \quad (2.8.14)$$

As distinct from the plane problem, here we have $\Delta p = \rho av = 0$ on the leading characteristic $\eta = 1$. A new feature is also the quadratic law for the pressure. This result could be easily explained. In fact, the work of an expanding piston $A \sim pr_b^{1+v}$ is spent, in particular,

for an increase in the internal energy $E \sim \Delta p R^{1+\nu}$. Hence, we have $\Delta p/p \sim (U_0/a)^{1+\nu}$, which gives a linear (at $\nu = 0$) and quadratic (at $\nu = 1$) dependence of Δp on U_0^2 . A relatively small correction coefficient $\ln U_0$ does not change the situation.

Using the unsteady analogy of Section 2.7 (relations 2.7.16), solutions 2.8.11 through 2.8.14 can be transformed for the case of a thin cone with a vertex angle $2\theta_c$ and the vertex at point $x = 0$ in a supersonic flow

$$\begin{aligned} v &= \theta_c U_\infty V_0(\eta), & \tilde{p} &= \frac{p - p_\infty}{\rho_\infty U_\infty^2 \theta_c^2} = P_0(\eta) \\ && \tilde{p}_c &= \ln \frac{2}{\eta_c} = \ln \frac{2}{\theta_c \beta_+} \\ \eta &= \frac{r}{x} \beta_+, & \eta_0 &= \theta_c \beta_+, & \beta_+ &= \sqrt{M_\infty^2 - 1} \end{aligned} \quad (2.8.15)$$

Here, \tilde{p} is the normalized pressure coefficient (cf. 2.7.11), while the functions $V_0(\eta)$ and $P_0(\eta)$ are determined by formulas 2.8.13. As follows from Figure 2.13, the pressure on a thin cone is smaller than that on a wedge and almost proportional to θ_c^2 . However, as will be seen later, on the nonlinear range, for $\Delta p \sim p$, pressures on a wedge and a cone follow a quadratic law and for $M_\infty \gg 1$ differ only slightly. As follows from Figures 2.13 to 2.15, the accuracy of the linear theory is, on the one hand, satisfactory up to the values of $K = \theta_c \beta_+ \leq 0.5$, which are not so small, and, on the other hand, even on the transonic range, $M_\infty \geq 1.015$. The latter is a result of the fact that, as $M_\infty \rightarrow 1$, the solution obtained

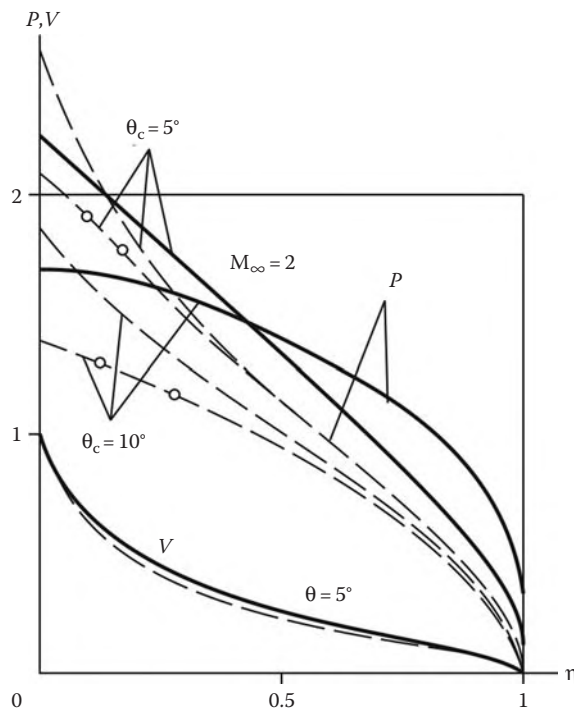


FIGURE 2.15

Pressure and transverse velocity profiles on cones; dashed curves relate to the linear theory for P_0 and V_0 , circles to the modified theory, and solid curves to the exact calculations.

has a considerably weaker singularity than in the plane problem ($\ln \beta_+$ instead of β_+^{-1}), and, in general, theoretical conditions under which the linear theory could be applied to axisymmetric flows are not so strong as conditions 2.8.5 for plane flows

$$\Delta u \sim \Delta p / \rho U_\infty^2 \sim \theta^2 |\ln \beta_+ \theta| \ll 1, \quad v/U_\infty \sim \theta \ll 1 \quad (2.8.16)$$

The functions $P_0(\eta)$ and $V_0(\eta)$ are plotted in Figure 2.15. They are similar to the exact ones for $K \approx 0.15$ (for $M_\infty = 2$ and $\theta = 5^\circ$), but the agreement deteriorates when this parameter is doubled. In contrast to the wedge, the pressure decreases with the distance from the body. This can be explained by convergence of stream tubes and concavity of streamlines, since the streamline slope on the bow wave, which is zero within the framework of the linear theory, is smaller than that on the cone surface; in accordance with Equation 2.2.6, this leads to an increase in the pressure. This pressure behavior is specific for flows past cones with relatively small θ_c and M_∞ .

We note that the solution obtained is not bounded as $\eta \rightarrow 0$, while near the points $\eta \approx \eta_0$ and η_c the omitted-to-retained term ratio is of the order of $v(\partial/\partial y)/U_\infty(\partial/\partial x) \sim v/(U_\infty \eta_c) \sim 1$, that is, strictly speaking, linearization is not legitimate in this wall region. However, in view of the relative smallness of this region, its contribution to the total solution is also small. Nevertheless, we can partially take into account the omitted terms, thus improving the result for small K (Figures 2.13b and c, and Figure 2.15). This *modified* linear theory (Lighthill, 1947) will be considered in Section 6.4, together with the nonlinear theory.

The linear theory can give useful solutions in integral form and even in terms of elementary functions; for this reason, we will briefly describe it for the general case. Functions 2.8.13 gives a solution of the original system also when η is replaced by $\zeta = r/a(t - \tau)$. The functions can be chosen as elementary conical sources distributed along the τ axis; their superposition gives the general solution ($F = V, P$)

$$F = C_0 F_0(\eta) + \int_0^{\tau_m} C'(\tau) F_0(\zeta) d\tau, \quad \tau_m = t - r/a \quad (2.8.17)$$

The choice of the upper limit τ_m is obvious since disturbances arising at $\tau > \tau_m$ have no time to reach the point (t, r) during the time interval $t - \tau$. As $\tau_m \rightarrow 0$ the integral vanishes and the first term gives the solution for a piston as $t \rightarrow 0$. The singularity arising when differentiating the integral with respect to the upper limit can, usually, be avoided by substituting beforehand operators F with the upper limit of the integral $\tau_m - \varepsilon$ into Equation 2.4.4 and making ε tend to zero in the final result.

Finally, to determine the arbitrary function $C(\tau)$ we should make r to tend to r_b , v to v_b , and τ_m to t . In this case, $V_0 \approx a(t - \tau)/r$ for small $r \sim r_b$ and r^{-1} can be factored outside the integral sign. Integrating by parts and setting $C(0) = C_0 = 1$ we obtain

$$r_b v_b = \frac{1}{2} \frac{dr_b^2}{dt} = U_0^2 \int_0^t C d\tau, \quad C = \frac{1}{2U_0^2} \frac{d^2 r_b^2}{dt^2} \quad (2.8.18)$$

Thus, the solution of such problems can be obtained in an integral form. A possible way to find the solution in terms of elementary functions is to approximate the arbitrary function C by polynomials of the type $C = \sum_n C_n \tau^n$. A particular solution corresponds to each

term of the sum. For example, the sum $C = 1 + C_1\tau$ is associated with the following piston and solution

$$\begin{aligned} r_b &= U_0 t \left(1 + \frac{C_1 t}{3}\right)^{1/2}, & V(\eta) &= V_0(\eta) + C_1 V_1(\eta) \\ && P &= P_0(\eta) + C_1 P_1(\eta), \\ V_1(\eta) &= \frac{1}{2} t V_0 - \frac{1}{2} \frac{r}{a} P_0, & P_1 &= t P_0 - \frac{r}{a} V_0 \end{aligned} \quad (2.8.19)$$

the solution being obtained by the change of the variables $d\tau = (r/a\xi^2)d\xi$ and the use of Equation 2.8.12. Substituting P_0 and V_0 for $\eta = \eta_b$ and using the analogy of Section 2.7 we write the expression for the pressure on similar bodies in supersonic flow in a somewhat modified form:

$$\begin{aligned} \tilde{p}(z) &= \Delta p / \rho_\infty U_\infty^2 \theta_0^2 = \ln 2/\eta_b - 3z(\ln 2/\eta_b - 1) \\ r_b &= \theta_0 x(1-z)^{1/2}, \quad \eta_b = r_b \beta_+/x = K(1-z)^{1/2} \\ z &= cx, \quad \beta_+ = (M_\infty^2 - 1)^{1/2}, \quad K = \theta \beta_+ \end{aligned} \quad (2.8.20)$$

Here, c is the parameter having the dimension L^{-1} . This “basic” body and the pressure on it are shown in Figure 2.14b. Clearly, solution 2.8.20 is in good agreement with the exact one, except for a vicinity of the trailing edge $z \approx 1$, where the tangent to the body is vertical, which does not allow us to apply the linear theory in this vicinity. At point $x = 2/3$ the relative size of the body is $r_0/\theta_0 x = 3$. Cutting off any forepart of the body and setting $cL = \alpha$ we obtain a one-parameter family of the contours shown in Figure 2.14b, $r_b = \theta_0 x(1-\alpha x/L)^{1/2}$, the pressure on which is determined by the same formula 2.8.20. For $2cL = 1$ the forward part of this curve ($x \leq L/4$) is similar to the nose part of a parabolic arc, $r_b = \theta_0 x(1-x/L)$, of length L (Figure 2.14a). In this region the pressures on both bodies are the same, while further they are different.

In contrast to the plane airfoils, the pressure on axisymmetric bodies does not follow any local law. Thus, on an ogive body (Figure 12.14) a negative excessive pressure occurs already in a region $\theta = dr_b/dx > 0$, while the pressure behavior on the rear depends essentially on the shape of the latter. Thus, it grows on a parabolic arc in spite of a decrease in θ , which is the manifestation of the “cumulation” effect of converging flows, fairly typical for the axisymmetric case. At the same time, the decrease in the slope θ prevails over this effect on the body specified by Equation 2.8.20, so that the pressure decreases.

As follows from Figure 2.14b, the pressure curve (2.8.20) with $\alpha = 1$ passes through zero at $z \approx 0.5$; therefore, on the rear of this body with $\alpha = 1/2 \div 1/3$ the quantity Δp is negative at a positive slope $\theta > 0$. The rarefaction propagates further to the cylinder attached to the forebody, thus making the pressure distribution to oscillate (Figure 2.14c for $\alpha = 2/3$).

This effect leads to a certain decrease in the drag of such a body nose as compared with a cone with the same relative radius of the end section r_0/L ($c_x \approx 0.012$ for $\alpha = 2/3$ and $c_x \approx 0.015$ for an equivalent cone with $\theta = r_0/L = 0.058$). Solutions of linearized problems of the minimum-drag body lead to an ogive similar to the body with $\alpha = 2/3$ (Ferrari, 1965).

Similarly, within the framework of the linear theory a wedge is an optimal plane nose. In fact, giving any variation to the wedge surface with fixed ends, $\theta = \theta_0 + \theta_1$, $\theta_1 \ll \theta_0$, we obtain a drag increment proportional to the integral of $\theta^2 - \theta_0^2$, which is always positive.

At the same time, on an airfoil of a given thickness h and length L composed of two rectilinear segments passing through sharp edges and intersecting at $x_l = l$, the drag $X \sim (h/l)^2 + [h/(1-l)]^2$ is minimum at $l = L/2$ (a rhombus). If, however, the trailing

edge of this airfoil has a finite thickness d and the base pressure is preassigned, $p_d < p_\infty$, then an extremum takes place for a finite $d > 0$ (Kraiko and Pudovikov, 1997).

These examples show that, in spite of intense development of computational gas dynamics, we have a long way to go before we are able to abandon the linear theory, since its analytical solutions make it possible to obtain qualitative and generalizing results. In particular, we point to the fairly developed linear theory of three-dimensional supersonic and subsonic flow around thin finite-span wings, which, unfortunately, is absent from this book. Within the framework of this theory, rather general results, both qualitative and quantitative, were obtained.

2.9 Subsonic Flow Past Thin Bodies

As in Section 2.8, we will construct a solution only for a very simple problem of the flow past a slender symmetric body using the *source method* that is easy to outline and will be also useful in obtaining a number of general results. We note that the general theory of these problems is associated with the conformal mapping method (see Section 2.10) and the theory of singular integral equations (Sedov, 1965; S. M. Belotserkovskii, 1965; Vorobyev, 1986; and others).

The method consists of replacing the body in gas flow by fictitious sources distributed along the x axis and having such intensities $q(x)$ that the streamline separating two flows (internal and external) coincides with the contour of the body, as shown in Figure 2.12.

Each elementary source at a point $(x', 0)$ has its own potential, which is a *fundamental solution* of Equation 2.7.3 and is dependent on the dimensionality of the problem under consideration.

For plane flows ($v = 0$), this potential has the form

$$d\varphi(x, y, x') = q(x') \ln r' dx', \quad r' = \sqrt{(x - x')^2 + \beta_-^2 y^2} \\ \beta_-^2 = 1 - M_\infty^2 > 0 \quad (2.9.1)$$

Here r' is the distance from the point (x, y) to the source $(x', 0)$. The radial velocity induced by the source is $v_r = q/r'$, which ensures the constancy of the source flow rate. Since Equation 2.7.3 is linear, we can seek a solution of the problem in the form of the integral

$$\varphi = \int_{x_1}^{x_2} q(x') \ln r' dx', \quad q = 0 \quad \text{for} \quad x < x_1 = -\frac{1}{2}L, \quad x > x_2 = \frac{1}{2}L \quad (2.9.2)$$

Here, anticipating the final result, we have let $q = 0$ outside the segment (x_1, x_2) , which gives the integration limits.

The disturbed velocity field is also determined in terms of this integral

$$u_1 = u - U_\infty = \frac{\partial \varphi}{\partial x} = \int_{x_1}^{x_2} \frac{q(x')(x - x')}{r'^2} dx' \\ v = \frac{\partial \varphi}{\partial y} = \beta_-^2 y \int_{x_1}^{x_2} \frac{q(x')}{r'^2} dx' \quad (2.9.3)$$

In order for the potential to be a solution of the original boundary-value problem, it must satisfy the impermeability condition 2.7.5 on the body contour $y_b(x)$. Then the function $q(x)$ must satisfy an integral equation obtained by putting $v[x, y_b(x)] = U_\infty \theta(x)$ in the second formula 2.9.3.

The fact that the kernel of this equation is singular simplifies considerably the situation. In fact, as $y, (x - x') \rightarrow 0$, the singularity gives the main contribution of the interval $|x' - x| \sim y_b$ to the integral. The order of this contribution in this region is not smaller than y_b^{-2} , as compared with the order of the contribution of the remainder of the integration region. Hence, as $y \rightarrow 0$, the integral is determined in this vicinity by the quantity $q(x')$. Then setting $q(x') = q(x) + q'(x)(x - x')$ we obtain the following solution valid for $y \sim y_b \sim \theta L$

$$\begin{aligned} v &= \beta_- q(x) (\arctan z_2 - \arctan z_1) + \frac{1}{2} q'(x) \beta_- y \ln \frac{z_2^2 + 1}{z_1^2 + 1} \quad (y \sim \theta L) \\ z &= \frac{x' - x}{\beta_- y}, \quad z_{1,2} = \frac{x_{1,2} - x}{\beta_- y}, \quad z_1 < 0, \quad z_2 > 0 \end{aligned} \quad (2.9.4)$$

We next require that this function satisfy the boundary condition on the airfoil. The second term of the solution is equal to zero on the y axis and, hence, is small in its vicinity (the orders of the contributions of the subsequent omitted terms to the expansion of $q(x')$ are even smaller). In the first term the coordinates $z_{1,2} \sim \theta^{-1}$, and, therefore, they can be replaced by their limiting values $z_{1,2} \rightarrow \mp\infty$. Then

$$v[x, y_b(x)] \rightarrow v(x, 0) = \beta_- \pi q(x) = U_\infty \theta(x), \quad y \rightarrow 0 \quad (2.9.5)$$

This determines the required function $q(x)$. It appears to be possible to sweep the boundary condition to the axis $y = 0$ in spite of a singularity in the general solution. Due to the symmetry of the problem, the same formula gives also the solution for the wing undersurface, in the region $y < 0$.

As an example, we will give a solution for the airfoil considered in Section 2.8. It consists of two symmetrical parabolic arcs 2.8.10 having the chord length L and edge slope θ_0 . Substituting $\theta = -2\theta_0 x/L$ in Equation 2.9.3 we obtain

$$\begin{aligned} u' &= \frac{u_1 \beta_-}{\theta_0 U_\infty} = \frac{2}{\pi} + \frac{x}{\pi L} \ln \frac{\beta_-^2 y^2 + (L/2 - x)^2}{\beta_-^2 y^2 + (L/2 + x)^2} - \\ &\quad 2 \frac{\beta_- y}{\pi L} \left(\arctan \frac{L/2 - x}{\beta_- y} + \arctan \frac{L/2 + x}{\beta_- y} \right) \end{aligned} \quad (2.9.6)$$

The right-hand side has a limit as $y \rightarrow 0$; therefore, in evaluating velocity and pressure distributions over the body surface, $\Delta p = -\rho_\infty U_\infty u_1$, we can set $y = 0$. The corresponding longitudinal velocity distributions along the x and y axes are plotted in Figure 2.16.

The convergence of integral 2.9.3 as $y \rightarrow 0$ despite its singularity requires explanation. To do this, we will write the sum (for $\beta_- = 1$)

$$u_{1\varepsilon} = q(x) \left[\int_{x_1}^{x-\varepsilon} \frac{dx'}{x - x'} + \int_{x+\varepsilon}^{x_2} \frac{dx'}{x - x'} \right] + I \quad (2.9.7)$$

Here, the integral I contains the difference $q(x') - q(x)$ in its numerator, thus being non-singular, while the integrals in the brackets contain the same singular terms $\ln \varepsilon$ having opposite signs and vanishing when being added. Thus, the sum in the brackets is finite as

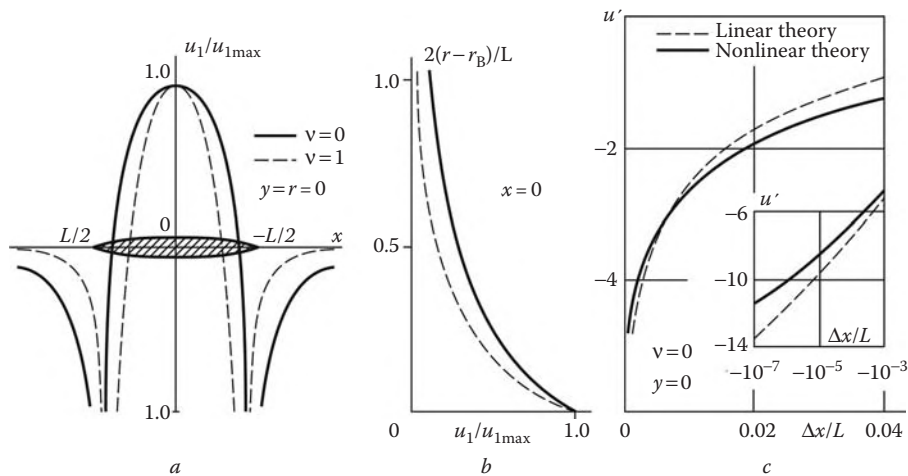


FIGURE 2.16
Longitudinal velocity component near a thin body.

$\varepsilon \rightarrow 0$ and, hence, $u_{1\varepsilon} \rightarrow u_1$ (similar singular integrals are called *convergent in the Cauchy meaning*).

The solution obtained satisfies the similarity law formulated in Section 2.7 and is expressed in terms of fundamental formulas of type 2.7.10. The singularity it has as $M_\infty^2 \rightarrow 1$ is of the same order as that for $M_\infty > 1$ in Section 2.8.

A comparison of the data obtained and those of Section 2.8 shows an essential qualitative difference between subsonic and supersonic flows, namely: in subsonic flows there are no discontinuities and sharply outlined zones of disturbance concentrations; they cover the entire flow region decaying asymptotically in all directions at a distance of the order of the body size. The solution is no longer of a local nature. For example, at the midpoint $x = 0$ of a body the velocity u' is equal to $2/\pi$, in contrast to the supersonic flow, in which, due to the locality law, $\Delta p = u_1 = 0$ at this point.

The second difference between solution 2.9.3 and that obtained in Section 2.8 is a logarithmic singularity of Equation 2.9.3 on the wing edges, $u_1 \sim \ln |x - x_{1,2}| \rightarrow -\infty$ and $p_1 \rightarrow \infty$, as $x \rightarrow x_{1,2}$. Theoretically, this is an evidence that the linearization is not legitimate, while from the physical point of view this means that disturbances in edge vicinities are finite in spite of the smallness of the disturbing angle. Thus, the complete problem of flow past a thin airfoil is *nonlinear* (if no special measures of precaution concerned with edge shapes are taken) and will be considered in Section 2.11. We will only note that the velocity at the leading edge is zero and compare the results in the vicinity of the wing edge obtained from both the exact and the linear theories (Figure 2.16c).

A parabolic arc in subsonic flow (in contrast to the supersonic one) exhibits no drag owing to the symmetry in the pressure distribution on the forward and rear parts. This result could be explained by a particular form of the profile or by the approximate formulation of the problem, but, in fact, this is a particular manifestation of the general law to be considered in Section 2.12.

Axisymmetric problems will be only sketched here. In this case Equation 2.7.3 for the potential has the fundamental solution $\varphi' = -q(x')/r'$ ($v = 1$), which leads to the general solution

$$\begin{aligned}\varphi &= - \int_{x_1}^{x_2} \frac{q(x') dx'}{r'}, \quad r' = \sqrt{(x - x')^2 + \beta_-^2 r^2} \\ u_1 &= \frac{\partial \varphi}{\partial x} = \int_{x_1}^{x_2} \frac{(x - x') q(x') dx'}{r'^3}, \quad v = \frac{\partial \varphi}{\partial r} = \beta_-^2 r \int_{x_1}^{x_2} \frac{q(x') dx'}{r'^3}\end{aligned}\quad (2.9.8)$$

Here, it is assumed that $q = 0$ outside the segment $[x_1, x_2]$. The boundary condition $v \rightarrow v_b = U_\infty dr_b/dx$ on the body surface $r = r_b(x)$ leads, as earlier, to an integral equation for the source $q(x')$. As in the plane problem, the singularity of the integral as $r' \rightarrow 0$ makes it possible to set $q(x') = q(x)$ and to factor out the function $q(x)$ from the integral. However, we cannot set $r_b = 0$ in the denominator; therefore, as in Section 2.8, the body shape enters in the solution for bodies of revolution directly rather than in terms of the slope $\theta_b(x)$ only.

However, the same singularity gives a possibility to replace $r_b(x')$ by $r_b(x)$ in the integral, which leads to the solution

$$\begin{aligned}U_\infty \frac{dr_b}{dx} = v_b &= \frac{(x' - x)q(x)}{r_b \sqrt{(x' - x)^2 + \beta_-^2 r_b^2(x)}} \Big|_{x'=x_1}^{x'=x_2} = 2 \frac{q(x)}{r_b} \\ q(x) &= \frac{1}{4} U_\infty \frac{dr_b^2}{dx}, \quad r_b^2 \beta_-^2 \ll (x_i - x)^2\end{aligned}\quad (2.9.9)$$

We note that this solution is valid only for bodies with sharp ends (x_1, x_2), at which the body shape follows the law $r_b = \theta_0 |x_i - x|^\alpha$, $\alpha \geq 1$, $\theta_0 \ll 1$, and at these points $q(x_i) = 0$. We also note that, as distinct from the plane problem, the quantity q is independent of the Mach number M_∞ .

Integrating by parts, Equation 2.9.8 for u_1 is brought to the form:

$$u_1 = \frac{q(x')}{r'} \Big|_{x'=x_1}^{x'=x_2} - \int_{x_1}^{x_2} \frac{q' dx'}{r'}, \quad q' = \frac{dq(x')}{dx'} \quad (2.9.10)$$

As shown previously, the first term vanishes for $q(x_i) = 0$.

Integrals 2.9.8 and 2.9.10 are reduced to elementary functions if $q(x')$ (i.e., the body shape $r_b(x)$) is given in terms of a polynomial in x . We will write the solution u_1 for the same parabola arc 2.8.10 with the ends $x = \pm L/2$ as in the plane case

$$\begin{aligned}\tilde{u}_1 &= \frac{u}{U_\infty \theta_0^2} = \frac{1}{4} \left(1 - 3\bar{x}^2 + \frac{3}{2} \beta_-^2 \bar{r}^2 \right) \ln \frac{\Delta_- - \bar{x} + 1}{\Delta_+ - \bar{x} - 1} - \\ &\quad \frac{3}{8} (3\bar{x} + 1) \Delta_- + \frac{3}{8} (3\bar{x} - 1) \Delta_+ \\ \Delta_\pm &= \sqrt{(1 \pm \bar{x})^2 + \beta_-^2 \bar{r}^2}, \quad \bar{x} = 2x/L \\ \bar{r} &= 2r/L, \quad \bar{r}_b = \frac{\theta_0}{2} (1 - \bar{x}^2)\end{aligned}\quad (2.9.11)$$

Passing to the limit, $r \rightarrow r_b \rightarrow 0$ for $|\bar{x}| < 1$ and $r \rightarrow 0$ for $|\bar{x}| > 1$, that is, along the x axis, we obtain

$$\begin{aligned}\tilde{u}_{1b} &= \frac{1}{4} (1 - 3\bar{x}^2) \left[\ln \frac{16}{K_-^2(1 - \bar{x}^2)} - 3 \right], \quad |\bar{x}| < 1, \quad K_- = \theta_0 \beta_- \\ \tilde{u}_{10} &= \frac{1}{4} \left[(3\bar{x}^2 - 1) \ln \frac{|\bar{x}| - 1}{|\bar{x}| + 1} + 6|\bar{x}| \right], \quad |\bar{x}| > 1\end{aligned}\quad (2.9.12)$$

For $\theta_0 \ll 1$ this solution is of the same order, $u_1 \sim \Delta p \sim \theta_0^2 \ln K_-$, as that for supersonic flow considered in Section 2.8. As in the plane problem, the function $u_{1b}(x)$ is symmetric about the body center and has a singularity of the same order, $u_1 \sim \ln |x - x_i|$, as $x \rightarrow x_i$. The singularity is integrable in evaluating the body drag. In contrast to the plane problem, the solution is not symmetric with respect to the endpoints and, moreover, is independent of M_∞ at the axis of symmetry outside the body. The profiles of \tilde{u}_1 along the x and y axes are plotted in Figure 2.16a and b.

We will now consider briefly one more important class of problems for which the source method appears to be insufficient; this is the class of plane circulatory flows around nonsymmetric airfoils. The Tomson theorem admits the presence of vortex sources with arbitrary distribution inside the body and the total circulation Γ around any contour enclosing the body. In this case the flow outside the body is again irrotational, but the solution becomes nonunique, since within the framework of the inviscid flow model the circulation itself cannot be determined without additional physical assumptions.

So far, such an assumption is known only for a very particular class of thin airfoils with an infinitely thin trailing edge (Figure 2.17). Experience shows that for small angles of attack a flow around such an airfoil is separationless, with smooth flow shedding from the trailing edge. Within the framework of the inviscid model this assumption corresponds to a specific value of the circulation. This assumption, or the *Joukowskii hypothesis*, was very fruitful in its time and made the theory important for applications.

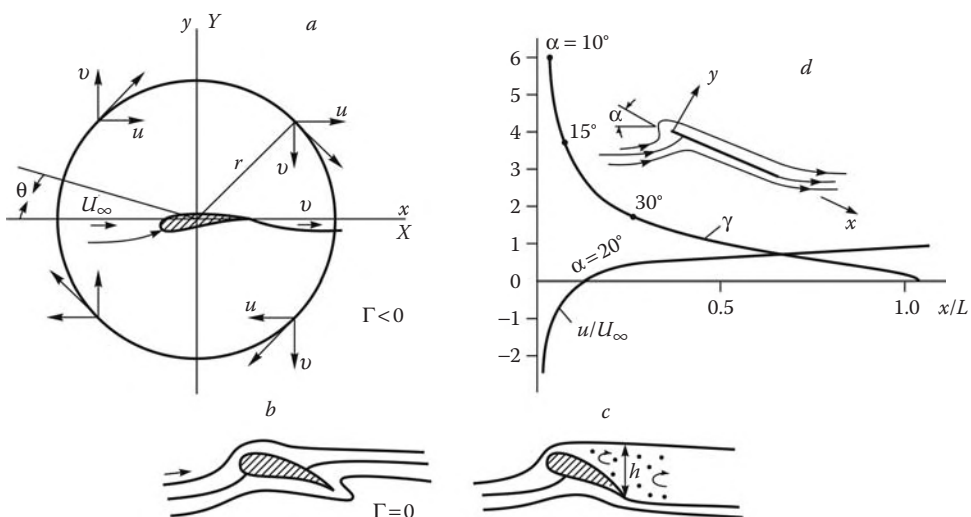


FIGURE 2.11

Nonsymmetric flow past bodies: a, circulation flow in accordance with the Joukowskii scheme; b, circulation-free flow; c, jet model of Kirchhoff; and d, plate at an angle of attack.

Let us explain how this flow pattern is formed. In a circulation-free flow around an airfoil there are two stagnation points on its sides (Figure 2.17b); however, this flow is physically unfeasible, since a separationless flow past a sharp edge is impossible (as the theory and experiments show). Therefore, this flow must rearrange itself; as an alternative, Kirchhoff suggested a jet model with a dead-air stagnation zone of infinite extent behind the body enclosed by external streamlines (Figure 2.17c). The pressure p_d in this zone is constant but cannot be determined from the solution of the problem. However, actually external jets entrain or eject fluid from the stagnation zone (due to viscous forces) and form a rotational flow inside the zone. Thus, a developed zone of a viscous recirculatory, or separated, flow is formed, but if the width h of the zone is relatively small (which takes place for angles of attack smaller than a certain critical value, $\alpha < \alpha_{cr}$), the external jets can completely “suck out” the zone, which leads to the Joukowski circulation model for a separationless flow past a wing.

We will illustrate the nature of the problems of this kind with reference to the example of the incompressible flow past a zero-thickness plate of length L (Figure 2.17a) set at an angle of attack α , subject to the condition of smooth flow shedding from the trailing edge. As distinct from the previous problem, the plate does not exert a displacing effect on the freestream, so that the flow past the plate can be simulated only by the lengthwise distribution of vortices with the specific intensity $\gamma(x)$. Then each plate element dx' induces a peripheral velocity field $v^{(y)} = [\gamma(x')/2\pi r]dx'$ at a certain point (x, y) , while the total fields of the induced velocities are determined by the integrals

$$u_\Gamma = -\frac{y}{2\pi} \int_0^L \frac{\gamma(x') dx'}{r^2}, \quad v_\Gamma = \frac{1}{2\pi} \int_0^L \frac{\gamma(x')(x - x') dx'}{r^2}$$

$$r^2 = (x - x')^2 + y^2 \quad (2.9.13)$$

The total velocity fields are as follows:

$$u = u_\infty + u_\Gamma, \quad v = v_\infty + v_\Gamma$$

$$u_\infty = U_\infty \cos \alpha, \quad v_\infty = U_\infty \sin \alpha \quad (2.9.14)$$

On the plate surface we have $v = 0$; for $y \rightarrow 0$ this leads to an integral equation in $\gamma(x)$

$$\int_0^L \frac{\gamma(x') dx'}{x - x'} = -2\pi U_\infty \sin \alpha \quad (2.9.15)$$

The integral on the left-hand side converges in the Cauchy sense and—which might appear at first glance surprising—is independent of x . This equation has the solution

$$\gamma = -2U_\infty \bar{\gamma} \sin \alpha, \quad \bar{\gamma} = [(1 - \bar{x})/\bar{x}]^{1/2}$$

$$\Gamma = \int_0^L \gamma(x') dx' = -\pi U_\infty L \sin \alpha, \quad \bar{x} = x/L \quad (2.9.16)$$

Clearly, $\gamma \rightarrow \infty$ as $x \rightarrow 0$ and $\gamma \rightarrow 0$ as $x \rightarrow L$. This function is plotted in Figure 2.17d. It can be easily seen that the velocity u_Γ is determined by integral 2.9.3 for v , if in the latter β_- is taken to be unity and q is replaced by $\mp\gamma/2\pi$. Here and in what follows, the upper

and lower signs relate to the upper and lower sides of the plate, respectively. Then on the plate we have $u_{\Gamma\pm} = \pm\gamma/2$, while the total velocities are as follows

$$u_{\pm} = U_{\infty}(\cos \alpha \pm \bar{\gamma} \sin \alpha) \quad (2.9.17)$$

For $\alpha = 20^\circ$ the function u_- is plotted in Figure 2.17d. The stagnation points, marked by symbols in the figure, are the points with $\bar{\gamma} = \cot \alpha$ on the plate undersurface. Outside the plate, at $y = 0$ we have $v = [(L - x)/x]^{1/2} \sin \alpha$. Immediately behind the trailing edge we have $v = 0$ and $u = u_{\infty}$, that is, the solution obtained actually satisfies the smooth flow shedding condition, though with an infinite curvature of the outgoing streamline, $K \sim \partial v / \partial x \sim (L - x)^{-1/2}$. On the leading edge $u_{\pm} \rightarrow \infty$ as $\pm x^{-1/2}$, while ahead of it again $v \sim (-x)^{1/2}$ (in Section 2.11 we shall revert to an analysis of this singularity from the general standpoint).

The pressure on the plate calculated from the Bernoulli equation has a nonintegrable singularity of the order $\bar{\gamma}^2 \sim 1/x$ as $x \rightarrow 0$; however, in calculating the pressure difference Δp on the plate sides, this singularity is compensated, which leads to the following expressions for the distributed force and the total normal force N acting on the plate

$$\begin{aligned} \Delta p &= p_- - p_+ = \rho_{\infty} U_{\infty}^2 \bar{\gamma} \sin 2\alpha \\ N &= -\rho_{\infty} \Gamma U_{\infty} \cos \alpha = \frac{1}{2} \pi \rho_{\infty} U_{\infty}^2 \sin 2\alpha \end{aligned} \quad (2.9.18)$$

However, apart from the normal force, the plate is under the action of the longitudinal (along the x axis) *drawing*, or *suction*, force applied to the leading edge; as will be shown in Section 2.12, this force is equal to $T = -N \tan \alpha$. This is due to the centripetal acceleration of the flow turning on the edge at an infinite velocity and an infinite (within the framework of the incompressible fluid model) negative pressure. The presence of this force is obvious for an edge with a finite thickness x ; however, this force turns out to have a limit, as $h/L \rightarrow 0$. Physically, this paradox can be removed either by a local flow separation above the plate's leading edge or by the gas compressibility effect taken into account (see Section 5.6).

2.10 Cylinder, Sphere, and Other Bodies in an Incompressible Flow

Since Equation 2.7.7 for the incompressible flow potential is linear, it is possible to split the problem into two subsequent ones, the linear problem of determining the potential and, hence, the velocity field and that of calculating the pressure from the Bernoulli equation using the velocity field previously obtained.

To do this, we will use a polar coordinate system (r, θ) with the origin at the body center and the ray $\theta = 0$ aligned with the vector $-\mathbf{U}$. In this case the continuity Equation 1.13.16 at a constant density is reduced by virtue of 2.1.12 to an equation for the potential

$$\frac{1}{r^v} \frac{\partial}{\partial r} \left(r^v \frac{\partial \Phi}{\partial r} \right) + \frac{1}{r^2 (\sin \theta)^{v-1}} \frac{\partial}{\partial \theta} \left[(\sin \theta)^{v-1} \frac{\partial \Phi}{\partial \theta} \right] = 0 \quad (2.10.1)$$

Here, $\nu = 1$ for a cylinder and $\nu = 2$ for a sphere. The boundary conditions are the flow impermeability on the circle $r = r_0$ and the disturbance decay at infinity

$$\begin{aligned} \frac{\partial \Phi}{\partial r} &= v_r = 0, & r = r_0 \\ \frac{\partial \Phi}{\partial r} &\rightarrow -U_\infty \cos \theta \\ \frac{1}{r} \frac{\partial \phi}{\partial \theta} &= v_\theta \rightarrow U_\infty \sin \theta, & r \rightarrow \infty \end{aligned} \quad (2.10.2)$$

Since the flow region has a very simple form, we can use a simple method of separation of variables, the mere form of conditions 2.10.2 predetermines the form of the solution

$$\Phi = -R(r) \cos \theta, \quad v_r = -R' \cos \theta, \quad v_\theta = \frac{R}{r} \sin \theta \quad (2.10.3)$$

The solution of this form satisfies the original equation for the potential at an appropriate choice of the function $R(r)$ satisfying the boundary conditions

$$R' \rightarrow U_\infty, \quad r \rightarrow \infty, \quad R' = 0, \quad r = r_0 \quad (2.10.4)$$

In the plane case, substituting 2.10.3 in Equation 2.10.1 we obtain the following equation

$$r(rR')' = R \quad (2.10.5)$$

This equation has two solutions, $R = cr^n$, where $n = \pm 1$. Combining these we can satisfy boundary conditions 2.10.4 and obtain the required solution

$$R = U_\infty \left(r + \frac{r_0^2}{r} \right) \quad (2.10.6)$$

From the Bernoulli Equation 2.2.10 the corresponding velocity and pressure distributions on the cylinder surface have the form:

$$\begin{aligned} \frac{U}{U_\infty} &= \bar{U} = 2 \sin \theta \\ C_p = 2\bar{p} &= \frac{p - p_\infty}{\frac{1}{2}\rho_\infty U_\infty^2} = 1 - \frac{U^2}{U_\infty^2} = 1 - 4 \sin^2 \theta \end{aligned} \quad (2.10.7)$$

We note that in aerodynamical applications the *pressure coefficient* means precisely the quantity C_p rather than the quantity \bar{p} introduced in Section 2.7 and used in high-speed gas dynamics.

Similarly, for an axisymmetric flow past a sphere we obtain

$$(r^2 R')' = 2R, \quad R = U_\infty \left(r + \frac{r_0^3}{2r^2} \right) \quad (2.10.8)$$

On the body surface we have

$$\bar{U} = \frac{3}{2} \sin \theta, \quad C_p = 1 - \frac{9}{4} \sin^2 \theta \quad (2.10.9)$$

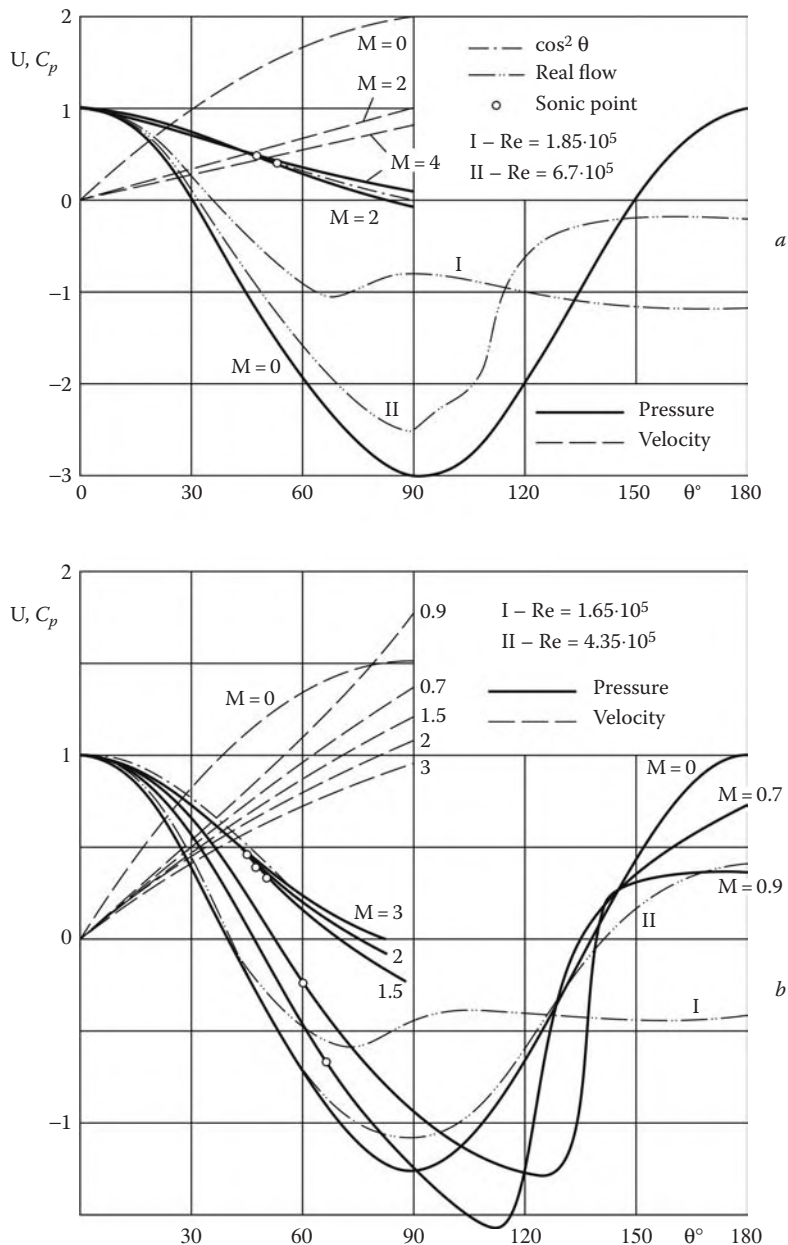


FIGURE 2.18
Pressure and velocity distributions over a cylinder (a) and a sphere (b).

The curves $\bar{U}(\theta)$ and $C_p(\theta)$ are plotted in Figure 2.18. Even at $\theta > 30^\circ$ for a cylinder and $\theta > 42^\circ$ for a sphere the body pressure is less than the static pressure in the freestream, which can be explained by centrifugal force action on convex streamlines (Figure 2.19). The velocity maximum on the body $U^{(m)}$ is achieved at $\theta = \pi/2$ and is equal to $2U_\infty$ for a cylinder and $3U_\infty/2$ for a sphere.

For a circulatory flow past a circular cylinder the superposition of circular velocities $v_\theta = -\Gamma/2\pi r$ on the flowfield obtained previously considerably changes the flow pattern.

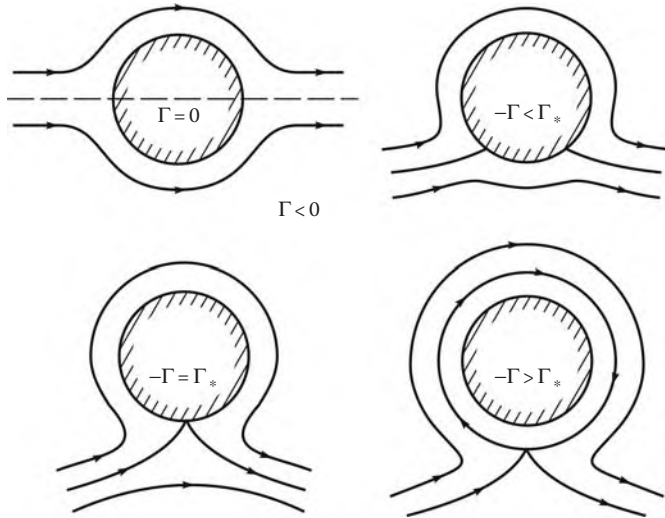


FIGURE 2.19

Streamlines in the circulation flow past a cylinder.

In particular, the stagnation points $\theta = \theta_0$ are displaced from the axis of symmetry, their new position being determined from the condition $U = 0$ on the cylinder surface $r = r_0$

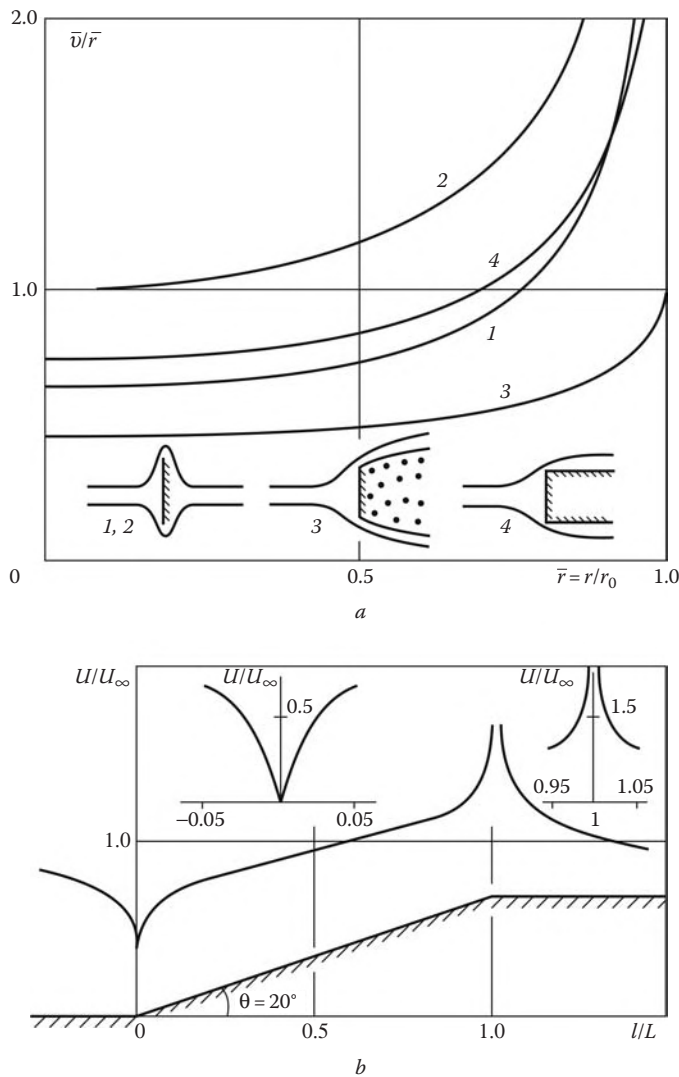
$$\frac{U}{U_\infty} = 2 \sin \theta_0 + \Gamma_0 = 0, \quad \Gamma_0 = -\frac{\Gamma}{2\pi U_\infty r_0} \quad (2.10.10)$$

For the critical value $\Gamma_0 = \Gamma_* = 2$ both stagnation points merge to a single point $\theta_0 = -\pi/2$ (or $\theta_0 = 3\pi/2$), while for $\Gamma_0 > \Gamma_*$ the solution of Equation 2.10.10 no longer exists. In the latter case the stagnation point "buoys" from the surface in the flow (Figure 2.19). A similar physical flow pattern can be implemented by spinning a cylinder that can produce the *Magnus lift*. The historical role of this solution was that it could be recalculated for wing airfoils using conformal mappings (see the following).

Analytical solutions, though very cumbersome, are known for ellipses and ellipsoids, as well as for some other bodies. We will present certain solutions without derivation.* Thus, in Figure 2.20a we have plotted the velocity distributions over a disc (1) and a flat plate (2-4) orthogonal to the flow

$$\begin{aligned} 1. \bar{v} &= \frac{2}{\pi} \frac{\bar{r}}{\sqrt{1 - \bar{r}^2}} \\ 2. \bar{v} &= \frac{\bar{r}}{\sqrt{1 - \bar{r}^2}}, \quad \bar{v} = \frac{v}{U_\infty}, \quad \bar{r} = \frac{r}{r_0} \\ 3. \bar{r} &= \frac{4}{4 + \pi} \left[\frac{(3 + \bar{v}^2)\bar{v}}{(1 + \bar{v}^2)^2} + \arctan \bar{v} \right] \\ 4. \bar{r} &= \frac{2}{\pi} \left[\frac{\bar{v}}{(1 + \bar{v}^2)} + \arctan \bar{v} \right] \end{aligned} \quad (2.10.11)$$

* Solutions 2.10.11 through 2.10.13 were given to the author by G. Yu. Stepanov; they had been obtained by the complex potential method (see the following discussion and the books of Sedov, 1950; Lavrent'yev and Shabat, 1973; and others).

**FIGURE 2.20**

Velocity distributions over blunt bodies (a) and a wedge-shaped step (b) in an incompressible flow.

Formulas 1 and 2 correspond to separationless flow and differ with respect to a coefficient only; formula 3 describes a jet flow (similar to that in Figure 2.17c) with an open infinite stagnation zone with $p_d = p_\infty$; while formula 4 relates to the face of a semi-infinite step.

The last problem is of methodical interest and represents a particular case of the flow past a wedge-shaped step (Figure 2.20b). The analytical solution of this problem gives the velocity distribution over the body surface in the parametric form:

$$U = U_\infty \left| \frac{\xi}{\xi - 1} \right|^\varepsilon, \quad l = A \int_0^\xi \left| \frac{\xi - 1}{\xi} \right|^\varepsilon d\xi \quad (2.10.12)$$

Here, θ is the wedge angle, $\varepsilon = \theta/\pi$, and l is the distance measured along the wedge generator; the values $\xi = 0$ and $\xi = 1$ correspond to $l = 0$ (wedge nose) and $l = L$ (rear). The constant A is chosen from the latter condition. For $\theta = \pi/2$ this solution is reduced to formula 2.10.11 for the plane step (variant 4). The velocity distribution along the step with $\theta = 20^\circ$ ($\varepsilon = 1/9$) is plotted in Figure 2.20b; for this and smaller values of θ we have $A \approx L$.

In the vicinity of the corner points $l = 0$ and $l = 1$ the function $U(l)$ has singular asymptotics of the type

$$U = U_\infty \left| \frac{(1-\varepsilon)l}{A} \right|^{\varepsilon/(1-\varepsilon)}, \quad U = U_\infty \left| \frac{A}{(1+\varepsilon)(L-l)} \right|^{\varepsilon/(1+\varepsilon)} \quad (2.10.13)$$

The general character of this result for bodies with corner points will be shown in the next section.

However, in reality, inviscid calculations give an incorrect idea on the flow pattern at $\theta > \pi/2$ because of the formation of viscosity-driven return flows. Without going into the reasons for their formation and their mechanisms, we will demonstrate the degree to which they alter the inviscid flow pattern by comparing the theoretical results with the experimental data for incompressible high-Reynolds-number ($Re > 10^5$) flows (Schlichting, 1968) under the conditions of highly developed separation flows (the same as in Figure 2.18). These data coincide with the theoretical results for spherical and cylindrical noses at $\theta \leq 40^\circ \div 60^\circ$, depending on the Reynolds number, while the region of larger θ is affected by the separation zone.

Thus, inviscid solutions for the bodies of this type cannot be used for calculating the forces acting on the body, though they give fairly accurate velocity distributions on the body nose (which can be of interest if only for evaluating heat fluxes).

It might be expected that these results could be extended to the noses of other blunt bodies of the same class (not too flattened ellipsoids, etc.). However, opposite examples are also known: thus, the plate velocity distributions presented in Figure 2.20 differ considerably for the cases in which the plate is in separationless and jet flows.

Thus, one should be careful in estimating the upstream effect of the conditions imposed behind a body in a fluid (at least, incompressible) flow.

In conclusion we will outline one more method for solving the problems of the two-dimensional potential fluid flows. This is the *complex potential* or *conformal mapping method*. The essence of this technique is as follows. We introduce a complex potential w and a complex variable z

$$w = \varphi(x, y) + i\psi(x, y), \quad z = x + iy \quad (2.10.14)$$

where φ and ψ are the velocity potential and the stream function, while $i^2 = -1$. The flow plane (x, y) is treated as the plane of the complex variable z , and the total velocity is $U = u + iv$, where u and v are the velocity projections onto the x and y axes. By virtue of the *Cauchy-Riemann equations*

$$u = \frac{\partial \varphi}{\partial x} = \frac{\partial \psi}{\partial y}, \quad v = \frac{\partial \varphi}{\partial y} = -\frac{\partial \psi}{\partial x} \quad (2.10.15)$$

the function $w(z)$ is analytical.

For analytical functions the derivative dw/dz is independent of a direction chosen in the z plane and is equal to

$$\frac{dw}{dz} = \frac{\partial \varphi}{\partial x} + i \frac{\partial \psi}{\partial x} = \frac{1}{i} \frac{\partial \varphi}{\partial y} + \frac{\partial \psi}{\partial y} = \bar{U}, \quad \bar{U} = u - iv = \overline{u + iv} \quad (2.10.16)$$

Here, \bar{U} is the *complex velocity*, which is complex-conjugate (this is denoted by the bar above the letter) with the true velocity U .

Let now a body contour L_z be specified in the z plane; we will study the flow around this contour. Along with the z plane, we will consider an auxiliary plane $\xi = \xi + i\eta$ and specify a relation between the variables $z = f(\xi)$ or $\xi = F(z)$ or the conformal mapping of one plane onto the other, subject to the condition that the L_z contour in the z plane passes to a certain contour L_ξ in the ξ plane. In this case, the complex potential is transformed as follows:

$$w(z) = w[z(\xi)] = W(\xi) = \Phi(\xi, \eta) + i\Psi(\xi, \eta) \quad (2.10.17)$$

Let the contour L_ξ be so chosen that the fictitious potential $W(\xi)$ corresponding to the flow around this contour is known. Then, using simple transformations, we obtain the required potential $w(z)$ corresponding to the flow around the original contour L_z in the physical plane (x, y) . Thus, the problem of the flow past a body is reduced to the search for the corresponding conformal mapping of the z plane onto the ξ plane.

It is in this way that solutions 2.10.11 through 2.10.13 of the problems presented previously were derived. The detailed presentation of this theory and the examples of the problems solved are given in many classical handbooks on fluid mechanics cited previously.

2.11 Stagnation Points and Singular Lines

Stagnation points can be elements of a wide variety of gas dynamic flows. They always occur in flows past blunt bodies and in subsonic flows past sharp bodies as well. Since velocities near stagnation points are small, the local flow in their vicinities can be considered incompressible and, in accordance with 2.2.15, having a constant density. Since in subsonic flow all separate subdomains interact with each other, the solutions obtained in what follows involve a number of free parameters characterizing special features of the global problem or the flow as a whole (the incident flow velocity, typical dimensions, etc.). These parameters can be determined only by matching the global and local solutions, which will be done below for several examples.

We will consider the following problems.

2.11.1 Plane Rotational and Irrotational Flows

We place the origin of a coordinate system (x, y) at the stagnation point and align the x axis with the $y = 0$ streamline. The plane incompressible flow equations in this system have a simple particular solution (Figure 2.21a and b)

$$u = ax + 2\omega y, \quad v = -ay, \quad p = p_0 - \frac{1}{2}\rho a^2(x^2 + y^2), \quad a, p_0, \omega = \text{const} \quad (2.11.1)$$

Here, the constants p_0 and ω are the pressure and the vortex (see Section 1.8) at the stagnation point. In its vicinity on a blunt body of the shape $y = y_0(x)$ with a finite radius of curvature R at the origin these expressions can be considered the first terms of a series-expansion of the general solution. In order to take into account a deviation of the body shape from a plane, we should retain quadratic terms in these expansions, for example

$$u = ax, \quad v = -ay - \frac{3}{2} \frac{a}{R} x^2, \quad y_0 = -\frac{1}{2} \frac{x^2}{R} \quad (2.11.2)$$

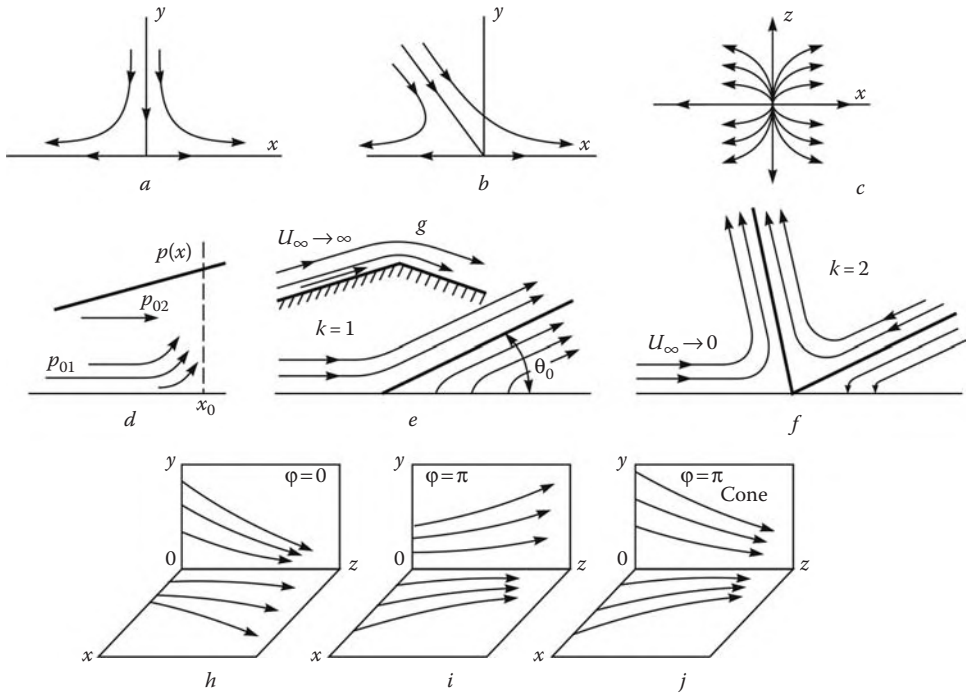


FIGURE 2.21
Stagnation points and divergence and convergence lines.

In what follows, the terms of this order will be omitted and we will restrict ourselves by an analysis of streamlines only as $x, y \rightarrow 0$. Thus, we have

$$\frac{dx}{dy} = \frac{u}{v} = -\frac{x}{y} - \frac{2\omega}{a}, \quad (x + ky)y = C, \quad k = \frac{\omega}{a} \quad (2.11.3)$$

This is a family of hyperbolas with a singular saddle point. Their asymptotes, $y = 0$ and $x + ky = 0$, are also streamlines passing through the origin. The irrotational flow pattern is symmetric, while in rotational flows streamlines entering the stagnation point have the angle coefficient equal to K (Figure 2.21b). Nevertheless, according to 2.11.1, the pressure distribution near the stagnation point is symmetric in this approximation and shear vorticity has no effect on it.

In the case of a cylinder at $\omega = 0$ a comparison with solution 2.10.7 gives $a = 2U_\infty R$, thus making the matching of the local and global solutions exhausted.

2.11.2 Axisymmetric Flow

Let the y axis be the axis of symmetry. In this case the velocity and pressure fields

$$u = ax, \quad v = -2ay, \quad p = p_0 - \frac{1}{2}\rho a^2(x^2 + 4y^2) \quad (2.11.4)$$

satisfy the equations of motion. The streamlines described by the equation $dy/dx = v/u$ have the form $yx^2 = \text{const}$ and tend to the plane $y = 0$ more rapidly than in the plane

flow. They form in space hyperboloids of revolution, coaxial with the y axis. For a sphere, $a = 3U_\infty/2R$. For ellipses and ellipsoids of revolution with the longitudinal and transverse axes b and a the dimensionless velocity gradients are

$$\bar{u}'_a = \frac{a}{U_\infty} \frac{\partial u}{\partial x}, \quad \bar{u}'_R = \frac{R}{U_\infty} \frac{\partial u}{\partial x}$$

where R is the radius of curvature at the stagnation point. These quantities are plotted in Figure 2.22 against b/a . It can be seen that the \bar{u}'_R curves tend to unity as $b/a \rightarrow \infty$ (for ellipses $\bar{u}'_R = (b+a)/b$); this hints at the fact that this quantity is independent of shapes of similar bodies. At the same time, for oblate bodies these data are hardly universal in view of the data (presented in Section 2.10) on different flow regimes past a plate. In separationless flows past plates $\bar{u}_a = 1$, while for a disc $\bar{u}_a = 2/\pi$.

2.11.3 Two Planes of Symmetry

Let the x and z axes of a Cartesian coordinate system be aligned with these planes, the $y = 0$ plane being, as earlier, the flow plane. In this coordinate system the equations of motion have the solution

$$\begin{aligned} u &= ax, \quad w = cz, \quad v = -by, \quad b = a + c \\ p &= p_0 - \frac{\rho}{2} (a^2 x^2 + b^2 y^2 + c^2 z^2) \end{aligned} \quad (2.11.5)$$

In each plane of symmetry the streamline family forms a saddle

$$\begin{aligned} yx^\chi &= \text{const}, \quad \chi = \frac{b}{a}, \quad z = 0 \\ yz^\chi &= \text{const}, \quad \chi = \frac{b}{c}, \quad x = 0 \end{aligned} \quad (2.11.6)$$

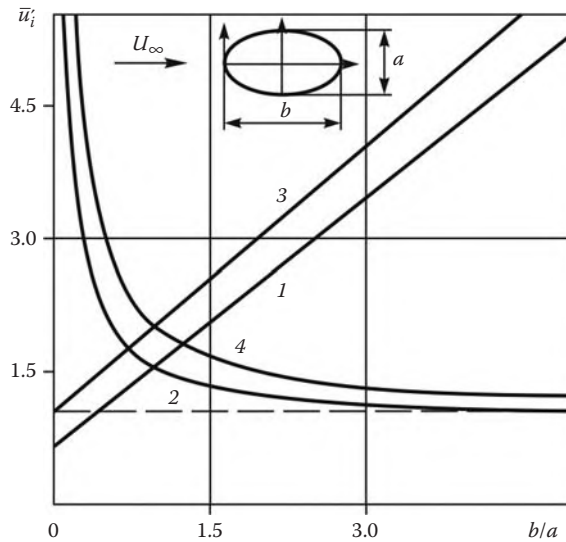


FIGURE 2.22

Dimensionless velocity gradients \bar{u}_a (1 and 3) and \bar{u}_R (2 and 4) at the stagnation points on ellipses (3 and 4) and ellipsoids (1 and 2).

In the $y = 0$ plane they form a node

$$\frac{dz}{dx} = \frac{cz}{ax}, \quad z = x^\kappa, \quad \kappa = \frac{c}{a} \quad (2.11.7)$$

These curves are plotted in Figure 2.21c for $\kappa < 1$ (for $\kappa > 1$ the x and z axes must be interchanged). All the cases considered have a common property that the streamlines form a singular family of curves at a regular behavior of the velocity field.

We considered stagnation points as the points of flow spreading (or divergence). Mathematically, these flows are reversible: it is sufficient to assign opposite signs to velocity components in order to obtain flow convergence points. However, from the physical point of view these flows cannot be realized owing to near-wall viscous effects at $y \approx 0$ and the no-slip condition imposed on the wall (see Section 1.16). A partial explanation of this situation is given by the following problem.

2.11.4 Stagnation Point with a Positive Pressure Gradient

Let a pressure distribution along a wall coinciding with the x axis be given, such that the pressure increases and takes at a certain point x_0 a value p_0 corresponding to the stagnation pressure in the near-wall streamtube in which the velocity vanishes at this point. At the same time, the pressure gradient is assumed to be positive, $dp/dx = \rho q > 0$.

Such a situation can be realized, for example, in a two-layer flow past a surface (Figure 2.21d), where the stagnation pressure and width of the upper layer are greater than those of the lower one ($p_{02} > p_{01}$), the lower layer width being so small that it has almost no effect on the formation of the total pressure field.

However, in reality the presence of a near-wall low-pressure sublayer (even as thin as wished) can lead to global restructuring of the entire flow pattern. In fact, let us assume that the opposite situation occurs: we will neglect the pressure difference in the sublayer and evaluate the velocity field in the immediate vicinity of the surface. Setting $v = 0$ we obtain from the equations of motion

$$u \frac{\partial u}{\partial x} = -\frac{1}{\rho} \frac{\partial p}{\partial x} = -q, \quad u = \sqrt{2q(x_0 - x)}, \quad q > 0 \quad (2.11.8)$$

First of all, this solution cannot be continued to the region $x > x_0$, where it is merely impossible to construct a meaningful inviscid solution with a continuous velocity field, that is, with $u \rightarrow 0$ as $x \rightarrow x_0$ from the right.

Moreover, there is no meaningful solution corresponding to the assumptions accepted in the region $x < x_0$ as well. In fact, it follows from the continuity equation (with 2.11.8 taken into account) that

$$v = q^{1/2} y [2(x_0 - x)]^{-1/2} \quad (2.11.9)$$

This means that as $x \rightarrow x_0$ streamlines with $y \neq 0$ turn up forming a barrier to the external flow and thus give rise to the global flow restructuring.

From the physical point of view, this situation can be eliminated by the viscosity influence due to which the external flow ejects the low-pressure sublayer thus helping to overcome the adverse pressure gradient, as it is the case, for example, in a boundary layer (Section 1.16) with a positive pressure gradient. However, in this situation recirculatory flow zones can occur.

2.11.5 Wedge in Incompressible Flow

A salient feature of the solution obtained in Section 2.9 is the existence of logarithmic singular points (with infinitely increasing velocity and pressure) at the leading and trailing edges of an airfoil. We will now consider an incompressible flow in the vicinity of a sharp wedgelike body (with an angle θ_0 , Figure 2.21e). The equation for the potential, 2.10.1, has a family of solutions

$$\begin{aligned}\Phi &= CU_\infty r^n \Theta(\theta), & C &= \text{const} \\ v_r &= nCU_\infty r^{n-1} \Theta, & v_\theta &= CU_\infty r^{n-1} \Theta' \end{aligned}\quad (2.11.10)$$

We recall that here a polar coordinate system with the $\theta = 0$ ray directed counter the external flow is used. The constant C has the dimension L^{-n} and must be determined by matching the unknown local solution with the global one. In the plane case, when $v = 1$ in Equation 2.10.11, we obtain from it a simple equation for Θ with the solution

$$\begin{aligned}\Theta'' + n^2 \Theta &= 0, & \Theta &= -\cos n\theta \\ v_r &= -nCr^{n-1} \cos n\theta, & v_\theta &= nCr^{n-1} \sin n\theta \\ U &= (v_r^2 + v_\theta^2)^{1/2} = nCU_\infty r^{n-1} \end{aligned}\quad (2.11.11)$$

This solution satisfies the symmetry condition $v_\theta = 0$ on the axis $\theta = 0$ and—for $C > 0$ —the condition $v_r < 0$. Setting $v_\theta = 0$ on the body surface $\theta = \pi - \theta_0$ we obtain a set of eigenvalues of the problem, $n = k\pi/(\pi - \theta_0)$, where k is an integer, with a corresponding set of nontrivial eigenfunctions Θ_k .

Since all $n > 1$, the velocities v_r and v_θ vanish at the edge as $r \rightarrow 0$, while the pressure tends to the stagnation value, $p_0 = p_\infty + (1/2)\rho_\infty U_\infty^2$. Hence, disturbances introduced by a wedge in an incompressible flow (as well as in subsonic flow, since in this case the governing equations are also elliptic) are not locally small at any θ_0 and are responsible for the appearance of a singularity on a thin airfoil in the linear problem (Section 2.9).

Of the whole family of eigensolutions, the first solution ($k = 1$) is the main one, since other solutions decay much more rapidly as $r \rightarrow 0$. For $\theta_0 = \pi/2$ or $n = 2$ this solution coincides with that obtained earlier for the plane stagnation point. The limiting case $\theta_0 \rightarrow 0$ corresponds to the undisturbed flow. A solution for a trailing wedge-shaped edge of a wing can be obtained from the previous solution by a simple turn of the flow through an angle θ or by changing velocity signs.

For $k \geq 2$ eigensolutions involve additional (in addition to the axis of symmetry and the wedge surface) rays, which represent streamlines, the number of which is equal to $k - 1$. For example, at $k = 2$ this is a bisector of the angle between the x axis and the wedge. These solutions describe rather exotic flows in angles between these rays (Figure 2.21f) and can be of interest only as terms of the solution expansion for a finite-length wedge. Therefore the case $k \geq 2$ will not be considered in what follows.

The continuation of the eigensolutions to a region inside the wedge describes a flow (except for the case of integer n) with a nonzero peripheral velocity on the axis $\theta = \pi$, that is, with a source (of the intensity of the type r^{n-1}) distributed on the axis or a sink of a fluid coming from the right from the infinity.

We also note that for a flow past a convex angle, that is, for $\theta_0 < 0$ (Figure 2.21g), the minimum of n is $n = \pi/(\pi + |\theta_0|) < 1$. Therefore, in this case the velocity components $v_i \sim r^{n-1} \rightarrow \infty$ as $r \rightarrow 0$, which was used earlier, in considerations of Section 2.10. In this case it follows from the Bernoulli equation that the pressure $p \rightarrow -\infty$; within the framework of the incompressible fluid model this singularity could be eliminated only by introducing the jet flow model (Figure 2.20a).

An unbounded solution for $r \rightarrow 0$ can be also obtained at $\theta_0 > 0$, however for certain $n < 0$ only. This solution corresponds to a certain source-sink at the point $r = 0$ with zero total fluid flow rate. Clearly, the variety of possible solutions of this local problem considerably exceeds the possibility of fitting them to any real flows.

We will now match this local solution with that obtained in Section 2.9 for a thin parabolic arc of length L . For $\theta_0 \ll 1$ we have $n - 1 = \theta_0/\pi$; then in a vicinity of the wedge the velocity v_r in solutions 2.11.11 can be represented in a series form:

$$\frac{v_r}{C_1 U_\infty} = \left(\frac{r}{L}\right)^{\theta_0/\pi} = 1 + \frac{\theta_0}{\pi} \ln \frac{r}{L} + \dots \quad (2.11.12)$$

where C_1 is a new constant. Let us compare this expansion with the limiting solution 2.9.6 in the vicinity of the leading edge

$$\begin{aligned} u' &= \frac{\pi}{\theta_0} \frac{u_1}{U_\infty} = 2 + \ln \frac{r}{L} \approx \ln \frac{r}{L} \\ \Delta x &= r = x + \frac{1}{2}L \rightarrow 0, \quad y \rightarrow 0 \end{aligned} \quad (2.11.13)$$

For small θ_0 the relation $v_r = U_\infty + u_1$ holds near the wedge surface; therefore, both formulas coincide for $C_1 = 1$. Therefore, in the domain in which both expressions 2.11.12 and 2.11.13 are valid simultaneously,

$$1 \ll \left| \ln \frac{r}{L} \right| \ll \frac{\pi}{\theta_0}$$

the original solutions 2.9.6 and 2.11.11 also coincide. These solutions are presented in Figure 2.16c; they are similar over a fairly wide range of small but nonvanishing r .

Another example of matching a local solution with the global one is furnished by a thin wedge-shaped step; for $A = L$, L being the step length, the limiting solution 2.10.13 for the step coincides with 2.11.10 or 2.11.12 for $C_1 = 1$.

We note in conclusion that in constructing a series from an infinite set of eigensolutions we could introduce a set of coefficients C_k and using them satisfy any conditions on the trailing edge of a wedge.*

2.11.6 Singular Surfaces and Lines

Generally, the three-dimensional stagnation point considered previously is an exceptional case in three-dimensional flows. More frequently, singular *divergence* and *convergence* stream surfaces and streamlines occur. As an example, we will consider a flow at a velocity U_∞ past an infinite cylinder C set at an angle of attack α , the cylinder axis coinciding with the z axis. In this case the longitudinal velocity component $w = U_\infty \cos \alpha$ is constant and the flow in cross-sections $z = \text{const}$ is the same as in the case of the plane flow at a velocity $U_{n\infty} = U_\infty \sin \alpha$ past the body with the contour C_n . As will be shown in what follows, such a flow model is applicable to flows past arbitrary elongated slender bodies.

Let the cylinder and the flow have the plane of symmetry $\varphi = 0$ and π . In this case stagnation points on the contour C_n are on the windward ($L_+, \varphi = 0$) and leeward ($L_-, \varphi = \pi$)

* The matching procedure was described in Van Dyke (1972); however, the analysis performed in that book is usually restricted to the first approximation.

cylinder generators. In their vicinities the velocity distribution in a cross-section is given by formulas 2.11.2 with $\omega = 0$. The spatial distribution of streamlines in vicinities of the lines L_{\pm} is obtained by taking into account the component w and Equation 1.8.2

$$x = x_0 \exp(az/w), \quad y = y_0 \exp(-az/w) \quad (2.11.14)$$

Clearly, as $az \rightarrow \infty$, all these lines tend to their *convergence surface* $y = 0$ moving away (at $x_0 \neq 0$) from the *divergence surface* $x = 0$. Since the roles of these surfaces are simply interchanged as $az \rightarrow -\infty$, they are mathematically equivalent. We term them *singular stream surfaces*.

On these surfaces, there are singular streamlines, both divergence and convergence, coinciding in this case with the lines L_{\pm} . They satisfy Equation 2.11.15 and are similar to singular nodal lines, but with infinitely far poles $z \rightarrow \pm\infty$. Of course, not every convergent or divergent family of curves includes a singular line.

Whenever the flow is directed along the z axis from the windward side of a cylinder, on which $a > 0$, the plane of symmetry is a divergence surface, while the cylindrical surface is a convergence one. The generator L_{+} is a convergence line on the first surface and a divergence line on the second surface. On the leeward side ($a < 0$) singular surfaces and lines interchange (Figure 2.21).

Thus, in the general case the nature of singular streamlines depends on the choice of a stream surface passing through them. Therefore, these singular lines are *surface singular* lines. However, *spatial* singular lines are also possible; their nature is the same for all the stream surfaces involving these lines (Figure 2.21).

We note in conclusion that, in contrast to the case of the flow past a plane blunt body (Section 2.10, Figure 2.18), a separationless flow past a yawed cylinder with the formation of convergence lines on the leeward side can be realized (as experience shows) even at small angles of attack.

2.12 Forces in Subsonic Flows

As shown in Sections 2.8 and 2.9, there is a principal difference between forces acting on bodies in inviscid supersonic and subsonic flows, namely, the body exerts a drag in the first but not in the second case. Although this result was obtained for bodies of particular shapes, it is of a general nature. In supersonic flows the drag is a result of the formation of a shock wave; this will be substantiated in Section 3.6. Here, we will consider the forces that act on bodies in a subsonic flow, as well as their properties.

As shown in Section 1.7, an important role is played by the asymptotic behavior of solutions far from the body. We consider first the asymptotics of the solution of the problem of subsonic irrotational flow past bodies. As follows from Section 2.10, velocity disturbances in an incompressible flow past a cylinder or a sphere decrease as $\Delta U \sim r^{-(2+v)}$. The same result can be obtained from formulas 2.9.3 and 2.9.8 as $r' \rightarrow \infty$. At the same time, for a circulatory flow past a cylinder $\Delta U \sim r^{-1}$.

We extend now this result to bodies of arbitrary shapes. To do this, we will use the expansion

$$r' = \sqrt{(x - x')^2 + r^2} = r_0 - 2 \frac{xx'}{r_0} + \dots, \quad r_0^2 = x^2 + r^2, \quad |x'| \ll L \ll r_0 \quad (2.12.1)$$

Substituting this expansion into formulas 2.9.2 and 2.9.7 for the potentials we obtain

$$\begin{aligned}\varphi &= C_1 \ln r_0 - C_2 \frac{2x}{r_0^2} + \dots, & \nu = 0 \\ \varphi &= \frac{C_1}{r_0} + C_2 \frac{2x}{r_0^3} + \dots, & \nu = 1 \\ C_1 &= \int_{x_1}^{x_2} q(x') dx', & C_2 = \int_{x_1}^{x_2} x' q(x') dx'\end{aligned}\tag{2.12.2}$$

Here, the coefficient C_1 is the total intensity of internal fictitious sources, which is equal to zero, since all streamlines emanating from them are confined by the body contour separating the external real and internal fictitious flows. Hence, the second term of expansions 2.12.2 is the principal one, determining the flow asymptotics, as $r_0 \rightarrow \infty$, while omitted terms are of higher orders.

In the general case the coefficient C_2 is not equal to zero and is termed the resulting *dipole* intensity, the dipole being oriented along the x axis. We will consider, for example, two sources of opposite signs, q_1 and $q_2 = -q_1$, spaced at a distance Δx . All the streamlines leave one source and arrive at the other. As $\Delta x \rightarrow 0$ and $q_1 \rightarrow \infty$, their product being, however, constant, $q_1 \Delta x = \text{const}$, we obtain a dipole.

We note that the three-dimensional Laplace equation has, in the general case, the same fundamental solution $\varphi \sim (r')^{-1}$ corresponding to a spherical source; in this solution the radius vector r' may be measured from any point (x', y', z') inside an arbitrary body, including bodies of not so small thickness.

Hence, the general solution of this problem can be sought in the form of integrals of distributed sources $q(x', y', z')$ with zero total intensity. Far from the body, they can be considered a set of dipoles of different orientations. This generalization adds terms proportional to y'/r_0 and z'/r_0 in expansion 2.12.1, while in 2.12.2 instead of a single term with the coefficient C_2 three similar terms of the same order will appear.

This result is valid for compressible flows as well. Since disturbances of all parameters are small far from the body, in the general case of subsonic flows with finite $M_\infty > 0$ they can be also described by linear Equation 2.7.3. The asymptotics of solution 2.12.2 are also conserved, but with a correcting coefficient β_- according to formula 2.9.1. Obviously, in this case $C_1 = 0$ as well, since the total flow rate through any contour enclosing the body is equal to zero.

Thus, the disturbance potential decays at infinity as $\varphi_0 \sim r_0^{-(1+\nu)}$ and in the case $\nu = 1$ this takes place for any finite three-dimensional body. Velocity disturbances decay as $\Delta U \sim \partial \varphi_0 / \partial r \sim r_0^{-(2+\nu)}$, which coincides with the asymptotics of formulas 2.9.3 and 2.9.8.

We will now consider the asymptotics of the solutions for plane irrotational circulatory flows around airfoils. They are simulated by vortices of the total circulation Γ distributed inside wings (Section 2.9). Far from the body these vortices are equivalent (in the principal term of the approximation) to a resulting vortex concentrated at point $x, r = 0$ and inducing, according to Section 2.1, the circular velocity field, $v_\theta = \Gamma / 2\pi r_0$, which dies out considerably slower than the circulation-free velocity field. Thus, we have the following law of the velocity disturbance decay far from a body in a subsonic potential flow

$$\Delta U \sim r_0^{-(2+\nu)}, \quad \nu = 0 \text{ and } 1, \quad \Gamma = 0; \quad \Delta U \sim r_0^{-1}, \quad \nu = 0, \quad \Gamma \neq 0\tag{2.12.3}$$

where r_0 is the distance from the body.

We will use this result for evaluating the forces \mathbf{X} and \mathbf{Y} acting on a body along and normally to the incident velocity vector U_∞ on the basis of formulas 1.7.18 and 1.7.19. These formulas give expressions for the forces in terms of integrals of flow parameters taken over an external control surface Σ (Figure 1.16c).

We will now evaluate the asymptotic order of these forces as the control surface recedes to infinity, that is, as $\Sigma \rightarrow \infty$. Let ΔU be the order of velocity disturbances on the surface Σ . Then $Y \sim \Delta U \Sigma$, while $X \sim (\Delta U)^2 \Sigma$. The first estimation is evident, while the second one follows from the fact that not only the last term of the first formula 1.7.18 is of this order, but also the first two terms since their integrands $\rho U \Delta u + \Delta p$ are equal to zero in the linear approximation and, hence, they are of the second order, $(\Delta U)^2$.

We will prove the following theorem: *a separationless, steady, inviscid, subsonic, potential, and circulation-free flow does not act on an immersed body.* The theorem is called the *Dalembert paradox*.

To prove it, we will take into account that, according to 2.12.3, velocity disturbances ΔU are of the order $r_0^{-(2+\nu)}$, while $\Sigma \sim r_0^{1+\nu}$. Hence, evaluating forces on a sufficiently distant surface we obtain that, at least, $X < Y \sim r_0^{-1}$, as $r_0 \rightarrow \infty$, which proves the statement.

In a circulatory irrotational flow the peripheral velocity $v_\theta \approx \Gamma / 2\pi r_0$ is predominant for large r_0 , while $\Sigma \sim r_0$, as before. It is sufficient for the longitudinal force $X \sim (\Delta U)^2 \Sigma \sim r_0^{-1}$ to be considered equal to zero, but the force $Y \sim \Delta U r_0$ remains finite. We can evaluate it using a control surface Σ in the form of a circle of a large radius r_0 (Figure 2.17a) and applying formula 1.7.16. In this case the flow parameters on an area element $d\Sigma = r_0 d\theta$ are as follows

$$\begin{aligned} U_n &= U_\infty \cos \theta, & U_N &= v = v_\theta \cos \theta, & n &= n_y = \sin \theta \\ p - p_\infty &= \rho U_\infty (U_\infty - u) = -\rho v_\theta \sin \theta & & & & \end{aligned} \quad (2.12.4)$$

Substituting these expressions in 1.7.16 and integrating over a circle we obtain the *Joukowski formula*

$$Y = -\rho_\infty U_\infty \Gamma \quad (2.12.5)$$

This force is directed upward and downward along the y axis for $\Gamma < 0$ (clockwise flow rotation, as shown in Figure 2.17a) and $\Gamma > 0$, respectively. Intuitively, its appearance can be explained by the fact that, due to velocity superposition, the total velocity is greater and the pressure is smaller on the upper side of a wing than on its undersurface.

Thus, for a plane body in separationless flow the lift calculation is reduced to the determination of a physically possible circulation around the body.

For a thin plate of length L at an angle of attack α , in accordance with Section 2.9, the circulation is $\Gamma = -\pi U_\infty L \sin \alpha$ and, hence, the lift is $Y = \pi \rho_\infty U_\infty^2 L \sin \alpha$. The projections of this force onto the normal and the plane of the plate are $N = Y \cos \alpha$ and $T = -Y \sin \alpha = -N \tan \alpha$; the causes of the occurrence of the suction force T were discussed in Section 2.9.

For small $\alpha \ll 1$ the similarity law 2.7.10 makes it possible to automatically take the gas compressibility into account

$$\Gamma = \oint u_1 dx = (1 - M_\infty^2)^{-1/2} \Gamma_0, \quad c_y = \frac{2Y}{\rho_\infty U_\infty^2 L} = \frac{2\pi\alpha}{\sqrt{1 - M_\infty^2}} \quad (2.12.6)$$

Clearly, as $|1 - M_\infty| \rightarrow 0$, the flat plate lift increases following a law similar to the law in 2.8.9 for a plate in supersonic flow. However, in subsonic flow the drag remains zero.

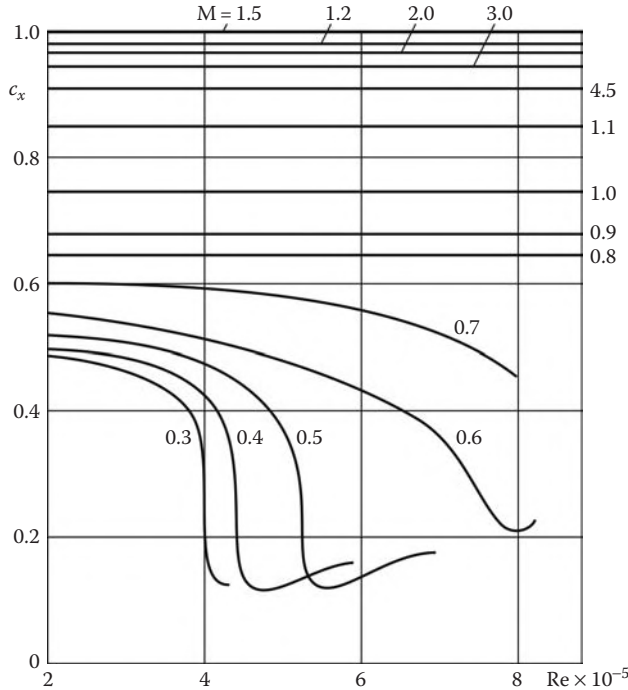


FIGURE 2.23
Drag coefficients c_x of spheres for different Mach and Reynolds numbers.

We note that two models are used for describing the subsonic three-dimensional flow over thin wings, namely, that of a *vortex surface* for the wing itself and that of a *vortex sheet* shed from the wing's trailing edge and containing streamwise distributed vortices. The intensity of these vortices is determined from the same condition of their smooth shedding from the trailing edge. The vortices induce both the lift Y and, as distinct from the plane flows, the *induced drag* X (see, e.g., S.M. Belotserkovskii, 1965). These mathematically sophisticated problems are not considered here. At the same time, bodies in supersonic flow exert a drag (Section 2.8). As shown in Figure 2.23, drag coefficients sharply increase with the Mach number even at $M_\infty < 1$, which will be explained in what follows by the formation of shock waves.*

We will now consider the effect of viscosity on subsonic flows around bodies. As shown in Section 1.16, real bodies in real fluid flows always exert a friction drag due to the fact that there is no fluid slip along the body surface that is not taken into account in the inviscid theory. However, for high Reynolds numbers, $Re > 10^3$, this effect is relatively small and, therefore, the principal role of viscosity is manifested in the formation of separated and recirculation flows, which are qualitatively shown in Figure 1.23. These flows change drastically the general pattern of the flow around bluff bodies (Figure 2.18) which can also be termed *ill-streamlined* with respect to this criterion.

* Figures 2.23 to 2.25 are taken from Schlichting (1968) in which many other results useful in illustrating our reasoning are given.

Without considering the mechanism of the formation of separation zones in detail, we will only point out that separation is formed, since low-pressure streamtubes in the viscous wall layer are not able to overcome a rather high pressure in the convergent flow on the body rear. The qualitative example of such a kind was considered in Section 2.11.

For well-streamlined bodies (like thin airfoils at small angles of attack) in incompressible fluid the inviscid theory with separationless flow around a trailing edge (Section 2.9) agrees quite well with experimental data (Figure 2.24). However, we recall that even in this case viscosity plays a crucial role in the formation of the separationless flow pattern and is important in the choice of the circulation (Section 2.9). However, as the angle of attacks increases, the agreement between the theory and experiment sharply deteriorates, since on the leeward side flow separation occurs, which results in the pressure growth and makes the body ill-streamlined.

Ill-streamlined, or bluff, bodies in incompressible flow have nonzero drag, which is shown in Figure 2.25. Putting aside the $Re \leq 10^3$ range on which the drag coefficient $c_x(Re)$ calculated from the formula $c_x = 2X/\rho_\infty U_\infty^2 S_0$ (S_0 is the cross-sectional area of the body), more general than formula 2.8.7 varies considerably, we will pay attention to the $Re = 10^3 \div 2 \cdot 10^5$ range on which c_x is near-constant ($c_x(Re) \approx 0.4 \div 0.5$), that is, the flow stabilization region formed by viscosity, which does not influence the body drag. In Figure 2.18 experimental curves I correspond to this range; they give near-constant low base pressure $\bar{p}_d = -(0.5 \div 1)p_\infty$, which is typical for flow separation regions with relatively low velocities.

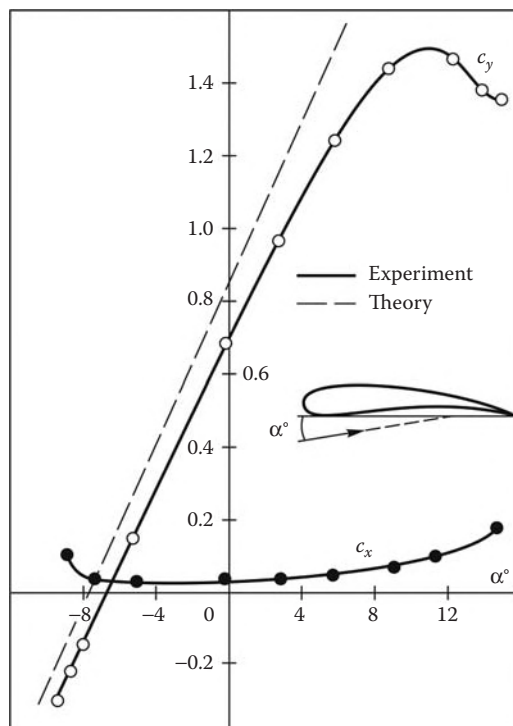
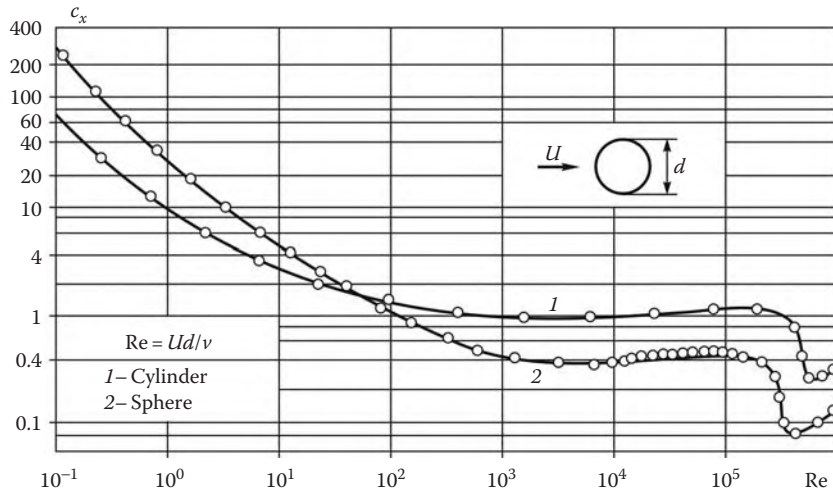


FIGURE 2.24
Drag and lift coefficients of a wing airfoil.

**FIGURE 2.25**

Reynolds number dependence of the drag coefficients for cylinders and spheres in an incompressible flow.

However, in both cases a sharp decrease in the drag down to the small values $c_x \approx 0.1 \div 0.3$ is observed at a certain value $Re \geq 5 \cdot 10^5$. This effect is termed a *drag crisis* and can be explained by the near-wall boundary layer turbulization. Since in this case the velocity profile becomes more convex than that in a laminar flow (Figure 1.26), the separation point is displaced considerably downward and the flow pattern looks similar to that for inviscid flow (curves II in Figure 2.18). This effect is frequently used to reduce the drag of an ill-streamlined body by means of artificial preliminary boundary-layer turbulization, thus postponing flow separation.

Naturally, the previous description of viscous effects is very brief, but, nevertheless, it gives an idea of the range of the inviscid fluid model applicability.

2.13 Aerodynamic Characteristics

The coefficients of the drag, c_x , and the transverse force, c_y , were introduced in Section 2.8 by formula 2.8.9. However, engineering practice usually involves a wider set of similar aerodynamic coefficients, which will partially be done in the following. According to Section 1.7, the projection F_l of the force \mathbf{F} acting on a body onto a direction \mathbf{l} is as follows

$$F_l = - \iint_{\Sigma_b} (p - p_\infty) n_l d\Sigma = \frac{1}{2} q S_0 c_l, \quad n_l = (\mathbf{n} \cdot \mathbf{l}) \quad (2.13.1)$$

Here, S_0 is a characteristic cross-sectional area of the body, $q = \rho_\infty U_\infty^2$ is the ram pressure, \mathbf{n} is the outward normal to the body surface Σ_b , and c_l is the *aerodynamic force coefficient* of F_l . Two coordinate systems are usually used in dynamics of body motion, namely, the *flow-fitted system* (x, y, z) with the x axis aligned with the velocity vector \mathbf{U}_∞ and the *body-fitted system* (τ, n, b) (Figure 2.26a). The τ axis is usually directed along the body surface or along the axis of symmetry as in Figure 2.26b, while the n axis is placed in the plane of symmetry of the body if there are any. The angle α between the x and τ axes is called the *angle of attack*.

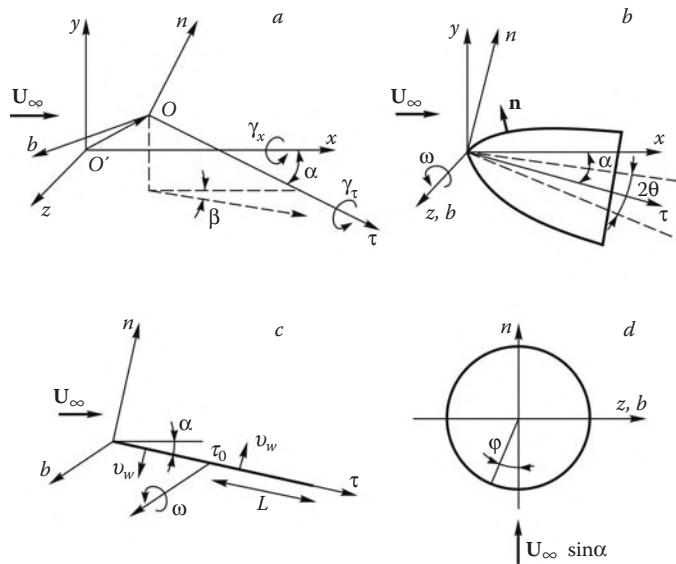


FIGURE 2.26
Flow- and body-fitted reference frames.

and the plane in which the two axes lie is termed the *plane of the angle of attack*. The angle β between the x axis and the projection of the τ axis onto the (x, y) plane is called the *slip angle*. Moreover, we must also specify the mutual displacement OO' of the body-fitted and flow-fitted reference frames and the angles γ_τ and γ_x of their rotations about the τ and x axes, respectively. Thus, we have

$$F_l = X, Y, Z, T, N, B, \quad l = x, y, z, \tau, n, b \quad (2.13.2)$$

Here, X is the body drag and Y is the lift, T and N are the *axial* (longitudinal) and *normal* forces, while Z and B are the lateral forces in their own coordinate systems.

Moreover, a body in a flow exhibits the action of moments of the forces relative different \mathbf{l} axes

$$\mathbf{M}_l = - \iint_{\Sigma_b} (p - p_\infty)[(\mathbf{n} - n_l \mathbf{l}) \times \mathbf{r}_l] d\Sigma = \frac{1}{2} q L S_0 c_{ml} \mathbf{l} \quad (2.13.3)$$

Here, $\mathbf{n} - n_l \mathbf{l}$ is the component of the normal \mathbf{n} orthogonal to \mathbf{l} , L is the body length, \mathbf{r}_l is the vector distance from a point on the body surface to the \mathbf{l} axis, and c_{ml} are the *moment coefficients*. Together with c_l , these form a set of the *aerodynamic characteristics* of a body. Apart from the body shape, they depend on the law of its motion and the similarity criteria M_∞ , Re_∞ , and so on. In the previous formulas only normal pressure forces are taken into account, but one can without difficulty include tangent forces of viscous friction.

When the \mathbf{l} axis is displaced parallel to itself by the vector \mathbf{r}_{l0} orthogonal to \mathbf{l} , the moment varies in accordance with the known law of mechanics

$$\mathbf{M}_l = \mathbf{M}_{l0} + \mathbf{F}'_l \times \mathbf{r}_{l0} \quad (2.13.4)$$

Here, \mathbf{F}'_l is the component of the force \mathbf{F} orthogonal to the vector \mathbf{l} .

In a steady flow past an axisymmetric body the x, y and τ, n planes can be brought into coincidence with the plane of the angle of attack, so that the angle of attack α remains to

be an only governing parameter. This is shown in Figure 2.26b and c, where the dashed line relates to the cone or wedge surface with the vertex angle 2θ . In this case the following relations hold

$$c_y = c_n \cos \alpha - c_\tau \sin \alpha, \quad c_x = c_n \sin \alpha + c_\tau \cos \alpha \quad (2.13.5)$$

If $\mathbf{M}_0 = \mathbf{M}_z(0)$ is a moment about a z axis passing through the origin, then the moment about the same axis passing through a point τ_0 is as follows

$$\mathbf{M}(\tau_0) = \mathbf{M}_0 - \tau_0 N, \quad c_m = c_{m0} - c_n \tau / L \quad (2.13.6)$$

The moment about the point $\tau_0 = \tau_d = L c_d$, where $c_d = c_{m0}/c_n$, is zero, that is, a body with the z axis passing through this point does not rotate. This is the case, for example, when the point coincides with the center of gravity of a body in free flight. The point τ_d is the *center of pressure*, while c_d is the *center of pressure coefficient* dependent on α and other governing parameters. Obviously, τ_d is the point of intersection of the resultant force and the τ axis.

The quantity c_d is one of most important aerodynamic characteristics responsible for the stability of a free ballistic flight (for the flow to be stable, the point τ_d must be located behind the center of gravity) or, in general, for the controllability of a vehicle. For a body of general shape, the center of pressure is a point with respect to which $\mathbf{M} = 0$. When α , β , and γ vary, these points are displaced along a certain surface.

Obviously, for a body of revolution $c_m = c_n = 0$ at $\alpha = 0$, so that for small α we can set

$$c_n = c_n^\alpha \alpha, \quad c_m = c_m^\alpha \alpha, \quad c_d = c_{d0} = c_m^\alpha / c_n^\alpha \quad (2.13.7)$$

Here, c_n^α , c_m^α , and so on are the *aerodynamic derivatives*. It is important that in the general case the quantity $c_{d0} \neq 0$; however it can be evaluated only in solving a three-dimensional problem (e.g., linearizing in α , Section 2.4). In a supersonic flow past a flat plate at a small angle of attack the pressure is constant, $\Delta p \sim \alpha$, and the center of pressure is at the plate center, $c_{d0} = 1/2$.

One more characteristic important in gliding flight and controlled flight in general is the *lift-drag (L/D) ratio* $K = c_y/c_x$ characterizing the vehicle gliding range in free, near-horizontal flight: the greater c_y and smaller c_x , the greater the distance covered by the glider before landing. The greatest permissible, theoretical L/D is achieved, in accordance with Section 2.8, by the previously mentioned flat plate at an angle of attack: $K \sim \alpha^{-1}$. However, for any real body of finite thickness we have $c_{x0} > 0$, so that actually $K \sim \alpha/c_{x0}$ as $\alpha \rightarrow 0$.

We will now consider *unsteady* characteristics of bodies in a flow. To begin with, we will analyze an example. Let a plate of length L set at an angle of attack α acquire suddenly (at $t = 0$) an angular velocity ω due to rotation around a point τ_0 (Figure 2.26d). Then each of its points acquires the normal velocity $v_\omega = \pm\omega(\tau - \tau_0)$, where the upper and lower signs relate to the upper and lower sides of the plate, respectively. Within the framework of the linear theory this problem is reduced to the solution of Equation 2.4.9 with the boundary condition $v_n = U_\infty \alpha + v_\omega$; in this case the steady ($v_n = U_\infty \alpha$) and unsteady ($v_n = v_\omega$) problems can be separated. At small t , when the acoustic wave induced is near-plane, the latter problem has a simple local solution $\Delta p = \rho_\infty a_\infty v_\omega$. In this case, according to 2.13.1 and 2.13.3, the force and the moment about point τ_0 acting on the undersurface of a plate of unit width are as follows:

$$\begin{aligned} N_\omega &= -\frac{1}{2} \rho_\infty a_\infty \omega (1 - 2\bar{\tau}_0) L^2, & \bar{\tau} &= \frac{\tau}{L} \\ M_\omega &= -\frac{1}{3} \rho_\infty a_\infty \omega (1 - 3\bar{\tau}_0 + 3\bar{\tau}_0^2) L^3 \end{aligned} \quad (2.13.8)$$

Here, in the latter formula the sum in the parentheses is positive for $\bar{\tau}_0 \leq 1$; therefore, the arising moment hinders rotation.

In the general case rotation can be due both to oscillations of the plate about, for example, a center of mass and to motion of the center of mass along a curvilinear trajectory, including the case of constant angles of attack and slip to be considered in Section 8.7. Thus, making a generalization, we may anticipate that the forces and moments acting on a body are dependent not only on the instantaneous position of the body in the flow but also on its angular velocity and even translational acceleration. Moreover, the body can change its shape due to deflection of controls, which extends the set of the governing parameters of the unsteady flow. In general, a nonrigid surface of the body can execute flexural oscillations (flutter).

The Strouhal numbers, Sh , characterizing unsteady body motions accompanying the flight (Section 1.12) are usually very small. For example, for a body of length $L = 1$ m moving at a speed $U_\infty \geq 1000$ m/s and executing oscillations at a rather high frequency, $v = 10$ Hz, we have $Sh = vL/U_\infty \leq 10^{-2}$, which allows us to neglect unsteady terms in the equations and to use quasisteady solutions taking into account unsteady terms as linear corrections of the form $M_\omega = M^\omega\omega$. We can also introduce *rotational aerodynamic coefficients* c_ω and their *derivatives* c^ω in accordance with the same scheme 2.13.3 (Belotserkovskii, 1956, 1965).

However, these quantities, though small, can considerably influence, say, ballistic reentry dynamics. In fact, let us write the equation for small oscillations in the form:

$$J\ddot{\alpha} = -M^\dot{\alpha}\dot{\alpha} - M^\alpha\alpha \quad (2.13.9)$$

Here J is the body's moment of inertia, while $M^\dot{\alpha}$ and M^α are the corresponding derivatives of the force moments. Obviously, M^α must be positive, otherwise the body would overturn. For small α and $\dot{\alpha}$ the solution of this equation can be written in the form:

$$\alpha = \alpha_0 e^{-\varepsilon t/2} e^{ivt}, \quad v^2 = \frac{M^\alpha}{J}, \quad \varepsilon = \frac{M^\dot{\alpha}}{J} \quad (2.13.10)$$

Here, v is the *oscillation frequency* and ε is the *oscillation decrement*. No matter how small ε may be, over a long period of time the oscillation amplitude grows infinitely at $\varepsilon < 0$, whereas for $\varepsilon > 0$ the oscillations die out. Precisely the latter case was realized in example 2.13.8 in which for any $\bar{\tau}_0 \leq 1$ the rotational derivative $M^\dot{\alpha} > 0$ (since $\omega = -\dot{\alpha}$).

2.14 Accelerated Motion of Bodies

The problems considered in Section 2.13 were concerned with steady flows around bodies, but, as was shown, in unsteady flows qualitatively new forces, proportional to the body acceleration, arise. Naturally, these forces must arise in accelerated translational motion of bodies. In fact, when a body is accelerated from a velocity U up to $U + \Delta U$ during a time interval Δt , the entrained fluid mass m acquires an additional momentum $m\Delta U$, which results in generation of the drag force $F \sim m\Delta U/\Delta t$. If the disturbed region size and the body size d are of the same order, then $m \sim \rho d^3 \sim \rho V$, V being the body volume, so that we can write

$$F = m \frac{dU}{dt}, m = \lambda' \rho d^3 = \lambda \rho V \quad (2.14.1)$$

This formula is a counterpart of the Newton law. The quantity m is termed an *apparent mass*, while λ' and λ are its coefficients.

Clearly, the apparent mass effect can be essential in hydrodynamics, since m can be comparable with the moving body mass M ; however, in aerodynamics usually $m \ll M$ owing to a small gas density. Moreover, the force F can be comparable with the force in a steady flow, $X = (1/2)c_x\rho U^2 S$, S being the body midsection, only for accelerations $\dot{U} \sim U^2/d$ (for $c_x, \lambda \sim 1$), which corresponds to the velocity increment $\Delta U \sim U$ over a very small time interval d/U . In considering flows at considerably lower accelerations, we can restrict ourselves to the quasisteady approximation. For this reason, in aerodynamics only unsteady effects of lateral motions are taken into account; their role was considered in Section 2.13. Since in this case the forces are proportional to angular, or rotational, velocities, the concept of rotational derivatives, rather than the apparent mass coefficients, is conventionally used to represent these forces.

Nevertheless, from methodical considerations, we will consider the problem of the accelerated motion of a cylinder or a sphere in an incompressible fluid and show that in this case the Dalembert theorem (Section 2.12) does not hold. Let a body move in a quiescent fluid at a variable velocity $-U_\infty(t)$ along the x axis. Since within the framework of incompressible hydrodynamics the speed of sound is infinite, $a = \infty$, the potential Equation 2.4.8 is reduced to the Laplace equation for steady flows with the same instantaneous quasisteady velocity field in the body-fitted coordinate system (x, y, z) . In this case, however, both the velocity field and the pressure distribution are time dependent and the pressure distribution in the flow and over the body should be evaluated by means of the Lagrange integral 2.2.11.

It is not convenient to apply this integral directly to the reversed unsteady flow past a fixed body, since in this case one should introduce a fictitious pressure gradient $\partial p/\partial x \sim \dot{U}_\infty$ in order to compensate the fluid mass acceleration and the effect under consideration would be not so clear. For this reason, we shall use the laboratory coordinate system x', y', z' , in which the fluid at infinity is at rest, and introduce a perturbed velocity \mathbf{U}' and its potential φ' as follows

$$\begin{aligned} \mathbf{U}' &= \mathbf{U} - \mathbf{U}_\infty, & \varphi'(t, x', y', z') &= \varphi(t, x, y, z) - xU_\infty \\ x' &= x + x_0(t), & y' &= y, & z' &= z, & \dot{x}_0 &= -U_\infty \\ &&&&&\varphi &= U_\infty(t)\bar{\varphi}(x, y, z) \\ \varphi' &\rightarrow 0 \quad \text{as} \quad x' \rightarrow \pm\infty, & \varphi &\rightarrow xU_\infty \quad \text{as} \quad x \rightarrow \pm\infty \end{aligned} \quad (2.14.2)$$

Here, \mathbf{U} and φ are the velocity and potential of the quasisteady flow determined by the solutions of Section 2.10. They are proportional to the velocity $U_\infty(t)$ and only in terms of it depend on time. Setting $C(t) = h_\infty$ in the Lagrange integral 2.2.11 we obtain

$$\frac{\Delta p}{\rho} = h - h_\infty = - \left(\frac{\partial \varphi'}{\partial t} + \frac{U'^2}{2} \right) \quad (2.14.3)$$

Substituting in Equation 2.14.3 the relations

$$\begin{aligned} (U')^2 &= (u')^2 + (v')^2 + (w')^2 = U^2 - 2uU_\infty + U_\infty^2 \quad (u' = u - U_\infty) \\ \frac{\partial \varphi'}{\partial t} &= \dot{U}_\infty(\bar{\varphi} - x) + U_\infty(u - U_\infty), \quad u = \frac{\partial \varphi}{\partial x} \end{aligned} \quad (2.14.4)$$

we obtain finally

$$\frac{\Delta p}{\rho} = \frac{1}{2}(U_\infty^2 - U^2) - \dot{U}_\infty(\bar{\varphi} - x) \quad (2.14.5)$$

The force F acting on the body is equal to the surface integral of $\Delta p n_x$; in accordance with the Dalembert theorem, the first, quasisteady term does not contribute to this integral. Hence, the force F is determined by the second term in 2.14.5. Then using the corresponding solutions from Section 2.10 and calculating the surface integral of $\Delta p \cos \theta$, we obtain $\lambda = 1$ for a cylinder and $\lambda = 1/2$ for a sphere in formula 2.14.1 (other examples and the general theory of apparent masses are presented in Loysianskii, 1966).

In conclusion, we will consider a problem of unsteady expansion of a symmetric piston ($r = r_0(t)$) in an incompressible fluid. As previously, the instantaneous velocity distribution is as follows: $v = \dot{r}_0(r_0/r)^\nu$, where $\nu = 1$ and 2 for cylindrical and spherical pistons, respectively. The pressure distribution is determined by the Lagrange integral 2.14.3, where

$$\varphi' = \varphi = \dot{r}_0 r_0 \ln(r/r_0), \quad \nu = 1; \quad \varphi = \dot{r}_0 r_0^2 / r^2, \quad \nu = 2 \quad (2.14.6)$$

In the case of a cylindrical piston, the pressure (or the apparent mass) becomes infinite as $r \rightarrow \infty$, since $\Delta p \sim \ln r$. We can avoid this physically meaningless result by taking into account the end effects for a cylinder of finite dimensions and the compressibility effect (the speed of sound in water is $a \approx 1500$ m/s). We note that the medium compressibility should be also taken into account in considering pulsed motions of a body ($\dot{U}_\infty = \infty$) for which formula 2.14.1 gives infinite force.

At the same time, the problem of a spherical piston has a bounded solution, which decreases at infinity as $\Delta p \sim r^{-1}$. This solution can be used in the problem of gas bubble expansion in water occurring, for example, in underwater explosions or underwater rocket launching.

3

Shock Waves

3.1 Introduction: Formulation of Problems

In the previous chapter the process of the propagation of disturbances was considered in the linear approximation. However, as was shown in Section 2.6, successive compression waves overtake each other with the result that the initial disturbance is enhanced and a *shock wave* forms. The process of the generation of a shock wave from an initially continuous compression wave is an important element of the theory and will be described in Chapter 4. However, in this chapter we will consider a shock wave as an already formed and isolated flow element.

Examples of shock waves near bodies in supersonic flows are shown in Figure 3.1. With respect to their outward appearance they could be subdivided into *bow* shocks, which represent a forward front of all disturbances, and *internal* ones. With respect to their origin, shock waves can be subdivided into *attached* (to the body's leading edge or a bend in the body surface as in Figure 3.1c and d), *detached* (from the body as in Figure 3.1a, b, and d), *submerged* (formed by compression waves inside the flow region as in Figure 3.1d), and other which will be considered in what follows.

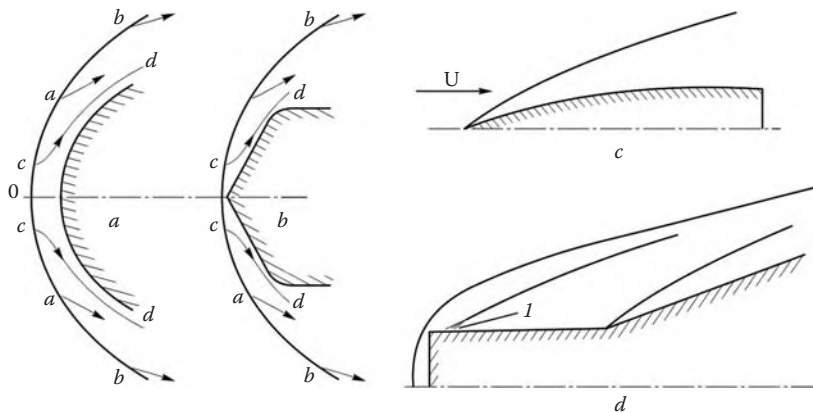
When a steady discontinuity is formed, the mass, momentum, and energy conservation laws 1.7.12 derived in Section 1.7 must be satisfied on either side of the discontinuity.

We will first consider *normal shock waves* whose fronts are orthogonal to the velocity vector of the gas flow across the shock. In this case, the velocity vector direction does not change across the shock, so that the gas flow is one-dimensional and relations 1.7.12 can be simplified somewhat. Moreover, we will consider (up to Chapter 11) only *adiabatic* shock waves with $q_m = 0$ in equations 1.7.12. We will further assume that the dissipative terms in these equations can be neglected in end sections 1 and 2 (Figure 1.16d); this gives relations between flow parameters on either side of an inviscid shock

$$\begin{aligned} \rho_1 u_1 &= \rho_2 u_2 \quad (u = v_n), & p_1 + \rho_1 u_1^2 &= p_2 + \rho_2 u_2^2 \\ H_1 &= h_1 + \frac{u_1^2}{2} = h_2 + \frac{u_2^2}{2} = H_2 \end{aligned} \tag{3.1.1}$$

Bringing sections 1 and 2 together we obtain in a limit a discontinuity front of zero thickness with the quantities on the two sides of the front being related by formulas 3.1.1. The internal structure of the front is of no importance if only there are no sources of mass, momentum, and energy inside. Thus, if the flow parameters are preassigned, say, at left, an equation of state should be invoked to close the system of three equations in four unknown parameters u_2 , ρ_2 , p_2 , and h_2 .

We will assume for a while that this equation has the form $\rho = \rho(p, h, \lambda)$ where λ is a parameter. Such equations are encountered in studying nonequilibrium flows, where λ can be the concentration of a chemical component in the equation of state 1.3.4. In this case an additional condition for the change in λ across the shock is required. However, for an

**FIGURE 3.1**

Different shapes of shock waves.

equilibrium gas state behind the shock, the equation of state $\rho = \rho(p, h)$ is a two-parameter equation (Section 1.3); thus, the formulation of the problem of an *inviscid shock wave* is closed.

However, the question arises (which is beyond the framework of the inviscid theory), whether the concept itself of a zero-thickness shock could be an element of an inviscid flow, since in substituting a discontinuous solution 3.1.1 in the Navier–Stokes equations we obtain unbounded dissipative terms, which were omitted in passing to the Euler equations.

This question of a fundamental nature will be answered in the next section in considering examples of viscous shock structures. It will be shown that the physical thickness δ of a shock front considered as a zone of dissipative effect concentration is extremely small, being of the order of molecular free path; this makes it possible to consider the shock wave front as a *mathematical surface*, at least, for flows inviscid as a whole. This postulate will be used starting from Section 3.3 up to Chapter 12.

The smallness of the shock thickness makes it possible to consider shocks as *quasisteady* in coordinate systems fitted to the shocks themselves (i.e., to neglect time-dependent terms in the integral conservation laws of Section 1.7). In fact, for a control surface enclosing the viscous shock transition zone of thickness δ , the ratio of the time-dependent term, say, in the mass conservation law 1.7.1 to the rate of the gas flowing at a velocity D through this zone is of the order of $(\rho\delta/t_0)/(\rho D) \sim \delta/Dt_0 \ll 1$ due to the assumption on a relative smallness of the shock thickness. Here t_0 is a time scale of the gas dynamic problem.

Thus, in a shock-fitted coordinate system, the flow parameters on either side of the shock are related by inviscid steady conservation laws 1.7.12 or by relations 3.1.1 for one-dimensional shocks.

The second critical point of shock wave theory is related to two physically opposite situations, which are admitted by relations (Equation 3.1.1)

$$\begin{aligned} u_2 < u_1, \quad p_2 > p_1, \quad \rho_2 > \rho_1, \quad h_2 > h_1, \quad e_2 > e_1 \\ u_2 > u_1, \quad p_2 < p_1, \quad \rho_2 < \rho_1, \quad h_2 < h_1, \quad e_2 < e_1 \end{aligned} \quad (3.1.2)$$

Here, $e = h - p/\rho$ is the internal energy. The inequalities for e written previously follow from formulas 3.3.5 or 3.4.22, which will be considered later. In both cases this is flow 1 that

flows in the discontinuity front. In other words, if the conservation laws alone are involved, then both *compression* and *rarefaction* shocks are admissible.

However, for the reasons outlined in Section 2.6 these situations are not physically equivalent. In Sections 3.3 and 3.4 this question will be considered in more detail; until the rigorous substantiation would be done, we will assume that only compression shocks can exist in gases. Media anomalous in this regard will be considered in Section 4.12.

In connection with gas properties we note (returning to Section 1.3) that equations of state for high-temperature gases may have rather complicated forms. Therefore, all further considerations will be performed for gases with the most general properties restricted only by conditions necessary for compression waves to exist.

Finally, in this chapter we will consider *equilibrium adiabatic shock waves* for which the gas states on either side of the shock are equilibrium and are associated with the same equation of state in the sense that there exists a reversible equilibrium process transforming one state into the other. Thus, air heated in a shock up to high temperatures triggering gas dissociation returns to its initial state if the pressure and temperature are restored to their initial values. The simplest example of this kind is provided by a perfect gas.

An opposite example is furnished by a shock wave propagating in a nonequilibrium gas. The well-known detonation and deflagration waves, ahead of which a medium is in a metastable rather than equilibrium state, are also phenomena of this kind. For example, as a result of oxyhydrogen gas explosion with subsequent cooling, water vapors are formed but not the initial mixture. The properties of these *nonequilibrium* shock waves, as well as those of *nonadiabatic* shocks, will be considered in Chapter 11, which is devoted to nonequilibrium flows.

3.2 Shock Wave Structure in a Viscous Gas

The concept of inviscid shock front as a mathematical surface adopted previously is elegant and fruitful for a wide class of inviscid flows. However, owing to dissipative effects, a real shock front must have a finite thickness δ and a continuous structure.

The first step in describing such a structure is to apply the Navier–Stokes equations. In so doing we will set $\tau = \frac{4}{3}\mu(\partial u/\partial x)$ and $J = -\lambda(\partial T/\partial x)$ in relations 1.7.12 and take advantage of the possibility of putting control sections in an arbitrary way. Then these relations can be presented in the form of integrals of the Navier–Stokes equations

$$\begin{aligned} \rho u &= m, & p + \rho u^2 - \frac{4}{3}\mu \frac{\partial u}{\partial x} &= I \\ mH - \lambda \frac{\partial T}{\partial x} - \frac{4}{3}\mu u \frac{\partial u}{\partial x} &= mH_0 \\ H = h + \frac{1}{2}u^2, & & m, I, H_0 &= \text{const} \end{aligned} \quad (3.2.1)$$

These integrals can be obtained by direct integration of the equations of viscous one-dimensional flows (Section 1.2).

For the sake of definiteness, we will assume that the gas flows from left to right, with entry parameters u_1, ρ_1, p_1 , and h_1 . The problem has no scale length; therefore, in bringing the equations to the dimensionless form the length x can be referred only to the combination $\delta_1 = \mu_1/(\rho_1 u_1)$. More particularly, the ratio δ/δ_1 can be obtained only after the problem 3.2.1 has been solved.

This system of equations has a simple solution (Becker, 1912) for a particular case of a perfect gas with the Prandtl number $Pr = \mu c_p / \lambda = 3/4$, which is close to the value $Pr \approx 0.7$ for diatomic gases. In this case the energy Equation 3.2.1 can be brought to the form:

$$\frac{\lambda}{c_p} \left(\frac{\partial h}{\partial x} + \frac{4}{3} Pr \frac{\partial u^2}{\partial x} \right) = \frac{\lambda}{c_p} \frac{dH}{dx} = m(H - H_0) \quad (3.2.2)$$

This equation has a family of solutions $H - H_0 = \text{const} \cdot \exp(mc_p x / \lambda)$ but only the bounded solution $H = H_0$ is of interest. Thus, in this flow, as well as in an inviscid flow, the total enthalpy of the gas is conserved.

Taking this into account and eliminating by means of the equation of state the pressure $p = [(\gamma - 1)m/(\gamma u)]h$ from the momentum equation we obtain

$$\frac{4}{3} \mu u \frac{du}{dx} = m \frac{\gamma + 1}{2\gamma} u^2 - Iu + m \frac{\gamma - 1}{\gamma} H_0 \quad (3.2.3)$$

The right-hand side of this equation is a quadratic trinomial in u whose roots u_1 and u_2 are known, since, as $du/dx \rightarrow 0$ and $x \rightarrow \pm\infty$, the equation is readily apparent from system 3.1.1. Bearing this in mind we transform the equation to the form:

$$\begin{aligned} \bar{u} \frac{d\bar{u}}{dz} &= (\bar{u} - 1)(\bar{u} - \bar{u}_2), & \bar{u} &= \frac{u}{u_1} = \frac{\rho_1}{\rho} \\ dz &= \frac{3(\gamma + 1)\rho u}{8\gamma\mu} dx, & \bar{u}_2 &= \frac{\rho_1}{\rho_2} = k \end{aligned} \quad (3.2.4)$$

This solution has no maxima in a domain of its definition; therefore, as z increases, the function \bar{u} can only decrease ($u_2 \leq u \leq u_1$) or increase ($u_2 \geq u \geq u_1$). However, the latter case is impossible since in any of these situations the right-hand side of the equation is negative. Hence, in the flow under consideration the first condition holds always (i.e., the gas always decelerates). The solution has the form:

$$\begin{aligned} \left(\frac{u_1 - u}{u_1 - u_2} \right) \left(\frac{u_1 - u_2}{u - u_2} \right)^k &= 2^{k-1} \exp[(1-k)z], & u_2 &= ku_1 \\ u \rightarrow u_1, \quad x \rightarrow -\infty; \quad u &\rightarrow u_2, \quad x \rightarrow +\infty \end{aligned} \quad (3.2.5)$$

This solution is shown in Figure 3.2, in which the section $z = 0$ is at the point where $u = (u_1 + u_2)/2$.

The results obtained allow us to make two fundamental conclusions. The first is that in a viscous one-dimensional flow across a discontinuity front (shock wave) only compression is possible, that is, of two situations 3.1.2 only the first one corresponding to a compression shock is possible.

This conclusion, though based only on a particular example, is of a universal nature for gases. In what follows (Section 3.4) we will confer to it a more general form based upon the restrictive properties of the second thermodynamics law.

The second conclusion is that the thickness δ of the shock front smeared by viscosity is of the order of the mean free molecular path l in the gas. In fact, let us define a front thickness, for example, from the condition $\Delta z(1 - k) \sim 1$. Then invoking the simplest considerations of kinetic theory of gases, in particular, formula 1.4.9 for the viscosity, $\mu = \rho V l / 2$, where V is the thermal velocity of molecules, we obtain the following estimate

$$\delta \sim \Delta x \sim \frac{\mu}{\rho u(1 - k)} \sim \frac{lV}{u(1 - k)} \quad (3.2.6)$$

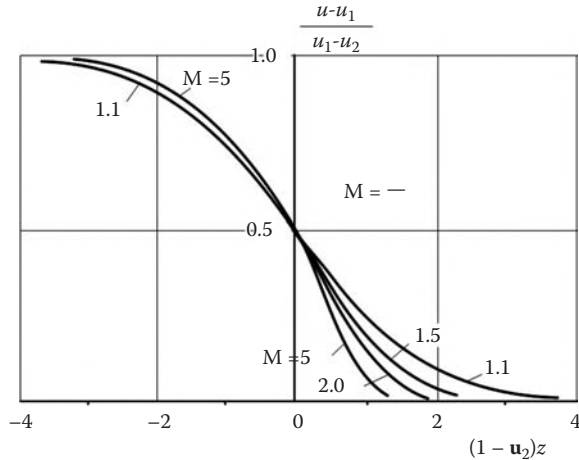


FIGURE 3.2
Velocity profiles in a viscous shock front (a is the speed of sound).

Actually, the quantity δ is of the order of several (up to 10) free molecular paths, depending on the governing parameters of the flow 3.2.6.

Obviously, this result casts some doubt on the validity of describing the shock wave structure within the framework of the Navier–Stokes equations. However, experience and more accurate calculations within the framework of the Boltzmann equation show that the results obtained previously are qualitatively valid (see, e.g., Kogan, 1969). Here, our purpose was only to demonstrate that taking dissipative effects in gas into account eliminates adiabatic and equilibrium rarefaction waves from consideration and allows the existence of compression shock waves only.

We note an interesting property of the solution obtained: the front thickness δ increases without bound as the front intensity decreases, that is, for $(u_1 - u_2)/u_2 \ll 1$. This paradox cannot be removed within the framework of the flow model adopted; however, it should be kept in mind than an unbounded or even very large thickness of the front is irreconcilable with the possibility of considering it as a plane in any real flow with a scale length $L \sim \delta$, the more so for $\delta \gg L$.

3.3 Normal Shock Waves in Perfect Gases

In what follows we will mainly use three forms of the equation of state

$$\frac{p}{\rho h} = \frac{\gamma - 1}{\gamma}, \quad \frac{p}{\rho h} = \frac{\gamma_* - 1}{\gamma_*}, \quad \rho = \rho(p, h) = \rho(p, s) \\ \gamma_* = \gamma_*(p, h) \quad (3.3.1)$$

These are the equations for a perfect gas and a quasiperfect gas with a weakly varying function γ_* , as well as the equation of a general form to be used in Section 3.4. In this section we will mainly consider perfect gases for which the relations on a shock have simple solutions.

Let us write relations 3.1.1 in a shock-fitted coordinate system in terms of relative normal inflow (v_{n1}) and outflow (v_{n2}) velocities. For time-independent and time-dependent processes (Section 1.6) they are, respectively, as follows

$$v_{n1} = u_1, \quad v_{n2} = u_2, \quad v_{n1} = D, \quad v_{n2} = D - u \quad (3.3.2)$$

Here, the quantity u can be called the *entrainment velocity*, that is, a velocity of a gas entrained by a shock wave propagating at a velocity D through a gas at rest. Then relations 3.1.1 takes the form:

$$\begin{aligned} \rho_1 v_{n1} &= \rho_2 v_{n2}, & p_1 + \rho_1 v_{n1}^2 &= p_2 + \rho_2 v_{n2}^2 \\ h_1 + \frac{v_{n1}^2}{2} &= h_2 + \frac{v_{n2}^2}{2} = H_n \end{aligned} \quad (3.3.3)$$

The quantity H_n is a normal component of the total enthalpy that is conserved across a shock.

Eliminating the velocity v_{n2} from this system we obtain

$$\begin{aligned} p_2 &= p_1 + \rho_1 v_{n1}^2 (1 - k), & k &= \frac{\rho_1}{\rho_2} \\ h_2 &= h_1 + \frac{1}{2} v_{n1}^2 (1 - k^2), & v_{n2} &= k v_{n1} \end{aligned} \quad (3.3.4)$$

Written in this form, for v_{n1} , p_1 , h_1 , and ρ_1 given, the system makes up, together with the equation of state, a closed group of thermodynamic relations.

Another form of these equations, which was partially derived in Section 1.6, is more convenient for time-dependent waves (cf. 3.2.2)

$$\begin{aligned} u &= v_{n1} - v_{n2} = D(1 - k), & p_2 &= p_1 + \rho_1 D u \\ e_2 &= h_2 - \frac{p_2}{\rho_2} = e_1 + (1 - k) \frac{p_1}{\rho_1} + \frac{1}{2} u^2, & D &= v_{n1} \end{aligned} \quad (3.3.5)$$

Introducing the normal Mach numbers M_n by formulas

$$M_{n1}^2 = \frac{v_{n1}^2}{a_1^2} = \frac{v_{n1}^2}{(\gamma - 1) h_1} = \frac{\rho_1 v_{n1}^2}{\gamma p_1}, \quad M_{n2}^2 = \frac{v_{n2}^2}{a_2^2} \quad (3.3.6)$$

and substituting p_2 and h_2 from 3.3.4 in the equation of state for a perfect gas we obtain a quadratic equation in k the first root of which, $k = 1$, corresponds to the absence of disturbances, while the second root corresponds to a shock wave

$$k = \frac{\rho_1}{\rho_2} = \frac{\gamma - 1}{\gamma + 1} + \frac{2}{\gamma + 1} \frac{1}{M_{n1}^2} = \frac{a_*^2}{v_{n1}^2} \quad (3.3.7)$$

Here, a_* is the critical velocity of sound (Section 2.2).

Eliminating then k from 3.3.4 we obtain the formulas

$$\begin{aligned} \frac{p_2}{p_1} &= \frac{2\gamma}{\gamma + 1} M_{n1}^2 - \frac{\gamma - 1}{\gamma + 1} = 1 + \frac{2\gamma}{\gamma + 1} (M_{n1}^2 - 1) \\ \frac{h_2}{h_1} &= \frac{T_2}{T_1} = 1 + \frac{2(\gamma - 1)}{(\gamma + 1)^2} (M_{n1}^2 - 1) \left(\gamma + \frac{1}{M_{n1}^2} \right) \end{aligned} \quad (3.3.8)$$

Formally, the relations on a shock are reversible; therefore, along with formula 3.3.7, we can write down the equation

$$\frac{\rho_2}{\rho_1} = \frac{\gamma - 1}{\gamma + 1} + \frac{2}{\gamma + 1} \frac{1}{M_{n2}^2} = \frac{a_*^2}{v_{n2}^2} \quad (3.3.9)$$

Combining with 3.3.7 yields the formulas

$$v_{n1}v_{n2} = a_*^2, \quad M_{n2}^2 = \frac{2 \left(1 + \frac{\gamma-1}{2} M_{n1}^2 \right)}{2\gamma M_{n1}^2 - (\gamma - 1)} \quad (3.3.10)$$

The first relation is called the *Prandtl formula*.

Eliminating M_{n1} from 3.3.7 and 3.3.8 we obtain the *shock adiabat* (Rankine, 1870, Hugoniot, 1895) called so to distinguish it from the adiabat-isentrope

$$\bar{p} = \frac{p_2}{p_1} = \frac{\bar{\rho} - k_0}{1 - k_0 \bar{\rho}}, \quad \frac{\rho_1}{\rho_2} = \frac{1}{\bar{\rho}} = \frac{\bar{h}}{\bar{p}} = \frac{k_0 \bar{p} + 1}{\bar{p} + k_0}, \quad \bar{h} = \frac{h}{h_1}, \quad k_0 = \frac{\gamma - 1}{\gamma + 1} \quad (3.3.11)$$

All these and other functions for a normal shock in a perfect gas are plotted in Figure 3.3.

The formulas obtained make it possible to formulate two theorems of shock wave theory that will be proved for the general case in Section 3.4.

Theorem 1 (Zemplen, 1905)

In a perfect gas only compression shock waves can exist.

To prove the theorem, we will rewrite the equation of state 1.5.9 for a perfect gas in terms of Equation 3.3.11, thus obtaining the expressions for the entropy function $\bar{\Theta}(s) = \bar{p}^{1/\gamma}/\bar{\rho}$ behind the shock and its derivative with respect to \bar{p}

$$\bar{\Theta} = \frac{(k_0 \bar{p} + 1) \bar{p}^{1/\gamma}}{\bar{p} + k_0}, \quad \frac{d\bar{\Theta}}{d\bar{p}} = B(\bar{p})(\bar{p} - 1)^2, \quad B(\bar{p}) > 0 \quad (3.3.12)$$

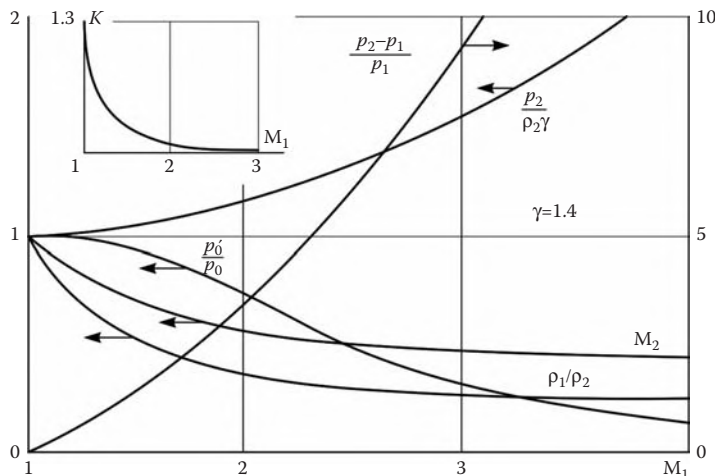


FIGURE 3.3

Dependence of the flow parameters behind a normal shock on the Mach number $M_1 = v_{n1}/a_1$; p_0 and p'_0 are the stagnation pressures ahead of and behind the shock, K is the ratio of the exact pressure increment $p'_0 - p_1$ at the stagnation point to its approximate value (Section 3.6).

The quantity Θ is more convenient in evaluating the difference between entropy changes in shock and isentropic processes, since at equal pressures it gives directly a difference in density. We do not write down the expression for the function $B(\bar{p})$, since only the sign of this function is important. Thence it follows that the derivative $d\bar{\Theta}/d\bar{p} > 0$, that is, the function $\bar{\Theta}$ and, hence, the difference $s - s_1$, monotonically increase with \bar{p} or M_{n1} . Since $\bar{\Theta} = 1$ for $\bar{p} = 1$, the important conclusion follows: *the gas entropy grows in compression shocks and decreases in rarefaction shocks.*

However, the state of a gas changes steeply across a shock wave, so that this process is, evidently, irreversible, according to the classification of Section 1.5. The second law of thermodynamics states that in irreversible adiabatic processes the entropy can only grow; hence, *in perfect gases only compression shock waves can exist*, which proves the statement.

Theorem 2

The gas flows in a compression shock at a supersonic velocity and flows out of it at a subsonic velocity, that is, $M_{n1} > 1$ and $M_{n2} < 1$ (the opposite statement would be valid for steady rarefaction shocks, if such discontinuities could exist).

The result follows immediately from formulas 3.3.7 and 3.3.9, since $M_{n1} = M_{n2}$ for $\rho_2 = \rho_1$.

Thence it follows that a shock wave overtakes and takes up all shock and acoustic waves traveling ahead of the initial wave, while all disturbances traveling behind it overtake and transform it, which was assumed in Section 2.6. This is an important and even underlying factor in forming gas flow structures.

Two more results could be formulated. A *monotonic* increase of the pressure, enthalpy, internal energy, density, and entropy with M_{n1} follows from the previous formulas. At the same time, the entrainment velocity decreases as M_{n1} increases. All these quantities depend univalently on this parameter.

From 3.3.12 it follows that for small $\bar{p} - 1$ the difference $\bar{\Theta} - 1 \sim (\bar{p} - 1)^3$, that is, the *entropy change in a weak shock is of the third order of smallness*.

The function $\bar{p}_2/\bar{\rho}_2^\gamma$ for a perfect gas with $\gamma = 1.4$ is plotted in Figure 3.3. Behind the shock we have always $\bar{p}_2/\bar{\rho}_2^\gamma > 1$. However, for $M_{n1} \leq 1.5$ we can assume that $\bar{p}_2/\bar{\rho}_2^\gamma \approx 1$ thus restricting the range of isentropic weak shocks. In this case the relative pressure increase is $\Delta p/p_1 \leq 1/3$. For higher M_{n1} the gas density behind the shock is noticeably smaller than in the case of the isentropic gas compression to the same pressure, this difference increasing with M_{n1} .

We will now consider limiting regimes with respect to the shock intensity. As $M_{n1} \rightarrow 1$ we have $p \rightarrow p_1$ and so on, while the shock wave itself degenerates, in accordance with Section 1.6, into an acoustic wave in which $v_{n1} = D \rightarrow a_1$. The ratios $\Delta p/\Delta\rho \rightarrow a_1^2$ and $\Delta h/\Delta p \rightarrow \rho_1^{-1}$ remain finite, while the increments themselves are linear in $\Delta M_{n1}^2 = M_{n1}^2 - 1$. For p_2 and h_2 this is evident, while for ρ_2 it follows from 3.3.7 that

$$\frac{\rho_2 - \rho_1}{\rho_1} = \frac{\Delta\rho}{\rho_1} = 1 - k = \frac{2}{\gamma + 1} \left(1 - \frac{1}{M_{n1}^2}\right) \rightarrow \frac{4}{\gamma + 1} (M_{n1} - 1) \quad (3.3.13)$$

A similar M_{n2} -dependence of $\rho_1 - \rho_2$ follows from 3.3.9. Summing these dependences and omitting all the terms of the order $(M_{n1} - 1)^2$ we obtain

$$1 - M_{n2} = M_{n1} - 1, \quad M_{n2} + M_{n1} = 2 \quad (M_{n1} \rightarrow 1) \quad (3.3.14)$$

In the other limiting case of strong shocks, $v_{n1} \gg a_1$, the density ratio and Mach number behind a steady shock have limits depending only on γ

$$k = k_0 = \frac{\rho_1}{\rho_2} = \frac{\gamma - 1}{\gamma + 1}, \quad M_{n2}^2 = \frac{\gamma - 1}{2\gamma} \quad (3.3.15)$$

At the same time, the pressure and temperature ratios, together with the gas velocity u behind a traveling wave, increase without bound.

There is no explicit solution for the equation of state of general form, but for strong shocks (behind which real gas properties are usually manifested) some general results can be obtained using the equilibrium equation of state in quasiperfect form 3.3.1. Let the Mach number M_{n1} be so high that the conditions

$$\begin{aligned} \frac{p}{p_1} &\approx \frac{\rho_1 v_{n1}^2}{p_1} = \gamma_{e1} M_{n1}^2 \gg 1, \\ \frac{h}{h_1} &\approx \frac{v_{n1}^2}{2h_1} = \frac{1}{2}(\gamma_{*1} - 1) \frac{\gamma_{e1}}{\gamma_{*1}} M_{n1}^2 \gg 1 \end{aligned} \quad (3.3.16)$$

are satisfied. Here, $\gamma_e = \rho a^2/p$ (Section 1.6). For a shock propagating through a cold gas $\gamma_{e1} = \gamma_{*1} = \gamma$. In this case formula 3.3.4 is simplified

$$p_2 = \rho_1 v_{n1}^2 (1 - k), \quad h_2 = \frac{1}{2} v_{n1}^2 (1 - k^2) \quad (3.3.17)$$

Substituting them in the quasiperfect equation of state we obtain

$$k = k_* = \frac{\gamma_* - 1}{\gamma_* + 1}, \quad \gamma_* = \frac{h}{e} = \frac{1 + k}{1 - k} \quad (3.3.18)$$

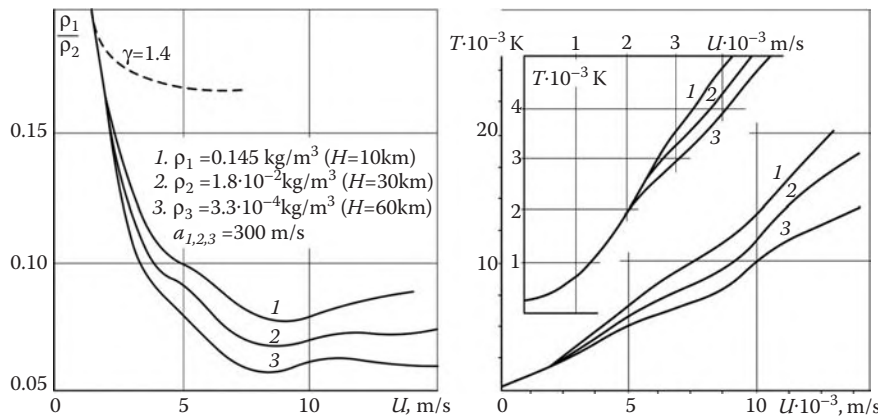
which formally coincides with the expressions for a perfect gas.

We note that the constraint $h_2 \gg h_1$ in 3.3.16 is more severe than $p_2 \gg p_1$ owing to the fact that the difference $(\gamma_* - 1)$ is small.

These relations show that the *gas state behind a strong shock depends on the normal velocity of the shock propagation and on the gas density in front of it rather than on the temperature or the static pressure*. We note that the ratios $p_2/\rho_1 v_{n1}^2$ and h_2/v_{n1}^2 remain finite, as $M_{n1} \rightarrow \infty$. This is the so-called *hypersonic stabilization* of shock waves. However, for real gases the density ratio can depend on the density ρ_1 and velocity U_1 ahead of the shock in terms of the equation of state or the relation $\gamma_* = \gamma_*(p, h)$. This is a typical situation for shocks in atmospheric air, that is, for $T_1 = 300^\circ\text{K}$ and $a_1 = 350 \text{ m/s}$. Thus, the “minimal hypersonic” Mach number, $M_{n1} \geq 6$ (or $k/k_0 \leq 1.15$) is associated with the velocity $v_{n1} \geq 2000 \text{ m/s}$ and the temperature $T_2 \geq 2500^\circ\text{K}$ (Figure 3.4). Under these conditions, oxygen dissociation is already significant (Section 1.3). Only for $M_{n1} \leq 4$, that is, $k/k_0 \geq 4/3$, we have $T_2 \leq 1200^\circ\text{K}$ and the perfect gas model becomes adequate for air if excitation of vibrational degrees of freedom is neglected (Figure 1.3). At the same time, in wind tunnels with not very high stagnation temperatures hypersonic stabilization is realized in its classical form.

For air or carbon dioxide at high temperatures the quantity $\gamma_* = 1.1 \div 1.2$ is near-unity (Section 1.3, Figure 1.9). Thus, the value of k is small: if for a perfect gas with $\gamma = 1.4$ the minimum value of k is $1/6$, for equilibrium air, as follows from Figure 3.4, $k = 0.05 \div 0.1$. Hence, accurate to terms of the order k for the pressure and k^2 for the enthalpy, we can let $k = 0$ in Equation 3.3.17, which yields

$$p_2 = \rho_1 v_{n1}^2, \quad h_2 = \frac{1}{2} v_{n1}^2 \quad (3.3.19)$$

**FIGURE 3.4**

Dependence of the density ratio across a normal equilibrium shock and the temperature behind the shock on the shock propagation velocity U at different altitudes H in the Earth's atmosphere.

In this approximation, the pressure and the enthalpy (as distinct from the density and the temperature) are independent of the gas state behind the shock.

A simple iteration procedure of determining equilibrium parameters behind the shock is based on this property. Setting $k = 0$ in Equation 3.3.4 we obtain the pressure and, especially, the enthalpy with a sufficient accuracy. Substituting then these results in the equation of state, we obtain a density value close to that in a real situation. Repeating the process we can rapidly approach the exact solution.

Finally, we will mention one more property of strong shocks. From Equation 3.3.5 at $p_1 = 0$ it follows that

$$e - e_1 = h - h_1 - \frac{p}{\rho} = \frac{1}{2} u^2 \quad (3.3.20)$$

In other words, the increment of the internal energy per unit mass behind a shock traveling through a gas at rest is equal to its kinetic energy.

The terms e_1 and h_1 are retained here for generality; for $M_\infty \gg 1$ their relative role in formula 3.3.4 is greater than that of the term p_1 . In this sense, the formula

$$\frac{1+k}{1-k} = \frac{h-h_1}{e-e_1} \quad (3.3.21)$$

is more exact than 3.3.18. Equation 3.3.21 can be obtained by combining formulas 3.3.4 at $p_1 = 0$ and 3.3.20.

3.4 Shock Waves in Normal Gases

The analysis presented here is a generalization and development of that given in the book of Sedov (1965). We will consider gases with the general equation of state, $\rho = \rho(p, h)$ or $\rho = \rho(p, s)$, and separate out those for which equilibrium shocks have the same properties as in perfect gases (Section 3.3), namely:

- A. Only compression shocks can exist in which the entropy, pressure, and internal energy increase, while the relative gas velocity decreases (the Zemplen theorem).

- B. The gas velocity relative to the shock is greater than the local speed of sound ahead of the shock and smaller than that behind the shock.
- C. The entropy, pressure, enthalpy, and velocity of the gas entrained by the shock increase monotonically with the relative velocity of the gas flowing in the wave; therefore, for a given shock there is a unique gas state behind the shock (under a natural assumption that the functions $\rho(p, h)$, $e(p, h)$, and so on are single-valued).
- D. Weak shocks are isentropic and the entropy increments in them are of the third order in the pressure increment.

As distinct from the perfect gas, the density is not required to be monotonic; this requirement is too severe, e.g., for air (Figure 3.4). Such gases are called *normal*.^{*} It will be shown that their equations of state obey the following restrictions

$$\left(\frac{\partial^2 \rho^{-1}}{\partial p^2} \right)_s = \frac{1}{\rho^6 a_e^6} \left[\frac{\partial^2 p}{\partial (\rho^{-1})^2} \right]_s = \frac{2A}{\rho^3 a^4} > 0, \quad A = 1 + \frac{1}{2} \rho \left(\frac{\partial a^2}{\partial p} \right)_s$$

$$p \left(\frac{\partial \rho^{-1}}{\partial h} \right)_p < L, \quad L = 1 \quad (3.4.1)$$

The latter condition is sufficient but not necessary. In particular, it is not required for weak shocks. At the same time, if the requirement of the entrainment velocity monotonicity is excluded from item C, it is sufficient to let $L = 2$, that is, to weaken the second restriction 3.4.1 in order for the other properties to be retained. The uniqueness of the gas state behind a shock is conserved in this case, since the monotonicity of the pressure and enthalpy is sufficient for this.

Conditions in 3.4.1 do not follow from any theorem of thermodynamics. Nevertheless, one can consider all known gases to be normal (until a disproof appears). For quasiperfect gases (Section 1.3) these conditions take the form:

$$A = \frac{\gamma_e + 1}{2} + \frac{p}{2} \left(\frac{\partial \gamma_e}{\partial p} \right)_s > 0, \quad \gamma_e = \frac{\rho a_e^2}{p}, \quad \frac{p}{\rho h} = \frac{\gamma_* - 1}{\gamma_*}$$

$$p \left(\frac{\partial \rho^{-1}}{\partial h} \right)_p = \frac{\gamma_* - 1}{\gamma_*} + \frac{h}{\gamma_*} \left(\frac{\partial \gamma_*}{\partial h} \right) < 1 \quad (3.4.2)$$

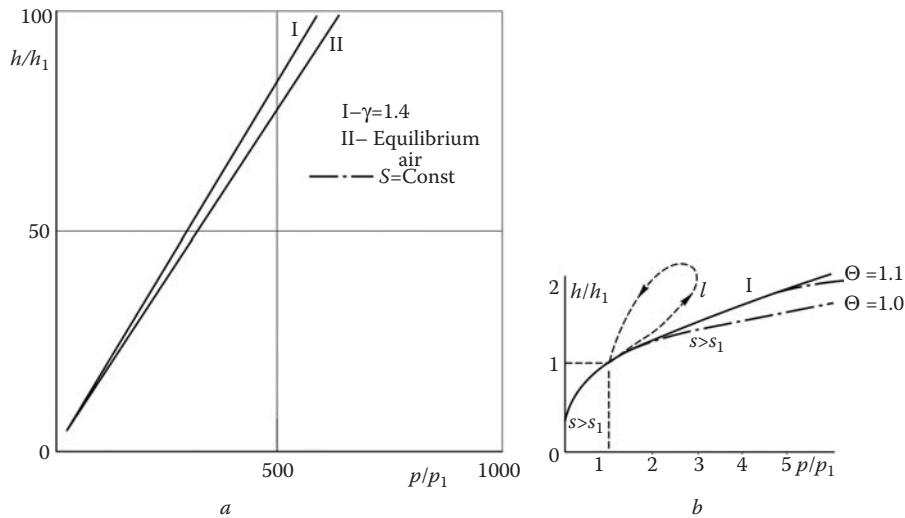
Since the functions γ_e and γ_* are weakly dependent functions of their arguments (see Figures 1.9 and 1.10 from Section 1.3), we can easily believe that the last terms in these formulas are relatively small.

To prove the previously formulated statements on shock wave properties, we eliminate the parameter $v_{n1} = v_1$ from formula 3.3.4, which leads to the relation (here subscripts 2 and n are omitted)

$$h - h_1 = \frac{1}{2} \left(\frac{1}{\rho_1} + \frac{1}{\rho} \right) (p - p_1), \quad \rho = \rho(p, h) \quad (3.4.3)$$

Together with the equilibrium equation of state, this dependence represents the *shock adiabat*, $h = h(p, p_1, h_1)$, which relates all the possible states behind shocks to a given initial state 1. Examples of shock adiabats are presented in Figure 3.5.

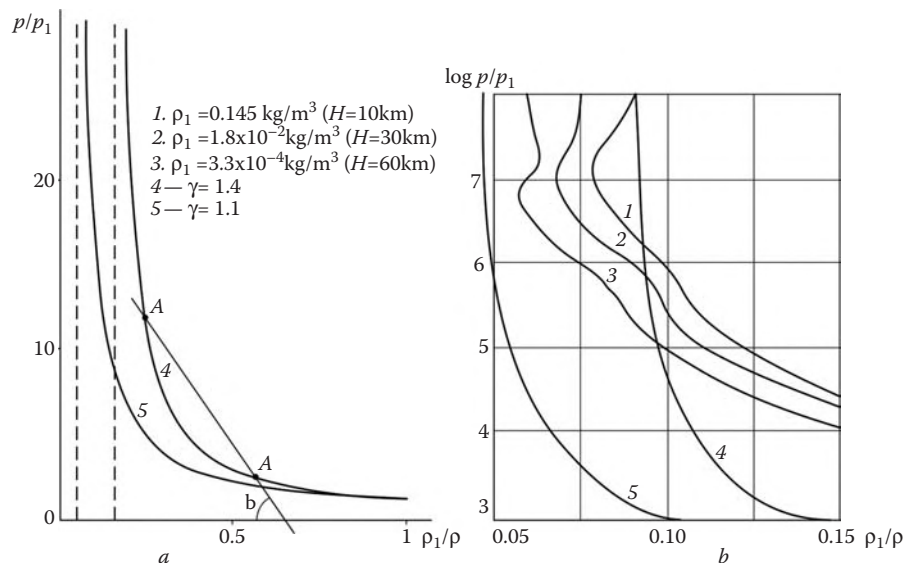
* We note that the frequently used term *normal* gas can have different meaning with respect to the second condition 3.4.1, which is variously, if at all, formulated in the works of different authors.

**FIGURE 3.5**

Shock adiabats in a perfect gas (I) and equilibrium air at $p_1 = 1$ atm and $T = 300$ K (II).

The shock adiabat can be also expressed in terms of other variables, for example, in the form of the dependence $p = p(\rho^{-1})$ presented in Figure 3.6 or by formula 3.3.11. In this phase plane the slope β of the secant AB in Figure 3.6a is related with the shock propagation velocity by the following formula, which can be derived from Equation 3.3.4

$$\frac{p_B - p_A}{V_A - V_B} = V_A^{-2} v_{nA}^2 = V_B^{-2} v_{nB}^2 = \tan \beta, \quad V = \rho^{-1} \quad (3.4.4)$$

**FIGURE 3.6**

Shock adiabats in equilibrium air (under the same conditions as in Figure 3.4) and in a perfect gas.

Here, the subscripts A and B refer to the parameters ahead of and behind the shock. However, in the general case these adiabats can be nonmonotonic (Figure 3.6b), which makes their analysis fairly difficult. As to monotonicity of curve 3.4.3, it will be established for normal gases in what follows.

In the phase plane (h, p) the shock adiabat is represented by a curve passing through point 1 with the parameters p_1, h_1, s_1 , and so on. The curve describes also a certain reversible, generally speaking, nonadiabatic process that transfers the gas from state 1 to a given state (p, h) behind the shock with a chosen propagation velocity v_1 . Precisely this auxiliary process is used in the following to evaluate the entropy behind the shock.

To do this, we will consider the shock adiabat in the parametric form, $h = h(v_1^2)$, $p = p(v_1^2)$ (formula 3.3.4) and differentiate these formulas; thus, we evaluate the entropy variation rate along the shock adiabat

$$Tds = dh - \frac{1}{\rho} dp = \frac{1}{2} \left(1 - \frac{\rho_1}{\rho}\right)^2 dv_1^2 \quad (3.4.5)$$

Thus, the entropy behind the shock increases with the shock propagation velocity. Near point 1 the shock degenerates into a sound wave in which $v_1 \rightarrow a_1$, $p_2 \rightarrow p_1$, and so on. Therefore, the entropy increases across the shock ($s > s_1$) at $M_1 = v_1/a_1 > 1$ and decreases ($s < s_1$) at $M_1 < 1$. Thence and from the second law of thermodynamics it follows that *the shock wave as a discontinuity front of parameters can propagate in a gas only at a supersonic velocity*.

Since from formulas 3.3.7 and 3.3.8 it follows that the density, the pressure, and the enthalpy increase with the Mach number M_1 , this proves that in perfect gases only shock compression can exist.

We will generalize this result to arbitrary gases. To do this, we will analyze the behavior of the solution in the vicinity of point 1 expanding the function $\rho(p, s)$

$$\begin{aligned} \frac{\rho_1}{\rho} &= 1 - \frac{p - p_1}{\rho_1 a_1^2} + \frac{1}{2} \rho_1 \left(\frac{\partial^2 \rho^{-1}}{\partial p^2} \right)_{s,1} (p - p_1)^2 + \\ &\rho_1 \left(\frac{\partial \rho^{-1}}{\partial s} \right)_p (s - s_1) + \dots, \quad \left(\frac{\partial \rho^{-1}}{\partial p} \right)_s = -\frac{1}{\rho^2 a^2} \end{aligned} \quad (3.4.6)$$

The subscripts of derivatives s and p indicate the parameters that are held constant at the differentiation, while the subscript 1 refers to point 1.

By virtue of 3.4.5, the order of smallness of the last term is greater than Δp^2 ; thus, this term can be omitted. Taking into account formula 3.4.1 and combining 3.4.6 with the first formula in 3.3.4 we obtain

$$\frac{1}{2} \rho_1^2 a_1^2 \left(\frac{\partial^2 \rho^{-1}}{\partial p^2} \right)_{s,1} (p - p_1) = A_1 \frac{p - p_1}{\rho_1 a_1^2} = M_1^2 - 1 \quad (3.4.7)$$

Substituting ρ_1/ρ from 3.4.6 into 3.4.5 and replacing the differential $dv_1^2 = a_1^2 dM_1^2$ from 3.4.7 by dp we obtain after integration the fundamental relation of shock wave theory

$$T_1(s - s_1) = \frac{1}{12} \left(\frac{\partial^2 \rho^{-1}}{\partial p^2} \right)_{s,1} (p - p_1)^3 + \dots \quad (3.4.8)$$

Since $s > s_1$, the sign of the difference $p - p_1$ for weak shocks is dependent on the sign of the derivative $(\partial^2 \rho^{-1}/\partial p^2)_s$, which is positive according to 3.4.1. Since the entropy in a shock always grows, weak shocks can be compression shocks only.

Extension of these results to a shock of finite intensity is evident. The shock adiabat $h(p)$ is continuous, since for $p \geq p_1$ the density satisfies the inequality $\rho \geq \rho_1 > 0$. Therefore, a shock wave could be a rarefaction shock only in the case in which the shock adiabat originating at point 1 in Figure 3.5b starts to the right with an increase in $v_1 > a_1$ and intersects again the line $p = p_1$ (curve l). However, at the point of intersection, relations 3.3.4 give $\rho = \rho_1$ and $h = h_1$. This means that the intersection could occur only at point 1 itself. At this point the entropy as a function of state is equal to $s = s_1$, which contradicts to condition 3.4.5 of monotonic entropy increase along the shock adiabat.

Hence, for gases under consideration the physically realized branch of the shock adiabat lies entirely to the right of point 1, that is, in the compression region, which proves the statement.

The adiabat branch to the left of point 1 corresponds to a rarefaction region, $p < p_1$ and so on, to subsonic Mach numbers, $M_1 < 1$, and, which is most important, to a decrease in the entropy. For this reason it cannot be realized. Obviously, the continuation of this branch to a region of decreasing v_1 leads, according to 3.4.5, only to a subsequent entropy decrease. Hence, as in previous considerations, the line $p = p_1$ cannot be intersected in such a way and even formally one cannot obtain a compression shock wave with an entropy decrease.

As follows from relation 3.4.8, the *shock adiabat at point 1 has the tangency of the second order with the isentrope*. In fact, let us expand the equation of state in the vicinity of point 1

$$h - h_1 = \frac{p - p_1}{\rho_1} - \frac{(p - p_1)^2}{2\rho_1 a_1^2} + \frac{1}{6} \left(\frac{\partial^2 \rho^{-1}}{\partial p^2} \right)_s (p - p_1)^3 + T_1(s - s_1) + \dots \quad (3.4.9)$$

On the isentrope we have $s = s_1$, while, according to 3.4.8, on the shock adiabat $\Delta s \sim (\Delta p)^3$, which proves the statement. Generally, according to 3.4.5, the shock adiabat is always located above a local isentrope (behind the shock) on which $\rho dh = dp$. Their relative position is shown in Figure 3.5b.

We will now prove that the flow behind a weak wave is subsonic. Since the relations across the shock are symmetric with respect to subscripts 1 and 2, the expansion in the vicinity of point 2 similar to 3.4.7 leads to a symmetrical relation

$$\frac{1}{2} \rho_2 a_2^2 \left(\frac{\partial^2 \rho^{-1}}{\partial p^2} \right)_s (p_1 - p_2) = M_2^2 - 1 \quad (3.4.10)$$

Since $p_2 > p_1$, the inequality $M_2 < 1$ holds.

Thus, all the statements A to D have been proved, though statements B and C are proved only for weak shocks. The monotonic behavior of the entropy for finite-intensity shocks has already been proven by relation 3.4.5, while the same for the enthalpy is ensured by the monotonicity of the pressure, by virtue of the second law of thermodynamics

$$\frac{dh}{dv_1} = \frac{1}{\rho} \frac{dp}{dv_1} + T \frac{ds}{dv_1} \quad (3.4.11)$$

We will now consider the pressure and the entrainment velocity u and prove the inequality $M_2 < 1$ for the general case. To do this, we differentiate Equations 3.3.4 and 3.3.5 along the shock adiabat

$$\frac{dp}{dv_1^2} = \rho_1(1 - k) - \rho_1 v_1^2 \frac{dk}{dv_1^2}, \quad k = \frac{\rho_1}{\rho} \quad (3.4.12)$$

and

$$\frac{du}{dv_1} = (1 - k) - 2v_1^2 \frac{dk}{dv_1^2} \quad (3.4.13)$$

Combining the previous equations we obtain

$$\frac{1}{\rho_1} \frac{dp}{dv_1^2} = \frac{1}{2}(1 - k) + v_1 \frac{du}{dv_1^2} \quad (3.4.14)$$

Clearly, the monotonicity of the pressure $p(v_1)$ follows from that of $u(v_1)$ but not *vice versa*. Setting $\rho = \rho(p, s)$ yields

$$\frac{d\rho^{-1}}{dv_1^2} = \left(\frac{\partial \rho^{-1}}{\partial p} \right)_s \frac{dp}{dv_1^2} + \left(\frac{\partial \rho^{-1}}{\partial s} \right)_p \frac{ds}{dv_1^2} = -\frac{1}{\rho^2 a^2} \frac{dp}{dv_1^2} + \left(\frac{\partial \rho^{-1}}{\partial h} \right)_p T \frac{ds}{dv_1^2} \quad (3.4.15)$$

Substituting the derivative of the pressure (3.4.12) in this relation and using formulas 3.3.3 and 3.4.5 we obtain

$$v_1^2 \frac{dk}{dv_1^2} = -\frac{1 - k}{1 - M^2} \left[M^2 - \frac{1}{2}(p - p_1) \left(\frac{\partial \rho^{-1}}{\partial h} \right)_p \right] \quad (3.4.16)$$

The Mach number M behind the shock introduced here is as follows

$$M^2 = \frac{v^2}{a^2} = \frac{\rho_1^2 v_1^2}{\rho^2 a^2} = -\rho_1^2 v_1^2 \left(\frac{\partial \rho^{-1}}{\partial p} \right)_s \quad (3.4.17)$$

Then formula 3.4.13 takes the form:

$$(1 - M^2) \frac{du}{dv_1} = (1 - k) \left[1 + M^2 - (p - p_1) \left(\frac{\partial \rho^{-1}}{\partial h} \right)_p \right] = W_1 > 0 \quad (3.4.18)$$

The inequality in the previous formula is valid by virtue of the second condition 3.1.1. Clearly, this condition is somewhat stronger than is necessary; on the other hand, it depends only on gas properties rather than on particular conditions.

Thus, the following inequalities have been proven for shock compression fronts

$$\begin{aligned} \frac{ds}{dv_1} &> 0, & (1 - M^2) \frac{du}{dv_1} &> 0, & (1 - M^2) \frac{dp}{dv_1} &= W_2 \\ W_2 &= 2\rho_1 v_1 (1 - k) \left[1 - \frac{1}{2}(p - p_1) \left(\frac{\partial \rho^{-1}}{\partial h} \right)_p \right] > 0 \end{aligned} \quad (3.4.19)$$

In order to prove that the functions $p(v_1)$, $h(v_1)$, and $u(v_1)$ are monotonic, we must assure ourselves that the condition $1 - M^2 > 1$ holds over the entire shock velocity range.

As was proved previously, for weak waves near point 1 $M < 1$, while the expression within the brackets in 3.4.18 is positive; therefore, $du/dv_1 > 0$, together with $dp/dv_1 > 0$. However, these derivatives can change their signs only with the difference $1 - M^2$. In this case from Equations 3.4.18, 3.4.14, and 3.4.5 there follows the sequence of relations along the shock adiabat

$$M \rightarrow 1, \quad \frac{du}{dv_1}, \frac{dp}{dv_1} \rightarrow \infty, \quad \frac{ds}{dp} = \frac{ds}{dv_1} \frac{dv_1}{dp} \rightarrow 0 \quad (3.4.20)$$

Since for weak shocks $M < 1$, the Mach number M must increase when approaching unity.

We will prove that this is impossible. To do this, we will evaluate the total derivative of M^2 with respect to p along the shock adiabat; at the sonic point, in view of limiting relations 3.4.20 and conditions 3.4.1, it is as follows

$$\begin{aligned} \frac{dM^2}{dp} &= -\rho_1 v_1^2 \left(\frac{\partial^2 \rho^{-1}}{\partial p^2} \right)_s + \left[\rho_1 \left(\frac{\partial \rho^{-1}}{\partial p} \right)_s + \rho_1 v_1^2 \left(\frac{\partial^2 \rho^{-1}}{\partial p \partial s} \right) \frac{ds}{dv_1} \right] \frac{dv_1^2}{dp} \\ &= -\rho_1 v_1^2 \left(\frac{\partial^2 \rho^{-1}}{\partial p^2} \right)_s < 0 \end{aligned} \quad (3.4.21)$$

This contradicts the condition that the sonic point can be obtained, that is, the condition $dM/dp > 0$ at this point. Thus, the last theorem, item B, has been proven for normal gases.

It should be noted that in order to prove the theorem we have needed only the condition $dv_1/dp = 0$ at the sonic point, that is, the condition $W_2 > 0$ in 3.4.19. In order for the latter inequality to hold, it is sufficient to let $L = 2$ in 3.4.1. All the properties A to D of shock waves formulated previously are conserved in this case, with the exception of the monotonic behavior of the $u(v_1)$ dependence.

We will explain in more detail the situation concerned with possible abnormal behavior of the density along the shock adiabat. For $M_1 \gg 1$ the relation $M^2 \approx k \ll 1$ usually holds, so that the expression in the brackets in 3.4.16 can change the sign under condition 3.4.1 as well, which is shown in Figures 3.3 and 3.6 for equilibrium-state air.

We will now touch on the internal energy e . A monotonic behavior of e with the shock velocity v_{n1} does not follow from the counterpart of Equation 3.4.11, $de = Tds - pd\rho^{-1}$, without any additional (relative to 3.4.1) assumption on the gas medium properties. We will not dwell on this question, the more so as this circumstance (as well as nonmonotonic behavior of the density) does not violate the uniqueness of the solution of the shock relations (for single-valued functions $\rho(p, h)$, $e(p, h)$, etc.). In time-dependent problems, adiabats of the form

$$e - e_1 = \frac{1}{2}(p + p_1) \left(\frac{1}{\rho_1} - \frac{1}{\rho} \right), \quad p = p(e, \rho) \quad (3.4.22)$$

are sometimes used. A possible nonmonotonicity of the function $\rho(v_{n1})$ can lead to non-monotonicity and even nonuniqueness of the function $e(\rho^{-1})$ similarly to the case of the function $p(\rho^{-1})$ in Figure 3.6b.

In conclusion, we will return to weak shocks. According to Equation 3.3.14, for perfect gases we have $M_1 + M_2 = 2$. However, within the accuracy of Equations 3.4.7 and 3.4.10, the coefficients on the left-hand sides can be considered to be equal. Therefore, summing these formulas for $M_1 \approx 1$ we obtain the same result in the general case as well. Thence, using the entrainment velocity $u = v_{n1} - v_{n2}$, we obtain

$$v_{n1} - a_1 = a_2 - v_{n2}, \quad v_{n1} = \frac{1}{2}(a_1 + a_2 + u) \quad (3.4.23)$$

Another useful formula can be obtained by subtracting Equation 3.4.10 from 3.4.7

$$(M_1^2 - 1) - (M_2^2 - 1) = M_1^2 - M_2^2 = 2A_1 \frac{p_2 - p_1}{\rho_1 a_1^2} \quad (3.4.24)$$

We emphasize that formulas 3.4.22 through 3.4.24 were derived with no regard for second-order terms and are by no means connected with restrictions 3.4.1.

3.5 Oblique Shocks

We are now coming to the study of *oblique* shocks. For these shocks, the plane in which they lie is inclined by an angle α to the inflowing gas velocity vector \vec{U}_1 . As earlier, the discontinuity front is considered to be quasisteady in its own coordinate system and its thickness sufficiently small, as compared with the radius of curvature of the shock and, generally, with a flow scale length, for a shock element could be assumed to be plane and dissipative terms on the boundary of the control volume Ω , for which the integral conservation laws have been written in Section 1.7, could be neglected.

Let \mathbf{U} be a local gas velocity in the coordinate system fitted to the shock front. From symmetry considerations it is obvious that across a plane shock the velocity vector varies only in the flow plane (or in the plane of the angle of attack) in which the velocity vector \mathbf{U}_1 and the outward normal \mathbf{n} directed to the inflowing gas lie. The flow pattern in this plane is shown in Figures 1.16d and 3.7 (we note that in these figures the directions of the normals are opposite; however, at the corresponding change in the vector signs, this does not alter the form of Equation 1.7.12).

We will take two planes parallel to the shock, in front of and behind it, such that the region of viscosity and heat conduction influence, that is, the region of shock transition, is completely confined between these planes. In this case we can apply to these planes Equations 1.7.12 with dissipative terms omitted, to relate the parameters in front of and behind the inviscid shock (subscripts 1 and 2, respectively). We will rewrite these relations in the form:

$$\begin{aligned} \rho_2 v_{n2} &= \rho_1 v_{n1}, \quad v_n = -\mathbf{n} \cdot \mathbf{U}, \quad \rho_2 v_{n2} \mathbf{U}_2 - p_2 \mathbf{n} = \rho_1 v_{n1} \mathbf{U}_1 - p_1 \mathbf{n} \\ \rho_2 v_{n2} \left(e_2 + \frac{1}{2} U_2^2 \right) - p_2 \mathbf{n} \cdot \mathbf{U}_2 &= \rho_1 v_{n1} \left(e_1 + \frac{1}{2} U_1^2 \right) - p_1 \mathbf{n} \cdot \mathbf{U}_1 = \\ \rho_1 v_{n1} \left(e_1 + \frac{1}{2} U_1^2 + \frac{p_1}{\rho_1} \right) &= \rho_1 v_{n1} \left(h_1 + \frac{1}{2} U_1^2 \right) \end{aligned} \quad (3.5.1)$$

As earlier, here v_n is the normal velocity of the gas flow across a fixed shock.

Let $\vec{\tau}$ be a vector tangent to the shock front and v_τ be the velocity vector projection onto the front. Multiplying scalarly the second Equation 3.5.1 by $\vec{\tau}$ and taking into account the first equation we obtain that $v_{\tau_2} = v_{\tau_1}$, that is, the *tangent component of the velocity does not change across the shock front*.

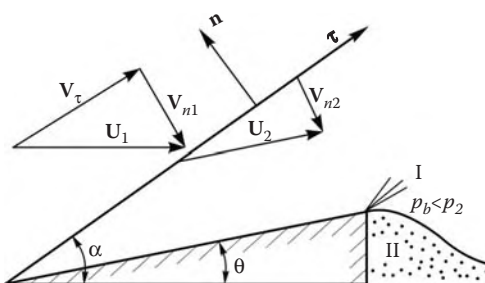


FIGURE 3.7
Oblique shock and flow past a wedge; I, expansion fan and II, base region.

Projecting the same equations onto the normal \mathbf{n} yields Equation 3.3.3 or 3.3.4, which determine completely shock thermodynamics; the properties of these equations were studied in detail in Sections 3.3 and 3.4.

Combining Equations 3.3.4 and 3.5.1 we obtain an expression for the velocity vector behind the shock

$$\mathbf{U}_2 - \mathbf{U}_1 = \frac{p_2 - p_1}{\rho_1 v_{n1}} \mathbf{n} = v_{n1}(1 - k) \mathbf{n}, \quad k = \frac{\rho_1}{\rho_2} = \frac{v_{n2}}{v_{n1}} \quad (3.5.2)$$

From the last equation of 3.5.1 it follows that

$$H_2 = h_2 + \frac{1}{2} U_2^2 = h_1 + \frac{1}{2} U_1^2 = H_1 \quad (3.5.3)$$

This means that *the stagnation enthalpy is conserved across a steady shock*, that is, *the constant of the Bernoulli equation from Section 2.2 does not change*. This is the generalization of the result for the normal component H_n of the total enthalpy H obtained in Section 3.3 (we note that it can easily be obtained from 3.5.3 by subtracting $v_\tau^2/2$ from both sides of the equality).

If α is the shock inclination angle in the flow plane, then we have $v_{n1} = U_1 \sin \alpha$ and the previously mentioned relations for the shock take the form:

$$p_2 - p_1 = \rho_1 U_1^2 \sin^2 \alpha (1 - k) \quad (3.5.4)$$

and

$$h_2 - h_1 = \frac{1}{2} U_1^2 \sin^2 \alpha (1 - k^2) \quad (3.5.5)$$

The previous relations were obtained for a fixed shock wave. Let now a shock element move in the space at a velocity \mathbf{U}_0 , \mathbf{U} being the velocity in the shock-fitted coordinate system and \mathbf{U}' the velocity in the fixed laboratory coordinate system. Then we have

$$\mathbf{U}' = \mathbf{U} + \mathbf{U}_0, \quad v_{n1} = -\mathbf{n}\mathbf{U} = -\mathbf{n}\mathbf{U}' + D, \quad D = \mathbf{n}\mathbf{U}_0 \quad (3.5.6)$$

Here, D is the component of the velocity \mathbf{U}_0 normal to the front. It was shown in Section 1.7 that the integral conservation laws for a volume Ω are invariant with respect to any inertial coordinate system. Therefore, relation 3.5.1 is unchanged in a new coordinate system if \mathbf{U} is replaced by \mathbf{U}' and the velocity v_{n1} is determined from 3.5.6 in terms of \mathbf{U}' and \mathbf{U}_0 .

In order to determine the components u , v , and w of the velocity vector \mathbf{U} in an arbitrary Cartesian coordinate system (x, y, z) we project Equation 3.5.2 onto the coordinate axes

$$u_2 - u_1 = n_x v_{n1}(1 - k), \quad v_2 - v_1 = n_y v_{n1}(1 - k), \quad w_2 - w_1 = n_z v_{n1}(1 - k) \quad (3.5.7)$$

Here, n_x , n_y , and n_z are the direction cosines of the normal \mathbf{n} . If the shock shape is given in the general form, $F(x, y, z, t) = 0$, the cosines and the normal velocities of the shock and the gas, D and v_n , are determined by formulas 1.11.3 to 1.11.7. If the formulas do not correspond to the normal direction chosen, the signs of their right-hand sides should be changed for opposite.

We will consider some intrinsic (i.e., independent of a coordinate system) properties of shocks. Let α be the local shock inclination angle in the flow plane and θ be the angle of the flow deflection across the shock; the latter is equal to the semivertex angle of a wedge in gas flow (Figure 3.7). Then, from geometrical considerations it follows

$$\begin{aligned} \frac{v_{n2}}{v_\tau} &= \tan(\alpha - \theta) = \frac{\tan \alpha - \tan \theta}{1 + \tan \alpha \tan \theta} = k \tan \alpha, \\ v_{n1} &= U_1 \sin \alpha, \quad v_\tau = U_1 \cos \alpha, \quad v_{n2} = k v_{n1}, \quad k = k(\alpha) = \frac{\rho_1}{\rho_2} \end{aligned} \quad (3.5.8)$$

Thence it follows

$$\zeta = \tan \theta = \frac{(1-k)\eta}{1+k\eta^2}, \quad \eta = \tan \alpha \quad (3.5.9)$$

$$k\zeta\eta^2 - (1-k)\eta + \zeta = 0, \quad k = k(\eta) \quad (3.5.10)$$

For small angles $\theta, \zeta \rightarrow 0$, two limiting solutions can exist. The first solution, $\eta \rightarrow \infty$, $\alpha \rightarrow \pi/2$, corresponds to a normal shock, while the second solution, $k \rightarrow 1$, corresponds to a shock of a very small intensity. The function $\zeta(\eta)$ (we will call it a *shock polar*) has a maximum at a point (ζ_0, η_0) , as shown in Figure 3.8 and for perfect gases in Figure 3.9. Thus, there exists a *limiting angle* of the flow deflection in a shock θ_0 such that if a sharp body has a semivertex angle $\theta > \theta_0$, then the shock wave detaches from the body (Figure 3.1b).

Clearly, the function $\zeta(\eta)$ is one-valued, but the inverse function $\eta(\zeta)$ is two-valued and has two branches. The branch $\eta > \eta_0$ with the greater pressure behind the shock is termed a *strong shock branch*, while the branch $\eta < \eta_0$ is called a *weak branch*. The branching point (η_0, ζ_0) is determined from the equation $d\zeta/d\eta = 0$, where

$$\begin{aligned} \frac{d\zeta}{d\eta} &= \frac{(1-k)(1-k\eta^2) - \eta(1+\eta^2)\frac{dk}{d\eta}}{(1+k\eta^2)^2}, \\ v_1 \frac{d}{dv_1} &= \eta(1+\eta^2) \frac{d}{d\eta} \end{aligned} \quad (3.5.11)$$

Relative position of the branching point and the *sonic point* (η_*, ζ_*) is of importance; here, $\eta_* = \tan \alpha_*$ and α_* is the *sonic angle* of the shock behind which we have

$$M_2^2 = \frac{v_{n2}^2 + v_\tau^2}{a^2} = \frac{1+\eta^2}{\eta^2} M_{n2}^2 = 1 \quad (3.5.12)$$

We will consider this situation for normal gases described in Section 3.4. Let us show that for $M_2 \geq 1$ the derivative $d\xi/d\eta \geq 0$, which means that one more property, in addition to A to D introduced in Section 3.4, of normal gases is manifested:

E. *A sonic point behind the shock cannot belong to the strong shock branch (i.e., $\eta_* \leq \eta_0$).*

To prove this statement, one should show that the numerator of 3.5.11 is positive for $M_2 \geq 1$. To do this, we eliminate the derivative of k and replace the last term in brackets of

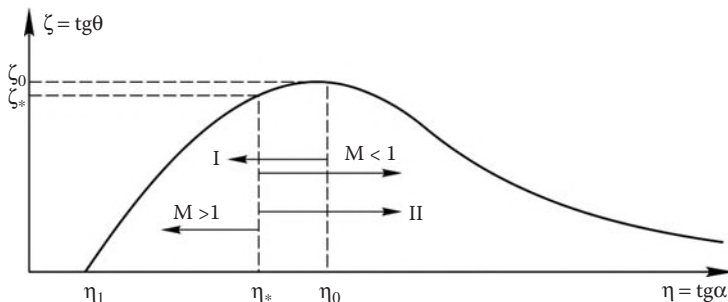
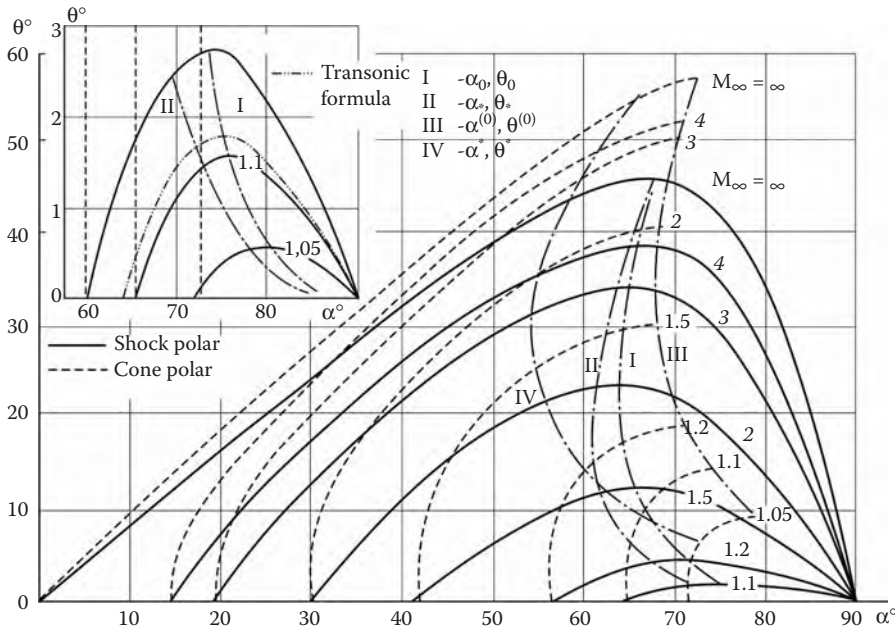


FIGURE 3.8
Shock polar; I and II relate to the weak and strong branches of a shock.

**FIGURE 3.9**

Shock and conical polars (cf. Section 6.4) for $\gamma = 1.4$. I to IV are the limiting and sonic angles on the $M = \text{const}$ curves; I and II relate to the wedge and III and IV to the cone.

3.4.16 by its maximum value equal to $1/2$, according to 3.4.1. This procedure only diminishes the numerator; therefore, expressing $M_3 = M_{n2}$ in 3.4.16 in terms of M_2 and using 3.5.12 we obtain the inequality

$$(1 - M_{n2}^2)(1 + k\eta^2) \frac{d\xi}{d\eta} \geq \frac{\eta^2(1 - k)}{1 + \eta^2} \Phi(\eta)$$

$$\Phi = (M_2^2 - k) + (M_2^2 - 1)k\eta^2 \quad (3.5.13)$$

Since $k \leq 1$, we have $\Phi \geq 0$ and, hence, $d\xi/d\eta \geq 0$ for $M_2 \geq 1$.

Thus, we have a sequence of inequalities

$$\eta \leq \eta_* \quad M_2 \geq 1; \quad \eta_* \leq \eta_0, \quad \eta \geq \eta_* \quad M_2 < 1 \quad (3.5.14)$$

At the point of maximum (ξ_0, η_0) separating the weak and strong branches of a shock (the curve $\xi(\eta)$) and generally behind the strong branch, $\eta \geq \eta_0$, the flow is subsonic. Behind the weak branch, $\eta < \eta_0$, the flow is supersonic, with the exception of a narrow range of the values $\Delta\eta = \eta_0 - \eta_*$.

For a perfect gas $a^2 = \gamma p/\rho$ and from Equations 3.5.12, 3.3.7, and 3.3.10 it follows (with $v_{n1} = U_1 \sin \alpha$ taken into account)

$$v_{n1} \frac{dk}{dv_{n1}} = -\frac{4}{(\gamma + 1)M_{n1}^2} = -2(k - k_0), \quad k_0 = \frac{\gamma - 1}{\gamma + 1} \quad (3.5.15)$$

and

$$M_2^2 = \frac{(1 + k\eta^2)(1 - k_0)}{k\eta^2(1 - kk_0)} \quad (3.5.16)$$

Substituting 3.5.15 in 3.5.11 and setting $d\xi/d\eta = 0$ in this equation and $M_2 = 1$ in Equation 3.5.16 we obtain the equations for η_0 and η_*

$$k(1 - k)\eta_*^2 = 1 - k_0, \quad k(1 - k)\eta_0^2 = 1 + k - 2k_0, \quad k = k(\eta) \quad (3.5.17)$$

Substituting the dependence $k(\eta)$ obtained at the solution of the relations on the shock, we get the equations for η_0 and η_* . For a perfect gas with $\gamma = 1.4$ these angles are shown in Figure 3.9. Clearly, the difference $\alpha_0 - \alpha_*$ is small, just greater than 4° for $M_1 \approx 1.5$. Since $d\xi/d\eta = 0$ for $\eta = \eta_0$ the difference $\theta_0 - \theta_*$ amounts to only a few fractions of a degree.

In the general case the choice of a shock branch is not always obvious and is determined by the entire form of the body in gas flow and, in general, by global conditions of the problem. Experience shows that in the flow past sharp bodies whose slope is everywhere smaller than the limiting angle, $\theta < \theta_0$, a weak branch is always realized due to the influence of rarefaction in the base region (regions I and II in Figure 3.7), which appears to be inconsistent with a subsonic flow behind the strong shock. For this reason, at the numerical solution of time-dependent problems of the flow past a sharp body starting from arbitrary initial conditions (with conditions behind the body taken into account) the limiting steady flow with a weak shock is obtained.

At the same time, it is also easy to obtain a solution with the strong shock attached to the sharp edge of a body. To do this, it is sufficient to consider the body surface as a streamline cd (Figure 3.1a and b) intersecting a strong shock branch Oc , the point a being the branching point at which $\theta = \theta_0$. Such a body (a body with a channel in the axisymmetric case) has a sharp edge with a strong shock attached to it. In this case a high pressure behind the body is maintained by a concave form of the body surface. It is another matter that such a flow pattern cannot actually be implemented owing to the effect of viscosity, which results in the formation of forward separation zones. However, within the framework of inviscid solutions, this example clarifies the essence of the question.

We emphasize a *threshold* nature of the shock transition from one branch to another. In fact, for a wedge angle $\theta < \theta_0$ the shock is attached, but, no matter how small the positive difference $\Delta\theta = \theta - \theta_0 > 0$ may be, a detached shock, normal on the axis, forms in front of the body. Thus, formally the solution has different limits from below and from above as $\Delta\theta \rightarrow 0$. However, the ratio of the extent of the nonrectilinear part of the shock to the wedge length decreases with $\Delta\theta$, which explains the paradox.

We will now consider some particular limiting properties of oblique shocks. In the hypersonic limit, when $M_1 \rightarrow \infty$ and $k \rightarrow k_0$, the characteristic angles α_0 and α_* coincide. As γ decreases they increase being determined by the relation

$$\begin{aligned} \eta_* &= \eta_0 = k_0^{-1/2} = \left(\frac{\gamma + 1}{\gamma - 1} \right)^{1/2}, & \eta &= \tan \alpha \\ \xi_* &= \xi_0 = \frac{1}{2}(1 - k_0)k_0^{-1/2} = \frac{1}{\gamma + 1} \left(\frac{\gamma + 1}{\gamma - 1} \right)^{1/2}, & \xi &= \tan \theta \\ \sin \theta_0 &= \frac{1 - k_0}{1 + k_0} = \frac{1}{\gamma}, & \sin \alpha_0 &= \frac{1}{\sqrt{1 + k_0}} = \left(\frac{\gamma + 1}{2\gamma} \right)^{1/2} \end{aligned} \quad (3.5.18)$$

The pressure behind the shock at this point is $p = \rho_\infty U_\infty^2 / \gamma$. These angles are shown in Figure 3.10a.

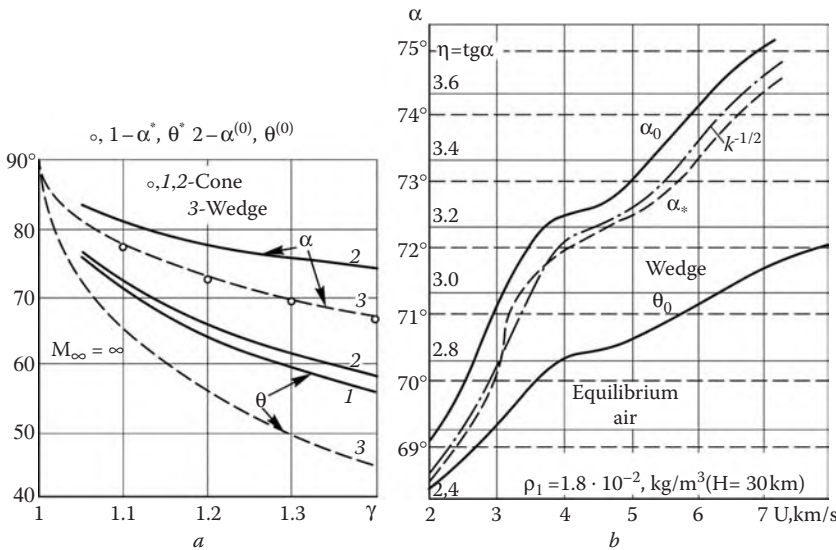


FIGURE 3.10
Sonic and limiting angles for cones (1 and 2) and wedges (3).

One more result is associated with this point. Taking 3.5.8 into account we obtain

$$\tan(2\alpha - \theta) = \frac{(1+k)\tan\alpha}{1-k\tan^2\alpha} \quad (3.5.19)$$

Thence it follows that for $\alpha = \alpha_0$ and $k = k_0$ the relation $2\alpha_0 = \theta_0 + \pi/2$ holds; obviously, this relation is independent of γ .

As to equilibrium air, its properties as an imperfect gas are manifested only for high Mach numbers M_1 and, as shown in Section 3.3, for small $k = (\gamma_* - 1)/(\gamma_* + 1)$. Therefore, neglecting the derivative $dk/d\eta$ in 3.5.11 and setting $a^2 = \gamma_e p/\rho$ and $\gamma_e = \gamma_*$ in 3.5.12 we obtain the same formulas as for a perfect gas

$$\eta_0^2 = \eta_*^2 = k^{-1/2} = \left(\frac{\gamma_* + 1}{\gamma_* - 1} \right)^{1/2} \quad (3.5.20)$$

The corresponding quantities for equilibrium air are shown in Figure 3.10b. As expected, the quantity $\eta_0 > \eta_*$ is close to $k^{-1/2}$.

For near-normal shocks, passing to the limit in 3.5.9 as $\alpha \rightarrow \pi/2$ we obtain

$$k = (1-k)\omega, \quad \omega = \pi/2 - \alpha \quad (3.5.21)$$

For hypersonic flows and $k \ll 1$ we have $\theta \gg \omega$, that is, the angle of the deviation of a shock from the normal shock is considerably smaller than the flow deflection angle in the shock.

We will consider the total velocity behind an oblique shock. It follows from 3.5.8 that behind the shock

$$U_2^2 = v_\tau^2 + v_{n2}^2 = U_1^2[1 - (1-k)\sin^2\alpha], \quad u_2 = U_2 \cos\theta \quad (3.5.22)$$

Thus, the total velocity is nearly conserved in a shock in two cases, namely, at $M_{n1} \approx 1$ as $1-k \rightarrow 0$ and for shocks with small inclination angles, $\alpha \ll 1$ (within the second-order

accuracy in α^2). In the latter case the longitudinal velocity behind the shock is $u \approx U_1$, since $\theta < \alpha$. In a word, *longitudinal and total gas velocities are conserved in a slightly inclined shock, irrespective of its intensity.*

For the Mach number behind the shock the inequality

$$M_2^2 = \frac{v_\tau^2}{a_2^2} + M_{n2}^2 \leq \frac{v_\tau^2}{a_1^2} + M_{n1}^2 = M_1^2 \quad (3.5.23)$$

always holds. This is obvious, in view of inequalities $M_{n2} < 1$, $M_{n1}^2 > 1$, and $a_2 > a_1$, which were proved in Section 3.4. Let now the conditions $M_1 \gg 1$ and $\alpha \ll 1$ be simultaneously satisfied. Naturally, in this case the inequality $M_1\alpha \geq 1$ is valid. Then, by virtue of 3.5.4, we have

$$\begin{aligned} a_2^2 &= \gamma \frac{p_2}{\rho_2} = \gamma k U_1^2 \alpha^2 \left[\frac{1}{\gamma M_1^2 \alpha^2} + (1 - k) \right] \\ M_2^2 &> \frac{v_\tau^2}{a_2^2} \sim \frac{1}{k\alpha^2} \gg 1 \end{aligned} \quad (3.5.24)$$

Thus, for $\alpha \ll 1$ the flow remains hypersonic in passing across the shock, but the Mach number M_2 has a finite, though high, limiting value as $M_1 \rightarrow \infty$.

Consider weak waves, $M_{n1}^2 - 1 \ll 1$. In this case $\Delta p/p_1 \ll 1$, where $\Delta p = p_2 - p_1$, and $\theta \ll 1$. For oblique shocks we bring 3.4.7 to the form:

$$M_1^2 A_1 \bar{p} = M_{n1}^2 - 1 = M_1^2 \sin^2 \alpha - 1, \quad \bar{p} = \Delta p / \rho_1 U_1^2 \quad (3.5.25)$$

Expressing k from kinematic relation 3.5.8 and substituting the result in the first formula in 3.5.4 we obtain the general relation

$$\bar{p} = \sin^2 \alpha \frac{\tan \alpha - \tan(\alpha - \theta)}{\tan \alpha} = \frac{\sin \alpha \sin \theta}{\cos(\alpha - \theta)} \quad (3.5.26)$$

Since an extremely weak shock tends to a characteristic, $\alpha \rightarrow \alpha^*$ and $\sin \alpha^* = M_1^{-1}$, as $\bar{p} \rightarrow 0$, we obtain from these formulas for small \bar{p} and θ that

$$\Delta \alpha = \alpha - \alpha^* = \frac{A_1 \bar{p} M_1^2}{2 \sqrt{M_1^2 - 1}}, \quad \bar{p} \frac{\theta}{\sqrt{M_1^2 - 1}} \quad (3.5.27)$$

The latter formula is already known from the linear theory, while the former gives a possibility to distinguish between a weak shock and a characteristic; for a perfect gas $\Lambda_1 = (\gamma + 1)/2$ (see 3.4.1).

We are coming now to the description of the properties of transonic shocks. As $M_1 \rightarrow 1$ and $\alpha \rightarrow \alpha^* \rightarrow \pi/2$ formula 3.5.25 should be written in the form:

$$\begin{aligned} A_1 \bar{p} &= M_1^2 - 1 - \cos^2 \alpha = M_1^2 - 1 - \omega^2 = \omega^{*2} - \omega^2 \\ \omega &= \pi/2 - \alpha, \quad \omega_* = \pi/2 - \alpha^* \end{aligned} \quad (3.5.28)$$

Combining with the limiting form of 3.5.26 for $\theta \ll 1$ and $\alpha \approx \pi/2$ yields relations for a transonic shock

$$\theta = \omega \bar{p} = A_1^{-1} \omega (M_1^2 - 1 - \omega^2) = \bar{p} (M_1^2 - 1 - A_1 \bar{p})^{1/2} \quad (3.5.29)$$

We note that from this equation, as well as from 3.5.21 for transonic velocities ($k \approx 1$), there follows the condition opposite to the hypersonic condition follows $\theta \gg \omega$, which follows from 3.5.21.

Formulas 3.5.28 and 3.5.29 are valid for both shock branches and give, as $\theta \rightarrow 0$, a solution for the normal shock, $A_1\bar{p} = M_1^2 - 1$. The curve $\theta = \theta(\omega)$ peaks at the point

$$\omega_0 = \frac{\pi}{2} - \alpha_0 = \left(\frac{M_1^2 - 1}{3} \right)^{1/2}, \quad \theta_0 = \frac{2}{3\sqrt{3}A_1}(M_1^2 - 1)^{3/2} \quad (3.5.30)$$

Clearly, at transonic velocities the deflection of streamlines across the shock is extremely small. Thus, for $M_1 = 1.05$ the deflection angle does not exceed one degree, while for $M_1 = 1.005$ it is about two minutes, which makes practically impossible the existence of attached shocks in flows past bodies of a reasonable relative thickness.

To obtain the values of ω and θ at the sonic point behind the shock we will use formula 2.2.20 in which we set $p = p_1$ and $M = M_1$. Combining with 3.5.28 and 3.5.29 yields

$$\theta_* = \frac{(M_1^2 - 1)^{3/2}}{2A_1\sqrt{2}}, \quad \omega_* = \frac{\pi}{2} - \alpha_* = \left(\frac{M_1^2 - 1}{2} \right)^{1/2} \quad (3.5.31)$$

We note that the characteristic angles ω and ω_* are independent of the equation of state.

Finally, using Equations 3.5.28, 3.5.30, and 3.5.31 we obtain the relations for the pressures behind the shock $\bar{p} = \bar{p}_0$ at the point ω_0 and \bar{p}_* at the point ω_*

$$A_1\bar{p}_0 = \frac{2}{3}(M_1^2 - 1), \quad A_1\bar{p}_* = \frac{M_1^2 - 1}{2} \quad (3.5.32)$$

Thus, the pressure increase in transonic shocks is small, being of the order of $\bar{p} \sim M_1^2 - 1$. Substituting \bar{p}_0 in formula 3.4.23, in which M_1 and M_2 can be considered as the total Mach numbers for $\alpha \approx \pi/2$, we obtain an expression for the Mach number M_0 behind the shock for $\omega = \omega_0$

$$M_0 = 1 - \frac{1}{3}(M_1^2 - 1) \quad (3.5.33)$$

The formulas obtained are convenient for analytical study and have a sufficient accuracy when $M_1 \leq 1.1$ (Figure 3.9).

3.6 Losses across Shock Waves

We will consider some consequences of the entropy increase in a shock. This growth is responsible for an important effect: the stagnation (or total) pressure p_{02} behind the shock is always smaller than the isentropic stagnation pressure p_{01} . In fact, the stagnation enthalpy H is conserved in the shock, while the entropy grows, $s_2 > s_1$. Therefore, by virtue of the first condition 1.5.1, we have

$$\left(\frac{\partial p}{\partial s} \right)_h = -\rho T < 0, \quad \left(\frac{\partial h}{\partial s} \right)_p = T > 0 \quad (3.6.1)$$

Thence it follows that at the stagnation point behind the shock

$$p_{02} = p(H, s_2) < p_{01} = p_0 = p(H, s_1) \quad (3.6.2)$$

Both theory and experiment show that actually it is impossible to decelerate a supersonic flow isentropically, so that in front of a blunt body in supersonic flow a shock always is formed (Figure 3.1); at the axis of symmetry the shock is normal. Hence, at the stagnation point of the body the pressure is equal to p_0 for $M_1 \leq 1$ and $p_{02} = p'_0$ for $M_1 \geq 1$. One should bear in mind this fact in interpreting Pitot probe measurements of the total pressure, as mentioned in Section 2.2.

Using formula 2.2.14 we obtain for a perfect-gas flow behind the normal shock

$$p'_0 = p_2 \left(1 + \frac{\gamma - 1}{2} M_2^2 \right)^{\gamma/(\gamma-1)} \quad (3.6.3)$$

The quantities p_2 and M_2 behind the normal shock are determined by formulas 3.3.8 and 3.3.10. The resulting formula is too cumbersome and is not written down here.

The quantities p'_0 and p_0 were compared in Figure 3.3 (Section 3.3). Clearly, for weak shocks $p_0 \approx p'_0$, but for $M_1 \gg 1$ $p_0 \gg p'_0$. In this case the quantity $M_2^2 = (\gamma - 1)/2\gamma$ is fairly small; expanding formula 3.6.3 in this quantity with 3.3.8 taken into account, we obtain a simple expression

$$p'_0 = \frac{(3 + \gamma)\gamma}{2(\gamma + 1)} p_1 M_1^2 \ll p_0 \approx p_1 \left(\frac{\gamma - 1}{2} M_1^2 \right)^{\gamma/(\gamma-1)} \quad (3.6.4)$$

This formula can be obtained in a more general way so that the result will not depend on γ . In view of the smallness of M_2^2 , the flow behind a normal shock can be considered to be incompressible and have a constant density $\rho = \rho_2$. In this case, it follows from the Bernoulli integral for an incompressible fluid (with 3.3.3 and 3.3.4 taken into account) that

$$p'_0 = p_2 + \frac{\rho_2 v_{n2}^2}{2} = p_1 + \left(1 - \frac{k}{2} \right) \rho_1 U_1^2, \quad k = \frac{\rho_1}{\rho_2} \quad (3.6.5)$$

A comparison with the exact solution (Figure 3.3) shows that for $\gamma = 1.4$ this simple formula is sufficiently accurate already at $M_1 \geq 2$. For perfect gases, at high M_1 this formula coincides with 3.6.4. Clearly, for small k (or $\gamma_* - 1$) the pressures behind the shock and at the stagnation point are similar (see Equation 3.3.17).

We can assure ourselves that the effect of the entropy growth in a shock and the associated effect of the total pressure decrease are negative with reference to the example of a jet issuing from a supersonic nozzle into an ambient medium at rest (Figure 1.6e, Section 1.7). In this case sufficiently far from the nozzle an inviscid plane-parallel flow with the pressure p_∞ is established and the engine thrust (formula 1.7.22) is as follows

$$T = \int_{\Sigma_2} \rho U^2 a d\Sigma = \int_G U dG, \quad dG = \rho U d\Sigma \quad (3.6.6)$$

Here, the integral is finite, as well as the gas flow rate G in the jet. If the initial (say, at a nozzle throat) entropy s_0 is conserved in the jet flow, then the velocities of all streamtubes in the jet are the same and equal to $U_0(p_\infty, s_0)$, while the thrust is $T_0 = G U_0$. However, if the entropy in the flow increases owing to the shock formation, then the gas velocity decreases by virtue of 3.6.1, the thrust decreases by the quantity $\Delta T = G \Delta U$, and *thrust loss across the shock* occurs. Thus, the maximum thrust is provided by a *perfectly designed, shock-free nozzle* with flow parameters uniformly distributed over the exit section, the exit pressure being p_∞ and the entropy s_0 .

Another similar effect of a fundamental nature is the wave drag of a body. It was shown in Chapter 2 that bodies in subsonic irrotational flows exert no drag (the Dalembert paradox, Section 2.12), as distinct from the case of supersonic flow. The point is that the barotropic dependence $\rho = \rho(p)$ necessary for a flow to be potential is violated when a shock is formed and entropy grows. To demonstrate this effect, we will choose a control surface in Figure 1.16c in such a way that its lateral side Σ_δ is beyond the entropy disturbance region and its limiting contribution in formula 1.7.18, as well as the contribution of the surface Σ_1 , is zero. Since we study the entropy growth effect, which in an inviscid flow does not die out at infinity, we will let $p = p_\infty$, $u = U$, and $v = 0$ in evaluating the limit of the integral over the surface Σ_2 . Using the Bernoulli equation and the equation of state $h = h(p, s)$ for section Σ_2 we obtain (T_* is the average value of T)

$$\begin{aligned} h - h_\infty &= \Delta h = \frac{1}{2}(U_\infty + u)(U_\infty - u) = T_* \Delta s \\ \Delta s &= s - s_\infty, \quad T_* > T_\infty \end{aligned} \quad (3.6.7)$$

Then the formula for the drag takes the form:

$$X = \int_{\Sigma_2} \rho u (U_\infty - u) d\Sigma = \int_{\Sigma_2} \frac{2U}{U + U_\infty} \rho T_* \Delta s d\Sigma \quad (3.6.8)$$

To evaluate these integrals it is sufficient to preassign the entropy distribution over streamlines, since for a given pressure, $p = p_\infty$, all the flow parameters (ρ, T, U) depend on entropy only.

Thus, the drag of a body in an inviscid flow is expressed in terms of the entropy increment. Therefore, a drag always arises when a shock is formed and this is why it is termed the *wave drag*. It can also arise in initially subsonic flows, if local supersonic zones appear inside a flow (Section 5.1).

Thence there follows the problem of minimizing the entropy growth at the supersonic flow deceleration (e.g., in diffusers of supersonic wind tunnels or in air intakes of air-breathing engines shown schematically in Figure 3.11). At the outlets of these devices it is desirable to produce the stagnation pressure as high as possible in order to facilitate ejection

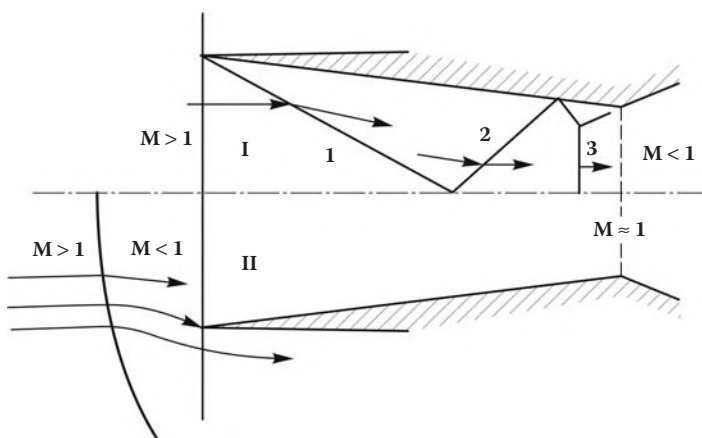


FIGURE 3.11

Flow in a supersonic diffuser with deceleration in a sequence of shocks (I) and in a solitary normal shock (II).

of working gas in the first case and to increase the thrust in the second case (primarily, by increasing the flow rate $G_* = \rho_* a_* \sigma_* \sim p_*$ at the channel throat OO with $M \approx 1$, Section 2.3). This can be achieved by organizing a sequence of shocks in which the gas is decelerated. For example, regime I in Figure 3.11 with a sequence of shocks 1, 2, 3, and so on terminated by a closing near-normal shock and regime II with a solitary detached shock at the outlet can be considered alternative flows. It turns out that the entropy of the gas flow that has passed through a sequence of shocks is lower, while the total pressure is higher than the flow that has passed through a single shock of an equivalent (in some sense or another) intensity.

This statement is made evident if a single shock with the pressure difference Δp is replaced by such a great number N of weak shocks that in each of these shocks the entropy increment is small (according to 3.4.8), $\Delta s_N \sim (\Delta p/N)^3$, as well as the total increment $\Delta s \sim N^{-2}$. Such a wave sequence is equivalent to isentropic gas compression. Then within the framework of the one-dimensional theory of Section 2.3 the diffuser in Figure 3.11 can be considered a reversible Laval nozzle (curve $b^+ a^-$ in Figure 2.3b) with a supersonic inlet and subsonic outlet. However, as will be shown in Chapter 4, in practice such a shock-free nozzle flow could hardly be implemented.

This conclusion is naturally generalized to the case of the turn of a flow by a given angle, for example, in the flow past a multi-wedge convex wall and in many other, qualitatively similar situations, when the introduction of each new bend in the surface generator accompanied by a shock leads to an increase in the resulting entropy. Analytically this can be proved only in certain particular cases, although the experience of numerous calculations has shown that there can be no doubt in its truth.

3.7 Piston and Wedge Problems

These problems are reduced to the derivation of the dependence of the flow parameters behind a shock on the velocity behind the same shock. These solutions are local and relate to very simple problems concerned with the supersonic flow past a wedge and the one-dimensional flow in front of a piston in a tube. We will restrict ourselves to the flows corresponding to weak shock branches, with supersonic flow regimes behind them. Only such regimes are associated with constant flow parameters and are usually implemented at leading edges of vehicles.

For a perfect gas the direct problem of the piston has an explicit solution; we will write the solution for the gas entrainment velocity $u = v_{n1} - v_{n2}$, which is positive at any direction of the piston motion. To do this, the quantity k from Equation 3.3.7 should be substituted in 3.3.5, which gives a quadratic equation in the induced wave velocity $D = v_{n1}$. The solution of this equation is as follows:

$$\frac{D}{a_1} = \frac{\gamma + 1}{4} \frac{u}{a_1} + \sqrt{\frac{(\gamma + 1)^2}{16} \frac{u^2}{a_1^2} + 1}, \quad p - p_1 = \rho_1 D u \quad (3.7.1)$$

The plus sign in front of the radical sign corresponds to compression waves. As to the formula for the pressure, it was obtained already in Section 1.6.

We note that the dependences $D(u)$ and $u(D)$ are monotonic, which ensures the uniqueness of the solution of the direct problem of the piston, as distinct from the wedge problem having two solutions (Section 3.5).

The problem for a wedge reduces to the solution of Equation 3.5.8 or 3.5.9 for the shock inclination angle α at a given wedge angle θ . In this case there is no simple solution of type 3.7.1, while the numerical results were presented in Figures 3.9 and 3.10. However, some explicit solutions can be obtained for separate limiting flow regimes behind a weak shock branch. Precisely these solutions are presented in the following.

3.7.1 Linear and Quadratic Approximations

In Chapter 2 the problems of an acoustic wave in front of a piston moving at a small velocity u and a supersonic flow past a thin airfoil with a small angle θ were solved. The corresponding solutions are as follows

$$\Delta p_{lin} = p - p_1 = \rho_1 a_1 u, \quad \sqrt{M_\infty^2 - 1} \Delta p_{lin} = \rho_\infty U_\infty^2 \theta \quad (3.7.2)$$

Here, the subscript ∞ refers to the parameters of the flow incident on the wedge. Within the framework of the linear theory, the disturbance front is represented by the acoustic wave $dx/dt = a_1$ in the first case and the Mach line with the slope $\alpha^* = \arcsin M_\infty^{-1}$ in the second case.

The question arises on the relation between the linear and exact theories of the piston motion or the flow past a thin body. Within the framework of the exact theory, boundary conditions for the problem should be imposed on an unknown bow shock, the position of which cannot be obtained from the classical linear theory treated in Chapter 2. However, on the basis of the considerations of Section 2.4, in linearizing these exact problems for perturbations boundary conditions can be transferred from the shock X_s directly to the leading characteristic X_0 , since in the main approximation the solution is constant. This leads to the solutions of Chapter 2. The bow shock position is then determined from 3.4.7 and 3.5.27.

We will now obtain a second-order correction to the linear theory. To do this in the piston problem, the quantity D should be excluded from relations 3.3.5 and the dependence thus obtained be expanded in Δp using 3.4.6 and 3.4.1 with the following result

$$\begin{aligned} u &= \left[\frac{1}{\rho_1} (1 - k) \Delta p \right]^{1/2} = \frac{\Delta p}{\rho_1 a_1} \left(1 - \frac{1}{2} A_1 \frac{\Delta p}{\rho_1 a_1^2} + \dots \right) \\ \frac{p - p_1}{\rho_1 a_1^2} &= \frac{Du}{a_1^2} = \frac{u}{a_1} + \frac{1}{2} A_1 \frac{u^2}{a_1^2} + \dots \end{aligned} \quad (3.7.3)$$

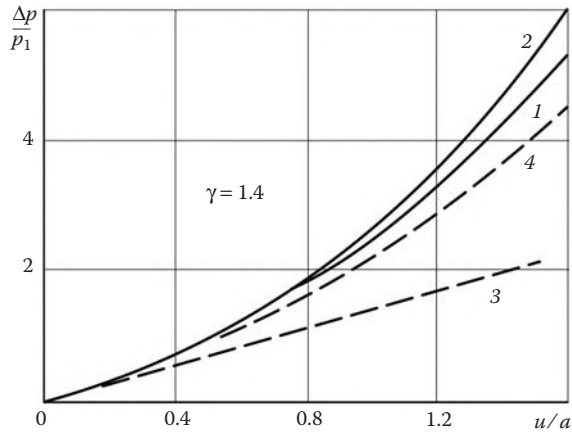
As follows from Figure 3.12, the range of applicability of the latter formula, which is obtained by inverting the former, extends almost to sonic velocities of the piston, $u \leq a$. This result is not accidental if one takes into account the smallness of the term with u^2 under the radical sign of 3.7.1 on this range.

A similar result for the wedge follows from formula 3.5.26, which, having been expanded in a series and with 3.7.2 and 3.5.27 taken into account gives

$$p' = \frac{\Delta p}{\Delta p_{lin}} = 1 + \frac{1}{2} BK, \quad K = \theta \sqrt{M_\infty^2 - 1} \quad (3.7.4)$$

Here, K is the similitude parameter introduced in Section 2.7, while the coefficient B is determined by the formula

$$(M_\infty^2 - 1)^2 B = A_1 M_\infty^4 - 2(M_\infty^2 - 1) \quad (3.7.5)$$

**FIGURE 3.12**

Relative pressure increase in shock (1) and simple (2, see Section 4.6) waves; 3 and 4 are the linear and quadratic approximations.

At $M_\infty \geq 2.5 \div 3$ we have $B \approx A_1$ accurate to a few percents, which leads to a linear dependence of p' on the parameter K . In this form the formula practically coincides with the data in Figure 2.13 and, as follows from Figure 3.13a, provides a good accuracy far beyond the theoretical limits of the region of the linear theory applicability (up to $\Delta p/p_\infty \leq 4$ for moderate Mach numbers M_∞). In the transonic region, the term $BK \rightarrow \infty$, as $M_\infty \rightarrow 1$. Nevertheless, as follows from Figure 3.13b, this formula retains its validity for all $\theta < 2\theta_0/3$, θ_0 being the limiting wedge angle for which, according to 3.5.30 the term BK is finite, $BK = 2/3^{3/2} < 1$. On this range formula 3.5.29 for the wedge is valid; in view of 3.5.30, its expansion in $\bar{p}/(M_\infty^2 - 1)$ has the form $p' = 1 + \theta/(3\sqrt{3}\theta_0)$ and coincides with 3.7.4 as $M_1 \rightarrow 1$.

3.7.2 Hypersonic Approximation of a Thin Shock Layer: Newton Formula

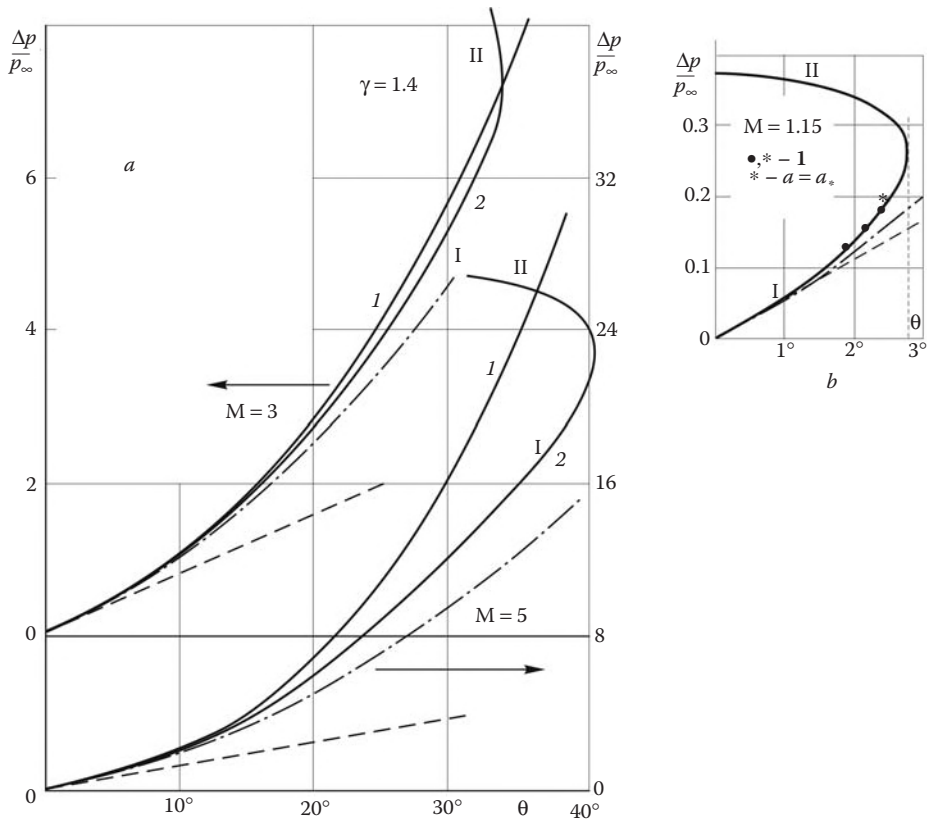
As was shown in Section 3.3, in a hypersonic flow at $M_\infty \sin \alpha \gg 1$ the density ratio across a shock is fairly small, $k = (\gamma_* - 1)/(\gamma_* + 1) = 0.05 \div 0.2$ (Figure 3.4). This prompts us to use k as a small parameter and to construct asymptotic solutions as $k \rightarrow 0$ or, which is the same, $M_\infty \rightarrow \infty$ and $\gamma_* \rightarrow 1$.

As to the direct piston problem, its limiting solution is elementary. In this case one should replace D by u in the formula for $k = k(D/a_1)$ in the exact solution 3.3.5.

Passing on the wedge problem we take into account that, according to 3.5.8, for moderate values of $\tan \alpha \sim 1$ we have

$$\alpha - \theta = k \tan \theta + O(k^2), \quad \sin \alpha = (1 + k) \sin \theta \quad (3.7.6)$$

From the previous relations follows an important conclusion that when the gas is highly compressed in the shock, the thickness of the *shock layer*, that is, the disturbed layer between the shock and the body, is relatively small as if the shock clings loose to the body, as distinct from the linear theory, in which the shock is similar to the leading undisturbed characteristic and, hence, depends on the body shape only weakly.

**FIGURE 3.13**

Pressure increase on a wedge: 1, in a simple wave (Section 4.6) and 2, behind a weak (I) and strong (II) branches of a shock. Dashed and dot-and-dash curves relate to the linear and quadratic formulas, respectively.

The following parameters on a wedge are obtained in the same approximation as 3.7.6 by substituting 3.7.6 in 3.5.4 and 3.5.5

$$\begin{aligned} p - p_\infty &= \rho_\infty U_\infty^2 (1 + k) \sin^2 \theta \\ h - h_\infty &= \frac{1}{2} U_\infty^2 (1 + k)^2 \sin^2 \theta, \quad k(\alpha) = k(\theta) \end{aligned} \quad (3.7.7)$$

We will separate out the main term in the first formula (as $k \rightarrow 0$)

$$\Delta p = p - p_\infty = \rho_\infty U_\infty^2 \sin^2 \theta = \rho_\infty U_n^2, \quad U_n = U_\infty \sin \theta \quad (3.7.8)$$

Although this formula is elementary, it provides a correct order of the pressure and the tendency of its variation but, of course, beyond the limits of the linear theory, according to which $\Delta p \sim \theta$. In what follows it will be shown that this is valid for any part of a body surface inclined to the flow at an angle $\theta > 0$. For this reason the formula is widely used in engineering estimations. It is called the *Newton formula* and, indeed, it was derived by Sir Isaac Newton himself within the framework of his body drag law.

Newton assumed that in a sufficiently rarefied gas, particles reach a surface without collisions. Their interaction with a surface was assumed to be absolutely inelastic, with the loss of the normal component of the velocity but with the conservation of the tangent

component. The mass of particles incident on an area element $d\sigma$ of the body at a local angle of attack θ per unit time (Figure 3.14) is equal to $\rho_\infty U_\infty \sin \theta d\sigma$. Multiplying this by the normal component of the velocity, $U_n = U_\infty \sin \theta$, we obtain the normal component of the momentum lost by the gas, which is equal to the normal force $(p - p_\infty)d\sigma$ acting on a gas. This results in formula 3.7.8.

For moderate M_∞ the disturbed layer thickness is comparable with the body size; therefore, the Newtonian theory of the drag does not give satisfactory results and for this reason it was forgotten by scientists in hydrodynamics. However, for hypersonic velocities and small k the shock layer thickness is small so that Newton's flow scheme is realized, at least, superficially.

The Newton concept and formula will be discussed in more detail in Chapter 7; here, we restrict ourselves to its testing.

In Figures 3.15 and 3.16 we have plotted the pressure on a wedge calculated from formula 3.7.8 (the pressure is referred to Δp) and the relative shock layer thickness $(\alpha - \theta)/k \tan \theta$, respectively. Clearly, the exact and approximate curves are fairly similar if the angle θ is not too small and not too close to the limiting angle of the flow deflection in the shock θ_0 , since in these two cases the condition $\alpha \approx \theta$ is violated. In fact, for small θ and finite M_∞ the parameter k is no longer small, while for a wedge with the limiting angle of flow deflection at $k \ll 1$ we have, in accordance with 3.5.18, $\tan \alpha / \tan \theta \approx 2$, which gives a quite different value for the angular shock-layer thickness, namely, $\alpha - \theta \approx \sqrt{k}$. At $\theta = \theta_0$ the Newton formula gives the pressure $\Delta p = \rho_\infty U_\infty^2 / \gamma^2$, which is γ times smaller than the exact value.

The accuracy of the Newton formula 3.7.8 on the parameter range of Figure 3.15 is not worse than 10–30%, which one should bear in mind in estimating the usefulness of the formula. The relative error in determining the pressure at the stagnation point of a blunt body is $k/2$ (cf. 3.6.5). Substituting the Newton formula in 2.12.7 we obtain the drag coefficient for a wedge $C_x = 2 \sin^2 \theta$.

As an example of useful application of the Newton formula we will consider the problem of a double wedge in hypersonic flow, Figure 3.17. Behind the first shock the pressure is $p_1 = \rho_\infty U_\infty^2 \sin^2 \theta_1$, while the density is $\rho_1 = \rho_\infty / k \gg \rho_1$. The pressure behind the second

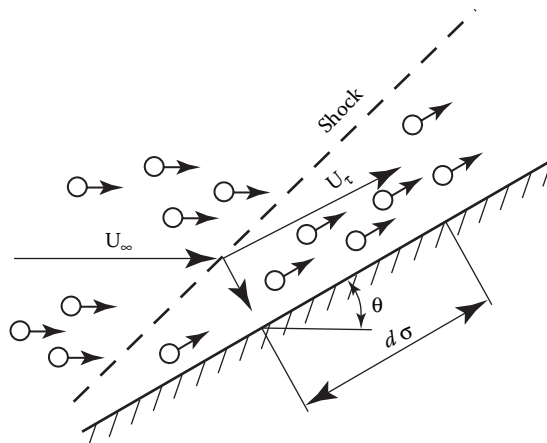


FIGURE 3.14

On the Newtonian drag model (dashed line is the shock).

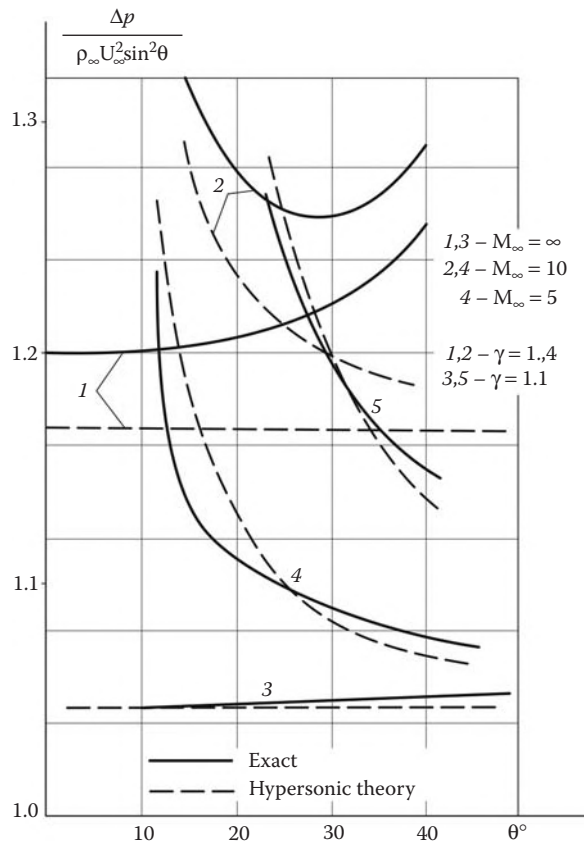


FIGURE 3.15
Ratio of the excess pressure on a wedge to its Newtonian value.

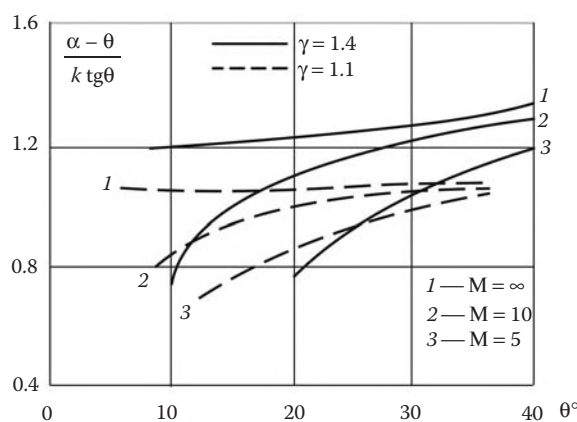


FIGURE 3.16
Ratio of the thickness of the shock layer on a wedge to its approximate (hypersonic) value.

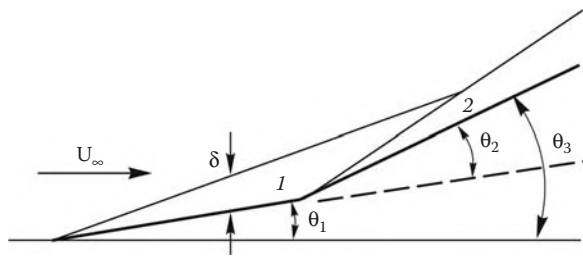


FIGURE 3.17
Flow past a double wedge.

shock can be obtained by applying the “local” Newton formula 3.7.8 to the second wedge

$$p_2 = p_1 + \rho_1 U_1^2 \sin^2 \theta_2 = p_1 + k_1^{-1} \rho_\infty U_\infty^2 \sin^2 \theta_2 \cos^2 \theta_1 \quad (3.7.9)$$

This pressure can be significantly greater than that on the second isolated wedge, $p_3 = \rho_\infty U_\infty^2 \sin^2(\theta_1 + \theta_2)$, at least, for $\theta_1 \sim \theta_2$ (compare with the similar result for a piston in an unsteady problem, Section 3.6).

We also note that although the elevated pressure p_2 acts only on a small part (of the order of k) of the second wedge, which is immersed in the shock layer of the first wedge, the force applied to this part of the wedge is of the order $X \sim k_1 p_2 \sim \sin^2 \theta_2$. This effect should be borne in mind in estimating forces acting on superstructures or controls of vehicles.

To continue the analysis of Section 3.6, we will now compare the stagnation pressure behind the normal shock in the incident flow with those behind the oblique shocks in regions 1 and 2 in Figure 3.17. We will denote these pressures by p'_0 , p'_{01} , and p'_{02} , respectively. For $k_2 \ll 1$ in thin shock layers the gas velocities in the regions 1 and 2 are approximately the same, $U_1 = U_\infty \cos \theta_1$ and $U_2 = U_1 \cos \theta_2$, so that for small θ_i we can put $U_i \approx U_\infty$. Then we obtain the sequence of inequalities

$$p'_0 \approx \rho_\infty U_\infty^2 \ll p'_{01} \approx \frac{1}{k_1} p'_0 \ll p'_{02} \approx \frac{1}{k_1 k_2} p'_0 \quad (3.7.10)$$

This example supports the statement made in Section 3.6 that the wave loss associated with supersonic flow stagnation can be reduced by replacing a single shock by a sequence of weaker shocks with the same resulting flow deflection angle.

4

Theory of Characteristics

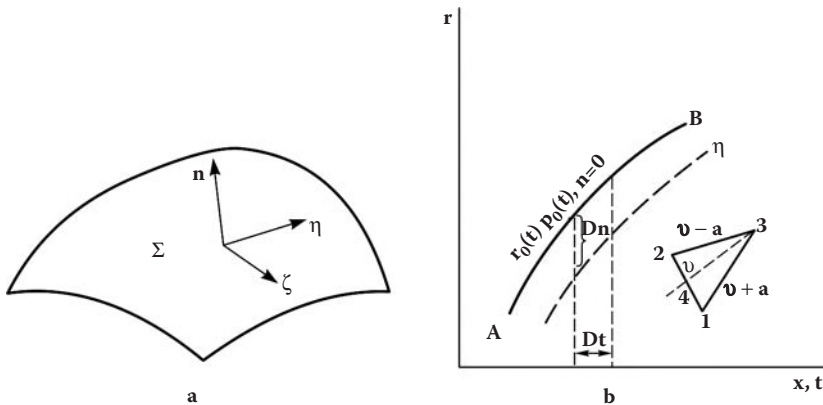
The concept of characteristics as trajectories of small disturbances in supersonic and unsteady subsonic flows was presented in Chapter 2 (and even earlier, in Section 1.6, where they were treated as Mach lines). In what follows, the theory of characteristics (as a part of the theory of mathematical physics equations) is outlined as applied to gas dynamic equations. Most of the chapter is devoted to gas dynamic applications of the theory to an analysis of general and local flow properties. It involves solutions for compression and expansion waves, shock wave initiation, and interaction of disturbances with flow inhomogeneities, such as, for example, shock waves.

4.1 Formulation of the Problem

We will consider equations in three independent variables governing, for example, time-dependent plane and axisymmetric flows or steady three-dimensional flows, such as in Equation 2.4.2 or Equation 1.9.11 supplemented by the continuity of Equation 2.4.1 with omitted time derivatives.

We will indicate the basic properties of such flows and the corresponding restrictions that are important for the theory under consideration. First of all, for the sake of generality, we will not specify the equation of state. Thus, the speed of sound may be considered here not only as isentropic ($a = a_e$, as in previous chapters) but also as any speed of disturbance propagation typical for processes in a gas. Similarly, the effective source Q_{eff} in 2.4.2 can involve not only the influence of axial symmetry and external heat sources but also the effect of other, for example, chemical sources. In general, the only restriction imposed on this function is its *local* nature and independence of the derivatives of the flow parameters. This restriction can be essential in radiation gas dynamics (Chapter 14), where a heat source can depend not only on local flow parameters but also on an integral of their spatial distributions. Theory of such integro-differential equations is not considered here.

An important property of such systems is their *quasilinearity*, that is, they are linear in higher-order derivatives only. Their solutions are determined by additional conditions formulated in the general form in Section 1.11. However, the key to determining the fundamental properties of systems of differential equations with respect to their type (hyperbolic or elliptic, cf. Chapter 2) is the *initial value or Cauchy problem*. The problem is reduced to specifying all unknown functions (p , u , and so on) on a certain “initial” surface Σ in the three-dimensional space, (t, x, r) or (x, y, z) , and, hence, their derivatives along two arbitrary directions (ξ, η) tangent to Σ (Figure 4.1a). Let us replace the original variables by (n, ξ, η) , where n is any coordinate line that does not lie on Σ , for example, a normal to it. Then in the transformed system of equations two of the three first-order derivatives of each required function are known on the surface Σ , while the unknown *outward derivatives* with respect to n can be determined from the system itself, which is a closed system of

**FIGURE 4.1**

Formulation of the Cauchy problem and definition of characteristics.

linear algebraic equations with respect to these derivatives. Similarly, subsequently differentiating the equations and initial data we can also determine the higher-order outward derivatives and, hence, represent the solution in the vicinity of the initial surface ($n = 0$) in a series form

$$f_i(n, \xi, \eta) = f_{i0} + n \left(\frac{\partial f_i}{\partial n} \right) + \frac{1}{2} n^2 \left(\frac{\partial^2 f_i}{\partial n^2} \right) + \dots \quad (4.1.1)$$

Here f_i stands for p, u , and so on.

From the previous considerations it follows that for solving the Cauchy problem it is sufficient to specify only required functions (but not their derivatives) on the initial surface.

However, series 4.1.1 can be used only when the outward derivatives on the initial surface can be uniquely determined from the previously mentioned system of linear algebraic equations. To do this requires that the determinant D composed of the coefficients of these derivatives is nonzero ($D \neq 0$). At $D = 0$ the solution of the system either does not exist or is not unique, so that in this case the Cauchy problem either has no solution at all or has infinitely many solutions passing through the surface Σ . Such a surface is referred to as a *characteristic surface*.

In mathematics, for systems of partial differential equations of the general form the following *Cauchy-Kovalevskaya theorem*, which states the existence and uniqueness of the solution of the Cauchy problem, can be proved: series 4.1.1 is convergent in the vicinity of the initial surface Σ if all the functions of the problem are analytic and, which is most important, the initial surface is not tangent to a characteristic one.

As a very simple example, we will consider the isentropic equation for an adiabatic equilibrium gas flow (Section 1.5)

$$\frac{ds}{dt} = U \frac{ds}{dl} = u \frac{\partial s}{\partial x} + v \frac{\partial s}{\partial y} + w \frac{\partial s}{\partial z} = 0 \quad (4.1.2)$$

Here, dl is the differential of an arc along a streamline. Clearly, the equation does not involve derivatives with respect to a normal to streamlines, and, hence, with respect to a normal to any streamsurface (Section 2.1) formed by these streamlines, which is the characteristic surface for this equation. Specifying the entropy on this surface gives no information on its distribution in the vicinity of this surface. Moreover (and this is important), one cannot specify the entropy on a streamsurface arbitrarily since, according to the previous

equation, the entropy is constant along streamlines. The special role of streamlines as generators or *bicharacteristics* of *characteristic* streamsurfaces or, simply, characteristics of the given equation is evident.

This result can be extended to a more general case of the time-dependent equation of the first law of thermodynamics

$$\frac{dh}{dt} = \frac{\partial h}{\partial t} + u \frac{\partial h}{\partial x} + v \frac{\partial h}{\partial y} + w \frac{\partial h}{\partial z} = \frac{1}{\rho} \frac{dp}{dt} + q \quad (4.1.3)$$

The characteristics of this equation are the particle trajectories

$$\frac{dx}{dt} = u, \quad \frac{dy}{dt} = v, \quad \frac{dz}{dt} = w \quad (4.1.4)$$

The derivatives dh/dt and dp/dt are calculated along precisely these curves. At the same time, it is impossible to determine the outward derivatives of h when flow parameter (e.g., pressure) distributions are specified along the characteristics.

This preliminary information shows an important role played by characteristic surfaces in mathematical physics. We will begin their study with systems of equations in two independent variables, (t, r) or (x, r) . For these equations the characteristics introduced in Section 2.5 play the same role as the characteristic surfaces considered previously.

There are different equivalent methods of deriving the equations of characteristics. The first method is to replace the variables in the equations of motion by (n, η) , where $n = 0$ is the equation of an initial curve $r = r_0(t)$ or $r = r_0(x)$, while η is a variable measured along this curve (Figure 4.1.b). The transformed system should then be checked for the solvability in the derivatives of the unknown functions with respect to n . As can be easily seen, the number of unknown derivatives coincides with the number of equations for them.

The second method is to extend the initial system of equations by adding differential relations obtained by differentiating initial functions f_{i0} along the initial curve. This results in additional relations for the derivatives of these functions, which makes it possible to obtain a local solution of type 4.1.1, while the impossibility to determine them means that the initial curve coincides with a characteristic.

The first method of determining characteristics is more visual, while the second one is more formal and preferable for cumbersome systems. In what follows both these methods will be used.

For the problem under consideration a linear algebraic system for outward derivatives breaks up into two independent sets mentioned in Section 2.4. The momentum and continuity equations of system 2.4.2 belong to the first set involving the pressure and velocity derivatives along all the directions. The second group involves the energy equation of system 2.4.2 and Equation 1.6.8 relating the derivatives of the pressure and density; in a particular case this is isentropic Equation 4.1.2. Therefore, the characteristics of these two sets can be considered separately (though this is not necessary); this fact will be used in what follows.

As follows from the previous analysis, the gas dynamic equations of all types possess the streamline characteristics, which are also called *trajectory characteristics*. However, in this chapter our prime interest is in the *wave characteristics*, like those introduced in Section 2.8; the existence of precisely these characteristics determines the type of the equations. In other words, the entire analysis of this chapter concerns the hyperbolic equations.

We will now consider one more property of partial differential equations with respect to the Cauchy problem. As shown in Chapter 2, the hyperbolic wave equation, which can govern time-dependent or steady supersonic flows, possesses a pair of characteristics, while

the elliptic Laplace equation, which can govern subsonic flows, has not any. Thus, it would seem that in the latter case the constraints on the formulation of the Cauchy problem on an arbitrary initial surface are fewer.

However, this is not the case. We will explain it in terms of Equation 2.7.3 for the perturbation potential (with $v = 0$); using the change of variables, it can be reduced to the form:

$$\omega \frac{\partial^2 \varphi}{\partial x^2} + \frac{\partial^2 \varphi}{\partial y^2} = 0 \quad (\omega = \pm 1) \quad (4.1.5)$$

This is the Laplace equation ($M_\infty < 1$) for $\omega = 1$ and the wave equation ($M_\infty > 1$) for $\omega = -1$. It has the following set of solutions (the *Hadamard solutions*)

$$\begin{aligned} \omega = 1 : \quad u_n &= (C_{1n}^{(+)} e^{\pi ny} + C_{2n}^{(+)} e^{-\pi ny}) \sin \pi nx \\ v_n &= -(C_{1n}^{(+)} e^{\pi ny} - C_{2n}^{(+)} e^{-\pi ny}) \cos \pi nx \\ \omega = -1 : \quad u_n &= C_{1n}^{(-)} \cos \pi n(x+y) + C_{2n}^{(-)} \cos \pi n(x-y) \\ v_n &= C_{1n}^{(-)} \cos \pi n(x+y) - C_{2n}^{(-)} \cos \pi n(x-y) \end{aligned} \quad (4.1.6)$$

These periodic solutions (with the period equal to $\Delta x = 2/n$) correspond to the Cauchy problem posed on the x axis, the choice of a particular problem being determined by the coefficients $C_{in}^{(\pm)}$.

For $\omega = -1$ the solution consists of two waves propagating along the $x \pm y = \text{const}$ characteristics. It is bounded everywhere, so that small variations of the initial data (the coefficients $C_{in}^{(\pm)}$) are associated with the equally small variations of the solutions. Such problems are called *well posed*. On the other hand, the solution corresponding to $\omega = 1$ increases in the general case (when $C_{1n}^{(+)} \neq 0$) without bounds as $ny \rightarrow \infty$; therefore, any variation ("error") in the initial data, however small it may be, can lead to the discrepancies in the results, which can be made as large as is wished.

This is the reason why none of the reasonably formulated physical problems can be reduced to the Cauchy problem for elliptic equations. Typical of these equations are boundary-value problems posed on a closed curve; moreover, if the problem is formulated for the outward domain, then some conditions should be imposed infinitely far from the curve (a body in the flow in gas dynamic problems). The problems of Sections 2.9 and 2.10 were formulated in precisely this fashion; the theorems of existence and uniqueness were proven for a wide class of similar problems posed for elliptic equations.

We note in conclusion that within the framework of the linear theory of Sections 2.7 to 2.9 solution 4.1.6 is applicable to the problem of the longitudinal flow (along the x axis) above an unbounded wavy wall described by the equation $y = (\theta_0/n\pi) \sin \pi nx$, where θ_0 is its maximum slope. For subsonic flows, the solution boundedness should be required as $y \rightarrow \infty$; to do this, we put $C_{1n}^{(\pm)} = 0$, thus formulating, as it was done in Chapter 2, a boundary value problem, typical of elliptic equations. In supersonic flows there are no waves arriving from the outside along the second-family characteristics $x+y = \text{const}$; then, by analogy with Section 2.8, $C_{1n}^{(-)} = 0$ should also be put in the solution.

4.2 One-Dimensional Unsteady Flows

We will begin our study with time-dependent one-dimensional flows, plane ($v = 0$), cylindrical ($v = 1$), and spherical ($v = 2$). In this case rewriting the systems of Equations 1.13.10

through 1.13.16 in terms of transformation 2.4.1 gives the following form of the first group of equations:

$$\frac{\partial v}{\partial t} + v \frac{\partial v}{\partial r} + \frac{1}{\rho} \frac{\partial p}{\partial r} = 0, \quad \frac{1}{\rho} \frac{\partial p}{\partial t} + \frac{v}{\rho} \frac{\partial p}{\partial r} + a^2 \frac{\partial v}{\partial r} = a^2 Q_{\text{eff}}, \quad Q_{\text{eff}} = -Q - \frac{vv}{r} \quad (4.2.1)$$

According to 1.6.8, $Q = 0$ in equilibrium adiabatic flows. We will carry out the change of variables

$$(t, r) \rightarrow (t', n), \quad t' = t, \quad n = r - r_0(t) \\ \frac{\partial}{\partial t} = \frac{\partial}{\partial t'} - \dot{r}_0 \frac{\partial}{\partial n}, \quad \frac{\partial}{\partial r} = \frac{\partial}{\partial n} \quad (4.2.2)$$

Here, n is the outward coordinate for the initial curve $r = r_0(t)$, while t plays the role of a longitudinal coordinate η (Figure 4.1b). Solving system 4.2.1 for derivatives with respect to n we bring it into the form:

$$D \frac{\partial v}{\partial n} = D_1 = \frac{1}{\rho} \frac{\partial p}{\partial t} - (v - \dot{r}_0) \frac{\partial v}{\partial t} - a^2 Q_{\text{eff}} \\ D \frac{\partial p}{\partial n} = D_2 = -(v - \dot{r}_0) \left[\frac{1}{\rho} \frac{\partial p}{\partial t} - \frac{a^2}{v - \dot{r}_0} \frac{\partial v}{\partial t} - a^2 Q_{\text{eff}} \right] \quad (4.2.3)$$

Here, D is the determinant of system 4.2.1 composed of the coefficients of derivatives with respect to n

$$D = (v - \dot{r}_0)^2 - a^2 \quad (4.2.4)$$

If $D \neq 0$, we can determine the outward derivatives with respect to n for given initial distributions of the functions $p_0(t)$ and $v_0(t)$, that is, solve the Cauchy problem. However, it cannot be done in the case in which the required functions are so specified on the initial curve that it turns out to be a characteristic, or satisfies the equation

$$D = 0, \quad \dot{r} = \frac{dr}{dt} = v \pm a \quad (4.2.5)$$

Here, the subscript 0 is omitted, while the plus and minus signs refer to characteristics of the first and second families, respectively. We note that, as distinct from the linear equations of Chapter 2, where characteristics did not depend on the required solution and were known beforehand, in the general case of nonlinear equations the characteristics can be obtained only in the process of the problem solution.

Noteworthy are two main properties of characteristics

1. For $D = 0$ outward derivatives do not enter in system 4.2.3. Hence, characteristics represent lines of possible discontinuity in normal derivatives of solutions. Such discontinuities are referred to as *weak*. At the same time, *strong discontinuities* mean discontinuities of the functions themselves; this is the case of, for example, shock waves or contact discontinuities.
2. Equation 4.2.3 is equivalent to the original ones since it is obtained by means of nondegenerate transformations. However, for $D = 0$ the left-hand sides of the equations vanish on a characteristic and, hence, $D_1 = D_2 = 0$. It can be easily seen that both these equations degenerate into a single equation involving only longitudinal derivatives along these characteristics. Thus, the data on characteristics,

p_0 and v_0 , cannot be specified arbitrarily but must satisfy certain equations called *compatibility relations* (the subscript 0 is omitted)

$$dp \pm \rho a dv = \rho a^2 Q_{\text{eff}} dt = \rho a^2 Q_{\text{eff}} \frac{dr}{v \pm a} \quad (4.2.6)$$

Here, dt and dr are the differentials along characteristics, the plus and minus signs being referred to the same characteristics as the previous equation. Naturally, these conditions are automatically satisfied in the course of the solution.

It is important to note that since there exist two characteristics, Equations 4.2.5 and 4.2.6 are equivalent to the original system of equations. In order to make certain that this is the case, we introduce new *characteristic variables* (η_+ , η_-) for which the conditions

$$d\eta_{\pm} = dr - (v \pm a)dt \quad (4.2.7)$$

are satisfied. The variables η_+ and η_- are constant on the first- and second-family characteristics, respectively. Since for this transformation the relation $2adt = d\eta_- - d\eta_+$ holds, we obtain from 4.2.6

$$\begin{aligned} \frac{\partial p}{\partial \eta_-} + \rho a \frac{\partial v}{\partial \eta_-} &= \frac{1}{2} \rho a Q_{\text{ef}}, & \eta_+ = \text{const} \\ \frac{\partial p}{\partial \eta_+} - \rho a \frac{\partial v}{\partial \eta_+} &= -\frac{1}{2} \rho a Q_{\text{ef}}, & \eta_- = \text{const} \end{aligned} \quad (4.2.8)$$

Consider now the second group of equations involving derivatives along particle trajectories only

$$\frac{dr}{dt} = v \quad (4.2.9)$$

If a Cauchy problem is formulated on these lines, we are able to determine the outward derivatives of p and v from Equation 4.2.4; however, the derivatives of h and ρ or s cannot be determined from the equations of the second group. Hence, particle trajectories are also characteristics of the complete system of equations, while the equations themselves (e.g., Equation 4.1.2 or 4.1.3) are the compatibility relations.

Characteristics 4.2.5 are called *wave characteristics*; they play the crucial role in determining the types and the qualitative properties of equations and their solutions. Geometrical and physical meaning of the characteristics is evident: they are trajectories of disturbances, or acoustic waves, propagating to both sides at the speed of sound relative to moving particles.

As distinct from the wave characteristics, the *trajectory characteristics* 4.2.9, transfer information only along particle trajectories. From the standpoint of fundamental properties of equations or flows, they play, generally speaking, a secondary role. This follows even from the example of barotropic gases for which $\rho = \rho(p)$ and $h = h(p)$, so that Equation 4.1.2 can be omitted. Clearly, the trajectory characteristics are bisectors of angles between wave characteristics of different families.

The general theory of characteristics is well known; here, we will present only its main results as applied to gas dynamics. It is convenient to investigate the structure of solutions of various typical problems and the intuitive or heuristic substantiation of their solvability with reference to the *method of characteristics* with its transparent algorithm.

For this purpose, we will “freeze,” or assume to be constant, the coefficients of all the equations within a small triangle 1 – 2 – 3 at whose vertices 1 and 2 all the parameters are preassigned and whose sides, 1 – 3 and 2 – 3, are characteristics (Figure 4.1b). Then

along these lines the differential relations in Equations 4.2.5 and 4.2.6 can be replaced by finite-difference equations

$$\begin{aligned} r_3 - r_1 &= (v + a)(t_3 - t_1) \\ p_3 - p_1 + \rho a(v_3 - v_1) &= \rho a^2 Q_{\text{eff}}(t_3 - t_1) \\ r_3 - r_2 &= (v - a)(t_3 - t_2) \\ p_3 - p_2 - \rho a(v_3 - v_2) &= \rho a^2 Q_{\text{eff}}(t_3 - t_2) \end{aligned} \quad (4.2.10)$$

Solving these equations we obtain the coordinates of point 3 and the required quantities p_3 and v_3 at this point. The coefficients can be referred to any midpoint of the elementary triangle.

To evaluate the enthalpy and density at point 3, we will let out a particle trajectory from this point in the direction opposite to the flow until it intersects the segment 1–2 at a point 4 (Figure 4.1b; this is most typical but not the only version). Then the following relations hold

$$\begin{aligned} r_3 - r_4 &= v(t_3 - t_4), \quad h_3 - h_4 = \frac{1}{\rho}(p_3 - p_4) + q(t_3 - t_4) \\ h_4 &= \frac{1}{2}(h_1 + h_2) \end{aligned} \quad (4.2.11)$$

which close the problem at point 3. A similar algorithm is appropriate for other trajectory equations.

We now need to focus on the properties of wave characteristics and their role; in so doing we assume, for example, the gas to be barotropic. Let us formulate the Cauchy problem on a noncharacteristic curve AB (Figure 4.2) specifying p and v distributions on it. Subsequently applying solution 4.2.10 to each of the elementary triangles covering the domain ABC between characteristics AC and BC we can construct the solution within the entire

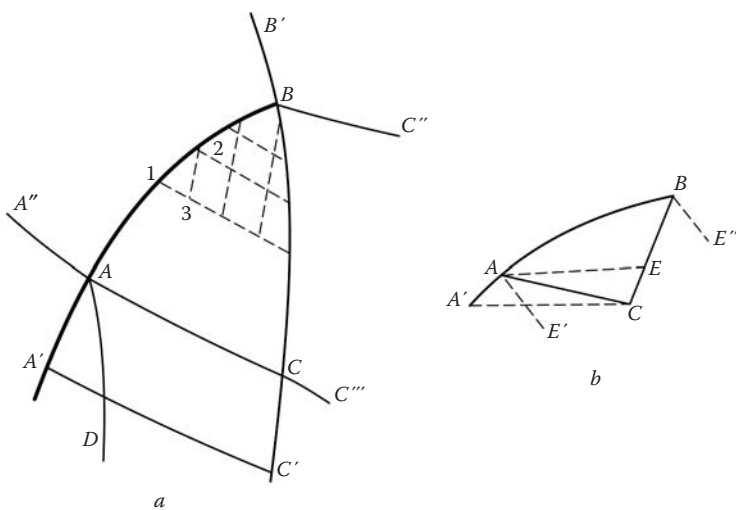


FIGURE 4.2

Domains of influence, dependence, and definiteness of the solutions separated by characteristics and particle trajectories.

region. Hence, the initial data preassigned on a noncharacteristic curve determine completely the solution in a curvilinear triangle formed by this curve and intersecting wave characteristics of different families passing through its ends (the *Riemann theorem*). This triangle gives the *domain of definiteness* of the solution for a given segment of the initial curve (when the process “develops” on the right of curve AB).

The extension of the solution to the region $ACC'A'$ is also determined by the conditions imposed on the continuation AA' of the initial curve; the latter conditions can be changed arbitrarily, thus generating discontinuities in normal derivatives of the solution on the boundary characteristic AC .

Further, if AD and BC'' are characteristics of different families, then the solution in the region $DABC''$ between them depends on the data preset on the curve AB . This region is a *domain of influence* of this curve on the solution. Extending the characteristics BC and AC up to $B'C'$ and $A''C'''$ we define an unbounded domain $B'CA''$ as the *domain of dependence* for the point C , while $C'CC'''$ is the domain of influence of the solution for the point C . Evidently, the concepts of the influence and dependence domains are reversible from the mathematical (but not physical) point of view.

Thus, *characteristics are the boundaries of the domains of influence, definiteness, or dependence of the solution on initial or boundary conditions and also the lines of possible discontinuity in normal derivatives*.

Consider now the contribution of the trajectory characteristics to these concepts. Obviously, taking them into account does not change the influence domain of the initial curve if this region, ABC in Figure 4.2b, lies between particle trajectories AE' and BE'' passing through the ends of the curve AB . The flow behind a shock wave, which will be identified with the segment AB , is an example of the opposite situation. Specifying the shock trajectory determines all the parameters behind it, corresponding to the Cauchy problem formulation. Since the relative normal velocity of the gas behind a shock is smaller than the speed of sound (Section 3.4), the first-family characteristic CB always overtakes the shock, while the particle trajectory AE is located between the shock and the second-family characteristic AC , thus narrowing the initial definiteness domain of the curve AB since particle trajectories filling the triangle ACE carry the information from the other, preceding part of the shock $A'A$.

We will consider several typical problems and substantiate their solvability based, as earlier, on the algorithm of the characteristic method and restricting ourselves to the first group of equations and wave characteristics.

The first problem is the *Goursat problem*: distributions of both functions, p and v , are preassigned on two intersecting characteristics of different families (AC and CB in Figure 4.3a). The solution at point 3 and so on in the entire triangle ACB between the given characteristics is determined by 4.2.10.

The second problem is posed on a characteristic of the first family (AC in Figure 4.3b), on which both parameters p and v are specified, and on a line AD located inside the angle formed by the AC and AB characteristics; only one of the required functions is specified on AD . This can be a trajectory of a piston moving at a velocity $v_p(t)$ or a boundary of a quiescent gas region with a given pressure $p_p(t)$. Using difference relations 4.2.10 along characteristic 1 – 2, together with the additional condition $v = v_p$ or $p = p_p$ at point 2, we can determine completely the solution at this point. Then the Goursat problem for point 3 should be solved, and so on.

In this problem the characteristic AC can be replaced by a noncharacteristic curve AE located as shown in Figure 4.3c. In this case the Cauchy problem posed on AE determines completely the solution within the triangle AEC ; a further solution is reduced to that for

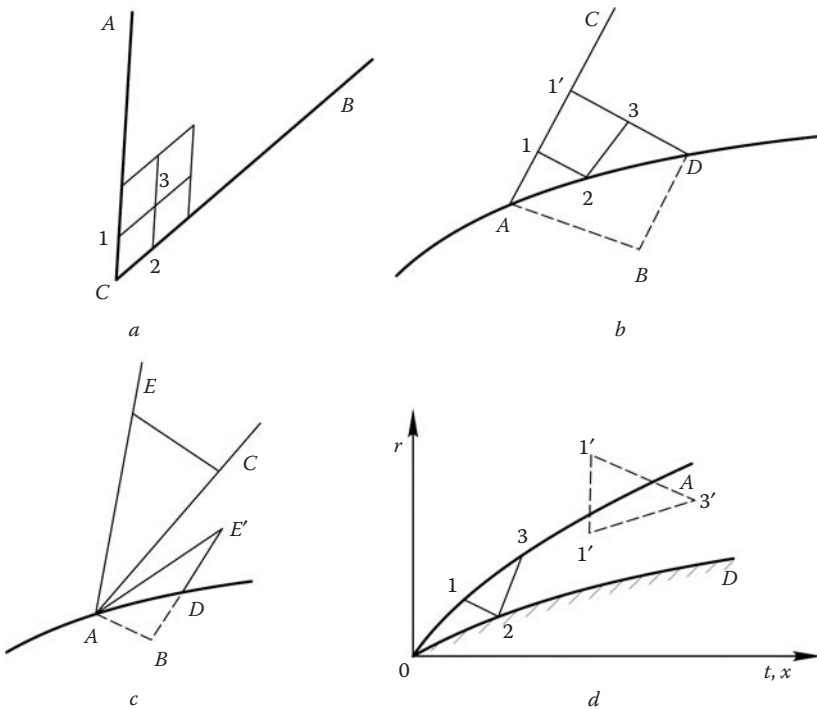


FIGURE 4.3
Typical problems of the theory of characteristics.

the previous problem. However, if both parameters are specified on the line AE' , this determines the solution within the triangle $AE'B$, with the line AD located inside it, so that we are no longer able to specify any parameter distributions on this line.

Finally, we consider one more problem concerned with a particular type of a flow. Let at $t = 0$ a piston begin to move according to a law $r_p(t)$ and in front of it a shock wave $R(t)$ be formed (lines OD and OA in Figure 4.3d). According to Section 3.7, the initial piston velocity $v_0 = \dot{r}_p(0)$ determines the initial shock velocity $\dot{R}(0)$ and, hence, the flow parameters at a near point 1. The technique of determining the flow parameters at point 2 on the characteristic $1 - 2$ has been already described. The first-family characteristic $2 - 3$ originating from this point intersects the shock continuation at point 3. Equation 4.2.10 for this characteristic gives a linear relation between p_3 and v_3 . The same quantities can be also expressed in terms of the relations on the shock (Section 3.3) written in the general form $p_3 = p_s(\dot{R}_3)$ and $v_3 = v_s(\dot{R}_3)$. The parameters p_3 , v_3 , and \dot{R}_3 can be determined from these three equations, as well as other parameters, $h_3 = h_s(\dot{R}_3)$ and $\rho_3 = \rho_s(\dot{R}_3)$, necessary to continue the calculations in the adjacent region.

The problem is easily generalized to the case of a nonuniform external medium in front of a traveling shock wave, since the parameters in the ambient medium are determined irrespective of the state behind the shock, which always passes inside the definiteness domain, for example, the segment $1' - 1'$ of the external flow (Figure 4.3d).

The solution can be continued by successive small portions using some appropriate numerical technique; this approach to constructing the solution is termed the *marching method*.

Theory of characteristics not only provides the basis for the formulation and analytical solution of gas dynamic problems and the interpretation of flow patterns, but must also be taken into account in developing numerical difference methods. It appears, in particular, that a no difference scheme gives a possibility to obtain a stable solution at a point outside the definiteness domain of initial and boundary conditions, thus imposing the main constraint on the space-to-time step ratio of a finite-difference grid.

The *grid-characteristic method* developed by Magomedov and Kholodov (1969) (Figure 4.4) provides a simple illustration of this general statement. It differs from the standard method of characteristics in that the information only at grid points on the r axis is stored in the course of computations, while the parameters at points 1 and 2 that enter in formulas in formula 4.2.10 are determined by interpolation using the gridpoints r_{k-1} , r_k , and r_{k+1} . In this case the method is stable and fruitful.

Formally, the calculations could also be carried out using points 1' and 2' outside the segment $[r_{k-1}, r_{k+1}]$. In that case, the flow parameters at these points could be determined using the same gridpoints, though by means of extrapolation, which would make it possible to determine the solution at point 3' with a greater time step Δt . However, point 3' lies exterior to the definiteness domain of the segment $[r_{k-1}, r_k]$ and, therefore, as both experience and theory show, this method of calculation turns out to be unstable.

As can be easily seen, point 3 lies within the definiteness domain of the initial interval if the condition

$$\Delta t = t_3 - t_k \leq \frac{\Delta r}{a + |v|}, \quad \Delta r = r_{k+1} - r_k = r_k - r_{k-1} \dots \quad (4.2.12)$$

is satisfied. This is a particular case of the *Courant criterion*, which must be satisfied in order for the calculation of hyperbolic equations by a difference method to be stable.

In conclusion, we will give some other forms of compatibility relations; they can be used instead of 4.2.6 and are based on the transformation

$$dp = a^2 d\rho + \left(\frac{\partial p}{\partial \rho} \right)_s ds \quad (4.2.13)$$

In this case, the compatibility relations involve three differentials and the inconvenience of this form follows from the previously written algorithm of the characteristic method. This disadvantage, however, disappears for isentropic one-dimensional flows

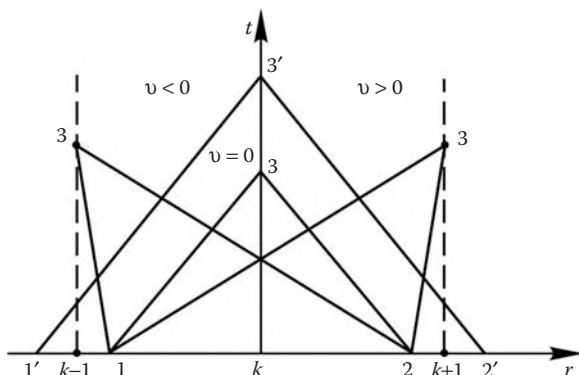


FIGURE 4.4
Grid-characteristic method scheme.

($s = \text{const}$, $Q_{\text{eff}} = 0$) for which conditions 4.2.6 can be written in an equivalent form (the last one is written for a perfect gas)

$$\pm dv = \frac{dp}{\rho a} = \frac{a}{\rho} d\rho = \frac{dh}{a} = \frac{2}{\gamma - 1} da \quad (4.2.14)$$

4.3 Steady-State Two-Dimensional Flows

In Cartesian or cylindrical coordinates (x, r) with velocity components u and v the original system of Equation 2.4.2 for steady-state two-dimensional (plane, $\nu = 0$, and axisymmetric, $\nu = 1$) flows has the form:

$$u \frac{\partial u}{\partial x} + v \frac{\partial u}{\partial r} = -\frac{1}{\rho} \frac{\partial p}{\partial x}, \quad u \frac{\partial v}{\partial x} + v \frac{\partial v}{\partial r} = -\frac{1}{\rho} \frac{\partial p}{\partial r} \quad (4.3.1)$$

$$\frac{u}{\rho a^2} \frac{\partial p}{\partial x} + \frac{v}{\rho a^2} \frac{\partial p}{\partial r} + \frac{\partial u}{\partial x} + \frac{\partial v}{\partial r} = Q_{\text{eff}}, \quad Q_{\text{eff}} = -Q - \frac{vv}{r} \quad (4.3.2)$$

$$\frac{dh}{dt} = u \frac{\partial h}{\partial x} + v \frac{\partial h}{\partial r} = \frac{1}{\rho} \frac{dp}{dt} + q \quad (4.3.3)$$

The system of Equations 4.3.1 and 4.3.2 belongs to the first group, according to the classification of Sections 4.1 or 2.4, while Equation 4.3.3 is an equation of the second group. The first set involves derivatives of three unknown functions u , v , and p ; however, it can be split, thus reducing the order of the determinant D in determining the characteristics. To do this, instead of the unknown functions u and v we will use the velocity magnitude U and the angle θ of its inclination to the x axis ($u = U \cos \theta$, $v = U \sin \theta$).

Multiplying the first and second equations in Equation 4.3.1 by u and v , respectively, summing and using the first law of thermodynamics 4.3.3, we obtain again Equation 2.2.8, which is known from Section 2.2

$$\frac{1}{2} \frac{dU^2}{dt} = -\frac{1}{\rho} \frac{dp}{dt}, \quad \frac{d}{dt} \left(h + \frac{U^2}{2} \right) = \frac{dh}{dt} = q \quad (4.3.4)$$

For adiabatic flows ($q = 0$) hence follows the Bernoulli equation, $h + U^2/2 = H(\psi)$, where ψ is the stream function (see Section 2.1). Multiplying now the first and second equations of 4.3.1 by $\sin \theta$ and $\cos \theta$, respectively, and subtracting we obtain

$$-\zeta \frac{\partial p}{\partial x} + \frac{\partial p}{\partial r} + \rho U^2 \left(\frac{\partial \theta}{\partial x} + \zeta \frac{\partial \theta}{\partial r} \right) = 0, \quad \zeta = \tan \theta \quad (4.3.5)$$

Let us now transform the continuity equation 4.3.2. Passing to the variables U and θ we obtain an intermediate equality

$$\frac{\partial u}{\partial x} + \frac{\partial v}{\partial r} = \cos \theta \frac{\partial U}{\partial x} + \sin \theta \frac{\partial U}{\partial r} - U \sin \theta \frac{\partial \theta}{\partial x} + U \cos \theta \frac{\partial \theta}{\partial r}$$

Since the sum of the first two terms on the right-hand side is $U^{-1}dU/dt$, we can bring the continuity equation (using the first formula of 4.3.4) to the form:

$$\frac{M^2 - 1}{\rho U^2} \left(\frac{\partial p}{\partial x} + \zeta \frac{\partial p}{\partial r} \right) - \zeta \frac{\partial \theta}{\partial x} + \frac{\partial \theta}{\partial r} = \frac{Q_{\text{eff}}}{U \cos \theta}, \quad M^2 = U^2/a^2 \quad (4.3.6)$$

Thus, Equations 4.3.5 and 4.3.6 involve only the derivatives of p and θ with respect to x and r and, similarly to Section 4.2, form the first group of equations whose characteristic property is manifested independently of equations of the second group (these are Equations 4.3.3 and 4.3.4).

Consider the first system. Let in the (x, r) plane a curve $r = r_0(x)$ be given with a Cauchy problem posed on it. This means that on this curve the distributions of the functions $p_0(x)$ and $\theta_0(x)$ are preassigned and, hence, their total derivatives along this curve are as follows

$$\frac{\partial f}{\partial x} + r'_0 \frac{\partial f}{\partial r} = \frac{df_0}{dx}, \quad f = p, \theta \quad (4.3.7)$$

As shown in Section 4.1, in order to obtain the solution in the vicinity of the initial curve the outward derivatives on this curve, that is, the derivatives of p and θ with respect to x and r , must be determined. In accordance with the second method of obtaining the characteristics (Section 4.1), we determine these derivatives from the system 4.3.5 through 4.3.7, which is possible if the determinant composed of their coefficients is nonzero (here, the derivatives of p are divided by ρU^2)

$$D = \begin{vmatrix} -\zeta & 1 & 1 & \zeta \\ \beta^2 & \beta^2 \zeta & -\zeta & 1 \\ 1 & r'_0 & 0 & 0 \\ 0 & 0 & 1 & r'_0 \end{vmatrix} = \beta^2(r'_0 - \zeta)^2 - (1 + \zeta r'_0)^2, \quad \beta^2 = M^2 - 1 \quad (4.3.8)$$

However, as follows from the theory of linear algebraic equations, this cannot be done if $D = 0$, that is, if the initial curve is a characteristic and is governed by the equation (the subscript 0 is omitted)

$$\begin{aligned} \frac{dr}{dx} = r' &= \frac{\beta \zeta \pm 1}{\beta \mp \zeta} = \tan(\theta \pm \alpha^*) \\ \sin \alpha^* &= \frac{1}{M} = \frac{a}{U}, \quad \beta = \cot \alpha^* \end{aligned} \quad (4.3.9)$$

At $M > 1$ this equation determines two families of real wave characteristics (upper and lower signs indicate the first and second families, respectively).

In accordance with the classification of differential equations, such a system is termed *hyperbolic*. Obviously, the equations of unsteady motion considered in Section 4.2 are of this type. However, for those equations real characteristics exist always, while in subsonic steady flows ($M < 1$) the system of equations is *elliptic* and has no real wave characteristics.

Finally, at a sonic velocity ($M = 1, \beta = 0$), which can usually be achieved only on isolated sonic lines, the two characteristic families merge, which leads to the *parabolic degeneration* of the equations, so that in the near vicinity of the sonic line, where $|M^2 - 1| \ll 1$, the equations are of a *mixed*, or *transonic*, type (see Chapters 5 and 6).

We will consider supersonic flows in more detail. For $D = 0$ the system of algebraic equations is either incompatible or has many solutions; in the latter case, all the determinants obtained from D by replacing any of its columns with the column of right-hand sides of equations are zero.

We denote this column by B , while A_n are the columns of the determinant D . Then the compatibility relations for the system can be written as follows

$$\begin{aligned} D &= |A_1, A_2, A_3, A_4| = 0, \quad D_1 = |B, A_2, \dots| \\ D_2 &= |A_1, B, \dots| = 0, \quad D_3 = 0, \quad D_4 = 0 \end{aligned} \quad (4.3.10)$$

The condition $D_1 = 0$ means the linear dependence of the columns

$$B = \sum_{n=2}^4 \alpha_n A_n, \quad \alpha_n = \text{const}$$

Substituting these expressions into D_2 and using the superposition rule we obtain

$$D_2 = \alpha_2 D + \alpha_1 |A_1, A_1, A_3, A_4| + \dots = 0$$

since $D = 0$ by the assumption, while other determinants vanish owing to the fact that they possess identical columns.

Thus, all the compatibility relations lead to the same result, which, after some algebra, can be represented in the form:

$$\begin{aligned} N dp \pm d\theta &= \frac{1}{MU} Q_{\text{eff}} dl_{\pm} \\ N = \frac{\beta}{\rho U^2}, \quad \beta^2 = M^2 - 1, \quad dl_{\pm} &= \frac{dr}{\sin(\theta \pm \alpha^*)} = \frac{dx}{\cos(\theta \pm \alpha^*)} \end{aligned} \quad (4.3.11)$$

Here, the upper and lower signs correspond to the first and second families of characteristics, respectively, while dl_{\pm} are the length differentials along them. These are the *compatibility conditions* to be satisfied by the p and θ distributions along each characteristic; as in Section 4.2, they are equivalent to the original system of equations written in the characteristic variables (η_+, η_-)

$$d\eta_{\pm} = dr - \tan(\theta \pm \alpha^*) dx = 0 \quad (4.3.12)$$

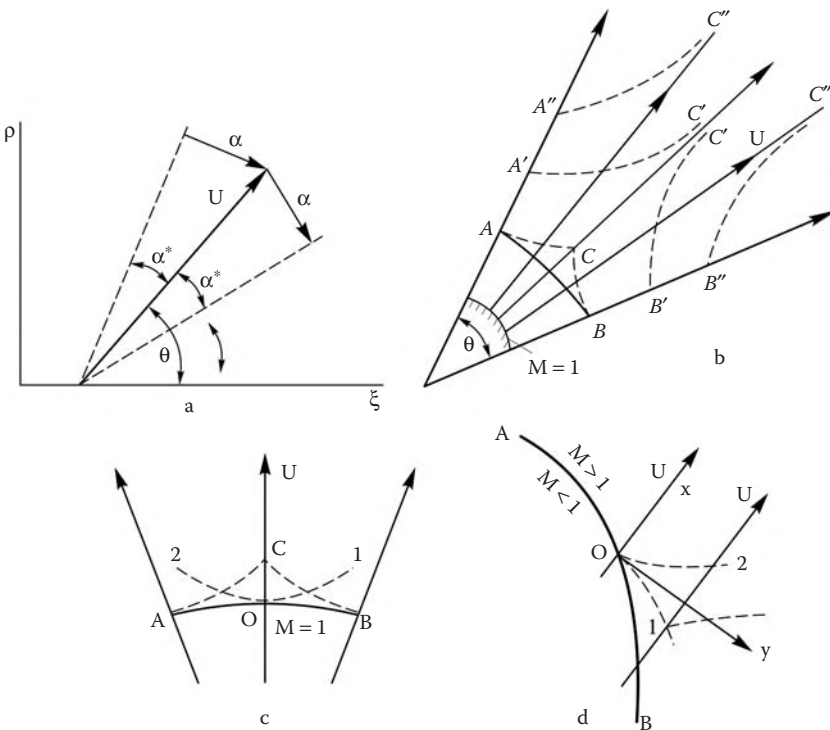
The characteristics of the group of trajectory Equations 4.3.3 and 4.3.4 are represented by the streamlines

$$\frac{dr}{dx} = \frac{v}{u} = \tan \theta \quad (4.3.13)$$

while the compatibility relations are represented by the equations themselves, as in Section 4.2. It is important to emphasize that the streamlines are characteristics for any Mach numbers, including the case of incompressible flows, where their characteristic properties are manifested in rotational flows (with the total enthalpy $H(\psi)$ varying across streamlines, Section 2.1).

We note that in the previous considerations the characteristics could be obtained without preliminary splitting of the general system of equations into the first and second groups. In this case the determinant of the system would be of the tenth rather than the fourth order (as in 4.3.8) and would naturally have the same roots 4.3.9 and 4.3.13.

The formulation of typical problems and their classification does not differ from those considered in Section 4.2, only the variable t should be properly replaced by x . In particular, the situation in Figure 4.3d is also pertinent to the supersonic flow past a sharp-nosed body with an attached shock (curves OD and OA). We will note only that *the velocity projection onto the normal to a characteristic is equal to the speed of sound*, which follows immediately from the definition of α^* in formula 4.3.9 and Figure 4.5a. As earlier, *the streamlines are bisectors of the angles between characteristics*, and their geometrical and physical meaning is the same as in the case of unsteady flows (which was explained in Section 4.2): they are trajectories of acoustic disturbances propagating at equal angles to streamlines (particle trajectories).

**FIGURE 4.5**

Characteristics (dashed curves) and streamlines. Definiteness and influence domains in hypersonic and transonic flows.

The analogy between one-dimensional unsteady and two-dimensional steady supersonic flows is particularly clear for high-Mach-number flows in narrow regions. It is sufficient to set

$$\theta \ll 1, \quad M \gg 1, \quad u = U = U_{\max} = \text{const}, \quad v = \theta U, \quad x = Ut \quad (4.3.14)$$

in Equations 4.3.9, 4.3.11, and 4.3.13, in order to bring the equations to the form analogous to that of equations of Section 4.2. This is a particular case of the *unsteady analogy* of hypersonic steady flows past thin bodies, which will be considered in Chapter 8.

However, supersonic steady flows have their own specific properties, in particular, in limiting cases of hypersonic and transonic flows. In the first case, as $\alpha^* = \arcsin M^{-1} \rightarrow 0$, both families of the wave characteristics tend to the single family of the streamlines, which can lead, under certain conditions, to a new effect, namely, to the appearance of unbounded domains of definiteness of the solution.

We will explain this effect with reference to the example of a gas jet expanding into a vacuum along a divergent bundle of almost rectilinear streamlines with the Mach number increasing approximately in accordance with the local source flow law (Section 2.3). Let θ be the divergence angle of the velocity vectors at the end points A and B of the initial curve in Figure 4.5b. If on this curve and in its vicinity $M \sim 1$, the characteristics of different families originating from these points intersect at point C and form a closed and bounded domain of definiteness of the solution. This is not the case if on this curve and downstream of it the conditions $\alpha^* \ll \theta$ or $K = M\theta \gg 1$ are satisfied. In that case, the extreme characteristics $A'C'$ and $B'C'$ tend asymptotically to streamlines and, as M increases, the point of their

intersection C' goes to infinity and these characteristics ($A''C'', B''C''$) no longer intersect, so that the definiteness domain of this initial curve becomes unbounded, while the influence domain is bounded, in the limit, by streamlines.

Contrariwise, in the transonic limit, as $M \rightarrow 1$, on the sonic line the angle $\alpha^* \rightarrow \pi/2$, while both characteristics tend to the normal to a streamline. If in this case the sonic line is orthogonal to a streamline, then it is tangent to characteristics $O1$ and $O2$ originating from point O (Figure 4.5c). Then the definiteness domain of the initial transonic curve occupies only the immediate vicinity of this curve. A rectilinear sonic line orthogonal to streamlines, which is realized under certain conditions in the Laval nozzle throat (line OA in Figure 4.6a), is an envelope of characteristics.

At the same time, if the sonic line is not orthogonal to streamlines, certain downstream-propagating characteristics ($O1$ in Figure 4.5d) can again reach the sonic line at point O , thus transmitting disturbances upstream, through the subsonic region.

These effects can occur both in nozzle flows (Figure 4.6b) and in flows past bodies and should be taken into account in formulating corresponding problems (Chapter 5).

Usually, characteristics have a singularity on the sonic line. To show this, we align the x axis of a Cartesian coordinate system with the vector \mathbf{U} and the y axis with the normal to it, the origin being at the sonic point O (Figure 4.5.d). Then by virtue of relation 2.2.21 and the smallness of the quantities Δp , θ , and $M - 1$ we can transform the characteristic Equation 4.3.9 in the vicinity of the sonic point to the form:

$$\frac{dx}{dy} = \cot(\theta \pm \alpha^*) = \theta \pm \sqrt{M^2 - 1} = \theta \pm \left(2A \frac{\Delta p}{\rho_* a_*^2} + B \frac{T_* \Delta s}{a_*^2} \right)^{1/2}$$

$$\Delta p = p - p_*, \quad \Delta s = s - s_* \quad (4.3.15)$$

Clearly, the term θ on the right-hand side can be neglected, if the flowfield is regular ($\Delta p, \theta, \Delta s \sim x, y$); then the solution of this equation has the form $x \sim y^\kappa$. For a simple plane-parallel isobaric vortical flow with the entropy distribution $\Delta s \sim y$ we have $\kappa = 3/2$. In the vicinity of the sonic line of the source flow (Figure 4.5c) in accordance with 2.3.7, the solution is singular and has the form $\Delta p \sim \sqrt{x}$, so that $\kappa = 4/3$. Of course, the cases in which the behavior of characteristics is regular can also exist (e.g., for $\theta \sim x, y$ and $\Delta p, \Delta s \sim x^2, y^2$) but rather as exceptions.

Consider briefly degeneration of equations, as $M \rightarrow \infty$ and $M \rightarrow 1$, associated with the merging of two families of wave characteristics. In the first limit, a streamline is the only characteristic; however, in actual fact, this *trajectory degeneration* is exactly realized only for $M = \infty$, for instance, for gas expansion into a vacuum. For finite, though as high as wished,

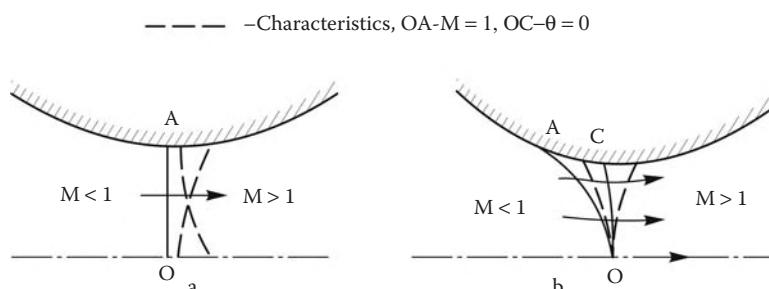


FIGURE 4.6
Transonic flow in a nozzle.

Mach numbers, the role of disturbances transverse to streamlines is conserved, although the velocity of their propagation is small as compared with the convective velocity of the disturbance transfer.

In contrast, the velocity of transverse disturbance propagation is relatively high as $M \rightarrow 1$, which is specific for parabolic equations, for example, for the heat conduction equation; therefore, such a degeneration is referred to as *parabolic*. However, as will be shown in Section 5.2, where simple examples were given, the parabolic sonic approximation (for $M = 1$) is even qualitatively inadequate for the description of transonic flows. Such a description appears to be possible only on the basis of the special von Kàrmà̄n equation to be given in Chapter 5.

In conclusion, we will give another frequently used form of the characteristic Equation 4.3.9, by transforming it as follows

$$\frac{dr}{dx} = \frac{\beta\zeta \pm 1}{\beta \mp \zeta} = \frac{v\sqrt{M^2 - 1} \pm u}{u\sqrt{M^2 - 1} \mp v} = \frac{uv \pm a\sqrt{U^2 - a^2}}{u^2 - a^2}$$

$$U^2 = u^2 + v^2, \quad u = U \cos \theta, \quad v = U \sin \theta \quad (4.3.16)$$

This form of the characteristic equations is obtained in deriving them directly from the original system of gas dynamic equations, that is, without passing to the unknown functions p and θ . From physical and geometrical points of view, this form is less visual than 4.3.9, particularly as the replacement of the pressure by the dependence $p = p(U, s)$ (using the Bernoulli and state equations) leads (as in Section 4.2) to the appearance of the third differential ds in the compatibility relations.

One more remark: the above characteristic equations were obtained for systems of first-order equations. However, in Chapter 2 the linearized version of this system was reduced to one second-order wave equation for a potential φ , for example, to the canonical equation of the form $\varphi_{xx} = \varphi_{yy}$ (subscripts denote the differentiation with respect to the appropriate variables). By the change $u = \varphi_x$, $v = \varphi_y$ the equation is reduced to the system of two first-order equations, $u_x = v_y$ and $u_y = v_x$. To this system the considerations of this section are applicable; as a result we obtain the characteristic system $y' = \pm 1$ (which is already obvious from the results of Sections 2.5 and 2.8) with the compatibility relations $du \mp dv = 0$ or $d\varphi_x \mp d\varphi_y = 0$.

4.4 Three-Dimensional Flows

To avoid employing the matrix theory, which is typical in treating such problems, we will reduce the consideration of the characteristic properties of three-dimensional equations to the generalization of the previously considered two-dimensional equations. To the point, this makes it possible to obtain more visual geometrical interpretation of the results. To do this, we will write the system of Equation 1.9.11, together with continuity Equation 2.4.1, in the form:

$$\frac{\partial u}{\partial t} + u \frac{\partial u}{\partial x} + v \frac{\partial u}{\partial y} + \frac{1}{\rho} \frac{\partial p}{\partial x} = -w \frac{\partial u}{\partial z} = Q_u \quad (4.4.1)$$

$$\frac{\partial v}{\partial t} + u \frac{\partial v}{\partial x} + v \frac{\partial v}{\partial y} + \frac{1}{\rho} \frac{\partial p}{\partial y} = -w \frac{\partial v}{\partial z} = Q_v \quad (4.4.2)$$

$$\begin{aligned} \frac{1}{\rho a^2} \frac{\partial p}{\partial t} + \frac{u}{\rho a^2} \frac{\partial p}{\partial x} + \frac{v}{\rho a^2} \frac{\partial p}{\partial y} + \frac{\partial u}{\partial x} + \frac{\partial v}{\partial y} &= Q_{\text{eff}} \\ Q_{\text{eff}} &= -Q - \frac{\partial w}{\partial z} - \frac{w}{\rho a^2} \frac{\partial p}{\partial z} \end{aligned} \quad (4.4.3)$$

$$\frac{\partial w}{\partial t} + u \frac{\partial w}{\partial x} + v \frac{\partial w}{\partial y} = -\frac{1}{\rho} \frac{\partial p}{\partial z} - w \frac{\partial w}{\partial z} = Q_w \quad (4.4.4)$$

According to Section 4.1, to obtain characteristic surfaces we should pose the Cauchy problem on a surface and find the conditions under which it is impossible to determine outward derivatives on it. Since characteristic properties of equations are local, we shall put the origin O of a coordinate system (t, x, y, z) at the point under consideration and draw a surface Σ through the z axis. Then all the derivatives with respect to z are known and can be substituted into the right-hand sides of the equations, as had been done previously.

We call attention to Equation 4.4.4. Given the quantity Q_w , the equation has the same form as Equations 4.1.2 and 4.1.3 and, hence, has the same characteristic surfaces formed by particle trajectories passing through the z axis (streamlines in a steady flow), which are bicharacteristics of these surfaces. Thus, Equations 4.4.4 and 4.1.3 belong to the equations of the second group, according to the classification of Section 4.1.

Consider the remaining equations, which belong to the first group. We begin with steady three-dimensional flows letting the derivatives $\partial/\partial t = 0$. To reduce the problem to the two-dimensional one treated in Section 4.3 we introduce a coordinate system in which the local velocity vector \mathbf{U} at the point O lies in the plane $z = 0$. Then at this point $w = 0$ and $U^2 = u^2 + v^2$, so that Equations 4.4.1 through 4.4.3 differ from those considered in Section 4.3 only by the derivative $\partial w/\partial z$ known on Σ , that is, by the right-hand side Q_{eff} . Hence, these equations have the same wave characteristics 4.3.9 with r replaced by y . Then in variables x, y, z , where the x axis is aligned with the vector \mathbf{U} and the angle $\theta \ll 1$, these characteristics take the form:

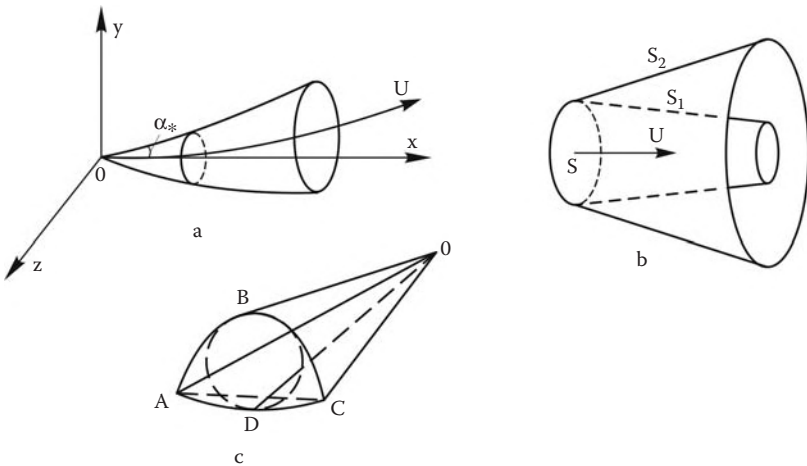
$$\frac{dy}{dx} = \pm \tan \alpha^* = \pm(M^2 - 1)^{-1/2}, \quad \alpha^* = \arcsin \frac{1}{M} \quad (4.4.5)$$

Thus, the surface Σ is *characteristic* if a *characteristic plane* tangent to it is inclined to the local streamline at the Mach angle α^* . Evidently, the velocity projection onto the normal to this surface is equal to the speed of sound. Turning the coordinate system around the x axis we obtain that the envelope of all the characteristic surfaces passing through point O is a *characteristic cone* whose axis of symmetry coincides with the velocity vector and the semi-vertex angle is equal to the Mach angle

$$y^2 + z^2 = x^2(M^2 - 1)^{-1} \quad (4.4.6)$$

Obviously, this is the Mach cone introduced in Section 1.6. Its generators, or characteristics 4.4.5, are bicharacteristics of three-dimensional equations and a set of characteristic surfaces can be drawn through each of them. Quite naturally, in a finite vicinity of point O bicharacteristics are three-dimensional curves inclined at the angle α^* to local streamlines, while the characteristic cone is a *curvilinear conoid* (Figure 4.7a).

The properties of characteristic surfaces are, in general, identical to those for two-dimensional flows described in Section 4.3. The conoid with the vertex at point O is the domain of influence of this point. The domain of definiteness of a part of the initial surface Σ is bounded by a characteristic surface S_1 being the inner envelope of the Mach conoids

**FIGURE 4.7**

Characteristic surfaces and conoid.

outgoing from the boundary, while the domain of its influence is the outer envelope of these conoids S_2 (Figure 4.7b).

Considering plane flows as the limiting case of three-dimensional flows we obtain that characteristics of plane flows are the lines of intersection of characteristic surfaces normal to the flow plane by the plane itself. Characteristics of axisymmetric flows are the lines of intersection of characteristic surfaces passing through circles in planes normal to the axis of symmetry, on which the centers of the circles are located, by meridional planes.

Generally speaking, the characteristic surfaces can be of different shapes. By way of illustration, we have plotted in Figure 4.7c a surface $OABCD$ confining the influence domain of a triangle AOC lying outside of the leading Mach cone with the vertex at the point O . Such surfaces are sometimes considered in developing and substantiating difference methods for solving similar problems.

The compatibility relations on characteristic surfaces follow from 4.3.11, the function Q_{eff} being determined from 4.4.3

$$\pm \frac{\partial \theta}{\partial l_{\pm}} + \frac{1}{MU} \frac{\partial w}{\partial z} + \frac{\sqrt{M^2 - 1}}{\rho U^2} \frac{\partial p}{\partial l_{\pm}} = -\frac{Q}{UM} \quad (4.4.7)$$

Here, dl_{\pm} are the differentials along the bicharacteristics in the $z = 0$ plane, which, as in 4.4.5, is orthogonal to the vector \mathbf{U} at the origin, θ is the angle of the inclination of this vector to the x axis, and the plus and minus signs relate to surfaces of the first and second families. Any of these relations is a partial differential equation on its characteristic surface, which follows from the impossibility of determining the normal derivative on it.

We will now consider the equation for the two-dimensional unsteady flow in the y, z plane; to do this, we set $u = 0$ in Equations 4.4.1 through 4.4.4. System 4.4.2 and 4.4.3 differ from the similar one of in Section 4.2 only by the right-hand sides of the equations and, hence, has the same characteristics $dy/dt = (v \pm a)$ in the y, t plane. The planes passing through them and the z axis correspond to a pair of wave characteristic surfaces. Similarly, the characteristics $dz/dt = (w \pm a)$ correspond to surfaces passing through the y axis. Obviously, turning the coordinate system around the point O or the t -axis in the t, y, z space

gives a set of similar characteristic surfaces whose envelope is the characteristic cone with the vertex at point O . For small t the equation of this cone is as follows

$$(y - vt)^2 + (z - wt)^2 = a^2 t^2 \quad (4.4.8)$$

Geometrical interpretation of the characteristic properties of the time-dependent system is the same as that shown in Figure 4.7, where one should only replace x by t , while the domain of influence of disturbances at a certain point O in a fixed coordinate system is formed by a circle expanding at a velocity a with the origin coinciding with the particle moving at a velocity \mathbf{U} , as shown in Figure 1.14 (Section 1.6).

To derive compatibility relations along the wave characteristic surfaces it is not sufficient to use relation 4.2.6 since its right-hand side does not allow for the contribution of the term Q_v to Equation 4.4.2. We will obtain the required relations by other means as in Section 4.2, namely, by multiplying Equation 4.4.2 by ± 1 and Equation 4.4.3 by a and summing them. This results in the differential equations

$$\begin{aligned} \pm \frac{Dv}{Dt} + \frac{1}{\rho a} \frac{Dp}{Dt} &= Q_{\pm}, & \frac{D}{Dt} &= \frac{\partial}{\partial t} + (v \pm a) \frac{\partial}{\partial y} \\ \tilde{Q}_{\pm} = aQ_{\text{eff}} \pm Q_v &= -a \left(Q + \frac{\partial w}{\partial z} + \frac{w}{\rho a^2} \frac{\partial p}{\partial z} \right) \mp w \frac{\partial v}{\partial z} \end{aligned} \quad (4.4.9)$$

Here, the operator D/Dt stands for the derivatives along the characteristics $dy/dt = v \pm a$ in the plane $z = 0$. The upper and lower signs relate to the first- and second-family curves, respectively. These equations, as well as Equation 4.4.7, are written for characteristic surfaces passing through the z axis, since they do not involve outward derivatives. We note that here, as distinct from 4.4.7, there are no restrictions on orientation of the y and z axes, but the equations are brought to their simplest form when the y axis is aligned with the vector \mathbf{U} , since in this case $w = 0$.

Finally, we will outline briefly the general case of three-dimensional time-dependent flows. Mathematically, in this case the Cauchy problem could be posed on any hypersurface $\Sigma(t, x, y, z) = 0$ inside a hypervolume $\Omega_t(t, x, y, z)$ in the four-dimensional space. However, physically, of exceptional importance is the initial-value problem posed on a surface $t = t_0 = \text{const}$, such that the projection of the previously mentioned hypervolume onto this surface is represented by the corresponding volume $\Omega_0(x, y, z)$ of the physical space. In other words, the initial distribution of the unknown functions must be preassigned in the volume Ω_0 at the moment t_0 .

The generalization of the notion of characteristics or characteristic surfaces to the general case is represented by characteristic surfaces $S(t, x, y, z) = 0$. For initial-value problems posed at $t = t_0$ these surfaces are constructed as the envelopes of all domains of influence for each point $O(x_0, y_0, z_0)$ inside an initial volume $\Omega_0(x_0, y_0, z_0)$. These domains are, in their turn, formed by the envelopes of all three-dimensional fronts of acoustic disturbances generated by each gas particle moving along a trajectory $x^*(t), y^*(t), z^*(t)$ (cf. Section 1.8). For each moment this domain of influence is confined in a volume bounded by the surface

$$\begin{aligned} (x - x^*)^2 + (y - y^*)^2 + (z - z^*)^2 &= R^2 \\ x^* = \int_{t_0}^t u dt, \quad \dots, \quad R = \int_{t_0}^t a dt \end{aligned} \quad (4.4.10)$$

Simple examples of such point influence domains were shown in Figure 1.14 from Section 1.6; for supersonic velocities ($U > a$) this is simply the Mach cone (or curvilinear conoid), while for $U < a$ this domain contains the initial point O in the interior of itself.

As in the case of two-dimensional flows, the equations of characteristic surfaces and the relations on them are effectively used for developing numerical methods for solving gas dynamic equations or, at least, for substantiating these methods. The time-dependent equations are frequently used to obtain stationary solutions by relaxing a time-dependent numerical simulation to an asymptotic steady state under the assumption that at constant boundary conditions all unsteady transition processes in flows decay in time. The hyperbolicity of the equations thus obtained makes it possible to avoid difficulties associated with solving sophisticated boundary-value problems for nonlinear elliptic equations.

4.5 Simple Waves

The compatibility relations along characteristics (for time-dependent one-dimensional and steady-state two-dimensional flows, Equations 4.2.6 and 4.3.11, respectively) can be integrated in a finite form when $Q_{\text{eff}} = 0$ and all the coefficients depend on the pressure p only. These conditions are realized in plane adiabatic flows ($\nu = 0, q = 0$) of a two-parameter gas with the total enthalpy H and entropy s constant throughout the entire flowfield, since in this case the quantities ρ, a, h , and U depend only on p . This very simple and at the same time important for applications case will be considered in the following.*

We will write the integrated compatibility relations for steady and unsteady problems in the form:

$$\begin{aligned} J^{(\pm)} &= v \pm P_1(p) = C_{\pm}(\eta_{\pm}), & P_1 &= \int \frac{dp}{\rho a} \\ d\eta_{\pm} &= dr - (v \pm a)dt = 0 & & \end{aligned} \quad (4.5.1)$$

$$\begin{aligned} I^{(\pm)} &= \theta \pm P_2(p) = C_{\pm}(\eta_{\pm}), & P_2 &= \int \frac{\sqrt{M^2 - 1}}{\rho U^2} dp \\ d\eta_{\pm} &= dr - \tan(\theta \pm \alpha^*)dx = 0 & & \end{aligned} \quad (4.5.2)$$

The constants C_{\pm} are determined in terms of the flow parameters at some point, while the combinations $J^{(\pm)}$ and $I^{(\pm)}$, constant along the corresponding characteristics, are termed the *Riemann invariants*.

For a perfect gas the integrals P_i are reduced to elementary functions

$$P_1 = \frac{2}{\gamma - 1}(a - a_0), \quad \frac{a}{a_0} = \left(\frac{p}{p_0} \right)^{(\gamma - 1)/2\gamma} \quad (4.5.3)$$

* The integrability conditions formulated previously are sufficient but not necessary. In Sedov (1965) a particular integrable case for a vortical flow with a special distribution $H(\psi)$ and $s(\psi)$ is presented.

$$P_2 = \sqrt{\frac{\gamma+1}{\gamma-1}} \arctan \sqrt{\frac{\gamma-1}{\gamma+1} (M^2 - 1)} - \arctan \sqrt{M^2 - 1}$$

$$\frac{p}{p_*} = \left(\frac{2}{\gamma+1} + \frac{\gamma-1}{\gamma+1} M^2 \right)^{\gamma/(1-\gamma)} \quad (4.5.4)$$

Here, the integration limits are so chosen that $P_1 = 0$ for a certain $a = a_0$ and $P_2 = 0$ at the sonic point of the flow, where $a = a_*$, $p = p_*$, and $M = 1$. Other expressions for P_2 are also known, but all of them can be reduced, correct to constant terms, to each other by means of the well-known trigonometric relations.

Let the region under consideration be adjacent to a constant flow zone, for example, region I to the left of the characteristic ac in Figure 4.8. Then the constant C_- is the same throughout the entire region II filled by second-family characteristics $\eta_- = \text{const}$ originating in region I. If the constant flow-parameter region is bounded by a second-family characteristic, then the roles of the two families are interchanged.

Such solutions and flows described by them are generally termed *simple waves* or the *Prandtl-Meyer waves* or *flows* in steady cases and the *Riemann waves* in unsteady cases.

The Riemann invariants give one-valued dependence between the flow parameters throughout the entire region II including body surfaces

$$v - P_1(p) = v_1 - P_1(p_1), \quad \theta - P_2(p) = \theta_1 - P_2(p_1) \quad (4.5.5)$$

Here, p_1 , v_1 , and θ_1 are some constant parameters in region I.

Since the combinations C_+ are constant along characteristics of the first family, the required functions are also constant on them, while the characteristics themselves are straight lines. The slopes of characteristics and the parameters on them are determined from the boundary condition on the piston, $r = r_p(t)$, or on the body surface in a flow, $r = r_b(x)$, where $v = \dot{r}_p(t)$ or $\tan \theta = r'_b(x)$. The pressure on the body surface is determined from Equation 4.5.5 and the slopes of the characteristics from Equations 4.2.5 and 4.3.9. If the wall slope to the right of point d (Figure 4.8) is constant (or the piston has a constant

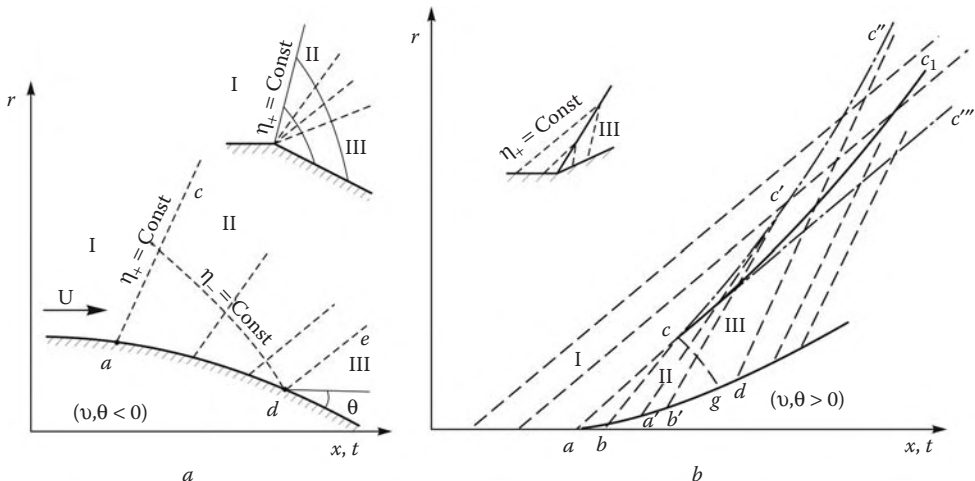


FIGURE 4.8

Simple waves: (a) expansion and (b) compression.

velocity), then behind the characteristic de there is a constant flow-parameter region III with parallel characteristics.

Of crucial importance is the law of the characteristic slope variation in a simple wave. For unsteady and steady problems the following relations hold on characteristics of the first (for definiteness) family

$$\begin{aligned} d(v+a) &= \frac{dp}{\rho a} + da = A \frac{dp}{\rho a}, \quad A = 1 + \frac{1}{2} \rho \left(\frac{\partial a^2}{\partial p} \right)_s \\ d(\theta + \alpha^*) &= d\theta + d \arcsin \frac{1}{M} = \frac{A}{\sqrt{M^2 - 1}} \frac{dp}{\rho a^2} \end{aligned} \quad (4.5.6)$$

Here we used the fact that in simple waves under consideration the differentials dv and $d\theta$ are related with dp by the compatibility relations along second-family characteristics; in evaluating the differential $dM^2 = d(U^2/a^2)$ we take into account that in a uniform isentropic flow the equality $\rho dU^2 = -2dp$ holds throughout the entire flowfield, which follows from the Bernoulli equation.

As shown in Section 1.6 (and used in Chapter 3), for normal gases the coefficient A is always positive; therefore, in a simple wave the slope of rectilinear characteristics changes in the same direction as the pressure.

From the previous considerations it follows that in the flow past a convex wall ($d\theta/dx < 0$, Figure 4.8a), in which both the slope and pressure decrease, the first-family characteristics originating on the curvilinear part of the surface ad form a divergent straight-line bundle. The same occurs for decelerating piston motion ($v_p = \dot{r}_p, \ddot{r}_p < 0$) in the piston problem. This means that in expansion flows no subsequent disturbance overtakes a preceding one, thus excluding the formation of expansion shock waves (this result was already obtained in Sections 2.6, 3.3, and 3.4).

On the contrary, in flows past concave walls ($d\theta/dx > 0$, Figure 4.8b) the characteristics form a convergent bundle (i.e., disturbances overtake one another) and since each characteristic carries its own constant values of the flow parameters, a region of a multivalued solution appears after these have been intersected. For unsteady one-dimensional flows the same results hold for an accelerating piston ($\ddot{r}_p > 0$).

The point of intersection of two close characteristics, $\eta_+ = \text{const}$, remains at a finite distance from the surface, as the distance between the characteristics on the surface tends to zero. First, we will show this for unsteady flows. Let (t_a, r_a) and (t_b, r_b) be the points of intersection of two close characteristics with the curvilinear piston trajectory in the t, r plane. The characteristics intersect at point c

$$t_c = t_a + \frac{(v+a)_b(t_b - t_a) - (r_b - r_a)}{(v+a)_b - (v+a)_a}, \quad r_c = r_a + (v+a)_a(t_c - t_a) \quad (4.5.7)$$

Let $t_b = t_a + \Delta t, \Delta t \rightarrow 0$. Then, using the limiting difference relations rewritten in terms of 4.5.6

$$\begin{aligned} (v+a)_b - (v+a)_a &= \frac{d(v+a)}{dp} \Delta p = \frac{A}{\rho a} \Delta p \\ \frac{\Delta r}{\Delta t} \rightarrow v_a, \quad \frac{\Delta p}{\Delta t} &= \rho a \frac{\Delta v}{\Delta t} \rightarrow \rho a \ddot{r}_p, \quad \Delta p = p_b - p_a \rightarrow 0 \end{aligned} \quad (4.5.8)$$

we obtain the coordinates of the point of intersection of two limitingly close characteristics

$$t_c = t_a + a(A\ddot{r}_p)^{-1}, \quad r_c = r_a + a(v+a)(A\ddot{r}_p)^{-1} \quad (4.5.9)$$

To obtain the analogous results for steady flows, we should replace t and $(v + a)$ by x and $\tan(\theta + \alpha^*)$, respectively, and set $dr/dx = \tan \theta$. Substituting, for simplicity, $\theta_a = 0$ we get

$$x_c = x_a + \frac{(M^2 - 1)^{3/2}}{AM^4} R, \quad \frac{1}{R} = \frac{\partial \theta}{\partial l}, \quad r_c = r_a + (M^2 - 1)(AM^4)^{-1} R \quad (4.5.10)$$

Here, l is the arc length measured along the body contour and R is its radius of curvature; all the parameters in both formulas are referred to the initial point a .

Above point c a region covered by intersecting first-family characteristics can be formed. Since, according to the theory, each of them carries constant values of the flow parameters, this is the region of *multivalued solutions*. To determine its boundaries, we take into account that similar considerations are valid for any pair of limitingly close characteristics, say, $a'c'$ and $b'c'$ originating on the curve ad . A set of such points c' forms an envelope of the characteristic family. For example, for a piston moving at a constant acceleration, $\ddot{r}_p = \text{const}$, it follows from 4.5.9 that the lengths of segments $a'c'$ and $b'c'$ increase, together with the velocity a , toward the right; therefore, the envelope cc'' lies above the continuation cc''' of the characteristic ac . In this case the two curves bound the region of the multivalued solution, as shown in Figure 4.8b.

In the general case the configuration of this region can be different; however, this presents no interest since such a multivalued solution has no physical meaning. In this case there is no physically meaningful continuous solution, so we must introduce a discontinuity line cc_1 with one-valued solutions on either side. Thus, to the left of this curve there is undisturbed region I, while the region to the right of it is filled with first-family characteristics starting from a piston or a wall.

From the mathematical point of view the discontinuity could be arbitrary, but to describe a real situation we must require the conservation laws to be satisfied on it, that is, this discontinuity can be a compression shock only (the submerged shock, according to the classification of Section 3.1) with point c being the point of its initiation. The process of shock wave formation was treated in Section 2.6, but here it is based on the more rigorous theory.

As shown in Section 3.4, a shock wave propagates through undisturbed gas at a supersonic velocity, while relative to disturbed gas it travels at a subsonic velocity. Therefore, in region III characteristics of the first family enter in the shock both from the right and from the left. The problem of constructing such a shock was considered in Section 4.2 (Figure 4.3).

Thence it follows that the simple wave region II to the right of the leading characteristic ac is bounded by the second-family characteristic cg and the solution in region III is not strictly a simple wave.

We note that real flow patterns can be more complicated since several shocks can simultaneously arise in a compression wave with their subsequent interference (Section 4.9). The location of the shock generation point depends significantly on M ; thus, at a constant A (for perfect gases $A = (\gamma + 1)/2$) the distance $x_c - x_a$ is maximum at $M = 2$, while for $M \rightarrow 1$ or $M \rightarrow \infty$ a shock is formed immediately at the point of discontinuity in the wall curvature.

4.6 Properties of Expansion and Compression Waves

In this section, some additional (as compared to Section 4.5) physical and mathematical properties of expansion and compression waves are outlined.

4.6.1 Expansion Waves

In Figure 4.9 we have plotted the pressure dependences $p(v)$ associated with perfect gas expansion in a channel from the rest ($v_1 = 0, a_1 = a_0$) and $p(\Delta\theta)$ for the turn of an initially sonic flow along a wall ($p_1 = p_*$, $\Delta\theta = \theta_1 - \theta$); the plots are obtained from formulas 4.5.3 through 4.5.5. Clearly, the influence of γ is relatively small for $\Delta v \leq a_0/2$ or $\Delta\theta \leq 15^\circ$, but it is appreciable for high-expansion ratios; the pressure difference in the expansion wave decreases with γ .

Generally, there are no similar analytical dependences for arbitrary gases, but, nevertheless, we can approximately use relations 4.5.3 and 4.5.4 for real gases with an effective adiabat exponent $\gamma = \gamma_*$ (Section 1.3) determined by the initial state. The data given in Figure 4.9 for equilibrium air confirm the possibility of this simplified approach.

Somewhat anticipating we note that in Figure 4.9 the curves for perfect gases with the so-called *frozen adiabatic exponent* γ_f (Figure 1.10) are also plotted; this exponent corresponds to an initially equilibrium gas composition ahead of the expansion wave. This process will be considered in detail in Chapter 11. Here we note only that the physics of the process under consideration has a considerable effect (via the corresponding adiabat exponent) on the flow parameters in the expansion wave.

Since high temperatures of air are associated with near-unity values of γ_* (Section 2.3, Figure 1.9), it is interesting to give limiting (as $\gamma \rightarrow 1$) forms of formulas 4.5.3 through 4.5.5

$$\frac{v}{a_0} = -\frac{2}{\gamma - 1} \left[1 - \left(\frac{p}{p_0} \right)^{\frac{\gamma-1}{2\gamma}} \right] \rightarrow \ln \frac{p}{p_0} \quad (4.6.1)$$

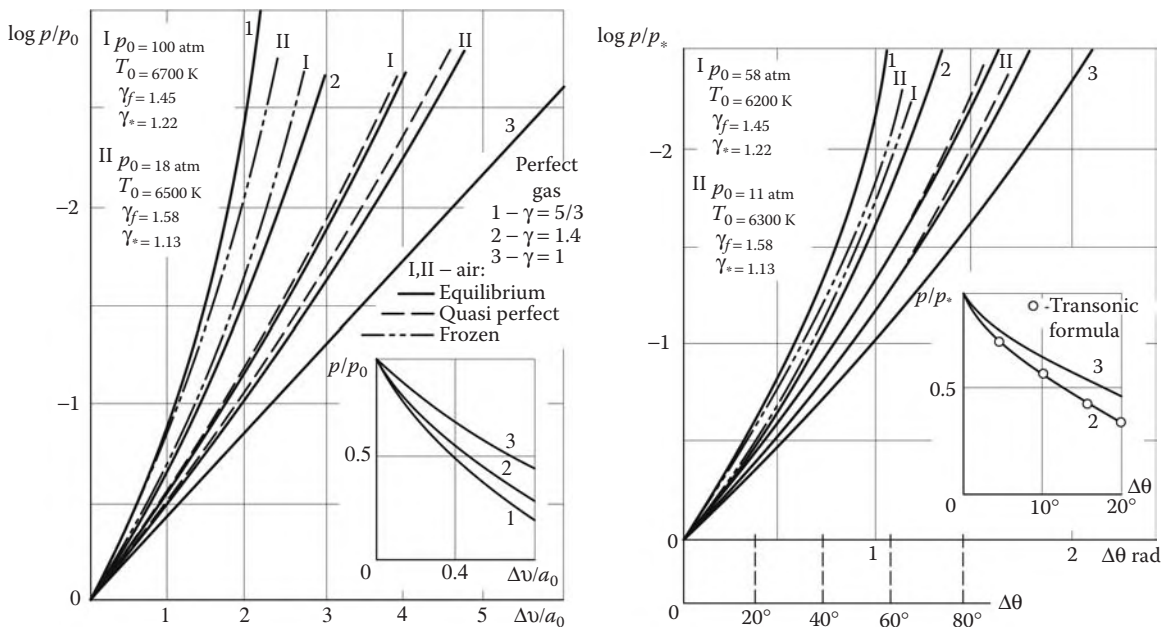


FIGURE 4.9

Pressure in simple waves: (a) Riemann waves and (b) Prandtl-Meyer waves.

$$\theta_1 - \theta = \Delta\theta \rightarrow \left(-2 \ln \frac{p}{p_*} \right)^{1/2} - \arctan \left(-2 \ln \frac{p}{p_*} \right)^{1/2} \quad (4.6.2)$$

The limiting curves are presented in Figure 4.9 and can be used as reference values for small ($\gamma - 1$).

Flows around a corner point or behind a piston suddenly starting to move at a constant velocity are special cases of simple expansion waves. One can easily imagine such a flow by letting the arc length ad in Figure 4.8 vanish, the flow parameters at points a and d being unchanged. Then in the limit we obtain a compression shock attached to the vertex of the angle or a *centered expansion wave* with a characteristic fan

$$\eta = \eta_+ = \frac{r}{t} = v + a, \quad \eta = \eta_+ = \frac{r}{x} = \tan(\theta + \alpha^*) \quad (4.6.3)$$

Together with dependence 4.5.5, formula 4.6.3 gives flow parameter distributions in the wave in the form of a self-similar solution $p(\eta)$, $v(\eta)$, or $\theta(\eta)$ with discontinuous derivatives with respect to η on the leading and trailing characteristics. Naturally, centered compression waves are impossible since in a gas flow around such an angle a compression shock is formed.

In Figure 4.10 the examples of simple waves in supersonic flows are presented, namely, the flows in a channel and past a sharp-nosed body. In the general case the centered wave abc originates at the corner point a and a region occupied by the simple wave is bounded from the right by the characteristic bd reflected from the line of symmetry or the shock.

Consider the behavior of the Prandtl-Meyer wave near the sonic characteristic. Expanding formula 4.5.2 for P_2 in series in $\Delta p = p_* - p$ and taking into account the limiting formula 2.2.20 yields

$$\frac{\Delta p}{p_*} = C(\Delta\theta)^{2/3}, \quad C = \frac{3^{2/3} \rho_* a_*^2}{2A^{1/3} p_*} = \frac{\gamma}{2} \left(\frac{18}{\gamma + 1} \right)^{1/3} \quad (4.6.4)$$

For $\gamma = 1.4$ the coefficient $C = 1.38$. The formula is sufficiently accurate for $\Delta\theta \leq 20^\circ$ ($M < 5$, Figure 4.9b). For a surface of finite curvature R^{-1} we can write $\theta = x/R$, so that $\Delta p \sim x^{2/3}$ and $\partial p/\partial x \rightarrow \infty$ as $x \rightarrow 0$. The singularity manifests itself in the distributions of the first-family characteristic slope, which can be demonstrated by integrating 4.5.6 with 2.2.20 taken into account

$$\varphi = \Delta(\theta + \alpha^*) = \left(2A_* \frac{\Delta p}{\rho_* a_*^2} \right)^{1/2} \sim x^{1/3} \quad (4.6.5)$$

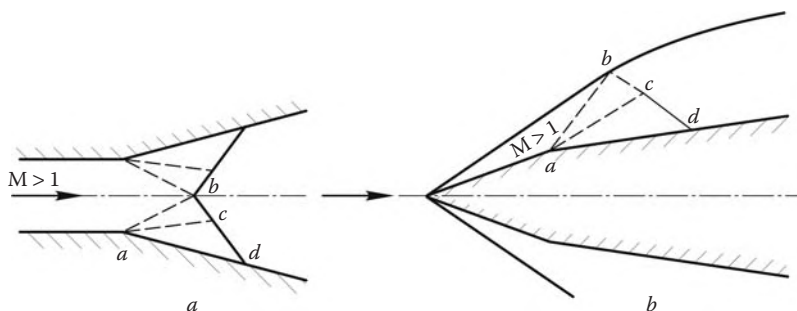


FIGURE 4.10
Two-dimensional supersonic flows with simple waves.

In a centered expansion wave in which the polar angle φ is the only coordinate, inversion of 4.6.5 gives dependences $\Delta p \sim \varphi^2$ and $\theta \sim \varphi^3$, that is, the pressure and the flow deflection angle near the initial characteristic have zero derivatives with respect to the angular coordinate. Hence, the second-family characteristic nearest to the sonic line intersects a characteristic of the first family at an angle 2φ and its equation in polar coordinates (r, φ) is $2\varphi dr/d\varphi = -r$ which has the solution $r\varphi^{1/2} = \text{const}$. These characteristics go to infinity as $\varphi \rightarrow 0$, that is, when the leading sonic characteristic is approached.

In the other limiting case of a large flow deflection angle, for high local Mach numbers and $U \sim U_{\max}$ formulas 4.5.2 and 4.5.4 give the following result

$$\begin{aligned}\Delta\theta_{\max} - \Delta\theta &= \frac{2}{\gamma - 1} \frac{1}{M} \\ \Delta\theta_{\max} &= \frac{\pi}{2} \left(\sqrt{\frac{\gamma + 1}{\gamma - 1}} - 1 \right) \quad (M \gg 1)\end{aligned}\quad (4.6.6)$$

When a flow with an initially high $M_1 \gg 1$ expands, it can turn only through a small angle $\Delta\theta \leq 2[(\gamma - 1)M_1]^{-1}$, the relative pressure change $p/p_1 = (M_1/M)^{2\gamma/(\gamma-1)}$ being as high as is wished.

Replacing $\Delta\theta U_{\max}$ by v we can reduce the relation 4.6.6 to the first integral of 4.5.3 for unsteady waves which is a particular manifestation of the previously mentioned unsteady hypersonic analogy.

The limiting deflection angle $\Delta\theta_{\max}$ for a flow expanding into a vacuum increases as γ decreases and is equal to $\pi/2, 0.72\pi$ (or 130°), and π for $\gamma = 5/3, 7/5$, and $5/4$, respectively. For $\gamma < 5/4$ the limiting turn cannot theoretically exist and the pressure at $\theta = \pi$ remains finite. In real situations, deflection angles are considerably smaller than the limiting ones due to viscosity influence and flow separation.

We note that for unsteady gas expansion into a vacuum the velocities v_{\max} are greater than those in steady expansion from the same stagnation conditions

$$-v \rightarrow v_{\max} = \frac{2a_0}{\gamma - 1} > U_{\max} = \sqrt{\frac{2}{\gamma - 1}} a_0 \quad (4.6.7)$$

4.6.2 Compression Waves

As shown previously, these waves are accompanied by internal compression shocks. This brings up the question of comparing the pressure increase in a simple wave and a shock for the same piston velocities or flow deflection angles. This comparison was given in Figures 3.12 and 3.13, where it was demonstrated that the pressure in a simple wave is always higher than in a shock, at least, for the weak branch of the shock.

To make the situation more visual, we will compare the pressures for one-dimensional unsteady waves ahead of the piston in the case of extremely high compression of a perfect gas, $p \gg p_0$. The corresponding pressure increase behind the simple and shock waves is as follows

$$\frac{p}{p_0} = \left(\frac{\gamma - 1}{2} \frac{v}{a_0} \right)^{2\gamma/(\gamma-1)}, \quad \frac{p}{p_0} = \frac{\gamma(\gamma + 1)}{2} \left(\frac{v}{a_0} \right)^2, \quad \frac{v}{a_0} \gg 1 \quad (4.6.8)$$

Clearly, for $v \gg a_0$ the pressure in a simple wave is an order greater than in a shock. A similar result can be obtained for steady compression waves: according to 3.3.8, in $M_1 \gg 1$

flows the pressure in a shock increases by a factor of $p/p_1 \sim M_1^2$ only, while in an isentropic compression wave, in accordance with 2.2.16, for $\gamma = 1.4$ it increases by a factor of $p/p_1 \sim M_1^7$. In a simple compression wave a flow can formally turn through the angle $\theta_{\max} = 130^\circ$, while in an oblique shock $\Delta\theta = 45^\circ$ (all these results are given for $\gamma = 1.4$). However, since it is very difficult to implement shock-free compression of supersonic flows, all these estimates should be considered only as reference points.

For weak waves the integral P_1 in 4.5.5 can be represented (up to the second-order terms) in the form:

$$\begin{aligned}\Delta v = v - v_1 &= \int_{p_1}^p \frac{dp}{\rho a} = \frac{\Delta p}{\rho_1 a_1} - \frac{1}{2} a_1 A_1 \left(\frac{\Delta p}{\rho_1 a_1^2} \right)^2 + \dots \\ \Delta p &= p - p_1, \quad A = 1 + \frac{1}{2} \rho \left(\frac{\partial a^2}{\partial p} \right)_s\end{aligned}\quad (4.6.9)$$

Here, the first term $\Delta p = \rho_1 a_1 \Delta v$ corresponds to the linear theory of Section 2.5. Substituting it into the second term we can write (with the same accuracy)

$$\frac{\Delta p}{\rho_1 a_1^2} = \frac{\Delta v}{a_1} + \frac{1}{2} A_1 \left(\frac{\Delta v}{a_1} \right)^2 + \dots \quad (4.6.10)$$

This formula (with u substituted for Δv) coincides with the similar expansion 3.7.3 for *weak unsteady shock waves*. Expanding in similar fashion the integral P_2 we obtain the same formula 3.7.4 for weak oblique shocks from which an important conclusion follows: expressions for $p(v)$ or $p(\theta)$, as well as those for the entropy increment from Section 3 differ only by the third-order terms (of the order $(\Delta p)^3$). Hence, *in weak shock waves the Riemann invariants, $v - P_1(p)$ or $\theta - P_2(p)$, are conserved with the same accuracy*.

Thus, the quadratic formulas obtained (valid for both simple and shock waves) hold on any streamline (*de* in Figure 4.11; see Section 4.8 for details) intersecting the waves. The data in Figures 3.12 and 3.13 show the range of the quadratic formula applicability for simple compression waves. Obviously, the previous formulas hold and can be useful for expansion waves as well.

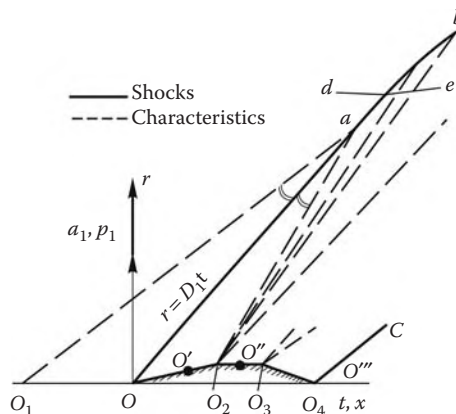


FIGURE 4.11
Weak-shock/expansion-wave interaction.

We note one more interesting peculiarity of the relative position of weak shocks and characteristics. As follows from formula 3.4.23, the velocity at which such a wave propagates is equal to a half-sum of the sonic wave velocities in front of and behind the shock. Thence it follows that in unsteady one-dimensional flows *a weak shock wave is a bisector of the angle between the characteristics in front of and behind the shock*. We can easily obtain the similar result for steady waves by integrating Equation 4.5.6 over a small region and taking into account 3.4.7

$$\theta + \alpha^* - \alpha_1^* = \frac{2}{\sqrt{M_{n1}^2 - 1}} \frac{v_{n1} - a_1}{a_1} = 2 \frac{\sin \alpha - \sin \alpha_1^*}{\cos \alpha} = 2(\alpha - \alpha_1^*)$$

$$v_{n1} = U_1 \sin \alpha, \quad a_1 = U_1 \sin \alpha_1^* \quad (4.6.11)$$

Here, α is the shock angle, while α_1^* and $\theta + \alpha^*$ are the slopes of characteristics in front of and behind the shock. Using 3.4.7 we can reduce this formula to 3.5.27.

4.7 Propagation of Disturbances in Nonuniform Media

Propagation of disturbances in the form of simple waves is possible only in uniform unbounded plane flows, that is, for $Q_{\text{eff}} = 0$ in relations 4.2.6 and 4.3.11. In real flows around bodies of complicated shape, disturbances interact both with the nonuniform non-isentropic vortex flow formed behind a curvilinear shock and with the shock itself; they can also be distorted due to the nonplane nature of the flow. To elucidate these effects, we will consider two groups of problems, namely, the problem of disturbance evolution in a continuous flow and that of disturbance reflection from a surface with given properties (such as discontinuity surface, and so on).

4.7.1 Waves in Continuous Media

Let a weak disturbance wave in the form of a narrow bundle of first-family characteristics 0 – 1, 0 – 2 (Figure 4.12a and b) propagate along the x axis starting from point O (e.g., from a bend in the body contour) in an isobaric plane-parallel (or axisymmetric) adiabatic supersonic flow. In particular, this can be the front of a finite-strength expansion wave. Such a wave is termed *short* (Ryzhov and Khristianovich, 1958), since its transverse dimension is considerably smaller than the longitudinal one. For such a wave the compatibility relations 4.3.11 are valid along characteristics 4.3.9

$$Ndp \pm d\theta = Q^{(\text{eff})} dl_{\pm}, \quad Q^{(\text{eff})} = \frac{Q_{\text{eff}}}{MU}, \quad N = \frac{\sqrt{M^2 - 1}}{\rho U^2} \quad (4.7.1)$$

The function Q_{eff} is determined by formulas 4.3.2 and 4.2.1. In what follows, Q_{eff} will be set equal to zero unless otherwise is stated. The general case will be considered at the end of the section.

Let a short wave be intersected by a segment of the second-family characteristic 1 – 2. Obviously, the segment length Δl_{12} is small; therefore, along it the coefficient N can be taken constant. If in the incident flow the function $Q^{(\text{eff})} = 0$, then, in view of continuity, it is small inside the short wave as well and the term $Q^{(\text{eff})} \Delta l$ is of the second order. Then along the segment 1 – 2, that is, across the short wave, the Prandtl-Meyer relation is valid

$$\theta - N \Delta p = 0 \quad (4.7.2)$$

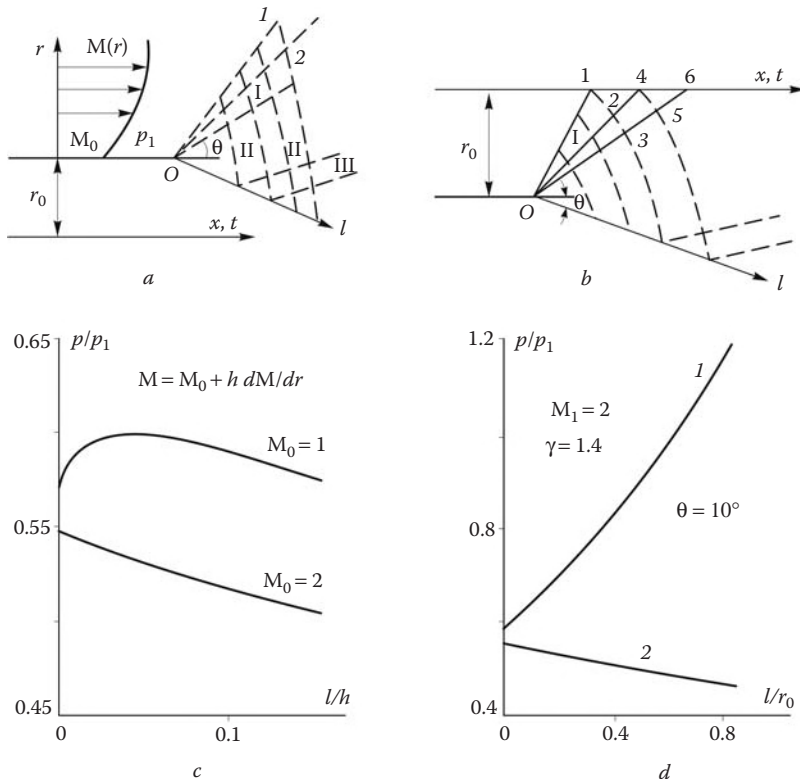


FIGURE 4.12
Flow turn around a corner point.

The coefficient N in a nonuniform vortex flow is a function of the distance measured along the short wave, while in a uniform flow it is constant.

Consider some typical examples.

4.7.2 Short Wave in a Vortex Flow

We consider a flow with continuous nonuniform transverse distributions of all the parameters, with exception of the pressure $p = p_1$ and the flow inclination angle $\theta = 0$ which are taken to be constant. A short disturbance wave propagates along characteristics of the first family. Such a situation occurs, for example, in a flow past a body with curvilinear shock inducing downstream of it a flow with transverse entropy gradients distorting the Prandtl–Meyer waves.

In this case eliminating the variable coefficient N from the compatibility relation 4.7.1 taken with the upper sign and from integral 4.7.2 we obtain a differential equation and its integral

$$\frac{dp}{p - p_1} + \frac{d\theta}{\theta} = 0, \quad \frac{\Delta p}{\Delta p_0} = \frac{p - p_1}{p_0 - p_1} = \frac{\theta_0}{\theta} = \left(\frac{N_0}{N} \right)^{1/2} \quad (4.7.3)$$

Here, p_0 , θ_0 , and N_0 are the parameters at point O on the given characteristic, which correspond to a small turn of the potential flow in the local Prandtl–Meyer wave. For a perfect gas the function $N/p = (M^2 - 1)^{1/2}/\gamma M^2$ is maximum for $M = \sqrt{2}$. Therefore, if, for

example, the Mach number is $M = M_0 \geq \sqrt{2}$ increasing with the distance from the wall, then the initial streamline bending at point O decreases, while the pressure disturbance grows as $(M/M_0)^{1/2}$ for high Mach numbers.

Let in a *uniform axisymmetric flow* a weak centered expansion wave be formed at point O at a distance r_0 from the axis of symmetry (Figure 4.12a and b). Equation 4.3.11 for characteristics near the wave front in the case of $v = \theta U$ and $\theta \ll \alpha^*$ ($\sin \alpha^* = M^{-1}$) takes the form:

$$d\theta \pm Ndp = -\theta \frac{dr}{r} \quad (4.7.4)$$

The coefficient N in a narrow wave can be considered to be constant. For a finite $r \sim r_0$, the right-hand side of 4.7.4 is of the second order of smallness; therefore, Equation 4.7.2, $N = \theta/\Delta p$, holds along the wave. By virtue of this fact, Equation 4.7.4 taken with the upper sign, that is, along the short wave, has the solution

$$\frac{\theta}{\theta_0} = \frac{\Delta p}{\Delta p_0} = \frac{\Delta K}{\Delta K_0} = \left(\frac{r_0}{r} \right)^{1/2}, \quad K = \tan(\theta + \alpha^*) \quad (4.7.5)$$

Relations for the increments of the angular coefficients of the characteristics follow immediately from Equation 4.5.6, which is valid in a short wave by virtue of Equation 4.7.2.

Thus, the initial disturbance decays away from the axis of symmetry (Figure 4.12a) and, vice versa, grows when the axis is approached (Figure 4.12b). In the latter case solution 4.7.5 has a singularity on the axis and is no longer valid in its vicinity, since the width of a divergent short wave becomes comparable with the distance from the axis as r decreases. In this case the last term in Equation 4.7.4 cannot be neglected and integral 4.7.2 is inapplicable.

Letting $\Delta p_0, \theta \sim \varphi$ for a centered simple wave in the vicinity of the leading characteristic we obtain from 4.7.5 the estimate $\partial p/\partial\varphi, \partial\theta/\partial\varphi \sim (r_0/r)^{1/2}$ as $\varphi, r \rightarrow 0$, where φ is the angle of the characteristic turn in the simple wave. These derivatives are unbounded at point 1 on the axis. Along the characteristic 1–3 (Figure 4.12b) bounding the domain of influence of the axis of symmetry the relation $r \sim r_0\varphi$ holds; therefore, the pressure and the angle θ along the characteristic vary as $\Delta p, \theta \sim \sqrt{\varphi}$.

Consider *unsteady flows* with cylindrical ($\nu = 1$) and spherical ($\nu = 2$) symmetry, for example, an expansion wave starting from a piston of the radius r_0 suddenly beginning to expand or compress. According to 4.2.1 and 4.2.6, the equation

$$dv \pm \frac{dp}{\rho a} = -v \frac{dr}{r} \quad (4.7.6)$$

is in this case a counterpart of Equation 4.7.4. Obviously, the plane Riemann invariant, $\rho av = \Delta p$, is conserved across the short shock wave and the solution along the short wave is

$$\frac{\Delta p}{\Delta p_0} = \frac{\Delta v}{\Delta v_0} = \frac{\Delta K}{\Delta K_0} = \left(\frac{r}{r_0} \right)^{-\nu/2}, \quad K = v + a \quad (4.7.7)$$

For $\nu = 1$ the solution coincides with 4.7.5, while the spherical wave decays for $r > r_0$ or is enhanced for $r < r_0$ more rapidly than the cylindrical one.

It is interesting to consider the behavior of a characteristic bundle in these waves. According to 4.7.7 or 4.7.5, the slopes of characteristics tend to those for the undisturbed flow;

however, they do not become parallel. To show this, we will write down the characteristic equations in terms of 4.7.7, which yields

$$\frac{dr}{dt} = K = K_1 + \Delta K_0 \left(\frac{r}{r_0} \right)^{-\nu/2} \quad (4.7.8)$$

Here, the subscript 1 refers to parameters ahead of the wave.

Since in a narrow wave $\Delta K \ll K_1$, we set $r = r_0 + K_1(t - t_0) \approx K_1 t$ on the right-hand side of 4.7.8 to obtain the following asymptotic forms of characteristics for $r \gg r_0$ and $t \gg t_0$

$$\begin{aligned} r &= K_1 t + 2\Delta K_0 \left(\frac{r_0 t}{K_1} \right)^{1/2}, & \nu &= 1 \\ r &= K_1 t + \frac{r_0 \Delta K_0}{K_1} \ln \frac{K_1 t}{r_0}, & \nu &= 2 \end{aligned} \quad (4.7.9)$$

The parameter that separates out an individual characteristic of the bundle is the quantity ΔK_0 . Clearly, the second term in 4.7.9 increases as $t \rightarrow \infty$, though slower than the plane wave width $\Delta r \sim K_0 t$. The characteristic shape in a steady cylindrical wave is derived from 4.7.9 by substituting x for t at $\nu = 1$ and $K = \tan(\theta + \alpha^*)$.

We note that formula 4.7.5 is also applicable to waves induced by a small roundness of the corner. Far from the body, where the wave width considerably exceeds its initial value, the wave slightly differs from a centered one characterized by an effective value r_0 .

The results obtained are easily generalized to more complicate functions $Q^{(\text{eff})}$ (see 4.7.1) which have the meaning of inner sources of disturbances. To show this, it is sufficient, for example, to represent these functions in the form $Q_r^{(\text{eff})} = \alpha_\theta \Delta\theta + \alpha_p \Delta p$, $\alpha = \alpha(x, r)$ and using integral 4.7.2 to solve the compatibility Equation 4.7.1 along the characteristics of the other family.

4.7.3 Short Wave/Contact Discontinuity Interaction

Let short waves of disturbances I and II be incident on either side of the segment 1–3 of a streamline ab separating regions I and II in Figure 4.13a; we will specify the intensities of these waves by the pressure differences $p_2 - p_1$ between points 2 and 1 in region I and $p'_2 - p_1$ between points 2' and 1 in region II, on the second- and first-family characteristics 2–1 and 2'–1, respectively. In region I we will consider a triangle 1–2–3, so small that the coefficients of Equation 4.7.1 could be assumed to be constant within it. Then, writing down the difference counterpart of Equation 4.7.1 along the first-family characteristic 2–3 (by analogy with 4.2.10) and subtracting the sum $Np_1 + \theta_1$ from either of its sides, we obtain the equations

$$\begin{aligned} \Delta L_{31} &= N(p_3 - p_1) + (\theta_3 - \theta_1) = \Delta L_{21} + Q^{(\text{ef})} \Delta l_{32} \\ \Delta L_{21} &= N(p_2 - p_1) + (\theta_2 - \theta_1) = \\ 2N(p_2 - p_1) - Q^{(\text{ef})} \Delta l_{21} &= 2(\theta_2 - \theta_1) + Q^{(\text{ef})} \Delta l_{21} \end{aligned} \quad (4.7.10)$$

Here, two last equations for the operator ΔL_{21} follow from Equation 4.7.1 for the second-family characteristic (first formula 4.7.10 in its original form is valid for any line 2–1). In view of the formulas 4.3.11 for the differentials dl_{\pm} , the quantities Δl_{32} and Δl_{21} are positive and, therefore, represent the lengths of the segments of characteristics 3–2 and 2–1.

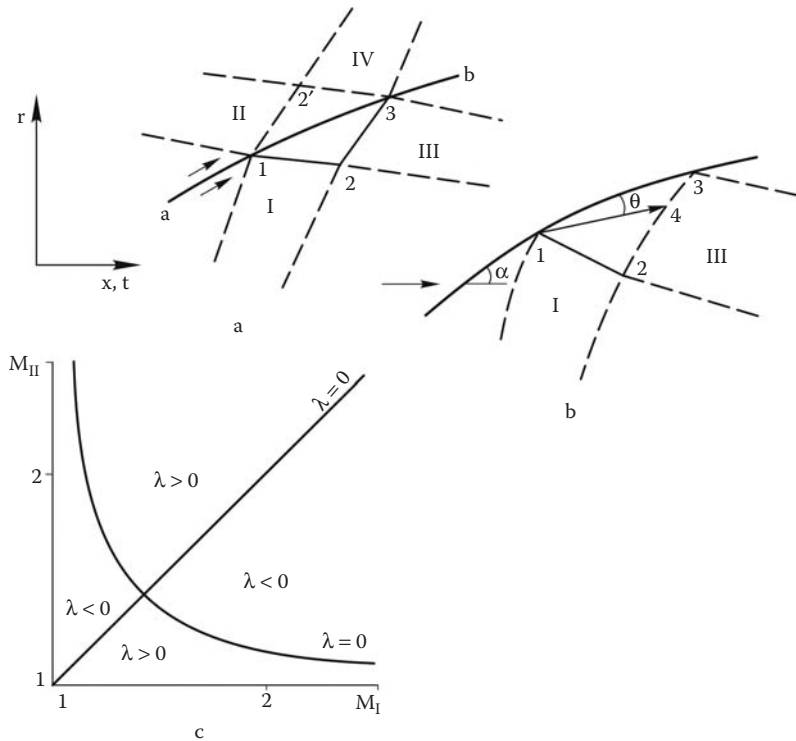


FIGURE 4.13
Interaction of disturbances with a contact discontinuity (a, c) and shocks (c).

Writing down the relations for the triangle $1 - 2' - 3$ in domain II, similar to 4.7.10, and taking into account the continuity of the pressures and the inclination angles on the contact discontinuity, we obtain a system of equations determining the flow parameters at point 3

$$\begin{aligned}
 N_I(p_3 - p_1) + (\theta_3 - \theta_1) &= 2N_I(p_2 - p_1) + Q_I^{(ef)} \Delta l_I^{(-)} = \\
 &\quad 2(\theta_2 - \theta_1) + Q_I^{(ef)} \Delta l_I^{(+)} \\
 \Delta l^{(-)} &= \Delta l_{32} - \Delta l_{21}, \quad \Delta l^{(+)} = \Delta l_{32} + \Delta l_{21} \\
 N_{II}(p_3 - p_1) - (\theta_3 - \theta_1) &= 2N_{II}(p'_2 - p_1) + Q_{II}^{(ef)} \Delta l_{II}^{(-)} = \\
 &\quad -2(\theta'_2 - \theta_1) + Q_{II}^{(ef)} \Delta l_{II}^{(+)}
 \end{aligned} \tag{4.7.11}$$

Since ab is a streamline, we have $\Delta l_{32} = \Delta l_{21}$ and $\Delta l^{(-)} = 0$. In the absence of a contact discontinuity ($N_I = N_{II}$, etc.), the disturbances can simply be summed up

$$p_3 - p_1 = p_2 - p_1 + p'_2 - p_1, \quad \theta_3 - \theta_1 = \theta_2 - \theta_1 + \theta'_2 - \theta_1 \tag{4.7.12}$$

In the general case the effects of the disturbances incident on either side of the discontinuity can be considered separately. Because of this, choosing wave I, that is, putting $p'_1 = p_1$

and $Q_{II}^{(eff)} = 0$ in system 4.7.11, we obtain the solution

$$\begin{aligned} p_3 - p_2 &= \lambda(p_2 - p_1), & p_3 - p_1 &= (1 + \lambda)(p_2 - p_1) \\ \theta_3 - \theta_2 &= -\lambda(\theta_2 - \theta_1) + (1 - \lambda)Q_I^{(ef)} \Delta l_{32} \\ \theta_3 - \theta_1 &= N_I(1 - \lambda)(p_2 - p_1) = (1 - \lambda)(\theta_2 - \theta_1 + Q_I^{(ef)} \Delta l_{21}) \end{aligned} \quad (4.7.13)$$

Here, the coefficient λ is as follows:

$$\lambda = \frac{N_I - N_{II}}{N_I + N_{II}} = \frac{M_{II}^2(M_I^2 - 1)^{1/2} - M_I^2(M_{II}^2 - 1)^{1/2}}{M_{II}^2(M_I^2 - 1)^{1/2} + M_I^2(M_{II}^2 - 1)^{1/2}} \quad (4.7.14)$$

Here, the latter formula is valid for a perfect gas only. The function λ is of alternate signs and $|\lambda| \leq 1$; on the lines $M_I = M_{II}$ (i.e., in the absence of the discontinuity) and $M_I^2 M_{II}^2 = M_I^2 + M_{II}^2$ we have $\lambda = 0$ (see Figure 4.13c in which the $M_I M_{II}$ plane is presented).

Clearly, the flow parameters at point 3 and the difference $p_3 - p_2$ expressed in terms of the difference $p_2 - p_1$ are independent of the function $Q^{(eff)}$; the difference $p_3 - p_2$ characterizes the intensity of the reflected wave III, λ being the *reflection coefficient*. The difference $p_3 - p_1$ is the intensity of the refracted wave IV with the *refraction coefficient* $1 + \lambda \geq 0$. For the disturbances of the angles θ , the reflection and refraction coefficients are the quantities $-\lambda$ and $1 - \lambda \geq 0$ with additional, internal sources of disturbances proportional to the function $Q^{(eff)}$.

Let us consider some examples. Let a wave interact with a rigid rectilinear wall ab (otherwise, a curved part itself would be a source of disturbances). In this case $\theta_3 = \theta_1$ and from the first relation 4.7.11 we obtain that the pressure disturbance is doubled, $p_3 - p_1 = 2(p_2 - p_1)$. The same result can be derived from 4.7.13 under the assumption that $\lambda = 1$ or $N_I \gg N_{II}$. In this case the reflected and incident disturbances are equal, $p_3 - p_2 = p_2 - p_1$. On the contrary, at $\lambda = -1$ we have $p_3 = p_1$, that is, the pressure disturbance is neutralized on the discontinuity, and $\theta_3 - \theta_1 = 2(\theta_2 - \theta_1)$, that is the angle disturbance is doubled (with a corresponding addition due to the function $Q^{(eff)}$). In accordance with 4.7.14, the value $\lambda = 1$ can be obtained, for example, by letting $M_{II} \rightarrow 1$ or $M_{II} \rightarrow \infty$ at a fixed value of M_I ; the case $\lambda = -1$ can be obtained when $M_I \rightarrow 1$ or $M_I \rightarrow \infty$ at a fixed value of M_{II} .

The analogous solution for the one-dimensional unsteady flow (or, in the limiting case, for the hypersonic flow on either side of a discontinuity with the same velocities $U_I = U_{II}$, Section 4.3) is very illustrative. In this case one should replace θ by v and N by $(\rho a)^{-1}$ in 4.7.11 through 4.7.14, which yields

$$\lambda = \frac{(\rho a)_{II} - (\rho a)_I}{(\rho a)_{II} + (\rho a)_I} = \frac{\rho_{II}^{1/2} - \rho_I^{1/2}}{\rho_{II}^{1/2} + \rho_I^{1/2}} \quad (4.7.15)$$

Here, the second equality is written for a perfect gas.

If a disturbance arrives at a denser medium, the inequality $\lambda > 0$ holds and vice versa. At $\rho_I \ll \rho_{II}$ (e.g., on reflection from a rigid wall) we have $\lambda \approx 1$, so that the pressure disturbance is doubled. At $\rho_I \gg \rho_{II}$, that is, at expansion into a vacuum, $\lambda \approx -1$ and $p_3 = p_1$, so that the pressure disturbance vanishes, while the velocity disturbance is doubled, $v_3 - v_2 = 2(v_2 - v_1)$. A typical example is provided by the air–earth (water) pair. Even the most intense, city-destroying earthquakes do not harm flying birds.

Finally, we will dwell on the disturbance reflection from the axis of symmetry. Let us consider the triangle 4 – 5 – 6 in Figure 4.12b; replacing the differentials in 4.7.4 by finite

differences, putting $\theta/r = \theta_5/r_5$, and taking into account the conditions on the axis, we arrive at the following relations

$$2\theta_5 = N(p_6 - p_5) = N(p_5 - p_4), \quad p_6 - p_4 = 2(p_5 - p_4) \quad (4.7.16)$$

that is, the disturbance incident on the axis of symmetry is doubled as in the case of its reflection from a rigid wall at $\lambda = 1$.

Naturally, this local analysis of the interaction of disturbances with a contact discontinuity holds only when the flow in region II is supersonic. Otherwise, the disturbance incident on region II propagates upstream within this region and, therefore, within region I as well. This problem will be treated in Section 5.8.

The only exception is provided by the limiting case in which the gas in region II is at rest, with a constant pressure $p = p_1$ and zero Mach number $M_{II} = 0$. On reflection from this contact discontinuity, the disturbance simply changes the sign, which corresponds to $\lambda = -1$.

4.7.4 Reflection of Disturbances from Sonic Lines

Let ab in Figure 4.13a be a sonic line, although in this case the figure is not absolutely accurate, since, as $M \rightarrow 1$, both families of characteristics are tangent to each other and to the line itself if it is normal to streamlines as in Figure 4.5c, Section 4.3, which is not shown in the figure. However, at present this circumstance is not of crucial importance. In this case the response of the flow in region II to disturbances cannot be determined as simply as earlier owing to the subsonic nature of the flow. However, irrespective of the disturbance of the sonic line shape, the speed of sound on it is equal to the critical velocity, $a = a^*$, which is constant in a perfect gas. In this case, the pressure is a function of the entropy s , $p = p^*(s)$, and $\partial p^*/\partial s < 0$. In a uniform isentropic flow $p^* = \text{const}$ and the first formula 4.7.11 gives the reflection coefficient $\lambda = -1$, as in the case of the reflection from a contact surface with a constant pressure in region II. In other words, disturbances incident on the sonic line change the sign on reflection.

At the same time, when the entropy varies along the sonic line, the given difference $p_3 - p_1$ in the previous relations should be considered as an additional disturbance imposed on the reflected one (as well as $\theta_3 - \theta_1$ on reflection from the wall). In this case the definition of the reflection coefficient as $\lambda = (p_3 - p_2)/(p_2 - p_1)$ is meaningless.

4.7.5 Flow behind the Point of the Flow Turn

By way of illustration, we will consider the flow behind a centered expansion wave (I in Figure 4.12), along the rectilinear wall Ol . We begin with the case in which the flow ahead of the corner point is plane and isobaric, though vortical, and the Mach number increases with the distance from the wall. The evolution of the initial (at the point O) disturbances in the centered wave I is determined by formula 4.7.3 and depends on the ratio N_0/N , the function N having a maximum $N = N_m = (2\gamma p)^{-1}$ at $M = \sqrt{2}$. Because of this, if we have $M = M_0 < \sqrt{2}$ on the wall, then the expansion wave is attenuated as r increases; therefore, in the wave the pressure increases, while the deflection angle θ decreases. Thus, waves II intersecting wave I are compression waves and are reflected from the rectilinear wall Ol again as compression waves III. In their turn, these waves interact with the subsequent compression waves II, which, in accordance with 4.7.12, leads to the pressure increase in the region downstream of wave I and along the surface Ol .

The pattern is opposite at $M_0 > \sqrt{2}$; in this case, the pressure decreases in wave I and downstream of it, including the surface Ol . If the point $M = \sqrt{2}$ is within wave I, then the pressure behind the corner point first increases and then decreases along the wall. The two cases are shown in Figure 4.12c.

Let now the earlier-considered axisymmetric flow, which is originally uniform and directed along the cylinder axis, turn either toward the axis of symmetry or away from it. In the former case, in accordance with Equation 4.7.5, the intensity of disturbances decreases in wave I; therefore, the pressure raises and waves II are compression waves. In this case the pressure increases along the wall Ol , that is, we deal with *cumulation* of disturbances with which we have already met in Chapter 2 (Figure 2.14). On the contrary, when the flow turns away from the axis of symmetry, as in a divergent nozzle, the pressure decreases in wave I, while waves II are expansion waves with the associated decrease in the pressure along the wall Ol . The two cases are shown in Figure 4.12d (curves 1 and 2).

4.8 Interaction of Sound and Shock Waves

In this section we will consider only the interaction of a solitary shock wave with an overtaking short sound wave.

Let ab in Figure 4.13b be a shock with a supersonic flow behind it and α be the angle at which the shock is inclined to the velocity vector of the incident uniform supersonic flow, the segment 1 – 3 of which is exposed to a short disturbance wave. In this case, the first relation 4.7.11 should be supplemented by the relations at a shock (Section 3.5), $p = p_s(\alpha)$ and $\theta = \theta_s(\alpha)$, or by the differences of the form:

$$\begin{aligned} p_3 - p_1 &= p'_s(\alpha_3 - \alpha_1), & (\theta_3 - \theta_1) &= \theta'_s(\alpha_3 - \alpha_1) \\ p'_s &= dp_s/d\alpha, & \theta'_s &= d\theta_s/d\alpha \end{aligned} \quad (4.8.1)$$

For unsteady waves here, as in formula 4.7.11, the quantities N^{-1} and θ should be replaced by ρa and v , while the derivatives p'_s and θ'_s should be replaced by $p'_D = dp_D/dD$ and $v'_D = dv_D/dD$, where $p_D(D)$ and $v_D(D)$ are the gas density and velocity behind the shock and D is the shock propagation velocity. As distinct from Figure 4.13a, in this case the segments of the characteristics are no longer equal, $\Delta l_{32} \neq \Delta l_{21}$, while $\Delta l^{(-)} = \Delta l_{34}$ is the length of the segment cut off Δl_{32} by streamline 1 – 4. Taking this into account and eliminating α or D from 4.8.1 we obtain relations similar to 4.7.13

$$\begin{aligned} p_3 - p_2 &= \lambda(p_2 - p_1) + \Delta p_Q, & p_3 - p_1 &= (1 + \lambda)(p_2 - p_1) + \Delta p_Q \\ \theta_3 - \theta_2 &= -\lambda_s(\theta_2 - \theta_1) + \Delta\theta_Q, & v_3 - v_2 &= -\lambda_D(v_2 - v_1) + \Delta v_Q \\ \lambda &= \lambda_s, \lambda_D, & 2N\Delta p_Q &= (1 + \lambda)Q^{(ef)} \Delta l_{34} \\ \lambda_s &= \frac{Np'_s - \theta'_s}{Np'_s + \theta'_s}, & \lambda_D &= \frac{p'_D - \rho a v'_D}{p'_D + \rho a v'_D} \end{aligned} \quad (4.8.2)$$

Here, the term Δp_Q is written only for steady-state shocks. Other terms, $\Delta\theta_Q$ and Δv_Q , which are not written here, can be derived in the same fashion. For normal gases (in the sense of Section 3.4) the derivatives p'_s , p'_D , and v'_D are positive; the inequality $\theta'_s > 0$ and, hence, $|\lambda| \leq 1$ corresponds to a supersonic flow behind the shock. The terms Δp_Q , $\Delta\theta_Q$, and Δv_Q make allowance for the flow nonuniformity effect on the shock evolution. At $Q = 0$

the function $Q^{(\text{eff})} \sim -vv/r$, so that the sign of the quantity Δp_Q is opposite to that of the radial velocity. In particular, in the situation presented in Figure 4.13b we have $v > 0$ and, therefore, the axial symmetry of the flow itself induces shock attenuation, as compared with plane flows.

Formulas for the reflection coefficients can be derived from the relations of Sections 3.3 to 3.5; here we will not present them, since they are too cumbersome. For weak shocks, using the quadratic formulas 3.7.3 and 3.7.4 and expanding the coefficients N and ρa in the pressure increment Δp across the shock, in the general case we obtain

$$\lambda_D, \lambda_s \sim (\Delta p)^2 \quad \text{or} \quad \lambda_s \sim (\alpha - \alpha^*)^2, \quad \Delta p \rightarrow 0, \quad \sin \alpha^* = M_1^{-1} \quad (4.8.3)$$

At the same time, weak shocks are isentropic and the previously mentioned quadratic formulas are the same for shock and continuous compression waves (Sections 3.4, 3.7, and 4.6) with a higher accuracy of the order $(\Delta p)^3$. For a perfect gas, the functions λ_s and λ_D are plotted in Figure 4.14. If λ_D is a decreasing function of D/a_1 , then the behavior of λ_s is more complicated and is characterized by the change of the sign. As the sonic point behind the shock is approached, the derivative θ'_s remains positive; therefore, for any bounded value of the Mach number ahead of the shock, $M_1 < \infty$, and $M_2 \rightarrow 1$ behind the shock the quantity $\lambda_s \rightarrow -1$.

At the same time, letting $M_1 = \infty$ and $k = k_0$ in formulas 3.5.4, 3.5.11, and 3.5.16, from 4.8.2 we obtain the limiting formula

$$\begin{aligned} \lambda_s = \lambda_{s\infty} &= \frac{\sqrt{2(\gamma - 1)} - \sqrt{\gamma(1 - k\eta^2)}}{\sqrt{2(\gamma - 1)} + \sqrt{\gamma(1 - k\eta^2)}} \\ k &= (\gamma - 1)/(\gamma + 1), \quad \lambda_{D\infty} = \lambda_{s\infty} \quad (\eta = 0) \end{aligned} \quad (4.8.4)$$

The curves $\lambda_{s\infty}(\eta)$ are also plotted in Figure 4.14a for different values of γ . At the sonic point, for $k\eta^2 = 1$, we have $\lambda_{s\infty} = 1$, while as $\eta \rightarrow 0$ we have $\lambda_{s\infty} \neq 0$, that is, at the extreme points of the interval $[0, \alpha_*]$ the limiting curve $\lambda_{s\infty}(\eta)$ does not coincide with the limiting values of the function $\lambda_s(\eta)$ for any large but finite M_1 . This is quite natural, since formula 4.8.4 is valid only for $M_1\alpha \rightarrow \infty$, while the applicability of our analysis is dubious in the case $M_2 \rightarrow 1$ in view of the fact that the displacement of the sonic point on the shock under the action of a disturbance incident on its vicinity is not taken into account.

As follows from Figure 4.14, for $\gamma = 1.4$ on a wide range of angles of attack far from the "sonic" value (see Section 3.5) the reflection coefficients of the disturbances incident on the shock (along characteristics 1 – 2 in Figure 4.15) are fairly small, say $|\lambda| < 0.1 – 0.15$. This makes it possible to neglect disturbances reflected from the shock, since for $\lambda = 0$ the Prandtl-Meyer wave proceeding from the wall would reach the shock without changing. For this reason, the flow downstream of the plane wedge-shaped nose of a two-dimensional airfoil near its curved afterbody and, generally, in the triangle 0 – 2 – 3 can be determined from the Prandtl-Meyer relations from Section 4.6 (shock expansion method, or SEM), at least, until a considerable vorticity induced by a fairly curved shock occurs in the flow. The efficiency of this method is demonstrated by the data presented in Figure 4.15.

We will now consider the case of *weak waves*. Their interaction seems to be impossible since in this case all the characteristics become almost parallel. However, in reality any shock overtakes and absorbs all preceding disturbances and, vice versa, all following disturbances overtake it (Sections 2.6 and 3.4). According to 3.4.23 and 4.6.11, a shock in the (x, r) or (t, r) planes (e.g., Oa in Figure 4.11 of Section 4.6) is the bisector of the angle between two characteristics, O_1a and O_2a , ahead of and behind the shock.

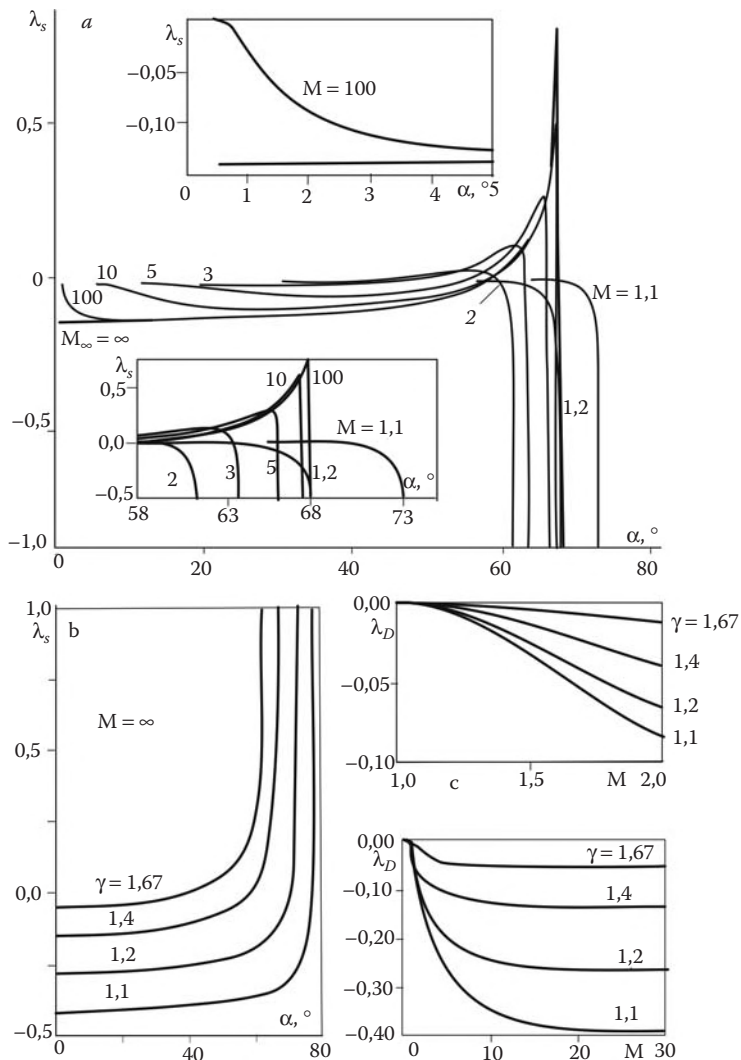


FIGURE 4.14
Coefficients of the disturbance reflection from steady-state (λ_s) and unsteady (λ_D) shocks.

Using this fact we are now able to elucidate an intractable question of the linear theory (Sections 2.5 and 2.8), namely, that of the disturbance decay in a flow past a thin airfoil or in a flow induced by a piston (Figure 4.11). The leading Oa and trailing Oc characteristics originating from the airfoil edges represent weak shocks interacting with each other and with expansion waves far from the body.

As an example, we consider a particular (but important for understanding the phenomenon) problem of the interaction of the bow shock and the centered expansion wave O_2ab originating from point O_2 under the assumption that there are no subsequent disturbances (Landau, 1944). This is the case of an airfoil in the shape of an infinite strip with a wedgelike nose or of a suddenly stopped piston.

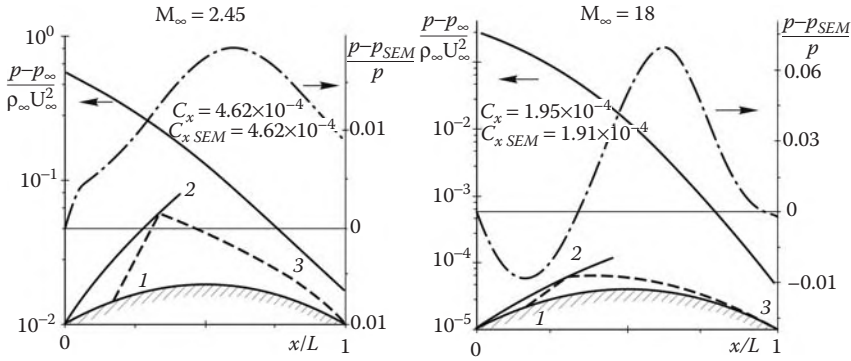


FIGURE 4.15
Shock-expansion method (SEM) accuracy.

On a weak shock the reflection coefficient $\lambda \approx 0$; therefore, an expansion wave reaches the shock without distortion and, hence, determines the parameters behind the shock in the interaction region ab . For an unsteady one-dimensional problem in a centered wave O_2ab the relation $v + a = (r - r_0)/(t - t_0)$, where t_0 and r_0 are the coordinates of point O_2 , holds along the curve ab . Putting $u = v$ and $a_2 = a$ in formula 3.4.23, as well as $t > t_a \gg t_0$ and $r > r_a \gg r_0$, where t_a and r_a are the parameters at point a , leads to the equation for the shock wave front r_s

$$\frac{dr_s}{dt} = D = \frac{1}{2}(a_1 + v + a) = \frac{1}{2}a_1 + \frac{1}{2}\frac{r_s}{t} \quad (4.8.5)$$

Hence follows

$$r_s = a_1 t + C_a \left(\frac{t}{t_a} \right)^{1/2}, \quad C_a = r_a - a_1 t_a$$

$$r_a = D_1 t_a, \quad t_a = (a_2 t_0 - r_0)(D_1 - a_2)^{-1}, \quad t \geq t_a, \quad r \geq r_a \quad (4.8.6)$$

Here, a_1 and a_2 are the speeds of sound ahead of and behind the shock.
Using formula 3.4.7 we obtain the law of the shock intensity decay

$$D - a_1 = v_{n1} - a_1 = \frac{1}{2}A \frac{p - p_1}{\rho_1 a_1} = \frac{1}{2}C_a \left(\frac{t}{t_0} \right)^{-1/2}, \quad t \geq t_a \quad (4.8.7)$$

Clearly, far from the body the shock slope tends to that of the leading characteristic, while the relative distance between them, $(r_s - a_1 t)/a_1 t$, decreases as $t^{-1/2}$.

In deriving similar dependences for axisymmetric ($\nu = 1$) and spherical ($\nu = 2$) flows a more general approach can be applied. Let us set $\Delta K_0 = K_0 - K_1$ ($K_1 = a_1$) in relations 4.7.7 through 4.7.9. Then we have

$$K = v + a = a_1 + \Delta K_0 \left(\frac{r}{r_0} \right)^{-\nu/2} \quad (4.8.8)$$

This is quite possible, since the flow parameters in weak shocks and simple waves coincide to small quantities of the third order (Section 4.6), so that the entire compression-expansion region $O_1O' O''$ in Figure 4.11 can be considered as a single simple wave without paying attention to characteristic intersection and shock formation. Here the quantity ΔK_0

is constant along characteristics given by formulas 4.7.9. The last terms in the formulas, together with $\Delta K_0/K_1$, are small, as in 4.8.8; however, one cannot neglect them since the deviation of these characteristics from the shock manifests itself in quantities of the same order, so that by omitting them one would make a large error in determining the point of intersection of these curves. Therefore, for solving Equation 4.8.5 (the first equality) we express the term $v + a$ in terms of 4.8.8 eliminating ΔK_0 in the latter formula by means of 4.7.9 and setting $r = a_1 t$ in the term $(r/r_0)^{-v/2}$. Thus, we obtain the following equations for the shock shape and intensity

$$\begin{aligned} \frac{dr_s}{dt} - a_1 &= \frac{d(r_s - a_1 t)}{dt} = \frac{1}{4t}(r_s - a_1 t), \quad v = 1 \\ r_s &= a_1(t - t_a) + r_a \left(\frac{t}{t_a} \right)^{1/4}, \quad D - a_1 = \frac{r_a}{4t_a} \left(\frac{t_a}{t} \right)^{3/4} \end{aligned} \quad (4.8.9)$$

$$\begin{aligned} \frac{dr_s}{dt} - a_1 &= \frac{r_s - a_1 t}{2t} \left(\ln \frac{a_1 t}{r_0} \right)^{-1}, \quad v = 2 \\ r_s &= r_a + a_1(t - t_a) + r_a \left(\ln \frac{t}{t_a} \right)^{1/2} \\ D - a_1 &= \frac{r_a}{2t} \left(\ln \frac{t}{t_a} \right)^{-1/2} \end{aligned} \quad (4.8.10)$$

Here, t_a and r_a are referred to as a point of the shock starting from which we can consider the assumptions made to be valid. We note that the quantity r_0 is not involved in these relations, which makes them to be of a general character. In particular, the relations remain valid when the corner of the body contour in Figure 4.11 is smoothed by a curve $O' O_2 O''$. Clearly, the shock decay rate grows as the space dimensionality is increased.

The results obtained within the framework of the unsteady analogy of Section 2.7 can also be extended to steady supersonic flows using the change of variables $t = x/U_\infty$, $a = U_\infty \sin \alpha^* = U_\infty/M_\infty$.

As for the flow past the airfoil or body of revolution presented in Figure 4.11 taken as a whole, the weak shock $O_4 c$ overtakes and absorbs the expansion wave proceeding from point O_3 ; in this case the shock intensity becomes zero. The problem of this flow may be of its own interest; however, it will not be considered here. We only note that the region $O' O'' O'''$ of the surface generates an expansion wave that overtakes the shock $O_1 a b$, reducing its intensity, which becomes zero in the limit.

The preceding provides an explanation to the observable “long-range action” (many kilometers) of the acoustic and even shock effect of supersonic aircraft.

4.9 Breakdown of an Arbitrary Discontinuity

To begin with, we consider a very simple time-dependent problem of the one-dimensional flow in a channel. At $t = 0$ on either side of a channel section I let there be the regions II and III with constant but different flow parameters. These can be the regions of a gas at rest or of constant-velocity flows. We shall call a flow occurring at $t > 0$ the *discontinuity breakdown* in section I. Some of the possible realizations of this process are sketched in

Figure 4.16, a to c. Clearly, either shocks or centered expansion waves are formed on both sides of the discontinuity depending on its initial parameters; thereupon they propagate with the formation of constant-parameter regions behind them (IV and V) separated by a contact discontinuity. The parameters in these regions are related to each other and the initial data by *equilibrium conditions*, or conditions of the *dynamic compatibility*, namely, the conditions of the pressure and velocity equality on either side of the contact discontinuity. These conditions can be symbolically written as follows

$$p_{IV}(II, u_{IV}) = p_V(III, u_V), \quad u_{IV} = u_V \quad (4.9.1)$$

Roman numerals in parentheses indicate the dependence of the functions on parameters in the corresponding flow regions. These dependences are determined by the relations for compression shocks (Sections 3.3 and 3.4) or rarefaction waves (Sections 4.5 and 4.6). The solvability of these problems is obvious from physical considerations.

These problems are widely met in *shock tubes*, which are test facilities for studying the high-temperature flow properties. A schematic diagram of such a setup is presented in Figure 4.16d. In this tube the compartments with pushing (II) and working (III) gases, initially at rest, are separated by diaphragm I, which breaks at a certain predictable pressure difference, $p_{II} > p_{III}$. In this case, the discontinuity breaks down in accordance with the diagram in Figure 4.16b., that is, an expansion wave VI with a constant-parameter region IV travels to the left, while a shock wave S with an adjacent constant-parameter region V propagates to the right. The latter region (a gas lock) is a region of high velocities and temperatures (up to 10^4 K). Modern measurement techniques make it possible to perform physical and gas dynamic investigations of gas locks in spite of short duration of the processes ($\Delta t \sim 10^{-5}$ s). To accelerate the gas in a gas lock multicasade schemes are used, for example, with one

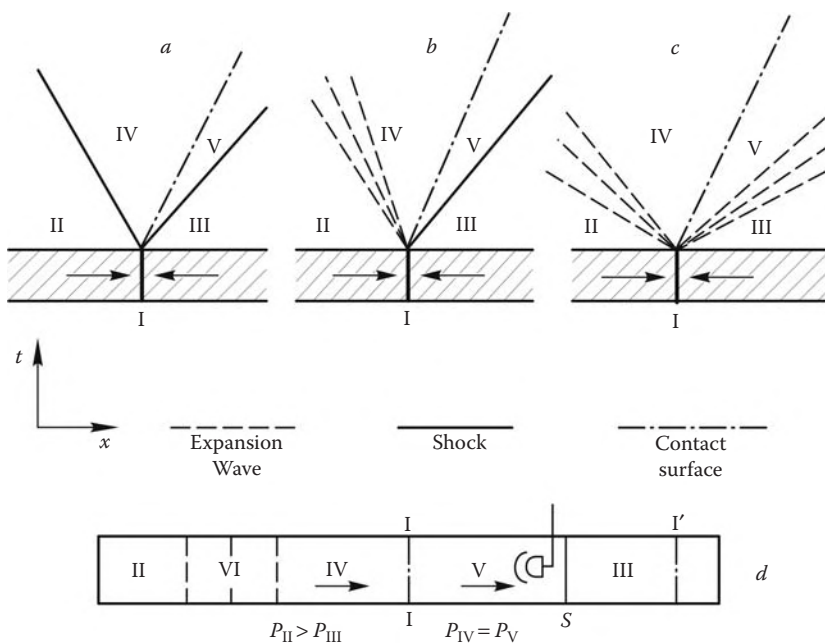


FIGURE 4.16

Time-dependent breakdown of arbitrary discontinuities (a, b, and c) and shock tube (d).

more diaphragm I' in front of the shock S and the breakdown of this new discontinuity in accordance with the scheme presented in Figure 4.16b.

We will now consider the steady discontinuity breakdown. We will distinguish interactions of *countermoving* and *overtaking* shocks (Figures 4.17a and 4.17b, respectively). Shocks 1 – 2 and 1 – 3 will be referred to as *primary*, or *incident*, since their slopes and parameters behind them (in regions II and III) are preassigned. *Secondary*, or *resulting*, waves (reflected or refracted) are to be determined. These can be shocks 1 – 4, centered expansion waves 1 – 5, and contact discontinuities 1 – 6. Moreover, for the sake of convenience, we will distinguish, likewise to the case of characteristics, the first- and second-family shocks in which the flow turns upward and downward, respectively (in the plane of the figure).

The dynamical compatibility relations between regions II and III for countermoving shocks and between regions I and III for overtaking shocks are reduced to the equality of the pressures and the flow directions in the regions IV and V on the contact discontinuity 1 – 6

$$\begin{aligned} p_V &= p_s(\text{II}, \theta_V) = p_{\text{IV}} = p_s(\text{III}, \theta_{\text{IV}}) \\ p_{\text{IV}} &= p_s(\text{I}, \theta_{\text{IV}}) = p_V = p_s(\text{III}, \theta_V), \quad \theta_{\text{IV}} = \theta_V \end{aligned} \quad (4.9.2)$$

Here, θ is the angle of the flow deflection with respect to the velocity vector in the outer flow I. The first and second equalities correspond to Figures 4.17a and 4.17b, respectively. In general the functions p_s are expressed in terms of the shock relations of Section 3.5 or those for centered expansion waves of Section 4.6. For shocks these functions were determined in parametric form, $p = p_s(\alpha)$, $\theta = \theta_s(\alpha)$, in Section 3.5; here, α is the shock slope. The solution of these systems determines the angles θ_i (or α_i) and the pressures p_i in secondary waves; other flow parameters in regions IV and V are determined in terms of θ_i and p_i .

We will describe briefly the properties of these solutions under the assumption that the flows behind secondary discontinuities are supersonic. Transitions III – IV and II – V for countermoving shocks always have the shock nature since they are generated by converging flows II and III.

On the contrary, discontinuity 1 – 5 in the overtaking shock interaction can be both a shock and an expansion wave. The weak shock 3 – 1 may be replaced by a weak compression wave, which, according to Section 4.8 (Figure 4.14), can be reflected from the main

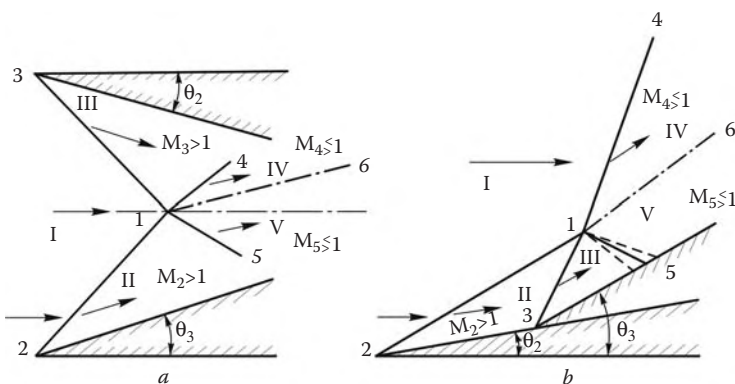


FIGURE 4.17
Examples of steady shock interference.

shock 2 – 1 – 4 both as an expansion wave and as a compression wave or a weak shock, as in the case under consideration. At the same time, at the interaction of strong waves the pressure on the double wedge is usually greater than on the single wedge whose slope is equal to the total slope of the double wedge (Section 3.7), that is, $p_{III} > p_{IV}$. In this case, as in the general case, the wave 1 – 5 must be an expansion wave. All these situations are demonstrated in Figure 4.17b.

Usually the solution of system 4.9.2 is very cumbersome even for a perfect gas. A rare exception is provided by the case of very weak shocks close to characteristics. Within the framework of the linear theory, $p_{IV} = p_{III} = p_I + N^{-1}\theta_{III}$ for overtaking shocks, so that discontinuity 1 – 5 does not exist at all (the coefficient N is determined by formula 4.3.11). Similarly, for countermoving shocks in the situation shown in Figure 4.17a, where $\theta_{II} > 0$ and $\theta_{III} < 0$, the following relations can be obtained

$$p_V = p_{IV} = p_I + N^{-1}(\theta_{II} + |\theta_{III}|), \quad \theta_{IV} = \theta_V = \theta_{II} - |\theta_{III}| \quad (4.9.3)$$

In a symmetric flow $\theta_{III} = -\theta_{II}$, $\theta_{IV,V} = 0$, and $p_{IV,V} - p_I = 2(p_{II} - p_I)$, that is, the pressure increment in a reflected shock is doubled, as in the case of short wave reflection from a wall (Section 4.7). As the incident shock intensity grows, the quantity $p_{IV,V}$ increases and follows in the supersonic flow the same laws as those obtained in Section 3.7 for double wedges.

In view of the two-valuedness of the function $p_s(\theta)$, the secondary shocks 1 – 4 or 1 – 5 may belong both to the weak and strong branches (in the sense of Section 3.5). The flow is usually supersonic behind the former and always subsonic behind the latter. As in the case of the flow past bodies, the choice of a reasonable flow scheme is determined by additional downstream conditions, for example, by the shape of the afterbody of a vehicle (not shown in Figure 4.17) whose nose has induced the primary shock.

The previous considerations relate to the breakdown of a discontinuity between supersonic flows II and III or I and III, as shown in Figures 4.17a and 4.17b, respectively. In these cases the number of resulting discontinuities (not counting the contact discontinuity) is equal to the number of primary ones (i.e., two). These shock interactions are referred to as *regular*, though frequently this term is referred only to the flows with secondary shocks of the weak branch (i.e., with supersonic flows behind shocks).

Let a shock 1 – 4 in Figure 4.18 with a subsonic flow behind it (no matter to which family it belongs) be attached to a shock 1 – 2 of the weak branch. There are no discontinuities in subsonic flows, so the quantities p_{IV} and θ_{IV} in region IV must be the same as in the region V behind the discontinuity 1 – 3, which is formed in the supersonic flow II. Only one (maybe two, due to the two-valuedness of the function $p_s(\theta)$) pair of values p_{IV} and p_{II} and shock angles α_{12} and α_{24} for shocks 1 – 2 and 1 – 4 corresponds to the compatibility relations at a triple point

$$p_{IV} = p_s(I, \theta_{IV}) = p_s(II, \theta_V) = p_V, \quad \theta_{IV} = \theta_V \quad (4.9.4)$$

One should bear in mind that state II depends only on state I and the angle α_{12} . Thus, *these shocks are interrelated and cannot be independently specified*. The secondary shock 1 – 3 (Figure 4.18) can belong to any branch; thus, in versions *a*, *b*, and *d* it belongs to the second, while in version *c* to the first family, the last version representing a particular case of overtaking shocks. In versions *b* and *c* shocks 1 – 4 belong to the first and in version *a* to the second families. In this regard, version *d* is intermediate; it is characterized by the fact that the flow in the zones IV and V retains its direction after the interaction.

The interaction of two given shocks with subsonic flows behind them is impossible, since one cannot construct discontinuities behind these shocks.

The graphical *shock polar method* is very illustrative in analyzing shock interference patterns, the examples of which are qualitatively illustrated in Figure 4.19. They represent

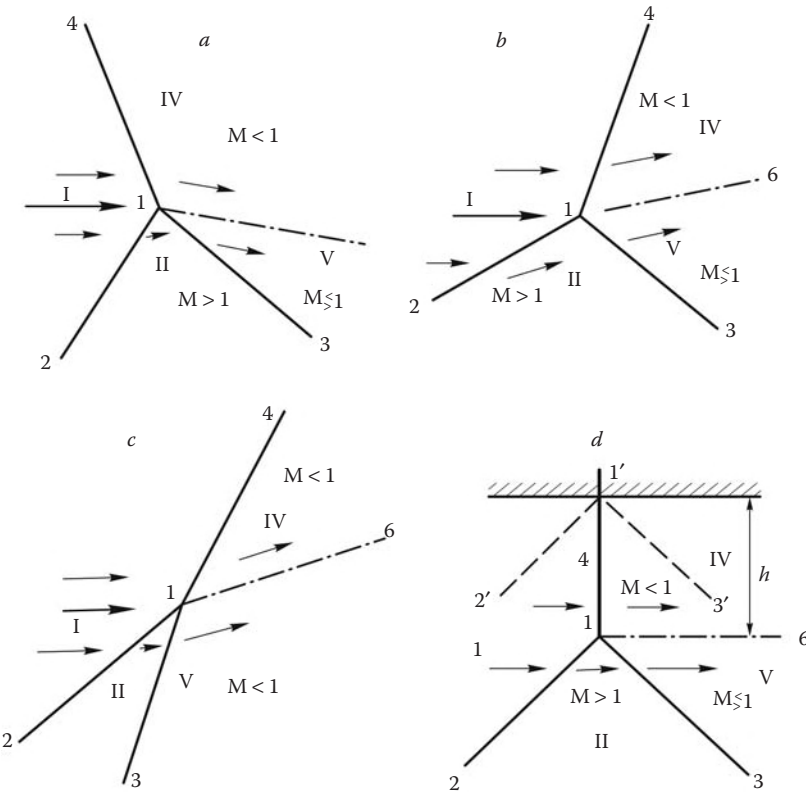


FIGURE 4.18
Shock configurations at triple points.

possible states behind a shock with a given initial state denoted by points 1 to 3 which relate to the regions I – III in Figures 4.17 and 4.18. These polar diagrams are symmetric about the vertical axis, their right and left sides presenting the shocks of the first ($\theta > 0$) and second ($\theta < 0$) families, respectively. The upper and lower parts of the polar diagram (above and below point O) correspond to the shocks of the strong and weak branches, respectively.

In solving interference problems for countermoving shocks the secondary polars II and III are attached to the primary polar I. Points 4 and 4' of the secondary polar intersections (Figure 4.19a) give the values of p and θ in regions IV and V in Figure 4.17a. For overtaking shocks at point 3 (Figure 4.19b) on polar II we construct polar III, whose points of intersection 4 and 4' with polar I give the values of flow parameters behind shock 1 – 4 (Figure 4.17b) if discontinuity 1 – 5 is a shock. Otherwise, transition from point 3 to point 5 of polar I is possible only along the descending curve $p(\theta)$ for the expansion wave 3 – 5 plotted in Figure 4.19c. Points 6₂ and 6₃ of intersection of polar I with the secondary polars II or III in Figure 4.19a or points 4 and 4' in Figure 4.19b correspond to states behind triple points.

Consider the interaction of symmetric countermoving shocks 2 – 1 and 3 – 1 in Figure 4.17a, which is equivalent to the reflection of one of these shocks, say, 2 – 1, from a rigid wall. The result of this interaction is represented by intersection points 5, 5' and 5_i, 5'_i, if they exist (cf. polar II₄), of polars II and II_i with the axis of symmetry of polar I (Figure 4.19a

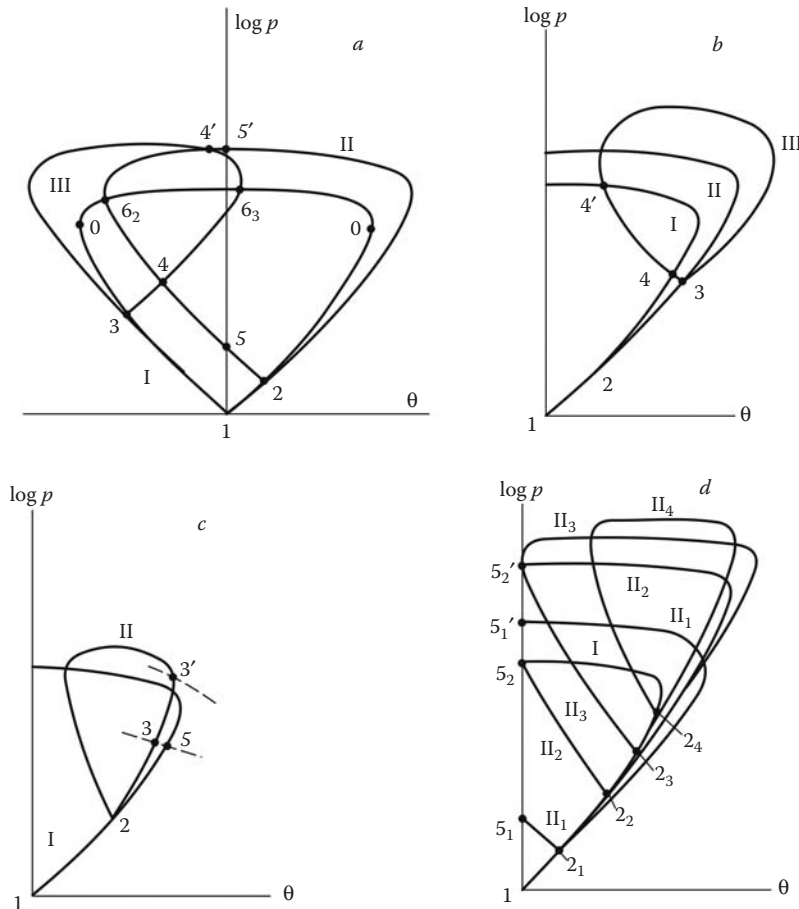


FIGURE 4.19
Types of shock polar diagrams.

and d). We note the case of polar II₂ (Figure 4.19d), the point 5₂ of which coincides with the upper point of polar I. This type of interaction is shown in Figure 4.18d; it is characterized by possible existence of both regular reflection of the shock 2' – 1' from the wall plotted in the same figure and the flow regime with a triple point 1, which is positioned at an arbitrary distance h from the wall.

This type of the relative position of shock polar diagrams results sometimes in rather paradoxical results. Consider polar II in Figure 4.19a with the initial point 2 close to point 1; the closeness of these points means that shock 2 – 1 in Figure 4.18a is weak. In this case, point 6₂ of intersection of this polar with polar I corresponds to a near-limiting slope of shock 1 – 4; therefore, when the weak shock 2 – 1 is incident, for example, on a normal shock ahead of a blunt body (Figure 4.20a), this can lead to a not so small local disturbance of the latter, as shown in Figure 4.20b. This brings up the question: how to relate this paradoxical result to the data of experiments in which undistorted shocks are observed even in wind channels where, as a rule, there are numerous small disturbances. The answer is that it is the distorted region extent rather than the shock shape distortion that vanishes together with the disturbance owing to the rapid decay of disturbances in the subsonic

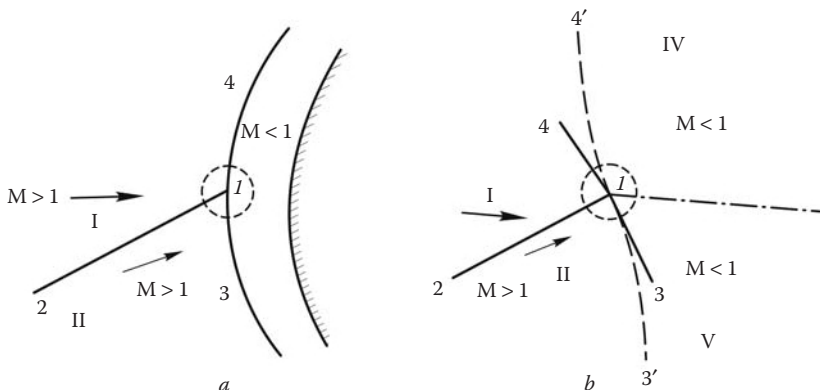


FIGURE 4.20
Interaction of weak and strong shocks.

flow behind the shock. As to accompanying entropy disturbances behind the shock, they are smeared due to viscosity effect. In Figure 4.20b we have plotted, though rather arbitrarily, the true position of the disturbed shock $4' - 1 - 3'$; the disturbed region is enclosed in a circle.

4.9.1 Irregular Shock Interactions

So far, only the point interactions of discontinuities satisfying conditions 4.9.2 or 4.9.4 were studied. However, these equations may have no solutions at all. The symmetric situation in Figure 4.17a is a very simple example; in this case a shock reflects from a wall at an angle θ_2 greater than the greatest possible flow deflection angle θ_0 across a shock in flow II. The flow with an attached shock past the wedge with this angle is impossible, so that polars II and III in Figure 4.19a do not intersect at all. In considering overtaking shocks we can imagine this situation assuming that the angle of the turn in the centered expansion wave $1 - 5$ (Figure 4.17b) is greater than the angle θ_0 for the external flow, even when the pressure p_{IV} is the same as behind the normal shock in flow I. In this case the corresponding trajectory of the expansion wave at point $3'$ (Figure 4.19c) cannot intersect polar I.

It is quite natural to ask what is the flow in this case. In a flow past a wedge with an angle $\theta > \theta_0$ a detached shock arises in front of the wedge, but in the case under consideration this shock interacts with primary shocks forming triple points that could be considered as modules in constructing a general irregular shock pattern. Thus, the *irregular*, or *Mach*, regime of shock interaction is formed whose integral part is a central Mach shock of the strong branch, or the *Mach disk*. The simplest version of this regime, namely, the reflection of shock 2 from a wall or an axis of symmetry at an angle greater than the limiting one, is presented in Figure 4.21 in which $1 - 0 - 1'$ is precisely the Mach disk. It is realized, in particular, in the case of jets, both plane and axisymmetric, issuing into an ambient constant-pressure medium at rest.

More complicated examples of irregular interactions given in Figure 4.22 relate to interference of shocks induced by a fuselage of supersonic or hypersonic aircraft, blunt edges

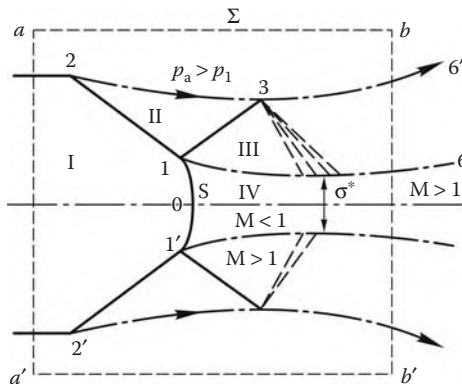


FIGURE 4.21
Overexpanded jet outflow.

of control surfaces and wings in planes of symmetry.* The first example, (a), is a non-symmetric version of the Mach interference of countermoving shocks similar to that in Figure 4.21. Two other examples (b and c) are associated with the interference of an incident shock $2 - 1$ and a shock $4 - 1 - 1' - 3$ detached from the wall. Version (d) relates to overtaking shocks. Its regular counterpart is shown in Figure 4.17b; in the case in which it cannot be realized, one must subsequently (from top to bottom) introduce three triple points ($1, 1',$ and $1''$) of the type shown in Figure 4.18. Only in such a way is it possible to satisfy the compatibility relations at each point. Generally, these configurations are very complicated and the procedure of their construction is difficult to formalize, thus requiring a great deal of imagination and scrupulousness.

We will call attention to two typical elements of the flow pattern presented in Figure 4.22d.[†] These are the secondary shock $1 - 5$ incident on a wall and a supersonic low entropy jetlet 6 containing numerous compression and expansion waves. Owing to, at least, three-fold passage across oblique shocks, the entropy of the jetlet is essentially lower than in neighboring regions and, hence, both the ram pressure and stagnation pressure are higher. Generally speaking, the formation of low-entropy jetlets is typical of shock interference and frequently leads to serious problems (especially concerned with heat transfer) when jets are incident on obstacles. However, this situation is not necessarily realized, since this sufficiently narrow jet can be swept away from the body due to the pressure difference $p_{III} - p_{IV}$ (in Figure 4.22c both cases are shown).

Let us make an important remark. The effect of the irregular configuration formation is of threshold nature (as for a wedge with an angle θ close to the angle θ_0 of the maximum flow deflection, Section 3.5), that is, the interaction may be either regular or irregular and has no intermediate stages. However, the widths of both jets, low entropy $1 - 1'$ and subsonic $1' - 1''$ (Figure 4.22d), decrease with the body slope β and they are carried by the flow. The expansion wave 7 tends to a centered one, thus attenuating the shock $1 - 5$ until it vanishes. Thus, a smooth passage from one regime to the other is provided.

* The classification of these interaction patterns was given by Edney (1968) and Roslyakov, Starykh, and Uskov (1987).

[†] See, for example, Zemlyanskii, Lesin, Lunev, and Shmanenkova (1982).

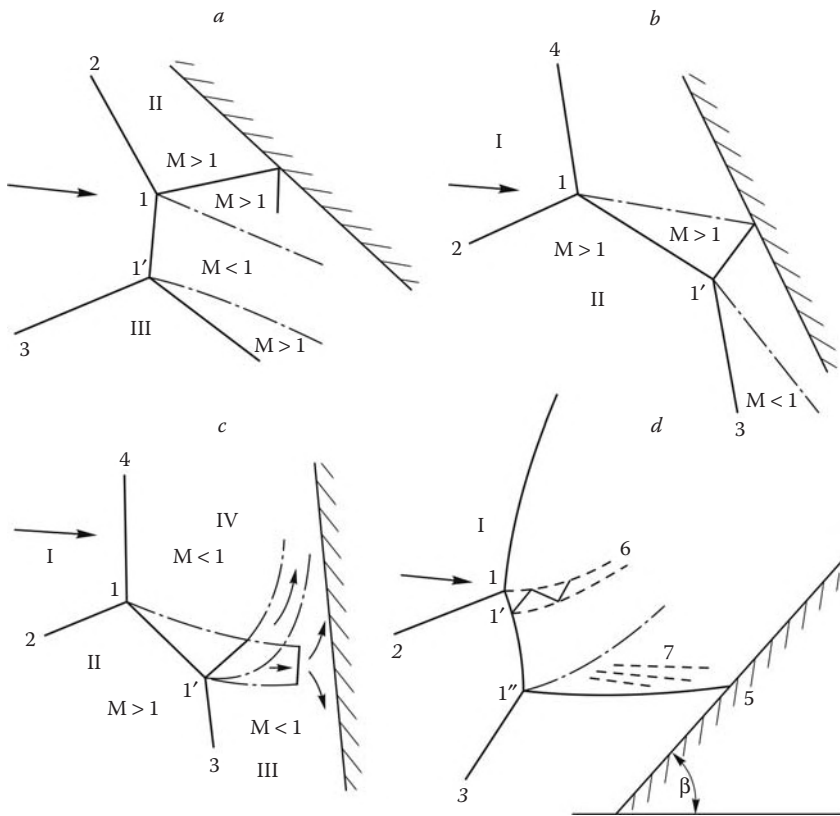


FIGURE 4.22
Types of irregular interaction of shock waves.

We note, however, that the threshold at which the irregular shock interaction arises, as determined from the greatest possible flow deflection across a shock, is actually only the upper theoretical limit. For example, in the case of the shock reflection from a wall, the triple configuration with a Mach disk arises often already when the regime of the type presented in Figure 4.18d is attained. This regime corresponds to points 2_2 and 5_2 of polar II_2 in Figure 4.19d (*the von Neumann criterion*), while the reflection regimes represented by segments $2_2 - 2_3$ become unstable and are not realized at all. In this case the normal shock I – 1 in Figure 4.18d is replaced by a curvilinear Mach disk.

Finally, the flow behind a Mach disk (as well as behind all the shocks of the strong branch) is subsonic, so that special conditions are required to maintain it. Therefore, the dimensions and shapes of such shock patterns cannot be governed only by local interaction conditions and are also determined by downstream conditions and, possibly, by dissipation effects. Such examples will be given in Section 5.5.

4.10 Disturbances in Thin Layers

In Section 4.7 the propagation of disturbances across isolines in a nonuniform flow was considered. We will now study the propagation of longitudinal disturbances under the same

conditions. Such phenomena occur in nature, for example, in the case of sound propagation in a relatively warm (cool) atmospheric boundary layer. Similar situations also occur in certain three-dimensional hypersonic flows around blunt bodies (the latter problem will be considered in detail in Section 9; see also Lunev, 1965). However, certain effects associated with this question will be discussed in the following with reference to the example of a limiting model problem.

Let a gas flow in a plane channel of constant width R (Figure 4.23) from left to right; the gas velocity in the lower sublayer of width δ is w . The density and speed of sound in the sublayer, ρ_2 and a_2 , differ from those, ρ_1 and a_1 , in the outer layer, that is, in the upper part of the channel. We assume that the inequalities $\rho_2 \ll \rho_1$ and $a_2 \gg a_1$ hold (i.e., the sublayer is highly heated). Initially all the quantities are constant and the gas in the outer layer is at rest. Such a flow could be obtained by suddenly shutting off a gas flow issuing from a slot in a baffle at $z = 0$ by a damper. It corresponds to the following conditions

$$t = 0, \quad z > 0, \quad f = f_A, \quad t > 0, \quad z = 0, \quad w = 0 \quad (4.10.1)$$

In a rigorous formulation the flow is described by the system of time-dependent equations (Section 4.4), while the disturbed region is bounded from the right by a characteristic surface $z^*(y)$ (Figure 4.23a) intersecting the lower surface of the channel along the bicharacteristic

$$z_0 = (w + a_2)_A t \gg z_1 = a_1 t \quad (4.10.2)$$

Here, the subscript A refers to the undisturbed gas in region A (Figure 4.23). In the thin sublayer $\delta \ll z_0$ we can neglect the transverse pressure difference, so that the equations of the gas motion in the sublayer (generalized one-dimensional equations of Section 1.2) take the form:

$$\begin{aligned} \frac{\partial \rho_2 \delta}{\partial t} + \frac{\partial \rho_2 \delta w}{\partial z} &= 0 \\ \frac{\partial w}{\partial t} + w \frac{\partial w}{\partial z} &= -\frac{1}{\rho_2} \frac{\partial p}{\partial z} = -\frac{a_2^2}{\rho_2} \frac{\partial \rho_2}{\partial z} \end{aligned} \quad (4.10.3)$$

From an equation similar to the latter equation it can be obtained that the induced longitudinal velocity in the outer layer is of the order $w_1 \sim (t/\rho_1)(\Delta p)/(\Delta z) \sim p/\rho_1 a_2$ if $\Delta p \sim p$ at a distance $\Delta z_2 \sim a_2 t$. Hence, a relative longitudinal displacement of gas particles is $w_1 t / \Delta z_2 \sim (a_1/a_2)^2 \ll 1$. In this case the longitudinal velocity of sound waves in the outer layer is relatively small and disturbances penetrate into it only through the sublayer, so that the gas in the outer layer and disturbances in it, as it were, remain in planes $z = \text{const}$.

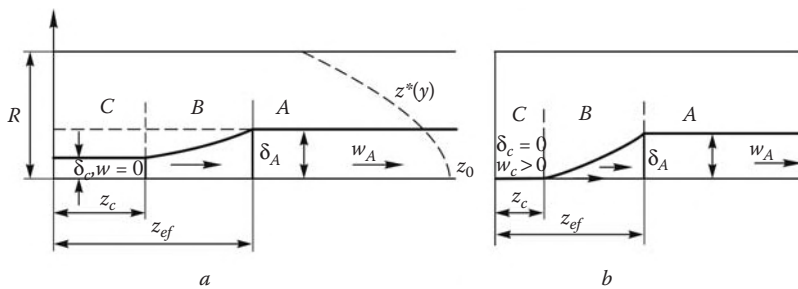


FIGURE 4.23
Disturbance propagation in a long channel with a heated sublayer.

System 4.10.3 involves two equations with respect to three unknown functions p_2 , w , and δ ; thus, one more relation should be obtained from the condition of the interaction between the inner and outer layers. In the rigorous formulation it could be derived from the condition of equal pressures on the layer-layer interface $y = \delta(t, z)$ and that of equal velocities normal to this surface. However, in order to obtain visible results, we will modify these equalities performing the analysis for the following flow regions:

1. The central region, where at $z = a_1 t \gg R$ the pressure is constant over the section $z = \text{const}$ due to multiple disturbance reflections from the channel walls.
2. An immediate front vicinity, $z \approx z_0(t)$, where disturbances in the outer layer on their reflection from the upper wall have not yet reached the sublayer boundary.

We will begin with the first region. Here the closure condition is obtained from the equation of gas state in the outer layer, where the mass is constant in each section $z = \text{const}$, and in the sublayer, where $\rho_2 \sim p^{1/\gamma}$:

$$p(R - \delta)^\gamma = p_A(R - \delta_A)^\gamma, \quad \rho_2(R - \delta) = \rho_{2A}(R - \delta_A) \quad (4.10.4)$$

Introducing a new unknown function, namely, the mass of the gas $m = \rho_2 \delta$, taking into account that $R \Delta \rho_2 = -\Delta m$, and using 4.4.10 we transform system 4.10.3 to the form:

$$\begin{aligned} \frac{\partial m}{\partial t} + \frac{\partial mw}{\partial z} &= 0, & \frac{\partial w}{\partial t} + w \frac{\partial w}{\partial z} &= -a_{\text{eff}}^2 \frac{1}{m} \frac{\partial m}{\partial z} \\ a_{\text{eff}}^2 &= a_2^2 \frac{\delta}{R} < a_2^2 \end{aligned} \quad (4.10.5)$$

The system differs from that for one-dimensional unsteady isentropic flows of Section 4.2 only in designations; therefore, it has the same characteristics 4.2.5 and compatibility relation 4.2.6 on them

$$\frac{dz}{dt} = w \pm a_{\text{eff}}, \quad a_{\text{eff}} dm = \mp mdw \quad (4.10.6)$$

The *effective speed of sound* a_{eff} is smaller (for $\delta < R$) than the thermodynamic one a_2 ; therefore, the disturbance front, $z_{\text{eff}} = (w + a_{\text{eff}})t$, propagates at a velocity that is less than the speed of sound. For the problem so formulated precisely this front separates the undisturbed (A) and disturbed (B) regions (Figure 4.23).

The compatibility relations 4.10.6 give integrals (the counterparts of the Riemann invariants) of the type of centered expansion waves with the same constant C_- determined on the forward front $z_{\text{eff}}(t)$

$$w - P_m = -C_- = w_A, \quad P_m = \int_{m_A}^m \frac{a_{\text{eff}}}{m} dm \quad (4.10.7)$$

Relations on rectilinear characteristics of the first family, $z/t = w + a_{\text{eff}}$, with constant w and a_{eff} close the problem.

Let $\delta \ll R$. Then the gas pressure and density are close to the initial ones, so that in evaluating a_{eff} and P we can set $m = \rho_{2A}\delta$ and $a_2 \approx a_{2A}$, which leads to the following form of formulas 4.10.7

$$2a_2 \sqrt{\frac{\delta}{R}} - w = 2a_2 \sqrt{\frac{\delta_A}{R}} - w_A \quad (4.10.8)$$

Setting $w = w_C = 0$ we obtain the relative sublayer thickness and the pressure in the central quiescent-gas region C with the leading characteristic z_C (Figure 4.23a)

$$\begin{aligned} w_C = 0, \quad \frac{\delta_C}{\delta_A} &= \left(1 - \frac{w_A}{2a_{\text{eff},A}}\right)^2, \quad z \leq z_C = a_2 \sqrt{\frac{\delta_C}{R}} t \\ \frac{p_C}{p_A} &= 1 - \gamma \frac{\delta_A}{R} \left(1 - \frac{\delta_C}{\delta_A}\right) \end{aligned} \quad (4.10.9)$$

The solution is similar to that for the standard centered Riemann wave in one-dimensional channel flows. However, at $w_A \geq 2a_2(\delta_A/R)^{1/2}$ it becomes meaningless and must be replaced by the following one

$$\delta_C = 0, \quad w_C = w_A - 2a_{\text{eff},A} > 0, \quad z \leq z_C = w_C t, \quad \frac{p_C}{p_A} = 1 - \gamma \frac{\delta_A}{R} \quad (4.10.10)$$

In this case the gas outflows from the sublayer completely (Figure 4.23b) and the characteristic z_C is, at the same time, a closing trajectory of particles.

A decrease in δ in a centered expansion wave is accompanied by the pressure decrease in the center region determined by formulas 4.10.9 and 4.10.10. Thus, the gas in the sublayer spreads, as it were, by its own momentum in spite of a counterpressure gradient. For this reason, such a gas spreading is termed *inertial*; it will be frequently used in what follows in analyzing three-dimensional supersonic flows.

The question arises as to what happens between the true disturbance front and the effective front z_{eff} , which appears only owing to asymptotic degeneration of the problem. To answer this question, let us analyze the solution in an immediate vicinity of the true front $z_0(t)$. As the sublayer thickness δ varies, a disturbance wave propagates upward into the outer layer; this wave may be considered to be a one-dimensional linearized wave (in a plane $z = \text{const}$) with the condition on the sublayer boundary in the form $\Delta p = \rho_1 a_1 \dot{\delta}$ (Sections 2.5 and 4.2). To clarify the problem it is sufficient to restrict oneself by the case of small velocity, $w \ll a_2$, which makes Equation 4.10.3 to be linear

$$\frac{1}{\rho_2 a_2^2} \frac{\partial \Delta p}{\partial t} + \frac{\partial w}{\partial z} = -\frac{1}{\delta} \frac{\partial \delta}{\partial t} = -\frac{\Delta p}{\rho_1 a_1 \delta}, \quad \frac{\partial w}{\partial t} = -\frac{1}{\rho_2} \frac{\partial \Delta p}{\partial z} \quad (4.10.11)$$

The compatibility relations for this system have the general form 4.2.6. As in Section 4.7, in the vicinity of the short wave front the integral

$$\Delta p - \rho_2 a_2 \Delta w = 0 \quad (4.10.12)$$

is valid along second-family characteristics. Eliminating w from the compatibility relation 4.2.6 along a first-family characteristic we obtain the equation and its solution

$$\frac{d \Delta p}{dt} = -\frac{1}{2} \frac{\rho_2 a_2^2}{\rho_1 a_1 \delta} \Delta p = -\frac{1}{2} \frac{a_1}{\delta} \Delta p, \quad \frac{\Delta p}{(\Delta p)_0} = \exp(-a_1 t / 2\delta) \quad (4.10.13)$$

Clearly, each initial disturbance in a short wave near the front decays with time and, therefore, it is the characteristic z_{eff} that becomes with time the real disturbance front, though smeared by disturbances induced ahead of it.

4.11 Shock Front Equation

In Section 4.8 the decay of weak shocks was analyzed on the basis of Equations 4.8.5 through 4.8.10, which will be referred to as the *equations of shock front propagation*. They follow from the relations on shocks and along sound waves overtaking the former. In what follows we will introduce a more general shock front equation for two-dimensional unsteady waves traveling through a gas at rest in a (y, z) plane in accordance with an $y = R(t, z)$ law. This equation can be useful both in analytical studies and for substantiating the correctness of numerical methods for solving gas dynamic hyperbolic problems.

We will write, first, the equation for the one-dimensional problem with a shock $y = R(t, 0)$ shown as curve ab in Figures 4.24a and 4.13b. To do this, we apply the compatibility relation 4.2.6 to interval 2 – 3 of the first-family characteristic plotted in the same figure. This leads to the counterpart of Equation 4.7.10

$$\begin{aligned} p_3 - p_1 &= \rho a(v_3 - v_1) = \Delta L_{21} + \rho a^2 Q_{\text{eff}} \Delta t_{32} \\ \Delta L_{21} &= p_2 - p_1 + \rho a(v_2 - v_1), \quad \Delta t_{32} = t_3 - t_2 \end{aligned} \quad (4.11.1)$$

Here, the term ΔL_{21} is assumed to be known from the preceding (in time) solution and point 2 is arbitrarily located on the first-family characteristic 2 – 3 on which the compatibility relation was used in deriving this equation. We write down the relations on the shock in the plane $z = 0$

$$\begin{aligned} v &= D(1 - k), \quad k = \rho_\infty / \rho, \quad D = R_t = \partial R / \partial t \\ p &= p_\infty + \rho_\infty D^2(1 - k) = p_\infty + \rho_\infty v D \end{aligned} \quad (4.11.2)$$

Here, the subscript “ ∞ ” refers to the undisturbed flow parameters. Thence it follows

$$\begin{aligned} p_3 - p_1 &= p'_D R_{tt} \Delta t, \quad v_3 - v_1 = v'_D R_{tt} \Delta t \\ \Delta t &= t_3 - t_2, \quad v'_D = dv / dD \\ p'_D &= dp / dD = \rho_\infty(v + Dv'_D) \end{aligned} \quad (4.11.3)$$

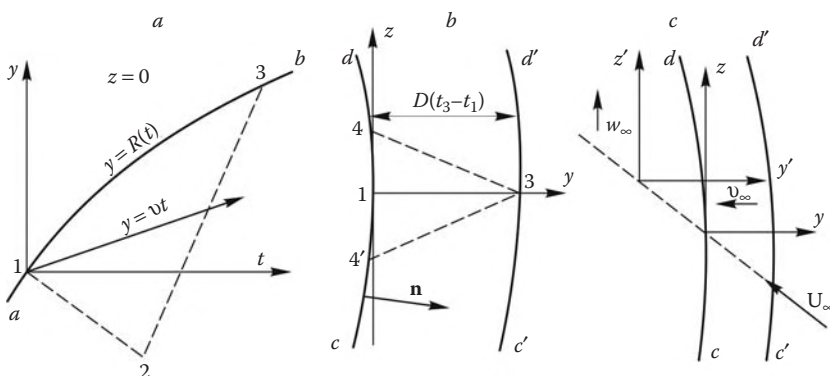


FIGURE 4.24
On the derivation of the shock front equation.

Let $\Delta t \rightarrow 0$; then we can reduce Equation 4.11.1 to the required differential equation

$$\begin{aligned} \kappa \frac{\partial^2 R}{\partial t^2} &= \omega - \rho a^2 \Delta Q_{\text{eff}}, & \kappa = p'D + \rho a v'_D \\ \omega &= \lim \frac{\Delta L_{21}}{\Delta t}, & \delta = \lim \frac{\Delta t_{32}}{\Delta t}, & \Delta t, \Delta t_{32} \rightarrow 0 \end{aligned} \quad (4.11.4)$$

As noted previously, point 2 is taken arbitrarily; however, if interval 1 – 2 belongs to a second-family characteristic, then from the geometry of triangle 1 – 2 – 3 and characteristic Equation 4.2.5, $dy/dt = v \pm a$, we can obtain

$$\delta = \frac{D + a - v}{2a} = \frac{a + kD}{2a} \quad (4.11.5)$$

As distinct from 4.8.5, Equation 4.11.4 is of the second order; however, for weak shocks overtaken by a centered expansion wave, $y/t = v + a$, it can be reduced to a first-order equation. In fact, in this case the functions $a(p)$ or $a(v)$ for shocks and simple waves coincide, so that, in view of equality $a + v + a_\infty = 2D$ (3.4.23) and condition $v \ll Dv'_D$, we obtain

$$\Delta L_{21} = 2\rho a \Delta v = 2\rho a B^{-1} \Delta(v + a), \quad p'_D = \rho a v'_D, \quad B = 1 + (da/dv), \quad v'_D = \frac{2}{B}$$

Then for $Q_{\text{eff}} = 0$ Equation 4.11.4 takes the form $R_{tt} = \frac{1}{2} \frac{d(y/t)}{dt}$ and, being integrated, it gives Equation 4.8.5.

We will now consider the two-dimensional problem, either plane or axisymmetric. As shown in Section 4.4, the compatibility relations (Equation 4.4.9) in the (y, z) plane have the same “one-dimensional unsteady” form (4.2.6) with aQ_{eff} replaced by \tilde{Q}_\pm defined by formula 4.4.9. Equation 4.11.1 can be applied to this problem. To simplify the form of the function \tilde{Q}_\pm we will fit the coordinate system (y, z) to the instantaneous form of the shock, $y = R(0, z)$ (cd in Figure 4.24b), directing the y axis along the normal to it. In the vicinity of the origin the deviation of the normal \mathbf{n} from the y axis is of the order of z^2 and within this accuracy we have $n_y = 1$ and $n_z = -R_z$, while the z -projection of the velocity \mathbf{U} behind the shock is

$$w = Dn_z(1 - k) = -vR_{zz}z \quad (R_z = \partial R / \partial z) \quad (4.11.6)$$

This quantity, as well as other coefficients, can be ascribed to the entire small triangle 1 – 2 – 3 and, hence, taking 4.4.3 into account we can put in the compatibility relations 4.4.9

$$\tilde{Q}_\pm = -a \left(Q + \frac{\partial w}{\partial z} \right), \quad \frac{\partial w}{\partial z} = -vR_{zz} \quad (4.11.7)$$

Since in this vicinity, as earlier, the shock velocity is $D = R_t$, we obtain, instead of 4.11.4, the following partial differential equation

$$\kappa \frac{\partial^2 R}{\partial t^2} - \chi \frac{\partial^2 R}{\partial z^2} = \omega - \rho a^2 \delta Q, \quad \chi = \rho a^2 v \delta \quad (4.11.8)$$

Since $\kappa, \chi > 0$, this equation is hyperbolic and has two wave characteristics

$$\frac{dz}{dt} = \pm a \beta, \quad \beta^2 = \frac{\rho v \delta}{\kappa} \quad (4.11.9)$$

The coefficient β is determined from Equations 4.11.2 and 4.11.5.

These characteristics cut off on the shock the domain of its influence on the solution at point 3. In the (t, y, z) space their projections onto the (y, z) plane (triangle 4–3–4' in Figure 4.24b) can be obtained by putting $y = Dt$ along the shock, so that we have

$$z = \pm\beta_1(y_3 - y), \quad \beta_1 = \bar{a}\beta, \quad \bar{a} = a/D \quad (4.11.10)$$

Then emitting the characteristic cone from point 3 backwards and letting $y = 0$ we obtain the domain of dependence of the solution at this point on the data on the wave cd

$$|z| \leq \beta y_3 = \beta D t_3 \quad (4.11.11)$$

We will evaluate the coefficient β for a perfect gas for which, according to 3.3.5 through 3.3.8, the following formulas hold

$$\begin{aligned} k &= \frac{\gamma - 1}{\gamma + 1} + \frac{2}{\gamma + 1}\bar{a}_{\infty}^2, \quad \bar{a}_{\infty} = a_{\infty}/D, \quad v = \frac{2}{\gamma + 1}D(1 - \bar{a}_{\infty}^2) \\ a^2 &= \gamma \frac{p}{\rho} = kD^2 \left(\frac{2\gamma}{\gamma + 1} - \frac{\gamma - 1}{\gamma + 1}\bar{a}_{\infty}^2 \right) \end{aligned} \quad (4.11.12)$$

Substituting these expressions into 4.11.9 yields

$$\beta^2 = \frac{(1 - \bar{a}_{\infty}^2)(\bar{a} + k)}{2\bar{a}[2k + \bar{a}(1 + a_{\infty}^2)]} \quad (4.11.13)$$

The dependence $\beta(\bar{a}_{\infty}, \gamma)$ is plotted in Figure 4.25. The quantity β is maximum at $\bar{a}_{\infty} = 0$, that is, as $D/a_{\infty} \rightarrow \infty$, and decreases monotonically as \bar{a}_{∞} increases; for all \bar{a}_{∞} and $\gamma > 1.32$ we have $\beta < 1$. However, for smaller γ (this is the case of hypersonic shocks, $D \gg a_{\infty}$, with physicochemical reactions behind them; cf. Sections 1.3 and 3.4) the parameter β may be greater than unity, for example, on the ranges $\bar{a}_{\infty} < 0.28$ at $\gamma = 1.1$ and $\gamma < 1.32$ at $\bar{a}_{\infty} = 0$; we note that at $\bar{a}_{\infty} = 0$ β increases without bounds ($\beta \sim k^{-1/4}$) as $\gamma \rightarrow 1$.

For weak waves ($D - a_{\infty} \ll a_{\infty}$) 4.11.13 is reduced to its limiting form

$$\beta^2 = (D - a_{\infty})/2a_{\infty} \quad (4.11.14)$$

and for $a_{\infty} \geq 0.8$ gives results close to exact ones. Clearly, $\beta \rightarrow 0$ as $D \rightarrow a_{\infty}$, that is, for an acoustic front the solution at point 3 is determined by the one-dimensional Equation 4.11.4 or by flow parameter distributions along the normal to the front. Of course, this conclusion is valid only for local properties of shock waves, but not for the inner flow region. We note, however, that in approaching this limit the domain of influence of point 3 shrinks very slowly, as $\beta \sim (D - a_{\infty})^{1/2}$.

We will now compare characteristics 4.10.10 with the wave characteristics proceeding from point 3; for this purpose we let $y = Dt$ in formula 4.4.8

$$\begin{aligned} z &= a\beta_2(t_3 - t) = \bar{a}\beta_2(y_3 - y) \\ a^2\beta_2^2 &= [a^2 - (D - v)^2] = a^2 - k^2D^2 \end{aligned} \quad (4.11.15)$$

For a perfect gas the curves $\beta_2(\bar{a}_{\infty})$ are shown in Figure 4.25 as well. For weak shocks we have

$$\beta_2^2 = 2(D - a_{\infty})/a_{\infty} \quad (4.11.16)$$

In this case the coefficient $\beta_2 = 2\beta$, that is, the shock region cut out by the characteristic cone, is twice as large as its dependence domain, both regions being infinitely small as

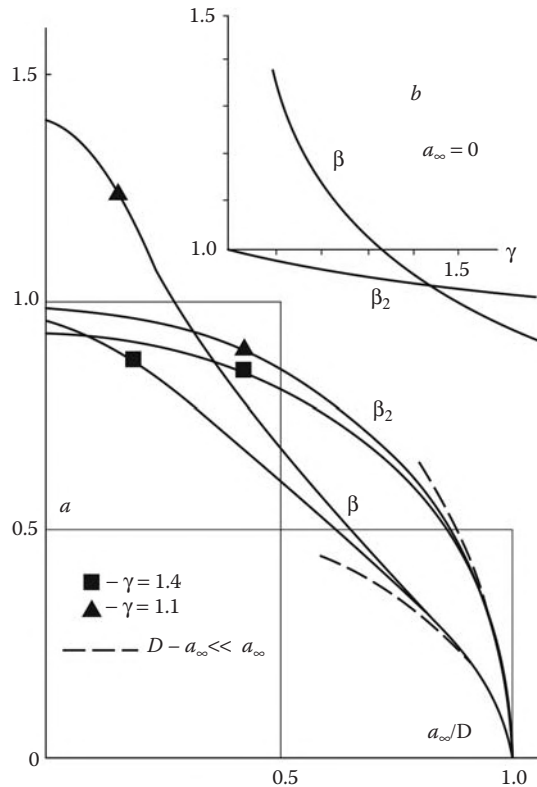


FIGURE 4.25
Coefficients β and β_2 in Equations 4.11.9 and 4.11.15.

$D \rightarrow a_\infty$. However, for strong waves the coefficient $\beta_2 = [(\gamma + 1)/2\gamma]^{1/2}$ is close to unity (in this case $\beta_2 \rightarrow 1$ as $\gamma \rightarrow 1$ and $\bar{a}_\infty \rightarrow 0$). The inequality $\beta_2 > \beta$ remains valid at $\gamma > 1.43$ for all \bar{a}_∞ . However, for smaller γ and strong shocks the inequality reverses sign.

Thus, under certain conditions the angular span of the domain of dependence of solution Equation 4.11.8 can exceed that of the characteristic cone in the internal flow region.

The equation obtained can be naturally generalized to the case of a shock propagating relative a fixed coordinate system (y, z) fitted to the instantaneous position of the shock at $t = 0$ (*cd* in Figure 4.24c) in a gas moving relative to the same fixed coordinate system at a velocity \mathbf{U}_∞ with the projections $-v_\infty$ and w_∞ onto the y and z axes. In this case in the coordinate system $y' = y + v_\infty t$, $z' = z - w_\infty t$ fixed to the undisturbed gas. Equation 4.11.9 retains its form, however, with the coefficients determined by the relative velocity $D' = D + v_\infty$ of the shock propagation. In the original coordinate system y, z this equation takes the form:

$$\kappa \frac{\partial^2 R}{\partial t^2} + 2\kappa w_\infty \frac{\partial^2 R}{\partial t \partial z} - (\chi - \kappa w_\infty^2) \frac{\partial^2 R}{\partial z^2} = \omega - \rho a^2 \delta Q \quad (4.11.17)$$

This equation has the characteristics $dz/dt = w_\infty \pm a\beta$, which are the natural generalization of characteristics 4.11.9.

An equation analogous to Equation 4.11.9 is also known for three-dimensional steady shocks with supersonic flow behind them (Lunev, 2000). The corresponding coefficient β is in this case smaller than unity for weak and greater than unity for strong shocks. We

note that the extension of the domains of influence and dependence of the solutions to the shock front equations as compared with those determined by the wave characteristic cone behind the shock (for $\beta > \beta_2$ or $\beta > 1$) can require the correction of the stability criteria for difference methods of the solution of inviscid problems, such as the Courant criterion (cf. Section 4.2).

In conclusion, we will make some general remarks on the shock propagation equations. The normal velocity D of the shock propagation is related with the front shape $y = R(t, z)$ in an arbitrary coordinate system by the differential equation

$$D = \frac{\partial n}{\partial t} = n_y R_t, \quad n_y = (1 + R_z^2)^{-1} \quad (4.11.18)$$

Here, n_y is the local normal projection onto the front and n is the distance along it. For an acoustic front $D = a$ and the shape of such a front is determined without solving the problem of the flow behind the front. At sound propagation in a highly nonuniform medium quite unusual shapes of the front (of the type shown in Figure 4.23a) are possible if the velocity w is taken to be zero. The problem of weak shock decay under the action of a centered expansion wave (Section 4.8) is a more complicated example; in this case one manages to express the shock velocity in terms of coordinates and time using the shock relations, which leads to analytic solutions of Equation 4.11.18.

Equation 4.11.18 describes not only shock propagation, but, for example, ablation fronts due to intensive aerodynamic heating. In a very simple formulation in this case we have $D = D(n_y)$, this equation being a nonlinear first-order equation of the type $R_t = \Phi(R_z)$ with sometimes nontrivial properties. A similar three-dimensional problem leads to partial differential equations of the type $x_{tyy} = x_{zzz}$ (Lunev, 1987).

The wave equation for a shock front was obtained previously. Clearly, the problems of propagation of shocks of various types lead to different types of equations of mathematical physics whose solutions have considerably different properties.

4.12 Waves in Anomalous Media

In Chapters 2 to 4 the analysis of wave processes was performed for normal gases and, in general, for media-satisfying conditions 3.4.1. In these media only compression shock waves, which possess properties A–E formulated in Sections 3.4 and 3.5, can occur. Thus, continuous compression waves have the property of convergence, while, on the contrary, rarefaction waves diverge in propagating. All the known gases and homogeneous liquids (which possess always a finite compressibility, which manifests itself at high compression) fall in this category. Moreover, most, if not all, solid substances (at least, metals) are found to belong to normal media, though at superhigh pressures far exceeding their elastic limits. Such pressures, of the order of 10^5 atm and higher, together with the accompanying high temperatures of several thousand degrees and more, are achieved at explosions in solid bodies or at high-speed impacts on bodies, for instance, at the impingement of space garbage elements or meteoroids on space vehicles (thus, at collision velocities of 5 km/s and higher, a pressure $p \sim 10^6$ atm is achieved in metals). In these conditions the behavior of such substances could be described by equations of state of the type $p = p(\rho, e)$, together with the inviscid gas dynamic equations. Then the whole general theory of wave processes outlined previously can be applied to these problems, though making allowance for their

specific features associated with fairly complicated forms of the equation of state (e.g., with a finite density at zero pressure, which differs qualitatively from the properties of gases).

However, in nature there are substances or media that do not obey these conditions; wave processes in such media are sometimes characterized by anomalous properties, qualitatively differing from those considered previously. First of all, these are condensed substances that undergo phase transitions accompanied on this range by an anomalous decrease in the speed of sound as the pressure increases at a constant entropy. These phases will arbitrarily be called "ice-water" phases (at standard conditions the speed of sound is about 4 km/s in ice and 1500 m/s in water).

In what follows we will outline some properties of wave processes in such media restricting ourselves to isolated examples that explain the essence of the problem within the framework of the gas dynamic model of these processes. A more detailed analysis of these effects could be found, for example, in Zeldovich and Raizer (1967).

The curves corresponding to the equations of state for these media can schematically be presented by piecewise-smooth curves. Thus, the isentropic curve of the $p - V$ diagram ($V = \rho^{-1}$ shown as curve II in Figure 4.26) consists of curve 1-2-3 corresponding to the "ice" phase, curve 5-6-8 for the "water" phase, and a rather arbitrarily chosen segment 3-4-5 of the two-phase state. Each of these regions can be considered to be normal from the standpoint of condition 3.4.1; however, in smoothing out region 2-3-5 by a single curve we obtain a region with the derivative $(\partial^2 V / \partial p^2) < 0$, which contradicts condition 3.4.1.

We will begin with shock waves. Now by curve II in Figure 4.26 is meant a shock adiabat, which is qualitatively similar to an isentrope. The slopes β of secants 1-6 and so on, connecting the states of media ahead of and behind the shocks, are determined in terms of the shock velocity D_{1i} from relation 3.4.4, where the subscript i refers to the state behind the shock ($D_{12} = v_{n1}$ in formula 3.4.4). For normal media (curve I in Figure 4.26) this secant

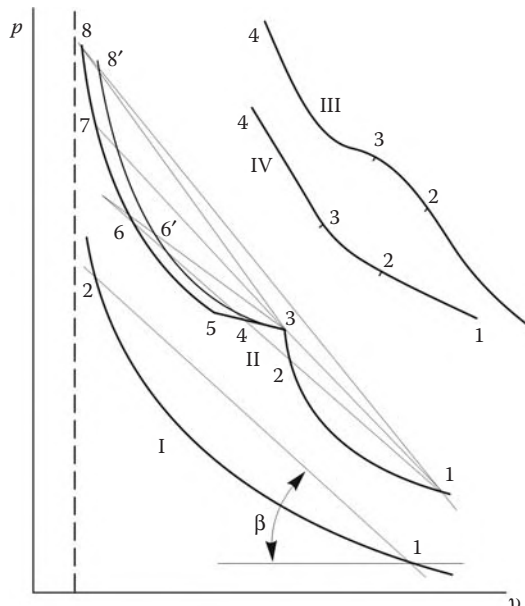


FIGURE 4.26
Shock adiabats and isentropes in normal and anomalous media.

intersects the adiabat—apart from point 1—only at one point 2, which ensures the uniqueness of the state behind the shock at this point and the uniqueness of the solutions of the shock equations. On the contrary, an indication of the anomalous nature of a medium is, in particular, the nonuniqueness of these solutions that can be realized for shock adiabats of type II. Here, the arc 1-2-3 presents the shock adiabat of “ice”; at point 3 the values p_3 , T_3 , and V_3 corresponding to the phase transition onset are achieved; the angle β_3 or the shock velocity D_{13} are maximum for this phase.

The last segment of curve II (i.e., arc 3-5-8), describes a two-phase medium and the “water” phase. In this case, secant 1-6 intersects the adiabat at points 2, 4, and 6; as $\beta \rightarrow \beta_3$, there are crossings at points 3 and 7 and only at $\beta > \beta_3$ or $D > D_{13}$ the solution of this problem is one-valued (point 8), as in the case of normal media.

Thus, for this shock adiabat there are several possible states behind a shock corresponding to a given velocity. To elucidate the situation, we will consider the following process. Let a piston gain jumplike the limiting velocity u_3 such that the limiting values of the parameters for the existence of the “ice” phase are realized behind the shock propagating at a velocity D_{13} . Similar to Section 2.6, we will impart a velocity increment Δu to the piston in a time interval Δt . This will generate an internal or *repeated* compression wave traveling at a velocity D_{3i} through the medium in the state 3; precisely behind this wave the previously mentioned phase transition is realized. Within the framework of a sketchy description of the problem we will assume that this transition occurs instantaneously, the “ice” state 3 being transformed to equilibrium states, namely, the two-phase state 4 and “water” state 6. This transition occurs following its own, *repeated* adiabat by which is arbitrarily meant curve 3 – 6’ – 8’ in Figure 4.26, without saying anything on the relative position of the two adiabats.

Let D_{3i} be greater than the shock velocity D_{13}^* relative to the gas behind the shock. This is fulfilled, for example, for secant 3-8. In this case, the repeated shock wave overtakes the leading shock and forms a single front with the latter; it should be expected that as $\Delta t \rightarrow 0$, that is, when an initial velocity $u = u_3 + \Delta u > u_7$ is imparted to the piston, a solitary shock wave is formed, whose velocity is determined by secant 1-8, where point 8 lies on the primary shock adiabat.

However, if $D_{3i} < D_{13}^*$, the repeated wave cannot overtake the leading shock; on the contrary, it will fall behind the latter. In this case, the total disturbance front consists of two successive fronts traveling at different velocities. This *shock front splitting* takes place also as $\Delta t \rightarrow 0$, that is, when a velocity $u < u_7$ is suddenly imparted to the piston. Only for $u > u_7$, that is, at shock velocity $D > D_{13} = D_{17}$, the two fronts coalesce at $\Delta t = 0$ and the substance under consideration behaves as a normal medium.

It is important to emphasize that the previously mentioned process with two fronts is essentially time-dependent; therefore, the steady-state conservation laws could not be written down for a control surface embracing the two fronts (Figure 1.16d in Section 1.7). Hence, a certain segment of the primary shock adiabat, namely, segment 3-5-7 to the left of point 3, cannot be physically realized in a solitary shock wave traveling in the medium with state 1.

We note that repeated shocks are characteristic of metals in which two successive compression fronts, elastic (or rapid) and plastic (or slow), are observed on the pressure range, on which the elasticity-plasticity transition occurs.

Now we will explain the process of formation of repeated shock waves by evolution of continuous compression waves. Let a piston accelerating in accordance with an $x = x_p(t)$ law compress a half-space $x \geq 0$ filled by a medium characterized by isentrope III in Figure 4.26. The piston trajectory is presented in Figure 4.27a; the points at the curve correspond to the states of the same name on isentrope III. In this case, as in a gas (Figure 4.8b) a simple

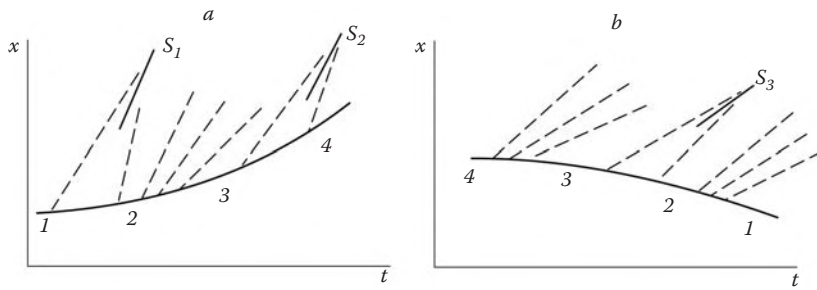


FIGURE 4.27
Different types of waves in anomalous media.

compression wave starts to propagate to the left, such that the characteristic slopes increase on the trajectory segment 1-2 when displacing to the right. In accordance with the theory of Section 4.5, this results in formation of a submerged shock S_1 . However, the speed of sound decreases on segment 2-3, while the derivative $\partial^2 V / \partial p^2 < 0$; hence, the characteristic slopes decrease here down to the “normal” region 3-4, where the slope starts again to increase. In this case, the converging characteristic bundles 2-3 and 3-4 initiate a repeated shock S_2 . If the slope of this shock is smaller than that of the shock S_1 , these shocks do not merge even at a decrease of the time interval $t_4 - t_1$, which will lead to formation of a pair of successive shocks, as was established previously in another way.

Let us now consider rarefaction waves induced by piston expansion in the medium under study (Figure 4.27b); the initial state is 4. In this case, this is a simple rarefaction wave that starts to travel to the right; the characteristic slope decreases on segment 4-3 and increases on segment 3-2. This leads to intersection of characteristics and, as a consequence, to formation of a submerged *rarefaction shock* S_3 , the states on either side of which are related by the same formulas of Section 3.3, however with the second group of inequalities 3.1.2, that is, with $p_1 \geq p_2$ and so on.

We note, however, that the shock nature of rarefaction waves is not innate to all two-phase media. Thus, for example, the isentrope of a “liquid-vapor” medium has a qualitatively different form IV, since the speed of sound of a liquid and, hence, the slope of isentrope 3-4, is considerably greater than that for vapor (segment 1-2). Correspondingly, the characteristic slope decreases in a characteristic bundle originated from the piston.

We note in conclusion that the previous analysis deals only with volumic waves and cannot be extended to waves in rods that are studied in the theory of elasticity, usually in the one-dimensional approximation; for this case there is its own, specific “quasi-one-dimensional” equation of state or the stress-strain relation.

5

Mixed (Subsonic–Supersonic) Flows

The properties of supersonic and subsonic flows were discussed in Chapter 2 with reference to some particular problems admitting very simple solutions. In Chapters 3 and 4 we studied local and certain general properties of both stationary supersonic and time-dependent subsonic flows, that is, hyperbolic problems. In what follows, we will consider certain properties of mixed flows containing both supersonic and subsonic zones, as well as transonic transition zones with the local Mach numbers $M \approx 1$. The same term *transonic* is reserved for the flows with the freestream Mach number $M_\infty \approx 1$.

5.1 Formation of Mixed Flows

The mixed flow zones occur, first of all, in the supersonic flow past blunt bodies with a subsonic flow behind the normal and near-normal bow shock and a supersonic flow behind its peripheral part (see, e.g., Figure 3.1 from Section 3.1). And, vice versa, local supersonic zones can arise in an originally subsonic flow. Thus, the maximum gas velocity in an incompressible flow past a cylinder is equal to the double freestream velocity, $U^{(m)} = 2U_\infty$ (cf. Section 2.10). Hence, at the same velocity distribution, the sonic velocity at $\theta = \pi/2$ is achieved already for $M_\infty \geq M_\infty^* \approx 0.5$. Under the same conditions, the critical Mach number for a sphere is $M_\infty^* \approx 2/3$.

Actually, the sonic velocity on a spherical surface is attained at even lower Mach numbers owing, in particular, to a decrease in the speed of sound, as shown by curves in Figure 2.18 from Section 2.10; these “compressible” curves are no longer symmetric, as they were in the case $M_\infty = 0$. Downstream of the sonic points, the pressure on the sphere continues to decrease, while the local Mach number M increases; however, approximately at $\theta \approx 130^\circ$ the pressure steeply increases and the flow becomes again subsonic. This is the manifestation of a shock smeared in the numerical calculation; the supersonic flow decelerates precisely across this shock.

This effect represents a compromise between two effects, which offset one another, and could roughly be explained as follows. On the one hand, in accordance with what was said in Sections 4.5 and 4.6, the supersonic wall flow, which streams along a convex surface, must constantly accelerate, while the pressure must diminish (cf. Figures 2.8 from Section 2.5, 2.14 from Section 2.7, and 4.15 from Section 4.8). But, on the other hand, the expansion of the external subsonic flow near the body base is accompanied by the pressure rise, so that, in accordance with Section 4.7, the reflection of disturbances from “subsonic” and, moreover, concave streamlines in the supersonic zone induces compression waves that cumulate to a shock. Obviously, the second effect is predominant.

Local supersonic zones also arise on thin airfoils, however, at higher subsonic Mach numbers M_∞ . In fact, at the upper point of an airfoil (Section 2.9) the velocity deficit is $U_\infty - u \approx 0.7\theta_0(1 - M_\infty^2)^{-1/2}U_\infty$. Letting $u = a_\infty$ in this formula we obtain an estimate for the conditions under which the sonic velocity is achieved: $1 - (M_\infty^*)^2 \sim \theta_0^{2/3}$. For this reason,

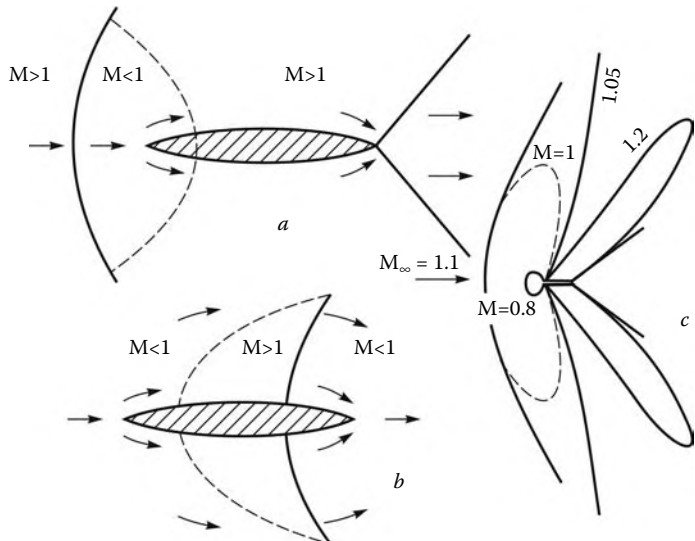


FIGURE 5.1
Spectra of the transonic flow past thin airfoils.

as the leading edge slope θ_0 and the Mach number M_∞ increase, the solution obtained in Section 2.9 is no longer adequate even qualitatively.

Mixed zones appear almost always in the transonic flow past even very thin bodies. Local supersonic zones in a subsonic flow were outlined previously. In a supersonic flow, as $M_\infty \rightarrow 1$, the limiting flow deflection angle decreases as $\theta_0 \sim (M_\infty - 1)^{3/2}$ (Section 3.5), so that in reality any sharp wing edge causes shock detachment (Figure 5.1a). Thus, sharp edges become stagnation lines like those considered in Section 2.11. The spectra of these flows are presented in Figure 5.1, a and b, while Figure 5.1c shows the Mach number contours, or isomachs, for $M_\infty = 1.1$.*

The velocity (Mach number) distribution over an airfoil presented in Figure 5.2a is very characteristic. At $M_\infty > 1$ the velocity increases along the wing in accordance with the laws of the supersonic flow past bodies. However, on the $0.75 < M_\infty < 1$ range the supersonic zone occurring outside the nose vicinity is terminated by a shock, across which the supersonic-to-subsonic transition occurs.

We note that this terminating shock can also be an effect of the flows converging at the trailing edge. That they cannot deflect in shocks “attached” to the trailing edge (shown in Figure 5.1a) can result in their upstream propagation. The same effect may also occur on a blunt body.

We note that the $M(x/L)$ curves presented in Figure 5.2a are weakly dependent on the freestream Mach number M_∞ along the full airfoil length for $M_\infty > 1$ and behind the closing shocks for $M_\infty < 1$, which is a particular manifestation of the *transonic flow stabilization law* (Diesperov, Yu. B. Lifshitz, and Ryzhov [1974]).

We also note that the flow spectra presented are in a sense ideal, that is, they do not allow for the shock-induced local viscous separation of boundary layers.

* The data presented in Figures 5.1 and 5.2 were kindly provided by Yu. B. Lifshitz.

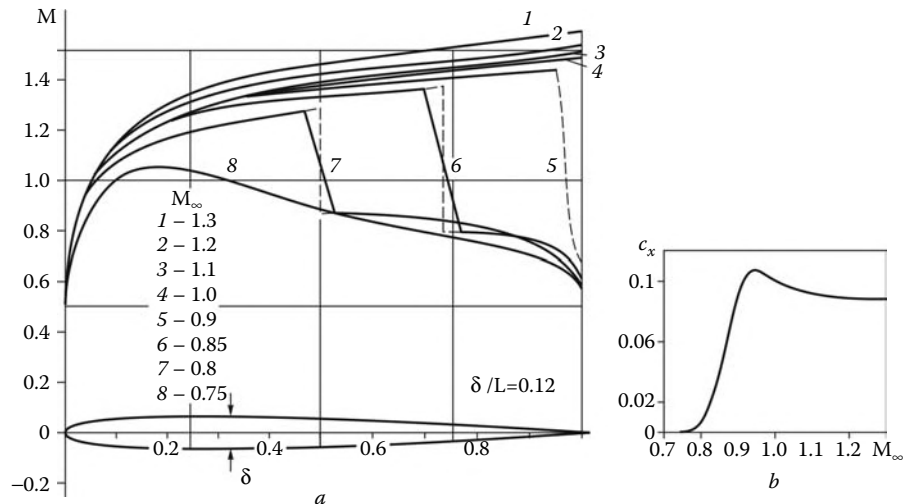


FIGURE 5.2

Mach number distribution over the NASA-0012 airfoil surface (a) and the airfoil drag coefficient (b).

Thence an important conclusion follows: as supersonic zones and terminating shocks appear in the flow past a body, the Dalembert theorem or paradox (Section 2.12) no longer holds. Really, the entropy s grows across shocks, so that after the passage of a shock the equation of state of a gas $\rho = \rho(p, s)$ no longer satisfies the barotropic condition $\rho = \rho(p)$ which lies in the foundation of the theorem. But it was shown in Section 3.6 that the drag of a body in an inviscid flow is expressed in terms of the entropy rise. Therefore, this drag appears always together with shock waves and precisely for this reason it is called the *wave drag*.

Thus, at $M_\infty < 0.75$ the wing airfoil drag (Figure 5.2b) is zero in accordance with the Dalembert theorem, since in this case the flow is potential. However, as M_∞ increases, shock waves are formed in the flow and the drag rapidly increases (although later, at $M_\infty > 1$, it is stabilized somewhat). Similarly, the drag coefficient of the sphere in Figure 2.23 sharply increases with M_∞ on the Re-range from 10^5 to 10^6 , where the viscosity effect is minimum, owing precisely to the wave drag. At the same time, the pressure on the spherical nose at $M_\infty \geq 3$ exceeds the static freestream pressure everywhere at $\theta \leq \pi/2$, while the base pressure p_d remains, as was shown experimentally, small, $p_d \leq p_\infty$, which leads to the stabilization of the drag coefficients at $M_\infty > 1$.

The appearance of a body drag must be accompanied by an asymmetry in the pressure distribution over the body surface, as it is the case in the supersonic flow (Figures 2.8, 2.14, and 4.15). However, the pressure curve on the wing airfoil in the subsonic flow with $M_\infty = 0.75$ is asymmetric in the absence of any drag (Figure 5.2a).

We will now dwell on the drag of thin bodies. It is of the order of $X \sim \theta^2$ for two-dimensional and θ^4 for axisymmetric bodies (Section 2.8). This result could not be derived using the control surface method, since the entropy increment Δs in a weak bow shock cannot be determined within the framework of the linear theory. In this case, the smallness of the increment $\Delta s \sim \theta^3$ is compensated by the extent of the disturbance propagation region, which is unbounded within the framework of the linear theory but becomes finite when the attenuation of the bow shock is taken into account (Section 4.8).

We note that here we have established only some reasons for the drag appearance. More particular laws and data on the body drag in supersonic flows will be presented in Chapter 7.

5.2 Transonic von Kàrmà̄n and Chaplygin Equations

The problem of the transonic flow around thin bodies outlined previously cannot be described by the linear theory of Chapter 2, since this theory, apart from an unlikely growth of the solution as $M_\infty \rightarrow 1$, rules out the presence of mixed flow zones owing to the constancy of the $M_\infty^2 - 1$ coefficient in Equation 2.7.3. At the same time, in the more exact Equation 2.4.9 (with the derivatives $\partial/\partial t = 0$) the higher-order derivative with respect to x has the coefficient $M^2 - 1$; in order to replace this coefficient in the process of linearization by the constant coefficient $M_\infty^2 - 1$, that is, to change over to Equation 2.7.3, it is necessary that the variation of ΔM^2 in the flow be small compared with the difference $1 - M_\infty^2$. By virtue of Equation 2.2.20, this requirement leads to the condition

$$(M_\infty^2 - M^2)\beta^{-2} = 2A_*\bar{p}_*\beta^{-2} \ll 1$$

$$\bar{p}_* = \Delta p/\rho_* a_*^2, \quad \beta^2 = |M_\infty^2 - 1|, \quad \Delta p = p - p_\infty \quad (5.2.1)$$

Here, the asterisked parameters are taken at the sonic point of the flow. For a perfect gas $2A_* = \gamma + 1$. However, in accordance with Sections 2.8 and 2.9, within the framework of the linear theory $\bar{p}_* \sim \theta/\beta$ for plane bodies ($\nu = 0$) and $\bar{p}_* \sim \theta^2 |\ln K|, K = \theta_0 \beta$ for axisymmetric bodies ($\nu = 1$). Thence we obtain the following restrictions on the maximum body slope

$$\theta_0 \ll \theta_0^* = \beta^3 / 2A_* M_\infty^2 \sim |1 - M_\infty^2|^{3/2}, \quad \nu = 0$$

$$\theta_0 \ll \theta_1^* = \beta |\ln K|^{-1/2}, \quad \nu = 1 \quad (5.2.2)$$

These restrictions are very strong, especially in two-dimensional flows (e.g., for $|M_\infty - 1| = 0.05$ the value of θ_0 must be at least smaller than 1° , which rules out the linear theory applicability to any realistic airfoils in transonic flow). At the same time, if this condition is violated, then the coefficient $M^2 - 1$ of the higher-order derivative may be not only variable but even have alternate signs, which results in the appearance of mixed flow zones, as described previously.

The unlimited growth of these solutions as $M_\infty \rightarrow 1$ requires accounting for nonlinear terms in the original Equation 2.4.8 for the potential. In this case, some alternatives seem to be possible. Thus, letting $M = 1$ in Equation 2.4.8 we obtain for plane flows

$$-2\bar{v} \frac{\partial \bar{v}}{\partial x} + \frac{\partial \bar{v}}{\partial y} = 0, \quad \bar{v} = \frac{v}{U_\infty} = -\frac{x - x_b}{2(y - y_b)} \quad (5.2.3)$$

Here, the velocity $v = U_\infty \bar{v}$ is constant along the characteristics of this equation (which are similar to the streamlines of Equation 4.1.3) passing through the points (x_b, y_b) on the airfoil contour. However, the pressure derived from the equation of motion for this velocity distribution increases as $\Delta p \sim \ln y$ far from the body. Hence, the term with $\partial^2 \varphi / \partial x^2$ omitted from Equation 5.2.3 plays the crucial role and must be retained even if its coefficient $M^2 - 1$ is small.

With these remarks in mind, the transonic small-perturbation theory for $\Delta M \sim M^2 - 1 \ll 1$ is constructed as follows. We discard all the second-order terms in Equation 2.4.8 and arrive at Equation 2.4.9 but with the coefficient $M^2 - 1$ dependent on Δp . To

do this, we will consider the small perturbations to be the deviations of the flow parameters from their critical, or sonic, values by letting

$$\begin{aligned} u_1 &= u - a_* = \frac{\partial \varphi}{\partial x} \ll a_*, & v &= \frac{\partial \varphi}{\partial r} \ll a_* \\ u_1 &\rightarrow U_\infty - a_*, & v &\rightarrow 0, & x &\rightarrow -\infty, & r &\rightarrow \pm\infty \end{aligned} \quad (5.2.4)$$

Then using Equations 2.2.20 and 5.2.1 we obtain

$$M^2 - 1 = -2A_* \frac{p - p_*}{\rho_* a_*^2} = 2A_* \frac{u_1}{a_*} \quad (5.2.5)$$

Then Equation 2.4.9 governing the transonic flow past thin bodies takes the form:

$$2A_* \frac{\partial \varphi}{\partial x} \frac{\partial^2 \varphi}{\partial x^2} = \frac{a_*}{r^v} \frac{\partial}{\partial r} \left(r^v \frac{\partial \varphi}{\partial r} \right) \quad (5.2.6)$$

This is the *von Kàrmàn equation* for thin bodies. It is valid in the vicinity of an internal sonic point in the flow if the x axis is aligned with the velocity direction at the sonic point.

An important consequence of this equation is the transonic similarity law for the flows past thin bodies of affinely similar shape. Let $\varphi = \kappa_\varphi La_* \varphi_t$, $r = \kappa_r L r_t$, and $x' = x/L$, where κ_φ and κ_r are certain coefficients to be determined, while the subscript t refers to dimensionless quantities, characteristic of transonic flows. For $\kappa_\varphi = \theta_0 \kappa_r$, θ_0 being the characteristic body slope, the boundary condition on the body $\partial \varphi / \partial r = a_* dr_b / dx$ takes the universal form $\partial \varphi_t / \partial r_t = dr_{bt} / dx'$. Transforming Equation 5.2.6 and putting the coefficient of its first term $2A_* \theta_0 \kappa_r^3 = 1$ we arrive at the following set of dimensionless variables

$$\begin{aligned} x' &= \frac{x}{L}, & r_t &= (2A_* \theta_0)^{1/3} \frac{r}{L}, & \varphi'_t &= (2A_*)^{1/3} \theta_0^{-2/3} \frac{\varphi}{La_*} \\ u'_t &= \frac{\partial \varphi'_t}{\partial x'} = (2A_*)^{1/3} \theta_0^{-2/3} \frac{u_1}{a_*}, & v' &= \frac{\partial \varphi'_t}{\partial r_t} = \frac{v}{\theta_0 a_*} \\ p'_t &= -u'_t = (2A_*)^{1/3} \theta_0^{-2/3} \frac{p - p_*}{\rho_* a_*^2}, & \theta' &= \frac{\theta}{\theta_0} \end{aligned} \quad (5.2.7)$$

In these variables, the equation for φ'_t has the same form as 5.2.6, provided $2A_* = 1$ and $a_* = 1$ in the latter equation.

Finally, from the freestream boundary condition $u_1 = u_{1\infty}$ and by virtue of 5.2.5 we arrive at the required similarity criterion

$$K_t = u'_{t\infty} = (2A_*)^{1/3} \theta_0^{-2/3} \frac{U_\infty - a_*}{a_*} = \frac{M_\infty^2 - 1}{(2A_* \theta_0)^{2/3}} \quad (5.2.8)$$

Relations 2.2.19 and 2.2.20 were used in the latter transformation. Clearly, this parameter includes—through the parameter A —the gas properties.

It is often convenient to refer the quantities p and u to the freestream rather than sonic values. By virtue of 2.2.20, the recalculation of the corresponding similarity variables reduces to formulas

$$\begin{aligned} p_t &= (2A_*)^{1/3} \theta_0^{-2/3} \frac{p - p_\infty}{\rho_* a_*^2} = p'_t + K_t \\ u_t &= (2A_*)^{1/3} \theta_0^{-2/3} \frac{u - U_\infty}{a_*} = u'_t + K_t, & u_t &\rightarrow 0, & x &\rightarrow -\infty \end{aligned} \quad (5.2.9)$$

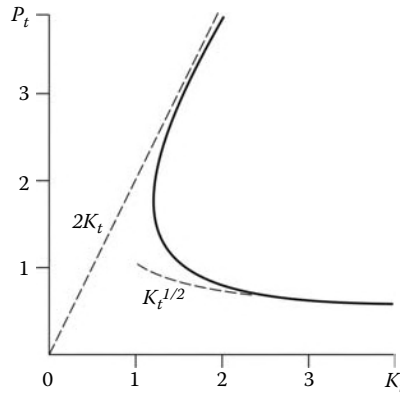


FIGURE 5.3
Pressure behind a shock in the similarity variables.

Other parameters in 5.2.7 do not change.

As for the dependences of the dimensionless quantities $p_t(K_t)$ and so on, they could be derived only by solving particular problems.

The similarity law derived can quite naturally be extended to the flows with shock waves (Figure 5.3). To demonstrate this, it is sufficient to write down relations 3.5.29 in similitude variables with the velocity deflection angle in the shock θ taken as the angle θ_0

$$p_t(K_t - p_t/2)^{1/2} = 1, \quad \omega_t = \omega(2A\theta_0)^{-1/3} = p_t^{-1} \quad (5.2.10)$$

The $p_t(K_t)$ curve is plotted in Figure 5.4; it embraces both branches of the shocks. As $K_t \rightarrow \infty$, relations 5.2.10 change over to the linear-theory dependence for a wedge, $p_t = K_t^{-1/2}$, and the relation at the normal shock, $p_t = 2K_t$.

The von Kàrmàn equation is widely used in theoretical studies, for example, of transonic flow asymptotics far from a body (Cole and Cook, 1986) or of local properties of transonic flows (see Section 6.3). At the same time, its applicability for calculating the flow past thin bodies is highly conjectured and, apparently, is restricted to a narrow range of supersonic flows with attached shocks. In other cases, the subsonic flow deceleration leads to near-zero velocities even on sharp edges and noses, thus bringing local disturbances beyond the small perturbation range with the same qualitative effect as in Section 2.9.

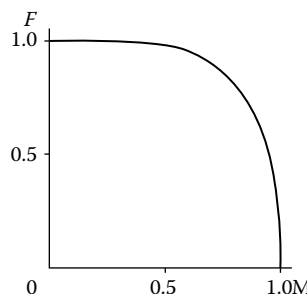


FIGURE 5.4
Function $F(M)$ for $M < 1$.

Finally, for substantiating the derivation of Equation 5.2.6 we will evaluate the role of the omitted term with mixed derivatives in the original Equation 2.4.8. In the similitude variables, the ratio of the second term to the third term of the equation is of the order

$$\frac{2v}{a_\infty} \frac{\partial v}{\partial x} : \frac{\partial v}{\partial r} = 2\theta_0^{2/3} \left(\frac{\partial v'}{\partial x'} : \frac{\partial v'}{\partial r'} \right) \quad (5.2.11)$$

Clearly, this term vanishes from Equation 2.4.8 as $\theta_0 \rightarrow 0$, that is, the higher-order nonlinear term is in this case the first nonlinear term with the second derivative $\partial^2 \varphi / \partial x^2$.

We will now dwell on the *Chaplygin equations*. In investigating the plane potential flows, *hodograph variables* are sometimes used, the independent variables being the absolute magnitude U of the velocity and the angle θ of its inclination to the x axis, while the unknown functions are the velocity potential φ and the streamfunction ψ . The derivation of the equations of motion in these variables can be sketched as follows. Equating the expressions for the differentials $d\varphi$ and $d\psi$ in the (U, θ) and (x, y) variables, we obtain the following expressions

$$dx = A_x dU + B_x d\theta, \quad dy = A_y dU + B_y d\theta \quad (5.2.12)$$

where the coefficients A and B contain the derivatives of the functions φ and ψ with respect to U and θ . These coefficients must satisfy the reciprocity relation $\partial A / \partial \theta = \partial B / \partial U$. Using these relations and the fact that the second derivatives of φ and ψ are mutually cancelled, we arrive at the Chaplygin equations

$$\frac{\partial \varphi}{\partial U} = -\frac{\rho_0(1-M^2)}{\rho U} \frac{\partial \bar{\psi}}{\partial \theta}, \quad \frac{\partial \varphi}{\partial \theta} = \frac{\rho_0 U}{\rho} \frac{\partial \bar{\psi}}{\partial U}, \quad \bar{\psi} = \frac{\psi}{\rho_0} \quad (5.2.13)$$

Here, ρ_0 is considered to mean the density at the stagnation point of the flow. The system is linear, since in the isentropic flow ρ and M are functions of U only. Making the change of variables (Leybenson, 1935)

$$ds = \frac{\beta}{U} dU, \quad \beta^2 = |1 - M^2| \quad (5.2.14)$$

we can transform system 5.2.13 into the symmetric form:

$$\begin{aligned} \frac{\partial \varphi}{\partial s} &= jF \frac{\partial \bar{\psi}}{\partial \theta}, & \frac{\partial \varphi}{\partial \theta} &= F \frac{\partial \bar{\psi}}{\partial s}, & F &= \frac{\rho_0}{\rho} |1 - M^2|^{1/2} \\ M > 1 : \quad j &= 1, & M < 1 : \quad j &= -1 \end{aligned} \quad (5.2.15)$$

For $M < 1$ the function F is plotted in Figure 5.4; clearly, for $M \leq 0.5$ it is near-unity. In this case we can put $F = 1$ with the result that system 5.2.15 becomes equivalent to the Laplace equation.

Finally, for transonic flows, $|1 - M^2| \ll 1$, in view of relation 5.2.5, the system 5.2.13 is reduced to the linear *Tricomi-type equation* (1952) for the potential φ and an analogous equation for $\bar{\psi}$

$$\frac{\partial^2 \varphi}{\partial U^2} = \frac{2A_*}{a_*^3} (U - a_*) \frac{\partial^2 \varphi}{\partial \theta^2} \quad (5.2.16)$$

Naturally, the Chaplygin equations retain the original characteristic properties: they are hyperbolic for $M > 1$ and elliptic for $M < 1$. The linearity of these equations makes them attractive in analytical studies of the intrinsic properties of gas flows. Their shortcoming lies in the difficulty of formulating the boundary conditions on the contours of bodies in

gas flow. Nevertheless, historically, the first solutions for compressible flows were obtained using precisely the Chaplygin equations. Thus, the solutions for jet flows were obtained by Chaplygin himself (1901), while the problem of the flow past a wing airfoil was solved by Khristianovich (1940) on the basis of Equation 5.2.15 with $F = 1$.

5.3 Formulation of Gas Dynamic Problems

The formulation of gas dynamic problems reduces to the choice of the governing equations (in our case the Euler equations), together with a set of initial and boundary conditions, which were formulated in the very general form in Section 1.11. The theory outlined in the following chapters makes it possible to specify these conditions for more particular classes of problems. In what follows, the rather obvious impermeability conditions on rigid surfaces of the type $v_n = 0$ will not receive mention; thus, we will restrict ourselves to the external conditions imposed on a certain surface Σ embracing a body in a gas flow (Figures 5.5 and 5.6) putting more emphasis on the minimization of the extent of the computational domain Ω bounded by this surface. Inappropriate reduction of this domain could misrepresent the results of the solution even qualitatively (an example is provided by the effect of the wind-tunnel wall on the pressure on an airfoil; see Figure 2.8). At the same time, both in running experimental studies and in constructing numerical algorithms there is little sense in enlargement of the domain Ω from the cost-saving standpoint. For this reason, a procedure of a correct transfer of the boundary conditions from infinity to a surface Σ located at a finite, though, possibly, quite large distance from the body is very important.

As shown in Section 1.11, in the problem of the unbounded flow (let it be uniform) past a body we could specify arbitrarily only the flow parameters at infinite distance ahead of the body, as $x \rightarrow -\infty$ (these are the absolute magnitude of the velocity, the angle θ_∞ which it makes with the x axis, the pressure p_∞ , etc.). Moreover, from the physical considerations, the damping of acoustic perturbations in all the other directions at infinity should be required

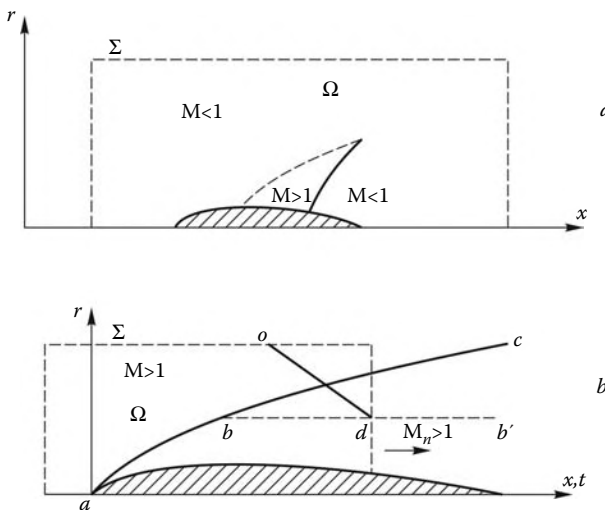
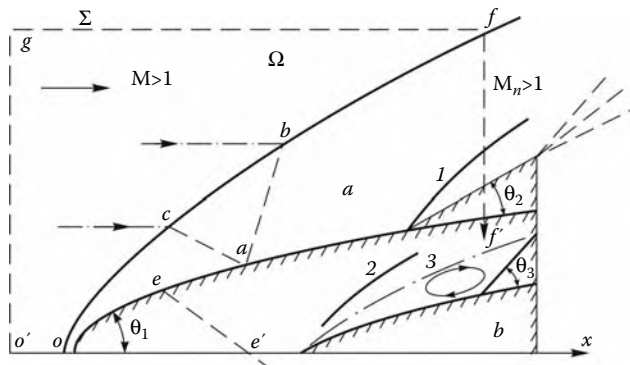


FIGURE 5.5

On the formulation of boundary conditions for gas dynamic problems.

**FIGURE 5.6**

On the formulation of boundary conditions in the problem of supersonic flow past bodies.

$$p \rightarrow p_\infty, \quad \theta \rightarrow \theta_\infty, \quad U \rightarrow U(p, s), \quad |x|, r \rightarrow \infty \quad (5.3.1)$$

The limiting gas velocity depends on the entropy s , the value of which in the wake behind the body, that is, at the exit of the Σ boundary, can differ from the freestream value s_∞ owing to its increase in shock waves, which can occur in the flow.

In the problems dealing with the propagation of time-dependent disturbances of finite total energy in an unbounded space, the disturbances are expected to die out as the distance r or time t increases without bounds.

These general remarks pertain equally to elliptic and hyperbolic problems; however, the approaches to the transfer of boundary conditions to a surface located at a finite distance differ for these problems and, therefore, will be considered separately.

5.3.1 Supersonic Flows

In this case the surface Σ must embrace the body in such a way that the bow shock intersects its exit section, for example, $f - f'$ in Figure 5.6. As noted in Chapter 4, any boundary conditions should not, rigorously speaking, be imposed on this section if the normal Mach number is $M_n > 1$. Such sections or boundaries will be referred to as *free*. However, there are finite-difference algorithms that require for their closure imposing boundary conditions on the free boundaries as well. Usually, the first or, which is more seldom, second derivatives with respect to the normal to the surface Σ are equated to zero. For generality, we will write this condition in the form:

$$\alpha_1 \left| \frac{\partial f}{\partial n} \right| + \alpha_2 \left| \frac{\partial^2 f}{\partial n^2} \right| \leq \varepsilon \ll 1 \quad (5.3.2)$$

Here, f is a particular function, α_i are the weight coefficients, and the quantity ε is determined by the accuracy required in the problem under consideration; in numerical algorithms it is most frequently taken to be zero.

It is quite naturally assumed that downstream of free surfaces there are no steps on body surfaces or barriers in jet and nozzle flows, and so on, such that disturbances produced by these obstacles could propagate (in the form of shock waves or forward separation zones) upstream to the free surface. Otherwise, the domain of definiteness of the solution must include these barriers as well.

Consider in detail the formulation of the problem of the supersonic flow past sharp and blunt bodies of the type shown in Figure 5.6. In these problems the lateral surfaces of the bodies are exposed to a supersonic flow (an analysis of the subsonic and transonic flow regions ahead of the blunt body will be given in Section 5.4). The most general formulation of the boundary conditions is that in which they are specified at the boundary $\Sigma(o'gff')$ embracing totally the disturbed region under consideration. There are some methods—referred to as *discontinuity-capturing techniques*—which make it possible to determine the solution of these problems with automatic localization of shock waves, that is, without imposing any special conditions on them. In this case the freestream parameters are preassigned on the sides $o'g$ and gf and conditions 5.3.1 are preset, if required, at ff' . The point f must be located above the shock.

The discontinuity-capturing techniques are based on Equations 1.9.7 through 1.9.10 in the conservation-law form; owing to the scheme viscosity effect, these algorithms smear a discontinuity to a certain stripe h , usually as large as several computational cells. For $h \ll L$, where L is the extent of the domain Ω , the derivatives along this stripe could be neglected in these equations, so that their integration across the stripe h gives the same conservation laws 1.7.12 relating the flow parameters on either side of it (Figure 1.16d). On the Ω domain scale, the stripe h , thus separated out, could be considered an isolated surface, that is, a shock wave with the corresponding relations on it. This situation is similar to the case of shock waves in viscous gases with $Re \gg 1$ (Section 3.2).

However, a more economically attractive formulation involving only a domain Ω_{\min} , as small as possible, is reduced to imposing the boundary conditions immediately ahead of an unknown shock on which the conservation laws of Chapter 3 should hold. The shape of the body must be specified only in the region where the solution is sought. Thus, preassigning the body contour oa we can obtain the solution in the domain oab bounded by shocks and a first-family characteristic. At the same time, the body shape at $x > x_a$ does not influence the sought solution.

Correspondingly, in a nonuniform freestream, the flow to the left of the characteristic ac is influenced only by the parameter distributions in the streamtube oc . Naturally, this is true only if the ram pressure of the gas in the streamtube cb is not too high; otherwise, the characteristic ac transforms to a shock with far-reaching consequences.

The question of the uniqueness of the solutions of these problems is associated with the realization of the weak and strong shock branches. It can be answered within the framework of reasoning of Section 3.5, with regard to the global conditions. However, a new situation arises if the body has a bend in its generator (such as a shield-equipped body). In an inviscid gas a set of solutions with various discontinuities of type 3 (Figure 5.6) could be constructed; these discontinuities would confine different constant-pressure dead-air zones. Actually, the gas is ejected from such a zone by the outer flow with the result that the shield is in a separationless flow at bend angles $\theta \leq \theta_{cr}$ (in accordance with the experimental data, $\theta_{cr} \approx 5^\circ$ for laminar and $\theta_{cr} \approx 10^\circ$ for turbulent boundary layers, although there can be strong variations in the angle θ_{cr} depending on the outer conditions). Thus, taking viscosity into account, though indirectly, allows us to choose a unique inviscid solution for this case (as in choosing the circulation around a wing airfoil, Section 2.9). However, at $\theta > \theta_{cr}$ the pressure jump results in boundary layer separation (as on a cylinder, see Section 2.10), so that a separation zone preceded by shock 2 is formed ahead of the shield. At high Reynolds numbers the flow outside this zone is inviscid; however, a unique solution of this problem could be obtained only by taking particular viscous effects into account.

In three-dimensional problems it is sufficient to imagine the characteristics ab and ca , as well as other lines, to be the traces of corresponding characteristic surfaces, shock waves,

and so on, especially for bodies qualitatively similar to axisymmetric ones. However, the flow three-dimensionality involves its own peculiarities. Thus, in the three-dimensional flow past the body shown in Figure 5.6 the domain of influence of the upper half-plane of symmetry is bounded on the body by the bicharacteristic ee' . For the bodies like delta wings, the questions of the domains of influence of the edges, the plane of symmetry, and so on, are very important; however, these questions are essentially three-dimensional (see Chapter 6).

In the problems outlined previously, the calculation must generally involve the entire domain between the shock and the body bounded by a corresponding characteristic. This requirement could be weakened in the case of two-dimensional isentropic flows behind a sufficiently weak shock induced, for example, by a thin elongated body or by a slowly moving piston. Precisely the latter problem will be outlined in the following.

Let the shock ahead of a piston be sufficiently weak starting from point b (Figure 5.5b), so that, in accordance with Section 4.6, it is equivalent to a simple wave. By virtue of Equation 4.8.3, the reflection coefficient for perturbations arriving at a weak shock is zero. Then for $Q_{\text{eff}} = 0$ the Riemann integral 4.5.1, $J^{(-)} = v - P(p) = 0$, holds along the characteristic od . Therefore, this condition can be used as a boundary condition on the line bb' . In the analogous steady-state problem, the integral 4.5.2 and, additionally, the Bernoulli equation for the longitudinal velocity component should be used.

However, the possibility of transferring the boundary condition from the shock to a surface closer to the body exists, rigorously speaking, only for two-dimensional isentropic flows, since, in accordance with Equation 4.2.6, in the general case the quantity $J^{(-)}$ is variable along the characteristic od at $Q_{\text{eff}} \neq 0$ and cannot be accurately swept from the shock to the line bb' . In this case, disturbances going from the body do not reflect from the shock as well; however, they reflect from the region $b'bc$ in which there are no simple waves. Nevertheless, the conditions of the type $J^{(-)} = 0$ are sometimes used on free boundaries instead of 5.3.2.

5.3.2 Subsonic Flows

In this case, the domains of influence are unbounded, while the boundary conditions 5.3.1 imposed infinitely far from the body are of asymptotic nature (this follows both from the general theory of elliptic equations and the examples presented in Chapter 2). These circumstances require that the surface Σ , on which the boundary conditions are imposed, be rather distant from the body, with conditions in Equation 5.3.2 as a possible criterion for the remoteness.

In accordance with Sections 2.9, 2.10, and 2.12, velocity disturbances in a potential flow die out far from the body as $U' \sim (r/r_0)^{-n}$, where r_0 is the body dimension, r is the distance from the body, $n = 1$ and 2 for circulatory and circulation-free flows around wing airfoils, and $n = 3$ for axisymmetric flows. Therefore, the following modified soft conditions at Σ

$$\frac{\partial U' r^n}{\partial r} \leq \varepsilon \ll 1, \quad U' = (U_\infty - u), v \quad (5.3.3)$$

are more accurate than the preceding ones; here, U_∞ is the freestream velocity. In calculating the flow past airfoils with $n = 1$ under conditions 5.3.3 it may be expected that the effect of the scheme viscosity itself can lead to a solution with a smooth shedding of the flow from the sharp trailing edge (Joukowski postulate, see Section 2.9). Otherwise, the circulation Γ required for this to happen is determined by an iteration procedure subject to the condition $U' \sim \Gamma/r$ for $r \gg r_0$.

We recall that all the aforesaid refers only to well-streamlined bodies (as defined in Section 2.12), for which separation zones and wakes downstream from them do not affect the preceding flow or are absent at all. Such flow patterns were sketched in Section 2.12 and we will not dwell on this question.

5.3.3 Transonic Flows

As the subsonic Mach number ($M_\infty < 1$) increases, the asymptotics of the solution of the Laplace equation in a stripe above the body have, in accordance with 2.9.1, the form $(\beta_- r/r_0)^{-n}$, where $\beta_- = (1 - M_\infty^2)^{1/2}$. In this case the disturbed region expands in the transverse direction as $\beta_-^{-1/2}$. For $M_\infty > 1$ the linear theory does not ensure the disturbance damping at all and the true asymptotics of the solutions as $r \rightarrow \infty$ are determined by the laws of shock attenuation (Section 4.8). For these reasons, for $M_\infty \approx 1$ in both cases the disturbance dies out in the direction normal to the external velocity vector \mathbf{U}_∞ , much slower than in the longitudinal direction; this must be correspondingly reflected in the choice of the surface Σ . For $M_\infty = 1$ the transonic theory* gives the following asymptotics of the solution as $r \rightarrow \infty$

$$\begin{aligned} u' &= U_\infty - u \sim r^{-n}, & v &\sim r^{-m} \\ v = 0 : & n = 2/5, & m &= 3/5 \\ v = 1 : & n = 6/7, & m &= 9/7 \end{aligned} \quad (5.3.4)$$

The slower damping of the u' component is not coincidental, since the linear theory also gives the estimate $u'/v \sim \beta_\pm^{-1} \rightarrow \infty$ as $M_\infty \rightarrow 1$. Correspondingly, the appropriate boundary conditions at Σ can have the form 5.3.3.

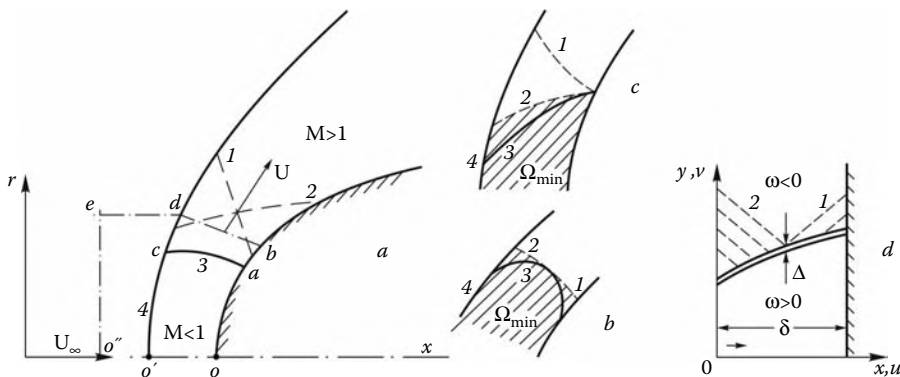
We note in conclusion that in general the transfer of the boundary conditions to the boundary Σ is not trivial, often borders on the art, and can usually be tested in numerical experiments. All the aforesaid can serve only as a reference in this procedure.

5.4 Supersonic Flow Past Blunt Bodies

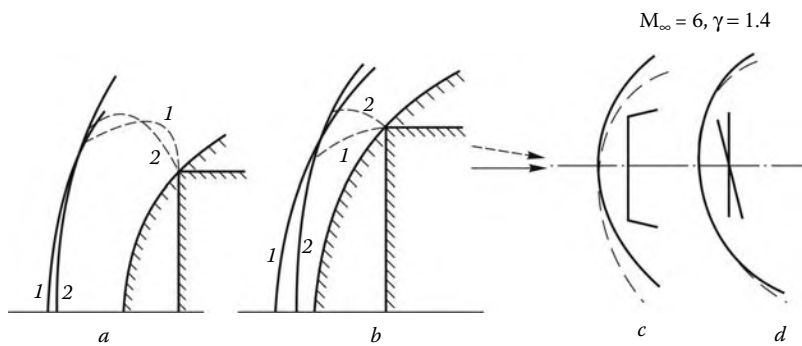
This section is devoted to an analysis of mathematical difficulties associated with the blunt-body problem, which is one of most sophisticated in mathematical physics. The purely gas dynamic features of these flows will be discussed in Chapter 7.

The general flow pattern is sketched in Figure 5.7. The most general formulation of the problem oriented at the numerical calculation on the basis of a shock-capturing technique is the same as in Section 5.3 with the condition $M_n > 1$ imposed on the closing boundary bd of the domain Ω with the boundary $o''edbo$ (Figure 5.7a). The minimum domain Ω_{\min} , in which the problem can be formulated correctly, is bounded by the bow shock 4 and the limiting characteristics 1 and 2 (Figures 5.7b and c), which still have the opportunity to arrive at the sonic line 3 and transmit disturbances to the subsonic region, thus affecting the flow as a whole. In Figure 5.7b the waves originating from the body arrive at the sonic line, which, in its turn, exchanges disturbances with the bow shock. In Figure 5.7c the sonic line is, as

* See, for example, the book of Cole and Cook (1986).

**FIGURE 5.7**

On the theory of the supersonic flow past blunt bodies.

**FIGURE 5.8**

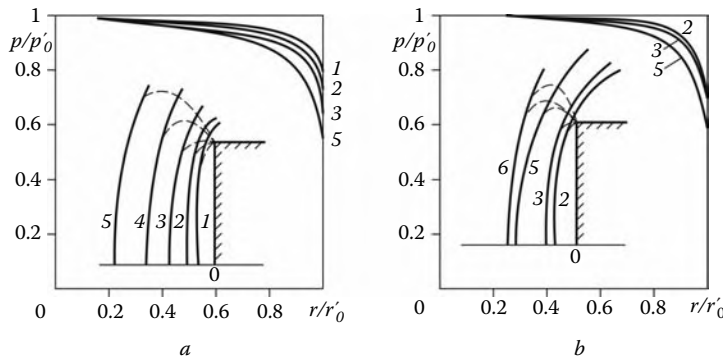
Shapes of the bow shocks and sonic lines in the flows past (a) a cylinder 1 and a flat plate 2 and (b) a sphere 1 and a disk 2. Bow shocks ahead of a disk at incidence in the body-fitted (c) and flow-fitted (d) reference frames.

it were, put up between the body and the shock and interacts only with the latter via the characteristics. As follows from Figures 5.8 through 5.11,* the first situation is characteristic of the flat plate and flat-ended cylinder set normally to the flow and the similar bodies, as well as for bodies like a sphere at $M_\infty \leq 2$. The second situation is typical of a sphere at high Mach numbers ($M_\infty \geq 3$).

The simplest (from the standpoint of validation) formulation of the problem is that using the method of the steady-state attainment described in Section 4.4.[†] Experience has shown that at stationary boundary conditions and for practically any initial conditions, time-dependent solutions usually converge to steady-state ones. In this case, it is sufficient to impose the free condition 5.3.2 on the "exit" boundary (db in Figure 5.7a) in the transonic region with $M_n > 1$ on this line.

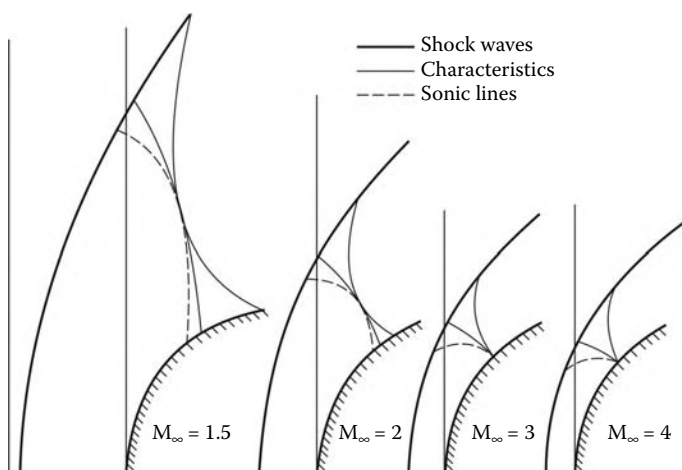
* The data for smooth bodies at moderate M_∞ were taken from O. M. Belotserkovskii (1966) and at high M_∞ from Lunev, Magomedov, and Pavlov (1968); the data for the flow past a disk were kindly supplied by Kholodov; the data in Figures 5.8c and d are experimental.

[†] Godunov (1959, 1975), Magomedov and Kholodov (1969), Lyubimov and Rusanov (1970), and others.

**FIGURE 5.9**

Pressure distributions over a flat plate (a) and a flat-faced cylinder (b), bow shocks in front of the bodies, and sonic lines (dashed curves) in the shock layers for $M_\infty = \infty$ and $\gamma = 1.02$ (1), 1.05 (2), 1.1 (3), 1.2 (4), and 1.4 (5) and $M_\infty = 6$ and $\gamma = 1.4$ (6).

Other methods based on the properties of precisely steady-state solutions also received wide acceptance at different times. These are, first of all, *inverse methods* based on preassigning the shape of the bow shock and, therefore, the flow parameters behind it. In accordance with the Cauchy-Kovalevskaya theorem (Section 4.1), this problem has a unique solution that, at an appropriate choice of the shock shape, can contain in the domain of its analyticity, (i.e., in the domain where there are no singular points), a certain streamsurface, which could be taken for the shock-inducing blunt body. Varying the shape of this shock one can in principle achieve a good fit of the body contour obtained to the desired one. Thus, parabolic bow shocks correspond to the flows past a sphere in the subsonic and transonic regions.

**FIGURE 5.10**

Pattern of the flow past a sphere.

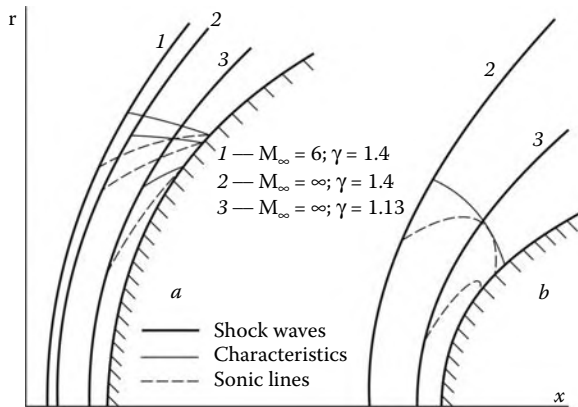


FIGURE 5.11
Patterns of the flow past a sphere (a) and a circular cylinder (b).

The inverse methods were used for solving the problems of the flows past a sphere, a cylinder, and similar bodies.* However, these methods turned out to be inadequate for treating the flow past bodies like a flat-ended cylinder with singular corner points or even with somewhat smoothed corners. One of the reasons for this is that the shock shape is not very sensitive to variation of the body shape (Figure 5.8). In particular, for this reason these methods were nearly ousted by the direct time-dependent methods mentioned previously. However, the inverse methods conserved their significance as an element of some iteration procedures that are to a certain degree equivalent to time-dependent methods (e.g., Telenin and Tinyakov, 1961).

As shown in Section 4.1, the Cauchy problem for elliptic equations is ill-posed. However, in our case there is a stabilizing factor, namely, the necessity of the agreement between the elliptic solution of the Cauchy problem with the hyperbolic one in the supersonic region located above the sonic line. In the latter domain the Cauchy problem is well-posed and gives a restricted solution, so that there is reason to believe that the general solution will be restricted and correct as well. In any case, it is interesting to reveal the mechanism of the subsonic/supersonic flow region interaction precisely for the steady-state boundary-value problem. This will be done in the following with reference to the example of a linear model system of equations

$$\omega \frac{\partial u}{\partial x} + \frac{\partial v}{\partial y} = q = \text{const}, \quad \frac{\partial v}{\partial x} - \frac{\partial u}{\partial y} = 0 \quad (5.4.1)$$

In the x, y coordinate system presented in Figure 5.7d the functions u and v simulate the velocity components across and along a disturbed layer, or *shock layer*, of thickness δ mapped onto a stripe, where the lines $x = 0$ and $x = \delta$ represent the shock and body surfaces. For $q = 0$ and $\omega = \pm 1$ this system reduces to Equation 4.1.5 for the potential. At $\omega = 1$ this is the Laplace equation, which is the model equation for the subsonic flow region, $v < a_*$, whereas at $\omega = -1$ this is the wave equation being the model equation for the supersonic region, $v > a_*$, where the speed of sound is taken to be constant (a more

* Garabedian (1957), Vaglio-Laurin and Ferri (1958), Van Dyke (1959), Lunev and Pavlov et al. (1966).

rigorous condition $u^2 + v^2 \geq a^2$ does not change the essence of the matter). This discontinuous transition from the equation of one type to that of another type can be regarded as the limiting case for the continuous transition $-1 \leq \omega(v) \leq 1$ in a vanishingly thin (Δ -thick) "transonic" vicinity of the sonic line. In this region too, Equation 5.4.1 can be regarded as the counterpart of the nonlinear von Kàrmà̄n Equation 5.2.6.

For the sake of illustration, we will formulate the following simple boundary-value problem for Equation 5.4.1

$$x = 0, \quad u = A = \text{const} > 0; \quad x = \delta, \quad u = 0; \quad y = 0, \quad v = 0 \quad (5.4.2)$$

which has the solution

$$\begin{aligned} u &= u_0 = A(1 - \bar{x}), & \bar{x} &= x/\delta, & \bar{y} &= y/\delta \\ v &= v_0^{(+)}(\bar{y}) = (q + A)\bar{y}, & \bar{y} &\leq \bar{y}_*^{(0)} = a_*(q + A)^{-1} \\ v &= v_0^{(-)}(\bar{y}) = a_* + (q - A)(\bar{y} - \bar{y}_*^{(0)}), & \bar{y} &\geq \bar{y}_*^{(0)} \end{aligned} \quad (5.4.3)$$

In order to make this problem more or less realistic, one should set $q - A > 0$. The position of the line $\bar{y} = \bar{y}_*^{(0)}$, which is in this case a straight line, is determined from the condition that the solution is continuous on it, though the derivative $\partial v / \partial y$ is here discontinuous. Then, preassigning on the basis of other considerations the position of the sonic point on the body $y = h$ and thus taking indirectly its characteristic dimensions into account, we can determine the thickness $\delta = \bar{y}_*^{(0)}h$.

In order to determine the mechanism ensuring the uniqueness of the problem, we will consider a homogeneous problem corresponding to the solution obtained by putting $A = q = 0$. This problem is associated with nontrivial eigen solutions 4.1.6 satisfying conditions 5.4.2 (for $A = 0$) with integer values of n

$$\begin{aligned} \omega = 1 : \quad u_n^{(+)} &= C_n^{(+)} F_n^{(+)} \sin \pi n \bar{x} \\ v_n^{(+)} &= -C_n^{(+)} F_n^{(-)} \cos \pi n \bar{x} \\ F_n^{(\pm)} &= e^{\pi n \bar{y}} \pm e^{-\pi n \bar{y}} \end{aligned} \quad (5.4.4)$$

$$\begin{aligned} \omega = -1 : \quad u_n^{(-)} &= C_n^{(-)} \sin \pi n \bar{x} \cos \pi n \bar{y} \\ v_n^{(-)} &= -C_n^{(-)} \cos \pi n \bar{x} \sin \pi n \bar{y} \end{aligned} \quad (5.4.5)$$

Here, $C_n^{(\pm)}$ are arbitrary constants, that is, in each of these separate domains, for $\omega = \pm 1$ the solution is nonunique. The situation can be corrected only by requiring the continuity of the solution as a whole on a sonic line $\bar{y}_* = \bar{y}_*^{(0)} + \bar{y}_*^{(n)}$. For determining this line and the constants $C_n^{(\pm)}$, which are assumed to be small, we have the following three conditions

$$u_n^{(+)}(\bar{y}_*^{(0)}) = u_n^{(-)}(\bar{y}_*^{(0)}), \quad v^{(\pm)} = v_0^{(\pm)}(\bar{y}_*) + v_n^{(\pm)}(\bar{y}_*^{(0)}) = a_* \quad (5.4.6)$$

In this case it turns out that $\bar{y}_*^{(n)} = C_{*n} \cos n \pi \bar{x}$ and Equation 5.4.6 are reduced to a system of homogeneous equations in C_{*n} and $C_n^{(\pm)}$; for discrete n nontrivial solutions of this system seem to be impossible. Hence follows the unique solvability of the problem as a whole (at a fixed sonic point on the body surface the condition $C_{*n} = C_n^{(\pm)} = 0$ is automatically fulfilled).

The same results can be easily obtained by simulating an inverse method of solution with the preliminary calculation of the supersonic region, as suggested previously. In this case the condition $u_n^{(-)} = v_n^{(-)} = 0$ should be imposed on a certain line $\bar{y} = \bar{y}_0(x)$; this procedure can also result only in the trivial solution.

Obviously, this reasoning, rather intuitive than rigorous, even within the framework of the example presented previously, cannot serve as a proof for the original, nonlinear gas dynamic problem. It is aimed only at elucidating the mechanism of the interaction between elliptic and hyperbolic regions and the correctness and uniqueness of the formulation of the mixed problem based on this mechanism. Experience, together with theoretical studies closer to the original problem,* have shown that precisely this situation is realized in the problem of the supersonic flow past blunt bodies. We will content ourselves with this assertion.

We will now consider the properties of these problems from another standpoint, which shows more illustratively the gas dynamic mechanism governing these flows and is based partly on the analogy between the shock layer flow and the nozzle flow from Section 2.3. We will consider a model example of a flat plate normal to the external velocity vector with the y and x axes directed along and normal to the plate (Figure 5.7d). As a rough approximation, we will average the flow parameters across the shock layer setting $p = p(y)$, $u = u(y)$, and so on. This makes the flow similar to the nozzle flow with a distributed flow rate $G'(x) = \rho_\infty v_{1n} = \rho_\infty U_\infty \cos \omega$ through the shock $x = \delta(y)$, where $\tan \omega = \delta'$. Since all the flow functions at the shock depend on δ' only, letting the gas velocity within the shock layer to be the same as at the shock itself, $v = v_s(\delta')$, we thus impart the following general form to Equation 2.3.16

$$(1 - M^2)\delta'' = \Phi(\delta', \delta, y), \quad M^2 = v^2/a^2 \quad (5.4.7)$$

We have a single symmetry condition, $\delta'_0 = \delta'(0) = 0$, for this, now second-order, equation; this gives a family of integral curves with the parameter $\delta_0 = \delta(0)$. This parameter is determined from the condition of regular behavior of an integral curve passing through the singular point $y = y_*$, $M = 1$, at which one should set, in accordance with (2.3.9), $\Phi = 0$. For the plate (or disk) under consideration this point is quite naturally brought into coincidence with the corner $y_* = r_0$ (cf. Section 6.3), while for smooth bodies the additional condition for its determination can be obtained, for example, starting from the value of the sonic angle δ' at the shock.

Naturally, all the mathematical and gas dynamic properties of the problems under consideration should be taken into account in designing methods of their solution, including numerical ones. Thus, equations of the type like Equation 5.4.7 form the basis of the integral relation method of Dorodnitsyn (1956), which was the first direct method for solving these problems.[†]

We note that the list and classification of the methods used for solving the problems considered extends further. In Chapter 7 we will outline some other methods, intermediate between inverse and direct ones, which are specific for the problem of the hypersonic flow past blunt bodies (the so-called *global iteration* methods).

* These studies are usually based on the Tricomi equation (1950). However, the use of this rather specific and fairly vast theory is beyond the scope of this book (cf. monographs cited in Sections 5.2 and 5.3).

[†] This method was implemented by O. M. Belotserkovskii (1957) and Chushkin (1957) for supersonic and subsonic flows past blunt bodies, respectively.

5.5 Nozzle and Jet Flows

In this section we will outline the salient features of the problems associated with flows in nozzles and in gas jets issuing into an ambient medium at rest or into a cocurrent stream.

The most general requirement that can be imposed upon a nozzle as an element of a jet engine, either liquid or solid, or of a wind tunnel is that the flow is uniform and isentropic at the exit section bb (Figure 5.12). This requirement results from the thrust optimization purpose in the former case (Section 3.6) and from the necessity of modeling the body flight in the undisturbed atmosphere in the latter one.

Methodically, the entire nozzle flow problem could be broken down into two successive problems. Problem 1 is formulated for the flow region from the nozzle inlet to the approximate, completely supersonic, free (in the sense of Section 5.3) section aa , where $M_n > 1$. Problem 2 deals with the following, purely supersonic flow region.

Clearly for problem 1 it is practically impossible to describe the entrance effects at locations of gas feeding into precombustion chambers and those of fuel combustion within the framework of inviscid gas dynamics. For this reason, an idealized treatable formulation of the problem is possible only for a relatively long chamber. In this case the stagnation pressure and the total enthalpy H must be specified at a certain cross-section OO of area σ_0 assumed to be initial. In the hydraulic approximation (Section 2.3) the Mach number in this section is the function $M_0 = M(\sigma_0/\sigma_*)$ that determines all the other parameters at this section, that is, the velocity u_0 , the pressure p_0 , the entropy s , the gas flow rate G , and so on (here, σ_* is the critical, or sonic cross-section of the nozzle). At the same time, in the exact formulation the quantity u_0 (or M_0) is, as it were, an *eigenvalue* of this problem which is to be determined in the course of solution. Generally speaking, the conditions $u = u_0$, and so on, must be satisfied rigorously only infinitely far from the nozzle throat, as $x \rightarrow -\infty$, the derivatives of these functions being zero. Therefore, the choice of the section OO in Figure 5.12 is determined by conditions 5.3.2.

Problem 2 has, at least, two versions. The first one is that with a given nozzle contour ab . Then the Cauchy problem posed on the line aa (Section 4.2) has a solution within the characteristic triangle aca . Further, the problem shown in Figure 4.3b is successively solved, first in the region between the characteristic cb and the wall ab and then between the characteristic cb and the axis of symmetry.

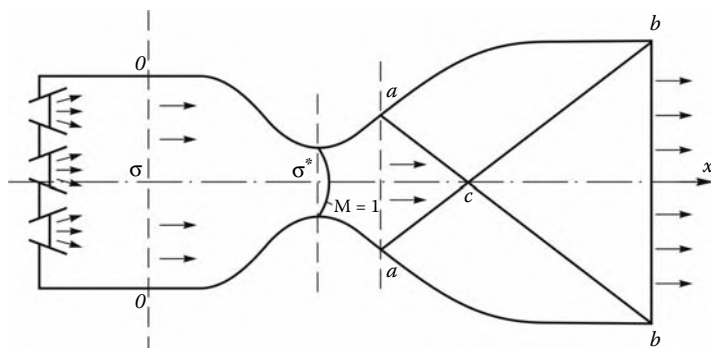


FIGURE 5.12
Supersonic nozzle.

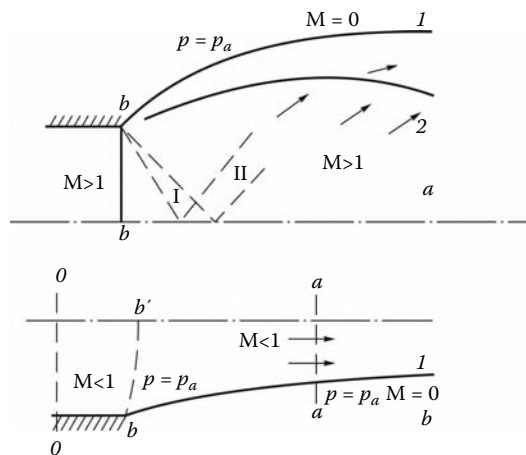


FIGURE 5.13
Outflow of supersonic (a) and subsonic (b) jets.

The second version is the construction of a contoured nozzle with uniform parameter distributions in section bb' . In this case the flow parameters in the triangle ccb are taken to be constant and the solution of the Goursat problem posed on the characteristics ac and cb determines the required nozzle contour ab , which produces the preassigned glow. Quite naturally, the preceding nozzle contour at $x < x_a$ must ensure the fulfillment of the condition $M_c = M_b$, thus excluding the possibility of the formation of shock waves with increase in entropy.*

5.5.1 Supersonic Jets

We will begin with supersonic jets issuing into an ambient space with a given constant pressure $p = p_a$. In order for the supersonic jet flow problem to have a solution, the initial parameters at the nozzle exit (section bb' in Figure 5.13a) should also be specified. Then the solution can be obtained using a marching technique, for example, the method of characteristics (Sections 4.2 and 4.3).

The jet outflow pattern depends considerably on the *nozzle-to-ambient pressure ratio* $n = p_b/p_a$; here, p_b is the nozzle exit pressure, while p_a is the atmosphere pressure. In *underexpanded* jets ($n > 1$) the gas accelerates in the expansion wave I centered at the nozzle edge, the flow pattern somewhat differing in axisymmetric and two-dimensional jets.

Typical of axisymmetric jet flows is the formation of an internal shock 2 below the jet boundary 1 (Figures 5.13a and 5.14a); the gas of the central overexpansion region flows across this shock to the *shock layer* between the shock itself and the jet boundary. The formation of this shock is due to an additional (caused by the axial symmetry of the flow) gas expansion in wave II originating from wave I, so that the pressure in this wave turns out to be smaller than p_a as the jet boundary is approached. Because of this, the wave is reflected from the jet boundary as a compression wave III (Figure 5.14a); the submerged shock 2 is formed precisely in this wave, due to disturbance accumulation. The shock can be directed

* The nozzle theory is presented in Pirumov and Roslyakov (1985).

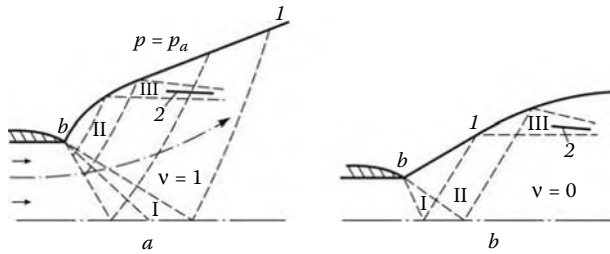


FIGURE 5.14
Shock formation in underexpanded jets.

either downward, as in Figure 5.14a, or, at high values of n , upward, as in Figure 5.13a. Subsequent expansion waves reflected from the axis of symmetry interact with this shock. In this case the jet boundary is curved along its whole length.

In a two-dimensional jet (Figure 5.14b) the initial region of the jet boundary 1 is rectilinear until the expansion wave II reflected from the plane of symmetry arrives at it. This wave is, in its turn, reflected from the jet boundary as a compression wave III within which an internal shock 2 may also be formed, however, at a fairly large distance from the nozzle exit. In both cases, the gas in the jet core is overexpanded with respect to the ambient gas. This circumstance leads eventually to the flow convergence far from the nozzle with interference of the incident shocks 2, which can be either regular (in the sense of Section 4.9) or, more often, irregular, as shown in Figures 4.21 and 5.15.

The outflow of *overexpanded jets* ($n < 1$) is always accompanied by this interference. In these jets, the pressure is recovered up to the value $p = p_a$ in the shocks originating at the nozzle edges. As n is decreased, the interference becomes irregular; its shock pattern is shown in Figure 4.21 (Section 4.9).

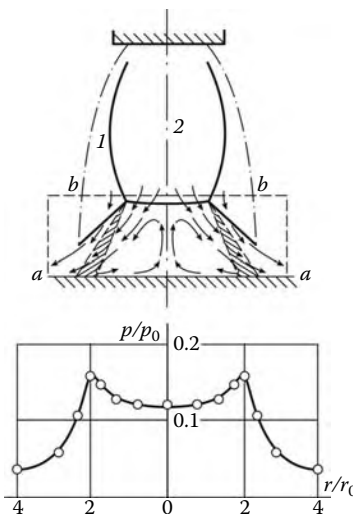


FIGURE 5.15
Interaction of an underexpanded jet with a barrier.

In this case the pressure in the subsonic jetlet behind the central shock is $p_{IV} > p_a$. Therefore, this jetlet must accelerate, which is ensured by a rarefaction wave formed at the reflection of the secondary shock 1–3 from the external jet boundary 2–6' at point 3. In the region, where this wave is incident on the internal jet boundary 1–6, a sonic cross-section is formed in the latter; the sonic-to-initial area ratio was determined in Section 2.3. However, the pressure in the central jet must decrease even to this section, which must be correlated with the behavior of the external supersonic flow III. Precisely these conditions in their totality determine the geometric flow pattern as a whole. A similar mechanism governs irregular shock configurations with central subsonic jets (Figure 4.22 of Section 4.9).

In the exact formulation of the problem, the contour $\Sigma(abb'a')$ in Figure 4.21 must contain the entire flow region (as in the case of the flow past blunt bodies). All the flow parameters must be preassigned at the entrance section and the condition of the undisturbed atmosphere, $p = p_a$, must be imposed on the lateral sides of the contour, its right boundary being free, with the condition $M_n > 1$ on it.

This flow pattern can break down as the nozzle-to-ambient pressure ratio p_b/p_a decreases. In this case, the Mach disk can displace into the nozzle, so that the outflowing jet is subsonic.

5.5.2 Subsonic Jets

The subsonic jet outflow is possible only at the exit pressure $p_b \geq p_a$; otherwise, the flow in the channel restructures itself with a reduction in the gas flow rate (Section 2.3). The isobar bb' with $p = p_a$ is located outside the nozzle (Figure 5.13b), since disturbances from the extreme point b are partially convected by the flow. However, these disturbances manifest themselves also in a certain region inside the channel, between the OO and bb' sections.

When the external pressure p_a is lower than the sonic pressure p_* , the jet becomes supersonic; it involves the sonic line bb' and an expansion wave, which is originated from the point b (it is not plotted in the figure). In this case, the formulation of the problem is the same as for the nozzle in Figure 5.12 with the condition 5.3.1 imposed on the OO section. At $p_a > p_*$ the jet is subsonic. The ultimate section area σ_a of the convergent jet is easily determined from the flow rate equation $G = \rho U \sigma_a$ in terms of the known pressure p_a . In the exact formulation, asymptotic conditions in Equation 5.3.2 are imposed on the subsonic sections oo and aa .

The problem of a jet in a cocurrent stream is solved in a similar fashion; in this case the surface Σ embraces a required part of the cocurrent stream and the standard conditions are imposed on the interface between the two flows.

Usually an important role (at least, qualitatively) in forming extended jet flows is played by a zone of viscous (chiefly turbulent) mixing on the interfaces between the flows. The ejection of the internal flow by the external one plays the same part as suction in a nozzle.

5.5.3 Interaction of Jets with Barriers

This problem (Figure 5.15) is similar to that of the flow past blunt bodies; as in Section 5.4, boundary conditions are imposed on the contour $aabb$. Here we will dwell only on a nontrivial example of an underexpanded jet incident on a barrier. In this case inviscid solutions may be absent.* In fact, due to internal shocks an external annular jet is formed; the ram pressure in this jet is higher than that in the central region 2, while the stagnation

* Gubanova, Lunev, and Plastinina (1971).

pressure behind the central Mach disk is lower than the pressure at the periphery induced by the annular jet turn. For this reason, the gas in the inviscid stationary stream cannot flow out from the central region, which indicates the absence of a steady-state solution. The stationary flow observed in experiments is viscosity-stabilized. Jet 1 ejects the central jetlet through the mixing zone with the formation of a central separation zone in the flow core. Frequently, such flows turn out to be fluctuating. Such situations should be expected in the problems of the nonuniform flow, both subsonic and supersonic, past bodies, for example, when a trailing body is placed in the wake of a leading body.

5.6 Subsonic Flow Past a Convex Corner

Problems of this kind arise in studying the flows past bluff bodies like a disk or a flat plate (Figures 5.8 and 5.9), the flows in nozzles with a bend in the wall near the nozzle throat, and so on. Here we consider some properties of these flows on the assumption that the flow is isentropic in the transverse direction and, which is most important, is accelerated only due to the presence of the corner point, other factors, such as, for example, the preceding contraction of the channel or the bending of its walls, being absent.

The main issue of this problem is that of the mutual location of the corner and sonic points. Obviously, the sonic point cannot be located downstream of the corner, since a subsonic flow cannot withstand infinite pressure gradients arising in such a flow. In fact, for an incompressible fluid (or a gas with the Mach number $M \ll 1$) the solutions of this problem 2.11.10 (Figure 2.21g of Section 2.11) or, in a particular case, 2.10.13 (Figure 2.20b of Section 2.10), give physically unfeasible infinite velocity at the corner point, the law of the velocity increase being as follows: $U = C_m U_\infty (r/L)^{-m}$, $m = \theta/(\pi + \theta)$, where r is the distance from the corner, θ is the deflection angle (Figure 5.16a), U_∞ and L are the scale velocity and length, and $C_m \sim 1$ is the form parameter of the body as a whole.

For incompressible flows, this paradox is removed by the formation of a vapor-filled cavitation zone downstream of the corner point; on the other hand, for gases this solution simply does not hold inside a circle with its center at the corner point O and radius r_0 determined from the condition

$$U \geq M_0 a_\infty, \quad r \leq r_0 = L(C_m M_\infty / M_0)^{1/m} \quad (5.6.1)$$

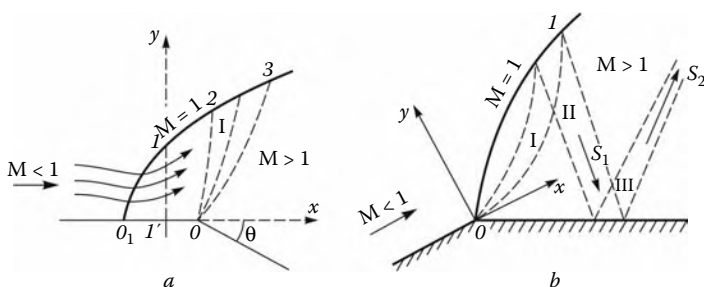


FIGURE 5.16
Subsonic flow past a corner.

where a_∞ is the speed of sound and M_0 is a certain Mach number, which sets a limit on the application of the incompressible theory. Clearly, the domain of influence of compressibility contracts as the freestream Mach number M_∞ and the exponent m (or the angle θ) decrease. For low Mach numbers M_∞ , this zone is extremely small and embedded in a viscous boundary layer and can thus be neglected on the scale of the flow as a whole.

Thus, only two locations of the sonic point are possible: either at the point O_1 at a certain distance h upstream the corner O (Figure 5.16a) or at the point O itself when approached from the left (Figure 5.16b). These cases share the common property that the disturbances can propagate upstream via the interaction of the characteristic bundle I originating from the corner with the sonic line.

However, the first case could hardly be realized in conventional flows. In fact, by assuming the flow to the right of the sonic line $O_1 - 1 - 3$ to be supersonic, we allow it to accelerate near the surface from the point O_1 to the point O with the result that the streamlines diverge and are convex with respect to the wall, as shown in Figure 5.16a. However, this pattern must be accompanied by a negative pressure gradient $\partial p/\partial y$ along the wall normal $1'-1$, this being in contradiction with the fact that the pressure at the sonic point 1 must be higher than that at point $1'$ where the flow is supersonic.

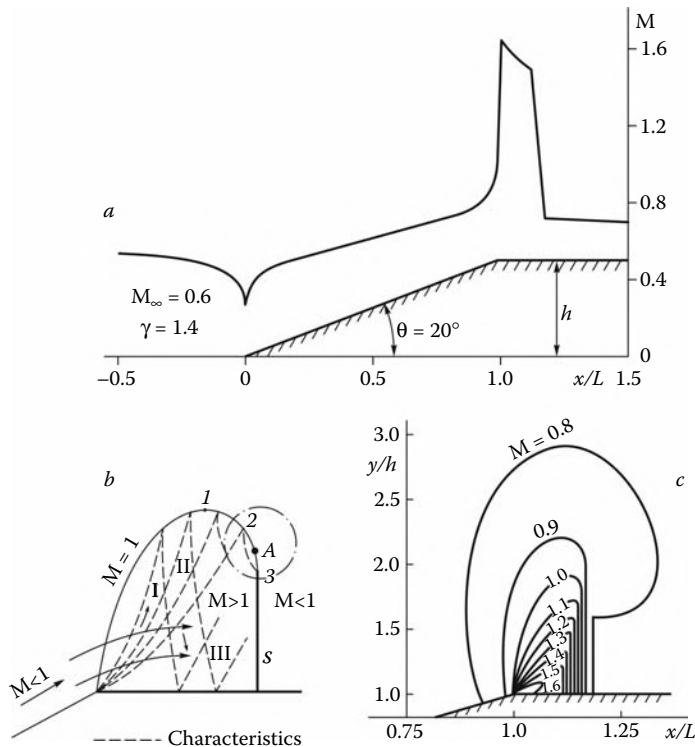
Therefore, the most probable situation in these flows is that in which the sonic point coincides with the corner, as the latter is approached from the left (Figure 5.16b). Though this assertion has not been rigorously proved, it is usually beyond question and, which is most important, is supported by the results of many calculations, as those presented in Figures 5.8 and 5.9 from Section 5.4 and Figures 5.17 through 5.19.*

In what follows we will analyze the flow turning around the corner on the basis of precisely this assumption. The centered expansion wave I originates from the corner point (Figure 5.16b), the characteristic fan corresponding to the Prandtl-Meyer wave at the point itself and being curved at a distance from the corner (a local analysis of this problem will be carried out in Section 6.3). Thus, downstream of the corner there appears a supersonic zone, where the expansion waves I are reflected from the sonic line as the compression waves II with their subsequent reflection from the wall as compression waves again (waves III). The cumulation of these compression waves can lead to the generation of shocks (S_1 or S_2 in Figure 5.16b) of one or another family.

We will now consider the flows of this type with reference to the example of a wedge-shaped step with a small angle θ (the same as in Figure 2.20b from Section 2.10) in subsonic flow. The Mach number distribution over its surface is plotted in Figure 5.17a; ahead of the corner point O it behaves as in the incompressible flow in Figure 2.20b, with the same monotonic velocity increase along the surface. The wave pattern in the supersonic flow region downstream of the corner is sketched in Figure 5.17b, while in Figure 5.17c the calculated Mach number contours in the vicinity of the corner are plotted. The sonic line and the closing shock S form the horseshoe-shaped supersonic zone boundary.

The shock S in Figure 5.17b belongs to the second family and is initiated due to convergence of the characteristics reflected from the descending region 1–2–3 of the sonic line. This analysis has no pretensions on the description of the wave pattern in the vicinity of the shock initiation point A and the transition of the sonic line into the shock. Moreover, in spite of many analytical studies of this problem, the flow pattern in this region is not as yet completely understood and, apparently, would be essentially dependent on the particular conditions if a wider class of the problems associated with the subsonic and transonic flows past thin airfoils and bodies of revolution is considered.

* The data presented in Figures 5.17 through 5.19 were obtained by Kovalev.

**FIGURE 5.17**

Subsonic flow past a wedge-shaped step.

Another example is provided by the supersonic flow ($M_\infty = \infty$) past a flat plate ($\nu = 0$) or a flat-faced cylinder ($\nu = 1$). The flow pattern downstream of the corner points of these bodies is presented in Figure 5.18. Here, the sonic lines have the shape that has been already described in Section 5.4, while the reflected wave patterns are similar to that shown in Figure 5.16b. The shock initiates within wave III reflected from the wall and is clearly visible both from the isobar pattern in Figure 5.18a and b, and directly from the pressure distributions over the lateral surfaces of the bodies (Figure 5.19). The pressure level on the initial regions of the lateral surfaces of these bodies, before the formation of the shock, is determined by the flow turn in the Prandtl-Meyer wave originating from the sonic point.

At the same time, the pressure increases by an order in the subsequent shock, which is due to large local Mach numbers ahead of the shock. The pressure over the lateral surfaces of these bodies far from the sonic point is determined by quite different laws, which will be considered in Chapter 9.

The qualitative behavior of the curves is somewhat different in the plane and axisymmetric flows, which is apparently due to the accompanying vorticity and axial symmetry effects considered in Section 4.7.

5.7 Interaction of Disturbances with a Subsonic Region

Earlier, in Section 4.7, we performed an analysis of the reflection of disturbances from a contact discontinuity with supersonic flow on either side of it. The interaction was only

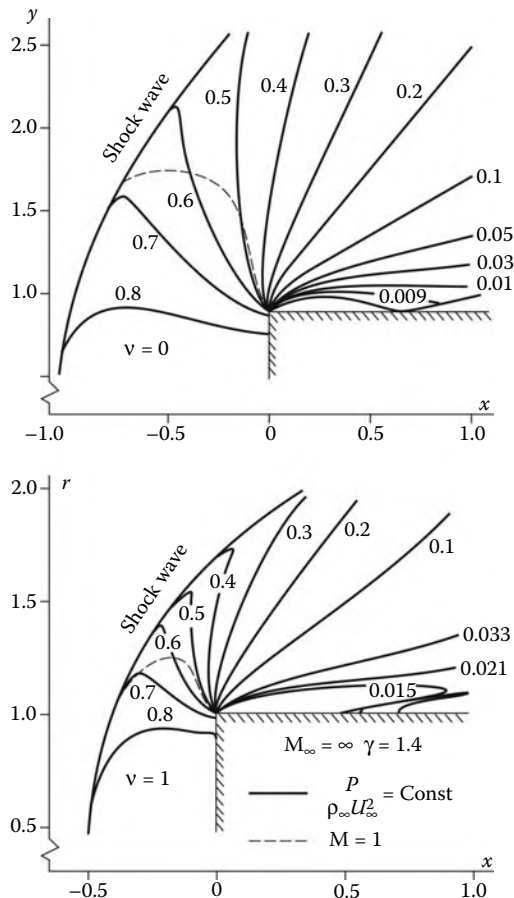


FIGURE 5.18
Patterns of the flow past a flat plate ($v = 0$) and a flat-faced cylinder ($v = 1$).

local in the sense that its result was dependent only on the conditions in the vicinity of the interaction point, while its effect propagated only downstream. However, a similar problem becomes nonlocal when disturbances are incident on a subsonic flow from a supersonic one, owing to the upstream propagation of disturbances in the subsonic flow.

By way of illustration, we will consider the problem of a two-layer flow along a wall aligned with the x axis, the upper flow I being supersonic and the lower sublayer flow II

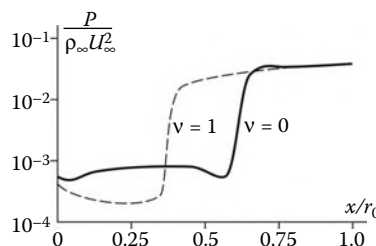


FIGURE 5.19
Pressure distributions over lateral flat-nosed surfaces of the bodies presented in Figure 5.19.

subsonic, with the thickness $\delta(x)$ and the velocity u . Let a weak, steplike disturbance wave be incident from region I on the point O ($x = 0$) of the subsonic sublayer (Figure 5.20a and b). We represent this wave as the characteristic aO with a given initial pressure difference $p_2 - p_1$ or the flow deflection angle θ_2 ($\theta_1 = 0$), where the subscripts 1 and 2 refer to the parameters in the initial domains (1) and (2) to the left and the right of the characteristic aO , fairly far from the point O . The incident wave can be either a shock ($\theta_2 < 0$, Figure 5.20a) or a narrow expansion fan ($\theta_2 > 0$, Figure 5.20b), which will be conditionally replaced by a line.

The disturbance propagates upstream along the subsonic sublayer and generates wave W_3 in flow I. We will call this region (region 3 in Figure 5.20) the *free interaction* region. Obviously, the disturbances induced in this region can decay only asymptotically, as $x \rightarrow -\infty$, which makes the boundary between regions 1 and 2 rather conditional.

Within the framework of the linear supersonic theory, which will be used in our analysis, at $x < 0$ the flow parameters on the sublayer boundary, referred to by the subscript 3, and on the characteristic aO far from the point O are related by the linear Equation 4.5.2, which can be written in the form:

$$\begin{aligned} N\Delta p_3 &= \theta_3, & N\Delta p_2 &= -\theta_2 \\ \Delta p_i &= p_i - p_1, & (\rho u^2)_I N &= \sqrt{M_I^2 - 1} \end{aligned} \quad (5.7.1)$$

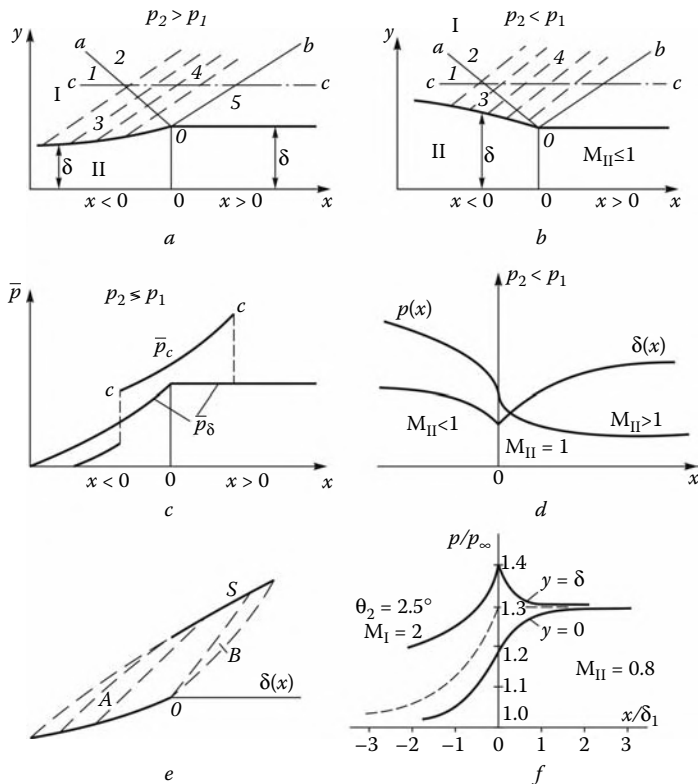


FIGURE 5.20

Interaction of disturbances with a subsonic flow.

Here, the subscripts I and II refer to the flow parameters in the corresponding layers.

In region 4 between the incident *aO* and reflected *Ob* characteristics, the flow parameters are determined by interference of two waves W_3 and W_2 propagating along the first-family (from beneath) and second-family (from above) characteristics, respectively. On these characteristics, Equation 4.5.2 is valid

$$\begin{aligned} W_2 : \quad N(p_4 - p_2) &= \theta_4 - \theta_2; \quad W_3 : \quad N(p_4 - p_3) = \theta_3 - \theta_4 \\ \text{or } \Delta p_4 &= \Delta p_3 + \Delta p_2, \quad \theta_4 = N\Delta p_4 + 2\theta_2 \end{aligned} \quad (5.7.2)$$

The wave W_2 extends also to region 5, to the right of the reflected characteristic *Ob*; this gives a relation between the pressure and the inclination angle $\theta = \delta'$ of the sublayer boundary. In view of 5.7.1 and 5.7.2 we obtain

$$\begin{aligned} N(p - p_1) &= \frac{d\delta}{dx} + N(p_i - p_1) \\ x < 0 : \quad p_i &= p_1, \quad x > 0 : \quad p_i - p_1 = 2(p_2 - p_1) \end{aligned} \quad (5.7.3)$$

To derive qualitative, illustrative results for the sublayer flow, we will consider it in the one-dimensional, hydraulic approximation (Section 2.3) by putting $dp = -\rho u du$ in Equation 2.3.4 and casting it to the form:

$$\begin{aligned} \varphi(p) \frac{dp}{dx} &= \frac{d\delta}{dx} \\ \varphi(p) = \frac{G(1 - M_{\text{II}}^2)}{(\rho^2 u^3)_{\text{II}}}, \quad G &= \rho u \delta = \rho_1 u_1 \delta_1 \end{aligned} \quad (5.7.4)$$

where G is the gas flow rate in the sublayer.

Combining this equation with Equation 5.7.3 we obtain the equation for the pressure in the sublayer

$$\varphi \frac{dp}{dx} = N(p - p_i) \quad (5.7.5)$$

Naturally, this equation is satisfied by the constant solution $p = p_i$. Assuming the disturbances in the sublayer to be small, we also put $\varphi = \text{const}$ in Equation 5.7.5, thus obtaining the solution

$$p - p_i = C_1 e^{\kappa x} + p_i - p_1, \quad \kappa = \frac{N}{\varphi} = \frac{M_{\text{II}}^2 \sqrt{M_{\text{I}}^2 - 1}}{\delta_1 M_{\text{I}}^2 (1 - M_{\text{II}}^2)} \quad (5.7.6)$$

The equality for κ is written for the case in which we deal with the flow of a perfect gas, the same in both layers. The first term vanishes as $x \rightarrow -\infty$; however, it is unbounded as $x \rightarrow \infty$, so that $C_1 = 0$ should be possible. In view of the continuity of the pressure and the layer interface slope at the point $x = 0$ we can present the solution as a whole in the same form for compression and expansion waves

$$\begin{aligned} x < 0 : \quad \bar{p} &= \frac{p - p_1}{p_2 - p_1} = C_2 e^{\kappa x}, \quad C_2 = 2 \\ x > 0 : \quad \bar{p} &= 2, \quad p = p_5 = p_1 + 2(p_2 - p_1), \quad \theta = 0 \end{aligned} \quad (5.7.7)$$

The sublayer II thickness is determined from the flow rate equation $\delta(x) = G/\rho u$, its boundary having a bend at the point $x = 0$. The first solution 5.7.7 relates to the region $x < 0$, while the second one relates to the region $x > 0$ and—outside of sublayer II—to the

entire region 5 to the right of the characteristic Ob and corresponds to the reflection of a weak disturbance from a solid wall. The boundary shape $\delta(x)$ is presented in Figure 5.20a and b, for the compression and expansion waves (everywhere for $M_{II} < 1$).

By the way, we note the qualitative difference of the interaction of disturbances with subsonic and supersonic sublayer flows: at $M_{II} > 1$ we have $\kappa < 1$ in the sublayer, so that the solution, bounded as $x \rightarrow -\infty$, can be obtained only for $C_1 = 0$, that is, when the solution for the sublayer is constant up to the point $x = 0$.

We will now investigate the disturbance field in flow I. The wave W_2 is simple; therefore, all the flow parameters on the first-family characteristics are constant in regions 3 and 4, though they have a discontinuity on the characteristic aO . From Equations 5.7.2 and 5.7.7 it follows that as the characteristic Ob is approached from the left, we have $\bar{p}_4 \rightarrow 3$ and $\theta_4 \rightarrow -\theta_2$. However, on the right of characteristic Ob we have $\bar{p}_5 = 2$ and $\theta_5 = 0$. Therefore, this characteristic is a discontinuity line of the solution, with the parameter jumps $\Delta\bar{p} = -1$ and $\Delta\theta = -\theta_2$, as shown in Figure 5.20c in which we have sketched the pressure coefficient \bar{p} distributions over the sublayer boundary II, that is, the wall, and in a certain longitudinal section $c-c$. In the case in which the incident waves are compression ones, the characteristic Ob represents an expansion wave; on the contrary, when the incident waves are expansion ones, ob represents a compression wave, or a weak shock. In other words, the wave structure formed from reflection of an acoustic wave from the subsonic flow region contains an intermediate zone in which the disturbance intensity exceeds the resulting intensity of the reflected wave as a whole.

Solution 5.7.7 is invalid in two limiting cases, in which either the pressure in the sublayer is close to the stagnation pressure p_0 or the sublayer flow is transonic; in fact, in these two cases the coefficient $\varphi(p)$ in Equation 5.7.5 cannot be taken to be constant, which lays in the basis of solution 5.7.6. In the first case, putting $\varphi \sim u^{-3}$ and $2(p_0 - p) = \rho u^2$ in Equation 5.7.5 and rewriting it in terms of the velocity u , it is easy to derive its integral-form solution, which is qualitatively similar to 5.7.6.

If flow II is initially transonic and the intensity of the incident expansion wave is sufficiently large that the flow accelerates up to a supersonic velocity, then the coefficient $\varphi(p)$ changes the sign at $M_{II} = 1$, this point being singular for Equation 5.7.5. The sublayer thickness is minimum in the sonic cross-section, which must include the point O at which the disturbance arrives, since in the free interaction zone the pressure can only decrease monotonically along the sublayer due to the decrease in its thickness. Putting $\varphi = \alpha(p - p_*)$, where $\alpha > 0$ is a constant and p_* is the sonic pressure (at $M_{II} = 1$), we obtain the following solution for the vicinity of the singular point

$$\begin{aligned} \alpha(p - p_*)^2 &= 2(p_* - p_i)x > 0 \\ x < 0 \quad p_i &= p_1 > p_*, \quad x > 0 \quad p_i = p_5 < p_* \end{aligned} \tag{5.7.8}$$

This solution is similar to the solution 2.3.8 for channels. The derivative dp/dx is unbounded at the point $x = 0$; however, in accordance with 5.7.3, the slope of the sublayer boundary $\theta = N(p_* - p_i)$ is bounded and, as earlier, discontinuous. In this approximation, Equation 5.7.5 can again be integrated in quadrature form. This solution is sketched in Figure 5.20d; it has the same asymptotics as 5.7.6, though propagating to both sides of the x axis ($x \rightarrow \pm\infty$).

We note that, in accordance with 5.7.6, the dimensions of the disturbance decay domain are in any case of the order $\Delta x \sim 1/\kappa$; they increase as the Mach number M_{II} decreases and decrease with the difference $|1 - M_{II}|$. Naturally, the interaction of the compression wave with a subsonic flow is possible only if the resulting pressure p_5 is smaller than the

stagnation pressure in layer II. Otherwise, the subsonic flow turns out to be choked, which is accompanied by the global restructuring of the flow.

In the linear formulation, the wave pattern obtained extends to infinity; however, it changes appreciably if nonlinear effects are taken into account. In particular, nonlinear expansion waves are continuous and diverging, which, generally speaking, must result in the smoothing of all discontinuities and bends in the sublayer boundary and pressure profiles in Figure 5.20. The problem of the incidence of a continuous expansion wave on a subsonic sublayer is, in particular, related with the outflow of an overexpanded jet from a nozzle with the formation of a subsonic jetlet behind the bridge-shaped shock, as described in Section 5.5 (see also Figure 4.21 in Section 4.9).

Here, we will dwell in detail only on nonlinear compression waves. The expected nonlinear wave pattern in the vicinity of the point of the compression wave reflection from the subsonic sublayer is shown in Figure 5.20e. In this case the first-family characteristics in waves 3 and 4 form the divergent bundle A , within which the shock S is initiated. However, since in this wave $\theta > 0$, the flow turns in the vicinity of the point O , thus generating the expansion wave B .

This wave interaction pattern was obtained by Chernyi (1952) in solving the problem for the two-dimensional flow in sublayer II in the nonlinear formulation. Characteristic of this solution is that it also contains the point O at which the sublayer boundary bends; in the case in which this point is, in accordance with Section 2.11, in the internal subsonic flow, it turns out to be the stagnation point of the flow with the pressure $p = p_0$. Quite naturally, the two-dimensional theory leads to different parameter distributions along the sublayer boundary and the wall, which is demonstrated in Figure 5.20f with reference to the example from the previously mentioned work; however, the one-dimensional theory (dash line) gives an adequate result for the wall pressure and the extent of the disturbed region.

A similar corner point is apparently inevitable at the point interaction of a shock with a subsonic flow region, including a semi-infinite one, since in this case the external flow must turn at the interaction point by a finite angle $\Delta\theta$ determined from the supersonic flow by the pressure differences $p_0 - p_1$, $p_0 - p_2$, or $p_0 - p_5$. In the incompressible ($p \approx p_0$) internal flow around such an angle with $\Delta\theta \neq \pi/2$ the corner point is singular (Section 2.11) with an unbounded derivative dp/dx , as shown in Figure 5.20f.

5.8 Existence of Steady-State Solutions

In gas dynamics it is usually assumed that the time-dependent problems always have a solution. Let us write down the time-dependent equations in the form:

$$\frac{\partial f}{\partial t} = L(f), \quad f = u, v, \dots \quad (5.8.1)$$

Here, $L(f)$ is a differential operator, which does not contain derivatives with respect to time. Then, specifying an arbitrary initial field $f = f_0$ at $t = t_0$, we can make a temporal, or evolutionary, step: $\Delta f = \Delta t \cdot L(f)$, and so on. This means that one or another process develops in any case. Another point is whether this process becomes stationary, as $t \rightarrow \infty$. However, this is the only fashion of attainment of the steady state.

The positive answer to this question is usually accepted without saying. A typical example of this kind is presented in Figure 1.22. A vast experience of running wind-tunnel

experiments, in which a certain time interval for starting the setup is necessarily envisaged, as well as of applying various numerical methods based on steady-state attainment (Section 4.4), also supports this point of view.

However, previously we have outlined many examples of the nonuniqueness of steady-state inviscid solutions or even of their absence. One of the examples of this kind, the interaction of a jet with a barrier (Figure 5.15), was described in Section 5.7. A similar situation can also occur in inviscid flows past bodies in the presence of bow and internal shocks. Since in this case the entropy is usually higher in the vicinity of the body, the stagnation pressure at near-wall streamlines is lower than that on peripheral ones, which are responsible for the pressure level on the body rear in a hypothetical separationless flow. This can result in the same situation as in Section 2.11 (Figure 2.21b), with a low-ram-pressure sublayer at a positive pressure gradient. In that case an inviscid steady-state flow was impossible owing to an inviscid separation of the flow, which was not balanced out by any other factor. Indeed, this effect has only theoretical implications, since in reality this separation is absorbed by a viscous separation base region, which always forms downstream of bluff bodies. In this case, viscosity plays a crucial part in the formation of the flow pattern and its uniqueness, as in the subsonic flow past bodies (Sections 2.10 and 2.12) and in the formation of forward separation zones (Section 5.3).

We note in conclusion that all these effects may appear in the numerical solution of similar inviscid problems due to the difference-scheme viscosity effect, which is qualitatively similar to the physical one. In particular, these solutions can contain inviscid separation zones, though any attempts of attributing them a physical reality are, quite naturally, not justified.

Finally, there exists a possibility that an unsteady periodic flow arises instead of the steady-state one under the same external conditions. An example in engineering is provided by the surge effect in air-breathing engines with a detached shock ahead of them (see the bottom panel in Figure 3.11, Section 3.6) or in a subsonic flow past bodies in general. This very undesirable effect consists of intense pressure and flow-rate fluctuations in engines. Such fluctuations arise in a supersonic flow past bodies with a closed forward cavity (e.g., at a cut-off entrance channel, as in Figure 3.11). We can even see this in a dancing lid of a boiling kettle, the gurgle of water pouring from an overturned bottle, and so on.

The variety of the examples of this kind is naturally much vaster than those presented here, especially if the range of the physical factors taken in consideration is extended to include such phenomena as viscosity, nonequilibrium, and so on. Therefore, we will repeatedly turn back to these questions.

6

Self-Similar or Group Solutions

In this chapter we have collected fairly miscellaneous problems with reference to a unified methodological criterion, namely, their self-similarity (cf. Section 1.12), which leads to reduction in their dimensionality, thus simplifying their solution. At the same time, the problems thus made canonical, together with their solutions, allow one to make more definite conclusions on local and global properties of the flows of more general classes.

6.1 Basic Concepts

We will consider a class of problems having a *solution group** of the type

$$\begin{aligned}\varphi(x, r) &= B_1 r^n f(\zeta) = \bar{B}_1 x^m \tilde{f}(\zeta), \quad \zeta = B_2 x r^{-k} \\ \tilde{f} &= \zeta^{-n/k} f, \quad m = n/k, \quad \bar{B}_1 = B_1 B_2^{n/k}, \quad B_i = \text{const}\end{aligned}\tag{6.1.1}$$

Here, x and r are any independent variables (e.g., time or coordinates), while φ and $f(\zeta)$ can be columns composed of several unknown functions. In this case, the problem can be reduced to a single ordinary differential equation with respect to the function $f(\zeta)$ or to a system of such equations, that is, a mathematically two-dimensional problem is reduced to a one-dimensional one, a three-dimensional problem to a two-dimensional one, and so on. The lines $\zeta = \text{const}$ are curvilinear for $k \neq 1$ and form a bundle of rays for $k = 1$. Earlier we have already met with such problems. Thus, the problems of the supersonic flow past a cone and a wedge (Section 2.8) correspond to $n = 0$ and $k = 1$, while for a wedge in incompressible flow (Section 2.9) we have $k = 1$ with the exponent n dependent on the wedge vertex angle.

The solutions of the type 6.1.1 are also referred to as *self-similar*, since they are similar to themselves in all sections $x = \text{const}$. An important role in their *a priori* construction is played by similarity and dimensional methods (see Section 1.12). For example, we recall conical bodies, the surfaces of which are formed by a bundle of rays with an arbitrary generator originating from a pole representing the body nose. The problem of the steady-state supersonic flow past these bodies lacks a scale length, so that dimensionless combinations of the parameters in parentheses in Equation 1.12.9 could be composed solely under the assumption that the solution depends on two variables only: $p' = p'(y/x, z/x)$. We will devote several sections of this chapter to these conical flows. As for subsonic flow past a cone or wedge nose, this flow is not conical owing to the influence of the body length L .

* The group analysis in gas dynamics is described in Ovsyannikov (1980).

Another example is provided by the one-dimensional time-dependent gas flow induced by piston expansion according to a $r_p = ct^n$ law. If the velocity of the piston-induced shock is so high that the following conditions hold

$$R \gg a_\infty, \quad p_\infty \ll \rho_\infty \dot{R}^2, \quad e_\infty \ll \dot{R}^2 \quad (6.1.2)$$

then the external gas parameters a_∞ and e_∞ no longer enter in the shock relations of Section 3.3; hence, for example, relation 1.12.9 must have the following form:

$$p = p(r, t, c, \rho_\infty, n, \gamma), \quad [c] = Lt_0^{-n}, \quad t_0 = [t] \quad (6.1.3)$$

Obviously, in this case the shock propagates following a $R \sim ct^n$ law; then the roles of uniquely possible dimensional pressure and velocity are played by the combinations $\rho_\infty c^2 t^{2(n-1)}$ and ct^{n-1} , while the independent variable is represented by the quantity $\eta \sim r/ct^n$. In other words, this solution belongs to class 6.1.1. In Section 6.8 it will be shown that the classical problem of the strong blast also belongs to the self-similar class, while the simplest version of this problem ($n = 1$) corresponds to piston expansion at a constant velocity, $v_p = r_p/t$. In this case, there is no need to put $a_\infty = 0$; simply, a new similitude parameter v_p/a_∞ appears. These problems were considered in Sections 2.8 and 3.7.

We note that there exists a fundamental difference between the two types of problems. For the conical problems, both exponents n and k are determined beforehand, from the similarity and dimensionality theory. At the same time, in the local problem of the incompressible flow past a wedge, these exponents are determined as eigenvalues in the process of the problem solution. The problems of the first class (apart from the conical flows, this class also includes the strong blast problem; see the following) are sometimes called the *self-similar problems of the first kind* (in accordance with the classification given by Zeldovich, 1966). The problems of the second class (wedge and cone in incompressible flow, transonic asymptotics) are referred to as the *self-similar problems of the second kind*.

Usually, the self-similar solutions reflect local asymptotics, either temporal or spatial, of particular fragments of more general, or *global*, solutions describing the flow as a whole. In this case the mode of matching of these local solutions with global ones depends on the kind of the self-similarity. Thus, a very simple and typical example of the first-kind self-similarity is provided by the supersonic flow around an airfoil with a wedge-shaped nose or a body of revolution with a conical nose; in these cases, the local self-similar solution at the nose is determined independently and is then continued downstream in the longitudinal coordinate. However, in a subsonic flow the local solution in the vicinity of a nose must necessarily include free parameters, for example, some coefficients B_i , which would allow for certain conditions imposed downstream of the nose. It should be noted that this matching can be made purely analytically in exceptional cases only (as in the problem of the wedge, Section 2.11); thus, the question of whether a local solution obtained is intrinsic to the global solution is usually solved upon intuition or using a special processing of numerical solutions.

We note that the choice of the problems, which are presented in the following, is rather fragmentary and is mainly related with supersonic flows (Sections 6.4 through 6.7). Sections 6.8 and 6.9 are devoted to strong blast theory, which has, as will be shown in Chapter 9, applications in hypersonic flow theory. Only two sections deal with incompressible (Section 6.2) and transonic (Section 6.3) flow theory. Finally, Section 6.10 is devoted to viscous self-similar problems.

6.2 Cone in Incompressible Flow

In this section we will derive an asymptotic solution for the vicinity of a conical nose in the same fashion as it was done for a wedge in Section 2.11. Using the substitution $\Phi = CU_\infty r^n \Theta(\theta)$ we reduce Equation 2.10 for the potential to an ordinary differential equation with respect to the function $\Theta(\theta)$

$$\begin{aligned} (\Theta' \sin \theta)' + [n(n+1) \sin \theta] \Theta &= 0 \\ \theta = 0, \pi - \theta_0 : \quad v_\theta, \Theta' &= 0 \end{aligned} \quad (6.2.1)$$

This is a homogeneous equation with homogeneous boundary conditions imposed on the axis of symmetry and on the surface of the cone with the semivertex angle θ_0 . As Equation 2.11.11 considered, this equation has nontrivial solutions only for certain eigenvalues $n = n(\theta_0)$.

Changing t for $\cos \theta$ we bring Equation 6.2.1 to the *Legendre equation*

$$\frac{d}{dt} \left[(1-t^2) \frac{d\Theta}{dt} \right] + n(n+1)\Theta = 0 \quad (6.2.2)$$

In these variables, the function $\Theta(t)$ must satisfy the conditions

$$\begin{aligned} \theta = 0, \quad t = 1 : \quad \frac{d\Theta}{d\theta} = -\sin \theta \frac{d\Theta}{dt} = 0, \quad \frac{d\Theta}{dt} &< \infty \\ \theta = \pi - \theta_0, \quad t = t_0 = -\cos \theta_0 : \quad \frac{d\Theta}{dt} &= 0 \end{aligned} \quad (6.2.3)$$

Thus, the problem is reduced to the search for a minimum eigenvalue n for this boundary value problem. The Legendre equation possesses a sequence of eigensolutions, namely, the *Legendre polynomials* $P_n(t)$ corresponding to integer eigenvalues n and bounded at the segment ending $t = \pm 1$. However, of all these solutions only two apply to our conditions: the first solution ($n = 1$) corresponds to the undisturbed flow and the second one ($n = 2$) to the vicinity of the stagnation point of a blunt body

$$\begin{aligned} \Theta_1 &= -P_1 = -t, \quad \theta_0 = 0, \quad t_0 = -1, \quad n = 1 \\ \Theta_2 &= -P_2 = -\frac{3}{2}t^2 + \frac{1}{2}, \quad \theta_0 = \pi/2, \quad t_0 = 0, \quad n = 2 \end{aligned} \quad (6.2.4)$$

At the same time, in the solution of Section 2.11 for a wedge, the value $n = 2$ corresponded to the stagnation point of a blunt body, $\theta_0 = \pi/2$. For an acute angle, $\theta_0 < \pi/2$, we have $1 < n < 2$ with a nonanalytical velocity distribution $v_\theta, v_r \sim r^{n-1}$ in its vicinity. It is quite natural to expect the same result in the case of a cone. However, the similar eigenvalue problem for a cone has no simple solutions. Equation 6.2.2 has two singular points, $t = \pm 1$, with the following solutions in their vicinities

$$\Theta = (1-mz)(C_1 + C_2 \ln z), \quad z = 1 \pm t, \quad m = \frac{n(n+1)}{2} \quad (6.2.5)$$

In these vicinities the derivative $d\Theta/d\theta \approx C_2 z^{-1}(\sin \theta) \sim C_2 z^{-1/2}$; using the boundary condition 6.2.3 as $t \rightarrow 1$ or $\theta \rightarrow 0$ we should set $C_2 = 0$. Then, since the general solution contains already an arbitrary constant, in what follows we set $C_1 = -1$. Then the single

condition $d\Theta/d\theta = 0$ at the cone surface $\theta = \pi - \theta_0$ suffices for the determination of the eigenvalues $n(\theta_0)$. This dependence, which can be determined solving the problem numerically (using either difference methods or expansion in hypergeometric series; Selezneva, 1998), is presented in Figure 6.1. The same figure presents the quantity $\Theta_0 = \Theta(t_0)$ on the cone surface (for a wedge $\Theta_0 = 1$).

However, in the problem for a slender cone $\theta_0 \rightarrow 0$, so that the conical surface lies within the domain of influence of the second singular point $t \rightarrow -1$ the extent of which is $\Delta z = 1 + t \sim \theta_0^2$. In this case, an asymptotic solution of Equation 6.2.2 can be derived by linearization. This solution is linear in θ and nonlinear with respect to the eigenvalue problem, since both Θ and n depend on θ_0 .

We will seek the solution of this problem for small θ_0 in a series form:

$$\Theta = -t + \varepsilon\Theta_1 + \dots, \quad n = 1 + \varepsilon \quad (6.2.6)$$

Substituting this expansion into Equation 6.2.2 and retaining the terms of the order of ε only, we obtain an equation for Θ_1

$$[(1 - t^2)\Theta'_1]' + 2\Theta_1 = 3t \quad (6.2.7)$$

It has a general solution (Gonor, 1989)

$$\Theta_1 = -\frac{1}{2}t \ln(1 - t^2) + C'_1 \left(\frac{1}{2}t \ln \frac{1+t}{1-t} - 1 \right) + C'_2 t \quad (6.2.8)$$

Setting $C'_1 = -1$ in this solution we exclude the singularity as $t \rightarrow 1$; by an appropriate choice of the constant C'_2 we ensure the fulfillment of the condition $\Theta_1(1) = 0$.

As a result, the solution takes the form:

$$\Theta_1 = -t[\ln(1+t) - \ln 2] + 1 - t \quad (6.2.9)$$

Since at small θ_0 we have $1 + t_0 = \theta_0^2/2$ on the cone, then, neglecting the terms of the order $\varepsilon \ln \varepsilon$, from the condition $d\Theta/dt = 0$ at $t = t_0$ we obtain

$$n = 1 + \frac{1}{2}\theta_0^2 \quad (6.2.10)$$

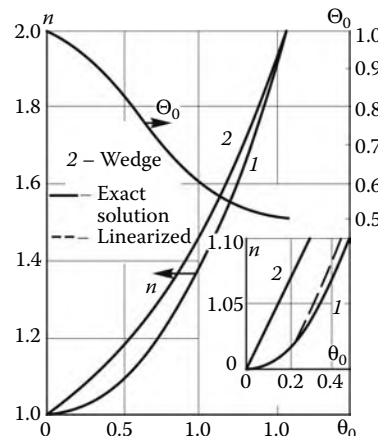


FIGURE 6.1

Eigenvalues $n(\theta_0)$ for a cone and a wedge and function Θ_0 on the conical surface.

Comparison of the data in Figures 6.1 and 6.2 demonstrates a good accuracy of the asymptotic solutions 6.2.9 and 6.2.10 already at $n - 1 \leq 0.05 - 0.08$ or at $\theta_0 \leq 20^\circ - 25^\circ$, that is, for not-too-slender cones.

As distinct from the problem of a wedge of Section 2.11, here we obtained only the minimum eigenvalue n determining the main term of the solution asymptotics as $r \rightarrow 0$. As for the arbitrary constant C entering in the solution, it should be determined, as noted previously (see Sections 2.11 and 6.1), by matching the solution obtained with the global solution for the body with a conical nose. In this connection, we note that the solution obtained applies also to compressible subsonic flows, since, as the flow decelerates or as the body surface is approached, the local Mach number M vanishes, so that the terms of the order M^2 associated with fluid compressibility drop off of the potential Equation 2.4.8 (in which the time-dependent terms are omitted).

6.3 Some Transonic Problems

In this section attention will be devoted to the flow in the vicinity of the corner point of a convex body in subsonic flow. When discussing in Section 5.6 the question of the relative position of the corner point and the sonic point, which occurs in this flow, we made the most plausible assertion that the two points coincide, at least, in the cases in which the turn of the flow around the corner point is the only reason for the attainment of the sonic velocity by the gas. In what follows we shall derive under this assumption a local self-similar solution for the vicinity of a corner point, originally in a subsonic flow. In anticipation, we note that, similarly to the problems of the wedge (Section 2.11) and the cone (Section 6.2) in incompressible flow, the solution to be obtained pertains to the self-similar solutions of the second class (as distinct from the Prandtl–Meyer waves) and involves an indefinite arbitrary constant, which, as in Section 2.11, could be determined only by matching the local solution with the global one, owing to their mutual influence, which is unavoidable in subsonic flow.

In considering subsonic channel flows in Section 2.3 we revealed the fact that in the sonic section the solution is singular if special measures for preventing it (e.g., an appropriate choice of the channel contour) are not taken. A similar singularity should be expected in

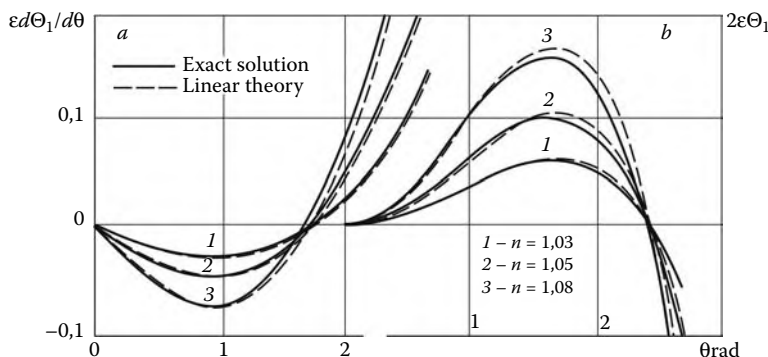


FIGURE 6.2
Comparison of the exact and linearized solutions.

our case as well. Because of this, in analyzing a small vicinity of the sonic point one should seek, in accordance with the notes made in Section 6.1, a solution of the von Kàrmà̄n Equation 5.2.6 in its general form 6.1.1 with r replaced by y . We will align the x axis with the wall ahead of the sonic point and place the coordinate origin ($x, y = 0$) at this point, as in Figure 5.16. The relation between the exponents n and k is determined from the condition that the ratio of the terms of Equation 5.2.6 must depend on ζ only

$$\varphi_x \varphi_{xx} : \varphi_{yy} \sim y^\chi F(\zeta) = F(\zeta), \quad \chi = n - 3k + 2 = 0 \quad (6.3.1)$$

We will change variables as follows:

$$x' = B_2 x, \quad y' = y, \quad \varphi' = C_0 \varphi, \quad \zeta = x'/(y')^k, \quad C_0 = 2A_* B_2^3 B_1 \quad (6.3.2)$$

In what follows the primes are omitted. Substituting 6.3.2 in 5.2.6 we obtain an equation for the function f of 6.1.1

$$L(f) = k^2 \zeta^2 f'' - 5k(k-1)\zeta f' + 3(k-1)(3k-2)f = f'f'' \quad (6.3.3)$$

The velocity components are as follows:

$$\varphi_x = y^{2(k-1)} f', \quad \varphi_y = y^{3(k-1)} \psi(\zeta), \quad \psi = (3k-2)f - k\zeta f' \quad (6.3.4)$$

We recall that in the von Kàrmà̄n approximation we have $U - a_* \sim \varphi_x$, so that on the sonic line $\varphi_x = 0, f'(\zeta) = 0$, and $\zeta = \zeta_* = \text{const}$, while in the subsonic and supersonic flow regions $\varphi_x < 0$ and $\varphi_x > 0$, respectively. The required solution must satisfy, first, the impermeability condition at the wall, $\varphi_y = 0$ at $y = 0$ and $x < 0$ ($\varphi_x < 0$) and, second, become a centered expansion fan downstream of the sonic line at $\varphi_x > 0$; such an expansion wave is necessarily formed in the flow past a corner point. Moreover, the sonic line $\zeta_* = \text{const}$ can pass through a corner point only for $k > 0$; precisely this case will be considered in the following.

Since $\zeta \rightarrow -\infty$, as $y \rightarrow 0$ and $x < 0$, the estimates $f \sim (-\zeta)^{3-2/k}$ and $f'/\zeta^2 \sim (-\zeta)^{-2/k} \rightarrow 0$ must be fulfilled in order for the quantity φ_x not to be zero or infinite. Thus, in this region the right-hand side of Equation 6.3.3 could be neglected, so that it becomes a linear homogeneous equation $L(f) = 0$. With allowance for this fact, the asymptotic expansion of the solution, as $\zeta \rightarrow -\infty$, takes the form:

$$f = C_1(-\zeta)^{3-2/k} + C_2(-\zeta)^{3-3/k} + C_3(-\zeta)^{3-4/k} \quad (6.3.5)$$

The first two terms of this expansion represent the general solution of the linear equation with arbitrary constants C_1 and C_2 . The third term is due to nonlinearity of the equation and is obtained by substituting the first, higher-order term into the right-hand side. For this reason, the coefficient $C_3 \sim C_1^2$. For $y \rightarrow 0$ this solution yields

$$\varphi_x = -C_1(-x)^{2-2/k}, \quad \varphi_y = -C_2(-x)^{3(k-1)/k} \quad (6.3.6)$$

Specifying the values $C_1 > 0$ and $C_2 = 0$ in this solution we can satisfy the conditions at the wall for $x < 0$. However, in this case a whole family of integral curves with different C_1 is reduced to a single curve by a transformation of the type 6.3.2. In view of this fact, one can satisfy the conditions in the domain $\varphi_x > 0$ only by an appropriate choice of the exponent k , that is, the eigenvalue of the problem.

This solution corresponds to the exponent $k = 5/4$ and was first obtained numerically (Vaglio-Laurin, 1960) and then in a parametric form (Falkovich and Chernov, 1964):

$$\begin{aligned} f &= \frac{C}{21}(t-1)^{-7/8}(7t^2 - 140t + 160) \\ \zeta &= C^{1/3}(t-1)^{-5/8}(t-8/5) \\ C > 0, \quad 1 < t < \infty \end{aligned} \quad (6.3.7)$$

In view of 6.3.4 and 6.3.6, this solution satisfies the condition $\varphi_y = 0$ as $y \rightarrow 0$ and $x < 0$, that is, for $t \rightarrow 1$ and $\zeta \rightarrow -\infty$. At the same time, as $t \rightarrow \infty$ and $\zeta \rightarrow \infty$, this solution has the asymptotics

$$f \rightarrow f_3 = \frac{1}{3}\zeta^3, \quad \varphi_x = (x/y)^2, \quad \varphi_y = -\frac{2}{3}(x/y)^3 \quad (6.3.8)$$

In this case $\zeta \sim y^{-1/4} \rightarrow \infty$, as $y \rightarrow 0$ at rays $x/y = \text{const}$. At $x/y > 0$ this solution describes a centered expansion wave and coincides with the Prandtl–Meyer wave asymptotics in the vicinity of the sonic line obtained in Section 4.6. It is interesting to note that the function $f_3(\zeta)$ is a k -independent solution of Equation 6.3.3 (at $x < 0$ it governs a certain compression wave, which would be difficult to interpret physically).

On the sonic line, $\zeta = \zeta_*$, solution 6.3.7 yields

$$\begin{aligned} f'(\zeta_*) &= 0, \quad t = 4, \quad \zeta_* > 0, \quad f_* = f(\zeta_*) < 0 \\ x &= \zeta_* y^{5/4} > 0, \quad \varphi_y = 7/8 f_* y^{3/4} < 0 \end{aligned} \quad (6.3.9)$$

Since on the sonic line characteristics are orthogonal to streamlines, the angles, which the former make with the y axis are $dx/dy \sim y^{3/4}$, which at small y are considerably less than the sonic line slope, $dx/dy \sim y^{1/4}$. Therefore, the bundle of characteristics originating from the corner point enters the sonic line in accordance with the scheme in Figure 5.16b, thus forming an interrelated flow fragment with a subsonic region $\varphi_x < 0$. It should be added that the expansion wave, which is centered as a whole, is no longer a simple expansion wave owing to nonuniformity of the preceding subsonic flow induced by the wave itself (an exception is provided by the corner point itself, where solution 6.3.8 is valid). The solution obtained gives unbounded velocity disturbances, φ_x and φ_y , as $y \rightarrow 0$ and $x > 0$; however, this testifies only to the inadequacy of the von Kármán equation in describing flows with finite disturbances.

The solution thus obtained is singular, which was assumed beforehand. The gas velocity tends to the sonic velocity following the law $\varphi_x \sim (-x)^{2/5}$ along the wall (in the channel flow we had $\varphi_x \sim (-x)^{1/2}$, Section 2.3) and $\varphi_x \sim y^{1/2}$ along the y axis. This singularity is illustrated, for example, by the calculated curves for the pressure on a flat-faced cylinder and a flat plate (Figures 5.8 and 5.9) with unbounded derivatives in the vicinities of corner points and sonic velocities at the points themselves. The transverse nonisentropicity of these flows does not change the nature of the singularity, though it can have an effect on the extent of the domain, where the singularity shows itself.

In conclusion, we will call attention to some other self-similar transonic solutions. For $k = 2$ Equation 6.3.3 has a solution

$$\begin{aligned} f &= f_2 = C\zeta^2 + 2C^2\zeta + C^3/3, \quad \zeta = x/\zeta^2 \\ \varphi_x &= 2Cx + 2C^2y^2, \quad \varphi_y = 4C^2xy + 4C^3y^3/3 \end{aligned} \quad (6.3.10)$$

It corresponds to a certain regular transonic flow along the streamline $y = 0$, $\varphi_y = 0$ and is usually derived by series-expansion of the solution of the original von Kàrmà̄n equation. In this case, the sonic line $\varphi_x = 0$ has the shape $x = \zeta_* y^2$, $\zeta_* = -C_1$ and is backward-facing at $C > 0$ (see curve OA in Figure 4.6b, Section 4.3). We have $\varphi_x < 0$ to the left of the sonic line and $\varphi_x > 0$ to the right of it. This case could be assigned to a vicinity of the sonic point on the axis of symmetry of a convergent-divergent nozzle. In this case line OC of zero velocity slope, $\varphi_y = 0$ and $x = -Cy^2/3$, is located in the supersonic region. On the contrary, the situation, in which $C < 0$ and $\zeta_* > 0$ corresponds to supersonic flow deceleration and cannot be related to any known flow.

We note, finally, that the approach outlined is also appropriate for studying the asymptotics of solutions far from a body in the transonic flow.* The solution of this problem is reduced to Equation 6.3.3 for two-dimensional flows and to a similar equation for axisymmetric flows with parametric solutions of the type 6.3.9. It turns out that $k = 4/5$ and $4/7$ in the first and second cases, respectively, which results in the velocity asymptotics $\varphi_x \sim y^{-2/5}$, $\varphi_y \sim y^{-3/5}$ and $\varphi_x \sim y^{-6/7}$, $\varphi_y \sim y^{-9/7}$, which were already presented in Section 5.4.

6.4 Cone in Supersonic Flow

We will deal with the flow past a circular cone with the semivertex angle θ_c at zero incidence. In a cylindrical coordinate system the solution of this problem is dependent on the angular coordinate $\eta = r/x$ only; thus, the governing Equations 4.3.5 and 4.3.6 are reduced to the form (here, θ is the angle of inclination of a streamline to the x axis):

$$\begin{aligned} \eta D\zeta' &= -\zeta(1 + \zeta\eta)(1 + \zeta^2), & \zeta = \zeta(\eta) &= \tan \theta \\ \eta Dp' &= -\zeta(\eta - \zeta)\rho U^2 \\ D &= (1 + \zeta\eta)^2 - \beta^2(\eta - \zeta)^2 = (1 + \zeta\eta)^2[1 - \beta^2 \tan^2(\varphi - \theta)] \\ \beta^2 &= M^2 - 1, & \varphi &= \arctan \eta \end{aligned} \quad (6.4.1)$$

The conventional relations of Section 3.5 are imposed as the boundary conditions on the shock wave ($p = p_s(\eta_s)$ and $\zeta = \zeta_s(\eta_s)$), while at the conical surface we have $\eta = \eta_c = \zeta_c$. This system has a singular point at $D = 0$ or at $\sin(\varphi - \theta) = M^{-1}$. In this case the ray η must coincide with a characteristic, while the velocity normal to the ray is $v_\varphi = a$. However, this is impossible, since first-family characteristics intersect the disturbed layer between the cone and the shock and enter the latter. Therefore, this system has no singularities within the disturbed region (within the framework of the linear theory the singularity appears on the outer boundary of the layer, that is, on the characteristic (Section 2.8)). Thus, the solution of the problem could be sought, in particular, from a given shock with the corresponding cone obtained in the course of solution (the inverse problem).

In the general case, the problem has no analytical solutions. Therefore, we will draw an analysis on the basis of the results of numerical solutions. As in the case of a wedge, the solution has two branches, a weak and strong conical ones. The *conical polar diagram* $\alpha(\theta_c)$ for the first branch is plotted in Figure 3.9 of Section 3.5. The *conical limiting angle of the shock* $\alpha^{(0)}$, which is still attached to the cone, is somewhat greater than the shock angle α_0 .

* The details of this theory can be found in Cole and Cook (1986).

on the wedge with the limiting angle θ_0 . At the same time, the *limiting angle of the cone* $\theta^{(0)}$, the shock in front of which is still attached, is greater than the angle θ_0 , especially for small supersonic M_∞ (cf. Figures 3.9 and 3.10). The same is true for the cone angle, at which the shock angle α_* is sonic. Moreover, one can also distinguish the *sonic angle of the cone* θ^* with $M_c = 1$ on the conical surface; this angle is limiting for the existence of a conical flow, since at $M_c < 1$ a subsonic region appears in the flow.

For small $M_\infty \leq 2$ the pressure is nonuniform across the shock layer; however, as M_∞ increases, the pressure equalizes and becomes near-constant (Figure 6.3). Due to the constancy of the entropy, the same property is inherent in the density and total velocity profiles.

The pressure over the cones at $\gamma = 1.4$ is plotted in Figure 6.4. Representing the pressure in the form of the *normalized pressure coefficient* \tilde{p} in the dependence

$$p_c - p_\infty = \tilde{p}_c \rho_\infty U_\infty^2 \sin^2 \theta_c \quad (6.4.2)$$

which generalizes the Newtonian formula (3.7.8), leads to the magnitudes of the same order, including the case of slender cones, which is evident from Figure 2.13 (Section 2.7).

We will further consider some limiting flow regimes, which admit analytical treatment of the problem.

Small disturbances. In Section 2.8 within the framework of the linear theory we obtained solution 2.8.15, which is quite acceptable for the pressure on the cone. The modified solution (Lighthill, 1947) mentioned in that section can be derived as follows. Omitting the terms of the order of ζ^2 and $\zeta\eta$ in system 6.4.1 and setting $\beta^2 = \beta_\infty^2 = M_\infty^2 - 1$ we bring it into the form:

$$\begin{aligned} \eta D\zeta' &= -\zeta, & D &= 1 - \beta_\infty^2 \eta^2 \\ \eta D\bar{p}' &= -\zeta(\eta - \zeta), & \bar{p} &= (p - p_\infty)/\rho_\infty U_\infty^2 \end{aligned} \quad (6.4.3)$$

However, in contrast to Section 2.8, we retained the quadratic term ζ^2 , which is important only near the wall, on the right-hand side of the second equation. The solution of this system is analogous to 2.8.13 and, with account taken of condition $\bar{p} = 0$ (together with the

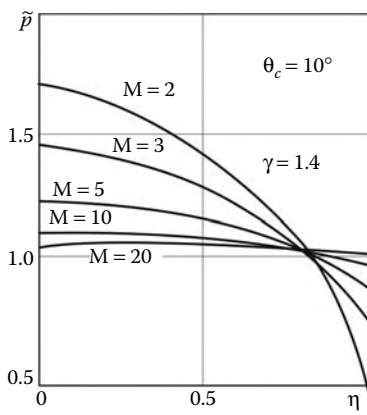


FIGURE 6.3
Pressure profiles in conical shock layers.

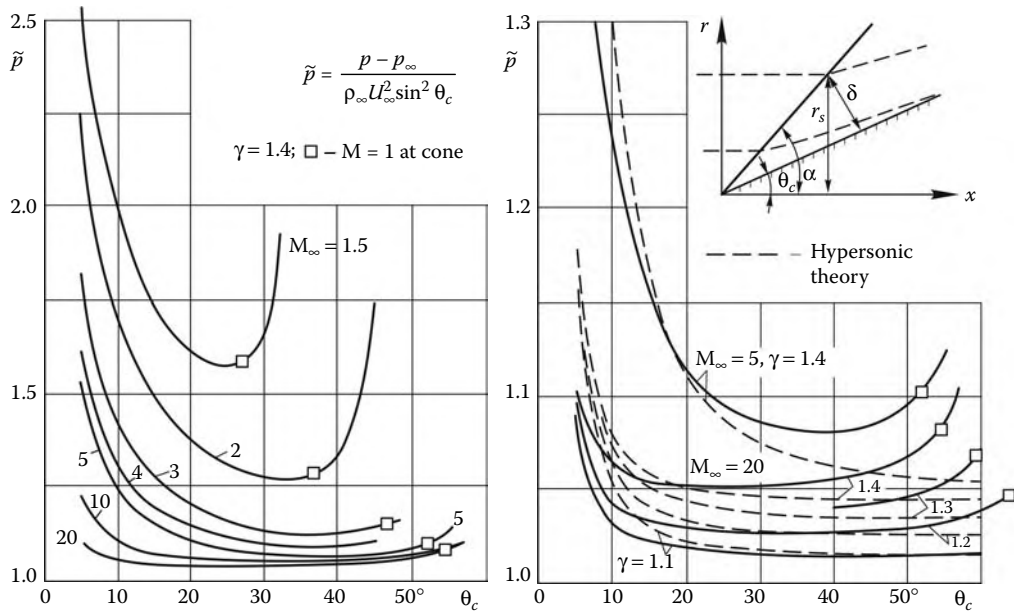


FIGURE 6.4
Pressure on cones.

solution $\zeta = 0$), for $\beta_\infty \eta = 1$ it takes, correct to quadratic terms, the form:

$$\zeta = \frac{\zeta_c^2}{\eta} \sqrt{D}, \quad \bar{p} = \zeta_c^2 \left[\frac{1}{2} \ln \frac{1 + \sqrt{D}}{1 - \sqrt{D}} - \frac{\zeta_c^2}{2\eta^2} \right] \quad (6.4.4)$$

On the conical surface ($\eta = \zeta_c$) we have

$$\tilde{p}_c = \ln(2/K) - 1/2, \quad K = \zeta_c \beta_\infty \quad (\zeta_c = \theta_c) \quad (6.4.5)$$

The correction term $-1/2$ to 2.8.15 improves the results for small $K \leq 0.2$, including those for the $p(\eta)$ and $\zeta(\eta)$ profiles, but deteriorates them for greater K ; however, in the latter case we are beyond the applicability range of the theory (Figures 2.13 to 2.15). Theoretically, this partial inclusion of quadratic terms is not rigorous, especially in the presence of the singular point $\eta = \eta_s$, in the vicinity of which linearization is incorrect. The linear theory gives zero disturbances $\zeta_c = \tilde{p}_c = 0$ at the bow shock, which does not allow one to evaluate its intensity (as was done in the case of the wedge) and its action on the environment. However, the ratios \tilde{p}_s/\tilde{p}_c are sufficiently small for $K \leq 0.1$ (Figure 6.5), together with the deviation $\Delta\alpha$ of the shock slope from that of the freestream characteristic. This is clearly visible in Figure 3.9b, where the conical polar $\alpha(\theta)$ is near-vertical for small θ . As an example, we determine from Figure 2.15 that $\tilde{p}_s = 0.0025$ for $M_\infty = 2$ and $\theta_c = 5^\circ$; then we obtain from formula 3.5.27 that $\Delta\alpha \approx 0.2^\circ$ and $\theta_s \approx 0.25^\circ$. Under the same conditions for the wedge we had $\Delta\alpha = 4^\circ$.

We emphasize that within the limits of the conditions of Figure 2.13 the pressure on the cone depends only on the parameter $K = \theta_c \beta_\infty$ down to $M_\infty = 1.015$ and up to $\theta \approx \theta^{(0)}$, that is, it follows the similarity law of Section 2.7 without the manifestation of specific transonic effects noted in Section 5.2. However, this is not inherent in the flow as a whole. Thus, the curves \tilde{p}_s/\tilde{p}_c in Figure 6.5 (the data of Lipnitskii) coalesce to a single curve for $K \geq 0.3$

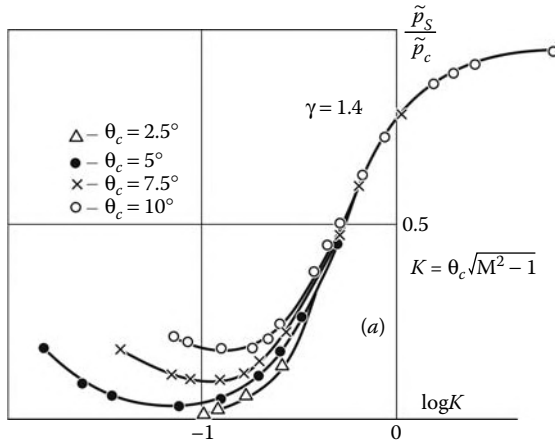


FIGURE 6.5
Pressure on cones.

but diverge at smaller K , their minima decreasing with θ_c ; thus, the solution is, as it were, brought into correspondence with the linear theory. Nevertheless, a growth of these curves with further decrease in K , which would appear rather unexpected, can be explained only by the manifestation of nonlinear transonic effects. At the same time, these curves do not follow the transonic similitude law of Section 5.2, owing to the fact that a too rigorous condition 5.2.7 is not fulfilled on the calculated parameter range.

Hypersonic approximation. In Section 3.7 we derived a simple solution for the flow past a wedge under the assumption that the density ratio across the shock is high, $k = \rho_\infty / \rho_s \ll 1$, or within the framework of the thin shock layer scheme. Here, we will obtain a similar solution for the cone. We will evaluate the shock layer thickness in the same fashion for the cone ($v = 1$) and the wedge ($v = 0$). From the condition of the equality of the rates of the gas flowing into the shock $r_s(x)$ from outside and that flowing out of a shock layer cross-section δ it follows (Figure 6.4)

$$\begin{aligned} (\pi r_s)^v r_s \rho_\infty U_\infty^2 &= (2\pi r_a)^v \rho_a U_a \delta \\ \delta/r_a &= k_a/2^v \cos \alpha, \quad k_a = \rho_\infty / \rho_a \ll 1 \end{aligned} \quad (6.4.6)$$

Here, ρ_a and other parameters are the quantities averaged over the shock-layer cross-section; for a thin shock layer it is taken that $r_a = r_s$ and $U_a = U_\infty \cos \alpha$. Moreover, at small pressure difference across the shock layer (cf. Figure 6.5) we have $\rho_a = \rho_s = \rho_\infty/k$. For the angles θ_c not too close to the limiting angles θ_0 and $\theta^{(0)}$, that is, when $\cos \alpha \approx 1$, it can be that $\alpha \approx \theta_c$ and $r_s = L \sin \theta_c$, where L is the length measured along the body. Then from Equation 6.4.6 we obtain

$$\delta/l = \tan(\alpha - \theta_c) = \alpha - \theta_c = \frac{1}{2^v} k \tan \theta_c \quad (6.4.7)$$

Clearly, the shock layer on the wedge is twice as thick as that on the cone. In this approximation, the first Equation 6.4.1 for the cone has the solution $\zeta = 2\zeta_c - \eta$. Using this solution and the shock condition written with account of Equation 6.4.7 $\bar{p}_s = (1 - k) \sin^2 \alpha \approx \sin^2 \theta_c$

we obtain the solution for the second equation (Chernyi, 1966)

$$\tilde{p} = \bar{p}_c - \frac{(\eta - \zeta_c)^2}{k_0(1 + \zeta_c^2)^2}, \quad \bar{p}_c = \left(1 + \frac{k_0}{4}\right) \sin^2 \theta_c, \quad k_0 = k(\theta_c) \quad (6.4.8)$$

In Figures 6.4 and 6.6 we have compared the approximate solution obtained with the exact one. As in Section 3.7, the agreement is quite satisfactory on the range $K = M_\infty \sin \theta_c \geq 1$ and for the pressure even for angles θ_c close to the limiting ones (within several percents). A comparison with Figure 3.15 shows that the practical accuracy of the hypersonic theory is higher for the cone than for the wedge. This is explained by the fact that the thickness of the shock layer on the cone is smaller by a factor of two than that on the wedge; hence, the addition to the Newtonian pressure 3.7.8 corresponding to the zero-thickness shock layer is smaller by a factor of four. We note that the range of applicability of the Newtonian formula is broader than the range of the conditions determining the smallness of the shock layer thickness. In fact, in accordance with Section 3.5, the latter is determined by the condition that $M_\infty \sin \alpha \gg 1$ or $K = M_\infty \sin \theta_c \gg 1$. Moreover, for $\theta_c \approx \theta^{(0)}$ we have $\tan \theta_c \sim k^{-1/2}$ (Section 3.5) and, in accordance with 6.4.7, $\alpha - \theta_c \sim k^{1/2}$ instead of the earlier result $\alpha - \theta_c \sim k$. At the same time, it follows from Figure 3.15 that the Newtonian formula gives reasonable values of the parameters even for $K \sim 1$. (We note that as $M_\infty \rightarrow \infty$ this parameter K coincides with the parameter K of Section 2.7).

6.5 Conical Flows

The conical flow equations, which in what follows are referred to as the *conical equations*, are degenerate in the sense that the number of the independent variables is less than in the original equations. This leads to the transformation of the properties of the equations, so that even their type may change due to the appearance of ellipticity regions in supersonic flows. A very simple example is provided by the problem of the flow past a cone, in which the original, partial differential equations degenerate into a system of ordinary differential

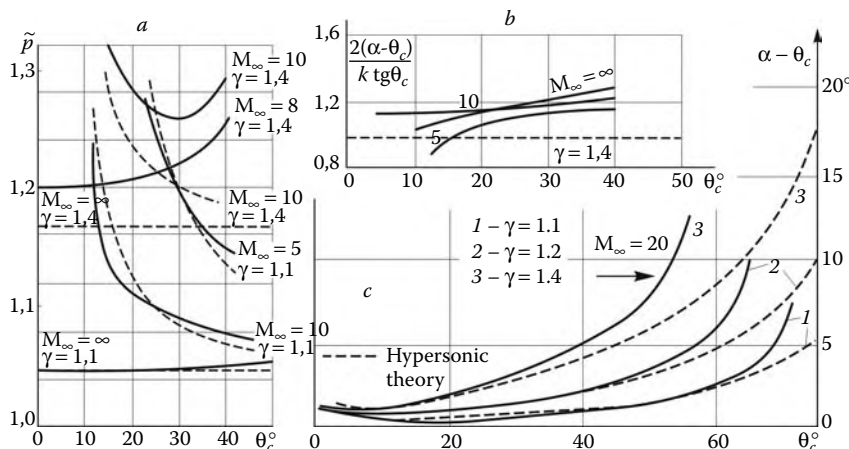


FIGURE 6.6

Pressures and angular thicknesses of the shock layers on cones.

equations with boundary conditions that do not contain any singularities related with the transonic transition.

To elucidate these questions, we will use the gas flow Equation 1.13.15 in a spherical coordinate system (Figure 6.7) and equate in them all the derivatives with respect to r to zero, since in our case all the flow parameters depend on the angular variables, θ and φ , only. Here, we do not write down these equations; however, for the sake of convenience, we will introduce a new notation writing u , v , and w for v_r , v_θ , and v_φ .

At all the points of the unit sphere we will introduce a local Cartesian coordinate system; taking into account expressions 1.13.14 for the scale factors we have

$$dx = dr, \quad dy = r d\theta, \quad dz = r \sin \theta d\varphi \quad (6.5.1)$$

Then the following relations are fulfilled along an arbitrary streamline

$$\frac{dr}{u} = \frac{dy}{v} = \frac{dz}{w}, \quad r \frac{d\theta}{v} = r \sin \theta \frac{d\varphi}{w} \quad (6.5.2)$$

In these variables, the entropy equation takes the form:

$$\frac{ds}{dt} = \frac{v}{r} \frac{\partial s}{\partial \theta} + \frac{w}{r \sin \theta} \frac{\partial s}{\partial \varphi} = v \frac{ds}{dx} + w \frac{ds}{dz} = \frac{1}{r} Q \quad (6.5.3)$$

In adiabatic flows $Q = 0$. We note that the first Equation 1.13.15 for the radial velocity u is of the same type; the only difference is that in that case $Q = u^2 + v^2$. According to the classification given in Sections 4.1 through 4.7, these equations belong to the second group; thus, they have, as in Section 4.3, the trajectory characteristics

$$\frac{d\varphi}{d\theta} = \frac{w}{v \sin \theta} \quad (6.5.4)$$

In accordance with Equation 6.5.2, these *conical streamlines* are the projections of the physical streamlines onto the unit sphere. Their shape is r -independent; therefore, they form a family of streamsurfaces generated by the rays $\theta = \text{const}$, $\varphi = \text{const}$ in the three-dimensional space. These surfaces are isentropic; however, as they are intersected by conical shocks along the rays, the entropy varies jumplike.

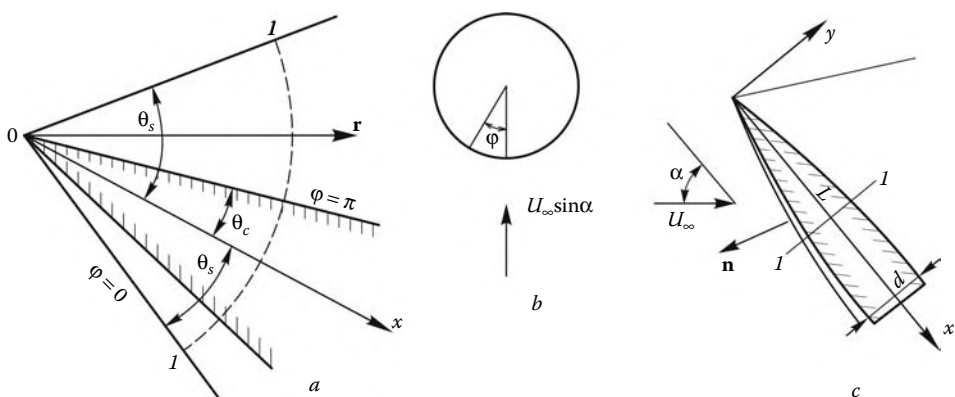
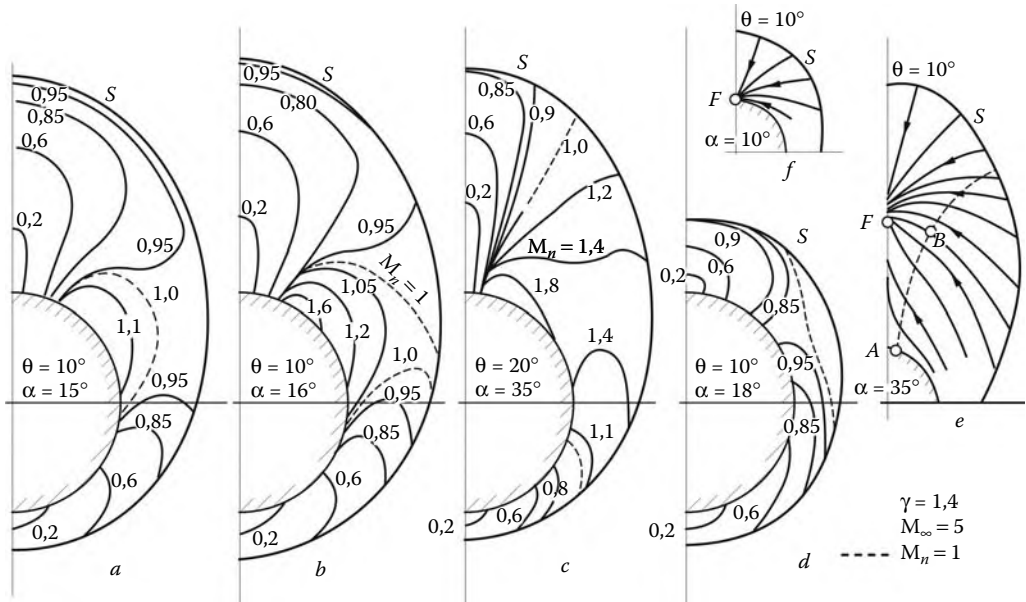


FIGURE 6.7
Coordinate systems for the problem of the flow past bodies at incidence.

**FIGURE 6.8**

Shocks (S), Mach number contours (a–d) and streamlines (e and f) in conical flows.

We will now consider the second, third, and fourth equations in 1.13.15. They form a first-group system, closed with respect to the derivatives, their differential operators coinciding in x, y variables with the same operators for two-dimensional flows of Section 4.3. Hence, they must have the same *wave characteristics*, though *conical*, which will be written in the form 4.3.16:

$$\frac{dy}{dx} = \frac{1}{\sin \theta} \frac{d\theta}{d\varphi} = \frac{vw \pm \sqrt{v^2 + w^2 - a^2}}{w^2 - a^2} \quad (6.5.5)$$

The difference in the right-hand sides of these systems addresses the compatibility conditions only. These characteristics exist only in the case in which the velocity component U_n , normal to a $\theta = \text{const}, \varphi = \text{const}$ ray, is greater than the speed of sound

$$U_n^2 = v^2 + w^2 \geq a^2, \quad M_n^2 = U_n/a \geq 1 \quad (6.5.6)$$

Only in this case the conical equation system is hyperbolic, whereas at $M_n < 1$ it is elliptic. Thus, the conical equation system may be elliptic, even if the original problem of the conical flow is hyperbolic.

A typical arrangement of elliptic and hyperbolic conical flow regions is shown in Figure 6.8 for circular cones at an angle of attack α .* We have $v = 0$ on the cone itself, $w = 0$ in the planes of symmetry $\varphi = 0$ and π , and $v_s = U_n < a$ in the same planes immediately behind the shock. Thus, it might be expected that the ellipticity conditions in these planes

* These data, as well as those of Section 6.6, were obtained by Bachmanova, Lapygin, and Lipnitskii (1973).

are always fulfilled. The same is true throughout the entire conical flow region at $\alpha = 0$ and, in view of the continuity of the solution with respect to α , over a certain range of small α 's. However, the velocity component w increases with α , its maximum value in the flow being reached near $\varphi \sim \pi/2$. Approximately in this vicinity, a conical hyperbolic flow region arises. On slender cones it appears at first near the body surface and then propagates toward the shock, thus becoming "open." This transition is near-jumplike (cf. the data for $\alpha = 15^\circ$ and 16° in Figure 6.8). However, in the flow convergence region ($\varphi \approx \pi$) we have again $|v| < a$, so that an elliptic region appears again. This supersonic-subsonic transition can occur across a shock (AB in Figure 6.8e); the lines $M_n = 1$ in other parts of Figure 6.8 are, possibly, also weak shocks. On the contrary, at large θ the hyperbolic region occurs near the shock, while near the cone itself the flow is elliptic.

The previous discussion gives a basis for the formulation of the problem of the supersonic flow past conical bodies. The equations were described previously; the boundary condition imposed on the body surface is the conventional impermeability condition $v_n = 0$ (or $v = 0$ in the case of a circular cone). On the shock $\theta = \theta_s(\varphi)$ we have, in accordance with Section 3.5, the following relations

$$\begin{aligned} p_s &= p_s(v_{n\infty}^2), & h_s &= h_s(v_{n\infty}^2) \\ \rho_s &= \rho(p_s, h_s) = \rho_\infty/k, & \vec{U} &= \vec{U}_\infty - \vec{n}v_{n\infty}(1-k) \end{aligned} \quad (6.5.7)$$

Here, the quantities p_∞ , ρ_∞ , and h_∞ are preassigned.

Bringing then the half-planes $\varphi = 0$ and $\varphi = \pi$ into coincidence with the windward and leeward sides of the plane of the angle of attack, respectively, we can derive the following formulas for the direction cosines of the outward normal \vec{n} and the corresponding components of the freestream velocity \vec{U} at the shock

$$\begin{aligned} n_r &= 0, & n_\theta &= \Delta^{-1}, & n_\varphi &= -\theta'_s(\Delta \sin \theta_s)^{-1} \\ v_{n\infty} &= -\frac{1}{\Delta} \left(v_\infty - w_\infty \frac{\theta'_s}{\sin \theta_s} \right), & \Delta &= \left(1 + \frac{(\theta'_s)^2}{\sin^2 \theta_s} \right)^{1/2} \\ u_\infty &= U_\infty (\cos \theta_s \cos \alpha - \sin \theta_s \sin \alpha \cos \varphi) \\ v_\infty &= -U_\infty (\sin \theta_s \cos \alpha + \cos \theta_s \sin \alpha \cos \varphi) \\ w_\infty &= U_\infty \sin \alpha \sin \varphi \end{aligned} \quad (6.5.8)$$

In the general case, these conditions are imposed on a closed curve $\theta_s(\varphi)$ for $\varphi = 0 \div 2\pi$ (or for $\varphi = 0 \div \pi$ in the presence of the plane of symmetry). However, in the presence of an open hyperbolic zone, the windward region can be calculated independent of the leeward one and separated from it by any boundary line, on which the local normal velocity is supersonic, $v_n > a$. This is necessary, in particular, in the case in which a cone is set at a high angle of attack, when a viscous separation zone appears and the inviscid solution is no longer realistic. Besides that, the conical solution can be applied in this case also to "half-cones" with a deformed contour (which can be even nonconical) at the leeward side, above the separating line.

Mathematically, this problem is identical to that of the supersonic flow past a body considered in Section 5.5 and requires similar algorithms for its solution. Thus, a counterpart of the stabilization method is provided by the marching method for the original hyperbolic problem; the method is applied along the r axis until the solution stabilizes and becomes conical. When the computational domain is reduced, a free boundary condition (Section 5.3) is imposed on the boundary line.

6.6 Cone at Incidence

The mathematical formulation of the problem was given in Section 6.5. Here we will perform the gas dynamic analysis of this flow, many properties of which could be extended to bodies of revolution having approximately the same shape. The analysis is carried out on the basis of numerical calculations and the Newtonian formula 3.7.8, which was shown to perform well, particularly at high Mach numbers M_∞ . In this formula, the quantity U_n is determined from relation 6.5.8 for $v_{n\infty}$ with θ_s replaced by θ_c . Thus, for $v_{n\infty} = v_\infty$ we have

$$p - p_\infty = \rho_\infty U_\infty^2 \bar{p} = \rho_\infty v_\infty^2 = \rho_\infty U_\infty^2 \sin^2 \theta_l \quad (6.6.1)$$

Here, θ_l is the local angle of attack for a given cone generator.

$$\sin \theta_l = \sin \theta_c \cos \alpha + \cos \theta_c \sin \alpha \cos \varphi \quad (6.6.2)$$

The data in Figure 6.9a and b demonstrate a satisfactory accuracy of these formulas, including the case of small angles $\theta_c + \alpha$, for $K_{\alpha+\theta} = M_\infty \sin(\alpha + \theta_c) \geq 1$. This allows us to hope that some particular cases, which can be derived from these formulas and are considered in the following, are also adequate. Thus, at small θ_c and α we have

$$\begin{aligned} \theta_l &= \theta_c + \alpha \cos \varphi \\ \tilde{p}_\theta &= \bar{p} / \sin^2 \theta_c = 1 + 2\bar{\alpha} \cos \varphi + \bar{\alpha}^2 \cos^2 \varphi, \quad \bar{\alpha} = \alpha / \theta_c \end{aligned} \quad (6.6.3)$$

The function \tilde{p}_θ depends on the parameter $\bar{\alpha}$ only, which is confirmed by the data in Figure 6.9c. For slender cones at high angles of attack, $\theta_c \ll \alpha$, we can derive another limiting relation

$$\tilde{p}_\alpha = \bar{p} / \sin^2 \alpha = (K_1 + \cos \varphi)^2, \quad K_1 = \theta_c \cot \alpha \quad (6.6.4)$$

This function depends on the parameter K_1 only, this being confirmed by the data in Figure 6.10, while the shock shapes are also dependent on the normal Mach number $M_n = M_\infty \sin \alpha$. As $K_1 \rightarrow 0$, the flow in the conical cross-sections is identical to the flow past a circular cylinder at the same Mach number M_n (in Chapter 8 we shall relate all these facts with the general similarity laws for hypersonic flows and shall present some additional data on this issue).

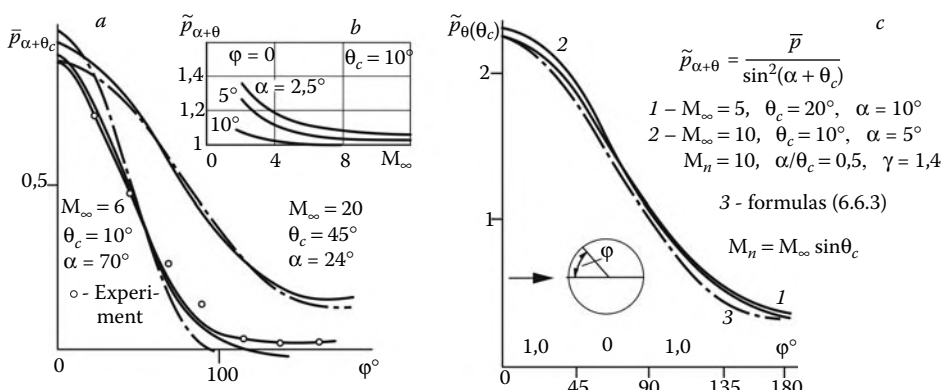
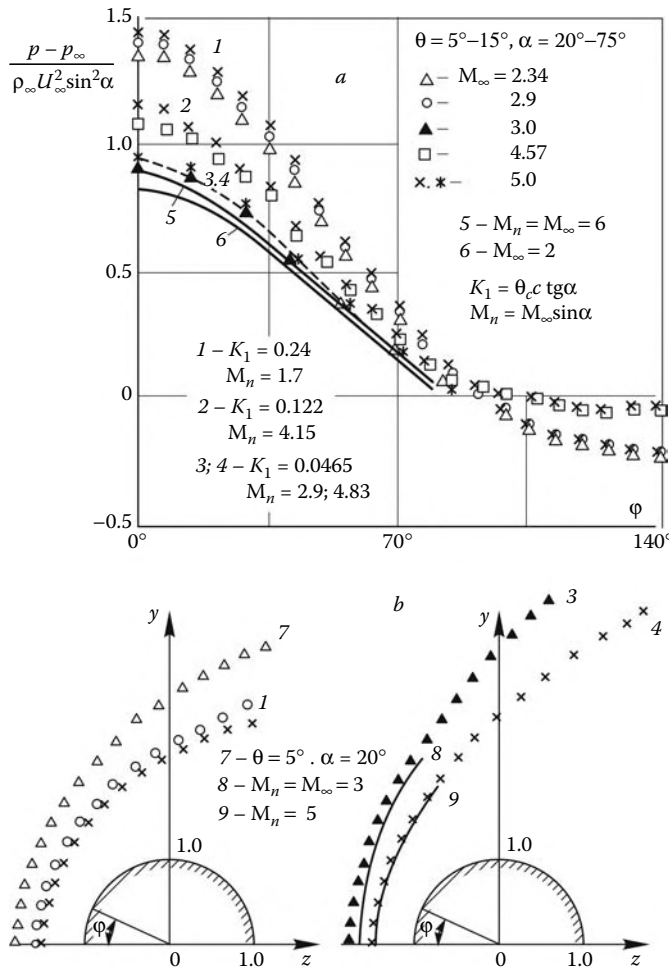


FIGURE 6.9

Pressure on cones: exact solutions vs. Newtonian theory.

**FIGURE 6.10**

Pressure (a) and shock waves (b) in conical cross-sections at high angles of attack; solid lines relate to the two-dimensional flow past a circular cylinder.

The shapes of the conical shocks $\theta_s(\varphi)$ presented in Figures 6.8 and 6.11 relate to a sphere $r = \text{const}$, or $1 - 1$ in Figure 6.7a. However, in the vicinity of the slender cone surface, this sphere is close to the cross-section $x = \text{const}$, or $1 - 1$ in Figure 6.7c. At high α this section may not intersect the conical shock having always a positive local angle of attack and transforming in a characteristic as $\alpha \rightarrow \pi/2$ and $\varphi \rightarrow \pi$. In this case, the section $x = \text{const}$ intersects the shock along a hyperbola-like curve, so that the shock is not closed in this plane, as demonstrated in Figure 6.10b.

In Figure 6.8 the shock layer thickness for $\varphi = 0$ is smaller than that for $\varphi = \pi$. However, at $M_\infty \gg 1$ the situation can be reverse, as shown in Figure 6.11 (this fact will be explained in Section 7.11).

We note that, strictly speaking, the flow past a cone remains conical only until the velocity in the shock layer is supersonic. However, a mathematical conical solution may exist even if this condition is violated, if only the shock is attached to the nose.

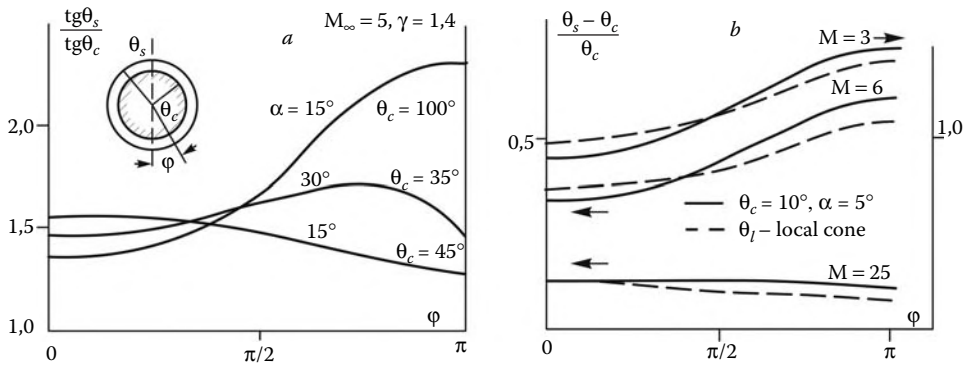


FIGURE 6.11
Shapes of conical shocks.

Consider now a cone at small angles of attack. In Figure 6.12 for the cone with $\theta_c = 10^\circ$ we have plotted the functions

$$\lambda(\varphi) = \frac{\bar{p} - \bar{p}_c}{\bar{p}_0 - \bar{p}_c}, \quad \tilde{p}_\theta(\theta_l) = \frac{\bar{p}}{\sin^2 \theta_l}, \quad \tilde{p}_\theta(\theta_c) = \frac{\bar{p}_c}{\sin^2 \theta_c} \quad (6.6.5)$$

Here, $\bar{p}_0 = \bar{p}$ for $\varphi = 0$ and $\bar{p}_c = \bar{p}$ for $\alpha = 0$. At $\bar{\alpha} \ll 1$, omitting the term with $\bar{\alpha}^2$ in Equation 6.6.3 we obtain $\lambda = \cos \varphi$. In fact, the exact solution in Figure 6.12a presented by symbols follows this law, except for the leeward side with $\varphi \geq 3\pi/4$.

Figures 6.11b and 6.12b demonstrate the results of testing the *local cone method*, in accordance with which the parameters of the flow past a cone at incidence in a $\varphi = \text{const}$ plane are taken to be the same as for the cone with the semivertex angle $\theta_c = \theta_l$ at $\alpha = 0$. Clearly, in the $\varphi \leq 3\pi/4$ region the local cone method is preferred for the pressure, as compared

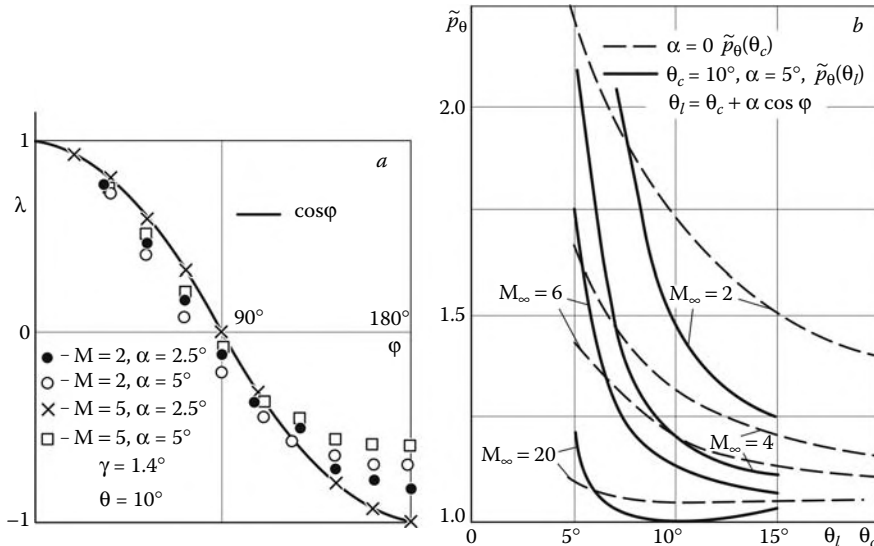


FIGURE 6.12
Peripheral pressure distribution in conical flows: exact solutions vs. local cone method (Equation 6.6.5).

with the Newton formula with $\tilde{p}_\theta = 1$, though its accuracy is not very high; moreover, one could speak of any accuracy of this method only for $M_\infty \geq 4$. At $M_\infty = 20$ both curves, $\tilde{p}_\theta(\theta_1)$ and $\tilde{p}_\theta(\theta_c)$, are equally close to the line $\tilde{p} = 1$. At the same time, the local cone method predicts fairly well the shock standoff distance.

At small α the exact solution also follows the laws established. In fact, the general form of the expansion of the boundary conditions at the shock is as follows

$$\begin{aligned} f &= f_0 + \alpha f_1 \cos \varphi, & w &= \alpha w_1 \sin \varphi \\ f &= u, v, p, \rho, \theta_s \end{aligned} \quad (6.6.6)$$

Substituting the solution in this form in Equation 1.13.15 and discarding the terms of the order α^2 , the equations can be brought to a system of ordinary differential equations with respect to the functions $f_1(\theta)$ and $w_1(\theta)$. These solutions are important for determining transverse forces and moments acting on a body at small α (see Section 2.13). It is unnecessary to determine these functions from the linearized system; it could also be done by solving the exact problem at $\alpha = 0$ and at a certain small α .

We note that the peripheral velocity on the cone follows well relation 6.6.6 up to $\bar{\alpha} \leq 1/2$; this can be seen from Figure 6.13. However, as $\bar{\alpha}$ is increased, the w peak is displaced somewhat toward larger φ .

However, the solution of the linear problem gives a qualitatively incorrect behavior of the entropy and the streamsurfaces near the body. In Equation 6.5.3 the term $w \partial s / \partial \varphi \sim \alpha^2$; omitting this term in linearizing gives $\partial s / \partial \theta = 0$, that is, the entropy is constant in meridional planes: $s = s_0 + \alpha s_1 \cos \varphi$. Generally speaking, the true isentropic surfaces, which have, in accordance with 6.5.4, the shape $\varphi = \varphi_0 + \alpha \varphi_1(\theta)$, differ from the meridional planes with the same initial ray at the shock by a quantity of the order of α . However, in view of the constancy of s_0 , the entropy difference on the isentropic surfaces and meridional planes is of the order of α^2 .

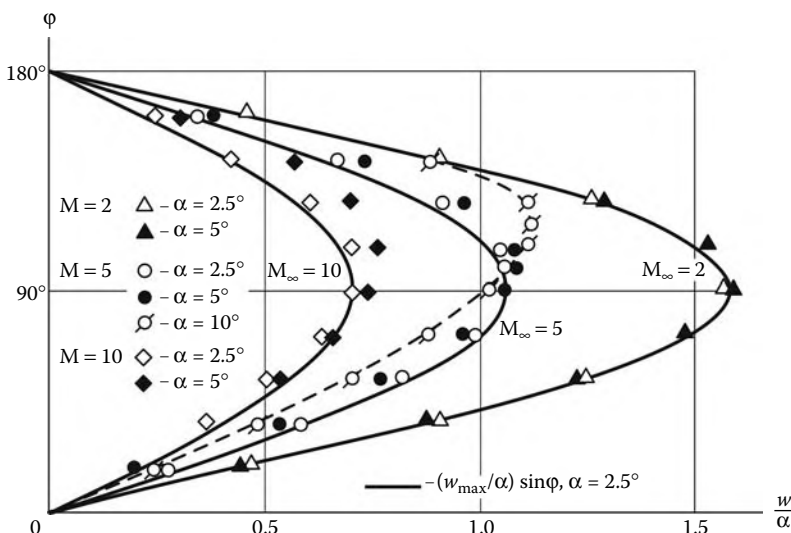


FIGURE 6.13
Relative profile of the peripheral velocity on a cone at incidence.

However, we have $v = 0$ at the conical surface, so that the two terms of Equation 6.5.3 may be of the same order in a certain wall *vortex sublayer*. We will study this question in more detail. In the vicinity of the cone, we have $v < 0$, in view of the fact that the streamlines converge to the body; thus, it may be accepted that

$$v = -a(\theta - \theta_c), \quad w = \alpha b \sin \varphi, \quad a, b > 0 \quad (6.6.7)$$

Hence, in this vicinity Equation 6.5.4 and the shapes of the conical streamsurfaces take the form:

$$\kappa \frac{d(\theta - \theta_c)}{\theta - \theta_c} = -\frac{d\varphi}{\sin \varphi}, \quad \kappa = \kappa(\varphi) = \frac{a}{b} \bar{\alpha} > 0 \quad (6.6.8)$$

Within the small vicinities of planes of symmetry solution 6.6.8 takes the form:

$$\theta - \theta_c = C\varphi^{-1/\kappa} \quad (\varphi \approx 0), \quad \theta - \theta_c = C(\pi - \varphi)^{1/\kappa} \quad (\varphi \approx \pi) \quad (6.6.9)$$

In the vicinity of the stagnation point the first-family streamlines form a saddle of the type shown in Figure 2.21a (Section 2.11). However, in the region $\varphi \approx \pi$ the streamlines form a node, as shown in Figure 6.14. Obviously, for $\alpha \ll \theta_c$ we have $\kappa < 1$ and all the streamlines are in this case tangent to the body surface (except for the vertical singular line, see Figure 6.14a). Thus, all the conical streamlines converge to the upper cone generator at the *Ferri point* F , which is the entropy many-valuedness point. The flow convergence at the leeward side of the cone is apparently the reason why in this region the pressure distribution deviates from the cosinusoidal one (Figure 6.12a).

The quantity κ increases with α . Extending qualitatively this result to finite values $\alpha \sim \theta_c$ we can attain the $\kappa > 1$ range. In this case the singular conical streamline lies on the conical surface, while the streamlines converging to the point F are tangent to the plane of symmetry (Figure 6.14b), which in this case, as later in Figure 6.14c, is the convergence plane (Section 2.11). This situation could be discerned on the calculated flow pattern plotted in Figure 6.8f.

Finally, at higher angles of attack the flow in the leeward region exhibits a qualitative restructuring. A regular convergence point O , similar to that behind a cylinder in an incompressible inviscid flow, appears on the cone, while the Ferri point F , as it were, buoys inside the flow (Figure 6.14c). The value of κ expected in this case is greater than unity ($\kappa > 1$); because of this, the conical streamsurfaces are tangent to the plane of symmetry, as in the previous case. An example of this flow pattern is shown in Figure 6.8e. The point F is the image of the spatial convergence line to which all the streamlines of the disturbed region converge.

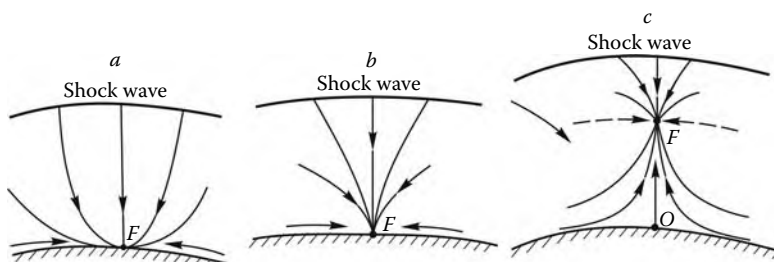


FIGURE 6.14

Different types of the streamlines in the vicinities of the stagnation points in conical flows.

We will now consider the surface distribution of the peripheral velocity w in φ . In our designations, the third Equation 1.13.15, when written on the body surface, takes the form:

$$w \frac{\partial w}{\partial \varphi} + uw \sin \theta_c = -\frac{1}{\rho} \frac{\partial p}{\partial \varphi} = -\frac{\partial h}{\partial \varphi} \quad (6.6.10)$$

We will restrict ourselves to the case $\alpha < \theta_c$ and use for our estimates the Newtonian pressure distribution 6.6.1

$$\begin{aligned} \frac{1}{\rho} \frac{\partial p}{\partial \varphi} &= -\beta a^2 \sin \varphi, \quad a^2 = \gamma p / \rho \\ \beta &= \frac{2 \cos \theta_c \sin \theta_l \sin \alpha}{M_\infty^{-2} + \gamma \sin^2 \theta_l} \end{aligned} \quad (6.6.11)$$

That the density is absent from this formula is convenient, since the pressure dependence of the squared speed of sound $a^2 \sim p^{(\gamma-1)/\gamma}$ is much weaker than that of ρ . For $\alpha \ll \theta_c$ the first term on the left-hand side of Equation 6.6.10 can be omitted, which leads to the formula

$$w = ug \sin \varphi, \quad g = \frac{\beta}{M^2 \sin \theta_c}, \quad M = \frac{u}{a} \quad (6.6.12)$$

The Mach number M increases with M_∞ ; therefore, the coefficient g decreases, as shown in Figure 6.13. At $\alpha \sim \theta_c$ both terms on the left-hand side of Equation 6.6.10 are of the same order, the equation is nonlinear, and the $w(\varphi)$ distribution is no longer sinusoidal.

Finally, for $\alpha \gg \theta_c$, this is the first term that contributes mainly to the left-hand side; this gives the Bernoulli equation for the peripheral velocity $(1/2)w^2 + h = h_0$, where h_0 is the enthalpy on the $\varphi = 0$ ray. In this case, the $w(\varphi)$ distribution is identical to the velocity distribution over the circular cylinder in the transverse supersonic flow with the freestream Mach number equal to the normal Mach number M_n . Obviously, this solution could not be continued up to $\varphi = \pi$ in a shockless or even separationless fashion.

We will now consider the flow near the divergence ($\varphi = 0$) and convergence ($\varphi = \pi$) lines. To do this, we put

$$\begin{aligned} w &= Ug\psi, \quad \frac{1}{\rho} \frac{\partial p}{\partial \varphi} = -\beta a^2 \psi, \quad u = U \\ \varphi \approx 0 : \quad \psi &= \varphi, \quad \varphi \approx \pi : \quad \psi = \pi - \varphi \end{aligned} \quad (6.6.13)$$

In this case, Equation 6.6.10 has the solution

$$\begin{aligned} g_{\pm} &= -\frac{1}{2} j \sin \theta_c \pm \Delta, \quad \Delta^2 = \frac{1}{4} \sin^2 \theta_c + j\bar{\beta}M^{-2} \\ \varphi = 0 : \quad j &= 1, \quad \varphi = \pi : \quad j = -1 \end{aligned} \quad (6.6.14)$$

The obvious condition $g \rightarrow 0$ as $\beta \rightarrow 0$ ($\alpha \rightarrow 0$) is associated with the root g_+ for $j = 1$ and g_- for $j = -1$ (both roots are positive for $\beta > 0$). However, in the latter case, for $\beta > 0$ the solution exists only for $\Delta^2 > 0$, that is, on a restricted range of the angle α . Thus, as α increases, the pressure behavior in the vicinity of the convergence line must so change, that the coefficient β decreases (which can be observed in Figure 6.12a) and even changes the sign, which corresponds to the appearance of a local pressure maximum (Figure 6.9a). In this case ($\beta < 0, j = -1$) the convergence line $\varphi = \pi$ is associated with the root g_+ , now positive.

6.7 Thin Delta Wing in a Supersonic Flow

We will consider a triangular plate with the vertex angle 2β (Figure 6.15) as a base and draw two surfaces close to the plate through its edges, so that the distance d between the surfaces (the wing thickness) is much smaller than the plate length L and half-width l . Precisely these conditions $d \ll L, l$ are distinctive features of a wing, as compared with bodies of other shapes. The ratio $l/L = \tan \beta$ is called the *wing span*, while its reverse $L/l = \tan \chi$ is called the *aspect ratio* or the *wing sweep*, χ being the *sweep angle*; thus, $\beta + \chi = \pi/2$. Finally, the shape of the wing section in the vicinity of an edge in the plane normal to the edge is referred to as the *edge section contour* (Figure 6.15c and d).

Generally speaking, the wing base may be presented by any part of a plane or a weakly curved surface (Figure 6.15d). However, even in the latter case a conditional *wing plane* is distinguished; the wing projection onto this plane gives the *wing planform*. In this case, the effective wing thickness must satisfy the conditions $d' \ll l$ and $d' \ll L$ (Figure 6.15d).

The reference frame x, y in Figure 6.15 is fitted to the wing plane; here, the origin O is at the plate vertex and the y axis is normal to the plate. Then we assume that the freestream velocity vector \vec{U}_∞ lies in the x, y plane and forms an angle of attack α with the x axis. In Figure 6.15 (x, y) is the plane of symmetry, though this condition is not obligatory. The same is true for the assumption that the wing has a conical shape; however, we will adhere to this assumption. The only important requirement is that the flow is supersonic throughout the entire domain, which imposes certain restrictions on the angle of attack, $\alpha \leq \alpha_{\max}$, since otherwise the subsonic flow is exposed to end effects.

In the x, y, z coordinates the freestream velocity components are as follows:

$$u_\infty = U_\infty \cos \alpha, \quad v_\infty = U_\infty \sin \alpha, \quad w_\infty = 0 \quad (6.7.1)$$

We will attach another reference frame τ, y, n to the wing edge. The corresponding freestream velocity components U_τ and U_n are equal to:

$$U_{\tau\infty} = U_\infty \cos \beta \cos \alpha, \quad U_{n\infty} = U_\infty \sin \beta \cos \alpha \quad (6.7.2)$$

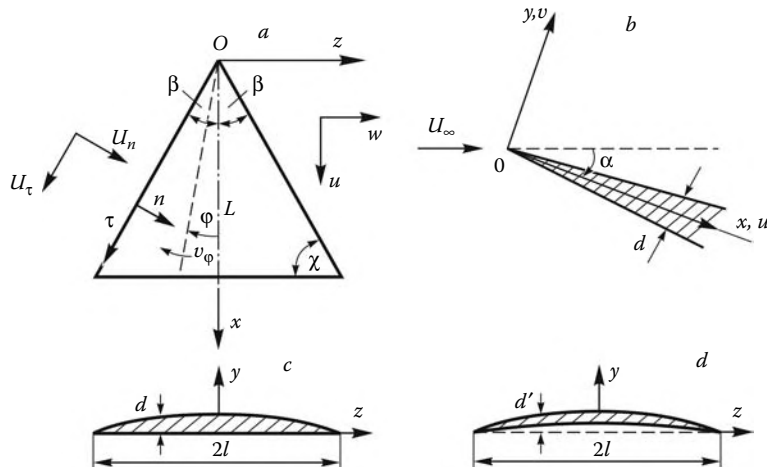


FIGURE 6.15
Delta wing at incidence.

We will introduce the projection $U^{(n)}$ onto the plane normal to the wing edge. Then for the freestream velocity we have

$$U_{\infty}^{(n)} = (U_{n\infty}^2 + v_{\infty}^2)^{1/2} = U_{\infty}(\sin^2 \alpha + \cos^2 \alpha \sin^2 \beta)^{1/2} \quad (6.7.3)$$

In what follows we will demonstrate that the wing flow regimes are mainly determined by the *normal Mach number* $M_{\infty}^{(n)}$ and the *normal angle of attack of the wing edge* ε

$$M_{\infty}^{(n)} = U_{\infty}^{(n)}/a_{\infty}, \quad \tan \varepsilon = v_{\infty}/U_{n\infty} = \tan \alpha / \sin \beta \quad (6.7.4)$$

For $M_{\infty}^{(n)} < 1$ the wing is entirely embedded in the outer leading Mach cone having the semivertex angle $\alpha^* = \arcsin M_{\infty}^{-1}$. This is the *subsonic edge regime*. In this case, the governing equations in the conical variables are, in accordance with Section 6.5, elliptic, that is, the flow is conically subsonic and all the wing elements affect each other. In this case the near-edge flow is qualitatively similar (but not identical) to the subsonic flow past its contour at a local Mach number $M^{(n)} < 1$. This flow is demonstrated in Figure 6.16a and b, for $\alpha = 0$; however, the main conclusions are also valid for $\alpha \neq 0$.

On the contrary, for $M_{\infty}^{(n)} > 1$ the wing is beyond the leading Mach cone, which in the general case is replaced by a shock. This is the *supersonic edge regime* demonstrated in Figure 6.16c and d, with reference to the example of the wing with a wedge-shaped edge, the vertex angle 2θ of its cross-section contour, and the shocks attached to the edge. Since the flow velocity component parallel to the edges is conserved across the shocks, $U_{\tau} = U_{\tau\infty}$, the flow in the n, y plane is the same as that past a wedge with the semivertex angle θ at the Mach number $M_{\infty}^{(n)}$. Behind the oblique weak-family shock we have $M^{(n)} > 1$; therefore, in the region between the bow shock and the internal vertex Mach cone, shaded in Figure 6.16d, the equations of motion in conical variables are hyperbolic and the interaction between the upper and lower wing surfaces does not take place. However, within the internal vertex Mach cone the corresponding equations are elliptic owing to the effect of the plane of symmetry, so that the flow is conically subsonic.

However, if the angle θ of this example is increased up to the values exceeding the limiting angle θ_0 for the flow past a wedge at a given $M_{\infty}^{(n)}$, then a detached shock forms, such

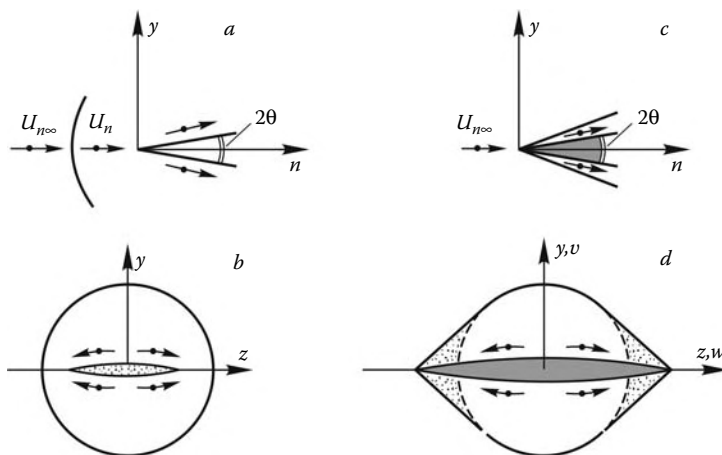


FIGURE 6.16

Wing at zero incidence: (a) and (b), subsonic edge and (c) and (d), supersonic edge (cross-section).

that behind it we have $M^{(n)} < 1$ (as in Figure 6.16a), that is, the local flow past the edge is subsonic. However, the shock remains attached to the vertex and the flow as a whole is conical. In this case the conical equations are elliptic; however, local hyperbolic zones, similar to those in transonic flows discussed in Section 5.1, can arise as we recede from the edges.

Another example is provided by a triangular plate at an angle of attack α (Figure 6.17). For $M_\infty^{(n)} > 1$ the flow in the vicinity of the edge is in the n, y plane the same as in the two-dimensional flow past a plate at an angle of attack ε , possibly with an attached shock on the windward side (the leeward side will be discussed separately). We have again a hyperbolic zone near the edges and an elliptic zone inside the internal Mach cone (Figure 6.17a and b). However, this flow can be realized only at $\varepsilon < \theta_0$; at $\varepsilon > \theta_0$ the shock detaches from the edge on the windward side and the Mach number behind it is smaller than unity ($M^{(n)} < 1$), so that the local flow past the edge in the n, y plane is subsonic (Figure 6.17c and d). We emphasize that, since $\varepsilon > \alpha$ and $\theta_0(M_\infty^{(n)}) \leq \theta_0(M_\infty)$, the limiting deflection angle in the shock is attained on the edge earlier than on the plate with the same angle of attack α but with the zero sweep.

We will now consider the *streamline pattern* and other elements of the structure of the flow around the plate. To do this, we shall calculate the velocity projection onto the z axis near the edge in terms of Equation 6.7.2

$$\begin{aligned} w &= -U_\tau \sin \beta + U_n \cos \beta = \Delta U_n \cos \beta \\ \Delta U_n &= U_n - U_{n\infty} \end{aligned} \quad (6.7.5)$$

Consider first the case $\alpha = 0$. Then in the vicinity of the edge, either subsonic or supersonic, it should be expected that $U_n > 0$, that is, in a $\tau = \text{const}$ plane the gas flows away from the edge. However, in an $x = \text{const}$ plane (the left part of Figure 6.15a) we have $\Delta U_n < 0$ and $w < 0$ owing to the total pressure loss across the shock; thus, the gas flows away from the plane of symmetry, which represents in this case the divergence, or spreading, plane (Figures 6.17b and 6.18a).

However, as distinct from the flows considered in Section 2.11, the pressure does not peak at the spreading line at the plate center. On the contrary, the pressure maximum in

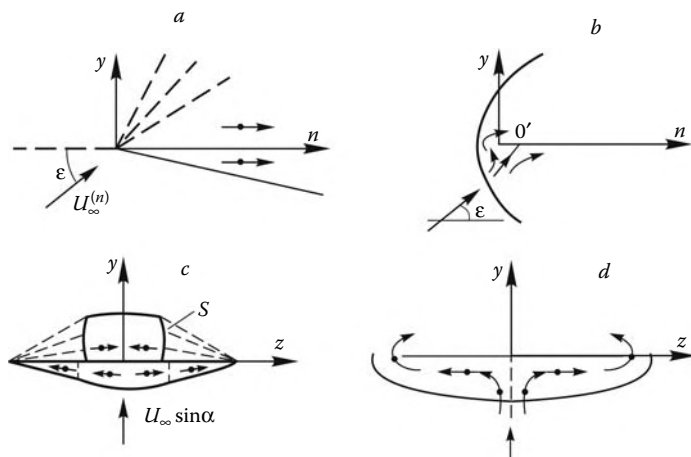


FIGURE 6.17
Triangular plate at an angle of attack (cross-section).

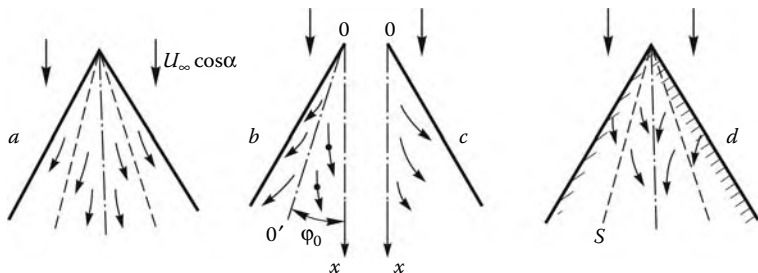


FIGURE 6.18
Streamlines on the surface of a triangular plate.

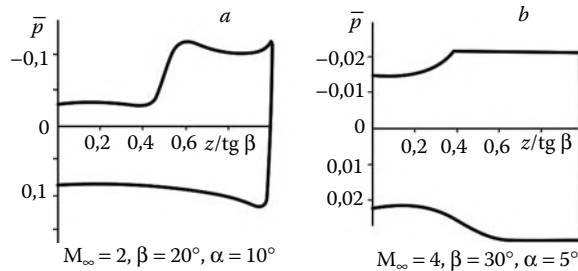
these flows is usually achieved precisely on the edges. The point is that the model of this flow in $x = \text{const}$ planes is provided rather by the time-dependent piston expansion, as though formed from the wing flow by substituting time t for the coordinate x . The expanding piston entrains the gas at the velocity w , thus leading to the gas outflow from the central region with the pressure reduction in it.

This type of gas spreading, caused by the given initial gas velocity (in our case, on the edge) rather than by a local pressure peak, was called the *inertia-like spreading* in Section 4.10; it is widespread in three-dimensional flows. For $\alpha > 0$, in the unsteady counterpart of the triangular plate flow used previously, the expanding piston acquires also the normal translation velocity $U_\infty \sin \alpha$. The flow behind an attached shock on the windward side of the triangular plate with a supersonic edge at $M_\infty^{(n)} > 1$ and a small angle $\varepsilon < \theta_0$ does not qualitatively differ from that considered previously (Figures 6.17a and b and 6.18a).

However, the situation changes at $\varepsilon > \theta_0$ when the shock detaches from the edge so that the edge is exposed to the subsonic normal flow behind the shock ($M^{(n)} < 1$) or, generally, when the wing is totally submerged in the leading Mach cone and has a subsonic edge. At not-too-high angles α or at an angle ε that is still close to θ_0 it might be expected that the stagnation point on this plate (O' in Figure 6.17c) is at an only slight distance from the edge (as in the flow around an airfoil in Figure 2.17), while the sonic speed $|U_n| = a$ is reached as the corner point itself is approached from below. On a delta wing, the points O' form a ray OO' , or $\varphi = \varphi_0$ (Figure 6.18b). On this line, the velocity component v_φ normal to it (Figure 6.15) vanishes; thus, this is the line of local pressure maxima and, simultaneously, the spreading line, while the axis of symmetry is the convergence line with its own pressure peak.

In other limiting subsonic cases, where $\varepsilon \approx \pi$ and $\alpha \approx \pi$, the flow around a triangular plate is more similar to the flow past a blunt body with a pressure peak in its plane of symmetry. Thus, there exists a high-angle-of-attack range, where the spreading line lies in the plane of symmetry of the plate. This situation is shown in Figures 6.17d and 6.18c; it does not change qualitatively when changing from a sharp edge to a blunt one.

On the leeward side of the plate at $\varepsilon < \theta_0$ a centered expansion wave attached to the edge forms; the normal flow behind it is necessarily supersonic. In this case $\Delta U_n > 0$ and $w > 0$, so that the gas flows away from the edges toward the plane of symmetry. However, since the local Mach number is $M^{(n)} > 1$, this supersonic flow decelerates across an internal shock S plotted in Figures 6.17b and 6.18d. At $\varepsilon > \theta_0$, that is, in the subsonic edge regime, the flow pattern is generally the same, since the gas flowing around the edges from below also accelerates up to supersonic normal velocities on the windward side. However, in

**FIGURE 6.19**

Pressure on the windward (bottom) and leeward (top) sides of a triangular plate.

both cases this inviscid flow pattern can be violated by the formation of separation zones induced by closing shocks, particularly at high angles of attack.

We note in conclusion that the pressure on a sharp plate is generally near-constant. Because of this, all flow nonuniformities, in particular, the arrangement of spreading lines, and so on, are caused precisely by the distributions of small pressure additions. The examples of the pressure distribution over a wing are presented in Figure 6.19. In the case "a" of the subsonic edge, the pressure maximum on the windward side is located near the edge (the same situation as in Figure 6.17c). In the case "b" of the supersonic edge, the pressure plateau adjacent to it transforms in a central rarefaction zone. A central compression zone behind the shock is clearly visible on the leeward side (the shock itself was smeared in the calculation).

The salient features of the hypersonic flows around wings will be discussed additionally in the corresponding chapters. The flow analysis and classification for wings at high incidence was given by Chernyi (1965) and Bashkin (1984).

6.8 Strong Blast

We will deal with a high-power atmospheric blast, where the size l and the mass m of the explosive device are much smaller than the explosion zone extent and the mass of the gas entrained in the zone. Thus, the damage zone of a nuclear bomb having its own size of the order of 1 meter can extend over several kilometers with the air mass $M \approx 5 \cdot 10^6$ kg, considerably exceeding m_0 , being concentrated in the ground zone of radius $R = 100$ m. Hence, at $R \gg l$ the quantities l and m_0 are no longer the relevant parameters of the problem and can be excluded from the set of parameters 6.1.3. Then the only control parameter of the process (apart from those characterizing the gas properties) is the energy E_0 released in the blast, in the zone of which the following integral is valid

$$E = 2^\nu \pi^\delta \int_0^R \rho \left[\frac{1}{2} v^2 + (e - e_\infty) \right] r^\nu dr = E_0$$

$$\delta = 0 \quad \nu = 0, \quad \delta = 1 \quad \nu = 1 \text{ and } 2 \quad (6.8.1)$$

Generally speaking, the energy dimensionality is $[E] = ML^2 t_0^{-2}$, where M , L , and t_0 are the mass, length, and time symbols (Section 1.12); however, this is true for the three-dimensional

problem ($\nu = 2$), while in the axisymmetric one ($\nu = 1$) the energy should be referred to a unit length L (e.g., an exploding wire, an electric discharge in its near vicinity); in the plane problem ($\nu = 0$) it should be referred to a unit area L^2 . Thus, $[E_0] = ML^\nu t_0^{-2}$. Dividing this quantity by the density ρ_∞ we obtain the required parameter C in Equation 6.1.13 in the form:

$$C = (E_0/\rho_\infty \pi^\delta)^{1/(3+\nu)}, \quad [C] = Lt_0^{-n}, \quad n = \frac{2}{3+\nu} \quad (6.8.2)$$

Then for a perfect gas in the strong stage of the blast (the real gas effects will be considered in the next section), that is, under conditions 6.1.2, we can, scaling the pressure and velocity on the combinations $\rho_\infty \dot{R}^2$ and \dot{R} , present the solution in the form:

$$\begin{aligned} R &= \chi_\nu(\gamma) \left(\frac{E_0}{\rho_\infty \pi^\delta} \right)^{1/(3+\nu)} t^{2/(3+\nu)}, & p &= \rho_\infty \dot{R}^2 P(\eta, \nu, \gamma) \\ v &= \dot{R} V(\eta, \nu, \gamma), & \rho &= \rho_\infty \bar{\rho}(\eta, \nu, \gamma), & \eta &= \frac{r}{R} \end{aligned} \quad (6.8.3)$$

Another representation of the pressure can be obtained by eliminating \dot{R}

$$\begin{aligned} p/\rho_\infty &= \kappa_\nu(\eta, \gamma) (E_0/\rho_\infty \pi^\delta)^{2/(3+\nu)} t^{-2(1+\nu)/(3+\nu)} = \\ &\chi_\nu^{1+\nu} \kappa_\nu \frac{E_0}{\pi^\delta R^{1+\nu}}, & \kappa_\nu &= \chi_\nu^2 \frac{4}{(3+\nu)^2} P(\eta) \end{aligned} \quad (6.8.4)$$

Clearly, the strong blast wave propagates following the laws $R \sim t^{2/3}$, $t^{1/2}$, and $t^{2/3}$ for $\nu = 0, 1$, and 2 , respectively, while the pressure is proportional to the blast energy and to the inverse of the explosion zone volume.

We will outline in the following the mathematical formulation of the problem in the general form, which includes, in particular, that for the piston expansion in accordance with the $r_p = ct^n$ law (Section 6.1). The functions $P(\eta)$, $V(\eta)$, and $\bar{\rho}(\eta)$ satisfy a system of ordinary differential equations, which do not include the coefficient χ_ν . On a strong blast wave (i.e., in accordance with Equation 3.3.16, under the condition $(\gamma - 1)\dot{R}^2 \gg 2a_\infty$) the following relations are valid

$$\eta = 1, \quad P(1) = \frac{2}{\gamma + 1}, \quad V(1) = \frac{2}{\gamma + 1}, \quad \bar{\rho}(1) = \frac{\gamma + 1}{\gamma - 1} \quad (6.8.5)$$

Relations 6.8.5 determine the initial conditions for a Cauchy problem. The ratio $\eta_p = r_p/R$, which is not known beforehand, is determined from the relations on the piston

$$v_p = \frac{dr_p}{dt}, \quad v(\eta_p) = n\eta_p \quad (6.8.6)$$

In the case of a blast, $\eta_p = 0$ and the coefficient χ_ν is determined in terms integral 6.8.1. A mathematical analysis shows (Sedov, 1946, 1972) that integral curves satisfying conditions 6.8.5 and 6.8.6 exist only for $n \geq 2/(3+\nu)$, while the condition $\eta_p = 0$ is possible only for $n = 2/(3+\nu)$, that is, for the strong blast only. To explain this result, we will evaluate the gas energy, say, kinetic one, using relations 6.8.3

$$E_{\text{kin}} \sim \rho_\infty R^{1+\nu} \dot{R}^2 \sim t^\omega, \quad \omega = (3+\nu)n - 2 \quad (6.8.7)$$

Clearly, at $\omega > 0$ the energy grows as the piston expands, while it is constant at $\omega = 0$ and $n = 2/(3+\nu)$, as it is the case for the strong blast. However, at $\omega < 0$ it is infinite as $t \rightarrow 0$, which is unrealistic and reflected by the mathematical solution.

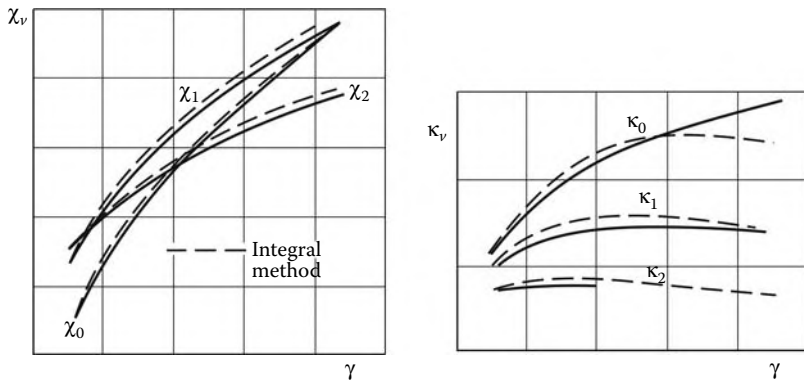


FIGURE 6.20
Coefficients in the strong blast solution.

Using Equation 6.8.3 it can be easily seen that at $\omega = 0$ the energy E_{12} is constant in the volume Ω bounded by surfaces $\eta_1 = \text{const}$ and $\eta_2 = \text{const}$. Hence, the energy fluxes across any surfaces $\eta = \text{const}$ are also constant (*Sedov integral*; see 6.10.2).

Sedov had derived an analytical solution of the strong blast problem; being too cumbersome, it is not presented here. The coefficients χ_v and $\kappa_v(0)$ are presented in Figure 6.20, while the flow parameter profiles are plotted in Figure 6.21. From these profiles there follows an important property of blast flows: within a considerable central part of the explosion zone the density is near-zero, while the pressure is near-constant. To explain this fact, we will introduce a Lagrangian coordinate m being the mass of the gas confined by a fluid surface $r = r_m(t)$. On the blast wave we have $m = m_s = M$ and $r_M = R$. Since the gas entropy is constant at $r_m(t)$, we obtain from the adiabatic equation using Equations 6.8.3 and 6.8.4

$$\frac{\rho(m)}{\rho_s(m)} = \left[\frac{p(m)}{p_s(m)} \right]^{1/\gamma} = \left[\frac{p(m)}{p_s(M)} \frac{m}{M} \right]^{1/\gamma} \quad (6.8.8)$$

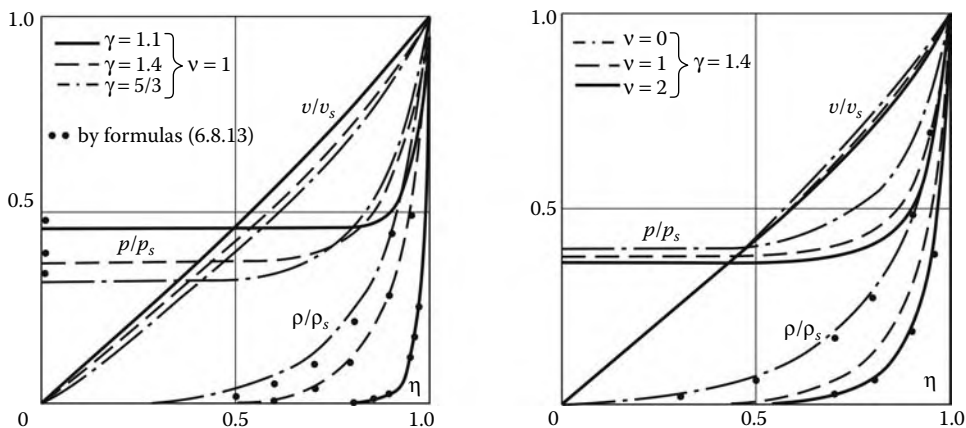


FIGURE 6.21
Parameters in the strong blast zone.

Here, p_s and ρ_s are the parameters immediately behind the shock, which has passed the point with the coordinate m . Obviously, $p(m) \sim p_s(M)$; therefore, from the relation $dm = 2^\nu \pi^\nu \rho r^\nu dr$ we obtain the following estimates

$$\frac{m}{M} \sim \eta^{\nu(\nu+1)/(\gamma-1)}, \quad \frac{\rho}{\rho_s} \sim \eta^{(\nu+1)/(\gamma-1)}, \quad r_m \sim \left(\frac{m}{\rho_\infty} \right)^{(\gamma-1)/\gamma(1+\nu)} R^{1/\gamma} \sim t^{2/\gamma(3+\nu)} \quad (6.8.9)$$

For $\gamma > 1$ the trajectories $r_m(t)$ always propagate slower than the blast wave. From the previous estimates it follows that the density $\rho = 0$ and the temperature $T = \infty$ at the center $\eta = 0$; for other η the smaller $\gamma - 1$, the smaller the density. The main mass of high-density gas is concentrated in a thin layer near the blast wave. The estimate for the thickness of this layer, $\Delta\eta \sim (\gamma - 1)/(1 + \nu)$, can be obtained by setting $\eta^{(1+\nu)/(\gamma-1)} = \text{const} \sim 1$ as $\gamma \rightarrow 1$.

To derive the mass distribution of the pressure, we change to the variables t and m in the momentum equation; then, taking into account that $dm/dt = 0$ along particle trajectories, we obtain

$$\frac{dv}{dt} - \frac{1}{\rho} \frac{\partial p}{\partial r} = \left(\frac{\partial v}{\partial t} \right)_m - 2^\nu \pi^\delta r^\nu \frac{\partial p}{\partial m} = 0 \quad (6.8.10)$$

In the vicinity of the blast wave, where most of the gas is concentrated, at $\gamma - 1 \ll 1$ we can set $r = R$ and $v = v_s = \dot{R}$. Then, making the integration, we obtain

$$\frac{p}{p_s} = 1 + B \left(1 - \frac{m}{M} \right), \quad B = \frac{R \ddot{R}}{(1 + \nu)p_s} = \frac{(\gamma + 1)(n - 1)}{2n(1 + \nu)} \quad (6.8.11)$$

The second equality was obtained at $p_s = 2\rho_\infty \dot{R}^2 / (\gamma + 1)$ and $R \sim t^n$, that is, including the case of a power-law piston. For the blast we have

$$\tilde{p} = \frac{p}{p_s} = \frac{3 - \gamma}{4} + \frac{\gamma + 1}{4} \frac{m}{M}, \quad \kappa_\nu(0) = \frac{2(3 - \gamma)}{(\gamma + 1)(3 + \nu)^2} \chi_\nu^2 \quad (6.8.12)$$

Here, the ratio $\tilde{p}(\eta)$ is ν -independent; it should be noted that exact curves $\tilde{p}(\eta)$ in Figure 6.21 exhibit a not too strong dependence on ν .

We will also present the formulas that are derived by passing to the limit $\gamma \rightarrow 1$ in the exact solution of Sedov and correcting the expressions thus obtained somewhat in order to improve their accuracy; as follows from Figure 6.21 the resulting accuracy is fairly good.

$$\begin{aligned} \tilde{p} &= \frac{3 - \gamma}{4} \left(1 - \frac{\gamma + 1}{4} \eta^\beta \right)^{-1}, & \tilde{\rho} &= \frac{\rho}{\rho_s} = \frac{1}{4} \eta^\beta \left(1 - \frac{1}{2} \eta^\beta \right)^{-2} \\ \tilde{v} &= \frac{v}{v_s} = \eta \left(\frac{\gamma + 1}{2\gamma} + \frac{\gamma - 1}{2\gamma} \eta^\beta \right), & \beta &= \frac{1 + \nu}{\gamma - 1} \end{aligned} \quad (6.8.13)$$

The linear term in the formula for \tilde{v} is exact for small η and ν -independent.

We note one more important result for small $\gamma - 1$: the kinetic-to-internal energy ratio in the explosion zone is of the order

$$E_{\text{kin}}/E_e \sim \frac{1}{2} M \dot{R}^2 / [p_0 M / \rho_\infty (\gamma - 1)] \sim \gamma - 1 \quad (6.8.14)$$

This means that most of the blast energy is transformed to the internal energy of the gas. For $\gamma \rightarrow 1$ the pressure in the blast zone is equal to $p_0 = (\gamma - 1) \rho_\infty E/M$.

These properties of blast flows provide the basis of the *integral relation method* by Chernyi (1962). The essence of the method is as follows. If the whole mass of the gas is concentrated

near the shock, then its kinetic energy is approximately equal to $Mv_s^2/2$. The internal energy can be determined by letting the pressure $p = p(0) = p_0$ throughout the entire volume $r \leq R$. Then the integral-form energy equation, analogous to Equation 6.8.1, takes a simple form:

$$\frac{1}{2}\rho_\infty R^{1+\nu} v_s^2 + \frac{p_0 - p_\infty}{\gamma - 1}(R^{1+\nu} - r_p^{1+\nu}) = \frac{1+\nu}{2^\nu \pi^\delta} E_0 + (1+\nu) \int p_0 r_p^\nu \dot{r} dt, \quad v_s = \frac{2}{\gamma + 1} \dot{R}(1 - a_\infty^2/\dot{R}^2) \quad (6.8.15)$$

For the sake of generality, we have also included the case of an expanding piston and the case with *counterpressure* by retaining the terms with p_∞ and a_∞ . Combining the previous result with Equation 6.8.12 we obtain for the strong blast

$$\chi_\nu = \left[\frac{(3+\nu)^2(1+\nu)(\gamma-1)}{2^{1+\nu}\alpha(\gamma)} \right]^{1/(3+\nu)}, \quad \alpha(\gamma) = \frac{6\gamma - \gamma^2 - 1}{(\gamma+1)^2} \quad (6.8.16)$$

The values of χ_ν and $\kappa_\nu(0)$ thus obtained are close to exact ones at $\gamma \leq 5/3$, together with the ratio p_0/p_s (Figures 6.20 and 6.21), which justifies the formal inadequacy of the terms of order $\gamma - 1$ in the factor $\alpha(\gamma)$ ($\alpha \rightarrow 1$ as $\gamma \rightarrow 1$).

For a weak stage of the blast, the external gas parameters p_∞ and h_∞ in the shock relations cannot be omitted or, in other words, the *counterpressure* cannot be neglected. In this case, the parentheses in formula 6.1.3 must also include the speed of sound $a_\infty = (\gamma p_\infty / \rho_\infty)^{1/2}$, which, together with the parameter c , contain the length and time dimensionalities. This makes it possible to separate out the time (t_0) and length (L) scales of the problem, so that the functions P , V , $\bar{\rho}$, χ_ν , and κ_ν in solutions 6.8.3 and 6.8.4 are dependent not only on η but also on one more dimensionless variable τ

$$\tau = a_\infty t/L, \quad L = (E_0 / \pi^\delta \rho_\infty a_\infty^2)^{1/(1+\nu)} \quad (6.8.17)$$

These functions satisfy partial differential equations (see, e.g., Korobeinikov, 1991) and depend on the parameters γ and ν only.

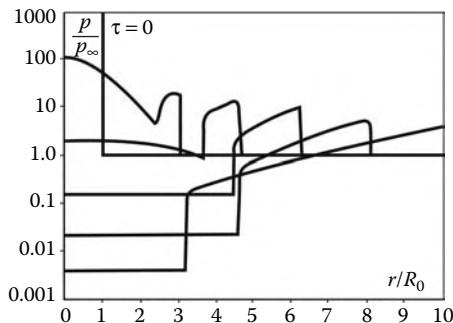
The limit $\tau \rightarrow 0$ corresponds to the strong blast; the self-similar solution for this case is used as the initial data in calculating the later stage of the blast using numerical or any other methods. As $\tau \rightarrow \infty$, the functions $p \rightarrow p_\infty$, $v \rightarrow 0$, $\rho_s \rightarrow \rho_\infty$, and $\dot{R} \rightarrow a_\infty$. For this reason, the solution with the counterpressure is often written in the form:

$$p = p_\infty P_1(\gamma, \nu, \eta, \tau), \quad R = L \bar{R}(\gamma, \nu, \eta, \tau) \quad (6.8.18)$$

However, the density $\rho(p_\infty, s)$ at the central explosion zone does not tend to ρ_∞ , since the entropy s remains high in the zone, while at the zone center we have $s = \infty$ and $\rho = 0$ (this makes the role of dissipation effects considered in Section 6.10 and neglected in the inviscid solution to be crucial). Precisely this low-density fireball buoys then in the atmosphere under the action of the Archimedes force.

We will present one more important parameter of the blast flow, namely, its momentum J . In a symmetric flow the total momentum vector is zero; for this reason, we will determine J for one-half of the flow at $\nu = 0$ and for a unit meridional angle $d\varphi$ at $\nu = 1$ and unit solid angle $d\Omega$ at $\nu = 2$

$$J = \int_0^R \rho v r^\nu dr = C \rho_\infty \dot{R} R^{1+\nu} \quad (6.8.19)$$

**FIGURE 6.22**

Pressure profiles in the blast zone (in the earlier stage).

where C is a dimensionless coefficient. In accordance with 6.8.3 and 6.8.4, for the strong blast stage we have

$$\frac{1}{\rho_\infty} J = \frac{2C\chi^{2+\nu}}{3+\nu} \left(\frac{E_0}{\rho_\infty \pi^\delta} \right)^{(2+\nu)/(3+\nu)} t^{(1+\nu)/(3+\nu)}, \quad C = \frac{1}{(2+\nu)\gamma - 1} \quad (6.8.20)$$

Here, the constant C is calculated from solution 6.8.13 for the pressure averaged over the compression zone $\bar{p} = 3/4$; this rather crude approximation is, however, sufficient for making estimates. Clearly, the momentum $J = 0$ at $t = 0$ and increases without bounds with t due to pressure forces acting from adjacent flow regions on the previously mentioned angles $d\varphi$ and $d\Omega$ at $\nu = 1$ and 2 and on the plane of symmetry at $\nu = 0$.

To demonstrate the rate at which the exact solution converges to the point blast model, we will present the calculated results for a sudden expansion of a spherical volume V of a perfect gas with $\gamma = 1.4$; the initial radius is R_0 , the pressure is $p_0 = 10^3 p_\infty$, the temperature is $T_0 = 10T_\infty$, and the density is $\rho_0 = 100\rho_\infty$. The initial energy of the sphere is $E_0 = \rho_0 V_0 / (\gamma - 1)$, hence $L_0 = 13.3R_0$ in Equation 6.8.17.

In the initial stage of the flow development, that is, at $t \sim R_0/a_0$ or $\tau \sim 0.1$, this problem is the discontinuity breakdown problem (Section 4.9), which involves complicated wave processes and does not obey any self-similar laws (Figure 6.22). Only after multiple travels of expansion waves throughout the disturbed region, when the pressure becomes sufficiently low, $p_s/p_\infty \leq 1.5$, the pressure profile in the disturbed zone starts to correspond to the point blast theory (Figure 6.23).* At the same time, the pressure behind the shock and the shape of the latter start to follow the point blast theory considerably earlier (Figure 6.24).

In this example, we have simulated the initial state of a detonated charge by a volume of compressed gas at rest. At the same time, during the charge explosion the gas behind the shock expanding into the ambient medium possesses not only an energy but a momentum as well. The same situation occurs at gas acceleration by a piston, after its short-duration expansion and stop. In both cases, the formulation of the problem might appear to involve two integral initial parameters, the energy E_0 and the momentum J_0 . This problem is non-self-similar and involves the length L and time t_L scales, which enter in the dimensionalities of the parameters

* The tables of the parameters for the blast with counterpressure are presented, for example, in Roslyakov, Kestenboim, and Chudov (1974). The data in Figure 6.21 are also taken from that book, while the data in Figures 6.22 to 6.24 were obtained by Kovalev.

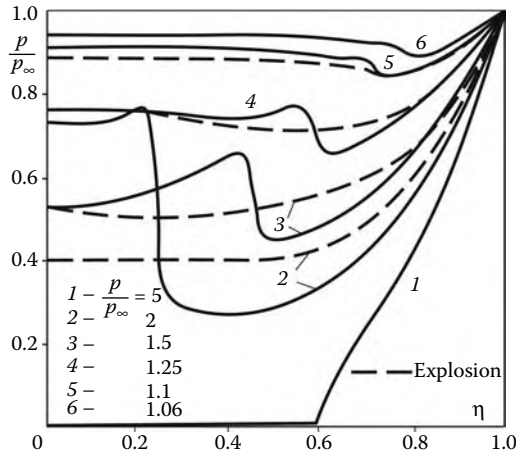


FIGURE 6.23
Pressure profiles in the blast zone.

$$E_0 \sim \rho_\infty \dot{R}_0^2 R_0^{1+v} \sim L^{3+v} t_L^{-2}, \quad J_0 \sim \rho_\infty \dot{R}_0 R_0^{1+v} \sim L^{2+v} t_L^{-1} \quad (6.8.21)$$

Here, R_0 and \dot{R}_0 are the initial position and velocity of the shock wave at $t = 0$. However, this problem has no solution in the point formulation, since at a finite momentum J_0 the energy $E_0 \sim J_0^2/R_0$ increases without bounds as $R_0 \rightarrow 0$. Therefore, the solution of this problem is possible only at finite initial R_0 and \dot{R}_0 and requires preassigning certain initial profiles of the flow parameters (p , v , and so on), the effect of the details of which attenuates with time. However, in accordance with 6.1.20, the total momentum in the flows of this kind increases, so that the effect of the parameter J_0 also vanishes with time and the solution asymptotics are determined by the point blast theory.

The moment at which these asymptotics are attained could apparently be accelerated by displacing forward the effective startup of the point explosion by a time interval t_0 determined in terms of J_0 via Equation 6.8.20. In Chapter 9, where the blast theory is applied to the hypersonic flow past thin blunt bodies, we shall make sure that this possibility really exists.

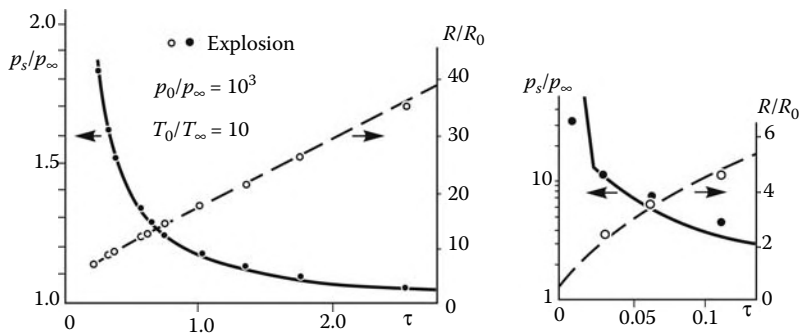


FIGURE 6.24
Shock wave and pressure at a blast.

6.9 Blast in Real Gases

We will now consider the effect of physical and chemical processes accompanying the high-temperature state in the explosion zone. It should be noted that these effects are always involved in limitingly intense shock waves in air, for which condition 3.3.16, $(\gamma - 1)\dot{R}^2 \gg 2a_\infty^2$, holds (thus, at $\dot{R} \gg 2000$ m/sec the temperature behind the shock $T_s \geq 2500^\circ\text{K}$ is sufficient for the dissociation onset). Using the equation of state in its quasiperfect form, $p/\rho h = (\gamma_* - 1)/\gamma_*$, $h = \gamma_* e$ (for high-temperature air the effective adiabatic exponent is $\gamma_* = 1.1 \div 1.2$; see Figure 1.9 of Section 1.3), for a given R we obtain a reduction in the shock velocity and the pressure behind the shock in the form $p_0 \sim \dot{R}^2 \sim (\gamma_* - 1)/(\gamma - 1)$, as compared with the case of the perfect gas with $\gamma = 1.4$.

However, it is rather difficult to attribute a certain value γ_* to the blast wave, owing, for example, to the fact that in the perfect gas the temperature at the center of the explosion zone is infinite. Moreover, as the shock velocity reduces down to the values of $\dot{R} \leq 4a_\infty$, $p_s/p_\infty \leq 20$, the air behind it can be considered to be a perfect gas (Section 3.3); therefore, the domain, within which real properties of the air manifest themselves, is bounded by a certain fixed value of the mass coordinate m_* .

Obviously, this problem is non-self-similar, since the equation of state in its general form involves additional physical scales p_c and h_c (Section 1.12).

The solution of this problem (e.g., a numerical one) requires preassigning a certain plausible parameter distribution within a small initial mass m_0 satisfying the energy integral 6.8.1 (the effect of the charge explosion products could be allowed for in a similar fashion). In this case the plausibility of the parameter behavior description in the $m > m_0$ region might be expected if the expansion of the initial mass m_0 and the transfer of the energy from this mass to the external gas are properly accounted. The effect of the gas imperfection within the mass $m \leq m_*$ can be taken into account within the framework of the solutions obtained for a perfect gas using a simple *effective energy method* (Lunev, 1968). To do this, we represent the internal energy of the gas in Equation 6.8.1 in the form:

$$\begin{aligned} E_e &= 2^\nu \pi^\delta \int_0^R \rho e r^\nu dr = \frac{2^\nu \pi^\delta p_0 R^{1+\nu}}{(1+\nu)(\gamma-1)} + \Delta E \\ \Delta E &= \int_0^M \left(e - \frac{p}{\gamma-1} \right) dm = \int_0^M \frac{\gamma - \gamma_*}{\gamma-1} e dm = \frac{\gamma - \bar{\gamma}_*}{\gamma-1} E_e \end{aligned} \quad (6.9.1)$$

Here, $\bar{\gamma}_*$ is the mass-averaged value of γ_* , while the term ΔE is the difference between the internal energies of the real and perfect gases for the same R within the explosion zone. Since $\gamma \geq \gamma_*$, we have $\Delta E > 0$. Substituting the expression 6.9.1 in Equation 6.8.1 we reduce the latter to the approximate form 6.8.15 with E_0 at the right-hand side replaced by the *effective energy* E_* , where

$$\frac{E_*}{E_0} = 1 - \frac{\Delta E}{E} = 1 - \frac{\gamma - \bar{\gamma}_*}{\gamma-1} \frac{E_e}{E} \approx \frac{\bar{\gamma}_* - 1}{\gamma-1} \quad (6.9.2)$$

This equality was derived at $E_e \approx E$, which is justified in view of 6.8.14, at least for a strong blast. However, the quantity E_* is not constant; at a fixed mass m_* it is a function of the pressure, $E_* = E_*(p_0)$. Therefore, substituting this solution, say, in Equation 6.8.15, results in the appearance of additional terms of the order of the derivatives $\partial(\gamma_* - 1)/\partial p$ at

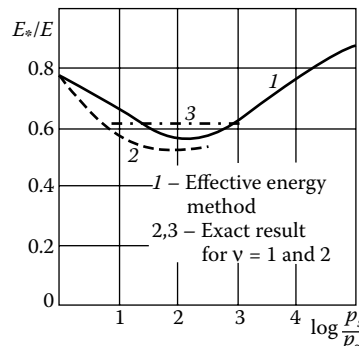


FIGURE 6.25
Relative effective energy for a blast in air.

a constant entropy. However, in accordance with Figure 1.13 (Section 1.5) these derivatives are very small for equilibrium air, so that these additional terms can be discarded. Therefore, solution 6.8.12 through 6.8.16, together with the exact solution, can be used in the case of a real gas if the energy E_* in these solutions is taken to be a time-dependent, or, more exactly, a pressure (p_0)-dependent, parameter.

The enthalpy profile in the explosion zone, necessary for calculating E_*/E_0 , can be obtained by integrating the adiabatic equation $\gamma_* d \ln h = (\gamma_* - 1)d \ln p$ along the particle trajectory $r_m(t)$ at any initial enthalpy profile for a small value of m_0 and an approximate pressure profile given, for example, by formula 6.8.12. An example of such a calculation for a ground spherical explosion is presented in Figure 6.25. At $p_s/p_\infty \approx 100$ the effective energy has a minimum, $E_*/E_0 \approx 0.5 \div 0.6$, which is due to the peaks of the curves $Z(T)$ in Figure 1.8 (Section 1.3). As $p \rightarrow p_\infty$, the ratio $E_*/E_0 \approx 0.8$, which can be explained by the conservation of high temperatures at the explosion zone center for a non-heat-conducting and non-radiating gas.

A weak pressure dependence of the equilibrium air properties results in a weak dependence of the ratio E_*/E on the density ρ_∞ , that is on the explosion altitude. Moreover, for a strong blast at $\gamma = 1.4$ we have $p_s M / \rho E = 0.70 \div 0.66$ for all v . Therefore, the entropy distribution over the mass and, hence, the ratio E_*/E_0 depend on the space dimensionality only slightly. This is confirmed by the curves presented in Figure 6.25 which were obtained by processing the data of the exact calculations of Brode (1959) for $\nu = 2$ and Rose (1962) for $\nu = 1$.

The solution obtained does not cover all the aspects of the gas physics influence on the blast process development, especially, in its initial stage.* In particular, reduction in the energy owing to gas luminosity was not taken into account; in a very simple approximation the energy E_* entering in the solution should be diminished by the energy radiated by the gas.

Moreover, even for a perfect gas the unbounded temperature growth at the blast center involves the necessity of making allowance for thermal conductivity of the gas which is not taken into account within the framework of the inviscid flow model. This question will be considered in the next section.

* See for details the books of Raizer and Zeldovich (1966) and Korobeinikov (1991).

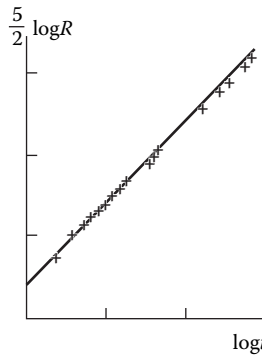


FIGURE 6.26
Strong blast theory vs. experiment.

Nevertheless, all these factors do not change the basic, power-law development of the strong blast. This is confirmed by the results of processing the data of the observations of a nuclear explosion (Taylor, 1950) presented in Figure 6.26.

6.10 Self-Similar Time-Dependent Dissipative Flows

The previous sections of this chapter were devoted only to inviscid flows. For the sake of generality, below we consider some time-dependent self-similar problems for a viscous, heat-conducting gas, which demonstrate clearly the role played by dissipative effects in the formation of such flows.

The presence of dissipative terms in the equations of motion of Section 1.9 involves new governing parameters of the problems, namely, viscosity μ and thermal conductivity λ .

If the heat flux vector 1.2.9 through 1.2.11 is written in the form

$$p_2 = \frac{c_p \mu}{\lambda}, \quad J = -\lambda \frac{\partial T}{\partial r} = -\frac{\lambda}{c_p} \frac{\partial h}{\partial r} = -\frac{\mu}{\text{Pr}} \frac{\partial h}{\partial r} \quad (6.10.1)$$

where h is the gas enthalpy, c_p is its specific heat, and Pr is the Prandtl number (see Section 1.3), then the gas temperature no longer enters in the equations of motion of Section 1.9 and the equation of state $\gamma p = (\gamma - 1)\rho h$ for a perfect gas. Then, combining with the density ρ_∞ , we get two more parameters, namely, the kinematic viscosity μ/ρ_∞ and the *thermometric conductivity* $\kappa = \lambda/c_p \rho_\infty$, in addition to the relevant parameters of the problems considered previously; both parameters have the same dimensionality L^2/t_0 . Naturally, this makes the construction of self-similar solutions more difficult. However, such solutions can exist; certain of these are presented in what follows.

Blast in a heat-conducting gas. The solution of the strong blast problem given in Section 6.8 has a singularity at the blast center: as the center is approached, the gas temperature grows as $T \sim \eta^{-(1+\nu)/(\gamma-1)}$ (see formula 6.8.9; here and in what follows the designations are the same as in Section 6.8); thus, heat conduction in the gas grows drastically in importance. At the same time, in the blast zone the Reynolds number $Re \sim \rho R \dot{R}/\mu$ is sufficiently high and, in accordance with the conclusions of Section 1.16, the flow in this zone should be considered as nondissipative everywhere, except for a vicinity of the central singular point.

Since, as shown in Section 6.8, in the blast zone the contribution of the kinetic energy is relatively low, its viscous dissipation can be neglected and the corresponding terms in the energy equation can be omitted. This reduces the problem to that of the blast in an inviscid, though heat-conducting gas; the initial, limitingly intense stage of the blast will be considered in the following.

However, this problem is self-similar only for some particular forms of the enthalpy dependence of the parameter λ/c_p , since the dimensionality of this parameter, L^2/t_0 , coincides with the dimensionality $[E/\rho_\infty] = L^{(3+\nu)/2}/t_0^2$, where E is the blast energy, only for $\nu = 1$ and a constant λ/c_p . If this function has a more general form, $\lambda/c_p = Ch^m$, then the dimensionality $[C/\rho_\infty] = L^{2(1-m)}/t_0^{(1-2m)}$ ($[h] = L^2/t_0^2$) can be made equal to $[E/\rho_\infty]$ only by letting $m = -1/2$ for $\nu = 0$, $m = 0$ for $\nu = 1$, and $m = 1/6$ for $\nu = 2$.

In these self-similar problems the energy equation has an integral that follows from the integral Equation 1.7.3 written for a movable volume Ω_η bounded by a surface $r = \eta R$ with a constant value of the self-similar variable η . The velocity at which the gas flows across this boundary is $\eta \dot{R} - v$, while the left-hand side of Equation 1.7.3 is zero in view of the constancy of the energy within the volume Ω_η . Then Equation 1.7.3 takes the form:

$$\rho(\eta \dot{R} - v) \left(e + \frac{1}{2} v^2 \right) - pv + \frac{\lambda}{c_p} \frac{\partial h}{\partial r} = 0, \quad e = \frac{1}{\gamma}, \quad \rho e = \frac{p}{\gamma - 1} \quad (6.10.2)$$

Here, we have used the condition of the solution smoothness, $\partial h/\partial r = 0$ for $r = 0$, which is inherent in the heat-conducting gas. At $\lambda = 0$ hence follows the Sedov integral mentioned in Section 6.8.

In the following we will consider only a rather simple axisymmetric problem ($\nu = 1, m = 0$) letting the parameter

$$\varepsilon = \frac{\lambda}{c_p \rho_\infty} \left(\frac{\rho_\infty}{E} \right)^{1/2} \ll 1 \quad (6.10.3)$$

to be small. In this case we should expect (and this will be shown later) that the domain of influence of heat conduction $\eta \leq \eta_\varepsilon$ would be deeply embedded in the isobaric central region $\eta < \eta_p$ of the blast zone ($\eta_p \sim 0.6 \div 0.7$ in Figure 6.21).

By virtue of the specific features of the strong blast flow described in Section 6.8, the internal energy redistribution in the isobaric region does not alter its total value proportional to $pR^{(1+\nu)/(y-1)}$ and, hence, has no effect on the pressure $p_0(t)$ in this region and the blast wave $R = R(t)$ determined by the solutions 6.8.3 and 6.8.4. In the isobaric region, the pressure can be let to be the function of time only, while the kinetic energy (the term $v^2/2$) can be neglected; then passing to variables 6.8.3 and introducing a new variable by the formula $h = 0.5\dot{R}^2H(\eta)$ we can bring Equation 6.10.2 to the form:

$$\begin{aligned} \bar{\varepsilon} \frac{dH}{d\eta} &= \eta(\gamma U - 1), & U &= \frac{V}{\eta}, & \eta &= \frac{r}{R} \\ \bar{\varepsilon} = \frac{(\gamma - 1)\lambda}{4c_p \rho_\infty R \dot{R} P_0} &= \frac{(\gamma - 1)(3 + \nu)}{4P_0} \varepsilon t^{(\nu-1)/(3+\nu)}, & P_0 &= P(0) \end{aligned} \quad (6.10.4)$$

In our case, $\nu = 1, \lambda/c_p = \text{const}$, and the parameter $\bar{\varepsilon}$ is constant.

The second equation for the isobaric region, in which the pressure is given, is the continuity equation, which in the self-similar variables (for $\nu = 1$) takes the form:

$$\frac{1}{\rho} \eta^2 (1 - U) \frac{d\rho}{d\eta} = -\frac{1}{H} \eta^2 (1 - U) \frac{dH}{d\eta} = \frac{d}{d\eta} (\eta^2 U) \quad (6.10.5)$$

For $\varepsilon = 0$ (in the absence of heat conduction) these equations have an inviscid, or external, solution

$$U = \frac{1}{\gamma}, \quad V = \frac{1}{\gamma}\eta, \quad H = H_e = C_1\eta^{-2/(\gamma-1)}, \quad C_1 = \frac{4\gamma(3\gamma-1)}{(\gamma+1)^2} \quad (6.10.6)$$

The constant C_1 is obtained by matching with formulas 6.8.13. This solution represents a limit for an internal solution of the heat-conducting problem. To obtain this solution we pass to the variables

$$\bar{H} = H/H_0, \quad \zeta = \bar{\eta}^2 = \eta^2/\bar{\varepsilon}H_0 \quad (6.10.7)$$

where the quantity $H_0 = H(0)$, which is unknown beforehand, is referred to the blast center. Equations 6.10.4 and 6.10.5 take the form:

$$\frac{d\bar{H}}{d\zeta} = \gamma U - 1, \quad U = \frac{V}{\eta} \quad (6.10.8)$$

$$\bar{H} \frac{d}{d\zeta}(\zeta U) = -\zeta(1-U) \frac{d\bar{H}}{d\zeta} = \zeta(1-U)(1-\gamma U) \quad (6.10.9)$$

For $\eta = 0$ the required solution must satisfy the conditions $\bar{H} = 1$ and $V = 0$. The latter condition is satisfied only by the sole bounded (as $\eta \rightarrow 0$) local solution of Equation 6.10.9 $U = \zeta/2$ and is not satisfied by the sole unbounded solution $U \sim (\zeta \ln \zeta)^{-1}$. For $\zeta \gg 1$ the system of Equations 6.10.8 and 6.10.9 has—with an error of the order of $\zeta^{-\gamma/(\gamma-1)}$ —the following asymptotic solution

$$\gamma U \rightarrow 1, \quad \bar{H}\zeta^{1/(\gamma-1)} = \frac{H}{H_0} \left(\frac{\eta^2}{\bar{\varepsilon}H_0} \right)^{1/(\gamma-1)} \rightarrow C_2 \quad (6.10.10)$$

The constant C_2 is determined in the process of solution. The constant H_0 , which is as yet indefinite, and the relation between the variables ζ and η are determined from the condition of matching solutions 6.10.10 for large ζ and 6.10.6 for small $\eta \leq \eta_\varepsilon$

$$H_0 = \beta \bar{\varepsilon}^{-1/\gamma}, \quad \zeta = \bar{\eta}^2 = \eta^2/\beta \bar{\varepsilon}^{(\gamma-1)/\gamma}, \quad \beta = (C_1/C_2)^{(\gamma-1)/\gamma} \quad (6.10.11)$$

The curves $\bar{H}(\bar{\eta})$ and $\bar{V}(\bar{\eta})$, where $\bar{V} = V(\beta \bar{\varepsilon}^{(\gamma-1)/\gamma})^{-1/2}$, are plotted in Figure 6.27 for $\gamma = 1.4$ ($C_2 = 0.487$) and $\gamma = 1.1$ ($C_2 = 1.71$); for the sake of comparison in the same

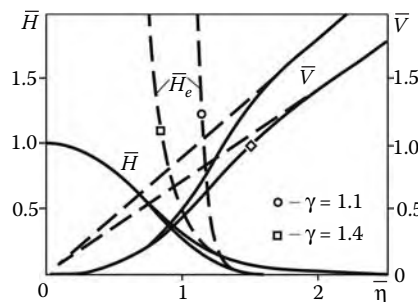


FIGURE 6.27
Enthalpy and velocity near the blast center in a heat-conducting gas.

figure the limiting external dependences $\bar{V} = \bar{\eta}/\gamma$ and $\bar{H} = \bar{H}_e(\bar{\eta})$ determined from 6.10.6 are also presented as dotted curves. The internal solution is close to the limiting curves for $\bar{\eta} \approx \bar{\eta}_e \approx 1.5$, which is associated with the heat-conduction influence boundary $\eta_e = \eta(\zeta_e) \approx 1.2\beta^{1/2}\bar{\varepsilon}^{(\gamma-1)/2\gamma}$. From 6.10.11 it follows that the temperature at the blast center increases, while η_e decreases when ε decreases.* Near the blast center this solution has the form: $H = 1 - \bar{\eta}^2$ and $\bar{V} = \bar{\eta}^3/2$.

Thermal source problem. We will now consider the later, or far-off, stage of the strong blast in which the pressure has completely equalized but the temperature profile in the central zone remains nonuniform, the temperature being unbounded at the center $r = 0$. We will simulate the evolution of this profile in a heat-conducting gas as follows. Let for $t = 0$ in a gas at rest with a temperature T_∞ occupying a three-dimensional ($v = 2$), two-dimensional ($v = 1$, “thermal filament”), or one-dimensional ($v = 0$, “thermal plane”) domain, a heat Q per unit length or area, for $v = 1$ and $v = 0$, respectively, release instantaneously at the point $r = 0$. All the other parameters, except for the temperature T or the enthalpy h , are assumed to be constant, while the gas is at rest; then the energy Equation 1.9.6 is reduced to the heat equation

$$\frac{\partial T}{\partial t} = \frac{\kappa}{r^v} \frac{\partial}{\partial r} \left(r^v \frac{\partial T}{\partial t} \right), \quad \kappa = \frac{\lambda}{c_p \rho_\infty} \quad (6.10.12)$$

We require that the solution be bounded for $r = 0$ and decay ($T \rightarrow T_\infty$) for $r \rightarrow \infty$. By the replacement $T - T_\infty = \Delta T$ the temperature T_∞ is eliminated from the relevant parameters of this linear problem and the scale for T is now represented by the quantity $Q/\rho_\infty c_p L^{1+v}$, where L is a parameter having the dimensionality of the length. In view of the absence of the scale length in our problem, we take for L the combination $(\kappa t)^{1/2}$, since $[\kappa] = L^2/t_0$. Therefore, the solution of the problem can be presented in the form:

$$\Delta T = C \frac{Q}{\rho c_p} (\kappa t)^{-(1+v)/2} e^{-\zeta/4}, \quad \zeta = \frac{r}{\sqrt{\kappa t}} \quad (6.10.13)$$

The arbitrary constant C is determined from the following condition of heat conservation in space

$$2^v \pi^\delta \rho c_p \int_0^\infty \Delta T r^v dr = Q \quad (6.10.14)$$

where $\delta = 0$ for $v = 0$ and $\delta = 1$ for $v = 1$ and 2.

The constants have the following values: $C_0 = 1/\sqrt{\pi}$, $C_1 = 1/4$, and $C_2 = 1/8\pi$. At the point $r = 0$ the temperature is infinite for $t = 0$ and decreases with time. The zone disturbed by heat transfer propagates as $r \sim \sqrt{\kappa t}$, that is, lags appreciably behind the blast wave, which, in the limit, represents an acoustic wave $a_\infty t$.

Plane starting at a longitudinal velocity. Let at a moment $t = 0$ the plane $y = 0$ with a gas of a fluid above it ($y > 0$), being at rest and characterized by the density ρ_∞ , enthalpy h_∞ , speed of sound a_∞ , and so on, acquire suddenly a constant longitudinal velocity U . The flow thus generated is dependent on time and the coordinate y normal to the plane and

* Similar conclusions for the strong blast were made earlier by Korobeinikov (1957, 1991) for the self-similar case and Sychev (1965) who derived a more general non-self-similar solution valid in the central blast region for any v and $\lambda/c_p \sim h$ using the method of external and internal expansions.

does not depend on the longitudinal coordinate x . In this case the equations of motion from Sections 1.8 to 1.10 take the form:

$$\rho \left(\frac{\partial u}{\partial t} + v \frac{\partial u}{\partial y} \right) = \frac{\partial}{\partial y} \left(\mu \frac{\partial u}{\partial y} \right) \quad (6.10.15)$$

$$\rho \left(\frac{\partial v}{\partial t} + v \frac{\partial u}{\partial y} \right) = - \frac{\partial p}{\partial y} + \frac{4}{3} \frac{\partial}{\partial y} \left(\mu \frac{\partial v}{\partial y} \right) \quad (6.10.16)$$

$$\frac{\partial \rho}{\partial t} + \frac{\partial \rho v}{\partial y} = 0 \quad (6.10.17)$$

$$\begin{aligned} \rho \left(\frac{\partial h}{\partial t} + v \frac{\partial h}{\partial y} \right) &= v \frac{\partial p}{\partial y} + \frac{1}{Pr} \frac{\partial}{\partial y} \left(\mu \frac{\partial h}{\partial y} \right) + \mu \left(\frac{\partial u}{\partial y} \right)^2 + \frac{4}{3} \left(\frac{\partial v}{\partial y} \right)^2, \\ Pr &= \frac{\mu c_p}{\lambda} \end{aligned} \quad (6.10.18)$$

Here, u and v are the velocity projections on the x and y axes; the Prandtl number Pr is taken to be constant. We will impose the following initial and boundary conditions

$$\begin{aligned} t = 0, \quad y \geq 0 : \quad u &= v = 0, \quad \rho = \rho_\infty, \quad h = h_\infty \\ y = 0 : \quad u &= U, \quad v = 0, \quad h = h_w = \text{const} \\ t > 0, \quad y \rightarrow \infty : \quad u &\rightarrow 0, \quad h \rightarrow h_\infty \end{aligned} \quad (6.10.19)$$

In the general case the problem formulated is non-self-similar, since, apart from the external parameters ρ_∞ , and so on, and the velocity U , it involves also the kinematic viscosity $\nu = \mu/\rho_\infty$ having the dimensionality L^2/t_0 . However, the problem can be reduced to a self-similar problem in two limiting cases, which will be discussed in the following.

The first case is the *Rayleigh problem* in its classical version. Let the ambient medium be an incompressible fluid and the velocity U be so small that viscous dissipation of the energy could be neglected. Then the density and the entropy can be assumed to be constant, the velocity component $v = 0$, and Equation 6.10.15 takes the same form as the heat Equation 6.10.12

$$\frac{\partial u}{\partial t} = \nu \frac{\partial^2 u}{\partial y^2}, \quad \nu = \frac{\mu}{\rho} \quad (6.10.20)$$

These flows with parallel streamlines are called layered. The problem is linear and the ratio u/U is U -independent, being dependent on the parameters t , y , and ν only; this gives the single (as in the thermal source problem) self-similar variable $\zeta = y/2\sqrt{\nu t}$. In this case Equation 6.10.20 is reduced to an ordinary differential equation $u'' + 2\zeta u' = 0$ whose solution is expressed in terms of the error integral as follows

$$\frac{u}{U} = \bar{u}(\zeta) = 1 - \Phi(\zeta), \quad \Phi(\zeta) = \frac{2}{\sqrt{\pi}} \int_0^\zeta e^{-\xi^2} d\xi \quad (6.10.21)$$

This solution is presented in Figure 6.28. The form itself of the variable ζ leads to the law $\delta = 2\zeta_\delta \sqrt{\nu t}$ for the stratified flow front with exponential decay of disturbances.

The flow considered previously corresponds to the condition $U \ll a_\infty$ (cf. Section 2.2). Let, contrariwise, the velocity be hypersonic, $U \gg a_\infty$ (the *Stewartson problem*, 1955). In this

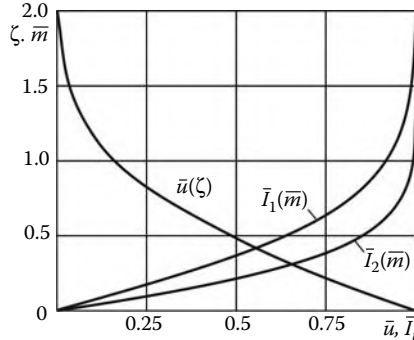


FIGURE 6.28
On the Rayleigh and Stewartson problems.

case, the gas is heated through viscous dissipation of the kinetic energy, which leads to the formation of a *viscous high-temperature sublayer* of thickness $y = \delta(t)$, whose expansion, apart from the longitudinal, quasistratified flow, induces also a transverse flow at a velocity $v > 0$ and a shock wave $y = R(t)$. We will assume that this shock wave is limitingly strong, with the velocity $\dot{R} \sim \dot{\delta} \gg a_\infty$ and the pressure $p \sim \rho_\infty \dot{\delta}^2$.

Mathematically, the sublayer heating is caused by the term $\mu(\partial u/\partial y)^2$ in Equation 6.10.18. Since $u \sim U$, this term is proportional to the product μU^2 , which makes it possible to form, along with the density ρ_∞ , the governing parameter $\mu U^2/\rho_\infty$ having the dimensionality L^4/t_0^3 , as well as the self-similar variable ζ , where

$$y = \zeta \chi^{1/4} t^{3/4}, \quad \chi = \mu_0 U^2 / \rho_\infty \quad (6.10.22)$$

Here and in what follows μ_0 , ρ_0 , h_0 , and so on, are the scale parameters of the viscous sublayer flow. By analogy with 6.8.3 this self-similarity is associated with the solution of the type

$$\begin{aligned} R &= A_R \chi^{1/4} t^{3/4}, & \rho &= \rho_\infty \bar{\rho}(\zeta) \\ p &= \rho_\infty \dot{R}^2 \bar{p}(\zeta) = A_p (\chi/t)^{1/2} \bar{p}(\zeta), & v &= \dot{R} \bar{v}(\zeta) \\ h &= 0.5 \dot{R}^2 \bar{h}(\zeta), & A_p &= 9A_R^2/16, \quad A_R = \text{const} \end{aligned} \quad (6.10.23)$$

We will now evaluate the viscous sublayer parameters; naturally, we assume that $\delta \sim R$, $\dot{\delta} \sim \delta/t$, and the orders 6.10.23 of the flow parameters p and v are conserved within the sublayer. Following the procedure of Section 1.16 and equating the orders of the left and right sides of Equation 6.10.15, we obtain $\rho_0 \delta^2 \sim \mu_0 t$, while comparing the first term on the left and the third term on the right of Equation 6.10.18 we obtain $\rho_0 h_0 \delta^2 \sim \mu_0 U^2 t$ (since $\Delta h_0 \sim h_0$ for $h_0 \gg h_\infty$ and, as we will assume, $h_w \leq h_0$). Combining these estimates with the equation of state we obtain the estimates for the sublayer thickness and the orders of the flow parameters therein

$$\begin{aligned} \delta &= A_\delta \chi^{1/4} t^{3/4}, & h \sim h_0 &= U^2 \\ \rho &\sim \rho_0 = \frac{\gamma}{\gamma-1} \frac{p_0}{h_0} = A_\rho \frac{\rho_\infty}{U^2} \left(\frac{\chi}{t} \right)^{1/2} \\ A_\rho &= \frac{9\gamma}{16(\gamma-1)} A_R^2 \bar{p}_0, & \bar{p}_0 &= \bar{p}(0) \end{aligned} \quad (6.10.24)$$

Thus, the solution in the sublayer should be sought in the form:

$$\bar{u}(\xi) = u/U, \quad \tilde{h}(\xi) = h/h_0, \quad \tilde{\rho}(\xi) = \rho/\rho_0 \quad (6.10.25)$$

for the same functions p and v as in Equation 6.10.23. However, this form of the solution for the functions h and ρ is inconsistent with 6.10.23.

These difficulties can be avoided for an *intermediate* stage of the process satisfying the condition

$$U^2 \gg \delta^2 \sim (\chi/t)^{1/2} \gg a_\infty^2 \quad (6.10.26)$$

Allowing for our estimates $\mu_0 \sim \mu_\infty (h_0/h_\infty)$, where $h_0 \sim U^2$ and $h_\infty \sim a_\infty^2$, we can bring these conditions to the form:

$$\frac{\delta^2}{U^2} \sim \frac{M_\infty}{\sqrt{Re_t}} \ll 1, \quad \frac{\delta^2}{a_\infty^2} \sim \frac{M_\infty^3}{\sqrt{Re_t}} \gg 1, \quad M_\infty = \frac{U}{a_\infty}, \quad Re_t = \frac{\rho_\infty U^2 t}{\mu_\infty} \quad (6.10.27)$$

Here, Re_t is the Reynolds number based on the path Ut traveled by the plate. In this case, the relative quantities—the pressure difference $\Delta p/p$, the gas density ρ_0/ρ_∞ and the gas mass $m_0/m_R \sim \rho_0/\rho_\infty$ in the viscous sublayer ($m_R \sim R\rho_\infty$)—are of the order δ^2/U^2 and, therefore, are negligibly small.

This makes it possible to subdivide the disturbed domain to two subdomains, namely, the *viscous sublayer* with a limitingly small mass and pressure, constant across the sublayer thickness, and the *shock layer* adjacent to the shock wave in which, as in the case of the strong blast, almost the whole mass of the disturbed gas is concentrated.

In the shock layer, the dissipative terms of the equations can be neglected, since, as compared with the viscous sublayer, the density in it $\rho \sim \rho_\infty \gg \rho_0$, while viscosity $\mu \ll \mu_0$ owing to much lower temperatures. Therefore, the flow in this layer is inviscid and is similar to that induced by a piston, whose role is played by the viscous sublayer; the thickness δ of the latter grows in accordance with a power law (cf. 6.10.24). The corresponding solution has the form 6.10.23; it was described in detail in Section 6.8, so we will not dwell on it.

To solve the problem of the viscous sublayer, we pass to a Lagrangian coordinate, namely, the gas mass m . Rewriting Equation 6.10.15 in terms of 2.1.4 yields

$$\frac{\partial u}{\partial t} = \frac{\partial}{\partial m} \rho \mu \frac{\partial u}{\partial m}, \quad \frac{\partial m}{\partial y} = \rho, \quad \frac{\partial m}{\partial t} = -\rho v \quad (6.10.28)$$

In Equation 6.10.18 with 6.10.26 taken into account we will drop the term with $\partial p/\partial y$ and the last term on the right; then, summing this equation with Equation 6.10.15 multiplied by u we obtain an equation for the *total enthalpy* of the gas H in which, for the sake of simplicity, we let $Pr = 1$

$$\frac{\partial H}{\partial t} = \frac{\partial}{\partial m} \left(\rho \mu \frac{\partial H}{\partial m} \right), \quad H = h + \frac{1}{2} u^2 \quad (6.10.29)$$

For the initial ($t = 0$) and boundary ($y = 0$) conditions we take the same conditions (6.10.19). However, on the outer edge of the viscous sublayer it should be $u = 0$ and, which is new, $h = H = 0$, since the enthalpy ratio in the shock layer and the viscous sublayer is, in accordance with 6.10.23 and 6.10.26, of the order $\delta^2/U^2 \ll 1$, and, by virtue of the condition $m_0/m_R \ll 1$, the conditions $u \rightarrow 0$ and $H \rightarrow 0$ can be fulfilled asymptotically for $m \rightarrow \infty$, which will be confirmed later.

Equations 6.10.28 and 6.10.29 differ from Equation 6.10.20 only by the variable quantity $\rho\mu$ instead of ν . To obtain illustrative results we assume that $\mu \sim h$ (instead of $\mu \sim h^{0.7}$ for air; cf. 1.3.11), that is, in view of 6.10.24 we put

$$\mu\rho = \mu_0\rho_0 = C^2t^{-1/2}, \quad C^2 = A_\rho \chi^{3/2} \frac{\rho_\infty^2}{U_\infty^4} \quad (6.10.30)$$

Then we introduce a new variable \bar{m} (a counterpart of ζ in 6.10.21) and functions

$$\begin{aligned} \bar{m} &= \frac{m}{2\sqrt{2}Ct^{1/4}}, & \bar{u} &= \frac{u}{U} \\ \bar{H} &= \frac{H}{H_w}, & H_w &= h_w + \frac{1}{2}U^2 \end{aligned} \quad (6.10.31)$$

Then the solutions of Equations 6.10.28 and 6.10.29 have the same form $\bar{H} = \bar{u} = 1 - \Phi(\bar{m})$ as 6.10.21; this solution is shown in Figure 6.28. We note that the relation $\bar{H} = \bar{u}$ obtained previously is a particular case of the *Crocco integral* with which we shall deal in Chapter 12.

Using the inverse transformation $dy = \rho^{-1}dm$, in view of 6.10.24 and 6.10.31, we obtain the relation between the original variables ζ and \bar{m}

$$\begin{aligned} \zeta &= \frac{2\sqrt{2}}{A_\rho^{1/2}} I(\bar{m}) = \frac{8}{3} \sqrt{\frac{2(\gamma-1)}{\gamma}} \frac{I(\bar{m})}{\bar{p}_0^{1/2} A_R}, & I(\bar{m}) &= \int_0^{\bar{m}} \tilde{h}(\bar{m}) d\bar{m} \\ \tilde{h} &= H_w(1 - \Phi) - \frac{1}{2}(1 - \Phi)^2, & I &= H_w I_1(\bar{m}) - I_2(\bar{m}), & \tilde{H}_w &= \frac{H_w}{U^2} \end{aligned} \quad (6.10.32)$$

The integral $I(\bar{m})$ converges exponentially to its limiting value I_∞ , which justifies the asymptotic substitution of the external boundary conditions for the functions \bar{u} and \bar{H} , as accepted previously. In this case $I_{1\infty} = 0.565$ and $I_{2\infty} = 0.165$, while the $\bar{I}_i = I_i/I_{i\infty}$ curve is plotted in Figure 6.28. Using 1.2.9, 6.10.28, and 6.10.31 it can easily be shown that the heat flux to the wall is $\partial T/\partial y \sim (1 - \tilde{H}_w)t^{-3/4}$. For a thermally insulated plate with the condition $\partial h/\partial y = 0$ at $y = 0$ we have $H_w = U^2$ and $h_w = U^2/2$; for $h_w = 0$ we have $H_w = U^2/2$.

Finally, letting $I = I_\infty$ in 6.10.32 we obtain the coefficient $A_\delta = \zeta_\delta$ in formula 6.10.24 for δ expressed in terms of A_R and the sublayer pressure \bar{p}_0 . Another relation between A_δ and A_R follows from the solution of the problem for a power-law piston, which for $\gamma = 1.4$ gives $A_\delta/A_R = 0.59$ and $\bar{p}_0 = 0.61$ (the latter value is close to the value $\bar{p}_0 = 0.6$ calculated from formula 6.8.11), which closes the problem.

Vortex diffusion. Let at $t = 0$ in a fluid there be a rotational flow with a vortex concentrated at the point $r = 0$ and zero elsewhere, circular streamlines, a constant circulation Γ_0 , and a peripheral velocity $w = \Gamma_0/2\pi r$ on the streamlines (cf. Section 2.1). The evolution of this flow is governed by the Navier-Stokes Equation 1.14.11; the initial flowfield thus preassigned satisfies these equations automatically and it would seem that there is no reason for its further evolution. However, in a viscous fluid the flowfield must be continuous everywhere including the point $r = 0$; thus, at this point we should let $w = 0$, as distinct from the inviscid problem in which $w \rightarrow \infty$.

As in the Rayleigh problem, the ratio Γ/Γ_0 can be dependent on the variable $\zeta = r/\sqrt{vt}$ only. Then Equation 1.14.11 has the general solution

$$2\pi rw = \Gamma = C_1 + C_2 e^{-\zeta^2/4} \quad (6.10.33)$$

The initial and boundary conditions for the problem are as follows

$$\begin{aligned}
t \rightarrow 0, \quad r > 0 : \quad \Gamma \rightarrow \Gamma_0 \\
t > 0; \quad r \rightarrow 0 : \quad \Gamma \rightarrow 2\pi w r \rightarrow 0 \\
r \rightarrow \infty : \quad \Gamma \rightarrow \Gamma_0, \quad p \rightarrow p_0
\end{aligned} \tag{6.10.34}$$

Thence it follows that $C_1 = -C_2 = \Gamma_0$. For small r the velocity field obtained, $w \approx r/8\pi vt$, corresponds to solid body rotation at an angular velocity decreasing as t^{-1} ; the extent of this quasisolid domain grows as \sqrt{t} .

We will also calculate the radial profile of the pressure for this flow. As follows from Equations 1.13.10 and 1.14.10, for $v = 0$ the equation of motion projected onto the r axis has the form $\partial p / \partial r = \rho w^2 / r$. Letting $p \rightarrow p_0$ as $r \rightarrow \infty$, we can represent the complete solution of this problem in the self-similar (since the dimensionality $[\Gamma_0] = [v]$, where v is kinematic viscosity) form:

$$\bar{w} = \frac{2\pi\sqrt{vt}}{\Gamma_0} w = \frac{1}{\zeta} (1 - e^{-\zeta^2/4}), \quad \frac{4\pi^2 vt(p - p_0)}{\rho \Gamma_0^2} = \bar{p} = - \int_{\bar{r}}^{\infty} \frac{\bar{w}^2}{\zeta} dr \tag{6.10.35}$$

The $\bar{w}(\zeta)$ and $\bar{p}(\zeta)$ curves are plotted in Figure 6.29. For $\zeta > 3.5$ they coincide with the initial inviscid curves $\bar{w} = 1/\zeta$ and $\bar{p} = -1/2\zeta^2$ and for $\zeta < 0.6$ with the quasisolid solution $\bar{w} = \zeta/4$ and $\bar{p} = \bar{p}(0) + \zeta^2/32$. At the point $\zeta_m = 2.24$ the function \bar{w} has a minimum $\bar{w}_m = 0.319$, while $\bar{p}(0) = -0.173$. In the original variables, the quantities $w_m \sim (vt)^{-1/2}$ and $-p(0) \sim 1/vt$ decrease with time, while the point $r_m = \zeta_m \sqrt{vt}$ moves away from the center of the vortex.

Let us consider one more similar problem. Let a time-independent rotational moment M_0 be suddenly applied to a fluid, initially at rest, at the point $r = 0$ (this is the counterpart of the Rayleigh problem considered previously). This problem is associated with the boundary condition $2\pi r^2 \mu (\partial w / \partial r) \rightarrow M_0$ for $r \rightarrow 0$, which, in its turn, is associated with solution 6.10.33 with $C_1 = 0$ and $C_2 = M_0 / \mu = \Gamma_0$. For $\zeta \ll 1$ or $r \ll \delta = 2\sqrt{vt}$ this solution gives $w = \Gamma_0 / 2\pi r$, that is, a time-independent irrotational velocity field induced by the concentrated vortex, which embraces the entire disturbed flow region for $t \rightarrow \infty$. Technically, this solution can be realized by rotating an unbounded cylinder of radius r_0 at a constant angular velocity $\Omega = \Gamma_0 / 2\pi r_0^2$ after the time interval $t \gg t_0 = r_0^2 / 4v$. In this case, the total moment of momentum $I = M_0 t$ increases with time without bound, which also corresponds to a concentrated vortex in an unbounded inviscid fluid.

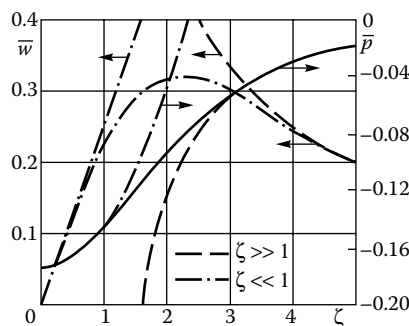


FIGURE 6.29

Velocity and pressure distributions in an unbounded viscous vortex.

7

Flows with Strong Shocks

From this chapter on, we turn to the presentation of hypersonic flow theory, that is, the theory of the flows with high Mach numbers, $M_\infty \gg 1$. In particular, the chapter is devoted to the flow past bodies in the presence of strong shocks. This circumstance, which often makes the physics of the phenomenon more difficult, at the same time facilitates the purely gas dynamic analysis due to the corresponding simplification of the governing equations. This simplification is based on the use of some small parameters whose appearance is due to strong shock waves accompanying hypersonic flows. At the same time, it turns out that many properties of these flows can be carried over to moderately supersonic flows.

7.1 Hypersonic Stabilization and Compressed Shock Layer

Methodically, the following analysis is based on the use of the quantities

$$M_{n\infty}^{-2} \ll 1, \quad k = \rho_\infty / \rho_s \ll 1 \quad (\gamma - 1 \ll 1) \quad (7.1.1)$$

as the small parameters of the problem. Here, $M_{n\infty}$ is the freestream Mach number normal to the shock (for an oblique shock with an angle α we have $M_{n\infty} = M_\infty \sin \alpha$), while k is the density ratio across the shock (the density values ahead of and behind the shock are referred to by the subscripts ∞ and s , as well as other quantities introduced in the following). For a perfect gas, $k \rightarrow (\gamma - 1)/(\gamma + 1)$ as $M_{n\infty} \rightarrow \infty$, so that $k \rightarrow 0$ as $\gamma \rightarrow 1$ (which is reflected by conditions 7.1.1). However, for air we have $\rho_s/\rho_\infty = 5 \div 20$ for $M_{n\infty} \geq 5$ (Section 3.3, Figure 3.4); thus, we will assume both parameters, $M_{n\infty}^{-2}$ and k , to be small. Obviously, this assumption is valid for the flows past blunt bodies, in which $\sin \alpha \sim 1$; the theory discussed in the following deals chiefly with precisely these flows.

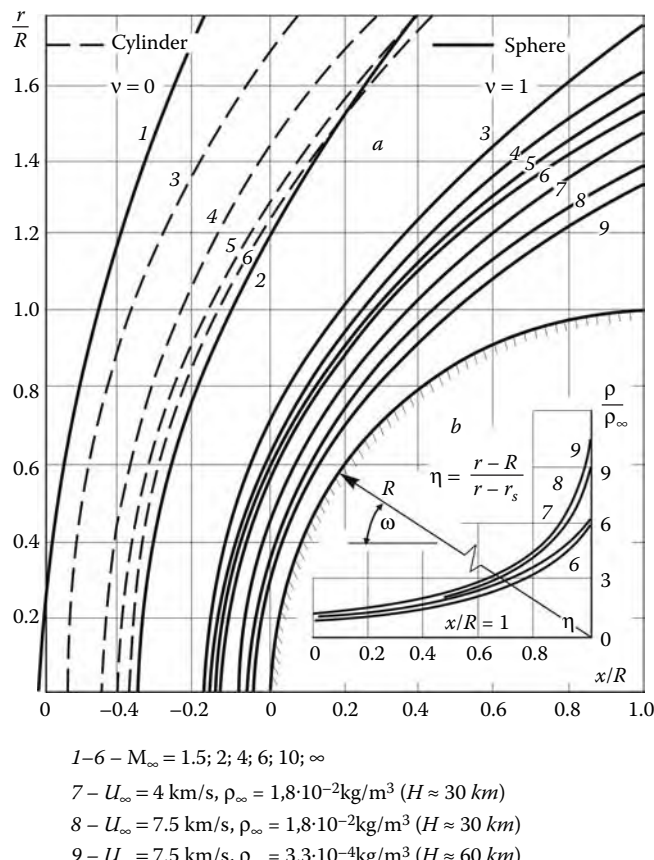
Conditions 7.1.1 imply two important properties of the flows past bodies, namely, their *hypersonic stabilization* and a small thickness of the *compressed shock layer*. Precisely these distinctive features will be considered here.*

As shown in Section 3.3, for high Mach numbers, $M_{n\infty} \gg 1$, or, to be more precise, for $(\gamma - 1)M_{n\infty}^2 \gg 2$ (cf. Equation 3.3.16), relations 3.3.4 for a shock wave no longer depend on the freestream parameters p_∞ and h_∞ , that is, on $M_{n\infty}$, and take the form 3.3.17 or, for an oblique shock

* In what follows, the shock layer is considered to mean a gas layer adjacent to the body, where the flow parameters are of the same order as immediately behind the shock. This layer is not necessarily compressed; see, for example, Chapters 8 and 9. However, generally speaking, this term is sometimes carried over to any gas layer between the body and the shock.

$$\begin{aligned}\bar{p}_s &= \frac{p_s}{\rho_\infty U_\infty^2} = (1 - k)s, & \bar{h}_s &= \frac{h_s}{U_\infty^2} = \frac{1}{2}(1 - k^2)s \\ \bar{\rho}_s &= \frac{\rho_s}{\rho_\infty} = \frac{\gamma_* + 1}{\gamma_* - 1}, & s &= \frac{U_{n\infty}^2}{U_\infty^2} = \sin^2 \alpha\end{aligned}\quad (7.1.2)$$

Here, for the sake of generality, we have used the equation of state $p/\rho h = (\gamma_* - 1)/\gamma_*$ in its quasiperfect form (Section 1.3); for a perfect gas $\gamma = \gamma_*$. We will now assume that the hypersonic conditions are fulfilled at the point c of the shock characterized by the angle α_c (Figure 5.6, Section 5.3). Then they are also fulfilled upstream of point c , since there we have $\alpha \geq \alpha_c$. Therefore, the Mach number M_∞ no longer enters in the boundary conditions in the region to the left of the characteristic ca and no longer affects the flow parameters \bar{p} , \bar{h} , $\bar{\rho}$, $\bar{U} = U/U_\infty$, and so on; thus, it disappears from the similarity criteria introduced in Section 1.12. This is the *hypersonic stabilization law*, which was formulated in Section 3.3 for shock waves and is now generalized to the flow as a whole. For $M_n \gg 1$ the range of its applicability is dependent not only on the freestream Mach number M_∞ but also on the body shape. Thus, from Figure 7.1a it follows that in the flow past blunt bodies the shock

**FIGURE 7.1**

Shapes of bow shocks in front of a sphere and a circular cylinder and density profiles in the shock layer on the sphere.

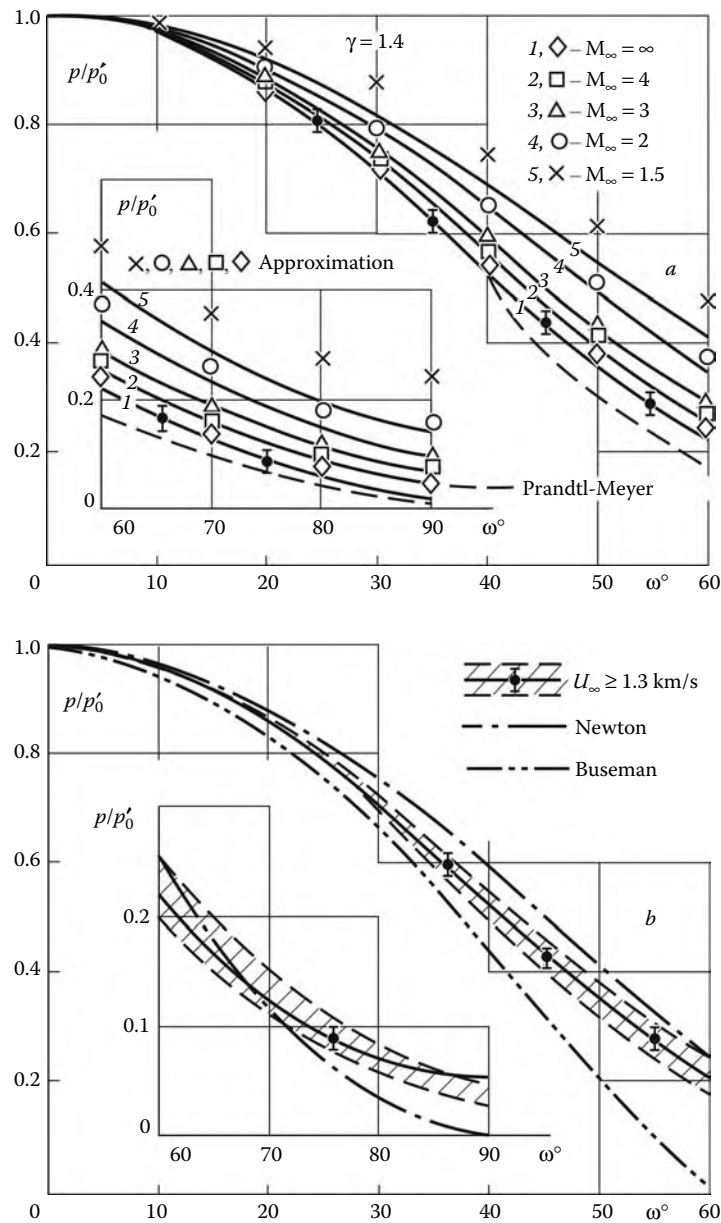


FIGURE 7.2
Pressure distributions over the spherical surface.

shapes are stabilized for $M_\infty \geq 10$ or, with a worse accuracy, for $M_\infty \geq 6$. At the same time, the pressure on the spherical nose ($\omega \leq 60^\circ$) is almost stabilized even at $M_\infty \geq 3$ (Figure 7.2a), though at $\omega \geq 70^\circ$ the pressure curves diverge considerably.* It should be also

* The calculated data presented in this chapter are mainly taken from Lunev, Magomedov, and Pavlov (1971).

noted that the shock waves and pressure distributions on a weakly blunted circular cylinder (Figure 7.3) start to diverge along the cylinder length sooner or later at any finite M_∞ . Moreover, while for $M_\infty \geq 6$ all the curves are similar, at least qualitatively, for $M_\infty \leq 2$ the shock waves go far from the body and the elevated pressure zone on the body is absent, that is, $\Delta p < 0$.

For a real gas (dissociated air) the hypersonic flow is also dependent on the freestream velocity U_∞ and, though only slightly, on the density ρ_∞ . At the same time, though the shock shapes and density profiles may considerably differ (Figure 7.1a and b), all the pressure profiles for $\omega \leq 70^\circ$ at hypersonic velocities $U_\infty \geq 1.3$ km/sec, $M_\infty \geq 4$ lie in a relatively narrow band shaded in Figure 7.2b.

The hypersonic stabilization law implies a simple form of the isentropic relation, which holds along a streamline

$$\bar{h} = \bar{h}_{ss}(\bar{p}/\bar{p}_{ss})^{(\gamma-1)/\gamma} = \frac{1}{2}q(\gamma)s^{1/\gamma}\bar{p}^{(\gamma-1)/\gamma}$$

$$q(\gamma) = (1+k)(1-k)^{1/\gamma} = 1 + k^2 + \dots, \quad k = \frac{\gamma-1}{\gamma+1} \quad (7.1.3)$$

Here, the quantity s plays the part of the gas entropy and is determined by the shock angle on the streamline under consideration, which is characterized by the quantities \bar{h}_{ss} and \bar{p}_{ss} immediately behind the shock. For $\gamma = 1 \div 5/3$ the quantity q ranges from 1 to 1.05, so that in what follows we assume that $q = 1$. Thus, we have

$$\bar{h} = \frac{1}{2}s^{1/\gamma}\bar{p}^{(\gamma-1)/\gamma}, \quad \bar{\rho} = \frac{\gamma}{\gamma-1}\frac{\bar{p}}{\bar{h}} = \left(\frac{1}{k}+1\right)s^{-1/\gamma}\bar{p}^{1/\gamma} \quad (7.1.4)$$

Downstream of the hypersonic stabilization region, the quantities \bar{p} and \bar{h} on these streamlines depend on M_∞ only via the local pressure.

For a real gas, the general form of these isentropic relations is as follows:

$$\bar{h} = \bar{h}(s, \rho_\infty, U_\infty), \quad \bar{\rho} = \bar{\rho}(s, \rho_\infty, U_\infty) \quad (7.1.5)$$

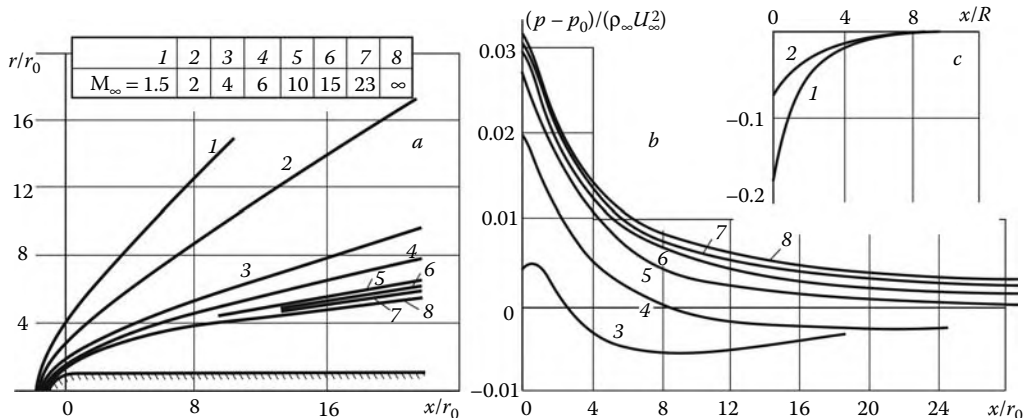


FIGURE 7.3

Shocks and pressures on a blunt cylinder with the bluntness radius r_0 .

However, making allowance for a weak change of γ_* along the isentropic lines (Figure 1.15), we can use formulas 7.1.4 substituting γ_* for γ in these formulas, the former being calculated from the relation $k = (\gamma_* - 1)/(\gamma_* + 1)$ behind the shock.

We are now coming to the question of the *compressed shock layer*. A high gas compression in the shock for $k \ll 1$ results in a small thickness δ of the shock layer on a body in gas flow (Figure 7.4). Using formulas 6.4.6 derived from the gas flow rate balance and the designations of that formula, we can write this condition in the form:

$$\delta/L = 2^{-v} (U_\infty r_a / U_a L) k_a \ll 1, \quad k_a = \rho_\infty / \rho_a \ll 1 \quad (7.1.6)$$

Here, L is the body scale length, for example, its radius of curvature or diameter. This condition is obvious if the mean values of the shock layer parameters are taken: $U_a \sim U_\infty$, $\rho_a \sim \rho_s \gg \rho_\infty$, and, hence, $r_a \sim L + \delta \approx L$. In particular, for a cone and a wedge with the semivertex angle θ we derived in Sections 3.7 and 6.4 the formula $\alpha - \theta = (1/2^v) \tan \theta$.

Generally speaking, this estimate follows from the condition $k_a \ll 1$, that is, under the assumption that the density in the shock layer is high on all streamlines, $\rho_a \gg \rho_\infty$ (e.g., $\rho_a \approx \rho_s$). In view of the relation $\rho/\rho_{ss} \sim (p/p_{ss})^{1/\gamma}$, this is possible only if *the order of the pressure is conserved along a streamline*, or if the order of the angle θ is conserved. On the contrary, in the neighborhood of the lateral surface of a flat-ended cylinder we have $p/p_{ss} \ll 1$

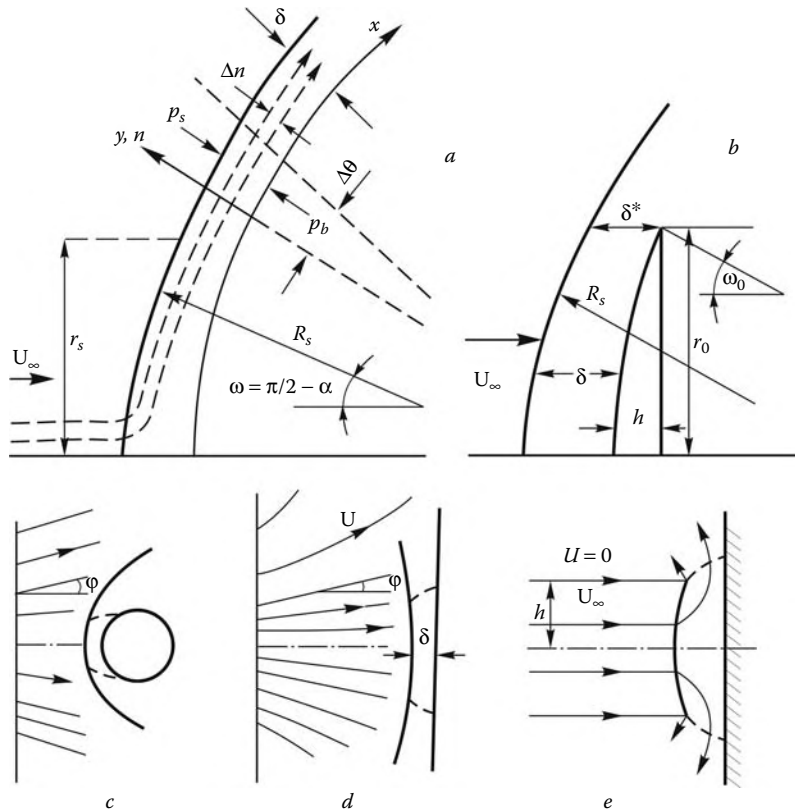


FIGURE 7.4
On the shock layer theory.

and the shock goes far from the body in this region, so that the ratio δ/L increases (Figure 7.4b).

Formula 7.1.6 contains an indeterminate form in the vicinity of the blunt body axis, since in this case $r_a \rightarrow 0$ and $U_a \rightarrow 0$. Then letting

$$r_a \approx r, \quad U_a \approx U_s = U_\infty \cos \alpha \sim U_\infty r/R_s \quad (7.1.7)$$

where R_s is the radius of curvature of the shock, we obtain the limiting formula

$$\delta/R_s \approx k_a/2^v \ll 1, \quad k_a \approx \rho_\infty/\rho_s \ll 1 \quad (7.1.8)$$

This formula leads to different implications for bodies of different shape. For *moderately blunt bodies* with the radius of curvature $R \sim r_0 = L$, we obtain that as $k \rightarrow 0$, that is

$$R_s - R \sim kR \quad \text{or} \quad K_s - K \sim kK \ll 1 \quad (7.1.9)$$

where $K_s = R_s^{-1}$ and $K = R^{-1}$ are the shock and body curvatures, the shock follows the body shape as in Figure 7.1a. Then from condition 7.1.8 there follows condition of 7.1.6. However, for *limitingly blunt bodies* with $R \gg r_0$, such as a flat plate or a flat-ended cylinder set normal to the flow, the limit $R_s \rightarrow R$ can be unattainable. In this case, in accordance with Section 6.3, the flow in the vicinity of the body "shoulder" (corner points in Figure 7.4b) must be assumed to be transonic, with $U_a \approx a_* \approx U_\infty k^{1/2}$. This follows from the arrangement of sonic lines in Figure 5.8 (Section 5.4). Then we have

$$\delta \sim \delta^* \approx 2^{-v} r_0 k^{1/2}, \quad R_s \sim 2^v r_0 k^{-1/2} \quad (7.1.10)$$

We note that the same estimate, $\delta \sim k^{1/2}L$, was obtained in Section 3.7 for wedges and cones with near-limiting angles. Thus, condition 7.1.6 is fulfilled in any case, though the particular laws of the decrease in δ with k can be different. Precisely this condition, together with the thin shock layer model based on it, lies in the foundation of the theory discussed in this chapter.

We note that the division of blunt bodies in different types, as accepted previously, is rather conditional. Thus, spherical segments with central half-angles ω_0 (Figure 7.4b) can be considered as moderately blunt for $\omega_0 > k^{1/2}$ and limitingly blunt for $\omega_0 < k^{1/2}$.

The method of the shock layer thickness evaluation based on the gas flow rate balance, as outlined previously, is rather universal and can easily be extended to other types of flows (three-dimensional, nonuniform, etc.) with an adequate consideration of the orders of the velocities in the shock layer. Thus, in the transverse flow past a prolate ellipsoid, the order of the spreading velocities in the shock layer is determined by the minimum radius of curvature R_{\min} of the body surface, so that $\delta \sim kR_{\min}$.

Another example is a body in a nonuniform divergent-jet flow (cf. Section 2.3). For $R_s \sim R$ the velocity at the shock near the axis of symmetry (Figure 7.4c and d) is as follows:

$$\begin{aligned} U_s/U_\infty &\approx \cos(\alpha + \varphi) \approx \omega_l = \omega + \varphi = r/R_{\text{eff}} \\ R_{\text{eff}}^{-1} &= R_s^{-1} + m, \quad m = \frac{\partial \varphi}{\partial r} \end{aligned} \quad (7.1.11)$$

Here, ω_l is the complementary angle to the local angle of the shock (or body) inclination, while R_{eff} is the *effective radius of curvature* of the body in nonuniform flow. Thus, substituting R_{eff} for R_s in 7.1.8 we obtain $\delta \sim kR_{\text{eff}}$. In a divergent flow we have $m > 0$, so that $R_{\text{eff}} < R$ and the shock layer thickness on the axis of symmetry and in its vicinity is smaller

than in the uniform flow. On the contrary, in a convergent flow $m < 0$; the shock layer thickness sharply increases as $mR \rightarrow -1$, and the previous estimate is, to say the least, of little use. It is interesting to note that the thickness of the shock layer on the flat plate in the expanding jet field (Figure 7.4d) is finite, $\delta \sim k/2^v m$, though $R_s \rightarrow \infty$, which is impossible in a uniform (or, the more so, convergent) flow.

Jet flow past a flat-ended cylinder is somewhat similar to the interaction of a bounded jet of half-width h (Figure 7.4e) with a plane barrier. In this case, the sonic velocity on the shock is attained at the point of its intersection with the jet boundary, while the shock layer thickness is $\delta \sim \delta^* \sim h\sqrt{k}$.

In making these estimates, we, quite naturally, discarded some nonordinary situations in which the assumed flow pattern is violated. Thus, in the impingement of an underexpanded jet on a barrier (see Section 5.5) peripheral shocks occurring in the jet lead to the formation of the forward zones of return flow (Figure 5.15).

We note in conclusion that each limiting theory may be valuable in applications only if it is reliable in the case of really attainable values of small parameters. The limit of the hypersonic flow stabilization was established previously quite unambiguously (its lower limit $M_\infty \geq 5 \div 6$ can conditionally be taken for the onset of the hypersonic law applicability range; we shall assure ourselves of this in the following chapters). However, the situation with certain properties of the compressed shock layers is more complicated. The theory possesses a long history and is very vast; however, in what follows it is reflected only in that its part, which, along with illustrative gas dynamic images and simple results, retains its validity at real values $k \geq 0.05$, which is not always fulfilled.*

7.2 Busemann and Newton Formulas

The smallness of the shock layer thickness allows us to derive some simple solutions for the wedge and cone flows, which was done in Sections 3.7 and 6.4. The same assumption made for the case $k \rightarrow 0$ makes it possible to obtain the Newton formula 3.7.8 for the pressure

$$\Delta p = p_N - p_\infty = \rho_\infty U_n^2 = \rho_\infty U_\infty^2 \sin^2 \theta, \quad \bar{p}_N = \sin^2 \theta \quad (7.2.1)$$

Newton himself derived this formula based upon his corpuscular model, in accordance with which gas particles reach the body surface without being disturbed and give their normal momentum to the body. Thence it follows that the formula is applicable to any element of the body surface exposed to any flow, either uniform or nonuniform, including time-dependent flows, if U_n in formula 7.2.1 is considered to mean the relative normal velocity of the particles and the surface element.

Naturally, this very simplified model does not take into account a variety of even qualitative factors.[†] We will note the following factors.

First, it would seem that the model could be applicable for a strongly rarefied gas, in which molecules arrive at the surface almost without mutual collisions. However, in this

* In more detail, this theory is outlined in the books of Hayes and Probstein (1966), Chernyi (1966), Lunev (1975), and others.

[†] It has been stated not to reproach the man of genius. Simply, all in its good time.

case tangent stresses are important. In particular, if a surface reflects gas molecules at velocities much smaller than U_∞ (see Section 12.1), then molecules lose in the impingement almost all their momentum, so that a force $\rho_\infty U_\infty^2 \Delta\sigma$ directed along the freestream velocity vector acts on each surface element $\Delta\sigma$. Thus, the Newton formula is inapplicable to the case of a rarefied gas.

Second, the Newton formula is inapplicable to the leeward side of a body placed in its *aerodynamic shadow*. However, this is not even put in a claim; in engineering practice, the base pressure p_d is determined separately; moreover, at high Mach numbers M_∞ it can be neglected in evaluating aerodynamic forces.

Finally, the incident, fairly high-density flow interacts with a gas layer, which has already reached the body surface and moves along it, rather than with the surface itself. As this passes, centrifugal forces are generated in the gas flowing along a curved surface, these forces being determined by formula 2.2.5 $\partial p/\partial n = \rho U^2/R_l$ for the pressure gradient along the normal n to a streamline with the curvature R_l^{-1} .

In a limitingly thin shock layer on a moderately blunt body the streamlines, together with the shock $r_s(x)$, fit closely the body surface $r_b(x)$. Therefore, as $\delta/L \rightarrow 0$ we have

$$dl = dx, \quad R_l = R_s = R, \quad n = y, \quad r_s = r_b(x), \quad u = U \quad (7.2.2)$$

Here, x, y is the curvilinear coordinate system fitted to the body surface (see Figures 7.4a and 1.24c of Section 1.13) and u is the velocity projection on the x direction.. Then, integrating the previous formula for $\partial p/\partial n$, we obtain the *Busemann formula*

$$\begin{aligned} p &= p_s - p_B, & p_s &= p_N = \rho_\infty U_\infty^2 \sin^2 \theta \\ && p_b &= p_s - p_B(0) \\ p_B &= \int_y^\delta \frac{\rho U^2}{R} dy = \frac{I(\psi)}{r_b^{1+v} R}, & I(\psi) &= \frac{1}{(2\pi)^v} \int_\psi^{\psi_s} U d\psi \\ d\psi &= (2\pi r)^v \rho U dy, & \psi_s &= \pi^v r_s^{1+v} \rho_\infty U_\infty \end{aligned} \quad (7.2.3)$$

Here, ψ is the stream function, while ψ_s is the gas flow rate across the shock layer. The integral $I(\psi)$ is the absolute magnitude of the momentum flux vector $\vec{I}(\psi)$ of the gas between the shock and a $\psi = \text{const}$ streamline. This vector, directed along the body surface, is calculated for one-half of a symmetric plane flow ($v = 0$) or for a unit angle $\Delta\varphi$ between two close meridional planes in the axisymmetric case. The centrifugal forces and the Busemann pressure difference p_B are due precisely to the turn of the vector \vec{I} .

In the same approximation the shock layer thickness is

$$\delta = \frac{1}{(2\pi r)^v} \int_0^{\psi_s} \frac{d\psi}{U} \quad (7.2.4)$$

As the shock angle $\alpha \rightarrow \theta$, the pressure p_s behind the shock tends to the Newtonian pressure 7.2.1, which turns out to be applied to the outer edge of the shock layer. We note that the first equality 7.2.3 for p_B is more general and can be applied in the more general case than that of a limitingly thin shock layer; then each streamline should be considered as having its own curvature R^{-1} . The equality is also applicable to three-dimensional flows.

Naturally, the Busemann formula does not give a final solution, since the quantities p_s and U entering in it are not known in advance (in what follows, we shall derive the limiting

solution as $k \rightarrow 0$). However, it allows us to gain a notion of the pressure behavior on bodies of different shapes based on purely mechanical concepts. Thus, on *convex* bodies with $R > 0$ we have $p_B > 0$, so that the pressure decreases from the shock to the body. However, on *concave* bodies ($R < 0$) the effect is opposite ($p_B < 0$). In the flows with rectilinear streamlines $p_B = 0$; this circumstance made it possible to derive effective limiting solutions for the flows past a wedge and a cone in Sections 3.7 and 6.4.

It would seem that the Busemann formula calls into question the Newton formula applicability. However, as shown in Section 6.4, the Newton formula gives fairly good results, both quantitative and qualitative, even in the flows around cones at incidence, in which centrifugal forces are unquestionably present. This is mainly explained by the fact that, first, the term p_s in 7.2.3 is usually predominant and close to the Newtonian term at $\alpha \approx \theta$, and, second, the inequality $p_s > p_N$ following from 3.5.26 for convex bodies at $\alpha > \theta$ is to some degree offset by negativity of the term p_B in 7.2.3. Therefore, in what follows we will orient only to the Newton formula, which gives a very simple, local pressure law irrespective of the body shape and the flow conditions. Naturally, this formula requires extensive checking for various classes of bodies; precisely this will be done in the following.

For blunt bodies, a *modified Newton formula* is usually used

$$\bar{p}' = \frac{p_b}{p'_0} = \sin^2 \theta = \cos^2 \omega, \quad p'_0 = p_\infty + \rho_\infty U_\infty^2 \left(1 - \frac{1}{2}k\right) \quad (7.2.5)$$

Here, p'_0 is the stagnation pressure behind the normal shock (see formula 3.6.5). The modified formula takes the flow conditions into account only via p'_0 , their influence being only slight, especially for hypersonic velocities (cf. Section 7.1). Thus, for a sphere moving in the terrestrial atmosphere on different heights at a velocity $U_\infty \geq 1.3$ km/sec ($M_\infty \geq 4$) the \bar{p}' curves in Figure 7.2b lie within a narrow band, the central line of which can be approximated by the formula valid for $\omega \leq 80^\circ$

$$\bar{p}' = \frac{p_b}{p'_0} = 1 - \frac{7}{6} \sin^2 \omega + 0.225 \sin^6 \omega, \quad \omega = \frac{\pi}{2} - \theta \quad (7.2.6)$$

Of course, this is incorrect for the shock layer structure: its thickness, the density distribution over it, and so on, considerably depend on the physical and chemical state of the gas. However, for a perfect gas with $\gamma = 1.4$ there is an even more exact approximation (Figure 7.2a) dependent on the Mach number M_∞

$$\bar{p}' = 1 - \left(1.2 - \frac{1.5}{M_\infty^2}\right) \sin^2 \omega + \left(0.27 - \frac{1.1}{M_\infty^2}\right) \sin^4 \omega \quad (7.2.7)$$

In Figure 7.5 we have plotted the pressure \bar{p}' profiles for ellipses and ellipsoids. The curves are close to each other and to the Newtonian curve. In Figure 7.6 we have also presented the pressure distributions in an underexpanded jet field and over a sphere embedded in the jet for various γ and scale lengths of the problems (Luney and Khramov, 1970). Though widely diffusing in original coordinates, these curves coalesce to a narrow bundle when plotted as $\bar{p}'(\omega_l)$ dependences, $\omega_l = \omega + \varphi$ being the local angle and the value p'_0 being calculated at $\varphi = 0$. This bundle is located somewhat below the $\bar{p}'(\omega)$ curve for the sphere in uniform flow due to the transverse decrease in the local ram pressure $\rho_l U_l^2$, or p'_{0l} , on a given streamline. For the same reason, the formula $\bar{p}' = \cos^2 \omega_l$ gives a somewhat overestimated pressure value, so that using the formula $p = p'_{0l} \cos^2 \omega_l$ would be more correct.

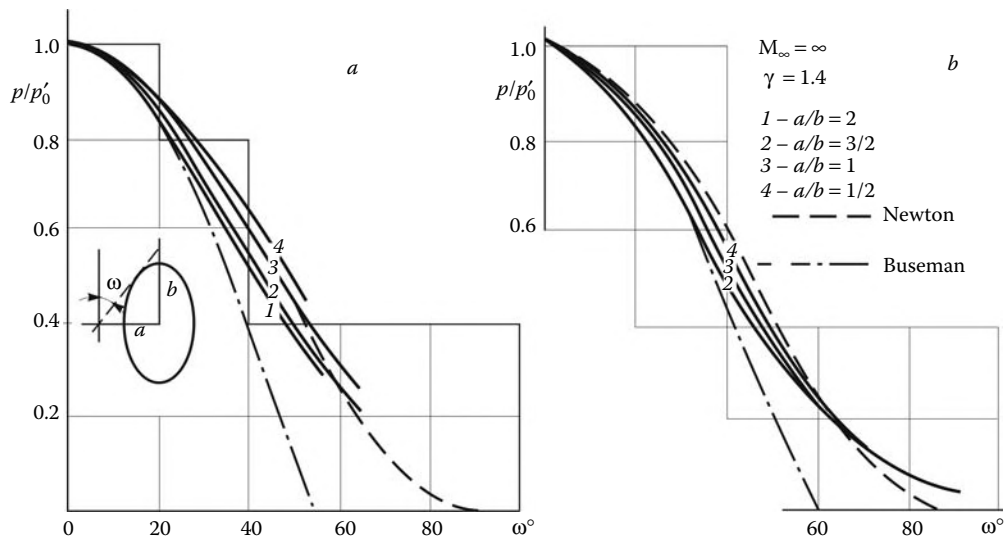


FIGURE 7.5
Pressure distributions over ellipses (a) and ellipsoids (b).

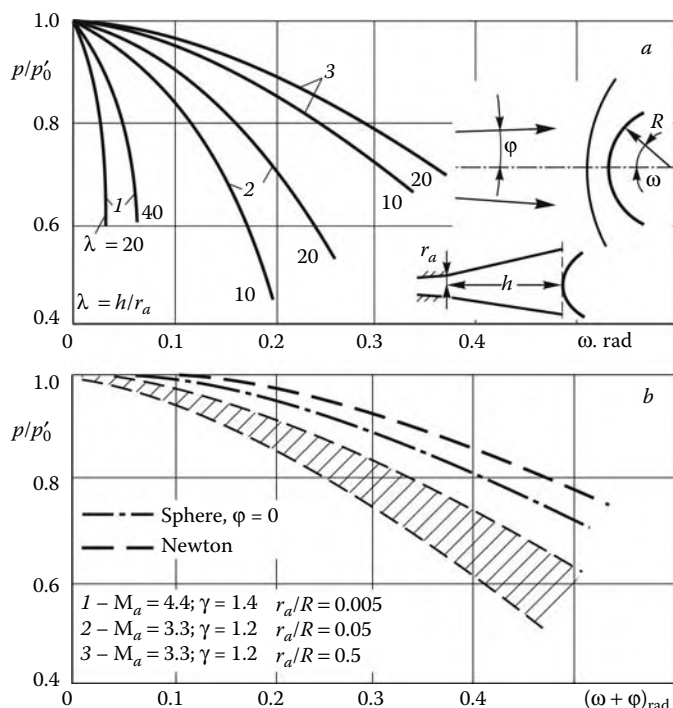


FIGURE 7.6
Pressure distributions over a sphere in an underexpanded jet flow.

The Newton formula is quite naturally generalized to the flow past two-dimensional sharp bodies as the *local wedge method*, which can be extended to the lower values of the angle θ and the freestream Mach number M_∞ due to the local character of the pressure law on thin bodies in the linear and quadratic approximations (Sections 2.8, 3.7, and 4.6). Figure 7.7 illustrates the successful use of this method for calculating the pressure on a flare joined to a blunt cone; the flow around the flare is essentially nonuniform and is characterized by local Mach numbers of about 2.5. Precisely the local flow parameters immediately ahead of the flare at each point were used as the oncoming flow parameters. At the same time, the calculation of the pressure using the freestream parameters (the “outer” Newton formula 7.2.1) gives rather crude approximation for the flare.

In addition to the data for cones at incidence presented in Section 6.6, we present in Figure 7.8 the results for slender ogive-shaped sharp bodies. The Newton formula, as well as its generalization, the *local cone method*, give fairly good results already at $M_\infty \geq 3$. As in the case of the flow past a cone, the pressures, both exact and Newtonian, are similar for $\alpha = 0$ and in the plane $\varphi = \pi/2$ for $\alpha > 0$.

We will now evaluate the Newton formula applicability range (except for the aerodynamic shadow region; see previous discussion), illustrating what will be said by most typical examples.

1. On the periphery of the spherical nose, along with the pressure p_s decrease on the shock, the centrifugal component p_B in formula 7.2.3 increases, while the relative pressure p_b/p_s decreases sharply (Figure 7.9a). The volume-average density ρ_a in the disturbed layer also decreases (Figure 7.9c). In accordance with Section 7.1, this results in shock detachment from the body. In this region, the estimates of Section 7.1 and, hence, the Newton formula are inapplicable (see Section 7.5 for details).
2. The qualitative properties predicted by the Busemann formula are distinctively observed on a concave body (Figure 7.10). Here, due to the contribution of

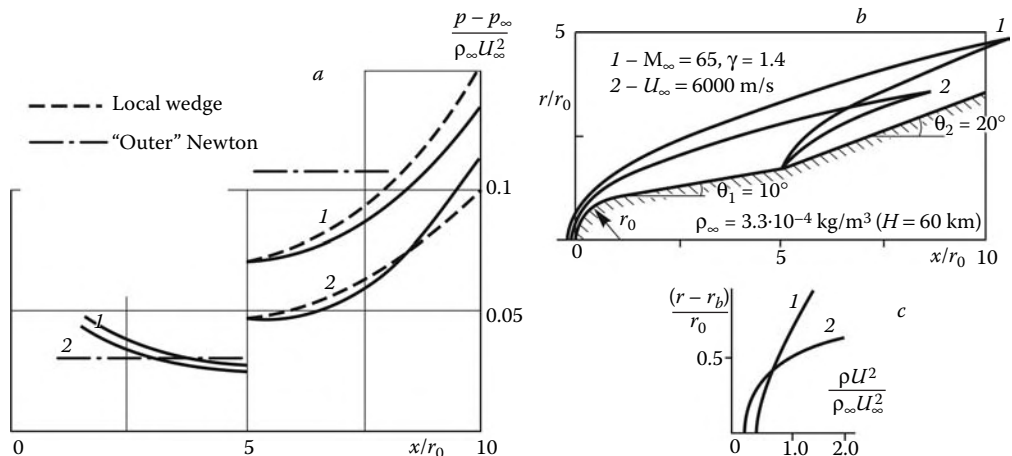
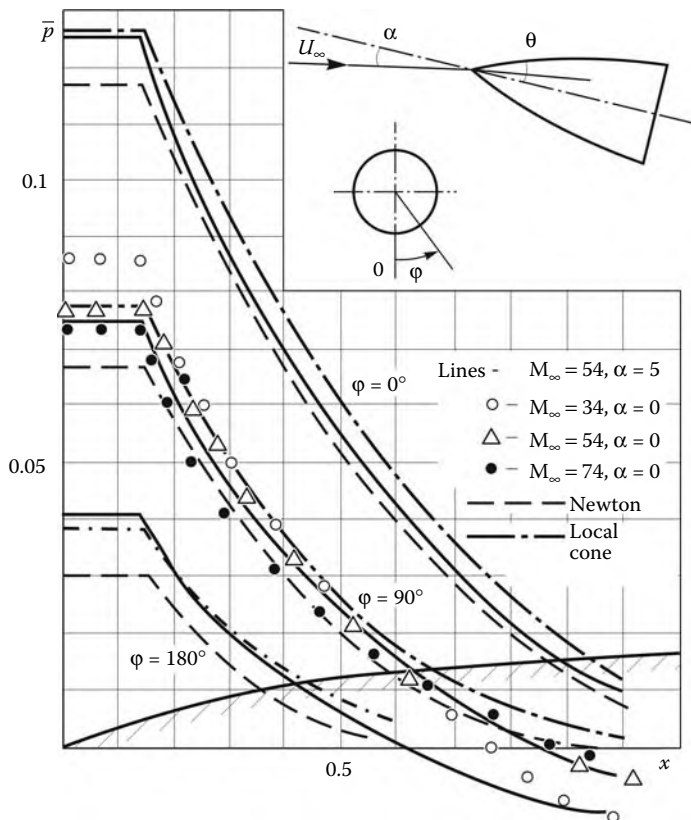


FIGURE 7.7

Pressure distributions over a blunt cone-flare body (a), shock shapes (b), and ram pressure distribution ahead of the flare (c).

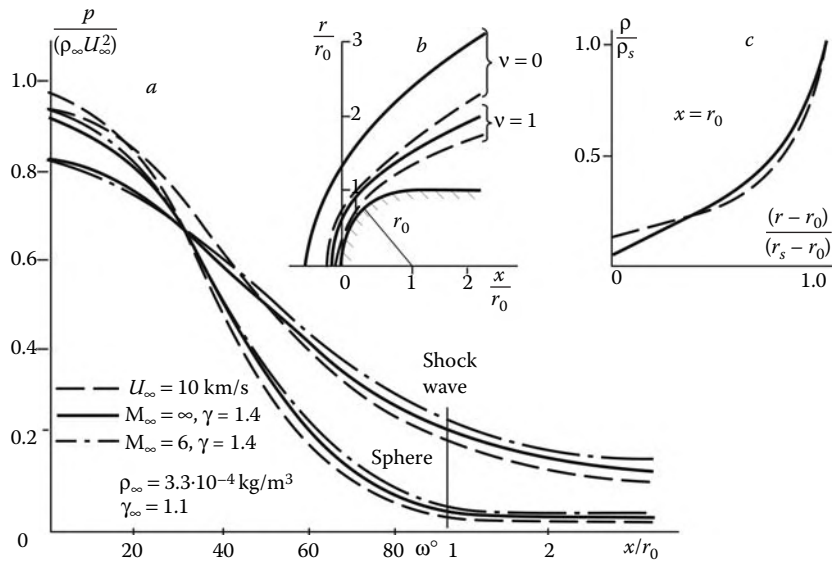
**FIGURE 7.8**

Pressure distribution over an ogive with a conical nose.

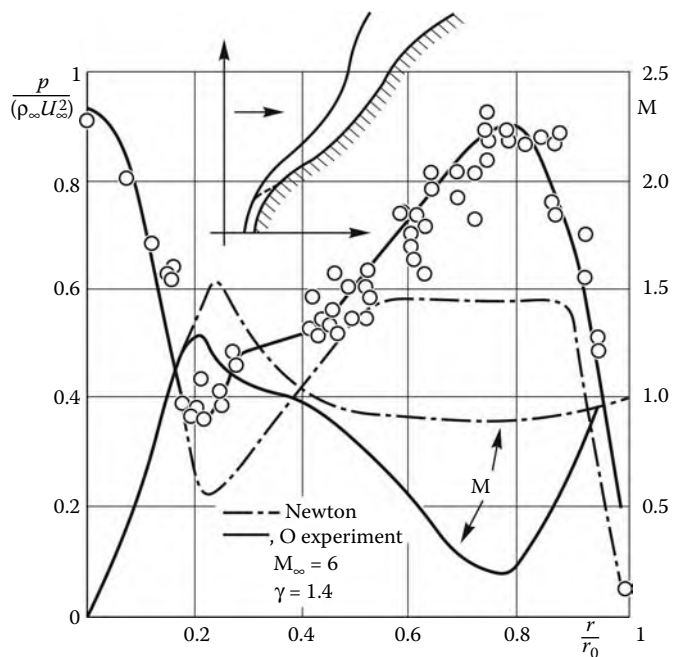
centrifugal forces, the experimental pressure increases up to the values nearly as high as the stagnation pressure p'_0 and exceeds the Newtonian pressure* (in this region a local viscous separation zone is formed). A similar, though somewhat smaller, pressure rise is observed in the vicinity of a discontinuity in the surface curvature, where it leads to the appearance of the streamline concavity regions. An example is presented in Figure 7.11. In these cases, the Busemann effects hinder the use of the Newton formula.

- Finally, Newtonian concepts are inapplicable in the flow region downstream of the point of a negative bend in the body generator, as well as in a flow region in the shade. The supersonic flow around the corner point is accompanied by generation of expansion waves, which in principle could not be described by the Newtonian flow model. If the flow upstream the corner point is subsonic, then the flow expansion due to the bend in the surface generator propagates upstream, so that, in accordance with Section 5.6, the flow in the vicinity of the corner point

* This example is by no means pedantic. Such body shapes can arise as a body (vehicle nose or meteoroid) burns in the atmosphere due to intense aerodynamic heating. See, for example, Voronkin, Lunev, and Nikulin (1978).

**FIGURE 7.9**

Pressure distributions over the body and the bow shock (a), shock shapes (b), and density distribution in the shock layer (c).

**FIGURE 7.10**

Experimental and Newtonian pressure and Mach number distributions over a convex-concave body and the shock in front of the body.

becomes transonic, irrespective of the local body slope. An example is provided by limitingly blunt bodies presented in Figures 7.11 and 7.12.

However, the examples presented show that, except for some particular situations (as those listed previously and certain others), which are quite obvious from the general considerations, the Newton formula and its generalization give quite acceptable accuracy for evaluating the pressure on sharp bodies and blunt convex bodies with smoothly varying contour curvature and for understanding the mechanisms responsible for the pressure behavior. This explains the attractiveness and wide use of the formula in hypersonic and even supersonic aerodynamics.

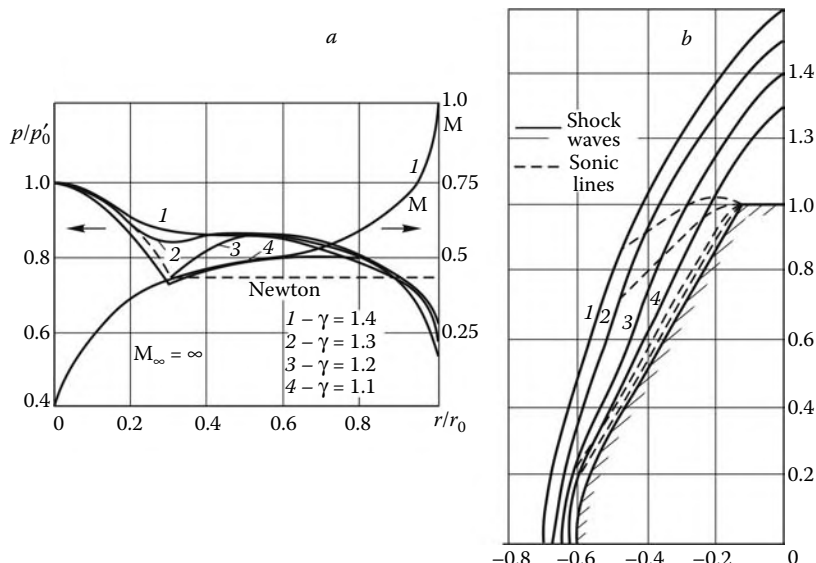


FIGURE 7.11

Pressure and Mach number distributions over a spherically blunted cone (a) and the shapes of the shocks and the sonic lines (b).

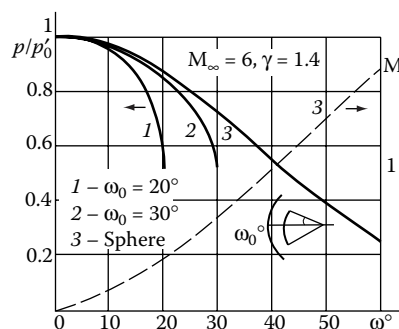


FIGURE 7.12

Pressure on spherical segments and Mach number distributions over a sphere.

7.3 Blunt Bodies: Similarity Law

The properties of subsonic and transonic flows behind the shock on a blunt body and the formulation of the corresponding problems were described in Section 5.4. In Figures 5.8 through 5.11 from that section we showed typical flow patterns. Here we will determine the shape and extent of the subsonic and transonic flow regions on the basis of the results obtained in this chapter and derive a similarity law involving the effective adiabatic exponent γ_* or the shock density ratio $k = (\gamma_* - 1)/(\gamma_* + 1)$ as a sole similarity parameter.

From formulas 2.2.13 and 2.2.14 it follows that the pressure p_* and the enthalpy h_* at the sonic point depend on γ comparatively weakly:

$$\begin{aligned} p_*/p'_0 &= [2/(\gamma + 1)]^{\gamma/(\gamma+1)} = 0.605 \div 0.525 \\ h_*/H &= 2/(\gamma + 1) = 1 \div 0.83, \quad \gamma = 1 \div 1.4 \end{aligned} \quad (7.3.1)$$

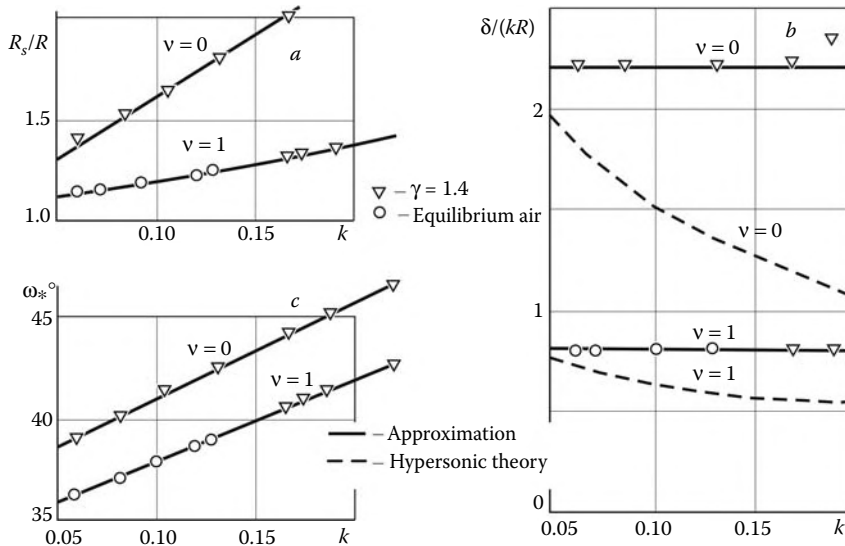
On the other hand, from the Newton formula $p_*/p'_0 = \cos^2 \omega_*$ it follows that the sonic point position and, in general, the Mach number distribution over the blunt body surface depend on the flow conditions, or on γ , only slightly. Thus, the central sonic angle ω_* for the flow past a sphere varies from 36° to 41° at $M_\infty \geq 4$. The shock slope at the sonic point α_* is determined from the condition $\tan \alpha_* = k^{-1/2}$ from Section 3.5. Assuming that the shock shape is similar to the body shape, we obtain that as $k \rightarrow 0$ the sonic point is displaced to the axis of symmetry in accordance with the $\omega_* \approx k^{1/2}$ law, as can be seen in Figures 5.11 and 7.11.

Let us now consider bodies with corner points, for example, spherical segments. If the central angle ω_0 of the segment is greater than the angular coordinate ω_1 of the limiting characteristic on the sphere, then the sonic point does not affect the transonic flow region. Otherwise (that is, in the case $\omega_0 < \omega_1$), the abrupt pressure fall behind the corner point propagates upstream throughout the subsonic region, thus resulting, in accordance with an analysis made in Section 5.6, in the displacement of the sonic point toward the corner. The pressure distribution over spherical segments is shown in Figure 7.12. The limiting case of these bodies is the flat-ended cylinder (Figure 7.4b). On the flat end the pressure decreases from the value $p = 0.9p'_0$ down to the sonic value $p_* \approx 0.6p'_0$ over a distance $\Delta r \approx 2\delta^*$, where, in accordance with 7.1.9, $\delta^* \sim k^{1/2}r_0$; together with the data on the sonic line shape, this indicates that the transonic zone length on the flat end is of the order $\delta^* \sim k^{1/2}r_0$.

The sonic point position ω_* on the circular cylinder and a sphere in nonuniform flow (Figures 7.4c and 7.6) is determined by the condition $p_*/p'_0 = \cos^2 \omega_{l*}$, $\omega_{l*} = \omega_* + \varphi_*$, while that on the shock in front of the body is determined from the formula $\omega_{s*} + \varphi_{s*} \approx k^{1/2}$ (here, φ_* and φ_{s*} are the angles of inclination of the streamlines arriving at the sonic points). On a plane barrier we have $p_*/p'_0 = \cos^2 \varphi_*$, $\varphi_* \approx k^{1/2}$.

All the aforesaid pertains to limiting blunt bodies and can be extended to the bodies of similar classes only. In intermediate cases, for example, for spherical segments with central angles smaller than the sonic angle on the sphere, $\omega_0 < \omega_*$, the sonic line passes through corner points, while on the shock it approaches the axis of symmetry as $\gamma_* \rightarrow 1$ in the same fashion as in the case of the sphere. The same is true for the body presented in Figure 7.11.

The information outlined previously allows us to derive a very simple similarity law for an equilibrium shock layer on the blunt body nose. Generally speaking, the rigorous similarity conditions for a given gas are the equality of the freestream velocities U_∞ and,

**FIGURE 7.13**

Geometric parameters of the flow past a sphere. Dashed curves represent the solution of Section 7.8.

to a smaller degree, densities ρ_∞ (Section 1.12). However, the pressure and enthalpy in the subsonic and transonic flow regions vary from maximum values at the stagnation point down to minimum values in the vicinity of the limiting characteristic, the difference between these values being not too great. Thus, for the sphere we have in this region $p/p'_0 \geq 0.5$ and $h/H \geq 0.7$. At the same time, as shown in Sections 1.3 and 1.6, the local real-gas flow can be characterized by the local value of the effective adiabatic exponent γ_* and the equilibrium exponent $\gamma_e = \rho a_e^2 / p$ determining the equilibrium speed of sound and dependent on γ_* and its derivatives (formula 1.6.12). Usually the quantities γ_* and γ_e vary only slightly as the enthalpy varies by a factor of 1.5 to 2 and the pressure by an order of magnitude (Figures 1.9 and 1.10, Section 1.3). Thus, for the flow region under consideration, they could be taken to be constant, so that the whole variety of the conditions determining the equilibrium flows past bodies is described by two parameters only, γ_* and γ_e .

However, the ratio γ_e/γ_* for air differs from unity by no more than 10% up to the temperatures $T \leq 10,000$ K or the flight velocities $U_\infty \leq 10 \div 15$ km/sec. Since the quantity γ_e enters in the equations directly, while γ_* enters in them via the small difference $\gamma_* - 1$, the former can be replaced by γ_* .

Thus, under the constraints accepted previously, the flow in the subsonic and transonic regions of the shock layer on the blunt body in hypersonic gas stream depends on the sole parameter γ_* , which is usually chosen in accordance with the value $k = (\gamma_* - 1)/(\gamma_* + 1)$ behind the normal shock. In general, it is precisely the quantity k that is often used as a similarity criterion (instead of γ_*), in any case, in correlation formulas.

This similarity law has a wide use and a good accuracy, which is visible, for example, in Figure 7.13 in which we have presented the shock standoff distance δ , the radius of curvature of the shock on the axis of symmetry R_s , and the values of the sonic angle ω_* on the sphere ($v = 1$) and the circular cylinder ($v = 0$) of radius R over a wide parameter range typical of the equilibrium-dissociating air and perfect gas flows past these bodies. The data presented are satisfactorily approximated by the formulas

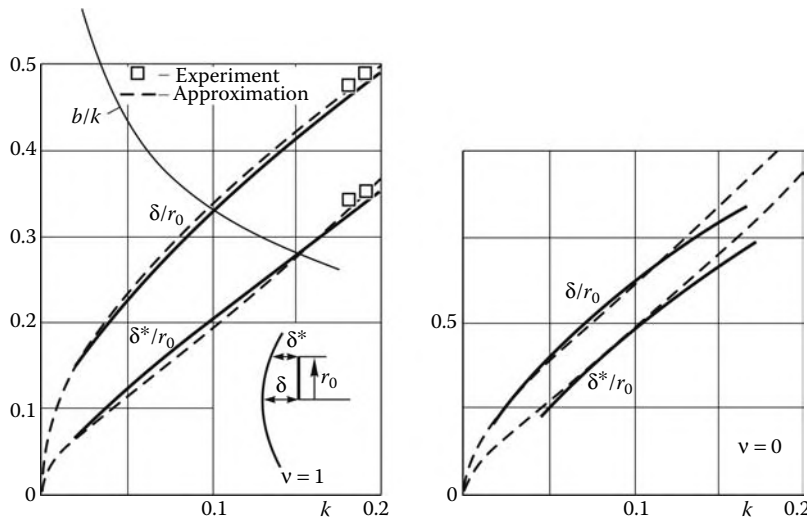


FIGURE 7.14
Shock layer thickness in the flows past a disk and a plate.

$$\begin{aligned} v = 1 : \quad & \delta = 0.78kR, \quad R_s = (1.05 + 1.65k)R, \quad \omega_*^\circ = 34 + 40k \\ v = 0 : \quad & \delta = 2.2kR, \quad R_s = (1.02 + 6.1k)R, \quad \omega_*^\circ = 36 + 43.5k \end{aligned} \quad (7.3.2)$$

For a disk and a flat plate set normal to the flow, the k -dependence of the shock layer thickness is presented in Figure 7.14. The curves are approximated by the formulas

$$\begin{aligned} v = 1 : \quad & \delta/r_0 = (1 + 0.6k)^{1/2}, \quad \delta^*/r_0 = (0.4 + 2.1k)^{1/2} \\ v = 0 : \quad & \delta/r_0 = (1.5 + 4.5k)^{1/2}, \quad \delta^*/r_0 = (0.9 + 6k)^{1/2} \end{aligned} \quad (7.3.3)$$

In the same figure the quantity $b = (r_0^2/x)(\partial p/\partial x)/p'_0$ characterizing the pressure gradient on the axis of symmetry of the flow past the disk is presented.

As to the pressure distribution, the fact that it depends on k only is confirmed by the universal formula 7.2.6 for the sphere in which p'_0 depends, in accordance with 7.2.5, on k only.

7.4 Aerodynamic Characteristics

The formal definition of the aerodynamic characteristics of bodies was given in Section 2.13. Here, we will calculate the aerodynamic coefficients for some particular cases using the Newton formula and study their properties. The pressure in the aerodynamic shadow will be taken to be the same as the external pressure, $p_d = p_\infty$.

We will start with a plate of arbitrary shape placed at an angle of attack $\alpha + \theta$ to the incident flow (the angle θ was introduced in Figure 2.26b for a wedge at an angle of attack). Dividing all the forces by the plate surface area Σ , as is usually done for wings, in the coordinate system presented in Figure 2.26b we obtain

$$\begin{aligned} c_\tau &= 2\bar{p} \sin \theta, & c_n &= 2\bar{p} \cos \theta, & \bar{p} &= \sin^2(\alpha + \theta) \\ c_x &= 2\bar{p} \sin(\alpha + \theta), & c_y &= 2\bar{p} \cos(\alpha + \theta) \\ K &= c_y/c_x = \cot(\alpha + \theta) \end{aligned} \quad (7.4.1)$$

Here, K is the lift-drag ratio of the plate.

For finite-thickness bodies these forces are usually referred to the area S_0 of their maximum cross-section, or midsection. For a wedge (or cone) $S_0 = \Sigma \sin \theta$, so that all the coefficients 7.4.1 should be divided by $\sin \theta$. We present their expressions for small $\alpha \ll \theta$

$$c_x = c_\tau = 2 \sin^2 \theta + 3\alpha \sin 2\theta, \quad c_n^{(\alpha)} = 2 \sin 2\theta \cos \theta \quad (7.4.2)$$

Here, $c_n^{(\alpha)} = (\partial c_n / \partial \alpha)_{\alpha=0}$ is the aerodynamic derivative of c_n introduced in Section 2.13. For a double-sided wedge shown by dotted lines in Figure 2.26, the quantity $c_n^{(\alpha)}$ should be doubled, while $c_x = 2 \sin^2 \theta + O(\alpha^2)$.

For a zero-thickness plate (planar wing) it should be let $\theta = 0$ in formulas 7.4.1. In this case the formulas, as well as the quadratic law for the pressure, are no longer applicable for small $\alpha < \alpha^* = \arcsin M_\infty^{-1}$; the pressure follows now a $\bar{p} \sim \alpha$ law with a finite value of $c_n^{(\alpha)}$ and a quadratic $c_x \sim \alpha^2$ law (cf. Sections 2.8 and 2.13).

The coefficients of the moments of the plate of length L and area Σ about the forward point O can easily be determined taking into account that at a constant pressure the resultant force directed along the normal passes through the center of inertia of the plate. If τ_d is the distance from the latter to the origin, then the corresponding moment and its coefficient (in accordance with 2.13.3) are equal to

$$M_0 = \tau_d(p - p_\infty)\Sigma, \quad c_{m_0} = 2\tau_d/L \quad (7.4.3)$$

For a rectangular plate the center-of-pressure coefficient is $c_d = c_{m_0}/c_n = \tau_d/L = 1/2$, while for a triangular plate $c_d = 2/3$.

For a wedge with the vertex angle 2θ and length L (Figure 2.26b) the normal passing through the midpoint of the generator of length $L_b = L/\cos \theta$ intersects the τ axis at the point $\tau_d = L_b/2 \cos^2 \theta$. Comparing this result with 7.4.2 and referring the moment to L and to the midsection area $S_0 = L \tan \theta$ we obtain

$$\begin{aligned} c_d &= \tau_d/L = (2 \cos^2 \theta)^{-1} \\ c_{m_0} &= c_d c_n = 2 \sin^2(\alpha + \theta)/\sin 2\theta, \quad c_{m_0}^{(\alpha)} = 2 \end{aligned} \quad (7.4.4)$$

We are now coming to bodies of revolution and similar bodies. For a circular cone at zero incidence, as well as for a wedge, we have $c_x = 2\bar{p} = 2 \sin^2 \theta$; the same value of the drag coefficient is appropriate for any polyhedron circumscribed about the cone. In fact, the pressure on each side of the polyhedron is in this case the same as on the inscribed cone; factoring out the pressure from the integral sign in 2.13.1 we obtain the forces in the form $X = T = (p - p_\infty)S_0$ and the coefficients in the form $c_x = c_\tau = 2\bar{p}$.

A simple formula for c_x can be also derived for elliptic cones

$$c_x = 2 \sin \theta_1 \cdot \sin \theta_2 \quad (7.4.5)$$

Here, θ_1 and θ_2 are the semivertex angles of the cone in the meridional planes of symmetry.

On the surfaces of bodies of revolution, the projections of the normal \vec{n} onto the τ , n , and b axes of the fitted coordinate system (Figure 2.26b) are as follows:

$$n_\tau = -\sin \theta, \quad n_n = -\cos \theta \cos \varphi, \quad n_b = -\cos \theta \sin \varphi \quad (7.4.6)$$

To calculate the forces and the moments acting on the body we separate out an annular element of length $\Delta\tau$ and within it an area element on the surface cut out by the meridional angle $\Delta\varphi$. The components of the forces acting on this area are $\Delta_\varphi \bar{T} = \bar{p}r\Delta r\Delta\varphi$ and $\Delta_\varphi \bar{N} = \bar{p}r \cos \varphi \Delta r \Delta\varphi$ (here, $\bar{T} = T/\rho_\infty U_\infty^2$, etc.). The first component produces the moment $\Delta M = \Delta_\varphi \bar{T}r \cos \varphi$ about the z axis, while the second gives the moment $\Delta \bar{M} = \Delta_\varphi \bar{N}\tau$. Using then the Newton formula (6.6.1) at $\alpha \leq \theta$ and integrating successively with respect to φ and r we obtain

$$\begin{aligned} S_0 \Delta c_\tau &= 2\pi J_1 r \Delta r = 2\pi J'_1 r \Delta\tau, & S_0 \Delta c_n &= 2\pi J_2 r \Delta\tau = 2\pi J'_2 r \Delta r \\ L S_0 \Delta c_{m0} &= 2\pi(r^2 \Delta r J_1 + \tau r \Delta\tau J_2) \\ J_1 &= \frac{2}{\pi} \int_0^\pi \bar{p} d\varphi = 2 \sin^2 \theta \cos^2 \alpha + \cos^2 \theta \sin^2 \alpha, & J'_1 &= J_1 \tan \theta \\ J_2 &= \frac{2}{\pi} \int_0^\pi \bar{p} \cos \varphi d\varphi = \cos \theta \sin \theta \sin 2\alpha, & J'_2 &= J_2 \cot \theta \\ c_\tau &= \frac{2\pi}{S_0} \int_0^{r_0} J_1 r dr, & c_n &= \frac{2\pi}{S_0} \int_0^L J_2 r d\tau \\ c_{m0} &= \frac{2\pi}{S_0 L} \int_0^{r_0} r^2 J_1 dr + \frac{2\pi}{S_0 L} \int_0^L r \tau J_2 d\tau & & (7.4.7) \end{aligned}$$

Here, $2r_0$ is the diameter of the body cross-section, while Δc_τ , and so on, are the aerodynamic coefficients of annular elements.

For a sharp cone, $r_0 = L \tan \theta$ and $dr = \tan \theta d\tau$; thus, we derive the following expressions for the aerodynamic coefficients

$$\begin{aligned} c_\tau &= 2 \sin^2 \theta \cos^2 \alpha + \cos^2 \theta \sin^2 \alpha \\ c_n &= \cos^2 \theta \sin 2\alpha, & c_{m0} &= \frac{2}{3} \sin 2\alpha \\ c_d &= \frac{c_{m0}}{c_n} = \frac{2}{3 \cos^2 \theta} & & (7.4.8) \end{aligned}$$

Clearly, the center of pressure of the cone is located farther from the vertex than that for the wedge; both coefficients are independent of the angle of attack. For small $\theta, \alpha \ll 1$ from 7.4.8 it follows that

$$c_x = 2\theta^2 + 3\alpha^2, \quad c_y = c_n = 2\alpha, \quad c_d = 2/3 \quad (7.4.9)$$

The lift-drag ratio of these cones is determined by the formula

$$K = c_y/c_x = 2\alpha/(2\theta^2 + 3\alpha^2) \quad (7.4.10)$$

In accordance with 6.6.1, the pressure \bar{p} vanishes for $\alpha > 0$ at the point $\varphi = \varphi_0$, $\cos \varphi_0 = -\tan \theta \cot \alpha$. Obviously at $\varphi > \varphi_0$ the Newton formula is inapplicable even from the formal point of view; therefore, in this domain we let $\bar{p} = 0$. For this case we do not present the cumbersome, though easy-to-derive, formulas for the aerodynamic coefficients; we only note that in this case, as earlier, $c_d = 2/(3 \cos^2 \theta)$.

The curves $K(\alpha, \theta)$ thus obtained are plotted in Figure 7.15. These curves have a maximum at $\theta < 30^\circ$; for slender cones it is attained at the point $\alpha = (2/3)^{1/2}\theta$ and equal to $K_{\max} = 1/(3\alpha)$, which is smaller than the value $K_{\max} = \alpha^{-1}$ for a thin plate in the Newtonian approximation. For $\alpha > \alpha_0$, where $\tan^2 \alpha_0 = 2(1 - \tan^2 \theta)$, the quantity K is negative, together with c_y (this follows from 7.4.8 and 2.13.5), which is attributable to an increase in the contribution of the axial force T directed to the region $y < 0$; for $\theta \geq 45^\circ$ this takes place for any α . As $\theta \rightarrow 90^\circ$, we have $K = -\tan \alpha$. A comparison with more exact results shows a fairly good accuracy of the Newton formula for calculating the lift-drag ratio of cones at high Mach numbers M_∞ , at least, for $\alpha \leq \theta$, that is, within the applicability range of inviscid gas dynamics (for $\alpha > \theta$ the effect of separation zones on the leeward side of the cone can be appreciable).

As for blunt bodies, we will present formulas for c_x at $\alpha = 0$ for spherical segments with the central angle $\omega_0 = \pi/2 - \theta_0$ calculated from the pressure distributions 7.2.6 at $M_\infty = \infty$

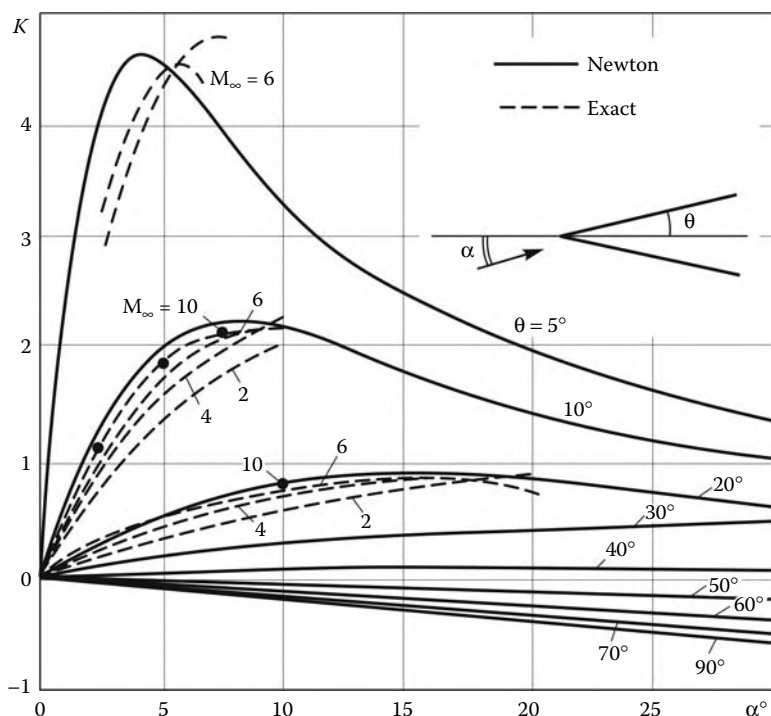


FIGURE 7.15
Lift-drag ratios of sharp cones.

$$\begin{aligned} v = 0 : \quad c_x &= 2\bar{p}'_0 \left(1 - \frac{1}{3} \sin^2 \omega_0 \right) \\ v = 1 : \quad c_x &= 2\bar{p}'_0 \left(1 - \frac{1}{2} \sin^2 \omega_0 \right) \\ \bar{p}'_0 &= p'_0 / \rho_\infty U_\infty^2 \end{aligned} \quad (7.4.11)$$

For a circular cylinder we have $c_x = \frac{4}{3}\bar{p}'_0$, while for a sphere $c_x = \bar{p}'_0$ ($\bar{p}'_0 = 0.92$ for $M_\infty = \infty$ and $\gamma = 1.4$). These formulas have a fairly good accuracy (cf. Figure 7.16). The maximum value $c_x = 2\bar{p}'_0$ is attained at $\omega_0 = 0$, that is, for a disk or a flat plate set normal to the flow. Obviously, in this approximation a plate of arbitrary shape placed normal to the flow has the same drag coefficient.

On the basis of the Newton formula we can also derive some useful laws of general nature. One such law can be obtained by eliminating $\cos^2 \theta$ from relations 7.4.7 for J_1 and J'_2 (this formula was suggested by Krasilnikov)

$$(2 - 3 \sin^2 \alpha) c_n = \sin 2\alpha (2 \cos^2 \alpha - c_\tau) \quad (7.4.12)$$

The testing of this formula with respect to the exact data, both calculated and experimental, is presented in Figure 7.17. It is interesting to note that for $\sin^2 \alpha = 2/3$ ($\alpha = 54.7^\circ$) the c_τ coefficient is equal to $2/3$ for any bodies (of course, within the framework of the Newtonian theory). However, it should be noted that formula 7.4.12 is valid only for $\alpha \leq \theta$. For small α from 7.4.12 and 2.13.15 there follows

$$c_n = \alpha (2 - c_\tau), \quad c_y = 2\alpha (1 - c_\tau), \quad c_x = c_\tau + 2\alpha^2 \quad (7.4.13)$$

We note that in using formulas 7.4.12 and 7.4.13 for blunt bodies, c_n and c_τ should be replaced by c_n/\bar{p}'_0 and c_τ/\bar{p}'_0 .

On the basis of the Newton formula we can also obtain the *area rule* for the drag of near-axisymmetric bodies. Let in a cylindrical flow-fitted coordinate system the shape of a body in gas flow differ only slightly from that of a certain axisymmetric body

$$r_b = r_\varepsilon(x, \varphi) = r_0(x) + \varepsilon r_1(x, \varphi), \quad \varepsilon \ll 1 \quad (7.4.14)$$

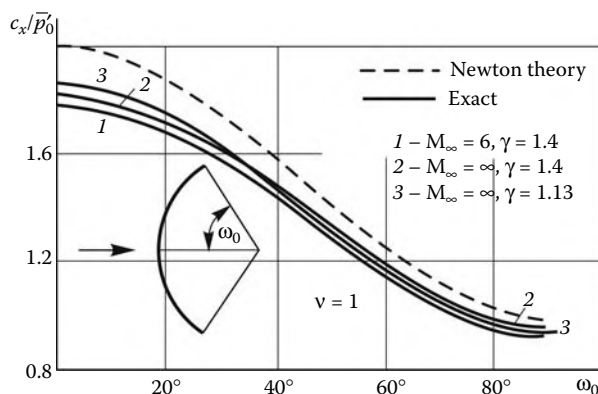
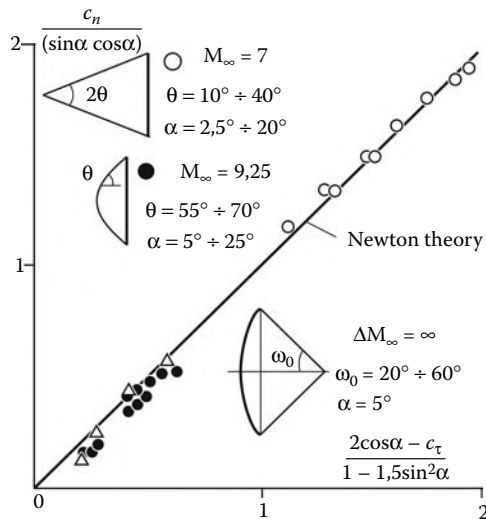


FIGURE 7.16
Drag coefficients of spherical segments.

**FIGURE 7.17**

Correlation between aerodynamic characteristics for different bodies of revolution.

We will choose the body $r_0(x)$ so that in an arbitrary cross-section $x = \text{const}$ its area and the area of the original body are the same. Then we have

$$S = \frac{1}{2} \int_0^{2\pi} r_e^2 d\varphi = \pi r_0^2 + \varepsilon r_0 J, \quad J = \int_0^{2\pi} r_1 d\varphi = 0 \quad (7.4.15)$$

In accordance with the Newton formula, $\bar{p} = n_x^2$, the force dX acting along the x axis on each area element of the body surface with the normal \vec{n} is proportional to $n_x^3 r_\varepsilon$. Correct to second-order terms, we have

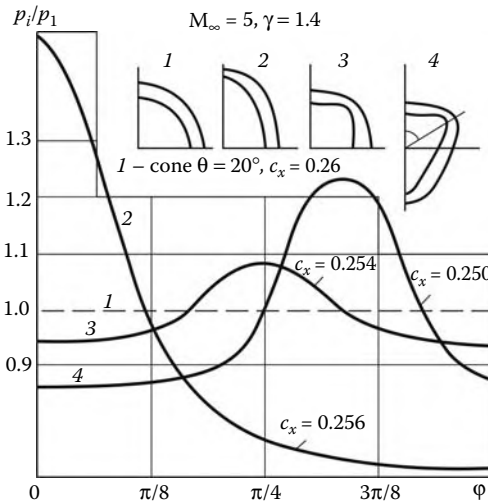
$$\begin{aligned} n_x &= -\Delta^{-1} r'_\varepsilon = n_{x_0} - \varepsilon \Delta_0^{-3} r'_1 \quad (r' = \partial r / \partial x) \\ n_{x_0} &= -\Delta_0^{-1} r'_0, \quad \Delta_0^2 = 1 + (r'_0)^2 \\ dX &\sim n_x^3 r_\varepsilon = r_0 n_{x_0}^3 - \varepsilon (r_0 \Delta_0^{-3} r'_1 - n_{x_0}^3 r_1) \end{aligned} \quad (7.4.16)$$

In view of the condition $J = 0$, the integral with respect to φ of the latter expression in the parentheses is also zero. Therefore, for the force acting on the body we obtain, correct to the second order, $X = X_0 + \varepsilon X_1 = X_0$, that is, $X_1 = 0$. Thus, the difference in the drag of the bodies compared is of a higher order than the deviation of their shapes, the areas of their cross-sections being the same.

This effect is called the *area rule*.* Its particular case is the flow past an axisymmetric body at a small angle of attack $\alpha \ll \theta$; in this case the body incidence results in the change in the body drag only by a value of the order $\Delta c_x^2 \sim \alpha^2$.

The area rule has been proved for near-axisymmetric bodies, but its applicability range is considerably wider. Thus, in Figure 7.18 conical bodies of different cross-sections are

* In rigorous formulation the area rule was proved by Kogan (1961) and Kraiko (1974).

**FIGURE 7.18**

Pressure distributions and shock shapes for sharp conical bodies with the same lengths and cross-sectional areas.

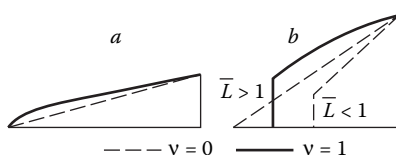
shown; correspondingly, the peripheral pressure distributions are also different, but the drag coefficients of the bodies differ only slightly.

However, this result is not a rule. Thus, for an elliptic cone (cf. 7.4.5) with the midsection area $S_0 = \pi L^2 \bar{S}$, $\bar{S} = \tan \theta_1 \tan \theta_2$ and small $\theta_1, \theta_2 \ll 1$ the quantity $c_x = 2\bar{S}$ is independent of the ratio θ_2/θ_1 , that is, the area rule holds. However, for finite θ_1 and θ_2 and $\bar{S} = \text{const}$ the value of c_x is maximum for a cone and vanishes as $\theta_2/\theta_1 \rightarrow 0$, that is, for an elliptic wing.

The Newton formula makes it possible to simplify the solution of certain variational problems of minimum drag bodies. This will be demonstrated with reference to some simple examples. Thus, for a thin power-law body, $r = Cx^n$, the Newtonian pressure coefficient is $\bar{p} = n^2 C^2 x^{2(n-1)}$, while the drag coefficient is

$$c_x = 2^{1+v} N(n) (r_b/x)^2, \quad N = n^3 [(3+v)n - 2]^{-1} \quad (7.4.17)$$

For $n < 1$ this body has a blunt nose, for which the thin-body approximation is incorrect; however, we will neglect this effect. Letting $dN/dn = 0$ at the same body aspect-ratio r_b/x , we obtain $n = 1$ and $N = 1$ for $v = 0$ and $n = 3/4$ and $N = 27/64$ for $v = 1$ (Figure 7.19a). Thus, the plane minimum-drag body is a wedge, while the minimum-drag body of revolution is a convex ogive-shaped body, though its gain over the cone is not too great (for the cone we have $N = 1/2$). We note that the exact self-similar solution of Section 6.8 and

**FIGURE 7.19**

Contours of the bodies of optimal shape.

Chapter 8 gives $n = 0.71$ for the latter problem, while within the framework of the linear theory the optimal body of revolution is also ogive-shaped (cf. Section 2.8).

Another example is a body whose longitudinal section is a trapezoid of length L with the radii of the forward and rear faces r_0 and r_m , and the angle θ of the lateral surface inclination (Figure 7.19b). For this body the Newton formula gives

$$\begin{aligned} \frac{1}{2}c_x &= (1 - \bar{r}_0^{1+\nu}) \sin^2 \theta + \bar{r}_0^{1+\nu} \\ \bar{r}_0 &= r_0/r_m = 1 - \bar{L} \tan \theta, \quad \bar{L} = L/r_m \end{aligned} \quad (7.4.18)$$

In the two-dimensional case ($\nu = 0$) the coefficient $c_x = 2 - \bar{L} \sin 2\theta$ decreases as the angle θ increases; the latter is, in its turn, bounded by either the condition $\bar{r}_0 \geq 0$ and $\bar{L} \tan \theta \leq 1$ at $\bar{L} \geq 1$ or the condition $\sin 2\theta = 1$ ($\theta = 45^\circ$) at $\bar{L} \leq 1$. Therefore, the optimal body is a wedge with the angle $\theta = \arctan 1/\bar{L}$ in the former case and a frustum of a wedge with the angle $\theta = 45^\circ$ and the flat nose of radius $\bar{r}_0 = 1 - \bar{L}$ in the latter case. For a body of revolution, the equation $dc_x/d\theta = 0$ has the solution $\tan 2\theta = 2/\bar{L}$. Since $\tan 2\theta > 2 \tan \theta$, we have $\bar{L} \tan \theta < 1$ and the required body has a finite nose radius, $r_0 > 0$.

We will note, however, that the simplicity of the solutions obtained is due to the analytical nature of the expression for c_x in the previous examples, which is an exception rather than a rule. Invoking arbitrary contours of the lateral surface of the bodies, as in Figure 7.19, requires using the apparatus of the variational calculus even within the framework of the Newtonian theory. However, in the examples considered previously this affects the results only slightly, though the optimal lateral surface of the body of revolution, sketched in Figure 7.19b, turns out to be ogive shaped.*

Finally, we will touch the calculation and properties of time-dependent aerodynamic characteristics. Let v'_n be a local velocity of a body area element along the surface normal \vec{n} in an inertial coordinate system x, y, z (Figure 2.26). As shown in Section 2.13, in aerodynamics the unsteady effects are usually small; thus, we adopt the condition

$$v'_n \ll U_{n\infty} = -(\vec{U}_{\infty} \cdot \vec{n}) \quad (7.4.19)$$

We will also present the Newton formula in the form:

$$\begin{aligned} \Delta p &= \rho_{\infty} v_{n\infty}^2 = \rho_{\infty} (U_{n\infty} + v'_n)^2 = \Delta p_0 + p'_n \\ \Delta p_0 &= \rho_{\infty} U_{n\infty}^2, \quad p'_n = 2\rho_{\infty} U_{n\infty} v'_n \end{aligned} \quad (7.4.20)$$

Here, Δp_0 is the quasistationary and p'_n the unsteady components of the excess pressure. For an L -long plate at an instantaneous angle of attack α rotating with an angular velocity ω about the center τ_0 we have (see Figure 2.26d from Section 2.13)

$$\begin{aligned} v'_n &= v_{\omega} = -\omega L(\bar{\tau} - \bar{\tau}_0), \quad \bar{p}_{\omega} = -2\bar{\omega}(\bar{\tau} - \bar{\tau}_0) \sin \alpha \\ U_{n\infty} &= U_{\infty} \sin \alpha, \quad \bar{\omega} = \omega L/U_{\infty}, \quad \bar{\tau} = \tau/L \end{aligned} \quad (7.4.21)$$

As distinct from the analogous example from Section 2.13, here we consider only the windward side of the plate (Figure 2.26d), the Newton formula being applicable to this

* The corresponding solution was obtained by Newton himself. See also the paper of Gonor and Kraiko in the book edited by Miele (1969).

side only. In accordance with this and formula 2.13.3, the rotational moment coefficient is as follows

$$c_\omega = \frac{M_\omega}{0.5\rho_\infty U_\infty^2 L^3} = -\frac{4}{3}\bar{\omega}(1 - 3\bar{\tau}_0 + 3\bar{\tau}_0^2) \sin \alpha \quad (7.4.22)$$

Clearly, the moment M_ω thus obtained differs from M_ω in formula 2.13.8 derived in another approximation only by a positive factor, so that, as in Section 2.13, the coefficient $c_{\dot{\alpha}} > 0$ for $\omega = -\dot{\alpha}$.

However, the quantity p_ω determined by formula 7.4.21 takes into account the contribution of plate rotation to the induced pressure only partially. In fact, gas particles entering the shock layer move along the plate at a near-constant velocity $u = U_\infty \cos \alpha$ following a curvilinear trajectory in space. In a fixed coordinate system (n', τ') coinciding for $t = 0$ with the fitted (n, τ) system (Figure 2.26), the particle trajectories on the plate undersurface ($\alpha > 0$) are described by the equations $dn'/dt = -v_\omega$, $d\tau'/dt = u$ or (for $\tau \approx \tau'$ and $\omega = -\dot{\alpha}$)

$$\frac{dn'}{d\tau} = \frac{\dot{\alpha}}{u}(\tau_0 - \tau), \quad n' = \frac{\dot{\alpha}}{u}(\tau \tau_0 - 0.5\tau^2) \quad (7.4.23)$$

Here, the integration constant is dropped. Curvilinearity and time dependence of these trajectories induce the centrifugal, or inertial, component in the time-dependent pressure, in addition to the Newtonian component 7.4.21. This component can be estimated using a counterpart of the Busemann formula based on the general Equation 2.2.5. Formula 7.4.21 does not take into account in full measure the contribution of body rotation due to its motion along the curvilinear trajectory. For thin bodies in hypersonic flow these effects will be taken into account in Section 8.7.

7.5 Limiting Solution: Free Layer

The Busemann formula, 7.2.3, derived in Section 7.2 is still unclosed, since the velocity distribution $U(\psi)$ under the integral sign in this formula is not known beforehand. However, using subsequently the asymptotic conditions $k \rightarrow 0$ and $\delta/R \rightarrow 0$, the problem could be closed, at least for moderately blunt bodies (in the sense of Section 7.1). For this purpose, we will evaluate the velocity increment in the shock layer and, for adiabatic flows, the enthalpy increment along the streamlines, taking the estimate $p \sim \rho_\infty U_\infty^2$ into account. Thus, we have

$$\Delta h = -\frac{1}{2}\Delta U^2 \sim \frac{1}{\rho}\Delta p \sim kU_\infty^2 \frac{\Delta p}{p} \quad (7.5.1)$$

As $k \rightarrow 0$ the increments Δh and ΔU vanish, that is, the velocity and the enthalpy are conserved along the streamlines. Thus, the limiting solution for the shock layer has the following general form in x, ψ variables

$$\begin{aligned} U &= U_0(s), \quad h = h_0(s), \quad \rho = \rho(p, s), \quad p = p_N(x) - p_B(x, s) \\ p_N &= p_s = \rho_\infty U_\infty^2 \sin^2 \theta, \quad r_s(x) = r_b(x), \\ s(\psi) &= \sin^2 \alpha_\psi, \quad \alpha_\psi = \alpha(\psi) \end{aligned} \quad (7.5.2)$$

Here, α_ψ is the angle of attack of the bow shock at the point of intersection with a given streamline $\psi = \text{const}$.

This solution contains only one arbitrary function, namely, the shock shape $r_s(x)$, which determines the entropy function $s(\psi)$. Since for moderately blunt bodies $r_s(x) = r_b(x)$ when

$\delta/R \rightarrow 0$, the solution is determined by the body shape only. We will add that, as $k \rightarrow 0$ the normal velocity behind the shock $v_n = kU_\infty \sin \alpha \rightarrow 0$; therefore, the total velocity is equal to the tangential one, $U_s = U_\infty \cos \theta$.

As an example, we will present the velocity distribution behind a spherical shock of radius R_s . In this case we have

$$\begin{aligned} U_s &= U_\infty \cos \alpha = U_\infty r_s/R_s = U_\infty (\psi_s/\psi_0)^{1/(v+1)} \\ U &= U_s \bar{\psi}^{1/(v+1)}, \quad \bar{\psi} = \psi/\psi_s, \quad \psi_0 = \pi^v R_s^{1+v} \rho_\infty U_\infty \end{aligned} \quad (7.5.3)$$

This limiting solution has an obvious physical meaning: a finite pressure gradient is not able to change the velocity and enthalpy (internal energy) of a gas having infinitely large density, so that these quantities are constant along streamlines, while the gas particles move along them as though by inertia. We will refer to these limiting mechanical flows as *Newtonian*, though Newton himself was not, obviously, acquainted with their properties in full measure.

We note some important properties of these flows. *The pressure, velocity, and enthalpy distributions in streamlines are independent of the physical properties of a gas and are determined by the body shape only.* At the same time, this assertion could not be extended to the distributions of the density, temperature, and physicochemical composition of the gas, which are determined in terms of the given p and h from the equation of state. In nonadiabatic flows the enthalpy is determined by the equation $dh/dt = q$, which is the only differential relation of the theory and must be integrated along streamlines with the conventional initial conditions at the shock and a certain preassigned function q .

A very simple nature of the solution obtained may tempt one to improve it by introducing corresponding correction terms, for example, using expansions of the type $U = U_0(\psi) + kU_1(x, \psi)$, and so on (see Chernyi, 1966 where this method was suggested). Precisely in this way the solutions for the cone and the wedge were derived in Sections 3.7 and 6.4. However, this method turns out to be inadequate as applied to blunt bodies. We shall demonstrate this by calculating the shock layer thickness δ on the axis of symmetry by means of formulas 7.2.4 and 7.5.3 with ρ_s substituted for ρ

$$\delta_0 = \frac{1}{2^v} kR_s \int_{\bar{\psi} \rightarrow 0}^1 \frac{d\bar{U}}{\bar{U}} = \begin{cases} kR, & v = 1 \\ -kR \ln \bar{\psi} \rightarrow \infty, & v = 0 \end{cases} \quad (7.5.4)$$

Clearly, in the two-dimensional case the flow rate integral diverges. This absurd result is attributable to the neglect of a nonzero velocity at the body surface ($U \neq 0$ at $\psi = 0$). In fact, using 7.5.1 and the Newton formula for the pressure we obtain for the velocity in the wall sublayer the estimate $U \sim U_s k^{1/2}$; taking this result into account would eliminate the divergence of the integral in Equation 7.5.4.

Thus, the solution of the problem is nonanalytic near the point $k = 0$, so that the search for corrections to the limiting solution could not be performed by regular expansion. This result is common for many other flows containing stagnation points and attachment lines.

At the same time, comparison with 7.5.3 indicates that the relative gas flow rate in this sublayer is $\bar{\psi} \sim k^{(v+1)/2}$; the velocity in the sublayer being $U \sim k^{1/2}$, this result makes a negligible contribution of the order $\Delta p_B \sim k^{1+v/2}$ to the integral 7.2.3 for p_B . Using formulas 7.2.3, 7.2.5, and 7.5.3 we can write for the pressure over a cylinder and a sphere

$$\frac{p}{p'_0} = \sin^2 \theta - \frac{\cos^2 \theta}{1 + \nu} \int_0^1 \bar{\psi}^{1/(\nu+1)} d\bar{\psi} = 1 - \beta \sin^2 \omega$$

$$\beta = (3 + \nu)/(2 + \nu) \quad (7.5.5)$$

For a cylinder $\beta = 3/2$, while for a sphere $\beta = 4/3$. The Newton formula gives $\beta = 1$ for both bodies, while approximation 7.2.6 for the sphere gives $\beta = 7/6$. Clearly, formula 7.5.5 gives zero pressure for $\sin^2 \omega' = (2 + \nu)/(3 + \nu)$, that is, at $\omega' = 55^\circ$ for $\nu = 0$ and 60° for $\nu = 1$. At this point both terms in 7.5.5 turn out to be equal; this means that the Newtonian pressure applied to the outer edge of the shock layer, that is, to the shock itself, is completely balanced by centrifugal forces.

However, in this case $\rho \rightarrow 0$ as $p \rightarrow 0$ on the body; thus, the volume-average density ρ_a can also become small, which would result in the growth of the disturbed layer thickness δ and in the violation of the theory applicability conditions in the vicinity of this singular point.

At the same time, the pressure at the point ω' behind the shock is $p/p'_0 = (3 + \nu)^{-1}$, thus having the order of unity. The same is true for a certain band adjacent to the shock in which the integral p_B in formula 7.2.3 still considerably differs from p_s . Therefore, the thickness of this band δ_f is small and in the vicinity of the *separation point* ω' , as it were, detaches from the body and forms a *free layer* adjacent to the shock (Lighthill, 1957), which is not propped up by the body owing to the smallness of the pressure on it, and changes its shape only under the action of the outer stream ram pressure. The free layer model is qualitatively supported by Figure 7.9 from Section 7.2 and Figure 7.20b, in which the pressure on the shock p_s is several times greater than the body pressure p_b in the region of the sharp increase in the disturbed layer thickness immediately behind the blunt body.

To determine the free layer shape, we will use the components I_x and I_r of the momentum flux vector \vec{I} introduced in Section 7.2 by formula 7.2.3

$$I_x = \int_{r_b}^{r_s} \rho u^2 r^\nu dr, \quad I_r = \int_{r_b}^{r_s} \rho u v r^\nu dr \quad (7.5.6)$$

We note that the quantity I_r is not equal to the force Y acting on the separated region of the body, since it is determined not only by the pressure distribution over the body surface (Oa in Figure 7.21d) but also by the pressure on the axis of symmetry for $\nu = 0$ (line OO') or on the previously mentioned (see comments to formula 7.2.3) meridional planes for $\nu = 1$ (the shaded region $O'Oab$ in Figure 7.21d).

The quantity I_x is determined from the longitudinal momentum conservation law, 1.7.13, which will be written down at $p_\infty = 0$ for a control volume bounded by the shock and an $x = \text{const}$ section

$$\pi^\nu r_s^{1+\nu} \rho_\infty U_\infty^2 - (2\pi)^\nu I_x - (2\pi)^\nu \int_{r_b}^{r_s} p r^\nu dr =$$

$$X = \frac{1}{2} C_x r_b^{1+\nu} \rho_\infty U_\infty^2 \quad (7.5.7)$$

Here, X is the drag of the body with the local radius r_b (or that of the half-body for $\nu = 0$). In what follows the last term on the left-hand side will be omitted, since the pressure in this region is small outside a layer of thickness $\Delta r \sim kr_s$.

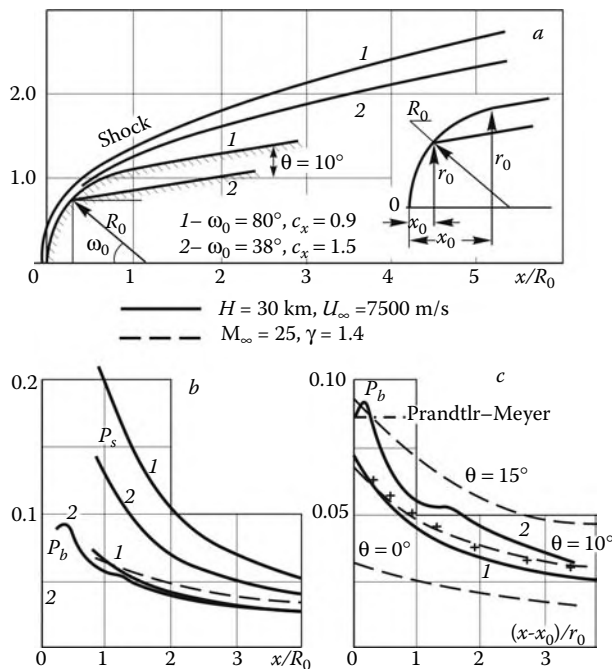


FIGURE 7.20
Shocks and pressures on blunt cones.

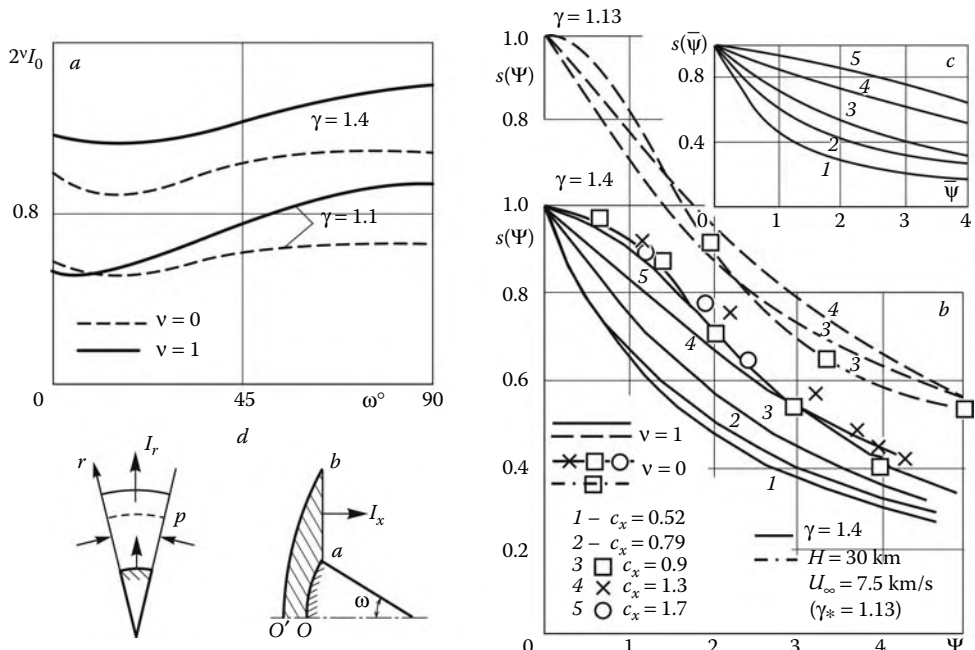


FIGURE 7.21
Relative momentum and entropy distributions over blunt bodies.

Since in the compressed shock layer the momentum flux vector \vec{I} is directed along the shock $r_s(x)$, from 7.5.6 and 7.5.7 there follows the relation

$$\begin{aligned} \frac{dr_{1s}}{dx_1} &= \tan \alpha = \frac{I_r}{I_x} = \frac{2^\nu I_0}{\Psi - 1} \\ I_0 &= \frac{2I_r}{c_x \rho_\infty U_\infty^2 r_0^{1+\nu}}, \quad \Psi = \frac{2r_s^{1+\nu}}{c_x r_0^{1+\nu}} = \frac{2\bar{\psi}_s}{c_x} \\ x_1 &= \frac{x}{r^{(0)}}, \quad r_1 = \frac{r}{r^{(0)}}, \quad r^{(0)} = \left(\frac{X}{\pi^\nu \rho_\infty U_\infty^2} \right)^{\frac{1}{1+\nu}} = \left(\frac{c_x}{2} \right)^{\frac{1}{1+\nu}} r_0 \end{aligned} \quad (7.5.8)$$

The profiles of the relative transverse momentum I_0 for spherical segments are plotted in Figure 7.21a. Within the framework of our model the quantity I_r and the body drag X can be regarded as constant in each section of the free layer; within the framework of the condition $c_x r_0^{1+\nu} = \text{const}$ this allows us to vary the quantity c_x and the midsection radius r_0 within certain limits. Under these assumptions, Equation 7.5.8 has the solution

$$\frac{1}{2+\nu} r_{1s}^{2+\nu} - r_{1s} = 2^\nu I_0 x_1 + C \quad (7.5.9)$$

where C is a constant determined from the condition at the separation point.

An excessively limiting nature of these solutions as $\gamma \rightarrow 1$ does not allow us to believe that they are quantitatively reliable. However, they lead to a conclusion having the meaning of a similarity law, namely, that, in accordance with 7.5.8, the distribution of the entropy function $s(\Psi)$ introduced in Section 7.1 over the *reduced stream function* depends on the parameter $2^\nu I_0$ only. In other words, the entropy distribution in streamlines behind the shock in the vicinity of a blunt body depends only on the force action exerted by the flow from the body. In support of this conjecture, we have plotted in Figure 7.21b the $s(\Psi)$ curves for different bodies under given flow conditions; for $c_x > 0.5$ they form fairly narrow bands, common for two-dimensional and axisymmetric flows. At the same time, the discrepancy in the curves $s(\bar{\psi})$ constructed in the original coordinates (Figure 7.21c) is considerably greater. Of course, ahead of the free layer separation point, that is for $\Psi < 1$, these curves depend on the body shape; however, this difference is not too large, the more so that in this region we have $s \approx 1$.

As for the pressure on the body downstream of the free layer separation point, it is chiefly determined by wave processes accompanying the turn of the flow around a convex wall and, for example, in the case of the flow past a sphere (Figure 7.2a of Section 7.1) is obeyed to the laws governing Prandtl-Meyer waves, in spite of the axisymmetric and highly vortical nature of the flow.

At the same time, the pressure p_b on the lateral surface of the short blunt cone with the semivertex angle 10° and the nose in the form of a spherical segment with the central angle ω and radius R_0 (Figure 7.20a) in equilibrium air decreases monotonically and already at $x/R_0 \geq 3$ reaches the Newtonian level (Figure 7.20b).

In Figure 7.20c we have also plotted by dots a curve whose abscissae are displaced in the ratio $(c_{x2} : c_{x1})^{1/2} = 1.3$ relative to curve 1. Curves 1 and 2 could be compared using the similarity variable x_1 introduced by formula 7.5.8. In fact, this procedure makes the curves closer to each other (with the exception of the segment $x_1 - x_0 \leq r_0$). This similarity law will be considered from other positions in Chapter 9.

7.6 Piston Problem

We will now consider the time-dependent problem of piston expansion, $r = r_p(t)$, in the plane, cylindrical, and spherical cases ($\nu = 0, 1$, and 2). We will assume that the shock wave $R(t)$ ahead of the piston propagates at a hypersonic velocity, $\dot{R} \gg a_\infty$, as does the piston itself, $\dot{r}_p \gg a_\infty$, and the density ratio across the shock is high, $\rho_s/\rho_\infty = k^{-1} \gg 1$. Apart from a methodical interest, the problem is pertinent to the hypersonic flow past thin sharp bodies within the framework of the time-dependent analogy (Chapter 8).

The shock layer thickness $\delta = R - r_p$ can be evaluated from the mass conservation law applied to the disturbed layer, as in Equation 6.4.6

$$\begin{aligned} M &= 2^\nu \pi^\kappa \rho_a \delta r_a^\nu = \pi^\kappa \rho_\infty R^{1+\nu}, & \delta/R \sim k_a = \rho_\infty/\rho_a \ll 1 \\ \kappa &= 0 \quad \nu = 0, \quad \kappa = 1 \quad \nu = 1, 2 \end{aligned} \quad (7.6.1)$$

As in Section 7.1, the condition that the pressure is of the same order along particle trajectories, $p/p_{ss} \sim 1$, p_{ss} being the particle pressure immediately behind the shock, must be fulfilled. This is a necessary condition for the order of the volume-average density to be conserved, $\rho_a \sim \rho_s$. Thus, this condition is fulfilled for a not too strongly decelerating piston, but is violated in the case of a blast (Section 6.8).

The Newton formula 7.2.1 gives the pressure $\Delta p = \rho_\infty \dot{r}_p^2$. However, in formula 6.8.11, in which it could be taken $p_s/\rho_\infty \approx \dot{R}^2 \approx \dot{r}_p^2$ as $\gamma \rightarrow 1$, there is one more term with the piston acceleration, $\ddot{R} \approx \ddot{r}_p$; this is proportional to the inertia force of a gas layer compressed between the shock and the piston. This formula is an analogue of the Busemann formula 7.2.3 for time-dependent flows under consideration.

We will also present a simpler scheme of this flow. If the compressed layer is thin, the piston $r_p(t)$ pushes the gas mass $M = \rho_\infty R^{1+\nu}/(1+\nu)$ (within a unit but small solid angle $d\Omega$), whose momentum $M\dot{R}$ grows due to the pressure difference

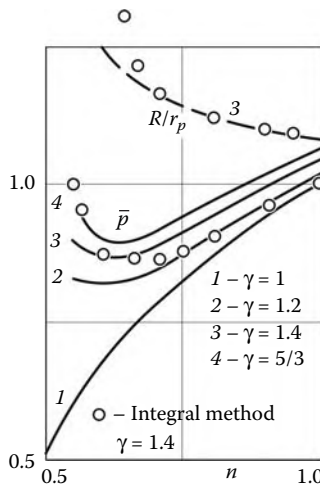
$$\Delta p = p - p_\infty = \frac{\rho_\infty}{(1+\nu)R^\nu} \frac{d}{dt}(R^{1+\nu}\dot{R}) = \rho_\infty \dot{R}^2 + \frac{\rho_\infty R \ddot{R}}{1+\nu} \quad (7.6.2)$$

For $\dot{R} \approx \dot{r}_p$ the first term in the last equation is the Newtonian pressure, while the second term is a counterpart of the Busemann term p_B in 7.2.3, which is due to the inertia force of the accelerating mass M . This formula coincides with 6.8.11 for $m = 0$ and $\gamma = 1$. The pressure is greater than the Newtonian one on an accelerating piston and smaller on a decelerating piston, as it is the case for convex and concave bodies (Section 7.2).

For a power-law piston, $r_p = ct^n$, the ratio of the excess pressure on the piston to the Newtonian one $\bar{p} = (p - p_\infty)/\rho_\infty \dot{r}_p^2$ is presented in Figure 7.22 for $\nu = 1$. Here, curve 1 for $\gamma = 1$ was obtained from formula 7.6.2 for $R = r_p$, while 2 to 4 are exact curves. In the general case, the quantity \bar{p} is close to unity for $\gamma > 1.2$ and n not too close to the blast value $n = 2/(3+\nu) = 1/2$. As $n \rightarrow 1/2$, the Newtonian pressure $\rho_\infty \dot{r}_p^2 \rightarrow 0$, while $R/r_p \rightarrow \infty$, so that the replacement of R by r_p is incorrect. The integral method of Section 6.8 (Equations 6.8.11 and 6.8.15) gives satisfactory results for this problem already for $n \geq 0.7$.

We note in this connection that for $n = 2/(3+\nu)$ the Newton formula applied to the equal mass lines $r_m(t)$ gives, in accordance with 6.8.9, an incorrect law of motion

$$p_m/p_s \sim \dot{r}_m^2/\dot{R}^2 \sim t^{-q}, \quad q = \left[\frac{2(\gamma-1)}{\gamma(3+\nu)} \right]^2, \quad M \sim \rho_\infty R^{1+\nu} \quad (7.6.3)$$

**FIGURE 7.22**

On the problem of a cylindrical power-law piston.

different from the solution $p_m/p_s = \text{const}$ for the central part of the blast zone (Section 6.8).

Having noted the similarity of this time-dependent problem with the steady-state problem of Section 7.2, we will now lay stress on their difference: in the latter case the gas velocity is conserved along the particle trajectories (streamlines), while in time-dependent flows the gas velocity is in the general case variable, together with the piston velocity (for $v \sim \dot{r}_p$) and the shock velocity (for $v \sim \dot{R}$).

We will now dwell on the unsteady analogue of the free layer described in Section 7.5. At a sudden stop of a piston, $\dot{r}_p = 0$, an expansion wave with a sharp pressure fall is formed on its surface. Then putting limiting values $p = 0$ and $p_\infty = 0$ in Equation 7.6.2 we obtain its integral and solution similar to 7.5.8

$$\begin{aligned} \dot{R}R^{1+\nu} &= \dot{R}_0 R_0^{1+\nu} = J_0/\rho_\infty, \quad t \geq 0 \\ R &= [R_0^{2+\nu} + (2+\nu)tJ_0/\rho_\infty]^{1/(2+\nu)} \end{aligned} \quad (7.6.4)$$

Here, R_0 and \dot{R}_0 are the initial parameters at $t = 0$ and J_0 is the gas momentum per unit meridional ($d\varphi$) and solid ($d\Omega$) angles for $\nu = 0$ and $\nu = 1$ (see Section 7.5). This momentum is constant in free inertia-driven motion of the increasing gas mass $M \sim \rho_\infty R^{1+\nu}$ but only until the pressure rise in the thin shock layer propagates to the entire disturbed region. Then the gas momentum J starts to grow and solution 7.6.4 is no longer valid. With time, this solution becomes quantitatively, and for $J \gg J_0$ even qualitatively, similar to the solution describing the point blast flow with the energy $E_0 \sim R_0^2 R_0^{1+\nu}$ equal to the piston work before its stop. As shown in Section 6.8, the solution for this effective blast represents the asymptotics of the piston problem.

We note that the parameter R_0 in solution 7.6.5 could be omitted as $t \rightarrow \infty$ and $R/R_0 \rightarrow \infty$; thus, we obtain a solution for a concentrated, or point, initial momentum. However, such a formulation of the problem is unrealistic, since the energy $E_0 \sim J_0/R_0$ corresponding to it becomes unbounded as $R_0 \rightarrow 0$. This question was already discussed at the end of Section 6.8.

In conclusion, within the framework of this flow model we will consider a simple variational problem similar (within the framework of the time-dependent analogy of Chapter 8)

to that solved in Section 7.4, namely, what value of n in the piston expansion law $r_p = ct^n$ is associated with minimum work done by the piston. Substituting r_p for R in Equation 7.6.2, for the pressure on the piston we obtain the following formula ($p_\infty = 0$):

$$p = \rho_\infty c_0^2 t^{2(n-1)}, \quad c_0^2 = c^2 \left(n^2 + \frac{n(n-1)}{1+\nu} \right) \quad (7.6.5)$$

The work made by the piston is proportional to the integral

$$\begin{aligned} E &= \int_0^t pr^\nu r dt = c^{3+\nu} \bar{N} t^\omega, \quad \omega = (3+\nu)n - 2 \\ \bar{N} &= AN, \quad A = 1 + \frac{n-1}{n(1+\nu)}, \quad N = \frac{n^3}{\omega} \end{aligned} \quad (7.6.6)$$

Here, the coefficient N is the same as in Equation 7.4.17, that is, in the problem of the minimum drag of a power-law body $r \sim x^n$; in the Newtonian approximation, or for $A = 1$, a minimum of E is reached for the same $n_\nu = 3/(3+\nu)$, or for $n_0 = 1$, $n_1 = 3/4$, and $n_2 = 3/5$ for $\nu = 0, 1$, and 2, respectively. At the same time a minimum of the function $\bar{N}(n)$ is reached for the same ν at $n_0 = 0.95$, $n_1 = 0.71$, and $n_2 = 0.565$. As for the second roots of the equation $d\bar{N}/dn = 0$ ($n_0 = 0.175$, $n_1 = 0.14$, and $n_2 = 0.12$), these have no physical meaning, since they give $\omega < 0$ (see Section 6.8).

7.7 Truncation Series Method for the Vicinity of a Stagnation Point

The limiting ($k \rightarrow 0$) solution of Section 7.5 with constant velocities $U(\psi)$ and enthalpies $h(\psi)$ along streamlines turned out to be incorrect for a wall layer on a blunt body, since zero velocity on the wall, $U(0) = 0$, does not allow us to calculate the two-dimensional shock layer thickness. In this case, the quantity $U(0) \sim k^{1/2}$ determined in Section 7.5, which, as shown in the same section, could be neglected in calculating the integral p_B in the Busemann formula 7.2.3, is not, generally speaking, small for realistic values $k \geq 0.05$.

In what follows, we will derive local equations and their solutions for a vicinity of the axis of symmetry of a blunt body, which are free of this flaw. These solutions are also asymptotic and correspond to the conditions

$$\varepsilon = \max\{k, \delta/L, \delta K_s, \delta K\} \ll 1, \quad M_\infty^{-2} \ll 1 \quad (7.7.1)$$

Here, as earlier, L is the body scale length, δ is the shock layer thickness, and K_s and K are the characteristic curvatures of the shock and the body. The relation between the parameters entering in 7.7.1 can be established only by analyzing particular flows, though some preliminary suggestions were made in Section 7.1.

We call attention to a contradiction between the local character of this solution and the ellipticity of the problem as a whole, which seems to exclude a possibility of constructing a solution in a subdomain embedded in the minimal domain of definition of the problem Ω_{\min} (cf. Section 5.4). However, it turns out that as $\varepsilon \rightarrow 0$, the governing equations become *degenerate*, thus losing their elliptic type, so that they could be solved using the *truncated series method* by constructing a local solution in the vicinity of the axis of symmetry. We will analyze this degeneration mechanism in the process of constructing the solution for a

flow in the vicinity of the axis of symmetry of a moderately blunt body, that is, satisfying condition $K_s - K \ll K_s$ (7.1.9), carrying away the general theory to Section 7.13.

We will use body-fitted curvilinear coordinates x, y (Section 1.13, Figure 1.24c). Let l be the scale length of the flow region under consideration along the axis of symmetry x , so that near the axis the angles of inclination of the shock α and the body surface θ to the vector \vec{U}_∞ can be evaluated as follows:

$$\omega_s = \frac{\pi}{2} - \alpha \sim K_s l \ll 1, \quad \omega = \frac{\pi}{2} - \theta \sim Kl \ll 1 \quad (7.7.2)$$

The following relations are valid for the velocity components v_n and v_τ , normal and tangent to the shock, and u and v , directed along the x and y axes (see Figure 7.4a of Section 7.1; the subscript s refers to the flow parameters behind the shock)

$$\begin{aligned} v_n &= -\vec{n} \cdot \vec{U}, & v_{n\infty} &= U_\infty \sin \alpha, & v_{ns} &= kv_{n\infty} \\ && v_{\tau s} &= v_{\tau\infty} = U_\infty \cos \alpha \\ v_s &= v_{\tau s} \sin(\alpha - \theta) - v_{ns} \cos(\alpha - \theta) \\ u_s &= v_{\tau s} \cos(\alpha - \theta) + v_{ns} \sin(\alpha - \theta) \end{aligned} \quad (7.7.3)$$

Then under conditions 7.7.1 and 7.7.2 the pressure and the velocity components behind the shock are as follows:

$$\begin{aligned} p &= p_\infty + \rho_\infty U_\infty^2 (1 - k) \sin^2 \alpha \approx \rho_\infty U_\infty^2 (1 - \sin^2 \omega_s) \\ \Delta p &= p - p'_0 \approx -\rho_\infty U_\infty^2 \sin^2 \omega_s \sim \rho_\infty U_\infty^2 K_s^2 l^2 \\ u_s &\approx U_\infty \sin \omega_s \sim U_\infty K_s l \\ v_s &\approx U_\infty [-k + \sin \omega_s \sin(\alpha - \theta)] \sim -U_\infty [k + K_s (K_s - K) l^2] \end{aligned} \quad (7.7.4)$$

We are now coming to an analysis of the equations of motion 1.13.21. Letting in these equations the velocity w , together with the derivatives $\partial/\partial t$ and $\partial/\partial\varphi$, to be zero and taking Equation 2.4.1 into account (with the same function Q), we write down the equations in the form:

$$\frac{u}{H_x} \frac{\partial u}{\partial x} + v \frac{\partial u}{\partial y} + \frac{uv}{H_x R} = -\frac{j_1}{\rho H_x} \frac{\partial p}{\partial x} + Q_1 \quad H_x = 1 + y/R \quad (7.7.5)$$

$$j_2 \left(\frac{u}{H_x} \frac{\partial v}{\partial x} + v \frac{\partial v}{\partial y} \right) - \frac{u^2}{H_x R} = -\frac{1}{\rho} \frac{\partial p}{\partial y} + Q_2 \quad (7.7.6)$$

$$\begin{aligned} \frac{1}{r^v H_x} \left[\frac{\partial(r^v \rho u)}{\partial x} + \frac{\partial(H_x r^v \rho v)}{\partial y} \right] &= \frac{j_3}{\rho a^2} \left(\frac{u}{H_x} \frac{\partial p}{\partial x} + v \frac{\partial p}{\partial y} \right) + \\ \frac{1}{r^v H_x} \left(j_5 \frac{\partial(r^v u)}{\partial x} + \frac{\partial(r^v H_x v)}{\partial y} \right) &= -Q + Q_3 \end{aligned} \quad (7.7.7)$$

$$\frac{u}{H_x} \frac{\partial h}{\partial x} + v \frac{\partial h}{\partial y} = \frac{j_4}{\rho} \left(\frac{u}{H_x} \frac{\partial p}{\partial x} + v \frac{\partial p}{\partial y} \right) + q + Q_4 \quad (7.7.8)$$

In Equation 7.7.7 we have used transformation 1.6.8. The coefficients j_i are introduced formally in order to indicate in what follows the terms to be neglected in one or another

approximation, while the fictitious terms Q_i will be used in Section 7.13; until then we let all $Q_i = 0$. For the original system of equations all $j_i = 1$.

We will evaluate the orders of individual terms of these equations based on the estimates 7.7.4 for the shock wave

$$\begin{aligned} u \frac{\partial u}{\partial x} &\sim U_\infty^2 K_s^2 l, & \frac{1}{\rho} \frac{\partial p}{\partial x} &\sim \frac{k}{\rho_\infty} U_\infty^2 K_s^2 l \\ u \frac{\partial v}{\partial x} &\sim U_\infty^2 K_s^2 (K - K_s) l^2, & u^2 K &\sim U_\infty^2 K_s^2 K l^2 \\ v \frac{\partial v}{\partial y} &\sim \frac{1}{\delta} U_\infty^2 [k + K_s(K_s - K)l^2]^2 \\ \frac{u}{\rho a^2} \frac{\partial p}{\partial x} &\sim U_\infty K_s^2 l, & \frac{\partial u}{\partial x} &\sim U_\infty K_s \end{aligned} \quad (7.7.9)$$

For moderately blunt bodies the first two terms on the left-hand side of Equation 7.7.6 are small as compared with the last term and can be omitted; this leads to a fundamental—as will be seen later—simplification of the system of equations of motion, which is derived from the original system for

$$j_2 = 0, \quad j_1 = j_2 = j_3 = j_5 = 1 \quad (7.7.10)$$

These equations play an important role in hypersonic flow theory and are called the *thin shock layer equations*.

Equating j_1 , j_2 , and j_4 to zero and j_3 and j_5 to unity we obtain the limiting Newtonian solution of Section 7.5. However, in this case the terms with the longitudinal pressure gradients are retained, since otherwise we would obtain zero velocities on the body surface instead of finite ones of the order of $u \sim k^{1/2}$, that is, precisely the shortcoming that should be remedied. From the first two estimates, 7.7.9, it follows that the ratio of these terms is of the order of k near the shock, that is, the role of the pressure gradient is essential only within a small wall sublayer with relative velocities $u/u_s \sim k^{1/2}$. Moreover, the Newtonian approximation is qualitatively inadequate in the vicinity of the axis of symmetry where there always exists a domain of extent l_k and flow rate ψ_k ; the orders of two last quantities are as follows

$$K_s l_k \leq k, \quad \psi_k \leq \psi_0 k^{1+\nu}, \quad \psi_0 = \pi^\nu \rho_\infty U_\infty^2 R_s^{1+\nu} \quad (7.7.11)$$

where, in accordance with 7.7.4, the condition $v \ll u$ is not fulfilled and the streamlines are not parallel to the shock. Precisely this domain, specified by the condition 7.7.2 $K_s^2 l^2 \ll 1$, will be considered in the following.

From the comparison of the two last estimates in 7.7.9, it follows that the terms with pressure gradients in Equation 7.7.7 have the relative order $K_s^2 l^2$ and can be thus omitted. Thus, in what follows we set $j_3 = 0$. In this case the density can vary along the axis only due to the presence of heat sources or physicochemical processes responsible for the term Q_{eff} in Equation 7.7.7. However, we shall deal for a moment only with flows for which $Q_{\text{eff}} \equiv 0$ (the general case will be considered in Section 7.9). In this case there is no need in Equation 7.7.8, so that it will be put aside for the present.

It should be noted that this *incompressibility* of the gas is due to the increase in the stagnation density along the shock, $\rho'_0 = \rho'_0(s)$, with the subsequent small Mach number variation ΔM^2 along a streamline in this vicinity, rather than by small local Mach numbers M in the sense of the dependence $\rho/\rho'_0 = 1 - 1/2M^2$ for isentropic flows (Section 2.2). The previously-mentioned shock vicinity can contain supersonic regions as well. In fact, at the sonic point

on the shock we have $x/R \approx \omega_{s*} \sim k^{1/2}$ (Section 7.3), so that as $k \rightarrow 0$, the subsonic region on the shock can be submerged in the region $x \ll R_s$, in which the theory under consideration is applicable, since the smallness parameters k and x/R are independent of this region.

We will further simplify the equations setting in them $H_x = 1 + Ky \approx 1$ and omitting the term uv/R in Equation 7.7.5, which is small compared with the term $v\partial u/\partial y$. Bearing in mind this assumption, we are now coming to the construction of the solution in the vicinity of the axis of symmetry of a blunt body of relative extent $K_s l \ll 1$ and $kl \ll 1$. We will retain for a time the factor j_2 in Equation 7.7.6 in order to be able to analyze the role of this term and let the other j_i be equal to unity.

In view of these assumptions, setting $l = x$ in 7.7.2 and 7.7.4 we obtain the first terms of the series expansions of the unknown functions at the shock

$$\begin{aligned} p_s &= \rho_\infty U_\infty^2 [1 - K_s^2 x^2 + O(x^4)] \\ u_s &= U_\infty \{K_s x + O[x^3 + k(K_s - K)x]\} \\ -v_s &= U_\infty \{k + K_s(K_s - K)x^2 + O[x^4 + k(K_s - K)^2 x^2]\} \end{aligned} \quad (7.7.12)$$

The shock shape is determined from 7.7.2, δ being the shock layer thickness at the axis

$$dy_s/dx = \omega - \omega_s, \quad y_s = \delta + \frac{1}{2}x^2(K - K_s) + O(x^4) \quad (7.7.13)$$

Then we seek the solution of the problem in the form of the following expansions

$$\begin{aligned} v &= -U_\infty [kf_0(\zeta) + K_s(K_s - K)x^2 f_2(\zeta) + \dots] \\ u &= U_\infty K_s x f_1(\zeta) + \dots, \quad p = \rho_\infty U_\infty^2 [p_0(\zeta) - K_s^2 x^2 p_2(\zeta) + \dots] \\ \rho &= \frac{\rho_\infty}{k} [\rho_0(\zeta) + K_s^2 x^2 \rho_2(\zeta) + \dots] \\ r &= x + O(x^3), \quad \zeta = y/\delta \end{aligned} \quad (7.7.14)$$

From the equation valid on the axis, $\rho v \partial v / \partial y = -\partial p / \partial y$, at a constant density $\rho = \rho_\infty/k$ we obtain the same Bernoulli equation as Equation 3.6.5

$$\begin{aligned} p'_0 &= -kf_0 f'_0, \quad p_0(1) = 1 - k, \quad f_0(1) = 1 \\ p_0 &= 1 - \frac{1}{2}k - \frac{1}{2}kf_0^2 \end{aligned} \quad (7.7.15)$$

Since $f_0 \sim 1$, we have $p_0 - 1 \sim k$, that is within the accuracy of our theory we have $p_0 = 1$ and $\rho_0 = 1$.

Substituting expansion 7.7.14 in the continuity Equation 7.7.7 and equating the sum of the terms of the order x to zero, we obtain the first relation between the unknown functions

$$\lambda(1 + \nu)f_1 = \frac{df_0}{d\zeta} = f'_0, \quad \lambda = \frac{\delta}{kR_s} \quad (7.7.16)$$

In terms of this relation, Equations 7.7.5 and 7.7.6 give

$$(f'_0)^2 - (1 + \nu)f_0 f''_0 = 2(1 + \nu)k\lambda^2 p_2 \quad (7.7.17)$$

$$\lambda(1 + \nu)^2 p'_2 = -R_s K (f'_0)^2 + j_2 \lambda R_s (K_s - K) [(1 + \nu)^2 (f_0 f_2)' - 2(1 + \nu) f'_0 f_2] \quad (7.7.18)$$

The function ρ_2 does not enter in these equations, so that in this approximation the gas density can be assumed to be constant in the equations of motion as well.

Boundary conditions 7.7.4 should be transferred from the shock y_s to the line $\zeta = y/\delta = 1$, since the functions f_0 and others no longer depend on x . To do this, we should use the procedure described at the end of Section 2.4, that is, the expansions

$$\begin{aligned} -\frac{v_s}{U_\infty} &= kf_0(1) + \frac{k}{\delta}f'_0(1)(y_s - \delta) + K_s(K_s - K)x^2f_2(1) + \dots = \\ &\quad k + K_s(K_s - K)x^2 \\ \frac{p_s}{\rho_\infty U_\infty^2} &= p_0(1) + \frac{1}{\delta}p'_0(1)(y_s - \delta) + x^2K_s^2p_2(1) = \\ &\quad 1 - K_s^2x^2 + \dots \end{aligned} \quad (7.7.19)$$

At the same time, the similar procedure for the velocity u or the function f_1 affects only higher-order terms, which have not been taken into account. Therefore, in view of the relation $p'_0(1) = -kf'_0(1)$ and expansions 7.7.13 for y_s , we obtain the following boundary conditions for the unknown functions

$$\begin{aligned} \zeta = 1, \quad f_0 = 1, \quad f'_0 = \lambda(1 + \nu), \quad f_2 &= \frac{3 + \nu}{2} \frac{K_s - K}{K_s} \\ p_2 &= 1 + \frac{1 + \nu}{2} \frac{K_s - K}{K_s} \\ \zeta = 0, \quad f_0 = f_2 = 0 \end{aligned} \quad (7.7.20)$$

We note the crucial point of the theory outlined: the system of the two Equations 7.7.17 and 7.7.18 thus obtained contains three unknown functions, f_0 , f_2 , and p_2 , as well as two unknown parameters, K_s and δ , so that conditions 7.7.20 are insufficient for determining them. We note that the function f_2 can be got rid of by neglecting the term dv/dt in Equation 7.7.6, that is, putting $j_2 = 0$ in that equation. However, this does not resolve the problem of determining the parameters K_s and δ . But for moderately blunt bodies, $|K_s - K| \ll K$, the last term in Equation 7.7.18 could be omitted, together with the function f_2 , so that the system becomes resolvable. Then the four boundary conditions, 7.7.20, for the third-order system of equations make it possible to determine also the parameter λ or, for $K_s = K$, the value of δ .

In the general case, the procedure of determining the subsequent terms of the series in x results in the appearance of new unknown functions f_3, f_4 , and so on, and the higher-order derivatives of the shock curvature. In other words, these series are not recurrent and the previously-mentioned problem of the solvability of the equations is simply displaced to next approximations. The series could be done recurrently only by *truncating* them, that is, by discarding the subsequent terms by an act of will, though based upon the assumptions of one or other type.

Nevertheless, the truncated series method in the first approximation, as outlined previously, is widely used in hypersonic aerodynamics when studying the influence of various gas dynamic and physical factors on the flows in shock layers near stagnation points or attachment lines on the windward side of bodies. Some of these problems will be discussed in Sections 7.8 to 7.11.

7.8 Constant-Density Flow in the Vicinity of the Axis of Symmetry of a Blunt Body

The formulation of this problem was given in preceding sections; within the framework of the truncated series method for a flow the system of the governing Equations 7.7.17 and 7.7.18 was derived for the coefficients of expansions 7.7.14. For moderately blunt bodies (sphere, etc.) we can set $j_2 = 0$ in these equations, thus closing the system. Moreover, we take into account that the right-hand side of Equation 7.7.17 is essential only in the wall sublayer; therefore, we set there $p_2 = p_2(0) = \beta$, where a constant β is as yet unknown. Thus, the problem is reduced to the system of equations (Li and Geiger, 1957)

$$(f'_0)^2 - (1 + \nu)f_0 f''_0 = 2(1 + \nu)^2 k \lambda^2 \beta \quad (7.8.1)$$

$$\lambda(1 + \nu)^2 p'_2 = -R_s K (f'_0)^2, \quad \lambda = \delta/k R_s \quad (7.8.2)$$

These equations must be solved subject to the conditions

$$\zeta = 0 \quad f_0 = 0, \quad \zeta = 1 \quad f_0 = p_2 = 1, \quad f'_0 = \lambda(1 + \nu) \quad (7.8.3)$$

The additional boundary condition imposed on f_0 serves for determining the shock layer thickness $\delta = \lambda k R_s$ which is as yet unknown.

In view of the equality $2f''_0 = d(f'_0)^2/d\zeta$, we transform Equation 7.8.1 to a linear equation with respect to the function $f'_0(f)$ having the integral

$$\frac{u}{u_s} = \frac{f'_0}{\lambda(1 + \nu)} = [2k\beta + (1 - 2k\beta)f_0^{2/(1+\nu)}]^{1/2} \quad (7.8.4)$$

This solution gives the velocity distribution $u(\psi)$ in the stream function $\psi = f_0 \psi_s$, which coincides with 7.5.3 for $k = 0$. Clearly, the terms of the order k are essential only in the sublayer $f_0 \leq k^{(1+\nu)/2}$, as indicated in Section 7.5. Omitting these terms we obtain the solution

$$p_2 - \beta = -\frac{R_s}{(2 + \nu)R} f_0^{(2+\nu)/(1+\nu)}, \quad \beta = p_2(0) = \frac{3 + \nu}{2 + \nu} \quad (7.8.5)$$

Here, β is the same as in Equation 7.5.5. Differentiating Equation 7.8.1 we obtain

$$(1 - \nu)f'_0 f''_0 = (1 + \nu)f_0 f'''_0, \quad f'_0(0) = \lambda(1 + \nu)\sqrt{2k\beta} \quad (7.8.6)$$

The additional condition for $f'_0(0)$, which is required due to the increase in the order of the equation, is derived from the original equation at $\zeta = 0$.

A further course of solution differs for two-dimensional and axisymmetric flows. Thus, for $\nu = 0$ we have

$$f_0 f'''_0 = f'_0 f''_0, \quad f''_{0\pm} = \pm \kappa^2 f_{0\pm} \quad (7.8.7)$$

Here, κ is an arbitrary constant. The latter equation has a solution satisfying the condition $f_0(0) = 0$

$$f_{0+} = \frac{1}{2} C(e^{\kappa\zeta} - e^{-\kappa\zeta}), \quad f_{0-} = C \sin \kappa\zeta \quad (7.8.8)$$

Here, C is a constant.

However, for small k the other conditions could not be satisfied by means of the latter solution. In fact, the conditions for f'_{0-} having been satisfied at $\zeta = 0$ and 1, we obtain for κ

the equation $\sqrt{2\beta k} \cos \kappa = 1$, which has no solutions at $2\beta k < 1$. Therefore, for small k only the first solution, $f_0 = f_{0+}$, is valid.

From the boundary conditions 7.8.3 and 7.8.6 it follows

$$\kappa C = \lambda \sqrt{2\beta k}, \quad C \sinh \kappa = 1, \quad \lambda = C \kappa \cosh \kappa, \quad \sqrt{2\beta k} \cosh \kappa = 1 \quad (7.8.9)$$

The latter equation can be brought to a quadratic equation with respect to e^κ . For $k \ll 1$ the solution of this equation has the form:

$$e^\kappa = \frac{1 + \sqrt{1 - 2k\beta}}{\sqrt{2k\beta}} \approx \frac{2}{\sqrt{2k\beta}}, \quad C = \sqrt{2k\beta} \quad (7.8.10)$$

$$\lambda = \frac{\delta}{kR_s} = \frac{1}{2} \ln \frac{2}{k\beta}, \quad \beta = \frac{3}{2} \quad (7.8.11)$$

The minus sign in front of the radical sign in the upper formula has been omitted, since from the first two equations of 7.8.9 it follows that $\kappa > 0$. Thus, in view of 7.8.10, the solution takes the form:

$$f_0 = \sqrt{2k\beta} \sinh \kappa \zeta = \sqrt{\frac{k\beta}{2}} (e^{\kappa\zeta} - e^{-\kappa\zeta}) = \\ \left(\frac{1}{2} \beta k \right)^{(1-\zeta)/2} - \left(\frac{1}{2} \beta k \right)^{(1+\zeta)/2} \quad (7.8.12)$$

In the axisymmetric case ($\nu = 1$) Equation 7.8.6 has a solution satisfying conditions of Equation 7.8.3 and the condition for $f'_0(0)$

$$\lambda = \delta/kR_s = (1 + \sqrt{2k\beta})^{-1}, \quad \beta = 4/3 \quad (7.8.13)$$

$$f_0 = \frac{2\sqrt{2k\beta}}{1 + \sqrt{2k\beta}} \zeta + \frac{1 - \sqrt{2k\beta}}{1 + \sqrt{2k\beta}} \zeta^2 \quad (7.8.14)$$

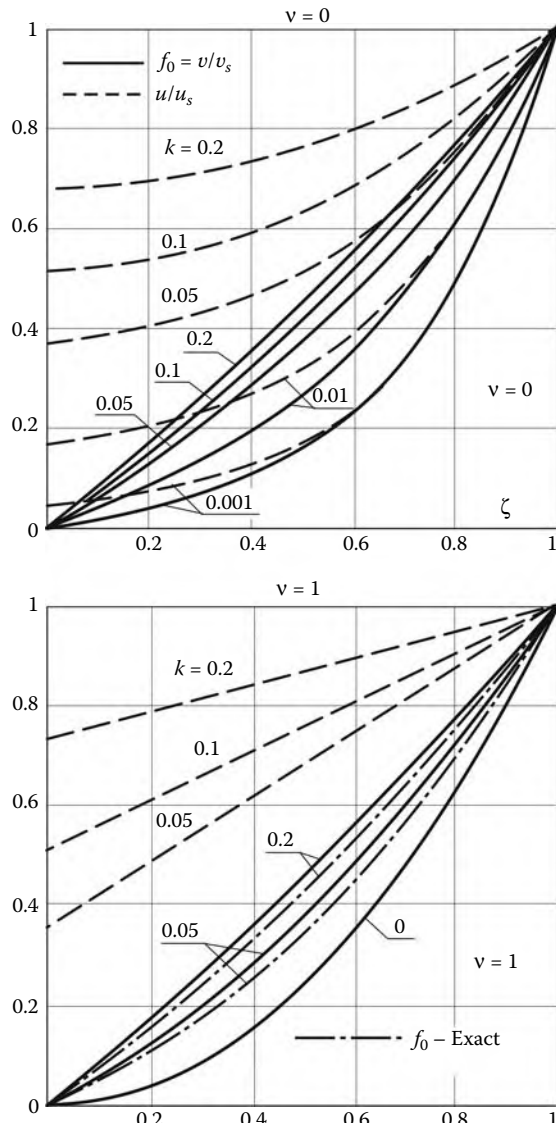
The profiles of the normal (f_0) and tangential ($u/u_s = f'_0/(1 + \nu)\lambda$) velocity components thus obtained for two-dimensional and axisymmetric flows are presented in Figure 7.23. In the same figure we have plotted the exact curves for f_0 , which are close to approximate ones. For $\nu = 1$ the limiting (as $k \rightarrow 0$) u/u_s profile is independent of the wall pressure gradient and corresponds to the purely Newtonian flow. However, for two-dimensional flows a k -dependence exists always. At the same time, on a realistic range $k = 0.05 - 0.2$ the u/u_s profiles are near-linear and depend on k only slightly.

We note that in an immediate vicinity of the wall both velocity components are linear: $u = ax$ and $v = -(1 + \nu)ay$, as was assumed in Section 2.11 in constructing streamlines in the vicinity of the stagnation point. In our case $a = \sqrt{2k\beta}U_\infty K_s$.

For $\nu = 0$ the tangential velocity is near-constant near the body, while for $\nu = 1$ it is linear everywhere. This crucial difference is due to the vortex behavior in the vicinity of the attachment line or point

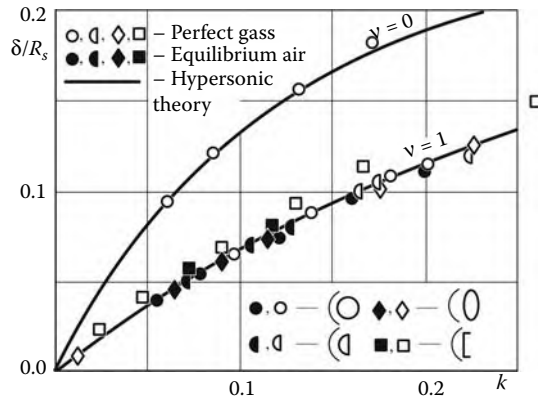
$$\Omega = \frac{\partial v}{\partial x} - \frac{\partial u}{\partial y} \approx -\frac{\partial u}{\partial y} = -\frac{xK_s^2 U_\infty f''_0}{\lambda^2(1 + \nu)k} \quad (7.8.15)$$

The vorticity grows as k decreases; however, for $\nu = 0$, in accordance with 7.8.7 we have $f''_0(0) = 0$ and $\Omega = 0$ on the wall; then, in accordance with the vortex conservation theorem, this property can be extended to the entire surface of a blunt body.

**FIGURE 7.23**

Velocity profiles between the body and the shock in the vicinity of the axis of symmetry of a blunt body.

Although the solution obtained is valid for moderately blunt bodies, it is more general than that. In fact, Equation 7.8.1 depends on Equation 7.8.2, or on the more general Equation 7.7.18, only in terms of the quantity β , which enters in the small term of the order k , though it itself is of the order of unity. Therefore, letting $\beta = 1$ we can give a more universal, though more approximate, form to our results. That this assertion is correct is demonstrated by Figure 7.24, in which the k -dependences of δ/R_s for bodies of different shape, including a disk, are close to the curves determined by formulas 7.8.10 and 7.8.13 with $\beta = 1$ let in

**FIGURE 7.24**

Bow shock stand-off distance referred to its radius of curvature for different bodies.

them

$$\frac{\delta}{kR_s} = \frac{1}{2} \ln \frac{2}{k} \quad (\nu = 0), \quad \frac{\delta}{kR_s} = \frac{1}{(1 + \sqrt{2k})^{1/2}} \quad (\nu = 1) \quad (7.8.16)$$

For moderately blunt bodies we can further take $R_s = R$, which was actually assumed from the beginning. The ratios δ/kR taken in this form are plotted as dotted curves in Figure 7.13. Their accuracy is satisfactory for axisymmetric flows; however, for two-dimensional flows on the realistic range $k = 0.05 \div 0.2$ the error is considerable, as well as the error of the assumption that $R_s = R$.

Finally, the results obtained make it possible to evaluate the small parameter ε in formula 7.7.1

$$\varepsilon \sim -k \ln k \quad \nu = 0, \quad \varepsilon \sim k \quad \nu = 1 \quad (7.8.17)$$

However, actually we have $-\ln k = 1.5 \div 3$ for $k = 0.2 \div 0.05$, so that for $\nu = 0$ particular significance should not be attached to different asymptotics for k and ε .

These previous results are related with the case of a uniform oncoming flow and a constant density in the near-axis region. In the following we will consider more complicated flows starting from *nonuniform flow* past bodies. This problem was touched on in Sections 7.1 and 7.2. In those sections we showed the determining role played by the effective curvature of a body $K_{\text{eff}} = m + K$, where $m = \partial\varphi/\partial x$ is the derivative of the angle of inclination of the external streamline and $R^{-1} = K = K_s$ are the body and shock curvatures near the stagnation point. In a divergent flow, for example a jet flow, the gas density decreases in accordance with the $\rho \sim h^{-2}$ law, h being the distance to the effective pole of the source (Section 2.3). Therefore, the variation of the external density along the body or the shock, $\Delta\rho/\rho = -2\Delta h/h$, leads to the expansion

$$\rho_\infty = \rho_{\infty 0}(1 - bx^2), \quad b = (m + K_s)m, \quad m = h^{-1} \quad (7.8.18)$$

We will discard the similar variation of the absolute magnitude of the velocity assuming the flow to be hypersonic, $U \approx U_\infty$. Then for the functions behind the shock in the flow past a moderately blunt body instead of 7.7.12 we obtain

$$\begin{aligned} u_s &= U_\infty \sin(\omega + \varphi) = U_\infty x K_{\text{eff}}, & v_s &= -kU_\infty \\ p_s &= \rho_\infty U_\infty^2 (1 - K_{\text{eff}}^2 \beta_s x^2), & \beta_s &= 1 + bR_{\text{eff}}^2 \end{aligned} \quad (7.8.19)$$

Using then expansions 7.8.14 with the curvature K_s replaced by K_{eff} , we obtain eventually the same Equation 7.8.1 with the same solution involving the parameter $\lambda_{\text{eff}} = \delta K_{\text{eff}}/k$ instead of λ and the same formulas 7.8.11 and 7.8.13 to determine it. Since all these formulas depend on β only slightly, the shock layer thickness is governed, first, by the effective curvature K_{eff} (as it is in the estimates given at the end of Section 7.1) and only to a slight degree depends on the coefficient b in the density expansion.

In Figure 7.25 the exact ratios δ/kR for the axisymmetric underexpanded jet flow past a sphere are presented for the same conditions as in Figure 7.6. The curves are plotted against k or the ratio $R/h = mR$ (Lunev and Khramov, 1970). There is no regular trend in the behavior of these curves; however, when plotted versus the ratio δ/kR_{eff} , they form a unique k -dependence determined by formula 7.8.16 (the data for a flat plate with $K = 0$ also obey this dependence).

Equation 7.8.2 with λ_{eff} substituted for λ and subject to the condition $p_2(1) = \beta_s$ has the solution

$$p_2(0) = \beta = \beta_s + \frac{1}{2 + v} \frac{K}{K_{\text{eff}}} \quad (7.8.20)$$

Generally speaking, the quantity β is dependent on b and K but actually the assumption $\beta = 1$ made previously is in agreement with the universal character of the curves $p(\omega)$ in Figure 7.6.

We will now consider the problem of *weak injection* of a gas through the surface of a body in a gas flow; the injected gas density, normal velocity, and speed of sound are ρ_w , v_w , and a_w , respectively. We will assume the relative thickness of the injected gas sublayer to be small, $\delta_w/R \ll 1$, so that both the interface $y = \delta_w(x)$ between the injected and outer gases and the bow shock fit close to the body, their curvatures being the same: $K_s = K_w = K$. This can be injection through the porous surface of a body or due to material evaporation under the action of radiation of an overheated shock layer. As earlier, the pressure induced by the hypersonic outer flow past the outer boundary of the injected gas acts on this surface and leads to gas spreading in the injected gas sublayer. In the vicinity of the stagnation point this pressure is $p = \rho_\infty U_\infty^2 (1 - K_s^2 \beta x^2)$, the coefficient β being the same as in the absence of injection; we will assume that β is constant across the sublayer.

In the inner sublayer the gas motion equations are the same as in the shock layer. On the interface the impermeability conditions must be fulfilled for both flows. On the body surface the normal velocity component is preassigned, while the tangential component is

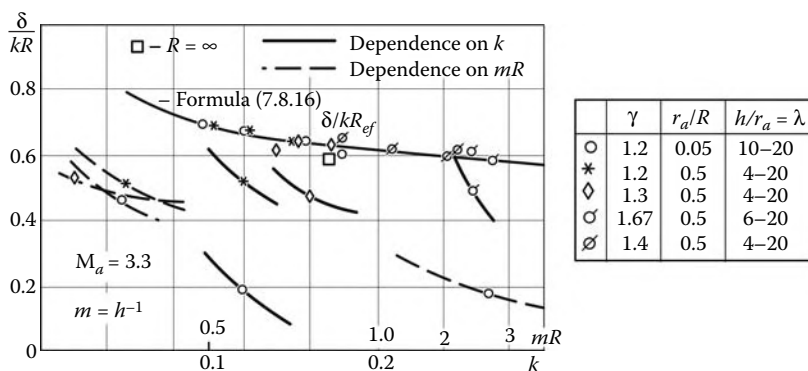


FIGURE 7.25
Shock layer thickness on a sphere in underexpanded jet flowfields.

set to be zero. As previously, we present the solution for the sublayer in the form:

$$v = v_w f_0(\zeta), \quad u = a_w K x f_1(\zeta), \quad \zeta = y/\delta_w \quad (7.8.21)$$

Substituting these expressions in the equations of motion we obtain a system of equations similar to 7.8.16, 7.8.17, and boundary conditions

$$\begin{aligned} f'_0 &= -(1 + \nu) \lambda_w f_1, & \lambda_w &= \delta_w K / M_w, & M_w &= \frac{v_w}{a_w} \\ (f'_0)^2 - (1 + \nu) f_0 f''_0 &= \frac{2}{\gamma_w} \lambda_w^2 (1 + \nu)^2 \beta, & \gamma_w &= a_w^2 \rho_w / p \\ \zeta = 0 \quad f'_0 &= 0, \quad f_0 = 1; & \zeta = 1 \quad f_0 &= 0 \end{aligned} \quad (7.8.22)$$

The problem has the solution (for $\nu = 0$, solution 7.8.7 of the type f_{0+} does not satisfy the boundary conditions)

$$\begin{aligned} \nu = 1 : \quad f_0 &= 1 - \zeta^2, & \lambda_w &= \left(\frac{\gamma_w}{2\beta} \right)^{1/2} \\ \nu = 0 : \quad f_0 &= \cos(\pi \zeta / 2), & \lambda_w &= \frac{\pi}{2} \left(\frac{\gamma_w}{2\beta} \right)^{1/2} \end{aligned} \quad (7.8.23)$$

The relative thickness of the sublayer $\delta_w K \sim M_w$ is small for $M_w \ll 1$; precisely this is the condition of the applicability of the solution obtained. For example, for a sphere $\beta = 1.17$ (see Section 7.2), so that for $\gamma_w = 1.4$ we obtain $\delta_w = 0.77 R M_w$.

We will also compare the tangent velocities on either side of the constant surface; to do this, we refer the subscripts 1 and 2 to the outer and inner layer parameters and write down the relation

$$\frac{u_1}{u_2} = \frac{U_\infty \sqrt{2\beta k}}{a_w \sqrt{2\beta/\gamma_w}} = \frac{U_\infty \sqrt{\gamma_w k}}{a_w} \approx \frac{a_*}{a_w} \quad (7.8.24)$$

where a_* is the critical speed of sound in the outer gas. If both counterstreaming gases are perfect and the same, then for $M_\infty \gg 1$ we obtain $u_1/u_2 \approx (T_0/T_w)^{1/2}$, where T_0 and T_w are the stagnation temperatures of the outer and injected flows. Since in hypersonic atmospheric flight we usually have $T_0 \geq T_w$, that is, making allowance for viscosity, we obtain that the inner flow is ejected by the outer flow. We note that the solution obtained is physically plausible only in the case in which the injected layer thickness is considerably greater than the thicknesses of the viscous mixing zone and the boundary layer, which are of the order $\delta \sim R \cdot Re^{-1/2}$, where Re is the Reynolds number (see Section 1.16).

7.9 Variable-Density Flow along the Axis of Symmetry

In the previous examples the constancy of the density along the axis of symmetry in a hypersonic shock layer was due to the constancy of the pressure and the isentropic nature of the flow. However, in hypersonic real gas flows this is the exception rather than the rule, since the gas density can vary due to radiative change of the temperature or chemical reactions (see Chapters 10 to 14). Gas dynamic features of these flows are considered in the following.

We will make it with reference to a very simple example of a nonisentropic process described by the equation $dh/dt = q$. At $q = q(h)$ this equation has the integral

$$\int_h^{h_s} \frac{dh}{q} = \int_y^\delta \frac{dy}{v} = -t \quad (7.9.1)$$

We recall that in the coordinate system adopted in the preceding sections the y axis is directed from the body counter to the flow, so that $v < 0$ and the gas inflows to the layer at the point $y = \delta$ with the initial enthalpy $h = h_s$.

Here, the function t has the meaning of the time it takes a gas particle to travel from the shock to the stagnation point. Since $t > 0$, we have $h > h_s$ for $q > 0$ and $h < h_s$ for $q < 0$. In the general case, this is not a solution of Equation 7.9.1, since the functions q and v are not defined. However, there follows an important conclusion: setting $v = -v_0 y/R$ in the vicinity of the stagnation point, v_0 and R being scale constants, we obtain

$$t = -(R/v_0) \ln(y/R) + \text{const} \rightarrow \infty, \quad y/R \rightarrow 0 \quad (7.9.2)$$

Therefore, the integral t must also be singular as $y \rightarrow 0$. However, this is possible only provided that $q \rightarrow 0$ as $y \rightarrow 0$, that is, the stagnation point is the point of thermal equilibrium of the flow. Neglecting this factor in the physical formulation of the problem can lead to physically unrealistic results. Thus, for a constant q we have $h - h_s = qt$, so that as $t \rightarrow \infty$ we obtain either $h \rightarrow \infty$ when $q > 0$ (heating) or zero temperature $T = T_0$ at a certain point $y = y_0$ when $q < 0$; the continuation of the solution beyond this point has no physical meaning.

This problem will be considered in Chapter 14; here we will dwell only on the flowfield description in the problems with a variable density without specifying the reasons producing this variability (Lunev, 1971). It can be easily shown that the density variation does not alter the estimates for the orders of velocities and pressure differences and does not prevent using expansions 7.7.14. In particular, it is obvious that, as before, the term ρ_2 does not enter in the analogs of Equations 7.7.16 through 7.7.18 (with $j_2 = 0$), while the terms with the pressure gradient in the continuity Equation 7.7.7 can be omitted. However, in the latter equation the right-hand side Q does not vanish; this quantity enters in the relation between the functions f_1 and f_0 , thus making the form of the subsequent equations much more complicated. However, we will introduce a new variable (*Dorodnitsyn variable*, 1940) and the function

$$\eta = \int_0^y \rho_0 dy, \quad \zeta = \frac{\eta}{\eta_\delta}, \quad \rho_0 = \frac{\rho k}{\rho_\infty}, \quad \rho_0 v = -k U_\infty f_0(\zeta) \quad (7.9.3)$$

Then from the continuity equation simplified for a thin shock layer

$$\frac{\partial \rho u x^\nu}{\partial x} + \frac{\partial \rho v x^\nu}{\partial y} = 0 \quad (7.9.4)$$

we derive the earlier expression for the tangential velocity

$$\bar{\lambda}(1+\nu)u = xU_\infty f'_0, \quad \bar{\lambda} = \eta_\delta K_s/k \quad (7.9.5)$$

Thence, under the same assumptions as in Section 7.8, instead of Equation 7.8.1 we obtain the equation

$$(f'_0)^2 - (1+\nu)f_0 f''_0 = 2(1+\nu)^2 \bar{\lambda}^2 k \beta / \rho_0 \quad (7.9.6)$$

which differs from Equation 7.8.1 only by a variable density $\rho_0 \neq 1$ on the right-hand side; the latter is of the order of k and is essential only in the wall sublayer with small f_0 . We write down an analog of integral 7.8.4 for this equation

$$\begin{aligned} f'_0 &= \bar{\lambda}(1+\nu)(f_0^{2/(1+\nu)} + 2k\beta/\tilde{\rho}_0)^{1/2} \\ \frac{1}{\tilde{\rho}_0} &= \frac{1+\nu}{2}f_0^{2/(1+\nu)} \int_{f_0}^1 \frac{1}{\rho_0} f_0^{-(3+\nu)/(1+\nu)} df_0 \end{aligned} \quad (7.9.7)$$

Equation 7.9.6 or 7.9.7 must be closed by the following equations:

$$\begin{aligned} \rho_0 &= \rho_0(h_0), \quad f_0 \frac{dh_0}{d\zeta} = f'_0 f_0 \frac{dh_0}{df_0} = -q_0 \\ h_0 &= 2h/U_\infty^2, \quad q_0 = 2q\eta_\delta/(U_\infty^3 k) \end{aligned} \quad (7.9.8)$$

Eliminating f'_0 from these equations via 7.9.7, we obtain for $q = q(h)$ an integro-differential equation for the function $h_0(f_0)$. However, this equation also has no simple solutions and, for this reason, we will restrict ourselves to a qualitative analysis of the problem and some numerical examples.

Integral 7.9.7 is improper; if the function ρ_0 is bounded when $f_0 \rightarrow 0$, which will be assumed in what follows, then passing to the limit for small f_0 we obtain $\tilde{\rho}_0 = \rho_0$. Then for small f_0 formula 7.9.7 takes the form:

$$f'_0 = \bar{\lambda}(1+\nu)\sqrt{2k\beta/\rho_0} \quad (\rho_0 f_0^{2/(1+\nu)} \ll 2k\beta) \quad (7.9.9)$$

Here, the inequality determines the applicability range of the solution. Substituting it in Equation 7.9.8 and letting from physical considerations $q = c(h_{0e} - h_0)$, where $h_{0e} = h_0(0)$, $c > 0$, we obtain, as $f_0 \rightarrow 0$, the asymptotics $h_e - h \sim f_0^\alpha$, where $\alpha = c/f'_0(0) > 0$.

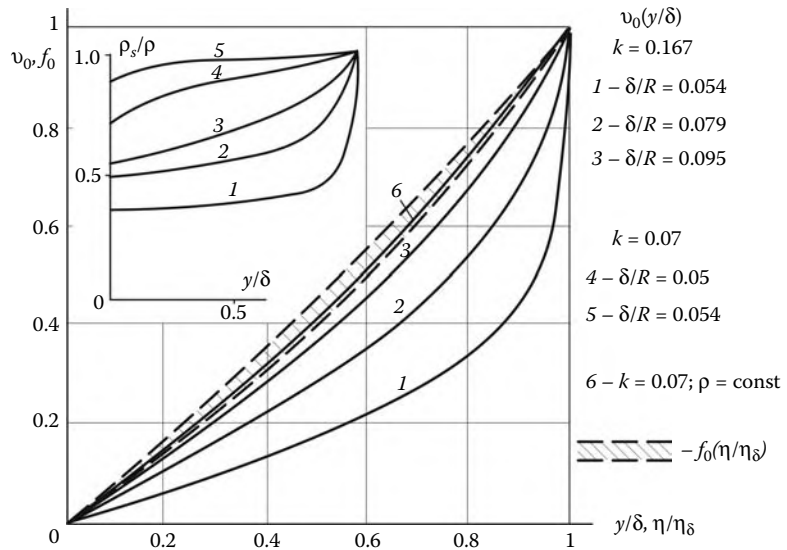
Outside this wall sublayer, integral 7.9.7 has the same form $f'_0 = \lambda(1+\nu)f_0^{1/(1+\nu)}$ as in Section 7.8; thus, Equation 7.8.2 has the earlier solution for $p_2(\zeta)$ with the same $\beta = (3+\nu)/(1+\nu)$.

Replacing then ρ_0 in 7.9.6 by an appropriate mean value $\bar{\rho}_0$, we arrive at the earlier solution, with $k_0 = k/\bar{\rho}_0$ substituted for k . The same relations determine the generalized thickness of the shock layer

$$\begin{aligned} \nu = 0 : \quad \frac{\eta_\delta}{kR_s} &= \frac{1}{2} \ln \frac{2}{\beta k_0} \\ \nu = 1 : \quad \frac{\eta_\delta}{kR_s} &= \frac{1}{1 + \sqrt{2\beta k_0}} \end{aligned} \quad (7.9.10)$$

In Figure 7.26 we have plotted the exact velocity profiles $v_0(y/\delta) = -v/U_\infty k$ for a sphere in the original coordinates corresponding to the density profiles ρ_s/ρ presented in the same figure and pertinent to both radiating and chemically nonequilibrium gases. They diverge considerably; however, in the f_0, ζ variables they converge to a narrow bundle. The shock layer thicknesses for the same cases also differ significantly: $\delta/kR_s = 0.3 \div 0.8$; however, the corresponding generalized thicknesses turn out to be close to the same quantity $\eta_\delta \approx 0.8kR_s$ as in the case of a constant density (Section 7.3).

This result has the meaning of a similarity law declaring the universality of the solution in the Dorodnitsyn variables for various density profiles between the shock and the body

**FIGURE 7.26**

Density and velocity profiles along the axis of symmetry in the chemically nonequilibrium flow (curves 1–3) and in the equilibrium radiation flow (curves 4 and 5) past a sphere.

in the vicinity of the axis of symmetry of a blunt body. However, within the wall sublayer this result is incorrect and, in view of 7.9.7, the velocity profiles depend directly on the density profiles.

In conclusion, setting the parameter k_0 to be constant and using the solution of Section 7.8 for the function f_0 we express time t in terms of the variable ζ

$$\begin{aligned} \frac{U_\infty t}{R_s} &= -\frac{U_\infty}{R_s} \int_y^\delta \frac{dy}{v} = \frac{\eta_\delta}{k R_s} \int_0^1 \frac{d\varphi}{\varphi_0} = \frac{\ln \varphi_v}{2(1+\nu)a}, \quad a = \sqrt{\frac{\beta k_0}{2}} \\ \varphi_0 &= \frac{(1-a)(1+a^\zeta)}{(1+a)(1-a^\zeta)}, \quad \varphi_1 = \frac{4a + (1-2a)\zeta}{(1+2a)\zeta} \end{aligned} \quad (7.9.11)$$

Near the stagnation point, as $\zeta \rightarrow 0$, the functions φ_v and t have the following asymptotics

$$\begin{aligned} \varphi_v &\rightarrow \frac{b_v}{\zeta}, \quad b_0 = \frac{2(1-a)}{(1+a)(-\ln a)}, \quad b_1 = \frac{4a}{1+2a} \\ \frac{U_\infty t}{R_s} &\rightarrow \frac{1}{2(1+\nu)a} \left(\ln \frac{1}{\zeta} + \ln b_v \right) \end{aligned} \quad (7.9.12)$$

7.10 Thin Three-Dimensional Shock Layers

In what follows we will make an analysis of the gas flow properties for three-dimensional shock layers under the same limiting conditions 7.1.1 or 7.7.1, as earlier, thus generalizing the previously obtained results.

First, we will show that the streamlines of the limiting flow in a thin shock layer, which coincide with their projections onto the body surface as $\delta \rightarrow 0$, are geodesic lines of the body surface, whose projections on the tangent plane have zero geodesic curvature at each point (see Section 1.13). Let $K_l = R_l^{-1}$ be the normal curvature of a streamline, \vec{n}_e be the principal normal to the streamline lying in its osculating plane, $\vec{\tau}_l$ and $\vec{\tau}_g$ be the tangent and normal unit vectors with respect to the streamline in the plane tangent to the body surface, and \vec{n} be the normal to it. Then the *normal curvature vector* \vec{K}_l has the components

$$\vec{K}_l = K_l \vec{n}_l, \quad (\vec{K}_l \vec{n}) = K, \quad (\vec{K}_l \vec{\tau}_g) = K_g, \quad (\vec{K}_l \vec{\tau}_l) = 0 \quad (7.10.1)$$

Here, K is the *curvature of the normal section* of the body surface, while K_g is the *geodesic curvature* of a streamline on the surface, that is, the curvature of the streamline projection on the plane tangent to the surface.

From formula 2.2.6 it follows that the pressure gradient ∇p projection on the plane normal to the streamline is parallel to the principal normal \vec{n}_p and equal to

$$\vec{n}_l \frac{\partial p}{\partial n_l} = \rho U^2 \vec{K}_l = \rho U^2 (\vec{n} K + \vec{\tau}_g K_g) \quad (7.10.2)$$

Thence it follows

$$\frac{\partial p}{\partial n} = \frac{\rho U^2}{R}, \quad \frac{\partial p}{\partial \tau_g} = \rho U^2 K_g, \quad \frac{1}{R} = K \quad (7.10.3)$$

Comparing the second formula of 7.10.3 and the Newton formula $p \sim \rho_\infty U_\infty^2$ for the flow scale length L in the $\vec{\tau}_g$ direction we obtain

$$\frac{\partial p}{\partial \tau_g} \sim \frac{\rho_\infty U_\infty^2}{L}, \quad L K_g \sim k \frac{U_\infty^2}{U^2} \quad (7.10.4)$$

Thus, for the streamlines on which $U \sim U_\infty$ we have $K_g \rightarrow 0$ as $k \rightarrow 0$, so that in the limit these streamlines actually coincide with the geodesic lines of the surface in the flow, while the principal normal to these coincides with the normal to the surface, as was to be proved. In this case, the initial direction of a streamline and the constant value of the velocity U are determined from the condition on the shock lying on the body in terms of its local angle of attack (for $k \rightarrow 0$, see Section 7.5). Thus, the construction of the limiting flow streamlines is reduced to a purely geometric problem. Then from the first formula 7.10.3 (with n replaced by y) there follows the same Busemann formula 7.2.3; however, in this case each of the streamlines has its own radius of curvature R , in accordance with Section 7.2.

However, this limiting solution is, first, rather cumbersome and, second, as shown in Section 7.5, is inapplicable in the wall layer on a blunt body, in particular, in the vicinities of stagnation points, where the role played by tangential pressure gradients is important. Therefore, bearing in mind the generalization of the results of Sections 7.7 and 7.8 to three-dimensional flows, we will derive the limiting form of the thin shock layer equations.

We will make use of the orthogonal coordinate system x_1, x_2, x_3 introduced in Section 1.13 and let $x_2 = 0$ on the body surface. Then for a thin shock layer on a moderately blunt body with a shock lying on the body, the following simplifications can be made in Equation 1.13.25.

First, all the curvatures K_{ik} of the x_1 and x_3 coordinate lines can be replaced by their values on the body surface $x_2 = 0$. We will write K_1 and K_2 for the principal curvatures K_{12} and K_{32} and K_{1g} and K_{3g} for the geodesic curvatures K_{13} and K_{31} .

Second, we will drop all the terms containing the velocity component normal to the surface, which is of the order $u_2 = v \sim kU_\infty$, except for the terms $v\partial/\partial x_2$ in the convective derivatives, since in the shock layer $\Delta x_2 \sim \delta \sim kR_{\min}$, where $R_{\min} = \min R$.

Third, we will replace the coordinate x_2 by the normal y to the body surface, since their difference is of a higher order of smallness.

Finally, in a thin shock layer we can assume that the scale factor $H_2 = 1$. Then the momentum Equation 1.13.25 takes the form:

$$\begin{aligned} & \frac{u_1}{H_1} \frac{\partial u_i}{\partial x_1} + v \frac{\partial u_i}{\partial y} + \frac{u_3}{H_3} \frac{\partial u_i}{\partial x_3} + u_i u_k K_{1g} - \\ & u_k^2 K_{kg} = -\frac{1}{H_i} \frac{1}{\rho} \frac{\partial p}{\partial x_i}, \quad i = 1 \quad k = 3, \quad i = 3 \quad k = 1 \end{aligned} \quad (7.10.5)$$

$$\rho(u_1^2 K_1 + u_3^2 K_3) = \partial p / \partial y \quad (7.10.6)$$

If θ is the angle between the local velocity vector \vec{U} and the x_1 axis, then $u_1 = U \cos \theta$ and $u_3 = U \sin \theta$; using the *Euler formula* for the curvature of an arbitrary normal section of the surface, $K = K_1 \cos^2 \theta + K_3 \sin^2 \theta$, we can reduce formula 7.10.6 to the first formula 7.10.3.

We are now coming to the solution of the problem of the flow in the vicinity of the central streamline arriving at the stagnation point $x_i = 0$ on a blunt body with two planes of symmetry with coordinates x_1 and x_2 along them and the scale parameters $H_1 = H_3 = 1$.*

Since the shock and the body surface in each plane of symmetry can be locally represented as circles of radii R_1 and R_2 , all the conclusions made in Section 7.7 for the pressure and velocity in two-dimensional flows are valid for these surfaces; as a result, we obtain the following expansions at the shock

$$\begin{aligned} p_s &= \rho_\infty U_\infty^2 (1 - k)(1 - x_1^2 K_{1s} - x_3^2 K_{3s}) \\ u_{is} &= U_\infty x_i K_{is}, \quad k\rho_s = \rho_\infty, \quad v_s = -U_\infty k, \quad y_s = \delta \end{aligned} \quad (7.10.7)$$

As in Section 7.8, in the equation for v it is assumed that $K_{is} = K_i$. As previously, we seek the solution of the problem in the form of truncated series:

$$\begin{aligned} u_i &= U_\infty x_i K_{is} \bar{u}_i(\zeta), \quad v = -U_\infty k f_0(\zeta) \\ p - p_\infty &= \rho_\infty U_\infty^2 [p_0(\zeta) - x_1^2 K_{1s}^2 p_{21}(\zeta) - \\ & x_3^2 K_{3s}^2 p_{23}(\zeta)], \quad \zeta = y/\delta \end{aligned} \quad (7.10.8)$$

The pressure distribution along the axis of symmetry is the same as 7.7.15, so that we assume that $p_0 = 1$. Substituting then expansions 7.10.8 into Equations 7.10.5 and 7.10.6 and into the continuity equation $\operatorname{div}(\rho \vec{U}) = 0$ (with the parameters $H_i = 1$ in the divergence operator 1.13.2) and letting, as in Section 7.7, $\rho = \text{const}$, we obtain a system of ordinary differential equations

$$\lambda_1 \bar{u}_1 + \lambda_3 \bar{u}_3 = f'_0, \quad \lambda_i = \delta K_{is}/k \quad (7.10.9)$$

$$f_0 \bar{u}'_i - \lambda_i \bar{u}_i^2 = -2\lambda_i \beta_i k, \quad \beta_i = p_{2i}(0) \quad (7.10.10)$$

* Lunev and Magomedov (1963).

$$K_{is} p'_{2i} = -\lambda_i K_i \bar{u}_i^2, \quad i = 1, 3 \quad (7.10.11)$$

Here, as for two-dimensional problems, the quantity $p_2(0)$ is replaced by its wall value. The boundary conditions are as follows:

$$\zeta = 0 \quad f_0 = 0, \quad \zeta = 1 \quad f_0 = \bar{u}_i = p_{2i} = 1 \quad (7.10.12)$$

The superfluous (with respect to the order of the system) condition serves for determining the unknown shock stand-off distance. After the change of the variable $d\xi = (f_0/2t)dt$ with $t = 0$ at $\xi = 0$ we obtain the following solution of Equation 7.10.10 and then of Equation 7.10.9

$$\begin{aligned} \bar{u}_i &= \kappa_i \frac{c_i + t^{\mu_i}}{c_i - t^{\mu_i}}, & \mu_i &= \lambda_i \kappa_i, & \kappa_i &= \sqrt{2k\beta_i} \\ f_0 &= c_0 t^{(\mu_1+\mu_3)/2} [(c_1 - t^{\mu_1})(c_3 - t^{\mu_3})]^{-1} \end{aligned} \quad (7.10.13)$$

Here, the condition $f_0(0) = 0$ is fulfilled. Bringing then the point $t = 1$ into coincidence with the shock ($\xi = 1$), from condition 7.10.12 we obtain

$$c_0 = (c_1 - 1)(c_3 - 1), \quad c_i = \frac{1 + \kappa_i}{1 - \kappa_i}, \quad \int_0^1 \frac{f_0}{t} dt = 2 \quad (7.10.14)$$

The latter integral serves for determining δ .

As $k^{1/2} \rightarrow 0$ the solution obtained takes the limiting form:

$$\bar{u}_i = \left(1 - \frac{1}{2} \lambda_i \ln t \right)^{-1}, \quad f_0 = \bar{u}_1 \bar{u}_3 \quad (7.10.15)$$

This solution gives the values $\bar{u}_i = 0$ at the wall, where actually we have $\bar{u}_i \sim k^{1/2}$. However, as earlier, this solution could be used for calculating p_2 from Equation 7.10.11 to the error of the order k ; this leads to the formula

$$\begin{aligned} \beta_1 &= 1 + \frac{1 - 3\omega}{2(1 - \omega)^2} - \frac{\omega^2 \ln \omega}{(1 - \omega)^3} \\ \beta_3 &= 1 - \frac{\omega(3 - \omega)}{2(1 - \omega)^2} - \frac{\omega \ln \omega}{(1 - \omega)^3}, \quad \omega = \frac{K_3}{K_1} \end{aligned} \quad (7.10.16)$$

These curves are plotted in Figure 7.27a. Clearly, for $\omega \geq 0.5$ the coefficients β_i differ from the value $\beta = 4/3$ for the sphere ($\omega = 1$) only slightly. The case $\omega = 0$ with $\beta_1 = 3/2$ and $\beta_3 = 1$ corresponds to an infinite cylinder normal to the flow, that is, to a two-dimensional problem.

The shock layer thicknesses, or the λ_1 curves, are presented in Figure 7.27b. The extreme curves correspond to the circular cylinder ($\omega = 0$) and the sphere ($\omega = 1$).

Finally, the curves for \bar{u}_i and f_0 are plotted in Figure 7.28. The axial velocity is almost independent of ω . The longitudinal velocity coefficient \bar{u}_1 for $\omega \geq 0.25$ varies slightly as well, while for $\omega = 0$ it corresponds to the case of a circular cylinder. As $\omega \rightarrow 0$ the coefficient $\bar{u}_3 \rightarrow 1$ everywhere with exception of the wall region, where $\bar{u}_3 = \sqrt{2\beta_i k}$. Thus, a longitudinal vortical sublayer is formed near a strongly elongated body with $K_3 \ll K_1$; however, this sublayer is of no interest from the physical standpoint, since in this case the velocity

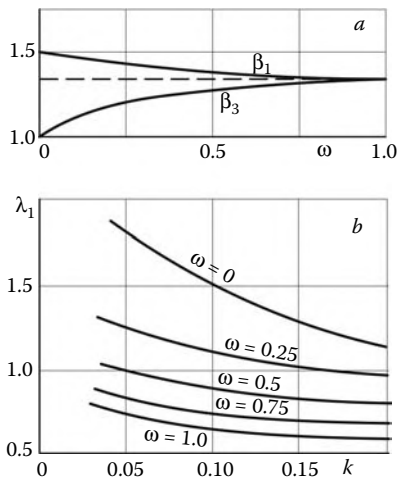


FIGURE 7.27
Parameters of the three-dimensional shock layer near a stagnation point.

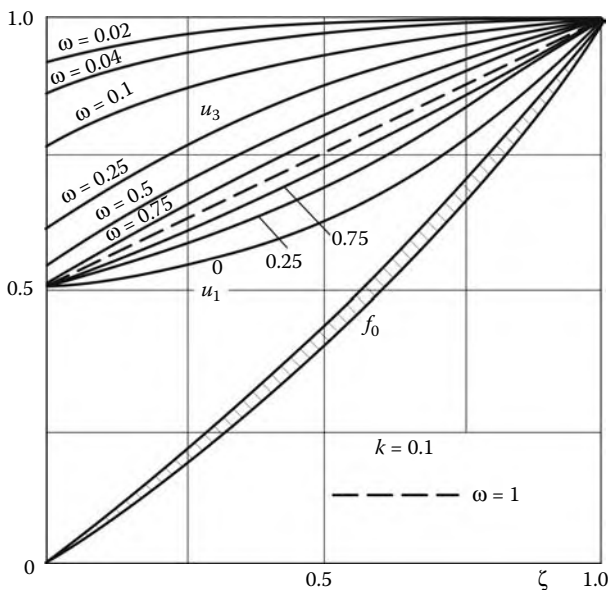


FIGURE 7.28
Axial (f_0) and longitudinal (u_i) velocity profiles.

component ratio $u_3/u_1 \sim \omega \rightarrow 0$. The streamlines on the body surface were considered in Section 2.11.

We note that the solution obtained is explicitly dependent on the shock curvature, while it depends on the body curvature in terms of β_i ; it can be applied to limitingly blunt bodies with two planes of symmetry, though the shock shape remains in this case indefinite.

We will now touch on flows, which are nonsymmetric as a whole. On moderately blunt bodies with shocks lying on them, as $\delta/R \rightarrow 0$ the central streamline passes through the

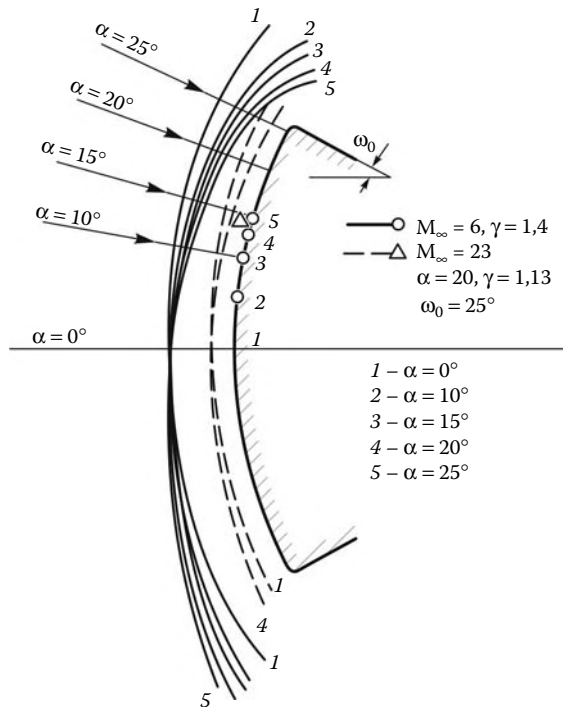


FIGURE 7.29
Shock shapes and stagnation point positions (symbols) in the flow past a spherical segment at incidence.

stagnation point along the common normal \vec{n}_0 to the body and the shock, parallel to the freestream. Since any surface possesses locally two planes of symmetry passing through the tangents to the curvature lines and the normal \vec{n}_0 , the solution obtained previously is applicable to this vicinity.

However, with an increase in the shock layer thickness on a body, which is not symmetric in a large vicinity of its forward point, the flow symmetry is violated due to the influence of the subsonic region periphery. In this case the central streamline may become curved and intersect the shock at a point, where the local angle of attack is $\alpha < \pi/2$. Then the pressure p''_0 at the stagnation point can in principle become greater than the stagnation pressure behind the normal shock p'_0 . However, this difference is usually small.

The most noticeable effect is related to the detachment of the stagnation point from the forward point of the body. This is clearly visible in Figure 7.29, in which the flow past a spherical segment at incidence is shown; in this flow an intense expansion originates from the corner as though push off the stagnation point of the flow.

7.11 Flow in the Vicinity of the Planes of Symmetry of a Conical Body

We will now continue the construction of local solutions using the truncated series method. We will first make an analysis for a circular cone with the semivertex angle θ_c at an angle of attack α ; then we will outline the procedure of the generalization of the solutions obtained.

We will deal not only with the windward side of the body, which is quite natural in using the truncated series method, but also with the leeward side, with appropriate restrictions on the applicability range of such a solution. In the latter case, the solution is bounded by the condition $\alpha \leq \theta_c$, otherwise the leeward generator is in the aerodynamic shadow. For the unification of the formulas, the two flow sides will differ only by the angles of attack ($\alpha > 0$ and $\alpha < 0$, respectively) for the same vicinity of the half-plane $\varphi = 0$.

In spherical coordinates r, θ, φ the velocity components u, v , and w (or v_r, v_θ , and v_φ of Equations 1.13.15), together with other flow parameters, are independent of r . Therefore, the shock is also conical and near the planes of symmetry has the shape

$$\begin{aligned}\theta &= \theta_s(\varphi) = \theta_{s0} + \frac{1}{2}\theta''_s\varphi^2 + \dots \\ \theta_{s0} &= \theta_c + \varepsilon, \quad \varepsilon \sim k = \rho_\infty/\rho_s \ll 1\end{aligned}\tag{7.11.1}$$

where ε is the angular shock-layer thickness.

The derivative θ''_s cannot be determined within the framework of the local problem, as well as the difference in the shapes of the body and the shock in the axisymmetric problem. However, since $\theta''_s \rightarrow 0$ as $\varepsilon \rightarrow 0$, we will truncate series 7.11.1 letting $\theta''_s = 0$, that is, in the same fashion as it was done in Section 7.7.

Then omitting the terms with the derivatives with respect to t and r in system 1.13.15 and taking 6.5.8 and 6.6.1 into account, we will seek its solution in the form of a truncated series* in φ

$$\begin{aligned}u &= U_\infty u_0(\zeta) \cos \alpha_0, \quad v = -kU_\infty f_0(\zeta) \sin \alpha_0 \\ w &= \varphi U_\infty f_1(\zeta) \sin \alpha, \quad \alpha_0 = \theta_c + \alpha \\ \zeta &= (\theta - \theta_c)/\varepsilon\end{aligned}\tag{7.11.2}$$

$$\begin{aligned}p - p_\infty &= \rho_\infty U_\infty^2 [p_0(\zeta) \sin^2 \alpha_0 - \\ &\quad \varphi^2 p_2(\zeta) \sin \alpha_0 \cos \theta_c \sin \alpha]\end{aligned}\tag{7.11.3}$$

Here, $\alpha > 0$ and $\alpha < 0$ correspond to the windward and leeward sides of the cone, respectively. Correspondingly, the plane $\varphi = 0$ is the flow divergence plane in the former case ($w > 0$) and the flow convergence plane in the latter case ($w < 0$).

The boundary conditions for these functions can be obtained from 6.5.8 letting $\theta_s = \theta_c$ in these equations, that is, neglecting the quantity ε

$$\zeta = 0 \quad f_0 = 0, \quad \zeta = 1 \quad u_0 = f_0 = f_1 = p_2 = 1\tag{7.11.4}$$

However, we will make an exception for the function p_0 in order for this function to involve the terms of the order k , as was done in Section 6.4. From relations 6.5.7 it follows that a rigorous expansion of p in φ at the shock is determined by formula 7.11.3 with θ_c replaced by θ_s . Expanding the latter formula in φ we obtain

$$\begin{aligned}p_0(1) &= 1 - k + 2\lambda k(1 - \omega), \quad \lambda = \varepsilon/k \tan \theta_c \\ 1 - \omega &= \tan \theta_c / \tan \alpha_0, \quad \omega = \sin \alpha / \cos \theta_c \sin \alpha_0\end{aligned}\tag{7.11.5}$$

* Lunev (1975). The integral-form solution for the entire conical shock layer was obtained by Gonor (1958).

The parameter λ is the same as in the previously considered problems, while the parameter ω ranges within the following limits

$$\begin{aligned} 0 \leq \omega \leq 1, \quad & 0 \leq \alpha \leq \pi/2 - \theta_c \\ -\infty \leq \omega \leq 0, \quad & -\theta_c \leq \alpha \leq 0 \end{aligned} \quad (7.11.6)$$

We are now coming to the construction of the solution. On the cone the velocity $v = 0$, while in the shock layer it is of the order k ($v \sim k$). Therefore, from the first Equation 1.13.15, $\partial u / \partial \theta = v$, in the plane of symmetry ($w = 0, \varphi = 0$) we obtain for the radial velocity $u = u_s = \text{const}$ or $u_0 = 1$. Further, only two terms, $v \partial v / \partial \theta$ and uv , remain in the second Equation 1.13.15. Therefore, integrating this equation we obtain

$$p_0(\zeta) - p_0(1) = \frac{1}{2}k(1 - f_0^2) - \lambda k(1 - \omega) \int_{\zeta}^1 f_0 d\zeta \quad (7.11.7)$$

As distinct from the case of the blunt-body stagnation point, this formula does not give a finite result, since the quantities $f_0(\zeta)$ and λ are as yet unknown.

In calculating other functions in the expansions 7.11.2 and 7.11.3 we will correspondingly simplify Equation 1.13.15 setting in them $p_0 = 1$ and omitting all the terms involving the function $v \sim kU_\infty$, except for the terms with $v \partial / \partial \theta$, since in the shock layer $\Delta\theta \sim \varepsilon$. Then, substituting these expansions in the equations and grouping the terms of the same order in powers of φ together, we obtain a system of ordinary differential equations

$$f_0 f'_1 = \lambda \omega (f'_1)^2 + \lambda(1 - \omega)f_1 - 2k\lambda\beta \quad (7.11.8)$$

$$f'_0 = \lambda \omega f_1 + 2\lambda(1 - \omega), \quad p'_2 = \lambda \omega f_1^2 \quad (7.11.9)$$

As earlier, in the single term of the order k retained in the equations, the function $p_2(\zeta)$ is replaced by its wall value $p_2(0) = \beta$. We will make a change of variables $\lambda t d\zeta = f_0 dt$ and let $t = 0$ at $\zeta = 0$ and $t = 1$ at $\zeta = 1$, which, as in Section 7.10, will serve for determining λ . Then, with allowance made for the boundary conditions, we obtain the solution

$$\begin{aligned} f_0 &= \frac{(\kappa_1 - \kappa_2)t^{1-\omega}}{(\omega - \kappa_2)t^{\kappa_2} - (\omega - \kappa_1)t^{\kappa_1}} \\ f_1 &= \frac{\kappa_1(\omega - \kappa_2)t^{\kappa_2} - \kappa_2(\omega - \kappa_1)t^{\kappa_1}}{\omega[(\omega - \kappa_2)t^{\kappa_2} - (\omega - \kappa_1)t^{\kappa_1}]} \\ \kappa_{1,2} &= -\frac{1}{2}(1 - \omega) \pm \sqrt{\frac{1}{4}(1 - \omega)^2 + 2k\beta\omega} \end{aligned} \quad (7.11.10)$$

For $k = 0$ we have $\kappa_1 = 0$ and $\kappa_2 = -(1 - \omega)$, so that the solution takes its limiting, or Newtonian, form:

$$f_1 = \frac{(1 - \omega)t^{1-\omega}}{1 - \omega t^{1-\omega}}, \quad f_0 = f_1 t^{1-\omega} \quad (7.11.11)$$

This solution gives zero peripheral velocities $f_1 = 0$ on the wall. Actually, as $t \rightarrow 0$ from 7.11.10 there follows

$$\begin{aligned} f_1 &= 2k\beta/(1 - \omega) & |1 - \omega| \gg 2k\beta \\ f_1 &= \sqrt{2k\beta} & |1 - \omega| \ll 2k\beta \end{aligned} \quad (7.11.12)$$

In the first case, to the accuracy of our order k theory, solution 7.11.11 is applicable everywhere; however, in the second case, at high angles of attack, the situation is similar to that of the two-dimensional problem of Section 7.8, in which the role played by the wall sublayer is crucial. This situation is realized only for $\omega \approx 1$, that is, on the windward side of the cone.

Applying solution 7.11.11 we obtain the following results

$$\lambda = \frac{\theta_s - \theta_c}{k \tan \theta_c} = \int_0^1 f_0 \frac{dt}{t} = -\frac{1}{\omega^2} \ln(1 - \omega) - \frac{1}{\omega} \quad (7.11.13)$$

$$p_0 = 1 - \frac{1}{2}k + k\Phi(\omega), \quad 2\omega^4\Phi(\omega) = \\ (1 - \omega)[3\omega(2 - \omega + \omega^2) - 2(3 - 3\omega + 2\omega^2)\ln(1 - \omega)] \quad (7.11.14)$$

Finally, the last equation of 7.11.9 has the solution

$$p_2(0) = \beta = 1 - \frac{6 - 9\omega + 2\omega^2}{2\omega^2} - \frac{3(1 - \omega)^2}{\omega^3} \ln(1 - \omega) \quad (7.11.15)$$

In Figure 7.30 these results are compared with the exact data for $M_\infty = 5$ and $\theta_c = 10^\circ$. On the windward generator ($\omega > 0$), formula 7.11.13 gives a value of λ close to the exact one, in spite of the fact that k is in this case not so small; the exception is provided by the high angle-of-attack range, $\alpha \approx \pi/2 - \theta_c$. At the same time, formula 7.11.14 gives an almost exact pressure on the cone over the entire α -range. As in two-dimensional problems, the Busemann formula 7.11.15 gives an overestimated value of the peripheral pressure gradient, the Newtonian value $\beta = 1$ being closer to reality.

We will now make the general analysis of solutions 7.11.13 through 7.11.15. The ω -dependences of λ , Φ , and β are presented in Figure 7.31 for the entire range of 7.11.6.

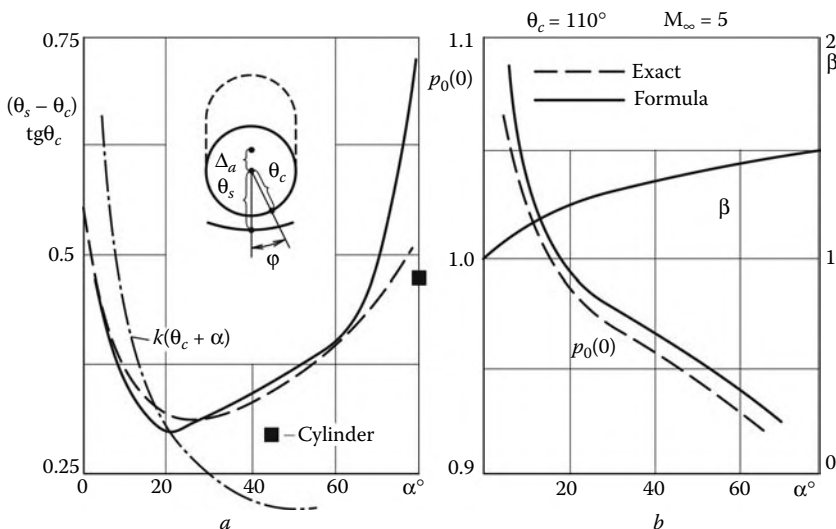
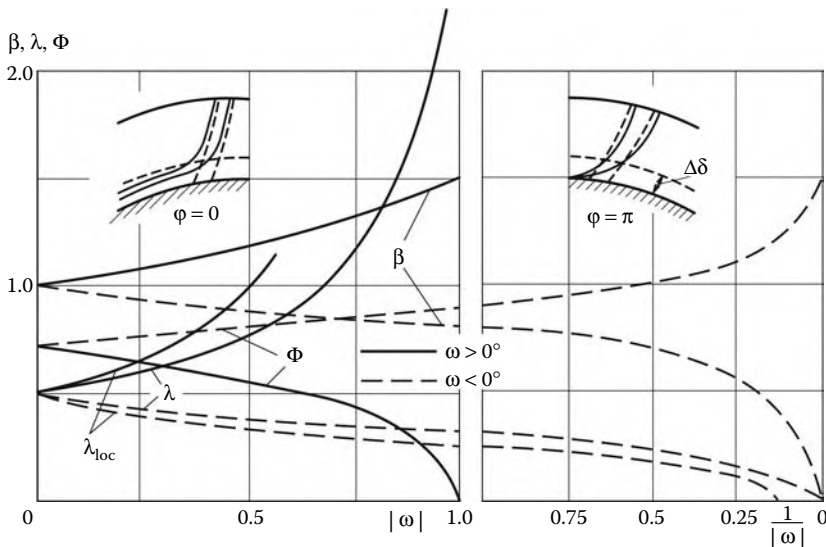


FIGURE 7.30
Pressure and shock layer thickness on the windward side of a cone.

**FIGURE 7.31**

Flow parameters on the attachment lines of sharp cones.

As $\omega \rightarrow 0$, or $\alpha/\theta_c \rightarrow 0$, this solution coincides with that for the cone at zero incidence (Section 6.4). At low angles of attack, or $|\omega| \ll 1$, we have

$$\begin{aligned} \lambda &= \frac{1}{2} + \frac{1}{3}\omega, & \beta &= 1 + \frac{1}{4}\omega \\ p_0(0) &= 1 + \frac{1}{4}k - \frac{7}{30}k\omega \end{aligned} \quad (7.11.16)$$

In another limiting case, $\omega \rightarrow 1$ or $\alpha/\theta_c \rightarrow \infty$, we have $\beta = 3/2$ and $p_0 = 1 - \frac{1}{2}k$, as for a circular cylinder set normal to the flow. However, the limiting formula 7.11.11 gives in this case $\lambda \rightarrow \infty$, as in the two-dimensional problem. To improve this result, one should use the original solution 7.11.10. However, in order not to become involved in a cumbersome analysis, we will restrict ourselves to a note that for $\omega = 1$ system, 7.11.8 and 7.11.9 coincide exactly with the system for the two-dimensional problem of Section 7.8, which must lead to the same solution with a finite value of λ . By and by, the quantity δ/R for a cylinder in the same flow conditions, as presented in Figure 7.30a, agrees well with the exact ratio $(\theta_s - \theta_c)/\tan \theta_c$ for a cone.

We will now dwell on the conical streamlines, which were defined in Section 6.5. We obtain the equations for them using 6.5.2 and 7.11.2

$$\frac{d\varphi}{\varphi} = -\frac{\varepsilon \sin \alpha}{k \sin \theta_c \sin \alpha_0} \frac{f_1}{f_0} d\xi = -\omega f_1 \frac{dt}{t} \quad (7.11.17)$$

Within the framework of the result 7.11.11 this equation has the solution

$$\varphi/\varphi_1 = (1 - \omega t^{1-\omega})(1 - \omega)^{-1} \quad (7.11.18)$$

Here, φ_1 is the shock coordinate of a streamline (streamsurface). For $\omega > 0$ the angle φ increases and for $\omega < 0$ decreases with t , that is as the wall is approached. However, in any

case the angle $\varphi = \varphi_0 = \varphi_1(1 - \omega)^{-1}$ is finite for $t = 0$. This means that within the framework of the limiting Newtonian theory the isentropic streamsurfaces in the shock layer are confined between the rays φ_1 on the shock and φ_0 on the cone, the rays being streamlines. A similar result was obtained in Section 6.6 within the framework of the linear theory for small α . However, in that section it was shown that taking a real velocity distribution in the wall region into account leads to formation of a vortex sublayer with streamsurfaces almost parallel to the cone surface, which itself is a streamsurface with the entropy corresponding to the shock slope $\theta_s + \alpha$ in the plane of symmetry on the windward side. The same qualitative result can be obtained in our problem when using velocities 7.11.12 in the wall sublayer $\Delta\delta$ sketched in Figure 7.31 (here, dotted curves are streamlines given by formulas 7.11.18 and bold ones are exact streamlines).

The previous discussion makes it possible to answer the question of whether the solution obtained is applicable on the windward side of the cone. It is actually applicable to the outer, Newtonian part of the shock layer, in which pressure gradients do not play any part, so that the right-hand side of the first Equation 7.11.8 could be dropped. However, in the wall sublayer ($\Delta\delta$ in Figure 7.31) the entropy on the oncoming streamlines at $\omega < 0$ is not determined by a local solution; neither is the density ρ , which actually enters in the coefficient k in Equation 7.11.8, or in the first formula for f_1 , 7.11.12. We can only assert that this density is smaller than that immediately behind the shock, their ratio being equal to $(p_-/p_+)^{1/\gamma}$, where p_+ and p_- stand for the pressures on the windward and leeward cone generators. This leads to an increase in the shock layer thickness, which could not be determined from the solution obtained and, eventually, to the change in the pressure, as observed, for example, in Figure 6.12 of Section 6.6.

In this connection, one should consider with caution the fact that the quantity λ in Figure 7.31, or the shock layer thickness, is smaller on the leeward than on the windward side. Nevertheless, from Figure 6.11 (Section 6.6) it follows that such a situation can actually take place.

A singular case is the situation in which $\alpha \rightarrow -\theta_c$, or $\omega \rightarrow -\infty$, when $\lambda \rightarrow 0$, $\beta \rightarrow 0$, and $\Phi \rightarrow 3/2$. This is a zero-thickness shock layer with zero peripheral gradient and, in accordance with 7.11.12, with zero peripheral velocity on the body. However, for zero shock slope, $\theta_s + \alpha = 0$, this parameter range cannot be described by our theory.

Finally, we dwell on the applicability of the solution obtained to the vicinities of the planes of symmetry of other conical bodies. Obviously, in order for this theory to be applicable, the surface of such a body in the coordinate system aligned with the external velocity vector must coincide in this vicinity with a certain equivalent osculating circular cone. For an elliptic cone at $\alpha = 0$ the cross-sections of these cones are presented in Figure 7.30a. In this case, the equivalent cone must be set at a positive angle of attack $\Delta\alpha$.

In conclusion, we will compare the shock slopes λ obtained with the same slopes for the local cone with the vertex angle $\theta_{loc} = \alpha_0 = \alpha + \theta_c$ set at zero incidence. For this cone in our notation formula 6.4.7 takes the form:

$$\lambda_{loc} = \frac{\theta_s - \theta_c}{k \tan \theta_c} = \frac{1}{2} \frac{\tan \alpha_0}{\tan \theta_c} = \frac{1}{2(1 - \omega)} = \frac{1}{2} + \frac{1}{2}\omega \quad (7.11.19)$$

As follows from Figure 7.31, this formula, as compared with 7.11.13 or 7.11.16, overestimates the shock slope on the windward generator ($\alpha > 0$) and underestimates it on the leeward generator ($\alpha < 0$); in the latter case it is in reasonable agreement with formula 7.11.13 for λ over the entire ω range. However, even for $\alpha > 0$ both formulas give comparatively close values up to $\omega \leq 1/2$ ($\alpha \leq \theta_c$ for slender cones). Within this accuracy and taking

into account that in the hypersonic approximation the pressure is close to the Newtonian one, one can say there is applicability of the local cone rule to cones at incidence.

7.12 Jet Flowing Counter to a Hypersonic Flow

In this section we will touch on the problem of the uniform hypersonic flow with the parameters ρ_∞ and U_∞ around a highly underexpanded axisymmetric jet (I in Figure 7.32a) directed against the flow or a spherical high-intensity source flow. In the case of a counterstreaming supersonic jet in an unbounded supersonic flow (II in Figure 7.32a), the two flows are separated by an interface Σ , which is convex relative to the outer flow; on either side of this surface shocks S are formed. Far downstream of the nozzle, the highly underexpanded jet flow is also hypersonic; therefore, the shock layers behind the shocks S can be assumed to be thin, so that the previous theory for compressed shock layers can be extended to this case.

The shape and position of the contact discontinuity Σ are determined by the condition of equal pressures on either side of Σ ; calculating these pressures from the Newtonian formula we obtain the relation

$$p = \rho_\infty U_n^2 = \rho_\infty U_\infty^2 \cos^2 \omega = \rho_1 U_1^2 \cos^2(\omega - \varphi) \quad (7.12.1)$$

Here, ρ_1 and U_1 are the parameters of flow I ahead of the interface Σ , while ω and φ are the angles by which this surface and the streamlines to the right of it are inclined to the axis of symmetry oo' (Figure 7.32b).

As shown in Section 2.3 (see Figures 2.6 and 2.7), the flow in a certain vicinity of the axis of symmetry of a highly underexpanded jet is similar to the flow generated by an equivalent spherical source with the effective center o (Figure 7.32b) and the sonic surface $r = r_*$ with the flow parameters ρ_* and $U = a_*$ on it. The streamlines of this flow are straight lines, while the variation of the density ρ and the velocity $U(\rho)$ with the distance r from the center is governed by the relation $\rho U r^2 = \rho_* a_* r_*^2$ which is exact for the spherical source. Under this assumption and letting also that jet expansion is fairly intense, so that the velocity U can be equal to its maximum value $U_m = [(\gamma+1)/(\gamma-1)]^{1/2} a_*$, from the equality $\rho_\infty U_\infty^2 = \rho_1 U_m^2$ on the axis of symmetry we obtain the distance $r = L$ between the center o and the stagnation point o' , as well as the density ρ_{10} ahead of the inner shock (the subscript 0 refers to the axis of symmetry)

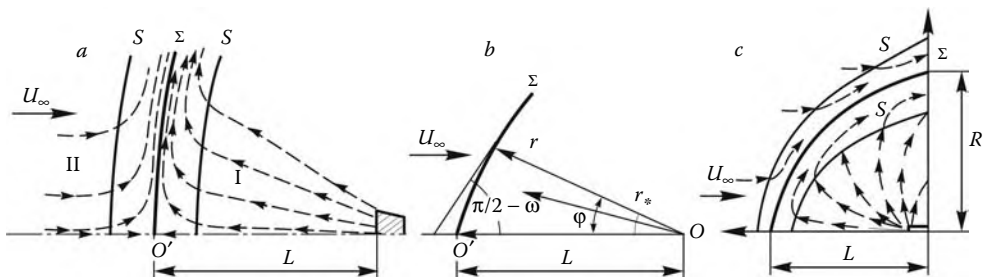


FIGURE 7.32
Injection counter to the oncoming hypersonic flow.

$$\begin{aligned} L &= \left(\frac{\gamma + 1}{\gamma - 1} \right)^{1/4} L_0, & L_0 &= r_{*0} \Omega^{1/2} \\ \frac{\rho_{10}}{\rho_{*0}} &= \frac{\gamma - 1}{\gamma + 1} \frac{1}{\Omega}, & \Omega &= \frac{\rho_{*0} a_{*0}^2}{\rho_\infty U_\infty^2} \end{aligned} \quad (7.12.2)$$

Thence it follows that the flow ahead of the inner shock is actually hypersonic provided that (cf. Section 2.2)

$$M_1 \sim (\rho_*/\rho_1)^{(\gamma-1)/2} \sim \Omega^{(\gamma-1)/2} \gg 1 \quad (7.12.3)$$

The curvature K_Σ of the interface Σ on the axis of symmetry can be obtained by applying Equation 7.8.19 for the pressure to either side of this surface

$$\begin{aligned} \beta_{sI} K_\Sigma^2 &= \beta_{sII} K_{\text{eff}}^2, & K_{\text{eff}} &= m - K_\Sigma \\ m &= \frac{\partial \varphi}{\partial l}, & K_\Sigma &= \frac{\partial \omega}{\partial l} \end{aligned} \quad (7.12.4)$$

where l is the curvilinear coordinate (denoted as x in Section 7.8) measured along the meridional section of the surface Σ . The surface Σ is concave relative to the inner flow I, which is taken into account in formula 7.12.4.

For $\beta_{sI} \approx \beta_{sII} \approx 1$ from 7.12.4 it follows that $K_\Sigma \approx K_{\text{eff}} \approx m/2$; hence, we have $\omega = \varphi/2$. For both flows the shock layer thicknesses are determined by the corresponding formula of Section 7.8.

In a wider vicinity of the axis of symmetry and for a given function $\rho(\varphi)$ in the polar coordinate system (Figure 7.32b), Equation 7.12.1 can be brought to the following form:

$$\begin{aligned} (\gamma - 1) \bar{r}^2 \bar{\Omega} \cos^2 \varphi &= (\gamma + 1) \cos^2(\omega - \varphi) \\ \bar{r} &= \frac{r}{L_0} = \frac{r}{r_{*0}} \Omega^{1/2}, & \bar{\Omega}(\varphi) &= \frac{\rho_{*0} a_{*0}^2 r_*^2}{\rho_{*0} a_{*0}^2 r_{*0}^2} \end{aligned} \quad (7.12.5)$$

Here, the parameter $\bar{\Omega}(\varphi)$ characterizes the distribution of the local parameters $\rho_{*0} a_{*0}^2$ and r_{*0}^2 of the effective spherical source in the angle φ . In this case, Equation 7.12.5 determines the function $\omega(\bar{r}, \varphi, \gamma)$ and, via the equation $d\bar{y}/d\bar{x} = \tan \omega$, where $\bar{x} = x/L_0$ and $\bar{y} = y/L_0$ are the dimensionless Cartesian coordinates, the shape of the surface Σ . This shape is dependent only on γ and the function $\bar{\Omega}(\varphi)$; for a spherical source with $\bar{\Omega} = 1$ it depends on γ only. In other words, in the hypersonic approximation ($\Omega \gg 1$) the length L_0 is the sole scale length of the problem unifying the source intensity (the parameters ρ_* and a_*) and its dimension r_* .

An example in Figure 7.33 confirms this similarity law; it presents the calculated pattern of the supersonic $M_\infty = 3$ flow past a spherical source:^{*} when plotted in the similitude variables \bar{x}, \bar{y} , this pattern is almost independent of Ω . It is interesting to note that on the rear side of the flow the inner shock is deflected toward the axis of symmetry with further reflection from the axis, as in the case of the supersonic underexpanded jet issuing into the ambient medium (see Section 5.5). In this example, the sonic line is continuous on Σ , since for equal γ on either side of the interface, the Mach number distributions along Σ are also the same. For different γ on either side of Σ the Mach number distributions are

* The data of Lebedev and Sandomirskaya (1981). In the hypersonic approximation this problem for a spherical source was solved by Baranov, Krasnobaev, and Kulikovskii (1970) as applied to the interaction of solar wind with the interstellar medium, and, for a more general situation, by Vasil'kov and Murzinov (1973).

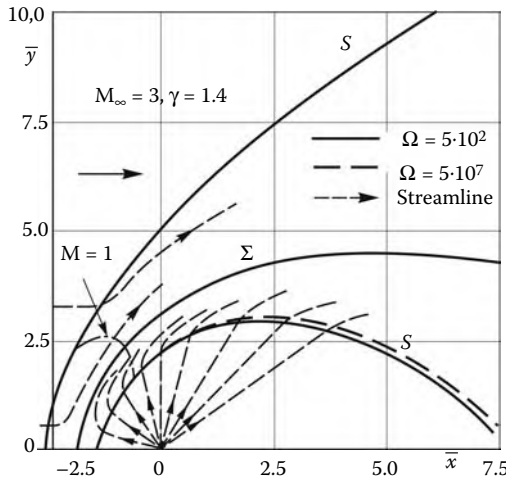


FIGURE 7.33
Supersonic flow past a spherical source.

also different, which can lead to nontrivial interference of the flows in the subsonic and transonic regions (see Section 5.7).

Consider in more detail the case of a collimated jet flowing out from a nozzle of radius r_a with the flow parameters ρ_a and U_a at the gas flow rate $G = \pi r_a^2 \rho_a U_a$. In this case Equation 7.12.5 describes the surface Σ only in a certain central region of the jet in which streamtubes bear a sufficiently high ram pressure. At the jet periphery, where the pressure and density are relatively low, the flow in the inner shock layer turns under the action of the external flow, like the free layer of Section 7.5, up to the complete, 180° turn of the jet, which becomes, as it were, fountain-shaped, as sketched in Figure 7.32c.

To evaluate the transverse dimension R of this jet we let, for the sake of simplicity, $M_a \gg 1$. Then the momentum of the jet flowing out from the nozzle is $I_a = GU_a = GU_m$. Letting the Mach number and velocity in the turned jet to be again $M \gg 1$ and $U \approx U_m$, we obtain the same momentum of the jet, only with the opposite sign: $I = -I_a$. Thus, the jet turns under the action of the force $X = 2I_a$ applied from the outer flow to the interface, which plays for this flow the role of a solid surface and exhibits, say, in the region of the nozzle exit (Figure 7.32c), the drag $X = 0.5c_x\pi R^2 \rho_\infty U_\infty^2$, where c_x is the drag coefficient of the interface. Then equating the two expressions for X we obtain the jet dimension

$$R \approx \frac{2}{\sqrt{c_x}} \bar{I}_a^{1/2} \approx \frac{2}{\sqrt{c_x}} \frac{U_m}{U_\infty} \left(\frac{\rho_a}{\rho_\infty} \right)^{1/2} r_a, \quad \bar{I}_a = \frac{I_a}{\pi \rho_\infty U_\infty^2} \quad (7.12.6)$$

Obviously, the realization of this flow model requires the fulfillment of the condition $R \gg r_a$.

The same estimate $L \sim \bar{I}_a^{1/2}$ can be obtained for the longitudinal extent of the jet by replacing ρ_a by ρ_* , U_a by U_* , and r_a by r_* in 7.12.2. Obviously, this effective, jet-formed body, having the same extent in different directions, must have $c_x \sim 1$.

Thus, in the problem of the highly underexpanded jet flow counter to a hypersonic stream, subject to the condition $\Omega_a = \rho_a U_a^2 / \rho_\infty U_\infty^2 \gg 1$, the effective scale length is the parameter $\bar{I}_a^{1/2}$. This similitude law generalizes to a certain degree the law established previously for

the spherical source; it was many times confirmed experimentally, including the case of jet arrays.*

7.13 Degenerate Shock Layer Equations

Previously, within the framework of the thin shock layer model, we derived two types of the blunt body flow problem solution, namely, the limiting Newtonian solution (Section 7.5) and the local solution for the vicinities of the axis of symmetry and of the spreading line (Sections 7.9 to 7.11) embedded in the elliptic subsonic flow region. The derivation of these solutions was possible due to the fact that we refused the exact equations and used their degenerate counterparts obtained by discarding their separate terms on the basis of asymptotic (as $k = \rho_\infty/\rho_s \ll 1$) estimates so that the elliptic nature of the equations has been lost. In the cases considered previously, the equations governing the local solutions of Sections 7.7 to 7.9 were obtained from the original systems 7.7.5 through 7.7.8 for $j_2 = 0$ and $j_{i \neq 2} = 1$, while those governing the limiting solutions of Section 7.5 were obtained for $j_1 = j_2 = j_4 = 0$ and $j_3 = j_5 = 1$.

In this connection, we will exhibit the responsibility of individual terms of these equations for their salient features by assuming the right-hand sides Q_i to be independent of the derivatives of the unknown functions. In principle, for the sake of generality it would be well to introduce coefficients $j_i^{(k)}$ in front of all, or at least many, terms of these equations and to study the effect of their variations. However, we restrict ourselves only to the variation of the coefficients j_1 and j_2 studied before and let the other coefficients be equal to unity (the case $j_5 \neq 1$ will be considered in Section 12.14). The aim of the investigation is to determine the shape of the characteristics $x(y)$ or $y(x)$ and the domain of existence for various values of the parameters j_1 and j_2 from the range $0 \leq j_1, j_2 \leq 1$.

Equation 7.7.8 has the streamlines $uy' = H_x v$ as its characteristics. Supplementing the system 7.7.5 through 7.7.8 by relations of type 4.3.7 and making the same operations as in Section 4.3, we obtain a characteristic equation, one of the roots of which relates to the same streamlines, though with a modified, as compared with the Bernoulli equation, compatibility equation

$$du^2 + j_1 j_2 dv^2 = -2j_1 \rho^{-1} dp + Q' dt, \quad Q' = uQ_1 + j_1 v Q_2 \quad (7.13.1)$$

Moreover, we obtain two more roots for a pair of wave characteristics equivalent to 4.3.16 at $j_1 = j_2 = 1$

$$\begin{aligned} H_x(a^2 - j_2 v^2)x'_\pm &= -j_2 uv \pm \Delta \\ \Delta^2 &= j_2 a^2(u^2 + j_1 j_2 v^2 - j_1 a^2) = j_1 j_2 a^2(M_{\text{eff}}^2 - 1) \\ M_{\text{eff}}^2 &= (j_1 a^2)^{-1}(u^2 + j_1 j_2 v^2) \end{aligned} \quad (7.13.2)$$

The effective Mach number M_{eff} plays the same role in the degenerate equations as the conventional Mach number in the exact solutions. For $\Delta^2 > 0$ or $M_{\text{eff}} > 1$ this formula gives a pair of real wave characteristics, while for $\Delta^2 < 0$ ($M_{\text{eff}} < 1$) the characteristics are imaginary, these two cases corresponding to the equations of hyperbolic and elliptic type.

* Gubanova, Karpman, and Lunev (1988).

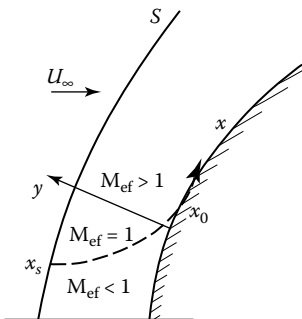


FIGURE 7.34
 $M_{\text{eff}} = 1$ lines in the shock layer on a blunt body.

For $j_2 = 0$ we have a single characteristic family, $x = \text{const}$, these lines being the normals to the body surface. Since such characteristics are inherent in parabolic equations (e.g., the heat equation), the case $j_2 = 0$ will be referred to as the *parabolic degeneration* of the original equations (though this term is more appropriate for viscous shock layers to be considered in Chapter 12).

For $j_1 = 0$ and $j_2 \neq 0$ formula 7.13.2 gives a pair of wave characteristics $\sqrt{j_2}uy'_\pm = \pm H_x(a \pm \sqrt{j_2}v)$ for any local Mach numbers; these characteristics are similar to the time-dependent ones of Section 4.2. While for $M > 1$ the characteristics of the equations simply change their form, for $M < 1$ we deal with the *hyperbolic degeneration* of originally elliptic equations. The same degeneration could be conserved for $j_1 \neq 0$ by choosing this parameter from the following conditions (see Vigneron, 1978)

$$j_1 = 1, \quad \Delta_*^2 = u^2 + j_2 v^2 - a^2 > 0, \quad M_{\text{eff}} \geq 1 \quad (7.13.3)$$

$$j_1 \leq j_{1*} = u^2(a^2 - j_2 v^2)^{-1}, \quad \Delta_*^2 < 0, \quad M_{\text{eff}} \leq 1 \quad (7.13.4)$$

The first condition signifies that there is no need to change j_1 in the system, which is hyperbolic in itself. The second condition ensures the hyperbolicity of the system for $M < 1$ as well. In the subsonic thin shock layer on a blunt body we have $v^2/a^2 \sim k \ll 1$ and $j_{1*} \approx u^2/a^2$. One of the $j_{1*} = \text{const}$ or $M_{\text{eff}} = 1$ lines corresponding to the solution of Section 7.8 is sketched in Figure 7.34, the ratio of its shock coordinates x_s and x_0 being of the order $x_s/x_0 \sim k$ on the body. As the axis of symmetry is approached, in accordance with 7.3.14, the coefficient j_1 must decrease as $j_1 \sim x^2k$, together with the gas velocity on the body $u_b \sim xk^{1/2}$. Qualitatively, the $M_{\text{eff}} = 1$ lines are similar to the Mach number contours $M = \text{const}$, while the properties of the characteristics in the $M_{\text{eff}} > 1$ region are similar to those outlined in Section 4.3.

These properties of the degenerate equations form the basis of rather effective and cost-saving (as compared, say, with stabilization methods) *global iteration methods*.* In these methods, a degenerate system is formed starting from the exact one by replacing its individual terms by sums of the type

$$\varphi_k = j_i \varphi_k^{(n+1)} + (1 - j_i) \varphi_k^{(n)} \quad (7.13.5)$$

* The global iteration methods were developed and used in the works of Davis (1979), Vigneron (1978), Glazkov, Tirsikii, and Shcherbak (1990), Blotner (1991), Vlasov and Gorshkov (2001), and others, mainly for the viscous shock layer problems (see Section 12.14).

in such a way that this degenerate system could be solved using a marching technique in the coordinate x . In 7.13.5 the second term is determined from the previous, n th iteration cycle (the n th layer), while in calculating the $(n+1)$ th cycle it is transferred to the right-hand side Q_i of the system. Provided the iteration procedure is convergent, we obtain in the limit the exact terms φ_k , together with the solution as a whole. Usually, φ_k is considered to mean either the derivative $\partial p / \partial x$ in the equation for the longitudinal momentum, 7.7.5, or the derivative dv/dt in the transverse momentum equation, 7.7.6.

The equations thus obtained can be transformed to the form:

$$(j_1 a^2 - u^2) \frac{\partial \psi_k^{(n+1)}}{\partial x} = \Phi_k, \quad j_2 u \frac{\partial v^{(n+1)}}{\partial x} = \Phi_3 \\ k = 1, 2 \quad \psi_1 = u, \quad \psi_2 = p \quad (7.13.6)$$

where the right-hand sides Φ_k contain only coordinates, unknown functions on layers n and $n+1$, and their derivatives with respect to y . For $j_2 = 0$ the derivative v_x vanishes from the second Equation 7.13.6 or 7.7.6 of the parabolized system, the equation taking the form $\Phi_3 = 0$. On the singular lines $y = y^*(x)$, with the conditions $j_1 u^2 = a^2$ imposed on these lines, the derivatives $\psi_{kx}^{(n+1)}$ also vanish from these equations.

This form of the equations expects to use a marching (in the x coordinate) technique of solution, which is, however, possible only if the normal (to the $x = \text{const}$ lines) Mach number is $M_{\text{eff},n} > 1$, that is, if conditions 7.13.3 and 7.13.4 are fulfilled (cf. Section 5.3).

In order for the previously-mentioned marching techniques to be realized, initial conditions on the axis of symmetry $x = 0$ should be preassigned in each iteration cycle; then, in the vicinity of $x = 0$, using expansions of type 7.7.14, the system 7.7.5 through 7.7.8 is reduced to a system of two ordinary equations containing, however, three unknown functions: f_0 , f_1 , and p_2 . For this reason, initial conditions on the axis for the further solution could be preassigned only by presetting from the previous approximation one of the functions—either f_2 for parabolized equations or p_2 for hyperbolized ones.

However, the local solution thus obtained contains an unknown parameter, which cannot be determined from this solution: the curvature K_s of the shock on the axis (or the shock layer thickness δ , which is related with the former). Preassigning this parameter determines completely the initial conditions for the degenerate equations and, hence, makes it possible to construct subsequent solutions within the framework of the given iteration cycle using the marching technique. Thus, the degenerate formulation of the problem must possess the possibility of determining this parameter in each iteration cycle in terms of any conditions, which, in a way or another, must be related with the conditions of the passage through the transonic flow region (e.g., by analogy with the conditions of the regular behavior of the solution at singular points in the Dorodnitsyn method presented in Section 5.4).

Thus, the problem with an unknown boundary (the shock) retains elliptic features even for the degenerate system that has lost its ellipticity. Otherwise, one could not ensure the convergence of the iteration procedure based on degenerate equations to the solution of elliptic or mixed (in the sense of Chapter 5) problems.

In particular, an algorithm, in which the subsequent, or $(n+1)$ th, iteration cycle is calculated from the shock wave shape $y = \delta_n(x)$ obtained in the n th cycle, has gained acceptance; the derivative $\delta'_n(x)$ is used for preassigning the $(n+1)$ th boundary conditions on the shock, while an additional condition on the body surface is used for determining the new shock shape, $\delta_{n+1}(x)$. In essence, this algorithm is reduced to an iterative sequence of inverse Cauchy problems set on the shock (see Section 5.4), which favors the stability of their solutions, at least within the framework of each iteration cycle.

The global iteration methods of this type are used chiefly within the framework of hyperbolized equations with $\varphi_k = \partial p / \partial x$ in sum 7.13.5, the parameter j_1 being chosen from conditions 7.13.3 and 7.13.4, since in this case a certain fraction of the term $\partial p / \partial x$ is taken into account in the $(n + 1)$ th iteration cycle. At the same time, the parabolized version of the degenerate equations, which can be realized for $j_2 = 0$ only, was usually used in the first approximation (the *thin shock layer method*) in the past and is used to the present day only for obtaining closed initial conditions on the axis of symmetry (cf. Sections 7.7 and 7.8) with the additional preassigning of the shock curvature on the axis that is equal or close to the body curvature. However, in the last case the solution as a whole remains formally approximate whatever mode of its continuation to the following part of the shock layer is used.

Finally, we will dwell on the *three-dimensional shock layer equations*. Let \vec{U}_τ be the velocity projection on the coordinate plane $x_2 = \text{const}$ in the system of orthogonal coordinates (x_1, x_2, x_3) introduced in Section 1.13, with $x_2 = 0$ on the body surface. We will introduce one more, local Cartesian coordinate system (x, y, z) with the velocity projections u, v , and w ; here, the x axis is aligned with the vector \vec{U}_τ , the y axis is tangent to the x_2 line, that is, approximately normal to the body surface, and the z axis is orthogonal to them; at origin $w = 0$. Then, by analogy with Equations 7.7.5 through 7.7.7, we can write the equations of motion in the form:

$$u \frac{\partial u}{\partial x} + v \frac{\partial u}{\partial y} = -\frac{j_{11}}{\rho} \frac{\partial p}{\partial x} + Q_1 \quad (7.13.7)$$

$$j_2 \frac{dv}{dt} = j_2 \left(u \frac{\partial v}{\partial x} + v \frac{\partial v}{\partial y} \right) = -\frac{1}{\rho} \frac{\partial p}{\partial y} + Q_2 \quad (7.13.8)$$

$$\frac{u}{\rho a^2} \frac{\partial p}{\partial x} + \frac{v}{\rho a^2} \frac{\partial p}{\partial y} + \frac{\partial u}{\partial x} + \frac{\partial v}{\partial y} + \frac{\partial w}{\partial z} = -Q + Q_3 \quad (7.13.9)$$

$$u \frac{\partial w}{\partial x} + v \frac{\partial w}{\partial y} = -\frac{j_{13}}{\rho} \frac{\partial p}{\partial z} + Q_w \quad (7.13.10)$$

We will establish the characteristic properties of this system depending on the coefficients j_{12} and j_2 . The fictitious right sides Q_i have the same meaning as before. Our reasoning is analogous to that drawn in Section 4.4 with that difference that there we had $j_{1i} = j_2 = 1$ and the x axis was aligned with the total velocity vector \vec{U} . In formulating initial value problems on surfaces passing through the z axis, the terms $\partial w / \partial z$ and $\partial p / \partial z$ are known and can be rearranged to the right sides of the equations. This determines instantly the characteristics of the last equation: as in Section 4.4, these are represented by streamlines. However, the differential operators of Equations 7.13.7 through 7.13.9 are the same as in Equations 7.7.5 through 7.7.7 for the two-dimensional shock layer. For $j_2 = 0$ and $j_{11} = 1$ from these equations we obtain parabolically degenerate equations of a thin shock layer that take the forms 7.10.5 and 7.10.6 in the (x_1, y, x_3) coordinate system. For $j_2 = 1$ and under the condition

$$a^2 j_{11} < u_1^2 + u_3^2 = U_\tau^2 \quad (7.13.11)$$

we obtain a pair of wave characteristic surfaces, whose slopes to the local x_2 surface are determined by Equation 7.13.2. Along these surfaces disturbances propagate across the shock layer, from the body surface to the shock and vice versa.

We will now consider the characteristic surfaces passing through the y axis (or the x_2 line). On these surfaces, the derivatives with respect to y are known. Eliminating the derivative

$\partial u / \partial x$ from Equation 7.13.9 via Equation 7.13.7, from two last equations we obtain the following system

$$\begin{aligned} \frac{1}{\rho} \left(j_{11} - \frac{u^2}{a^2} \right) \frac{\partial p}{\partial x} + \frac{\partial w}{\partial z} &= Q_4 \\ u \frac{\partial w}{\partial x} + \frac{j_{13}}{\rho} \frac{\partial p}{\partial z} &= Q_5 \end{aligned} \quad (7.13.12)$$

where Q_4 and Q_5 are certain right sides, known on the y axis.

Provided condition 7.13.11 holds, for all j_{13} this system has a pair of wave characteristics with the slopes

$$\frac{dz}{dx} = \pm \left[\frac{j_{11} - u^2/a^2}{j_{13}} \right]^{-1/2} \quad (7.13.13)$$

The corresponding characteristic surfaces propagate on each side of the local stream-surface passing through the x_2 line, thus forming the domain of influence of the latter. In intersecting the shock and the body surface they form curvilinear characteristic triangles. We note that here the effect of the coefficients j_{11} and j_{13} is different, while in the domain, where the condition $j_{11} > u^2/a^2$ does not hold (a vicinity of the stagnation point), hyperbolization of the conditions is, as previously, impossible.

We will not touch upon this question. We only note that in implementing the method, its conceptual sketch outlined previously is complicated by many accompanying details that ensure the normal operation of the method but, at the same time, are of secondary importance. Thus, such purely empirical approaches as the calculation of other terms of the equations in the preceding iteration stage, the anticipating calculation of their derivatives of the type $(\partial p / \partial x)^{(n)} = (p_{k+2}^{(n)} - p_{k+1}^{(n)}) / \Delta x$ at point $k+1$ of the x axis, and so on, are used. Usually, many of these empirical approaches can be theoretically warranted by an analysis of the differential operator remaining in the $(n+1)$ -th iteration stage or, on the contrary, by introducing new fictitious equations (e.g., in the operation of smoothing in calculating the derivative $\delta^{(n+1)}$).

We note that the global iteration techniques were developed chiefly for calculating viscous shock layers (see Chapter 12). However, their validation is to a considerable degree related with the previously-mentioned properties of inviscid operators of Navier-Stokes equations. A limitation of these methods is that they are applicable only for fairly smooth bodies and rather high freestream Mach numbers. Moreover, these methods are as yet developed only for the flows having an axis or two planes of symmetry, in the vicinity of which there exist expansions 7.7.14 or 7.10.8, which makes it possible to determine local solutions as the initial conditions for marching algorithms. For three-dimensional flows, these solutions involve even two indefinite parameters, namely, the curvatures K_{1s} and K_{3s} of the shock on the axis (see Section 7.10).

We also note that, though all this reasoning is not formally related with the hypersonic nature of the flow, experience has shown that the primary area of application of these iterative methods is precisely hypersonic flows, since the reduction of the shock layer in thickness ensures the accuracy of even the first approximation and favors the iteration convergence.

In conclusion, we present a methodically and historically interesting example of superdegeneration of a problem, which turns out to be in principle unclosed. This is the Hayes problem (1959) for a circular disk, which is solved in the Newtonian approximation $j_1 = 0$, $j_2 = 0$, and, moreover, with the constant density $\rho = \rho_s$. The system of equations for

this problem, 7.7.5 and 7.7.7, is closed with respect to the velocities u and v and has the $x = \text{const}$ characteristics; thus, it is parabolic degenerate. Equation 7.7.6 serves in this case for determining the pressure field. In accordance with Section 7.5, the velocity distribution in streamlines, $u(\psi)$, is completely determined by the shock shape $y = \delta(x)$; the differential equation for the latter can be obtained by differentiating repeatedly integral 7.5.4. This equation has the integral (see Lunev, 1975)

$$t = Z(1 + 2Z)^{-3/2}, \quad Z = (\delta')^2/k, \quad t = x^2 K_s^2/k \quad (7.13.14)$$

The function $Z(t)$ is two-valued with the singular point $Z = 1$, $t = t_0 = 0.192$; at this point $\delta' \rightarrow \infty$ and $\partial p / \partial x \rightarrow \infty$. Only the branch $0 \leq Z \leq 1$ has the physical meaning. The solution contains a parameter, namely, the shock curvature K_s at the axis of symmetry, for determining which additional condition is required. However, in this degenerate formulation of the problem, which does not involve the speed of sound, there is no such condition and this miscarriage cannot be removed in any subsequent iteration cycles. At the same time, the temptation of bringing two characteristic points into coincidence (i.e., the singular point and the corner $x = r_0$) leads to results very different from those presented in Section 7.3, despite the fact that the curvature $K_s \sim \sqrt{k}/r_0 \rightarrow 0$ as $k \rightarrow 0$ and the constant density region, together with the velocity distribution 7.5.3, propagates to the increasingly large part of the disk.

8

Hypersonic Flow Past Thin Sharp Bodies

This chapter is devoted to the study of the hypersonic flow past thin sharp bodies (the case of thin, slightly blunted bodies will be considered in the next chapter). As the linear theory for the supersonic flow past thin bodies of Chapter 2, the theory presented here is asymptotic and becomes rigorous only for limitingly thin bodies and limitingly high Mach numbers. However, this theory deals with nonlinear equations, which generates new effects of both a qualitative and quantitative nature. Moreover, many general rules revealed within the framework of this essentially hypersonic theory can be extended, at least, qualitatively, to moderately supersonic Mach numbers.

The *nonlinear hypersonic theory of the flow past thin sharp bodies* has a long history, its foundation having been laid in the works of Tsien (1946), Falkovich (1947), Ilyushin (1948), and Hayes (1948). The systematic presentation of the theory was given in the books of Chernyi (1966), Hayes and Probstein (1966), and Lunev (1975).

8.1 Distinctive Features of the Nonlinear Theory

The following conditions (see Figure 8.1) are at the basis of the nonlinear theory of the hypersonic flow past thin sharp bodies

$$\theta_0 = \max \cos(\vec{n}, \vec{U}_\infty) \ll 1, \quad M_\infty = U_\infty/a_\infty \gg 1 \\ \varepsilon = M_\infty^{-1} + \theta_0 \ll 1 \quad (8.1.1)$$

Here, \vec{n} is the vector of the normal to the body, while \vec{U}_∞ , a_∞ , and M_∞ are the freestream velocity, speed of sound, and Mach number (Figure 8.1).

Usually θ_0 is considered to mean the relative thickness d/L , d and L being the body diameter and length; however, the first condition, 8.1.1, is more rigorous than the condition $d/L \ll 1$. Thus, the latter condition could be fulfilled in the longitudinal flow past a long cylinder, but the disturbance field is determined by its blunt nose, on which $\cos(\vec{n}, \vec{U}_\infty) \sim 1$.

The flow past thin bodies was considered in a part of Chapter 2. However, the applicability of the linear small-perturbation theory outlined in that chapter is determined, apart from the smallness of θ_0 , by the fulfillment of one more condition

$$v \sim U_\infty \theta_0 \ll a_\infty, \quad M_\infty \theta_0 \ll 1 \quad (8.1.2)$$

where v is the body-induced transverse (relative to the vector \vec{U}_∞) velocity component. This constraint is considerably narrower than 8.1.1.

As distinct from the linear theory, the hypersonic thin-body theory outlined in the following is essentially nonlinear (as it is the transonic theory of Section 5.2), though it passes into the linear theory when conditions 8.1.2 are fulfilled. The foundation of the theory is provided by the following limiting properties of the flows under consideration, which were established in the previous chapters as particular examples:

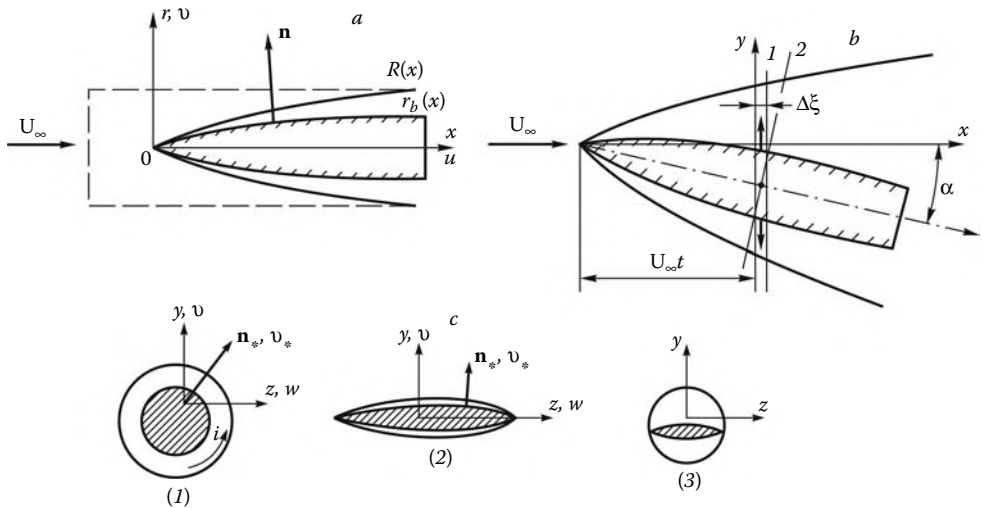


FIGURE 8.1

Flow past thin sharp bodies.

- Smallness of the transverse dimension of the disturbed region.* If it is bounded by an external characteristic, then its slope must satisfy the inequality $\alpha^* \approx M_\infty^{-1} \sim \varepsilon \ll 1$. If the boundary is an intense weak-family shock (only shocks of this family will be considered in the following), then, in accordance with Section 3.7, the angle of its inclination for a wedge with the vertex angle θ is $\alpha \approx \theta(1 + k)$, where $k = \rho_\infty / \rho_s$ is the density ratio across the shock. We emphasize that, in contrast to Chapter 7, the ratio k is no longer considered a small parameter.
- Finiteness of disturbances of the thermodynamic parameters (p , ρ , etc.), despite the smallness of the velocity disturbances.* In fact, for $M_\infty \theta \geq 1$ even the linear theory gives finite pressure disturbances $\Delta p/p \sim M_\infty \theta$ in a shock or in an expansion wave, which is also confirmed by the exact solutions of Sections 3.5 and 4.6.
- Conservation, correct to the second order, of the longitudinal flow velocities.* To an accuracy of M_∞^{-2} , the total velocity coincides with the limiting one, $U \approx U_m$, so that its projection onto the vector \vec{U}_∞ is $u = U \cos \theta = U_m(1 + O(\varepsilon^2))$. An analogous conclusion for the velocity behind a shock with the angle $\alpha \ll 1$ was made at the end of Section 3.5.
However, in this case the transverse velocity is of the order $v \sim U_\infty \theta_0$. Thence follows the *plane section law*. It can be formulated as follows. Let a body move at a velocity $-\vec{U}_\infty$ in a gas at rest. Then we can ignore the velocity $\Delta u = u - U_\infty \sim U_\infty \varepsilon^2$ of the longitudinal gas displacement from fixed thin layers $\Delta \xi$ orthogonal to the vector \vec{U}_∞ (Figure 8.1b), since the body in motion forces the gas in these layers apart without expelling it from the layers.
- Finally, smallness of the longitudinal velocity disturbances, $\Delta u/U \sim \varepsilon^2$, makes it possible to perform the following substitution in the steady-state equations*

$$u \frac{\partial}{\partial x} \rightarrow U_\infty \frac{\partial}{\partial x} \rightarrow \frac{\partial}{\partial t}, \quad x = U_\infty t \quad (8.1.3)$$

Then these equations pass into time-dependent equations in the space of a smaller dimension, which leads to the *hypersonic* version of the *time-dependent analogy* established for the linearized equations in Section 2.7. The manifestation of this analogy in a particular case was noted in Section 4.3, where the equations of the two-dimensional flow characteristics, subject to the conditions similar to 8.1.1, passed into the equations of the characteristics of the one-dimensional time-dependent flow of Section 4.2, the qualitative analogy thus changing to a quantitative one.

These properties, which will be generalized in the following, form the basis of the nonlinear hypersonic theory of the flow past bodies presented in the following.

8.2 Basic Equations: Time-Dependent Analogy

We will first consider the equations of two-dimensional flows, both plane ($v = 0$) and axisymmetric ($v = 1$), in a cylindrical coordinate system x, r with the x axis aligned to the vector \vec{U}_∞ . Let $r = r_b(x)$ be the shape of the body in the gas flow, while u and v are the velocity components in the x and r axes (Figure 8.1a). Then on the body surface we have

$$v/u = \tan \theta = r'_b(x) \sim \theta_0, \quad v \sim u\theta_0 \quad (8.2.1)$$

In a Cartesian coordinate system x, y, z the general relations on a shock (Chapter 3) have the form:

$$\begin{aligned} \Delta p = p - p_\infty &= \rho_\infty v_{n\infty}^2 (1 - k), & \Delta h = h - h_\infty &= (1/2)v_{n\infty}^2(1 - k^2) \\ u &= u_\infty + n_x v_{n\infty}(1 - k), & v &= v_\infty + n_y v_{n\infty}(1 - k) \\ w &= w_\infty + n_z v_{n\infty}(1 - k), & v_{n\infty} &= U_\infty \sin \alpha, & k &= \rho_\infty / \rho \end{aligned} \quad (8.2.2)$$

where $v_{n\infty}$ is the normal velocity at which the gas inflows into the shock and α is the angle of the shock inclination to the vector U_∞ . In our two-dimensional case we have

$$\begin{aligned} n_x &= -\sin \alpha, & n_y &= n_r = \cos \alpha \\ n_z &= 0, & v_\infty &= w_\infty = 0, & u_\infty &= U_\infty \end{aligned} \quad (8.2.3)$$

Since the disturbances in the gas flow are mainly induced by the flow deflection on the body surface, the maximum deflections are attained on the body itself, that is $v \sim \theta_0 U_\infty$ throughout the entire disturbed region including the shock. For the weak branch of the shock with $\cos \alpha \sim 1$ (see Section 3.5) from 8.2.2 it follows that

$$v/U_\infty \sim (1 - k) \sin \alpha \sim \theta_0, \quad u \sim U_\infty \quad (8.2.4)$$

If $1 - k \sim 1$, then $\alpha \sim \theta_0$; if $k \approx 1$, the shock is weak and the angle of its inclination is close to the Mach angle, $\alpha^* \approx M_\infty^{-1}$. Therefore, in the general case we have

$$\alpha \sim \varepsilon = \alpha^* + \theta_0 = M_\infty^{-1} + \theta_0 \ll 1, \quad \delta \sim \varepsilon L \ll 1 \quad (8.2.5)$$

where δ is the transverse dimension of the disturbed region. For a perfect gas this result could be obtained by substituting 8.2.4 in formula 3.3.7 for k ($M_{n\infty} = M_\infty \sin \alpha$)

$$(1 - k) \sin \alpha = \frac{2}{\gamma + 1} \left(1 - \frac{1}{M_{n\infty}^2} \right) \sin \alpha \sim \alpha - \frac{1}{M_\infty} \sim \theta_0 \quad (8.2.6)$$

The orders of the other parameters are obtained from 8.2.2

$$\begin{aligned}\Delta p &\sim \rho_\infty U_\infty \varepsilon \theta_0, & p &\sim \rho_\infty U_\infty^2 (M_\infty^{-2} + \varepsilon \theta_0) \sim \rho_\infty U_\infty^2 \varepsilon^2 \\ \Delta h &\sim U_\infty^2 \varepsilon \theta_0, & h &\sim U_\infty^2 \varepsilon^2, & \rho &= \gamma p / (\gamma - 1) h \\ \Delta u &= u - U_\infty \sim U_\infty \varepsilon \theta_0, & u &= U_\infty [1 + O(\varepsilon \theta_0)] \\ (\rho_\infty U_\infty^2 &= \gamma p_\infty M_\infty^2, & U_\infty^2 &= (\gamma - 1) M_\infty^2 h_\infty)\end{aligned}\quad (8.2.7)$$

Clearly, the ratios $p/\rho_\infty U_\infty^2$ and h/U_∞^2 are small together with ε^2 , whereas the ratios $\Delta p/p_\infty$ and $\Delta h/h_\infty$ may be arbitrary.

We will show that the orders thus obtained are conserved throughout the entire disturbed region. From the equation for the transverse component of the momentum we have

$$\frac{1}{\rho} \frac{\partial p}{\partial r} = -u \frac{\partial v}{\partial x} - v \frac{\partial v}{\partial r} \sim U_\infty^2 \left(\frac{\theta_0}{L} + \frac{\theta_0^2}{\varepsilon L} \right) \quad (8.2.8)$$

From this equation and from the adiabatic relation along streamlines we obtain the same estimates for the parameter increments in the disturbed layer

$$\begin{aligned}\frac{\Delta p}{\rho_\infty U_\infty^2} &\sim \varepsilon \theta_0 & \Delta h &\sim \frac{\Delta p}{\rho} \sim \varepsilon \theta_0 U_\infty^2 \\ \frac{\Delta \rho}{\rho} &\sim \frac{1}{\gamma} \frac{\Delta p}{p} \sim \frac{\theta_0}{\varepsilon}\end{aligned}\quad (8.2.9)$$

Finally, from the Bernoulli equation we obtain the estimate for the velocity deficit

$$\begin{aligned}u \Delta u &\sim U \Delta U - v \Delta v, & U \Delta U &\sim \Delta h \\ \Delta U &\sim \Delta u \sim U_\infty \varepsilon \theta_0\end{aligned}\quad (8.2.10)$$

This estimate, which was already given in Section 8.1, has now been derived as the general result. The plane section law formulated in that section is based precisely on this estimate.

The results obtained can easily be extended to the general three-dimensional case. Let in a Cartesian coordinate system with the x axis aligned to \vec{U}_∞ the body shape be $f(x, y, z) = 0$ with the direction cosines of the normal

$$\begin{aligned}n_x &= f_x \Delta^{-1} \ll 1, & n_y &= f_y \Delta^{-1}, & n_z &= f_z \Delta^{-1} \\ \Delta &= (f_x^2 + f_y^2 + f_z^2)^{1/2}\end{aligned}\quad (8.2.11)$$

We also introduce the normal \vec{n}_* to the cross-section contour $x = \text{const}$ (Figure 8.1c); for this normal we have

$$n_{*y} = f_y \Delta_*^{-1}, \quad n_{*z} = f_z \Delta_*^{-1}, \quad \Delta_* = (f_y^2 + f_z^2)^{1/2} \quad (8.2.12)$$

However, for a thin body (in the sense of conditions 8.1.1) we have

$$f_x^2 \sim \theta_0^2 (f_y^2 + f_z^2), \quad \Delta = \Delta_*, \quad n_y = n_{*y}, \quad n_z = n_{*z} \quad (8.2.13)$$

Thus, the impermeability condition on the body can be brought to the form:

$$v_n = u n_x + v n_y + w n_z = u n_x + v_* = 0, \quad v_* = v n_{*y} + w n_{*z} \sim \theta_0 U_\infty \quad (8.2.14)$$

Here, v_* is the velocity projection onto the normal \vec{n}_* . It would appear reasonable that precisely this velocity component determines the order of the transverse velocity throughout the entire disturbed region. Then for the local angle of the shock α we obtain the same condition 8.2.5 and, hence, the same estimates for the other flow parameters.

An additional estimate is required only for the transverse velocity component tangent to the body, whose value is determined by the circumferential pressure gradient rather than by the impermeability condition. Denoting this velocity by w_l and the corresponding direction by l and bearing in mind the possible condition $l \geq \delta \sim \varepsilon L$, we obtain from the equation of motion

$$\frac{dw_l}{dt} \sim \frac{1}{\rho} \frac{\partial p}{\partial l} \sim \frac{U_\infty^2 \theta_0 \varepsilon}{l}, \quad w_l \sim U_\infty \theta_0 \frac{\delta}{l} \leq U_\infty \theta_0 \quad (8.2.15)$$

Thus, the disturbances of the longitudinal velocity $\Delta u \sim U_\infty^2 \varepsilon^2$ are an order smaller than those of the transverse velocity $v, w_l \sim U_\infty \theta_0$, which was postulated in Section 8.1. This makes it possible to simplify the equations of gas motion 1.9.11. First, correct to second order, we can set $u = U_\infty$ in the total derivative operator d/dt in those equations. Second, the term

$$\frac{\partial u}{\partial x} \sim \varepsilon \theta_0 \frac{U}{L} \ll \frac{\partial v}{\partial y} + \frac{\partial w}{\partial z} \sim U \frac{\theta_0}{\varepsilon L} \quad (8.2.16)$$

in the divergence operator can be omitted. Then, correct to the order ε^2 , the system takes the form:

$$\begin{aligned} \frac{dv}{dt} &= -\frac{1}{\rho} \frac{\partial p}{\partial y}, & \frac{dw}{dt} &= -\frac{1}{\rho} \frac{\partial p}{\partial z}, & \frac{dh}{dt} &= \frac{1}{\rho} \frac{dp}{dt} \\ \frac{d\rho}{dt} + \rho \operatorname{div} \vec{U} &= 0, & \operatorname{div} \vec{U} &= \frac{\partial v}{\partial y} + \frac{\partial w}{\partial z} \\ \frac{d}{dt} \left(U_\infty \frac{\partial}{\partial x} + v \frac{\partial}{\partial y} + w \frac{\partial}{\partial z} \right) &= \frac{\partial}{\partial t} + v \frac{\partial}{\partial y} + w \frac{\partial}{\partial z} \\ x &= U_\infty t \end{aligned} \quad (8.2.17)$$

This system does not contain the longitudinal velocity u and, t being substituted for x , coincides with the system for the two-dimensional time-dependent flows in the y, z plane. We will consider the boundary conditions for this system on the body $f = 0$ and the shock $F = 0$ and associate these surfaces with time-dependent surfaces in the y, z plane

$$\begin{aligned} f(x, y, z) &= f(U_\infty t, y, z) = f_*(t, y, z) \\ F(x, y, z) &= F(U_\infty t, y, z) = F_*(t, y, z) \end{aligned} \quad (8.2.18)$$

Then the normal velocities of the body surface D_f and the shock D_F are determined by relations 1.11.15 through 1.11.17 as follows:

$$D_f = -\frac{f_{*t}}{\Delta_*} = v_* = -U_\infty n_x, \quad D_F = -U_\infty n_x = v_{n\infty} \quad (8.2.19)$$

As for the general shock relations 8.2.2, they are the same for stationary and time-dependent flows.

These results are particularly obvious for plane and axisymmetric flows, in which we have the following relations on the body $r_b(x)$ and the shock $R(x)$

$$\begin{aligned} v &= U_\infty \frac{dr_b}{dx} = \frac{dr_{*b}}{dt}, & v_{n\infty} &= U_\infty \sin \alpha = \frac{dR_*}{dt} \\ r_{*b}(t) &= r_b(U_\infty t), & R_*(t) &= R(U_\infty t) \end{aligned} \quad (8.2.20)$$

Thus, the stationary hypersonic flow past a thin body can be associated with a mathematically and physically equivalent time-dependent piston-induced flow, the piston expansion law being obtained from the original body shape by substituting $U_\infty t$ for x . All the flow parameters (except for Δu) in the stationary flow in an $x = \text{const}$ plane and in the equivalent time-dependent flow at the moment $t = x/U_\infty$ are the same. This is the content of the *hypersonic time-dependent analogy*.

As distinct from the equations of the linear small-perturbation theory, system 8.2.17 is nonlinear. The ratio of the convective terms in this system is of the order

$$(v\partial/\partial y)/(U_\infty\partial/\partial x) \sim \theta_0\varepsilon = M\theta_0(1 + M\theta_0)^{-1} \quad (8.2.21)$$

For $M\theta_0 \geq 1$ these terms are of the same order and only at $M\theta_0 \leq 1$, that is, when condition 8.1.2 is fulfilled, the nonlinear terms could be dropped from these equations. In this case, in accordance with 8.2.7, the ratios $\Delta p/p, \Delta\rho/\rho \sim M_\infty\theta_0$ and others are also small, so that the coefficients of the equations could be set to be constant ($\rho = \rho_\infty$, etc.) with the result that system 8.2.17 becomes linear. Since in this case the shock is close to the Mach line, $\alpha = \alpha^*$, we have $v_{n\infty} \approx a_\infty$, so that the shock relations degenerate into the relations on the forward characteristic, with which the shock coincides within the framework of the linear theory. These questions were covered adequately in Chapters 2 and 4.

The results obtained are also valid for the flows with internal shocks, whose angles α' are also small due to the hypersonic nature of the flow behind the bow shock, which follows from the estimate

$$M^2 = U^2/a^2 \sim \rho U_\infty^2/p \sim \varepsilon^{-2} \gg 1 \quad (8.2.22)$$

The estimates of the flow parameters behind the shocks, for which relations 8.2.2 are valid, do not differ from those presented previously.

A similar conclusion is valid for centered expansion waves originating from corner points on the surface, provided the flow turn angles at these points are small, $\Delta\theta \sim \theta_0$; the pressure difference in these waves is again $\Delta p/\rho U^2 \sim \varepsilon\theta_0$, which follows from the compatibility relations along the characteristics. Although in the vicinities of the corner points the gradients of all the parameters are great, the relative role of the terms of the differential equations does not change, since, due to the fact that the inclination of the centered wave is small for $\varepsilon \ll 1$, the longitudinal derivatives (with respect to x) in this wave are always smaller than the transverse ones by a factor of ε .

Previously the plane section law was formulated in the flow-fitted coordinate system with the x axis aligned to the vector \vec{U}_∞ . Let it now be inclined at a small angle α_0 . Then we have

$$\begin{aligned} u_\infty &= U_\infty \cos \alpha = U_\infty \left(1 - \frac{1}{2}\alpha_0^2\right), & v_\infty &= U_\infty \alpha, & w_\infty &= U_\infty \beta \\ \alpha_0^2 &= \alpha^2 + \beta^2, & \varepsilon &= \theta_0 + \alpha_0 + M_\infty^{-1} \end{aligned} \quad (8.2.23)$$

where α and β are, for example, the pitch and yaw angles (see Figure 2.26 in Section 2.13). Then, replacing U_∞ by u_∞ we arrive at the same conclusion as before, only for $x = \text{const}$ sections. This means that sections 1 and 2 in Figure 8.1b (or sections close to them) are equivalent with respect to the plane section law or the time-dependent analogy, with the sole difference that the equivalent piston now expands in section 2 at velocities v_∞ and w_∞ .

We note that, in distinction with the thin shock-layer theory of Chapter 7, we do not assume here that the density ratio $k = \rho_\infty/\rho$ is small, since our analysis is intended to reveal the asymptotic properties of the flows as $\varepsilon \rightarrow 0$, irrespective of k . However, in the

case of small k the results obtained remain the same. Obviously, the condition $u \approx U_\infty$ retains its validity; since, in accordance with Section 7.1, the disturbed layer thickness is $\Delta r \sim (\rho_\infty/\rho)\theta_0 L$, the estimate for the transverse pressure difference, 8.2.8 and 8.2.9, is also valid, while inequality 8.2.16 can only strengthen, since $\partial u/\partial x \sim k$. An analysis of the corresponding limiting (as $k \ll 1$) time-dependent flows was given in Section 7.5.

Finally, we note that, although in general the time-dependent analogy offers no major advantages in the numerical solution of the equations, since the reduction of the equation number by one is not of crucial importance, it plays a considerable part in establishing physical laws and in certain cases makes it possible to reduce the problem dimensionality, that is, to decrease the number of the independent variables. The examples will be considered in what follows.

8.3 Analogy for the Integral Conservation Laws

In continuation of Section 8.2, we will establish the analogy between the integral characteristics of the equivalent stationary and time-dependent flows. In considering the stationary flow past a body we will choose a cylindrical control surface (Figure 8.1a) coaxial to the x axis, that is, to the velocity vector \vec{U}_∞ and passing through the outer contour of the shock cross-section. Let S_R be the cross-section area confined by this contour and S_0 be the body cross-section area. Then the balance of the gas flow rates across this surface takes the form:

$$\rho_\infty U_\infty S_R = \int_{S_R - S_0} \rho u dS, \quad \rho_\infty S_R = \int_{S_R - S_0} \rho dS \quad (8.3.1)$$

where the second relation is obtained from the first one at $u = U_\infty$. Thus, the conservation law for the mass flow rate across $x = \text{const}$ sections is equivalent to the conservation law for the disturbed layer mass in the sections $\xi = x - U_\infty t = \text{const}$ of the time-dependent flow.

Let us consider the longitudinal momentum conservation law. For a piston expansion in a section $\xi = \text{const}$ there is no longitudinal coordinate at all; therefore, the analog for the longitudinal momentum conservation law in the equivalent time-dependent flow is the energy conservation law. To demonstrate this, we will set $\Sigma_2 = S_R$ in formula 1.7.21 for the body drag X and transform the term $p_\infty S_R$ in terms of the first Equation 8.3.1.

Then formula 1.7.21 takes the form:

$$\int_{S_R - S_0} \rho \left[u(U_\infty - u) - \frac{p}{\rho} + \frac{u}{U_\infty} \frac{p_\infty}{\rho_\infty} \right] dS = X \quad (8.3.2)$$

Invoking the Bernoulli equation and the relation $h = e + p/\rho$ we obtain

$$\begin{aligned} u(U_\infty - u) - \frac{p}{\rho} + \frac{u}{U_\infty} \frac{p_\infty}{\rho_\infty} &= e + \frac{v^2}{2} + \frac{w^2}{2} - \\ \frac{u}{U_\infty} e_\infty - \frac{1}{2}(U_\infty - u)^2 - \frac{U_\infty - u}{U_\infty} h_\infty \end{aligned} \quad (8.3.3)$$

Then Equation 8.3.3 can be brought to the form:

$$\begin{aligned} \int_{S_R-S_0} \rho \left(e + \frac{v^2}{2} + \frac{w^2}{2} \right) dS &= X + \rho_\infty e_\infty S_R + E_1 \\ E_1 &= \int_{S_R-S_0} \rho \left[\frac{1}{2}(U_\infty - u)^2 + \frac{U_\infty - u}{U_\infty} h_\infty \right] dS \end{aligned} \quad (8.3.4)$$

This relation is exact and valid for supersonic flows past arbitrary bodies. But if conditions 8.1.1 are satisfied, then, in view of the estimates made in Section 8.2, correct to the order ε^2 , the term E_1 could be dropped; thus, we obtain

$$\Delta E = E - E_\infty = \int_{S_R-S_0} \rho \left(e + \frac{v^2}{2} + \frac{w^2}{2} \right) dS = X, \quad E_\infty = \rho_\infty e_\infty S_R \quad (8.3.5)$$

This equation represents the energy conservation law in the time-dependent gas flow in the direction perpendicular to the body motion in a unit-width plane layer, the equivalent piston expansion work, or the energy $\Delta E = X$ imparted to the gas by the piston, being equal to the work of the drag X of the original body on a unit path.

Finally, we will consider the conservation law for the transverse momentum perpendicular to the x axis; for the sake of simplicity, we will let it be zero in the freestream. Let \vec{I} be the momentum flux vector (different from that introduced in Sections 7.2 and 7.5), acquired by the gas under the action of the transverse force $\vec{Y} = -\vec{I}$. Then, being projected onto the y axis, this law takes the form:

$$I_y = \int_{S_R-S_0} \rho u v ds = -Y_y, \quad J_y = \int_{S_R-S_0} \rho v ds = \frac{I_y}{U_\infty} = -\frac{Y_y}{U_\infty} \quad (8.3.6)$$

The second relation is derived from the first at $u = U_\infty$ and represents the conservation law for the momentum \vec{J} of a unit plane layer in the expansion of the piston, which has imparted the momentum J_y to the gas along the y axis.

Hence, the time-dependent analogy gives the following relations

$$\Delta E = X, \quad U_\infty \vec{J} = \vec{I} = -\vec{Y} \quad (8.3.7)$$

We note that, so far, the fulfillment of the plane section law at the end section of the control surface sufficed to derive the conservation laws Equations 8.3.5 and 8.3.6. However, if the body is thin everywhere, then these relations could be derived directly from the balance of the forces acting on the body

$$X = - \int_0^x \oint_l p n_x dl dx = \int_0^t \oint_l p v_* dl dt = \Delta E \quad (8.3.8)$$

$$-Y_y = \int_0^x \oint_l p n_y dl dx = U_\infty \int_0^t \oint_l p n_{*y} dl dt = U_\infty J_y \quad (8.3.9)$$

Here, l is the body cross-section perimeter, the integrals on the right-hand sides are the piston expansion work and the momentum imparted to the gas, \vec{n}_* is the normal to the body cross-section contour, and v_* is the velocity along this normal.

In symmetric flows the vectors $\vec{Y} = \vec{J} = 0$; for this reason, we should go over, as was done in Sections 6.8 and 7.5, to the momenta I_r and J_r in the second relations 8.3.6 writing it for one-half of a plane flow ($\nu = 0$) and for a region between two near meridional sections in an axisymmetric flow ($\nu = 1$). The relation $I_r = U_\infty J_r$ remains valid but the corresponding force Y_r is dependent not only on the pressure distribution over the body; the explanation of this fact is given in Figure 7.21 (Section 7.5).

We note in conclusion that the drag of a thin body in a hypersonic flow is of the order $X \sim \Delta p S_0 \sim \rho_\infty U_\infty^2 \theta_0 \varepsilon S_0$, which amounts to only a small fraction of the oncoming flow momentum $I_x \sim \rho_\infty U_\infty^2 S_0$ across the area S_0 . This fact should be borne in mind when checking the accuracy of calculations by means of the integral conservation laws.

8.4 Similarity Law

In accordance with the perturbation orders established in Section 8.2, we introduce the following dimensionless quantities

$$x' = x/L, \quad y' = y/L\theta_0, \quad z' = z/L\theta_0 \quad (8.4.1)$$

$$\begin{aligned} p' &= \frac{p}{\rho_\infty U_\infty^2 \theta_0^2}, & h' &= \frac{h}{U_\infty^2 \theta_0^2}, & \rho' &= \frac{\rho}{\rho_\infty} \\ u' &= \frac{u - U_\infty}{U_\infty^2 \theta_0^2}, & v' &= \frac{v}{U_\infty \theta_0}, & w' &= \frac{w}{U_\infty \theta_0} \end{aligned} \quad (8.4.2)$$

In these variables, we represent the body shape and the unknown shock surface in the general form for three-dimensional flows and in the explicit form for plane and axisymmetric flows

$$\begin{aligned} f(x', y', z') &= 0, & F(x', y', z') &= 0 \\ r'_b &= r_b(x')/L\theta_0, & R' &= R(x')/L\theta_0 \end{aligned} \quad (8.4.3)$$

In the new variables, Equation 8.2.17 do not change their form, as well as the boundary conditions of Equation 8.2.14 on the body surface

$$v'_n = n'_x + v' n_{*y} + w' n_{*z} = 0 \quad (\theta_0 n'_x = n_x) \quad (8.4.4)$$

However, relations 8.2.2 on the bow shock for a perfect gas in the freestream involve the parameters determining the flow past the body

$$p'_\infty = (\gamma M_n^2)^{-1}, \quad h'_\infty = [(\gamma - 1)M_n^2]^{-1}, \quad M_n = M_\infty \theta_0 \quad (8.4.5)$$

From the conjectured uniqueness of the solution of the problem it follows that the solutions of the same dimensionless equations coincide with the same dimensionless shapes 8.4.3 of the bodies compared and the same freestream parameters 8.4.5 in the sense that *the distributions of the dimensionless quantities p' , v' , and so on, with respect to the dimensionless*

variables x', y', z' in the flows compared are the same. This is the formulation of the *hypersonic similarity law for thin bodies*. For a perfect gas we have

$$\frac{p}{\rho h} = \frac{p'}{\rho' h'} = \frac{\gamma - 1}{\gamma}, \quad (a')^2 = \frac{a^2}{U_\infty^2 \theta_0^2} = \gamma \frac{p'}{\rho'} \quad (8.4.6)$$

In this case, the similarity criteria are the parameters

$$\gamma, \quad M_\infty \theta_0 \quad (8.4.7)$$

Thus, in the hypersonic perfect-gas flow past thin bodies the requirements of the general similarity law (Section 1.12), namely, the identity of the Mach number M_∞ and the body shape at the same adiabatic exponent γ , are considerably weakened. In this case, the flows past *affinely similar* bodies, which could be obtained one from another by uniform extension in directions normal to the freestream velocity, are similar. Thus, the flow past a thin body at a very high Mach number $M_{\infty 1}$ (hardly realizable in experiments) could be simulated by a flow with a smaller $M_{\infty 2}$ by increasing the relative body thickness in accordance with the equality $\theta_2 = \theta_1 M_{\infty 1} / M_{\infty 2}$. In this case, the pressures at the corresponding points of the similar bodies change as $p \sim \theta_0^2$, and so on.

If the body shape is preassigned in a system other than a flow-fitted coordinate system, then all the freestream velocity components, which appear in the shock relations 8.2.2, should be taken into account. Then, in accordance with 8.2.23, the following, purely kinematic criteria

$$v'_\infty = v_\infty / U_\infty \theta_0 = \alpha / \theta_0, \quad w'_\infty = \beta / \theta_0 \quad (8.4.8)$$

are added to those listed previously.

Using definitions given in Section 2.13, the aerodynamic coefficients of similar flows can be presented in the form:

$$\begin{aligned} c_x &= \theta_0^2 c'_x, & c'_x &= \frac{2}{s'_0} \int_0^1 \oint p' n'_x dl' dx' \\ c_y &= \theta_0 c'_y, & c_m &= \theta_0 c'_m \\ S'_0 &= s_0 \theta_0^{-2}, & l' &= l \theta_0^{-1} \end{aligned} \quad (8.4.9)$$

where c'_x, c'_y, c'_m , and so on, are the same for similar flows.

The similarity law derived is very useful and has a good accuracy over a wide range of θ_0 and M_∞ , which was already shown in Section 6.6 (Figure 6.10) with reference to the example of slender cones and is confirmed by the data in Figure 8.2. In this figure, as in Figure 2.13, the argument is taken in the form $K = \theta_0 \sqrt{M_\infty^2 - 1}$; this parameter was obtained within the framework of the linear theory of Section 2.7 and passes into $M_\infty \theta_0$ for $M_\infty \gg 1$. Thus, this quantity is the similarity criterion for the flows past thin bodies over the entire $M_\infty > 1$ range, except for transonic Mach numbers $M_\infty \approx 1$ (Section 5.2).

For $M_\infty^2 \theta_0^2 \gg 1$ we can set $p'_\infty = 0$ and $h'_\infty = 0$ in the shock relations; then the solution no longer depends on $M_\infty \theta_0$. In this case, the sole similarity criterion is the adiabatic exponent γ .

In Section 1.12 we also presented the derivation of the general similarity law from the similarity and dimensionality theory. Similar reasoning for our case within the framework of the time-dependent analogy presents no special problems. The perfect-gas flow at the

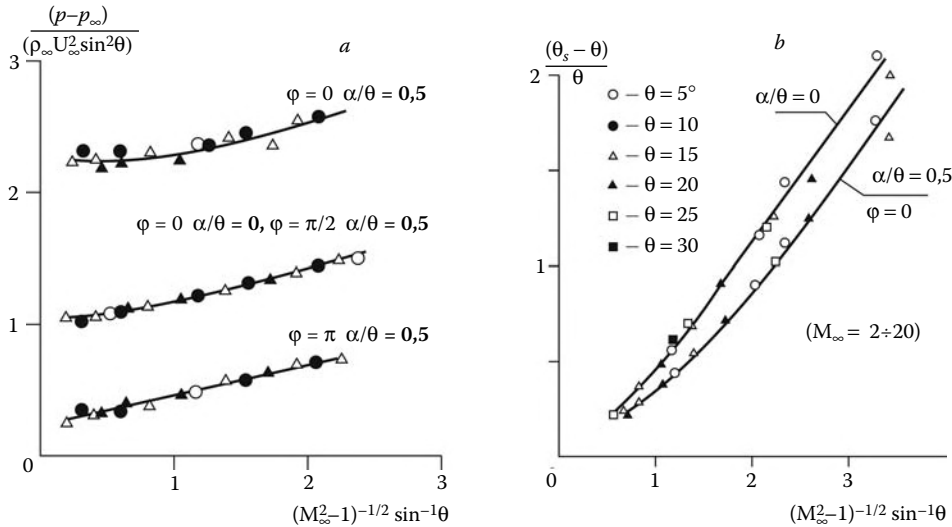


FIGURE 8.2
Pressure (a) and shock layer thickness (b) in the flows past slender cones.

expansion of a piston (for the sake of simplicity, we consider the one-dimensional case) depends on the parameters

$$t, \quad r, \quad T, \quad d, \quad \rho_\infty, \quad a_\infty \quad (8.4.10)$$

Here, T and d are the characteristic time and dimension in the piston expansion law. Then, forming dimensionless complexes of these parameters and bearing in mind that for the original stationary flow past a body we have $x = U_\infty t$, $L = U_\infty t$, and $d = \theta_0 L$, we can obtain the following structure of the solution, for example, for the pressure

$$p = \rho_\infty \frac{d^2}{T^2} P \left(\frac{t}{T}, \frac{r}{d}, \frac{d}{a_\infty T}, \gamma \right) = \theta_0^2 \rho_\infty U_\infty^2 P \left(\frac{x}{L}, \frac{r}{\theta_0 L}, M_\infty \theta_0, \gamma \right) \quad (8.4.11)$$

which reflects the similarity law.

The derivation of the similarity law in the original, stationary formulation is somewhat more complicated, since in this case all the independent variables have the same dimensionality. To do this, the characteristic velocity $U_\infty \theta_0$ should be introduced instead of U_∞ , as was done in the general similarity law of Section 1.12, and two independent scales L and $L \theta_0$ should be taken for measuring the distances in the longitudinal and transverse directions, respectively; when going over the equivalent time-dependent flows this is done automatically and more conveniently.

Previously we have written the similarity criteria, 8.4.7, for a perfect gas. For the sake of completeness of the theory we will also consider the general case of a two-parameter, equilibrium gas, whose equation of state is most conveniently presented in the quasiperfect form using the effective adiabatic exponent, as in Section 1.3

$$\begin{aligned} \frac{p}{\rho h} &= \frac{p'}{\rho' h'} = \frac{\gamma_* - 1}{\gamma_*} \\ \gamma_*(p, h) &= \gamma_*(\theta_0^2 \rho_\infty U_\infty^2 p', \theta_0^2 U_\infty^2 h') = \gamma'_*(p', h') \end{aligned} \quad (8.4.12)$$

In this case, the flows may be similar only if the functions $\gamma'_*(p', h')$ are the same; for a gas of a given sort this leads, in view of 8.4.5, to the following similarity parameters

$$U_\infty \theta_0, \quad \rho_\infty, \quad p'_\infty, \quad h'_\infty \quad (8.4.13)$$

The presence of dimensional quantities in the system of the similarity criteria should be meant in the same sense as in Section 1.12.

The distinction from the general similarity law of Section 1.12 consists only in that the velocity normal to the body, $U_\infty \theta_0$, rather than the total freestream velocity U_∞ is the governing parameter, since precisely this velocity determines the gas composition and state in the shock layer near the body. The corresponding points of the similar flows are characterized by the same values of the pressure, temperature, and other thermodynamic parameters.

For a gas, perfect in the undisturbed flow, criteria 8.4.5 are reduced to the similarity criterion $M_\infty \theta_0$, but the dependence of the solution on ρ_∞ and $U_\infty \theta_0$ is retained via the equation of state. However, for air the ρ_∞ -dependence could be neglected in view of the fact that the p -dependence of γ_* is weak (Section 1.3). Taking into account that the real gas properties usually manifest themselves in very intense shocks only, that is, for $M_\infty \theta_0 \gg 1$, the latter parameter could also be omitted within the framework of the hypersonic stabilization law. In this case the solution depends on the parameter $U_\infty \theta_0$ only.

8.5 Flow around Thin Wings

A particular class of bodies allowing for considerable simplification of the mathematical problem of the flow past them is represented by thin, sharp-edged wings with the wing span l far exceeding the thickness d . In this case, all the points on the wing surface are close to a certain plane $y = 0$ (plots 2 and 3 in Figure 8.1c). We will also require that the wing span be much larger than the Mach cone width and, moreover, that the angle, which the normal \vec{n} to the body makes with the y axis, be small everywhere. Thus, the following conditions must be fulfilled

$$\begin{aligned} \varepsilon &= \theta_0 + M_\infty^{-1} \ll 1, & \varepsilon_z &= \varepsilon L/l \ll 1, & M_\infty &\gg 1 \\ \theta_0 &= \max \cos(\vec{U}_\infty, \vec{n}) \ll 1 \end{aligned} \quad (8.5.1)$$

These conditions, more rigorous than Equation 8.1.1, are satisfied, for example, by contour 2 in Figure 8.1c, but are not satisfied by contour 3 in the same figure. Though the latter is also strongly flattened, we have for it $\varepsilon_z \sim 1$. The condition $\varepsilon \ll 1$ leads to the plane section law and the similarity law considered previously. However, the condition $\varepsilon_z \ll 1$ presents some new possibilities, which will be considered in what follows.

In this case the bow shock $F(x, y, z) = 0$ is attached to the leading edges and the direction cosines of its normal are as follows

$$\begin{aligned} n_x &= F_x \Delta^{-1} \sim \theta_0 \ll 1, & n_y &= F_y \Delta^{-1} \approx 1 \\ n_z &= F_z \Delta^{-1} \sim \varepsilon_z \ll 1, & \Delta &= (F_x^2 + F_y^2 + F_z^2)^{1/2} \approx F_y \end{aligned} \quad (8.5.2)$$

From Equation 8.2.2 we obtain for w

$$w \sim U_\infty \theta_0 \varepsilon_z \ll v \sim U_\infty \theta_0 \quad (8.5.3)$$

The same order of the peripheral velocity on the body is induced by the pressure gradient; this can be easily shown by setting $l \sim \varepsilon L / \varepsilon_z$ in formulas 8.2.15. Then we have

$$\left(w \frac{\partial}{\partial z} \right) : \left(v \frac{\partial}{\partial y} \right) \sim \varepsilon_z^2, \quad \frac{\partial w}{\partial z} : \frac{\partial v}{\partial y} \sim \varepsilon_z^2 \quad (8.5.4)$$

By virtue of these relations, we can drop the corresponding terms in Equations 8.2.17 through 8.2.20, thus introducing the error of the order ε^2 , and separate out an independent group from the equations of motion

$$\begin{aligned} \frac{dv}{dt} &= U_\infty \frac{\partial v}{\partial x} + v \frac{\partial v}{\partial y} = \frac{\partial v}{\partial t} + v \frac{\partial v}{\partial y} = -\frac{1}{\rho} \frac{\partial p}{\partial y} \\ \frac{d\rho}{dt} + \rho \frac{\partial v}{\partial y} &= 0, \quad \frac{dh}{dt} = \frac{1}{\rho} \frac{dp}{dt}, \quad x = U_\infty t \end{aligned} \quad (8.5.5)$$

with the following boundary conditions on the body $r_b(x, z)$ and the shock $R(x, z)$

$$v = U_\infty \frac{\partial r_b}{\partial x} = \frac{\partial r_*}{\partial t}, \quad v_{n\infty} = U_\infty \frac{\partial R}{\partial x} = \frac{\partial R_*}{\partial t} \quad (8.5.6)$$

The equations and boundary conditions thus obtained govern the plane time-dependent flow in the planes $z = \text{const}$ induced by the piston expansion $r_*(t, z)$ in these planes. The solutions in each plane are independent, which reduces the dimensionality of the original problem. If need be, the other velocity components, u and v , could be determined from the purely kinematic equations at known v , ρ , and p with the boundary conditions on the known shock.

This result is called the *stripe rule*. Its physical meaning is that the gas is near stagnant not only in the $x = \text{const}$ planes but in the $z = \text{const}$ planes as well.

However, these inferences are appropriate in the full measure only for the wings with a smooth planform of the edge, rounded at the wing tip, that is, in the case in which the wing span determines the order of the derivatives with respect to z . These conditions are not satisfied, for example, by the traces of the corner points of the wing's leading edges in Figure 8.3. In fact, the domains of influence of these points lie within the Mach cones with the transverse dimension of the order $\Delta z \sim \varepsilon L \sim \varepsilon_z l$, which determines the order of the derivatives with respect to z in these singular domains. The ratio of the terms of Equation 8.5.4 in these domains is ε_z rather than ε_z^2 ; thus, the accuracy of the stripe rule is naturally decreased by an order in the singular domains.

At the same time, taking into account the terms of the type $\partial w / \partial z$, and so on, in Equation 8.5.5, which are of the relative order ε_z , introduces a correction of the order ε_z in the

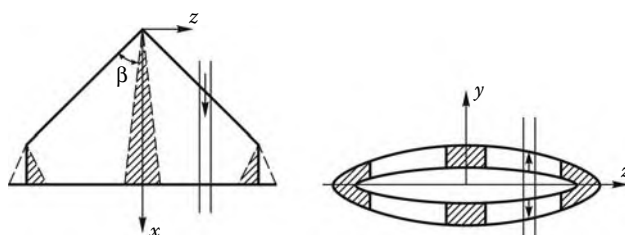
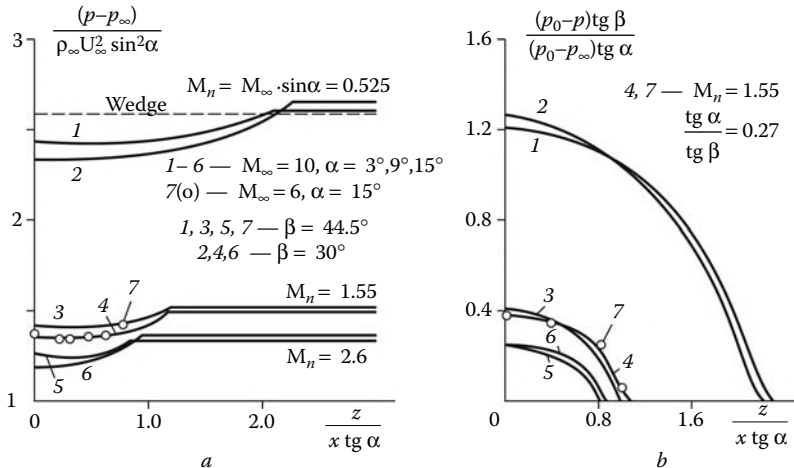


FIGURE 8.3
Concerning the stripe rule. Singular domains are shaded.

**FIGURE 8.4**

Pressure on the windward side of a delta wing.

solutions of these equations, so that the solution in the singular domain can be represented in the form:

$$p(x, y, z) = p_0(x, y, z) + \varepsilon_z p_1(x, y, z) \quad (8.5.7)$$

where the term p_0 corresponds to the stripe rule. However, for a finite number of singular domains their relative area is small (of the order ε_z) and the error of the order ε_z in the solutions in these domains introduces the same second-order error ε_z^2 in the integral characteristics, for example, in the lift, as the stripe theory itself.

By way of illustration, we will consider a triangular plate with the vertex angle 2β . The flow around this plate is conical and depends on the ratios y/x and z/x only. An analysis of these flows was made in Section 6.7; therefore, here we will note only their singularities related with the smallness of the angle of attack, $\alpha \ll 1$, so that $\varepsilon = \alpha + M_\infty^{-1}$ and $\varepsilon_z = \varepsilon \cot \alpha$. By virtue of Section 8.4, the similarity criteria of the problem are as follows:

$$M_\infty \alpha, \quad \alpha L/l = \alpha \cot \beta \quad (8.5.8)$$

As $\alpha / \tan \beta \rightarrow 0$, the stripe theory holds, so that the pressure on the plate is the same as on a wedge with the angle $\pm \alpha$ and depends on the parameter $M_\infty \alpha$ only. This is confirmed by the data for the windward side of the plate presented in Figure 8.4a. For this reason, the solution in the central, low-pressure region (see Section 6.7) depends on the parameter $\alpha \cot \beta$ comparatively weakly, though the coincidence of both criteria 8.5.8 for curves 4 and 7 makes them closer. The representation of the solution in the form 8.5.7 in Figure 8.4b gives almost coinciding additional terms p_1 .

8.6 Thin Bodies at High Incidence

The plane section law can also be realized in the supersonic flow past thin, high-aspect-ratio bodies at a large angle of attack α provided that the relative transverse dimension δ of the disturbed region is small. In Section 6.6 it was shown that for slender cones under these

conditions the law is realized even for moderately supersonic normal Mach numbers M_n . Thus, the following analysis will be subject to the conditions

$$\varepsilon = \max(\delta/L, d/L) \ll 1, \quad M_n = M_\infty \sin \alpha > 1 \quad (8.6.1)$$

Here, L is the body length and d is its diameter.

In essence, the second condition ensures the fulfillment of the first one. In this case $\delta \leq d$ for $M_n - 1 \sim 1$ or $M_n \gg 1$; however, the ratio δ/d increases as $M_n \rightarrow 1$, so that the real small parameter of the problem is $\varepsilon = \max(\delta/L)$. Thus, the theory outlined in the following goes beyond the scope of the hypersonic theory. Moreover, at the end of the section we shall also discuss a possibility of extending the results obtained to subsonic Mach numbers, $M_n < 1$.

We note that at high α the leeward flow region may be fairly thick (Section 6.6) and, moreover, contain viscous separation zones (which are not considered here). If this is the case, our analysis is appropriate only to the windward side.

As earlier, we will write down the body and shock shapes in the variables

$$\begin{aligned} f(x', y', z') &= 0, & F(x', y', z') &= 0 \\ x' &= x/L, & y' &= y/\varepsilon L, & z' &= z/\varepsilon L \end{aligned} \quad (8.6.2)$$

Then the direction cosines of the normal are as follows

$$\begin{aligned} n_x &= f_x \Delta^{-1} = \varepsilon f'_x \Delta_*^{-1} = n'_x \varepsilon \\ n_y &= f_y \Delta^{-1} = f'_y \Delta_*^{-1} = n_{*y}, & n_z &= n_{*z} \\ f'_x &= \frac{\partial f}{\partial x'}, & f'_y &= \frac{\partial f}{\partial y'}, & f'_z &= \frac{\partial f}{\partial z'} \\ \Delta &= (f_x^2 + f_y^2 + f_z^2)^{1/2} = \Delta_* / \varepsilon L, & \Delta_* &= [(f'_y)^2 + (f'_z)^2]^{1/2} \end{aligned} \quad (8.6.3)$$

where n_{*y} and n_{*z} are the direction cosines of the normal to the body cross-section contour $x = \text{const}$. We introduce the dimensionless variables

$$\begin{aligned} p &= p' \rho_\infty v_\infty^2, & \rho &= \rho' \rho_\infty, & h &= h' v_\infty^2 \\ u &= u' u_\infty, & v &= v' v_\infty, & w &= w' v_\infty \\ u_\infty &= U_\infty \cos \alpha, & v_\infty &= U_\infty \sin \alpha, & v_n &= v'_n v_\infty \end{aligned} \quad (8.6.4)$$

In these variables, only the formulas for the velocities in relations 8.2.2 change their form:

$$\begin{aligned} u' \cot \alpha &= \cot \alpha - \varepsilon n'_x v'_{n\infty} (1 - k) \\ v'_{n\infty} &= \varepsilon \cot \alpha u'_\infty n'_x + v'_\infty n_{*y} + w'_\infty n_{*z} \end{aligned} \quad (8.6.5)$$

The dimensionless freestream parameters are as follows

$$\begin{aligned} u'_\infty &= v'_\infty = \rho'_\infty = 1, & w'_\infty &= 0 \\ p'_\infty &= (\gamma M_n^2)^{-1}, & h'_\infty &= [(\gamma - 1) M_n^2]^{-1} \end{aligned} \quad (8.6.6)$$

In the new variables, the equations of motion take the form:

$$\begin{aligned} \frac{d}{dt'} (u' \cot \alpha) &= -\frac{\varepsilon}{\rho'} \frac{\partial p'}{\partial x'} \\ \frac{d}{dt'} &= u' \varepsilon \cot \alpha \frac{\partial}{\partial x'} + v' \frac{\partial}{\partial y'} + w' \frac{\partial}{\partial z'} \end{aligned} \quad (8.6.7)$$

$$\begin{aligned} \frac{dv'}{dt'} &= -\frac{1}{\rho'} \frac{\partial p'}{\partial y'}, & \frac{dw'}{dt'} &= -\frac{1}{\rho'} \frac{\partial p'}{\partial z'} \\ \frac{1}{\rho'} \frac{d\rho'}{dt'} + \varepsilon \cot \alpha \frac{\partial u'}{\partial x'} &+ \frac{\partial v'}{\partial y'} + \frac{\partial w'}{\partial z'} = 0 \\ \frac{dh'}{dt'} &= \frac{1}{\rho'} \frac{dp'}{dt'}, & \frac{p'}{\rho' h'} &= \frac{\gamma - 1}{\gamma} \end{aligned} \quad (8.6.8)$$

Finally, the boundary condition on the body is as follows:

$$v'_n = \varepsilon \cot \alpha u' n'_x + v' n_{*y} + w' n_{*z} = 0 \quad (8.6.9)$$

From 8.6.5 it follows that, correct to the order ε , the following relation on the shock holds

$$u' \cot \alpha = \cot \alpha + O(\varepsilon) \text{ or } u' = 1 \quad (8.6.10)$$

In view of Equation 8.6.7, the right-hand side of which is also of the order ε , this relation is fulfilled along streamlines. We can set $u' = 1$ in Equation 8.6.8, thus introducing an error of the order ε^2 only. These equations turn out to be independent of Equation 8.6.7, this situation being completely analogous to that of Section 8.2. Thence two consequences follow (Sychev, 1960).

The first is the *similarity law*: the hypersonic flows past affinely similar thin bodies at a finite angle of attack are similar provided the following criteria coincide

$$K_1 = (d/L) \cot \alpha, \quad M_n = M_\infty \sin \alpha, \quad \gamma \quad (8.6.11)$$

For similar cones these criteria were established in Section 6.6 (for cones we have $d/L = \theta_0$).

As before, the similarity manifests itself in the identity of the dependences of the dimensionless functions introduced previously on the dimensionless variables $p'(x/L, y/d, z/d)$, and so on, since the parameter ε used previously is determined by the solution and is thus dependent on the same similarity criteria.

For small α this law passes into the law established in Section 8.4

$$K_1 \rightarrow \theta_0/\alpha, \quad M_n \rightarrow M_\infty \alpha = M_\infty \theta_0/K_1 \quad (8.6.12)$$

The second consequence is the *plane section law* or the *time-dependent analogy* resulting from the condition 8.6.10. We will make the change of variables

$$x = t u_\infty = t U_\infty \cos \alpha \quad (8.6.13)$$

Then at $u' = 1$ Equation 8.6.8 passes into the equations of the time-dependent gas flow in the cross-section $\xi = x - u_\infty t = 0$, which follows from the transformation $u_\infty \partial / \partial x = \partial / \partial t$. The equivalent piston not only expands following the $f(U_\infty t, y, z) = f_s(t, y, z) = 0$ law, but also moves in the plane $\xi = \text{const}$ at the velocity $-v_\infty$. The conditions on the body and the shock also go automatically over time-dependent ones.

The physical meaning of this plane section law is the same as earlier: the gas, as it were, remains in the planes normal to the body axis and fixed in space. This can occur due to the velocity (u') constancy for $\cot \alpha \sim 1$ and thanks to the velocity smallness for small $\cot \alpha$. The parameter $(d/L) \cot \alpha$ represents the Strouhal number (cf. Section 1.12) of the time-dependent piston expansion with the scale length d and time $t_0 = L/u_\infty$ in the flow having the velocity $v_\infty = U_\infty \sin \alpha$. Clearly, the role played by this time dependence is

small, together with $(d/L) \cot \alpha$, and vanishes as $(d/L) \cot \alpha \rightarrow 0$. In this case the flow in each $x = \text{const}$ plane coincides with the flow past a plane airfoil of the same shape, as that of the local cross-section of the original body in the flow with the velocity v_∞ or, more exactly, in view of the presence of the longitudinal velocity $u \neq 0$ constant over the cross-section, with the flow past an infinite cylinder at the angle of attack α .

The accuracy of the similarity law can be judged from the data for cones presented in Figure 6.10 (Section 6.6). Clearly, the shock shapes and pressure distributions obey the similarity law, the pressure depending on the normal Mach number M_n only slightly. A failure of assumptions 8.6.1 leads to the violation of the similarity law for the shock shapes for $\theta_0 \geq 10^\circ$, though the similitude in the pressure distributions over the bodies is still good, apparently, thanks to its Newtonian nature. At $K \leq 0.05$ the solution coincides with that for a two-dimensional cylinder in the flow with the Mach number M_n .

By analogy with Sections 8.2 and 8.4, the results obtained could be extended to the body with bends in the generator (the flows with internal shocks or expansion waves) and to the case of the real gas flow with an equation of state of the general form. In the latter case, by analogy with Section 8.4 and with the same accompanying consequences, the dimensional criteria ρ_∞ and $v_\infty = U_\infty \sin \alpha$ should be added to the similarity criteria 8.6.12.

Some results obtained previously could be generalized to the case of nonuniform flow past thin bodies (e.g., to the case of a wing's leading edge, stabilizer, fin, etc., mounted on the fuselage inducing a curvilinear shock). For this purpose, it is sufficient that the transverse d_1 (in the $x = \text{const}$ plane) and longitudinal L_1 (along the x axis) nonuniformity scales satisfy the conditions

$$d \leq d_1, \quad d \ll \min(L, L_1) \quad (8.6.14)$$

For $d \ll d_1$ only the oncoming flow nonuniformity in the x direction could be taken into account; if, in addition to that, we have $L \ll L_1$, then the body is, as it were, in a uniform flow.

In the general case ($u_\infty \neq \text{const}$) the longitudinal velocity field may be nonuniform; then the plane section law does not hold. From Equation 8.6.7 it follows only that the variation of the velocity u' along the streamlines is small together with ε . As $(d/L) \cot \alpha \rightarrow 0$, all the derivatives with respect to x in Equation 8.6.8 and boundary conditions 8.6.5 vanish with the result that in each normal section the flowfield is the same as in the two-dimensional transverse flow past a blunt body with the local velocity v_∞ , except for the longitudinal velocity, which is either constant or small. In the latter case, internal stagnation points can occur in the shock layer if the pressure gradient along the body is positive; this can lead to qualitative changes in the flow pattern (see Section 9.8).

We will now touch on the possible extension of the results obtained to subsonic velocities ($M_n < 1$). Formally, the whole previous analysis retains its validity for these flows, since the freestream conditions 8.6.6 are independent of the presence or absence of a shock. However, the condition $\delta \ll L$ must be fulfilled. To estimate the ratio δ/d for small M_n we can use the data on the subsonic flow past a circular cylinder; in accordance with Section 2.10, the velocity disturbances in this flow decrease fairly rapidly, as $(d/r)^2$. By analogy with this flow, we can expect that the viscous zone downstream of a body, where the excess pressure level is comparable with that on the windward side, does not exert a considerable influence on the flow over that side, and that for a yawed cylinder of an appreciable extent ($d \ll L$) the windward flow in the normal sections far away from the body nose is adequately described by the inviscid solution of Section 2.10.

However, the time-dependent analogy cannot be directly applied to the case of a body of a variable cross-section in incompressible flow, since, as was shown in Section 2.14, the

problem of the two-dimensional piston expansion has no solution. Therefore, in a subsonic flow past an even rather long thin body at high incidence the finite length L of the body could not be ignored. In this case, in accordance with Section 2.12, disturbances far from the body die out as $(L/r)^3$.

At transonic velocities, $M_n \approx 1$, the disturbed flow region extent in an $x = \text{const}$ cross-section is considerably larger than the body cross-section size d (Figure 5.1, Section 5.2). This restricts considerably the applicability range of the plane section law by the Mach numbers $M_n < 2$. In other situations, this requires, at least, supplementary analysis and testing.

8.7 Time-Dependent Flows: Curved Body Rule

Let a thin body move at a hypersonic velocity $-\vec{U}_\infty$ in a fixed space (x'', y'', z'') and simultaneously maneuver relative to an inertial coordinate system (x, y, z) moving with the initial velocity (at the moment $t = 0$ when the body motion began to be tracked) $-\vec{U}_{0\infty}$. The coordinate axes of the same name of the two systems are parallel and the x and x'' axes are aligned with the vector $\vec{U}_{0\infty}$ (Figure 8.5a).

The body maneuver can consist of both spatial oscillations about a point O , for example, the center of mass, and the motion along a curvilinear trajectory accompanied by rotation

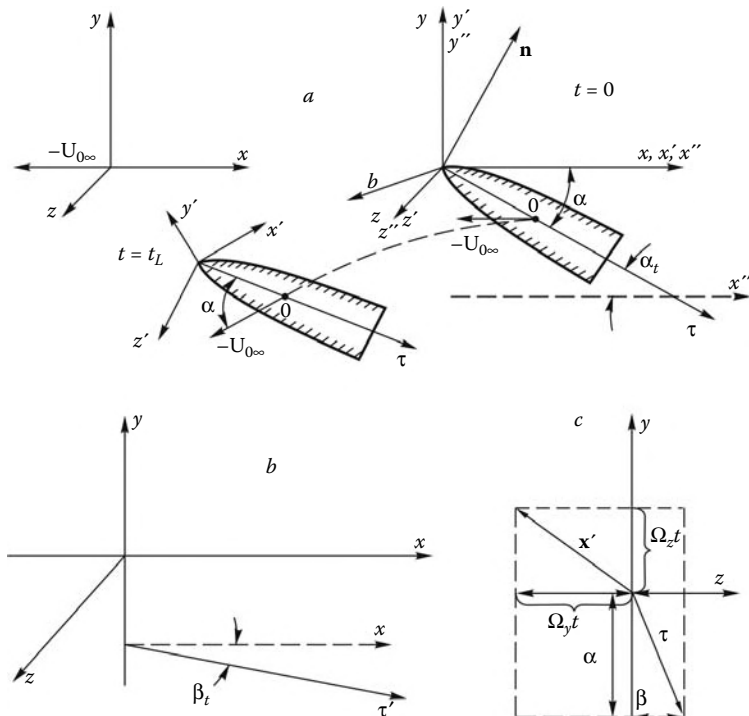


FIGURE 8.5
Unsteady motion of a thin body.

of the vector \vec{U}_∞ . For a time, we will assume the absolute magnitude U_∞ of the velocity vector to be constant and take into account only the variation of its direction.

We will also introduce the body-fitted (τ, n, b) and the flow-fitted x', y', z' coordinate systems; for $t = 0$ the latter coincides with the inertial system (see Section 2.13); in Figure 2.26a the flow-fitted system is denoted by (x, y, z) , while the inertial system is absent. The relative location of the body- and flow-fitted coordinate systems is determined by the angles of attack α and slip β (Figure 2.26a), while that of the body-fitted and inertial (or fixed) systems by the angles of pitch α_t between the τ axis and the (x, z) plane and yaw β_t between the projection τ' of the τ axis on the (x, z) plane and the x axis (Figure 8.5b), or, for small angles, between the τ axis and the (x, y) plane. Obviously, for $t = 0$ we have $\beta_t = \beta$. For the sake of definiteness, we must also preassign the angles of rotation of the flow- and body-fitted systems about the x and τ axes (γ_x and γ_τ in Figure 2.26a). Naturally, in unsteady problems all the coordinate angles introduced are time-dependent.

In the body- and flow-fitted systems, we preassign the body shape as follows:

$$f_0(t, \tau, n, b) = 0, \quad f(t, x, y, z) = 0 \quad (8.7.1)$$

In the general case, the fact that f_0 is time dependent signifies the variation of the shape of the body itself (deflection of controls, vibration, etc.). The change from the function $f_0(\dots)$ to $f(\dots)$ is determined by the corresponding coordinate transformation.

For the general theory we shall need only the body shape in the inertial system of coordinates; as for particular forms of the body shape and the mutual location of the coordinate systems, these data will be used only for applications.

Let now the body surface make a small angle of the order $\bar{\theta}$ with the x axis; we will also assume that the time-dependent component D_f of the body velocity in the inertial coordinate system is small, that is, the following condition is fulfilled

$$\begin{aligned} \varepsilon' &= \varepsilon + \bar{\omega} \ll 1, & \varepsilon &= M_\infty^{-1} + \bar{\theta} \\ \bar{\theta} &= \max |n_x|, & n_x &= \cos(\vec{n} \cdot \vec{x}) \\ \bar{\omega} &= D_{f0}/U_\infty, & D_{f0} &= \max |D_f| \end{aligned} \quad (8.7.2)$$

Here, \vec{n} is the instantaneous normal to the body surface, while the velocity D_f is determined in accordance with the procedure described in Section 1.11

$$D_f = \Delta^{-1} f_t, \quad \Delta = (f_x^2 + f_y^2 + f_z^2)^{1/2} \quad (8.7.3)$$

If the body of length L rotates about a certain point O at an instantaneous angular velocity $\bar{\omega}$, then $D_f \sim \bar{\omega}L$. In the particular case of oscillatory motion we have $\omega \sim \alpha_m/T$, α_m and T being the oscillation amplitude and period (these situations were discussed in Sections 7.4 and 7.6 in the approximate Newtonian formulation). The smallness of ω ensures the smallness of the angle $\omega L/U_\infty$ through which the body turns in the characteristic gas dynamic time interval $\Delta t \approx L/U_\infty$; during this interval the body traverses one or another plane fixed in space.

To start with, we will evaluate disturbances introduced into the flow by the body in motion. In the (x, y, z) coordinate system the normal component of the gas velocity on the body surface is $v_n = D_f$; therefore, by analogy with Equation 8.2.14, from the impermeability condition we obtain the following estimate for the velocity component v_* along the normal \vec{n}_* to the contour of an $x = \text{const}$ body cross-section:

$$v_* = v n_{*y} + w n_{*z} = D_f - n_x u \sim (\bar{\theta} + \bar{\omega}) U_\infty \ll U_\infty \quad (8.7.4)$$

This condition, as well as that of Section 8.2, determine the order of the transverse velocities in the shock layer. Then from the shock relations we derive an estimate for the velocity $v_{n\infty}$ with which the gas inflows into the bow shock

$$\begin{aligned} v_* &\sim v_{n\infty}(1 - k) \sim (\bar{\theta} + \bar{\omega})U_\infty \\ v_{n\infty} &= D_F - (\vec{n}_F \cdot \vec{U}_\infty), \quad k = \rho_\infty/\rho_s \end{aligned} \quad (8.7.5)$$

Here, D_F is the speed of the shock propagation and \vec{n}_F is the normal to the shock; they are determined in terms of the shock shape $F(t, x, y, z) = 0$, similar to 8.7.3.

Then, by analogy with 8.7.5, we obtain

$$D_F \sim a_\infty + D_f, \quad \frac{v_{n\infty}}{U_\infty} \sim \frac{1}{M_\infty} + \bar{\theta} + \bar{\omega} \sim \bar{\varepsilon} \ll 1 \quad (8.7.6)$$

The disturbed region thickness δ is determined by the shock angle α_s

$$\delta \sim \alpha L \sim \bar{\varepsilon}L \quad (8.7.7)$$

Substituting all these results into the shock relations, we obtain the estimates, which are, in essence, the same as in Section 8.2

$$\begin{aligned} \Delta p &\sim \rho_\infty U_\infty^2 \bar{\varepsilon}(\bar{\theta} + \bar{\omega}), \quad p \sim \rho_\infty U_\infty^2 \bar{\varepsilon}^2 \\ \Delta h &\sim U_\infty^2 \bar{\varepsilon}(\bar{\theta} + \bar{\omega}), \quad h \sim U_\infty^2 \bar{\varepsilon}^2 \\ \Delta u &= u' - U_\infty \sim U_\infty \bar{\varepsilon}(\bar{\theta} + \bar{\omega}) \end{aligned} \quad (8.7.8)$$

As in the steady-state flow, correct to the order $\bar{\varepsilon}^2$, the longitudinal velocity is $u' = U_\infty$. As in Section 8.2, these estimates are also valid for the internal flow region. This proves the validity of the plane section law, in accordance with which the gas does not leave the planes $x'' = \xi = x - U_\infty t = \text{const}$, fixed in space and orthogonal to the velocity vector $\vec{U}_{0\infty}$.

To generalize the time-dependent analogy to this case, we pass from the t, x to the t, ξ variables. Then, in view of the condition $\Delta u \sim \bar{\varepsilon}^2$, correct to the order $\bar{\varepsilon}^2$, we have

$$\frac{\partial}{\partial t} \Big|_x + u \frac{\partial}{\partial x} \Big|_t = \frac{\partial}{\partial t} \Big|_\xi + \Delta u \frac{\partial}{\partial \xi} = \frac{\partial}{\partial t} \Big|_\xi \quad (8.7.9)$$

The derivative $\partial u / \partial x$ can be dropped from the continuity equation. The boundary conditions are transformed to the purely time-dependent conditions in the same fashion as in Section 8.2. This follows directly from expression 8.7.4 for the normal velocity v_* and the coincidence of the normals \vec{n} and \vec{n}_* to the body and shock surfaces and to their cross-section contours. Thus, the problem of the three-dimensional, time-dependent flow past a thin body is reduced to a set of time-dependent two-dimensional problems of the piston expansion in the $\xi = \text{const}$ planes. In other words, we arrive again at the *plane section law* (Telenin, 1956) with that difference from the steady-state case of Section 8.2 that the original problem corresponds now to a continuous set of two-dimensional time-dependent problems.

We will now evaluate the body acceleration \dot{U}_∞ , at which the plane section law is not as yet violated. Obviously, to do this would require that the velocity increment ΔU_∞ of a body of length L in the time interval $t_L = L/U_\infty$ the body passes through a given section $\xi = \text{const}$, satisfies condition 8.7.8 for Δu

$$\Delta U_\infty \sim \dot{U}_\infty L / U_\infty \leq \bar{\varepsilon}^2 \quad (8.7.10)$$

This condition is by no means too heavy for all hypersonic flight conditions; precisely this gave motive to set above $U_\infty = \text{const}$.

We now return to the problem of the time-dependent motion of equivalent pistons in $\xi = \text{const}$ planes. Each of these pistons starts to expand at the time moment $t = t_0$ at the point of the intersection of the body nose $x = 0$ with the plane $\xi = -U_\infty t_0$. But, in accordance with the time-dependent analogy of Section 8.2, the same piston expansion law $f_*(t, \xi, y, z) = 0$ in this plane generates a certain body of the shape $f^*(\xi, x, y, z) = 0$, which is in the steady-state flow at the velocity $\tilde{U}_{0\infty}$; the body shape is obtained from the function $f_* = 0$ by the inverse change of variables $t = (x - \xi)/U_\infty = x/U_\infty + t_0$

$$\begin{aligned} f_*(t, \xi, y, z) &= f[t, U_\infty(t - t_0), y, z] = \\ f\left(\frac{x - \xi}{U_\infty}, x, y, z\right) &= f^*(\xi, x, y, z) = 0 \\ -U_\infty t_L &= -L \leq \xi = -U_\infty t_0 \leq 0 \end{aligned} \quad (8.7.11)$$

The body shape $f^* = 0$ represents a certain deformation of the original shape $f = 0$. Each plane $\xi = \text{const}$ corresponds to its own deformed, or *curved*, body; by solving the problem of the steady-state flow past this body, we obtain a solution of the form $p = p_\xi(\xi, x, y, z)$ in this plane. Hence, the set of these solutions for $t = t_L$ gives the solution of the original problem of the form:

$$p(x, y, z) = p_\xi(x - L, x, y, z) \quad (8.7.12)$$

This result will be called the *curved body rule* or *method*.* The method makes it possible to replace the solution of the original problem, four-dimensional in the general case, by a set of solutions of three-dimensional problems; the number of these solutions (or the number of the $\xi = \text{const}$ planes) is determined by the required accuracy of the solution of the original problem.

We will now consider in more detail the time-dependent motion of a thin rigid body of fixed shape $f_0(\tau, n, b) = 0$ (cf. 8.7.1) in the absence of its rotation about the τ axis (e.g., the case of a body of revolution). Since the instantaneous contours of the body cross-sections $x = \text{const}$ and $\tau = \text{const}$ coincide, correct to the second order, for determining the equivalent curved body shape it is sufficient to write down the expressions for the shape of its axis τ . The latter may be specified by the pitch (α_t) and yaw (β_t) angles shown in Figure 8.5 and by the displacement (Δ_y, Δ_z) of some point $O(x_0, y_0, z_0)$, for example, the center of inertia of the body, caused by the curvilinearity of the trajectory. Then the equation for the τ axis of the curved body is written in the form:

$$\begin{aligned} y - y_0 &= -(x - x_0)\alpha_{t0} + \Delta y_\tau, & \alpha_{t0} &= \alpha_t(0), & \dots \\ z - z_0 &= (x - x_0)\beta_{t0} + \Delta z_\tau, & \beta_{t0} &= \beta_t(0) \\ \Delta y_\tau &= -(x - x_0)\Delta\alpha_t + \Delta_y, & \Delta\alpha_t &= \alpha_t - \alpha_{t0}, & \dots \\ \Delta z_\tau &= (x - x_0)\Delta\beta_t + \Delta_z, & \Delta\beta_t &= \beta_t - \beta_{t0} \end{aligned} \quad (8.7.13)$$

* Lunev (1968, 1975). The method was generalized to the case of thin bodies at high angles of attack by Krasil'nikov (1969). The method, together with its applications, is presented in Krasil'nikov, Lipnitskii, Pokrovskii, and Shmanenkov (2003). On the intuitive level, the idea of the method was formulated by Vetchinkin (1918) under the assumption of the local nature of the pressure law and used by Gurzhenko (1934) for the experimental modeling of the motion of bodies along curvilinear trajectories at small subsonic velocities.

Substituting $t = t_0 + x/U_\infty$ in these equations, we obtain the displacements Δy^* and Δz^* of the points of the curved body axis from the original one and the body shape

$$\begin{aligned} f^*(x, y, z) &= f(x, y + \Delta y^*, z + \Delta z^*) \\ \Delta y^*(t_0, x) &= \Delta y_\tau(t, x), \quad \Delta z^*(t_0, x) = \Delta z_\tau(t, x) \\ t &= t_0 + x/U_\infty \end{aligned} \quad (8.7.14)$$

Let all the angular velocities be so small that the following conditions are fulfilled

$$\bar{\omega} = \frac{L}{U_\infty} \max(|\dot{\alpha}_t|, |\dot{\beta}_t|) \ll \bar{\theta} = \max(\theta_0, |\alpha_t|, |\beta_t|) \quad (8.7.15)$$

Here, θ_0 is the relative body thickness.

Then for $t \leq t_L = L/U_\infty$ the displacements Δy^* and Δz^* are also relatively small: $\Delta y^*, \Delta z^* \ll \bar{\theta}L$. Then, using a certain arbitrariness in the choice of the flow-fitted coordinate system, we can assume that this system does not rotate about the vector \vec{U}_∞ or the x' axis. Then the rotation velocity $\vec{\Omega}$ of this system has the projections Ω_y and Ω_z onto the y and z axes only (since for $\bar{\theta} \ll 1$ its projection Ω_x is negligibly small). Moreover, for $t = 0$ we will bring all the planes (x, y) , (x', y') , and (τ, n) into coincidence with the plane of the angle of attack. Then for $t = 0$ we have $\alpha_{t0} = \alpha_0$ and $\beta_{t0} = \beta_0 = 0$, while for $t > 0$ we obtain the following dependences

$$\begin{aligned} \alpha_t &= \alpha_0 + \Delta\alpha_t, \quad \Delta\alpha_t = \dot{\alpha}_{t0}t = (\dot{\alpha}_0 - \Omega_z)t = -\omega_z t \\ \beta_t &= \Delta\beta_t = \dot{\beta}_{t0}t = (\dot{\beta}_0 - \Omega_y)t = -\omega_y t \\ \Delta_y &= -\frac{1}{2}\Omega_z U_\infty t^2, \quad \Delta_z = \frac{1}{2}\Omega_y U_\infty t^2 \end{aligned} \quad (8.7.16)$$

Here, ω_y and ω_z are the total angular velocities of the body in the inertial coordinate system. The relation between the angles that enter in Equations 8.7.16 is demonstrated in Figure 8.5c in which we have plotted the projections of the unit vectors \vec{x}' and \vec{r}' on the (y, z) plane in the body- and flow-fitted coordinate systems and their projections on the y and z axes.

Substituting these expressions into Equation 8.7.13 and setting $t = t_0 + x/U_\infty$ we obtain

$$\begin{aligned} \Delta y^* &= \Delta y_0 - \alpha_1 x - \alpha_2 x^2 \\ \Delta z^* &= \Delta z_0 + \beta_1 x + \beta_2 x^2 \\ \alpha_1 &= \dot{\alpha}_0(t_0 - x_0/U_\infty) + x_0 \Omega_z/U_\infty \\ \beta_1 &= \dot{\beta}_0(t_0 - x_0/U_\infty) + x_0 \Omega_y/U_\infty \\ U_\infty \alpha_2 &= \dot{\alpha}_0 - \frac{1}{2}\Omega_z, \quad U_\infty \beta_2 = \dot{\beta}_0 - \frac{1}{2}\Omega_y \end{aligned} \quad (8.7.17)$$

We do not write down here the constants Δy_0 and Δz_0 , since these mean only the initial displacement of the curved body relative to the original one and do not affect the curved body shape and, hence, the solution for it. We note that for constant angles α and β , that is, when a body rotates only due to the curvilinearity of its trajectory, the parameter t_0 vanishes from Equation 8.7.17, so that the curved body is the same in all the $\xi = \text{const}$ sections.

Substituting 8.7.17 into 8.7.14 we obtain the curved body shape $f^* = 0$, which contains small parameters α_i and β_i ; the problem of the flow past this body could be represented in the form of expansions in these parameters:

$$p(t_0, x, y, z) = p_0 + \alpha_1(t_0)p_{1\alpha} + \alpha_2 p_{2\alpha} + \beta_1(t_0)p_{1\beta} + \beta_2 p_{2\beta} \quad (8.7.18)$$

The functions $p_i(x, y, z)$, and so on, are independent of the angular velocities and the parameter t_0 . They can be determined either by solving the corresponding linearized problems or by differentiating numerically (using the formulas of the type $(p(\alpha_i) - p_0)/\alpha_i = p_{i\alpha}$) the solutions $p(\alpha_i)$ of the nonlinear problems, which are obtained sequentially and independent from each other for small but finite values of α_i .

The solution for the original body at the moment $t_L = L/U_\infty$ is obtained from 8.7.18 by the substitution $t_0 = (L - x)/U_\infty$ in the formulas 8.7.17.

To demonstrate the curved body method, we will consider a plate in motion along a curvilinear trajectory at an angle of attack $\alpha(t) > 0$ assuming, as above, that $\bar{\omega}t_L \ll \alpha_0$. In accordance with Equations 8.7.13 and 8.7.17 for the windward side of the plate we will write the shape of the corresponding curved "band" as follows:

$$r = (\alpha_0 + \alpha_1)\tau + \alpha_2\tau^2, \quad \alpha_1 = \alpha_1(t_0) \quad (8.7.19)$$

Here, unessential constants are dropped and, as in Section 7.4, x is replaced by τ .

Within the framework of the time-dependent analogy and the flow model of Section 7.6, the pressure on the windward side of this band is determined by the formula $p = \rho_\infty U_\infty^2 \bar{p}$, where, in accordance with the method under consideration, the pressure coefficient $\bar{p} = (rr')'$ should be calculated at constant values of α_1 and α_2 , which leads to the solution

$$\bar{p} = (rr')' = \bar{p}_0 + 2\alpha_0\alpha_1(t_0) + 6\alpha_0\alpha_2\tau, \quad \bar{p}_0 = \alpha_0^2 \quad (8.7.20)$$

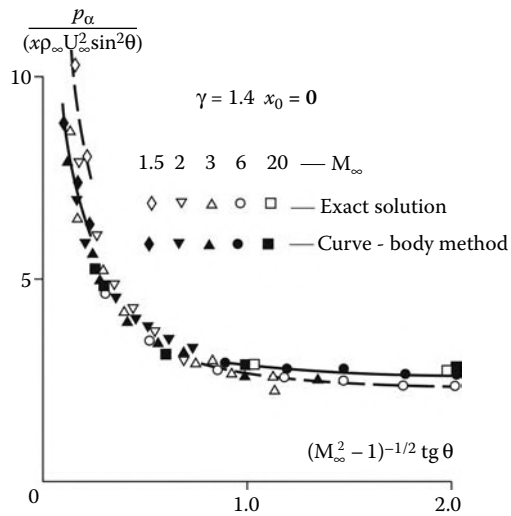
Comparing this result with Equation 8.7.18 we obtain $\bar{p}_{1\alpha} = 2\alpha_0$ and $\bar{p}_{2\alpha} = 6\alpha_0\bar{\tau}$ and, finally, substituting α_1 and α_2 from Equation 8.7.17 into Equation 8.7.20 for an L -long plate we obtain the following solution

$$\begin{aligned} p &= \bar{p}^{(0)} + \bar{\omega}_z \bar{p}^{(\bar{\omega})} + \bar{\Omega} \bar{p}^{(\bar{\Omega})}, \quad \bar{p}_0^{(0)} = \bar{p}_0 + 2\dot{\alpha}_0 t_L \approx (\alpha_0 + \dot{\alpha}_0 t_L)^2 \\ \bar{p}^{(\bar{\omega})} &= -2\alpha_0(2\bar{\tau} - \bar{\tau}_0), \quad \bar{p}^{(\bar{\Omega})} = \bar{\tau}, \quad \bar{\tau} = \tau/L \leq l \\ \omega &= \Omega_z - \dot{\alpha}_0, \quad \Omega = \Omega_z, \quad \bar{\omega} = \omega l/U_\infty, \quad \bar{\Omega} = \Omega l/U_\infty \end{aligned} \quad (8.7.21)$$

Here, $\bar{p}^{(0)}$ is the quasistationary solution corresponding to the instantaneous angle of attack $\alpha_1 = \alpha_0 + \dot{\alpha}t_L$. The term $\bar{p}^{(\bar{\omega})}$ differs from the similar term in Equation 7.4.21 in the item $2\bar{\tau}$, instead of τ , in the parentheses, which is due to the Busemann term rr'' in expression 8.7.20 for \bar{p}_ω . The latter term is not taken into account in the Newtonian formula 7.4.21, while its effect may be important. Finally, the presence of the term $\bar{p}^{(\bar{\Omega})}$, which is also not taken into account in formula 7.4.21, indicates that the effects of the angular velocities $\dot{\alpha}$ and Ω on the solution are different.

In conclusion, we will touch upon the similarity law for the time-dependent hypersonic flow past thin bodies. In this case, the criteria $\tilde{\omega}_i = \omega_i L/\bar{\theta}U_\infty$, $\omega_i = \dot{\alpha}, \dot{\beta}$, and $\bar{\Omega}$ should be added to the similarity criteria derived in Section 8.4; these have the meaning of the relative angles of the turn of bodies in their rotation during a time interval $t_1 = L/U_\infty$ (here, θ is the characteristic angle of inclination of the body surface to the vector U_∞).

By way of illustration, we will consider a wedge with the semivertex angle θ_0 executing small oscillations in supersonic flow. In this case, the linear term expression 8.7.8 also corresponds to a wedge; therefore, the quantity $p_{1\alpha}$ is constant. The quadratic term in the expansion for the curved body shape gives in the linear formulation a linear increase in the pressure: $p_{2\alpha} \sim x$. Therefore, in accordance with 8.7.20, the coefficient $p_{\dot{\alpha}}$ is also linear in x . The dimensionless complex calculated in the exact linear formulation and in the previous hypersonic approximation for $x_0 = 0$ (the data of Stepanov) is plotted in

**FIGURE 8.6**

Pressure on an oscillating wedge.

Figure 8.6 versus the generalized similarity criterion $K = \theta_0 \sqrt{M_\infty^2 - 1}$ covering, as earlier, the moderately supersonic velocity range. Clearly, the exact and approximate curves are close except for the range of small K corresponding to low supersonic Mach numbers $M_\infty < 2$, for which the hypersonic theory no longer holds.

9

Flows Past Thin, Slightly Blunted Bodies

From the engineering standpoint, thin sharp bodies are of limited utility in hypersonic flight owing to prohibitive heating and even destruction of sharp noses and edges. Because of this, they are usually made blunt; however, at hypersonic velocities even a slight bluntness can appreciably affect the body drag and, therefore, the flow pattern. A considerable influence of a small bluntness on the flow past thin bodies was experimentally revealed by Hammitt and Bogdonoff (1955) and Bertram (1956) and explained in the works of Cheng and Pallone (1956) and Chernyi (1956, 1966) who related this effect with strong blast theory. In what follows we will show that this theory with corresponding supplements (Lunnev, 1975) reflects adequately the mechanisms governing these flows, though it has no pretensions to playing the part of an exact calculation technique for the problem under consideration. This chapter is devoted to the study of these mechanisms and the qualitative features of these flows in general.

9.1 General Pattern of the Flow Past Thin Blunt Bodies

First, we will evaluate the domain of influence of a small bluntness for the bodies and flows satisfying the conditions

$$r_0 \ll R \ll L, \quad d \ll L, \quad \varepsilon = \theta_0 + M_\infty^{-1} \ll 1, \quad c_{x0} \sim 1 \quad (9.1.1)$$

Here, r_0 is the midsection radius of the blunt nose having its own drag coefficient c_{x0} , L is the body length, d is its diameter, $R(x)$ is the bow shock shape, and θ_0 is the maximum slope of the body's lateral surface $r = r_b(x)$ to the freestream velocity vector \vec{U}_∞ . Up to the final sections, we shall mainly deal with two-dimensional bodies ($v = 0$) and bodies of revolution ($v = 1$).

The characteristic nose slope is $\theta \sim \pi/2$, while the Newtonian pressure on the nose (Section 7.2) is $p \sim p'_0 \approx \rho_\infty U_\infty^2$. At the same time, the pressure on the lateral surface is $\Delta p = p - p_\infty \sim \rho_\infty U_\infty^2 \theta_0^2 \ll p'_0$. Therefore, the gas having passed the nose neighborhood experiences strong expansion with a more or less protracted transition process, as shown in Figure 9.1. Let c_{xb} be the drag coefficient of the lateral surface with the midsection area $S_0 \sim d^{1+v} \sim (\theta_0 L)^{1+v}$. Then the nose-to-lateral drag ratio is as follows

$$\frac{X_0}{X_b} \sim \frac{c_{x0} r_0^{1+v}}{c_{xb} S_0} \sim \bar{X} = \frac{1}{2} c_{x0} \left(\frac{r_0}{L} \right)^{1+v} \theta_0^{-(3+v)} \quad (9.1.2)$$

Setting $\bar{X} = 1$ in the previous formula we obtain the length and thickness of a body with the same contributions of the nose and the lateral surface to the total drag

$$L \sim r_0 (c_{x0}/2)^{1/(1+v)} \theta_0^{-(3+v)/(1+v)}, \quad d \sim L \theta_0 \quad (9.1.3)$$

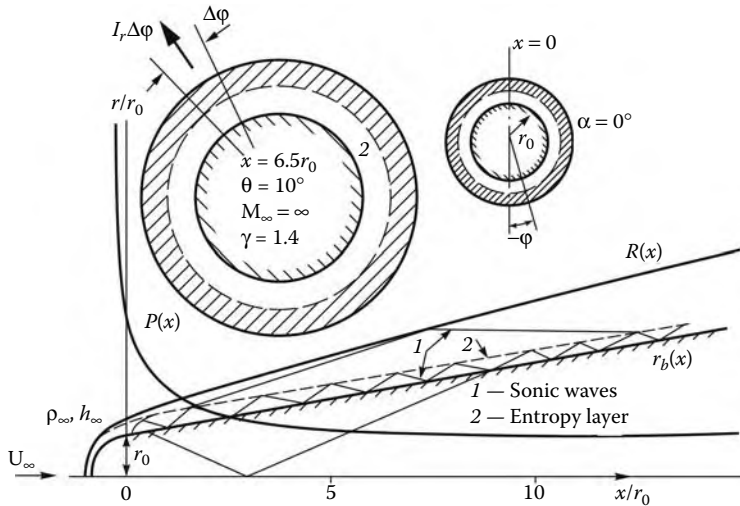


FIGURE 9.1

Flow past a thin blunt body.

Let now I_{r0} and I_{rb} be the fluxes of the momentum (in the sense of Section 7.5 for symmetric flows, see Figures 7.21 and 9.1) acquired by the gas in the transverse direction under the action of the nose and the lateral surface. For these quantities we can derive the estimates

$$\begin{aligned} I_{r0} &= \pi^\nu r_0^{1+\nu} \rho_\infty U_\infty^2 I, & I_{rb} &\sim \Delta p L R^\nu \sim \rho_\infty U_\infty^2 \theta_0^{2+\nu} L^{1+\nu} \\ \frac{I_{r0}}{I_{rb}} &\sim I \left(\frac{r_0}{L} \right)^{1+\nu} \theta_0^{-(2+\nu)} = \bar{X} I_0 \theta_0, & I_0 &= \frac{2I}{c_{x0}} \end{aligned} \quad (9.1.4)$$

The parameter I_0 was introduced in Section 7.5 (Equation 7.5.8). Setting then $I_{r0} \sim I_{rb}$ we obtain the length of the corresponding body

$$L' \sim L \theta_0^{1/(1+\nu)} \sim r_0 I_0^{1/(1+\nu)} \theta_0^{-(2+\nu)/(1+\nu)} \quad (9.1.5)$$

We will now evaluate the M_∞ effect on the extent L_M of the region of propagation of the elevated pressure induced by the nose as a separate blunt body. To do this, we equate the drag X_0 to the force $X_M \approx \pi^\nu R^{1+\nu} \Delta p$ acting on the end section of the disturbed region due to the pressure difference $\Delta p \sim p_\infty$. Letting the shock be a Mach cone, $R \approx L_M/M_\infty$, we obtain

$$L_M \sim r_0 M_\infty^{(3+\nu)/(1+\nu)} c_{x0}^{1/(1+\nu)} \quad (9.1.6)$$

Obviously, for $M_\infty \gg 1$ the extent of the domain of nose influence $L_M \gg r_0$, the ratio L_M/r_0 exceeding 10^3 and 10^2 for blunt plates and cylinders already for $M_\infty \geq 10$, whereas at moderate M_∞ the bluntness effect on the flow has only a local character. The corresponding example is presented* in Figure 7.3.

The estimates derived demonstrate the considerable influence of an even small bluntness on the hypersonic flow past thin bodies. Thus, for $c_{x0} \approx 1$ (cylinder or sphere) and

* Most of the calculated data presented in this chapter are taken from Lunev, Magomedov, and Pavlov (1968, 1971).

$\theta = 2.5 \div 15^\circ$ (or $\theta_0 = 0.045 \div 0.3$) we have $L/r_0 = 6000 \div 30$ for blunt wedges ($v = 0$) and $L/r_0 = 400 \div 10$ for blunt cones ($v = 1$). The ratio L'/r_0 is also large, but for $I_0 \sim 1$ (see Figure 7.21 in Section 7.5) it is $\theta_0^{1/(1+v)}$ times smaller than L_0/r . This means that the nose exerts the main influence precisely on the body drag.

We will now consider the structure of the disturbed layer between the body and the shock for thin blunt bodies. In Section 7.1 we expressed the dependences of the dimensionless enthalpy $\bar{h} = h/U_\infty^2$ and density $\bar{\rho} = \rho/\rho_\infty$ on the pressure $p = \bar{p}\rho_\infty U_\infty^2$ behind the strong shock in the vicinity of the nose in terms of the "entropy" distribution $s(\psi) = \sin^2 \alpha(\psi)$ over streamlines (formulas 7.1.2 through 7.1.5); here, $\alpha(\psi)$ is the shock slope corresponding to the given streamline. Near the lateral surface of the body the pressure in the disturbed layer is usually determined by the local shock slope α_l ; for $\alpha_l \ll 1$ it is of the order $\bar{p} \sim \alpha_l^2$. Thus, the orders of the enthalpy and density are determined here by the parameter s , which varies within wide limits, $s = \alpha_l^2 \div 1$.

Near the body surface the streamlines that have passed across the shock in the nose vicinity, where $s \sim 1$, form the *high-entropy layer*, which theoretically exists in an inviscid gas at any distance from the nose. In accordance with 7.1.4, the orders of the flow parameters in this layer are as follows

$$\begin{aligned} \bar{h} &\sim \alpha_l^{2(\gamma-1)/\gamma}, & \bar{\rho} &\sim (\gamma-1)^{-1} \alpha_l^{2/\gamma}, & M^2 &\sim \bar{\rho}/\bar{p} \sim (\gamma-1)^{-1} \bar{h} \\ \Delta u &= U_\infty - u \approx U_\infty - U \approx U_\infty \bar{h} \end{aligned} \quad (9.1.7)$$

Contrary to this, in the vicinity of the shock and sufficiently far from the nose the orders of the flow parameters on the streamlines that have crossed the shock with $s \sim \alpha_l^2 \ll 1$ are the same as in the flow past sharp thin bodies (Section 8.2)

$$\bar{h} \sim \alpha_l^2, \quad \bar{\rho} \sim 1, \quad M^{-2} \sim \alpha_l^2, \quad \Delta u \sim U_\infty \alpha_l^2 \quad (9.1.8)$$

These streamlines form the *low-entropy shock layer* with high Mach numbers $M \gg 1$; in the following we shall frequently call it simply *shock layer*. For this layer the plane cross-section law or the time-dependent analogy of Chapter 8 is valid. At the same time, the local Mach numbers in the high-entropy layer are comparatively low ($M \approx 2 \div 3$, as in Figure 9.2), while the velocity deficit Δu is of the smaller order of smallness, especially for small values of $\gamma - 1$. Thus, the plane cross-section law for this layer has lower accuracy than for the low-entropy shock layer.

Thus, the gas in the high-entropy layer has a high temperature and a low density as compared with the same parameters in the low-entropy shock layer (Figures 9.2 and 9.3); therefore, various physical and chemical processes can develop precisely in the high-entropy layer, while near the shock the gas may remain cold and near perfect. The low density in this layer results in the pressure equalization in the layer (similar to the explosion zone in Figure 6.21, Section 6.8) due to fairly frequent reflections of disturbances from the wall and the denser shock layer (cf. Section 4.7), while the disturbance paths in the shock layer are considerably longer due to rather high local Mach numbers (Figure 9.1).

The information presented previously makes it possible to simplify the formulation of the problem of the flow past thin blunt bodies as follows: due to a considerable extent of the domain of influence of the bluntness, the influence of the details of the initial parameter profiles in the section $x = 0$ between the lateral surface and the nose on the flow far from this section could be neglected, together with that of the nose shape (similar to the strong

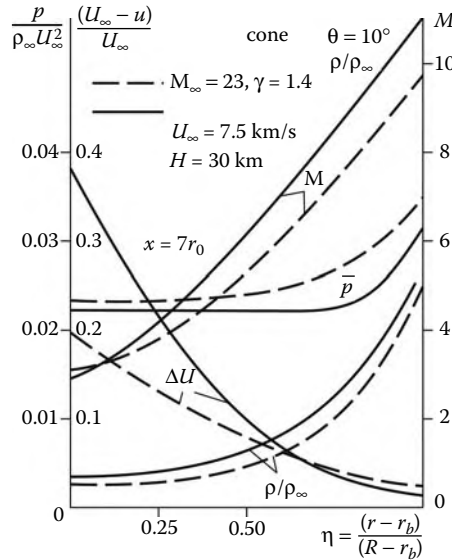


FIGURE 9.2
Flow parameters in the shock layer of a spherically blunted cone.

blast problem, Section 6.8), so that the initial conditions are taken into account only via the force parameters of the nose X_0 and I_{r_0} , these forces being applied in the region of small extent, $\Delta x, \Delta r \sim r_0 \ll L$. We recall that the same governing parameters were used in the free layer model (Section 7.5), with the difference that in that model the surface pressure effect on the shock shape was neglected.

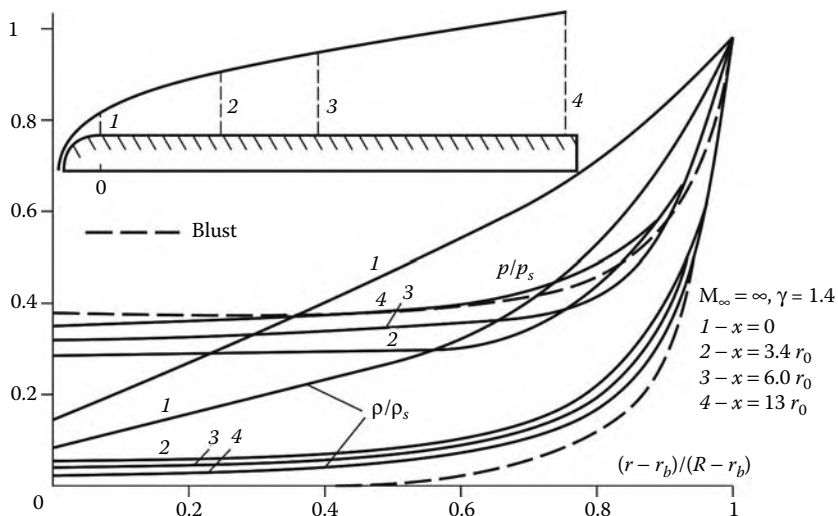


FIGURE 9.3
Densities and pressures in different sections between a blunt cylinder and the bow shock.

9.2 Similarity Law and Blast Analogy

The model of the flow past thin blunt bodies adopted at the end of Section 9.1 has an important consequence. This is the simplification of the similarity law derived in Section 1.12: in formulating this law it is now sufficient to require only the geometric similarity of the shape $r^{(b)}(x)$ of the body's lateral surface

$$\bar{r}^{(b)}(x') = r^{(b)}/L = (r_b - r_0)/L, \quad x' = x/L \quad (9.2.1)$$

Substituting the additional parameters X_0 and I_{0r} into the general relation 1.12.9 and taking their dimensionalities into account we obtain additional similarity criteria

$$\begin{aligned} \bar{X}_1 &= \frac{X_0}{\pi^\nu \rho_\infty U_\infty^2 L^{1+\nu}} = \left(\frac{r^{(0)}}{L}\right)^{1+\nu}, & \frac{r^{(0)}}{r_0} &= \left(\frac{2}{c_{x0}}\right)^{1/(1+\nu)} \\ I_0 &= I_{0r}/X_0 = 2I/c_{x0} \end{aligned} \quad (9.2.2)$$

Thus, the *effective size* $r^{(0)}$ of the nose is its only parameter, irrespective of its shape and dimensions. The parameter I_0 was introduced in Section 7.5, where we showed (cf. Figure 7.21) that for blunt bodies (noses) with $c_{x0} \sim 1$ this parameter depends on the body shape only weakly. Moreover, it was shown in Section 9.1 that for thin bodies the main nose effect is determined by its drag X_0 . For this reason, in what follows we will deal with the criterion \bar{X}_1 only. Then, in accordance with Section 1.12, the similarity criteria for the bodies of the same shape $\bar{r}^{(b)}(x')$ are as follows:

$$\bar{X}_1, \quad \gamma, \quad M_\infty, \quad \rho_\infty, \quad U_\infty \quad (9.2.3)$$

The two last parameters relate to real gas flows. If these parameters coincide, then the dimensionless functions

$$\bar{p} = p/\rho_\infty U_\infty^2, \quad \bar{h} = h/U_\infty^2, \quad \bar{\rho} = \rho/\rho_\infty, \quad \bar{v} = v/U_\infty \quad (9.2.4)$$

of the variables x/L and r/L are the same.

For blunt cones and wedges with the equation of the generator $r^{(b)} = \theta x$ the length L drops out, together with the parameter \bar{X}_1 ; however, the scale length $r^{(0)}$ still remains, which leads to the same similarity variables as in Section 7.5

$$x_1 = \frac{x}{r^{(0)}} = \frac{x}{r_0} \left(\frac{2}{c_{x0}}\right)^{1/(1+\nu)}, \quad r_1 = \frac{r}{r_0} \left(\frac{2}{c_{x0}}\right)^{1/(1+\nu)} \quad (9.2.5)$$

In Figure 9.4 we have presented the data characterizing the flows past spherically and segmentally blunted cylinders and cones in the similarity variables. Here, the shocks $R_1(x_1)$ on the bodies with different noses practically coincide (they are also the same for the cones and cylinders), while the pressures are close already for $x/r_0 \geq 2 \div 3$, in spite of the difference in transition processes in the region $x \sim r_0$ and the formation of internal shocks downstream of the segmental bluntness (cf. Section 5.6). The same conclusion follows from Figure 9.5 for the cylinders and flat plates with circular and elliptic noses.

We note that in Figure 9.4b the profiles of the pressure and entropy function $\bar{p}/\bar{\rho}^\gamma$ in similar cross-sections are also close to each other, including the high-entropy regions in which the entropy distribution is not described by our model. This result, somewhat unexpected

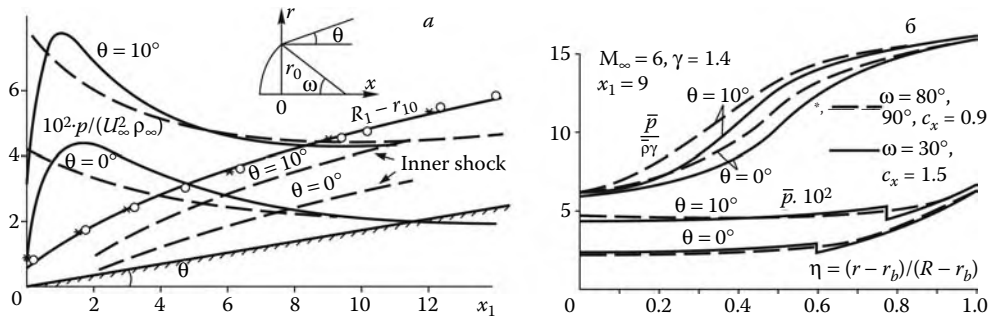


FIGURE 9.4
Flow past cones and cylinders with segmental noses.

for this formulation, can be explained as follows. The streamline distribution $r_{\Psi_1}(\Psi)$ in the high-entropy layer is determined by integrating the equation $d\Psi = (2\pi)^v \rho u r^v dr$. In the similarity variables 9.2.5 for $u \approx U$ we have

$$r_{\Psi_1}^{1+v} - r_{b1}^{1+v} = \int_0^\Psi \frac{d\Psi}{\bar{\rho} \bar{U}}, \quad \Psi = \frac{2\Psi}{\pi^v c_{x0} \rho_\infty U_\infty},$$

$$\bar{\rho} = \bar{\rho}(\bar{p}, s), \quad \bar{U}(\bar{p}, s) = U/U_\infty \quad (9.2.6)$$

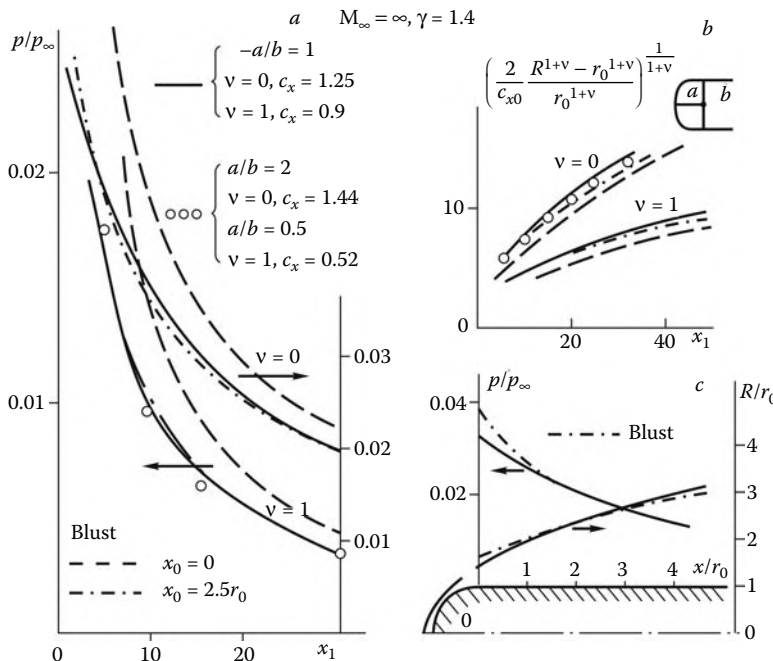


FIGURE 9.5
Shocks and pressures on a blunt cylinder and plate with elliptic noses.

Here, as in Section 9.1, the function $s(\Psi) = \sin^2 \alpha$ is determined by the angle $\alpha(\Psi)$ of the shock inclination on the given streamline $\Psi = \text{const}$ (the function Ψ was introduced in Section 7.5). We note that even when the ratio of the flow rate across the high-entropy layer $\psi_\delta \approx \pi^\nu r_0^{1+\nu} \rho_\infty U_\infty$ to the total flow rate ψ_R is small, $\psi_\delta/\psi_R \sim (r_0/R)^{1+\nu}$, the high-entropy layer thickness $r_\delta = r_\psi(\psi_\delta)$ may be fairly appreciable due to the low density in it (of the order $\rho \sim \rho_\infty \alpha_l^{2/\gamma}$; cf. formula 9.1.7).

The pressure $\bar{p}(x_1)$ is constant across the high-entropy layer (Section 9.1, Figures 9.2 and 9.3) and for the similar flows under consideration is dependent on the variable x_1 only. However, according to Figure 7.21, the function $s(\Psi)$ depends on the blunt body shape only weakly; hence follow the slight dependence of the function $s(r_1)$ on the body shape and the similarity of the flow as a whole.

The schematic representation of the problem, as outlined previously, can be easily interpreted within the framework of the time-dependent analogy of Chapter 8. In this case the force action of the nose on a gas confined in the stationary thin layer $\Delta\xi$, $\xi = x - U_\infty t$ is, in accordance with Section 8.3, equivalent to the energy release (explosion) equal to the work of the nose drag $E_0 = X_0$ imparting to the gas the momentum $J_0 = I_{r0} U_\infty^{-1}$ determined by formulas 9.1.2 and 9.1.4. At the same time, the action of the lateral surface is equivalent to the piston expansion in accordance with the law $r_p(t) = r^{(b)}(U_\infty t)$. This is the *explosion-piston model* or the *blast analogy* (Chernyi, 1956, 1966). We note that within the framework of the approximate equations of energy (6.8.15) and momentum (7.6.2 or 6.8.11 for $m = 0$ in the first formula) preassigning the parameters E_0 and J_0 is sufficient for determining the initial parameters p_0 and $R = R_0$ at $x = 0$.

The explosion-piston model based on the time-dependent analogy does not take into account the fact that the latter does not hold in the high-entropy layer. However, as will be shown in Section 9.3, this has only a slight effect on the flow as a whole.

The time-dependent analogy makes it possible to derive the similarity law for bodies with affinely similar lateral surfaces $r^{(b)}/d$; this law generalizes the similarity law of Section 8.4 to the case of blunt bodies (Chernyi, 1966). For this purpose, we introduce the scales of the problem $d = L\theta_0$ and $t_L = L/U_\infty$; in accordance with the dimensionalities of the quantities E_0 and J_0 (6.8.21) this gives two parameters

$$\bar{X}_2 = \frac{E_0 t_L^2}{\rho_\infty d^{3+\nu}} = \bar{X}_1 \theta_0^{3+\nu}, \quad \frac{J_0 t_L}{\rho_\infty d^{2+\nu}} = I_0 \theta_0 \quad (9.2.7)$$

Clearly, the sought similarity law could take place only for $I_0 \theta_0 \approx 0$. Then for the bodies of the same shape $r^{(b)}/L\theta_0$ the similarity criteria are as follows:

$$\bar{X}_2, \quad \gamma, \quad M_\infty \theta_0, \quad \rho_\infty, \quad U_\infty \quad (9.2.8)$$

The following formulation of this law and the similarity variables do not differ from those of Section 8.4.

As previously, for wedges and cones we obtain the scale length of the problem by putting $\bar{X}_2 = 1$; this leads to the variables (cf. 9.2.5)

$$x_2 = x_1 \theta^{(3+\nu)/(1+\nu)}, \quad r_2 = r_1 \theta^{2/(1+\nu)} \quad (9.2.9)$$

For blunt plates and cylinders we have $r^{(b)} = 0$, so that the equivalent time-dependent problem is that of the explosion. However, it was shown in Section 6.8 that the point explosion problem with the initial momentum $J_0 \neq 0$ has no solution. For this reason, in order to satisfy two conservation laws for small x/r_0 (instead of one) we locate the effective source

of the equivalent point explosion at a certain point $x = -x_0$ in front of the body, so that in the $x = 0$ plane the transverse momentum of the gas is equal to J_0 (the *modified explosion analogy*; Lunev and Pavlov, 1966). Then passing to the variable $x = U_\infty t$ and taking 6.8.17 into account we represent the solution 6.8.3 and 6.8.4 for the explosion in the form:

$$\begin{aligned}\bar{p} &= \kappa_v(\gamma, \eta, \tau) (x_1 + x_{10})^{-2(1+\nu)/(3+\nu)} \\ R_1 &= (R/r_0)(2/c_x)^{1/(1+\nu)} = \chi_v(\gamma, \tau) (x_1 + x_{10})^{2/(3+\nu)} \\ \eta &= r/R, \quad \tau = (x_1 + x_{10})M_\infty^{-(3+\nu)/(1+\nu)}, \quad x_{10} = x_0/r^{(0)}\end{aligned}\quad (9.2.10)$$

For $\tau = 0$ the coefficients κ_v and χ_v were given in Figure 6.20 (Section 6.8). The coordinate shift $x_0 = U_\infty t$ is determined by substituting the quantity $J_0 = r_0^{1+\nu} \rho_\infty U_\infty I$ into 6.8.20

$$x_{10} = [(3 + \nu)I_0/2C\chi]^{(3+\nu)/(1+\nu)} \quad (9.2.11)$$

Far from the nose ($x \gg x_0$) the parameter x_{10} may be dropped out; then formula 9.2.10 corresponds to the classical blast analogy, in which it is sufficient to know only the drag coefficient c_{x0} .

At $\gamma = 1.4$, formula 6.8.20 for C and the data in Figure 7.21 for I_0 give the values $x_{10} = 3.7$ for $\nu = 1$ and $x_{10} = 5$ for $\nu = 0$ (in both cases $x_0 \approx 2.5r_0$ for circular noses). This shift makes the curves considerably closer to the exact ones, including the near vicinity of the nose in Figure 9.5. In particular, for the spherically blunted cylinder the formulas

$$\bar{p} = \frac{0.9p_0}{x + 2.7r_0}, \quad R = 1.1r_0 \left(\frac{x}{r_0} + 2.7 \right)^{1/2} \quad (9.2.12)$$

thus obtained for $\gamma = 1.4$ (and slightly corrected) are accurate to a few percents for $x \leq 4r_0$ and are practically exact for greater values of x (by the way, the formula $R/r_0 = 1 + (x/r_0 + 0.2)^{1/2}$ has an even better accuracy).

In the case of a finite counterpressure, or the Mach number M_∞ , in accordance with 6.8.17 the solution could be presented in another form:

$$p - p_\infty = p_\infty P_1(\gamma, \nu, \eta, \tau), \quad R_1 = M_\infty^{2/(1+\nu)} \bar{R}(\gamma, \nu, \tau) \quad (9.2.13)$$

The processing of the data for the circularly blunted cylinder in these similarity variables with inclusion of the coordinate shift (Figure 9.6) brings all the curves for different M_∞ to the same bundles, though they may differ considerably when constructed in the original coordinates (Figure 9.2).

A similar result follows from the data in Figure 9.7 for the wakes behind blunt cones with small $c_x \approx 0.2 \div 0.5$. For these bodies the parameter $I_0 = 1 \div 2$, which leads to large values of x_{10} . We note the oscillatory nature of all the pressure curves (appropriate for the explosion process) having the rarefaction regions in which $p < p_\infty$.

Quite naturally, the coordinate shift denudes the blast analogy of simplicity; thus, its role is mainly reduced to the interpretation of the discrepancy between the analogy and reality. In the particular case of conical and wedge-shaped noses with small semivertex angles θ the parameter $I_0 \sim \theta^{-1}$ and the value $x_{10} \sim \theta^{-(3+\nu)/(1+\nu)}$. Another example is provided by the case of small $\gamma - 1$ when, in accordance with 6.8.20, we have $x_{10} \sim (\gamma - 1)^{-(2+\nu)/(1+\nu)}$. In both cases the blast analogy cannot explain the situation without resorting to the coordinate shift (see also Figure 9.9 of Section 9.3).

Finally, we will discuss the blast analogy applicability to far wake flows downstream of bodies. That it is applicable for the pressure is shown in Figure 9.7. However, far away from

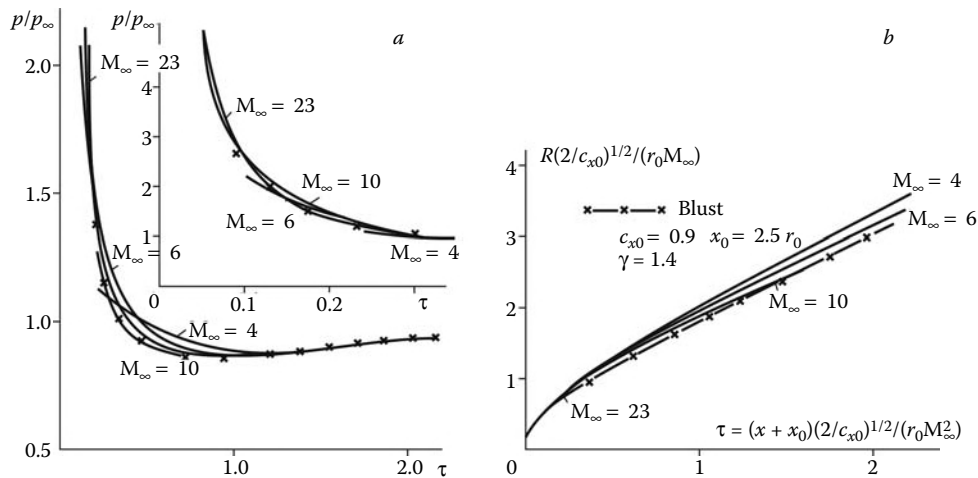


FIGURE 9.6
Pressures (a) and shocks (b) on a blunt cylinder.

a body dissipative effects are inevitable in the central part of the wake; to evaluate these effects we will neglect the influence of the boundary layer on the body surface (Section 1.16) and assume the flow in its end section to be inviscid. This can be done, for example, for a blunt short body of radius r_0 with $c_{x0} \sim 1$; precisely this case will be considered in the following. Then, in view of the relatively low velocity deficit in the high-entropy layer shed

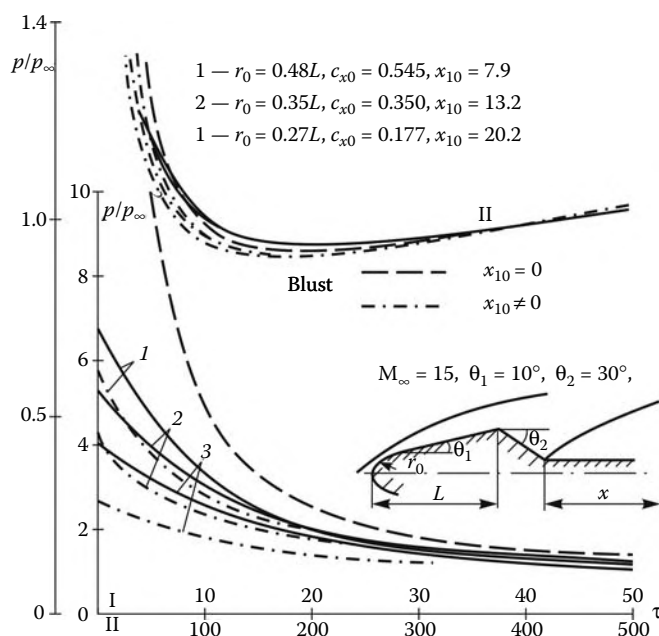


FIGURE 9.7
Pressure distribution in the wake downstream of a body.

from the body, we will neglect the viscosity effect in it and use the time-dependent analogy together with the problems of Section 6.10 of the blast in a heat-conducting gas.

In accordance with these solutions, we will carry on our analysis for bodies of revolution for two limiting cases, namely, at $M_\infty \gg 1$ for a wake with a fairly intense shock and, on the other hand, for the farthest region of the wake, where the pressure has been equalized ($p \approx p_\infty$). In the first case, the solution of Section 6.10 for the blast is dependent on the parameter ε 6.10.3 which for $E = 0.5c_x\pi r_0^2\rho_\infty U_\infty^2$ is equal

$$\varepsilon = \left(\frac{2}{c_x\pi} \right)^{1/2} \frac{\lambda}{c_p\rho_\infty r_0 U_\infty} \sim \frac{1}{Re} = \frac{\mu_0}{\rho_\infty U_\infty r_0} \quad (9.2.14)$$

Generally speaking, the viscosity μ_0 in the Reynolds number must be evaluated from the wake core parameters. For actual problems usually $Re \gg 1$ (see Figure 1.1) and, therefore, $\varepsilon \ll 1$, which was assumed in Section 6.10.

Letting $\bar{\varepsilon} \sim \varepsilon$ and $\beta \sim 1$ in formula 6.10.11 and taking 9.2.5 and 9.2.10 into account we obtain the order of the enthalpy in the near-axial region of the wake

$$h \sim \frac{1}{2}U_\infty^2(R')^2\varepsilon^{-1/\gamma} \sim \frac{U_\infty^2}{2} \frac{r_0}{x} Re^{1/\gamma} \quad (9.2.15)$$

At the same time, in an inviscid high-enthalpy layer the enthalpy is of the order

$$h \sim \frac{1}{2}U_\infty^2\bar{p}^{(\gamma-1)/\gamma} \sim \frac{U_\infty^2}{2} \left(\frac{r_0}{x} \right)^{(\gamma-1)/\gamma} \quad (9.2.16)$$

Obviously, the thermally insulated solution for the blast cannot be applied to the wake, at least until the enthalpy determined by formula 9.2.16 becomes greater than the enthalpy 9.2.15, that is, only for $x > r_0 Re$, since taking heat conduction into account can only reduce the temperature in the wake downstream of a body as compared with the original non-heat-conducting solution.

Similar asymptotics $c_p\Delta T \sim 0.5U_\infty^2(r_0/x)Re$ for the enthalpy increment in the far wake are also given by the solution 6.10.13 for a thermal source. This enthalpy also becomes lower than the stagnation enthalpy $U_\infty^2/2$ only for $x > r_0 Re$.

9.3 Role of the High-Entropy Layer in Real Gas Effects

In this section we will touch on, first, the effect of physical and chemical processes in the high-entropy layer on the gas flow past thin blunt bodies (from Figure 9.2 it follows that in the high-entropy layer the density and temperature depend considerably on the state of the gas in the layer) and, second, the effect of the violation of the time-dependent analogy in the high-entropy layer in which the velocity deficit is appreciably greater than in the low-entropy shock layer (thus, in Figure 9.2 we have $\Delta u/U_\infty \approx 0.4 \div 1$).

The blast analogy makes it possible to solve this problem using the same effective energy method as was applied for the explosion problem in Section 6.9. For this purpose, we pass

from the longitudinal momentum Equation 8.3.3 to the energy conservation law, 8.3.5, and, using 6.9.1, bring the latter to the form:

$$\begin{aligned}
 & (2\pi)^v \int_{r_b}^R \left(\rho \frac{v^2}{2} + \frac{p}{\gamma - 1} \right) r^v dr = E_* + \frac{\pi^v R^{1+v} p_\infty}{\gamma - 1} \\
 & E_* = E_0 + E_1 - E_2 \\
 & \frac{E_1}{E_0} = \frac{1}{2} \int_0^{\Psi_\delta} \frac{(U_\infty - U)^2}{U_\infty U} d\Psi, \quad \frac{E_2}{E_0} = \int_0^{\Psi_\delta} \frac{(\gamma - \gamma_*) h}{\gamma_* (\gamma - 1) U_\infty U} d\Psi \quad (9.3.1)
 \end{aligned}$$

Here, the function Ψ is the same as in formulas 9.2.6 and 7.5.8, while γ^* is the effective adiabatic exponent (see Section 1.3). As compared with expression 8.3.5 for E_1 , here we have dropped the term with h_∞ , as being of a relatively small order for $M_\infty^2 \gg 1$, and replaced the longitudinal velocity u by the total velocity U .

Outside the high-entropy layer, the integrand in the expression for E_1 is small in view of the condition $\Delta U/U \sim \alpha_f^2 \ll 1$ (cf. Section 9.1); because of this, the choice of the upper limit Ψ_δ is of no importance. The same is true for the integral E_2 if real gas properties manifest themselves in the high-entropy layer only, while outside of it the effective adiabatic exponent $\gamma_* \approx \gamma$ (for cones with $\theta \leq 10^\circ$ this holds at $U_\infty \leq 7$ km/sec).

As in Section 6.9, the quantity E_* will be called the *effective energy of the equivalent explosion*; in our problem we will also introduce the notion of the *effective drag coefficient* (Lunnev, 1959, 1975).

$$c_x^* = \lambda c_{x0}, \quad \lambda = E_*/E_0 = 1 - (E_2 - E_1)/E_0 \quad (9.3.2)$$

Due to the universal nature of the function $s(\Psi)$ noted in Section 9.2, we can neglect the dependence of the ratio λ on the nose shape and to consider it to be the function of the pressure only. However, its dependence on \bar{p} is only slight, as it is for the quantity $\bar{h} \sim \bar{p}^{(\gamma^*-1)/\gamma^*}$. This is confirmed by the data for the ratio c_x^*/c_{x0} calculated for blunt cones in equilibrium air flow, as presented in Figure 9.8. For this reason, as in Section 6.8, we will

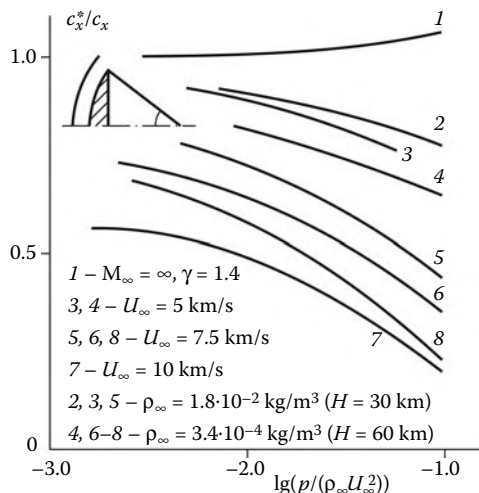


FIGURE 9.8
Effective-to-true nose drag coefficient ratio.

substitute precisely this energy for E_0 in solution 9.2.3, this being equivalent to introducing the variables

$$x_1^* = x_1, \quad r_1^* = r_1, \quad x_2^* = x_2, \quad r_2^* = r_2 \quad (9.3.3)$$

Estimates show that the role of the term E_1/E_0 is unimportant (curve 1 in Figure 9.8). Generally speaking, setting $\Delta U/U \approx \bar{h}$ we obtain $E_1/E_0 \sim \bar{p}^{2(\gamma-1)/\gamma} \ll 1$ for $\bar{p} \ll 1$. The only exception is provided by the case $\gamma \rightarrow 1$ in which, due to the fact that $U \rightarrow 0$ as $\Psi \rightarrow 0$ (cf. Section 7.5), the integral E_1 is not small for $v = 1$ and even diverges for $v = 0$. However, this rather speculative limiting case is of little interest for the problems under consideration.

Taking real processes in air into account reduces considerably the value of c_x^* and, hence, the bluntness effect on the flow past thin bodies. In support of this conjecture we have plotted in Figure 9.9 the pressure distributions over the blunt cylinder. For various flow conditions they can differ by nearly a factor of two. At the same time, when the shifted similarity coordinates x_1^* are used, the curves are brought close together; thus, the effective drag coefficient model adequately reflects the mechanism of the real gas effect on the flow past thin blunt bodies.

9.4 Flow Past Blunt Cones

Conical blunt-nosed bodies are widely used in rocket engineering, so we will dwell on the flows past these bodies in more detail. The illustrations presented in this section relate to the cones with the semivertex angles θ and, if otherwise is not stated, with spherical noses (with the midsection radius r_0) joined smoothly with the conical surface at the section $x = 0$ (see Figures 9.1 and 9.10). The following notation is used in the figures

$$\begin{aligned} \Delta \bar{R} &= (R - r_b)/r_0, & r_b &= r_0 + x \tan \theta \\ \Delta \bar{p} &= (p - p_\infty)/\rho_\infty U_\infty^2, & \bar{p} &= p/\rho_\infty U_\infty^2 \\ & & \tilde{p} &= \bar{p}/\sin^2 \theta \end{aligned} \quad (9.4.1)$$

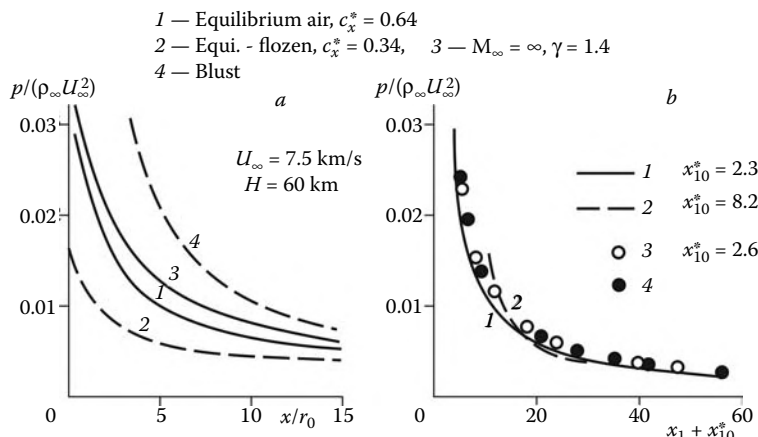


FIGURE 9.9
Pressure on a spherically blunted cylinder in air flow.

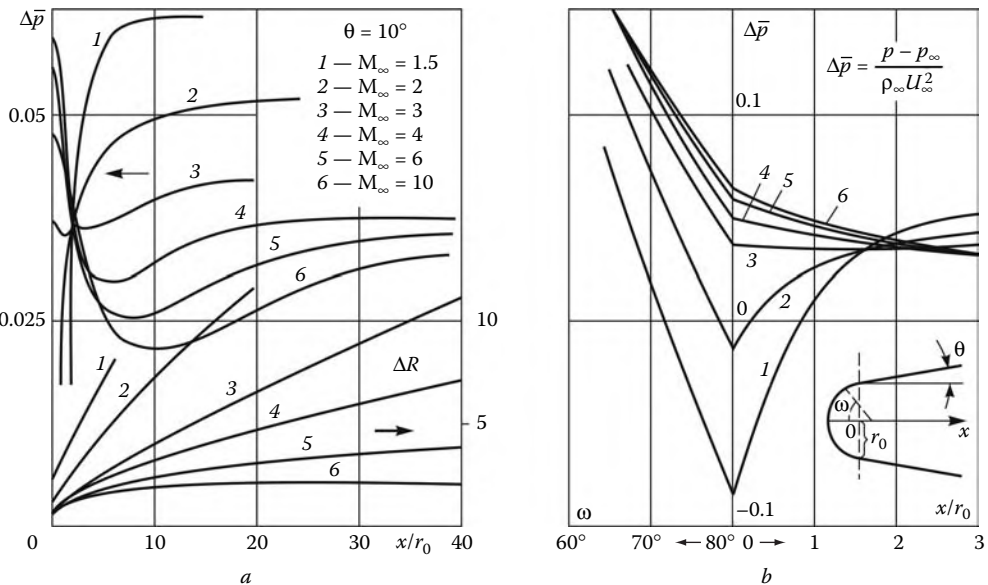
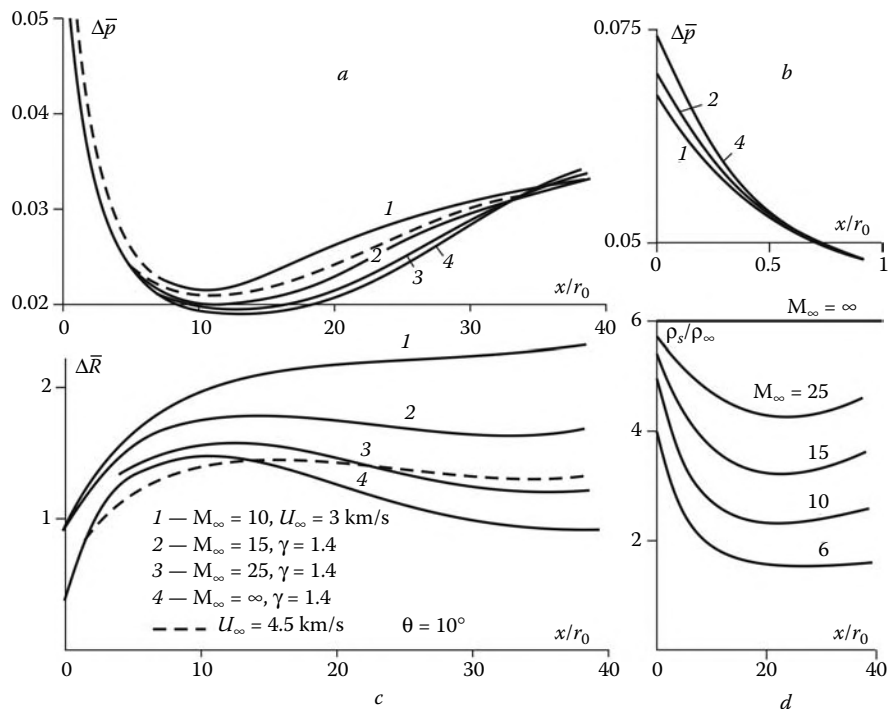


FIGURE 9.10
 M_∞ -dependence of the pressure and shock shape on cones.

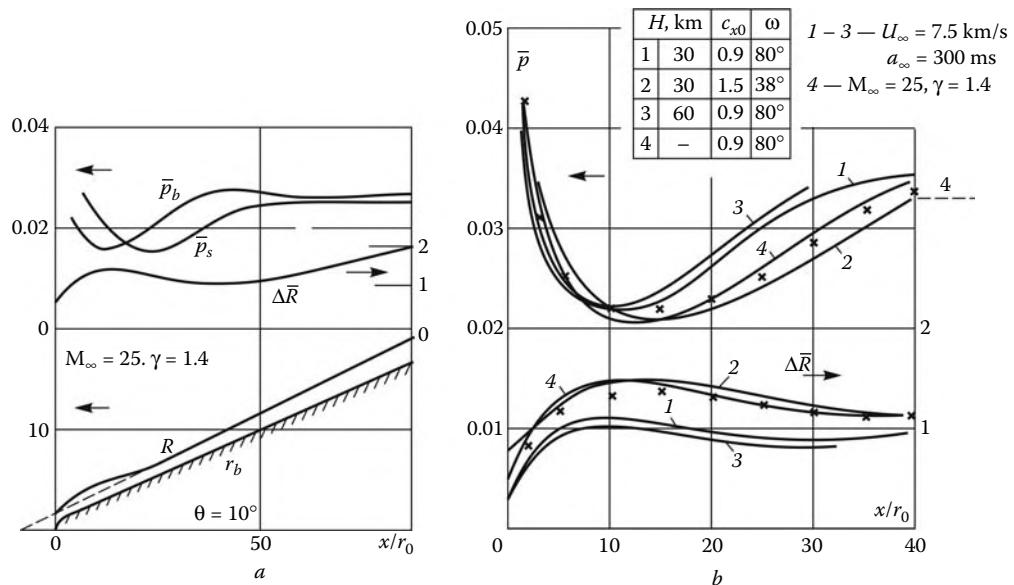
The Mach number effect (or that of the atmospheric flight conditions in the case of equilibrium air flows) on the flow past cones is illustrated in Figures 9.10 through 9.13. As follows from Figure 9.10, the pressure distribution over the sphere-cone body with $\theta = 10^\circ$ depends qualitatively on the Mach number M_∞ . For $M_\infty \leq 3$ the bluntness effect is only local (the zone of influence is $x \leq 2r_0$), while in the vicinity of the transition section $x = 0$ there forms a negative excess-pressure zone ($\Delta p < 0$), so that the pressure on the sphere far from the stagnation point is smaller than that on the sharp cone and approaches the conical distribution from below.

In contrast, at $M_\infty > 3$ the pressure on the sphere is greater than that on the cone, so that the further flow is determined by the expansion of the flow, which has not been totally expanded on the sphere. For $M_\infty \geq 4$ a pressure wave appears on the cone, this wave being the salient feature of the hypersonic flow past thin blunt cones. In accordance with Section 9.1, the extent of the wave increases with M_∞ , while its amplitude grows up to the value $\bar{p}_{\max}/\bar{p}_{\min} \approx 2$. The formation of this wave is due to the fact that the conical surface initially, as it were, falls behind the nose-induced shock, so that the pressure decreases. However, their trajectories are brought close as x/r_0 increases, and the pressure increases in the domain of the cone/shock interaction. Then the pressure p_b on the body and the shock slope (or the pressure p_s on the shock) become the same as for the sharp cone, the limiting position of the shock corresponding to that for the sharp cone with the vertex displaced with respect to the original cone nose (Figure 9.12a).

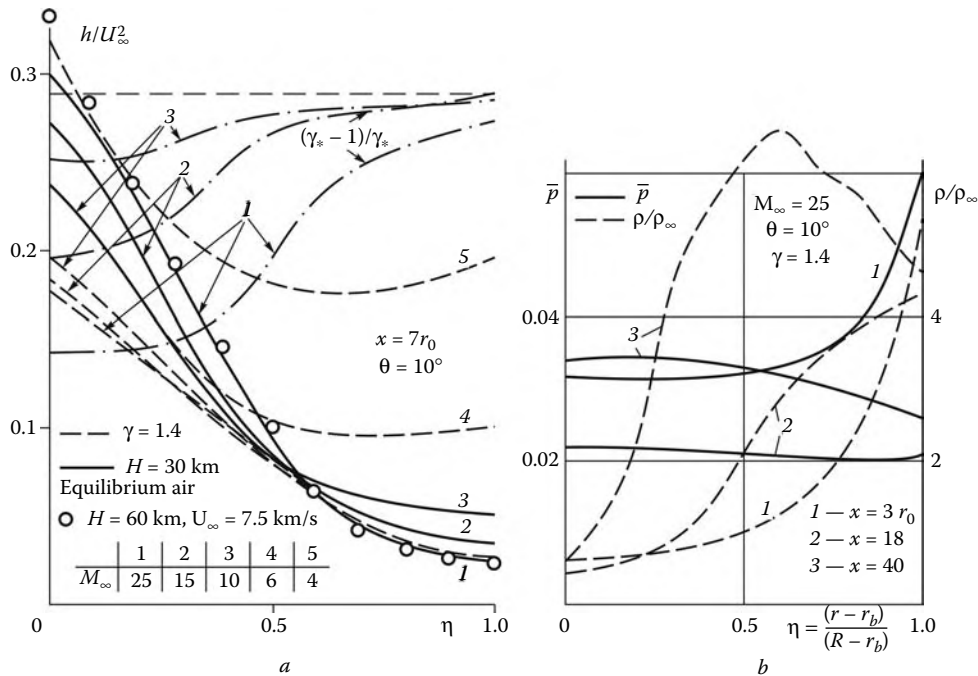
In Figure 9.14 the body pressure $p_b(x)$ is compared to the shock pressure $p_s(x)$, the latter parameter being the most sensitive to the shock shape. While the $\bar{p}_b(x)$ curves for different θ diverge already at $x > 0$, the $\bar{p}_s(x)$ curves for $M_\infty \gg 1$ in Figure 9.14a deviate from the curve for the cylinder ($\theta = 0$) consecutively and for $M_\infty = 4$ (Figure 9.14b) they almost coincide with it at $x < 30r_0$.

**FIGURE 9.11**

Pressures (a and b), shocks (c), and densities behind the shocks (d) in high-Mach-number flows past cones.

**FIGURE 9.12**

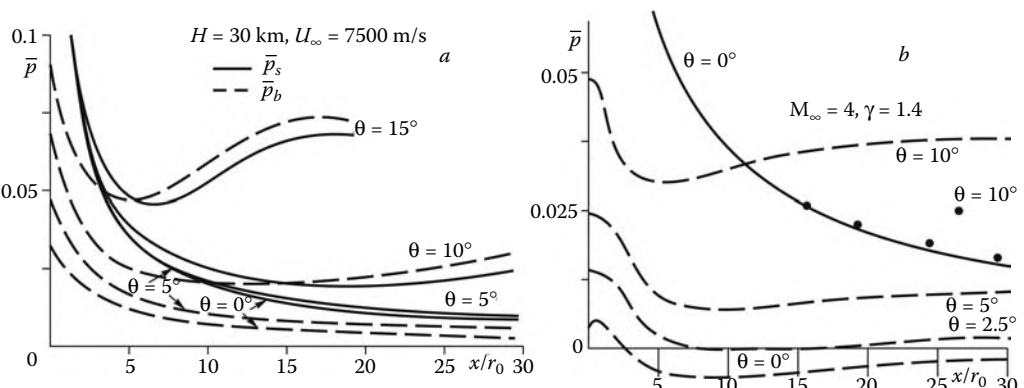
Pressures and shocks on a cone at high Mach numbers.

**FIGURE 9.13**

Flow parameters in the shock layer on a blunt cone.

The pressure waves, though weak, occur also on the blunt cylinder but only at finite M_∞ ; in these waves $\Delta p < 0$. The same effect is known for the explosion at a counterpressure (Section 6.8). At the same time, there is no pressure wave on wedges with $\theta \leq 15^\circ$; in this case the pressure decreases smoothly down to the value corresponding to the sharp wedge (Figure 9.15).

From Figures 9.10 and 9.11 it follows that for the cones with $\theta = 10^\circ$ the excess pressure Δp is almost independent of the Mach number already for $M_\infty \geq 10$ or $M_{\infty n} = M_\infty \sin \theta > 2$.

**FIGURE 9.14**

Pressures on cones and behind the shocks.

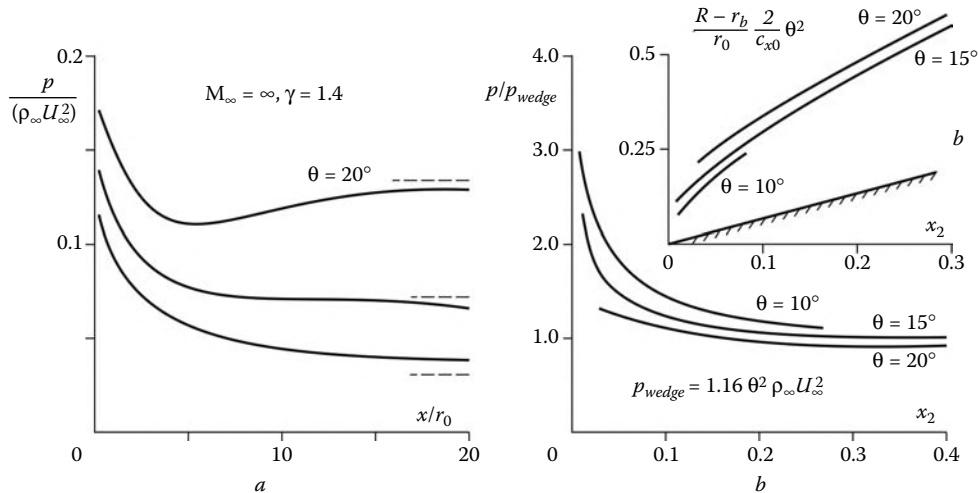


FIGURE 9.15
Pressures and shocks on wedges.

(for a perfect gas). At the same time, the shock layer thickness and structure are sensitive to the freestream Mach number for the values of M_∞ as high as almost 25 (or $M_{\infty n} \approx 5$), which determines the lower limit of the adequacy of the hypersonic stabilization law from Section 7.1.

The pressure waves diversify the shock layer structures. Thus, from Figure 9.13b it follows that the density has a peak inside the shock layer, which exceeds considerably the value of the density behind the shock. This occurs on the streamlines that have entered the shock layer in the pressure minimum region, with the subsequent pressure increase along these lines.

Physical and chemical processes in atmospheric flight start to affect the pressure and shock shape on the cone with $\theta = 10^\circ$ approximately at $U_\infty \geq 4.5$ km/s or $M_\infty \geq 15$ (Figure 9.11). However, the enthalpy and density profiles in the high-entropy layer are exposed to their influence considerably earlier (Figure 9.13). The real gas effects are readily illustrated by the profiles of the quantity $(\gamma_* - 1)/\gamma_*$; thus, for $U_\infty < 7.5$ km/sec (or, in the general case, for $U_{\infty n} \leq 1.5$ km/s) the effective adiabatic exponent is $\gamma \approx 1.4$ in the dense shock layer, while in the high-entropy layer it decreases down to the value $\gamma \approx 1.15$ (see also Figure 1.13 in Section 1.3). Under the conditions of that figure the density on the cone surface varies from $\rho_0/\rho_\infty = 0.4 \div 0.5$ in the perfect gas to $\rho_0/\rho_\infty = 0.7$ in real air. We will also note that, in accordance with Section 1.12, the variation of the density ρ_∞ by a factor of 100 (this corresponds to the atmospheric flight altitude H variation from 30 to 60 km) affects the results comparatively weakly (curves 1 and 3 in Figure 9.12 and curves and symbols in Figure 9.13a).

At first glance it would seem that the effect of the Mach number M_∞ and real gas properties on the pressure distribution over cones is unimportant (within the limits of 20% as in Figure 9.12). However, in view of rather high accuracy required from the calculated aerodynamic characteristics, this difference should be taken into account; in Section 9.5 we shall convince ourselves of that. The effect of M_∞ and gas properties on the shock layer thickness and structure is even more considerable (Figures 9.11 through 9.13).

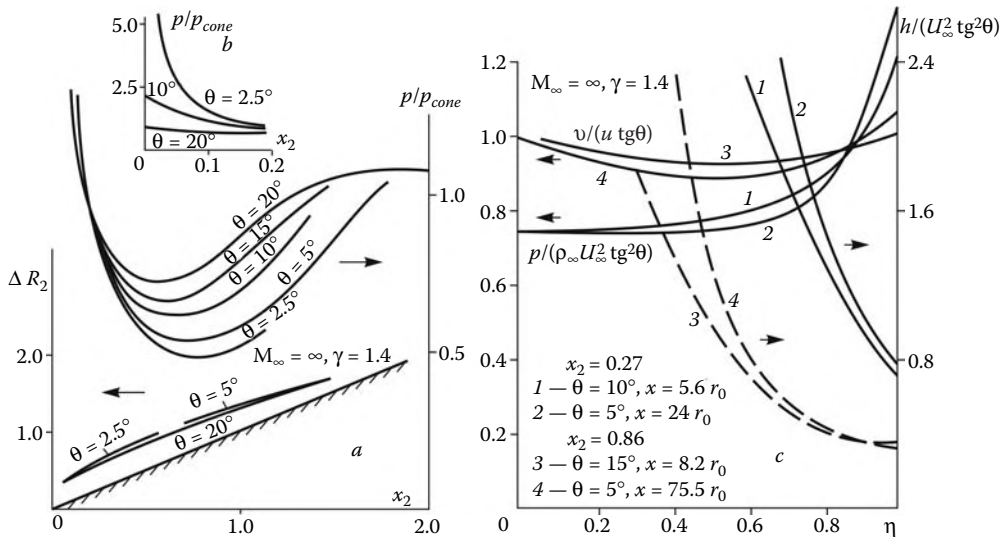


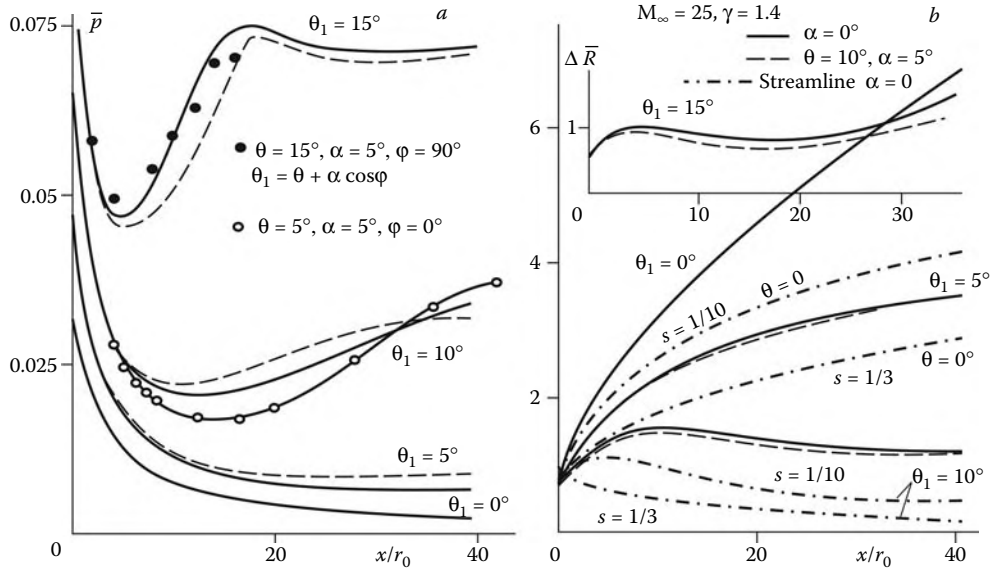
FIGURE 9.16
On the similarity law for blunt cones.

The nose shape effect on the flow past cones and the testing of the similarity law from Section 9.2 are presented in Figures 9.4 and 9.12b. In the latter figure curve 2 relates to the segmental nose with $\omega = 38^\circ$, $c_x = 1.5$, and the same flow conditions as for curve 1. The region of small values of x ($x \leq 3r_0$) for these conditions was shown in Figure 7.20c from Section 7.5. As in Figure 7.20c, curves 1 with the coordinates x and ΔR extended in the ratio $(c_{x2}/c_{x1})^{1/2} = 1.3$ (symbols) turn out to be close to curves 2; hence, they are close in the similarity coordinates x_1 and r_1 9.2.5. In the immediate vicinity of the nose the pressure on the body depends, quite naturally, not only on the nose drag but on its shape as well, though this dependence is weaker than that on the conical surface angle θ (Figure 7.20c).

Finally, we call attention to curves 2 and 4 in Figure 9.12b; the latter relates to the perfect gas, while the former to the equilibrium air, though in accordance with Figure 9.8, the effective drag coefficient is approximately the same: $c_x^* \approx 0.9$. The closeness of these curves confirms the similarity law of Section 9.3.

We will now consider the flow past cones with different θ . The corresponding data are presented in Figures 9.14 through 9.18. The flows obey the similarity law of Section 9.2, in accordance with which the pressure on the body \tilde{p} (see formula 9.4.1) and the shock shape $\Delta R_2 = (\Delta R_1)\theta^{-1}$ are dependent on the coordinate $x_2 = x_1\theta^2$ (formula 9.2.10). In these variables, the pressure curves and the shocks form fairly narrow bundles in Figure 9.16a, especially if we take into consideration the fact that in the original coordinates they could not even be compared (see, e.g., Figures 9.17 and 9.14; the data for $\alpha \neq 0$ in Figure 9.17 will be explained in the next section).

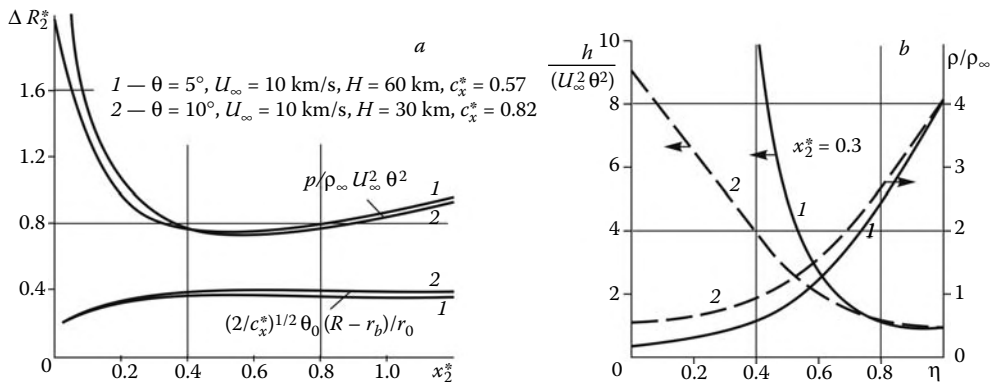
The similar data for wedges are presented in Figure 9.15b and for cones in real air in Figure 9.18; in the latter case the variables x_2^* and r_2^* (9.3.3) are used. As for the flow parameter profiles between the shock and the body surface, only the pressure and streamline slope distributions are similar for the cones with different θ . At the same time, the density and enthalpy distributions are similar only within a layer adjacent to the shock (Figures 9.16c and 9.18b).

**FIGURE 9.17**

Pressures (a) and shocks and streamlines (b) in the flows past cones with different semivertex angles θ at various angles of attack α .

However, from Figure 9.16b it follows that this similarity law no longer works for $x_2 \leq 0.2$; though for $\theta \geq 10^\circ$ this region is a comparatively small vicinity of the nose, for $\theta \leq 5^\circ$ it is fairly large and covers the region $x > 10r_0$. Here the shock stand-off distance is far in excess of the body thickness, so that its effect reduces to the appearance as though excess pressure on the cylinder (or on the flat plate). For this reason, as follows from Figure 7.20c of Section 7.5, the θ dependence of the pressure on short or very slender cones is near linear (Figure 9.14b); it is quadratic only for $x_2 \geq 0.2$.

We will now consider the behavior of streamlines within the high-entropy layer. In Figure 9.17b we have plotted the streamlines corresponding to the parameters $s = 1/3$ and $s = 1/10$ (cf. Section 9.1) for the blunt cone with $\theta = 10^\circ$ and for the cylinder ($\theta = 0$) at

**FIGURE 9.18**

Flow similarity for cones.

$M_\infty = 25$. The distances from the streamlines to the wall, as well as the high-entropy layer thickness in general, vary as $\delta/r_0 = (r_0/r_b)p^{-1/\gamma}$ as x increases. Because of this, on the cone we have $\delta/r_0 \rightarrow 0$ as $x/r_0 \rightarrow \infty$, this leading to the formation of a thin, strongly vortical wall sublayer (for $\theta = 10^\circ$ it is formed already at $x/r_0 > 30$). On the contrary, in the flow past the cylinder the streamlines diverge, at least, until the shock layer pressure becomes equal to the external pressure. At the same time, these streamlines appreciably deviate from the shock, which does not make it possible to use, in particular, the Newton formula for determining the pressure on the high-entropy layer edge (as in the explosion zone; see Section 7.6).

Finally, we will consider the drag coefficients of thin blunt bodies:

$$c_x = \frac{2(X_0 + X_b)}{\pi^\nu r_b^2 \rho_\infty U_\infty^2} = c_{x0} \left(\frac{r_0}{r_b} \right)^2 + c_{xb}$$

$$c_{xb} = \frac{4}{r_b^2} \int_{r_0}^{r_b} \Delta \bar{p} r_b dr_b \quad (9.4.2)$$

Here, the first and second terms represent the contributions of the nose and the lateral surface of the body. The corresponding examples for the spherically blunted cones are presented in Figure 9.19. In the original coordinates (Figure 9.19a) for comparatively small x/r_0 the coefficient c_x increases when θ decreases; this is caused by the decrease in the cone midsection area πr_b^2 and an appreciable contribution of the nose to the total drag of the cone. With the distance from the nose the situation is reversed, since as $x/r_0 \rightarrow \infty$, the coefficient c_x approaches its limiting value for the sharp cone $c_x = 2.08 \sin^2 \theta$ (Section 6.4). At the same time, c_x varies monotonically with θ if the coordinate x_2 is used. In accordance with the similarity law for thin bodies, the ratio c_x/θ^2 must be θ independent (for a fixed $M_\infty \theta$, see Sections 8.4 and 9.2). However, for this law to work, the term r_0 must be neglected in the expression for the body radius $r_b = r_0 + \theta x$ in formula 9.4.2; this could be done only if $x\theta \gg r_0$. Because of this, the more preferable correlation is the ratio c_x/c_{xN} of the exact value of the cone drag coefficient to the Newtonian one

$$c_{xN} = c_{x0} \left(\frac{r_0}{r_b} \right)^2 + 2 \sin^2 \theta \left[1 - \left(\frac{r_0}{r_b} \right)^2 \right] \quad (9.4.3)$$

These ratios are presented in Figure 9.19c and form a fairly narrow bundle of curves.

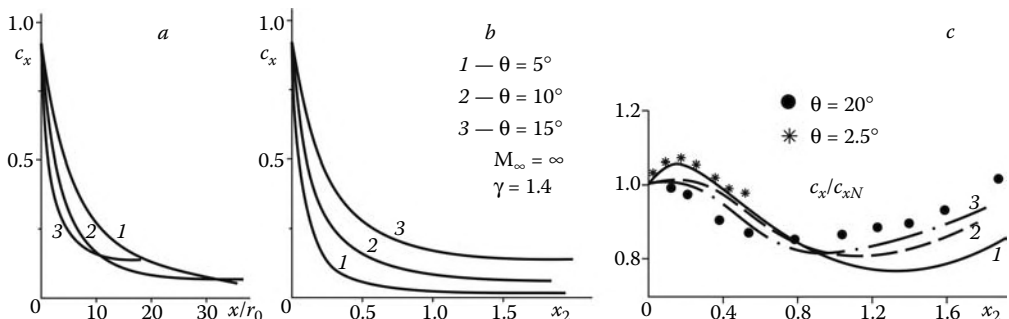


FIGURE 9.19
Drag coefficients of blunt cones.

We will now consider the particular features of the flows around protruding elements of bodies (such as shields, controls, etc.) embedded in the shock layer on a blunt cone, for example, on the vehicle fuselage. As follows from Figure 9.20, the pressures and shocks on double cones with different noses but with the same similarity parameter $X_1 = (2/c_{x0})^{1/2}r_0/L$ (see 9.2.2) differ only slightly, including the flow over the second cone (shield), which is indicative of the similarity of the shock layer flows past blunt bodies.

However, the main effect consists in an appreciable (by several times) increase in the pressure on the shield, due to the variation of the gas density across the shock layer by an order; this underlines the contribution of the denser part of the shock layer to the aerodynamic characteristics of the vehicles having superstructures on their frames (this was noted earlier, in Section 3.7). This effect can lead to fundamental consequences. To elucidate this effect, we have plotted in Figure 9.21 the approximate pressure and Mach number distributions over the shield or, say, the blunt edge of a swept control inclined to the conical surface with $\theta = \theta_1 = 10^\circ$ by an angle of $\theta_2 = 25^\circ$ (the local Mach number on the cone is $M_0 \approx 3$ and the limiting angle of the internal shock is $\alpha = 34^\circ$). Clearly, at a certain point η_* the local Mach number is $M = 1$; the further flow is subsonic, which, in accordance with Section 5.3, leads to the change in the flow problem formulation and the necessity (in the general case) of taking certain downstream boundary conditions into account.

Moreover, at a certain point $\eta = \eta_0$ we have $M = 0$; thus, in accordance with Section 2.11 (Figure 2.21), the further inviscid flow on the second cone is no longer possible without the global flow restructuring and the formation of viscosity-driven separated flows (of the jet type in Figure 5.15). The question of the existence of inviscid solutions for a blunt swept wing edge will be discussed in Section 9.9.

The manifestation of these effects via the shock layer structure and thickness depends considerably on the Mach number M_∞ ; because of this, the M_∞ effect on the aerodynamic characteristics of thin blunt bodies is more appreciable when these bodies have shields, controls, and so on, than in the case in which there are no superstructures on the frame.

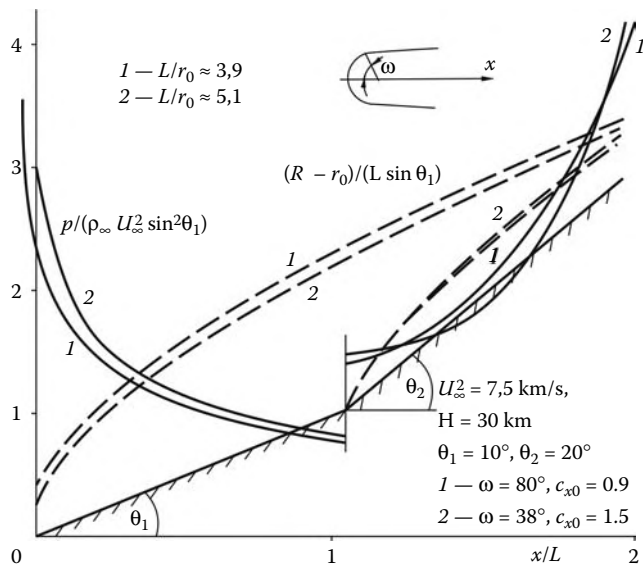
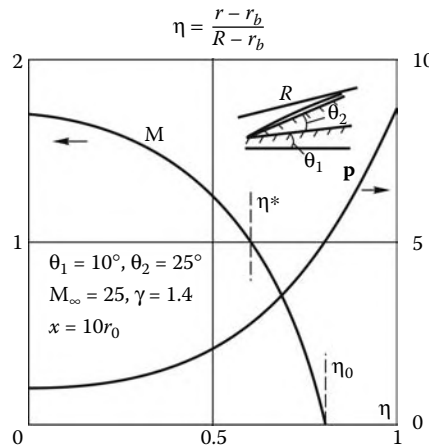


FIGURE 9.20

Pressure distributions and shocks on the cones with a broken generator.

**FIGURE 9.21**

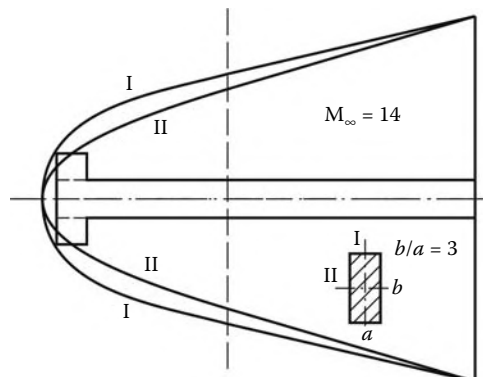
Pressures and Mach numbers on the second cone or on the swept edge of a control.

9.5 Bodies of Revolution at Incidence

In accordance with the subject matter of this chapter, we will consider only low angles of attack, $\alpha \ll 1$, thus satisfying conditions 9.1.1. In this case the three-dimensional effects are superimposed on the nose-induced effects, while at high angles of attack, $\alpha \sim 1$, the nose effect is only local and the flow obeys the same laws as those considered for sharp bodies in Sections 6.6 and 7.11 (except for a thin wall vortex layer, see Section 9.8).

As earlier, we will use the body-fitted cylindrical reference frame x, r, φ , where x is the axis of symmetry of the body, the origin $x = 0$ is located at the junction of the nose with the lateral surface, and the plane of symmetry $\varphi = 0$ relates to the windward side.

It would seem that in these conditions the logical consequence of the blast-piston model is the axial symmetry of the shock wave and the absence of peripheral pressure gradients in the central low-density blast zone with the body embedded in it, as is the case, for example, for the nonaxisymmetric charge explosion. In fact, such a flow is realized in the far wake behind a blunt body in Figure 9.22 (experimental data), when nothing prevents transverse

**FIGURE 9.22**

Shape of the shock in the flow past a rectangular plate in two perpendicular planes.

pressure equalization, so that the shock wave, initially nonsymmetric, becomes then symmetric. In this case, within the framework of the model of Section 9.2, the far wake flow is determined by the body drag X_0 and the transverse force Y_0 or, within the framework of the blast analogy, by the explosion energy $E_0 = X$ and momentum $J_0 = Y_0/U_\infty$. Taking the latter into account results in the drift of the center of mass $y = y^*(t)$ of the gas in the explosion zone at the velocity

$$\frac{dy^*}{dt} = U_\infty \frac{dy_0}{dx} = v, \quad \pi^\nu \rho_\infty R^{1+\nu} v = J_0 \quad (9.5.1)$$

In the original steady-state flow this corresponds to the bending of the wake axis in accordance with the law $y = y_0(x) = y^*(x/U_\infty)$. For $M_\infty \gg 1$ we have $R \sim t^{1/2} \sim x^{1/2}$ and $y_0 \sim \ln x$ in the axisymmetric wake ($\nu = 1$) and $R \sim x^{2/3}$ and $y_0 \sim x^{1/3}$ in the plane wake ($\nu = 0$) (Ryzhov and Terent'ev, 1974).

However, this model is, generally speaking, incorrect, as applied to the flow past a thin blunt body, since in the high-entropy layer with moderate local Mach numbers ($M_0 \approx 3$) the mean path of disturbances in the peripheral direction can be fairly large. This follows from the equation of the characteristics on the body surface; when the peripheral velocity $w = 0$, it has the form:

$$\frac{dx}{d\varphi} \approx M_0 r_b = M_0(r_0 + \theta x) \quad (9.5.2)$$

Integrating this equation from $\varphi = 0$ to $\varphi = 2\pi$ we obtain the length l_φ over which a disturbance traveling from an original meridional plane returns to it on reflection from the opposite meridional plane

$$l_\varphi \approx (r_0/\theta)(\exp 2\pi M_0 \theta - 1) \quad (9.5.3)$$

The ratio l_φ/r_0 increases with θ and is fairly high ($l_\varphi/r_0 \approx 2\pi M_0 \geq 20$) even for $\theta \approx 0$ ($M_0 \geq 3$). We note that the peripheral velocity $w \neq 0$, which is not taken here into account, can only increase the value of l_φ ; moreover, if w is supersonic, the disturbances cannot at all return from the leeward to the windward side.

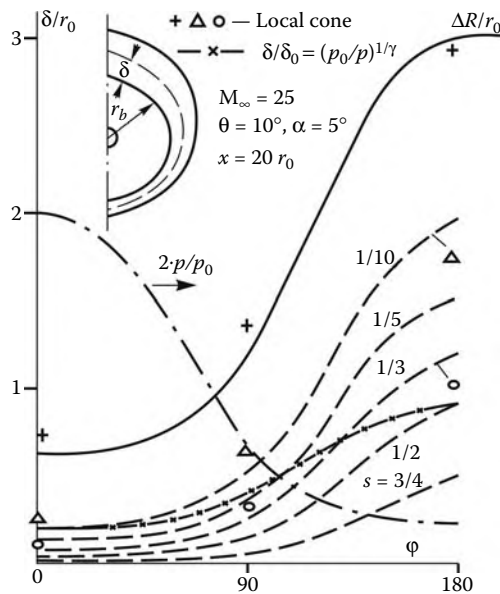
At the same time, the same disturbances cross twice the high-entropy layer of thickness δ over the distance of $l_r \approx 2M_0\delta$. In Figure 9.23 we have presented the shock layer thickness and the shapes of the isentropic surfaces $s = \text{const}$ (s is the parameter introduced in Sections 7.1 and 9.1) for a conical cross-section in the typical case $\theta = 10^\circ$ and $\alpha = 5^\circ$. Clearly, in this case $\delta \sim r_0$ and, hence, $l_r \ll l_\varphi$. In other words, the equalization of disturbances within the high-entropy layer is more rapid in the radial than in the peripheral direction.

Because of this, in generalizing the description of the nose effect in terms of its integral characteristics, we should also preassign their peripheral distributions, that is, the longitudinal force $X^{(\varphi)}\Delta\varphi$ and the longitudinal momentum fluxes $I_r^{(\varphi)}\Delta\varphi$ and $I_\varphi^{(\varphi)}\Delta\varphi$ in the transverse and peripheral directions for each small angle $\Delta\varphi$ between close meridional planes, as well as the gas flow rate $Q^{(\varphi)}(\psi_s)\Delta\varphi$ between the body surface and isentropic streamsurfaces $\psi_s = \psi(s, r, \varphi)$ and the entropy distribution $s(\psi_s)$ over them.

However, for a blunt body of revolution (nose) a small angle α introduces only small asymmetry in all the flow parameter distributions, which could be, hence, represented in the form:

$$F(\varphi) = F_0 + \alpha F_1(\varphi), \quad F = X^{(\varphi)}, \dots \quad (9.5.4)$$

At the same time, the angle-of-attack effect on the flow past the lateral surface is of the order α/θ , which follows, for example, from the Newtonian pressure distribution $p \sim (\theta + \alpha \cos \varphi)^2$ (Section 6.6). On this background, the influence of the terms of the order α in 9.5.4 may be neglected.

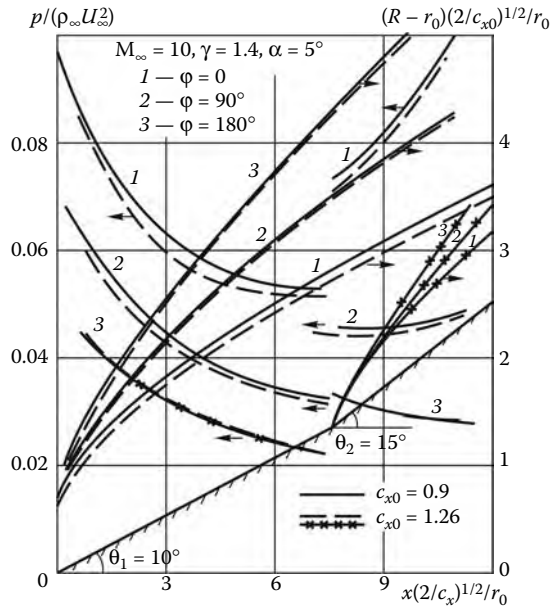
**FIGURE 9.23**

Shock shapes and isentropic surfaces $s = \text{const}$ in the shock layer on a spherically blunted cone.

Then, in accordance with the analysis made in Sections 9.1 and 9.2, the main parameter determining the nose effect on the flow is its drag $X_0 = 2\pi X_0^{(\varphi)}$ (Luney, Zemlyanskii, and Magomedov, 1969), the more so that at low angles of attack the bow shock ahead of a blunt body has a tendency to conserve its shape in the flow-fitted reference frame (Figure 5.8, Section 5.4). These results give ground to extend the laws and similarity criteria of Section 9.2 to the nonsymmetric flow past thin blunt bodies, though adding to them the parameter α/θ . The testing of this similarity law for geometrically similar double cones having different noses is given in Figure 9.24 for pressures and shocks, while the parameter profiles in the similar sections of the shock layers are compared in Figure 9.25.

Let us consider other properties of the flow past thin blunt bodies. In Figure 9.26 the shapes of the longitudinal and transverse sections of the shocks ahead of spherically blunted cones and cylinders are plotted in the flow-fitted coordinate system (the following illustrations also relate to the same bodies). These shocks conserve their symmetric, nose-induced shape at fairly great distances from the noses. Thus, the shape of the shock on the cone with $\theta = 10^\circ$ at an angle of attack $\alpha = 5^\circ$ varies only for $x > 10r_0$ on the windward side, while on the leeward side it remains unaltered even at $x \leq 30r_0$. As for the blunt cylinder, it is embedded in this wave up to the intersection with its near vicinity, which, in accordance with 9.2.2, takes place only for $x/r_0 \approx (\tan \alpha)^{-2} \geq 10^2$ at $\alpha \leq 6^\circ$. We note that these data relate to $M_\infty = \infty$; however, these effects are only enhanced as M_∞ decreases.

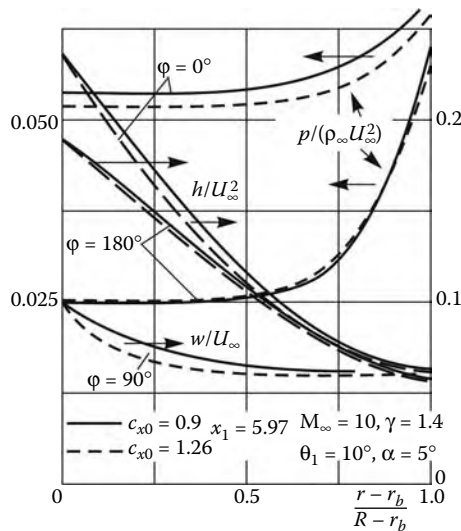
The previously mentioned properties of the shocks on the blunt cylinder are responsible for the peculiar features of the cylinder flowfield. As follows from Figure 9.27, the flow past the cylinder, apart from the near vicinity of the nose (of the order of its size) and up to the "contact" of the cylinder with the denser, near-shock part of the shock layer, is qualitatively similar (within the framework of the plane section law of Section 8.2) to the two-dimensional transverse flow past the circular cylinder at the Mach number $M_{0n} \approx M_0 \sin \alpha < 1$ (where M_0 is the characteristic Mach number in the high-entropy layer), the pressures at $\varphi = 0$ and

**FIGURE 9.24**

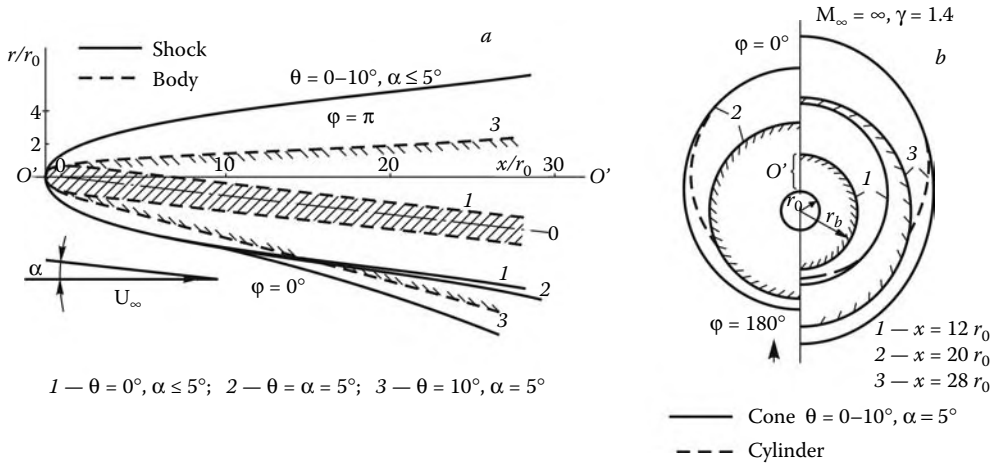
Surface pressures and shocks in the flow past a blunt cone with a conical flare.

$\varphi = \pi$ being approximately equal and the pressure at $\varphi = \pi/2$ being smaller than that at the same section for $\alpha = 0$. For finite M_∞ the pressure at $\varphi = \pi/2$ is even smaller than the external pressure p_∞ .

For the cones with $\alpha < \theta$ the following semi-empirical *local blunt cone rule* works: the pressure distributions over the conical surface and the shock shapes in the meridional planes of

**FIGURE 9.25**

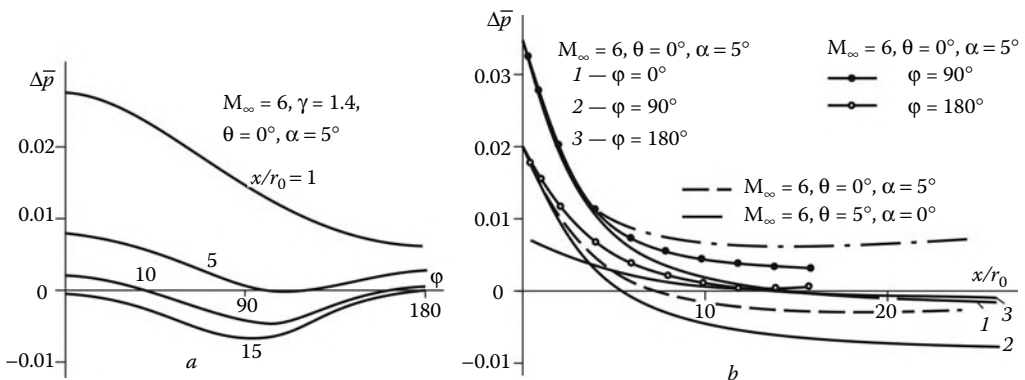
Flow parameters in the similar sections of the shock layer on a blunt cone.

**FIGURE 9.26**

Shock shapes in the flow past blunt cones at incidence in meridional (a) and transverse (b) sections.

the cone set at incidence coincide with the same quantities for the *local*, or *equivalent*, cone with the same nose set at $\alpha = 0$ but having the semivertex angle equal to the local angle of attack of the given generator $\theta_l = \theta + \alpha \cos \varphi$ of the original cone (Lunev, Murzinov, and Ostapovich, 1960). In support of this conjecture, in Figure 9.17 we have compared the pressure distributions, shock shapes, and flow parameters in the shock layer for the original and local cones with the same θ_l ; here, the curves and symbols relating to the same parameters form fairly narrow bundles, while the pressure on the $\varphi = \pi/2$ generator of the cone with the given θ is near independent of the angle of attack. The analogous rule for sharp cones was formulated in Section 6.6. At the same time, the rule is not extended to the blunt cylinder at an angle of attack and, apparently, to very slender cones with $\theta \leq 5^\circ$ at $\alpha \approx \theta$ (Figure 9.27b).

The local cone rule can also be extended to the case of cones with nonsymmetric noses. This follows from Figure 9.28, in which the nose asymmetry is due to the turn of the junction between the conical nose with the angle $\theta_1 = 45^\circ$ and the lateral conical surface, so that

**FIGURE 9.27**

Pressures in transverse (a) and meridional (b) sections of the flow past slender cones.

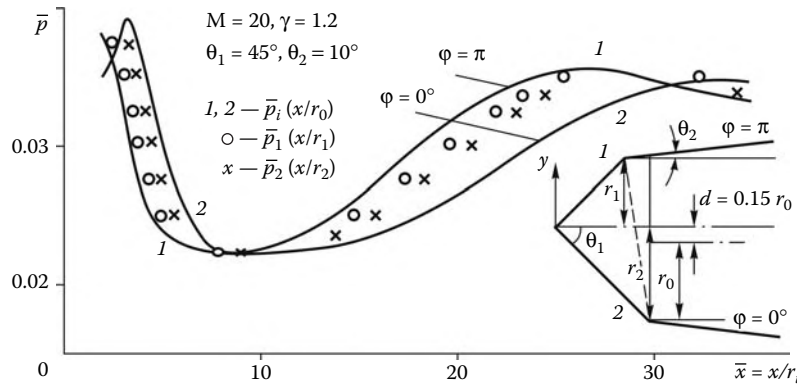


FIGURE 9.28
Pressure distribution over a blunt cone with a nonsymmetric nose.

in each meridional plane the nose has its own size r_i . Because of this, the local equivalent cones are in this case the cones with symmetric noses of the same shape but with their own sizes $r_0 = r_i$. Reconstructing these curves in the coordinates x/r_i (symbols) results in their almost complete coincidence.*

The local cone rule can be extended to the flow parameter distributions in the shock layer, at least, for not too long cones (at $x \leq 30r_0$, as in Figure 9.29, in which the density profiles are plotted for the cone with $\theta = 10^\circ$ at $\alpha = 5^\circ$). As follows from Figure 9.23, within these limits the shapes of the isentropic surfaces in the high-entropy layer are also similar, though the peripheral distribution of the high-entropy layer thickness δ does not follow in the general case the $\delta p^{1/\gamma} \approx \text{const}$ law corresponding to the uniform φ -distribution of the longitudinal gas flow rate within the layer.

However, with increasing x/r_0 , due to the peripheral flow effect, the agreement between the density profiles for the original and equivalent cones, both quantitative and even qualitative, is violated ($x = 40r_0$ in Figure 9.29), while the thickness of the high-entropy layer becomes smaller on the windward side of the cone and larger on the leeward side than on the equivalent cones.

The φ -distribution of the peripheral velocity w over the surface of the blunt cone follows approximately the sinusoidal law, as in the case of sharp cones (Section 6.6, Figure 6.13) with a maximum of this function on the ray $\varphi = \pi/2$ for small α and its displacement toward larger values of φ as α increases. Figure 9.30a presents the function $w/u \sin \alpha$ on the body (in the plane $\varphi = \pi/2$), which increases up to a certain limit with x/r_0 ; the transverse distribution of the velocity w in the same plane is plotted in Figure 9.30b for several cross-sections $x = \text{const}$. Clearly, the value of w increases by a factor of two to three as the body surface is approached. This effect is due to the simultaneous decrease in the density which, for the same orders of the peripheral pressure gradients, causes a greater peripheral acceleration of the gas in the high-entropy layer than in the denser shock layer.

The peculiar features of the pressure distribution over slender blunt cones reflect also on the nature of their aerodynamic characteristics. An example is shown in Figure 9.31 for the spherically blunted cones at $\alpha \leq \theta = 10^\circ$. Due to a considerable contribution of the

* The data in Figure 9.28 were obtained by Lipnitskii and those of Figures 9.26, 9.27, and 9.29 to 9.32 by Antonets.

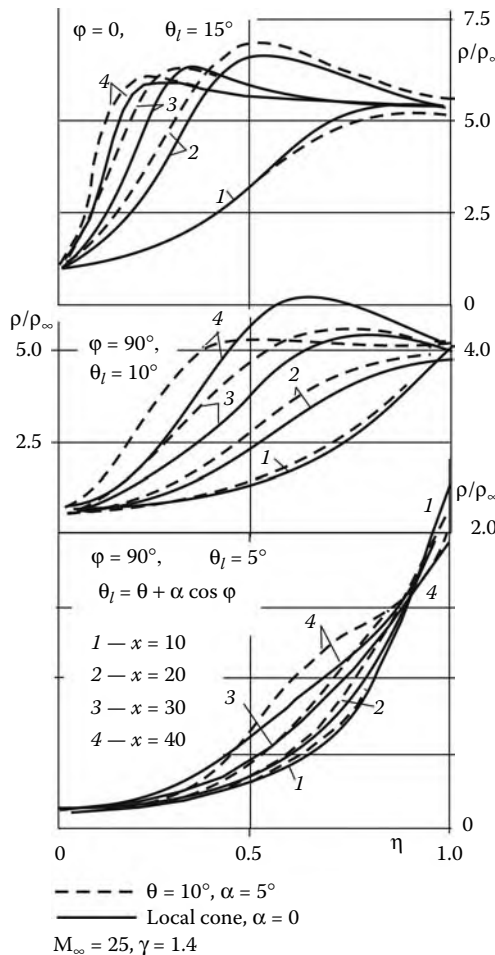


FIGURE 9.29
Density profiles in the shock layers on blunt cones.

nose, the tangential force coefficient c_τ depends on the angle of attack only slightly and, at least, more slightly than in the case of sharp cones, for which, in accordance with 7.4.8, $c_\tau = 2\theta^2 + \alpha^2$ for $\alpha, \theta \ll 1$.

In this connection, precisely the transverse aerodynamic characteristics, that is, the coefficients of the normal force c_n and of its moment c_m about the forward point of the body c_m , are of particular interest.

Representing these coefficients in the form of the ratios c_n/α and c_m/α makes these curves considerably closer, though the dependence on α is conserved. As $\alpha \rightarrow 0$ (e.g., for $\alpha = 1^\circ$) these ratios tend to the finite aerodynamic derivatives $c_n^{(\alpha)}$ and $c_m^{(\alpha)}$. The center of pressure c_d depends on the angle of attack only slightly, though it should be borne in mind that in engineering rather stringent requirements are imposed on the accuracy of determining it. In Figure 9.32 the values of c_d for the spherically blunted cone are presented for different flow conditions. Clearly, the effect of the Mach number M_∞ and the real gas properties on the value of c_d amounts to several percents, which is rather high for this parameter.

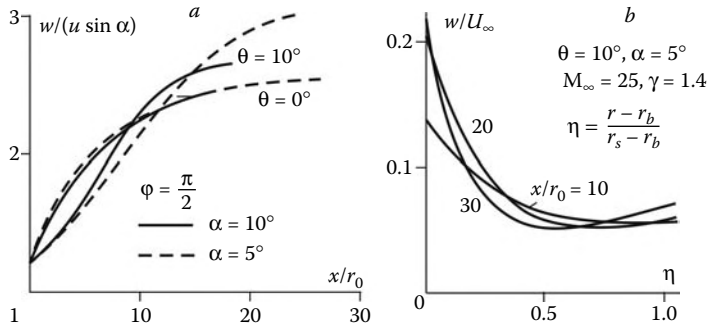


FIGURE 9.30
Peripheral velocity distributions in the shock layers on blunt cones.

The parameters c_n , c_m , and c_d are considerably affected by the pressure wave, which, in accordance with the local cone rule, contracts on the windward side and extends on the leeward one, this determining a fairly complicated nature of their distributions over the conical surface. In this connection, it is interesting to compare the exact and Newtonian data; this will be done using formulas 7.4.7 and 7.4.13 with allowance for the constancy of the integrals J_i . The final formulas (for $\alpha < \theta \ll 1$) are as follows:

$$\begin{aligned} c_\tau &= c_{x0}\lambda^2 + (2\theta^2 + \alpha^2)(1 - \lambda^2), & \lambda &= r_0/r_b \\ c_n &= c_{n0}\lambda^2 + 2\alpha(1 - \lambda^2), & c_{n0} &= \alpha(2 - c_{x0}) \\ c_m &= \frac{l_0}{L}c_{n0}\lambda^2 + \frac{4\alpha}{3\theta}\frac{r_b}{L}\left[1 - \frac{2}{3}\lambda + \frac{3}{2}\lambda^2 + \frac{3}{2}\lambda\theta(1 - \lambda^2)\right] \\ c_d &= \frac{c_m}{c_n} \end{aligned} \quad (9.5.5)$$

Here, L is the body length measured from its forward point, while l_0 is the distance from the center of pressure of the bluntness to the forward point. The terms with c_{x0} and c_{n0} are due to the nose contribution, while the other terms to that of the lateral surface. These curves are also plotted in Figure 9.31 for the spherically blunted cone ($c_{x0} = 1, l_0 = r_0$). As the cone thickness r_b/r_0 increases, the coefficients c_n and c_m approach the corresponding values for the sharp cone more rapidly than c_τ ; however, they differ considerably (up to a factor of two) from the exact values. This is attributable to the fact that the nose affects the transverse coefficients of the blunt cones via, primarily, the surface pressure which is considerably lower than on the sharp cone, this leading to a decrease in c_n and c_m . The position of the center of pressure also considerably differs from the exact value (Figure 9.32). We note that within the framework of formulas 9.5.5 the quantities c_n/α , c_m/α , and c_d do not depend on α at all.

As for time-dependent aerodynamic characteristics of thin blunt bodies, we will restrict ourselves only to an indication of the possibility of extending the curved body rule established in Section 8.7 for sharp bodies to the unsteady case. This possibility is based, first, on the quasisteady nature of the flow past the nose (the Strouhal number ratio for the flows past the nose and the long body as a whole is of the order $r_0/L \ll 1$, Section 1.12) and, second, on a comparatively weak effect of the violation of the time-dependent analogy in the high-entropy layers on thin blunt bodies on the main parameters of the flowfields for these bodies (Section 9.3).

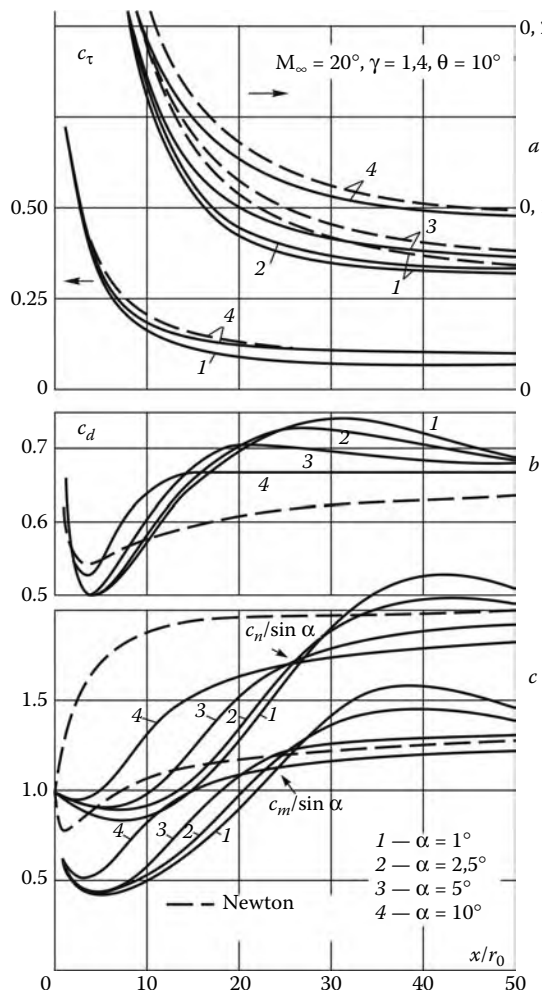


FIGURE 9.31
Aerodynamic characteristics of a spherically blunted cone.

For testing the curved blunt body rule in Figure 9.33 we have compared the coefficients p_i in Equation 8.7.18 determined in accordance with this method (for $l = r_0$, with account of Equation 8.7.21) with the solution of the exact time-dependent linear problem in the form:

$$p_1 = \bar{p}_i / \cos \varphi, \quad \bar{p}_1 = \bar{p}_{\alpha 1}, \quad p_2 = \bar{p}_{\alpha 2}, \quad \bar{p}_3 = \bar{p}^{(\bar{\omega})}, \quad \bar{p}_4 = \bar{p}^{(\bar{\Omega})} \quad (9.5.6)$$

Clearly, the curves for the same flow parameters are fairly close.

9.6 Wings with Blunt Edges

A very simple example of such a wing is furnished by a triangular plate with a hypersonic (in the sense of Section 7.1) blunt edge of small thickness r_0 (Figure 9.34) and a sharp nose in gas flow under the following conditions

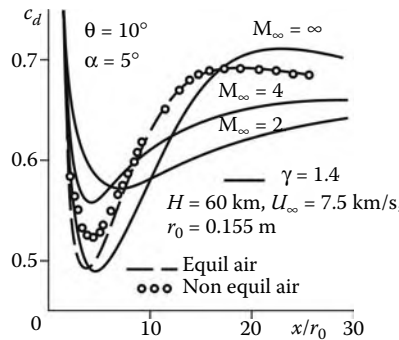


FIGURE 9.32
Center of pressure of a blunt cone.

$$\alpha \ll \beta, \quad \varepsilon = \alpha / \sin \beta \ll 1 \\ L \gg r_0, \quad l = L \tan \beta \gg r_0, \quad M_{n\infty} = M_\infty \sin \beta \gg 1 \quad (9.6.1)$$

Here, L is the length, $2l$ is the wing width (span), and ε is the normal angle of attack of the plate in the plane normal to the edge (formula 6.7.4; Figure 6.17). The restriction on the angle of attack α is caused by the fact that the distinctive features of the flow described in the following manifest themselves only when the flow is subject to these conditions, whereas in the case $\alpha \sim \beta$ the flow pattern is similar to that described in Section 6.7 for the wing with sharp edges.

We will first consider the flow domain A (Figure 9.34) adjacent to the edge and well off the nose so that the effect of the latter could be neglected. In accordance with 6.7.2 and 6.7.3 at $\alpha \ll \beta$ the components $U_{\tau\infty}$ and $U_{\infty}^{(n)}$ of the external velocity \vec{U}_∞ along the edge axis τ

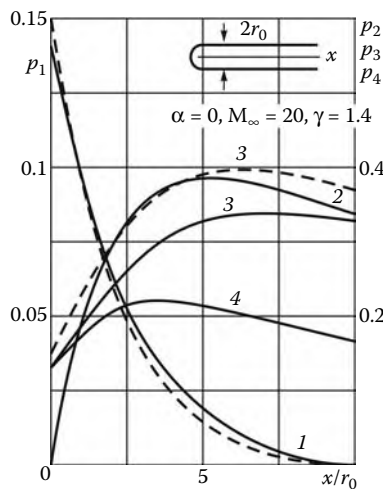


FIGURE 9.33
Unsteady parameters of the flow past a blunt cylinder (solid curves relate to the curved body method and dashed curves to the exact solution).

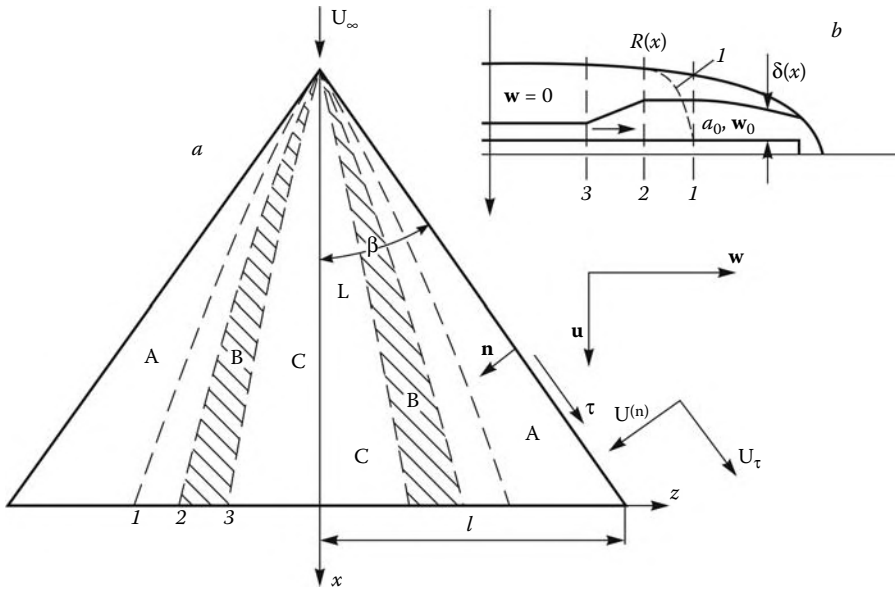


FIGURE 9.34
Flow past a triangular plate with blunt edges.

and in the plane normal to it and the projection $U_{n\infty}$ of the latter component onto the plate (or on the n axis) are as follows:

$$U_{\infty}^{(n)} = U_{n\infty} = U_{\infty} \sin \beta, \quad U_{\tau\infty} = U_{\infty} \cos \beta \quad (9.6.2)$$

When the edge is in the hypersonic stream with $U_{n\infty} \gg a_{\infty}$, then the flow in the domain A is the same as the flow past an infinite blunt plate set at the yaw angle β to the freestream and with the constant velocity component along the edge $U_{\tau} = U_{\tau\infty}$. The solution in the plane perpendicular to the edge is the same as for the flow with the velocity $U_{\infty}^{(n)}$ past a blunt plate set at a small angle of attack ε (Section 9.2), with the coordinate x replaced by n . In particular, the pressure, the shock shape, and, in accordance with 7.1.4, the distribution of the enthalpy in isentropic streamsurfaces are determined by the following formulas

$$\begin{aligned} \bar{p}_n(\bar{n}, \bar{y}) &= \bar{p}/\sin^2 \beta, \quad \bar{p} = p/\rho_{\infty} U_{\infty}^2 \\ \bar{R}(\bar{n}) &= R/r_0, \quad \bar{n} = n/r_0, \quad \bar{y} = y/r_0 \\ h/U_{n\infty}^2 &= \bar{h}_n(\bar{p}_n, \bar{s}_n) = \frac{1}{2} \bar{p}_n^{(\gamma-1)/\gamma} s_n^{1/\gamma} \\ s/\sin^2 \beta &= s_n(\bar{\psi}_{sn}) = \sin^2 \alpha_n, \quad \bar{\psi}_{sn} = \psi_n/r_0 \rho_{\infty} U_{n\infty} \\ s &= \sin^2 \alpha_s, \quad s_n = \sin^2 \alpha_n \end{aligned} \quad (9.6.3)$$

Here, ψ_n is the gas flow rate in the two-dimensional flow in the plane normal to the edge, α_n is the angle of the inclination of the shock section by this plane, α_s is the local angle of attack of the shock $R(n)$, and s is the entropy function (see Section 7.1). On the plate surface we have $s_n = 1$ and $s = \sin^2 \beta$.

In accordance with the classification adopted in Sections 9.1 and 9.2, we assign the flow domain with $s_n \sim 1$ to the high-entropy layer and the domain with $s_n \ll 1$ to the low-entropy shock layer. By analogy with Section 6.7, we write down the velocity projections onto the x and z axes

$$\begin{aligned} u &= U_\infty(1 - \bar{v} \sin^2 \beta), & w &= U_\infty \bar{v} \sin \beta \cos \beta \\ U_{n\infty} \bar{v} &= U_{n\infty} - U_n \end{aligned} \quad (9.6.4)$$

In domain A the velocity deficit v is determined from the Bernoulli equation

$$\bar{v} = 1 - \sqrt{1 - 2\bar{h}_n} \sim \bar{h}_n \quad (9.6.5)$$

The orders of the quantity \bar{v} in the shock and high-entropy layers are different, namely

$$\bar{v}_s \sim \bar{p}_n \sim (dR/dn)^2 \ll 1, \quad v_0 \sim \bar{p}_n^{(\gamma-1)/\gamma} \quad (9.6.6)$$

Here, the subscript 0 is refers to the flow parameters on the plate.

Hence, in the shock layer the stripe rule of Section 8.5 is correct to the second order; in accordance with this rule, the gas flows in the $z = \text{const}$ planes only. In the high-entropy layer the velocity deficit \bar{v} is greater; precisely this circumstance generates the effects considered in the following. The point is that the quasi-two-dimensional flow in domain A is violated in the domain of influence of the plane of symmetry where the following condition is imposed

$$w = 0, \quad z = 0 \quad (9.6.7)$$

This domain is bounded by the limiting characteristic surface passing through the nose vicinity. The line of intersection $z_0(x)$ of this surface with the plate $y = 0$ is a bicharacteristic whose equation at high local Mach numbers can be brought to the form:

$$U_\infty \frac{dz_0}{dx} = w_0 + a_0, \quad a^2 = (\gamma - 1) U_{n\infty}^2 \bar{h}_n \quad (9.6.8)$$

At the same time, the slope of the characteristics on the shock inclined at the angle α_s is determined by the local Mach number

$$U_\infty \frac{dz_s}{dx} \sim a_s \sim U_\infty \bar{p}^{1/2} \sim U_\infty \alpha_s \quad \bar{p} \sim (dR/dx)^2 \sim \alpha_s^2 \quad (9.6.9)$$

Therefore, we have

$$z_s/z_0 \sim (\alpha_s / \sin \beta)^{1/2} \ll 1 \quad (9.6.10)$$

Thus, the domain of influence of the plane of symmetry is much larger in the high-entropy layer than in the shock layer and, as distinct from the case of the sharp plate, even the relation $z_0 \sim l$ can take place. Because of this, the influence of the plane of symmetry propagates along the z axis only via the high-entropy layer, which is shown in Figure 9.34b, curve 1.

In this case the two-layer model could be used for making estimates; this model is based on the blast analogy and the integral equations of Section 6.8 for blunt plates in $z = \text{const}$ planes but takes into account also the gas flow toward the z axis in the high-entropy layer with some layer-averaged parameters a_a, w_a , and so on (Lunev, 1965, 1975). However, if it is desired to reveal qualitative effects only, this model could be further simplified by letting in the first approximation the shock shape $R(x, z)$ to be a constant parameter of the problem in each $x = \text{const}$ section. Then the problem is reduced to that considered in Section 4.10 (Figure 4.23) with the same principal qualitative effects. In particular, the disturbance propagation velocity along the z axis is also equal to $a_{\text{eff}} = a_a(\delta/R)^{1/2}$, thus being smaller than the average speed of sound a_a in the high-entropy layer. Hence, the boundary between

the undisturbed domain A and the centered expansion wave (domain B in Figure 9.34) is located within the theoretical Mach cone. In the immediate vicinity of the cone, the same conclusions on the disturbance decay, as in Section 4.10, are correct.

Due to gas spreading in the high-entropy layer, the pressure on the plate decreases; in the central region C bounded by the closing characteristic $z_c(x)$ of the expansion wave (line 3 in Figure 9.34) it is determined by formula 4.10.9 with all ensuing consequences discussed in Section 4.10.

In the first and second approximations this model solution from the previously mentioned work is presented in Figure 9.35 for different γ and sections $\tau = x \sin \theta / r_0 c_x$, where c_x is the drag coefficient of the plate edge. As γ decreases, the value of \bar{v} increases, thus enhancing the spreading effect and the pressure decrease. This effect advances a very long distance along the plate, $L \sim 10^3 r_0$. We note that in the second approximation, which takes the shock shape variation along the z axis into account, the $\bar{p}(z)$ curves have local maxima on the axis of symmetry. This secondary effect is due to a certain increase in the ratio δ/R , as the shock stand-off distance decreases with the pressure. These results were qualitatively confirmed in the experiments performed at the U-11 setup of the Central Research Institute of Machinebuilding (TsNIIMash) (Krasil'nikov and Ivanov, 1972); the observed pressure decrease was larger than the theoretical value, due, possibly, to the conicity of the nozzle used and the flow divergence within it (Figure 9.35c).

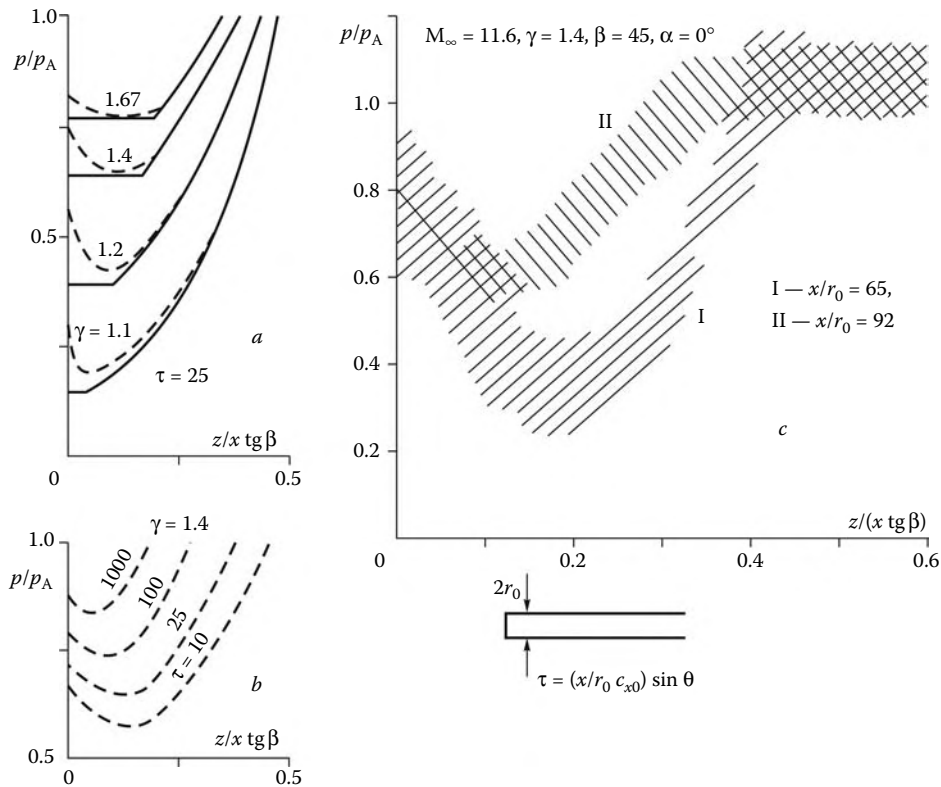


FIGURE 9.35

Relative pressure distributions over the plate span: (a and b) the model problem (solid and dashed curves relate to the first and second approximations); (c) experiment.

The flow considered is a typical example of the *inertia-driven* gas spreading caused by the boundary conditions on the edges rather than by the local pressure maximum (cf. Sections 4.10 and 6.7). Moreover, the induced pressure gradient even retards the gas spreading. As a result, the gas can completely flow out from the central high-entropy zone, the latter being filled by the streamlines from the shock layer — this effect takes place also in the solution of Section 4.10.

This effect is all the more probable as the angle of attack α increases. In this case the thin sublayer $\delta \ll R, \alpha x$ does not practically affect the pressure distribution, which is near constant, as on the sharp plate. In its turn, this leads to the constancy ("freezing") of the velocities along streamlines, as well as the constancy of the angles θ at which they are inclined to the x axis; this follows from Equation 2.2.6

$$\rho U^2 \frac{\partial \theta}{\partial l} = \frac{\rho U^2}{R} = \frac{\partial p}{\partial n} \quad (9.6.11)$$

Here, l and n are the coordinates along and normal to a streamline, while R is its radius of curvature. For $\partial p / \partial n \approx 0$ hence follows the constancy of the streamline slopes and their radial divergence, which is the required result.

9.7 Wings with Blunt Noses

We will consider a triangular plate with a nose of small radius r_0 and sharp or blunt (with a small bluntness radius r_1) edges set at a small angle of attack $\alpha \ll 1$. We will assume the angle β to be small (Figure 9.36a); at the same time, we assume that $M_\infty \sin \beta \gg 1$, since a rather nontrivial effect of the interference between the nose-induced shock and the edges or the wing plane manifests itself precisely in this case. This effect, on which we will concentrate our attention for reasons to be explained in the following, consists of the occurrence of divergence lines on the wing plane; they are approximately parallel to the axis $z = 0$ and pass through the region of intersection of the nose-induced shock with the edges, conditionally, point A .

The effect is illustrated in Figure 9.37 in which the distribution of the derivative $\partial \theta / \partial z = \theta'(z)$ of the angle of inclination of streamlines to the x axis in different $x = \text{const}$ cross-sections is plotted (the data of Kovalev). Curve 1 relates to the forward part of the plate, namely, the region $x < x_A$ preceding the point A (we will drop an analysis of the flow pattern in this region). As for curves 2 to 4 that relate to the $x > x_A$ region, these are qualitatively different from curve 1. On these curves the derivative $\theta'(z)$ is negative near the $z = 0$ axis, so that, as distinct from curve 1, this axis is a convergence line. However, as z increases, this derivative reverses sign and increases up to the maximum point O . In this case maximum divergence of the corresponding streamlines should be expected at points $z = z_A$ of inflection of the $\theta'(z)$ curves, at which $\theta''(z_A) = 0, \theta'''(z_A) > 0$, and the following expansion is valid

$$\theta - \theta_A = (z - z_A)\theta'(z_A) + \frac{1}{6}(z - z_A)^3\theta'''(z_A) \quad (9.7.1)$$

The $z_A(x)$ curve is a divergence line passing through a vicinity of point A at a distance $\Delta z \approx 2r_0$ from the axis $z = 0$. These distances correspond to the plate width at point A and are almost independent of the local plate width. The causes of the occurrence of precisely this flow pattern are analyzed in the following.

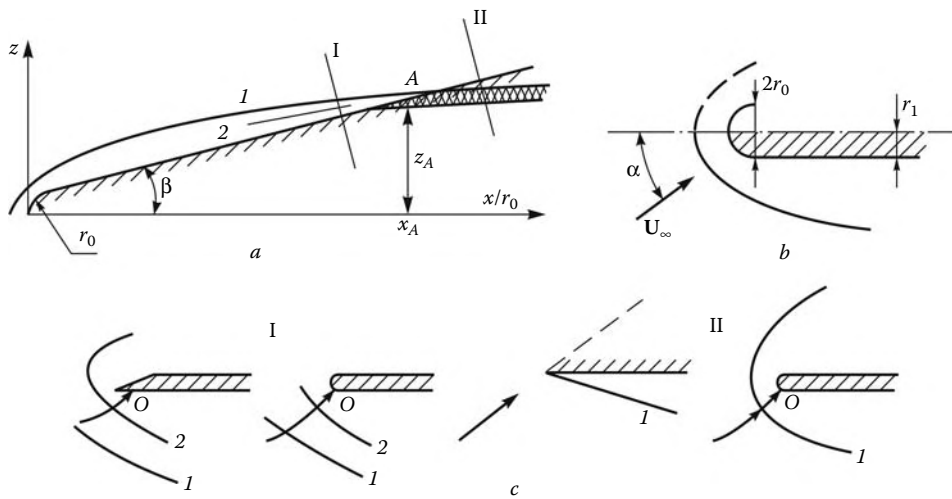


FIGURE 9.36
Diagram of the flow past a blunt-nosed triangular plate.

The shape $R(x, z)$ of the shock induced by the nose as by a blunt body is determined by the blast analogy laws (Section 9.2). Therefore, at a certain plate length $x \leq x_A$ its frame is located within this initially axisymmetric blast wave. The general plate-flow pattern is sketched in Figure 9.36 (a and b are the plan and side views), while in Figure 9.36c we have presented the flow diagrams in the vicinity of a conditional point A of the interaction of the bow shock with the sharp edges in different normal sections ahead of this point. In region I for $x < x_A$ behind the bow shock the Mach numbers $M^{(n)}$ normal to the edge are comparatively small. Thus, in the plane normal to the edge the flow around the latter is usually either subsonic or is accompanied by the detached shock 2. In region II the Mach numbers $M_\infty^{(n)} > 1$, so that a solitary shock, either attached or detached, is formed ahead of

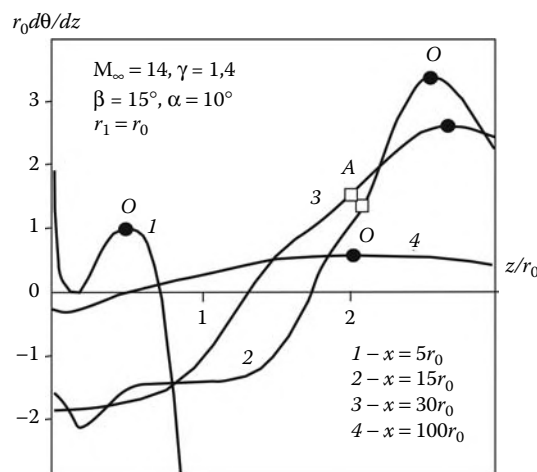
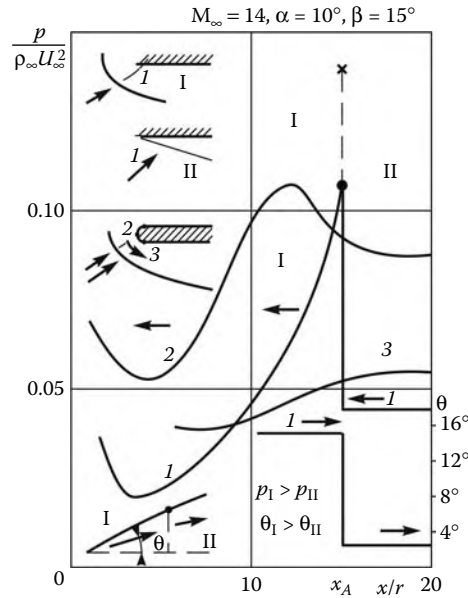


FIGURE 9.37
On the definition of the convergence and divergence lines on a plate.

**FIGURE 9.38**

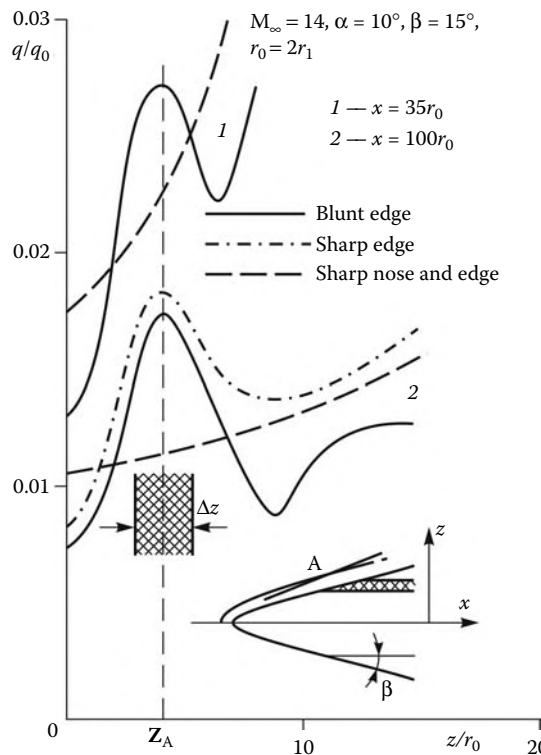
Pressure distribution over the wing edge.

the edge. For small α and β the interaction of shocks 1 and 2 is usually regular, though this is of no importance in our case.

The pressure distributions over the edges, both sharp and blunt, are plotted as curves 1 and 2 in Figure 9.38 for points O on the windward side of the plate (Figure 9.36c).^{*} The initial pressure decrease at $x < x_A$ is attributable to the pressure decrease along the shock, while its subsequent increase as $x \rightarrow x_A$ to the edge/shock-layer interaction. In the same figure, the angles θ between streamlines and the x axis are plotted. Clearly, a discontinuity in the pressure and in the angle θ arises on the edge near the point A ; the breakdown of this discontinuity (Section 4.9) results in the appearance of the elevated-pressure zones marked by an asterisk. A pressure maximum, though without a discontinuity, occurs on the blunt edge as well (curve 2).

Thus, in the region of the interaction between the shock layer and the wing edge a small elevated-pressure zone, or “spot,” arises; the subsequent enlargement of the spot generates a bundle of divergent streamlines on the lateral surface of the plate, together with a central divergence line ($z_A(x)$ in Figures 9.37 and 9.39). As follows, for example, from the comparison of curves 2 and 3 in Figure 9.38, the decrease in the edge pressure down to the value corresponding to the sharp plate occurs nearly immediately (at least, for $\alpha \sim \beta$); because of this, the previously mentioned divergent streamline bundle is, as it were, frozen. This means that, as in Sections 4.10, 6.7, and 9.6, we deal again with the *inertia-driven gas spreading* (though of somewhat different origin) leading to the convergence of the near-wall stream-surfaces in the vicinity of the line $z = z_A$ passing through the point A . It is hardly probable that the described effects of the inertia-driven gas spreading are essential for determining forces acting on a vehicle; however, they can affect the distribution of heat fluxes to the surface due to particular sensitivity of the fluxes to the behavior of near-surface streamlines.

* For a detailed discussion see Lesin and Lunev (1994).

**FIGURE 9.39**

Heat flux distribution over a triangular plate (q_0 is the heat flux at the stagnation point on the nose).

This is illustrated by Figure 9.39, in which the spreading effect at a near-constant pressure on the plate leads to the peak increase in the heat flux by a factor of 1.5 at distances up to $x \sim 100r_0$.^{*} These heat flux peaks are located within narrow bands Δz near the $z = z_A$ line and are attributable to peculiar features of the three-dimensional heat transfer, which are described in Section 12.15 (the experiments were performed at $r_0 = 2r_1$ (see Figure 9.36c); for this reason, region A in Figure 9.39 is about twice as far from the axis as in the calculation presented in Figure 9.37, which was carried out under the same conditions but for $r_0 = r_1$).

9.8 Some Properties of the Three-Dimensional Vortex Layers on Blunt Bodies

In Section 9.5 we described some properties of the three-dimensional flows in the high-entropy layers on thin blunt bodies on the basis of an analysis of the calculated data. Here, we will present the more general analytical investigation of these flows in the vicinity of the flow convergence and divergence lines in the plane of symmetry (Figure 9.40). We will restrict ourselves to the wall layer on the assumption that it is filled by isentropic stream-surfaces (determined by the parameter s ; see Sections 7.1 and 9.1) fitting closely the body

* This effect was detected in the experiments of Gubanova, Zemlyanskii, Lesin, Lunev, and Nikulin (1992).

surface. We will assume the pressure distribution over the body surface to be preassigned and the pressure normal to the surface to be constant within the sublayer. We will use the surface-fitted coordinate system x, y, φ 1.13.21 with the velocity projections u, v , and w on these axes and with the transverse radius of curvature of the body r_b . For blunt cones $r_b = r_0 + x \sin \theta$, where θ is the semivertex cone angle and r_0 is the nose midsection radius.

In the vicinity of the flow divergence ($\varphi = 0$) and convergence ($\varphi = \pi$) lines lying in the plane of symmetry, the following expansions for the pressure $p(x, y)$ and the peripheral velocity w hold

$$\begin{aligned} \frac{1}{\rho} \frac{\partial p}{\partial \varphi} &= -U_\infty^2 \beta a^2 \tilde{\varphi}, & w &= U_\infty g \tilde{\varphi} \\ \tilde{\varphi} &= \varphi, \quad \varphi \approx 0; & \tilde{\varphi} &= \pi - \varphi, \quad \varphi \approx \pi \end{aligned} \quad (9.8.1)$$

The expansions are similar to those for sharp cones (6.6.13). Here, U_∞ is a certain scale velocity, for example, the freestream velocity in the problem of the flow past cones. The density $\rho = \rho_0(p)s^{-1/\gamma}$ and the speed of sound $a = a_0(p)s^{1/2\gamma}$, together with the parameter s , are dependent on the isentropic surface under consideration (the subscript 0 refers to the surface parameters). In the reference frame adopted, the velocity w and its coefficient g (9.8.1) are positive everywhere, including the leeward convergence line. We also assume the coefficient β to be positive, except for specially specified situations in which there is a local pressure peak on the flow convergence line (e.g., those in Figure 6.9 of Section 6.6 for sharp cones and Figure 9.27 for blunt cones).

This introduction having been done, we will first investigate the isentropic streamsurface distributions in the vicinity of the convergence and divergence lines. For this purpose, we consider a narrow streamtube of thickness δ_m , confined by two isentropic streamsurfaces almost enveloping the body surface and two meridional sections determined by a small angle $\Delta\varphi$ (Figure 9.40). Then, as $\Delta\varphi \rightarrow 0$, the gas flow rate equation in the streamtube and

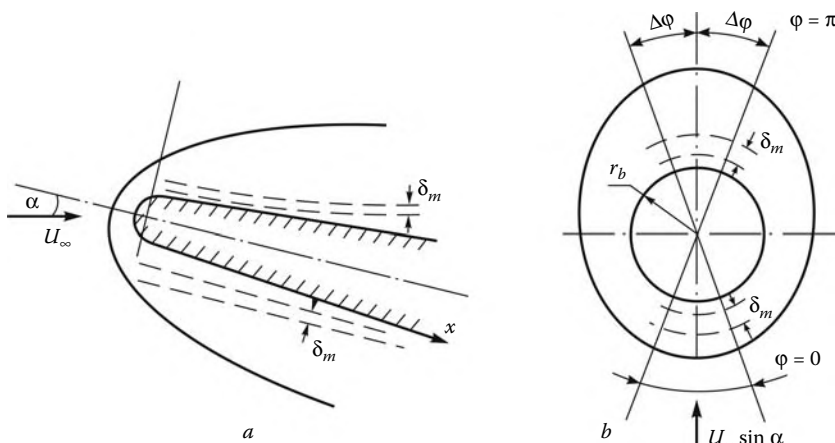


FIGURE 9.40

Problem of the flow in the vicinity of the planes of symmetry of a blunt body.

the isentropic streamsurface distribution over the vortex layer take the following forms:

$$\begin{aligned} \frac{\partial}{\partial l}(\rho\delta_m Ur_b) &= -\frac{\partial}{\partial\varphi}(\rho w\delta_m) = -jU_\infty\rho\delta_m g \\ \frac{\partial y}{\partial y_1} &= \frac{\delta_m}{\delta_{m1}}, \quad j=1, \quad \varphi=0; \quad j=-1, \quad \varphi=\pi \end{aligned} \quad (9.8.2)$$

We refer the subscript 1 to certain initial (for a certain $l = l_1$) parameters, the initial distance $y = y_1$ of the isentropic surface to the body being the Lagrangian coordinate of the former. The coefficient $j = 1$ relates to the flow convergence and $j = -1$ to divergence lines, while l is the distance measured along the streamtube; for isentropic surfaces close to the body surface, which are considered for the time being, l coincides with x . In view of 9.8.1, this equation has the solution

$$\begin{aligned} mr_b &= m_1 r_{b1} e^{-j\xi}, \quad m = \rho U \delta_m \\ \xi &= \int_{x_1}^x \frac{g}{r_b \bar{U}} dx, \quad \bar{U} = \frac{U}{U_\infty} \end{aligned} \quad (9.8.3)$$

For a cone at zero incidence, the estimate $\delta \sim (r_b p^{-1/\gamma})^{-1}$ at $g = 0$ and $\xi = 0$ leads to the asymptotics for the high-entropy layer thickness far from the cone nose obtained earlier in Section 9.4. Therefore, the flow past a cone at incidence ($g > 0$) results in the relative narrowing of the high-entropy layer on the windward side of the body ($\varphi = 0, j = 1$) and widening on the leeward side ($\varphi = \pi, j = -1$) with the respective increase and decrease in the high-entropy layer vorticity, which is confirmed, in particular, by the density profiles in Figure 9.29 (Section 9.5).

The factor e^ξ is not necessarily the exponential function of x . Thus, in a very simple case of constant $g = g_1$ and $U = U_1$ for blunt cones we obtain

$$\begin{aligned} r_b &= r_0 + x \sin \theta, \quad \xi = \omega \ln \frac{r_b}{r_0} \\ \frac{m}{m_1} &= \left(\frac{r_0}{r_b} \right)^{1+\omega}, \quad \omega = \frac{g_1}{\bar{U}_1 \sin \theta} \end{aligned} \quad (9.8.4)$$

On a divergence line we have always $dm/dx < 0$, while on a convergence line $dm/dx < 0$ for $\omega < 1$ and $dm/dx > 0$ for $\omega > 1$. In the latter case the convergence effect prevails over purely "conical" gas spreading. Near the nose (at least, spherical nose) of a blunt cone, at $x = x_1 = 0$ we can put $w \approx \alpha U \sin \varphi$, where α is the angle of attack, and, hence, $g_1 \approx \bar{U}_1 \alpha$. Therefore, for $\bar{U}_1 \approx 1$ we have $\omega < 1$ for $\alpha < \theta$ and $\omega > 1$ for $\alpha > \theta$. In the case of more complicated functions $g(x)$, solution 9.8.4 involves exponential terms with the derivatives dm/dx , whose signs alternate on convergence lines.

We are now coming to an analysis of the behavior of the peripheral velocity w on isentropic near-wall streamsurfaces. For conical surfaces (the case to which we will restrict ourselves) the corresponding Equation 1.13.21 in our variables takes the form:

$$r_b L(w) + uw \sin \theta = -\frac{1}{\rho} \frac{\partial p}{\partial \varphi}, \quad L(w) = u \frac{\partial w}{\partial x} + \frac{w}{r_b} \frac{\partial w}{\partial \varphi} \quad (9.8.5)$$

For near-wall streamsurfaces in the vicinity of the planes of symmetry it should be set $v = 0$ and $u = U$. In this case, preassigning the pressure distribution $p(x, \varphi)$ over the body

surface or in its immediate vicinity (as was accepted previously) transforms Equation 9.8.5 into a separate first-order equation with respect to the function w with the initial condition $w = w_1(\varphi)$ in the initial section $x = x_1$, from which the streamsurfaces with the inclination $r_b d\varphi/dx = w/u$ representing the characteristics of this equation originate. For $w > 0$ these characteristics approach the flow convergence line $\varphi = \pi$, which makes impossible to satisfy, in the general case, the symmetry condition $w = 0$ on this line without the corresponding "fitting" of the pressure distribution. Therefore, we will assume that the pressure distribution over the body obtained in the solution of the global problem is consistent with this symmetry condition. Later we shall return to this question.

For the vicinity of divergence and convergence lines we will use expansion 9.8.1, thus reducing Equation 9.8.5 to the form:

$$\begin{aligned} \frac{dg}{d\zeta} + G = 0, \quad \zeta = \int_{x_1}^x \frac{dx}{r_b \bar{U}} \\ G = jg^2 + g \bar{U} \sin \theta - \beta_0, \quad \beta_0 = \beta a^2 / U_\infty^2 \end{aligned} \quad (9.8.6)$$

Given the coefficients \bar{U} and β_0 , this equation can be solved subject to the initial condition $g = g_1$ at $x = x_1$. For small g (or α) the term g^2 in Equation 9.8.6 may be neglected. Then the equation has an integral-form solution, which, for cones at constant β_0 and \bar{U} , is as follows:

$$g - g_0 = (g - g_1)r_0/r_b, \quad g_0 = \beta_0/U \sin \theta \quad (9.8.7)$$

This solution is the same for the convergence and divergence lines and tends to the asymptotic limit $g = g_0$ fairly slowly as $x/r_0 \rightarrow \infty$. In the general case, the behavior of the solution of Equation 9.8.6 depends on whether the roots of the equation $G = 0$ analogous to 6.6.14

$$g_{\pm} = -j \frac{1}{2} \bar{U} \sin \theta \pm \Delta, \quad \Delta = \frac{1}{4} \bar{U}^2 \sin^2 \theta + j\beta_0, \quad g_+ - g_- = 2\Delta \quad (9.8.8)$$

are real or imaginary. For $\beta_0 > 0$ they are always real on the divergence lines ($j = 1$) and imaginary on the convergence lines ($j = -1$) if $\Delta^2 < 0$ or $\beta_0 > (1/4)\bar{U}^2 \sin^2 \theta$. Correspondingly, the function G can be presented in the form:

$$\begin{aligned} G = j(g - g_+)(g - g_-), \quad \Delta^2 > 0 \\ G = j[(g + (1/2)\bar{U} \sin \theta)^2 - \Delta^2], \quad \Delta^2 < 0 \end{aligned} \quad (9.8.9)$$

For constant β_0 and \bar{U} the solution of Equation 9.8.6 is reduced to simple tabulated integrals for the function $\zeta(g)$, which are not written down here. However, in the general case the integral form of the solution of this equation cannot be derived, so that we restrict ourselves to a qualitative analysis of the solution. For $j = 1$ we have for the roots $g_+ > 0$ and $g_- < 0$; therefore, the function g approaches g_+ from above at $g > g_+$ and from below at $g < g_+$ (Figure 9.41a) following the $g - g_+ \sim e^{-2\zeta\Delta}$ law at $g_+ = \text{const}$. For $j = -1$ but when $\beta_0 > 0$ and $\Delta^2 > 0$ we have for the roots $g_+ \geq g_- > 0$. In this case, for $g < g_+$ the function g approaches g_- increasing at $g < g_-$ and decreasing at $g > g_-$. However, for $g > g_+$ the function g increases near a certain point x_∞ as $g \sim (\zeta_\infty - \zeta)^{-1} = \text{const}(x_\infty - x)^{-1}$. In accordance with 9.8.9, the same result is obtained for $\Delta < 0$. In both cases, the asymptotics of the unbounded solutions are determined by the solution of the equation $g' = g^2$, which follows from the limiting inertial equation of the form, 9.8.5, $L(w) = 0$.

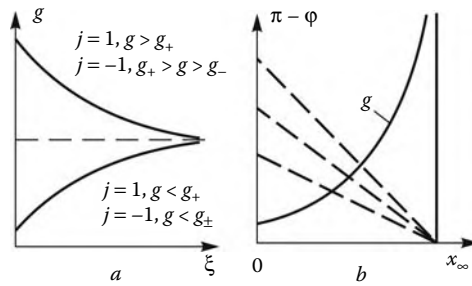


FIGURE 9.41
Behavior of the peripheral velocity coefficient and the streamlines.

The characteristics of this equation are the streamsurfaces $d\varphi/dx = w/ur_b$ with $w = \text{const}$ on them. When $u = \text{const}$ and the distribution of w in the initial section $x = x_1$ has the form $w_1 \sim \pi - \varphi$, the bundle of these characteristics (dotted lines in Figure 9.41b) converges to the line $\varphi = \pi$ at a point x_∞ , the derivative $\partial w/\partial\varphi \sim g$ increasing without bounds as this point is approached.

However, this intense flow toward the line $\varphi = \pi$ leads to unbounded growth of the vortex layer thickness in the vicinity of the singular point x_∞ ; in accordance with 9.8.3, the asymptotics of this thickness for the solution obtained are $\delta \sim (x_\infty - x)^{-\mu}$, where the exponent $\mu > 0$. It is impossible to continue this solution into the region $x > x_\infty$, so that the real flow must restructure itself with the formation of a local pressure peak on the convergence line. In this case, the parameter β_0 becomes negative with $\Delta^2 > 0$, as in the case $j = 1$ and $\beta_0 > 0$, and the corresponding behavior of the solution.

To evaluate the parameter β_0 we will apply the Newtonian formula (6.1.1) to slender blunt cones. Then, putting also $M_\infty \theta^2 \gg 1$ and $U \approx U_\infty$, from formulas 6.6.11 for β and 9.8.1 we derive the estimate $\beta_0 \sim \alpha/\theta_l M^2$, where $\theta_l = \theta + \alpha \cos \varphi$ and M is the local Mach number on the given isentropic streamsurface (in accordance with Sections 9.1 and 9.4, on the blunt cone surfaces M ranges from 2 to 4 increasing with the distance from the wall). Therefore, for $j = -1$ and $\beta_0 > 0$ the inequality $\Delta^2 > 0$ holds only at comparatively low angles of attack, $\alpha < (1/4)M^2\theta^2(\theta - \alpha)$.

We note one more important property of these flows. The quantities g_+ for $j = 1$ and g_- for $j = -1$ decrease with the parameter β_0 and, hence, with the entropy function s , since $\beta_0 \sim s^{1/\gamma}$. Since, in accordance with 9.8.3, the streamtubes get narrow on the windward side and, for small angles of attack, even on the leeward side, the limiting solution in the wall region possesses large gradients of not only the flow parameters in the meridional plane (as noted in Sections 9.4 and 9.5) but also the peripheral velocity w .

This problem is related with the flow past the edges of wings and controls embedded in the nonuniform shock layer on blunt bodies in a hypersonic stream (Figure 9.42). However, this pertains only to the flows with a finite nonvanishing velocity U and a bounded parameter g , where the isentropic surfaces that embrace the body surface and each other in the initial section, retain this mutual position further downstream, thus forming a thin vortex layer of infinite extent with a constant entropy on the body surface. On the divergence lines this situation occurs for any angles of attack $\alpha < \pi/2 - \theta$. A different case will be considered in the following.

We note that Equation 9.8.6 can be used for the effective checking of the accuracy of the numerical solutions for the flows with thin wall vortex layers, such that the numerical resolution of their structure is often troublesome.

9.9 Nonuniform Hypersonic Flow Past a Yawed Cylinder

Let a thin edge of a wing be exposed to an appreciably nonuniform flow with a possible considerable increase in the pressure resulting in the flow deceleration in the wall layer as shown in Figure 9.21 from Section 9.4. In this flow the assumption on the conservation of the order of the total velocity U along streamlines, which was adopted in Section 9.8, no longer holds.

We will consider the vortex layer of a gas in the divergence plane of a yawed cylinder of radius r_0 (Figure 9.42a) with the pressure increasing along the cylinder and attaining the stagnation value $p = p_m$ at certain points $x = x_m$ on the streamlines forming the layer. In the vicinities of these points we represent the pressure and velocity distributions (with the Bernoulli equation taken into account) in the form:

$$\begin{aligned} p_m - p &= \text{const}(x_m - x)^n \\ U &= [2(p_m - p)/\rho_m]^{1/2} = q(x_m - x)^{n/2}, \quad q = \text{const} > 0 \end{aligned} \quad (9.9.1)$$

Here, q is a coefficient, while the exponent $n = 1$ corresponds to the finite pressure gradient at the point x_m and $n = 2$ to the pressure peak. As shown previously, Equation 9.8.6 has no singularities on the flow divergence lines on the body, so that the function g is bounded there. In this case, at $n = 1$ expansion 9.9.1 for U cannot be continued into the region $x > x_m$, as in the similar two-dimensional problem of Section 2.11 (Figure 2.21d). The streamtube thickness also increases without bounds following the same $\delta_m \sim (x_m - x)^{-1/2}$ law, since in this case the integral in solution 9.8.3 converges at the point x_m . Strictly speaking, in this vicinity solution 9.8.3 itself is not valid, since we cannot let $dl = dx$ there; on the contrary, for this solution $dl/dx \rightarrow \infty$.

However, as distinct from the similar situation in the two-dimensional problem with inevitable flow separation and global restructuring of the flow pattern, which cannot be described within the framework of inviscid gas dynamics, in our case the enforced flow restructuring may remain within the framework of the inviscid flow model. In order to elucidate the possible flow pattern, we consider the shock-layer flow near the point x_0 of the pressure peak p_0 , that is the case $n = 2$ in formulas 9.9.1 for the streamlines with $p_m = p_0$. We will assume that at $x \leq x_0$ the stagnation pressures p_m on the streamlines increase normal to the shock layer. The flow pattern suggested is presented in Figure 9.43a. The streamlines with $p_m > p_0$ can be freely continued through the point x_m , thus forming the direct flow

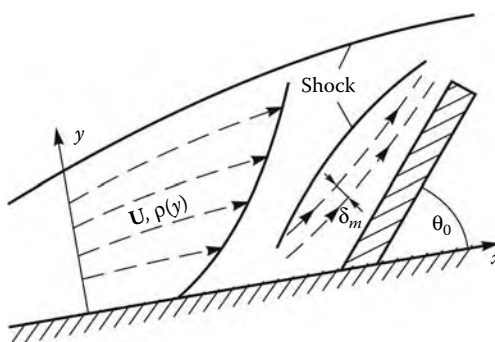
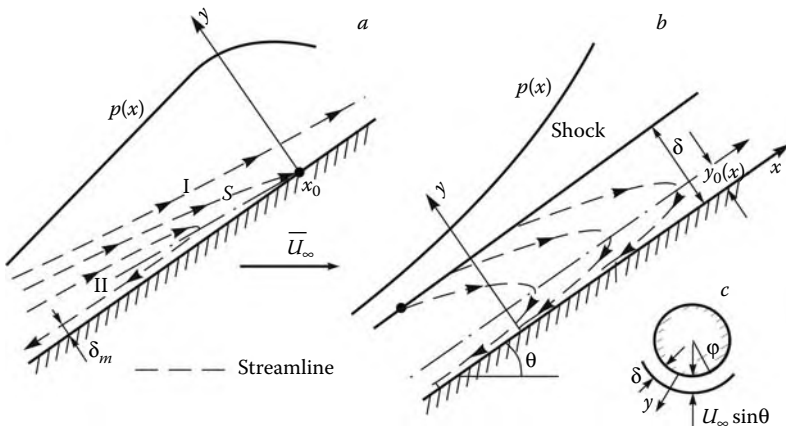


FIGURE 9.42
Flow in the shock layer near the wing edge.

**FIGURE 9.43**

Flow near the wing edge with the pressure increasing along the edge.

region I. At the same time, the streamlines with $p_m < p_0$ cannot overcome the barrier and are reversed, thus forming the return flow region II. The two flows are separated by the streamline S with the equation $y = y_s(x)$, passing through the stagnation point $x = x_0, y = 0$ on the body surface. Such a point may occur in the region of the intersection of the bow shock with the cylinder (the case shown in Figure 9.21) or if there exists a density maximum inside the shock layer (Figure 9.13b).

The problem of the flow near the point x_0 can be solved in the same fashion as in Section 2.11. Expanding the velocity field in this vicinity, by analogy with 2.11.1 and 2.11.5 and in view of 9.8.1

$$\begin{aligned} u &= ax' + 2\omega y, & x' &= x - x_0 \\ v &= -by, & w &= U_\infty g \varphi = cz \\ z &= r_0 \varphi, & a, b, c &= \text{const} > 0 \end{aligned} \quad (9.9.2)$$

from the continuity equation we obtain $b = a + c$ and the equation for a streamline in the plane of symmetry

$$\frac{dy}{dx} = \frac{v}{u} = -\frac{(a+c)y}{ax' + 2\omega y} \quad (9.9.3)$$

where ω is the vortex on the line S , positive by convention.

Equation 9.9.3 gives a family of streamlines of the type of "generalized" hyperbolas with a singular saddle-type point

$$(x' + \bar{k}y)^{a/(a+c)} = \text{const}, \quad \bar{k} = 2\omega/(2a + c) \quad (9.9.4)$$

In the plane $y = 0$ the streamlines form a node governed by the same equation (2.11.7). The separating singular streamline $y_s(x)$ (line S in Figure 9.43a) and the line $y = y_0(x)$ of zero longitudinal velocities $u = 0$ are as follows:

$$2\omega y_s = -(2a + c)x', \quad 2\omega y_0 = -ax' \quad (9.9.5)$$

The latter is independent of c and g . On this line the streamlines have a vertical tangent, a finite curvature K , a nonzero total velocity $U = |v|$, and the pressure $p < p_m$, while the longitudinal pressure gradient is balanced out by the centrifugal one $\rho v^2 K$.

In the vicinity of the line $y_0(x)$ solution 9.8.3 is not valid. However, this solution is applicable to the reversed streamlines in region II and gives an asymptotically decreasing mass flow rate $m \rightarrow 0$ as $x_0 - x \rightarrow \infty$. These streamlines do not leave anywhere the vicinity of the body surface.

In order to carry on an analysis of the behavior of the spreading coefficient g in the near-wall return flow, it is sufficient to change the direction of the x axis in Equation 9.8.6 and to put $u = -U$. Then the coordinate ζ remains positive and the previous analysis of the roots of this equation still holds.

To analyze the distinctive features of these flows, we will consider their limiting regime with a distant stagnation point $x_0 \rightarrow \infty$ that the entire flow region under consideration belongs to domain II, that is, the streamlines that have entered in this region the shock wave $y = \delta$ later reverse the direction, as shown in Figure 9.43b. This flow pattern can correspond to an unbounded nonuniform flow past an infinite (or limitingly slender) cylinder with the surface pressure monotonically increasing without bounds along the x axis. We will ascribe the flow nonuniformity only to an increase in the density ρ_∞ along the x axis and assume the stagnation enthalpy H to be constant, together with flow velocity and wash.

In this hypersonic shock layer on the cylinder the pressure p_δ and the density ρ_δ behind the cylinder-induced shock are proportional to the density ρ_∞ , while the function $s = p_\delta/\rho_\delta^\gamma \sim \rho_\infty^{1-\gamma}$ determining the entropy (here, the gas is perfect and γ is the adiabatic exponent) decreases monotonically along the x axis and, therefore, across the reversed streamlines as the body surface is approached.

Then in the direct flow from the shock to the $y_0(x)$ line the gas entropy s and enthalpy h increase, while the density ρ and the total velocity U decrease, whereas in the reverse flow from the $y_0(x)$ line to the wall $y = 0$ s and h decrease and ρ and U increase. As the section x_1 is displaced to the left, the velocity at the wall increases and the enthalpy and the density decrease due to the decrease in the pressure p_δ .

Naturally, this flow pattern is realized only in the case in which the streamtube expansion in the return flow due to the streamwise decrease in the pressure is offset by the gas flow in the azimuthal direction, which ensures the conservation of a relatively thin shock layer. Otherwise, global flow restructuring can occur.

10

Physicochemical Models of Relaxing Gases

10.1 Formulation of the Problem

So far, we have restricted ourselves to the study of the flows of *two-parameter*, or *simple* gases, whose state is completely determined by a pair of the *basic thermodynamic parameters*, say, the pressure p or the density ρ and any *energy-type* variable, such as the temperature T , the enthalpy h , the internal energy e , or the entropy s . Earlier (see Sections 1.1 to 1.4) we noted that only gases in *equilibrium state* or in *equilibrium process*, which is understood to be a *sequence of equilibrium states* superseding one another at an infinitely slow rate, could be assigned to the two-parameter gases (in what follows this fact will be rigorously proven). However, actual rates of these processes are always finite, so that in the general case the state of a gas is nonequilibrium and is determined by the set of *kinetic variables* λ_i as well. These can be the mass (or volume, etc.) concentrations of the species that form the gas mixture, or the degrees of excitation of their internal degrees of freedom, that is, the vibrational (for molecules) or electronic levels.

These parameters are determined by the differential equations of physicochemical kinetics governing the course of physical processes or chemical reactions and having the general form of Equation 1.2.8. The problem consists in the specification of their right-hand sides Λ_i . At equilibrium the parameters $\lambda_i = \lambda_{ie}(p, T)$ are single-valued functions of the pressure and the temperature, so that we deal again with a two-parameter gas (we refer the subscript e to the equilibrium state parameters). Naturally, this equilibrium solution must be a part of the totality of the relaxation equation solutions, that is, equilibrium gas dynamics outlined previously represents a particular case of the general nonequilibrium, or *relaxation*, gas dynamics.

The subject matter of nonequilibrium gas dynamics can be described under two headings (correspondingly, two chapters in this book). The first one contains the physicochemical model of the nonequilibrium mixture of *moderately dense* (in the sense of Sections 1.1 through 1.4) reacting or relaxing gases, that is, the description of their equations of state, the generating functions Λ_i , and so on, for given flow conditions. These questions are treated in this chapter. The model follows from theoretical and experimental studies within the framework of different divisions of physics and chemistry, such as quantum and statistical physics, kinetic theory of gases, theory of chemical reactions, and so on. For this reason, our presentation has only descriptive, or *phenomenological*, character, since we simply could not do otherwise within the scope of a book on gas dynamics.*

* The foundations and details of these theories can be found in Zeldovich and Raizer (1967), Clarke and MacChesney (1964), Hirschfelder, Curtiss, and Bird (1954), Gordiets, Osipov, and Shelepin (1980), Kuznetsov (1982), Chernyi and Losev (eds.) (1995), Maikapar (ed.) (1975), Bond, Watson, and Welch (1966), and others.

The second part of nonequilibrium gas dynamics is related with some specific effects of a gas dynamic nature caused by relaxation processes. They will be treated in the next chapter. In both chapters we will deal with inviscid flows only. Nonequilibrium dissipative effects will be considered in Chapter 13.

10.2 Basic Postulates of the Relaxing Medium Model

The aim of constructing a rational model of relaxing gases is the description of all the dependent thermodynamic variables and the right-hand sides Λ_i in the relaxation Equation 1.2.8 in the form of functions of, for example, the pressure p , the temperature T , and the kinetic variables λ_i

$$f = f(p, T, \lambda_i), \quad f = \rho, h, e, s, \Lambda_i \quad (10.2.1)$$

For the gases and conditions under consideration the possibility of this representation is based, as noted in Section 1.4, on the difference between the orders of the relaxation times for the molecular-kinetic and physicochemical equilibrium states that are different stages of the general nonequilibrium process. This postulate is at the basis of the entire gas flow model. The following reasoning provides support for this model. Only a few molecular collisions are needed to ensure the attainment of the *molecular-kinetic equilibrium* described by the Maxwellian distribution (Section 1.4); this makes it possible to introduce the notion of the isotropic temperature T of translational degrees of freedom and the static pressure p for the range of processes we are interested in, as noted in Section 1.1. This conclusion follows from kinetic theory of gases; however, on the level of estimates it can be deduced using simple reasoning within the framework of mechanics of *elastic hard body collisions*. Let two particles of masses m_1 and m_2 experience a straight-line collision at a relative velocity V_0 ; we will ascribe this velocity to the first particle. The result of this elastic collision is described by the momentum and energy conservation laws

$$m_1 V_0 = m_1 V_1 + m_2 V_2, \quad m_1 V_0^2 = m_1 V_1^2 + m_2 V_2^2 \quad (10.2.2)$$

This system has the well-known solution

$$\begin{aligned} V_1 &= \frac{\bar{m} - 1}{\bar{m} + 1} V_0, & V_2 &= \frac{2\bar{m}}{\bar{m} + 1} V_0, & \bar{m} &= \frac{m_1}{m_2} \\ \Delta E &= E_0 - E_1 = \frac{m_1}{2} (V_0^2 - V_1^2) = \frac{4\bar{m}}{(1 + \bar{m})^2} E_0 \end{aligned} \quad (10.2.3)$$

In gas mixtures, for example, in air, the masses of all the atoms and molecules are usually of the same order; therefore, for the present we will let $\bar{m} \sim 1$. Then the variations of the kinetic energy of the particles in the collision process are of the same order as the initial energy: $\Delta E \sim E_0$; thus, in the general case of arbitrary but elastic collisions it can be assumed that the energy of the particle m_1 moving at a velocity V_0 strongly different from velocities of other particles, for example, being nearly at rest, decreases in accordance with a power law and has the value $E_{n+1} = qE_n \sim q^{n+1}E_0$ ($q < 1$) after the $(n + 1)$ -th collision. Therefore, this particle loses its individuality after a few collisions, which is what we set out to prove.

Precisely this circumstance allows us to apply to these mixtures the *uniform energy distribution principle* of Sections 1.3 and 1.4 with the same translational temperature T for all the gas components and the energy $kT/2$ per each translational degree of freedom of any gas component. An exception of this rule can be provided only by the electronic gas for which $\bar{m} \ll 1$; it will be considered separately at the end of this section.

At the same time, hundreds and thousands of collisions are needed for the attainment of *physicochemical equilibrium* in a gas mixture, so that these processes occur as though on the background of molecular-kinetic equilibrium at the current values of the pressure and the temperature. We will explain this result using the following heuristic arguments. By way of illustration we will consider dissociation of some diatomic molecule AB with atoms A and B and excitation of some particles A , no matter whether atoms or molecules. In the symbolic form, these processes can be written as follows:



Here, A^* is the symbol of the excited particle and M is any third particle taking part in the energy and momentum exchange in the collisions. The first reaction applies also to ionization, if AB is considered to mean a neutral particle, A its positive ion AB^+ , and B an electron e^- . In these collisions the kinetic energy of particles is not conserved; with respect to this criterion they are referred to as *inelastic*, as distinct from the previously mentioned elastic collisions that result only in the redistribution of the translational energy of atoms and molecules. Usually, all these reactions proceed at a high absorption energy ε_D , which far exceeds the mean thermal energy of molecules $3kT/2$. Thus, the *characteristic temperatures* $\theta_D = \varepsilon_D/k$ of dissociation of oxygen (O_2), nitrogen (N_2), and nitric oxide (NO) molecules are equal to $59,000^\circ K$, $113,000^\circ K$, and $75,000^\circ K$, respectively, while ionization of these molecules and atoms takes place at temperatures $\theta_D \geq (10^5)^\circ K$ (the energy ε_D is also often measured in electronvolts, 1 eV corresponding to $\Delta\theta_D = 11,600^\circ K$).

However, the only result-producing collisions between the particles are those with the kinetic energy of the relative thermal motion $\varepsilon = mV^2/2 > \varepsilon_D$. Because of this, the relative number n_D/n of these particles, which decreases exponentially as θ_D/T increases (in accordance with the Maxwellian distribution 1.4.7), turns out to be fairly low on the conventional gas dynamic temperature range $T \leq 25,000^\circ K$. Actually, by no means each collision of particles is inelastic, even at high energies; this plays the crucial role in the decrease of the probability of a reaction between the particles in the collision.

Naturally, the decrease in the number of high-velocity molecules violates the Maxwellian distribution, which forms the basis of the molecular-kinetic equilibrium hypothesis, and can thus affect the rates of the physicochemical processes. However, in view of the postulate that the processes have different orders, this distribution is continuously restored.

In accordance with Section 1.4, the violation of the Maxwellian velocity distribution function does not prevent in itself to introduce the isotropic temperature and pressure if only the isotropic nature of the function is conserved.

This reasoning applies to forward reactions proceeding in accordance with the symbolism of formula 10.2.4, that is from left to right with energy absorption. On the contrary, in reverse reactions energy is released; here, of crucial importance is the part played by a third M particle, which must absorb this energy excess, provided the total momentum of the particles is conserved.

We will now dwell on the *internal degrees of freedom*. From quantum mechanics it is known that the energy (amplitude) of vibrations of, say, a diatomic molecule may take only discrete values, or it is distributed over its *quantum levels*. The excitation degree, or *population*, of a given k -th level is characterized by the portion of the corresponding particles. Within

certain limits, this portion may be arbitrary, so that each quantum level could in the general case be related with its own degree of freedom. We will call the totality of these levels of the same type a *group*, or *mode*, of the internal degrees of freedom. Thus, diatomic molecules of any species have a single vibrational mode, while polyatomic molecules have several such modes.

The orbits in which electrons rotate around atomic and molecular nuclei are also discrete, as are the corresponding energies that increase with the orbit size. Therefore, an individual degree of freedom can be ascribed to each orbit and a group of such orbits to each electron. The number of the quantum levels within each group can be fairly high (thus, oxygen and nitrogen molecules, as some others, have several tens of vibrational levels preceding molecular dissociation).

For a very simple case of diatomic molecule vibration, this situation is sketched in Figure 10.1 in the form of the potential Morse curve representing the dependence of the potential energy ε of the molecule on the interatomic distance, with the horizontal straight lines of the admissible quantum levels. This curve has the horizontal asymptote, $\varepsilon \rightarrow \varepsilon_D$, where ε_D is the dissociation energy or the mutual potential energy of free atoms.

Strictly speaking, the rotational energy of molecules is also distributed over quantum levels. However, for the gas dynamic problems of interest, the times of the attainment of equilibrium between the rotational degrees of freedom themselves and with the translational degrees of freedom are comparable with the times of the attainment of equilibrium between the translational degrees of freedom and, moreover, the rotation is excited in the *classical* fashion, in accordance with the uniform energy distribution principle (Sections 1.3 and 1.4), that is, with the energy $kT/2$ per each degree of freedom. For this reason, in gas dynamics of moderately dense gases the rotational and translational degrees of freedom are unified to a single group of the *external degrees of freedom* and characterized by the same translational temperature T .

At the same time, the model of the single translational temperature for all the components of a gas mixture can be inadequate for the electronic gas in the ionized gas mixture, or plasma. In fact, the molecular mass of electrons $\bar{M} \approx 1/2000$ is considerably smaller than those of atoms and molecules ($\bar{M} > 1$), which are in this sense *heavy* particles. In this case

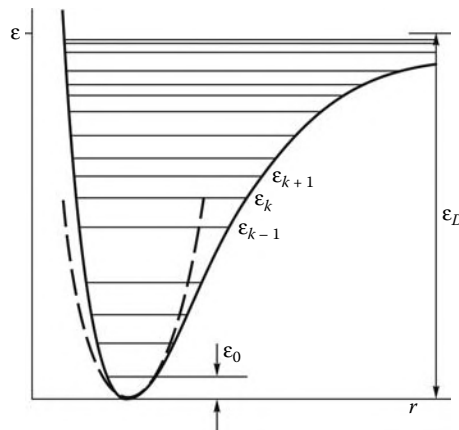


FIGURE 10.1

Curves of the potential energy of diatomic molecule vibration (solid and dashed curves are for the anharmonic Morse oscillator and the harmonic oscillator).

we have $\bar{m} \ll 1$ in relations 10.2.3; then relative losses of energy in collisions are very small, $\Delta E/E_0 \sim \bar{m}$, and the process of equalization of the kinetic energies of heavy particles and electrons can be prolonged. Nevertheless, all the electrons, being under approximately the same conditions, have usually the equilibrium Maxwellian velocity distributions, though with their own translational *electron temperature* T_{el} , which may not coincide with the temperature T of the heavy particles (to describe the situation there exists the term the *electron temperature discrepancy*). In this case, the quantity T_{el} is among the kinetic parameters λ_i . In view of its specific nature, this effect will be considered separately in Section 10.12; for now, we shall take $T_{el} = T$ without specifying this especially.

We note that the outlined model, based on different orders of the times of the attainment of the molecular-kinetic and physicochemical equilibrium, is in no way universal and is restricted to not very high gas temperatures, since at $\theta_D \approx T$ the rates of forward reactions can be comparable with the rate of the Maxwellian distribution recovery, while in the limit $T \gg \theta_D$ almost each collision leads to the molecule breakdown or its excitation immediately to one of the upper quantum levels.

We will now discuss one more aspect of the theory related with the possibility of applying the differential laws of equilibrium thermodynamics (in particular, its first and second laws) to nonequilibrium processes accompanying the change in the gas composition. Under the assumptions made previously, this possibility is supported by the following reasoning. For a gas mixture considered a thermodynamic system, the processes transforming one substance to another are equivalent to a decrease and increase in their quantities with simultaneous energy supply or absorption. This means that, as distinct from *closed thermodynamic systems* with a fixed, isolated mass of a matter, which are considered in equilibrium gas dynamics, the nonequilibrium systems considered here are modeled by *unclosed systems* being in the process of heat and mass exchange with the environment. Due to low rates of these processes, they can be considered as reversible, while each mixture component (the group of molecules of the same species) or even each internal degree of freedom can be regarded as a *local-equilibrium thermodynamic subsystem* with its own temperature, energy, entropy, and so on.

This situation is analogous to the example of a set of bodies with different temperatures in the process of slow mutual heat exchange considered in Section 1.5. In our case we agreed upon considering the temperature T to be the same for all heavy particles (the electronic temperature T_{el} was discussed previously). As for the internal degrees of freedom, in the general case the particles of the given species i of atoms or molecules with the same set of excited levels of arbitrary groups of degrees of freedom should be regarded as an individual component of the mixture. However, it can happen (e.g., in the case of vibrational degrees of freedom of molecules) that the distribution of such particles in quantum levels within a single, l -th, group turns out to be equilibrium (the sense of this situation will be explained in Section 10.7), but with its own temperature $T_l^{(v)}$ that is not necessarily equal to T . In the case of this internal equilibrium the group can be taken for a single degree of freedom and an individual locally equilibrium subsystem with the temperature $T_l^{(v)}$.

We will call such models of nonequilibrium gas mixtures *multi-temperature*, as distinct from *single-temperature* ones in which the previously mentioned temperatures coincide with the translational one.

The information presented previously represents only a set of postulates that form the basis of the model of the nonequilibrium gas mixture dynamics. Next we will fill this model by a concrete content and supply it with additional comments.

10.3 Equations of State for Gas Mixtures

The system of the equations of state for moderately dense gases contains, first, the generalized Clapeyron Equation 1.3.4

$$\begin{aligned} p &= \sum_i p_i = nkT = NRT = \rho RT/\bar{M} \\ n &= \sum_i n_i, \quad N = \sum_i N_i, \quad \bar{M}^{-1} = \sum_i c_i \bar{M}_i^{-1} \end{aligned} \quad (10.3.1)$$

Here, k is the Boltzmann constant, R is the gas constant, n_i and N_i are the numbers of the particles of species i and of their moles, n and N are the total numbers of the particles per unit volume of the mixture, and \bar{M}_i and \bar{M} are the molecular masses of species i and the mixture as a whole. Apart from the *mass* and *numerical* concentrations of the components c_i and n_i , the *molar concentrations* x_i and the *molar-mass concentrations* κ_i (the number of the moles of species i per unit mass of the mixture) are also often used

$$\begin{aligned} x_i &= \frac{n_i}{n} = \frac{N_i}{N} = \frac{p_i}{p} = \bar{M} \frac{c_i}{\bar{M}_i} = \bar{M} \kappa_i \\ \bar{M} &= \sum_i x_i \bar{M}_i, \quad \sum_i x_i = \bar{M} \sum_i \kappa_i = \sum_i c_i = 1 \end{aligned} \quad (10.3.2)$$

The quantity \bar{M} has all the properties characteristic of the molecular mass of a pure gas. In particular, \bar{M}/N_0 is the mean molecular mass of the mixture and $\rho = n\bar{M}/N_0$ is the mean density, while the number of the particles in a mass of the mixture equal to \bar{M} grams is equal to the *Avogadro number* $N_0 = 6.3 \cdot 10^{23}$. If $V_i = \bar{M}_i/\rho_i$ and V are the molar volumes of species i and the gas mixture, then $p_i V_i = pV = RT$.

In deriving the *calorimetric* equation of state we will take into account that the uniform energy distribution principle can be extended to rotational degrees of freedom as well (see Section 10.2). For each degree of freedom there is the same energy $RT/2$ per mole; for this reason, the translational and rotational degrees of freedom may be pooled to form a single group of the *external* degrees of freedom.

A diatomic molecule possesses two independent rotational degrees of freedom, or rotation axes, since the energy of rotation about the longitudinal axis passing through both atoms is negligibly small owing to the smallness of the corresponding moment of inertia. The atoms of the three-atom carbon dioxide (CO_2) molecule are arranged in line, so that the molecule also has two rotational degrees of freedom; however, the water (H_2O) molecules are arranged in a triangle and have three rotational degrees of freedom.

Along with the energy of the external degrees of freedom $E_i^{(0)}$, the total mole energy E_i and enthalpy H_i of species i include the energy $E_i^{(v)}$ of the internal degrees of freedom and the enthalpy of formation H_{0i}

$$\begin{aligned} E_i &= E_i^{(0)} + E_i^{(v)} + H_{0i}, \quad E_i^{(v)} = \sum_k E_{ik}^{(v)} \\ H_i &= E_i + p_i V_i = H_i^{(0)} + E_i^{(v)} + H_{0i} \\ E_i^{(0)} &= C_{vi}^{(0)} T, \quad H_i^{(0)} = C_{pi}^{(0)} T \\ C_{vi}^{(0)} &= \frac{1}{2} l_i R, \quad C_{pi}^{(0)} = \frac{1}{2} (l_i + 2) R \end{aligned} \quad (10.3.3)$$

Here, $C_{vi}^{(0)}$ and $C_{pi}^{(0)}$ are the molar specific heats of the external degrees of freedom, while l_i is their number. We have $l_i = 3$ for atoms, $l_i = 5$ for diatomic molecules and CO_2 molecules (cf. 1.3.7), and $l_i = 6$ for H_2O molecules. The terms $E_{ik}^{(v)}$ are the internal energies of a k -th degree of freedom of species i , which will be treated in Section 10.7.

In the general case the enthalpy of formation H_{0i} is a conditional quantity dependent on the origin from which the internal energy is measured, on the set of the physical processes under consideration, and, in general, on the mode of writing down the first law of thermodynamics. Thus, in the mutual transformation of the gaseous and condensed phases of a substance, we are free to ascribe the plus sign to the evaporation heat H_0 of the gaseous phase and the minus sign to that of the liquid (or solid) phase or, in general, as it is sometimes done in combustion problems, to eliminate this heat from the equations of state of both phases and introduce it into the energy equation for the phase transformation in the form of a heat source. With a corresponding caveat, this does not lead to any misunderstanding. In general, it is worthwhile to retain in H_0 only those terms that participate in energy exchange in the processes under consideration. Thus, in supersonic aerodynamic setups the expanding gas can cool down to the condensation temperature. However, since we do not touch on these questions, we will drop the corresponding evaporation heats from the expression for H_0 .

In gas dynamic problems of interest for us, due to a great number of the species and processes that should be allowed for, it is the practice to incorporate the energy of formation into the internal energy of the species. Moreover, we will let $H_{0i} = 0$ for the components that are present in the initial state of the mixture at standard temperature (e.g., for nitrogen, oxygen, and carbon dioxide molecules). Because of this, for atoms the quantity H_{0i} represents the energy of their formation at decomposition of the corresponding number of molecules, while for ions it is the ionization energy, and so on. For example, if ε_D is the dissociation energy of a diatomic molecule, then the molar energy of atom formation is equal to $H_{0a} = (1/2)N_0\varepsilon_D$.

The specific energy and enthalpy are derived from the molar ones 10.3.3 by dividing them by the molecular mass

$$\begin{aligned} e_i &= E_i \bar{M}_i^{-1} = e_i^{(0)} + e_i^{(v)} + h_{0i}, & e_i^{(v)} &= \sum_k e_{ik}^{(v)} \\ h_i &= e_i + \rho_i^{-1} p_i = H_i \bar{M}_i^{-1} \end{aligned} \quad (10.3.4)$$

The total specific molar quantities are determined as the sums

$$\begin{aligned} f &= \sum_i c_i f_i, & f_i &= h_i, e_i \\ F &= \sum_i x_i F_i, & f_i &= H_i, E_i \end{aligned} \quad (10.3.5)$$

We note that the specific quantities $h_i, e_i^{(v)}$, and so on, used here are referred to precisely the unit mass of species i , while $h, e^{(v)}$, and so on, to the unit mass of the gas mixture. The enthalpy formulas, 10.3.5, take the form:

$$\begin{aligned} h &= \sum_i c_i h_i = c_p^{(0)} T + e^{(v)} + h_0 \\ c_p^{(0)} &= \sum_i c_i c_{pi}^{(0)}, & e^{(v)} &= \sum_i c_i e_i^{(v)}, & h_0 &= \sum_i c_i h_{i0} \end{aligned} \quad (10.3.6)$$

$$\begin{aligned} H &= C_p^{(0)}T + E^{(v)} + H_0, & H_0 &= \bar{M}h_0 \\ C_p^{(0)} &= \sum_i x_i C_{pi}^{(0)} = \bar{M}c_p^{(0)}, & E^{(v)} &= \bar{M}e^{(v)} \end{aligned} \quad (10.3.7)$$

Here, $c_p^{(0)}$ and $C_p^{(0)}$ are the total specific and molar heats of the external degrees of freedom, $e^{(v)}$ and $E^{(v)}$ are the similar energies of the internal degrees of freedom, and h_0 and H_0 are the energies of formation of the gas mixture as a whole. To derive the expressions for the energies $e^{(0)}$ and $E^{(0)}$ it is sufficient to replace $c_{pi}^{(0)}$ by $c_{vi}^{(0)}$ in the previous formulas.

We note that as reactions proceed, the number of moles per a fixed mass of gas varies, so that a mole of the mixture has a variable mass.

In the previous formulas we did not separate out the electronic gas. In general it behaves as a monatomic gas with its own temperature T_{el} and the following partial pressure, enthalpy, and molar heats

$$\begin{aligned} p_{el} &= n_{el}kT_{el}, & E_{el} &= C_{v,el}T_{el} = \frac{3}{2}N_0kT \\ C_{v,el} &= \frac{3}{2}R, & C_{p,el} &= \frac{5}{2}R \end{aligned} \quad (10.3.8)$$

Since mass concentrations of electrons are infinitesimally small, while specific heats are very high, molar quantities are usually used to specify the electronic gas. At equilibrium ($T_{el} = T$) the electronic gas contribution to the pressure and molar enthalpy (energy) is taken into account by formulas 10.3.1 and 10.3.7. However, under conditions of the electron temperature discrepancy ($T_{el} \neq T$) this effect must be properly accounted for in sums 10.3.5.

We will represent the entropy of a nonequilibrium gas mixture by the formula

$$s = \sum_i c_i s_i, \quad s_i = s_i^{(0)} + s_i^{(v)}, \quad s_i^{(v)} = \sum_k s_{ik}^{(v)}, \quad S_i = \bar{M}_i s_i \quad (10.3.9)$$

Here, $s_i^{(0)}$ and $s_{ik}^{(v)}$ are the entropies of the external and internal degrees of freedom. For each individual component with its temperature T_i (e.g., translational or electronic) from 1.5.1 there follows the equality

$$T_i ds_i = dh_i - \frac{1}{\rho_i} dp_i = de_i + p_i d\rho_i^{-1} \quad (10.3.10)$$

Integrating this equation with allowance for 10.3.3 and 10.3.4, at $h_i = h_i^{(0)}$ we obtain the entropy of the external degrees of freedom, which is the same as 1.5.8 for a perfect gas

$$s_i^{(0)} = c_{pi}^{(0)} \ln T_i - \frac{R}{\bar{M}_i} \ln p_i + s'_{0i} \quad \ln p_i = \ln p + \ln x_i \quad (10.3.11)$$

Of interest in applications is usually only the difference of entropies in different states, so that the constant s_{0i} is unessential (cf. Equations 1.5.8 and 1.6.9). However, the quantity s_{0i} enters directly, for example, in the equilibrium conditions of Sections 10.6 to 10.8. This constant can be determined only within the framework of statistical physics.

To determine the entropies $s_{ik}^{(v)}$ of internal degrees of freedom, we should specify the notion of their temperatures $T_{ik}^{(v)}$ as individual locally equilibrium thermodynamic subsystems (Section 10.2) with given energies $e_{ik}^{(v)}$. Within the framework of such a model the

quantity $T_{ik}^{(v)}$ can naturally be determined as the temperature of an equilibrium medium in which all these energies are equal to the equilibrium energies $e_{ik}^{(v)} = e_{ike}^{(v)}(T_{ik}^{(v)})$ (the subscript e refers to the equilibrium parameters of the medium). The corresponding dependences $e_{ike}^{(v)}(T)$ are discussed in Section 10.7. Then the entropy $s_{ik}^{(v)}$ can be determined from the second Equation 10.3.10 with the term $p_i d\rho_i^{-1}$ dropped out, since it is already accounted for by 10.3.11. Thus, we have

$$T_{ik}^{(v)} ds_{ik}^{(v)} = de_{ik}^{(v)}, \quad s_{ik}^{(v)} = \int_0^{T_{ik}^{(v)}} \frac{de_{ik}^{(v)}}{T_{ik}^{(v)}}, \quad e_{ik}^{(v)} = e_{ike}^{(v)}(T_{ik}^{(v)}) \quad (10.3.12)$$

The convergence of this integral as $T \rightarrow 0$ will be proved in Section 10.7. At equilibrium between the internal and external degrees of freedom ($T_{il}^{(v)} = T$), the entropy of species i is determined from 10.3.10 as follows:

$$s_i = \bar{s}_i(T) - \frac{R}{M_i} \ln p_i + s_{0i}, \quad \bar{s}_i = \int_0^T \frac{dh_i}{T} \\ h_i = h_i^{(0)}(T) + e_i^{(v)}(T) \quad (10.3.13)$$

We will consider one more important property of the gas mixture entropy. Making the summation, for example, in formulas 10.3.13 we obtain

$$s = \sum_i c_i s_i = \bar{s}(T) - \frac{R}{\bar{M}} \ln p + s_0 + s_m \\ \bar{s} = \sum_i c_i \bar{s}_i, \quad s_0 = \sum_i c_i s_{0i} \\ s_m = -R \sum_i \frac{c_i}{\bar{M}_i} \ln x_i = -\frac{R}{\bar{M}} \sum_i \ln x_i \quad (10.3.14)$$

Clearly, the *entropy of mixing* s_m is always positive ($s_m > 0$), since $x_i < 1$; because of this, the gas mixture entropy is always greater than the sum of the entropies of the components, whose partial pressures are equal to the total pressure. This effect could easily be explained within the framework of the second law of thermodynamics. Let us imagine a vessel partitioned into separate sections in such a fashion that each section contains a single-component gas, while the temperature and the pressure are everywhere the same. Then, if the partitions are taken away, the gases mix with each other through diffusion without any changes in pressure and temperature; the irreversibility of this process results in an increase in the entropy.

Formula 10.3.14 leads to the *Gibbs paradox*, if separate portions of the single-component gas are regarded as different components. This is attributable to the fact that from the standpoint of the experiment with the vessel, the molecules initially in different sections, as though different from each other by this very fact, so that the process of their subsequent mixing is irreversible. Since taking this difference into account makes no sense, formula 10.3.14 is simply inapplicable in this case. This example demonstrates that the notion of entropy cannot be conclusively comprehended in the context of the classical thermodynamics and requires invoking the apparatus of statistical physics.

In conclusion, we will consider a very simple three-parameter gas model, the state of which is governed, apart from the main variables p and T , by the only parameter λ . Quite often this model is sufficient for establishing qualitative nonequilibrium effects in gas dynamics. Thus, it can be introduced in the case of solitary reactions of type 10.2.4, when other, neutral components are invariable.

A very simple example of the three-parameter mixture is the binary mixture of atoms and molecules of the same element (they will be denoted by the subscripts a and m) at equilibrium between the internal degrees of freedom, that is, for $e_i^{(v)} = e_{ie}^{(v)}(T)$. In this case we have

$$\bar{M}_a = \frac{1}{2}\bar{M}_m, \quad c_{pa}^{(0)} = 5\frac{R}{\bar{M}_m}, \quad c_{pm}^{(0)} = \frac{7}{2}\frac{R}{\bar{M}_m} \quad (10.3.15)$$

and Equations 10.3.1 and 10.3.6 take the form:

$$p = R\rho T(1 + c)/\bar{M}_m, \quad (c = c_a, \quad c_m = 1 - c) \quad (10.3.16)$$

$$\begin{aligned} h &= ch_a + (1 - c)h_m = c_p^{(0)}T + e^{(v)} + ch_0 \\ c_p^{(0)} &= cc_{pa}^{(0)} + (1 - c)c_{pm}^{(0)} = \frac{R}{2\bar{M}_m}(7 + 3c) \\ e^{(v)} &= ce_a^{(v)} + (1 - c)e_m^{(v)} \end{aligned} \quad (10.3.17)$$

Here, the energies of the internal degrees of freedom are not specified.

10.4 Relaxation Equations and Limiting Flow Regimes

In Section 1.2 the differential equations of relaxation for determining the kinetic variables λ_i (Equation 1.2.8) were derived from the conventional conservation laws. Here, we will determine the forms of the source functions Λ_i in these equations; this will be done only for a three-parameter mixture, which is nevertheless sufficient for understanding the principles of constructing these functions. The generalization to the case of a multicomponent gas will be given in Section 10.9.

It is obvious that any system in nonequilibrium must tend to an equilibrium state, as far as it is allowed by external conditions. Because of this, it should be suggested that, at fixed p and T , the quantity λ approaches its limiting value $\lambda_e(p, T)$, that is, λ_e is a root of the equation $\Lambda = 0$. Therefore, in the vicinity of the equilibrium state this function can be expanded in a series, with only one term retained in the expansion

$$\frac{d\lambda}{dt} = \Lambda = \frac{\lambda_e - \lambda}{\tau}, \quad \frac{1}{\tau} = \left. \frac{\partial \Lambda}{\partial \lambda} \right|_{\lambda=\lambda_e} > 0 \quad (10.4.1)$$

The fact that τ is positive follows from the physically obvious tendency to equilibrium of any thermodynamic system, which is possible only in the case in which $\Lambda > 0$ for $\lambda < \lambda_e$ and $\Lambda < 0$ for $\lambda > \lambda_e$, where $\lambda_e(p, T)$ is the *locally equilibrium value* of λ for local values of p and T .

However, this expression is applicable even when the value of the difference $\lambda - \lambda_e$ is not small, if the parameter τ is calculated at a certain midpoint λ' between λ and λ_e using the well-known mean value theorem. In this case the parameter $\tau = \tau(p, T, \lambda)$ is simply a more complicated function of the state.

This parameter has the meaning and name of the *relaxation time*.

In fact, let, for the sake of illustration, λ_e and τ be constant; then Equation 10.4.1 has the solution

$$\lambda_e - \lambda = (\lambda_e - \lambda_0)e^{-t/\tau}, \quad \lambda_0 = \lambda(0) \quad (10.4.2)$$

Clearly, $\lambda \rightarrow \lambda_e$, as $t/\tau \rightarrow \infty$, that is, the gas relaxes to a certain equilibrium state. Practically, any initial gas state is, as it were, "forgotten" already at $t/\tau \geq 2 - 3$, which justifies the term *relaxation time* in connection with the parameter τ . If the gas flows at a velocity U along the x axis, then the region $\delta_r \sim \tau U_\infty$ is the gas *relaxation zone*, in which the gas attains a near-equilibrium state $\lambda \approx \lambda_e$ for an arbitrary initial condition λ_0 .

The natural generalization to multicomponent mixtures leads to the equation

$$\frac{d\lambda_i}{dt} = \Lambda_i = \sum_j \frac{\lambda_{ej} - \lambda_j}{\tau_{ij}} \quad (10.4.3)$$

where the relaxation times τ_{ij} are the functions of all λ_j . However, as will be shown in what follows, actually the functions Λ_i have a more complicated nature and cannot always be reduced to such simple sums.

Most typical of the relaxation zones are those behind shock waves; a very simple model of such a zone suggests *frozen shock transition*, that is, the conservation of the kinetic parameters across the shock front, whose viscous thickness δ_v (Figure 10.2) determined by the solution of Section 3.2 is usually considerably smaller than the relaxation zone thickness δ_r for physical and chemical processes occurring behind the shock. In this case in solution 10.4.2 it should be let $\lambda_0 = \lambda_1$ and $\lambda_e = \lambda_{2e}$, where the subscripts 1 and 2 refer to the parameters ahead of and behind the shock. In this case the distinctive features of the relaxation zone depend on the relation between λ_1 and λ_{2e} , as shown in Figure 10.2. We will discuss these questions in more detail in Chapter 11.

We will now present another, *molecular-kinetic*, derivation of the formula for Λ_i , which helps to elucidate its structure for moderately dense gases. We will restrict ourselves to the case of certain particles A having only two states of an internal degree of freedom, namely,

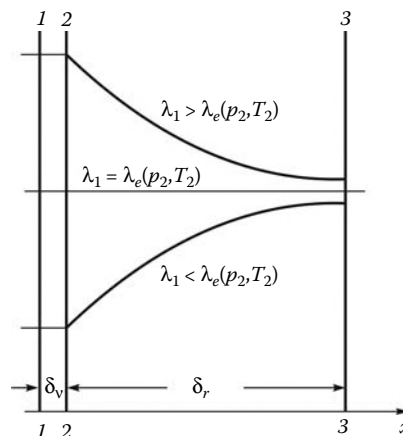


FIGURE 10.2
Shock wave and relaxation zone.

the excited A_2 and unexcited A_1 states, with *numerical concentrations* n_2 and n_1 , respectively. Symbolically, this process can be written in the form of Equation 10.2.4 as follows:



Here, M is any third component of the given gas mixture with concentration $n \geq n_A = n_1 + n_2$, which takes part in the collisional energy exchange. Strictly speaking, the result of the collision must depend on the kind of this component; however, so far we will neglect this circumstance.

Obviously, the *rate* r_f of the *forward reaction* (10.4.4) going to the right is proportional to the probability of the collision between the A_1 and M particles, that is, of their simultaneous appearance in the interaction volume element, whose dimensions for moderately dense gases are small as compared with the free mean path of the particles. The probability of these independent events is proportional to the product $n_1 \cdot n$; thus, $r_f = \bar{k}_f n_1 n$. As for the *reverse reaction rate*, it is $r_r = \bar{k}_r n_2 n$. The coefficients \bar{k}_f and \bar{k}_r are called the *forward and reverse reaction rate constants*, this name being purely historical, since the two quantities are, at least, functions of the temperature. The reaction rates are usually measured in (mole)/(volume)·(time).

The effective rate r of the formation of a *number of moles* of excited particles per unit volume is equal to

$$r = r_f - r_r = \bar{k}_f n(Kn_1 - n_2), \quad K = \bar{k}_f / \bar{k}_r \quad (10.4.5)$$

The function $K(T)$ is the *equilibrium constant* for this process, while the equilibrium concentrations $n_{1e}(T)$ and $n_{2e}(T)$ satisfy the *equilibrium condition*

$$\frac{n_{2e}}{n_{1e}} = \frac{p_{2e}}{p_{1e}} = \frac{x_{2e}}{x_{1e}} = K(T) \quad (10.4.6)$$

If locally equilibrium concentrations $n_{ie}(T)$ are ascribed to fixed parameters p and T , then the instantaneous values of the concentrations n_{1e} and n_{2e} must satisfy the conservation condition

$$n_1 + n_2 = n_{1e} + n_{2e} = n_A \quad (10.4.7)$$

Then rewriting formula 10.4.5 in terms of 10.3.1 and 10.3.2 yields

$$\begin{aligned} \frac{1}{\bar{k}_r} r &= \frac{n_A n}{n_{1e}} (n_{2e} - n_2) = \frac{n_A^2 n}{n_{1e}} (\bar{n}_{2e} - \bar{n}_2) = \\ &n^2 \frac{n_A}{n_{1e}} (x_{2e} - x_2) = n^2 \frac{n_A}{n_{1e}} \frac{\bar{M}}{\bar{M}_A} (c_{2e} - c_2) \\ &\frac{n_A}{n_{1e}} = 1 + K, \quad \bar{n}_i = n_i/n_A \\ &x_i = \frac{n_i}{n}, \quad c_i = \frac{\bar{M}_i}{\bar{M}} x_i \end{aligned} \quad (10.4.8)$$

Here, x_2 and c_2 are the molar and mass concentrations of the A_2 particles, while \bar{M}_A and \bar{M} are the molecular masses of the A particles and the mixture as a whole (see Section 1.3); the quantity n_i is called the *relative degree of the excitation* of the A particles or the *population of a level* of an internal degree of freedom (in our case this is level 2).

However, in order to pass from the function r to Λ in Equation 10.4.1, it should be borne in mind that the total derivative $d\lambda/dt$ is written for a fixed fluid particle, while the function r is written for a unit volume. Then we will take a fluid volume v with a fixed mass ρv .

The number of the A_2 particles in this volume is n_2v , while the rate of their formation is N_0vr , where N_0 is the Avogadro number. Then the relaxation equation ensuing from our reasoning takes the form:

$$\frac{dvn_2}{dt} = N_0vr \quad (10.4.9)$$

Clearly, the number n_2 varies not only via the rate r but also due to the variation of the volume v . Therefore, in order to derive an equation of type 10.4.1, we will pass from the number of moles of the A_2 particles in the volume v to their mass $mn_2v = \rho_2v = \rho vc_2$, where m is the mass of the A molecules. Then, in view of the fact that the mass ρv of a gas volume is constant along its trajectory, rewriting Equation 10.4.9 in terms of Equation 10.3.2 yields

$$\begin{aligned} \frac{dc_2}{dt} &= \Lambda = \frac{c_{2e} - c_2}{\tau}, \quad \Lambda = \frac{\bar{M}r}{\rho} \quad (\bar{M} = N_0m) \\ \frac{1}{\tau} &= \bar{k}_r n^2 \frac{m\bar{M}}{\rho\bar{M}} (K + 1) = \frac{(K + 1)p\bar{k}_r}{kT} \end{aligned} \quad (10.4.10)$$

Clearly, in this particular case $\tau \sim p^{-1}$, that is, τ is inversely proportional to the pressure, which is an important property of the relaxation time.

The parameter τ admits one more interpretation as the effective time interval between those particle collisions that are result-producing for the relaxation process. In this case $\tau = l_{\text{eff}}/V$, where V is the velocity of thermal motion, while l_{eff} is the corresponding effective free path of the particles. It is inversely proportional to their volume concentration n , so that setting $\sigma_{\text{eff}}l_{\text{eff}}n = 1$ we obtain

$$\tau = \frac{1}{nV\sigma_{\text{eff}}} \quad (10.4.11)$$

Here, σ_{eff} is the *effective cross-section* of the given reaction, usually very small; thus, for reactions and processes in air it varies on the range from 10^{-22} to 10^{-14} cm^2 .

We will now transform Equation 10.4.10 to the form that is more appropriate for the relaxation equation. To do this, we multiply it by the level excitation energy ε_2 of one particle and by the number N_0/\bar{M}_A of particles A per unit mass. Then we obtain the equation for the energy $c_A e^{(v)}$ of the excited particles per unit mass of the gas mixture (we recall that the energy $e_i^{(v)}$ introduced in Section 10.3 is related to the unit mass of component i)

$$\frac{dc_A e^{(v)}}{dt} = \frac{c_A (e_e^{(v)} - e^{(v)})}{\tau}, \quad e^{(v)} = \frac{c_2 \varepsilon_2 N_0}{c_A \bar{M}_A} \quad (10.4.12)$$

The equations thus obtained represent only particular and very simple versions of the relaxation equation. The more realistic equations for multilevel groups of the internal degrees of freedom or for chemical reactions have a considerably more complicated form and will be derived later, in Sections 10.9 to 10.11.

Given the relaxation Equation 10.4.1, we can present with reference to this simple example the more accurate definition of the limiting regimes of the equilibrium and frozen flows (see Section 1.1). The general case will be considered in Chapter 11. Let a gas flow at a velocity U in the domain Ω of size L ; then $t_0 = L/U$ is the residence of a particle in this domain, or the *gas dynamic time of the problem*. If this time is small compared to the relaxation time τ , then the variation $\Delta\lambda$ in the domain Ω is of the order

$$\Delta\lambda = \lambda - \lambda_0 \sim (\lambda_e - \lambda)t_0/\tau \ll \lambda_e - \lambda_0 \quad (t_0 \ll \tau) \quad (10.4.13)$$

In other words, the gas composition has no time to change till the gas particle leaves the domain Ω ; in this case the limiting solution, as $t_0/\tau \rightarrow 0$ is $\lambda = \lambda_0$. These *flows* and *processes* are called *frozen*.

Let, on the contrary, $t_0 \gg \tau$. Then the estimate $\Delta\lambda \sim t_0/\tau$ 10.4.13 is absurd and it is quite natural to assume the boundedness of the derivative $d\lambda/dt$. Then from 10.4.1 we derive another estimate

$$\begin{aligned}\lambda_e - \lambda &= \tau \frac{d\lambda}{dt} = \tau \frac{d\lambda_e}{dt} + \tau \frac{d(\lambda - \lambda_e)}{dt} \approx \tau \frac{d\lambda_e}{dt} \sim \Delta\lambda_e \frac{\tau}{t_0} \\ \frac{d\lambda_e}{dt} &= \frac{\partial\lambda_e}{\partial p} \frac{dp}{dt} + \frac{\partial\lambda_e}{\partial T} \frac{dT}{dt} \sim \frac{\Delta\lambda_e}{t_0}\end{aligned}\quad (10.4.14)$$

Here, $\Delta\lambda_e$ is the order of the variation of λ_e in a time t_0 in the flow domain under consideration. We will call the limiting solution $\lambda = \lambda_e(p, T)$, as $\tau/t_0 \rightarrow 0$, the *equilibrium approximation*, while the process (or flow) itself will be named the *equilibrium* or, to be more precise, *quasi-equilibrium* process. From the mathematical standpoint, this situation is the typical manifestation of the properties of equations with a small parameter at the higher derivative; being multiplied by τ , Equation 10.4.1 transforms to an equation of precisely this type.

An *equilibrium process* should be differentiated from an *equilibrium state*, since in the former the quantity $\lambda = \lambda_e(p, T)$ varies with p and T . In this case, *the rate of formation of the quantity λ is finite* and equal to the derivative $d\lambda_e/dt$ expressed in terms of the time derivatives of p and T , in accordance with Equation 10.4.14. At the same time, the gas composition and state in each gas particle can be as near to the equilibrium ones as is wished.

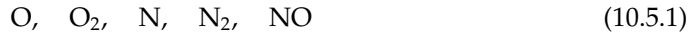
We emphasize an important property of the limiting flow regimes obtained: in both cases, $\lambda = \text{const}$ and $\lambda = \lambda_e(p, T)$, the differential relaxation equations can be replaced by finite relations or equations of state; thus, the gas is a two-parameter medium again (this will be discussed in more detail in Section 11.3).

In conclusion, we will make some remarks on the notion of locally equilibrium kinetic parameters $\lambda = \lambda_e$. In introducing these into Equation 10.4.1 it was assumed that the function $\Lambda = \Lambda(p, T, \lambda)$ is expressed in terms of the pressure and temperature, which resulted in the dependence of the form $\lambda_e = \lambda_e(p, T)$. However, formally some other pairs, such as (p, h) , (ρ, s) , and so on, could be chosen as the main thermodynamic variables. In this case, too, repeating the same reasoning as that used in deriving Equation 10.4.1, we would arrive at some locally equilibrium parameters $\lambda_e = \lambda_e(p, h)$, and so on, different, generally speaking, from $\lambda_e(p, T)$. These alternative locally equilibrium parameters are sometimes used in the general theory; however, as follows from Section 10.3, precisely p and T are the best-suited thermodynamic variables in the sense that the other thermodynamic parameters are expressed in terms of these most conveniently. Therefore, if otherwise not stated, in what follows the locally equilibrium parameters are considered to mean precisely the functions $\lambda_e(p, T)$.

10.5 Gas Composition and Basic Reactions

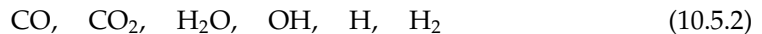
First of all, gas dynamics deals with our natural environment, that is, the air, which represents the mixture of oxygen (23% of mass) and nitrogen (76%) with inert argon, water vapors, carbon dioxide, and others present in minor amounts (about 1%). At high

temperatures, the air consists mainly of the following atoms and molecules



Moreover, the high-temperature air is a *plasma*, that is, it contains the positive ions of the previously listed components (NO^+ , etc.), free electrons, and, sometimes, negative ions (e.g., O_2^-).

The presence of carbon and hydrogen in the air atmosphere leads to the appearance of the following compounds



as well as various complex oxides of the type NO_n , hydrocarbons C_nH_m , cyanides CN , and so on. All these compounds are significant in ecological problems, which are beyond the scope of this book; however, gas dynamic models of high-temperature air medium do not take them into account because of their minute amounts. At the same time, all these compounds, especially 10.5.2, can play an important role in atmospheres of other planets promising for aeronautics (such as Mars, Venus, and Jupiter), as well as in the combustion products of thermal power plants and various thermal engines, including rocket ones. In gas dynamics we have to deal with even more complex mixtures formed due to evaporation of heat-insulating coatings containing sodium, fluorine, and other elements.

The general theory outlined in this chapter is concerned with all these gas mixtures. However, in what follows we will deal mainly with the air mixture, bearing in mind aerospace problems in the Earth's atmosphere.

The equilibrium air composition has been partially shown in Figure 1.4. We note that, in spite of the relative smallness of the nitrogen oxide (NO) concentration (not more than 10%) it plays an important part in chemical reaction kinetics and plasma generation. An even smaller fraction of ions and electrons plays the crucial role in radiophysics and in the kinetics of certain reactions.

The gas mixture composition varies depending on conditions (pressure, temperature); however, the *element composition conservation conditions* hold in each mixture. They are as follows:

$$\sum_i c_i d_{ij} = c_j^{(*)}, \quad \sum_j d_{ij} = 1, \quad \sum_j c_j^{(*)} = 1 \quad (10.5.3)$$

Here, $c_j^{(*)}$ is the mass fraction of element j of the mixture, while d_{ij} is its mass fraction in species i . For example, the oxygen atoms are contained in the O atoms, O_2 and NO molecules, and so on, as well as in their ions, which leads to the condition

$$c_{\text{O}} + c_{\text{O}}^+ + 2(c_{\text{O}2} + c_{\text{O}2}^+) + \frac{16}{30}(c_{\text{NO}} + c_{\text{NO}}^+) + \dots = c_{\text{O}}^{(*)} \quad (10.5.4)$$

where $c_{\text{O}}^{(+)}$, and so on, are the ion concentrations; the difference between the ion and neutral masses can be neglected. For the Earth atmosphere air we have $c_{\text{O}}^{(*)} = 0.23$ and $c_{\text{N}}^{(*)} = 0.76$; however, this relation can be different, for example, in the presence of diffusion, which leads sometimes to element separation in the flow region (see Chapter 13).

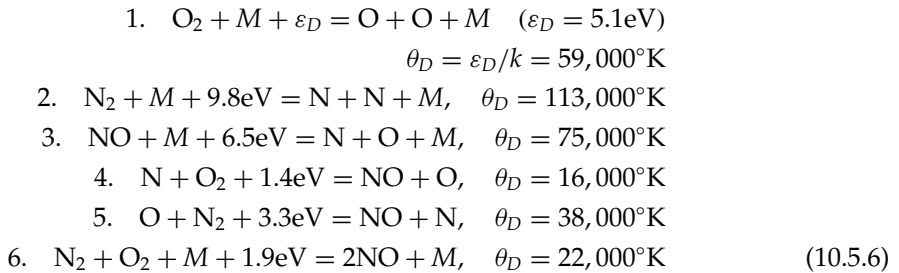
Similar additional conservation conditions exist for charged particles, namely, ions (both positive and negative) and electrons. In gas dynamic problems the gas is usually neutral, that is, there is no space charges in it if we deal with volume elements (in the gas dynamic sense, see Section 1.4) containing fairly large amount of particles, including charged ones. The point is that the Coulomb forces of the charged particle interaction are so large that,

in the absence of external electromagnetic forces, any considerable separation of charges is impossible. In other words, in gas dynamic problems the ionized gas may be treated (except in specifically stated situations) within the framework of the *quasineutral plasma* model. In such a plasma, all the processes obey the charge conservation law

$$n^+ - n^- - n_{\text{el}} = 0 \quad (10.5.5)$$

Here, n_{el} , n^+ , and n^- are the numerical concentrations of electrons and positive and negative ions of all the species.

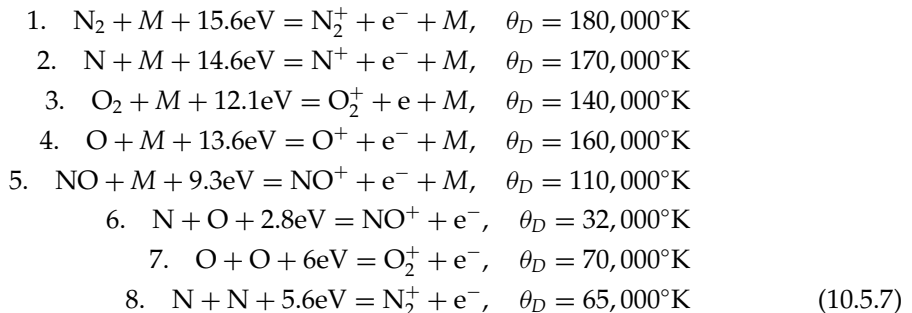
We are coming now to the description of some processes in the air mixture, as well as in some other gas mixtures. For the air mixture the following reactions are most important



Here, ε_D is the reaction energy absorbed (for $\varepsilon_D > 0$) or released ($\varepsilon_D < 0$) in each elemental act of the reactions proceeding to the right and θ_D is the *characteristic temperature* of the reactions. In all the previous reactions the energy is absorbed, that is, they are *endothermic*. On the contrary, in *exothermic* reactions ($\varepsilon_D < 0$) the energy is released (the sign of ε_D is, obviously, only conditional and depends on which reaction is taken as forward or reverse).

The first three reactions in the preceding list are those of molecule *dissociation* and atom *recombination* in which M is the third particle introduced in Equation 10.2.4, while the next two reactions are the *exchange reactions*. We note that the exchange reactions require appreciably smaller amounts of energy and, which is most important, do not require the presence of the third particle M ; this causes the important role played by these reactions in the air mixture kinetics, in spite of the fact that the concentration of NO molecules is usually small. Finally, the last reaction is formally equivalent to the dissociation reaction of two molecules, N_2 and O_2 , with the following formation of NO molecules. This reaction does not play any important role in the air mixture kinetics.

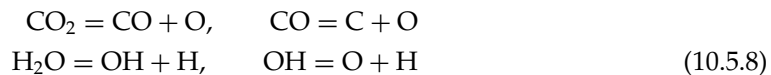
We write down now the basic ionization reactions in air



Here, reactions 1 to 5 are the direct ionization reactions, while the other reactions (6 to 8) relate to *associative ionization*; in view of the small amount of energy required, the sixth

reaction is the main supplier of electrons to the air plasma, at least, for atmospheric flight velocities, $U_\infty \leq 7$ km/s. In essence, this process is formally equivalent to the sequence of two processes: recombination of N and O atoms to an NO molecule (reaction 3 in list 10.5.6) and the direct ionization of this molecule (process 5 list 10.5.7).

The previously listed reactions are typical of diatomic molecules. For three-atom molecules the number of possible reactions increases; at least, instead of a single dissociation reaction two successive reactions can proceed. Thus, for example



Here, the particle M is omitted. The forward reactions relate to molecular dissociation, while the reverse ones relate to the ordinary processes of combustion and burnout of gaseous carbon and hydrogen and of their radicals CO and OH. Formally, these processes do not differ from the recombination process in list 10.5.6.

For the sake of convenience, we will introduce in conclusion a certain classification of the previously listed reactions. They can be divided into two groups with respect to their stoichiometric schemes. The first group of reactions, which will be referred to as *dissociative*, proceeds in accordance with the first scheme 10.2.4



and requires pair, or *binary*, particle collisions in order to be realized in the forward direction and triple collisions for reverse recombination and deionization processes. These are reactions 1 to 3 and 6 in 10.5.6, 1 to 5 in 10.5.7, and all reactions in 10.5.8. We will refer to reactions 4 and 5 in 10.5.6 and the associative ionization processes 5 to 8 in 10.5.7 as the second group of *exchange* reactions. They proceed in accordance with the scheme



and do not require the presence of the third particle M . Formally, the excitation processes 10.4.4 also correspond to this scheme when $B = D = M$, as well as the *electron exchange reaction* of the type



which is not mentioned in list 10.5.8. All these reactions proceed in both directions by the binary mechanism. However, for the sake of brevity, we will call *binary reactions* all the reactions of type 10.5.9 and 10.5.10, in which the direct reaction is binary.

10.6 Entropy and Equilibrium Conditions

In the aforesaid the equilibrium gas conditions, $\lambda_i = \lambda_i(p, T)$, and so on, were meant to be known; however, the approaches to determining them were not given. In what follows, we will show that the equilibrium conditions for thermodynamic systems are determined by the second law of thermodynamics and can be expressed in terms of the derivatives of the entropy s with respect to the kinetic variables λ_i .

The most general dependences of the form $s = s(p, h, \lambda_i)$ or $s = s(e, \rho, \lambda_i)$, equivalent to the original dependence $s = s(p, T, \lambda_i)$ (Section 10.3), will suffice in the first stage of our analysis. The differentials of these functions are as follows:

$$\begin{aligned} ds &= s_h^{(p,\lambda)} dh + s_p^{(h,\lambda)} dp + \sum_i s_{\lambda i}^{(p,h)} d\lambda_i = \\ &= s_e^{(\rho,\lambda)} de + s_\rho^{(e,\lambda)} d\rho + \sum_i s_{\lambda i}^{(\rho,e)} d\lambda_i \\ s_{\lambda i} &= \frac{\partial s}{\partial \lambda_i}, \quad f_\alpha^{(\beta,\gamma)} = \left(\frac{\partial f}{\partial \alpha} \right)_{\beta,\gamma} \end{aligned} \quad (10.6.1)$$

Here, the subscripts refer to the differentiation with respect to the corresponding parameters, while the superscripts relate to the parameters, that remain constant at the differentiation. At $\lambda_i = \text{const}$ the system is a two-parameter system, for which relations 1.5.1 of the second law of thermodynamics are valid. Therefore, we have

$$s_e^{(\rho,\lambda)} = s_h^{(p,\lambda)} = \frac{1}{T}, \quad s_p^{(h,\lambda)} = -\frac{1}{\rho T}, \quad s_\rho^{(e,\lambda)} = -\frac{p}{T\rho^2} \quad (10.6.2)$$

Obviously, for $\lambda_i = \text{const}$ by T is meant precisely the temperature of the external degrees of freedom.

In view of the first law of thermodynamics, whose form 1.2.7 is independent of the internal processes in the system, relation 10.6.1 can be reduced to the form:

$$ds = T^{-1} dQ + ds^{(q)}, \quad ds^{(q)} = \sum_i s_{\lambda i}^{(q)} d\lambda_i, \quad dQ = dh - \rho^{-1} dp \quad (10.6.3)$$

Here, dQ is the heat flux differential. The derivative $s_{\lambda i}^{(q)}$ will be called *adiabatic*, since it is taken not only for constant p and h or ρ and e but also along any adiabatic curves in the (p, h, λ) or (ρ, e, λ) variable spaces with the condition $dQ = 0$ imposed on these curves. Since relation 10.6.1 represents also the differentials of the functions $h = h(p, s, \lambda_i)$ or $e = e(\rho, s, \lambda_i)$, the following relationships are valid

$$s_{\lambda i}^{(q)} = s_{\lambda i}^{(p,h)} = s_{\lambda i}^{(\rho,e)} = -\frac{1}{T} h_{\lambda i}^{(p,s)} = -\frac{1}{T} e_{\lambda i}^{(\rho,s)} \quad (10.6.4)$$

From 10.6.3 it follows that *the entropy of a system can vary due to not only heat supply to the system (the term dQ) but also the change in the composition or the state of the system (the term $ds^{(q)}$)*. Then, invoking relaxation Equation 10.4.3 we obtain the *entropy production equation* for an arbitrary, nonequilibrium as a whole, process

$$\begin{aligned} \frac{ds}{dt} &= \frac{q}{T} + \frac{ds^{(q)}}{dt}, \quad q = \frac{dQ}{dt} \\ \frac{ds^{(q)}}{dt} &= \sum_i s_{\lambda i}^{(q)} \Lambda_i \end{aligned} \quad (10.6.5)$$

Although, in accordance with the model of Section 10.2, our gas mixture consists of locally equilibrium subsystems and is quasiclosed, it is actually nonequilibrium as a whole and, of course, closed; simply, the variations of the components in the mixture satisfy certain conditions that will be introduced later. However, in accordance with the second law of

thermodynamics, the total entropy of a closed, adiabatically insulated system may only increase, attaining a maximum at the equilibrium point. Hence, letting $dQ = 0$ in 10.6.3 and 10.6.5 we derive the conditions

$$ds^{(q)} = \sum_i s_{\lambda i}^{(q)} d\lambda_i \geq 0, \quad \frac{ds^{(q)}}{dt} = \sum_i s_{\lambda i}^{(q)} \Lambda_i \geq 0 \quad (10.6.6)$$

The first condition expresses the general tendency of the process development in an isolated system, while the second one is independent of the nature of the process, since $s_{\lambda i}^{(q)}$ and Λ_i are the *functions of the state* rather than of the process; thus, they are subject to certain constraints. Here, the equality sign relates to the state of equilibrium, in which the entropy attains a maximum; in the vicinity of this state the variations $d\lambda_i$ do not change the value of the entropy.

Thus, the *adiabatic* entropy variation with respect to kinetic variables, or λ variation, is zero in the vicinity of equilibrium state (at *equilibrium point*).

The logic pattern of the derivation of the equilibrium conditions of the type $f_i(\lambda_j) = 0$ from inequalities 10.6.6 is as follows. If parameters λ_i are independent, then, letting all the variations $d\lambda_{i \neq j}$, except a sole $d\lambda_j$, to be zero ($d\lambda_{i \neq j} = 0, d\lambda_j \neq 0$), we obtain the condition $s_{\lambda j}^{(q)} \geq 0$, which, when $d\lambda_j$ are of different signs, is possible only when $s_{\lambda j}^{(q)} = 0$ at the equilibrium point, this equality being the *equilibrium condition*.

However, in the general case the variations $d\lambda_i$ are not independent; they are related, first, by the condition representing the conservation of the element composition of the gas 10.5.3 and, second, by the conditions under which real processes proceed. These conditions dictate that in actually close systems disappearance of some components and appearance of others occurs in certain proportions determined by the structure of the reaction (e.g., decomposition of a single oxygen molecule generates two oxygen atoms). Because of this, we must eliminate these relationships and pass to a system of certain independent variables, adequate to our problem, in inequality 10.6.6.

In this connection, it is necessary to solve, first, two problems, namely, to express the derivatives $s_{\lambda i}^{(q)}$ in terms of the typical thermodynamic functions and variables and to specify the constraints imposed on the variations $d\lambda_i$. We will begin with the first question. The differential of the entropy of a gas mixture is as follows:

$$ds = d \sum_i s_i c_i = \sum_i s_i dc_i + \sum_i c_i ds_i, \quad ds_i = ds_i^{(0)} + \sum_k ds_{ik}^{(v)} \quad (10.6.7)$$

Here, c_i are the mass concentrations of the components entering the system, s_i are their specific entropies, and $s_i^{(0)}$ and $s_{ik}^{(v)}$ are the entropies of their external and k -th internal degrees of freedom as individual thermodynamic subsystems (see Sections 10.2 and 10.3).

We will invoke the first law of thermodynamics

$$\begin{aligned} dQ = dh - \frac{1}{\rho} dp &= d \sum_i h_i c_i - \sum_i \frac{c_i}{\rho_i} dp_i = \\ &\sum_i h_i dc_i + \sum_i c_i \left(dh_i - \frac{1}{\rho_i} dp_i \right) \end{aligned} \quad (10.6.8)$$

and, in view of Equations 10.3.4, 10.3.9, 10.3.10, and 10.3.12, represent the expression in parentheses in the form:

$$\begin{aligned} dh_i - \frac{1}{\rho_i} dp_i = dQ_i &= \sum_{k=0} dQ_{ik}, & dQ_{i0} = dh_i^{(0)} - \frac{1}{\rho_i} dp_i &= T_i ds_i^{(0)} \\ dQ_{ik} &= de_{ik}^{(v)} = T_{ik}^{(v)} ds_{ik}^{(v)}, & k &= 1, \dots \end{aligned} \quad (10.6.9)$$

For the sake of brevity, we will designate ds_i and $ds_{ik}^{(v)}$ by ds_n and the corresponding temperatures T_i and $T_{ik}^{(v)}$ by T_n with continuous numbering in n . Then for adiabatic processes ($dQ = 0$) relation 10.6.8 takes the form:

$$\sum_i h_i dc_i + \sum_n c_n T_n ds_n = 0 \quad (c_n = c_i \text{ for } n = i, ik) \quad (10.6.10)$$

Subtracting this equality from Equation 10.6.7 multiplied by T , that is, the temperature of external degrees of freedom of a conditionally basic component (i.e., heavy particles in the presence of, e.g., electronic gas with the temperature $T_{el} \neq T$) we obtain

$$T ds^{(q)} = - \sum_i [g_i - (T - T_i)s_i] dc_i + \sum_n (T - T_n)c_n ds_n \quad (10.6.11)$$

Here, g_i is the *specific thermodynamic potential* of the i -th component

$$g_i = h_i - T_i s_i \quad (10.6.12)$$

Thus, comparing Equation 10.6.11 with 10.6.3 we obtain

$$\begin{aligned} Ts_{\lambda i}^{(q)} &= -g_i + (T - T_i)s_i = -h_i + Ts_i, & d\lambda_i &= dc_i \\ Ts_{\lambda n}^{(q)} &= c_n(T/T_n - 1), & d\lambda_n &= T_n ds_n = dQ_n \end{aligned} \quad (10.6.13)$$

We call attention to the terms $T_n ds_n = dQ_n$ in formula 10.6.13, which are equal to the heat influx to individual species i or to their internal degrees of freedom due to energy transfer.

Thus, *the entropy in a nonequilibrium adiabatic process changes due to both mutual physicochemical transformations in the system and energy exchange between its separate subsystems*.

We are now coming to another problem, namely, that of the constraints imposed on the proceeding of reactions in gas mixtures. These constraints are called *stoichiometric relations* of reactions, or physicochemical processes in general; they are written in the form

$$\sum_i v'_i A_i \rightleftharpoons \sum_i v''_i A_i \quad (10.6.14)$$

Here, A_i are the symbols of the species (mixture components), which take part in each act of reaction by simultaneous collisions, while v'_i and v''_i are the *stoichiometric coefficients* of the reactions, which represent the number of particles A_i ensuring the proceeding of (conditionally) forward and reverse reactions. In each act of the forward process there appear $\Delta v_i = v''_i - v'_i$ particles of species i , while Δv_i particles disappear in the inverse process. We will call Δv_i the *stoichiometric difference* for a given reaction. Thus, for the dissociation-type reactions 10.5.9 we have

$$\begin{aligned} v'_{AB} &= v''_A = v''_B = 1, & v'_A &= v'_B = v''_{AB} = 0 \\ \Delta v_{AB} &= -1, & \Delta v_A &= \Delta v_B = 1 \\ v'_M &= v''_M = 1, & \Delta v'_M &= 0 \end{aligned} \quad (10.6.15)$$

For the exchange reactions 10.5.10, which do not include particle M , we have

$$\begin{aligned} v'_A = v'_B = v''_C = v''_D = 1, \quad v''_A = v''_B = v'_C = v'_D = 0 \\ \Delta v_A = \Delta v_B = -1, \quad \Delta v_C = \Delta v_D = 1 \end{aligned} \quad (10.6.16)$$

Hence it follows that the numbers of the particles that appear and disappear in each act of an s -th reaction must be in relation $\Delta n_{is} \sim \Delta v_{is}$, or for the mass concentrations

$$\Delta c_{is} = \bar{M}_i \Delta v_{is} \Delta R_s \quad (10.6.17)$$

Here, ΔR_s is a coefficient for the given reaction, proportional to the mass of the mixture reacted in the given process; we will call it the *displacement of this reaction* and relate it in what follows with the reaction rate. We note that thence and from the conservation condition for the mass and the element composition 10.5.3 the following conditions for each reaction are

$$\begin{aligned} \sum_i \Delta c_{is} = 0, \quad \sum_i \bar{M}_i \Delta v_{is} = 0 \\ \sum_i \Delta c_{is} d_{ij} = 0, \quad \sum_i \bar{M}_i d_{ij} \Delta v_{is} = 0 \end{aligned} \quad (10.6.18)$$

Substituting Equation 10.6.17 into 10.6.11 and summing over all species i we come to the following expression for the entropy differential in an adiabatic process

$$\begin{aligned} T ds^{(q)} = - \sum_s \chi_s dR_s + \sum_n c_n (T - T_n) ds_n \geq 0 \\ \chi_s = \sum_i G_i \Delta v_{is}, \quad G_i = \bar{M}_i g_i = H_i - TS_i \end{aligned} \quad (10.6.19)$$

Here, G_i is the *molar thermodynamic potential* at $T_i = T$.

This inequality forms the basis of the derivation of equilibrium conditions. We note, first, that an equilibrium system must be isothermal, with the obvious equality $T_n = T$ to be fulfilled; thus, the second term in 10.6.19 must be zero. The next step is related to the assumption of the possibility of an independent virtual (strictly theoretical) deviation of any s -th process from equilibrium, while all other processes remain at equilibrium. Then, letting any variation $dR_s \neq 0$, all other variations being zero, and taking into account that for any sign ahead of dR_s the condition $ds^{(q)} \geq 0$ holds when the system returns to equilibrium, we obtain the following equilibrium condition

$$\begin{aligned} ds^{(q)} = 0, \quad \chi_s = \sum_i G_i \Delta v_{is} = 0 \\ \Delta H_s = \sum_i H_i \Delta v_{is} = T \sum_i S_i \Delta v_{is} = T \Delta S_s \end{aligned} \quad (10.6.20)$$

Here, ΔH_s and ΔS_s are the total variations of the molar enthalpy and entropy of the gas mixture during the s -th reaction at the disappearance or appearance of Δv_{is} moles of the components taking part in the reaction. We emphasize that these quantities involve only the ultimate results of the reaction, namely, the differences Δv_{is} , rather than the parameters of auxiliary particles M , which enter in the reaction rates (cf. 10.2.4).

This condition must be obeyed by each process in the gas mixture, regardless of whether this process is isolated, that is, being the sole process in the system, or one of many processes, since the *system as a whole can be in equilibrium only if each process in the system is in internal equilibrium*.

This postulate, fundamental in thermodynamics, called the *detailed balancing principle*, is intuitively obvious; however, so far it has been rigorously proven by us only for the case in which the variations dR_s are actually independent; otherwise, it is only the sufficient criterion for the system equilibrium. In fact, if the gas composition, or the set of parameters λ_i , I in number, must satisfy J conservation conditions 10.5.3 or 10.5.5, then only $L = I - J$ parameters λ_i may be independent and determined by the equilibrium conditions $\chi_s = 0$ for $s \leq L$. Therefore, among these conditions and the parameters dR_s (the number of which can be fairly large, in accordance with the number of possible processes in the gas) only L ones may be independent in the meaning that their equilibrium involves equilibrium of other processes as well; other parameters χ_s and dR_s with the numbers $s > L$ are determined in the vicinity of the equilibrium state by linear equations of the type

$$dR_s = \sum_{l=1}^L \alpha_{sl} dR_l, \quad \chi_s = \sum_{k=1}^L \beta_{sk} \chi_k \\ s > L, \quad l, k = 1, \dots, L \quad (10.6.21)$$

where α_{sl} and β_{sl} are some coefficients or the functions of state.

In terms of these relations, conditions 10.10.19 yield

$$ds^{(q)} = \sum_{l=1}^L s_{Rl}^{(q)} dR_l \geq 0, \quad s_{Rl}^{(q)} = \chi_l + \sum_{k=1}^L \gamma_{lk} \chi_k \\ \gamma_{lk} = \sum_{s>L} \alpha_{sl} \beta_{sk}, \quad l, k = 1, \dots, L \quad (10.6.22)$$

In this inequality, the variations dR_l can be specified independent of each other; this leads to the required equilibrium conditions $s_{Rl}^{(q)} = 0$ or to a system of L linear homogeneous equations with respect to the variables χ_l . At a nonzero determinant, $\Delta \neq 0$, this system has only trivial solution $\chi_l = 0$, which proves the detailed balancing principle (the case $\Delta = 0$ is simply improbable in the space of, say, variables p and T on which the coefficients α_{sl} and β_{lk} depend).

We will now touch on the formulation of the equilibrium conditions in terms of the thermodynamic potential $g = h - Ts$, which is often used for this purpose in thermodynamics. In view of 10.6.3, the expression for the differential dg can be written in the form:

$$dg = dh - Tds - sdT = \frac{1}{\rho} dp - sdT - T \sum_i s_{\lambda i}^{(q)} d\lambda_i \quad (10.6.23)$$

Obviously, the derivative $g_{\lambda i}^{(p,T)} = -Ts_{\lambda i}^{(q)}$. Thence, comparing for $T_n = T$ (10.6.23, 10.6.13, and 10.6.6) we obtain a condition, valid for constant p and T

$$dg^{(p,T)} = \sum_i g_{\lambda i}^{(p,T)} d\lambda_i = -T \sum_i s_{\lambda i}^{(q)} d\lambda_i = \sum_i g_i dc_i \leq 0 \quad (10.6.24)$$

As before, the equality sign relates to the equilibrium state. Thus, the thermodynamic potential in an *isothermobaric* system ($p = \text{const}$ and $T = \text{const}$) can only decrease and attain

a minimum at the equilibrium state. The further specification of the equilibrium conditions does not differ from that outlined previously.

The results obtained make it possible to derive an entropy distribution in kinetic variables in the vicinity of the equilibrium state, which is important for further applications. For this purpose, we chose a system of *generalized independent kinetic variables* ξ_i , L in number; though, generally speaking, arbitrary, it possesses the property of completeness in the sense that each variable λ_i of the original system must be determined in terms of, at least, one variable ξ_l . By analogy with 10.6.3, we write the adiabatic entropy differential in these generalized variables as follows:

$$ds^{(q)} = \sum_{l=1}^L D_l d\xi_l, \quad D_l = s_{\xi_l}^{(q)} = s_{\xi_l}^{(p,h)} = s_{\xi_l}^{(\rho,e)} \quad (10.6.25)$$

Since the entropy has a maximum at the equilibrium point $\xi_l = \xi_{le}$, while all the variations $d\xi_l$ are independent, all the derivatives D_l are zero at this point. Hence, in the vicinity of this point and for fixed p and h the following expansions are valid

$$\begin{aligned} D_l &= \sum_{l=1}^L D_{lk} \Delta \xi_k, \quad \Delta \xi_k = \xi_k - \xi_{ke} \\ D_{lk} &= \left(\frac{\partial D_l}{\partial \xi_k} \right)_{p,h} = \left(\frac{\partial^2 s}{\partial \xi_k \partial \xi_l} \right)_{p,h} \end{aligned} \quad (10.6.26)$$

Then the adiabatic deviation of the entropy from the equilibrium value is as follows

$$s - s_e = \frac{1}{2} \sum_l \sum_k^L D_{lk} \Delta \xi_k \Delta \xi_l \leq 0 \quad (10.6.27)$$

Thus, in the vicinity of the state of equilibrium, in the space of kinetic variables an adiabatic deviation of the entropy from its equilibrium value is of second order. For the three-parameter system having a single kinetic variable λ , as introduced at the end of Section 10.3, of the expansion 10.6.27 takes the form:

$$\begin{aligned} s - s_e &= \frac{1}{2} s_{\lambda\lambda}^{(q)} (\lambda - \lambda_e)^2, \quad s_{\lambda\lambda}^{(q)} \leq 0 \\ s_{\lambda}^{(q)} &= s_{\lambda\lambda}^{(q)} (\lambda - \lambda_e) \end{aligned} \quad (10.6.28)$$

The quadratic form 10.6.27 is called *negatively defined*; it is of constant sign at any linear transformation of independent variables. Hence follows, in particular, the condition $D_{ll} \leq 0$ for all $l = k$.

According to quadratic form theory, there exists such a linear transformation of the system of variables

$$\Delta \xi_l = \sum_{k=1}^L \bar{c}_{lk} \Delta \tilde{\xi}_k, \quad \Delta \tilde{\xi}_l = \sum_{k=1}^L c_{lk} \Delta \xi_k \quad (10.6.29)$$

where \bar{c}_{lk} and c_{lk} are the elements of the direct and inverse matrices of the transformation, that reduces a quadratic form to its canonical form containing only the sum of squares

$$\begin{aligned} s - s_e &= \frac{1}{2} \sum_{l=1}^L \tilde{D}_{ll} (\Delta \tilde{\xi}_l)^2 \\ \tilde{D}_l &= \left(\frac{\partial s}{\partial \tilde{\xi}_l} \right)_{p,h} = \tilde{D}_{ll} \Delta \tilde{\xi}_l, \quad \tilde{D}_{ll} = \frac{\partial^2 s}{\partial \tilde{\xi}_l^2} \leq 0 \end{aligned} \quad (10.6.30)$$

These variables are called *canonical*.

10.7 Equilibrium of the Internal Degrees of Freedom: Boltzmann Distribution

This problem breaks up into two ones: that of the *partial* equilibrium between two arbitrary quantum levels inside one group, or mode, of the internal degrees of freedom (this notion was introduced in Section 10.2) and that of the *local*, or *internal*, equilibrium of this mode as a whole.

We begin with the equilibrium of two quantum levels of the particles of species A in a reaction of type 10.4.4, assigning the symbols A_1 and A_2 to the particles that are on these excitation levels. The stoichiometric differences of this reaction are $\Delta v_1 = -1$ and $\Delta v_2 = 1$. In this case $\Delta v_M = 0$ and condition 10.6.20 take the form:

$$\Delta H = H_2 - H_1 = T(S_2 - S_1) = T\Delta S \quad (10.7.1)$$

The meaning of this relation is obvious: in accordance with Equation 1.5.1, it gives the entropy increment ΔS in a reversible isothermal and isobaric process, which transforms a mole of the A_1 particles to a mole of the A_2 particles due to the heat flux ΔH .

The difference of the molar enthalpies of these levels is as follows

$$H_2 - H_1 = N_0(\varepsilon_2 - \varepsilon_1) = (R/k)(\varepsilon_2 - \varepsilon_1) \quad (10.7.2)$$

where N_0 is the Avogadro number, R is the gas constant, k is the Boltzmann constant (here and in the products kT or $k\theta$ in the following), and ε_2 and ε_1 are the level energies ($\varepsilon_2 > \varepsilon_1$), which in this case have the meaning of the formation enthalpies h_{0i} in Equation 10.3.4. The particles A_1 and A_2 can be considered individual species with their own pressures p_1 and p_2 and entropies S_{01} and S_{02} but with equal other thermodynamic parameters $h_i^{(0)}$ and energies $e_i^{(v)}$ which are not considered here. Then, in accordance with Equations 10.3.9 to 10.3.13, the difference between the molar entropies of these particles is as follows:

$$\Delta S = S_2 - S_1 = R(\ln p_1 - \ln p_2) + S_{02} - S_{01} \quad (10.7.3)$$

Therefore, the required equilibrium condition of Equation 10.7.1 takes the form:

$$\frac{p_2}{p_1} = \frac{n_2}{n_1} = K(T) = \frac{I_2}{I_1} e^{-(\varepsilon_2 - \varepsilon_1)/kT}, \quad \ln I_k = S_{0k}/R \quad (10.7.4)$$

Here the subscript e is omitted; n_2 and n_1 are the numerical concentrations of the A_2 and A_1 particles or the level *populations* of the A particles. This formula determines the power-law temperature dependence of the equilibrium constant $K(T)$, typical of all similar equilibrium conditions. As for the coefficients I_1 and I_2 , they are determined, as noted previously, only within the framework of statistical physics, where they are called the *degeneracy factors* of the *levels* with equal energies (e.g., the totality of the electron orbits, both circular and elliptic, in the *Sommerfeld atom model*).

We will now consider the set of particles of the same species possessing a system of quantum levels of the given group of the degrees of freedom. Obviously, the necessary conditions of the total equilibrium of this group require pairwise equilibrium of two of these levels satisfying condition 10.7.4. Let n_0 be the population of the zeroth, or basic, level of the same A particles. Then substituting the subscripts 0 and k for 1 and 2 in Equation 10.7.4 we obtain the *Boltzmann distribution* or the *detailed balancing principle* for the populations of levels k with the energies ε_k

$$\frac{p_k}{p_0} = \frac{n_k}{n_0} = \bar{I}_k e^{-(\varepsilon_k - \varepsilon_0)/kT}, \quad \bar{I}_k = \frac{I_k}{I_0} \quad (10.7.5)$$

This distribution is a particular case of the more general *Gibbs distribution* derived in statistical physics. For the sake of convenience, in what follows we will assume $\varepsilon_0 = 0$, thus taking the basic level energy as the reference point. The total number of all the particles of species A per unit volume is as follows

$$n_A = \sum_{k=0}^m n_k = n_0 Z, \quad Z = \sum_{k=0}^m \bar{I}_k e^{-\varepsilon_k/kT} \quad (10.7.6)$$

Here, $m = k_{\max}$ is the number of the upper level preceding particle dissociation or ionization. The function Z is the *statistical sum* of a given group of the degrees of freedom, in our case dependent on the temperature and subject to the condition that $Z \rightarrow 1$ as $T \rightarrow 0$. Eliminating n_0 from 10.7.5 we obtain

$$\bar{n}_k = \frac{n_k}{n_A} = \frac{\bar{I}_k}{Z} e^{-\varepsilon_k/kT} = K_{kA} \quad (10.7.7)$$

The total molar energy of all the levels of these particles can be obtained by letting $n_A = N_0$

$$E^{(v)} = \sum_{k=0}^m \varepsilon_k n_k = \frac{N_0}{Z} \sum_{k=0}^m \bar{I}_k \varepsilon_k e^{-\varepsilon_k/kT} = RT^2 \frac{\partial \ln Z}{\partial T} \quad (10.7.8)$$

As $T \rightarrow 0$, we obtain the asymptotics

$$E^{(v)} \approx N_0 \bar{I}_1 \varepsilon_1 e^{-\varepsilon_1/kT}, \quad Z - 1 \approx \bar{I}_1 e^{-\varepsilon_1/kT} \quad (10.7.9)$$

ensuring the convergence of the integral $s^{(v)}$ in 10.3.12.

The total energy $E_{\Sigma}^{(v)}$ of several groups l of the internal degrees of freedom can be associated with the general function Z_{Σ}

$$Z_{\Sigma} = \prod_l Z_l, \quad E_{\Sigma}^{(v)} = \sum_l E_l^{(v)} \quad (10.7.10)$$

Let us apply these results to diatomic molecule vibration. In this case, the level energies obey—to a certain approximation—the $\varepsilon_k = k\varepsilon_v$ law, where ε_v is the first level energy (for the zeroth, or basic, level it was assumed that $k = 0$ and $\varepsilon_v = 0$), and, moreover, all $I_k = 1$. This is the *harmonic oscillator* model that corresponds to the assumption of the linear dependence of the attraction forces between the atoms in a molecule on the distance (as in the case of loads on inelastic spring). In this case, sums 10.7.6 and 10.7.8 can be cast to the form:

$$\begin{aligned} Z = Z_m &= \sum_{k=0}^m q^k = \frac{1 - q^{m+1}}{1 - q} \\ q &= e^{-\theta_v/T}, \quad k\theta_v = \varepsilon_v \\ E_v^{(v)} = E_{vm} &= \frac{R\theta_v q}{1 - q} (1 - \beta_m), \quad \beta_m = \frac{(m+1)q^m}{Z_m} \end{aligned} \quad (10.7.11)$$

Here, E_v is the vibrational energy and θ_v is the *characteristic vibrational temperature*. For oxygen and nitrogen molecules we have $\theta_v = 2230^\circ\text{K}$ and 3340°K , which is considerably lower than the typical dissociation and ionization temperatures for the same molecules given in Section 10.2 ($\theta_D \geq 60,000^\circ\text{K}$). Since the upper vibrational level energy is $\varepsilon_m = m\varepsilon_v \approx \varepsilon_D$, that is, equal to the dissociation energy, it would seem that $m \approx \theta_d/\theta_v$. For nitrogen and oxygen this would result in the values $m \approx 26$ and $m \approx 34$. However, the harmonic oscillator model is incorrect for upper vibrational levels of molecules, their distribution being actually more frequent (see Figure 10.1 of Section 10.2). This *anharmonic* effect results, in particular, in a number of vibrations twice as large as that noted previously, $m \approx 2\theta_D/\theta_v$.

However, it is known that molecular dissociation, at least, equilibrium one, occurs on the temperature range $\theta_v \leq T \leq 3\theta_v$, that is, for $q = e^{-\theta_v/T} \leq e^{-1/3}$. Under these conditions, on upper levels the molecular concentrations are fairly small and do not contribute considerably to the total vibrational energy, which makes it possible to apply the harmonic oscillator model. Since any of the previous estimates give fairly large limiting values of m , the coefficient β_m and, the more so, the quantity q^m turn out to be negligible with the result that formulas 10.7.11 take the form corresponding to an infinite number of the levels ($m \rightarrow \infty$)

$$E_v^{(\infty)} = \frac{R\theta_v}{e^{\theta_v/T} - 1}, \quad Z = \frac{1}{1 - e^{-\theta_v/T}} \quad (10.7.12)$$

The functions $E_v^{(\infty)}$ and β_m are presented in Figure 10.3. Precisely these formulas correspond to the most widespread *classical harmonic oscillator model*, while formulas 10.7.11 can be assigned to the *truncated harmonic oscillator model*. For high values of T/θ_v functions 10.7.12 have the following asymptotics

$$E_v^{(\infty)} = RT \left(1 - \frac{\theta_v}{2T}\right), \quad Z = \frac{T}{\theta_v} \left(1 - \frac{\theta_v}{2T}\right) \quad (10.7.13)$$

As follows from Figure 10.3, these asymptotics are attained already at $T/\theta_v > 1$, while for $T/\theta_v \gg 1$ the energy $E_v^{(\infty)} \rightarrow RT$, which corresponds to the classical principle of the uniform energy distribution, if two degrees of freedom, kinetic and potential, are related

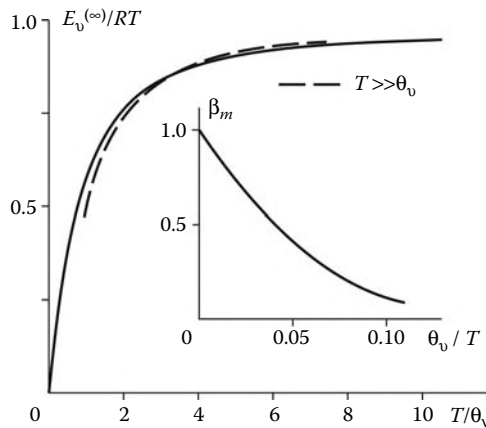


FIGURE 10.3
Vibrational energy of a harmonic oscillator.

with vibrations. In this case it should be set $l_i = 7$ in formulas 10.3.3, this giving the value of the adiabatic exponent $\gamma = 9/7$.

We note also that, with respect to the general formula 10.7.11 for the truncated oscillator, the limiting formula $E_v = RT$ represents only intermediate asymptotics, provided that the following inequalities

$$\theta_v/T \ll 1, \quad q^m = e^{-m\theta_v/T} \ll 1 \quad (10.7.14)$$

are simultaneously fulfilled. In fact, as $q \rightarrow 1$, expressions 10.7.11 for Z_m and E_{vm} have a removable singularity, which can be eliminated, for example, by expanding them in $\Delta = 1 - q \ll 1$. This leads to the following asymptotics

$$\begin{aligned} Z_m &= (m+1) \left(1 - \frac{1}{2} m \Delta \right) \\ E_{vm} &= -R\theta_v \frac{q}{Z_m} \frac{\partial Z_m}{\partial \Delta} = \frac{1}{2} m R \theta_v = \frac{1}{2} R \theta_D \\ \Delta &= 1 - q \approx \theta_v/T \ll 1 \end{aligned} \quad (10.7.15)$$

For $\Delta = 0$ these formulas give constant, temperature-independent, limiting values. In this limit, the level population distributions 10.7.7 turn out to be uniform, $n_k = n_A/m$. However, their energies, equal to $k\varepsilon_v n_A/m$, increase with k and, since within the framework of this model the molecular dissociation energy is $\varepsilon_D = m\varepsilon_v$, the limitingly attainable (as $T \rightarrow \infty$) energy of the equilibrium vibration of a mole is $E_{vm} = \frac{1}{2} N_0 \varepsilon_D$.

However, these limiting equilibrium states 10.7.13 and 10.7.15 of oxygen and nitrogen molecules are not actually realized, since on their applicability range there are scarcely any molecules in the equilibrium air mixture. At the same time, in Section 10.11 we shall use formulas 10.7.15, though in a somewhat different interpretation.

We will now touch on triatomic molecules with reference to the example of carbon dioxide, CO_2 . The atoms within this molecule are arranged in line and possess four vibration modes, two longitudinal (symmetric and antisymmetric) with $\theta_{v1} = 3380^\circ\text{K}$ and $\theta_{v2} = 1920^\circ\text{K}$, respectively, and two transverse in mutually perpendicular directions with $\theta_{v3,4} = 960^\circ\text{K}$. The latter modes are referred to as *multiple* or *degenerate*.

In view of the relative smallness of the quantities $\theta_{v3,4}$, with an increase in the temperature carbon dioxide starts to differ from a perfect gas considerably earlier than, say, oxygen and nitrogen (already for $T > 300^\circ\text{K}$; cf. Figure 1.3, Section 1.1).

For large T/θ_v the total molecular vibration energy for carbon dioxide $E_v = 4RT$ is fairly large. The total number of molecular degrees of freedom is, in accordance with 10.3.3, $l_i = 13$, so that the adiabatic exponent is $\gamma = 15/13$, this value being very close to unity even without taking dissociation effects into account. However, this limiting solution is not attained at the dissociation onset. This property is common for other degrees of freedom, for example, for electronic states of atoms and molecules.

However, there is an important exception to this rule. We mean rotational degrees of freedom, which, in accordance with quantum theory, also consist of discrete levels. The point is that the energies of these levels are comparatively small, so that on the range of moderate gas densities they are equilibrium-excited with the rotational temperature T_r . Moreover, for air molecules, as for many other molecules (with the exception, maybe, of hydrogen) the characteristic rotational temperatures θ_r are so small that even at the standard temperature the rotational degrees of freedom are excited in the classical fashion, with the molar energy $RT/2$ per each rotational mode. This made it possible to introduce the single group of the external degrees of freedom in Section 10.2.

We will now consider in more detail the problem of the internal, or local, equilibrium of individual groups of the internal degrees of freedom of a gas mixture, nonequilibrium as a whole. As noted previously, in the general case each quantum level can be considered as an individual degree of freedom. However, the hierarchy of the process rates is usually such that the equilibrium energy distribution in quantum levels 10.7.7 is attained considerably more rapidly within one group than between this group and other degrees of freedom. Then the whole group can be considered as a single degree of freedom and a separate thermodynamic subsystem with its own single temperature $T^{(v)}$ entering, instead of T , in the Boltzmann distribution 10.7.7 (the realization of which is the evidence of the internal equilibrium of the given mode) and in formula 10.7.8 for the energy $E^{(v)}$. Precisely the latter formula serves for determining the temperature $T^{(v)}$.

Most frequently, this approach is applied to molecular vibration; in this case the attainment of equilibrium is favored by the closeness of the energies of neighboring levels. As to the electronic states of atoms and molecules, they are usually fairly distant from the energetic standpoint, this hindering the attainment of their internal equilibrium against the background of ionization processes.

We note in conclusion that the number of separate quantum levels may even increase due to interference of different modes of the degrees of freedom. Thus, molecules with vibration level k may have l electron excitation levels, so that the total number of these levels can be of the order of the product kl of the number of the levels of individual modes.

10.8 Equilibrium of Chemical Reactions and Composition of Gases

We will now specify the equilibrium conditions for reactions with the general stoichiometric relations 10.6.14. Substituting expressions 10.3.3 and 10.3.13 for the molar enthalpies and entropies of the components into equilibrium conditions 10.6.20 and assuming the internal degrees of freedom to be equilibrium (otherwise, the general equilibrium of the system

cannot take place), we group the terms determined by the energy of the internal degrees of freedom, as follows:

$$\begin{aligned} E_i^{(v)} - TS_i^{(v)} &= E_i^{(v)} - T \int_0^T \frac{dE_i^{(v)}}{T} = -TRJ_i^{(v)} \\ J_i^{(v)} &= \sum_l J_{il}^{(v)}, \quad J_{il}^{(v)} = \frac{1}{R} \int_0^T E_{il}^{(v)} \frac{dT}{T^2} = \ln Z_{il} \end{aligned} \quad (10.8.1)$$

Here, $E_{il}^{(v)}$ is the energy of an l -th group of the internal degrees of freedom of species i , and Z_{il} is the corresponding statistical sum (see Equation 10.7.8). Then we introduce the quantities

$$\begin{aligned} \omega_s &= \frac{1}{R} \sum_i \Delta v_{is} C_{pi}^{(0)}, \quad \theta_s = \frac{1}{R} \sum_i \Delta v_{is} H_{0i} \\ J_s^{(v)} &= \sum_i \Delta v_{is} J_i^{(v)}, \quad \Delta v_s = \sum_i \Delta v_{is} \\ \ln I_s &= \frac{1}{R} \sum_i \Delta v_{is} (S_{0i} - C_{pi}^{(0)}) \end{aligned} \quad (10.8.2)$$

In view of 10.7.10, condition 10.6.20 can be brought into the form:

$$\begin{aligned} \prod_i p_i^{\Delta v_{is}} &= (kT)^{\Delta v_s} \prod_i n_i^{\Delta v_{is}} = K_s(T) = (kT)^{\Delta v_s} \bar{K}_s(T) \\ K_s(T) &= I_s T^{\omega_s} Q_s e^{-\theta_s/T} \\ Q_s &= \exp J_s^{(v)} = \prod_i Z_i^{\Delta v_{is}}, \quad Z_i = \prod_l Z_{il} \end{aligned} \quad (10.8.3)$$

These conditions are often called the *acting mass law*. As in Sections 10.4 and 10.7, the functions $K_s(T)$ and $\bar{K}_s(T)$ are the *equilibrium constants** expressed in terms of the partial pressures and the numerical concentrations of the components, respectively. The equilibrium conditions can also be written for the molar and mass concentrations in the form:

$$\prod_i x_i^{\Delta v_{is}} = \bar{M}^{\Delta v_s} \prod_i \left(\frac{c_i}{\bar{M}_i} \right)^{\Delta v_{is}} = p^{-\Delta v_s} K_s = K_{sp}(T, p) \quad (10.8.4)$$

We will now explain the meaning of different quantities entering in these formulas. The quantity $R\omega_s$ is the variation of the total heat of the mixture, the sum $R\theta_s$ represents the total heat of the given reaction, and the quantity θ_s is the *characteristic temperature* (the same as θ_D in Section 10.2). Usually this quantity is rather large; for this reason the temperature dependence of the function $K_s(T)$ in formula 10.8.3 is mainly determined by the factor $e^{-\theta_s/T}$. The factor Q_s is determined by the energy of the internal degrees of freedom and depends on the contributions of individual groups in accordance with a multiplicative law that follows from the definition of the integrals $J_{il}^{(v)}$ and the function Q_s . In this case, in view

* Obviously, the term *constant* used here and in what follows for variable quantities is of purely historical origin.

of Equation 10.7.9, $J_s \rightarrow 0$ as $T \rightarrow 0$ and, hence, the coefficient $Q_s \rightarrow 1$. At higher values of T the temperature dependence of this factor is a power-law one.

By way of illustration, we will calculate this factor for the vibrational energy $E^{(v)}$ of diatomic molecules in accordance with formula 10.7.12. In this case it should be let $\Delta v_{is} = -1$ for molecules and $E_i^{(v)} = 0$ for atoms in expression 10.8.2 for $J_s^{(v)}$, this leading to the formula

$$Q_s = 1 - e^{-\theta_v/T} \rightarrow \frac{\theta_v}{T} \quad \text{for } \frac{\theta_v}{T} \ll 1 \quad (10.8.5)$$

We note that at present it is generally agreed upon that the equilibrium constants of reactions are well known, at least for the most abundant gases; their tables are given in various handbooks, such as that of Glushko (1978) and JANAF Thermochemical Tables (1985).

We will further consider some properties of the equilibrium constants. In Section 10.6 we introduced the notion of dependent and independent reactions, the number of the latter being equal to the difference $L = I - J$, where I and J are the numbers of the mixture components and elements, respectively. For example, in the nitrogen-oxygen mixture there can proceed at least six reactions 10.5.6 with six equilibrium conditions. Together with two mass balance relations 10.6.3 for O and N elements, this is obviously too much for five components (O, O_2, N, N_2 , and NO). However, from 10.8.3 it follows that the terms $\prod_i p_i^{\Delta v_{is}}$ for the subsequent reactions are expressed in terms of the same terms for the first three reactions. Therefore, the equilibrium constants $K_s(T)$ must obey the same law. In this sense, three arbitrary reactions 10.5.6 could be referred to as independent and the other as dependent reactions.

In the general case, if an s -th reaction depends on the previous L reactions, from Equation 10.8.3 there follow the conditions for this reaction

$$K_s = \sum_{l=1}^L K_l^{\alpha_{ls}}, \quad \Delta v_{is} = \sum_{l=1}^L \Delta v_{il} \alpha_{ls} \quad (10.8.6)$$

We can convince ourselves that this is correct by taking the logarithm of Equation 10.8.3; then the dependent equations, linear with respect to $\ln p_i$, become linear combinations of the independent equations with the coefficients α_{ls} .

Thus, the number of the independent equations for determining the equilibrium gas composition is always equal to the number of the unknown variables. We note that the obvious conservation conditions $\sum_i c_i = 1$, $\sum_i x_i = 1$, and $\sum_j c_j^* = 1$, where c_j^* are the element concentrations (Section 10.5), could be used instead of each of the previously mentioned conditions.

We will now specify the general formulas for the binary reactions presented in Section 10.5. For reactions of type 10.5.9 the equilibrium conditions 10.8.3 and 10.8.4 rewritten in terms of 10.6.15 give the following result

$$\frac{p_A p_B}{p_{AB}} = T \frac{n_A n_B}{n_{AB}} = K(T) = IT^\omega Q e^{-\theta/T} \quad (10.8.7)$$

$$\frac{c_A c_B}{c_{AB}} = \frac{\rho_D}{\rho} e^{-\theta/T}, \quad \rho_D = \frac{\bar{M}_A \bar{M}_B}{R \bar{M}_{AB}} I T^{\omega-1} Q \quad (10.8.8)$$

Here, the subscript s is omitted.

The function ρ_D is termed the *characteristic density of a reaction*. In these cases formulas 10.8.2 take the form:

$$\begin{aligned} R\omega &= C_{pA}^{(0)} + C_{pB}^{(0)} - C_{pAB}^{(0)}, & R\theta &= H_{0A} + H_{0B} - H_{0AB} \\ J^{(v)} &= J_A^{(v)} + J_B^{(v)} - J_{AB}^{(v)}, & Q &= \exp J^{(v)} = Z_A Z_B Z_{AB}^{-1} \end{aligned} \quad (10.8.9)$$

For a binary reaction the quantity $R\theta$ is the decomposition energy of a mole of the original particles, while $\varepsilon_D = k\theta$ is the dissociation or ionization energy for a single particle. In accordance with 10.3.7, we have $C_p^{(0)} = 5R/2$ for atoms and $C_p^{(0)} = 7R/2$ for diatomic molecules, so that for the dissociation reaction of the latter we have $\omega = 3/2$. The molar heats of neutral particles and of their ions are the same, while the heat capacity of electrons is the same as for atoms; thus, for ionization reaction we have $\omega = 5/2$.

If particles A and B in a mixture are formed only as the result of the decomposition of molecules AB , then $n_A = n_B$, $p_A = p_B$, and $x_A = x_B$, while from 10.8.7 there follows

$$\frac{p_A^2}{p_{AB}} = \frac{Tn_A^2}{n_{AB}} = K(T), \quad \frac{x_A^2}{x_{AB}} = K_p = -\frac{1}{p}K \quad (10.8.10)$$

If A and B are an ion and an electron, then this dependence gives also the *Saha equation* relating the concentrations of the positive ions $n^+ = n_A$, the electrons $n_{el} = n^+$, and the neutral particles generating the charged ones $n_n = n_{AB}$. In the more general case, a similar formula can be written for the decomposition of the complex molecule AB to the positive (A) and negative (B) ions. In all these cases the gas mixture composition can be also described by the *dissociation or ionization degree* $\alpha = n_A/n_{AB}$ or by the relative number of disintegrated molecules. For the binary mixture of one-element atoms with $c_A = c$ and molecules with $c_{AB} = 1 - c$ formula 10.8.8 takes the form:

$$\frac{c^2}{1 - c} = \frac{\rho_D}{\rho} e^{-\theta/T} \quad (10.8.11)$$

Thence by virtue of the equation of state Equation 10.3.16 $\bar{M}_m p = (1 + c)R\rho T$ we obtain

$$c^2 = \frac{\varphi}{1 + \varphi}, \quad \varphi = \frac{\rho_D RT}{p\bar{M}_m} e^{-\theta/T} \quad (10.8.12)$$

The characteristic density is $\rho_D \approx 1.5 \cdot 10^5 \text{ kg/m}^3$ for oxygen and $\rho_D \approx 1.3 \cdot 10^5 \text{ kg/m}^3$ for nitrogen with a small (no higher than 15%) deviation to both sides over a wide temperature range $T \leq 7000^\circ\text{K}$. These enormous values (the standard air density is $\rho_a \approx 1.3 \text{ kg/m}^3$) are offset by the smallness of the quantity $e^{-\theta/T}$ under the same conditions (the values $\theta \geq 60,000^\circ\text{K}$ for gaseous components of air were already presented). This conservatism of the characteristic densities ρ_D makes it possible to consider them to be constant, at least in making estimates (the Lighthill model of the *ideally dissociated gas*). It is interesting to note that the constancy of ρ_D could be obtained by assuming molecular vibration to be excited by half, at the energy $E_v = RT/2$, and by neglecting the energies of other degrees of freedom. In this case we should let $C_p^{(0)} = 4R$, $C_v^{(0)} = 3R$, and $E_i^{(v)} = 0$ in 10.8.9 this gives $\omega = 1$ and $Q = 1$ and, hence, the constancy of ρ_D .

We will further consider the question of the variation of the equilibrium gas composition with the temperature and pressure, which is determined by the dependence of the equilibrium constants K_s and K_{ps} on these parameters. Differentiating expressions 10.8.3 and 10.8.4

for these constants, using the differential of the last relation 10.6.20, and taking 10.3.10 into account we obtain

$$\begin{aligned} d \ln K_{ps} &= d \ln K_s - \Delta v_s \frac{dp}{p}, & \Delta v_s &= \sum_i \Delta v_{is} \\ d \ln K_s &= \frac{\Delta H_s}{RT^2} dT, & \Delta H_s &= \sum_i \Delta v_{is} H_i \end{aligned} \quad (10.8.13)$$

Clearly, these functions increase with the temperature for $\Delta H_s > 0$, while the function K_{ps} decreases as the pressure increases, if the reaction results in an increase of the total number of the particles, $\Delta v_s > 0$, and vice versa. For binary reactions $\Delta v_s = 1$ and $\Delta H_s = H_A + H_B - H_{AB}$, so that for endothermic reactions proceeding with heat absorption (it is included to the internal energy of newly born particles H_A and H_B) we have $\Delta H_s > 0$. Because of this, from 10.8.10 and in view of the equation $x_{AB} = 1 - 2x_A$, it follows that the molar (and, hence, any other) concentration of the particles x_A and $x_B = x_A$ increases with the temperature and decreases as the pressure increases.

By way of illustration, for the binary gas mixture from 10.8.12 (with $\rho_D = \rho_D(T)$) we have

$$\left(\frac{\partial c}{\partial p} \right)_T = -\frac{c}{2p}(1 - c^2) < 0 \quad (10.8.14)$$

For an ideally dissociating gas* ($\rho_D = \text{const}$) we have

$$\left(\frac{\partial c}{\partial T} \right)_p = \frac{c}{2T}(1 - c^2) \left(1 + \frac{\theta}{T} \right) > 0 \quad (10.8.15)$$

These derivatives vanish for $c = 0$ and $c = 1$ and have an extremum at $c = 1/\sqrt{3}$. We note that the same inequalities are valid for oxygen and nitrogen atoms in equilibrium air; this was demonstrated, in particular, in Figure 1.4.

10.9 Reaction Rates

In Section 10.4 we derived the general form of the source functions Λ_i in Equation 10.4.10 for the relaxation of the internal degrees of freedom. In what follows we will obtain the more general expression for the rates of arbitrary physicochemical processes proceeded by the stoichiometric mechanism 10.6.14.

In accordance with this scheme, v'_i particles of each type must meet in an interaction volume in order for the forward reaction act to take place, while v''_i particles of each type are necessary for the reverse reaction act. From the reasoning of Section 10.4 it follows that the probabilities of these events and, hence, the rates of the forward r_f and reverse r_r reactions must be proportional to the products

$$r_f = \bar{k}_f \prod_i n_i^{v'_i} = k_f \prod_i p_i^{v'_i}, \quad r_r = \bar{k}_r \prod_i n_i^{v''_i} = k_r \prod_i p_i^{v''_i} \quad (10.9.1)$$

* The general formulas for the variations in the component concentrations at displacement of many reactions in a multicomponent gas mixture are presented in Lunev (1975).

where, as in Section 10.4, \bar{k}_f and k_f are the forward reaction rates, while \bar{k}_r and k_r are the reverse reaction rates.

On the other hand, the increase Δn_{is} in the number of particles of each species in the act of an s -th reaction must, in accordance with Equation 10.6.17, be proportional to the stoichiometric difference v_{is} . Therefore, by analogy with 10.4.4, the rates of the formation of a number of moles of species i in unit volume for the s -th reaction can be written in the form:

$$r_{is} = \Delta v_{is} r_s, \quad r_s = r_{fs} - r_{rs} = k_{fs} \prod_i p_i^{v'_{is}} - k_{rs} \prod_i p_i^{v''_{is}} \quad (10.9.2)$$

Here, r_s is the rate of the s -th reaction, proportional to the time derivative of the parameter R_s introduced by formula 10.6.17. Since the dependence of r_s on the particle concentration has been already chosen by products (10.9.1), this constant no longer depends on the pressure, but only on the nature of the process, the temperature, and the degree of the excitation of the internal degrees of freedom, or, in a particular case, on the temperature $T_{ik}^{(v)}$.

As for the dimensionalities of the rates r , r_f , and r_r , we will determine them, as in Section 10.4, as mole/(volume·time) (e.g., mole/m³·sec), no matter how these rates are expressed in terms of the particle number n_i or the mole number $N_i = n_i/N_0$ per unit volume, the partial pressures p_i , and so on. The dimensionalities of the reaction rates k_f , \bar{k}_f , and so on, are determined appropriately, the relations between them following from the equation of state $p_i = n_i kT$.

We will further transform the formula for r_s to the form:

$$\begin{aligned} r_s &= k_{rs} \prod_i p_i^{v'_{is}} \left(\tilde{K}_s - \prod_i p_i^{v_{is}} \right) = X_s \Phi_s \\ X_s &= k_{rs} \prod_i p_i^{v'_{is}} = k_{rs} p^{\beta_s} \prod_i x_i^{v'_{is}}, \quad \beta_s = \sum_i v'_{is} \\ \Phi_s &= \tilde{K}_s - \prod_i p_i^{\Delta v_{is}} = \tilde{K}_s - p^{\Delta v_s} \prod_i x_i^{\Delta v_{is}} \\ \tilde{K}_s &= k_{fs}/k_{rs}, \quad x_i = p_i/p, \quad \Delta v_s = \sum_i \Delta v_{is} \end{aligned} \quad (10.9.3)$$

Bearing this formula in mind, the quantity k_{rs} is often called simply the *reaction rate constant*. If $r_s > 0$, then the reaction goes to the right and vice versa. At equilibrium between the internal and external degrees of freedom, the function \tilde{K}_s coincides with the equilibrium constant introduced in Section 10.8. In the equilibrium state $r_s = 0$ and the equilibrium condition is presented by the acting mass law obtained in Section 10.8.

Equation 10.9.2 for mass concentrations is similar to Equation 10.4.10 and, in view of Equation 10.6.17, takes the form:

$$\frac{dc_{is}}{dt} = \Delta v_{is} \frac{\bar{M}_i}{\rho} r_s = \Delta v_{is} \frac{\bar{M}_i}{M} \frac{RT}{p} r_s, \quad r_s = \rho \frac{dR_s}{dt} \quad (10.9.4)$$

For dissociation-type reactions 10.5.9 we have $\beta_s = 2$ and $\Delta v_s = 1$; in this case from 10.9.3 and 10.9.4 there follows

$$\begin{aligned} \frac{dc_{is}}{dt} &= \Delta v_{is} \frac{\bar{M}_i}{M} [pF_{1s}(T, \lambda_n) - p^2 F_{2s}(T, \lambda_n)] \\ F_{1s} &= RTk_{fs}x_M x_{AB}, \quad F_{2s} = RTk_{rs}x_M x_{AXB} \end{aligned} \quad (10.9.5)$$

As before, by λ_n is meant the whole set of the kinetic variables. The first term in parentheses represents the rate of the forward reaction (dissociation and ionization) and is proportional to the pressure, while the second term represents the recombination rate and is proportional to the squared pressure.

At the same time, for the exchange processes 10.5.10 we have $\beta_s = 2$ and $\Delta v_s = 0$, so that formula 10.9.4 takes the form:

$$\frac{dc_{is}}{dt} = \Delta v_{is} \frac{\bar{M}_i}{\bar{M}} p F_{1s}(T, \lambda_n)$$

$$F_{1s} = RT(k_{fs}x_Ax_B - k_{rs}x_Cx_D) \quad (10.9.6)$$

As in the relaxation Equation 10.4.10, the right-hand side in the previous formula is proportional to the pressure.

If component i takes part in several reactions at one time, then the resulting equation has the form:

$$\frac{dc_i}{dt} = \sum_s \frac{dc_{is}}{dt} = \frac{\bar{M}_i}{\rho} r_i, \quad r_i = \sum_s \Delta v_{is} r_s \quad (10.9.7)$$

Thus, nitrogen atoms take part at one time in four reactions, 2 to 5 of list 10.5.6 and in processes 2, 6, and 8 of 10.5.7. However, in this case the number of summands in the total rate r_i is considerably greater, since reactions of type 10.5.8 proceeding with the given particles A and B but with different third particles M_k should be considered as different, since in the general case they are associated with different coefficients $X_s = X_{sk}$ in formula 10.9.3 and, generally speaking, with different functions $\tilde{K}_s = \tilde{K}_{sk}$, inasmuch as the reaction rates are dependent on the type of the M_k species.

However, at equilibrium of the internal and external degrees of freedom, the functions $\tilde{K}_s = K(T)$ and Φ_s no longer depend on the species of the third particle. In this case, all the reactions with the same functions Φ_s , that is, with the same equilibrium conditions, can formally be unified into a single reaction with the *effective* rate

$$k_{rs}^{(\text{eff})} = \sum_k k_{rsk}(x_{Mk}/x_M), \quad x_M = \sum_k x_{Mk} \quad (10.9.8)$$

where x_{Mk} are the concentrations of the M_k particles.

We will now dwell on the reaction rates. If the forward direction of reactions is taken to be that with energy absorption (e.g., endothermic reactions of molecular dissociation and molecular and atomic ionization), then the forward reaction rate is usually determined by the *Arrhenius law*

$$k_f = F(T, \lambda_n) e^{-\varepsilon_a/kT} \quad (10.9.9)$$

Here, ε_a is the *activation energy*, while $F(T, \lambda_n)$ is a function of the temperature (weak as compared with the exponential function) and, in the general case, of the kinetic variables λ_n . In the classical version of this formula $F = F_e(T)$. The presence of the exponential functions is due to the Maxwellian distribution 1.4.7, since the number of high-velocity molecules, the collisions of which can only result in endothermic processes, increases following precisely this law.

For many gases that are treated by gas dynamics, the energy ε_a is equal or very near to the dissociation or ionization energy ε_D . In these cases, the constants k_r of the reverse (exothermic) reactions do not include exponential factors, that is, they are relatively weak

functions of the temperature. They are determined experimentally and are usually dependent on the temperature in accordance with a power-law, $k_r \sim T^{-n}$, where for most of the gases of the air mixture n ranges from 1/2 to 3/2.

In the absence of equilibrium of the internal degrees of freedom, the dependence of the functions $F(T, \lambda_n)$ on the variables λ_n can be very considerable, which is due to the fact that the excited (e.g., vibrationally or electronically) molecules require for their decomposition an appreciably smaller collision energy than the unexcited ones. This can be realized in collisions involving a greater number of the particles. In the presence of partial (local) equilibrium within individual groups of the internal degrees of freedom, λ_n can be taken to mean the temperatures $T_n^{(v)}$ of these groups (Section 10.7). The dependences $F(T, \lambda_n)$ for the molecular dissociation processes under the conditions of the nonequilibrium excitation of their vibration (the *vibration-dissociation effect*) are known precisely in the form $F(T, T_n^{(v)})$; we will dwell on this question in Section 10.11.

10.10 Relaxation of Complex Systems

In Section 10.4 we considered the relaxation of the two-level system of the internal degrees of freedom and derived a very simple version of the relaxation Equation 10.4.10 for this system. In what follows we will consider the relaxation processes for multilevel groups of the degrees of freedom, for example, vibrational ones. We take a set of particles of species A with a concentration n_A and consider the evolution of a given group (mode) of their internal degrees of freedom. Due to different external actions and spontaneous effects, each particle carries the possibility of $j-k$ transition from the j -th to the k -th excited level and of reverse transition, that is, conversion of particle A_j to particle A_k , and inversely. If n_j and n_k are the numerical concentrations of these particles, then, by analogy with Sections 10.4 and 10.9, the volume rate r_k of the variation of the mole number of particles A_k can be presented in the form:

$$\begin{aligned} r_k &= \sum_j r_{jk}, \quad r_{jk} = r_{jk}^{(v)} + r_{jk}^{(T)} \\ r_{jk}^{(b)} &= n_b (\bar{k}_{jk}^{(b)} n_j - \bar{k}_{kj}^{(b)} n_k) \\ b = v \quad n_b &= n_A; \quad b = T \quad n_b = n_M \\ \sum_k^m n_k &= \sum_j^m n_j = n_A, \quad k, j = 1, \dots, m, \quad k \neq j \end{aligned} \tag{10.10.1}$$

Here, $\bar{k}_{jk}^{(v)}$ and $\bar{k}_{kj}^{(v)}$ are the rates of the intragroup exchange by energy quanta at collisions of particles A with each other, while $\bar{k}_{jk}^{(T)}$ and $\bar{k}_{kj}^{(T)}$ are the rates of excitation and deactivation (quenching) of particles A due to the energy exchange with external degrees of freedom at their collisions with any auxiliary particles M with concentration n_M (including collisions with each other). For molecular vibrations these are the V-V and V-T exchanges, respectively.

Summing over j we obtain

$$\begin{aligned} r_k &= r_k^{(v)} + r_k^{(T)}, & r_k^{(b)} &= \sum_j r_{kj}^{(b)} = n_b (\bar{k}_{Ak}^{(b)} n_A - \bar{k}_{kA}^{(b)} n_k) \\ \bar{k}_{Ak}^{(b)} &= \sum_{j \neq k} \bar{k}_{jk}^{(b)} (n_j / n_A), & \bar{k}_{kA}^{(b)} &= \sum_{j \neq k} \bar{k}_{kj}^{(b)} \end{aligned} \quad (10.10.2)$$

Here, $\bar{k}_{Ak}^{(b)}$ and $\bar{k}_{kA}^{(b)}$ are the total (with respect to j) effective constants of the appearance and disappearance rates for particles A_k . Applying then the procedure of the derivation of Equation 10.4.10 for the mass concentration c_k of particles A_k we arrive at the equation

$$\begin{aligned} \frac{dc_k}{dt} &= \Lambda_k = \Lambda_k^{(v)} + \Lambda_k^{(T)} = \frac{\bar{M}_A}{\rho} r_k \\ \Lambda_k^{(v)} &= \frac{\bar{M}_A}{\rho} r_k^{(v)}, & \Lambda_k^{(T)} &= \frac{\bar{M}_A}{\rho} r_k^{(T)}, & c_k &= \frac{n_k}{n_A} c_A \end{aligned} \quad (10.10.3)$$

Here, \bar{M}_A is the molecular mass of particles A and c_A is their mass concentration. This is the system of the *state-to-state kinetics equations* with which we will deal in the general case; the properties of this system will be considered in the following. We emphasize that this system was derived in the absence of other sources of the variation of the number of particles A_k . The more general case is considered at the end of this section.

At equilibrium, by virtue of the detailed balancing principle (Sections 10.6 through 10.8) all the terms on the right-hand sides of the previous equations must vanish separately, thus giving the following relation between the reaction rate constants and the equilibrium constants 10.7.5 and 10.7.7

$$\frac{n_k}{n_j} = \frac{\bar{k}_{jk}^{(b)}}{\bar{k}_{kj}^{(b)}} = K_{kj}^{(v)}(T), \quad \frac{n_k}{n_A} = \frac{\bar{k}_{Ak}^{(b)}}{\bar{k}_{kA}^{(b)}} = K_{kA}^{(T)}(T) \quad (10.10.4)$$

At known equilibrium constants, these equations cut the number of the coefficients $\bar{k}_{jk}^{(b)}$ to be determined in half.

However, the real situation is much more complicated. First, these coefficients are averaged over a set of more particular processes. For example, considering the processes in detail it would be well, by analogy with 10.9.8, to put

$$n_A \bar{k}_{fk}^{(v)} = \sum_l \bar{k}_{jkl}^{(v)} n_l, \quad n_M \bar{k}_{jk}^{(T)} = \sum_i \bar{k}_{jki}^{(T)} n_{Mi} \quad (10.10.5)$$

where the coefficients $\bar{k}_{jkl}^{(v)}$ and $\bar{k}_{jki}^{(T)}$ are proportional to the probability of A_j to A_k particle transition at collisions with a particle A_l and a particle M of species i with a concentration n_{Mi} ; these *primary coefficients* can be considered temperature-dependent only. We note that this detailing is not ultimate, since the coefficients $\bar{k}_{jkl}^{(v)}$, and so on, for the process of, say, vibrational relaxation of reacting molecules can also depend on the state of the electronic levels of all the components taking part in the process.

This splitting of a complex process to partial, elementary processes is necessary in solving quantum-mechanical problems of the interaction of particles on the atomic and molecular levels, the solution of which could in principle give the information on the primary coefficients $\bar{k}_{jkl}^{(v)}$, and so on. However, so far the problems of this kind have not been solved

exhaustively, while the possibility of the direct experimental determination of these coefficients is highly conjectural. Moreover, although the detailing of type 10.10.5 does not increase the number of equations in 10.10.3, it makes them considerably more complicated, which is attributable to a fairly large number of these equations.

This almost excludes the possibility of applying directly the state-to-state kinetics systems to gas dynamic problems (at least, in this stage), which prompts us to search for some simplified physical models for such processes. These models were developed for vibrational relaxation on the assumption that the V-V exchange rates are considerably greater than those of all other processes included in Equation 10.10.2. This implies the fulfillment of the conditions

$$n_A \bar{k}_{jk}^{(v)} \gg n_M \bar{k}_{jk}^{(T)} \quad (10.10.6)$$

Then a certain quasistationary solution must be attained in a system with arbitrary initial data after a certain small relaxation time $\Delta t \sim (n_A \bar{k}_{jk}^{(v)})^{-1}$ (see Section 10.4). However, since the terms $\Lambda_k^{(v)}$ in 10.10.3 describe the processes within the given vibrational mode, that is, the adiabatic process for this mode, this solution corresponds to a, as it were, constant initial total vibrational energy E_v per mole of molecules A. Because of this, the state governed by this solution (it was called the local equilibrium state in Section 10.2 if the given mode is considered an individual thermodynamic system) is described by the Boltzmann distribution 10.7.5 through 10.7.7 but with its own temperature T_v (determined by the energy E_v) instead of T

$$\frac{n_j}{n_k} = K_{jk}(T_v) = \frac{I_j}{I_k} e^{-(\varepsilon_j - \varepsilon_k)/kT_v} \quad (10.10.7)$$

In order to derive an equation for the evolution of the vibrational energy e_v per unit mass of molecules A, by analogy with the derivation of Equation 10.4.12, we multiply Equation 10.10.3 by ε_k/m_A , that is, by the specific energy of the k-th vibrational level of a single particle with the mass m_A , and then sum up these equations

$$\begin{aligned} \frac{dc_A e^{(v)}}{dt} &= \Lambda^{(v)} + \Lambda(T), & e_v &= \frac{1}{c_A m_A} \sum_k \varepsilon_k c_k \\ \rho \Lambda^{(v)} &= N_0 \sum_k \varepsilon_k r_k^{(v)} = 0 \\ \rho \Lambda^{(T)}(T, T_v, p) &= N_0 \sum_k \varepsilon_k r_k^{(T)}, & N_0 &= \bar{M}_A / m_A \end{aligned} \quad (10.10.8)$$

Here, as in Section 10.4, e_v is the vibrational energy per unit mass of particles A, while $c_A e_v$ is the energy per unit mass of the mixture.

The assumption $\Lambda^{(v)} = 0$ adopted here is based on the fact that the V-V process is adiabatic as a whole, while the concentrations n_k and n_j entering in the terms $\Lambda_k^{(T)}$ (see 10.10.3) can be expressed in terms of relations 10.10.7, which eventually leads to the functional dependence $\Lambda^{(T)} = \Lambda^{(T)}(T, T_v, p)$, as noted previously.

Specifying the form of these equations requires some additional assumptions on the nature of the processes under consideration. In particular, for V-T relaxation there exists the *Landau-Teller equation* obtained within the framework of the harmonic oscillator model

$$\begin{aligned} \frac{dc_A e_v}{dt} &= \Lambda^{(T)}(T, T_v, p) = \frac{c_A [e_v(T) - e_v(T_v)]}{\tau_v} \\ \tau_v &= p^{-1} B(T) e^{-\alpha T^{1/3}} \end{aligned} \quad (10.10.9)$$

Here, the constant α and the “slow” temperature function $B(T)$ depend on the particular gas. The form of this equation coincides with that of Equation 10.4.12; however, the former relates to the total vibrational energy. For more sophisticated models of molecules, the form of the function $\Lambda^{(T)}$ also becomes more complex; however, the arguments T , T_v , and p remain the same.

We will now consider a more complicated problem. The variation of the A_k particle concentration can also occur due to chemical reactions, in which particles A may appear and disappear with different excited levels (e.g., molecular dissociation by the scheme $A_k = B + C$ from a k -th vibrational level and recombination of atoms B and C to molecule A_k with the k -th excited level). In this case, Equation 10.10.3 should be replaced by a more general one; we will write this equation for the relative concentrations \bar{c}_k in terms of formula 10.9.4 with $\Delta\nu_A = -1$

$$c_A \frac{d\bar{c}_k}{dt} = \Lambda_k + \Lambda_k^{(w)}, \quad \Lambda_k^{(w)} = W_k - \bar{c}_k \frac{dc_A}{dt}, \quad \bar{c}_k = \frac{c_k}{c_A} = \frac{n_k}{n_A}$$

$$W_k = \frac{\bar{M}_A}{\rho} (r_{rk} - r_{fk}), \quad \frac{dc_A}{dt} = \frac{\bar{M}_A}{\rho} (r_r - r_f) \quad (10.10.10)$$

Here, r_{rk} and r_{fk} are the rates of formation and decomposition of particles A_k , while r_r and r_f are the same rates for particles A as a whole. The variation of the relative concentration \bar{c}_k is also dependent on the total variation of the concentration c_A , which is taken into account by the second term in the expression for $\Lambda_k^{(w)}$.

The results obtained represent a typical example of the construction and validation of *multitemperature* models for nonequilibrium gases. We note that the aforesaid is only a short review of this theory; we refer the reader for more detail to books cited in Section 10.1 (the same is true for the material outlined in the Section 10.11).

10.11 Relaxation–Reaction Interaction

We noted that reaction rate constants can depend on the state of the internal degrees of freedom. Obviously, an inverse relationship between these factors can also exist, since, for example, excited molecules reduce the total vibrational energy of a mixture in dissociating and augment it when appearing in recombination. We will call this interrelated process the *relaxation–reaction* (R–R) or, as applied to molecular vibration, the *vibration–dissociation* (V–D) interaction. In what follows we will study these effects on a model level with the aim of obtaining the general structure and nature of the governing equations and formulas.

We will consider reactions of dissociative type 10.5.9 and write them in the form $A = BC = B + C$. We represent the total rates of the forward (r_f) and reverse (r_r) reactions as the sums of the partial rates of decomposition processes for the A_k particles, that is, the A particles with an excited k -th level.

$$r_f = n_M n_A \bar{k}_f = \sum_k r_{fk}, \quad r_{fk} = n_M n_k \bar{k}_{fk}$$

$$r_r = n_M n_B n_C \bar{k}_r = \sum_k r_{rk}, \quad r_{rk} = n_M n_B n_C \bar{k}_{rk}$$

$$n_A \bar{k}_f = \sum_k n_k \bar{k}_{fk}, \quad \bar{k}_r = \sum_k \bar{k}_{rk} \quad (10.11.1)$$

Here, as previously, n_M is the concentration of the auxiliary neutral particles M , n_A is the total concentration of particles A , n_k is the concentration of particles A_k , that is, particles A excited on the k -th level, n_B and n_C are the concentrations of particles B and C , \bar{k}_f and \bar{k}_{fk} are the total and partial reaction rate constants for the forward reactions, and \bar{k}_r and \bar{k}_{rk} are the same constants for the reverse reaction.

To evaluate \bar{k}_{fk} we will use the following intuitive arguments. The reaction rate $\bar{k}_{fk} d\varepsilon / kT$ at collision of the particles, whose relative translational energy ranges from $\varepsilon + d\varepsilon$ to ε , is proportional to their concentration $d n_\varepsilon$ determined by the Maxwellian distribution (1.4.7); however, only collisions at an energy ε above a certain energetic threshold ε_{ak} , can be result producing. However, due to different reasons, even at $\varepsilon > \varepsilon_{ak}$ particle collisions do not always result in a reaction, whose probability decreases with the difference $\varepsilon - \varepsilon_{ak}$. We will allow for all these factors, which quite often compensate for each other, assuming that

$$\varepsilon_{ak} = \alpha \varepsilon_D - \beta \varepsilon_k, \quad kT \bar{k}_{fk} = B_k (\varepsilon - \varepsilon_{ak}) e^{-\varepsilon/kT}, \quad \varepsilon \geq \varepsilon_{ak} \quad (10.11.2)$$

where α , β , and B_k are some coefficients and a function, ε_k is the energy of the k -th level, ε_D is the energy of decomposition (dissociation or ionization) of particles, and only the exponential factor has been taken from formula 1.4.7. Integrating this formula we obtain

$$\bar{k}_{fk} = \frac{B_k}{(kT)^2} \int_{\varepsilon_{ak}}^{\infty} (\varepsilon - \varepsilon_{ak}) e^{-\varepsilon/kT} d\varepsilon = F_k e^{-\alpha \varepsilon_D / kT}, \quad F_k = B_k e^{\beta \varepsilon_k / kT} \quad (10.11.3)$$

Comparing Equations 10.9.9, 10.11.1, and 10.11.3 we obtain

$$\begin{aligned} \bar{k}_f &= F e^{-\varepsilon_a / kT}, & \varepsilon_a &= \alpha \varepsilon_D \\ F &= \sum_{k=0}^m F_k \bar{n}_k, & n_k &= \frac{\bar{n}_k}{n_A}, & m &= \max k \end{aligned} \quad (10.11.4)$$

In the general case n_k are independent and determined by the system of the state-to-state kinetics Equations 10.10.10, together with the corresponding physicochemical kinetics equations. The latter circumstance only aggravates the difficulties in realizing the complete formulation of the problem noted in Section 10.10; for this reason, in what follows we will restrict ourselves to the case of internal equilibrium of the quantum level groups, the state of which can, in accordance with Section 10.7, be characterized by a single vibrational temperature T_v with the Boltzmann distribution 10.7.7 or 10.10.7 for the populations n_k . In this case the sum 10.11.4 leads to a dependence of the type $\bar{k}_f = \bar{k}_f(T_v, T)$.

Let, for example, the coefficients B_k obey the law

$$B_k = B_0 e^{\gamma \varepsilon_k / k\theta_D}, \quad B_0 = \text{const}, \quad k\theta_D = \varepsilon_D, \quad \gamma \geq 0 \quad (10.11.5)$$

This law (see Marrone and Treanor, [1963]) implies an additional increase in the probability of the dissociation from upper levels at $\gamma > 0$ (for $\gamma = 0$ all $B_k = B_0$). In order to eliminate \bar{n}_k from 10.11.4 we will use formula 10.7.7 with T replaced by the vibrational temperature T_v . Then, summing over k we obtain

$$\begin{aligned} \bar{k}_f &= F e^{-\varepsilon_a / kT}, \quad F = F(T, T_v) = B_0(T) Z(T^*) Z^{-1}(T_v) \\ \frac{1}{T^*} &= \frac{1}{T_v} - \frac{B}{T} - \frac{\gamma}{\theta_D} \end{aligned} \quad (10.11.6)$$

The *fictitious* temperature T^* introduced previously can be of any sign, while the function $Z(T^*)$ determined by formula 10.7.6 is continuous at the point $T^* = \pm\infty$. For the truncated harmonic oscillator (formula 10.7.11) the function $Z_m(T^*)$ and the energy $E_{vm}(T^*)$ are plotted in Figure 10.4 for $m = 30$. Their limits, $Z_m(T^*) \rightarrow m + 1$ and $E_{vm}(T^*) \rightarrow (1/2)N_0\varepsilon_D$ as $T^* \rightarrow \infty$, are determined by formula 10.7.15. For $T^* < 0$ both functions lose their original physical meaning; in this case $Z_m(T^*) \rightarrow \infty$ and $E_{vm}(T^*) \rightarrow N_0\varepsilon_v m = N_0\varepsilon_D$, as $T^* \rightarrow -\infty$.

Introducing the equilibrium function $F = F_e$ for $T_v = T$, formula 10.11.6 can be brought into the form:

$$\begin{aligned} F &= F_e(T) \cdot F_v(T, T_v), \quad F_e(T) = B_0(T)Z(T_e^*)Z^{-1}(T) \\ F_v &= \frac{Z(T^*)Z(T)}{Z(T_e^*)Z(T_v)}, \quad \frac{1}{T_e^*} = \frac{1-\beta}{T} - \frac{\gamma}{\theta_D} \end{aligned} \quad (10.11.7)$$

The dependence of the function $F_v = F/F_e$ on the relevant parameters is presented in Figure 10.5. As the ratio T_v/T increases, the function increases by several orders; as $T_v \rightarrow 0$, or, to be more precise, when $T_v \ll \theta_v$ and $T_v \ll T$, it attains a minimum. The quantity F_v is also strongly dependent on the parameter γ , while the influence of the parameter β , on the range of its physically justified variation, is comparatively weak. In the same figure we have plotted the curve for the stepwise population of vibrational levels; it is Boltzmannian for the lower levels and zero for the upper ones with the corresponding δ -fold decrease in the vibrational energy, which leads to a considerable reduction of the dissociation rate. This model result characterizes qualitatively the influence of possible violation of the Boltzmann distribution due to molecular dissociation chiefly from the upper vibrational levels.

We will now dwell upon the reverse reaction rates. Atoms *B* and *C*, which recombine to molecule *BC*, cannot know the state of the vibrational degrees of freedom of molecules;

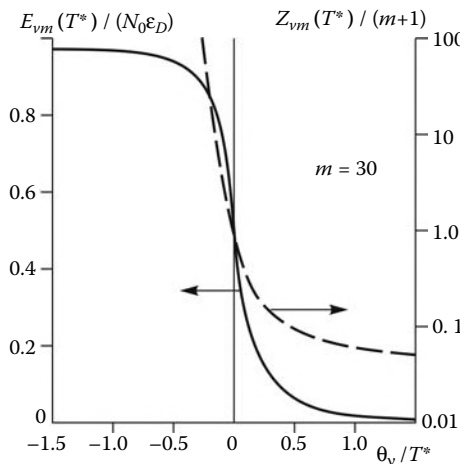


FIGURE 10.4

Dependence of the energy and the statistical sum of a truncated oscillator on the fictitious temperature.

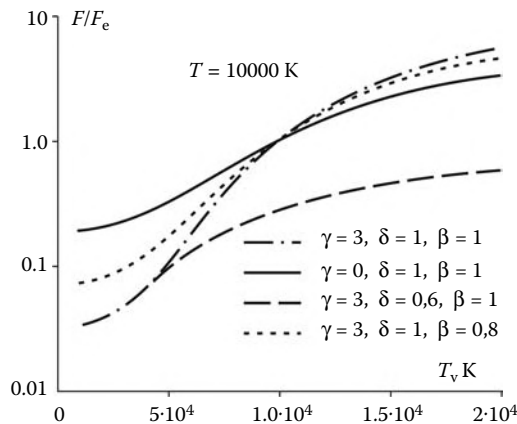


FIGURE 10.5
Vibrational temperature effect on the molecular dissociation rate.

therefore, the functions \bar{k}_{rk} and \bar{k}_k are generally independent of this state.* Thus, they can be assumed to be dependent on the temperature T only, but not on T_v . Nevertheless, a certain probability of atom recombination to a certain molecular level must exist. In this stage, this question is solved by applying the detailed balancing principle (Sections 10.6 through 10.8), in accordance with which and in view of 10.11.1 at equilibrium the following conditions are simultaneously fulfilled

$$\begin{aligned} r_{fk} &= r_{rk}, \quad r_f = r_r \\ \frac{n_B n_C}{n_A} &= \frac{\bar{k}_f}{\bar{k}_r} = \frac{n_k \bar{k}_{fk}}{n_A \bar{k}_{rk}} = \frac{1}{kT} K_s(T) \end{aligned} \quad (10.11.8)$$

Here, K_s is the equilibrium constant for the reaction as a whole, while the ratio n_k/n_A is determined by the Boltzmann distribution 10.7.7. Setting in 10.11.8 $\bar{k}_{fk}(T, T_v) = \bar{k}_{fk}(T, T)$, and so on, we determine the functions $\bar{k}_{fk}(T)$ and $\bar{k}_r(T)$, which are, therefore, as though always equilibrium in our formulation, if, of course, to abstract from the possible influence of the state of particles B and C on them. Similar conclusions are valid for ionization reactions in which particles B and C represent an ion and an electron.

Let us now consider an inverse process, namely, the effect of the reactions of the $A = B + C$ type on the relaxation of the vibrational degrees of freedom, with the aim of obtaining an equation of type 10.10.10 and in the same approximation for the total energy e_v of the given vibrational mode per unit mass of particles A . As in Section 10.10, we will assume the presence of internal equilibrium within this group, with its own temperature T_v . Then multiplying Equation 10.10.10 by the specific energy ε_k/m_A of a single particle and summing

* In principle, such a dependence can exist via “third” particles M (see 10.5.9 and 10.9.8); however, it could hardly be taken into account.

over k we obtain the required equation for e_v

$$\begin{aligned} c_A \frac{de_v}{dt} &= \Lambda^{(T)} + \Lambda^{(w)}, \quad \Lambda^{(w)} = \frac{1}{m_A} \sum_k \varepsilon_k \Lambda_k^{(w)} = \\ &\quad \frac{\bar{M}_A}{\rho c_A} [(e_r - e_v)r_r - (e_f - e_v)r_f] \\ m_A e_r r_r &= \sum_k \varepsilon_k r_{rk}, \quad m_A e_f r_f = \sum_k \varepsilon_k r_{fk} \end{aligned} \quad (10.11.9)$$

Here, the quantities e_v and $\Lambda^{(T)}$ are the same as in Equation 10.10.8, while the differences $e_f - e_v$ and $e_r - e_v$ give the decrease and the increase in the energy of this mode, respectively, at decomposition and formation of unit mass of particles A . At equilibrium, in accordance with the detailed balancing principle, we obtain the condition $e_f = e_r(T)$. In the absence of equilibrium the similar dependence of e_r on T only ($e_r = e_r(T)$) should be conserved in accordance with the previous reasoning about the reverse reaction rates. At the same time, the energy e_f and the forward reaction rate must depend on the state of the reacting particles A , that is, at least on the temperature T_v . Thus, the energies entering in Equation 10.11.9 have the functional form:

$$e_v = e_v(T_v), \quad e_f = e_f(T, T_v), \quad e_r = e_r(T) \quad (10.11.10)$$

By way of illustration, we will evaluate the energies e_f and e_r of diatomic molecule dissociation within the framework of the truncated harmonic oscillator model. Summing over k in the formulas for e_f and e_r , 10.11.9 and taking Equations 10.7.7, 10.7.8, 10.7.11, and 10.11.1 to 10.11.6 into account we obtain

$$\begin{aligned} N_0 \sum_k \varepsilon_k r_{fk} &= N_0 n_M n_A \sum_k \varepsilon_k \bar{n}_k \bar{k}_{fk} = \\ n_M n_A B_0 E_{vm}(T^*) e^{-\varepsilon_a/kT} &= \bar{M}_A e_f r_f \end{aligned} \quad (10.11.11)$$

Comparing these equations with Equations 10.11.1, 10.11.4, and 10.11.6 we obtain

$$\begin{aligned} e_f(T, T_v) &= e_f(T^*) = \frac{1}{\bar{M}_A} E_{vm}(T^*) \\ e_r(T) &= e_f(T, T) = e_f(T_e^*) = \frac{1}{\bar{M}_A} E_{vm}(T_e^*) \end{aligned} \quad (10.11.12)$$

The quantities T^* and T_e^* are determined by formulas 10.11.6 and 10.11.7; the function $E_{vm}(T^*)$ is presented in Figure 10.4. It is interesting to note that even under the equilibrium conditions, in the general case we have $e_f = e_r \neq e_v(T)$. For example, at $\beta = 1$ and $\gamma = 0$ from Equation 10.11.7 we have $T_e^* = \infty$ and, in accordance with 10.7.15, $E_{vm} = R\theta_D/2$, regardless of the temperature. At the same time, the equilibrium vibrational energy is

always $E_v \leq RT$, so that for $T \ll \theta_D/2$ we have $E_{vm}(T_e^*) > E_v(T)$ and, hence, $e_f, e_r > e_v(T)$. In other words, the mean vibrational energy of both dissociating molecules and molecules formed in recombination is greater than the mean vibrational energy of all the molecules of this species.

10.12 Relaxation of the Electron Temperature

The results obtained previously, namely, the equilibrium conditions (Section 10.8), the expressions for the reaction rates (Section 10.9), and so on, relate equally to ionized gases. In particular, the Saha Equation 10.8.10 determines the equilibrium conditions for electrons and ions, while the general formulas of type 10.11.4 determine the rates of *stepwise ionization* allowing for the nonequilibrium degree of the electronic excitation of neutral, or heavy, particles—atoms and molecules—entering an ionization reaction. Since electrons in a gas can be generated due to ionization of several components, the corresponding kinetic equations are usually written for positive ions and for negative ions, if the latter exist in the gas. The total electron concentration in the quasineutral plasma is determined by the charge conservation law 10.5.5.

We note that in most gas dynamic problems related to atmospheric flight we deal with only very low molar electron concentrations x_{el} which do not influence the total characteristics of the gas mixture (thus, for the spacecraft reentry conditions we have $x_{el} < 0.01$). However, even this *ionization degree* is important for the properties of radiowave propagation or decay in a plasma and, second, at high gas temperatures many kinetic processes (such as dissociation, ionization, excitation of the internal degrees of freedom) involve electrons through the *electron impact* mechanism, the rates of these processes being dependent precisely on the electron temperature T_{el} , which makes topical the problem of its determination.

Within the framework of the phenomenological model of a gas mixture as adopted in Section 10.2, the electronic gas represents only one component of this mixture, with the equation of state 10.3.8 for a monatomic gas and its own temperature T_{el} , which is in the general case different from the common translational temperature of heavy particles. The equation for T_{el} follows from the first law of thermodynamics written for a liquid volume

$$\frac{d}{dt} \left(\frac{3}{2} n_{el} k T_{el} v \right) + p_{el} \frac{dv}{dt} = \Lambda_{n,el} v, \quad p_{el} = n_{el} k T_{el} \quad (10.12.1)$$

Here, n_{el} is the numerical electron concentration determined by its own kinetic equation (Section 10.9), $\Lambda_{n,el}$ is the generating function, and the second term on the left-hand side signifies the electron pressure work at the variation of the volume v .

We note that a similar energy equation can be written for any individual component of the gas mixture having its own temperature T_i . However, at molecular-kinetic equilibrium all these equations must have the common temperature $T_i = T$ as their limiting solution, this temperature being determined by the equation for the total energy.

Acting in the same fashion as in deriving Equation 10.4.10 and replacing, in accordance with 1.8.11 the term $v^{-1}dv/dt$ by the gas velocity divergence $\operatorname{div} \bar{U}$, from 10.12.1 we obtain the equation for the specific electron density e_{el} (per unit mass)

$$\frac{de_{\text{el}}}{dt} + \frac{2}{3} e_{\text{el}} \operatorname{div} \bar{U} = \Lambda_{\text{el}} - \frac{e_{\text{el}}}{c_{\text{el}}} \frac{dc_{\text{el}}}{dt}$$

$$c_{\text{el}} = \frac{\rho_{\text{el}}}{\rho} = \frac{n_{\text{el}} m_{\text{el}}}{\rho}, \quad \Lambda_{\text{el}} = \frac{1}{\rho} \Lambda_{n,\text{el}}, \quad e_{\text{el}} = \frac{3}{2} \frac{k T_{\text{el}}}{m_{\text{el}}} \quad (10.12.2)$$

Here, m_{el} is the electron mass and c_{el} is their mass concentration determined by Equation 10.9.4 as follows:

$$\frac{dc_{\text{el}}}{dt} = \frac{1}{\rho} \bar{M}_{\text{el}} r_{\text{el}} = \frac{N_0 m_{\text{el}}}{\rho} r_{\text{el}}, \quad r_{\text{el}} = r_{f,\text{el}} - r_{r,\text{el}} \quad (10.12.3)$$

Here, $r_{f,\text{el}}$ and $r_{r,\text{el}}$ are the total (summed over all the reactions) rates of ionization and deionization. The function Λ_{el} is determined by the contributions of various processes

$$\Lambda_{\text{el}} = \Lambda_{\text{el}}^{(T,T_{\text{el}})} + \Lambda_{\text{el}}^{(T_l^{(v)},T_{\text{el}})} + \Lambda_{\text{ion}} \quad (10.12.4)$$

Here, we have written only one term of each type; in the general case by this term is meant the sum over the corresponding processes of the same type. The first two terms are determined by energy exchange between the electronic gas and the external or internal (with the temperature $T_e^{(v)}$) degrees of freedom. In the general case they include also individual quantum levels, if their distributions within their groups are different from the Boltzmann distribution. Reasoning in the same fashion as in deriving Equation 10.4.2, we can present these terms in the following schematic form:

$$\Lambda_{\text{el}}^{(m)} = k \frac{T_m - T_{\text{el}}}{\tau_{\text{el}}^{(m)}}, \quad T_m = T, T_l^{(v)} \quad (10.12.5)$$

Here $\tau_{\text{el}}^{(m)}$ are relaxation times and $\tau_{\text{el}}^{(m)} \sim n_{\text{el}}^{-1}$, since $\Lambda_{\text{el}}^{(m)} \sim n_{\text{el}}$. The last term of the sum 10.12.4 is caused by the electron energy variation due to their formation and disappearance in the ionization and deionization processes; by analogy with 10.11.9, we write it in the schematic form as follows:

$$\rho \Lambda_{\text{ion}} = k N_0 (T_{f,\text{el}} r_{f,\text{el}} - T_{r,\text{el}} r_{r,\text{el}}) \quad (10.12.6)$$

Here, $T_{f,\text{el}}$ and $T_{r,\text{el}}$ are the mean temperatures of the produced and disappeared electrons; as in the case of molecular vibration energies (Section 10.11), they are not equal to the local temperatures T and T_{el} , since in the ionization and deionization processes the preferential appearance and disappearance of electrons with energy different from the mean energy is possible. Generalizing the reasoning of Section 10.11 we note that the reverse reaction rate $r_{r,\text{el}}$ and the function $T_{r,\text{el}}$ must depend on the temperatures T and T_{el} only, while the functions $r_{f,\text{el}}$ and $T_{f,\text{el}}$ must in the general case depend also on the degree of the electron excitation of the interacting particles, by analogy with formula 10.11.10.

However, it should be noted that in gas dynamic problems related with flows around bodies or channel flows in the absence of electromagnetic fields (which transmit energy to the flow mainly by means of electrons), the equations obtained are seldom used in full measure. Most commonly, we restrict ourselves to some suitable approximation based on the limiting properties of some terms entering in 10.12.5. For example, based on the fact that the rate

of the energy exchange between electrons and one of the l -th molecular-vibrational modes ($V-T_{el}$ exchange) is usually greater than that for other modes, we can assume $T_{el} = T_l^{(v)}$, thus excluding Equation 10.12.4 from the system of the governing equations.

10.13 Conclusion

In conclusion, we will make some notes on the physicochemical model of nonequilibrium gas mixtures outlined previously. In determining the right-hand sides of the physicochemical kinetics equations, only their general structure was elucidated; some details of this structure were determined to a greater (Sections 10.10 and 10.11) or a smaller (Section 10.12) degree, accurate to coefficients, either constant or variable. The structures of these coefficients can, in their turn, be specified within the framework of the corresponding physical theories (this was partially done previously); however, ultimately they are determined from a comparison with experimental data.

In such experiments, optical or electrophysical techniques are used to measure only a restricted number of parameters, such as the density, temperature, electron concentration, and so on; the measurements are usually performed in the relaxation zones behind shock waves (cf. Sections 10.4 and 11.5) and, more rarely, in expansion flows, for example, in nozzles (Section 11.11). Isolated full-scale experiments on vehicles reentering in the terrestrial atmosphere are also known. The required information on the reaction rates is determined from the comparison with the solution of the corresponding problems. Because of this, the ultimate result is often dependent on an apriopi structure of the formulas, which is at the heart of the calculation.

In particular, in the formulas obtained in Section 10.11 the functions $B(T)$, the coefficients α , β , and γ , and, possibly, the number m are to be determined (the situation with the coefficient α is simpler, since, in view of the closeness of the values ε_a and ε_D , as mentioned previously, we may assume that $\alpha = 1$). If need be, the number of these coefficients could be appreciably increased by making the structure of the corresponding formulas more complicated, in particular, by allowing for additional physical effects. For example, effective values of the reaction rates can depend not only on the kind of auxiliary particles, but also on their excitation degree.

The factors of this kind are usually uncontrolled and manifest themselves in various ways in different experiments, which results in a wide scatter in the published data on reaction rates. At the same time, taking account of additional factors in the structures of the formulas for reaction rates requires determining their coefficients considerably wider sets of experiments over wide parameter ranges, which can frequently be beyond the scope of technical possibilities.

We also note that the attractive possibility of representing the reaction rates in the form of general formulas (of the type of those derived in Sections 10.10 and 10.11), is not necessarily the case; thus, it does not exist in describing the molecule and atom ionization in accordance with schemes 1 to 5 of the list 10.5.7. The point is that, due to the great difference between the energies of neighboring lower electronic levels, the excitation and particle ionization rates are comparable, so that, in the absence of their equilibrium with the external degrees of freedom, we cannot ascribe any single temperature to the set of electronic states. In this case, nonequilibrium ionization is described using formulas 10.11.1 together with the solution of the level-by-level relaxation equation for the level populations (the stepwise

ionization mechanism). Moreover, in Chapter 14 we shall show that the nonequilibrium ionization processes are appreciably affected by radiation of atoms and molecules.

In principle, similar effects must also accompany associative ionization (e.g., 6 to 8 in list 10.5.7), since the ionization rate depends on the excitation degree of the electronic states of N and O atoms. However, owing to the absence of reliable information on this question, these effects are not usually taken into account. For the same reason, the possible effect of the electronic excitation of molecules on the reaction rates is taken into consideration only very rarely.

A lot of similar examples could be given; in particular, all these notes are to an even greater degree true for the electronic (Section 10.12) or radiating (Chapter 14) gas relaxation processes.

For the previously discussed reasons, the published data on the reaction rates and the scale times of physical processes are quite frequently contradictory to one another, are not of ultimate nature, and necessitate supplementary testing; for this reason, they have not been presented here. On this point, we restrict ourselves only to the references made in Section 10.1.

11

Nonequilibrium Gas Flows

Chapter 10 was devoted to the physical models of nonequilibrium gases. In what follows, we will study the purely gas dynamic features of relaxing gas flows. Nonequilibrium effects, as well as those of viscosity, manifest themselves usually at small gas densities, say, at $H \geq 50$ km for bodies of standard dimensions in the atmospheric flight, the two effects often appearing simultaneously. As the viscous flows will be reviewed in the subsequent chapters, we defer an analysis of such situations until then. We note that methodically the main nonequilibrium gas dynamic effects can be established with reference to the example of the very simple three-parameter gas model of Section 10.3, which involves only one kinetic variable λ , along with two basic variables (the pressure p , the temperature T or the enthalpy h , etc.). In many cases, we will restrict ourselves to this model, using the more exact data on the flows of nonequilibrium multicomponent gas mixtures (usually, the air) for the purpose of illustration.

11.1 Equations of Nonequilibrium Gas Flows

For inviscid flows these equations can be written in the following general form:

$$\rho \frac{d\vec{U}}{dt} = -\text{grad}p \quad (11.1.1)$$

$$\frac{d\rho}{dt} + \rho \text{div}\vec{U} = \frac{\partial \rho}{\partial t} + \text{div}\rho\vec{U} = 0 \quad (11.1.2)$$

$$\frac{dh}{dt} - \frac{1}{\rho} \frac{dp}{dt} = \frac{de}{dt} + p \frac{d\rho^{-1}}{dt} = q \quad (11.1.3)$$

$$\rho = \rho(p, T, \lambda_n) = \frac{p\bar{M}}{RT}, \quad \frac{1}{\bar{M}} = \sum_i \frac{c_i}{\bar{M}_i}, \quad h = h(T, \lambda_n) \quad (11.1.4)$$

$$\frac{d\lambda_i}{dt} = \Lambda_i(p, T, \lambda_n) \quad (11.1.5)$$

This system differs from that for equilibrium gas flows, as described earlier, by the more general form of the equations of state 11.1.4 and the presence of the relaxation Equations 11.1.5 for the kinetic variables λ_i (here, λ_n is considered to mean the total set of the parameters λ_i), that is, the mass concentrations c_i of the components, the populations of quantum levels for individual groups of the degrees of freedom or the temperatures of these groups (if they are in internal equilibrium; see Section 10.7), the electronic gas temperature T_{el} , and so on. The form of the generating, or source, functions Λ_i was determined in Chapter 10.

The general formulation of gas dynamic problems for this case differs from that presented in Section 1.11 and the subsequent chapters only by the need to specify some initial distributions of the parameters $\lambda_i = \lambda_{i0}$ for all individual species.

We recall that the Bernoulli integral $h + U^2/2 = H$ obtained in Section 2.2 for steady-state adiabatic flows in which the total enthalpy H is constant along streamlines, is also valid for nonequilibrium adiabatic flows.

Other integrals of the governing equations include the conservation conditions 10.5.3 and 10.5.5; in these integrals, the independent species of the mixture must include differently excited atoms and molecules or their ions. Since these conditions are satisfied in each individual s -th reaction governed by Equation 10.9.4, they hold automatically in the solutions of systems 11.1.5 at the given initial data $\lambda_i = \lambda_{i0}$. Using these integrals, the number of the equations can be reduced, which is done sometimes in the process of their solution.

Equations 11.1.5 can have different forms: thus, the right-hand sides Λ_i of the equations of Section 10.9 determined by formulas 10.9.3, 10.9.4, and 10.9.7 are expressed in terms of the partial pressures p_i or the molar concentrations x_i , while on the left-hand sides of those equations we have $\lambda_i = c_i$. We will also express the equations in terms of *mass-molar concentrations* $\kappa_i = c_i/\bar{M}_i = x_i/\bar{M}$. These variables are convenient, in particular, for describing gas mixtures with highly differing molecular masses of various components (including the electronic gas with the negligible mass fraction c_i). In this case, in view of 10.9.3, Equation 10.9.4 takes the form:

$$\begin{aligned} \rho \frac{d\kappa_i}{dt} &= \sum_s \Delta v_{is} r_s, \quad r_s = X_s \Phi_s, \quad \Delta v_s = \sum_i \Delta v_{is} \\ X_s &= k_{rs}(p\bar{M})^{\beta_s} \prod_i \kappa_i^{v'_{is}}, \quad \beta_s = \sum_i v'_{is} \\ \Phi_s &= K_s - (p\bar{M})^{\Delta v_s} \prod_i \kappa_i^{\Delta v_{is}} = p^{\Delta v_s} \Phi_s^* \\ \Phi_s^* &= \bar{M}_e^{\Delta v_s} \prod_i \kappa_{ie}^{\Delta v_{is}} - \bar{M}^{\Delta v_s} \prod_i \kappa_i^{\Delta v_{is}}, \quad \bar{M}^{-1} = \sum_i \kappa_i \end{aligned} \quad (11.1.6)$$

Here, for the sake of simplicity it is assumed that $\tilde{K}_s = K_s(T)$.

The stoichiometric coefficients v'_{is} and the differences Δv_{is} were introduced in Section 10.6. From the condition $\Phi_s = 0$ the equilibrium constant $K_s(T)$ can be expressed in terms of the local equilibrium parameters $\kappa_{ie}(p, T)$.

In accordance with 10.6.15 and 10.6.16, for reactions of dissociative type 10.5.9 and exchange reactions 10.5.10 we have

$$\Delta v_s = 1, \quad \beta_s = 2 \quad \text{for} \quad (10.5.9)$$

$$\Delta v_s = 0, \quad \beta_s = 2 \quad \text{for} \quad (10.5.10) \quad (11.1.7)$$

It can be shown that the function Φ_s^* is reduced by successive substitutions $\kappa_{ie} = \kappa_i + (\kappa_{ie} - \kappa_i)$ to a sum of the differences $\kappa_{ie} - \kappa_i$ with the corresponding coefficients, which leads to an equation of type 10.4.3

$$\frac{d\kappa_i}{dt} = \sum_k \frac{\kappa_{ke} - \kappa_k}{\tau_{ik}} \quad (11.1.8)$$

Here, cumbersome expressions for τ_{ik} are omitted. In some cases, the equations written in this form can conveniently be solved. However, the parameters τ_{ik} thus introduced may be called relaxation times only conditionally, since they are not related with any particular processes.

In this regard, an exception is furnished by unit, or isolated, reactions, for which the sum over s in Equation 11.1.8 is reduced to a single term.

By way of illustration, we will consider the dissociation or ionization reactions proceeded by scheme 10.2.4 or 10.5.9, $AB + M = A + B + M$, provided that these species do not take part in other reactions proceeding in the gas mixture and the *mixture* of A and B particles is *stoichiometric* in the sense that these particles can unite to form AB particles without a balance. Then we have $\kappa_A = \kappa_{AB}$, while from condition 10.5.3 it follows that $\kappa_A + \kappa_{AB} = \kappa_{Ae} + \kappa_{ABe}$. In this case, letting $\kappa_{AB} = \kappa_1$ and $\kappa_A = \kappa_2$, we can bring Equation 11.1.6 into the form:

$$\frac{d\kappa_2}{dt} = \frac{\kappa_{2e} - \kappa_2}{\tau}, \quad \frac{1}{\tau} = k_r^{\text{eff}} p^2 R T \bar{M}_e \kappa_M E$$

$$\kappa_{1e} E = \bar{M} \kappa_1 (\kappa_{2e} + \kappa_1) + \bar{M} \kappa_2 (1 - \bar{M} \kappa_{1e}) \quad (11.1.9)$$

Here, k_r^{eff} is the effective reaction rate constant (of type 10.9.8) and κ_M is the concentration of the entire set of third particles M taking part in the reaction. The parameter τ has the meaning of the relaxation time; however, as distinct from τ in Equation 10.4.10 for the relaxation of internal degrees of freedom, the former is also dependent on the concentrations of the species taking part in the reaction. Using 11.1.6 for \bar{M}^{-1} and condition $\kappa_1 + \kappa_2 = \kappa_{1e} + \kappa_{2e}$, it can easily be shown that $\bar{M}^{-1} - \kappa_{1e} > 0$ and, hence, $E > 0$. Moreover, the positiveness of τ follows directly from physical considerations.

11.2 Limiting Flow Regimes

In Section 10.4 we gave the mathematical form to the notions of the frozen and equilibrium flows with reference to the particular example of the three-parameter gas, the state of which is determined by the basic parameters p and T and a single kinetic variable λ ; they were also associated with the limiting solutions of the relaxation equations that reduce the equations of state to conventional two-parameter equations. In the following we will generalize these results to multicomponent systems. To do this, we write Equation 11.1.5 in the following general form (taking Equation 11.1.6 into account):

$$\frac{d\lambda_i}{dt} = \Lambda_i = B_i \sum_s \Delta v_{is} \frac{\Omega_s}{\tau_s} \quad (11.2.1)$$

Here, τ_s are the parameters that, as distinct from τ_{ik} in 11.1.8, have the meaning of the relaxation times for individual physicochemical processes, while the functions Ω_s are made bounded by certain normalizing of the functions Φ_s and vanish at equilibrium simultaneously with Φ_s and the parameters χ_s introduced in Section 10.6. The coefficients B_i reflect the specific features of the parameters λ_i (e.g., $B_i = \bar{M}_i$ for $\lambda_i = c_i$ and $B_i = 1$ for $\lambda_i = \kappa_i$).

Furthermore, let $t_0 = L/U$ be a certain gas dynamic scale time (introduced in Sections 1.1 and 10.4) having the meaning of the stay of a fluid particle with a velocity U in a flow domain of extent L . Then the variations of the parameters in this domain are of the order

$$\Delta \lambda_i \sim t_0 \Lambda_i \quad (11.2.2)$$

and, as in Section 1.4, the following limiting situations are possible.

11.2.1 Frozen Flow

Let the following condition be fulfilled

$$t_0 \ll \tau_{\min} = \min \tau_s \quad (11.2.3)$$

Then the solution of system 11.2.1 as $t_0/\tau_{\min} \rightarrow 0$ is represented by the constant *frozen* quantities $\lambda_i = \lambda_{i0}$, with the same consequences as in Section 10.4. Obviously, the parameters can remain constant only in flow regions of restricted extent, $L \ll U\tau_{\min}$, which is not fulfilled, for example, in the far wake downstream of a body. Because of this, in the general case we can speak only of a *frozen approximation* for the solution of the relaxation equations. An exception can be provided only by the *hardening* effect considered in Section 11.11; this is the case of gas expansion into a vacuum, where the parameters τ_s increase with the size L , condition 11.2.3 being continuously fulfilled. Conditions 11.2.3 can also be violated in the vicinity of stagnation points of flows; in this case the flow can, on the contrary, be near equilibrium, which will be proved in what follows.

In the frozen state, a moderately dense gas behaves as a perfect gas, so that the equations of state of Section 10.3 can be cast to the form:

$$\begin{aligned} h &= c_p^{(0)} T + h_f, & h_f &= \sum_i c_i (e_i^{(v)} + h_{0i}) \\ \frac{p}{c_p^{(0)} \rho T} &= \frac{R}{\bar{M} c_p^{(0)}} = \frac{\gamma_f - 1}{\gamma_f}, & \gamma_f &= \frac{c_p^{(0)}}{c_v^{(0)}} \\ c_p^{(0)}, \bar{M}, h_f, \gamma_f &= \text{const} \end{aligned} \quad (11.2.4)$$

Here, $c_p^{(0)}$, $c_v^{(0)}$, and h_f are the *frozen specific heats* and the bound energy of physicochemical transformations, while γ_f is the *frozen adiabatic exponent* presented in Figure 1.10 (Section 1.3). Using then the adiabatic equation $\rho dh = dp$, the relations $p \sim \rho_f^\gamma$ and $T \sim p^{(\gamma_f-1)/\gamma_f}$ can be easily derived. They are analogous to Equations 1.5.9 from Chapter 1; however, in this case T cannot be replaced by h .

Obviously, the frozen flow model is simple only in the case in which its intrinsic parameters h_f and γ_f are the same throughout the entire flow, as is the case in the uniform flow of the cold atmospheric air past bodies in the absence of reactions in the shock layer. In the general case, in different flow regions the gas is differently frozen, so that the flow becomes nonuniform in this sense.

11.2.2 Equilibrium Flows

Equation 11.1.5 describes nonequilibrium flows in general, so that equilibrium processes must be described by these equations as particular limiting solutions corresponding to very rapidly proceeding reactions, that is, under the conditions

$$t_0 \gg \tau_{\max} = \max \tau_s \quad (11.2.5)$$

Estimate 11.2.2 leads in this case to an absurd situation; because of this, we will proceed from the assumption that the increments $\Delta\lambda_i$ are finite over the time interval t_0 . Then multiplying Equations 11.2.1 by the ratio τ_{\max}/t_0 and letting this ratio to tend to zero, we bring system 11.2.1 into an algebraic system, homogeneous with respect to the functions Ω_s . This system is satisfied by the equilibrium conditions $\Omega_s = 0$, of which, in accordance

with Section 10.6, only $L = I - J$ conditions are independent (here, I is the number of the components and J is the number of the additional constraints, or conservation conditions 10.5.3 or 10.5.5). This solution is realized for so vast a majority of the processes satisfying conditions 11.2.5, that it is usually assumed to be the only possible one.

At the same time, from neither a formal nor physical standpoint we can eliminate in the general case the existence of nontrivial solutions $\Omega_s \neq 0$ of system 11.2.1 with the dropped derivatives on the left-hand side. The examples of such *quasistationary* but nonequilibrium as a whole *processes* will be presented in what follows.

We recall (see Section 10.4) that, as distinct from the equilibrium state, the reaction rates in an equilibrium process are nonzero

$$\begin{aligned} \Lambda_i \approx \frac{d\lambda_{ie}}{dt} &= \left(\frac{\partial \lambda_{ie}}{\partial p} \right)_T \frac{dp}{dt} + \left(\frac{\partial \lambda_{ie}}{\partial T} \right)_p \frac{dT}{dt} = \\ &= \left(\frac{\partial \lambda_{ie}}{\partial p} \right)_s \frac{dp}{dt} + \left(\frac{\partial \lambda_{ie}}{\partial s} \right)_p \frac{ds}{dt} \end{aligned} \quad (11.2.6)$$

These rates can vanish simultaneously only if p and T are constant, that is, in an equilibrium state.

These formulas also determine the order of the increments $\Delta\lambda_i \approx \Delta\lambda_{ie}$, which turns out to be different from the general estimate 11.2.2, the latter being valid only for processes fairly far from equilibrium.

The results obtained make it possible to evaluate the accuracy of the fulfillment of the equilibrium conditions in a near-equilibrium process in terms of the gradients of the main flow parameters as follows

$$\Omega_s \sim \tau_{\max} \max(d\lambda_{ie}/dt) \quad (11.2.7)$$

These estimates generalize those obtained in Section 10.4 ($\lambda_e - \lambda \sim \tau d\lambda_e/dt$, formulas 10.4.14).

We note that near-equilibrium processes can be realized only in the regions with a smooth and rather slow variation of the flow parameters, so that physicochemical processes have time to adjust themselves to these variations. However, this requirement is not fulfilled at an abrupt change in the flow parameters, for example, across a shock wave, downstream of a bend in the body contour, and so on. In this case, relaxation zones appear in the flow; however, when the general condition $L \gg U\tau_{\max}$ is fulfilled, their relative dimension $\Delta L/L \sim \tau_{\max}/t_0$ is small and these zones have no effect on the flow as a whole. These issues will be analyzed when studying some particular types of nonequilibrium flows.

We will now consider the more general case of a *partially equilibrium* system, in which only a part of the processes with the numbers $s \leq m$ are at equilibrium, their relaxation times satisfying the condition

$$\tau_s \leq \tau^{\max} \ll t_0, \quad s = 1, \dots, m \quad (11.2.8)$$

The unconventional nature of this situation manifests itself in the fact that even if we have only one small parameter $\tau = \tau_k \rightarrow 0$, all the equations of system 11.2.1 involving this parameter degenerate to the same equation $\Omega_k = 0$, so that the system is undetermined. To avoid this situation, the expression for the term Ω_k/τ_k from one of the Equations 11.2.1 should be substituted into other equations, while the equation itself should be replaced by the equation $\Omega_k = 0$. Applying this procedure successively to the system with several

near-equilibrium processes we can reduce it (with the corresponding numbering of the variables λ_i) to the form:

$$\frac{d\lambda_i}{dt} + \sum_{k=1}^m A_{ik} \frac{d\lambda_k}{dt} = \sum_{s>m} C_{is} \frac{\Omega_s}{\tau_s} \quad (i = m+1, \dots, I) \quad (11.2.9)$$

Here, m is the number of independent near-equilibrium processes with the minimum values of the parameters $\tau_s = \tau_k$, while A_{ik} and C_{is} are certain constant coefficients; their constancy is due to the fact that in different equations the terms corresponding to the same s -th reaction differ, by virtue 10.9.4, only by the constant factors B_i and $\Delta\nu_{is}$. Together with the equilibrium conditions $\Omega_k = 0, k \leq m$, these equations form a closed system of equations that does not contain indeterminate terms.

The opposite case in which the first s reactions are frozen, while the others are arbitrary, leads generally only to the situation in which a part of the terms on the right-hand sides of Equation 11.2.1 are dropped. A qualitative simplification of the problem can be obtained only if some species i is formed as a result of only one reaction, which is frozen under the given conditions; this gives the solution $\lambda_i = \lambda_{i0} = \text{const}$.

We will also consider the *equilibrium-frozen* processes, in which the reactions with the numbers $s \leq m$ are equilibrium, while the other processes entering into the right-hand sides of Equation 11.2.9 are frozen with the scale times

$$\tau_s^{(\min)} \gg t_0, \quad s \geq m+1 \quad (11.2.10)$$

Then Equation 11.2.9 is homogeneous and has the integrals

$$\lambda_i + \sum_{k=1}^m A_{ik} \lambda_k = \lambda_{i0} + \sum_{k=1}^m A_{ik} \lambda_{k0} = \text{const} \quad (i = m+1, \dots, I) \quad (11.2.11)$$

Together with the equilibrium conditions $\Omega_s = 0, s \leq m$, this leads to the limiting equilibrium frozen solutions of the type

$$\lambda_i = \lambda_{ie}^{(m)}(p, T, \lambda_{j0}) \quad (i, j = 1, \dots, I) \quad (11.2.12)$$

However, as distinct from the local-equilibrium functions λ_{ie} , the newly introduced functions $\lambda_{ie}^{(m)}$ are dependent not only on p and T but also on the initial set of the parameters λ_{i0} at the point of partial freezing of the flow.

11.2.3 Isentropicity of the Limiting Flows

Previously we did not mean that the flow is adiabatic, so that the results obtained are in this sense of a general nature. Let now the flow be adiabatic ($q = 0$). Then extending in Equation 10.6.19 the designations χ_s and dR_s to the similar terms of the second sum and, correspondingly, expanding the numbering of the processes, and taking Equation 10.9.4 into account, we obtain the following expression for the time derivative of the entropy

$$\frac{ds}{dt} = \sum_s \chi_s \frac{dR_s}{dt}, \quad \frac{dR_s}{dt} = \frac{r_s}{\rho} = \frac{\Omega_s}{\tau_s} \quad (11.2.13)$$

For the sake of brevity, we will immediately consider the general equilibrium-frozen process subject to conditions 11.2.8 and 11.2.10. In this case, the derivatives dR_s/dt are finite

for the first m processes, but the parameters χ_s are small, together with Ω_s and the ratios $\tau^{(\max)}/t_0$, while for the other processes the derivatives $dR_s/dt \sim 1/\tau^{(\min)}$ are small. Finally, we obtain the following estimate for the entropy increment in these processes

$$\Delta s \sim \frac{\tau^{(\max)}}{t_0} + \frac{t_0}{\tau^{(\min)}} \ll 1 \quad (11.2.14)$$

which in the limit ensures the isentropic nature of equilibrium-frozen flows. Only the first term should be left in the sum 11.2.14 for purely equilibrium processes and only the second term for purely frozen ones.

At the same time, an actual nonequilibrium process can be associated with *locally equilibrium entropies*

$$s_e(f, \varphi) = s[f, \varphi, \lambda_{ie}(f, \varphi)], \quad f, \varphi = p, T; \quad p, h; \quad \rho, e \quad (11.2.15)$$

where $\lambda_{ie}(f, \varphi)$ are the locally equilibrium concentrations introduced in Section 10.4 and corresponding to a given pair of the basic variables f and φ ($\lambda_{ie}(p, s), \lambda_{ie}(\rho, s)$, and so on, can also be added to usual $\lambda_i(p, T)$). In the general case, all of the previously mentioned quantities of the same name do not coincide but in a completely near-equilibrium process with $\tau^{(\max)} = \tau_{\max}$ all the differences $\lambda_i - \lambda_{ie}(f, \varphi) \leq \varepsilon \ll 1$ are small. Therefore, in accordance with 10.6.27, the entropies $s_e(f, \varphi)$ are equal to each other and the local entropy s correct to the second ε^2 order. As regards estimate Equation 11.2.14, it relates to the increments $\Delta s_e(f, \varphi) \sim \tau_{\max}/t_0$.

We dwell on one more property of the entropy in equilibrium-frozen systems. Let a certain, initially frozen, $(m+1)$ -th adiabatic process be allowed to proceed approaching to an equilibrium process, while the other processes are in equilibrium. In accordance with the second law of thermodynamics, this is accompanied by an increase in the entropy from s_m to s_{m+1} . In other words, replacing any frozen process by an equilibrium one results in an increase in entropy, that is, for a given sequence of "defreezing" the processes the following sequence of inequalities holds

$$s_e \geq s_L \geq s_{L-1} \geq \cdots \geq s_{m+1} \geq s_m \geq \cdots \geq s_1 \geq s_f \quad (11.2.16)$$

where the subscripts refer to the numbers of equilibrium processes, while s_f is the initial energy of the fully frozen process.

11.2.4 Quasistationary Solutions

Equilibrium or partially equilibrium solutions are *degenerate*, since the corresponding partial differential equations of kinetics degenerate into ordinary equations, totally or partially, though in the latter case the flow remains nonequilibrium as a whole. However, even the solutions, which do not involve equilibrium at all, can be degenerate. We will show this with reference to the example of the relaxation Equations 10.11.9 and 10.12.2 written in the form:

$$\frac{d\lambda_i}{dt} = \frac{\Omega_i^{(T)}}{\tau_T} + \frac{\Omega^{(w)}}{\tau_w} \quad (11.2.17)$$

Here, the first term is responsible for collisions, while the second term is caused by the formation of component λ_i due to other factors and τ_T and τ_w are the scale times of these processes. The structures of the terms $\Omega^{(T)}$ and $\Omega^{(w)}$ are determined by comparison with the previously mentioned equations.

Let now these two scale times be small compared to the gas dynamic time, $\tau_T, \tau_w \ll t_0$, but be comparable with each other. Then Equation 11.2.16 may have a degenerate solution, which in the general case can differ from the equilibrium one

$$\tau_w \Omega^{(T)} + \tau_T \Omega^{(w)} = 0 \quad (11.2.18)$$

These regimes can also be generalized. For example, in the expression $\Omega^{(w)} = \Omega_f^{(w)} - \Omega_r^{(w)}$, where $\Omega_f^{(w)}$ and $\Omega_r^{(w)}$ are the forward and reverse reaction rates, one of the terms, say $\Omega_f^{(w)}$, can under given conditions turn out to be negligible. Then, instead of condition 11.2.18, we obtain $\tau_w \Omega^{(T)} = \tau_T \Omega_r^{(w)}$.

These regimes are also called *quasistationary*. They can be realized, for example, when excitation of vibrational or electronic levels of molecules is offset by their dissociation, ionization, or photoquenching (cf. Section 10.12). The examples will be presented in the following, in analyzing particular problems. We underline that these solutions represent only intermediate asymptotics of the solution as a whole, which approaches equilibrium, as $t \rightarrow \infty$, while $\tau_w \neq 0$ and $\tau_T \neq 0$.

In conclusion, we call attention to the distinctive features of numerical algorithms for near-equilibrium flows. The equality $\Omega_s \approx 0$ (usually approximate) or, to be more precise, the condition $\Omega_s \sim \tau_s \ll t_0$ is due to the mutual compensation of two terms in the quantities Φ_s in Equation 11.1.7, that is, by the smallness of the difference between two large quantities; this is open to great computational errors, if only the proper algorithms are not involved (see Voronkin, 1970).

11.3 Limiting Speeds of Sound and Their Hierarchy

In Section 1.6 the speed of the small perturbation propagation was determined as the limit

$$a^2 = \lim_{\Delta p, \Delta \rho \rightarrow 0} (\Delta p)/(\Delta \rho) = \partial p / \partial \rho \quad (11.3.1)$$

The derivative on the right-hand side of this formula is specified in accordance with the nature of a particular process in the sound wave. In the same section, we introduced by formulas 1.6.16 two limiting speeds of sound, namely, the isentropic speed a_e and the isothermal speed a_T ; they correspond to the processes of the same name in a simple two-parameter gas with the equation of state of the form $\rho = \rho(p, s)$ or $\rho = \rho(p, T)$. In the general case, the equations of state involve also the kinetic variables λ_i , whose behavior in the sound wave must be known for determining the derivative $\partial p / \partial \rho$.

We will choose the equation of state in the form $\rho = \rho(p, s, \xi_l)$, where ξ_l is the system of independent generalized kinematic variables introduced in Section 10.6. In these variables, the density differential takes the form:

$$d\rho = \rho_p^{(s, \xi)} dp + \rho_s^{(p, \xi)} ds + d\omega$$

$$d\omega = \sum_l \rho_{\xi l}^{(p, s)} d\xi_l, \quad \rho_{\xi l} = \frac{\partial \rho}{\partial \xi_l}, \quad \rho_\alpha^{(\beta, \gamma)} = \left(\frac{\partial \rho}{\partial \alpha} \right)_{\beta, \gamma} \quad (11.3.2)$$

In the absence of external heat sources, a discontinuity front is adiabatic as a whole and, as shown in Section 3.2, dissipative effects within the front, including the acoustic one,

are concentrated in a narrow zone of the order of the molecular free path; we will assume this width to be small compared with the general flow scale length. On the basis of this assumption, in Section 1.6 we determined the isentropic speed of sound a_e for the equilibrium equation of state $\rho = \rho(p, s)$ as a function of the gas state. In what follows, we demonstrate that similar speeds of sound, dependent on the gas state only, can also be determined for multicomponent media, though only for the limiting, in the sense of Section 11.2, processes, that is, frozen, equilibrium, and equilibrium-frozen ones. As shown in Section 11.2, these processes are isentropic, so that for them the differential ds drops out of expansions 11.3.2; in this sense, these speeds of sound are also isentropic, as distinct from the isothermal speed of sound a_T , which was treated at the end of Section 1.6.

Let physicochemical processes in the sound wave proceed so slowly that they can be regarded as frozen; then the increments $\Delta\xi_l$ in them can be taken to be zero: $\Delta\xi_l = 0$. Then from Equation 11.3.2 we obtain the expression for the *frozen speed of sound* a_f

$$\frac{1}{a_f^2} = \rho_p^{(s,\xi)} = \left(\frac{\partial \rho}{\partial p} \right)_{s,\xi} \quad (11.3.3)$$

Let now, on the contrary, the previously mentioned processes in the sound wave proceed so rapidly that they can be regarded as equilibrium. In this case, we can let $\xi_l = \xi_{le}(p, s)$ and $\rho = \rho(p, s)$. Then from Equation 11.3.2 we obtain the expression for the *equilibrium, or isentropic, speed of sound* a_e

$$a_e^{-2} = \left(\frac{\partial \rho}{\partial p} \right)_s = a_f^{-2} + \omega_p, \quad \omega_p = \sum_{l=1}^L \rho_{\xi l}^{(p,s)} \left(\frac{\partial \xi_{le}}{\partial p} \right)_s \quad (11.3.4)$$

Both speeds of sound are the functions of the state; however, the frozen speed of sound a_f can be determined in any case, whereas a_e can be determined only when the gas ahead of the acoustic wave is in total equilibrium.

The following theorem holds: *in an equilibrium gas the equilibrium speed of sound is always less than or equal to the frozen speed of sound*,* that is

$$a_e \leq a_f \quad (11.3.5)$$

To prove this statement we should verify that the sum ω_p in 11.3.4 is positive. Let us imagine that the differential Equation 10.6.1 is written down for the function $s = s(p, h, \xi_l)$ with the last sum replaced by sum 10.6.25. However, this relation can also be considered as an expression for the differential of the function $h(p, s, \xi_l)$ in terms of the differentials of its arguments; thence, in view 10.6.2, we obtain the reciprocity relation

$$\begin{aligned} \frac{\partial}{\partial \xi_l} \left(\frac{1}{\rho} \right)_{p,s} &= -\frac{\rho_{\xi l}^{(p,s)}}{\rho^2} = -\left(\frac{\partial TD_l}{\partial p} \right)_{s,\xi} = -T \left(\frac{\partial D_l}{\partial p} \right)_{s,\xi} \\ D_l &= s_{\xi l}^{(p,h)} = -\frac{1}{T} h_{\xi l}^{(p,s)} \end{aligned} \quad (11.3.6)$$

* On the basis of general physical considerations this assertion was substantiated by Mandelstam and Leonov (1937) and presented in Landau and E. M. Lifshitz (1983); the theoretical analysis was carried out by Napolitano (1964) and Lunev (1975).

Here, Equation 10.6.4 and the equilibrium condition $D_1 = 0$ are taken into account. However, in this case at a constant s the total derivative dD_1/dp is zero

$$\begin{aligned} \frac{dD_l}{dp} &= \left(\frac{\partial D_l}{\partial p} \right)_{s,\xi} + \sum_{k=1}^L D_{lk} \left(\frac{\partial \xi_{kl}}{\partial p} \right)_s = 0 \\ D_{lk} &= \left(\frac{\partial D_l}{\partial \xi_k} \right)_{p,s} = \left(\frac{\partial D_l}{\partial \xi_k} \right)_{p,h} \end{aligned} \quad (11.3.7)$$

Here, the latter equality for D_{lk} is obtained by differentiating the composite function $D_l = D_l(p, s, \xi_k) = D_l[p, h(p, s, \xi_k), \xi_k]$ with allowance for the equation $h_{\xi l}^{(p,s)} = 0$, which takes place at equilibrium. Eliminating the derivative $(\partial D_l / \partial p)_{s,\xi}$ from 11.3.6 and 11.3.7 we can calculate the derivative $\rho_{\xi l}^{(p,s)}$; then the function ω_p in 11.3.4 is equal to

$$\omega_p = -T\rho^2 \sum_{l=1} \sum_{k=1} D_{lk} \left(\frac{\partial \xi_{le}}{\partial p} \right)_s \left(\frac{\partial \xi_{ke}}{\partial p} \right)_s \geq 0 \quad (11.3.8)$$

The inequality in the previous formula follows from condition 10.6.27; thence follows also the inequality of Equation 11.3.5, namely $a_f \geq a_e$.

It is pertinent to remember that the similar hierarchy of the speeds of sound was already encountered in Section 1.6, where it was shown that the isothermal speed of sound a_T is always less than the isentropic one a_e (cf. formula 1.6.16).

We will now express the speeds of sound in terms of the equations of state 11.1.4 with the arguments p , T , and λ_i entering into them; we recall that almost all thermodynamic functions derived in this section, including Λ_i in Equation 11.1.5, are expressed in terms of these parameters. For this purpose, we write down the differentials

$$\begin{aligned} d\rho &= \rho_p^{(T,\lambda)} dp + \rho_T^{(p,\lambda)} dT + \sum_i \rho_{\lambda i}^{(p,T)} d\lambda_i \\ dh &= h_p^{(T,\lambda)} dp + c_p^{(0)} dT + \sum_i h_{\lambda i}^{(p,T)} d\lambda_i = \frac{1}{\rho} dp + dQ \\ dQ &= qdt, \quad c_p^{(0)} = h_T^{(p,\lambda)} \end{aligned} \quad (11.3.9)$$

Here, for the sake of generality we have taken the heat flux dQ and the term $h_p^{(T,\lambda)}$, equal to zero for Equation 11.1.4, into account. Eliminating the differential dT from the previous equations we obtain

$$\begin{aligned} d\rho &= \frac{1}{a_f^2} dp + d\bar{\omega} + \frac{\rho_T^{(p,\lambda)}}{c_p^{(0)}} dQ \\ \frac{1}{a_f^2} &= \rho_p^{(T,\lambda)} + \frac{\rho_T^{(p,\lambda)}}{c_p^{(0)}} \left(\frac{1}{\rho} - h_p^{(T,\lambda)} \right), \quad d\omega = \sum_i \delta_i d\lambda_i \\ \delta_i &= \rho_{\lambda i}^{(p,T)} - \frac{1}{c_p^{(0)}} h_{\lambda i}^{(p,T)} \rho_T^{(p,\lambda)} \end{aligned} \quad (11.3.10)$$

At equilibrium we have $\lambda_i = \lambda_{ie}(p, T)$ and in 11.3.10 it should be that

$$\begin{aligned} d\lambda_i &= \left(\frac{\partial \lambda_{ie}}{\partial p} \right)_s dp + \left(\frac{\partial \lambda_{ie}}{\partial s} \right)_p ds \\ \left(\frac{\partial \lambda_{ie}}{\partial p} \right)_s &= \left(\frac{\partial \lambda_{ie}}{\partial p} \right)_T + \left(\frac{\partial \lambda_{ie}}{\partial T} \right)_p \left(\frac{\partial T}{\partial p} \right)_s \\ \left(\frac{\partial \lambda_{ie}}{\partial s} \right)_p &= \left(\frac{\partial \lambda_{ie}}{\partial T} \right)_p \left(\frac{\partial T}{\partial s} \right)_p = \frac{T}{c_p} \left(\frac{\partial \lambda_{ie}}{\partial T} \right)_p \end{aligned} \quad (11.3.11)$$

The derivative $(\partial T / \partial p)_s$ is determined from Equation 1.6.14. Correspondingly, we have

$$\begin{aligned} d\omega &= \omega_p dp + \omega_s ds, \quad ds = T^{-1} dQ \\ \omega_p &= \sum_i \delta i \left(\frac{\partial \lambda_{ie}}{\partial p} \right)_s \\ \omega_s &= \sum_i \delta i \left(\frac{\partial \lambda_{ie}}{\partial s} \right)_p = \frac{T}{c_p} \sum_i \delta i \left(\frac{\partial \lambda_{ie}}{\partial T} \right)_p \end{aligned} \quad (11.3.12)$$

Substituting this result into 11.3.10 and comparing with Equation 1.6.8 for equilibrium gas we obtain

$$\begin{aligned} d\rho &= a_e^{-2} dp + \rho Q_e dt, \quad a_e^{-2} = a_f^{-2} + \omega_p \\ \rho Q_e &= q \left(\frac{\rho_T^{(p,\lambda)}}{c_p^{(0)}} + \frac{\omega_s}{T} \right) = q \left[\frac{\partial \rho(p, h)}{\partial h} \right]_p \end{aligned} \quad (11.3.13)$$

Thus, all the unknown quantities are expressed in terms of the derivatives of the functions of the form $f = f[p, T, \lambda_{ie}(p, T)]$ and of $\lambda_{ie}(p, T)$. Since $a_e \leq a_f$, we have also $\omega_p \geq 0$.

As shown in Section 11.2, a moderately dense gas in the frozen state behaves as a perfect gas with the frozen adiabatic exponent $\gamma_f = c_p^{(0)}/c_v^{(0)}$. Transforming formula 11.3.10 for a_f and using formulas 1.6.16 and 1.6.11 for a_e , we can write down both limiting speeds of sound in the form:

$$a_e^2 = \frac{c_p}{c_v} \left(\frac{\partial p}{\partial \rho} \right)_T = \gamma_e \frac{p}{\rho}, \quad a_f^2 = \frac{c_p^{(0)}}{c_v^{(0)}} \frac{p}{\rho} = \gamma_f \frac{p}{\rho} \quad (11.3.14)$$

where c_p and c_v are the specific heats for the equilibrium gas and γ_e is the *equilibrium coefficient of the speed of sound*. For air, both functions γ_f and γ_e are plotted in Figure 1.10 (Section 1.3), where their ratio can be as high as 1.5, the maximum value $\gamma_f = 5/3$ corresponding to monatomic gas.

We note further that the first formula 11.3.14 was derived in Section 1.6 for an arbitrary gas, if its state is dependent on p and T only; this pertains equally to all the limiting processes considered. Therefore, the speeds of sound can be determined from this formula, all the cofactors being calculated in accordance with the processes in the gas and using the equations of state for the corresponding equilibrium composition and state of the gas, that is, for $\lambda_i = \lambda_{ie}(p, T)$.

Let us carry on outlining the general theory of the speeds of sound. Along with the *total* equilibrium a_e and frozen a_f speeds of sound, a set of *equilibrium-frozen speeds of sound* $a_e^{(m)}$ corresponding to the equilibrium-frozen processes considered in Section 11.2 can also be

introduced; the number of these speeds is $2^L - 1$ including $a_e^{(L)} = a_e$. To generalize the previous theorem on the inequality $a_e \leq a_f$ we shall establish the inequality $a_e^{(m)} \leq a_f$, that is, the *equilibrium-frozen speeds of sound are always smaller than or equal to the frozen speed of sound*.

Let the first m independent processes of the chosen set L be equilibrium and correspond to the conditions $\Omega_l = 0$ or $\chi_l = 0$, where $l \leq m$, while the other $L - m$ processes are frozen and associated with the parameters 11.2.11 written down for the variables ξ_l . By analogy with 11.2.12, this process is associated with the set of the parameters $\xi_{le}^{(m)}(p, s)$ whose derivatives will enter in formula 11.3.8 for ω_p with the same coefficients D_{lk} ; therefore, the inequalities $\omega_p \geq 0$ and $a_e^{(m)} \leq a_f$ remain valid. Thus, the theorem is proved.

Another approach to the problem consists in the fact that in the analysis of the properties of the entropy carried out in Section 10.6 the frozen processes are assumed to be absent, while integrals 11.2.11 are considered additional constraints, like the mass balance equations from Section 10.5. Then only m kinetic variables with the equilibrium parameters $\bar{\xi}_{le}^{(m)}$ ($l \leq m$) are independent. In this case, the sum 11.3.8 includes only m terms, though, with other, generally speaking, coefficients \bar{D}_{lk}^m . Naturally, this change does not violate inequalities of 10.6.27 and 11.3.8, and, hence, the inequality

$$\begin{aligned} \omega_p^{(m)} &= -T\rho^2 \sum_{l=1}^m \sum_{k=1}^m \bar{D}_{lk}^{(m)} \left(\frac{\partial \bar{\xi}_{le}^{(m)}}{\partial p} \right)_s \left(\frac{\partial \bar{\xi}_{ke}^{(m)}}{\partial p} \right)_s \geq 0 \\ (a_e^{(m)})^{-2} &\leq a_f^{-2} + \omega_p^{(m)}, \quad a_e^{(m)} \leq a_f \end{aligned} \quad (11.3.15)$$

The possibility of representing the speed of sound in the form of a determinate function of the state is exhausted by the previously listed limiting cases. In the general case, the question of the actual speed and the nature of the propagation of small disturbances can be solved only on the basis of an analysis of the complete system of equations governing nonequilibrium gas flows, which will be done in Sections 11.4 and 11.6.

As for the relative hierarchy of the speeds of sound $a_e^{(m)}$, it would seem natural to expect their growth as a subsequent, hitherto equilibrium, m -th process is frozen. However, it should be noted that the inequality $a_e^{(m-1)} \geq a_e^{(m)}$ does not follow from the previous reasoning owing to the fact that the behavior of the function ω_p at the substitution of $\xi_{le}^{(m)}$ for ξ_{le} in the quadratic form 11.3.8 is unpredictable. The reduction in the number of the terms in sum 11.3.15 also does not necessarily lead to the inequality $\omega_p^{(m-1)} \leq \omega_p^{(m)}$ (an example is furnished by the quadratic form $f = (x_1 + x_2 - x_3)^2$ for all $x_i \geq 0$). Moreover, the quadratic forms $\omega_p^{(m-1)}$ and $\omega_p^{(m)}$ may be different, since in the general case they relate to gases in different states, that is, in essence, different gases with possible inequalities $\bar{D}_{lk}^{(m-1)} \neq \bar{D}_{lk}^{(m)}$ and $\bar{\xi}_{lk}^{(m-1)} \neq \bar{\xi}_{lk}^{(m)}$. Moreover, the previous analysis has not even established that the quantity $a_e = a_e^{(L)}$ is minimum, as compared with the other $a_e^{(m)}$.

However, the situations in which the freezing of a next process leads actually to an increase in the speed of sound $a_e^{(m)}$, are possible; we will assure ourselves that this is true with reference to the example of a mixture of excited atoms or molecules for which formula 11.3.14 for a_e^2 can be presented as follows:

$$\frac{p}{\rho} a_e^2 = \frac{c_p}{c_v} = \frac{c_p^{(0)} + c^{(p)}}{c_v^{(0)} + c^{(v)}}, \quad c^{(v)} = \sum_m c_m^{(v)}, \quad c_m^{(v)} = \frac{de_{me}^{(v)}}{dt} \quad (11.3.16)$$

Here, $e_m^{(v)}$ are the energies of different, m -th internal degrees of freedom; since $c_m^{(v)} > 0$ and $c_p^{(0)} > c_v^{(0)}$, for any order of freezing their sequence leads to the sequence of inequalities

$$a_e = a_e^{(1)} \leq \cdots \leq a^{(m)} \leq a^{(m-1)} \leq \cdots \leq a_f \quad (11.3.17)$$

with an ordered hierarchy of the equilibrium-frozen speeds of sound.

The discovery of more general examples is related with an analysis of fairly complicated situations in which the coefficients D_{lk} for different $l \neq k$ can be of opposite sign, as well as the coefficients $(\partial \xi_{le} / \partial p)_s$.

An exception is provided by the case in which each of the canonical variables $\tilde{\xi}_l$ introduced by Equation 10.6.29 is determined by a single, its own l -th process (either isolated from other processes or a certain exotic combined process determined in terms of "original" processes via relations of type 10.6.29), such that $\tilde{\xi}_l = \text{const}$ and $\tilde{\xi}_l = \tilde{\xi}_{le}$ when the process is frozen and equilibrium, respectively, regardless of other processes or variables $\tilde{\xi}_k, k \neq l$.

In this case, rewriting function 11.3.8 in terms of Equation 10.6.30 yields

$$\omega_p = -T\rho^2 \sum_{l=1}^L \tilde{D}_{ll} \left(\frac{\partial \tilde{\xi}_{le}}{\partial p} \right)_s^2, \quad \tilde{D}_{ll} \leq 0 \quad (11.3.18)$$

Therefore, at the freezing of each m -th process, that is, for $\tilde{\xi}_m = \text{const}$, the function ω_p may only decrease, which results in the sequence of inequalities 11.3.17.

11.4 Speed of the Propagation of Disturbances in Nonequilibrium Gases

The definition of the speed of sound in terms of the limit of the ratio $\Delta p / \Delta \rho$ in the sound wave, as given earlier in Section 1.6, gives a definite answer only in the limiting cases of the frozen and equilibrium processes in the wave; however, the question as to which speed of sound should enter in the mathematical theory of gas dynamics and determine the domains of disturbance propagation and their behavior still remains to be solved. At the same time, in the equilibrium gas dynamics the quantity a was considered to mean the equilibrium isentropic speed of sound.

To answer this question for nonequilibrium processes, we recall first that the speed of sound appears in the gas dynamic equations when the derivative of the density in the continuity equation is replaced by the derivative of the pressure in terms of formula 1.6.8 for equilibrium processes. The nonequilibrium generalization of that formula is given by Equation 11.3.10 derived previously. Dividing by dt we obtain the required equation with the same designations as in formula 11.3.10

$$\begin{aligned} \frac{d\rho}{dt} &= \frac{1}{a_f^2} \frac{dp}{dt} + \rho Q_f, \quad Q_f = Q_\Lambda + Q_q, \quad \rho Q_q = \frac{q \rho_T^{(p,\lambda)}}{c_p^{(0)}} \\ \rho Q_\Lambda &= \sum_i \delta_i \frac{d\lambda_i}{dt} = \sum_i \delta_i \Lambda_i, \quad \rho_T^{(p,\lambda)} = \left(\frac{\partial \rho}{\partial T} \right)_{p,\lambda} \end{aligned} \quad (11.4.1)$$

Substituting this result into the continuity equation, we bring it into the form similar to 2.4.1, namely:

$$\frac{1}{\rho a_f^2} \frac{dp}{dt} + \operatorname{div} \vec{U} = -Q_f \quad (11.4.2)$$

To make this representation more illustrative, we will also write down this equation for the three-parameter gas model with one kinetic variable λ and the relaxation Equation 10.4.1 for it ($q = 0$)

$$L_f = \frac{1}{\rho a_f^2} \frac{dp}{dt} + \operatorname{div} \vec{U} = -Q_\Lambda = -\frac{\delta}{\rho} \frac{d\lambda}{dt} = -\frac{\delta}{\rho} \frac{\lambda_e - \lambda}{\tau} \quad (11.4.3)$$

Clearly, these equations involve precisely the frozen speed of sound a_f .

Since the speed of sound does not enter into other gas dynamic equations at all, while the term Q_Λ , together with Λ_i , is the function of the state, which does not contain the derivatives of the unknown functions, it would suffice to let $a = a_f$ and $Q = Q_f$ in the theory of Chapter 4 in order to extend it to nonequilibrium flows. As for the kinetic equations $d\lambda_i/dt = \Lambda_i$, they enter in the second group of equations (see Sections 2.4 and 4.1), whose characteristics are particle trajectories.

Thus, precisely the frozen speed of sound enters in the equations for characteristics and determines the disturbance propagation speed and the positions of the disturbance fronts. For steady-state flows, the *frozen Mach number* $M_f = U/a_f$ determines the type of the corresponding equations, elliptic for $M_f < 1$ and hyperbolic for $M_f > 1$.

In particular, the method of characteristics is almost unchanged. From the data on the initial line AB (Figure 11.1), on which the kinetic variables λ_i should be specified in addition to those mentioned in Section 4.2, the pressure and velocity are determined at the point C using the same method. At the same time, along the streamline CD the increments $\Delta\lambda_i = \Lambda_i \Delta t$ are calculated apart from the enthalpy. We note that the theoretical domain of influence of the initial data bounded by the frozen characteristics is, in view of the condition $a_f \geq a_e$, always larger than that physically realized in the equilibrium flow ($A'B'C$ in Figure 11.1), so that the Courant criterion for the stability of the method of characteristics,

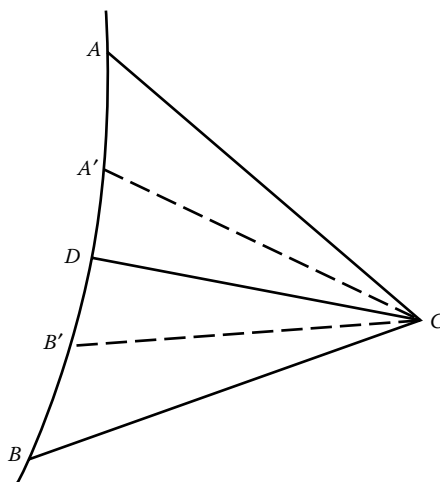


FIGURE 11.1
Equilibrium and frozen characteristics.

$a_f \Delta t \leq \Delta x$ (Section 4.2), calculated from the frozen speed of sound (or the Mach number M_f) is always sufficient for any flows.

In connection with the preceding discussion, the question arises of the equilibrium theory applicability even for the flows close to equilibrium as nearly as possible, since even for these flows the general Equation 11.4.2 still holds, the inequalities $a_f \neq a_e$ and $Q_\Lambda \neq 0$ being valid in the general case. Because of this, in order to construct the equilibrium theory, we should let by an act of will $a = a_e$ and $Q_f = Q_e$ in the continuity equation, that is, to write it as follows:

$$L_e = \frac{1}{\rho a_e^2} \frac{dp}{dt} + \operatorname{div} \vec{U} = -Q_e = - \left(\frac{\partial \rho}{\partial h} \right)_p \frac{q}{\rho} \quad (11.4.4)$$

Equation 11.4.2 could not be transformed to 11.4.4 by the formal passage to the limit (for $\tau_{\max} \rightarrow 0$ in the estimates of Section 11.2), since even at equilibrium we have, generally speaking, $a_e \neq a_f$, while the term Q_Λ is nonzero together with Λ_i and the reaction rates in the equilibrium processes. However, from the general physical considerations the possibility of using the equilibrium model under proper conditions is beyond question. In other words, in transition from the general nonequilibrium flow regime to the equilibrium one, the characteristic properties of the governing equations change abruptly.

This effect is called the *paradox of two speeds of sound*. The paradoxicality of the situation is illustrated by the following examples: for $a_e < U < a_f$ the flow is subsonic in the accurate nonequilibrium formulation and supersonic in the equilibrium formulation, which changes the type of the governing equations. For example, if disturbances introduced into a nozzle flow by a change in the nozzle contour propagate upstream through the gas at the frozen speed of sound, then they attain the nozzle throat and have an effect on the flow in its vicinity. However, if the disturbance propagation speed is equilibrium, they are convected by the flow, as is the case in the supersonic flow.

This paradox is solved in the following fashion: at the passage to the equilibrium limit, rather the solutions of the governing equation than their forms themselves are approached. It turns out that the frozen front intensity tends to zero with time, while the real disturbance front is the equilibrium one, determined by the equilibrium speed of sound. An analysis of these flows will be carried out in Sections 11.6 and 11.7.

We note in conclusion that similar paradoxes are typical of the situations with different speeds of sound relating to different fixed variables in the derivative $\partial p / \partial \rho$. In particular, it is appropriate to recall the example of the pair of the isothermal and isentropic speeds of sound satisfying the inequality $a_T < a_e$, which is the analogue of the inequality $a_e \leq a_f$.

11.5 Shock Waves and Relaxation Zones

We will now consider the physicochemical structure of a compression shock wave, to which we relate the entire gas layer confined between the entry section 1 in Figure 10.2 (Section 10.4), where the gas is undisturbed, and a certain exit section 3, where the gas is already at equilibrium. For this purpose, it would suffice, as shown in Chapter 3, to consider the parameter distributions along the normal to the front, that is, a normal stationary shock wave traveling in the gas at a velocity $v_{n1} = u_1$.

In Section 3.2 we considered the dissipative shock structure within the framework of the Navier-Stokes equations and showed that its thickness δ_v is of the order of several molecular free paths l . As shown in Section 1.4, several collisions experienced by the particles within

the dissipative shock would suffice for the establishment of the Maxwellian distribution 1.4.7, that is, for equilibrium of the translational (and rotational) degrees of freedom. The latter would, in its turn, suffice for introducing the notions of the temperature and other thermodynamic variables related to each other by equations of state. On these grounds, we assume, as it is done in the whole preceding and subsequent theory, that in the exit section of the dissipative shock there exists molecular-kinetic equilibrium of the gas that was treated in Section 1.4.

At the same time, the whole theory of Chapters 10 and 11 is based on the assumption that the scale time τ of physicochemical processes is considerably greater than the scale time $\tau_v \sim l/V$ of the collisions between individual particles (here, V is the speed of their chaotic thermal motion, which is of the order of the speed of sound). This gives a reason for considering these processes as proceeding against the background of molecular-kinetic equilibrium. Because of this, the logical consequence of this hypothesis is the following model of the shock transition consisting of two subsequent zones:

1. The frozen shock wave, that is, the zone of the shock transition itself (1–2 in Figure 10.2) including all the dissipative effects noted in Section 3.2, the physicochemical processes being frozen; and
2. The relaxation zone 2 – 3 behind the frozen shock, in which the gas attains a new state corresponding to the equilibrium shock transition.

This model of the compression wave and the wave itself are called *shock relaxation*. So far, we have not applied this term to equilibrium shock waves, since we have not taken interest in their structures.

Earlier it was assumed that the relaxation zone thickness δ_r is much smaller than the scale length L of the flow region under consideration, this giving reason for applying the model of an infinitely thin equilibrium shock transition zone. In this chapter we are mainly interested precisely in the regimes with $\delta_r \sim L$; however, up to Chapter 12, we will, as earlier, assume the actual thickness of the shock transition to be relatively small ($\delta_r \ll L$), thus representing the frozen shock wave as a mathematical surface.

The frozen shock transition is described by the same equations (3.3.3) supplemented by the equations of state

$$\begin{aligned} \rho_1 u_1 &= \rho_2 u_2, & \lambda_{n1} &= \lambda_{n2} \\ p_1 + \rho_1 u_1^2 &= p_2 + \rho_2 u_2^2, & h_1 + u_1^2/2 &= h_2 + u_2^2/2 \\ \rho &= \rho(p, T, \lambda_n), & h &= h(T, \lambda_n) \end{aligned} \quad (11.5.1)$$

Here, as before, λ_n are considered to mean the whole set of the kinetic variables that do not change in passing across the shock. If in the undisturbed flow the gas is perfect and has the adiabatic exponent γ , then it conserves this property behind the shock, the frozen exponent being $\gamma_f = \gamma$. In this case, all the relations derived in Sections 3.3 to 3.5 for a perfect gas are valid for the frozen shock front. The molecular mass of the gas mixture \bar{M} , the frozen specific heats $c_p^{(0)}$ and $c_v^{(0)}$, and the bound physicochemical energy h_f in the formula for the enthalpy $h = h_f + c_p^{(0)}T$ are conserved across the shock. Precisely this situation is typical of the conditions of the body flight in the undisturbed atmosphere.

As shown in Section 1.7, in the following relaxation zone relations 11.5.1 are valid in every section; these relations with the omitted subscript 2 are simply the integrals of the equations of the steady-state inviscid one-dimensional gas flow along the normal to the front; one can

convince oneself that this is true by omitting the dissipative terms in Equation 3.2.1. We will write these equations in the form:

$$\begin{aligned}\bar{\rho}u = u_1 &= v_{n1}, \quad \bar{\rho} = \rho/\rho_1, \quad \rho = \rho(p, T, \lambda_n) \\ \frac{p}{\rho_1} &= \bar{p} = \bar{p}_1 + u_1^2 - \bar{\rho}u^2 = \bar{p}_1 + u_1^2 \left(1 - \frac{1}{\bar{\rho}}\right) \\ h(T, \lambda_n) &= h_1 + \frac{1}{2}(u_1^2 - u^2) = h_1 + \frac{1}{2}u_1^2 \left(1 - \frac{1}{\bar{\rho}^2}\right)\end{aligned}\quad (11.5.2)$$

These relations must be supplemented by the equations of kinetics 11.1.5

$$\frac{d\lambda_i}{dt} = u \frac{d\lambda_i}{dx} = \Lambda_i(p, T, \lambda_n) \quad (11.5.3)$$

Finally, the problem is closed by conditions 11.5.1, which are automatically satisfied by relations 11.5.2.

This system describes also the steady-state relaxing flow in a constant cross-section channel; making the same transformations as in Section 2.3, but taking now Equation 11.4.3 into account, we obtain the following equation for a three-parameter gas

$$(1 - M_f^2) \frac{du}{dx} = -Q_\Lambda = -\frac{\delta}{\rho} \frac{\lambda_e - \lambda}{\tau} \quad (11.5.4)$$

This equation has a singular point at $M_f = 1$; in accordance with Section 2.3, the solution can be extended through this point only in the case in which it is made regular by turning its right-hand side to zero. In our case, this is attained under the equilibrium condition $\lambda_e - \lambda = 0$; for this reason, no relaxation zone can contain the point $M_f = 1$ within its internal region. Obviously, this condition is fulfilled in the conventional equilibrium shock, since behind the frozen front we have $M_f < 1$, while behind the equilibrium front we have $M_e < 1$ and, hence, $M_f < 1$ as well.

As $x \rightarrow \infty$, the solution of Equation 11.5.4 approaches asymptotically the equilibrium limit, since at $M_f \neq 1$ $du/dx \rightarrow 0$, as $\lambda - \lambda_e \rightarrow 0$, the latter difference decreasing exponentially (this follows from Equation 10.4.2).

The model thus formulated has the most general character and can equally be applied to shock waves in both gaseous and condensed (see Section 4.12) relaxing media; it does not involve any restrictions on the gas state ahead of the shock front, which can be both equilibrium and nonequilibrium (the latter case is considered at the end of this section).

At the same time, this model is naturally only relative and can be incomplete, for example, for gases at superhigh temperatures, at which reactions can start within the dissipative front.

The fundamental restriction of the previous shock-relaxation model is that it could be realized only for shock waves with velocities $u_1 > a_{f1}$, since the frozen shock front cannot travel at a velocity $u_1 < a_{f1}$. However, the condition $u_1 > a_{e1}$ would suffice for the existence of the resulting equilibrium shock front. Thus, the question arises of the structure of a shock wave traveling at an intermediate velocity satisfying the condition

$$a_{f1} \geq u_1 \geq a_{e1} \quad (11.5.5)$$

It turns out that in this case a continuous *relaxation compression wave* is formed instead of the shock front; this wave transforms the initial gas state to the equilibrium state behind

the shock corresponding to the given velocity u_1 . This problem can be solved (see Section 11.7), since, as the pressure increases and the velocity decreases in a compression wave, the local Mach number M_f also decreases, so that at $M_{f1} < 1$ the singular point $M_f = 1$ does not appear within the zone. At the same time, a similar continuous relaxation compression wave cannot exist for $M_f > 1$, since at $M_e < 1$ an impassable singular point $M_f = 1$ takes place inside the wave.

The presentation of the general theory of shock waves will be continued in Section 11.8; for the moment, we will consider some examples.

11.5.1 Hypersonic Shocks

At a velocity $u_1 \gg a$, the density ratio $k = \bar{\rho}_2^{-1}$ is usually fairly small (for diatomic gases it is equal to 1/6), so that the further variation of the density in the relaxation zone cannot change considerably the pressure and, the more so, the enthalpy in it. For this reason, these quantities can be considered constant in the first approximation, letting for the sake of simplicity $p = p_2$ and $h = h_2$. In this case, the solution of the problem is reduced to the solution of the relaxation equations, together with the equations of state at constant p and h . This solution can be presented in the general form, dependent on time only

$$\lambda_i = \lambda_i(t, p_2, h_2), \quad \rho = \rho(t, p_2, h_2), \quad T = T(t, p_2, h_2) \quad (11.5.6)$$

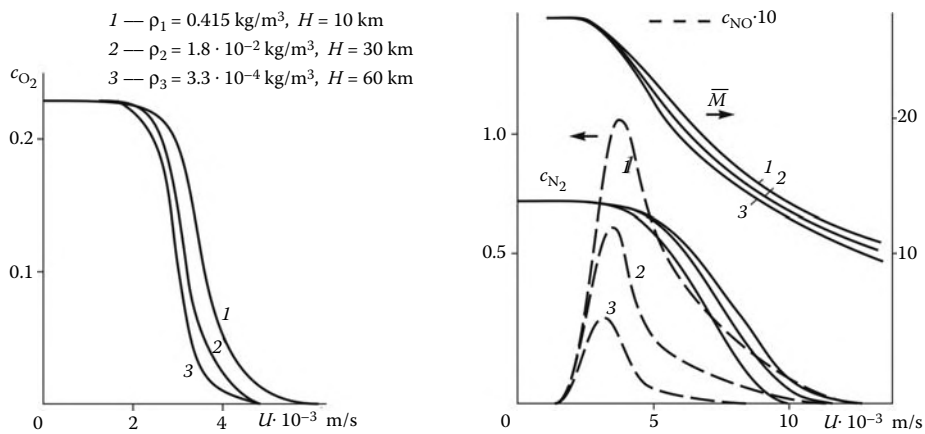
This solution does not include the velocity u , which makes it possible to extend its applicability range. The relation between t and x is determined by the equations

$$dx = u dt = \frac{u_1}{\bar{\rho}} dt, \quad x = u_1 \int_0^t \frac{dt}{\bar{\rho}} \quad (11.5.7)$$

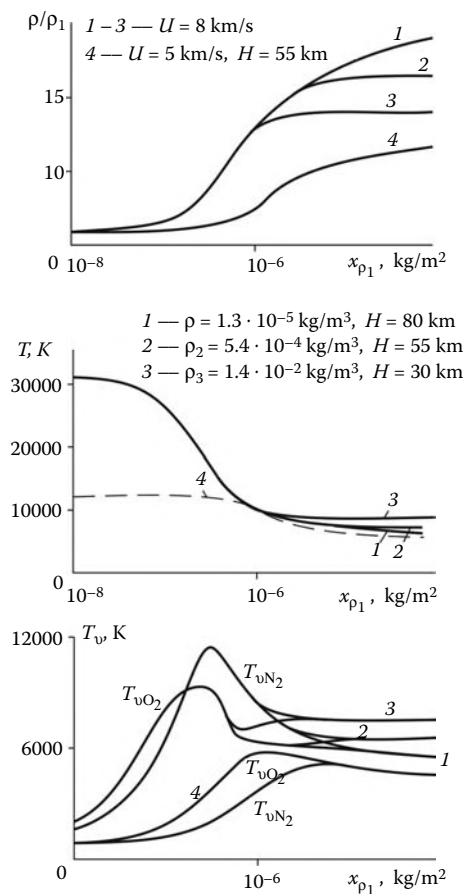
In accordance with the solution of Equation 10.4.2, all the parameters in the relaxation zone tend to their limiting equilibrium values following the power law. The dependence of these equilibrium parameters on the speed U of the shock propagation in the air atmosphere is shown in Figure 3.4 of Section 3.4 (for the density and the temperature) and Figure 11.2 (for the molecular mass and the component concentrations). Clearly, oxygen behind the shock is completely dissociated already at $U \geq 4.5$ km/sec and nitrogen at $U \geq 10$ km/sec, while the NO concentration has a maximum (up to 10%) at $U = 3 - 4$ km/sec. The molar concentration of electrons x_{el} is mainly determined by associative ionization of NO (reaction 5 in list 10.5.7) and, at higher velocities, by nitrogen and oxygen atom ionization.

The examples of the relaxation zones behind shock waves in air are presented in Figures 11.3 and 11.4 (in accordance with the model of Vlasov and Gorshkov, 2001). As in Figure 3.4, all these parameters presented in Figures 11.2 to 11.4 essentially depend on the shock velocity, that is, on the gas temperature behind the shock, while their dependence on the pressure, that is, the flight altitude H , is considerably weaker, even though the pressure may vary by a factor of 10^3 .

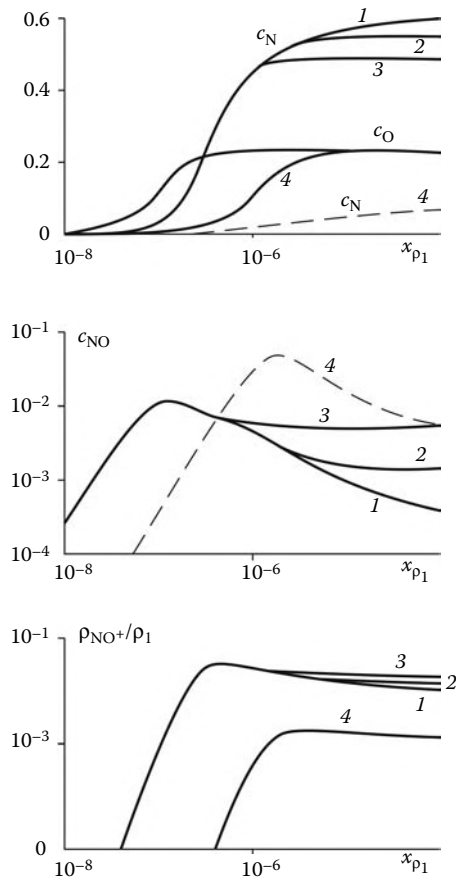
The relaxation zone thickness δ_r decreases with an increase in the gas velocity and, which is more important, a decrease in the flight altitude (Figure 11.5), which can be easily explained by the corresponding increase in the reaction rates (see Section 10.9). At high flight altitudes ($H \geq 70$ km) for the bodies of dimension $L \sim 10$ m the relaxation zone thickness is of the same order as the body size, which indicates the completely nonequilibrium nature of the flow past the body.

**FIGURE 11.2**

Concentrations of the components and molecular weight of air behind a normal shock under the same conditions as in Figure 3.4.

**FIGURE 11.3**

Distributions of the density and the translational and vibrational temperatures in relaxation zones.

**FIGURE 11.4**

Concentrations of the components and the NO^+ ions in relaxation zones under the same conditions as in Figure 11.3.

Finally, in Figure 11.6 the relaxation zone behind the shock in pure oxygen is shown. The distinctive feature of this zone is that it can be divided into two zones, namely, a short one of thickness δ_T , where a near-equilibrium temperature is attained, while the atom concentration is $C_O \approx 1$, and the extended zone of thickness $\delta \approx 20\delta_T$, where the vibrational temperature equilibrium is attained, while the oxygen molecule concentration on its own scale is $C_{O_2} \sim 10^{-4} - 10^{-5}$; within the latter zone there is a fairly extended region of near-constant vibrational temperature T_v , which differs appreciably from T . In this region of quasistationary solution (in the sense of Section 11.2) the terms on the right-hand side of Equation 10.11.9 nearly compensate one another, this resulting in the constancy of the temperature T_v against the background of vanishingly small molecular concentrations (in air this zone of vibrational temperature relaxation is almost imperceptible and is not shown in Figure 11.4).

However, the physicochemical gas model accepted previously can be brought in question for this example, since the assumption that the V-V exchange rate is much greater than the V-T exchange rate, which was a basis of this model (Section 10.7), can turn out to be inadequate for so small molecular concentrations.

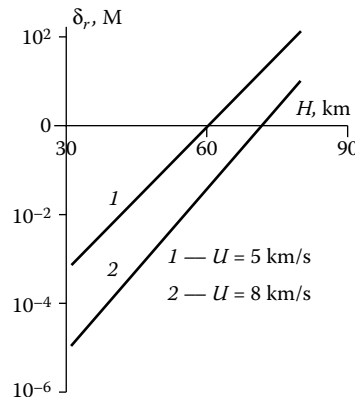


FIGURE 11.5
Relaxation zone thickness behind the normal shock in air.

11.5.2 Nonequilibrium Shock Waves

The previous examples pertain to equilibrium shock waves; however, as noted, the formulation of the problem is applicable to nonequilibrium shocks traveling in gases in nonequilibrium state. The general analysis of nonequilibrium shocks will be carried out in Section 11.8. Here, we only draw attention to some peculiar features of the relaxation shock waves satisfying the condition $v_{n1} > a_{f1}$, which can arise, for example, in nonequilibrium flows past bodies or in nozzle and jet flows. The whole totality of the states ahead of shocks can conditionally be divided into “underexcited” ones, in which the bound energy of physicochemical processes h_{f1} is smaller than the locally equilibrium energy h_{fe1} , and the “overexcited” ones with $h_{f1} > h_{fe1}$. For a three-parameter gas, in our problems these notions correspond to the conditions $\lambda_1 < \lambda_{e1}$ and $\lambda_1 > \lambda_{e1}$, if λ is considered to mean, say, the vibrational energy or the atom concentration.

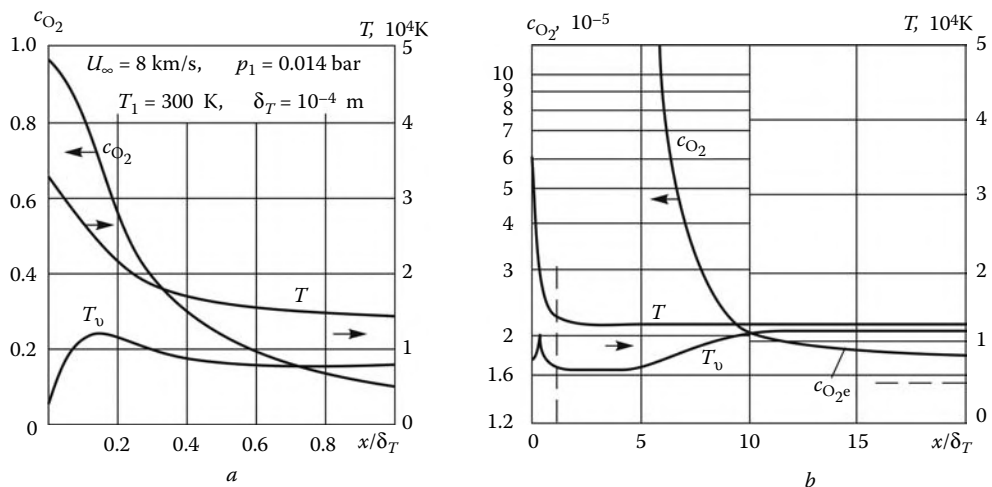


FIGURE 11.6
Relaxation zone in oxygen.

However, in this case the qualitative structure of the relaxation zone is determined by the relation between the parameter λ_1 and the locally equilibrium parameter λ_{e2} behind the frozen front 2-2 in Figure 10.2 (Section 10.4) rather than by the relation between the parameters λ_1 and λ_{e1} . Here, for $\lambda_1 < \lambda_{e2}$ the parameter λ increases along the relaxation zone, as in the case $\lambda_1 = 0$, while for $\lambda_1 > \lambda_{e2}$ it decreases. Finally, for $\lambda_1 = \lambda_{e2}$ the gas state behind the frozen shock is equilibrium, while the relaxation zone is absent.

We note one more property of the hypersonic nonequilibrium shocks, including frozen ones. When the gas state ahead of such a shock is overexcited, the quantity $h_1 = c_p^{(0)}T + h_{f1}$ can turn out to be not small, as compared with the total enthalpy of the gas; in this case formula 3.3.21 should be used instead of formula 3.3.18 for k .

11.6 Short Waves and Weak Shocks in Nonequilibrium Gases

As shown in Section 11.4, the theoretical front of small disturbances propagating in a nonequilibrium gas is always a frozen characteristic. Thus, the theoretical front of the expansion wave shown in Figure 11.7a and b, must be represented by the frozen characteristic Oa determined by the frozen speed of sound a_{f1} ahead of it. However, if the duration of the wave travel is fairly long, $t \gg \tau$, where τ is the relaxation time, that is, equilibrium is being approached, the wave front is rather the equilibrium characteristic bb' with the equilibrium speed of sound a_{e1} ahead of it.

The similar situation arises at propagation of a stationary equilibrium shock at a velocity D_e ranging from a_{e1} to a_{f1} .

Ahead of a piston, which has suddenly acquired a velocity $v_0 > 0$ at the moment $t = 0$, the induced shock wave propagates at a velocity $D_f > a_{f1}$ for fairly small times $t \ll \tau$, when the process is frozen (Figure 11.8), and only at large values of time $t \gg \tau$ the establishment of a stationary wave traveling at the velocity D_e should be expected.

In this connection, two principal questions arise: first, what happens with the disturbances behind the leading frozen front and, second, what is the flowfield in the vicinity of the resulting equilibrium front. The first question will be answered in this section, while the answer to the second question is put off until the next section.

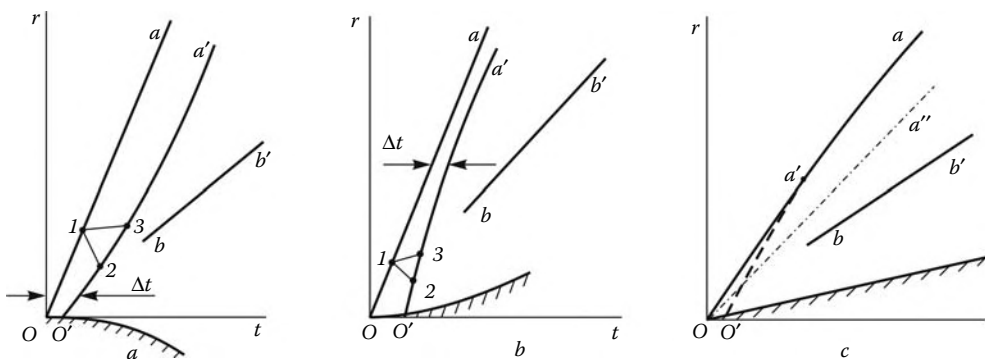


FIGURE 11.7
Wave propagation in a relaxing gas.

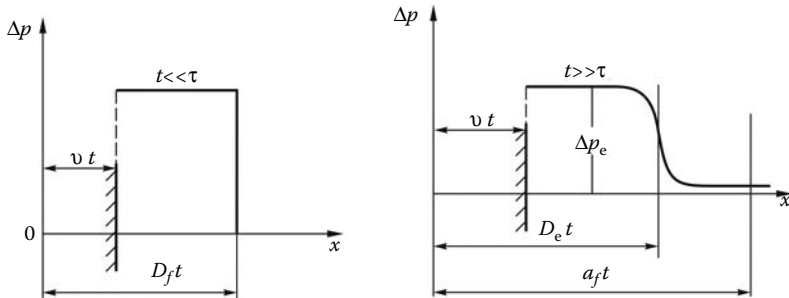


FIGURE 11.8
Pressure ahead of the piston in a relaxing gas with a weak compression shock.

We will first consider a plane, compression or expansion, wave traveling at the frozen speed of sound in an equilibrium gas at rest, the gas parameters being p_1 , λ_1 , and so on. The possible diagrams of this flow, induced, for example, by the displacement of a piston, are shown in Figure 11.7. The compression wave ($v > 0$, b) is assumed to be continuous (a compression shock, even a weak one, needs a special treatment, which will be carried out later), while the expansion wave ($v < 0$, a) may be centered. We will restrict ourselves to the case of a three-parameter gas; in this case, for the adiabatic ($q = 0$) nonequilibrium gas flow the characteristics of Equation 4.2.5 and the compatibility relations 4.2.6 take, in view of 11.4.1 and 11.4.3, the following form:

$$\frac{dr}{dt} = v \pm a_f \quad (11.6.1)$$

$$dp \pm \rho a_f dv = -\rho a_f^2 Q_\Lambda dt = -a_f^2 \delta \frac{\lambda_e - \lambda}{\tau} dt \quad (11.6.2)$$

Let us now consider a short wave (see Section 4.7) of width $\Delta t \ll \tau$ confined between the characteristics Oa and $O'a'$; here, Δt is the time measured along the second-family characteristic 1-2 or the particle trajectory 1-3; the increments of all the functions in this wave are small. Then for the second-family characteristics we can neglect the right-hand side in Equation 11.6.1, which leads, as in Section 4.7, to the Riemann integral 4.5.1 to 4.5.3

$$v = P = \int_p^{p_1} \frac{dp}{\rho a} = \frac{2}{\gamma_f - 1} (a_{f1} - a_f) \quad (11.6.3)$$

or, for small perturbations

$$\rho_1 a_{f1} v = \Delta p = p - p_1 \quad (11.6.4)$$

From Section 11.2 it follows that for $\Delta t \ll \tau$ the flow in the short wave is frozen, with $\lambda = \lambda_1 = \lambda_{e1}$, including the flow on the piston OO' ; thus, integral 11.6.4 is valid on the piston surface. In this case, the centered rarefaction wave includes a small frozen vicinity of the singular point embracing the entire fan of diverging characteristics within which integral 11.6.3 is valid.

Thus, the difference $\lambda_e - \lambda$ proportional to the function Q_Λ in Equation 11.6.2 changes only due to variation of the locally equilibrium parameter $\lambda_e(p, T)$, which is the reason for the appearance of nonequilibrium. This function varies with time following the law

$$\frac{d\lambda_e}{dt} = \left(\frac{\partial \lambda_e}{\partial p} \right)_T \frac{dp}{dt} + \left(\frac{\partial \lambda_e}{\partial T} \right)_p \frac{dT}{dt} = \alpha \frac{dp}{dt} + (1 - \beta) \frac{dT}{dt} \quad (11.6.5)$$

Here, the coefficients α and β are obtained by eliminating the derivative dT/dt by means of the second Equation 11.3.9

$$\begin{aligned}\alpha &= \lambda_{ep} + \frac{\lambda_{eT}}{c_p^{(0)}} \left(\frac{1}{\rho} - h_p^{(T,\lambda)} \right) \\ \lambda_{ep} &= \left(\frac{\partial \lambda_e}{\partial p} \right)_T, \quad \lambda_{eT} = \left(\frac{\partial \lambda_e}{\partial T} \right)_p \\ c_p^{(0)} \beta &= c_p^{(0)} + h_\lambda^{(T,p)} \lambda_{eT}, \quad c_p^{(0)} = h_T^{(p,\lambda)}\end{aligned}\quad (11.6.6)$$

In equilibrium state, the coefficient β is as follows:

$$\begin{aligned}\beta &= \frac{h_{eT}}{c_p^{(0)}} = \frac{c_p}{c_p^{(0)}}, \quad h_{eT} = \left(\frac{\partial h_e}{\partial T} \right)_p = c_p \\ h_e &= h[p, T, \lambda_e(p, T)]\end{aligned}\quad (11.6.7)$$

In an equilibrium process, in which $\lambda = \lambda_e(p, T)$, from Equations 11.6.5 and 11.4.3 there follows

$$\rho Q_\Lambda = \delta \frac{d\lambda_e}{dt} = \omega_p \frac{dp}{dt}, \quad \omega_p = \frac{\alpha \delta}{\beta} \quad (11.6.8)$$

In this case, $a_e^2 d\rho/dt = dp/dt$, so that, comparing Equation 11.6.8 with Equations 11.3.13 and 11.4.1 we obtain the following relation

$$\omega_p = \frac{\alpha \delta}{\beta} = \frac{1}{a_e^2} - \frac{1}{a_f^2} \geq 0 \quad (11.6.9)$$

In a frozen process, in which $d\lambda/dt = 0$, from Equation 11.6.5 it follows that $d\lambda_e/dt = \alpha dp/dt$, or, for a short wave

$$\lambda_e - \lambda = \lambda_e - \lambda_1 = \alpha(p - p_1) \quad (11.6.10)$$

Substituting relations 11.6.4 and 11.6.10 into Equation 11.6.2 for a first-family characteristic, along which time t increases without bounds, we obtain, in view of Equation 11.6.9, the following equation and its solution

$$\begin{aligned}\frac{d\Delta p}{\Delta p} &= -\frac{\kappa}{\tau} dt, \quad \frac{\Delta p}{(\Delta p)_0} = \frac{v}{v_0} = e^{-\kappa(t-t_0)/\tau} \\ \kappa &= \frac{\beta}{2} a_f^2 \omega_p = \frac{\beta}{2} \left(\frac{a_f^2}{a_e^2} - 1 \right) = \frac{1}{2} \beta \frac{\gamma_f - \gamma_e}{\gamma_e}\end{aligned}\quad (11.6.11)$$

Here, $(\Delta p)_0$, v_0 , and t_0 are the initial values of the parameters at point O on the piston, while the coefficients γ_f and γ_e were introduced by formula 11.13.14. In accordance with 11.6.7, $\beta > 0$, so that $\kappa > 0$ as well. Therefore, *the initial perturbations caused by the variations in the boundary conditions decay exponentially with time along the frozen first-family characteristics.*

To derive the form of these characteristics, we rewrite Equation 11.6.1 in terms of Equations 4.5.6 and 11.6.4

$$\frac{dr}{dt} = a_f + v = a_{f1} + (a_f - a_{f1}) + v = a_{f1} + Av, \quad A = \frac{\gamma_f + 1}{2} \quad (11.6.12)$$

Thence, in view of Equation 11.6.11 we obtain the form of the characteristics

$$\begin{aligned} r - r_0 - a_{f1}(t - t_0) &= \Delta r(1 - e^{-\kappa(t-t_0)/\tau}) = \Delta r(1 - v/v_0) \\ \Delta r &= Av_0\tau/\kappa \end{aligned} \quad (11.6.13)$$

Here, r_0 and t_0 are the coordinates of the initial point O' on the piston. For the expansion wave centered at the point O we have $t_0 = r_0 = 0$; however, $v_0 \neq 0$ and $\Delta p_0 \neq 0$. As $(t - t_0)/\tau \rightarrow \infty$, characteristics 11.6.13 acquire the same slope as in the undisturbed flow; at the same time, they are displaced at a distance Δr with respect to the undisturbed characteristic originating from the point O' . In this case, $\Delta r < 0$ for the expansion wave and $\Delta r > 0$ for the compression wave.

For the compression wave the solution obtained is valid only in the region up to the intersection of characteristics, the condition $t \leq t_c$ (formula 4.5.9 with the frozen speed of sound) determining the lower boundary of the previously mentioned region in view of the fact that the characteristic slope (11.6.13) decreases as time t increases. The intersection of characteristics leads to the formation of a weak submerged shock propagating at a velocity $D > a_{f1}$ and interacting with the subsequent compression waves weakened by the relaxation zone.

To reveal the nature of this interaction, we will consider the problem of the piston with a constant initial velocity $v_0 > 0$; this case corresponds to an equilibrium shock at a velocity $D_e < a_{f1}$. At the same time, for $t \ll \tau$ the induced frozen shock propagates at a velocity $D_f > a_{f1}$, so that the decay rate of this leading disturbance front should be determined. Schematics of the process are presented in Figure 11.7c, where Oa is the leading shock, while $O'a'$ is a characteristic overtaking the shock.

As shown in Section 4.8, for a weak frozen shock the same relations 11.6.4, as for a simple wave, are valid and, hence, the same characteristic relations 11.6.13 hold. The propagation speed for weak shock waves is determined by Equation 4.8.5, which can be rewritten in terms of Equation 11.6.12 as follows

$$\frac{dr_s}{dt} = D = \frac{1}{2}(a_{f1} + a + v) = a_{f1} + \frac{1}{2}Av \quad (11.6.14)$$

Here, the velocity v should be determined using the data on the first-family characteristics overtaking the shock, that is, from formula 11.6.13. To do this, we set $r = r_s$ in this formula and drop out the terms with t_0 and $r_0 \sim v_0 t_0$ by assuming that $t \gg t_0$. Then Equation 11.6.14 takes the form:

$$\frac{dR}{dt} = -\frac{\kappa}{2\tau}R, \quad R = r_s - a_{f1}t - \Delta r, \quad \Delta r = Av_0\frac{\tau}{\kappa} \quad (11.6.15)$$

The solution of this equation is similar to 11.6.13

$$r_s = a_{f1}t + \Delta r(1 - e^{-\kappa t/2\tau}) \quad (11.6.16)$$

As $t \rightarrow 0$, this solution determines the frozen shock shape $r_s = (a_{f1} + Av_0/2)t$, whereas, as $t \rightarrow \infty$, the shock front becomes parallel to the leading frozen characteristic $r_f = a_{f1}t$ (Oa'' in Figure 11.7c) with a positive displacement Δr and asymptotic decay of the disturbances on the front. The decay decrement $\kappa/2\tau$ is half as large as that for short waves in formula 11.6.11.

Thus, in the problems considered the theoretical front of weak disturbances ceases with time to bear real disturbances at all. The decay time for these disturbances $t \sim \tau/\kappa$ is of the

same order as the relaxation time, though it can be larger than the latter if the speeds of sound a_f and a_e are similar in value, since in this case $\kappa \ll 1$. Moreover, as $a_{f1} - a_{e1} \rightarrow 0$, or $\kappa \rightarrow 0$, the disturbances do not decay at all, and the difference between the frozen and equilibrium fronts no longer exists.

This study embraces only a small vicinity of the front $\Delta t \ll \tau$; however, considering successive narrow bundles of frozen characteristics, we can arrive at the similar conclusion that the disturbances decay along them as well. However, as $t/\tau \rightarrow \infty$, the flow as a whole must tend to equilibrium so that the propagation front for real disturbances must be represented by an equilibrium characteristic or an equilibrium shock ($b - b'$ in Figure 11.7), if the gas ahead of the front is at equilibrium. However, these equilibrium fronts are not rigorous from the standpoint of nonequilibrium theory, since the traces of nonequilibrium effects ahead of the fronts can disappear only asymptotically. The structures of these near-equilibrium fronts will be considered in Section 11.7.

The qualitative generalization of the results obtained to steady-state supersonic flows is obvious in view of the time-dependent analogy of Sections 2.7 and 8.3.*

11.7 Near-Equilibrium Flows and Viscosity-Relaxation Analogy

In Section 11.4 we posed the problem of the limiting passage of the system of nonequilibrium gas dynamic equations as the involved processes approach equilibrium. In what follows we derive the limiting form of the equations, which demonstrates clearly their near-equilibrium properties, and discuss the question about the *viscosity-relaxation analogy* that makes it possible to model some simple near-equilibrium flows. On this basis, we study the structure of the equilibrium fronts of weak disturbances in relaxing gases (this question remained unsolved in Section 11.6). We will restrict ourselves to the three-parameter gas with a single kinetic variable λ satisfying the relaxation equation $d\lambda/dt = (\lambda_e - \lambda)/\tau$ (Equation 10.4.1). Combining this equation with Equation 11.6.5 we derive its other form:

$$\frac{\tau}{\beta} \frac{d(\lambda_e - \lambda)}{dt} + (\lambda_e - \lambda) = \tau \frac{\alpha}{\beta} \frac{dp}{dt} \quad (11.7.1)$$

Then Equation 11.4.3 takes the form:

$$L_c = \frac{1}{\rho a_c^2} \frac{dp}{dt} + \operatorname{div} \vec{U} = \frac{\delta}{\rho \beta} \frac{d(\lambda_e - \lambda)}{dt}, \quad \frac{1}{a_c^2} - \frac{1}{a_f^2} = \omega_c = \frac{\alpha \delta}{\beta} \quad (11.7.2)$$

Eliminating the difference $\lambda_e - \lambda = -(\rho \tau / \delta) L_f$ from this equation and Equation 11.4.3, we obtain an equation that does not include explicitly the derivative from λ

$$L_c = -\frac{\delta}{\rho \beta} \frac{d}{dt} \left(\tau \frac{\rho}{\delta} L_f \right), \quad L_f = L_c - \frac{\omega_c}{\rho} \frac{dp}{dt} \quad (11.7.3)$$

The operators L_f and L_e (see 11.4.3 and 11.4.4) differ from L_c in that a_c is replaced by a_f or a_e and the function ω_c differs from ω_p in 11.6.9 in that the quantity a_e is substituted for

* Similar problems with the axial and spherical symmetry were considered by Ryzhov (1971). Within the framework of the linear theory, the problem was investigated by Kraiko and Tkalenko (1968).

a_c . We note that the quantity a_c in the operator L_c is not the speed of sound in the sense of Sections 11.3 and 11.4. Only for equilibrium flows can we let in Equation 11.7.3

$$\begin{aligned}\omega_c &= \omega_p(p, T, \lambda_e), & a_e &= a_c(p, T, \lambda_e) \\ \rho &= \rho_e = \rho(p, T, \lambda_e), & \lambda_e &= \lambda_e(p, T)\end{aligned}\quad (11.7.4)$$

thus reducing it to the equilibrium Equation 11.4.4 with $L_c = L_e = 0$ (for $q = 0$).

Equation 11.7.3 has appeared as the result of eliminating the derivative $d\lambda/dt$ from Equations 11.1.2 and 11.1.5, which has led to the increase of its order up to the second. The system of the basic gas dynamic equations thus obtained, namely, the equations of momentum 11.1.1, continuity 11.7.3, and energy 11.1.3, contain neither the derivatives from λ nor the term $(\lambda_e - \lambda)/\tau$ generating the indeterminate form at small τ . The variable λ enters now only in the coefficients of these equations and, in the general case, is determined by Equation 11.7.1.

This system is equivalent to the original system 11.1.1 through 11.1.5 and, naturally, conserves all the mathematical or characteristic properties of the latter for any τ . In particular, in spite of the presence of the second derivatives of the unknown functions on the right-hand side of Equation 11.7.3, which would seem to be unbounded on weak discontinuities, the appearance of weak discontinuities with the frozen speed of sound a_f is still possible. Therefore, the passage of the crucial role from the frozen speed of sound a_f to the equilibrium one a_e , coincidentally with the conservation of the property of more rapid propagation of nonequilibrium disturbances, as compared with equilibrium ones, which disappears at $\tau = 0$ and $a_c = a_e$, can be attained only at the cost of a certain *degeneration* of the original equations or, as it is in our case, by bringing them into the so-called *near-equilibrium* form that governs the near-equilibrium flows and allows for the main effects at small but finite values of τ .

For this purpose we will consider the flow satisfying the conditions

$$\lambda_e - \lambda \ll \lambda_0, \quad L_c = L_f + \omega_c \frac{1}{\rho} \frac{dp}{dt} \sim O(\lambda_e - \lambda) \quad (11.7.5)$$

Here, λ_0 is a certain scale of the parameter λ and two last conditions follow from the first one. These conditions infer the closeness of the flow to the equilibrium flow with $\lambda = \lambda_e$ and $L_c = L_e = 0$. A very simple example of such a flow is the flow with a given time scale $t_0 \gg \tau$ determining the orders of all the derivatives. In this case, by sequential substitution of the previous approximation into the first term of Equation 11.7.1 having the order of τ/t_0 , we obtain a series expansion in τ

$$\lambda_e - \lambda = \tau \frac{\alpha}{\beta} \frac{dp}{dt} + F_\lambda, \quad F_\lambda = -\frac{\tau}{\beta} \frac{d}{dt} \left(\tau \frac{\alpha}{\beta} \frac{dp}{dt} \right) + \dots \quad (11.7.6)$$

Here, F_λ is a series in τ in which only the leading term is written down. The subsequent terms of the series with increasing powers in τ contain the derivatives of the orders that also increase with the number of a term of the series.

Dropping the term L_c in expression 11.7.3 for the operator L_f and retaining only the terms of the order not higher than τ we arrive at the equation

$$L_c = \frac{\delta}{\rho\beta} \frac{d}{dt} \left(\frac{\tau}{\delta} \omega_c \frac{dp}{dt} \right) = -\frac{\delta}{\rho\beta} \frac{d}{dt} \left(\tau \frac{\rho}{\delta} a_c^2 \omega_c \operatorname{div} \vec{U} \right) \quad (11.7.7)$$

In the latter equation the derivative dp/dt is eliminated by means of Equation 11.7.2 with the dropped right-hand side of the order τ .

This equation has the most general form and is the most accurate among other near-equilibrium forms of the continuity equation. Superficially, it is of the same type as Equation 11.7.3; however, as will be shown later, the features of these two equations are radically different. Together with the equations of motion 11.1.1 and energy 11.1.3, Equation 11.7.7 forms a system qualitatively similar (with respect to the properties of their solutions) precisely to the Navier–Stokes equations.

The coefficients of Equation 11.7.7 are dependent on λ ; in order to give the completely near-equilibrium form to this equation, all these coefficients must be replaced by the equilibrium ones f_e using the expansion of the type $f = f_e + f_\lambda(\lambda - \lambda_e)$, where f_λ is the derivative with respect to λ . Introducing then the coefficient $\delta/\rho\beta$ under the sign of the outer derivative we bring Equation 11.7.7 into the form:

$$L_e = \frac{1}{\rho a_e^2} \frac{dp}{dt} + \operatorname{div} \vec{U} = -\frac{d}{dt} (\tau \chi \operatorname{div} \vec{U}) \quad (11.7.8)$$

Here, the locally equilibrium parameters ρ_e and a_e are determined by formulas 11.7.4, while the parameter χ is analogous to κ in 11.6.11 and equal to

$$\chi = \frac{1}{\beta} \left(1 - \frac{a_e^2}{a_f^2} \right) = \frac{\gamma_f - \gamma_e}{\beta \gamma_f} = \frac{2\kappa \gamma_e}{\beta^2 \gamma_f}, \quad \beta = \frac{c_p}{c_p^{(0)}}, \quad \gamma_e = \frac{\rho a_e^2}{p}, \quad \gamma_f = \frac{\rho a_f^2}{p} \quad (11.7.9)$$

The following term is omitted from the right-hand side of Equation 11.7.8

$$F = F_1 + F_2, \quad F_1 = \frac{\lambda_e - \lambda}{\rho a_e^2} \frac{\partial}{\partial \lambda} \left(\frac{1}{\rho a_c^2} \right)_{p,s} \frac{dp}{dt} = \\ \tau \frac{\alpha}{\beta} \frac{\partial}{\partial \lambda} \left(\frac{1}{\rho a_c} \right)_{p,s} \left(\frac{dp}{dt} \right)^2, \quad F_2 = C \tau \chi \left(\frac{dp}{dt} \right)^2 \quad (11.7.10)$$

The terms F_1 and F_2 are written with allowance for the isentropicity of near-equilibrium flows. The term F_1 is due to the transformation of the left-hand side of Equation 11.7.7 (the latter expression was obtained in terms of Equation 11.7.6 with the last term omitted from the right side), while the term F_2 is due to the transformation of the right-hand side of the equation; the expression for the coefficient C is not presented, since it is not needed in what follows. We note that the terms similar to F_1 must appear in the equations of momentum 11.1.1 and energy 11.1.3 due to the substitution of the equilibrium value ρ_e for the density ρ .

It is important to note that essentially nonlinear terms F_i can be, generally speaking, of the same order as the first term on the right-hand side of Equation 11.7.8. For this reason, a rational theory of near-equilibrium flows can be constructed only if there exists a possibility, supplementary to conditions 11.7.5, of neglecting these terms. Only after these transformations have been done, the variable λ disappears from the main gas dynamic equations with the result that their coefficients depend on the variables p and T for $\lambda = \lambda_e(p, T)$. The difference $\lambda_e - \lambda \sim \tau$ can then be refined from the equilibrium solution by means of Equation 11.7.1 or 11.7.6. Precisely this system will be considered as the *near-equilibrium system of equations*.

We will lay down one more constraint on the applicability of Equation 11.7.8 for transonic flows, which will be explained with reference to the example of one-dimensional flows for which, by analogy with Equation 11.5.4, the operator L_c contains the coefficient $M_c^2 - 1$ of

the derivative du/dx . Therefore, for $|M_c^2 - 1| \ll 1$, M_c can be replaced by M_e only provided that

$$|\lambda - \lambda_e| \ll |M_{e1}^2 - 1| \max |(\partial M_c^2 / \partial \lambda)_{p,T}|^{-1} \quad (11.7.11)$$

where M_{e1} is the characteristic Mach number in the domain under consideration.

Let us formulate some general results. Equation 11.7.8 is derived from the exact Equation 11.7.3 by dropping out some terms with higher-order derivatives. Therefore, this equation is *degenerate* with respect to the exact one and must, for this reason, possess somewhat other properties. In the same fashion, the term F can endow Equation 11.7.8 with some new qualitative properties; because of this, there are no *a priori* reasons to drop out this term justifying it by the more important role played by the term of the same order, but with the second derivative.

However, this degeneration must not be excessive. Thus, in the first approximation, it would seem natural to substitute the equilibrium solution into the terms with the coefficient τ in the original Equations 11.7.1 and 11.7.3 and even to organize some iteration procedure on this basis. However, in such a procedure, the type of the equations is completely distorted in each iteration stage, since the second derivatives on the right-hand side of Equation 11.7.3 are completely determined by the previous stage and thus enter into the right-hand side of this equation as known terms, which, as shown in Section 7.13, do not affect the type of the equation. In this case, the solution obtained gives simply a correction of the order τ to the solution of the equilibrium equations together with the continuity Equation 11.4.4. However, this method is totally inapplicable for obtaining non-smooth solutions in the equilibrium approximation, on which the operator L_f can be discontinuous or unbounded in the main approximation, as is the case in the problems considered in the following.

We specify that the equations obtained are not intended for using them in particular calculations, first of all, in view of their restricted applicability range and the difficulty of generalizing them to multicomponent systems. However, such asymptotic methods are often indispensable for obtaining qualitative illustrative results.

By way of illustration, we will apply this theory for studying the relaxation structure of near-equilibrium zones in the vicinity of equilibrium discontinuities. We begin with the flow near the leading characteristic of the expansion wave *Ob* (Figure 11.9a), whose frozen front was considered in Section 10.6. On this characteristic, the inviscid equilibrium solution experiences a *weak discontinuity* (in the first derivatives), which is incompatible with Equation 11.7.8 containing the second derivative of the velocity on its right-hand side. However, this derivative must be bounded due to the fact that the boundary region thickness δ , though small together with τ , is nonvanishing. We will determine the size of this region later, accepting until then the condition $\delta \ll a_{et}$.

To solve the problem, we make the change of variables

$$t, \quad r \rightarrow t, \quad \xi = a_{e1}t - r \quad (11.7.12)$$

The lines $\xi = \text{const}$ are parallel to the leading characteristic *Ob*, on which we will put $\xi = 0$. In a small vicinity of this line, $\Delta\xi \sim \delta$, the orders of the derivatives with respect to ξ and t are determined by the limiting equilibrium expansion wave, within which the derivatives with respect to ξ are finite and those with respect to t are proportional to the angle $\Delta\varphi$ of the deviation of the characteristics on which the solution is constant, from the line $\xi = 0$. In the boundary region the parameter perturbations are small, together with

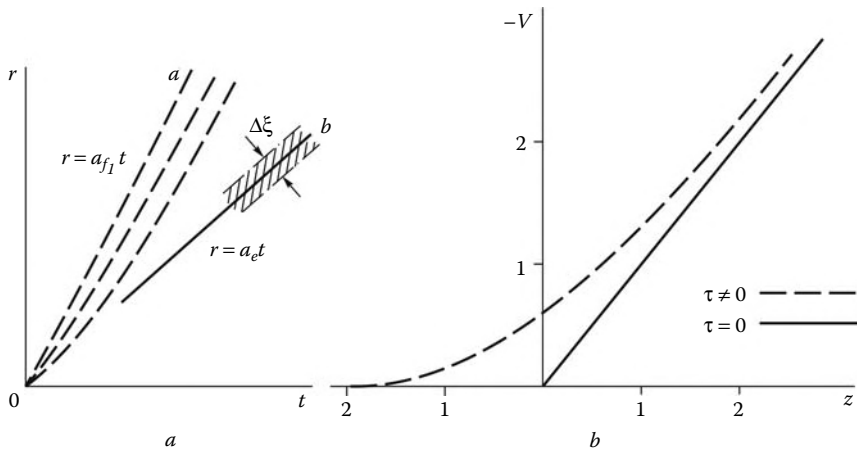


FIGURE 11.9
Structure of the rarefaction wave in a near-equilibrium gas.

$\Delta\varphi$; thus, in this region the following relations hold

$$\begin{aligned} \frac{\Delta p}{\rho a_e^2} &\sim \frac{v}{a_e} \sim \Delta\varphi \sim \frac{\delta}{a_e t}, & \frac{\partial}{\partial \xi} &\sim \frac{1}{a_e t} \frac{\partial}{\partial \varphi} \\ \frac{\partial}{\partial t} &\sim \Delta\varphi a_e \frac{\partial}{\partial \xi} \sim \frac{\Delta\varphi}{t} & (\tan \varphi = v + a) \end{aligned} \quad (11.7.13)$$

Here, $\partial/\partial\varphi$ is the derivative of the slope of the characteristics in an equilibrium rarefaction wave expanding in proportion to t with respect to the angle φ . Moreover, due to the isentropic nature of near-equilibrium processes (Section 10.6), the density and the speed of sound in the coefficients of the equations can be assumed to be the functions of the pressure only.

In the new variables, the equation of momentum 4.2.1 and Equation 11.7.8 take the form:

$$\begin{aligned} \frac{dv}{dt} &= \frac{\partial v}{\partial t} + (a_{e1} - v) \frac{\partial v}{\partial \xi} = \frac{1}{\rho} \frac{\partial p}{\partial \xi} = a_e \frac{\partial P}{\partial \xi} \\ \frac{\partial P}{\partial t} &+ (a_{e1} - v) \frac{\partial P}{\partial \xi} - a_e \frac{\partial v}{\partial \xi} = \\ a_e \left[\frac{\partial}{\partial t} + (a_{e1} - v) \frac{\partial}{\partial \xi} \right] \left(\tau \chi \frac{\partial v}{\partial \xi} \right) &= \\ a_e a_{e1} \frac{\partial}{\partial \xi} \left(\tau \chi \frac{\partial v}{\partial \xi} \right), & P = \int_{p_1}^p \frac{dp}{\rho a_e} \end{aligned} \quad (11.7.14)$$

Here, in view of their relative smallness (together with δ), the derivative $\partial/\partial t$ and the term v are omitted from the parentheses on the right-hand side of the second equation. However, if all the terms of the order $\Delta\varphi$ and τ are dropped out of system 11.7.14, then both equations of this system coincide with the compatibility relation along the second-family characteristics for $\xi \approx 0$, having the Riemann invariant $P = v$ as its solution. In

other words, in the $\xi \sim \delta$ region the two equations differ by small terms only. To find these terms, we sum up the equations and use the relations $P = v$ and $a_{e1} - a_e - v = Av$ (cf. Equation 11.6.12); then setting all the coefficients, except for v , to be constant, we arrive at the equation (Luney, 1975)

$$\frac{\partial v}{\partial t} - Av \frac{\partial v}{\partial \xi} = \frac{1}{2} a_{e1}^2 \tau \chi \frac{\partial^2 v}{\partial \xi^2} \quad (11.7.15)$$

In formulating the boundary conditions for this equation we take into account that the flow ahead of the relaxation zone is equilibrium and undisturbed, so that $v \rightarrow 0$, as $\xi/\delta \rightarrow -\infty$. On the right-hand side, as $\xi/\delta \rightarrow \infty$ in the supersonic flow, we can require only the asymptotic approach of the solution to a physically reasonable limiting form.

We will seek the solution of Equation 11.7.15 in the form:

$$v = a_e \sqrt{\frac{\tau \chi}{t}} V(z), \quad z = \frac{\xi}{a_e \sqrt{\tau \chi t}} \quad (11.7.16)$$

The function $V(z)$ satisfies the equation

$$V'' + (z + 2V)V' + V = (V' + V^2 + zV)' = 0 \quad (11.7.17)$$

Integrating this singly and using the complex $Y = Ve^{z^2/2}$ we reduce this equation to the form $Y' + Y^2 e^{-z^2/2} = 0$ and obtain the solution

$$V = -\frac{1}{\sqrt{2\pi}} e^{-z^2/2} (C - \Phi(z))^{-1} = -e^{-z^2/2} \left(\int_z^\infty e^{-z'^2/2} dz' \right)^{-1}$$

$$\Phi = \frac{1}{\sqrt{2\pi}} \int_{-\infty}^z e^{-z'^2/2} dz' \quad (11.7.18)$$

As $z \rightarrow -\infty$, this solution decreases as $V \sim e^{-z^2/2}$. Since $\Phi(\infty) = 1$, a bounded solution exists only for $C = 1$, which was assumed previously. The corresponding curve $V(z)$ is plotted in Figure 11.9b. As $z \rightarrow \infty$, $V \rightarrow -z(1 + z^2 + \dots)$; comparing this result with 11.7.16 we obtain that this solution passes into the solution $v = -\xi/t = -a_{e1} + r/t$ for the centered equilibrium expansion wave in the vicinity of the leading characteristic Ob (though more slowly than in the case $z \rightarrow -\infty$).

Letting $\Delta z \sim 1$ we determine the relative order of the boundary zone thickness $\delta/a_{et} \sim (\tau \chi/t)^{1/2}$, which, together with 11.7.13, determines the orders of the parameters within this zone. Thus, as t increases, the portion of the expansion wave embraced by this zone is progressively smaller, so that the flow pattern as a whole approaches the equilibrium one.

We note that Equation 11.7.15 was obtained from system 11.7.14 with the same relative accuracy of the order $(\tau/t)^{1/2}$. We will now evaluate the accuracy of the original Equation 11.7.8 with respect to the solution obtained. In accordance with 11.7.14 and 11.7.13, the first derivative $dp/dt \sim p/t$ both in the boundary region and in the expansion wave itself;

however, in evaluating the second derivative $(dp/dt)/\Delta t$, the estimate $\Delta t \sim \delta/a_e \sim (\tau t)^{1/2}$ should be borne in mind. Therefore, the ratios of the terms F_i (see 11.7.10) omitted in deriving Equation 11.7.8 to its right side decrease, as $\tau/t \rightarrow \infty$, not slower than $(\tau/t)^{1/2}$, which determines the asymptotic accuracy of this solution on weak discontinuities. The term F_λ on the right side of Equation 11.7.6 is of the same relative order $(\tau/t)^{1/2}$ and can be dropped out. At the same time, in accordance with 11.7.6, the difference $\lambda_e - \lambda \sim \tau/t$ is of the higher order of smallness (the same as for smooth solutions), which makes it possible to assume the flow to be quasi-equilibrium.

We note that the value of δ thus obtained is larger than that determined from a seemingly natural criterion of the equal orders of all the terms of Equation 11.7.8, which leads to the estimate $\Delta t \sim \tau$. However, when $\tau = 0$, the operator $L_e = 0$ as well, so that at small nonzero values of τ the leading terms compensate each other and this operator is actually of the same order $(\tau/t)^{1/2}$, as that of the right-hand side of Equation 11.7.8.

We are coming now to the problem of a weak steady-state shock, the gas parameters ahead of which are p_1 , ρ_1 , and $v_{n1} = u_1$, the velocity being aligned with the x axis. Using the one-dimensional equation of motion $dp = -\rho u du$ we reduce Equation 11.7.3 to the form:

$$\begin{aligned} L_c &= (M_c^2 - 1) \frac{du}{dx} = \frac{\delta u}{\rho \beta} \frac{d}{dx} \left(\tau \frac{\rho}{\delta} L_f \right) \\ L_f &= (1 - M_f^2) \frac{du}{dx}, \quad M_c = \frac{u}{a_c}, \quad M_f = \frac{u}{a_f} \end{aligned} \quad (11.7.19)$$

Equation 11.7.19 has a singular point at $M_f = 1$; based on this fact, in Section 11.5 we ruled out the possibility of constructing a continuous solution for shock waves on the velocity range $u_1 > a_{f1}$. This inference can easily be confirmed analytically for an equilibrium freestream with $M_{c1} = M_{e1} > 1$. In fact, for $x \rightarrow -\infty$ a bounded solution subject to the condition $u \rightarrow u_1$ must have the form:

$$u - u_1 = \text{const } e^{x/\bar{\kappa}}, \quad \bar{\kappa} = \frac{\tau u_1 (1 - M_{f1}^2)}{\beta (M_{e1}^2 - 1)} \quad (11.7.20)$$

This is possible only for $\bar{\kappa} > 0$, that is, for $M_{f1} < 1$ and $M_{e1} > 1$ (conditions 11.5.5) since, in accordance with 11.6.7, $\beta > 0$. As noted in Section 11.5, in this case a relaxation compression wave is realized; we will restrict its analysis to the case of limitingly weak waves satisfying the requirements

$$u_1 - a_{e1} \ll a_{f1} - a_{e1}, \quad M_{e1}^2 - 1 \ll 1 - M_{f1}^2 \quad (11.7.21)$$

In this case, we can put $M_f = M_{f1} = a_{e1}/a_{f1}$ in the difference $1 - M_f^2$ and take the difference $M_{e1} - 1$ as a small parameter of the problem. Other coefficients of Equation 11.7.19 can be assumed to be not only equilibrium, but constant as well, thus omitting the terms of the type F_i in 11.7.10 as being of the second order of smallness in $M_{e1}^2 - 1$ or τ . However, the replacement of M_c by M_e in Equation 11.7.19 is possible only with the constraint 11.7.11, which is too severe for this problem, since in a weak wave the pressure difference is $\Delta p \sim \rho a_e^2 (M_{e1}^2 - 1)$ and $\Delta \lambda \sim (\partial \lambda_e / \partial p)_s \Delta p$. Therefore, condition 11.7.11 can be fulfilled only for fairly small values of $(\partial \lambda_e / \partial p)_s$. In other words, the problem cannot be reduced with the asymptotic rigorousness to the solution of Equation 11.7.19 alone, separately from Equation 11.7.1, that is, to the near-equilibrium flow model formulated previously with its basic Equation 11.7.8.

However, the difference $M_c^2 - 1$ in Equation 11.7.19 is also of alternate signs, so that we can assume that its behavior is qualitatively similar to that of the difference $M_e^2 - 1$, especially in view of the fact that the two differences are the same at the equilibrium boundaries of the domain, $x \rightarrow \pm\infty$. Therefore, in what follows we will put $M_c = M_e$ for our qualitative analysis; then Equation 11.7.19 takes the form that coincides with that of Equation 11.7.8 under the conditions considered

$$(M_e^2 - 1) \frac{du}{dx} = \frac{d}{dx} \left(\tau u \chi \frac{du}{dx} \right) \quad (11.7.22)$$

We will assume the relaxation zone thickness to be small as compared with the distance between the frozen and equilibrium characteristics; then, as $x \rightarrow \pm\infty$, the asymptotic boundary conditions $du/dx \rightarrow 0$ can be preassigned for this equation. In view of formulas 2.2.19 and 2.2.20, we set $M_e^2 - 1 = (2A_*/a_*)(u - a_\infty)$ and integrating Equation 11.7.22 singly bring it into the form similar to that of Equation 3.2.3, with a quadratic trinomial in u on the right-hand side, and then, using integral 11.5.2, into the form 3.2.4, only with the variable $z = A_*x(\tau\chi u_1)^{-1}$, where $u_1 \approx a_*$. Therefore, the solution of this equation coincides with 3.2.5 with all that implies (which is not repeated here).

We note that an analogous solution of Equation 11.7.19 could be obtained in the case of the exact difference $M_f^2 - 1$ as well (Clarke and McChesney, 1966); however, it is qualitatively similar to that obtained previously, though not as illustrative.

Finally, we dwell on the case in which the speeds of sound a_f and a_e are similar in value and the distance between the frozen and equilibrium disturbance fronts is relatively small (of the order of χ). In this case, the solution for an expansion wave obtained previously is valid only when the boundary zone thickness $\delta \sim a_e(\tau\chi t)^{1/2}$ is small as compared with the distance $\bar{\delta} \sim a_e\chi t$ between the limiting characteristics, that is, when $t^{1/2} \gg (\tau/\chi)^{1/2}$. For smaller t the boundary zone thickness is comparable with the distance between the previously mentioned characteristics and the limiting formulation of our problems is no longer correct. At the same time, for a steady-state compression wave the ratio of the relaxation front thickness Δx to $\bar{\delta}$ is always of the order of τ . However, in accordance with 11.6.16, in order that disturbances should decay in the vicinity of the frozen front, the fulfillment of the earlier condition $\chi t/\tau \gg 1$ is required. Practically, these discontinuities become indistinguishable, as $\chi \rightarrow 0$.

We note that in actual flows only one of the limiting regions, namely, either $\tau \ll t$ or $\tau \gg t$, may be distinguishable.

The results obtained show that there exists a certain *viscosity-relaxation analogy* between near-equilibrium and viscous flows, which consists in qualitative similarity of their dissipative properties which, as it were, make the flowfields smoother. Mathematically, this dissipation is due to the second derivative in Equation 11.7.9, which allows us to assign the system of equations governing near-equilibrium flows to the same type as the system of Navier-Stokes equations. We recall that the original system of the basic equations of nonequilibrium gas dynamics does not possess these dissipative properties, although it contains the second derivatives with the coefficient τ in Equation 11.7.3. In this and only in this meaning can we speak of the *relaxation viscosity* of near-equilibrium flows. This viscosity, which will be denoted μ_f , is proportional to the product $\tau\chi$; in order that it has the same dimensionality as the physical viscosity, it is determined as follows

$$\mu_f = K\tau\rho(a_f^2 - a_e^2) \quad (11.7.23)$$

Comparing formulas 11.7.23 and 3.2.4 for the variable z gives that the coefficient K is of the order of unity; generally speaking it may depend on the nature of a problem if it is determined following precisely the viscosity-relaxation analogy.

The relaxation viscosity must be considerably larger than the physical viscosity, at least within the framework of the shock transition model of Section 10.5, which supposes that the relaxation zone thickness is appreciably greater than that of the viscous zone, which is of the order of a mean free path.

This viscosity, or, to be more precise, the parameter $\tau\chi$, enters into Equation 11.7.8 as a coefficient of the velocity divergence $\operatorname{div}\vec{U}$; therefore, it has a *bulk-associated* nature. In this connection, some scientists came up with an idea that the relaxation viscosity can be accounted for by introducing it into the isotropic (spherical) component p_* of the stress tensor 1.10.10, if this component is written in the form:

$$p_* = p + \left(\frac{2}{3} \mu - \mu_f \right) \operatorname{div}\vec{U} \quad (11.7.24)$$

Thus, μ_f is identified with the second viscosity $\mu^{(2)}$ mentioned in Section 1.10 without changing the equation of state $p = nkT$ (1.4.6) and the equilibrium form $L_e = 0$ of the continuity equation.

However, this model is mainly based on the comparison of the solutions of one-dimensional problems, in which the original equations of motion and continuity are simply summed. Thus, in the problem of the propagation of one-dimensional acoustic waves* with simultaneous account of the viscosities $\mu^{(2)}$ and μ_f in Equations 11.7.24 and 1.10.10 (with $\mu = 0$) and μ_f in Equation 11.7.8 the equation of motion after their linearization reduces to the system

$$\frac{\partial u}{\partial t} + \frac{1}{\rho} \frac{\partial p}{\partial x} = \frac{\mu^{(2)}}{\rho} \frac{\partial^2 u}{\partial x^2}, \quad \frac{1}{\rho a_e^2} \frac{\partial p}{\partial t} + \frac{\partial u}{\partial x} = -\frac{\mu_f}{\rho a_e^2} \frac{\partial^2 u}{\partial t \partial x} \quad (11.7.25)$$

We will consider waves traveling from left to right, for example, induced by a piston oscillating at $x = 0$ with a frequency ω and a velocity $u = u_0 e^{i\omega t}$

$$u = u_0 e^{i\omega(a_e t - x) - \varepsilon x}, \quad p = \rho a_e u_0 \bar{p} e^{i\omega(a_e t - x) - \varepsilon x} \quad (11.7.26)$$

In this case, Equations 11.7.25 are consistent provided that

$$\begin{aligned} \varepsilon + i\omega &= i\omega [1 + i\omega(\mu^{(2)} + \mu_f)/\rho a_e]^{-1/2} \\ \varepsilon &\approx \omega^2 (\mu^{(2)} + \mu_f)/2\rho a_e \quad \text{for} \quad \omega(\mu^{(2)} + \mu_f) \ll \rho a_e \end{aligned} \quad (11.7.27)$$

* The notion of the relaxation viscosity arose precisely in the similar problem of acoustic wave decay in a relaxing gas (Mandelshtam and Leontovich, 1937). This problem was also presented, albeit in a somewhat different form than in the following, in Landau and E. M. Lifshitz (1983), where the viscosity μ_f was identified with $\mu^{(2)}$. However, in view of the foregoing, this suggestion could hardly be agreed with. At the same time, the previous presentation does not exhaust the problem of the second viscosity. In some works, it is introduced within the framework of kinetic theory for gases with equilibrium-excited internal degrees of freedom, though it is absent from frozen or nonequilibrium flows and the passage to the limit when the flow tends to become equilibrium is indefinite (see, e.g., Kogan, 1947, E. M. Lifshitz and Pitaevskii, 1979). In this model the temperature is no longer the measure of the kinetic energy of molecular translation, while the pressure is not equal to one third of the sum of the normal stresses.

However, so far these results have pertained only to kinetic theory of gases and have not been introduced into the gas dynamic theory of viscous relaxing flows tested only within the framework of the model outlined in Section 1.10, which does not involve the second viscosity, and on physical laws based on the conventional notions for the temperature and the pressure.

The normal stress is as follows:

$$p_{xx} = -p + \mu^{(2)} \frac{\partial u}{\partial x} = \rho a_e u_0 \bar{p}_{xx} \cdot e^{i\omega(a_e t - x) - \varepsilon x}, \quad \bar{p}_{xx} = -\frac{i\omega}{\varepsilon + i\omega} \quad (11.7.28)$$

Thus, both relaxation and conventional viscosities lead to a decay of acoustic waves with increase in x and a shift in the velocity and pressure phases. Clearly, the coefficients $\mu^{(2)}$ and μ_f enter symmetrically into this solution, so that in this case we can actually retain the right-hand sides only in one of Equation 11.7.25 and obtain, letting $\mu^{(2)} = \mu_f$, the same solution.

However, these particular results do not allow us to make any generalizations, since the cases presented here are usually associated with *different* systems of equations.

Finally, from the derivation itself of the relaxation viscosity, it does not enter into the stresses in the equations of motion but only in the source term of the transformed equation of continuity 11.7.8 as a limiting product of precisely inviscid nonequilibrium gas model and is, therefore, already present in the latter. In other words, the exact solution of the system of equations governing inviscid nonequilibrium flows under near-equilibrium conditions gives also an exact description of all the dissipative relaxation effects mentioned previously.

11.8 General Theory of Stationary Waves in Relaxing Media

In Section 11.5 we formulated the problem of shock waves followed by relaxation zones. In the following, based on the properties of shock adiabats introduced in Section 3.4, we will give the general theory of these waves, both equilibrium and nonequilibrium (in the sense of Section 3.1), that is, propagating in equilibrium and nonequilibrium media, respectively; in the latter case, the final state of the medium is equilibrium. The states on either side of an equilibrium wave are related by the same equilibrium equation of state, which is impossible in the case of nonequilibrium waves. In this sense, frozen shocks (see Section 11.5) with the same variables $\lambda_i = \lambda_{i1}$ on either side of the shock, should be assigned to equilibrium ones.

Typical examples of these nonequilibrium adiabatic waves are also *detonation* and *combustion* waves; in these waves reactions proceed in the absence of external heat sources. Continuous stationary waves (zones) of relaxation and combustion can also be assigned to nonequilibrium waves; on either side of such a wave the states are related by the same equations as for shock waves.

Along with the nonequilibrium waves, we will consider *nonadiabatic waves*, which may incorporate sources (or sinks) of the external energy q_m , provided that their action is localized in a fairly narrow zone included in the wave structure. These sources can be due to gas heating by external radiation, or vice versa, energy release, plasma heating by an electromagnetic field, and so on.

Among nonadiabatic waves are also *sublimation waves* due to evaporation of condensed matter under the action of a powerful incident flux of energy (radiation, X-ray, electron flux, etc.).

We note that in any case by the wave is meant, as in Section 11.5, a region on the boundaries of which the dissipative terms are absent and relations 1.7.12 pass (for $q_m = 0$) to the conventional relations on discontinuities, such as 3.1.1, 11.5.1, and so on.

There is an analogy between all these waves; to demonstrate it, we pass from the enthalpy h in the adiabatic Equation 3.3.4 to the enthalpy of the external degrees of freedom $h^{(0)}$, or, actually, to the temperature, and bring Equation 1.7.12 (without dissipative terms) into the form:

$$\begin{aligned} \rho v &= \rho_1 v_1 = m, & p - p_1 &= \rho_1 v_1^2 - \rho v^2 \\ h^{(0)} - h_1^{(0)} &= \frac{1}{2} v_1^2 - \frac{1}{2} v^2 + q_0 \\ q_0 &= q_m + \Delta h_f, & \Delta h_f &= h_{f1} - h_f \\ h_f &= h - h^{(0)}, & h^{(0)} &= c_p^{(0)} T = \frac{\gamma_f}{\gamma_f - 1} \frac{p}{\rho} \end{aligned} \quad (11.8.1)$$

Here, subscript 2 is dropped out and h_f is the energy of physicochemical transformations, the variation of which is, as it were, a source of external energy with respect to the subsystem of the external degrees of freedom.

All the possible gas states behind these waves traveling in a gas at a velocity v_1 are presented in the phase plane (h, p) (as in Section 3.4) or $(p, V = \rho^{-1})$ (as in Section 4.12) by shock adiabats, which are obtained by the substitution of the equilibrium equations of state $\rho = \rho_e(p, h)$ or $h = h_e(p, \rho)$ in the dependence $h = h(p_1, \rho_1, h_1, p, \rho)$ (3.4.3). It is important to note that these adiabats represent the integral characteristics of the waves under consideration and are independent of their internal structure.

Excluding the parameter v_1 from Equation 11.8.1 we arrive, as in Section 3.4, at the *generalized* equation of shock adiabat, analogous to Equation 3.4.3 (we will retain this conventional term although it seems to be inconsistent with nonadiabatic and continuous waves)

$$h^{(0)} - h_1^{(0)} = \frac{1}{2} \left(\frac{1}{\rho_1} + \frac{1}{\rho} \right) (p - p_1) + q_0 \quad (11.8.2)$$

The outward appearance of this equation is the same for all the previously mentioned waves. As for the direct generalization of Equation 3.4.3, it is as follows:

$$h - h_1 = \frac{1}{2} \left(\frac{1}{\rho_1} + \frac{1}{\rho} \right) (p - p_1) + q_m \quad (11.8.3)$$

However, the form, 11.8.2, of this equation is more convenient for illustrative physical reasoning.

We are coming now to an analysis of adiabats and adiabat-governed processes. Following a common practice for the problems of this kind and in distinction to Section 3.4, we will choose for our analysis a plane (p, V) in which, for the given velocity v_1 , all intermediate and final states of these waves lie on straight lines (3.4.4) or on the rays

$$p - p_1 = \rho_1^2 v_1^2 (V_1 - V), \quad V = \rho^{-1} \quad (11.8.4)$$

Equations 11.8.1 through 11.8.4 can be applied to any internal section of continuous relaxation zones, provided that their structure is inviscid, which is for the moment assumed.

The frozen (I), equilibrium (II), and nonequilibrium (III and IV) adiabats are qualitatively shown in Figure 11.10a on the assumption that these curves are monotonic. For adiabatic equilibrium and frozen waves, adiabats I and II studied in Section 3.4, pass through point 1 with the tangent rays with $v_1 = a_{f1}$ and $v_1 = a_{e1}$, respectively. Since $a_f \geq a_e$, in the vicinity of point 1 adiabat II is located below adiabat I. At the same time, adiabats III and IV are

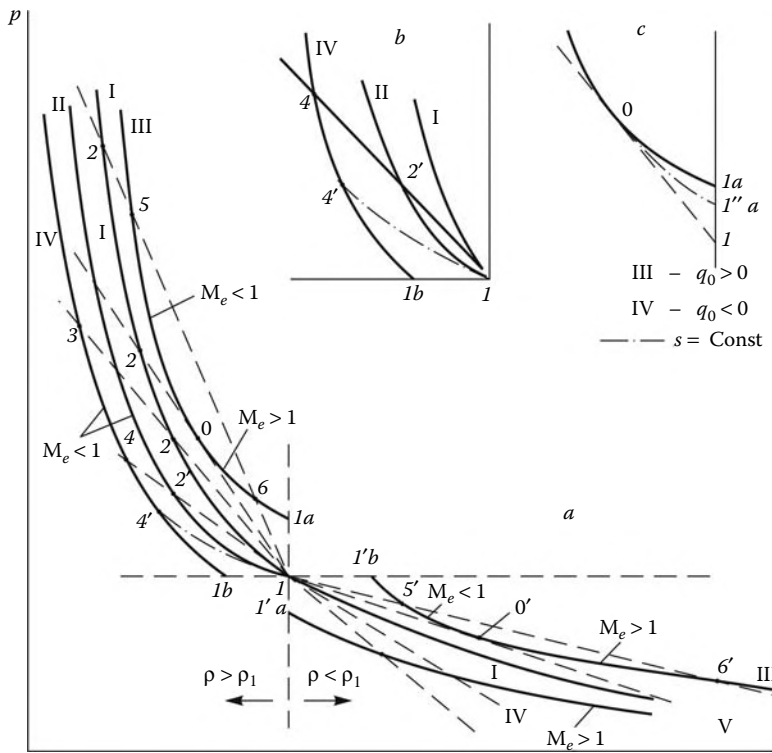


FIGURE 11.10
Shock adiabats in the p, V plane.

located on either side of adiabat I and are constructed for both compression and expansion waves, in accordance with two solutions 3.1.2 for the relations on a discontinuity. For $q_0 \neq 0$ these adiabats cannot pass through point 1, as it would be the case for equilibrium waves with $q_0 = 0$. At $q_0 > 0$ the passage from point 1 onto the adiabats is accompanied by gas heating and an increase in the pressure (at $\rho = \rho_1$) or specific volume (at $p = p_1$). On the diagram these states correspond to points 1a and 1'b. At $q_0 < 0$ the process is reversed, with the corresponding points 1'a and 1b. Thus, it should be expected that the case $q_0 > 0$ corresponds to adiabat III (we will conditionally call these waves *exothermal*) and the case $q_0 < 0$ to adiabat IV (*endothermal waves*). The regions of the adiabats omitted from the figure are unlikely, since they contradict to conditions 3.1.2 $\rho_2 > \rho_1$ for $p_2 > p_1$ and $\rho_2 < \rho_1$ for $p_2 < p_1$.

In the rarefaction region, adiabats I and II are physically unrealized, since in passing from state 1 onto these adiabats the entropy decreases, as shown in Section 3.4, which is forbidden for adiabatic processes by the second law of thermodynamics. However, this assertion cannot be extended to nonadiabatic and nonequilibrium rarefaction waves, in which the entropy rise is quite possible (e.g., in relaxation zones). For this reason, we will draw a simultaneous analysis of both compression and expansion waves based on relations 3.4.5 and 3.4.9 along adiabats

$$T \frac{ds}{dv_1} = v_1 \left(1 - \frac{\rho_1}{\rho}\right)^2, \quad (1 - M_e^2) \frac{dp}{dv_1} = W_2 \quad (11.8.5)$$

where $W_2 > 0$ for $\rho > \rho_1$ and $W_2 < 0$ for $\rho < \rho_1$. By generalizing the analysis performed in Section 3.4 one can be easily convinced that these relations hold also for adiabats that do not pass through point 1, at least for adiabatic nonequilibrium waves, which will be studied first.

The left and right branches of adiabat IV are singly intersected by rays 11.8.3, the condition $dp/dv_1 > 0$ being fulfilled on them. Therefore, on these branches $M_e < 1$ for $\rho > \rho_1$, that is, on the left of Figure 11.10a, and $M_e > 1$ for $\rho < \rho_1$, or on the right of this figure. At the same time, both branches of adiabat III are either twice intersected by these rays or not intersected at all. At points O and O' , called the *Jouguet points*, the rays are tangent to the adiabats. At these points $dv_1 = 0$, $ds = 0$, and $dp/dv_1 = \infty$; therefore, in accordance with 11.8.5, $M_e = 1$, that is, *behind these Jouguet waves the gas flows at the sonic velocity*. In accordance with the signs of the derivatives dp/dv_1 and the functions W_2 , we have $M_e < 1$ to the left and $M_e > 1$ to the right of these points.

At point O of adiabat III, the enthalpy $s = s_0$ is minimum; nevertheless, the inequality $s_0 > s_1$, which is necessary for the state O to be realized, still holds. In fact, at point O , the isentrope $p = p_e(V)$ is tangent to adiabat III. Thus, by virtue of the main condition of our analysis 3.4.1, namely, $(\partial^2 p / \partial V^2)_s > 0$, it intersects the vertical line 1-1a at point 1'a in Figure 11.10c lying above point 1. However, the equilibrium transition at a constant volume from point 1 to point 1a or 1'a is accompanied by the rise of the entropy (that is, $s_0 > s_1$), since it can be realized only at the cost of heat addition. For the same reason the equilibrium transition at a constant pressure from point 1 to point 1'b in Figure 11.10a is also accompanied by an increase in the entropy along the right branch of adiabat III to the point O' , where it attains a maximum. Thus, the branch 1'b-O' of this adiabat is also physically realizable.

Reasoning in the same fashion, we obtain that the entropy at points 1b and 1'a is less than at point 1; hence, the right branch of adiabat IV, along which the entropy decreases simultaneously with the ray slope, is physically unrealizable, as the right branches of adiabats I and II. As for the left (compression) branch of adiabat IV, only the points lying above point 4' of the intersection between this adiabat and isentrope 1-4', are attainable.

The $M_{f1} = 1$ ray is tangent to the frozen adiabat I at point 1 and lies everywhere below it; thus, in the vicinity of point 1 the $M_{f1} > 1$ rays are located above this adiabat for $\rho > \rho_1$ and below it for $\rho < \rho_1$, while for the $M_{f1} < 1$ rays the pattern is opposite. The points of the branch 1a-O of adiabat III can be attained in continuous waves along the "supersonic" rays 1-6 with $M_{f1} > 1$, only if at these points the condition $M_f > 1$ is fulfilled together with the condition $M_e > 1$, that is, when the internal singular point $M_f = 1$ is absent, which is hardly probable in a compression wave. On the contrary, adiabats II and IV and the branch 0-5 of adiabat III cannot be attained in continuous waves, owing to the condition $M_f < M_e < 1$ on these curves. However, they can be attained in the shock-relaxation process described in Section 11.5, in which the gas passes in the frozen shock from state 1 to state 2 on adiabat I with $M_f < 1$ on it and then passes continuously through continuous relaxation waves along the segments of rays 2-3 or 2-5 to the final state on the corresponding adiabats. Further motion along ray 5-6, as well as 6-5 transition, is no longer possible, since the gas having attained equilibrium at point 5 (or 6) has no urge for changing its state.

In the compression region, the subsonic rays with $M_{f1} < 1$ lie below adiabat I and tangent 1-2'-4 to this curve (Figure 11.10b); therefore, the states on the *equilibrium* adiabat II below point 2', that is, at the velocities $a_{f1} \geq v_1 \geq a_{e1}$, can be attained through continuous compression waves only. The region 4'-4 of adiabat IV can also be attained only through continuous waves.

Finally, the right branch of adiabat III is intersected by subsonic rays only; in this case, segment 1'b-O' can be attained along waves 1-5', while transition from state 5' to state 6' along ray 5'-6' is no longer possible for the same reasons as 5-6 and 6-5 transitions.

Let us consider in more detail the Jouguet points O and O' on the exothermal adiabat III, at which the Mach number $M_e = 1$. The waves corresponding to these points are noteworthy by the fact that they cannot be overtaken by any disturbances traveling behind them at the equilibrium speed of sound, and the pressure behind them is the least possible for waves of this type. The expression for the velocity $v_1 = D$ of these waves is derived as follows. We use formulas 11.3.14 and 11.2.4 written in the form:

$$a_e^2 = \gamma_e \frac{p}{\rho} = \gamma_e \frac{R}{M_e} T = \frac{\gamma_e(\gamma_f - 1)}{\gamma_f} c_p^{(0)} T, \quad (\gamma_f - 1) c_p^{(0)} T = a_f^2 \quad (11.8.6)$$

From Equation 11.8.1 at $v = a_e$ we obtain

$$\begin{aligned} a_e &= kD, & k &= \frac{\rho_1}{\rho} = \frac{\gamma_e}{\gamma_e + 1} \left(1 + \frac{p_1}{\rho_1 D^2} \right) \\ & & & (\gamma_e + 1)(p - p_1) = \rho_1 D^2 - \gamma_e p_1 \end{aligned} \quad (11.8.7)$$

Expressing the quantities T and k from these formulas and substituting them into the energy Equation 11.8.1 we reduce the latter to a biquadratic equation for D , the solution of which we write down only for a perfect gas replacing for this purpose the exponents γ_e and γ_{f1} by γ_f (since precisely the difference $\gamma_f - 1$ enters into the coefficient of the large quantity q_0)

$$D_{\pm} = \sqrt{\frac{1}{2}(\gamma_f^2 - 1)q_0 + a_{f1}^2} \pm \sqrt{\frac{1}{2}(\gamma_f^2 - 1)q_0}, \quad D_+ D_- = a_{f1}^2 \quad (11.8.8)$$

Here, the solution $D_+ > a_{f1}$ corresponds to the supersonic and $D_- < a_{f1}$ to the subsonic waves. Obviously, the Jouguet waves can exist only for $q_0 > 0$. In accordance with Figure 11.10a, the previous formulas impose restrictions on the least possible velocities of compression waves and the greatest possible velocities of expansion waves. If these waves propagate through a gas at rest, the *entrainment velocity* of the gas behind the waves is as follows (cf. Equation 3.3.5):

$$u_{\pm} = D_{\pm}(1 - k) = D_{\pm} - a_{\pm}, \quad u_{\pm} + a_{\pm} = D_{\pm} \quad (11.8.9)$$

In compression waves $k < 1$, $a_{\pm} < D_{\pm}$, and $u_{\pm} > 0$. However, in expansion waves $k > 1$, $a_- > D_-$, and $u_- < 0$; therefore, in this case it is more convenient to operate with the velocity of the gas *outflow* from a wave $u^{(-)} = -u_- > 0$.

We will now consider shock adiabats of mixed type with the sources q_0 of alternate signs with respect to v_1 , as shown in Figure 11.11. They are possible, for example, in a binary mixture of atoms and molecules or in a plasma in which the concentrations of atoms and electrons ahead of the wave are greater than the equilibrium values behind the wave, whose velocity is smaller than a certain critical value, $v_1 < D_*$ (the case $\lambda_1 > \lambda_{2e}$ in Figure 10.2 of Section 10.4). In this case, recombination or deionization reactions proceed behind the shock wave with $\Delta h_f > 0$. Therefore, the corresponding interval of adiabat V below point 7 (Figure 11.11a) is similar to the exothermal adiabat III in Figure 11.10. However, for $v_1 > D_*$ further dissociation or ionization with $\Delta h_f < 0$ occurs behind the shock, which becomes endothermal, while above point 7 adiabat V is located to the left of the frozen adiabat I. At $v_1 = D_*$ we have $\Delta h_f = 0$ and both adiabats intersect at point 7. In this case,

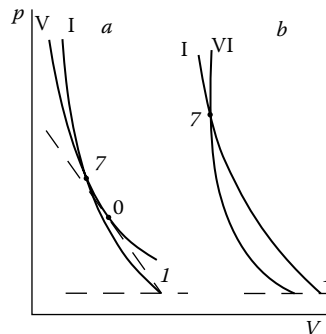


FIGURE 11.11
Shock adiabats of mixed type.

the Jouguet point lies always in the region $\Delta h_f > 0$, that is, below point 7, which follows, in particular, from Figure 11.12 for a nonequilibrium binary mixture of nitrogen atoms and molecules.

On the contrary, if the dissociation or ionization degree ahead of the wave is below the equilibrium value behind the wave (that is, $\Delta h_f < 0$; the case $\lambda_1 < \lambda_{2e}$ in Figure 10.2), but, with increase in the temperature (or the velocity v_1), some exothermal processes accompanied by the change of sign of Δh_f start in the gas mixture, then the corresponding adiabat VI, as well as the equilibrium adiabat II, may intersect adiabat I and then go to the right of it (Figure 11.11b).

For nonadiabatic waves, in the preceding reasoning Δh_f should be replaced by $q_0 = q_m + \Delta h_f$. This will not affect the inference about the relative position of the adiabats in Figures 11.10 and 11.11, although in this case adiabats III and IV can have other shapes due to the fact that the heat source q_m is usually considerably dependent on the gas temperature or composition behind the shock, that is, the velocity v_1 (for both radiative and electromagnetic nature of q_m). In this case, relations 11.8.5 hold only if in 11.8.1 $q_m = \text{const}$; then all the properties of the Jouguet points are conserved. However, even in this simple case the conclusions on the physical realization of individual adiabat branches based on the second law of thermodynamics require an additional analysis for $q_m \neq 0$.

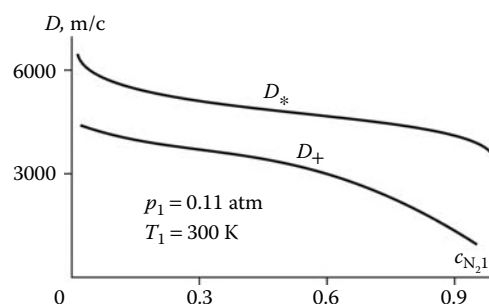


FIGURE 11.12
Detonation wave speed D_+ and critical velocity D_* of a shock wave in nonequilibrium nitrogen.

In particular, for an inviscid equilibrium flow in a thermal nozzle (Section 2.1) with a bounded zone of heat release or removal, which can also be considered as a wave, the singular point is the point $M_e = 1$ and the attainable states are those described by the branch 1'b-0' of adiabat III for $q_m > 0$ and the right branch of the endothermal adiabat IV on rays with $M_{e1} \geq 1$ and its left branch below point 4' for $q_m < 0$. An example of this thermal nozzle can be provided by the flow across the plane of rotation (in an electromagnetic field) of a voltaic arc in benchmark electric-arc setups.

An example of purely nonadiabatic waves is furnished by a wave traveling at a superhigh velocity, behind the front of which intense energy quenching occurs (schematically, in a thin layer behind the wave). Then in Figure 10.10a this wave is associated with transition from curve I to IV along segment 2-3. In another case, a shock wave induced by a laser beam nonabsorbed by cold gas is associated with transition from adiabat I to III along segment 2-5.

We note, however, that a similar analysis of the resulting adiabats of stationary waves can turn out to be inadequate for determining the conditions of their existence in the cases in which the quantities q_0 determined for each section of the relaxation zone reverse sign within the zone. A similar situation may also occur in gases with exothermal and endothermal reactions separated in time within the relaxation zone. This can result in the appearance of internal singular points with $M_f = 1$ (or $M_e = 1$), which are not predicted by the adiabat analysis.

We also note that considering the presence of the internal singular point with $M_f = 1$ in waves as an indication of the prohibition against the physical attainability of states corresponding to separate regions of adiabats in Figure 11.10a is generally legitimate only for waves with an inviscid structure (e.g., relaxation waves) within which relations 11.8.1 hold along rays 11.8.4. However, these relations are invalid for thermal waves (Sections 11.12), so that the prohibition against, for example, the realization of states 0'-6' on adiabat III requires additional validation (see Sections 11.12 and 11.13).

The application of this theory to detonation and combustion waves traveling through a *metastable nonequilibrium medium* is especially fruitful.* Among these media are almost all explosives, including gaseous ones, which at standard, or room, conditions can conserve their composition for years. Combustion processes in such media start only when the temperature increases up to a certain limiting value determined by the power-law temperature dependence of the reaction rate, for example, of the type $k_f \sim e^{-\theta/T}$ with fairly high values of θ , as considered in Section 10.9.

The shock detonation waves, as conventional ones described in Section 11.5, have *shock-relaxation structure* (Zeldovich, 1944, 1984) including a bow shock and a relaxation, or combustion, zone behind the former, with its own distinctive features of physicochemical reactions (burning processes) proceeding within it; they are initiated by the temperature increase behind the shock. As in relaxation zones behind conventional shock waves, the flow in these combustion zones may usually be assumed to be inviscid and adiabatic, which makes it possible to apply completely the previous analysis of adiabats in Figure 11.10 to the detonation waves.

The detonation waves propagate at a supersonic velocity and correspond to the region 0-5 of adiabat III to the left of point O in Figure 11.10a. The most widespread are the Jouguet detonation waves that can propagate, say, through a bar of solid explosive without being

* The detailed presentation of the physical and mathematical aspects of this theory can be found, for example, in Zeldovich, Barenblatt, Librovich, and Makhviladze, 1980.

attenuated by the disturbances arising behind the wave. Therefore, in order to accelerate the detonation front, the pressure behind it must be increased. This detonation wave is called *overcompressed*. At the same time, a decaying plane overcompressed detonation wave approaches the Jouguet wave only asymptotically, or at infinity, like a weak shock wave approaching an acoustic wave (Section 4.8). However, as distinct from the plane waves, the similar cylindrical and spherical waves can convert themselves to the limiting Jouguet waves already at a finite distance from their initiation (Levin and Chernyi, 1967).

The possible range of detonation wave intensity is very wide. Thus, in oxyhydrogen gas consisting of 7/8 mass fractions of oxygen and 1/8 of hydrogen, at $p = 1$ atm and $T_1 = 300$ K the Jouguet wave has the velocity $D_+ \approx 2900$ m/s and the following parameters behind it, $p/p_1 = 18$ and $T = 3600$ K. Behind the wave, the gas consists mainly of water (H_2O) molecules with an admixture of other molecules. At the same time, in condensed explosives, the pressure behind the detonation wave can be as high as 10^5 atm. As behind any other shock wave, gaseous combustion products can have the density exceeding that of the original condensed matter.

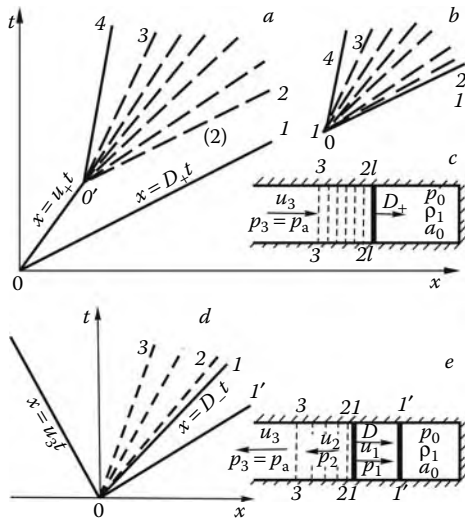
As distinct from detonation waves, combustion waves propagate at a subsonic velocity; they are associated with the right branch of adiabat III or, to be more precise, its region 5'-0' (see the following). In these waves, the combustion mixture heating and ignition is realized via heat transfer from heated combustion products, which determines the *natural velocity* D_0 of the wave propagation over a gas at rest. This velocity is dependent on the properties of a medium and, usually only slightly, the external conditions (usually D_0 is fairly small; thus, for oxyhydrogen gas under standard conditions it is of the order of a few m/s, while the Jouguet wave velocity, were it to be reached, would amount to, according to 11.8.8, several tens of m/s).

The same properties, that is, the existence of the natural propagation velocity determined by the internal wave structure, are inherent in other rarefaction waves (those in an electromagnetic high-frequency field, in an incident radiation flux, etc., under the condition that the gas subjected to the action is transparent in its original state, as well as sublimation waves). In what follows, all these waves, nonequilibrium and nonadiabatic, will be unified by the same term *thermal waves*.

We will consider the gas dynamic features of the propagation of nonequilibrium and nonadiabatic waves. In spite of their different physical nature, all stationary shock waves have something in common from the standpoint of the formulation of the problem. Thus, at an unknown velocity v_1 of their propagation, one more parameter behind the wave must be specified to determine it completely; this can be the pressure, the gas velocity, and so on, of course, on the range of existence of stationary waves. For example, for detonation waves a given pressure behind the wave cannot be less than that corresponding to the Jouguet point.

We will explain these properties of detonation waves with reference to a simple example of their propagation in a constant-area channel (Figure 11.13a to c). Let in this channel a Jouguet detonation wave $x = D_+t$ travel from left to right (lines 1 in Figure 11.13a and b) with states 1 and 2 ahead of and behind it and let it be followed by a piston with the entrainment velocity $u_+ = D_+/2 = a_+$. A sudden increase in the piston velocity (at point 0' in Figure 11.13a) induces a shock wave that overtakes the detonation wave, thus increasing its velocity up to $D > D_+$ and converting it to a previously mentioned overcompressed detonation wave.

On the contrary, a sudden deceleration of the piston to a velocity $u_0 < u_+$ at point 0' (trajectory 0'-4 in Figure 11.13a) results in the appearance of a centered rarefaction wave 2-0'-3 with the leading characteristic 0'-2 parallel to the shock front 0-1. As point 0' approaches

**FIGURE 11.13**

Detonation waves with reference to a simple example of their propagation in a constant-area channel.

point 0, characteristic 0'-2 coalesces with front 0-1, so that in the limit we arrive at a self-similar flow pattern with a stagnation zone 3-0-4 in Figure 11.13b. It can be assumed that this pattern is also limiting for any other transition trajectory with a final velocity $u_0 < u^{(+)}$ provided, naturally, that the temperature of the gas behind the primary shock wave is sufficient for ignition of the combustible mixture.

At the travel of a detonation wave in a channel with an open left end (Figure 11.13c) at an external pressure $p_a > p_+$, where p_+ is the pressure behind the Jouguet wave, the detonation wave will be overcompressed, with a velocity $D > D_+$. However, at $p_a < p_+$ a Jouguet wave is formed that has a velocity D_+ and is adjoined by a centered rarefaction wave 2-3 (Figure 11.13c) with the pressure $p_3 = p_a$ at its exit; when the detonation wave is formed in a channel with a dead left end ($u_0 = 0$), there is a stagnation region to the left of characteristic 0-3 in Figure 11.13b.

We will now consider rarefaction waves. For a given state 1 ahead of a thermal wave, the previously mentioned additional condition for its natural velocity D_0 , together with relations 11.8.1, completely determine state 2 behind the wave, which, in contrast to a shock wave, makes impossible the satisfaction of any conditions behind the wave without changing the state ahead of it.

By way of illustration, we will consider a channel with a dead right end and an open left end (Figure 11.13d) with an initial pressure p_0 ; we will begin with the case in which p_0 is equal to the external pressure p_a . Thermal wave 1 travels along the channel from left to right at a velocity D with states 1 and 2 ahead of and behind it. At a small wave intensity, the pressure in a subsonic jet issuing from the wave at a velocity u_2 is approximately equal to the atmospheric pressure $p_2 = p_a$; thus, using Equation 11.8.1 we can determine the pressure $p_1 > p_a$. Therefore, the wave is preceded by a compression wave 1' with a velocity u_1 behind it. Specifying the value $p_2 = p_a$ and the relations on both fronts closes the problem.

In a laboratory coordinate system, the wave and gas velocities (see Figure 11.13d) are as follows

$$D = D_0 + u_1, \quad u_2 = u^{(-)} - D, \quad u^{(-)} = D_0(\rho_1/\rho_2 - 1) \quad (11.8.10)$$

where D_0 is the natural velocity of the wave and $u^{(-)}$ is the relative velocity of the gas outflow from the wave. Sonic waves travel from left to right at a velocity

$$\frac{dx}{dt} = -u_2 + a_2 = a_2 - u^{(+)} + D \quad (11.8.11)$$

For $u^{(-)} < a_2$ these waves overtake wave 1 with the result that the external pressure p_a has an effect on the flow throughout the entire channel; then the parameters u_2, p_2 , and so on, immediately behind front 1 are the same as u_3, p_3 , and so on, at the channel exit.

This flow pattern is qualitatively conserved for all natural velocities D_0 (we will assume D_0 to be an independent parameter), up to the Jouguet wave velocity $D_0 = D_-$. However, for $D_0 = D_-$ and $u^{(-)} = a_2 = a_-$ waves (11.8.11) proceeding from the left channel end are no longer able to overtake front 1; thus, they have no effect on its velocity and the flow parameters to the right of it. Rigorously speaking, this inference does not concern compression waves, which, in accordance with Sections 4.5 to 4.7, travel somewhat faster than acoustic waves; however, rarefaction waves induced by a decrease in the pressure p_a can propagate up to front 1 (since, by virtue of Equation 11.8.10, $u_2 < a_2$ for $u^{(-)} = a_2$), thus forming a rarefaction wave 2-3 in Figure 11.13d and retaining the condition $p_3 = p_a$. Only when the condition $u_3 = a_3$ is fulfilled, that is, at sonic jet outflow from the channel, further decrease in the pressure p_a has no longer an effect on the channel flow. The velocity of this jet relative to the wave front 1 is supersonic. The limiting self-similar flow pattern at $D_0 = D_-$ is presented in Figure 11.13e, where 3-0-2 is a centered rarefaction wave. At $u_3 = a_3$ characteristic 0-3 coincides with the t axis.

Since $D_0 < a_1$, in a channel of finite size the compression front 1' arrives sooner or later to the right end and after repeated travel of these waves along the channel, a stagnation region with a pressure $p_1 = p_a + \rho_1 D_- u^{(-)} > p_a$ will occur ahead of wave 1; this channel represents a very simple model of a jet engine.

We note that, as mentioned previously, the theory outlined here does not involve a prohibition against the existence of rarefaction waves with a supersonic velocity $u^{(-)} > a_-$ corresponding to the region 0'-6' of adiabat III. For $p_3 > p_a$ the ambient medium has also no effect on them. However, such waves were never observed and any time-dependent process that would lead in the limit $t \rightarrow \infty$, all the boundary conditions being satisfied, to the attainment of their steady state, has not as yet been constructed, even theoretically. In other words, regimes with $u^{(-)} > a_-$ are *nonevolutionary*. Moreover, there is good reason to think that the solutions of the corresponding problems on the structure of these waves with regard for actual internal dissipation effects cannot lead to a supersonic flow behind the front, much as taking dissipative effects into account in Section 3.2 resulted in the existence of only equilibrium compression fronts with subsonic flows behind them.

Finally, we will dwell briefly on one more important question about the physical realization of one of two regimes permitted by adiabat III in Figure 11.11a, for example, detonation waves (region 5-0) or combustion waves (region 5'-0') for the same value of q_0 . This question can be solved theoretically by a search for a limiting regime for the corresponding time-dependent problem formulated with regard for not only the boundary conditions but also the fashion of combustible mixture ignition. At detonator explosion a detonation wave is usually formed, while at simple ignition this is a combustion wave. However, in principle an initially combustion wave can convert to a detonation wave at a fairly high intensity of the shock wave 1' in Figure 11.13d and, the more so, at its reflection from obstacles in the channel or from its dead end. However, detailed discussion of this question is beyond the scope of this book.

11.9 The Law of Binary Similarity

The formulation of the problem of a body in the flow of a relaxing gas described by Equations 11.1.1 through 11.1.5 is reduced to specifying the body shape $f(\bar{x}, \dots) = 0$, where $\bar{x} = x/L$, and so on, L being the scale length, and the freestream parameters $\rho = \rho_\infty$, and so on. Thus, the problem involves the parameters $p_\infty, \rho_\infty, T_\infty, \lambda_{i\infty}, \tilde{U}_\infty$, and L . The freestream gas can be in any state, either equilibrium or nonequilibrium, while the flow itself can be either supersonic or subsonic.

From the standpoint of the similarity and dimensionality theory (Section 1.12), taking the nonequilibrium effects into account makes the problem of the mutual simulation of gas flows more difficult, as compared with the case of an imperfect equilibrium gas with an arbitrary equation of state $\rho = \rho(p, h)$, for which the freestream parameters ρ_∞, U_∞ , and so on, cannot be eliminated from the set of the similarity criteria (Section 1.12).

These rigorous requirements to the simulation can be eased somewhat in the case of hypersonic flows, for which p_∞ and T_∞ can be eliminated from the set of the governing parameters, and thin affinely similar bodies within the framework of the similarity law of Section 8.4 with the similarity criteria $M_\infty \theta$ and $U_\infty \theta$, where θ is the relative body thickness. However, in the general case, the simulation of one nonequilibrium flow by another nonequilibrium flow is impossible.

This general formulation of the problem does not characterize the degree of the nonequilibrium effect on the flow. To do this, the reaction time scales τ_s should be separated out from the functions Λ_i in accordance with Section 11.2; this leads to the appearance of new relevant parameters $U_\infty \tau_s / L$ (instead of L) with the corresponding classification of the flows into frozen (for $U_\infty \tau_s / L \gg 1$), developed nonequilibrium (for $U_\infty \tau_s / L \sim 1$), and equilibrium (for $U_\infty \tau_s / L \ll 1$) ones.

However, in view of the complicated form of the functions $\tau_s(p, T, \lambda_j)$ themselves, this approach does not generally simplify the problem of the mutual simulation of the flows. The simplification turns out to be possible only for the times $\tau_s \sim p^{-1}$, that is, for gases with the kinetics equations of the particular form:

$$\frac{d\lambda_i}{dt} = \Lambda_i(p, T, \lambda_n) = p \bar{\Lambda}_i(T, \lambda_n) \quad (11.9.1)$$

Similar equations were obtained in Section 10.4 for relaxation of the internal degrees of freedom and in Section 10.9 for exchange reactions (Equation 10.9.6). Moreover, in the kinetics equations of more general type (Equation 10.9.5), the second term can be neglected for the forward part of the relaxation zone behind the shock in a cold gas, due to, first, the low concentration of atomic products of reaction in this zone and, second, a fairly high gas temperature, which underlines the role of the forward reaction rate coefficient k_f , exponentially dependent on the temperature. We note that the equilibrium conditions $\Lambda_i = 0$ for the processes described by Equation 11.9.2 are also independent of the pressure.

In this case, introducing the variables and functions

$$\bar{x} = x/L, \quad \bar{p} = p/p_\infty, \quad \bar{\rho} = \rho/\rho_\infty \quad (11.9.2)$$

we bring Equation 11.9.1 into the form:

$$\rho_\infty L \left(u \frac{\partial \lambda_i}{\partial \bar{x}} + \dots \right) = \bar{p} \bar{\Lambda}_i(T, \lambda_j) \quad (11.9.3)$$

Equations 11.1.1 through 11.1.4, the shock relations, 11.5.2, and the impermeability conditions on the body do not change their form in the new variables. Then inviscid nonequilibrium flows of the same gas with the equal parameters \bar{p}_∞ , T_∞ , \bar{U}_∞ , and $\rho_\infty L$ are similar in the sense of Section 1.12, that is, the distributions of the functions \bar{p} , $\bar{\rho}$, \bar{T} , and so on, are the same in the dimensionless variables \bar{x} , \bar{y} , and \bar{z} .

This is the *law of binary similarity*, while the product $\rho_\infty L$ is called the *binary similarity parameter*. As for the fact that this parameter and the gas dynamic functions are dimensional, it does not contradict similarity theory in light of the explanation made in Section 1.12 for imperfect gases.

The testing of this similarity law for bodies in hypersonic flow will be made in the next section, together with an analysis of the distinctive features of the flowfields involved. Here, in addition to Section 11.5, we will consider from this standpoint the shock structure, restricting ourselves to the case of normal shocks. In this case, there is no scale length L , so that introducing the new variables $\xi = \rho_\infty t$ and $\eta = \rho_\infty x$ (the x coordinate is directed along the shock normal) we reduce Equations 11.9.1 and 11.9.3 to the form:

$$\frac{d\lambda_i}{d\xi} = u \frac{\partial \lambda_i}{\partial \eta} = \bar{p} \bar{\Lambda}_i(T, \lambda_n) \quad (11.9.4)$$

The solution of this system, that is, the set of the functions \bar{p} , $\bar{\rho}$, h , T , λ_i , and u depends only on the binary similarity variables ξ and η and on the initial parameters ahead of the shock \bar{p}_∞ , T_∞ , $\lambda_{i\infty}$, and $u = v_{n\infty}$ but is independent of the density ρ_∞ ahead of the shock.

From the binary similarity law there follows a simple dependence $\delta_r = \eta_s / \rho_\infty$ for the relaxation zone thickness behind the shock. As applied to hypersonic atmospheric flight of bodies, the effect of the parameters \bar{p}_∞ and T_∞ can be neglected. Since the composition of the terrestrial atmosphere (parameters $\lambda_{i\infty}$) is actually the same everywhere, the solution thus obtained is independent of the flight altitude H . The data in Figures 11.4 and 11.5 from Section 11.5, in which ρ_∞ is denoted as ρ_1 , are processed precisely in the binary similarity variables. Clearly, even for densities ρ_∞ differing by a factor of 1000 (for $H = 30 - 80$ km), the curves for the forward part of the relaxation zone almost coincide when constructed in the similarity variable η , though they cannot even be presented on the same scale in the original coordinate. For most of the flow parameters (except for c_{NO}) these curves are also fairly close in the rear of the zone, where both terms in Equation 10.9.5 are comparable or, in the limit, even equal. This is attributable to a weak dependence of the equilibrium concentrations of the components on the pressure (which is proportional to the density ρ_∞ in this wave), at a constant or near-constant enthalpy h .

11.10 Nonequilibrium Flows Past Bodies

In this section we will study the distinctive features of the nonequilibrium hypersonic flow past bodies. Qualitatively, these flows are similar to the equilibrium flows discussed in Chapters 7 to 9. However, nonequilibrium results sometimes in some new qualitative effects.

As noted previously, the flow regimes related with nonequilibrium are determined by the ratio of the body scale length L to the longitudinal dimension l_r of the relaxation zone. Behind an oblique shock inclined at an angle of attack α , the quantity $l_r = \delta_r / \sin \alpha$, where δ_r is the relaxation zone thickness introduced in Section 11.5. The flow past bodies is frozen as

a whole for $L \ll l_r$ and equilibrium for $L \gg l_r$. The reservation as a whole is not accidental in this context; it suggests the possible existence of separate flow fragments with their own local scales $L_{\text{loc}} \neq L$, where the previous estimates are inadequate. An example is furnished by the vicinity of a corner point on the body contour (Section 10.6).

This introduction having been done, we will consider the flows past the plane ($\nu = 0$) and axisymmetric ($\nu = 1$) bodies of typical classes; up to a certain moment, the freestream with the parameters ρ_∞ , and so on, will be assumed to be equilibrium and corresponding to the conditions of the atmospheric flight of the bodies. The general case will be considered at the end of the section.

11.10.1 Flow Past Sharp Bodies with an Attached Shock

Very simple examples of this flow are the flows past a wedge and a cone shown in Figure 11.14; here, the x axis is aligned with the freestream velocity vector \vec{U}_∞ , while the l axis is directed along the body surface.

In a small vicinity of the nose, $x \ll l_r$, the flow near the shock Ob is frozen, while in the relaxation zone adjacent to the shock and having the rear front $cc'd$ it is different from an equilibrium flow. The flow to the right of this front is equilibrium; for $x \gg l_r$ it would be expected to be the same as for the original equilibrium flow past the body.

However, some evidence of nonequilibrium effects is conserved even for $x \gg l_r$. In fact, let the nonequilibrium influence on the shock shape be confined to its segment Oa , whose shape differs from that of the shock Oa' in the equilibrium flow past the body, while in the further flow the two shocks, ab and $a'b'$, are parallel and spaced Δ_s apart. For $l \gg \Delta_s$ this difference is no longer significant; however, the difference in the entropy distribution, which exists at the relaxation zone exit cc' , is conserved in the inviscid layer between the body and the boundary streamline $c'f$ with the gas flow rate across the layer $\psi_b \sim r_b^\nu U \Delta_r$, where $r_b(x)$ is the body cross-section radius, U is the gas velocity, and Δ_r is the thickness of this *relaxation-entropy layer* (Zhigulev, 1962). On the wedge the quantity Δ_r is constant, while on the cone it decreases as $\Delta_r \sim r_b^{-1} \sim x^{-1}$.

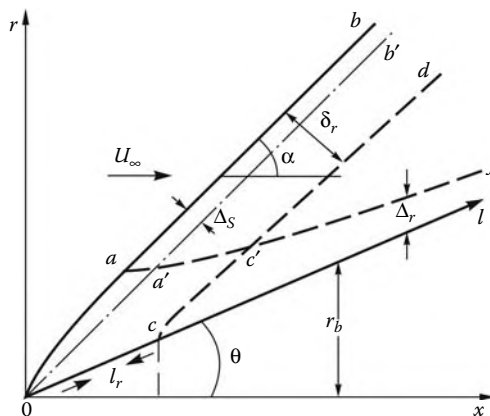


FIGURE 11.14
Nonequilibrium flow past a sharp body.

11.10.2 Thin Shock Layer in a Hypersonic Flow

As shown in Chapter 7, in a hypersonic flow past a body ($M_\infty \gg 1$), when the density ratio is very low, $k = \rho_\infty / \rho_a \ll 1$, where ρ_a is the characteristic density in the shock layer between the shock and the body, the shock layer thickness δ is so small that the shock fits closely the body, while the body pressure depends on γ only slightly and is mainly determined by the slope θ of the body surface to the velocity vector \vec{U}_∞ (e.g., as in the Newtonian theory, $p \approx \rho_\infty U_\infty^2 \sin^2 \alpha$). However, at the same time the shock layer structure, that is, the gas density, temperature, composition, and state, as well as the layer thickness, are dependent on the gas properties. In this case, the shock layer parameters can often be determined or, at least, evaluated by the *streamline method*, which is reduced to the joint solution of Equations 11.1.4 and 11.1.15 and the Bernoulli equation at a preassigned pressure distribution along a streamline l

$$\begin{aligned} U \frac{d\lambda_i}{dl} &= \Lambda_i(p, T, \lambda_n), & \rho &= \rho(p, T, \lambda_n) \\ h &= h(T, \lambda_n) = H - \frac{1}{2} U^2, & p &= p(l) \end{aligned} \quad (11.10.1)$$

The initial conditions for this system are provided by the relations on the frozen shock at the point of its intersection with a given streamline. Then the shock layer thickness is determined by integral 7.2.4, while the shock shape $r_s = r_s(x)$ and the pressure in the shock layer can be taken from the available data on the perfect or equilibrium gas flow past the body.

Generalizing the solutions of Sections 3.7 and 6.4 we can determine the thin shock layer on a wedge or a cone for $k \ll 1$ from solution 11.5.6 putting in it

$$\begin{aligned} p &= \rho_\infty U_{n\infty}^2, & h &= h_n = \frac{1}{2} U_{n\infty}^2, \\ v_1 &= U_{n\infty} = U_\infty \sin \alpha \approx U_\infty \sin \theta \end{aligned} \quad (11.10.2)$$

Here, α is the local angle of the shock inclination.

In this case, the stay t of a particle moving along a streamline $\psi = \text{const}$ in the almost plane relaxation zone is related with the distance $l - l_0$ from the shock along this streamline by the formula

$$\begin{aligned} Ut &= l - l_0, & U &= U_\infty \cos \theta \\ \psi / \pi^\nu \rho_\infty U_\infty &= r^{1+\nu}(l_0) \approx r_b^{1+\nu}(l_0) = (l_0 \sin \theta)^{1+\nu} \end{aligned} \quad (11.10.3)$$

Here, l_0 is the point of the intersection between the shock and the given streamline. Thus, all the shock layer parameters are the functions of the form $\rho = \rho(l - l_0)$. The shock layer thickness δ measured along the normal to the body surface, is determined by integral 7.2.4, as follows:

$$\delta_\nu = \frac{1}{(2\pi r_b)^\nu} \int_0^{\psi_s} \frac{d\psi}{\rho U} = \frac{\tan \theta}{l^\nu} \int_0^l \frac{\rho_\infty}{\rho} dl_0, \quad \psi_s = \psi(l) \quad (11.10.4)$$

For $\rho = \text{const}$ these formulas can be reduced to Equations 3.7.6 and 6.4.7. Differentiating δ_ν with respect to l and taking into account that $d\rho/dl = -d\rho/dl_0$, we determine the shock layer slope

$$\frac{d\delta_0}{dl} = \frac{\rho_\infty \tan \theta}{\rho_0}, \quad \rho_0 = \rho(\psi = 0)$$

$$\frac{d\delta_1}{dl} = \frac{\tan \theta}{l} \int_0^l \left(1 - \frac{l_0}{l}\right) \frac{\rho_\infty}{\rho} dl_0 \quad (11.10.5)$$

Obviously, in the wedge flow the angle between the shock and the body surface is inversely proportional to the wall density $\rho_0(l)$ at $\psi = 0$, which behind the relaxation zone l_r downstream of the shock approaches the equilibrium value ρ_{se} behind the shock. In the conical flow this passage to the equilibrium state is delayed due to presence of the weight factor $1 - l_0/l$ under the integral sign in Equation 11.10.5. Due to the fact that the thickness of the shock layer on the cone is half as large as that on the wedge, the relative thickness of the relaxation zone behind the shock on the cone is smaller than that on the wedge.

These inferences are supported by Figure 11.15. Taking nonequilibrium into account has almost no effect on the body pressure; however, it does affect the shock layer thickness distribution, so that the shock slope varies from the frozen value, as $x \rightarrow 0$, to the equilibrium one, as $x \rightarrow \infty$. The curves in the figure are plotted in the binary similarity variables and are hardly distinguishable though the densities ρ_∞ may differ by a factor of 100.

11.10.3 Stagnation Point on a Blunt Body

At this point the velocity $U = 0$; therefore, the streamline method, as outlined previously, is inapplicable to the vicinity of the axis of symmetry of a blunt body and the solution should be determined using the method of Section 7.9. At small $k = \rho_\infty/\rho_s$, where ρ_s is the density behind the shock, the pressure and the enthalpy in this vicinity are near constant; therefore, in this case we can apply solution 11.5.16 for the relaxation zone. In this solution, the relationship of the variable t with the distance $\delta - y$ from the shock (Figure 11.16) is determined by the equation $dy = -vdt$ or by integral 7.9.1. Since, in accordance with Section 7.8, $v \sim -y$ in the vicinity of the stagnation point, we have also $t \sim -\ln y$, as $y \rightarrow 0$ (cf.

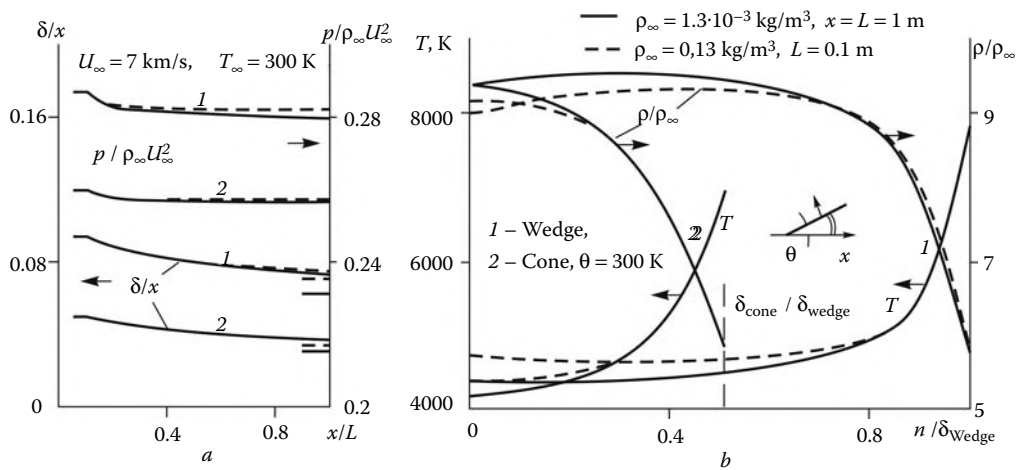


FIGURE 11.15

Relative shock layer thickness and pressure (a) and parameter distributions in the shock layer in nonequilibrium flows past a wedge and a cone.

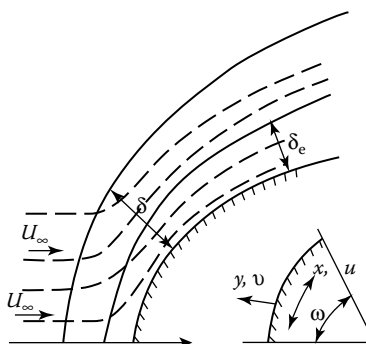


FIGURE 11.16
Flow past a blunt body.

Equation 7.9.2), that is, the infinitely distant point of the relaxation zone is mapped onto the stagnation point. In this case, the gas state approaches to equilibrium, $\rho \rightarrow \rho_e(p'_0, H)$, and so on, determined by the stagnation parameters $p = p'_0$ and $h = H$, which are close to those behind the normal equilibrium shock; therefore, the nonequilibrium structure of the shock layer has almost no effect on the stagnation point parameters.

The velocity distribution $v(y)$ is determined by Equation 7.9.6 which contains the variable density ρ on its right-hand side; therefore, Equations 7.9.6 and 11.5.6 must be solved jointly. For the sake of illustration, we will restrict ourselves to solution 10.4.3 of the relaxation Equation 10.4.1 with constant λ_e and τ . Then, using formulas 7.9.11 with the same functions $\varphi_v(\zeta)$, $\zeta = y/\delta$, we obtain

$$\begin{aligned}\Phi_v &= \frac{\lambda_e - \lambda}{\lambda_e - \lambda_\infty} = e^{-t/\tau} = \varphi_v^{-\kappa(1+v)} \\ \kappa &= \frac{R_s}{\tau U_\infty \sqrt{2k_0 \beta}}, \quad k_0 = \frac{\rho_\infty}{\rho_e}\end{aligned}\quad (11.10.6)$$

The functions Φ_v are plotted in Figure 11.17 for $k_0 = 0.05$, $\beta = 1$, and various values of κ . At $\kappa \gg 1$ a thin relaxation zone is formed near the shock, while the shock layer flow is

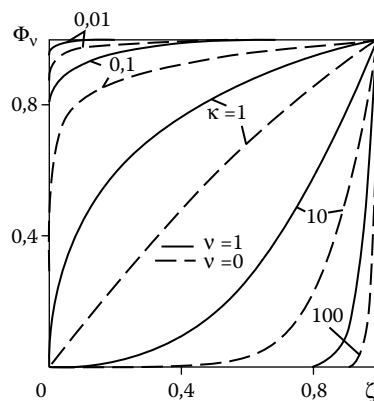
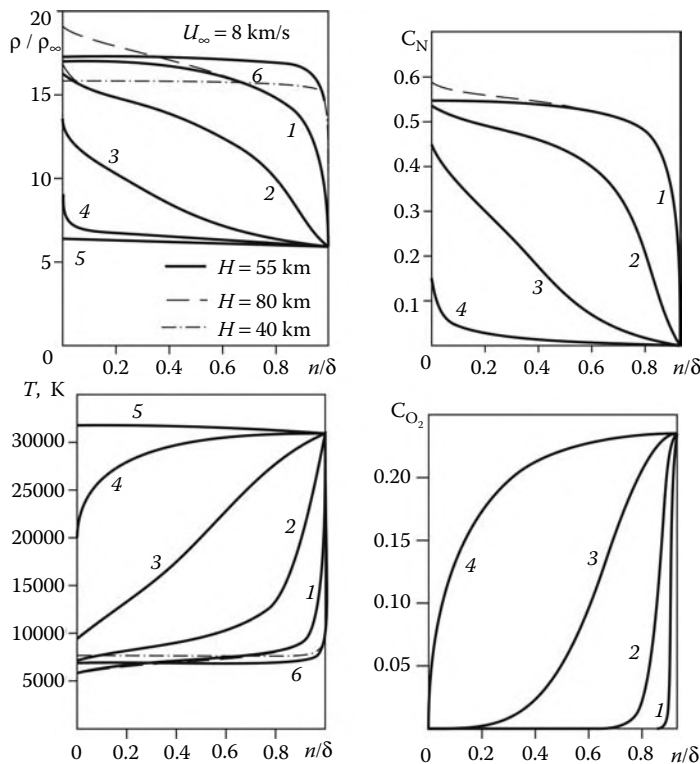


FIGURE 11.17
Concentration profiles along the axis of symmetry for blunt bodies.

**FIGURE 11.18**

Parameter profiles along the axis of symmetry in the shock layer on a sphere.

equilibrium almost everywhere. On the contrary, at $\kappa \ll 1$ the flow is frozen throughout the entire shock layer; however, at the stagnation point it is always equilibrium with the formation of a thin relaxation sublayer of small thickness $\Delta \ll \delta$, the plane sublayer being considerably thicker than the axisymmetric one.

Thus, nonequilibrium flows past blunt bodies tend to their frozen ($\tau \rightarrow \infty$) and equilibrium ($\tau \rightarrow 0$) limits only in the basic (with respect to volume) region with unremovable boundary relaxation zones, though decreasing in extent as $\tau \rightarrow 0$ or $\tau \rightarrow \infty$.

In Figure 11.18 we have plotted the distributions of the density, temperature, and concentrations of the nitrogen atoms (c_N) and oxygen molecules (c_{O_2}) along the axis of symmetry in the shock layers on spheres of different radii R_0 in the air flow at $U_\infty = 8 \text{ km/s}$ and different densities ρ_∞ corresponding to different flight altitudes H ; all these quantities, together with the binary similarity parameter $B = \rho_\infty R_0 \text{ kg/m}^2$ are given in the following table.

Tables of the parameters of the flows presented* in Figures 11.18, 11.19, and 11.23 to 11.26 (R_{ij} is the nose radius R_0 and $B_j = \rho_i R_{ij} \text{ kg/m}^2$, $U_\infty = 8 \text{ km/s}$)

* Data of Gorshkov for the model of Figures 11.3 and 11.4.

I	$H = 40 \text{ km}$	$\rho_I = 4 \cdot 10^{-3} \text{ kg/m}^3$
II	$H = 55 \text{ km}$	$\rho_{II} = 5.9 \cdot 10^{-4} \text{ kg/m}^3$
III	$H = 80 \text{ km}$	$\rho_{III} = 2.1 \cdot 10^{-5} \text{ kg/m}^3$

1	$B_1 = 2.1 \cdot 10^{-4}$	$R_{II1} = 0.35 \text{ m}$	$R_{III1} = 10 \text{ m}$
2	$B_2 = 2.1 \cdot 10^{-5}$	$R_{II2} = 3.5 \text{ m}$	$R_{III2} = 1 \text{ m}$
3	$B_3 = 2.1 \cdot 10^{-6}$	$R_{II3} = 0.35 \text{ cm}$	$R_{III3} = 0.1 \text{ m}$
4	$B_4 = 2.1 \cdot 10^{-7}$	$R_{II4} = 0.035 \text{ cm}$	$R_{III4} = 1 \text{ cm}$
5	$B_5 \rightarrow \infty$	$\gamma = 1.4$	
6	$B_6 = 2.1 \cdot 10^{-3}$	$R_{I6} = 0.52 \text{ m}$	$R_{II6} = 3.5 \text{ m}$

For $B < 10^{-7}$ the flow on the axis is chiefly frozen and, except for the wall relaxation sublayer, is close to the flow of the perfect gas with $\gamma = 1.4$. For $B \sim 10^{-3}$ the flow is near-equilibrium everywhere, except for a narrow relaxation zone behind the shock. The curves for intermediate values of B are located between the two limiting curves, similar to the curves in Figure 11.17; the B -dependence is monotonic. At the stagnation point itself,

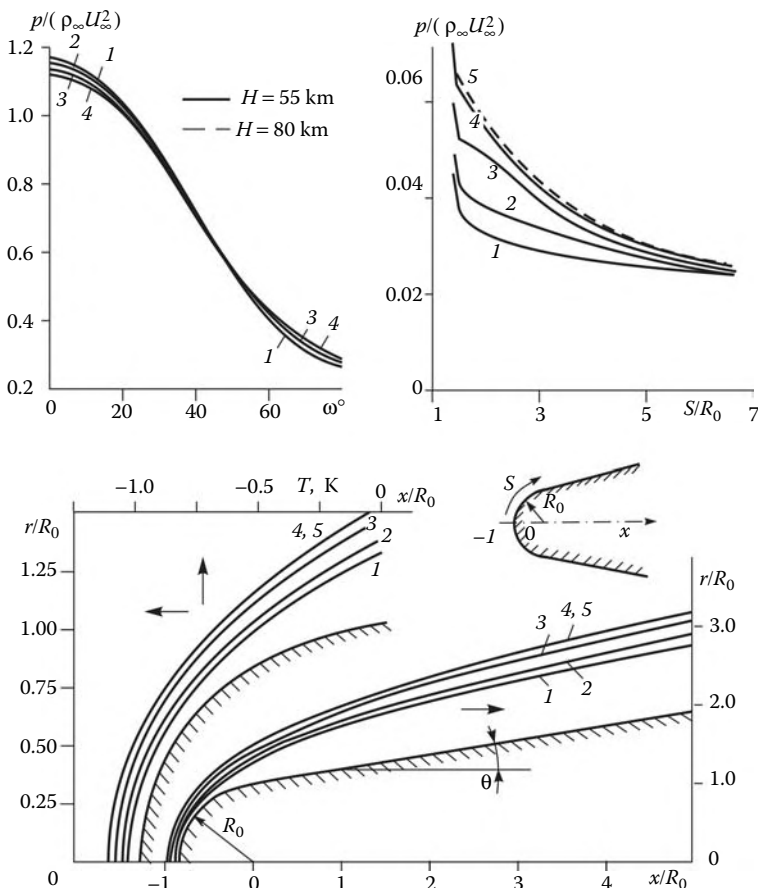


FIGURE 11.19
Pressures and shocks on a sphere and a blunt cone.

the values $\rho = \rho_e$ and $T = T_e$ are dependent in this case only on ρ_∞ but not on B (this is difficult to demonstrate for all B on the scale of the figure).

In Figure 11.18 most of the curves with the same values of B are hardly distinguishable, which supports the binary similarity law. An exception is provided only by the wall layer and the near-equilibrium curves corresponding to $B \approx 10^{-3}$. However, even in these cases, the discrepancy of the curves is comparatively slight, which is favored by a comparatively slight difference in the equilibrium parameters for these flow regimes. We note that this inference pertains also to the data in the following figures, which correspond to the same flow regimes for other bodies.

11.10.4 Sphere and a Slender ($\theta = 10^\circ$) Spherically Blunted Cone

The shock shapes and pressure distributions over these bodies are presented in Figure 11.19 for the same conditions, as in Figure 11.18. As the parameter B is increased, the corresponding curves are located between those for the quasi-equilibrium and perfect gases and follow qualitatively the theories of Chapters 7 and 9. In particular, the pressure distribution over the spherical nose is close to that plotted in Figure 7.2 (Section 7.1) and is consistent with approximation 7.2.6, while the nonequilibrium effect is appreciable only on the lateral surface of the sphere and on the blunt cone nose.

At the same time, the pressure on long blunt cones is less sensitive to nonequilibrium effects. Thus, in Figure 11.20 the nonequilibrium pressure curve is only slightly displaced with respect to the equilibrium one. However, it should be borne in mind that even this slight difference in the pressure distribution can be important in determining such a "fine" flow parameter, as the center of pressure of a body (see Figure 9.32 of Section 9.5).

As shown in Section 9.3, the influence of the real gas properties in the high-entropy layer on thin blunt bodies on the pressure and the shock shape is determined by the effective drag coefficient c_x^* , or, to be more precise, by the ratio c_x^*/c_{x0} , which for equilibrium flows is presented in Figure 9.8 (here, c_{x0} is the blunt nose drag coefficient). For spherically blunted cones with $\theta = 5 - 15^\circ$, in the domain where the binary similarity law performs well,

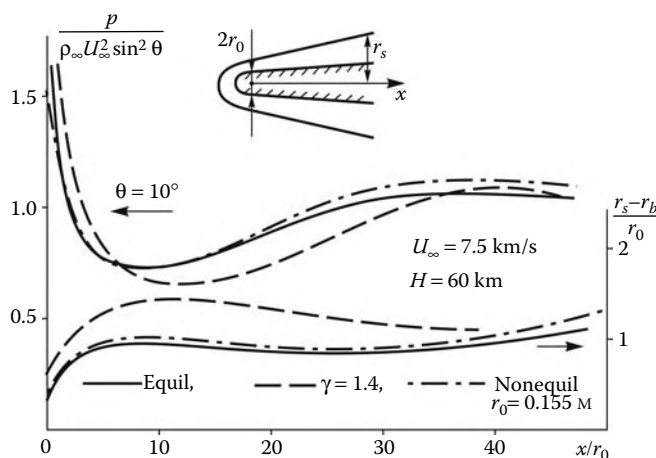
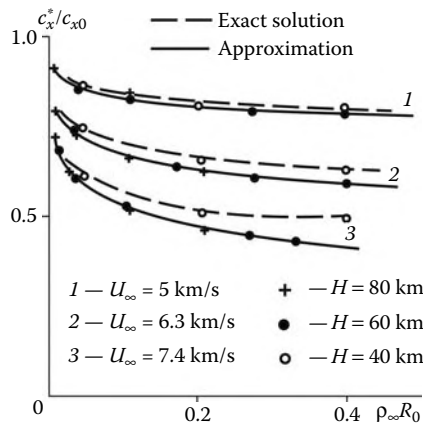


FIGURE 11.20
Pressure and shock layer thickness on a spherically blunted cone.

**FIGURE 11.21**

Effective drag coefficient for a nonequilibrium flow past blunt cones.

the ratios c_x^*/c_{x0} are plotted in Figure 11.21. They can be approximated by the formulas (Voronkin, 1970)

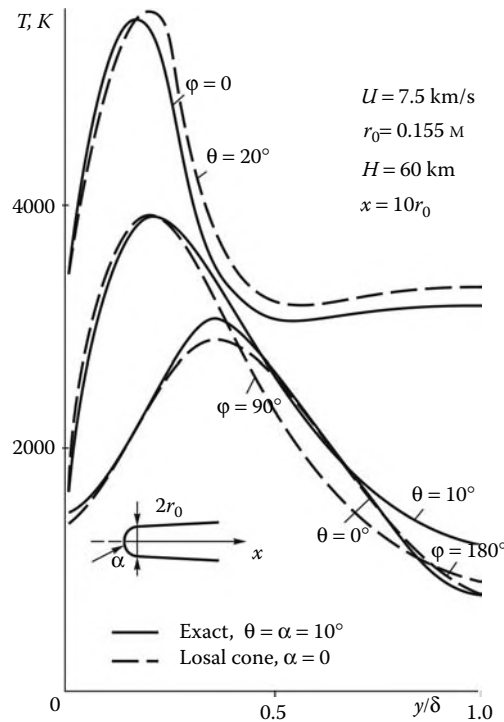
$$\frac{c_x^*}{c_{x0}} = 1 - 2.85[0.16(U_\infty \text{ km/s})^2 - 1]B^{1/6}, \quad B = \rho_\infty R_0 \text{ kg/m}^2 \quad (11.10.7)$$

The rule of local blunt cones (Section 9.5) can also be extended to nonequilibrium flows; this is confirmed by Figure 11.22 (the data of Antonets).

We are now coming to an analysis of the shock layer structure. Under the conditions of Figure 11.18 (see also the data in the table), reactions proceed in the shock layer on the sphere and in the high-entropy layer on the cone. Outside of the high-entropy layer, the gas in the shock layer on the cone is near perfect. This follows from the comparison of the curves for the species concentrations or for the densities in Figures 11.23 to 11.27. In this sense, the nonequilibrium shock layer structure is similar to the equilibrium one. However, there is an essential distinction. The gas in the wall layer (conditionally, for $y < \delta_e$ in Figure 11.16), which is in near-equilibrium state in the near-axis region, is being frozen during its subsequent expansion and conserves the excessive concentrations of atoms. This occurs also in the high-entropy layer on the thin blunt body, where the pressure is fairly low. We will call this flow *equilibrium-frozen*. In this case, the bound energy of the gas h_f is greater and the temperature is lower than those in the fully equilibrium flow; after the conditional freezing point with the parameters T_f , p_f , and so on, they are determined from the isentropic dependence

$$T/T_f = (p/p_f)^{(\gamma_f - 1)/\gamma_f}, \quad h = c_p^{(0)}T + h_f \quad (11.10.8)$$

In the limiting case of the gas freezing with the stagnation parameters (e.g., as $B \rightarrow \infty$), this temperature distribution over the blunt cone surface is plotted in Figure 11.28. Here, the temperature is several times smaller than the equilibrium one and by an order lower than that in the perfect gas under the same flight conditions. At the same time, the enthalpy on the cone surface in this equilibrium-frozen flow is somewhat greater and, hence, the flow velocity is smaller than those for the fully equilibrium and perfect gases. This fact is reflected in the temperature profiles in the shock layer on the cone, which are monotonic in equilibrium flows and have an internal maximum in nonequilibrium ones (Figures 11.22 to 11.24).

**FIGURE 11.22**

Temperature profiles between the body and the shock for a spherically blunted cone in a nonequilibrium flow.

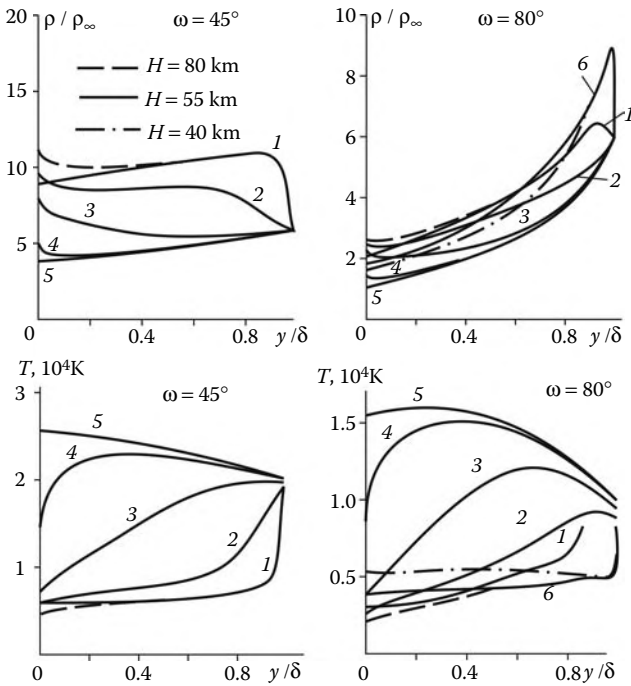
Naturally, this freezing zone is, rigorously speaking, only the leading part of the corresponding relaxation zone, so that on a body of a fairly large extent at a finite (nonzero) body pressure equilibrium is sooner or later attained (an exception is provided by the hardening effect at gas outflow in a vacuum outlined in Section 11.11).

We note that the calculation of the flow past the blunt cylinder presented in Figure 9.9 of Section 9.3 was performed within the framework of the limiting equilibrium-frozen flow model: the flow was assumed to be equilibrium up to limiting characteristics in the shock layer on the spherical surface and completely frozen downstream of it. Within the framework of this model the nonequilibrium effect on the pressure distribution on a thin blunt body and the shock layer is maximum.

We call the reader's attention to the distinctive features of the profiles of the concentrations of NO molecules and electrons in the shock layer (Figures 11.26 and 11.27). As for the relaxation zones behind the shock under the same conditions (Figure 11.4 from Section 11.5), typical of these profiles are peaks inside the shock layer. As the parameter B decreases, these peaks are displaced from the shock toward the body surface. We note that under these conditions electrons are supplied mostly by the associative ionization reaction in list 10.5.7; precisely this is the reason for the qualitatively similar behavior of the corresponding curves.

11.10.5 Bodies in a Nonequilibrium Supersonic Flow

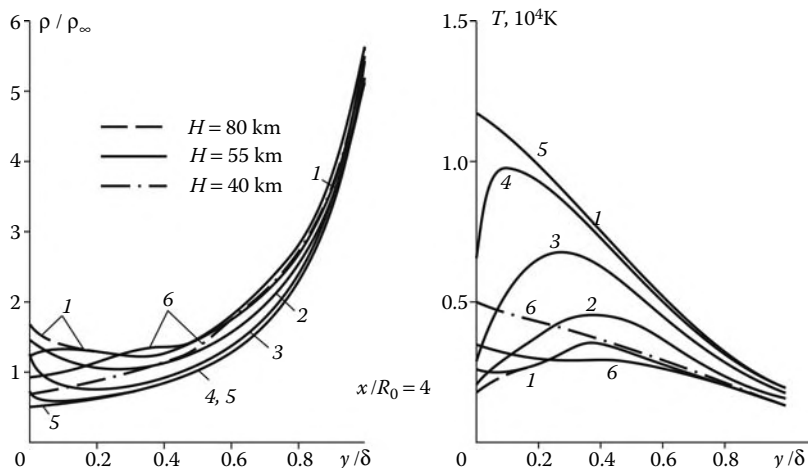
As shown in Section 11.8, the behavior of shocks is different in *underexcited* and *overexcited* gases. The former corresponds to the condition $\lambda_1 < \lambda_{2e}$ in Figure 10.2 (Section 10.4) or

**FIGURE 11.23**

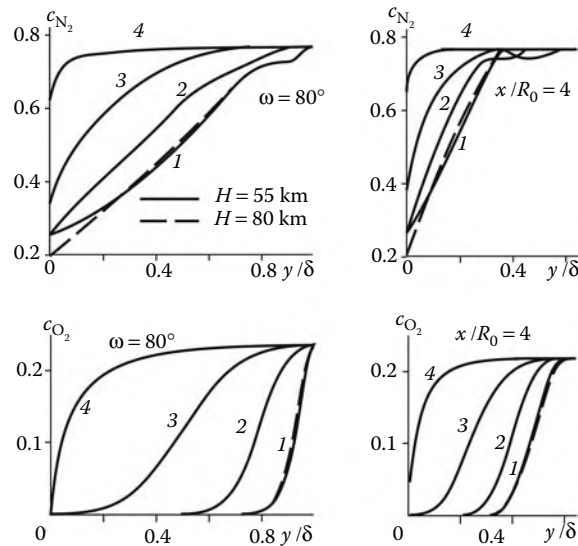
Density and temperature distributions in the shock layer on a sphere.

$h_{f1} < h_{f2}$ and adiabat IV in Figure 11.10 (Section 11.8), while the latter to the conditions $\lambda_1 > \lambda_{2e}$, $h_{f1} > h_{f2}$, and adiabat III. Correspondingly, in Section 11.8 these shocks were termed endothermal and exothermal.

The flow past bodies with endothermal shocks does not differ qualitatively from the equilibrium flow past the same bodies, though quantitative differences may be appreciable. However, the overexcited gas flow past a body (e.g., the combustible mixture flow)

**FIGURE 11.24**

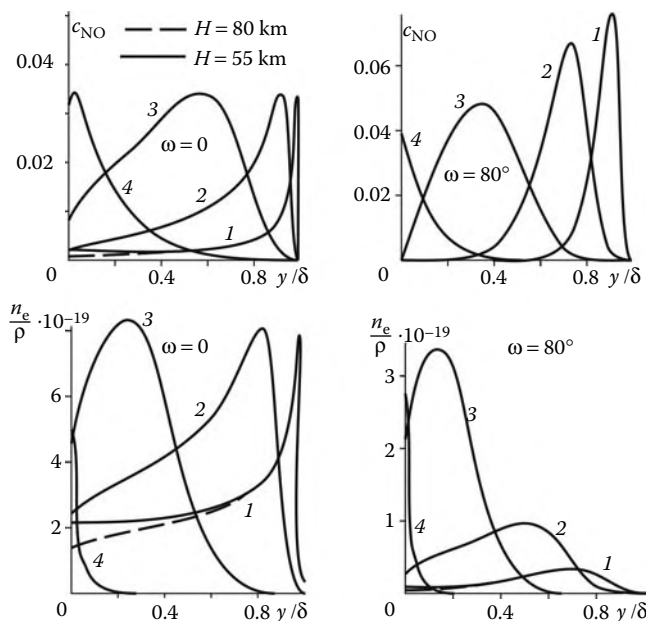
Density and temperature distributions in the shock layer on a blunt cone.

**FIGURE 11.25**

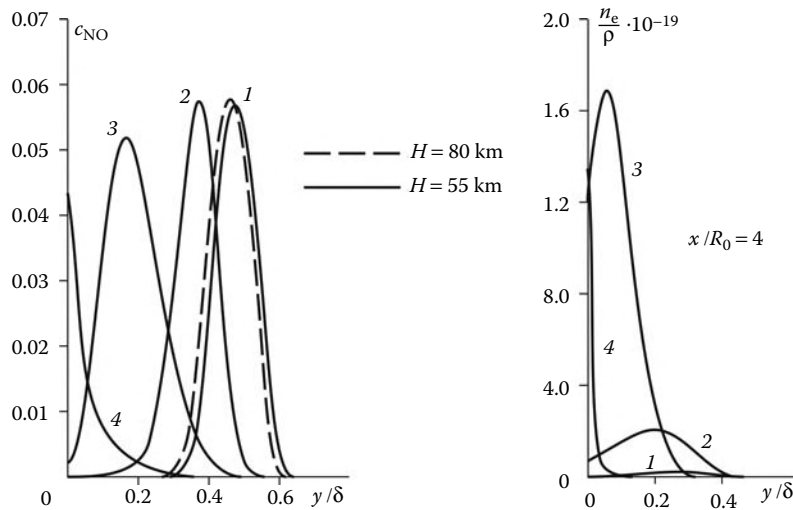
Concentrations of oxygen and nitrogen molecules in the shock layers on a sphere and a cone.

with exothermal shock waves is accompanied by new qualitative effects related with the occurrence of the Jouguet point. This case will be considered separately.

Let, first, the relaxation zone extent be small compared with the body dimensions, so that the shock ahead of the body can be considered as an equilibrium one. In this case, the situations described by the inequalities

**FIGURE 11.26**

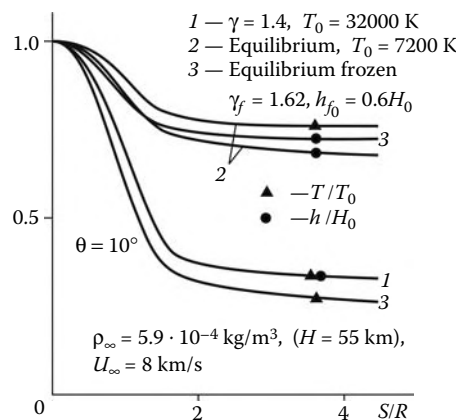
Concentrations of NO molecules and electrons in the shock layer on a sphere.

**FIGURE 11.27**

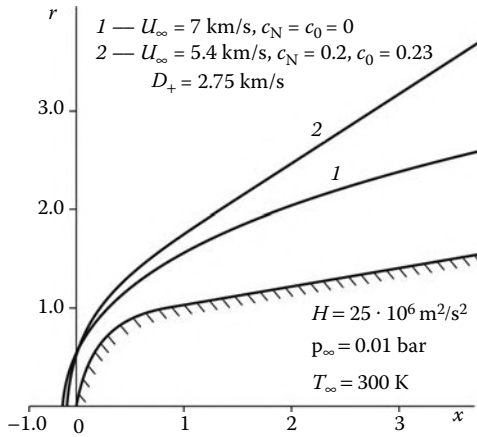
Concentrations of NO molecules and electrons in the shock layer on a blunt cone.

$$U_\infty < D_g, \quad D_g < U_\infty < D_+, \quad U_\infty > D_+ \quad (11.10.9)$$

are qualitatively different. Here, D_+ is the Jouguet wave velocity (e.g., the detonation wave) and D_g is the mixture “ignition” wave velocity, if we are dealing with detonation waves. In the first case, we have the conventional supersonic flow past a body; however, in the second case the steady-state flow past the body is impossible, since the body-induced shock wave travels over the gas at a velocity exceeding the freestream velocity. Thus, for example, in the case of a model mounted in the nozzle with a frozen flow (see Section 11.11) this wave propagates upstream until a new stationary flow, consistent with the experimental conditions, is attained. Finally, in the case $U_\infty > D_+$ the flow pattern is qualitatively similar to the conventional one, with the only though fundamental difference that in an unbounded

**FIGURE 11.28**

Enthalpy and temperature distributions over the surface of a spherically blunted cone.

**FIGURE 11.29**

Nonequilibrium flow past a body at a preassigned stagnation enthalpy.

space far from the body the shock wave has rather an oblique shock than a Mach wave as its asymptotics. The normal speed of this shock is equal to the Jouguet wave speed: $U_\infty \sin \alpha = D_+$.

For the sake of illustration, in Figure 11.29 we have plotted the shapes of the shocks ahead of a blunt body in hypersonic air flow with the equilibrium (there are no atoms) and partially frozen atom concentrations at the equilibrium and frozen flow in the shock layer. This example demonstrates that the state of the gas in the freestream can have a considerable effect on the flowfield ahead of the model embedded in the stream.

11.11 Nozzle and Jet Flows: Hardening Effect

In the exact formulation, the problems of the nonequilibrium flows in nozzles with a given contour and jets are not essentially different from those formulated in Section 5.5; the only, natural distinction is that the system of the governing equations involves the frozen speed of sound rather than the equilibrium one and is supplemented by the equations of physico-chemical kinetics. However, the problem of the flow in a contoured nozzle is in principle more complicated, since it is impossible to specify beforehand a uniform nonequilibrium flow in the exit section (as was done in Figure 5.12).

We will study the specific features of the flows under consideration in the simple one-dimensional, or hydraulic, approximation. Making transformations similar to those of Section 2.3 and taking into account also Equation 11.4.1 with the same Q_Λ and $q = 0$, we obtain an equation similar to Equation 2.3.3

$$(1 - M_f^2) \frac{du}{dx} = Q_{\text{eff}} = -Q_\Lambda - \frac{u}{\sigma} \frac{\sigma}{dx} \quad (11.11.1)$$

Here, $\sigma(x)$ is the cross-sectional area of the channel. Together with the equations

$$\begin{aligned} \frac{dp}{dx} &= -\rho u \frac{du}{dx} = \rho \frac{dh}{dx}, & u \frac{d\lambda_i}{dx} &= \Lambda_n \\ \rho &= \rho(p, T, \lambda_n), & h &= h(T, \lambda_n) \end{aligned} \quad (11.11.2)$$

Equation 11.11.1 forms the system of the governing equations. To solve this system, all the unknown flow parameters ($u = u_0$, etc.), including the set of the kinetic variables $\lambda_i = \lambda_{i0}$, should be specified in some initial section. As applied to the nozzles of high-temperature experimental setups or jet engines, the state of the gas in the initial section (in the plenum chamber) can be considered as equilibrium because of high temperatures and pressures involved (tens and hundreds of atmospheres).

This system has the singular point at $M_f = 1$; in a channel of a constant-area cross-section the solution cannot be continued through this point (this fact was used in analyzing the relaxation zone structure in Section 11.5); an exception is provided only by the case of the removable singular point with $Q_\Lambda = 0$, that is, the case in which rigorous equilibrium is attained at this point.

In the general case of a channel of variable cross-section, in particular, a convergent-divergent, or Laval, nozzle, the qualitative nature of the flow is determined by the sign of Q_{eff} , which is not known beforehand. The situation is more definite, when the flow in the vicinity of the nozzle throat is near-equilibrium and adiabatic. This situation occurs at high pressures and temperatures in the plenum chamber, when the flow becomes nonequilibrium only downstream of the throat, where the pressure decreases rapidly along the nozzle. In this case, the condition $M_e = u_e/a_e \approx 1$ holds in the vicinity of the nozzle throat; therefore, the condition $M_f = 1$ must be realized somewhat downstream of the throat, in the divergent region of the nozzle; then, in accordance with Section 2.3, in order for the solution to be regular, the condition $Q_{\text{eff}} = 0$ must be fulfilled at this point. We note that, as distinct from isentropic flows, the maximum of the density flux ρu is not associated with the $M_f = 1$ cross-section; as before, this maximum coincides with the nozzle throat, which follows from the condition $\rho u \sigma = G = \text{const}$.

An example of such a flow is shown in Figure 11.30 for dissociated oxygen. Typical of this example is the behavior of the molecular oxygen concentration: first, it increases starting from near-zero values in the plenum chamber; however, at a certain distance from the nozzle throat it becomes constant, though not equal to unity, in spite of the fact that the pressure and, hence, the temperature continue to decrease.

The occurrence of the gas composition freezing zone is due to a sharp decrease in the pressure and, therefore, the recombination rate. It is similar to the freezing zone on blunt cones (Section 11.10). In both cases, the extent of the zone is finite, but absolutely frozen flows can also exist.

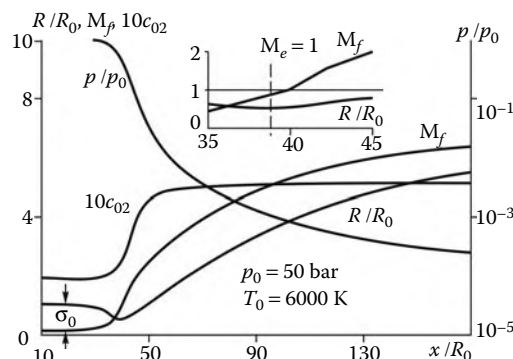


FIGURE 11.30

Parameter profiles along the axis of an axisymmetric nozzle with the $R(x)$ contour.

To elucidate this effect, we will consider the limiting case of the three-parameter gas expansion into a vacuum with a single relaxation Equation 10.4.1, in which the locally equilibrium quantity $\lambda_e(t)$ and the relaxation time $\tau(t)$ depend on time only. This equation has a solution, somewhat more general than 10.4.3

$$\begin{aligned}\lambda &= \lambda_0 e^{-z} + \lambda_e^*, \quad \lambda_0 = \lambda(0) \\ \lambda_e^* &= e^{-z} \int_0^z e^z \lambda_e dz, \quad z = \int_0^t \frac{dt}{\tau(t)}\end{aligned}\quad (11.11.3)$$

Here, the first term describes the structure of the domain of influence of the initial conditions, or the relaxation zone introduced in Section 10.4. As $t/\tau \sim z \rightarrow \infty$, this term vanishes and the solution takes the form $\lambda = \lambda_e^* = \lambda_e$. On the contrary, for small values of z the solution is near frozen.

However, for a variable $\tau(t)$ the situation can occur in which τ increases with t without bounds in such a way that the integral z remains bounded by a constant value: $z \leq z_0 < \infty$. Then from Equation 11.11.3 we obtain the limiting solution

$$\lambda = \lambda_f = \lambda_0 e^{-z_0} + \lambda_e^*(z_0) \quad t \rightarrow \infty, \quad z \rightarrow z_f \quad (11.11.4)$$

This is the *hardening effect*. This regime is usually realized at the gas expansion into a vacuum. Usually, τ is a decreasing function of the density, for example, $\tau \sim \rho^{-n}$, where $n \sim 1$. If the gas density decreases in accordance with a power law, $\rho \sim t^{-m}$, then the integral z is convergent for $nm > 1$ and divergent for $nm < 1$. If λ is the atom or ion concentration or the vibrational energy of molecules, then at strong gas expansion with simultaneous cooling (from the Poisson adiabat there follows $T \sim p^{(\gamma-1)/\gamma} \rightarrow 0$ as $p \rightarrow 0$), for example, at the exit of a high-altitude engine nozzle, it should be expected that $\lambda_e \rightarrow 0$, as $t \rightarrow \infty$. Therefore, when the integral z is divergent, the limiting solution $\lambda \rightarrow \lambda_e^* \rightarrow 0$ is, as it were, an equilibrium one. On the contrary, for a finite z_f the solution is frozen at the level $\lambda = \lambda_f$. This result is quite obvious, bearing in mind that the atoms that have bounced apart in a vacuum have not a slightest chance of mutual collisions and recombination to molecules; similarly, deactivation of molecular vibrations is no longer possible.

By way of illustration, we will consider a spherical source flow, or the flow on the axis of symmetry of an infinitely long conical nozzle (Section 2.3), or the gas jet expansion into a vacuum, which is equivalent to the two preceding flows. As, due to gas expansion, the local Mach number becomes very high, the gas velocity U approaches a constant maximum value. Then, invoking the flow rate equations, we can put $\rho U x^2 = \text{const}$. Since $x \sim Ut$, we have $m = 2$ and for $n \geq 1/2$ (which usually takes place) the integral is convergent and, therefore, the gas parameters are frozen at a certain finite degree of dissociation, ionization, vibrational energy, and so on.

The flow freezing effect leads to a decrease in the velocity of the gas expanding into a vacuum. In fact, as $\lambda \rightarrow \lambda_f$, the gas enthalpy remains finite: $h \rightarrow h_f(\lambda_f)$, as $p \rightarrow 0$; then from the Bernoulli equation there follows:

$$U_f^{(\max)} = \sqrt{2(H - h_f)} < U_{\max} = \sqrt{2H} \quad (11.11.5)$$

The same effect can be obtained at the high-altitude engine nozzle exit. The freezing in the nozzle leads, in accordance with Equation 1.7.22, to the loss in the engine thrust.

The fact that the nozzle flows in high-temperature benchmark setups could be frozen should be also borne in mind in interpreting the experimental results obtained on these setups; this follows, in particular, from the notes to Figure 11.29 of Section 11.10.

11.12 Thermal Rarefaction Waves

In Section 11.8 we outlined the general theory of steady-state nonequilibrium adiabatic waves and pointed to the probable existence of discontinuous, or shock, rarefaction waves propagating at subsonic velocities.

In contrast to compression shock waves, the distinctive feature of these waves is that the velocity of their propagation is determined by specifying not only the conservation laws 11.8.1 but also certain additional physical conditions that are beyond the framework of inviscid gas dynamics. In what follows, we will discuss briefly *thermal waves*, whose propagation velocity is determined by their internal dissipative structure.

The thermal waves include, first, combustion waves. These waves propagate over a specially prepared combustible mixture, gaseous or condensed, being at a *metastable state*; the ignition of the mixture is caused by heat transfer from the burnt portions of the gas to the medium ahead of the wave by heat conduction accompanied by diffusion of the combustion products and the original components rather than by shock heating, as is the case in detonation waves. The thermal waves also include the waves in which the gas flowing across them is heated by a high-frequency electromagnetic field. In these waves the energy is imparted to free electrons generated at thermal ionization of the gas and diffusing counterstream, together with the heat flux. We will also mention thermal waves induced by the counterflux of the radiant energy, which is absorbed by an already heated gas due to a considerable increase of the absorption coefficients (see Chapter 14).

Many and varied as these processes may be, they possess a common property of the *self-adjusted* heat release. In fact, in all these processes the cold gas ahead of the wave can usually be considered nonreacting, or transparent for the energy flux supplied to the wave front. Then, simplifying the matter, we can assume that the real heat release starts from a certain threshold temperature $T = T^*$ (or some other parameter). At the same time, heat release ceases at the wave termination, owing to combustion mixture burnout, complete absorption of electromagnetic or radiative energy fluxes in the terminating layer of a wave, and so on.

We are now coming to a model example of a thermal wave for the purpose of establishing the dependence of the propagation velocity $D = u_1$ of these waves on their internal structure. We will assume that the gas flows across the wave at a velocity u from left to right along the x axis. We derive the equation for this wave from Equation 1.2.7 taking 1.2.9 into account and retaining only the terms involving the temperature, as well as the source term of the special form; we also put $h = c_p T$, $c_p = \text{const}$, and $\lambda = \text{const}$. Thus, we obtain

$$c_p m \frac{\partial T}{\partial x} = \lambda \frac{\partial^2 T}{\partial x^2} + \bar{q}, \quad m = \rho u = \rho_1 u_1 = \text{const} \\ x \rightarrow -\infty, \quad T \rightarrow T_1; \quad x \rightarrow \infty, \quad \partial T / \partial x \rightarrow 0 \quad (11.12.1)$$

The condition for $x \rightarrow \infty$ follows from the boundedness of the solution at a finite total heat supply. The term \bar{q} simulates the source of chemical, or some other, energy, which is transformed in the course of reactions to the energy of translational degrees of freedom and is equal to the heat inflow rate per unit volume. We can simulate the previously noted self-adjustment property by putting the source term \bar{q} to be the function of the temperature only, subject to the following three-zonal condition

$$1) \quad \bar{q} = 0 \quad T < T^*, \quad 2) \quad \bar{q} \geq 0 \quad T^* \leq T \leq T_2, \quad 3) \quad \bar{q} = 0 \quad T^* > T_2 \quad (11.12.2)$$

The examples of the function $\bar{q}(T)$ satisfying conditions 11.12.2 are sketched in Figure 11.31a. The ascending branches of the curves simulate the increase in the combustion rate with the temperature, while the descending ones model the decrease in this rate in the process of the mixture burnout.

The final temperature T_2 attained at the thermal wave termination satisfies the condition

$$c_p m(T_2 - T_1) = \int_{-\infty}^{\infty} \bar{q} dx = mq_m \quad (11.12.3)$$

which is obtained by integrating Equation 11.12.1 over the entire x axis. Here, q_m is the heat acquired by a unit mass of the gas in passing across the wave. For combustion waves, precisely the parameter q_m is most often preassigned; therefore, the final temperature T_2 is also known. However, generally this is not the case.

We will make an important note. Problem 11.12.1 and 11.12.2 can also have the trivial solution $T = T_1$ and $\bar{q} = 0$. For example, burning in a combustible mixture can generally occur only in the presence of an initiating heat source with a local initial temperature $T_* \geq T^*$, under the action of which the transient process developed can be terminated by the formation of a steady-state thermal wave. The same is true for other previously mentioned processes that start at certain threshold values of the relevant parameters.

Let us now consider the solution of the problem thus formulated. The heat release zone is preceded by the gas preheating zone, in which Equation 11.12.1 is homogeneous for $\bar{q} = 0$ and has a solution that decays asymptotically, as $x \rightarrow -\infty$ (we let $x = 0$ for $T = T^*$)

$$T^{(1)} - T_1 = C_1 e^{kx}, \quad k = c_p m / \lambda, \quad C = T^* - T_1 \quad (11.12.4)$$

For an arbitrary function $\bar{q}(T)$ the problem under consideration is nonlinear; precisely this is the decisive factor in determining uniquely the wave propagation velocity u_1 , which cannot be done for the linear problems. We will demonstrate this with reference to the very simple example of a function $\bar{q}(T, T^*)$, which is linearly dependent on T near the initial and final heat release points (e.g., curve 2 in Figure 11.31a)

$$\bar{q} = \alpha(T - T^*), \quad T \geq T^*; \quad \bar{q} = \beta(T_2 - T), \quad T \leq T_2 \quad (11.12.5)$$

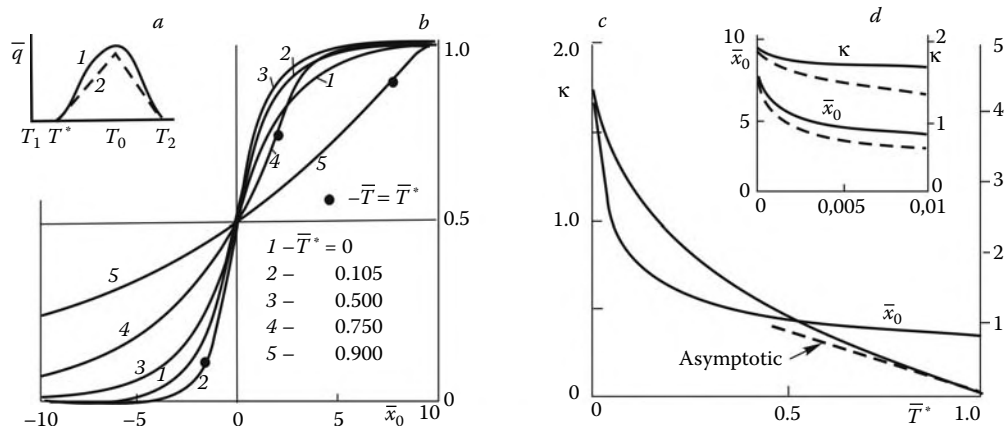


FIGURE 11.31
Temperature field in a thermal wave.

In these regions Equation 11.12.1 is linear, and near the initial point $T \approx T^*$ can have three types of local solutions

$$\begin{aligned} T^{(2)} - T^* &= C_1 e^{k_1 x} + C_2 e^{k_2 x} \\ k_{1,2} &= \frac{k}{2} \pm \Delta_1, \quad \Delta_1^2 = \frac{1}{4} k^2 - \frac{\alpha}{\lambda} > 0, \quad k = \frac{c_p m}{\lambda} \end{aligned} \quad (11.12.6)$$

$$T^{(2)} - T^* = e^{kx/2} (C_1 + C_2 x), \quad \Delta_1 = 0 \quad (11.12.7)$$

$$T^{(2)} - T^* = e^{kx/2} (C_1 \cos \Delta_2 x + C_2 \sin \Delta_2 x), \quad \Delta_2^2 = -\Delta_1^2 > 0 \quad (11.12.8)$$

For $T \approx T_2$ a local solution bounded as $x \rightarrow \infty$ takes the form:

$$T_2 - T^{(3)} = C_3 e^{k_3 x}, \quad k_3 = \frac{1}{2} k - \Delta_3, \quad \Delta_3 = \frac{1}{4} k^2 + \frac{\beta}{\lambda} \quad (11.12.9)$$

In this case, at $T = T^*$ solutions 11.12.6 through 11.12.8 must be matched with the solution of Equation 11.12.4 for the region $x \leq 0$ from the condition of the equality of the temperatures $T^{(1)} = T^{(2)} = T^*$, together with their derivatives, at point $x = 0$ (the condition of the absence of concentrated heat sources). This determines the constants C_1 and C_2 . Then the local solutions can be continued, in one way or another, to the region of higher T and solution 11.12.9 to the region of lower T ; matching these solutions at a particular point $x = x_0$ with a temperature T_0 we can, in principle, determine the constant C_3 and the *eigenvalue* k .

We note the difference between this nonlinear problem with $\bar{q} = \bar{q}(T, T^*)$ and the similar linear problem with $\bar{q} = \bar{q}(x)$ whose solution exists for any value of the parameter k . However, in the nonlinear problem subject to condition 11.12.2, the condition $T = T^*$ with a given value of T^* must be fulfilled at the initial point $x = 0$ of the heat release zone; precisely this determines uniquely the value of k , or u_1 , which makes such a solution possible.

We will demonstrate the procedure of matching the unilateral solutions with reference to the problem for a “triangular” function $\bar{q}(T, T^*)$ (curve 2 in Figure 11.31a) formed by straight lines, 11.12.5 continued inside the interval $[T^*, T_2]$ up to their intersection at the temperature $T_0 = (\alpha T^* + \beta T_2)(\alpha + \beta)^{-1}$. It turns out that in this case the problem formulated has a solution only in the class of functions 11.12.8. In this case, matching the functions $T^{(1)}$ and $T^{(2)}$ at point $x = 0$ we obtain the required solution for $T^{(2)}(x)$, which in the dimensionless form is as follows:

$$\bar{T}^{(2)} - \bar{T}^* = \frac{2\bar{T}^*}{\bar{\Delta}_2} e^{\kappa \bar{x}/2} \sin \frac{\kappa \bar{\Delta}_2 \bar{x}}{2}, \quad \bar{T} = \frac{T - T_1}{T_2 - T_1} \quad (11.12.10)$$

$$\bar{x} = \frac{x}{\delta}, \quad \delta = \sqrt{\frac{\lambda}{\alpha}}, \quad \kappa = \frac{c_p m}{\sqrt{\alpha \lambda}} = k \delta, \quad \bar{\Delta}_2 = \sqrt{\frac{4}{\kappa^2} - 1}$$

Solution 11.12.9 passing through point x_0 at which $\bar{T}^{(3)}(\bar{x}_0) = \bar{T}_0$ takes the form:

$$\begin{aligned} 1 - \bar{T}^{(3)} &= (1 - \bar{T}_0) e^{\bar{k}_3 (\bar{x} - \bar{x}_0)}, \quad \bar{T}_0 = \frac{\bar{T}^* + \beta}{1 + \beta} \\ \bar{k}_3 &= \frac{\kappa}{2} (1 - \bar{\Delta}_3) < 0, \quad \bar{\Delta}_3 = \sqrt{\frac{4\beta}{\kappa^2} + 1}, \quad \bar{\beta} = \frac{\beta}{\alpha} \end{aligned} \quad (11.12.11)$$

At point \bar{x}_0 Equation 11.12.10 gives one relation between \bar{x}_0 and κ

$$\frac{1}{\bar{\Delta}_2} e^{\kappa \bar{x}_0/2} \sin \varphi = \frac{\beta(1 - \bar{T}^*)}{2(1 + \beta)\bar{T}^*}, \quad \varphi = \frac{1}{2}\kappa \bar{\Delta}_2 \bar{x}_0 \quad (11.12.12)$$

Another relation between \bar{x}_0 and κ follows from the condition of smoothness of the solution at point \bar{x}_0 ; combining this condition with Equation 11.12.12 we obtain

$$\bar{\beta} \cot \varphi = \bar{\Delta}_2^{-1}(\bar{\Delta}_3 - \bar{\beta} - 1) \quad (11.12.13)$$

We recall that the solution obtained is valid for $\kappa \leq 2$. When $\kappa \rightarrow 2$, or $\bar{\Delta}_2 \rightarrow 0$, the expression in parentheses in 11.12.13 is negative; therefore, in the vicinity of $\kappa \approx 2$ from 11.12.13 we obtain

$$\varphi \approx \pi, \quad \cos \varphi \approx -1, \quad \bar{x}_0 \approx \frac{\pi}{\bar{\Delta}_2}, \quad \sin \varphi \approx A\bar{\Delta}_2, \quad A = \frac{\bar{\beta}}{1 + \bar{\beta} - \sqrt{1 + \bar{\beta}}} \quad (11.12.14)$$

From this equation and Equation 11.12.10 it follows that $\bar{T}^* \rightarrow 0$ as $\kappa \rightarrow 2$ and in this limit the following asymptotics are valid

$$\bar{x}_0 = \ln \frac{B}{\bar{T}^*}, \quad B = \frac{\beta}{2A(1 + \beta)}, \quad \kappa = 2 - \frac{\pi^2}{\bar{x}_0^2} \quad (11.12.15)$$

In another limiting case $\bar{T}^* \rightarrow 1$, from Equation 11.12.12 it follows that $\bar{\Delta}_2 \rightarrow \infty$, or $\kappa \rightarrow 0$; in this case, we have

$$\kappa \bar{\Delta}_2 / 2 \rightarrow 1, \quad \varphi \rightarrow \varphi_1 = \arctan \bar{\beta}^{1/2}, \quad \bar{x}_0 \rightarrow \varphi_1, \quad \kappa \rightarrow (1 - \bar{T}^*) \sqrt{\frac{\bar{\beta}}{1 + \bar{\beta}}} \quad (11.12.16)$$

By way of illustration, in Figure 11.31c and d, we have plotted the curves $\kappa(\bar{T}^*)$ and $\bar{x}_0(\bar{T}^*)$ for $\alpha = \beta$ and in Figure 11.31b for certain values of \bar{T}^* the curves $\bar{T}(\bar{x})$ passing through the point $\bar{x} = 0, \bar{T} = 1/2$. Clearly, the thermal wave thickness decreases with \bar{T}^* up to the value $\bar{T}^* = 0.105$ corresponding to the equality $\bar{\Delta}_3 = 2$ in 11.12.13 or $\kappa = 1.15$. With further decrease in \bar{T}^* ($\bar{T}^* \rightarrow 0$) the wave thickness increases somewhat. As for the parameter \bar{x}_0 , which increases without bound as $\bar{T}^* \rightarrow 0$, in this case it no longer characterizes the wave thickness.

In our example, the parameter $\kappa \rightarrow 0$ as $\bar{T}^* \rightarrow 1$; therefore, the natural velocity u_1 also decreases. The heat release region thickness remains finite at $x > 0$, whereas the extent of the preheating region (1) increases without bound, thus determining the wave thickness. However, these particular inferences cannot be extended to actual thermal waves, since the triangular function $\bar{q}(T, T^*)$ taken previously, as well as Equation 11.12.1 itself and the limit $T^* \rightarrow T_2$, are no more than a qualitative mathematical model for these waves.

The solution obtained supports the preliminary inferences about the uniqueness of the natural velocity of thermal wave propagation over a gas at rest. This result, fundamental for combustion theory, was rigorously proved for a wide class of functions $\bar{q}(T, T^*)$ satisfying conditions 11.12.2 and then generalized to more complicated systems of the same type that can involve the diffusion equation.* An analogous result is also valid for a thermal wave in

* See, for example, Zeldovich, Barenblatt, Librovich, and Makhviladze, 1980, cited in Section 11.8.

a high-frequency electromagnetic field; in this case, the equilibrium electron concentration depends on the temperature only, which reduces the problem to that of the previously considered type (Raizer, 1968; Meyerovich, 1971). As for nonequilibrium processes, they are governed by, at least, two equations, namely, those of heat conduction and production of electrons (with allowance for diffusion); in this case, the uniqueness of the problem solution was also proved (Lunev and Semin, 1989).

A particular place in the theory outlined is occupied by the classical problem on the combustion wave propagation over a mixture with the greatest admissible temperature $T^* = T_1$. In this case, we should let $T^* = T_1$ in Equation 11.12.5; then the preheating region (1) vanishes and formulas 11.12.6 through 11.12.8 give a decaying (since $k_{1,2} > 0$) solution as $x \rightarrow -\infty$. Matching the continuation of this two-parameter solution with the continuation of the one-parameter solution 11.12.9 at a certain point $T = T_0$ makes it possible to determine all the constants C_1 , C_2 , and C_3 for any k . On physical grounds, a solution of alternate sign of type 11.12.8 should be discarded, while solution 11.12.6 exists only in the case $\Delta_1^2 \geq 0$, or

$$\kappa \geq 2, \quad \rho_1 u_1 = m \geq m_{\min} = \rho_1 u_{1\min} = (2/c_p)(\alpha\lambda)^{1/2} \quad (11.12.17)$$

For smaller m , or for the velocities $u_1 < u_{1\min}$, propagation of a stationary thermal wave turns out to be impossible; however, for $m > m_{\min}$ there exists a multitude of solutions of this problem.

However, this uncertainty was solved as follows.* It was demonstrated that the time-dependent problem, arising when the term $\partial T / \partial t$ is added to Equation 11.12.1 with certain constraints imposed at $t = 0$ on the initial function $T = T_0(x) > T_1$ and the function $\bar{q}(T)$, has a limiting solution of the type of a running wave $T(x - u_{1\min}t)$ as $t \rightarrow \infty$ with a natural velocity $u_{1\min} = D_0$ determined by condition 11.12.17; for this velocity the steady-state solution described by Equation 11.12.7 at $T \approx T_1$ is actually realized in an evolutionary process.

This fundamental result was empirically (numerically) extended to various time-dependent problems of this kind, whose solution always leads to stationary waves traveling at a definite natural velocity. We note that precisely the solution of these time-dependent problems with the passage to the limit $t \rightarrow \infty$ is almost the main mean for the theoretical determination of the natural velocities of thermal waves.

We note that at $T \approx \bar{T}_1$ the limiting solution of the time-dependent problem obtained previously is associated with the solution of type 11.12.7. For the triangular profile $\bar{q}(T, T^*) = \bar{q}(T, T_1)$ used previously, matching unilateral solutions 11.12.7 and 11.12.9 at $T = T_0$ determines all the constants C_1 , C_2 , and C_3 . However, it can be shown that solution 11.12.10 and 11.12.13 obtained previously has the same limiting form as $\bar{T}^* \rightarrow 0$ (accurate to a shift in coordinates; curve 1 in Figure 11.31b). From general considerations it might be expected that this coincidence of two limiting solutions takes place also for functions $\bar{q}(T, T^*)$ of a more general form.

We will now explain the physical meaning of the eigenvalues for these problems. The quantity $\delta = (\lambda/\alpha)^{1/2}$ introduced in Equation 11.12.10 is of the order of the wave thickness determined from the condition that the terms on the right-hand side of Equation 11.12.1 are of the same order. Since the gas viscosity $\mu \sim \lambda c_p$ (see Section 1.3), the parameter

* In the fundamental work of Kolmogorov, Petrovskii, and Piskunov, 1937, which was not directly related with combustion theory but marked the beginning of the mathematical theory of thermal wave propagation.

$\kappa \sim \rho_1 u_1 \delta / \mu$ is of the order of the Reynolds number based on the wave thickness and the flow parameters at its entry. Therefore, $\delta \sim \mu / \rho_1 u_1$ for $\kappa \sim 1$, as in the problem of the shock wave structure (Section 3.2). On the other hand, the dimensionality and the order of the heat influx rate is $\bar{q} \sim \rho_0 \tau^{-1} c_p (T_2 - T_1)$, where ρ_0 is the characteristic density within the wave and τ is the scale time of the process, for example, the combustion relaxation time. Therefore, $\alpha \sim c_p \rho_0 / \tau$ and from the comparison of two formulas for δ we obtain the estimates ($\mu \sim \lambda / c_p$)

$$\delta = \sqrt{\frac{\lambda}{\alpha}} \sim \frac{\lambda}{c_p \rho_1 u_1}, \quad u_1 = \left(\frac{\lambda \rho_0}{c_p \rho_1^2 \tau} \right)^{1/2}, \quad \delta \sim \frac{\rho_1}{\rho_0} u_1 \tau \quad (11.12.18)$$

Thus, the parameter δ has the meaning of the relaxation zone thickness for these processes.

We note that for many processes, for example, combustion reactions, we have $\tau \sim 1/\rho$ and $\delta \sim 1/\rho$, so that the natural velocity of these waves is density (pressure) independent; generally speaking, this was meant in the gas dynamic analysis drawn at the end of Section 11.8, which will not be amplified here.

11.13 Sublimation Waves

In addition to the previous section, we will now consider one more type of rarefaction waves, namely, nonadiabatic (in accordance with the classification of Section 11.8) *sublimation waves*, which are generated under irradiation of condensed media by an intense energy flux (by a laser, X-ray, or electron beam, etc.).

Let a homogeneous radiation flux I be incident from the right on the semi-infinite surface W of a material (Figure 11.32a). The flux caused by an external source (minus its own radiation of the surface) leads to material sublimation; we will assume that the vapor flow is transparent for radiation. Near the surface W we separate out a control surface embracing the entire wave zone of thickness δ ; the latter includes, as the thermal wave of Section 11.12, three zones, namely, (1) a heating zone, (2) a sublimation front (W in Figure 11.32a), that is, a thin (possibly, of a monomolecular thickness) material layer in which energy is absorbed, and then (3) a wall layer (*Knudsen layer*) whose thickness l_k is of the order of a free molecular path (Section 1.4); within the latter vapors go over to a molecular-kinetic equilibrium state. Thus, on the left there is a solid body with the initial parameters ρ_1, T_1 , and so on, and on the right a gas with the parameters ρ_2, T_2 , and so on. We will fit the reference frame to the surface W putting $x = 0$ on it; then the original condensed material inflows into the wave at velocity u_1 and flows out of it at the velocity u_2 . Obviously, $\rho_1 > \rho_2$; therefore, the sublimation wave thus separated out is a rarefaction wave and equilibrium states behind it lie on the right branch of adiabat III in Figure 11.10a (Section 11.8).

The parameters on either side of the separated-out wave are related by Equation 11.8.1. For our case we can write these relations in the form:

$$\begin{aligned} m &= \rho_1 u_1 = \rho_2 u_2, & p_1 + m u_1 &= p_2 + m u_2 \\ q_0 &= c_{p2} T_2 + \frac{1}{2} u_2^2 = H_2 = c_{p2} T_0 = c_{p2} T_2 \left(1 + \frac{\gamma - 1}{2} M_2^2 \right) \\ q_0 &= \frac{I}{m} - \Delta h, & \Delta h &= c_{p1}(T_w - T_1) + h_0, & \rho_2 &= \frac{p_2 \bar{M}}{R T_2}, & M_2 &= \frac{u_2}{a_2} \end{aligned} \quad (11.13.1)$$

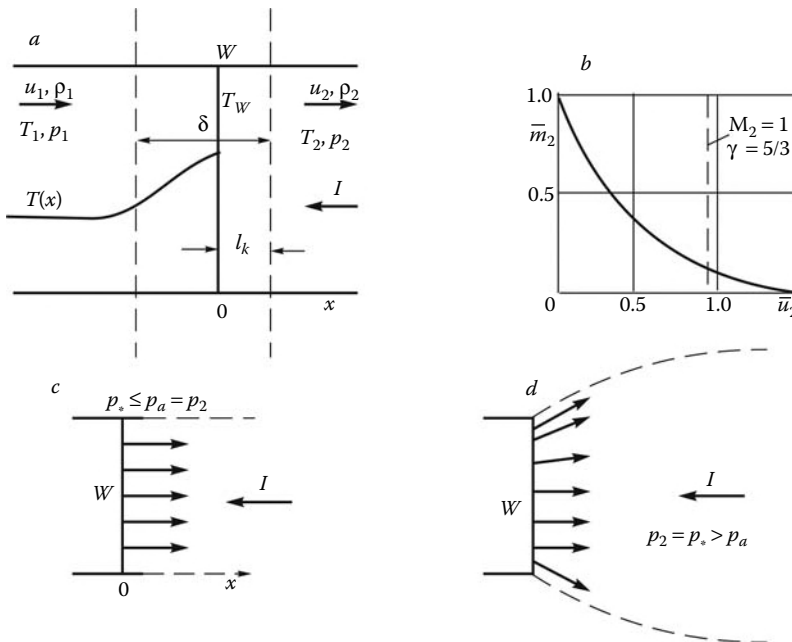


FIGURE 11.32
Evaporation waves.

Here, T_w is the surface temperature, h_0 is the phase transition heat, and H_2 is the total enthalpy of outgoing vapors with their own stagnation temperature T_0 , Mach number M_2 , and specific heat ratio γ . We assume the specific heats of the original material (c_{p1}) and its vapors (c_{p2}) to be constant.

The heating zone is described by solution 11.12.4 with $C = T_w - T_1$ (Figure 11.32a) determining the heat flux to the material

$$c_{p1}m(T_w - T_1) = -\lambda \left. \frac{\partial T}{\partial x} \right|_{x=0} \quad (11.13.2)$$

The system of Equation 11.13.1 involves four equations in seven unknown parameters: u_1 (or m), p_1 , u_2 , p_2 , ρ_2 , T_2 , and T_w at given parameters ρ_1 and T_1 ahead of the front, which, as distinct from the case of gases, can be assumed pressure-independent for the condensed media under consideration. As compared with thermal waves (Section 11.12), in this problem one more unknown quantity, that is, the temperature T_w , appears.

Specifying one of the parameters, p_1 or p_2 , gives the fifth relation, so that two more relations are needed for closing the problem. These relations can be obtained only by an analysis of the processes in the Knudsen layer, which can be drawn only within the framework of molecular-kinetic theory. In the following we will use a very simple model of this theory.

For this purpose, we will consider a control surface in Figure 11.32a embracing the Knudsen layer l_k between the surface W and its exit boundary. We define the total vapor flow rate across the surface W as follows:

$$\rho_1 u_1 = m = m_w - \alpha_m m_2, \quad m_2 = m_2(p_2, T_2, u_2) \quad (11.13.3)$$

Here, m_w is the *natural* mass flow rate of the material evaporation, which is caused by thermal emission of particles from the surface and should be determined, while m_2 is the

return mass flow rate of the material vapors flowing across the control surface from the right at a mean velocity V'_2 , and α_m is the *mass accommodation coefficient* determining the fraction of molecules incident on the surface W and absorbed by it. The velocity V'_2 is dependent on the temperature T_2 and the velocity u_2 , since in calculating it the function of molecular distribution in velocities (Section 1.4) must be averaged only over those molecules for which the thermal velocity component normal to the wall is greater than the mass-average velocity u_2 .

Using for estimates the Maxwellian distribution 1.4.7 we obtain the following formula for m_2 (see, e.g., Bird, 1976)

$$\bar{m}_2 = \frac{m_2}{m_{20}} = e^{-\bar{u}^2} - 2\bar{u} \int_{\bar{u}}^{\infty} e^{-\zeta^2} d\zeta, \quad \bar{u} = u_2 \sqrt{\frac{\bar{M}}{2RT}} \quad (11.13.4)$$

$$m_{20} = m_2(p_2, T_2, 0) = \frac{1}{2} \rho_2 V_2(T_2) = p_2 \sqrt{\frac{\bar{M}}{2\pi RT_2}}, \quad V_2 = \sqrt{\frac{2RT_2}{\pi \bar{M}}}$$

Here, V_2 is the mass-average velocity of the thermal molecular motion in the direction of the wall at $u_2 = 0$. The function $\bar{m}(\bar{u}_2)$ is presented in Figure 11.32b. The mass velocity of evaporation m_w can be determined from the following reasoning based on the detailed balancing principle (see Section 10.7). At vapor-solid equilibrium we have $u_2 = 0$, $T_2 = T_w$, $m_2 = m_{20}(T_w)$, and the pressure $p_2 = p_1 = p_e(T_w)$, where the *saturated vapor pressure* $p_e(T_w)$ is determined by the *Clausius-Clapeyron formula*

$$p_e = A(T_w) e^{-\theta/T_w}, \quad \theta = \bar{M}h_0/R \quad (11.13.5)$$

Here, θ is the *characteristic evaporation temperature*, while $A(T_w)$ is a “slow” function of the temperature. Letting then $m = 0$ in 11.13.3 we obtain

$$m_w = \alpha_m m_{20}[p_e(T_w), T_w] = m_w(\alpha_m, T_w) \quad (11.13.6)$$

Thus, in this approximation the quantity m_w for a given material (at a given accommodation coefficient α_m and a temperature θ) is a function of the surface temperature only. In view of the results obtained above, formula 11.13.3 takes the form:

$$m = \alpha_m \sqrt{\frac{\bar{M}}{2\pi RT_w}} \left[p_e(T_w) - \bar{m}_2 p_2 \sqrt{\frac{T_w}{T_2}} \right] \quad (11.13.7)$$

At a small deviation from equilibrium, letting $\bar{m}_2 = 1$ and $T_2 = T_w$ we obtain the Knudsen-Langmuir formula

$$m = m_w - \alpha_m m_2(p_2, T_w) = \frac{\alpha_m [p_e(T_w) - p_2]}{\sqrt{2\pi RT_w/\bar{M}}} \quad (11.13.8)$$

One more relation is required for closing the problem, namely, that between the pressures p_1 and p_2 . Let us consider the gas dynamic features of the issuing vapor jet. In this connection, all the notes made at the end of Section 11.8 about the general properties of rarefaction waves can be transferred to sublimation waves if we assume that the rarefaction wave is induced, as in Figure 11.13c, by a radiant energy flux I incident on it from the left (on the right part of Figure 11.32c). In particular, the maximum velocity of the vapor

outflow at a given value of q_0 is equal to the speed of sound $u_2 = a_2$ and corresponds to the Jouguet point $0'$ on adiabat III in Figure 11.10a. This condition leads to the relations

$$p_2 = p_* = \frac{1}{\gamma} \rho_2 a_2^2 = \frac{1}{\gamma} m a_2 = m \left(\frac{RT_2}{\gamma M} \right)^{1/2}, \quad p_1 = (\gamma + 1)p_2, \quad T_2 = \frac{2T_0}{\gamma + 1} \quad (11.13.9)$$

Here, the term mu_1 is dropped from the formula for p_1 , since it is small for $\rho_2/\rho_1 = u_1/u_2 \ll 1$. Substituting this quantity into 11.13.7, we obtain

$$\begin{aligned} Bm &= \alpha_m p_e(T_w) \sqrt{\frac{\bar{M}}{2\pi RT_w}}, & B &= 1 + \frac{\alpha_m \bar{m}_2}{\sqrt{\gamma}} \\ Bp_2 &= \alpha_m p_e(T_w) \sqrt{\frac{T_2}{2\pi \gamma T_w}} \end{aligned} \quad (11.13.10)$$

Hence follows that at $M_2 = 1$ the pressure p_2 is several times smaller than the equilibrium pressure $p_e(T_w)$. In accordance with Figure 11.32b, we have $\bar{m}_2 \approx 0.2$ for $M_2 = 1$, that is, the coefficient B is near-unity.

When the pressure p_2 is greater than the sonic pressure ($p_2 > p_*$), it should be set equal to the external pressure, $p_2 = p_a$, which determines the pressure p_1 . This inference can be extended, with one degree of approximation or another, to irradiated spots of finite size but sufficiently large in comparison with the heating zone thickness $\Delta x \sim \lambda/c_p m$ by equating the pressure on its surface to the external pressure $p_2 = p_a < p_1$ for $u_2 < a_2$ and to the sonic pressure $p_2 = p_*$ for $u_2 = a_2$; the shape of this jet is sketched in Figure 11.32d.

We note that the limiting evaporation regime $u_2 = a_2$ corresponds to a fairly intense irradiation of a material; at a large evaporation heat $h_0 \gg c_p T$, or $\theta/T_w \gg 1$ in formula 11.13.5, from the last Equation 11.13.1 we obtain $m(T_w) \approx I/h_0$, thus determining from Equation 11.13.10 the surface temperature T_w which, in view of the exponential dependence $P_e(T_w)$ 11.13.5, varies at θ/T_w considerably weaker than the parameter m .

Finally, we will establish a relation between the temperatures T_w and T_0 as the relation closing the problem; for this purpose, we will consider the flow parameters in the immediate vicinity of the surface (below they are referred to by the subscript g). Obviously, the wall region is predominantly filled (especially at $M_2 = 1$ and a small value of \bar{m}_2) by molecules emitted by the wall and having thermal velocities corresponding to the wall temperature T_w . For our qualitative estimates, we will assume their distribution to be Maxwellian, with the mass-average vapor outflow velocity equal to $V_2(T_w)$ (see Equation 11.13.4). In this flow the principle of uniform energy distribution (Sections 1.3 and 1.4) does not hold, since, in accordance with 1.4.4, the temperature components in directions orthogonal to the x axis are equal, as in an isentropic flow, $T_{yg} = T_{zg} = T_w$, but the x term $T_{xg} = \kappa T_w$, where the coefficient $\kappa < 1$ in view of the presence of the mass-average gas velocity u_g , which is smaller than the velocity $V_2(T_2)$ even in the limiting case $M_2 = 1$ due to the presence of the return mass flow $m_2(\bar{u}_2)$. Then the mean gas temperature in the wall region is equal to $T_g = (2 + \kappa)T_w/3$, while the stagnation enthalpy of the gas is as follows:

$$H_g = c_{p2} T_g + \frac{1}{2} u_g^2 = c_{p2} T_{0g} = c_{p2} T_w (1 - \chi), \quad \chi = \frac{1 - \kappa}{3} - \frac{(\gamma - 1)}{\pi \gamma} \frac{u_g^2}{V_2^2(T_w)} \quad (11.13.11)$$

Both terms in the expression for χ are small and compensate one another, so that for estimates we can let $T_{0g} = T_w$, the more so that as equilibrium is approached, we have

$T_2 \approx T_{0g} \approx T_w$. At the same time, the flow in the gas jet is adiabatic, so that it should be expected that the stagnation enthalpy $H_g = H_2$, equal to $c_{p2}T_w$ in our approximation, is conserved. To justify this model, we note that the parameters m and p_2 in Equations 11.13.7 and 11.13.10 are only slightly dependent on the ratio T_2/T_w .

We note that the inequality of the temperatures $T_x \neq T$ can be considered one of the principal macroscopic indications of the nonequilibrium nature of the process in this jet; on a model level, it can qualitatively be described by a relaxation equation for the x component of the temperature

$$\frac{dT_x}{dt} = \frac{T - T_x}{\tau} \quad (11.13.12)$$

where τ is a relaxation time.

The determination of the parameters κ and χ and the correct description of the flow in the Knudsen layer is possible only within the framework of rigorous molecular-kinetic gas theory; one of advanced computational tools of this theory is the *statistical modeling method* (Bird, 1976), whose essence lies in the direct calculation of molecular trajectories (in a limited ensemble, considerably smaller than the actual one) with allowance for the laws of their interaction at collisions. Such calculations were carried out also for $\gamma = 5/3$ (e.g., metal vapors) and for $M_2 = 1$ gave the temperatures $T_0 \approx 0.9T_w$ and $T_2 \approx 0.65T_w$ (the data of Vlasov and Kusov, 2000), similar in value to $T_0 = T_w$ and $T_2 = 3T_w/4$ in our model.

12

Viscous Flows and Boundary Layers

This chapter is devoted to real gas flows past bodies with due account for accompanying dissipative effects, such as viscosity and heat conduction, which were neglected in the preceding chapters, with the exception, maybe, of their separate fragments. Bearing in mind, first of all, high-Reynolds-number flows, the emphasis will be placed on boundary layer theory (see Section 1.16) and its generalization to thin shock layers.

In the introduction to the main content of the chapter (Sections 12.1 to 12.4) we will give some elements of the general theory of viscous and boundary-layer flows and present some simple reference problems, which provide useful insight into the role played by dissipative effects in the formation of flows as a whole. In more detail, the presentation of these general issues of the theory can be found in books already cited in the introduction to Chapter 1, as well as in the monographs of Schlichting, 1968, and Slezkin, 1960, to name but a few.

In the sections devoted to particular questions, the primary emphasis will be made upon hypersonic flows and, since purely hypersonic effects in viscous flows are associated with the flight at comparatively high altitudes (see Figure 1.2 of Section 1.1), where the laminar flow regime is usually realized, we will focus on precisely this flow regime unless otherwise indicated. As for the few examples of turbulent flows, these will be outlined using the available semi-empirical closure relations without discussing the relations themselves in detail.

As in the case of inviscid flows, all basic gas dynamic effects will first be studied with reference to the example of equilibrium gases, while nonequilibrium flows constitute the subject of Chapter 13. Finally, we will everywhere, except for Section 12.15, mean and consider only two-dimensional (plane and axisymmetric) flows. Unfortunately, the limitations on the volume of the book, as well as the shortage in time, hindered the author from describing in more detail this important division of three-dimensional viscous flows.

For the same reason, the boundary layer problems are considered only on an impermeable surface, that is, without regard for material melting or evaporation under the action of intense heat fluxes.

12.1 Boundary Conditions and Equations of Motion for Dissipative Viscous Gas Flows

As shown in Section 1.16, this is precisely the boundary conditions of no-slip on a rigid surface in a fluid or gas flow that make us to take account of viscous, or more generally, dissipative properties of fluids and gases. Similar effects are observable not only in the flows past rigid surfaces but also in arbitrary flows, which, were the fluid inviscid, would be accompanied by the formation of contact or shock discontinuities and singularities, impossible in dissipative media. Among these flows are, for example, those associated with the problems of the blast, the heat source, and the diffusion of a concentrated vortex in incompressible fluid discussed in Section 6.10.

The last example is characteristic in that the inviscid solution satisfies the Navier–Stokes equations everywhere except for the central singular point; because of this, the reasons for viscous effects to reveal themselves would not exist, if a vicinity of the center was “withdrawn” and the corresponding annular streamline replaced by a small-sized rigid annulus rotating together with the fluid. This example is a particular case of an incompressible flow governed by the Navier–Stokes Equations 1.10.12. These equations are satisfied by the velocity potential $\varphi(x, y, z)$ introduced in Section 2.4 and governed by the Laplace equation $\Delta\varphi = 0$, since in this case the viscous terms in Equation 1.10.12 also vanish. However, this solution can satisfy only one boundary condition on the surface, namely, the condition of impermeability or vanishing of the normal velocity component, $v_w = 0$, and cannot simultaneously satisfy the condition of no-slip or vanishing of the longitudinal velocity, $u_w = 0$, which is intrinsic in viscous flows (here and in what follows, the subscript w refers to the gas parameters directly at the wall). For this reason, viscous fluid or gas flows in a domain with fixed boundaries cannot be potential, so that taking the viscous terms in the Navier–Stokes equations into account becomes inevitable.

The most widespread and typical conditions imposed on rigid surfaces in gas and fluid flows are the no-slip condition and that of the equality of the fluid and surface temperatures

$$y = 0 : \quad u_g = u_w = 0, \quad T_g = T_w \quad (12.1.1)$$

Here, y is the distance to the wall measured along the normal, the subscript g refers to the gas parameters in the near vicinity of the wall, as $y \rightarrow 0$, and the subscript w relates to the flow parameters at the wall itself (in the following we show that these parameters may be different). Physically, these conditions arise as a result of intermolecular interaction of two contacting media, which is direct for fluids in view of the fact that their molecules are tightly packed, and is caused by gas atoms and molecules incident on a rigid surface for the case of gases. However, in the latter case the validity of the conditions 12.1.1 is not quite obvious, so that we will consider this question in more detail.

For this purpose, we will consider the processes that take place in the near-wall gas layer (*Knudsen layer*) on elementary molecular level, as done in Section 1.4; the layer boundary y_l is at a distance of a free-molecular path l from the wall. At a small distance from the wall, we will separate out one further thin sublayer g of thickness $y_g \ll l$ (Figure 12.1), on the boundary of which we will determine the parameters of the gas which is assumed to be single-component. Precisely these parameters, as $y_g \rightarrow 0$, will be taken as the boundary conditions imposed for the gas on the wall.

In gases, the molecules incident on a rigid surface are not all reflected elastically (as it was assumed in the Newtonian model, Section 3.7), but a fraction α , α being the *accommodation coefficient of tangential momentum*, different from the coefficient α_m in Section 11.13, is actually adsorbed by this surface and then leaves it at a thermal speed V (Section 1.4), which corresponds approximately to the surface temperature T_w , and with a diffuse near-uniform distribution in reflection angles, if a fairly large ensemble of reflected particles is considered. Obviously, the mass-average normal velocity of these molecules (see 1.4.1) in the sublayer g is zero.

Therefore, if the longitudinal mass-average velocity of molecules at a distance l from the rigid surface is u_l , on the surface itself y_g the velocity is equal to the half-sum $u_g = (1 - \alpha/2)u_l$ of the velocities of the molecules incident at the velocity u_l and reflected at the velocity $(1 - \alpha)u_l$, since the number of molecules of both types is the same. However, at the same time $u_l = u_g + l(\partial u / \partial y)$ (we will neglect the distance y_g as compared with l) and the *gas slip velocity* on the rigid surface is as follows

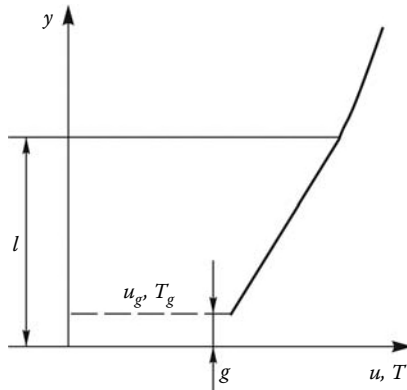


FIGURE 12.1
Velocity and temperature jumps at a wall.

$$u_g = l \frac{2 - \alpha}{\alpha} \frac{\partial u}{\partial y} \quad (12.1.2)$$

We recall that this formula pertains to a simple case of a single-component gas. For a multicomponent gas mixture, this formula determines only the velocity u_{ig} of species i having its own α_i , l_i , and concentration c_i . The overall slip velocity of the gas mixture is $u_g = \sum_i c_i u_{ig}$.

A similar reasoning leads to a formula for the near-surface temperature T_g . The particles incident on the surface at an energy ε_l are elastically reflected in ratio $1 - \beta$ (here, β is the *energy or temperature accommodation coefficient*) with the conservation of the energy ε_l ; however, their fraction β is adsorbed by the surface and emitted at an energy ε_w corresponding to the temperature T_w . Hence, the mass-average energy in the sublayer is as follows

$$\varepsilon_g = \frac{1}{2} \beta \varepsilon_w + \left(1 - \frac{1}{2} \beta\right) \varepsilon_l, \quad \varepsilon_l = \varepsilon_g + l \frac{\partial \varepsilon}{\partial y} \quad (12.1.3)$$

Thence, letting the energy ε be in proportion to T , we arrive at a condition for the *temperature jump* on the rigid surface

$$\Delta T = T_g - T_w = l \frac{2 - \beta}{\beta} \frac{\partial T}{\partial y} \quad (12.1.4)$$

For a multicomponent nonreacting mixture the mean temperature is $T_g = \sum c_i T_{gi}$.

This qualitative scheme (*Maxwell scheme*) provides only the orders of the quantities u_g and ΔT and the form of their dependence on flow parameter gradients on the surface. Clearly, both the slip velocity and the temperature jump are in proportion to the ratio l/δ , where δ is a scale length determining the orders of the velocity and temperature derivatives normal to the surface. Therefore, for $\delta \gg l$ boundary conditions 12.1.2 to 12.1.4 transform to the no-slip and no-temperature-jump conditions 12.1.1, classical for continuous media.

The ratio l/δ can be expressed in terms of the macroscopic parameters of the flow. In accordance with 1.4.9, $l \sim \mu/\rho V$, where μ is viscosity, while the mean thermal speed of molecules V is of the same order as the speed of sound a . Thus, we have

$$\frac{l}{\delta} \sim \frac{\mu}{\rho a \delta} = \frac{1}{\text{Re}_{a\delta}} = \frac{M}{\text{Re}_\delta} = \text{Kn}_\delta$$

$$\text{Re}_{a\delta} = \frac{\rho \delta a}{\mu}, \quad \text{Re}_\delta = \frac{\rho \delta U}{\mu}, \quad M = \frac{U}{a} \quad (12.1.5)$$

Here, U is the scale velocity of the flow, $\text{Re}_{a\delta}$ and Re_δ are the characteristic Reynolds numbers, and $\text{Kn}_\delta = M/\text{Re}_\delta$ is the *Knudsen number*, which was already introduced in Sections 1.4 and 11.13. As $\text{Kn} \rightarrow 0$ we have $l/\delta \rightarrow 0$, which leads to boundary conditions 12.1.1.

As shown in Section 1.16, the viscous boundary layer thickness is of the order $\delta \sim L/\sqrt{\text{Re}_L}$, where L is the longitudinal, or streamwise, scale length. In this case, $\text{Re}_\delta = \sqrt{\text{Re}_L}$, so that $\text{Kn}_\delta = M/\sqrt{\text{Re}_L}$.

The accommodation coefficients introduced previously are usually near-unity and dependent on many factors, such as the type of a gas and a surface material, the surface temperature and state, the presence of other gases, and so on. We note that in the idealized case in which $\alpha = 0$ and $\beta = 0$, boundary conditions 12.1.2 and 12.1.4 give zero derivatives $\partial u/\partial y = 0$ and $\partial T/\partial y = 0$ on the wall, as $y \rightarrow 0$.

We are now coming to the equations of motion for a viscous compressible gas. The continuity and momentum equations derived in Section 1.9 in conventional (Equations 1.9.1 through 1.9.4) and conservative (Equations 1.9.7 and 1.9.8) variables do not require any comments and, in view of the rheological relation 1.10.10 between the viscous (P_τ) and complete (P) stress tensors and the strain rate tensor E_ε (see Sections 1.8 and 1.10), together with the data of Sections 1.13 and 1.14, can easily be rewritten in Cartesian or other systems of coordinates.

Nevertheless, in the energy Equations 1.9.6 or 1.9.10 the term q_τ , responsible for the heat inflow due to viscous dissipation of mechanical energy, and the energy flux \vec{J} are to be clarified. We will determine the latter somewhat later, while for calculating q_τ we will express formulas 1.14.2 or 1.9.5 in terms of the strain rates ε_{ik} . Since these physical quantities are invariant about coordinate transformations, we will perform this for a simple Cartesian coordinate system with unit vectors \vec{l}_i letting $H_i = 1$ in Equation 1.14.2. Then letting

$$\vec{U} = \sum_i \vec{l}_i u_i, \quad \vec{\tau}_i = \sum_k \vec{l}_k \tau_{ik} \quad (12.1.6)$$

we bring Equation 1.14.2 into the form:

$$q_\tau = P_\tau \cdot A, \quad A = \left\| \frac{\partial u_i}{\partial x_k} \right\| \quad (12.1.7)$$

Using then transformations of Equations 1.8.5 to 1.8.10

$$\frac{\partial u_i}{\partial x_k} = \varepsilon_{ik} + \frac{1}{2} \omega_{ik}, \quad \omega_{ik} = \frac{\partial u_i}{\partial x_k} - \frac{\partial u_k}{\partial x_i} \quad (12.1.8)$$

where ω_{ik} are the components (1.8.7) of the vector $\vec{\omega}$, we present the matrix A in the form:

$$A = E_\varepsilon + B, \quad B = \frac{1}{2} \begin{vmatrix} 0 & -\omega_{21} & -\omega_{31} \\ \omega_{21} & 0 & -\omega_{32} \\ \omega_{31} & \omega_{32} & 0 \end{vmatrix} \quad (12.1.9)$$

It can be easily seen that the matrix product $P_\tau B = 0$, which is quite natural, since viscous stresses do not produce work when a gas is rotated as a solid body. Then using 1.10.10 we obtain

$$q_\tau = 2\mu E_\varepsilon^2 - \frac{2}{3}\mu(\operatorname{div} \vec{U})^2, \quad E_\varepsilon^2 = \sum_i \sum_k \varepsilon_{ik}^2 \quad (12.1.10)$$

The latter equation follows from the symmetry of matrix E_ε about the diagonal. Using simple transformations the formula can be cast to the form (Loitsyanskii, 1966):

$$q_\tau = 4\mu(\varepsilon_{12}^2 + \varepsilon_{13}^2 + \varepsilon_{23}^2) + \frac{2}{3}\mu[(\varepsilon_{11} - \varepsilon_{22})^2 + (\varepsilon_{11} - \varepsilon_{33})^2 + (\varepsilon_{22} - \varepsilon_{33})^2] \quad (12.1.11)$$

Clearly, we have always $q_\tau \geq 0$, which is natural due to dissipation irreversibility. At the same time, at adiabatic gas expansion, that is, for $\varepsilon_{ik} = 0, i \neq k$ and $\varepsilon_{11} = \varepsilon_{22} = \varepsilon_{33}$, the energy dissipation is zero.

The main gas dynamic properties of viscous gas flows can conveniently be established with reference to the simplest models of gas media. For this reason, we will let for a time the gas be at equilibrium state, with the equations of state and transport coefficients of the general form:

$$\rho = \rho(p, T), \quad h = h(p, T), \quad \mu = \mu(p, T), \quad \lambda = \lambda_{\text{eff}}(p, T) \quad (12.1.12)$$

Here, as before, p , ρ , T , and h are the gas pressure, density, temperature, and enthalpy, while μ and λ are viscosity and thermal conductivity, the parameter λ_{eff} having the same meaning as in formula 1.3.11. Viscous nonequilibrium flows will be considered in Chapter 13.

12.2 Some Exact Solutions of Navier–Stokes Equations

In addition to the problem of Section 3.2 on the shock wave structure and the problems of Section 6.10 grouped with respect to the criterion of self-similarity, we will present some further exact solutions of incompressible Navier–Stokes equations, the simple analytical form of which makes it possible to demonstrate clearly the role played by viscosity in the formation and properties of some flows.

These are, first, layered flows in which particles move along rectilinear trajectories parallel to a longitudinal x axis and the longitudinal velocity u and the temperature are dependent on the transverse y coordinate only. As for the transverse velocity and the pressure gradient $\partial p / \partial y$, these are zero. Among these flows are the Rayleigh flow (Section 6.10) and the *Couette* and *Poiseuille* flows, which will be discussed in the following (in what follows we will use the more general term *shear flows*, which will be also assigned to the flows qualitatively similar to the layered flow, that is, those in which the transverse gradients of the flow parameters are predominant over the longitudinal ones, as, e.g., in boundary layers; see Section 1.16).

In the *Couette flow* a fluid flows in a gap of width d formed by two infinite parallel plates with temperatures T_1 and T_2 , one of which is at rest, while the other moves at a longitudinal velocity U (Figure 12.2). This problem is related with the flow between two coaxial rotating cylinders with a so narrow gap between them that the effects of the streamline curvature and the transverse pressure gradient can be neglected.

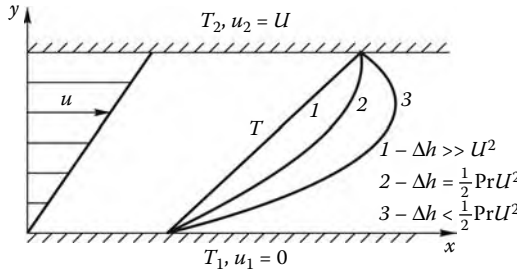


FIGURE 12.2
Couette flow.

In the *Poiseuille flow* a fluid flows in a plane or circular channel of height (or diameter) $2r_0$ and infinite extent. In this channel all cross-sections are the same and the streamlines are parallel to the channel walls or the axis, that is, the flow is stratified. Obviously, this duct can represent a model of only a relatively long channel with a length $L \gg r_0$.

To overcome friction and to force a fluid through the channel at a flow rate G , the pressure difference $\Delta p = \kappa L$ must be applied at the channel end sections.

In a cylindrical reference frame (Section 1.14) the equations of motion 1.10.12 and 1.9.10, common for both plane ($v = 0$) and axisymmetric ($v = 1$) flows, can be written in the form:

$$-\kappa = \frac{\partial p}{\partial x} = \frac{1}{r^v} \frac{\partial r^v \tau}{\partial r}, \quad \tau = \mu \frac{\partial u}{\partial r} \quad (12.2.1)$$

$$\kappa u = \frac{1}{r^v} \frac{\partial r^v \bar{J}}{\partial r}, \quad \bar{J} = -J_T + \tau u \quad (12.2.2)$$

$$-J_T = \lambda \frac{\partial T}{\partial r} = \frac{\lambda}{c_p} \frac{\partial h}{\partial r} = \frac{\mu}{\text{Pr}} \frac{\partial h}{\partial r}, \quad \text{Pr} = \frac{\mu c_p}{\lambda}$$

Here, \bar{J} is the total transverse energy flux, τ is friction, h is the enthalpy, μ and λ are viscosity and thermal conductivity, c_p is the specific heat of the gas, and Pr is the Prandtl number.

For the Couette flow we should let $\kappa = 0$ and $v = 0$ and pose the following boundary conditions

$$\begin{aligned} y = 0 : \quad u &= u_1 = 0, \quad T = T_1 \\ y = d : \quad u &= u_2 = U, \quad T = T_2 \end{aligned} \quad (12.2.3)$$

Here, r is replaced by y .

In this case, we have the integrals $\tau = \text{const}$ and $J = \text{const}$, that is, the conditions of the constancy of friction and the energy flux between the plates; for this reason, conditions 12.2.3 imposed on the plates cannot be replaced by preassigning the heat fluxes on both plates.

Since in isobaric flows the Prandtl number Pr and viscosity μ are dependent only on the enthalpy or the temperature (Section 1.3), the system of Equations 12.2.1 and 12.2.2 has the integral $h = h(u)$, which at a constant Pr can be brought into the form:

$$H = h + \frac{1}{2} u = c_1 + c_2 u + \frac{1}{2} (1 - \text{Pr}) u^2 \quad (12.2.4)$$

In other words, the total gas enthalpy H , which is constant along the streamlines of an inviscid adiabatic steady-state flow, is in our case a quadratic, and for $\text{Pr} = 1$ even a linear function of the velocity. In the latter case this integral is known as the *Crocco integral* (which was encountered earlier, in Section 6.10).

At constant transport coefficients, the velocity profile in the Couette flow is linear in y , while the enthalpy profile (or that of the temperature at $c_p = \text{const}$) is quadratic, as shown in Figure 12.2. For $\Delta h = h_2 - h_1 < \text{Pr}U^2/2$ the temperature maximum is displaced inward from one of the walls, so that the dissipative heat flux (the term τu in the second equation in Equation 12.2.2) is predominant over the external one and is incident on both plates. Contrariwise, for $\Delta h \gg U^2$ viscous dissipation of the energy is unessential and the enthalpy profile is linear.

For an incompressible isothermal fluid, the Couette solution is a limit of the solution of the Rayleigh problem (Section 6.10) on a suddenly starting plate in the presence of another, fixed plate, spaced apart of the starting plate at a distance d and with the no-slip condition imposed on it. For the sake of illustration, in Figure 12.3 we have plotted the exact solution of Equation 6.10.20, subject to the previously mentioned conditions, for different values of the dimensionless time $\tau = vt/d^2$. The disturbance front from the moving plate reaches the fixed plate at $\tau > 0.1$; at $\tau > 0.5$ the velocity profile becomes linear and the time-dependent Rayleigh flow degenerates to the stationary stratified Couette flow. However, at $\tau < 0.1$ the velocity profiles follow the self-similar Rayleigh solution (Figure 6.24).

We will now return to the *Poiseuille flow*. It is realized only when the density is pressure independent (incompressible flow regime). For a constant μ , Equation 12.2.1 is not connected with Equation 12.2.2 and has the solution

$$\frac{u}{u_0} = 1 - \frac{r^2}{r_0^2}, \quad u_0 = \frac{\kappa r_0^2}{2(1+\nu)\mu}$$

$$u_G = \frac{2}{3+\nu} u_0, \quad G = \frac{2\pi\nu}{3+\nu} r_0^{1+\nu} \rho u_0, \quad \tau = 2\mu u_0 \frac{r}{r_0^2} \quad (12.2.5)$$

Here, u_0 and u_G are the maximum velocity at the channel axis and the flow-rate-average velocity. The velocity (u/u_0) profile is plotted in Figure 12.4.

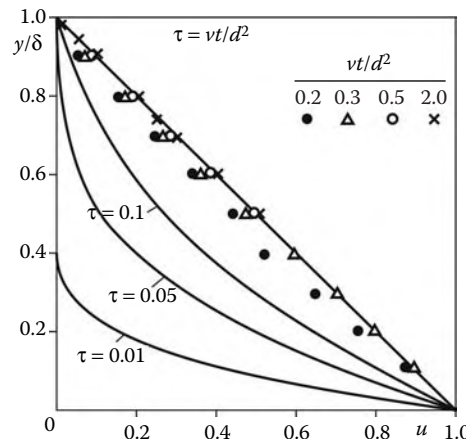


FIGURE 12.3
Rayleigh problem in a finite-thickness layer.

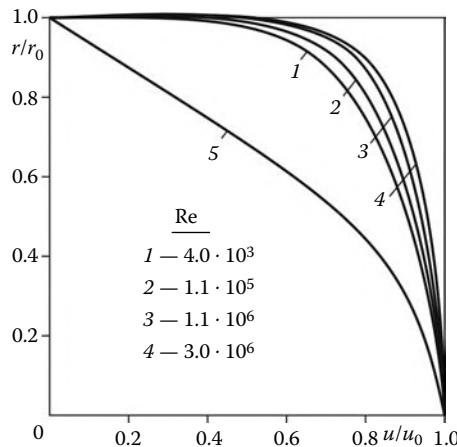


FIGURE 12.4
Velocity profiles in turbulent (1 to 4) and laminar (5) flows in a circular tube.

This solution is not adequate near the channel ends; however, far from the ends it gives the velocity and friction distributions in the main region of a very long tube and the dependence of the fluid flow rate in the tube on the pressure difference. There are no similar solutions for gases, since in this case the density and temperature vary with the pressure along the longitudinal axis of the channel. For a constant μ , the temperature field inhomogeneity has no effect on the velocity field 12.2.5, but at $\mu = \mu(T)$ this flow can be only isothermal, since any transverse variation of the temperature would result in heat fluxes to the walls and, therefore, the temperature and viscosity variation along the tube. An exception is provided only by a plane channel with different, though constant, wall temperatures; in such a channel the energy equation takes the form $\lambda dT/dy = \text{const}$. In this case, the velocity profile is simply nonsymmetric, though it is, as before, independent of the longitudinal coordinate.

In fairly long tubes universal velocity profiles are realized in turbulent flows as well. These profiles are also presented in Figure 12.4 for different Reynolds numbers $Re = \rho u_a d / \mu$ (d is the tube diameter, u_a is the mean velocity, and the walls are smooth); they are considerably more convex than the laminar profiles, which indicates that in tubes turbulent friction is appreciably greater than laminar friction. In fairly smooth tubes the flow is laminar for the Reynolds numbers as high as $2 \cdot 10^3$ and becomes turbulent usually for $Re > 10^4$. The initial, transition region of the tube up to the formation of the universal velocity profile has an extent of the order of several tens of the tube diameters, being somewhat longer in the turbulent and shorter in the laminar flow.*

Stagnation point in a viscous flow. In Section 2.11 we presented the solutions for the flow in the vicinity of a plane ($v = 0$) and axisymmetric ($v = 1$) stagnation points ($x = y = 0$, Figure 2.21) in an inviscid transverse flow over an infinite plane $y = 0$ in a Cartesian coordinate system. In the following we will derive an exact solution for the similar problem of the viscous flow over the same plane.

* In more detail this is outlined in the previously mentioned books of Schlichting (1968) and Loitsyanskii (1966).

By analogy with Equations 2.11.1 or 2.11.4 (with the constant a replaced by c), we seek a solution in the form:

$$\begin{aligned} u &= cx\varphi'_v(y), & v &= -(1+\nu)c\varphi_v(y) \\ p &= p_0 - \frac{1}{2}\rho c^2(x^2 + \bar{p}_v(y)), & c &= \text{const} \end{aligned} \quad (12.2.6)$$

This solution satisfies the incompressible continuity equation for any function φ_v and the inviscid system of equations for $\varphi_v = y$ and $\bar{p} = (1+\nu)^2y^2$.

Substituting expansion 12.2.6 into the first momentum equation in Equation 1.10.12 we obtain the following equation for the function φ

$$\frac{\mu}{\rho c}\varphi''' + (1+\nu)\varphi_v\varphi'' + (1-\varphi_v^2) = 0, \quad \varphi_v(0) = \varphi'_v(0) = 0 \quad (12.2.7)$$

For $\mu = 0$ this equation has an inviscid solution $\varphi = y$. This is a third-order equation and, apart from the no-slip conditions written previously, needs one more boundary condition. It is naturally related with the conditions posed far from the wall assuming the decay of the viscosity effect, that is, $\varphi'_v \rightarrow 1$ as $y \rightarrow \infty$, as in the case of an inviscid velocity field. Passing to the variables

$$\begin{aligned} \zeta &= \chi y, & \Phi_v(\zeta) &= \chi\varphi_v(y) \\ \chi &= \left[\frac{2(1+\nu)c\rho}{\mu} \right]^{1/2}, & \varphi'_v &= \frac{d\varphi_v}{dy} = \frac{d\Phi_v}{d\zeta} = \Phi'_v \\ \varphi''_v &= \frac{d^2\varphi_v}{dy^2} = \chi \frac{d^2\Phi}{d\zeta^2} = \chi\Phi'' \end{aligned} \quad (12.2.8)$$

we bring Equation 12.2.7 into the form:

$$2\Phi'''_v + (1+\nu)\Phi_v\Phi''_v + \beta(1-\Phi_v^2) = 0, \quad \beta = (1+\nu)^{-1} \quad (12.2.9)$$

Finally, from the second momentum in Equation 1.10.12, that is, projected on the y axis, we obtain a formula for the function \bar{p}_v in Equation 12.2.6 for the pressure

$$\bar{p}_v(y) = (1+\nu)^2\varphi_v^2 + (1+\nu)\frac{2\mu}{\rho c}\varphi'_v = (1+\nu)\frac{\mu}{\rho c}(\Phi_v^2 + 2\Phi'_v) \quad (12.2.10)$$

The solution of Equation 12.2.9 is shown in Figures 12.5 and 12.6, the profiles of the longitudinal $\Phi'_v(\zeta)$ and normal $\Phi_v(\zeta)$ dimensionless velocities being fairly similar for the plane ($\nu = 0$) and axisymmetric ($\nu = 1$) flows. Friction on the wall is equal to zero at the stagnation point itself, while in its vicinity it is determined by the formula

$$\begin{aligned} \tau &= \mu \frac{du}{dy} = x\sqrt{2(1+\nu)\rho\mu c^3}\Phi''_v(0) \\ \Phi''_0(0) &= 0.872, \quad \Phi''_1(0) = 0.655 \end{aligned} \quad (12.2.11)$$

The domain of influence of viscosity on the external inviscid flow is bounded from above by a certain value ζ_δ such that for $\zeta \geq \zeta_\delta$ the difference $1 - \Phi'_v \leq \varepsilon \ll 1$ and the function $\Phi'_v \approx 1$ corresponds to the external inviscid flow over the plane wall. Therefore, the quantity $\delta = \bar{\delta}_v(\mu/\rho c)^{1/2}$ is, as it were, the thickness of the boundary layer mentioned in Section 1.16, which develops within the near-wall part of the external inviscid flow ($\bar{\delta}_0 \approx 2.6$ and $\bar{\delta}_1 = 2.15$ for $\varepsilon = 0.005$).

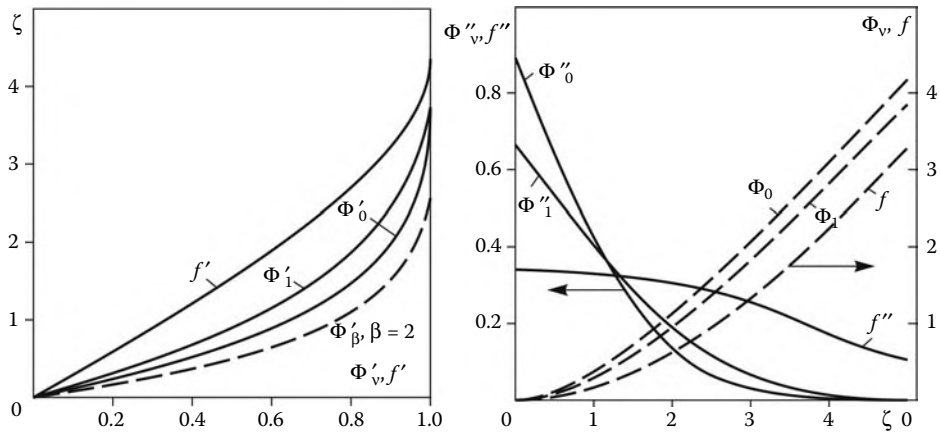


FIGURE 12.5
Velocity and friction profiles in an incompressible boundary layer.

However, in accordance with Figure 12.5, the function $\Phi_v = \zeta - \zeta^*$ ($\zeta^* = \text{const}$), proportional to the normal velocity v , approaches the external velocity $\Phi_v = \zeta$ only as ζ^*/ζ , that is, rather slowly. Therefore, in order to offset this boundary layer effect on the inviscid flow, the wall should be drawn back at a distance $\delta_v^* = y_v^* = \bar{\delta}_v^*(\mu/c\rho)^{1/2}$ called the *boundary layer displacement thickness* ($\bar{\delta}_0^* = 0.65$ at $v = 0$ and $\bar{\delta}_1^* = 0.58$ at $v = 1$).

The asymptotics of this solution for large values of ζ can be derived by letting $\Phi_v = \zeta - \zeta^*$ on the left-hand side of Equation 12.2.10 and neglecting (with the following checking) the right-hand side of this equation. Thus, we have

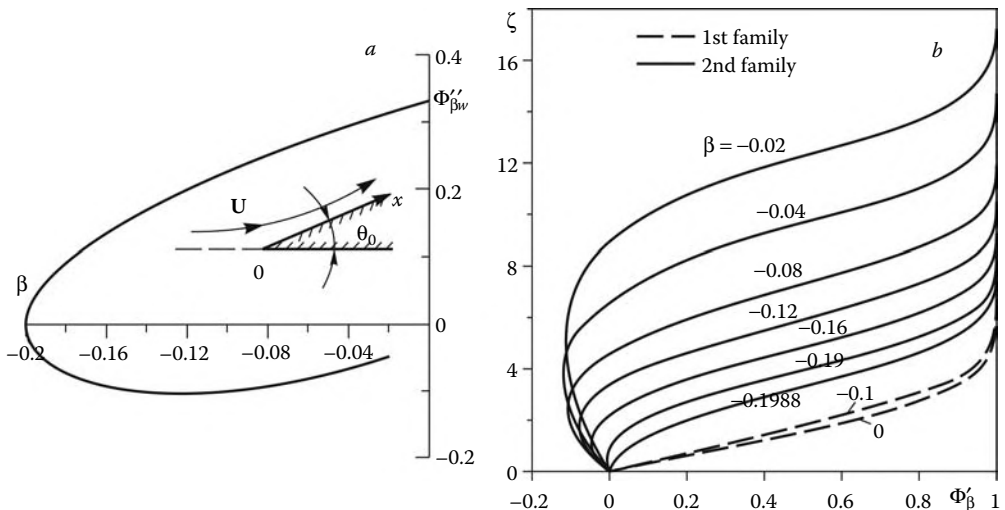


FIGURE 12.6
Parameter β (a) and velocity profiles (b) in a boundary layer with a power-law outer velocity.

$$\begin{aligned}
\Phi_v'' &\approx CE, \quad E = e^{-(\zeta - \zeta^*)^2} \\
1 - \Phi_v' &\approx C \int_{\zeta}^{\infty} Ed\zeta \approx \frac{1}{2}C(\zeta - \zeta^*)^{-1}E \\
\Phi - (\zeta - \zeta^*) &\approx -\frac{1}{4}C(\zeta - \zeta^*)^{-2}E, \quad \zeta^* = \int_0^{\infty} (1 - \Phi_v')d\zeta
\end{aligned} \tag{12.2.12}$$

In doing these transformations we applied the L'Hospital rule, while the relative order of the discarded right-hand side of Equation 12.2.9 is $(\zeta - \zeta^*)^{-2} \ll 1$, that is, the same as that of the terms discarded in 12.2.12. The constant C is determined by matching with the complete solution of the problem.

Thus, inherent in this problem, as well as, for example, in the Rayleigh problem of Section 6.10, is exponential decay of the viscous effect due to the no-slip condition imposed on the wall. This is particularly important, since the solution obtained has a meaning only for $\delta \ll L$, where L is the length scale of the blunt body modeled here by an infinite plane wall. Thus, as in Section 2.1, this formally exact solution can be only local with respect to actual flows in the vicinity of the stagnation point of a blunt body. It represents the first term of the exact solution expansion in x , similar to those obtained in Sections 7.7 and 7.8 by the truncated series method. Within the limits of the viscous flow zone, in accordance with 12.2.10, the transverse pressure difference is of the second order, $\Delta p/\rho U^2 \sim (\delta/L)$,* that is, the pressure can be taken to be constant across the boundary layer.

We note one more fundamental difference of viscous and inviscid flows, which follows from the solution obtained. At least in the vicinity of the stagnation point the inviscid flow is reversible, so that the same solution describes the vicinities of the divergence ($c > 0$) and convergence ($c < 0$) points. However, in the latter case a bounded solution of the viscous problem, that is, Equation 12.2.7 with the conditions $\varphi_v' \rightarrow 1$ and $\varphi_v'' \rightarrow 0$ as $y \rightarrow \infty$, does not exist at all, since, subject to these conditions, Equation 12.2.7 has an unbounded asymptotic solution $\varphi'' \sim e^{-\chi^2 y^2}$, where $\chi^2 < 0$. In this case, the flow is directed from the periphery to the center, so that near-wall particles that possess low velocities are not able to overcome the growing pressure, which, physically, must lead to the flow restructuring and, mathematically, manifests itself in the absence of a bounded solution.

At the same time, at low Reynolds numbers (possibly for $Re < 50$) a continuous separationless flow past a body is quite possible at the expense of the internal friction forces and the corresponding entrainment of near-wall jetlets by the external flow.

12.2.1 General Case $U_\delta = cx^m$

The solution presented previously is a particular case of the more general class of self-similar solutions corresponding to a power-law velocity distribution $U_\delta = cx^m$ in the vicinity of a sharp (at $x = 0$) edge of a wedge or a vertex of a cone with the vertex angle θ_0 (Figure 12.6 and Figure 2.21f and g, of Section 2.11) in an incompressible viscous flow. In the designations of Sections 2.11 and 6.2, where the corresponding inviscid flows were discussed, $m = n - 1$.

* The solution of Falkner and Skan (1931); see also Loitsyanskii (1966).

This problem can be reduced to Equation 12.2.9 in the variables

$$\xi = \sqrt{\frac{\rho c(m+1+2\nu)}{\mu}} \frac{y}{x^{(1-m)/2}}, \quad u = cx^m \Phi'_\beta(\xi), \quad \beta = \frac{2m}{m+1+2\nu} \quad (12.2.13)$$

The case $m = \beta = 0$, or $U_\delta = \text{const}$ corresponds to the boundary layer on a flat plate, which will be considered in Section 12.4; the cases $\beta = 1$ and $\beta = 1/2$ considered previously correspond to the stagnation points on a two-dimensional blunt body and a blunt body of revolution. The two cases are limiting for bodies with an acute semivertex angle ($\theta_0 \leq \pi/2$), so that the values $\beta > 1$ in the former and $\beta > 1/2$ in the latter case, that is, for $m > 1$, can relate only to the flows inside a backward-facing wedge or cone ($\theta_0 > \pi/2$, Figure 2.21f), while the velocity profile for $\beta = 2$ or $m \rightarrow \infty$, as shown in Figure 12.5a, relates to the limiting flow inside such a wedge when the angle $\theta_0 \rightarrow \pi$, since, in accordance with Section 2.11, $m = \theta_0/(\pi - \theta_0)$.

Solutions of Equation 12.2.9 can exist also for $m < 0$, that is, at a positive pressure gradient $\partial p/\partial x > 0$, which, in accordance with Section 2.11, corresponds to the flow downstream of the deflection point of a plane incompressible flow (Figure 2.21g) if, of course, the boundary layer thickness ahead of the corner point is neglected. In this case, for $\beta = \beta_0 = -0.1998$ (or $m = -0.0904$, $\theta_0 = -0.0994\pi = 17.9^\circ$ at $\nu = 0$) the friction on the wall vanishes ($\Phi''_{\beta w} = \Phi''_\beta(0) = 0$), while for $\beta < \beta_0$ there is no solution at all.

However, it turns out that on the $\beta_0 \leq \beta < 0$ range the solution of Equation 12.2.9 has two families, namely, the first with the velocity directed forward, $\Phi'_\beta > 0$, $\Phi''_{\beta w} > 0$, and the second with negative friction on the wall $\Phi''_{\beta w} < 0$ and a wall region of return flow. For both families, the curve $\Phi''_{\beta w}(\beta)$ is plotted in Figure 12.6a, while the second-family profiles are presented in Figure 12.6b.*

12.3 Parabolization of Incompressible Navier–Stokes Equations

The time-dependent, spatially one-dimensional problems were considered in Section 6.10, in particular, as applied to the Rayleigh problem.

For these problems the idea of *parabolic equations* is brought into use. A very simple and canonical example of these equations is the heat conduction Equation 6.10.12, as well as Equation 6.10.20 in the Rayleigh problem coinciding with the former if u is replaced by T and $\nu = \mu/\rho$ by $\kappa = \lambda/\rho c_p$. However, the self-similar degenerate problems with special initial conditions considered in Section 6.10 do not allow us to reveal in a full measure the properties of such equations; to a certain degree, this gap will be filled in what follows.

As distinct from elliptic and hyperbolic equations of inviscid fluid dynamics (e.g., the Laplace and wave equations), which, in essence, differ only in opposite signs of their second, higher-order derivatives (which leads to fundamental differences of the properties of their solutions), an indicator of parabolic equations is that the higher derivative with respect to one of the variables (in our case t) is of the first order, while the other derivatives are of the second order.

The distinctive feature of the parabolic equations, as the hyperbolic ones, is that they are *evolutionary* in the temporal variable in the sense that a solution known on an initial line (or

* The data of Shmanenkov and Pokrovskii (1979) used these profiles in solving problems of separated flows.

plane) $t = t_0$ can always be continued to the domain $t > t_0$. In fact, for example, in Equation 6.10.20 the derivative u_{yy} is known on the initial line,* therefore, the *outward derivative* u_t can also be determined from the equation. This gives us a theoretical possibility to make a step $\Delta u = u_t \Delta t$ in time for determining the solution on the subsequent line $t_1 = t_0 + \Delta t$.

However, it should be borne in mind that the possibility of determining the outward derivatives is insufficient for the realization of the solution, since the initial-value problem must also be well-posed. This well-posedness was proved for hyperbolic and parabolic equations, as distinct from the case of elliptic equations (cf. Section 4.1). We note that, as distinct from the Courant criterion $a\Delta t \leq \Delta x$ for the stability of an explicit numerical method of solution of the wave equation (Δx is the spatial size of a cell and a is the speed of sound; see Sections 4.2 to 4.4), for the heat conduction equation this criterion is provided by the condition $\Delta t \leq (\Delta x/\kappa)^2$. This difference is also an indicator of the fundamental difference of the compared equations.

For the heat conduction equation the lines $t = \text{const}$ are *characteristics*, though their meaning is different from those of the wave equation. Disturbances preassigned on these characteristics propagate only forward, into the future or the $t > t_0$ domain, and do not determine the solution at the preceding $t < t_0$ moments. Apparently, this is the most important property of these characteristics, which manifests itself in more general situations as well.

At constant boundary conditions the solutions of time-dependent parabolic equations approach the solutions of the corresponding elliptic equations governing the limiting steady state of the process under consideration. Thus, the time-dependent flow between two plates induced by a sudden start of one plate (Rayleigh problem) degenerates with time into the steady-state Couette flow (Figure 12.3). If an infinite channel of a constant cross-section with the walls parallel to an x axis is set in motion, then the flow thus generated is also x -independent and, hence, the system of Equation 1.10.14 is reduced to a single equation, more general than 6.10.20

$$\frac{\partial u}{\partial t} = v \Delta u, \quad \Delta u = \frac{\partial^2 u}{\partial x^2} + \frac{\partial^2 u}{\partial y^2} \quad (12.3.1)$$

This two-dimensional heat conduction equation is also parabolic and, when the steady state is attained, its solution degenerates into the solution of the elliptic Laplace equation $\Delta u = 0$, which was also encountered in Chapter 2 in connection with subsonic flows. Naturally, a class of these examples can be extended.

Departing from these examples, we will extrapolate the results formulated to the general Navier–Stokes equations. We recall that the classification of the equations of mathematical physics is performed in accordance with the order of the higher derivatives and the signs of their coefficients. For the time-dependent Navier–Stokes equations, these criteria, namely, the first order of the derivative with respect to time and the second order of the spatial derivatives, makes it possible to assign these equations to the parabolic type. For their solution they require preassigning the distributions of the initial flow parameters at $t = t_0$ and the boundary parameters on the domain boundaries. In the problem of unbounded flow past a body some conditions must be imposed far from the body in all directions.

Correspondingly, the steady-state Navier–Stokes equations are elliptic and require for their solution only imposing some conditions on a boundary or in the far periphery of the

* The subscripts t , x , and so on, will sometimes be referred to the partial derivatives with respect to the corresponding variables, as it is accepted in the mathematical literature.

flow domain. The conditions ahead of a body in a fluid flow are obvious: they correspond simply to the freestream. However, since the solutions of these equations have no simple analytical asymptotics as the Laplace equation of Chapter 2, the question of the formulation of conditions downstream of the body is less obvious, the more so that physically these conditions cannot be preset arbitrarily. This question will be answered as particular problems will be formulated. We will only note that the dependence of the solution on the conditions posed downstream of a body considerably weakens as the Mach number and, usually, the Reynolds number grow, that is, as the gas velocity increases.

Moreover, there is one more extended and even predominant (from the standpoint of practical importance) class of problems in which the role played by the conditions posed behind a body or, generally, downstream of a domain of our interest, is rather insignificant or even vanishes. This is possible for flows in narrow layers with a thickness $\delta \ll L$, where L is the scale length of the longitudinal flow, at the expense of *parabolization* of the originally elliptic steady-state Navier–Stokes equations.

The basic idea of this parabolization was demonstrated in Section 1.16 with reference to the example of the two-dimensional incompressible flow along a plane surface (in particular, a flat plate) with the coordinates x and y along and normal to the surface. This procedure reduces to discarding the second derivatives with respect to the longitudinal x coordinate in the viscous operator based on the fact that at high Reynolds numbers the longitudinal derivatives of the flow parameters are (according to 1.16.3), smaller than the transverse derivatives along the y axis by a factor of δ/L . In this case, the normal velocity component (along the y axis) is, in accordance with 1.16.4, of the order $v \sim U_0\delta/L \ll u$, where u is the longitudinal velocity component and U_0 is its scale value; therefore, $u \sim U$, where U is the total velocity.

Under these assumptions, the Navier–Stokes Equation 1.10.12 for two-dimensional incompressible flows take the form:

$$\begin{aligned} \rho(uu_x + vu_y) &= -p_x + (\mu u_y)_y \\ \rho(uv_x + vv_y) &= -p_y + (\mu v_y)_y \\ u_x + u_y &= 0 \end{aligned} \quad (12.3.2)$$

We note that both terms on the left-hand side of the momentum equation are of the same order $\rho u^2/L$ or $\rho uv/\delta$.

In relation to the original system 1.10.12, the obtained system 12.3.2 is *parabolized*, that is, it pertains to the parabolic type of equations with respect to the totality of the main indicators (the higher derivative with respect to the “temporal” variable x is of the first order), though the presence of the continuity equation in the system violates somewhat the purity of the classification.

System 12.3.2 is an example of the general parabolized system (we shall return to such systems and systems of a more general form in Section 12.5); however, in this case the system can additionally be simplified. For this purpose, we will evaluate the transverse (along the y axis) pressure difference caused by inertial and viscous terms of the second momentum equation taking into account that $u \sim U_0$ and $v/U_0 \sim \delta/L$

$$\begin{aligned} \frac{\Delta p}{\rho U_\delta^2} &\sim \frac{\delta}{U_0} \frac{\partial v}{\partial x} \sim \frac{\delta^2}{L^2} \\ \frac{\Delta p}{\rho U_0^2} &\sim \delta \frac{\mu}{\rho U_0^2} \frac{\partial^2 v}{\partial y^2} \sim \frac{\mu}{\rho u L} = \frac{1}{Re_L} \end{aligned} \quad (12.3.3)$$

Here, the pressure difference is divided by the ram pressure ρU_0^2 , since for an incompressible fluid the value of the pressure itself does not play any role.

Thus, for $\delta/L \ll 1$ and high Reynolds numbers $Re_L \gg 1$, the transverse pressure gradient can be neglected, which is equivalent to degeneration of the transverse momentum equation to the limiting equation $\partial p/\partial y = 0$. This result reduces Equation 12.3.2 to more simplified *boundary layer equations* or *Prandtl equations* (1904)

$$\begin{aligned} \rho uu_x + \rho vu_y &= -p_x + (\mu u_y)_y \\ u_x + v_y &= 0, \quad p = p(x) \end{aligned} \quad (12.3.4)$$

This system consists of two equations but involves three unknown functions u , v , and p , even if ρ and μ are constant. In order to obtain a missing equation we will consider two typical examples.

The *first example* is furnished by the flow in a plane narrow channel for which we have four boundary conditions $u = v = 0$ at $y = 0$ and $y = \delta$, which is quite unnecessary, since the continuity equation for v is a first-order equation and requires only one boundary condition, while the momentum equation is of the second order, so that having two boundary conditions for u is quite natural.

The extra boundary condition, which is equivalent to preassigning the fluid flow rate across the channel, serves for determining the function $p(x)$. Apparently, the problem conserves its evolutionary nature, since, the initial equations being preset in a certain section x_0 , the equations and the boundary conditions suffice for determining the velocity profile and the pressure p in the next $x = x_0 + \Delta x$ section (e.g., using one or another iteration procedure).

However, if at the end of the channel $x = L$ the pressure $p = p_L$ thus obtained would not coincide with the external pressure p_a , then, as in the hydraulic approximation of Section 2.3, the fluid flow rate should be so altered as to obtain $p_L = p_a$ for $p_a \geq p_*$ or $p_L = p_*$ for $p_a \leq p_*$, where p_* is a certain average sonic pressure. In any case, as in the one-dimensional problem of Section 2.3, for a parabolic channel flow *formally parabolic problem acquires elliptic features* owing to the presence of an additional unknown function (in our case, $p(x)$). We recall that analogous “elliptization” of parabolic and hyperbolic equations was encountered in the problem of a thin shock layer of Section 7.13.

Finally, under the condition $L \gg \delta Re_\delta$, where $Re_\delta = \rho u \delta / \mu$, the convective terms in the first equation of Equation 12.3.4 become unessential, so that for constant ρ and μ the solution of this equation passes over the Poiseuille solution 12.2.5 which can be treated as intermediate asymptotics valid at a certain distance from the channel ends. As for their immediate vicinities of extent $\Delta x \sim \delta$, in these regions the boundary layer Equations 12.3.4 are inadequate.

The *second example* of the application of Equation 12.3.4 is furnished by the problem of the thin boundary layer on a body surface, which was considered in Section 1.16. The boundary layer being limitingly thin, it does not almost introduce disturbances into the external inviscid flow and, hence, the pressure distribution over the body surface which can be assumed to be preassigned and equal to the surface pressure in the inviscid flow. The same is true for other flow parameters on the outer edge of the boundary layer (which are referred to in the following by the subscript δ) and, in particular, for the longitudinal velocity $u \approx u_\delta$, which, for $v \ll u_\delta$, is equal to the total velocity U_δ .

This formulation of the problem of a limitingly thin boundary layer will be termed *classical*; we will devote several of the following sections to the corresponding problems. In this case, system 12.3.4 is parabolic without any reservations. The parabolicity of this system is

most clearly demonstrated by passing from the x, y variables to the *von Mises variables* x, ψ , where $\psi(x, y)$ is the stream function (Equation 2.1.2); then the system of Equation 12.3.4 reduces to a single equation

$$\frac{\partial u}{\partial x} = \frac{\partial}{\partial \psi} \left(\rho \mu u \frac{\partial u}{\partial \psi} \right) + \frac{1}{\rho u} \frac{dp}{dx} \quad (12.3.5)$$

This equation is analogous to the nonlinear inhomogeneous heat conduction equation with the temporal coordinate x and the variable thermal conductivity $\rho \mu u$; for $p = \text{const}$ this equation is analogous to Equation 6.10.29, which was met earlier.

Finally, we will dwell on boundary conditions for the boundary layer equations. For an incompressible flow, these conditions are as follows:

$$\begin{aligned} y = 0 : \quad u = v = 0, \quad & y = \delta : \quad u = U_\delta \\ x = x_0 : \quad u = u_0(y) \end{aligned} \quad (12.3.6)$$

Under these conditions the initial function $v_0(y)$ cannot be arbitrary but must satisfy system 12.3.4 with the derivative u_x eliminated from it. This is, in particular, the manifestation of the characteristic nature of the $x = \text{const}$ section. Moreover, these conditions are not closed, since they do not determine the boundary layer edge δ , while the problem formulated can be solved for any chosen value of δ if we proceed from the total order of the system of equations in Equation 12.3.4.

The latter question is one of most fundamental for the whole boundary layer theory; it can be answered only based upon the general formulation of the problem of the viscous flow past a body. The answer is as follows: since at high Reynolds numbers the viscosity effect is concentrated only within a boundary layer of small thickness $\delta \ll L$, the *internal solution* corresponding to it must be matched smoothly, namely, with continuous second derivatives of the velocity field (and, in the general case, of other functions too), with the *external inviscid solution*. The conditional edge of the boundary layer is determined from precisely this condition. In a very simple case, in which in the external flow the normal derivatives $\partial u / \partial y$, and so on, are of the order of u/L , and so on, they can be neglected as compared with the similar derivatives in the boundary layer. Moreover, the variation of these functions across the thickness of the order δ is negligibly small, so that the effect of absorption of a portion of the inviscid flow by the boundary layer can also be neglected; thus, the same values of the flow parameters as on the body surface can be assigned to the outer edge of the boundary layer. Thus, the boundary layer thickness should be determined as a minimum, though ensuring the smooth matching of the internal and external solutions, value. This matching procedure is fundamentally facilitated by the fact that the boundary layer solutions tend *exponentially* to their outer boundary conditions, usually as $e^{-\alpha(y/\delta)^2}$, where $\alpha \sim 1$. This assertion follows from all the examples presented in Sections 6.10 and 12.2; in what follows we shall convince ourselves in that again (e.g., in Section 12.4). This makes it possible to formulate boundary conditions for the boundary layer equations as $y \rightarrow \infty$, thus excluding the parameter δ from conditions 12.3.7.

Further discussion of the question of the boundary layer interaction with an external inviscid flow will be continued in the following sections of this chapter.

12.4 Boundary Layer on a Flat Plate in an Incompressible Flow

In the formulation of Section 12.3 we will consider the problem of a classical thin boundary layer on a semi-infinite flat plate with a sharp leading edge at the origin $x = 0, y = 0$ (Figure 12.7) in a longitudinal incompressible flow. In this case, the pressure can be assumed to be constant and the system of Equations 12.3.4 and boundary conditions (Equation 12.3.6) take the form:

$$\begin{aligned} u \frac{\partial u}{\partial x} + v \frac{\partial u}{\partial y} &= \frac{\mu}{\rho} \frac{\partial^2 u}{\partial y^2} \\ \frac{\partial u}{\partial x} + \frac{\partial v}{\partial y} &= 0 \end{aligned} \quad (12.4.1)$$

$$\begin{aligned} x \geq 0, \quad y = 0 : \quad u &= 0, \quad v = 0 \\ y \rightarrow \infty : \quad u &\rightarrow U_\infty \\ x < 0 : \quad u &= U_\infty, \quad v = 0 \end{aligned} \quad (12.4.2)$$

The possibility of imposing an asymptotic (as $y \rightarrow \infty$) external boundary condition was mentioned at the end of Section 12.3 and will be validated additionally in the following. The last boundary condition of Equation 12.4.2 presupposes the absence of disturbances ahead of the plate, which seems to contradict the preceding views on the properties of incompressible flows. However, for the *degenerate* system 12.4.1 (with respect to the original Navier-Stokes equations) conditions 12.4.2 at $x < 0$ are acceptable.

Although the scale length L is absent from the problem, it is not self-similar, since the combination $\mu/\rho U_\infty$ has the dimension of the length, which makes it possible to form dimensionless variables $\text{Re}_x = (\rho U_\infty x)/\mu$ and Re_y , together with the dimensionless functions u/U_∞ and v/U_∞ . In this case, both the system of equations 12.4.1 and the boundary conditions 12.4.2 are not altered.

However, these dimensionless variables are not distinctive of the problem under consideration. In fact, it would be more appropriate to scale the variable y on the boundary

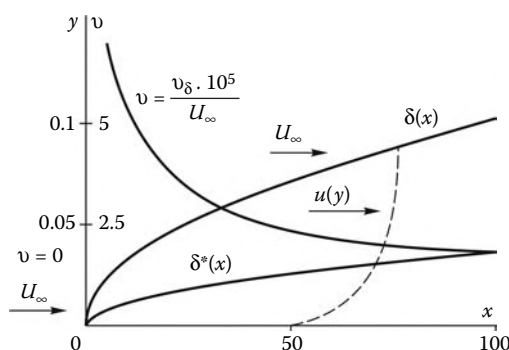


FIGURE 12.7
Parameters of an incompressible flat-plate boundary layer.

layer thickness δ and the velocity v on the quantity $U_\infty \delta / x$. For this reason, we will seek the solution of our problem in the form:

$$\begin{aligned} u &= U_\infty f'(\zeta), & \zeta &= y \sqrt{\frac{U_\infty \rho}{\mu x}} \\ v &= -\frac{\partial}{\partial x} \int_0^y u dy = \frac{1}{2} U_\infty \sqrt{\frac{\mu}{\rho U_\infty x}} (\zeta f' - f) \\ \psi &= \int_0^y \rho u dy = f \sqrt{\rho \mu U_\infty x} \end{aligned} \quad (12.4.3)$$

The previous solution is presented in the form of a group of type 6.1.1 in which the exponents m , n , and k corresponding to Equation 12.4.1 and the boundary conditions 12.4.2 are chosen beforehand. In particular, the formula for v is derived using the continuity equation, while the function f is proportional to the stream function ψ .

Substituting 12.4.3 in the first equation of Equation 12.4.1 we obtain the *Blasius equation* for the *Blasius function* f with the boundary condition 12.4.2 for the latter*

$$\begin{aligned} 2f''' + ff'' &= 0 \\ \zeta = 0 : \quad f = f' &= 0, \quad \zeta \rightarrow \infty : \quad f' \rightarrow 1 \end{aligned} \quad (12.4.4)$$

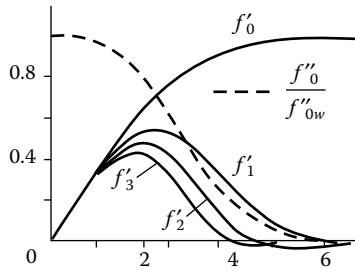
In addition to the reasoning made at the end of Section 12.3, we will explain the condition posed for $\zeta \rightarrow \infty$ in more detail. Equation 12.4.4 has a solution with the condition $f' = 1$ on any boundary $\zeta = \zeta_\delta < \infty$ with a piecewise-smooth continuation $f' = 1$ into the $\zeta > \zeta_\delta$ domain. However, in this case the point ζ_δ is a corner point for the velocity profile $u(y)$ if the solution of this problem is considered throughout the entire quadrant $x > 0, y > 0$, so that the second derivative of u with respect to y is infinite on the line $\zeta = \zeta_\delta$. At the same time, as $\zeta_\delta \rightarrow \infty$, the first and second derivatives with respect to y tend to zero, in accordance with the asymptotics given by Equation 12.2.12, in which it should be let $f'' \sim E = e^{-(\zeta-\zeta^*)^2/4}$, and so on. Therefore, the *internal boundary-layer solution* is fairly smoothly matched with the *external inviscid solution* already at finite ζ_δ , or at a fairly small distance from the wall $\delta \approx \zeta_\delta x \text{Re}_x^{-1/2}$. A conditional edge of the boundary layer can be determined by the quantity $\delta = \zeta_\delta (\mu x / \rho U_\infty)^{1/2}$, where ζ_δ ranges from 5 to 5.3; in this case, $f' = 0.99 \div 0.995$.

The functions f , f' , and f'' are presented in Figures 12.5 and 12.8†; the quantity ζ^* is as follows:

$$\zeta^* = \lim_{\zeta \rightarrow \infty} (\zeta - f) = \sqrt{\frac{\rho U_\infty}{\mu x}} \delta^* = \int_0^\infty (1 - f') d\zeta = 1.72 \quad (12.4.5)$$

* We note that in different handbooks Equation 12.4.4 is written in different forms. In particular, in variables $\zeta' = \zeta/2$ the coefficient 2 of the first term of this equation vanishes.

† Tables for these functions, as well as for Φ_v and other functions from Section 12.2, can be found in many handbooks on boundary layer theory and are not given here.

**FIGURE 12.8**

On the problem of the decay of stationary disturbances in a boundary layer.

Here, the *boundary layer displacement thickness* is introduced

$$\delta^* = \frac{1}{\rho U_\infty} \int_0^\delta \rho (U_\infty - u) dy = \int_0^\delta \left(1 - \frac{u}{U_\infty}\right) dy \quad (12.4.6)$$

The flow rate across this thickness is smaller than that in the external inviscid flow across the same thickness δ by the value $\rho U_\infty \delta^*$. Another interpretation of the quantity δ^* is the same as in Section 12.2. This is the shape of a thin body introducing into the external inviscid flow the same disturbances as the boundary layer, that is, in this approximation the boundary layer on the body of shape $y = -\delta^*(x)$ would not introduce any disturbances into the external flow. The normal velocity component $v = v_\delta$ on the outer edge of the boundary layer is expressed in terms of δ^* as follows

$$\frac{v_\delta}{U_\infty} = \frac{1}{2} \zeta^* \text{Re}_x^{-1/2} = \frac{d\delta^*}{dx} \quad (12.4.7)$$

The functions $\delta^*(x)$ and $v_\delta(x)$ are plotted in Figure 12.7.

Finally, we will write the formula for the friction τ_w at the plate surface

$$\begin{aligned} \tau_w &= \mu \left. \frac{\partial u}{\partial y} \right|_{y=0} = \frac{1}{2} \rho U_\infty^2 C_f, \quad C_f = 2f''_w \text{Re}_x^{-1/2} \\ f''_w &= f''(0) = 0.332 \end{aligned} \quad (12.4.8)$$

Here, C_f is the *friction coefficient*. The function τ_w is associated with the *momentum thickness* δ^{**} , which can be obtained, by analogy with Section 1.7, by multiplying the second equation of Equation 12.4.1 by U_∞ , subtracting the product from the first equation, and integrating the result with respect to y within the limits from 0 to δ and with respect to x within the limits from 0 to x . Thus, we obtain

$$\begin{aligned} \delta^{**} &= \frac{1}{\rho U_\infty^2} \int_0^\delta \rho u (U_\infty - u) dy = \sqrt{\frac{\mu x}{\rho U_\infty}} \zeta^{**} = \int_0^x \frac{\tau_w}{\rho U_\infty^2} dx \\ \zeta^{**} &= \int_0^\infty f' (1 - f') d\xi = 2f''_w = 0.664 \end{aligned} \quad (12.4.9)$$

Here, the first relation represents the longitudinal momentum conservation law, while the relation between ζ^{**} and f_w'' is easily derived by evaluating the integral by parts and using the original Equation 12.4.4.

The meaning of the quantity δ^{**} is that the flux of the longitudinal momentum through the boundary layer is smaller than that in the layer of thickness δ in the inviscid flow region by the value $\rho U_\infty^2 \delta^{**}$.

We note some properties of the solution obtained. The point $x = 0$ is singular, since, as $x \rightarrow 0$, the friction τ_w and the velocity component v_δ increase without bound, as $x^{-1/2}$. Outside the boundary layer, this component is, first, constant in the sections $x = \text{const}$, including the case $y \rightarrow \infty$, and, second, discontinuous at the $x = 0$ line, namely, it is unbounded to the right and zero to the left of the line, in view of the conditions 12.4.2, as shown in Figure 12.7. Thus, the boundary layer solution obtained is realistic and, hence, valid only within the boundary layer limits, with exception of a small-size region near the sharp edge of the plate, with the local Reynolds number $\text{Re}_x \sim 1$ and not so small relative boundary layer thickness $\delta/x \sim \text{Re}_x^{-1/2}$.

In this region, for a plate of precisely zero thickness with an absolutely sharp edge, the flow is described by the complete system of Navier–Stokes equations with a singular local solution in the vicinity of the sharp edge characterized by unbounded pressure growth as the edge is approached: $p \sim r^{-1/2}$, where r is the distance to the edge (Shmyglevskii, 1995, 1999). This seemingly unexpected result contradicting the views developed in inviscid fluid dynamics, is attributable to the fact that the deceleration of a viscous flow as the sharp edge is approached along the x axis (see the problem of a wedge of Section 2.11) is hindered by the entrainment of neighboring streamlines due to viscosity, which leads to unbounded growth of the stagnation pressure.

However, the difference of the Navier–Stokes solution from the boundary-layer one occurs only in the domain of small Reynolds numbers $\text{Re} \sim 1$. Therefore, the main error is introduced in the boundary layer solution by the plate nose having actually a certain bluntness; in this case, in the initial section $x = 0$ of the flat plate the boundary layer thickness δ_0 is finite. If in this section the velocity profile is taken to be that of Blasius, corresponding to an x_0 -long plate, then for $x/x_0 \rightarrow \infty$ the true solution, for example, that for friction, tends to the solution for the sharp plate with the origin at the point $x = 0$ as $(1 + x_0/x)^{1/2}$.

In this connection, we will consider a linearized problem of the velocity profile development in a boundary layer slightly different from that of Blasius in the initial section $x = x_0$. For this purpose we let

$$u = u_0 + u' = U_\infty [f'_0(\zeta) + \sum_n \varepsilon_n \bar{x}^{-n} f'_n(\zeta)] \\ |u'| \ll u_0, \quad \varepsilon_n \bar{x}^{-n} \ll 1, \quad \bar{x} = x/x_0 \geq 1 \quad (12.4.10)$$

where $f_0(\zeta)$ is the Blasius function 12.4.4, while the dimension of ε_n is $[\varepsilon_n] = L^{-n}$. In this formulation, system 12.4.1 for the coefficients of series 12.4.10, that is, the functions $f_n(\zeta)$, is reduced, correct to the terms of the order ε_n^2 , to the equation

$$2f'''_n + f_0 f''_n + f'_0 f_n = -2n(f'_0 f'_n - f''_0 f_n) \quad (12.4.11)$$

The functions f_n must also satisfy the conditions

$$\zeta = 0 : \quad f_n = f'_n = 0, \quad \zeta \rightarrow \infty : \quad f'_n \rightarrow 0 \quad (12.4.12)$$

By analogy with the preceding Equations 12.2.11 and 12.4.4, for $\zeta \rightarrow \infty$ the decreasing solution of Equation 12.4.11 has the asymptotics $f'_n \sim (\zeta - \zeta^*)^{-1} e^{-(\zeta - \zeta^*)^2/4}$ similar to 12.2.12. The functions f_n tend to finite values, $f_n \rightarrow \zeta_n^*$; because of this, in order to obtain the displacement thickness δ^* of this velocity profile, the quantity ζ^* on the left-hand side of formula 12.4.5 must be replaced by $\zeta^* + \varepsilon_n \bar{x}^{-n} n \zeta_n^*$.

Equation 12.4.11 is homogeneous, together with its boundary conditions; therefore, in accordance with the general theory of equations of this type, its nontrivial, nonzero solution can exist only at certain discrete eigenvalues n . After these eigenvalues and the corresponding eigenfunctions f_n have been determined, in a certain initial section $x = x_0$ we can expand the difference $u' = u - u_0$ in series 12.4.10 thus tracking the evolution of an initial disturbance u' with x .

The first eigenvalue n_1 and the first eigenfunction $f_n(\zeta)$ are determined by comparing two Blasius velocity profiles u_0 and u_1 corresponding to plates of lengths x and $x + x_1$, where $x \gg x_1$. Expanding the difference $u = u_1 - u_0$ into a series, we obtain

$$u'_1 = -\frac{1}{2\bar{x}} \zeta f''_0, \quad f'_1 = \zeta f''_0, \quad f_1 = \zeta f'_0 - f_0 \quad (12.4.13)$$

It is easy to verify that the function $f_1(\zeta)$ satisfies Equation 12.4.11. By solving numerically this equation, the following eigenvalues are obtained: $n_1 = 1$, $n_2 = 1.88$, and $n_3 = 2.81$, that is, the minimum value $n_1 = 1$ really satisfies expansion 12.4.13. Due to nonlinearity of the original system 12.4.1, the coefficients of the other discarded terms of series 12.4.13 do not satisfy Equation 12.4.11. The first three functions $f'_n(\zeta)$ with $f''_n(0) = f'_0(0)$ are presented in Figure 12.8.

The choice of the initial reference Blasius profile $u_0(y)$ and the coordinate x_0 corresponding to it is not, generally, uniquely defined. To do this, we will require that the profile have the same momentum thickness δ^{**} as the overall velocity profile $u(y) = u_0 + u'$ at $x = x_0$. Then we have

$$\begin{aligned} I &= \int_0^\infty u(U_\infty - u') dy = \int_0^\infty u_0(U_\infty - u_0) dy + I' \\ I' &= \int_0^\infty u'(U_\infty - 2u_0) dy \end{aligned} \quad (12.4.14)$$

Condition $I' = 0$ determines the initial profile $u_0(y)$ at $x = x_0$.

12.5 Parabolization of the Compressible Navier–Stokes and Boundary Layer Equations

In Section 12.3 we performed the parabolization of the Navier–Stokes equations and obtained the boundary layer equations for an incompressible flow over a flat plate. Below we will generalize these results to the plane ($\nu = 0$) and axisymmetric ($\nu = 1$) compressible flows in a thin layer adjacent to the surface of a two-dimensional or axisymmetric body of arbitrary shape subject to the basic condition that the ratio of the layer thickness δ to the scale length L of the surface is small: $\delta/L \ll 1$. The results to be obtained will pertain not only to limitingly thin boundary layers but also to the more general case of thin viscous

shock layers (similar to those considered in Chapters 7 to 9 for inviscid flows), in which the viscous region thickness is comparable to the overall thickness of the viscous layer.

We will use a curvilinear coordinate system x, y fitted to the surface in a flow, as shown in Figure 1.24c of Section 1.13 and in Figure 12.9; the velocity components along the axes are u and v . The subscripts δ and w refer to the flow parameters on the outer edge of the boundary layer and on the body surface, respectively. We assume that the radius of curvature of the longitudinal section of the body is of the order $R \sim L$ or $R \gg L$. However, in order to maintain the original form of the equations governing inviscid flows, we will neglect the terms of the order $\delta/L \ll 1$ only in the viscous operator of the Navier–Stokes equations. Taking this result into account and generalizing the procedure outlined in Section 12.3, we obtain the estimates for the flow parameters in the narrow layer and individual terms in the compressible Navier–Stokes equations. Since in this layer the longitudinal velocity is obviously of the order $u \sim u_\delta$, from the continuity Equation 1.13.21 there follows the estimate for the transverse velocity $v \sim u_\delta \delta/L \ll U_\delta$, the same as in Section 12.3, so that we have $u \approx U$, where U is the total gas velocity.

Since, as distinct from Section 7.7, the inviscid operators 1.3.18 through 1.3.21 of the Navier–Stokes equations remain unaltered, we will consider the viscous operators of these equations; using 1.14.1 we will write the divergence of the viscous stress tensor entering into the momentum Equation 1.9.2

$$H_x r^v \operatorname{Div} P_\tau = \frac{\partial r^v \tau_x}{\partial x} + \frac{\partial H_x r^v \tau_y}{\partial y}, \quad H_x = 1 + \frac{y}{R} \quad (12.5.1)$$

where r is the distance from a given point to the axis of symmetry. If \vec{i} and \vec{j} are the unit vectors of the x, y coordinate system, then from matrix 1.10.1 there follows

$$\tau_x = \vec{i} \tau_{xx} + \vec{j} \tau_{xy}, \quad \tau_y = \vec{i} \tau_{xy} + \vec{j} \tau_{yy} \quad (12.5.2)$$

where τ_{xy} is the vector τ_x projection onto the y axis, and so on.

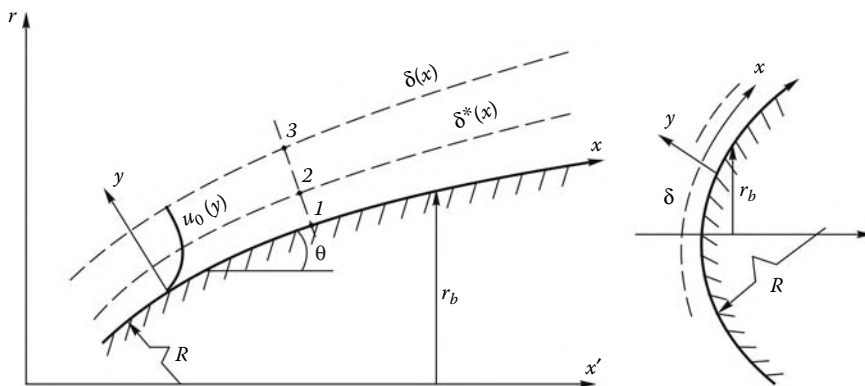


FIGURE 12.9
Boundary layer on a body of revolution.

Substituting these expressions in Equation 12.5.1 and taking 1.13.20 into account we obtain

$$\begin{aligned} H_x r^v \operatorname{Div} P_\tau &= \vec{F}_i + \vec{F}_j \\ F_i &= \frac{\partial r^v \tau_{xx}}{\partial x} + \frac{\partial H_x r^v \tau_{xy}}{\partial y} + \frac{r^v \tau_{xy}}{R} \\ F_j &= \frac{\partial r^v \tau_{xy}}{\partial x} + \frac{\partial H_x r^v \tau_{yy}}{\partial y} - \frac{r^v \tau_{xx}}{R} \end{aligned} \quad (12.5.3)$$

In order to obtain the resulting expression for $\operatorname{Div} P_\tau$, relations 1.10.10 and 1.14.8 should be used. However, owing to the fact that these expressions are rather cumbersome, we will write down only their leading terms, which are determined with account for the orders of the velocities, $u \sim U_\delta$ and $v \sim U_\delta \delta / L$, and the derivatives, $\partial/\partial x \sim 1/L$ and $\partial/\partial y \sim 1/\delta$

$$\begin{aligned} F_i &= \frac{\partial}{\partial y} \left(r^v \mu \frac{\partial u}{\partial y} \right) \sim \frac{r^v \mu U_\delta}{\delta^2} \\ F_j &= \frac{\partial}{\partial x} \left(r^v \mu \frac{\partial u}{\partial y} \right) + 2 \frac{\partial}{\partial y} \left(r^v \mu \frac{\partial v}{\partial y} \right) \sim \frac{r^v \mu U_\delta}{\delta L} \end{aligned} \quad (12.5.4)$$

With these simplifications, the longitudinal momentum and continuity equations of the Navier–Stokes system take the form:

$$\begin{aligned} \frac{\rho u}{H_x} \frac{\partial u}{\partial x} + \rho v \frac{\partial u}{\partial y} + \frac{uv}{H_x R} &= -\frac{1}{H_x} \frac{\partial p}{\partial x} + \frac{1}{r^v} \frac{\partial r^v \tau}{\partial y} \\ \frac{\partial \rho u r^v}{\partial x} + \frac{\partial H_x \rho v r^v}{\partial y} &= 0, \quad \tau = \tau_{xy} = \mu \frac{\partial u}{\partial y} \end{aligned} \quad (12.5.5)$$

As for the transverse momentum equation, it is written separately

$$\frac{\rho u}{H_x} \frac{\partial v}{\partial x} + \rho v \frac{\partial v}{\partial y} - \frac{\rho u^2}{R + y} = -\frac{\partial p}{\partial y} + \frac{1}{r^v} F_j \quad (12.5.6)$$

The energy Equation 1.9.6 is simplified in a similar fashion; for a while, we will consider only the equilibrium approximation reserving the application to chemically reacting and mutually diffusing gas mixtures for Chapter 13. In this case, the main terms on the right-hand side of Equation 1.9.6 are the energy flux along the y axis (in the term $\operatorname{Div} \vec{J}$) and, in accordance with Equations 12.1.11 and 1.14.8, the term $q_\tau = \mu(\partial u / \partial y)^2$ in the dissipative heat flux. Finally, this equation takes the form:

$$\begin{aligned} \frac{1}{H_x} \rho u \frac{\partial h}{\partial x} + \rho v \frac{\partial h}{\partial y} &= \frac{u}{H_x} \frac{\partial p}{\partial x} + v \frac{\partial p}{\partial y} - \frac{1}{r^v} \frac{\partial r^v J}{\partial y} + \mu \left(\frac{\partial u}{\partial y} \right)^2 \\ -J &= \lambda_{\text{eff}} \frac{\partial T}{\partial y} = \frac{\lambda_{\text{eff}}}{c_p} \frac{\partial h}{\partial y} = \frac{\mu}{\Pr} \frac{\partial h}{\partial y}, \quad \Pr = \frac{\mu c_p}{\lambda_{\text{eff}}} \end{aligned} \quad (12.5.7)$$

The energy equation can conveniently be written for the total enthalpy $H = h + U^2/2$. For this purpose, the first equation of Equation 12.5.5 should be multiplied by u and Equation 12.5.6 by v (at $F_j = 0$) and added to Equation 12.5.7

$$\frac{\rho u}{H_x} \frac{\partial H}{\partial x} + \rho v \frac{\partial H}{\partial y} = \frac{1}{r^v} \frac{\partial}{\partial y} [r^v (\tau u - J)] = \frac{1}{r^v} \frac{\partial}{\partial y} \left(\frac{r^v \mu}{\text{Pr}} \frac{\partial H}{\partial y} \right) - \frac{1}{r^v} \frac{\partial}{\partial y} \left[\left(\frac{1}{\text{Pr}} - 1 \right) r^v \mu \frac{\partial}{\partial y} \left(\frac{u^2}{2} \right) \right] \quad (12.5.8)$$

The convenience of this equation is that it does not incorporate the derivative $\partial p / \partial x$.

We will expand the system of equations obtained adding the equilibrium equations of state $\rho = \rho(p, T)$ and $h = h(p, T)$ and the relations for the coefficients $\mu = \mu(p, T)$ and $\lambda_{\text{eff}} = \lambda_{\text{eff}}(p, T)$ with the reservation as for the *element separation effect*, which will be considered in Section 13.2.

Strictly speaking, the system of Equations 12.5.5 through 12.5.7 cannot be assigned to the parabolic type, since Equation 12.5.6 incorporates the partial derivative u_{xy} in the term F_j on its right-hand side, which, in view of the continuity equation combined with the second term of F_j , vanishes from Equation 12.3.2 for plane incompressible flows. Therefore, rigorous parabolization of the system obtained is related with a possibility of neglecting the term F_j in Equation 12.5.6, which will be done if need be.

We will consider in more detail the limitingly thin boundary layer in the classical formulation of the problem. Let ρ_* and μ_* be the scale density and viscosity in the boundary layer corresponding to the *characteristic boundary layer temperature* T_* . Then from the condition that the viscous term in the first equation in Equation 12.5.5 and, for example, the first term on the left-hand side of this equation are of the same order, we obtain the following estimate for the boundary layer thickness

$$\delta \sim L(\text{Re}_L^*)^{-1/2}, \quad \text{Re}_L^* = \frac{\rho_* U_\delta L}{\mu_*} \quad (12.5.9)$$

Thus, the adopted model of a thin boundary layer is realized at Reynolds numbers characteristic for the internal boundary layer flow $\text{Re}_L^* \gg 1$. We note that the characteristic temperature T_* may be considerably different from the external temperature T_δ ; for this reason, the Reynolds number Re_L^* can appreciably differ from the Reynolds number $\text{Re}_L^{(\delta)} = \rho_\delta U_\delta L / \mu_\delta$ based on the external parameters of the boundary layer. To evaluate the temperature T_* or the enthalpy $h_* = h(T_*)$, we will estimate the contribution of viscous energy dissipation to the latter. For this purpose, we will equate the orders of the first term on the left and the last term on the right of Equation 12.5.7; in view of 12.5.9, this gives the following estimate

$$\Delta h_* = h_* - h_\delta \sim \frac{\mu_* U_\infty L}{\rho_* \delta^2} \sim U_\delta^2, \quad h_* \sim h_\delta + U_\delta^2 \sim H_\delta \quad (12.5.10)$$

Therefore, the characteristic enthalpy h_* in the boundary layer is of the same order as the external stagnation enthalpy H_δ , except for exotic cases in which $h_w \gg H_\delta$, where h_w is the gas enthalpy on the wall; in what follows these cases are ignored.

A similar result can be obtained from Equation 12.5.8; by analogy with 12.5.10, for $\text{Pr} \sim 1$ there follows the estimate

$$\Delta H_* = H_* - H_\delta \sim \frac{\mu_*}{\rho_*} \frac{H_\delta L}{\delta^2 U_\delta} \sim H_\delta \quad (12.5.11)$$

Therefore, in the boundary layer the stagnation enthalpy is equal to $H = h + u^2/2$ (for $v^2 \ll h_*$) and everywhere of the order of the external flow stagnation enthalpy H_δ . We note

that for $\text{Pr} = 1$ the contribution of energy dissipation to the total gas enthalpy is absent, since in this case the last term vanishes from Equation 12.5.8.

We will further generalize estimates of Equation 12.3.3 for the pressure difference Δp across the viscous layer. Evaluating the first and last terms on the left-hand side of Equation 12.5.6 and, with allowance for 12.5.9 on the right-hand side, we obtain the following contributions of these terms to the relative pressure difference

$$\frac{\Delta p}{\rho^* U_\delta^2} \sim \frac{\delta^2}{L^2} + \frac{\delta}{R}, \quad \frac{\Delta p}{p} \sim M_*^2 \rho_* U_\delta^2 \left(\frac{\delta^2}{L^2} + \frac{\delta}{R} \right) \\ M_*^2 \sim \frac{\rho_* U_\delta^2}{p} \quad (12.5.12)$$

Here, M_* is the characteristic Mach number inside the boundary layer which, in view of estimates 12.5.10, is limited even if on the outer edge the Mach number is $M_\delta \gg 1$. Thus, for $\delta \ll L$ the pressure difference across the boundary layer is small, so that Equation 12.5.6 can be omitted at all and replaced by the given pressure distribution $p = p(x)$ over the body surface in the inviscid flow. Clearly, for $R \sim L$ the main term of the estimates 12.5.12 is the term δ/R associated with the longitudinal curvature of the body surface; this means that the accuracy of the boundary layer equations on a curved surface is an order (by a factor of δ/R) lower than on a rectilinear surface.

At the same time, system 12.5.5 through 12.5.7 with dropped viscous terms governs the flow outside the boundary layer, that is, in the inviscid shock layer, whose thickness is determined by other estimates obtained earlier in Chapters 7 to 9 for both sharp and blunt bodies. Therefore, discarding the term F_j in Equation 12.5.6 we obtain a *composite* system of the parabolized Navier-Stokes equations or the *viscous shock layer equations*, which adequately describes the entire flow between the body surface and the shock, since outside the boundary layer the viscous terms in Equations 12.5.5 and 12.5.7 are small and, hence, have only a slight effect on the flow, while in the boundary layer zone the truncated Equation 12.5.6 may be dropped. However, we note in anticipation that the parabolized nature of the composite (with $F_j = 0$) system 12.5.5 through 12.5.7 does not generally ensure its evolutionary nature, that is, the same notes and reservations, as for systems 12.3.2 or 12.3.4, are valid for this system (in Section 12.14 this question will be discussed in more detail).

We will now return to the boundary layer. Since system 12.5.5 and 12.5.7 governing the boundary layer flow is parabolic, the corresponding initial (in a certain section $x = x_0$) and boundary conditions, more general than 12.3.6, should be formulated for it. These are as follows

$$y = 0 : \quad u = 0, \quad v = 0, \quad h = h_w \\ y_\delta(x) : \quad u = U_\delta(x), \quad h = h_\delta(x) \\ x = x_0 : \quad u = u_0(y), \quad h = h_0(y) \quad (12.5.13)$$

The remarks advanced in Section 12.3 are valid for these conditions as well, namely, the initial function $v_0(y)$ cannot be preassigned arbitrarily, while the boundary layer thickness δ is determined from the condition of smooth matching between the velocity and enthalpy profiles in the boundary layer and the external flow; due to the fact that the solution tends to its external boundary conditions imposed at $y = \delta(x)$ in accordance with a power law, these conditions can be replaced by asymptotic conditions valid as $y \rightarrow \infty$.

As applied to a thin boundary layer, we will assume one further constraint, which is concerned with axisymmetric flows, namely, we will assume the smallness of the boundary

layer thickness δ as compared with the radius r_b of the body cross-section. On this basis, we let $r = r_b(x)$ in Equations 12.5.5 through 12.5.8, so that the system takes the form:

$$\begin{aligned} \rho u \frac{\partial u}{\partial x} + \rho v \frac{\partial u}{\partial y} &= -\frac{\partial p}{\partial x} + \frac{\partial}{\partial y} \left(\mu \frac{\partial u}{\partial y} \right) \\ \frac{\partial \rho u r_b^v}{\partial x} + \frac{\partial \rho v r_b^v}{\partial y} &= 0 \\ \rho u \frac{\partial H}{\partial x} + \rho v \frac{\partial H}{\partial y} &= \frac{\partial}{\partial y} \left(\frac{\mu}{\text{Pr}} \frac{\partial H}{\partial y} \right) + \frac{\partial}{\partial y} \left(\mu \frac{\text{Pr} - 1}{2\text{Pr}} \frac{\partial u^2}{\partial y} \right) \end{aligned} \quad (12.5.14)$$

In this system $r_b(x)$ is retained only in the continuity equation. Precisely this formulation of the thin boundary layer problem will be called *classical*, this term being generalized somewhat as compared with Section 12.3.

We will dwell on one more important element of the thin boundary layer theory. This theory is based upon the smallness of the back boundary layer effect on the external flow, which was attributed in Section 12.4 to the smallness of the boundary layer displacement thickness δ^* determined by formula 12.4.6 (the first equation at $\rho \neq \text{const}$). Below we will discuss this question from a more general standpoint.

For this purpose, we will pose the question: which effective body contour in an inviscid flow would provide the proper pressure and velocity distributions on the outer edge of the boundary layer with allowance for its influence on the external flow (or, conversely, how should the body contour be changed in order to eliminate this influence)? Obviously, for this to happen, the gas flow rate across the outer edge of the boundary layer in the actual viscous flow (across section 1-3 in Figure 12.9) and in the equivalent inviscid flow (across section 2-3) must coincide. Precisely this condition determines the displacement thickness

$$\begin{aligned} (2\pi r_b)^v \int_0^\delta \rho u dy &= (2\pi r_b)^v \rho_\delta U_\delta (\delta - \delta^*) \\ \delta^* &= \int_0^\delta \left(1 - \frac{\rho u}{\rho_\delta U_\delta} \right) dy \end{aligned} \quad (12.5.15)$$

At a distance $\delta - \delta^*$ between points 2 and 3 the longitudinal velocity and the gas density in the equivalent inviscid flow vary only by small values of the order δ/L , so that they may be assumed to be constant within the boundary layer. We will now demonstrate that in the inviscid flow past the equivalent body, that is, displaced relative to the original body by the value δ^* , the normal velocity v_δ on the line $y = \delta(x)$ is the same as on the same line considered as the outer edge of the boundary layer on the original body. For this purpose, we will integrate the continuity equation taking 12.5.15 into account; as a result, we obtain

$$\begin{aligned} (\rho v r_b^v)_\delta &= - \int_0^\delta \frac{\partial}{\partial x} (\rho u r_b^v) dy = (\rho u r_b^v)_\delta \frac{d\delta}{dx} - \frac{d}{dx} [(\rho u r_b^v)_\delta (\delta - \delta^*)] \\ &= (\rho u r_b^v)_\delta \frac{d\delta^*}{dx} - (\delta - \delta^*) \frac{d}{dx} (\rho u r_b^v)_\delta \end{aligned} \quad (12.5.16)$$

However, by virtue of the continuity equation, the last term represents the difference $\Delta \rho v r^v = \rho_\delta r_b^v (v_\delta - v^*)$ between the $\delta(x)$ and $\delta^*(x)$ lines in the inviscid flow. Therefore, in

a coordinate system fitted to the original body surface, imposing on the equivalent body boundary the inviscid impermeability condition

$$\frac{v^*}{U_\delta} = \frac{d\delta^*}{dx} \quad (12.5.17)$$

we obtain the same v_δ in the original and equivalent flows, which proves the statement.

In conclusion, we will note that the applicability of the boundary layer equations obtained is not restricted to wall flows only. There exist, at least, two types of flow governed by these equations. First, this is the shear layer flow that is a result of dissipative smoothing of contact discontinuities, which can arise, for example, in the jet outflow into a cocurrent stream. Second, this is the flow in the far region of such a jet or in a wake downstream of a body.

12.6 Boundary Layer in a Compressible Gas

Here we will consider the main properties and problems of the laminar boundary layer in a compressible equilibrium (in the meaning of Section 12.5) gas flow. This can conveniently be done by passing to the *Dorodnitsyn variables* that were already used in Section 7.9

$$x, y \rightarrow x, \bar{\eta} = \int_0^y \rho dy \quad (12.6.1)$$

In these variables Equation 12.5.14 is reduced to the form:

$$\begin{aligned} u \frac{\partial u}{\partial x} + V \frac{\partial u}{\partial \bar{\eta}} &= -\frac{1}{\rho} \frac{\partial p}{\partial x} + \frac{\partial}{\partial \bar{\eta}} \left(\rho \mu \frac{\partial u}{\partial \bar{\eta}} \right) \\ \frac{\partial u r_b^v}{\partial x} + \frac{\partial V r_b^v}{\partial \bar{\eta}} &= 0, \quad V = \rho v + u \left(\frac{\partial \bar{\eta}}{\partial x} \right)_y \\ u \frac{\partial H}{\partial x} + V \frac{\partial H}{\partial \bar{\eta}} &= \frac{\partial}{\partial \bar{\eta}} \left(\frac{\rho \mu}{\text{Pr}} \frac{\partial H}{\partial \bar{\eta}} \right) + \frac{\partial H}{\partial \bar{\eta}} \left(\frac{\text{Pr} - 1}{2\text{Pr}} \rho \mu \frac{\partial u^2}{\partial \bar{\eta}} \right) \\ H &= h + \frac{1}{2} u^2 \end{aligned} \quad (12.6.2)$$

Clearly, here the role of the velocity v is played by the function V having the dimension of the mass flux density. In deriving these equations, the following auxiliary formulas were used

$$\begin{aligned} \left(\frac{\partial \rho u r_b}{\partial x} \right)_y &= \rho \left(\frac{\partial u r_b}{\partial x} \right)_{\bar{\eta}} + \rho \left(\frac{\partial u r_b}{\partial \bar{\eta}} \right)_x \left(\frac{\partial \bar{\eta}}{\partial x} \right)_y + u r_b \left(\frac{\partial \rho}{\partial x} \right)_y \\ \left(\frac{\partial \rho}{\partial x} \right)_y &= \frac{\partial^2 \bar{\eta}}{\partial x \partial y} = \rho \frac{\partial}{\partial \bar{\eta}} \left(\frac{\partial \bar{\eta}}{\partial x} \right)_y \end{aligned} \quad (12.6.3)$$

Compared with the original system, this system is more like that of an incompressible flow, since here the density is absent from the continuity equation and, moreover, as shown in Section 1.3, the dependence of the product $\rho \mu$ on the temperature is appreciably weaker ($\sim h^{-0.3}$) than those of ρ and μ taken separately. A considerable temperature dependence

is conserved only in the first equation of Equation 12.6.2, namely, in the term $\rho^{-1}dp/dx$ vanishing at constant pressure.

Then Equation 12.6.2 is conveniently written in variables in which the edge of the boundary layer varies only slightly

$$\begin{aligned}\xi(x) &= \frac{1}{\rho_* \mu_* U_\delta r^{2\nu}} \int_0^x \rho_* \mu_* U_\delta r^{2\nu} dx \\ \zeta(x, \bar{\eta}) &= \sqrt{\frac{U_\delta}{\rho_* \mu_* \xi}} \bar{\eta} = \sqrt{\frac{\rho_* U_\delta}{\mu_* \xi}} \eta, \quad \eta = \frac{\bar{\eta}}{\rho_*} = \int_0^y \frac{\rho}{\rho_*} dy\end{aligned}\quad (12.6.4)$$

Here, ρ_* and μ_* are some quantities governed by the local pressure p and a certain *determining enthalpy* h_* ; they are of the same order as the characteristic quantities in the boundary layer with the same name used in Section 12.5 for the estimates. The variables ξ and η have the same dimensions as x and y , while ζ is dimensionless and, in view of 12.5.9, is of the order of unity. The transformation inverse with respect to 12.6.4 is given by the formula

$$\begin{aligned}y &= \sqrt{\frac{\mu_* \xi}{\rho_* U_\delta}} \bar{\zeta} = \sqrt{\frac{\mu_* \xi}{\rho_* U_\delta}} \frac{\rho_*}{\rho_\delta} \tilde{\zeta} \\ \bar{\zeta} &= \int_0^\zeta \frac{\rho_*}{\rho} d\xi, \quad \tilde{\zeta} = \int_0^\zeta \frac{\rho_\delta}{\rho} d\xi, \quad \rho = \rho(\xi, \zeta)\end{aligned}\quad (12.6.5)$$

The formula with the integral $\tilde{\zeta}$ is often useful at comparatively low Mach numbers.

Simultaneously, by analogy with the Blasius problem of Section 12.4, we introduce new dimensionless functions

$$f'(\xi, \zeta) = \frac{\partial f}{\partial \zeta} = \frac{u}{U_\delta}, \quad \bar{H} = \frac{H}{H_\delta} \quad (12.6.6)$$

Here, primes refer to the differentiation with respect to ζ , while the subscripts ξ and x refer to the differentiation with respect to these variables. The functions f and \bar{H} must satisfy conditions 12.5.13

$$\begin{aligned}\zeta = 0 : \quad f &= f' = 0, \quad \bar{H} = \bar{H}_w = \bar{h}_w \\ \zeta \rightarrow \infty : \quad f' &\rightarrow 1, \quad \bar{H} \rightarrow 1 \\ \xi = \xi_0 : \quad f &= f_0(\zeta), \quad \bar{H}_0 = \bar{H}(\zeta)\end{aligned}\quad (12.6.7)$$

The ratio \bar{H}_w (or \bar{h}_w) is the *wall enthalpy factor*, while the ratio T/T_w is the *temperature factor* ($T_{0\delta}$ is the stagnation temperature of the external flow).

The stream function ψ is expressed in terms of the new variables by the formula

$$\psi = (2\pi)^v r_b^v \int_0^y \rho u dy = (2\pi)^v r_b^v f \sqrt{\rho_* \mu_* U_\delta} \quad (12.6.8)$$

Finally, we will express the wall friction τ_w and the heat flux to the wall q_w in terms of the new variables

$$\begin{aligned}\tau_w = \tau(0) &= \mu_w \frac{\partial u}{\partial y} \Big|_{y=0} = \omega_w \rho_* U_\delta^2 \sqrt{\frac{\mu_*}{\rho_* U_\delta \xi}}, \quad \omega_w = \frac{\rho_w \mu_w}{\rho_* \mu_*} \\ q_w = -J_w &= \lambda_{\text{eff},w} \frac{\partial T}{\partial y} \Big|_{y=0} = \frac{\omega_w \rho_* U_\delta H_\delta \bar{H}'_w}{\Pr_w} \sqrt{\frac{\mu_*}{\rho_* U_\delta \xi}}\end{aligned}\quad (12.6.9)$$

We note that on transition to the variables ξ and ζ and the functions ρ_* and μ_* formulas 12.6.4 through 12.6.9 took the form similar to that for the case of a flat plate in an incompressible flow. In this sense, the variable ξ plays the role of an *effective length* of the body surface, equal to the length L of an equivalent plate, which, as it were, is in a boundary layer with the same flow parameters (a more clear meaning will be assigned to this notion in Section 12.8).

When transforming Equation 12.6.2 to the new variables $\xi(x)$ and $\zeta(\xi, \bar{\eta})$ we take into account the following relations

$$\begin{aligned}\left(\frac{\partial}{\partial x}\right)_{\bar{\eta}} &= \xi_x \left(\frac{\partial}{\partial \xi}\right)_{\bar{\eta}} = \xi_x \left[\left(\frac{\partial}{\partial \xi}\right)_\zeta + \left(\frac{\partial \zeta}{\partial \xi}\right)_{\bar{\eta}} \left(\frac{\partial}{\partial \zeta}\right)_\xi \right] \\ \left(\frac{\partial}{\partial \bar{\eta}}\right)_x &= \left(\frac{\partial \zeta}{\partial \bar{\eta}}\right)_\xi \left(\frac{\partial}{\partial \zeta}\right)_\xi, \quad \xi_x(1 + \varphi) = 1, \quad \varphi = \xi \frac{(r_b^{2v} \rho_* \mu_* U_\delta)_\xi}{(r_b^{2v} \rho_* \mu_* U_\delta)} \\ V &= -\frac{1}{2} \sqrt{\frac{\rho_* \mu_* U_\delta}{\xi}} \left[f + 2\xi_x \xi f' \left(\frac{\partial \zeta}{\partial \xi}\right)_{\bar{\eta}} + 2\xi_x \xi f_\xi \right]\end{aligned}\quad (12.6.10)$$

Here, the formula for V is derived by integrating the continuity equation of system 12.6.2 in terms of the previous formula for ξ_x . Then in the new variables Equation 12.6.2 takes the form:

$$\begin{aligned}2(\omega f'')' + ff'' + F_p &= F_f = 2\xi_x \xi (f' f'_\xi - f_\xi f'') \\ 2\left(\frac{\omega}{\Pr} \bar{H}'\right)' + f \bar{H}' + 2B \left[\omega \frac{\Pr - 1}{\Pr} ((f')^2)'\right]' &= F_H = 2\xi_x \xi (f' \bar{H}_\xi - f_\xi \bar{H}') \\ F_p &= \beta \left(\frac{\rho_\delta}{\rho} - (f')^2\right), \quad \beta = -\frac{2\xi_x \xi}{\rho_\delta U_\delta^2} \frac{dp}{d\xi} = 2 \frac{\xi_x \xi}{U_\delta} \frac{dU_\delta}{d\xi}\end{aligned}\quad (12.6.11)$$

In the expression for F_p the relation $dp = -\rho_\delta U_\delta dU_\delta$ on the boundary layer edge is used. For isobaric flows the parameter $\beta = 0$. The function ω and the constant B are given by the following formulas

$$\begin{aligned}\omega &= \frac{\mu \rho}{\mu_* \rho_*} = \left(\frac{h}{h_*}\right)^{-n} \\ B &= \frac{U_\delta^2}{2H_\delta} = \frac{U_\delta^2}{2h_\delta + U_\delta^2} = \frac{(\gamma - 1)M_\delta^2}{2 + (\gamma - 1)M_\delta^2}\end{aligned}\quad (12.6.12)$$

Here, M_δ is the Mach number on the boundary layer edge. The second equation for ω follows from formula 1.3.11, where $n = 0.3$.

In what follows we will consider some particular problems.

12.6.1 Boundary Layer on a Flat Plate (in Particular, on a Wedge or a Cone in a Supersonic Flow).

For constant p and U_δ and rectilinear conical surface with the equation $r_b = bx$ the variables 12.6.4 take the form:

$$\xi = \frac{x}{2\nu + 1}, \quad \zeta = \sqrt{\frac{(2\nu + 1)\rho_* U_\delta}{\mu_* x}} \eta \quad (12.6.13)$$

In this case it should be let $F_f = F_H = F_p = 0$ in Equation 12.6.11, which transforms these equations to ordinary differential ν -independent equations whose solutions are dependent on ζ only. Correspondingly, formulas 12.6.9 for τ_w and q_w are transformed as follows:

$$\begin{aligned} \tau_w &= \omega_w f''_w \rho_* U_\delta^2 \sqrt{\frac{(2\nu + 1)\mu_*}{\rho_* U_\delta x}} \\ q_w &= \frac{\omega_w}{\text{Pr}_w} \bar{H}'_w \rho_* U_\delta H_\delta \sqrt{\frac{(2\nu + 1)\mu_*}{\rho_* U_\delta x}} \end{aligned} \quad (12.6.14)$$

The heat flux and friction on the cone ($\nu = 1$) are by a factor of $\sqrt{3}$ greater, while, in accordance with 12.6.5, the boundary layer thickness is by a factor of $\sqrt{3}$ smaller than those in the case of a plate or a wedge of the same length x .

We will study the basic properties of the solutions of system 12.6.11 with reference to some particular examples. The simplest case is that in which $\text{Pr} = 1$; in this case two equations of the system become identical for an arbitrary ω , which implies a linear relation between \bar{H} and f' or the *Crocco integral* (see also Section 12.2), which will be written down in different forms with account for the boundary conditions

$$\begin{aligned} H &= h + \frac{1}{2} u^2 = (H_\delta - h_w) \frac{u}{U_\delta} + h_w \\ \bar{H} &= \bar{h} + B f'^2 = f' + \bar{h}_w (1 - f'), \quad B = \frac{U_\delta^2}{2H_\delta} \\ \bar{h} &= \frac{h}{H_\delta}, \quad \tilde{h} = \frac{h}{h_\delta} = f' + \frac{h_w}{h_\delta} (1 - f') + \frac{1}{2} \frac{U_\delta^2}{h_\delta} f' (1 - f') \end{aligned} \quad (12.6.15)$$

Since the Prandtl number is near-unity, this integral can be used for, at least, a qualitative analysis of the properties of nonisothermal boundary layers.

Another example of a simple solution is provided by the case in which $\omega = 1$ (or $n = 0$) in 12.6.12 and $\text{Pr} = \text{const}$. In this case the first equation of Equation 12.6.11 becomes the Blasius equation with the solution given in Section 12.4; then, with account for this solution, the second equation of Equation 12.6.11 can be reduced to an equation in \bar{h} with the corresponding solution

$$\begin{aligned}
& 2 \left(\frac{\omega}{\text{Pr}} \bar{h}' \right)' + f h' + 4B\omega f''^2 = 0 \\
& \bar{h} = (1 - B) \frac{h}{h_\delta} = 1 - CJ_1 + 2B\text{Pr}J_2, \quad \bar{H} = \bar{h} + Bf'^2 \\
& CJ_{10} = 1 - \bar{h}_w + 2B\text{Pr}J_{20}, \quad J_{i0} = J_i(0) \\
& J_1 = \int_{\zeta}^{\infty} (f'')^{\text{Pr}} d\zeta, \quad J_2 = \int_{\zeta}^{\infty} (f'')^{\text{Pr}} \left[\int_0^{\zeta} (f'')^{2-\text{Pr}} d\zeta \right] d\zeta
\end{aligned} \tag{12.6.16}$$

This solution satisfies the conditions $\bar{H} \rightarrow 1$, or $h \rightarrow h_\delta$, as $\zeta \rightarrow \infty$, and $\bar{H} = \bar{H}_w$, or $h = h_w$, for $\zeta = 0$. For $\text{Pr} = 1$ this solution becomes the Crocco integral 12.6.15.

The curves $\bar{h}(\zeta)$ obtained in Equation 12.6.16 for different Mach numbers M_δ and the Prandtl numbers $\text{Pr} = 0.5, 0.725$, and 1 are presented in Figure 12.10a. The dependence of the curves on Pr increases with the Mach number M_δ ; however, generally, it is not too great. At low values of the enthalpy factor \bar{h}_w and large M_δ , the enthalpy within the boundary layer has a maximum; at $M_\delta = \infty$ and $\bar{h}_w = 0$ the maximum value is $h = H_\delta/4$ for $\text{Pr} = 1$ and $h = 0.15H_\delta$ for $\text{Pr} = 0.5$, that is, the ratio h/H_δ remains bounded, which supports the estimate $h_* \sim H_\delta$ (12.5.10) for the characteristic enthalpy. In Figure 12.10b we have plotted the velocity profiles $u/u_\delta = f'(y/\delta)$ at $\text{Pr} = 1$ and $n = 0$ for different Mach numbers M_δ ; in this case, the coordinate y is determined by formula 12.6.5: $\delta = y(\zeta_\delta)$, where $\zeta_\delta = 5.2$. We will point out the appreciable effect of the temperature factor on not only the enthalpy profiles, which is quite natural, but also the velocity profiles at $M_\delta = 0$.

In view of the solution obtained, the derivative \bar{H}'_w entering into formula 12.6.14 for the heat flux q_w can be written in the form:

$$\bar{H}'_w = kf''_w(\bar{H}_e - \bar{h}_w), \quad H_e = h_\delta + \frac{1}{2}\kappa U_\delta^2 \tag{12.6.17}$$

Here, H_e is the so-called *adiabatic wall enthalpy* realized on a thermally insulated surface at $q_w = 0$, while κ is the total enthalpy recovery coefficient.

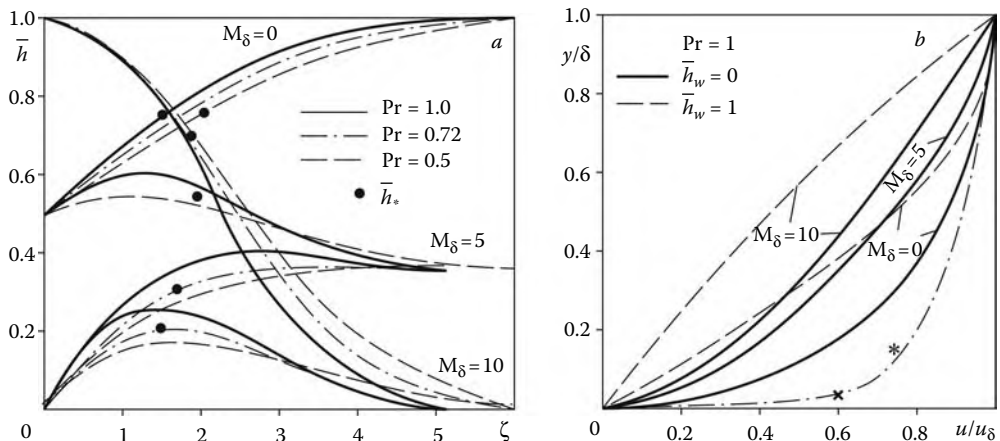


FIGURE 12.10

Enthalpy (a) and velocity (b) profiles in a boundary layer. Dash-and-dot curves relate to the velocity profiles in a turbulent boundary layer (Section 12.7).

Exact formulas for k and κ and their approximations for Pr ranging from 0.5 to 2 are as follows

$$k = (f_w'')^{\text{Pr}-1} J_{10}^{-1} = \text{Pr}^{1/3}, \quad \kappa = 2\text{Pr}J_2(0) = \text{Pr}^{1/2} \quad (12.6.18)$$

For $\text{Pr} = 1$ we have $J_{10} = 1$, $J_{20} = 1/2$, and $k = \kappa = 1$.

We will point out the qualitative influence of the Prandtl number on the adiabatic enthalpy, namely, $H_e < H_\delta$ for $\text{Pr} < 1$, $H_e = H_\delta$ for $\text{Pr} = 1$, and $H_e > H_\delta$ for $\text{Pr} > 1$, that is, for air we always have $H_e < H_\delta$. Further, making estimates for the heat-conduction term in the energy equation, the same as conducted before for the thickness δ , we obtain the order of the thermal layer thickness $\delta_T \sim \delta\text{Pr}^{-1/2}$, that is, for $\text{Pr} < 1$ temperature disturbances penetrate further into the external flow than the velocity disturbances, which is visible in Figure 12.10a. For gases, the difference between δ and δ_T is small and affects only the asymptotics of the function $h - h_w \sim (1 - f')^{\text{Pr}}$ for large ζ ; however, it can be quite appreciable for fluids, for which the Prandtl number can be rather high (from $\text{Pr} \approx 7$ for water to $\text{Pr} \approx 10^3$ for oils at standard temperature).

In the general case of the temperature-dependent functions $\omega(h)$ and $\text{Pr}(h)$, system 12.6.11 must be solved numerically, for example, using some iteration procedure based on relatively weak dependence of the velocity profile f' and the function $h(f')$ on the function ω (at an appropriate choice of the enthalpy h_*) and on the Prandtl number when the latter ranges from 0.6 to 1, which corresponds to the temperatures $T < 10^4\text{K}$, as shown in Figure 1.11d (Section 1.3).

On the basis of a set of calculations performed for the high-temperature air boundary layer, Eckert (1957) suggested an approximate formula for the determining enthalpy h_* , which should be used for calculating the parameters ρ_* and μ_* entering in the preceding formulas. In this approach we let $\rho\mu = \rho_*\mu_*$ (or $n = 0$ in formula 12.6.12), that is, use the Blasius formula for the function $f(\zeta)$ of Section 12.4. Thus, we have

$$\begin{aligned} h_* &= \frac{1}{2}(h_\delta + h_w) + 0.22(H_e - h_\delta) = h_{*0} - \left(\frac{1}{2} - 0.22\kappa\right) \frac{U^2}{2} = \\ &= \frac{1}{2}H_\delta \left[1 + \bar{h}_w - 0.31 \frac{2(\gamma - 1)M_\delta^2}{2 + (\gamma - 1)M_\delta^2} \right], \quad h_{*0} = \frac{1}{2}(H_\delta + h_w) \end{aligned} \quad (12.6.19)$$

Here, the latter formula is written for a perfect gas and $\text{Pr} = 0.71$, while the former is valid, at least, for the boundary layer temperatures $T \leq 8 \cdot 10^3\text{K}$ at $T_w \leq 2 \cdot 10^3\text{K}$. The quantity h_* is rather conservative; it is of the order of H_δ and for M_δ varying on the entire range from 0 to ∞ varies not more than threefold, even at $\bar{h}_w = 0$. The values of h_* are marked on the enthalpy profiles plotted in Figure 12.10a.

Finally, substituting 12.6.17 and 12.6.18 in 12.6.14 we obtain the following formula for the laminar ($q_w = q_l$) boundary layer on a flat plate (or a wedge or a cone in a supersonic flow)

$$\begin{aligned} q_w &= \alpha_l(H_e - h_w), \quad H_e = h_\delta + \frac{1}{2}\text{Pr}_w^{1/2}U_\delta^2 \\ \tau_w &= 0.332U_\delta \sqrt{\frac{(2\nu + 1)\rho_*\mu_*U_\delta}{x}} \\ \alpha_l &= 0.332\text{Pr}_w^{-2/3} \sqrt{\frac{(2\nu + 1)\rho_*\mu_*U_\delta}{x}} \end{aligned} \quad (12.6.20)$$

Here, α_l is the laminar *thermal-conductivity coefficient* (this name is often given to the ratio $q_w/(T_e - T_w)$, which is designated as α/c_p). Here, the product $\rho_*\mu_*$ is dependent on the local

pressure and the determining enthalpy h_* (as $h_*^{-0.3}$). The parameter $\text{Pr}_w = \text{Pr}(T_w)$ entering directly in formula 12.6.4 is taken instead of $\text{Pr}_* = \text{Pr}(h_*)$ (for a cold air $\text{Pr} = 0.71$).

It is the practice to express the friction and the heat flux on the wall in terms of the dimensionless *friction coefficient* C_f and the *Stanton number* St as follows

$$C_{f\delta} = \frac{2\tau_w}{\rho_\delta U_\delta^2}, \quad \text{St}_\delta = \frac{q_w}{\rho_\delta U_\delta (H_e - h_w)} = \frac{1}{2} \bar{k} C_f \quad (12.6.21)$$

The subscript δ of the coefficients refers to the fact that they are based on the parameters ρ_δ and U_δ , since, in principle, other representations are also possible.

This relation between the parameters C_f and St is called the *Reynolds analogy*; in view of 12.6.14 and 12.6.20, the *Reynolds analogy coefficient* is $\bar{k} = \text{Pr}_w^{-2/3}$.

We will also present some formulas for the displacement thickness δ^* . Putting $\rho_\delta/\rho = h/h_\delta = \tilde{h}$ and $\rho_*\mu_* = \rho_\delta\mu_\delta(h_\delta/h_*)^n$, taking into account 12.6.4 and 12.6.5, calculating integral 12.5.15, and determining $\tilde{h}(\xi)$ from 12.6.16 in the general case and from 12.6.15 for $\text{Pr} = 1$, we obtain

$$\begin{aligned} \delta^* &= \int_0^\infty \left(1 - \frac{\rho u}{\rho_\delta U_\delta}\right) dy = \left(\frac{h_\delta}{h_*}\right)^{n/2} \sqrt{\frac{\mu_\delta \xi}{\rho_\delta U_\delta}} \bar{\delta}^* \\ \bar{\delta}^* &= \int_0^\infty (\tilde{h} - f') d\xi = \frac{H_\delta}{h_\delta} K, \quad \xi = \frac{x}{2\nu + 1} \\ K &= \zeta^* \frac{h_w}{H_\delta} + f''_w \frac{U_\delta^2}{h_\delta} = 1.72 \frac{h_w}{H_\delta} + 0.332 \frac{U_\delta^2}{H_\delta} \quad (\text{Pr} = 1) \\ K &= 1.94 \frac{h_w}{H_\delta} + 0.58 \frac{U_\delta^2}{2H_\delta} - 0.21 \frac{h_\delta}{H_\delta} \quad (\text{Pr} = 0.72) \end{aligned} \quad (12.6.22)$$

We point out the proximity of the values of $\bar{\delta}^*$ for $\text{Pr} = 0.72$ and 1. Clearly, as compared with incompressible flows, for $M_\delta = 0$ and $h_w = h_\delta$ the displacement thickness increases with the Mach number M_δ and the wall enthalpy; contrariwise, for $M_\delta \approx 0$ and a strongly cooled wall, $h_w \ll h_\delta$, the displacement thickness is near-zero and can become even negative for $\text{Pr} < 1$.

Finally, using Equation 12.6.5 and the asymptotics derived in Section 12.4, $f \rightarrow \xi - \xi^*$, for $\xi \rightarrow \infty$, we obtain the boundary layer thickness in the form:

$$\delta = \left(\frac{h_\delta}{h_*}\right)^{n/2} \sqrt{\frac{\mu_\delta \xi}{\rho_\delta U_\delta}} \bar{\delta}, \quad \bar{\delta} = (f_\delta + \bar{\delta}^*), \quad f_\delta \approx 3.3 \quad (12.6.23)$$

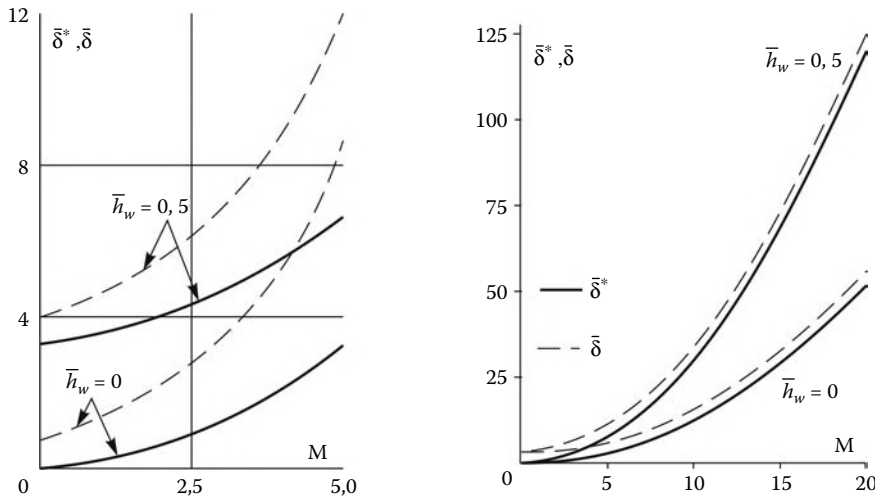
The M_δ dependence of $\bar{\delta}_*$ and $\bar{\delta}$ is presented in Figure 12.11 for $\text{Pr} = 1$.

We note that for $M_\delta \gg 1$ the quantity $\bar{\delta}^* \gg f_\delta$; therefore, in this case the error in determining the boundary values ξ_δ and f_δ introduces an only slight error into the entire boundary layer thickness.

12.6.2 Boundary Layer at the Blunt-Body Stagnation Point

In the vicinity of this point, by analogy with Section 7.7, it should be let

$$U_\delta = cx \left[1 + O\left(\frac{x^2}{L^2}\right)\right], \quad c \sim \frac{U_\infty}{L}, \quad r = x \left[1 + O\left(\frac{x^2}{L^2}\right)\right] \quad (12.6.24)$$

**FIGURE 12.11**

Mach number dependence of the dimensionless boundary layer thickness $\bar{\delta}$ and the displacement thickness $\bar{\delta}^*$.

Here, L is the scale of the flow (in particular, it can be the radius of curvature R of the body or the radius of curvature R_s of the shock) and U_∞ is the freestream velocity. As shown in Section 7.7, in this case the inviscid equations of gas flow are reduced to ordinary differential equations, correct to the second-order (of the order x^2/L^2) terms. Hence, within the same accuracy, we can neglect the terms F_f and F_H in Equation 12.6.11, since they are generated by precisely the inviscid part of the Navier-Stokes operator. Moreover, the orders of the viscous terms of this equation and the transverse pressure difference in the boundary layer estimated in Section 12.5 remain the same in the vicinity of the stagnation point, since these estimates are based only on the smallness of the ratio δ/L . Therefore, in expansions 12.6.24 we may restrict ourselves to only the first terms $U_\delta = cx$ and $r = x$, which leads to the following formulas for the variables 12.6.4 and the parameter β in 12.6.11

$$\xi = \frac{x}{2(1+\nu)}, \quad \zeta = \sqrt{\frac{2(1+\nu)c\rho_*}{\mu_*}}\eta, \quad \beta = \frac{1}{1+\nu} \quad (12.6.25)$$

For constant ρ and μ the variable ζ coincides with the same variable in 12.2.8. Thus, putting $F_f = F_H = B = 0$ in Equation 12.6.11 we reduce them to ordinary differential equations

$$\begin{aligned} 2(\omega\Phi_v'')' + \Phi_v\Phi_v'' + (1+\nu)^{-1}\left(\frac{\rho_\delta}{\rho} - \Phi'^2\right) &= 0 \\ 2\left(\frac{\omega}{\Pr}\bar{h}'\right)' + \Phi_v\bar{h}' &= 0 \end{aligned} \quad (12.6.26)$$

Here, in order to bring the equations into the same form as Equation 12.2.9, we designated the function f in 12.6.9 as Φ_v and, thanks to the smallness of the velocity u , put $\bar{H} = \bar{h}$.

In the general case, due to the existence of the relation of the form $\rho = \rho(h)$ (in a particular case, $\rho = \rho_\delta h_\delta/h$), Equation 12.6.26 forms an interrelated system. For this system,

the Crocco integral (12.6.15) obtained at $\text{Pr} = 1$ for a flat plate, is invalid, as it is for any flows with variable pressure $p = p(x)$, that is, for $\beta \neq 0$. This system can be split only for $\rho_\delta = \rho$ and $\omega = 1$, that is, for a limitingly small temperature variation in the boundary layer. In this case, the first equation of the system goes over to Equation 12.2.9, while the second equation takes the same form as Equation 12.6.16, where we should put $B = 0$ and substitute the function Φ_v for f . At the same time, a numerical solution of the system 12.6.26 presents no special problems if an iteration algorithm based on sequential solution of the equations of the system is used.

We note that these solutions can be used as initial conditions for more general problems of blunt-body boundary layers.

12.7 Models and Properties of Turbulent Flows

The salient features of turbulent flows were discussed in Section 1.15. Here we will present only brief information on the modern models of turbulent flows.*

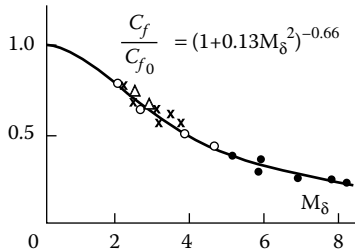
In the hierarchy of turbulence models with respect to the degree of their complexity and development in time, three large-scale levels, or stages, can apparently be distinguished. In the initial stage, the main properties of velocity profiles in boundary-layer and tube flows were investigated on the basis of experimental data and theory of similarity with the result that empirical criterion dependences for the friction and, later, heat transfer coefficients on the Reynolds number, the temperature factor $\bar{h}_w = h_w/H_\delta$, and other similarity criteria were obtained. In particular, for the turbulent heat flux q_w and friction τ_w on a flat plate in a high-temperature flow, the following formulas were derived

$$\begin{aligned} \tau_w &= 0.0296 \rho_* U_\delta^2 \text{Re}_*^{-0.2} \\ q &= A_t \rho_* U_\delta \text{Re}_*^{-0.2} (H_e - h_w) = A_t A_{t1} \rho_\delta U_\delta \text{Re}_\delta^{-0.2} (H_e - h_w) \\ A_{t1} &= \left(\frac{\rho_*}{\rho_\delta} \right)^{0.6} \left(\frac{\rho_* \mu_*}{\rho_\delta \mu_\delta} \right)^{0.2}, \quad H_e = h_\delta + \frac{1}{2} \kappa U_\delta^2 \\ \text{Re}_* &= \frac{\rho_* U_\delta x}{\mu_*}, \quad \text{Re}_\delta = \frac{\rho_\delta U_\delta x}{\mu_\delta} \\ A_t &= 0.0296 \text{Pr}^{-0.6} = 0.0363, \quad \kappa = \text{Pr}^{1/3} = 0.89 \quad (\text{Pr} = 0.71) \end{aligned} \quad (12.7.1)$$

The friction coefficient C_f is related with the Reynolds analogy 12.6.21 with the coefficient $\bar{k} = \text{Pr}^{-0.6}$. For calculating the characteristic parameters ρ_* and μ_* in this formula, the determining enthalpy of Eckert 12.6.19 can be used. This possibility is supported by Figure 12.12 in which the experimental values of the friction coefficient agree well with the calculated curve $C_f/C_{f0} = A_{t1}$, where C_{f0} is the value of C_f for $M_\delta = 0$, over a wide Mach number range (the data are taken from Hayes and Probstein, 1966; 12.7.1 will additionally be checked at the end of Section 12.8).

For a *three-regime* boundary layer characterized by the presence of successive *laminar*, *transition*, and *turbulent* regions of the boundary layer state, the heat flux is determined from a combined formula (see, e.g., Safiullin, 1971)

* The general theory of turbulence is presented in Schlichting (1968), Loitsyanski (1966), Hinze (1963), Lapin (1982), and others.

**FIGURE 12.12**

M_δ -dependence of the friction coefficient on a thermally insulated flat plate.

$$q_w = q_l(1 - \Gamma) + \Gamma q_t \quad (12.7.2)$$

where Γ is the *interruption coefficient* characterizing the degree of turbulence development in a boundary layer from zero ($\Gamma = 0, q_w = q_l$) to complete ($\Gamma = 1, q_w = q_t$). Thus, the $0 \leq \Gamma \leq 1$ range pertains to the transition (laminar-to-turbulent) boundary layer. The parameter Γ itself is preassigned as a certain monotonic function of the variable $\bar{x} = (x - x_1)/(x_2 - x_1)$, where x_1 and x_2 are the coordinates of the beginning and the end of the transition zone, whose length $x_2 - x_1$ is usually equal to the length x_1 of the preceding laminar region. The initial point x_1 is given by the transition Reynolds number Re_{cr} based on the local length x or some characteristic boundary layer thickness $\delta, \delta^*, \delta^{**}$, and so on. For smooth surfaces in a supersonic or hypersonic flow, in accordance with experimental data, transition takes place for the Reynolds numbers Re_x ranging from 10^5 to 10^6 with the twofold and even threefold (and even larger) scatter in the data obtained by different authors. This fact reflects objective difficulties in the interpretation of experiments of this type, since the boundary layer turbulization process is considerably affected by fluctuations and other, difficult-to-control disturbances of the external flow, which, quite naturally, are different for different wind tunnels. Of importance also are the state of the surface, the temperature factor, and so on. The theoretical prediction of the location where transition appears and the flow in the transition region is as yet impossible, despite great efforts made to solve the problem.

At the same time, the question is very important for practical applications, since at high local Reynolds numbers the turbulent heat flux q_t and friction τ_t are considerably larger than the laminar ones q_l and τ_l . In fact, comparing, for example, formulas 12.7.1 and 12.6.20 for a flat plate, we obtain the ratio $\lambda_q = q_t/q_l \approx \tau_t/\tau_l \approx 10^{-1}Re_x^{0.3}$ (for a compressible flow in these estimates the Reynolds number must be determined from the determining enthalpy h_*). Obviously, $\lambda_q \leq 1$ only for $Re_x \leq 10^3$, that is, far beyond the range of turbulence formation in boundary layers.

It would seem that the excess of the quantities q_t and τ_t over q_l and τ_l is due to the smaller turbulent boundary layer thickness δ_t as compared with the laminar thickness δ_l under the same conditions. Actually the pattern is opposite. In an incompressible flow the experimentally determined thickness of the turbulent boundary layer on a flat plate is $\delta_t \approx 0.38xRe_x^{-0.2}$, while the laminar boundary layer thickness is $\delta_l \approx 5xRe_x^{-0.5}$. Therefore, the thickness ratio $\delta_t/\delta_l \sim q_t/q_l$ is also greater than unity at high Re_x , which is sometimes used for determining the onset and extent of the transition zone by optical measurement techniques.

This fact indicates that the *turbulent viscosity* μ_t is appreciably greater than the molecular, or laminar, viscosity $\mu_l = \mu$. In fact, putting, for example, the viscous stress to be equal to $\tau_t = \mu_t \partial u / \partial y \sim \mu_t U_\delta / \delta_t$, we obtain the relation

$$\mu_t/\mu_l \sim \tau_t \delta_t / \tau_l \delta_l \sim 10^{-2} \text{Re}_x^{0.6} > 1 \quad \text{for } \text{Re}_x \geq 2.2 \cdot 10^3 \quad (12.7.3)$$

Hence follows, incidentally, that the apparent turbulent viscosity varies along the boundary layer in accordance with the $\mu_t \sim x^{0.6} \sim \delta_t^{3/4}$ law.

In Section 12.8 we shall give an engineering method that makes it possible to recalculate or extrapolate formulas 12.7.1 or 12.6.20 valid for a flat plate, to more general boundary layers. However, it seems attractive to use for this purpose the differential boundary layer Equations 12.5.14 as well; this possibility is provided by *algebraic turbulence models* or *second-level models*. These are based on the same equations in Equation 12.5.14 referred to the average motion, though with the appropriately chosen coefficients of viscosity μ_t , heat transfer λ_t , and so on. For example, for boundary layers the viscosity coefficient is usually preassigned in the form of an empirical dependence of the type $\mu_t(y/\delta, \Delta_i)$, where Δ_i are considered to mean a set of similarity criteria or some experimental constants. The first attempt at obtaining dependences of this type was undertaken by Prandtl who supposed that in a *shear flow*, that is, in a flow in which the parameters vary mainly along the coordinate y normal to the wall, the velocity fluctuations u' and v' entering into the stresses $p_{x,y} = \tau_t$ 1.15.6 are proportional to the derivative of the mean velocity, that is, $u' \sim v' \sim l_t \partial u / \partial y$, and so on, where l_t is the *turbulence scale* or the *mixing path length* introduced by analogy with the molecular-free path in the reasoning of Section 1.4. Eventually, this assumption leads to the formula

$$\tau_t = \rho l_t^2 \left| \frac{\partial u}{\partial y} \right| \frac{\partial u}{\partial y}, \quad \mu_t = \rho l_t^2 \left| \frac{\partial u}{\partial y} \right| \quad (12.7.4)$$

Here, from obvious considerations one of the cofactors $\partial u / \partial y$ is taken in absolute magnitude. Since turbulent fluctuations must decay near the wall, the scale l_t vanishes as the wall is approached, so that in the near vicinity of the wall a very thin *laminar sublayer* is formed; the flow in this sublayer is governed by molecular viscosity, appreciably smaller than a turbulent one. This leads to a considerably larger convexity of the turbulent velocity profile, as compared with the laminar one, which is demonstrated, in particular, by Figure 12.4 from Section 12.2 in which the velocity profiles in circular tubes are plotted, and Figure 12.10b from Section 12.6 for a flat plate. In the latter case, outside of the laminar sublayer, whose boundary is marked by a symbol, there is formed a *power-law* velocity profile $u/u_\delta = (y/\delta)^n$, where $n = 1/7$, usually independent of the Mach number and the temperature factor.

However, formula 12.7.4 is invalid in the outer part of the boundary layer or near the tube axis, where the derivative $\partial u / \partial y$ is small but the fluctuation intensity is still appreciable and the function μ_t is near constant. Therefore, the function μ_t is usually of a fairly complicated, composite shape.*

To close Equation 12.5.14, the *turbulent Prandtl number* Pr_t must also be preassigned; usually it is taken on the range from 0.9 to 1.

For the three-regime boundary layer the viscosity coefficient is replaced by a combined parameter

$$\mu^{(\Sigma)} = \mu_l(1 - \Gamma) + \Gamma \mu_t \quad (12.7.5)$$

where the intermittance coefficient Γ has the same meaning as in 12.7.2.

Using these models makes it possible to calculate more complicated boundary layer flows, including those in the presence of physical and chemical processes, with the establishment of the detailed flow pattern.

* A review and analysis of its numerous modifications can be found, for example, in Lapin (1982).

Finally, the *differential turbulence models*, or *third-level models*, make it possible to calculate separated and other similar flows, as distinct from the previously mentioned models that are adequate only for boundary layers or other shear flows.

These models are, in one way or another, based on the ideas of Kolmogorov (1942). Schematically, the essence of these models is as follows. First, it is assumed that the turbulent stress tensor 1.15.1 or 1.15.6 is proportional to the mean kinetic energy k of the velocity fluctuations u' , v' , and w' (in a Cartesian system of coordinates) determined by the formula

$$k = \frac{1}{2}(\bar{u'^2} + \bar{v'^2} + \bar{w'^2}) \quad (12.7.6)$$

It should be borne in mind that even in an on-the-average two-dimensional flow the fluctuation velocity component $w' \neq 0$ and, in accordance with the hypothesis adopted, is equal to the other components. The mean turbulent pressure p_t entering in the *pseudorheological* model 1.15.1 is, in view of 1.15.6, determined by the formula

$$p_t = \frac{2}{3}\rho k \quad (12.7.7)$$

This formula is analogous to 1.4.6 (with account for Equation 1.4.4) for the molecular pressure, while the quantity k is a counterpart of the mean kinetic energy of chaotic molecular motion. More generally, this turbulence model is to a certain extent analogous to the model of a gas in a state near to the local molecular-kinetic equilibrium. In particular, this turbulence model is valid under the assumption that, first, the turbulence scale l_t of the most energetic vortices is much smaller than the scale length L of the flow (e.g., the boundary layer thickness) and, second, turbulence is *near-locally-isotropic* or *near-equilibrium*. The essence of the latter assumption reduces ultimately to the equations

$$\bar{u'^2} = \bar{v'^2} = \bar{w'^2} = \frac{2}{3}k, \quad \bar{u'v'} = \bar{u'w'} = \dots = 0 \quad (12.7.8)$$

Small deviations from these equalities result in the formation of shear stresses and normal turbulent stresses.

We note, however, that the equilibrium nature of turbulence can be violated across shock waves or in the vicinities of singular (e.g., corner) points in turbulent flows, since behind the singularities certain *relaxation zones* (by analogy with nonequilibrium gas flows described in Chapter 11) can arise, in which the near-equilibrium state of turbulence is restored. However, any models for describing the flow in such relaxation zones are as yet lacking. In particular, in a passage across a shock wave (neglecting the thickness of its smearing by turbulent fluctuations), the conditions for the turbulence parameters behind the shocks are unclear.

Within the framework of equilibrium turbulence models, in accordance with the dimensionality analysis, turbulent viscosity μ_t , thermal conductivity λ_t , and diffusivity D_t must have the following structures

$$\mu_t = C_\mu \rho l_t k^{1/2}, \quad \lambda_t = \mu_t c_p / \text{Pr}_t, \quad \rho D_t = \mu_t / \text{Sc}_t \quad (12.7.9)$$

where the coefficient C_μ is a dimensionless constant or a function of some dimensionless variables and parameters, while the turbulent Prandtl Pr_t and Schmidt Sc_t numbers are usually assumed to be unity.

Under these assumptions, the equations of motion 1.9.7 and 1.9.8 taken, for example, in their integral form, retain, in accordance with the assumption, their form for the average

motion, only with a formal replacement of the molecular stress tensor P_μ by the overall tensor $P^{(\Sigma)} = P_\mu + P_t$ determined by formula 1.15.1, together with formulas 12.7.7 and 12.7.9. The average energy Equation 1.9.10 must also be supplemented and then takes the form:

$$\begin{aligned} \frac{\partial \rho E^{(\Sigma)}}{\partial t} + \operatorname{div} [(\rho E^{(\Sigma)} + p^{(\Sigma)}) \vec{U}] &= \rho q - \operatorname{div} \vec{J}^{(\Sigma)} + \operatorname{div} (P_\tau^{(\Sigma)} \vec{U}) \\ E^{(\Sigma)} &= e + \frac{1}{2} U^2 + k, \quad p^{(\Sigma)} = p + p_t \\ -\vec{J}^{(\Sigma)} &= (\lambda_{\text{eff}} + \lambda_t) \operatorname{grad} T + (\mu + \rho D_t) \operatorname{grad} k \end{aligned} \quad (12.7.10)$$

Here, the flux $\vec{J}^{(\Sigma)}$ differs from 1.15.2 in that it takes into account the turbulent energy diffusion k caused by the transport of macroscopic fluid particles accompanying turbulent fluctuations. In this formulation, the turbulent energy k is, as it were, the internal flow energy, which is in the state of exchange with its kinetic energy and thermodynamic energy e . Then the averaged total enthalpy with account of fluctuations is as follows:

$$H^{(\Sigma)} = h + \frac{1}{2} \overline{(U + U')^2} \approx h + \frac{1}{2} U^2 + k \quad (12.7.11)$$

We note that in many flows k is small, as compared with the energy $E = e + U^2/2$, and is usually discarded (in any case, always in algebraic turbulence models). Nevertheless, the presence of the terms involving k in the energy equation should always be borne in mind, particularly in separated flows in which an elevated fluctuation level is observed on the background of low local Mach numbers.

In any case, the energy k is an unknown parameter of the problem formulated, which enters into the coefficients μ_t , and so on, and, therefore, is to be determined. The turbulent energy evolution is usually described by a differential equation, which is presented here without derivation*

$$\rho \frac{dk}{dt} = \operatorname{div} [(\mu + \rho D_t) \operatorname{grad} k] + W_G - W_D, \quad W_G = P_t E_\varepsilon \quad (12.7.12)$$

Here, W_G and W_D are the volumic rates of turbulent energy generation and dissipation and E_ε is the strain rate tensor of the average motion. Equation 12.7.12 is, in essence, constructed in accordance with the plausibility criterion, by analogy with the structure of the viscous terms in the Navier–Stokes equations, as it was done before on transition from the Reynolds stresses 1.15.6 to the pseudorheological relations (Equation 1.15.1). The term $\rho D_t \operatorname{grad} k$ is the turbulent energy flux due to turbulent diffusion. The term W_G is defined by analogy with the molecular viscous energy dissipation q_τ determined by formula 12.1.7 with the substitution of the turbulent stress tensor P_t for the viscous stress tensor P_τ . This is based on the assumption that dissipation of the kinetic energy of the average flow exposed to turbulent stresses goes directly to an increase in the fluctuation energy k and transforms to the internal energy e only due to dissipation of the energy k , that is, at the expense of the term W_D in Equation 12.7.11. From the dimensional analysis there follows the structure of this term:

$$W_D = C_D \rho k^{3/2} / l_t \quad (12.7.13)$$

* See, for example, Launder and Spalding (1972) and Launder and Sharma (1974).

The coefficient C_D , as C_μ in 12.7.6, may be either a constant or a certain function of the corresponding dimensionless coordinates and other parameters.

However, apart from the coefficients C_μ and C_D , the functions μ_t and W_D incorporate also the turbulence scale l_t ; determining this parameter is the most sophisticated point in turbulence theory. This function can be presented in the form of some empirical algebraic formulas only for boundary-layer-type flows. However, this presentation denudes the differential turbulence model any advantages over the algebraic model. As for the construction of some equation for l_t on the basis of one or another conservation law like 12.7.12, it seems impossible.

Though attempts at deriving a differential equation for the function l_t are known (Glushko, 1970), the most commonly encountered approach is associated with the construction of equations of type 12.7.12 for combinations of the parameters k and l_t : directly for the function W_D (the k - ε model; see Launder and Sharma, 1974), for the function $\omega \sim \varepsilon/k$ (k - ω model; Wilcox, 1991), and so on. In these cases, the turbulence scale l_t is eliminated from Equation 12.7.9 via the functions presented previously. Moreover, there are versions of the models in which equations constructed directly for viscosity μ_t are used instead of Equation 12.7.12 for k .* We will drop an analysis of these models since it is beyond the scope of this book.

In conclusion, we note that the second and third-level turbulence models outlined previously are, in spite of their apparent mathematical rigorousness, actually *semiempirical*, since they are based on the equations derived from the considerations of similarity and dimensionality, general physical ideas on the structure of the flux and dissipative terms in the mathematical formulation of the conservation laws, and the set of empirical coefficients, C_μ , and so on, either constant or variable, which are chosen to fit the theory with the experimental data with respect to some, few in number, parameters open to measurements. For this reason, a combination of these parameters chosen for one class of flows, needs additional testing when applied to flows of other types. Nevertheless, the development of turbulence models, particularly, differential ones, must be taken as important progress. Some examples of the application of these theories will be given in Section 12.8.

12.8 Integral Relations and Approximate Methods: Boundary Layer on Blunt Bodies

Along with numerical solutions of the boundary layer equations, their approximate, simplified solutions are also known. Popular in the past, they are still of importance due to their simplicity, the accuracy of determining heat fluxes, friction, and boundary layer thicknesses, sufficient for engineering practice, and the clarity of the solutions obtained that reflect the basic properties of boundary layers.

These methods are usually based on the use of the integral form of the equations of motion presented in Section 1.9. However, in this case it would be more obvious to derive them directly from the boundary layer Equations 12.5.14. For this purpose, we multiply the first and third equations of that system by r_b^w and, in view of the continuity equation, bring

* Gulyaev, Kozlov, and Sekundov (1993), Spallart and Allmaras (1994).

them to the form:

$$\begin{aligned} \frac{\partial \rho u^2 r_b^v}{\partial x} + \frac{\partial \rho u v r_b^v}{\partial y} &= -r_b^v \frac{\partial p}{\partial x} + r_b^v \frac{\partial}{\partial y} \left(\mu \frac{\partial u}{\partial y} \right) \\ \frac{\partial \rho u r_b^v H}{\partial x} + \frac{\partial \rho v r_b^v H}{\partial y} &= r_b^v \frac{\partial}{\partial y} \left(\frac{\mu}{\text{Pr}} \frac{\partial H}{\partial y} \right) + r_b^v \frac{\partial}{\partial y} \left(\mu \frac{\text{Pr} - 1}{2\text{Pr}} \frac{\partial u^2}{\partial y} \right) \end{aligned} \quad (12.8.1)$$

Then, following the analogous procedure of Section 1.7, we subtract the continuity equation multiplied by U_δ from the first equation of Equation 12.8.1 and integrating the equation thus obtained with respect to y between the limits from 0 to δ obtain the resulting *integral momentum equation*

$$\begin{aligned} \frac{d}{dx} \left[r_b^v \int_0^\delta \rho u (U_\delta - u) dy \right] &= \frac{d}{dx} (r_b^v \rho_\delta U_\delta^2 \delta^{**}) = r_b^v \delta^* \frac{dp}{dx} + r_b^v \tau_w \\ \tau_w &= \left(\mu \frac{\partial u}{\partial y} \right)_{y=0} \\ \delta^* &= \int_0^\delta \left(1 - \frac{\rho u}{\rho_\delta U_\delta} \right) dy, \quad \delta^{**} = \int_0^\delta \frac{\rho u}{\rho_\delta U_\delta} \left(1 - \frac{u}{U_\delta} \right) dy \end{aligned} \quad (12.8.2)$$

Here, the *displacement thickness* δ^* is the same as in Equation 12.5.15; however, the form of the *momentum thickness* δ^{**} is more general than that for an incompressible flow in Equation 12.4.9.

Similarly, we subtract the continuity equation multiplied by H_δ from the second equation of Equation 12.8.1 and integrate the result with respect to y within the same limits from 0 to δ ; this yields the *integral energy equation*

$$\begin{aligned} \frac{d}{dx} (\rho_\delta U_\delta H_\delta r_b^v \Theta) &= r_b^v q_w, \quad q_w = \left(\frac{\mu}{\text{Pr}} \frac{\partial h}{\partial y} \right)_{y=0} \\ \Theta &= \int_0^\delta \frac{\rho u}{\rho_\delta U_\delta} \left(1 - \frac{H}{H_\delta} \right) dy = (1 - \bar{h}_w) \delta^{**}, \quad \bar{h}_w = h_w/H_\delta \end{aligned} \quad (12.8.3)$$

Here, Θ is the *total enthalpy thickness* of the boundary layer, while the second equation for Θ is derived using the Crocco integral 12.6.15.

For the laminar flat-plate boundary layer, passing in Equation 12.8.22 to variables 12.6.1 and 12.6.4 we obtain for δ^{**} the same formula 12.6.23 as for δ , though with the parameter $\delta^{**} = 0.664$ instead of $\bar{\delta}$. For an incompressible boundary layer ($\delta^* = 1.71$) the ratio $\delta^{**}/\delta \approx 0.12$ is fairly low and decreases, along with an increase in the boundary layer thickness (cf. 12.6.22 and 12.6.23), as M_δ increases.

The experimentally determined thickness of an incompressible turbulent boundary layer on a flat plate is usually described by the formula $\delta = 0.38x\text{Re}_x^{-0.2}$, while the velocity profile is approximated by a power law $u/U_\delta = (y/\delta)^n$, where $n = 1/7$. Substituting these expressions in the formula for δ^{**} and Equation 12.8.2 for a flat plate, we obtain

$$\delta^{**} = \frac{n\delta}{(1+n)(1+2n)} = \frac{7}{72}\delta, \quad \tau_w = 0.0296\rho_\delta U_\delta^2 \text{Re}_x^{-0.2}, \quad \text{Re}_x = \frac{\rho_\delta U_\delta x}{\mu_\delta} \quad (12.8.4)$$

Thus, in this case again the ratio δ^{**}/δ is fairly small. Incidentally, the preceding formula for friction explains, in view of the Reynolds analogy 12.6.21, the origin of the numerical coefficient in formula 12.7.1 for the turbulent heat flux.

First integral methods for solving the boundary layer problems were developed for incompressible flows and were based on preassigning the velocity profiles in the form $u/U_\delta = f(y/\delta, \Delta_i)$ (e.g., in the form of polynomials in y/δ as in the Pohlhausen method), where the number of the given *form parameters* $\Delta_i(x)$ is equal to the number of the conditions imposed on the wall and the outer edge of the boundary layer. Among these conditions can be some constraints on the higher derivatives of the function f determined directly from the governing differential equations. From the given velocity profile the displacement thickness δ^{**} and the friction τ_w in Equation 12.8.2 are then determined; thus, Equation 12.8.2 is transformed to an ordinary differential equation with respect to the thickness δ .

However, more accurate approximate methods of the boundary layer calculation, developed usually for determining heat fluxes, are based on the simpler and, as experience has shown, very plausible assumption that the friction τ_w and the heat flux q_w are dependent only on the local external parameters and, accordingly, on the thicknesses δ^{**} for τ_w and Θ for q_w . In accordance with the hypothesis adopted, the $\tau_w(\delta^{**}, \lambda_i)$ and $q(\Theta, \lambda_i)$ dependences, where $\lambda_i = \rho_\delta, U_\delta, H_\delta, h_w$, and so on, are taken to be the same as for a flat plate. Other, and very similar, versions of these methods were suggested by Lees (*local similarity method*, 1956) and Avduevskii (*effective length method*, 1962, 1975).

In its practical realization, the latter method is reduced to what follows. We write the formula for the heat flux to the plate in the general form:

$$\begin{aligned} q_w &= q_i = B_i x^{-m} \\ i = l : \quad m &= m_l = \frac{1}{2}, \quad B_l = 0.332 \text{Pr}^{-2/3} \sqrt{\rho_* \mu_* U_\delta} (H_{el} - h_w) \\ i = t : \quad m &= m_t = 0.2, \quad B_t = 0.0296 \text{Pr}^{-0.6} (\rho_* U_\delta)^{0.8} \mu_*^{0.2} (H_{et} - h_w) \end{aligned} \quad (12.8.5)$$

The expressions for m and B_i for the laminar ($i = l$) and turbulent ($i = t$) boundary layers follow from formulas 12.6.20 and 12.7.1. Substituting Equation 12.8.5 in 12.8.3 and integrating the latter for $v = 0$ we obtain a relation between Θ and x for a flat plate, together with the $q_i(\Theta_i)$ dependence

$$\bar{\Theta}_i = \rho_\delta U_\delta H_\delta (1 - m) \Theta_i = B_i x^{1-m} \quad (12.8.6)$$

$$q_i = B_i x^{-m} = B_i^{1/(1-m)} \bar{\Theta}_i^{-m/(1-m)} \quad (12.8.7)$$

We assume that the function $q_i(\Theta_i)$ is universal; then, rewriting Equation 12.8.3 in terms of this function of variables B_i yields

$$\frac{d}{dx} (r^v \bar{\Theta}_i) = (1 - m) (r^v B_i)^{1/(1-m)} (r^v \bar{\Theta}_i)^{-m/(1-m)} \quad (12.8.8)$$

Integrating this equation we obtain

$$(r^v \bar{\Theta}_i)^{1/(1-m)} = z_i(x) = \int_0^x (r^v B_i)^{1/(1-m)} dx \quad (12.8.9)$$

Finally, returning to Equation 12.8.7 we arrive at a formula for $q_i(x)$

$$q_i = r^{vm/(1-m)} B_i^{1/(1-m)} z_i^{-m} = B_i x_{\text{eff}}^{-m}, \quad x_{\text{eff}} = (r^v B_i)^{-1/(1-m)} z_i \quad (12.8.10)$$

Here, x_{eff} is the *effective length* of a given boundary layer or the length of a plate with the same heat flux to the wall, as for the body under consideration under the local boundary conditions. For the laminar and turbulent boundary layers the functions x_{eff} are as follows:

$$\begin{aligned} x_{\text{eff},l} &= \frac{\bar{z}_l}{\bar{B}_l}, \quad \bar{z}_l = \int_0^x \bar{B}_l dx, \quad \bar{B}_l = r^{2\nu} \rho_* \mu_* U_\delta (H_{el} - h_w)^2 \\ x_{\text{eff},t} &= \frac{\bar{z}_t}{\bar{B}_t}, \quad \bar{z}_t = \int_0^x \bar{B}_t dx, \quad \bar{B}_t = r^{5\nu/4} \rho_* \mu_*^{1/4} U_\delta (H_{et} - h_w)^{5/4} \end{aligned} \quad (12.8.11)$$

For a constant enthalpy difference $H_{el} - h_w$ the function x_{eff} coincides with the variable ξ 12.6.4; in this case, the result obtained is equivalent to the solution of Equation 12.6.11 for $F_p = F_f = F_H = 0$, that is, the solution of the locally self-similar problem for the equivalent plate with the length $x_{\text{eff}} = \xi$. Thence follows the second name of this method, namely, the *local similarity method*.

For $h_w = \text{const}$ or $h_w \ll H_\delta$ the differences $H_e - h_w$ disappear from the expressions for x_{eff} . From Equation 12.6.19 it follows that the dependence of the determining enthalpy h_* on the Mach number M_δ is comparatively weak; for this reason, on the range $M_\delta \leq 2 - 3$, typical of blunt bodies (see Figure 9.2), taking into account Equation 1.3.11, we set

$$(h_*/h_{*0})^{-0.3} = 1, \quad \rho_* \mu_* = \rho_{*0} \mu_{*0} \bar{p}, \quad \rho_* \mu_*^{1/4} = \rho_{*0} \mu_{*0}^{1/4} \bar{p}, \quad \bar{p} = p/p'_0 \quad (12.8.12)$$

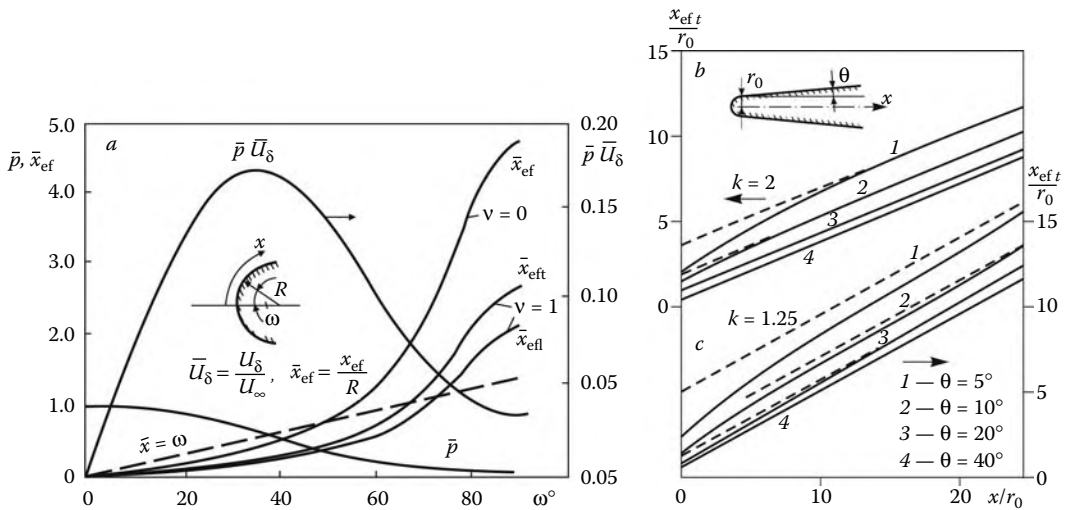
Here, p'_0 , h_{*0} , ρ_{*0} , and μ_{*0} are the blunt-body stagnation-point parameters. Then formulas 12.8.11 take the form:

$$x_{\text{eff},i} = \frac{\tilde{z}_i}{\bar{p} \bar{U}_\delta}, \quad \tilde{z}_i = \frac{1}{r^\kappa} \int_0^x r^\kappa \bar{p} \bar{U}_\delta dx, \quad \bar{U}_\delta = \frac{U_\delta}{U_*} \quad (12.8.13)$$

Here, $\kappa = 2\nu$ for a laminar and $\kappa = 5\nu/4$ for a turbulent boundary layer and U_* is a scale velocity, for example, the freestream velocity U_∞ . Clearly, in this approximation the functions x_{eff} have the same form for both laminar and turbulent boundary layers at $\nu = 0$ and are different for $\nu = 1$.

The effective length method for the skin friction τ_w can be constructed in a similar manner using the same relationship $\tau_w = \tau_w(\delta^{**})$ as for the plate. In this case, a stronger pressure-gradient effect should be expected, since this quantity enters directly in Equation 12.8.2. However, in engineering practice the friction coefficient is usually determined from the Reynolds number 12.6.21 in terms of the Stanton number.

We will use the results obtained for an analysis of the distinctive features of the heat flux distributions over body surfaces. In Figure 12.13a we have plotted the distributions of the quantity $\bar{x}_{\text{eff}} = x_{\text{eff}}/R$ (12.8.13) over a circular cylinder ($\nu = 0$) and a sphere ($\nu = 1$) of radius R for laminar and turbulent boundary layers at the same, spherical pressure distribution 7.2.6. Comparing the \bar{x}_{eff} curves with the straight line $\bar{x} = x/R = \omega$, where ω is the central angle, we can conclude that in the central region of the bodies $\omega < \omega_c$, where ω_c is a certain threshold angle, the inequality $x_{\text{eff}} < x_c = \omega_c R$ holds and, hence, in this region the heat flux is greater than on a flat plate with the local flow parameters and the length x equal to the length of the generators of these bodies; for $x_{\text{eff}} > x_c$ the opposite situation occurs. We note that the product $\bar{p} \bar{U}_\delta$ in formula 12.8.13 underlines the role played by precisely local flow parameters, while their previous distribution has an only averaged effect, via

**FIGURE 12.13**

Effective length on a sphere and a circular cylinder (a) and on a blunt cone with laminar (b) and turbulent (c) boundary layers.

the \tilde{z}_i integrals. This is particularly visible in such short regions of the surface, where the parameters \tilde{z}_i vary only slightly, though the variation of the pressure is appreciable (such as the vicinity of a corner point or a small roundness). In these regions, heat fluxes vary in proportion to the parameter $\bar{p}\bar{U}_\delta$, in the same fashion for laminar and turbulent boundary layers.

For $v = 0$ the x_{eff} curves in Figure 12.13a lie above those for $v = 1$; therefore, under the same external conditions the heat flux through an axisymmetric boundary layer $q_{v=1}$ is higher than that in the plane case $q_{v=0}$. For a laminar boundary layer this was shown in Section 12.6 with reference to particular examples, where it was obtained that the heat flux to a cone is greater than that to a flat plate in ratio $q_{v=1}/q_{v=0} = \sqrt{3}$. However, for a turbulent boundary layer the difference is smaller. Thus, setting $r \sim x$, $p = \text{const}$, and $U = \text{const}$ in 12.8.11 or 12.8.13, for a cone we obtain

$$\frac{x_{\text{eff}}}{x} = \frac{4}{5v + 4} = \frac{4}{9}, \quad \frac{q_{v=1}}{q_{v=0}} = \left(\frac{x}{x_{\text{eff}}} \right)^{0.2} = 1.176 \quad (12.8.14)$$

At stagnation points of blunt bodies, letting, as before, $U_\delta = cx$, $r = x$, and $\bar{p} = 1$ in their vicinity, for a laminar boundary layer from 12.8.5 and 12.8.11 we obtain the following formulas

$$\begin{aligned} x_{\text{eff},l} &= \frac{x}{2(1+v)}, & q^{(0)} &= A_v \text{Pr}^{-2/3} \omega_\delta^{-1/2} \sqrt{\rho_\delta \mu_\delta c} (H_{el} - h_w) \\ H_{el} &= H_0 = H_\infty, & \omega_\delta &= \frac{\rho_\delta \mu_\delta}{\rho_* \mu_*} = \left(\frac{h_*}{H_\delta} \right)^n = \left(\frac{1}{2} + \frac{1}{2} \bar{h}_w \right)^n \\ A_v &= 0.47 A'_v \sqrt{1+v}, & A'_0 &= 1.2, \quad A'_1 = 1.15 \end{aligned} \quad (12.8.15)$$

We note that the method itself gives the value of the coefficient $A'_v = 1$, while the values A'_v presented previously are correction coefficients leading to the exact values $A_0 = 0.57$ and $A_1 = 0.76$ obtained earlier by approximating the results of the calculations at moderate

temperatures. Thus, the heat flux ratio for the stagnation points on a sphere and a circular cylinder is $0.76/0.57 = 1.33$ (for $A'_v = 1$ it is equal to $\sqrt{2}$).

For hypersonic flows, the comparison of formulas 7.7.14, 7.7.16, and 7.8.6 (or, simply, the expansion $p = p'_0(1 - \beta x^2/R_s^2)$ (7.7.14) and the equation of motion $u(\partial u/\partial x) = -\rho^{-1}(\partial p/\partial x)$) yields the formula

$$R_s c = U_\infty \sqrt{2\bar{p}'_0 \beta k_0}, \quad \bar{p}'_0 = \frac{p'_0}{\rho_\infty U_\infty^2}, \quad k_0 = \frac{\rho_\infty}{\rho_0} \quad (12.8.16)$$

Here, p'_0 and ρ_0 are the pressure and the density at the stagnation point, β is a coefficient, different from the coefficient β in Equation 12.6.11, and R_s is the radius of curvature of the shock at the axis of symmetry. For $k_0 \ll 1$, in the hypersonic approximation of Chapter 7, letting $p/\rho = \text{const}$ along the axis of symmetry and taking Equation 3.6.5 with $M_\infty^2 \gg 1$ into account, correct to k_0^2 we obtain

$$\begin{aligned} \bar{p}'_0 &= 1 - \frac{1}{2}k, & k_0 &= k(1 - 0.5k), & \bar{p}'_0 k_0 &= k(1 - k) = \bar{k} \\ R_s c &= U_\infty \sqrt{2\beta \bar{k}}, & k &= \frac{\rho_\infty}{\rho_s} \\ \beta &= \bar{\beta} \frac{R_s^2}{R^2}, & c &= \frac{U_\infty}{R} \bar{c}, & \bar{c} &= \sqrt{2\bar{\beta} \bar{k}} \end{aligned} \quad (12.8.17)$$

where ρ_s is the density immediately behind the shock and R is the radius of curvature of a body; for a sphere $\bar{\beta} = 1.17$ (cf. 7.2.6).

At the same time, the relative laminar heat flux distribution $q_l/q^{(0)}$ over, say, a spherical surface obtained by the effective length method, almost coincides with the exact one presented in Figure 12.14a calculated at the hypersonic pressure distribution 7.2.6. This

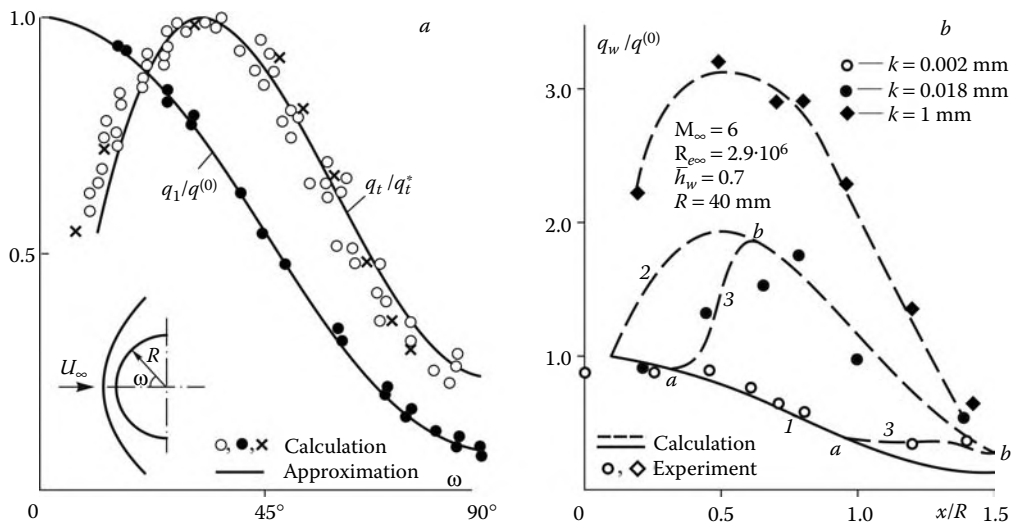


FIGURE 12.14

Distributions of laminar and turbulent heat fluxes over a sphere in a hypersonic flow: (a) • and ○, calculations in accordance with Sections 12.6 and 12.8; ×, calculation with the algebraic viscosity (Section 12.7) (Safarov and Tirsikii, 1977); (b) calculation and experiment (Marinin) for a smooth surface (1) and a rough surface (2 to 4) with a roughness height k ; ab is the transition zone.

distribution is universal, in the sense that it is almost independent of the flow conditions (at least, for $U_\infty < 7.5$ km/s) and can be approximated with a high degree of accuracy by the following formula (Murzinov, 1966)

$$\frac{q_t}{q^{(0)}} = 0.55 + 0.45 \cos 2\omega \quad (12.8.18)$$

Here, ω is the angular coordinate of a point; the dependence is plotted in Figure 12.14a.

For the turbulent boundary layer in the vicinity of the stagnation point, from Equations 12.8.10 and 12.8.13 it follows

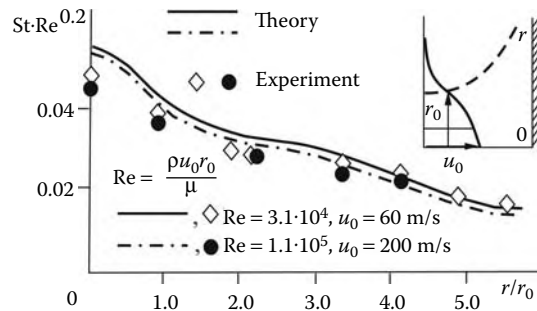
$$x_{\text{eff}} = \left(\frac{4}{5\nu + 8} \right) x, \quad q_t = 0.0296 \Pr^{-0.6} \left(\frac{5\nu + 8}{4} \right)^{0.2} (\rho_* c)^{0.8} \mu_{*0}^{0.2} x^{0.6} (H_{et} - h_w) \quad (12.8.19)$$

Here, in the axisymmetric flow the heat flux is by a factor of 1.27 greater than that in the two-dimensional case; however, most important is that in both cases the turbulent heat flux is zero at the stagnation point itself and has a singularity of the type $q_t \sim x^{0.6}$ in its vicinity. Because of this, on a spherical surface (as well as on other bodies) the q_t curve has a maximum $q_t = q_{t*}$ (Figure 12.14) located near the sonic point on the surface, but on the subsonic side of it, in accordance with the maximum of the $\bar{p}\bar{U}$ curve located at the point $M = \gamma^{-1/2}$. As for a laminar boundary layer, the q_t/q_{t*} curves are, to a certain degree, universal, so that the calculated results for hypersonic flight conditions ($M_\infty \geq 3$) with the pressure 7.2.6, as presented in Figure 12.13, can be approximated by the following formula (bold curve in Figure 12.14a)

$$\frac{q_t}{q_{t*}} = 3.75 \sin \omega - 3.5 \sin^2 \theta \quad (12.8.20)$$

(Zemlyanskii and Stepanov, 1981). Naturally, at the stagnation point the equality $q_t = 0$ is contradictory to the usual physical notion and the experience, since formally for even fairly high Reynolds numbers $\text{Re}_{\infty R}$ based on the sphere radius R and the freestream parameters, in the vicinity of the stagnation point $x \ll R$ there is always a region of low local Reynolds numbers $\text{Re} \sim U_\delta x / R \sim (x/R)^2$ associated with a laminar boundary layer followed by transition to the turbulent one in accordance with the pattern shown in Figure 12.14b.

The location of the transition region in Figure 12.14b (curves ab) depends on both external conditions, first of all, the local Reynolds number, and the state of the surface. Without going into detail of this complicated process, we will comment on Figure 12.15 in which the experimental heat fluxes on a rough spherical surface are presented. On a surface with a vanishingly small roughness the boundary layer is laminar and the calculated heat fluxes (curve 1) are in agreement with the experimental data. In this case, the transition region is located only on the peripheral part of the surface. As the roughness is increased, the transition region is displaced toward the axis of symmetry. As noted in Section 12.7, its length is approximately equal to that of the preceding laminar region. However, at the same time, in the turbulent region of the boundary layer the experimental heat fluxes are generally in agreement with the calculated ones (curve 2) obtained using the earlier described method for a smooth surface, the turbulent heat flux being twice as large as the laminar one. Finally, for large-sized roughness, the heat flux distribution follows almost everywhere the turbulent law (curve 4) defined by solution 12.8.14 for smooth bodies, though with a heat flux enhancement factor equal to about 1.5. In this case, in Figure 12.14a the ratio of the roughness height to the boundary layer thickness is equal to k/δ_l . For curve 1 $k/\delta_l \sim 10^{-2} \ll 1$, for curve 2 $k/\delta_l \sim 10^{-1} \ll 1$, and for curve 4 $k/\delta_t \sim 1$, where δ_l and δ_t are the thicknesses of laminar and turbulent boundary layers.

**FIGURE 12.15**

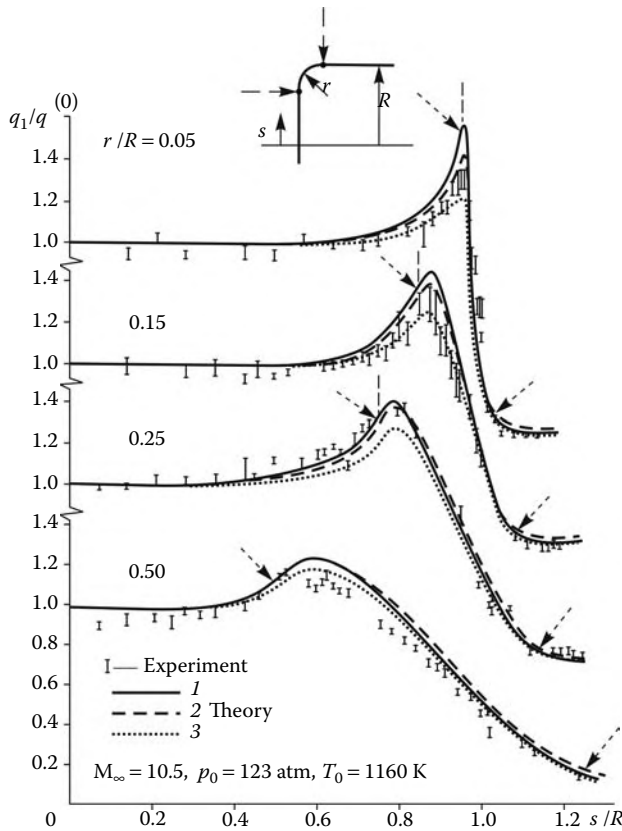
Heat flux distribution over a flat plate in a perpendicular axisymmetric heated turbulent jet.

We note that this relative position of the laminar and turbulent boundary layer regions pertains only to the case of the laminar undisturbed external flow. If the external flow is strongly turbulized (e.g., the case of a blunt body in a turbulent jet), then the observed behavior of the heat flux is quite different: at the stagnation point the pressure-dependence of the heat flux is “turbulent” ($\rho^{0.8}$), while the heat flux distribution over the body surface is “laminar” (Karpov, 1966). In support of this conjecture, in Figure 12.15 we have plotted the distributions of heat fluxes on a flat plate orthogonal to the axis of an axisymmetric turbulent jet. Here, the measured data are in good agreement with the results of calculations using the differential k - ε model (see Section 12.7).* In the vicinity of the stagnation point this model gives a finite value of q_m , as distinct from the standard turbulent model 12.8.19, in accordance with which at this point $q_w = 0$.

The preceding analysis indicates that the accuracy of the effective length method is fairly sufficient for engineering practice, at least for bodies of rather smooth shapes, that is, without regions characterized by excessively high pressure gradients (such as, e.g., vicinities of corner points on the contour), where the method needs additional checking. Figure 12.16, in which the calculated and measured heat flux distributions over a circular disk with rounded corner points are presented (Marvin and Sinclair, 1967) serves to illustrate the possibilities of the method discussed in similar situations. A fairly high accuracy is provided by the *generalized local similarity method* (curves 2), which differs from the method presented previously in that the coefficient B_1 in Equation 12.8.5 is determined from Equation 12.6.11 in which the right-hand sides are omitted but the term with the coefficient β determined from the local pressure gradient, that is, from the solutions of Falkner and Skan for a compressible flow (Section 12.2), is retained. However, this generalization of the method denudes it of simplicity.

As for slender blunt cones, owing to the high-entropy layer effect (Chapter 9) the boundary layer on these bodies cannot be regarded as classical in the meaning of Sections 12.3 and 12.5. This question will be discussed in Section 12.13. Here, we restrict ourselves to the estimate of the effective lengths for blunt cones and wedges; for this purpose, we will use formula 12.8.13 letting in it $pU = \text{const}$. Integrating we obtain

* The experimental data of Donaldson, Snedecker, and Margolis (1971) and the calculated results of Gorshkov, Lunev, and Selezneva (1997) obtained using the k - ε model in the modification of Lam and Bremhorst (1981).

**FIGURE 12.16**

Laminar heat flux distribution over a disk with rounded corner points: 1, exact calculation; 2, generalized local similarity method; and 3, effective length method; p_0 and T_0 are the stagnation parameters.

$$\begin{aligned}\bar{x}_{\text{eff}} &= \frac{x_{\text{eff}}}{r_0} = \frac{1}{\bar{r}_b^\kappa} \left(x_{\text{eff},0} + \frac{\bar{r}_b^{\kappa+1} - 1}{(\kappa + 1) \sin \theta} \right) \\ \bar{r}_b &= \frac{r_b}{r_0} = 1 + \bar{x} \sin \theta, \quad \bar{x} = \frac{x}{r_0}\end{aligned}\quad (12.8.21)$$

Here, $\kappa = 2\nu$ for the laminar and $\kappa = 5\nu/4$ for the turbulent boundary layer, r_0 and θ are the nose midsection radius and the semivertex angle of a cone or a wedge, the x axis is measured along the lateral surface of the body from the junction with the nose, and $x_{\text{eff},0}$ is the effective length of the nose surface. In the vicinity of the origin, for $\bar{x} \sin \theta \ll 1$, the following expansion is valid

$$\bar{x}_{\text{eff}} - \bar{x}_{\text{eff},0} = B\bar{x}, \quad B = 1 - \kappa \bar{x}_{\text{eff},0} \sin \theta \quad (12.8.22)$$

Usually, $B > 0$; however, the $B < 0$ case is also possible. In other limiting cases, $\bar{r}_b^\kappa \gg 1$, solution 12.8.21 has the following asymptotics

$$\bar{x}_{\text{eff}} = \frac{\bar{x}}{\kappa + 1} + \bar{x}_{\text{eff}}^{(0)}, \quad \bar{x}_{\text{eff}}^{(0)} = \frac{1}{(\kappa + 1) \sin \theta} \quad (12.8.23)$$

Only for $\bar{x} \sin \theta \gg 1$ the effective length of the blunt cone tends to the same limiting value $x/(\kappa + 1)$ as for the sharp cone.

For the sake of illustration, Figure 12.13 plots the curves $\bar{x}_{\text{eff}}(\bar{x})$ for blunt cones with a spherical nose of radius R (in this case $r_0 = R \cos \theta$) and the angles $\theta = 5$ to 40° in the cases of the laminar ($\kappa = 2$, Figure 12.13b) and turbulent ($\kappa = 5/4$, Figure 12.13c) boundary layers; the initial values $\bar{x}_{\text{eff},0}$ are determined from the data in Figure 12.13a. Clearly, the $\bar{x}_{\text{eff}}(\bar{x})$ curves fairly rapidly approach their asymptotics (12.8.23) (dashed curves), particularly for the laminar boundary layer ($\kappa = 2$) and the angles $\theta \geq 10^\circ$.

In conclusion, we will check formulas 12.8.15 and 12.7.1 by comparing their results with the experimental data obtained in shock tubes* for the stagnation parameters corresponding to the conditions of the flight in the Earth's atmosphere with velocities $U_\infty = 7$ to 8 km/s at altitudes $H = 7$ to 37 km in an equilibrium-dissociated air, at freestream Mach numbers $M_\infty = 2$ to 3 and low values of the enthalpy factor $\bar{h}_w = h_w/H_\delta \geq 0.02 - 0.1$. We will also use the available approximations of the experimental results.

The formula for the laminar boundary layer at the stagnation point was obtained by Fay and Riddell (1982) by approximating sets of calculations

$$\begin{aligned} q^{(0)} &= A_l A_{1l} \sqrt{\rho_\delta \mu_\delta} (H_\delta - h_w), & A_l &= 0.76 \text{Pr}^{-0.6}, & A_{1l} &= \omega_{\delta w}^{0.1} A_{2l} \\ A_{2l} &= 1 + (\text{Le}^{0.52} - 1) \frac{h_f}{H_\delta}, & \omega_{\delta w} &= \frac{\rho_w \mu_w}{\rho_\delta \mu_\delta} \end{aligned} \quad (12.8.24)$$

Here, h_f is the specific enthalpy or the air dissociation energy at the outer edge of the boundary layer. The calculations were carried out at $\text{Pr} = 0.7$ and a constant Lewis number $\text{Le} = \rho D C_p / \lambda$ (see 1.3.12, D is diffusivity); the latter enters in formulas 12.8.24 due to the solution of problems within the framework of *heat-conduction-diffusion model* (i.e., solving simultaneously the energy and diffusion equations (cf. Section 13.1) rather than using the effective thermal conductivity λ_{eff} (see 1.2.11)). For $\text{Le} = 1.4$ the formula is in good agreement with the experimental data, though it was derived using the Sutherland formula 1.3.9, which underestimates considerably (by a factor of greater than 1.5 for the temperatures of $(5$ to $6) \cdot 10^3$ K) viscosity in comparison with more accurate data (Figure 1.11b). Were the latter data (formula 1.3.11 for $\rho \mu$) used in formula 12.8.24, for good agreement with experiments it would be well to put $\text{Le} < 1$ in the formula. In view of this fact and taking into account formula 1.3.11 for $\rho \mu$ and Figure 1.8, the results given by formulas 12.8.15 and 12.8.24 are almost coincident. Thus, formula 12.8.15, simpler than formula 12.8.24, is in good agreement with the previously mentioned experimental data (the more so, with account for their considerable, up to a factor of about 1.5, scatter).

It should be noted that the testing of the formulas of this kind is, first, the testing of the adopted physical models, in particular, the transport coefficients used in the calculations, hardly measurable directly in experiments.

For the turbulent boundary layer the previously mentioned experimental data can be approximated by the formula

* The data of Rose and Stark (1958) for the laminar boundary layer at the stagnation point on a sphere and Rose, Probstein, and Adams (1958) for the turbulent boundary layer on the lateral surface of a blunt cylinder at $M_\infty \approx 2$ (see also Hayes and Probstein, 1966).

$$\begin{aligned}
 q_w &= A_t A_{1t} \rho_\delta U_\delta \text{Re}_{e_\delta}^{-0.2} (H_e - h_w), & A_t &= 0.0296 \text{Pr}^{-0.6} \\
 A_{1t} &= 1 + 0.4 \frac{h_f}{H_\delta}, & \text{Re}_\delta &= \frac{\rho_\delta U_\delta x}{\mu_\delta} \\
 \frac{h_f}{H_\delta} &\leq 0.3, & \bar{h}_w &\leq 0.2, & M_\delta &\approx 2
 \end{aligned} \tag{12.8.25}$$

The same estimates as previously used demonstrate the practical equivalency of this formula with formula 12.7.1 under experimental conditions. However, formula 12.7.1 is more general, since formula 12.8.25 is inadequate at high Mach numbers M_δ , as follows from Figure 12.12.

12.9 Viscous-Inviscid Interaction: Basic Effects

The boundary layer problem was considered in Section 12.8 in the classical formulation for a limitingly small value of the ratio of the boundary layer thickness δ to a problem scale L , $\delta/L \ll 1$. The scale L could mean not only the length of the surface exposed to the flow but also a cross-sectional radius r_b of an axisymmetric body, which makes it possible to let $r = r_b$ in system 12.5.5 through 12.5.8 on transition to system 12.5.14.

However, quite often we are forced to go beyond the framework of the classical boundary layer model, particularly in the problems of hypersonic flow past thin bodies, both sharp and blunt, under high-altitude flight conditions, that is, for moderate Reynolds numbers Re and fairly high Mach numbers M_∞ . In this case, certain specific effects associated with the so-called *viscous-inviscid interaction* of the boundary layer with the external flow can occur. These effects often show themselves in combination; however, to elucidate their role, we will consider them individually.

12.9.1 Displacement Effect

As shown in Sections 12.2, 12.4, and 12.5, in order to eliminate the boundary layer effect on the external inviscid flow, the surface in the flow must be moved at a distance equal to the displacement thickness $\delta^*(x)$; otherwise, in the external flow there appear additional disturbances of the order δ^*/L or $\text{Re}^{-1/2}$ for a laminar boundary layer (which will be meant in what follows if otherwise is not stated).

In the problems of hydrodynamics or aerodynamics with Mach numbers $M_\infty \sim 1$ and at moderate flight altitudes, the displacement effect is usually small and, with rare exceptions, is not taken into account. However, the relative boundary layer displacement thickness δ^*/L increases not only as the Reynolds number decreases or the flight altitude increases, but, in accordance with 12.6.22, with the local Mach number M_δ as well. Because of this, starting from certain regimes of the high-altitude hypersonic-vehicle flight, the boundary layer thickness $\delta(x)$ may become comparable with the shock layer thickness and even the thickness of the body itself if the latter is not too large (as shown in Figure 12.17a and b, where $r_s(x)$ is the bow shock). This can lead to an increase in the effective body thickness accompanied by an increase in the pressure, density, heat fluxes, and so on.

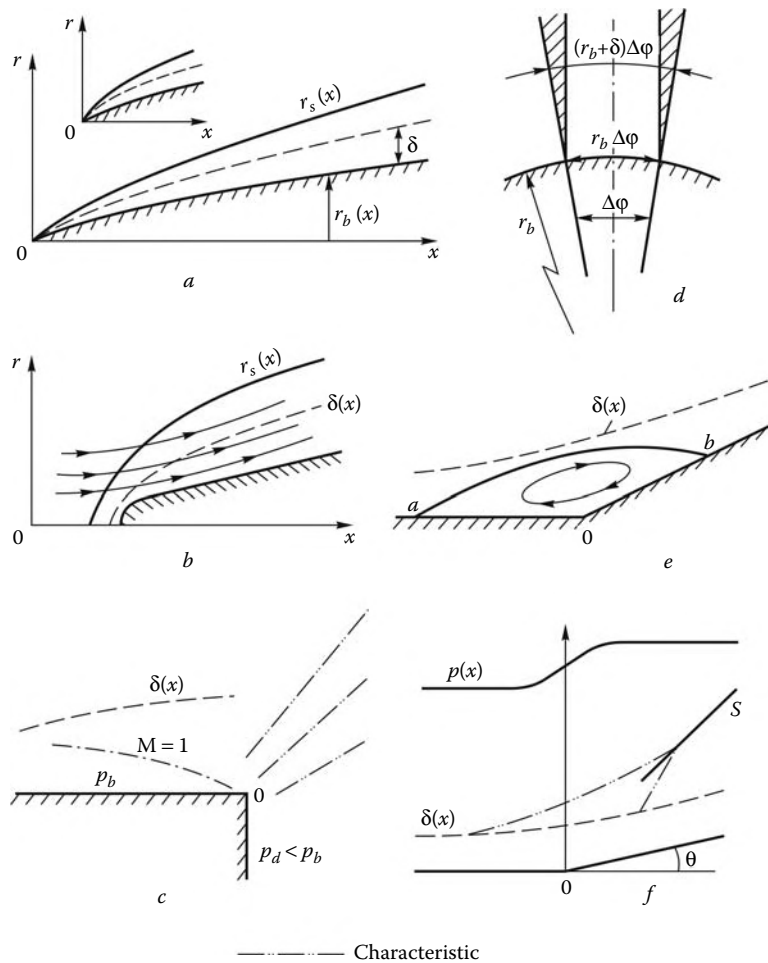
**FIGURE 12.17**

Illustration to viscous-inviscid interaction effects; dash-and-dot lines are characteristics.

12.9.2 Transverse Curvature Effect

At $\delta \sim r_b$ we cannot let $r \approx r_b$ in system 12.5.5 through 12.5.8 with the following transition to system 12.5.14; the former system must be used in its original form. The nature of this effect is obvious from an analysis of Figure 12.27d: due to cumulation of heat or momentum fluxes, fluxes from the peripheral parts of the element $\Delta\varphi$ of the meridional angle, shaded in the figure, are added to the heat flux or friction determined for $r = r_b$.

The transverse curvature effect can be realized in not only hypersonic, but also arbitrary flow regimes, for example, in the flow around a slender, zero-thickness spike with the no-slip condition imposed on its surface, together with that of a given temperature.

12.9.3 End Effects

A smooth surface of an arbitrary body, on which the boundary layer continuously grows, is, naturally, of a finite length and ends, for example, by a base section with the corner

point O (Figure 12.17c), the base pressure p_d being lower than the pressure p_b ahead of the corner point. If the external (with respect to the boundary layer) flow is subsonic, then in the vicinity of the corner point the same effects, as in Sections 5.6 and 6.3, show themselves; these are associated with upstream disturbance propagation. However, even in a supersonic external flow, the flow in the wall region of the boundary layer is subsonic, so that the base pressure inevitably propagates upwind, at least at a distance of the order of the subsonic sublayer thickness, while the sonic line $M = 1$ comes nearer to the corner point. However, in this case the solution of Section 6.3 is unacceptable owing to an appreciable viscosity effect near the wall caused by the no-slip condition imposed. For this reason, in the general case this local problem of the boundary layer turn near a corner point must be solved within the framework of the complete Navier-Stokes equations.

In another case, the body contour can include a concave angle θ and a corner point O , as in Figure 12.17e and g. In an inviscid supersonic flow the local wedge induces a shock S ; this compression wave propagates upwind along the subsonic sublayer of the boundary layer and, for a wedge angle θ larger than a certain limiting value θ_{cr} , produces boundary layer separation with the formation of a viscous return-flow zone bounded by the *separating line ab* (see Figure 12.17e, where $\theta_{cr} \approx 5^\circ$ for a laminar and $\theta_{cr} \approx 10^\circ$ for a turbulent boundary layer, these values being strongly dependent on the flow conditions). For such flows the boundary layer model, even with allowance for the displacement effect, is inadequate.

However, for $\theta < \theta_{cr}$ the compression wave propagating in the subsonic sublayer leads only to flow deceleration and boundary layer broadening (Figure 12.17). This problem pertains to the viscous-inviscid interaction problems.

Except for the flows with separation zones, the nature of the previously mentioned end effects is local and their upwind influence is more or less rapidly attenuated. However, in certain specific situations, the end effects may propagate, at least theoretically, up to the initial point of the boundary layer, like in the case of the subsonic flow past bodies with a corner point on the contour (Section 12.12).

12.9.4 External Flow Nonuniformity Effect

On a slender and fairly long blunt body, the boundary layer develops inside the entropy layer propagating along streamlines with different values s of the entropy (Figure 12.17b); this makes the boundary layer model go beyond the framework of the classical formulation. This situation may be considered more widely as a general problem of the boundary layer development in a nonuniform external flow, for example, behind a boundary-condition discontinuity point (e.g., a temperature discontinuity, as in Figure 12.18a) on the body surface or, say, on a flat plate in a longitudinal nonuniform jet or wake flow (Figure 12.18b).

12.9.5 Non-Thin (or Spread) Shock Effect

Previously we assumed the shock to be limitingly thin as compared with the flow scale length (if relaxation zones were not taken into account) and in a theoretical analysis replaced it by a mathematical surface with the flow parameters satisfying the conservation laws on either side of it. This model is based on the estimates of Section 3.2, in accordance with which the shock thickness Δ is of the order of the mean molecular free path l , while the Reynolds number $Re_\Delta \sim \rho U \Delta / \mu$ is generally of the order of unity and, formally, the ratio $\Delta/\delta \ll 1$, where δ is the boundary layer thickness.

However, actually the thicknesses Δ and δ might be of the same order at fairly high Reynolds numbers. This follows, for example, from Figure 12.19 in which the pressure and

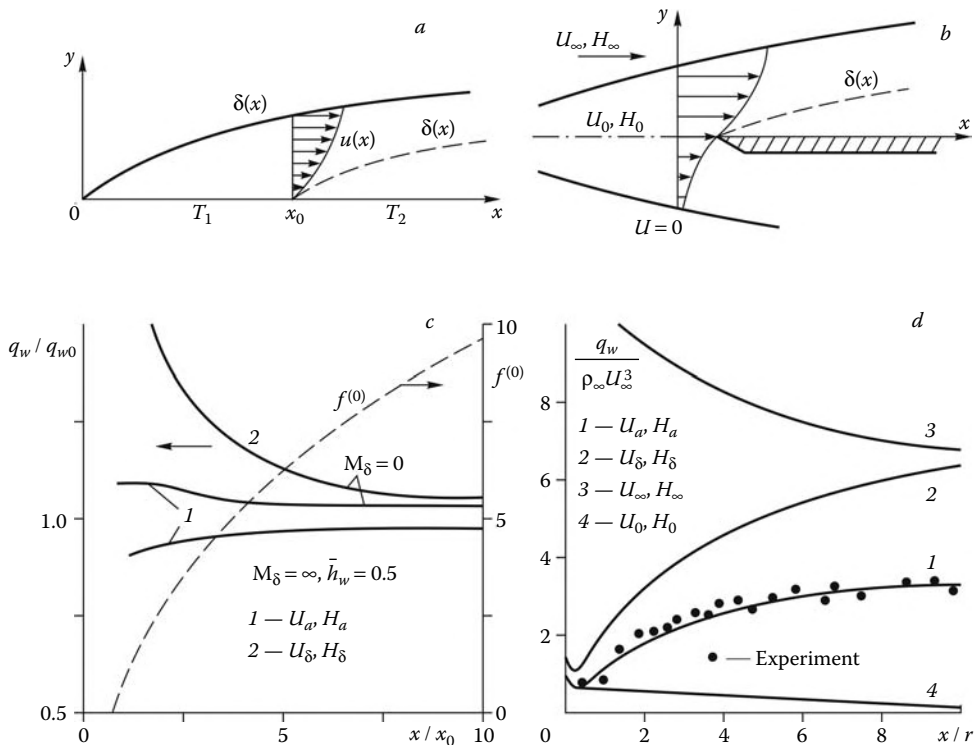


FIGURE 12.18
Boundary layer in a nonuniform flow.

temperature profiles in the shock layer on a sphere calculated (by Gorshkov) within the framework of Navier–Stokes equations are plotted for different Reynolds numbers Re_∞ ; as Re_∞ decreases from 10^4 to 10^2 , the flow behavior varies from near-completely inviscid, with narrow viscous sublayers on the shock layer edges, to completely viscous. In the latter case, the broadened shock front and the boundary layer are merged, the inviscid shock layer as a distinct fragment of the flow no longer exists, and the entire disturbed layer ahead of the body is viscous. This *continuous viscous layer* realized at low Reynolds numbers is governed by the complete system of Navier–Stokes equations.

In the hypersonic flow past bluff and slender blunt bodies (Chapter 9) at moderately high Reynolds numbers the *viscous shock layer* is realized* (*viscous flow model*). In this regime, the shock thickness is relatively small (though not obligatorily vanishingly small) but the boundary layer thickness is comparable with that of the entire disturbed layer, which, in turn, is small compared to the streamwise dimension. This pattern can be described within the framework of the simplified *composite* system of *parabolized Navier–Stokes Equations* 12.5.5 through 12.5.8 (for the sake of brevity, it will be referred to as *PNSE system* or *model*; it will be substantiated in Section 12.14).

* The word thin should be added to this term, since the model is valid only for thin layers. However, in the literature this term is usually applied to a more simplified model in which all the terms, except for the centrifugal Busemann terms, are dropped from the transverse momentum equation. This model was used in Sections 7.8 to 7.13 and will be mentioned in the following.

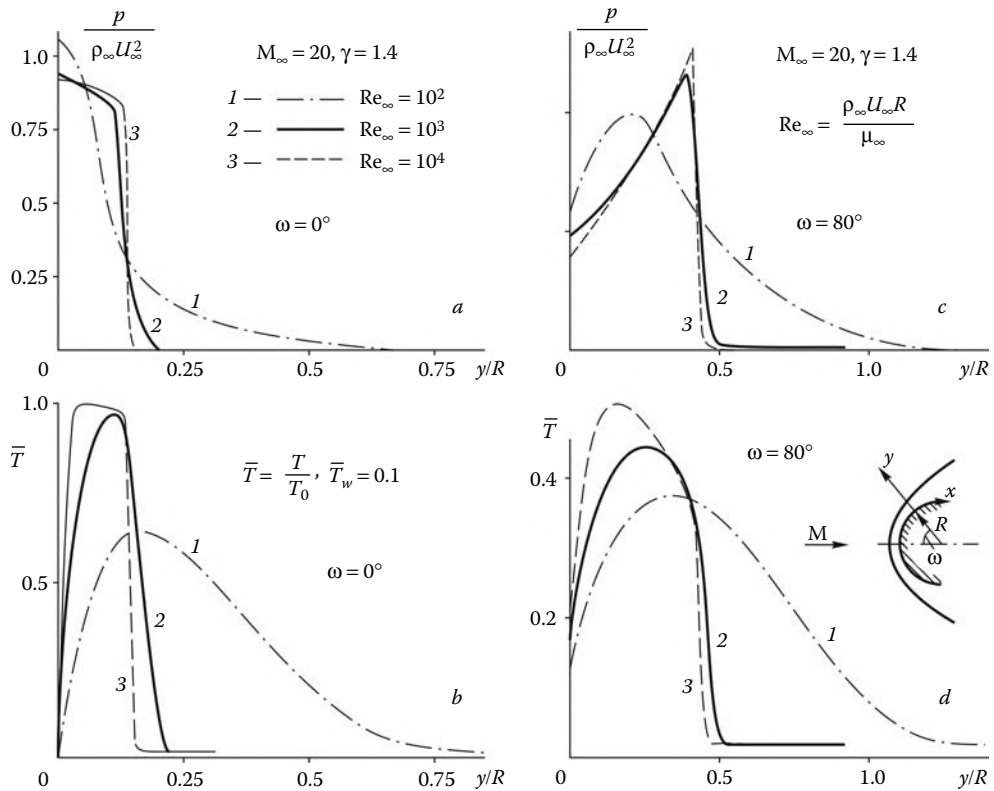


FIGURE 12.19
Pressure and temperature profiles in the shock layer on a sphere.

The conventional boundary-layer model of an inviscid shock layer with a thin shock and a relatively thin, or classical, boundary layer, in which the back influence on the body pressure is small, while the external parameters can be taken from the solution for the inviscid flow, is realized only at high Reynolds numbers.

Obviously, the boundaries of these regimes, as well as the values of the determining Reynolds numbers, are conditional and dependent on both the other flow parameters and the body shape; we shall convince ourselves that this is true in Sections 12.13 and 12.14.

12.10 Boundary Layer in a Nonuniform Flow

We will deal with the general problem formulated in Section 12.5 of the boundary layer subject to boundary conditions 12.5.13, that is, with given nonuniform velocity and enthalpy distributions in a certain initial section x_0 , as shown, for example, in Figure 12.18a and c. This problem is tractable numerically; nevertheless, it is useful to study its distinctive features associated with an *internal boundary layer* developing inside the nonuniform external flow at $x > x_0$ and limiting the domain of influence of the boundary conditions imposed on the surface $y = 0$ in the fluid flow.

A fundamental difference between this internal boundary layer and the classical one is the necessity of matching the former with a precisely nonuniform flow on a more or less conditional interface $\delta(x)$. As in the case of the classical, limitingly thin boundary layer (cf. Section 12.5) this boundary is determined from the condition of smooth matching of the solutions along the normal-to-wall coordinate y in both flow regions, thus separated out. In particular, for the velocity u the following conditions must be fulfilled

$$y = \delta(x), \quad u_I = u_{II}, \quad \frac{\partial u_I}{\partial y} \approx \frac{\partial u_{II}}{\partial y} \quad (12.10.1)$$

Here, the subscripts I and II refer to the quantities above and beneath the interface $\delta(x)$, as shown in Figure 12.20a.

However, in the general case the external velocity profile $U_I(y)$ entering into these conditions does not coincide with the initial profile $U^{(0)}(y)$ in the section $x = x_0$ and, even in an isobaric flow, is deformed with an increase in the longitudinal x coordinate due, first, to viscous dissipation and, second and most important, to the deflection of the external streamlines from the wall by the displacement thickness δ^* of the internal boundary layer.

These conditions can be simplified for a *weakly nonuniform* external flow with the transverse nonuniformity scale Δ much greater than the internal boundary layer thickness δ . Then the ratio of the dissipative terms in the boundary layer equations for the external and internal flow regions is of the order $(\delta/\Delta)^2 \ll 1$, so that the external flow dissipation can be neglected and the flow can be assumed to be inviscid with conservation of the initial distributions of the total energy H and entropy s in streamlines. In this case, the external flow nonuniformity, or *vorticity*, effect reduces to the variation of the flow parameters along

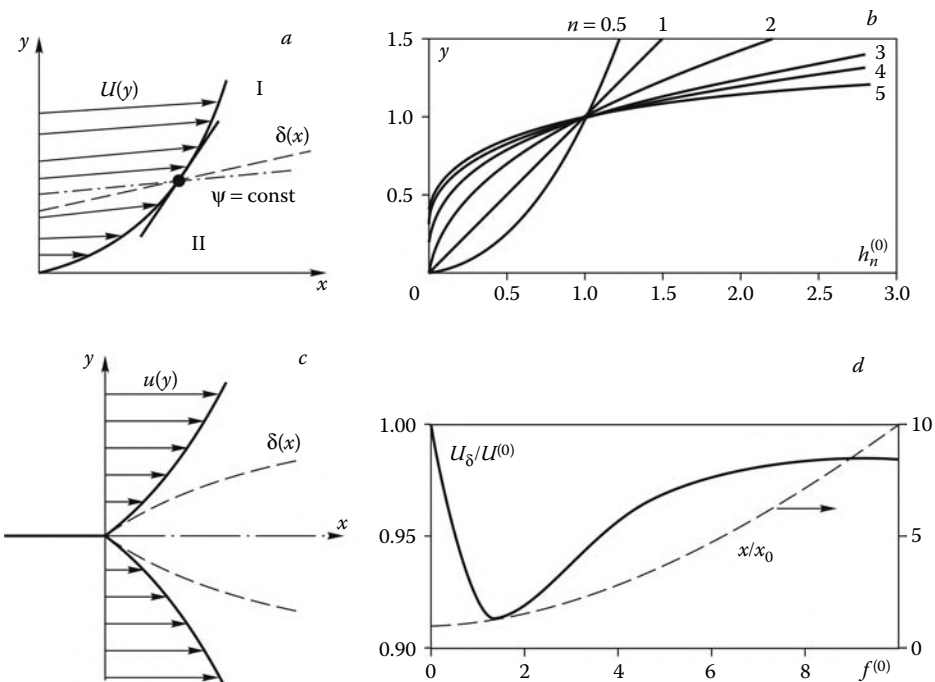


FIGURE 12.20
Boundary layer in a nonuniform flow.

the edge of the internal boundary layer by the quantities of order δ/Δ , which has the effect of the same order (at least, formally) on the internal boundary layer characteristics. Since in an inviscid two-dimensional flow at a given local pressure the distributions of the total enthalpy $H(\psi)$ and the entropy $s(\psi)$ in the streamlines determine also the distributions of the velocity $U(\psi)$ and the enthalpy $h(\psi)$, the conditions of the type 12.10.1 on the edge of the internal boundary layer can be written in a more general form:

$$\begin{aligned} y = \delta : \quad \psi = \psi_\delta, \quad H_{\text{II}}(\psi_\delta) &= H^{(0)}(\psi_\delta), \quad s_{\text{II}}(\psi_\delta) = s^{(0)}(\psi_\delta) \\ \frac{\partial H_{\text{II}}}{\partial \psi} &\approx \frac{\partial H^{(0)}}{\partial \psi}, \quad \frac{\partial s_{\text{II}}}{\partial \psi} \approx \frac{\partial s^{(0)}}{\partial \psi} \end{aligned} \quad (12.10.2)$$

Here, $H^{(0)}(\psi)$ and $s^{(0)}(\psi)$ are the corresponding functions in the initial section $x = x_0$ which do not vary in the inviscid, by assumption, external flow.

We will illustrate the internal boundary layer properties and its interaction with the external nonuniform flow with reference to an example that allows an analytic treatment (Luney and Rumynskii, 1966).

Let an incompressible flow with a constant velocity U_∞ and a nonuniform enthalpy distribution be preassigned in the section $x = 0$. The enthalpy distribution is governed by the following law:

$$\begin{aligned} x = 0 : \quad h_n^{(0)} &= h_c \psi^n \quad (\psi \geq 0), \quad h^{(0)} = 0 \quad (\psi \leq 0) \\ \psi &= \psi' (\rho \mu U_\infty L)^{-1/2}, \quad \psi' = \int_0^y \rho u dy \end{aligned} \quad (12.10.3)$$

Here, ψ' and ψ are the dimensional and dimensionless stream functions, the length scale L is a conditional parameter, and the density ρ , the viscosity μ , and the enthalpy h_c are constant. The family of these curves is schematically presented in Figure 12.20b in the form of the dependence $h_n^{(0)} \sim y^n$ for different n .

In the von Mises variables x, ψ (see 12.3.5) and notation 12.10.3 the system of equations for the longitudinal velocity u and the enthalpy h takes (for $\text{Pr} = \text{const}$) the form:

$$\frac{\partial u}{\partial x} = \frac{\partial}{\partial \psi} \left(u \frac{\partial u}{\partial \psi} \right), \quad \frac{\partial h}{\partial x} = \frac{1}{\text{Pr}} \frac{\partial}{\partial \psi} \left(u \frac{\partial h}{\partial \psi} \right) \quad (12.10.4)$$

Here, the parameters h, u , and x are divided by h_c, U_∞ , and L , respectively. For $u = 1$ the initial-value problem 12.10.3 for the second equation in Equation 12.10.4 has a known solution, which can be presented in the form:

$$h_n = x^{n/2} J_n^{(+)}(f), \quad J_n^{(+)} = \frac{\sqrt{\text{Pr}}}{2\sqrt{\pi}} \int_0^\infty \xi^n e^{-\text{Pr}(f-\xi)^2/4} d\xi, \quad f = x^{-1/2} \psi \quad (12.10.5)$$

As $f \rightarrow \infty$, we have $J_n^{(+)} \rightarrow f^n$ and $h_n \rightarrow \psi^n$, while as $f \rightarrow -\infty$, we have $h_n \rightarrow 0$.

We will now consider an analogous, but *semi-boundary-value*, problem for the domain $\psi \geq 0, x \geq 0$ with the condition $h = h_w = \text{const}$ imposed on the plate $\psi = 0$ (for the present, again with $u = 1$). In this case, the second equation of Equation 12.10.4 has a group solution of the form $h_n = x^{n/2} J_n(f)$, where the function $J_n(f)$ satisfies the equation

$$2J_n'' + \text{Pr}f J_n' - n\text{Pr}J_n = 0 \quad (12.10.6)$$

One of the linear-independent solutions of this equation coincides with $J_n^{(+)}(f)$, while the second solution can be determined from the *Liouville formula*

$$J_n^{(-)}(f) = CJ_n^{(+)} \int_f^{\infty} (J_n^{(+)})^{-2} e^{-f^2/4} df, \quad C = \text{const} \quad (12.10.7)$$

This solution vanishes as $J_n^{(-)} \sim f^n e^{-f^2/4}$ when $f \rightarrow \infty$. Thus, letting $J_n^{(-)}(0) = 1$, by an appropriate choice of C we obtain the general solution

$$\begin{aligned} h_n &= \bar{h}_n + h_0, \quad \bar{h}_n = h_n^{(+)} - h_n^{(-)}, \quad h_0 = h_w J_0^{(-)}(f) \\ h_n^{(+)} &= x^{n/2} J_n^{(+)}(f), \quad h_n^{(-)} = x^{n/2} J_n^{(+)}(0) J_n^{(-)}(f) \end{aligned} \quad (12.10.8)$$

This solution satisfies the conditions $\bar{h}_n = 0$ and $h_0 = h_w$ for $f = 0$ and $h_n \rightarrow \psi^n$ and $h_0 \rightarrow 0$ when $x \rightarrow 0$. The term $h_n^{(+)}$ in 12.10.8 represents the solution of the Cauchy problem formulated previously, while the terms $h_n^{(-)}$ and h_0 introduce corrections for the effect of the boundary condition. These terms decrease when $f \rightarrow \infty$, thus forming an internal boundary layer near the surface considered as the domain of influence of boundary conditions imposed on the latter.

We will now turn to the original, complete problems 12.10.3 and 12.10.4 with the no-slip condition $u = 0$ imposed for $y = \psi = 0$, $x > 0$. In this case, the problem admits a solution similar to 12.10.8, namely

$$u = u(f), \quad h_n = x^{n/2} I_n(f) + h_0 \quad (f \geq 0) \quad (12.10.9)$$

The first equation of the system in Equation 12.10.4 is independent of the second and its solution $u = u(f)$ is the Blasius solution of Section 12.4, though written in other variables, and is obtained by eliminating the variable ζ from the dependence $u = f'(\zeta)$, $f = f(\zeta)$ obtained in Section 12.4, where $f = x^{-1/2}\psi$ is the Blasius function. Therefore, we will turn to the solution for h_n . The function I_n is determined from an equation similar to 12.10.6, though having a more general form*:

$$2(uI'_n)' + \text{Pr}fI'_n - \text{Pr}nI_n = 0 \quad (12.10.10)$$

This equation has also two linearly independent solutions, $I_n^{(+)}$ and $I_n^{(-)}$, increasing and decreasing, respectively, as $f \rightarrow \infty$. For $f \rightarrow \infty$ the function $u \rightarrow 1$ in accordance with a power law (Sections 12.2 and 12.4), while Equation 12.10.10 coincides with Equation 12.10.7, so that it can be assumed that $I_n^{(+)} \rightarrow J_n^{(+)}$. Correspondingly, as $f \rightarrow \infty$, the second solution decreases, in accordance with the same law, as $J_n^{(-)}$. Therefore, by analogy with 12.10.8, the solution of this problem can be presented, letting $J_n^{(-)}(0) = 1$, in the form:

$$\begin{aligned} h_n &= \bar{h}_n + h_0, \quad \bar{h}_n = h_n^{(+)} - h_n^{(-)}, \quad h_0 = h_w I_0^{(-)}(f) \\ h_n^{(+)} &= x^{n/2} I_n^{(+)}(f), \quad h_n^{(-)} = x^{n/2} I_n^{(+)}(0) I_n^{(-)}(f) \end{aligned} \quad (12.10.11)$$

For $\text{Pr} = 1$ the function $I_0^{(-)} = 1 - u$, while the term h_0 is simply the Crocco integral 12.6.15. As previously, the terms $h_n^{(-)}$ and h_0 also have an effect on the boundary layer

* The tables of the functions $I_n(f)$ for $\text{Pr} = 0.71$ and $n \leq 5$ are presented in the paper cited previously.

formation, limiting the influence of the conditions imposed on the wall ($y = \psi = 0$) with an exponential decay of the effect of these conditions on the external solution as $f \rightarrow \infty$ or $\zeta \rightarrow \infty$.

Generally speaking, in the problems considered the initial enthalpy profile $h_n^{(0)}(\psi)$ varies with x due to the heat-conduction effect, so that in the general case $h_n(\psi) \neq h_n^{(0)}(\psi)$ for $x > 0$. However, it turns out that for comparatively small values $n < 2$ the enthalpy (temperature) distribution in streamlines is almost unaltered up to the intersection of the corresponding streamlines with the edge of the internal boundary layer $f = f_\delta$ or $\zeta = \zeta_\delta$. For the complete problems 12.10.9 and 12.10.10 this follows from the table data calculated for the ratio $\lambda_n = h_n/h_n^{(0)}$ at the boundary values $\zeta_\delta = 5.2$, or $f_\delta = 3.3$, and $\text{Pr} = 0.72$

n	1/2	1	2	3	4	5
λ_n	0.96	1.00	1.22	1.68	2.50	4.10
λ'_n	0.97	1.00	1.25	1.75	2.50	3.50
q_w/q_{w0}	0.97	0.98	0.96	0.86	0.71	0.51

We note that the deformation of the initial profile depends only on its form, but is independent of the Reynolds number. In fact, the deviation of the function $h_n(\psi)$ from the initial one $h_n^{(0)}(\psi)$ at the points where the corresponding streamlines $\psi = \text{const}$ enter the internal boundary layer, is, as follows from Equation 12.10.4 of the order

$$\Delta h_n \approx \frac{\partial^2 h_n^{(0)}}{\partial \psi^2} \approx \frac{1}{\text{Pr} f_\delta^2} \psi^2 \frac{\partial^2 h_n^{(0)}}{\partial \psi^2} \quad (12.10.12)$$

For the same value $f_\delta = 3.3$ and $\text{Pr} = 0.72$ the increment of the function h_n obtained from the Equation 12.10.12 is equal to $\Delta h_n = 0.125n(n - 1)h_n^{(0)}(\psi)$, while the ratio $\lambda'_n = h_n(\psi)/h_n^{(0)}(\psi)$ is given in the table and is similar in value to λ_n . For $n = 1$ the initial profile $h_n^{(0)}(\psi)$ remains, naturally, unaltered outside the boundary layer (as for $n = 0$); this follows directly from the second equation of Equation 12.10.4.

Another example is furnished by the development of an internal boundary layer from the point $x = x_0$ inside the boundary layer on a flat plate. The ratio $U_\delta/U^{(0)}$ of the velocity on the edge of the internal boundary layer to its initial (at $x = x_0$) value is shown in Figure 12.20d and is within the limits from 0.9 to 1. In the same figure, the function $f^{(0)} = x_0^{-1/2}\psi$ is plotted on the abscissa axis; the function is constant along streamlines, so that on the edge of the internal boundary layer we put $f^{(0)} = f_\delta(x'/x_0)^{1/2}$, where $x' = x - x_0$ and $f_\delta = 3.3$. The inverse dependence $x/x_0 = 1 + 0.1(f^{(0)})^2$ is also presented in Figure 12.20d.

Thus, for not too steep initial profiles of the flow parameters, the flow in the external, relative to the internal boundary layer, region can be assumed to be nondissipative and inviscid; moreover, in the previous examples the nonuniformity scales for the external and internal flow regions, Δ and δ , are of almost the same order, which is important for applications of the theory.

In the last problem considered, the initial velocity profile at point x_0 is linear in y near the wall, $u^{(0)} = \omega y$, where $\omega = \tau_w/\mu$, τ_w being the local friction on the wall; therefore, on

the edge of the δ -thick internal layer the velocity is of the order $u_\delta \sim \omega\delta$, and from estimate 1.16.6 we obtain

$$\delta \sim \left(\frac{vx'}{u_\delta} \right)^{1/2} \sim \left(\frac{vx'}{\omega\delta} \right)^{1/2}, \quad \delta \sim \left(\frac{vx'}{\omega} \right)^{1/3}, \quad x' = x - x_0, \quad v = \mu\rho \quad (12.10.13)$$

In this connection we will also mention the Goldstein problem (1930) on the development of the wake behind a zero-thickness plate (Figure 12.20c; this problem is, probably, one of the first problems of this kind). As the flow is shed from the plate's trailing edge at point $x = 0$, the flow accelerates in accordance with a law determined by the equation of motion on the axis, which, at a linear velocity profile ahead of the edge, $u^{(0)} = \omega y$, and in view of Equation 12.10.13, leads to the following law of the velocity u_0 variation on the wake axis ($y = \psi = 0$)

$$u_0^2 \sim vx \frac{\partial^2 u}{\partial y^2} \sim \frac{v\omega x}{\delta}, \quad u_0 \sim (\omega^2 vx)^{1/3} \quad (12.10.14)$$

A detailed description of this problem can be found, for example, in Sychev (1987).

12.11 Method of Mass-Average Parameters for the Boundary Layer in a Nonuniform Flow

In Section 12.8 we presented the engineering *effective-length method* for calculating the heat flux and friction distributions over bodies in the case of classical, that is, limitingly thin (see Sections 12.3 and 12.5) boundary layers. It might seem that this method could be generalized to the boundary layer in a nonuniform flow by using the flow parameters on the outer edge of the boundary layer (u_δ, H_δ , etc.) instead of those in the inviscid oncoming stream.

However, it turns out that such a generalization can lead to inaccuracies caused by the violation of the conservation laws in the internal boundary layer. In fact, using, say, the local velocity $u_\delta = u(\psi_\delta)$ in a certain section $x = x_1$ of the internal boundary layer on a flat plate is associated with the assumption, as applied to the analysis drawn in Section 12.8, that this is the longitudinal momentum flux $u_{\delta 1}\psi_{\delta 1}$ that has entered the internal boundary layer; however, this value can be overestimated, if, for example, on the interval $x_0 \leq x \leq x_1$ the velocity $u_\delta < u_{\delta 1}$, or $\psi_\delta < \psi_{\delta 1}$, as in the example in Figure 12.20a.

In this connection, it seems natural to assume that such basic boundary layer characteristics as the wall friction and the heat flux to the wall are determined by the overall momentum and total-enthalpy fluxes across the boundary layer edge rather than by the local parameters on this line. The implementation of this idea leads to a hypothesis that some *mass-average values* of the velocity U_a and the total enthalpy H_a must be used in the formulas of the effective length method (Section 12.8) rather than local external parameters. These mass-average parameters are expressed in terms of the integrals (Lunev, 1967)

$$U_a(p, \psi) = \frac{1}{\psi_\delta} \int_0^{\psi_\delta} U^{(0)}(p, \psi) d\psi, \quad p = p(x)$$

$$H_a = \frac{1}{\psi_\delta} \int_0^{\psi_\delta} H^{(0)}(\psi) d\psi, \quad h_a = H_a - \frac{1}{2} U_a^2 \quad (12.11.1)$$

Here, $p(x)$ is the local pressure, while $U^{(0)}(p, \psi)$ and $H^{(0)}(\psi)$ are the distributions of the corresponding parameters in the flow external with respect to the boundary layer; the external flow is assumed to be inviscid in accordance with the conclusions made in Section 12.10. The mass-average enthalpy h_a is expressed in terms of U_a and H_a from the Bernoulli equation.

To determine the mass-average values of the flow parameters on the outer edge of the boundary layer, the gas flow rate $\psi_\delta(x)$ across this line must be known. Under the same assumptions as those made previously and in Section 12.8, for a laminar boundary layer we set

$$\psi_{\delta l} = (2\pi)^v r^v f_{\delta l} (\rho_{*a} \mu_{*a} U_a x_{\text{eff},l})^{1/2} \quad (12.11.2)$$

where $f_{\delta l} = f_\delta = 3.3$, the effective length x_{eff} is determined from formula 12.8.11, and the parameters ρ_{*a} and μ_{*a} are calculated from the local pressure and the determining enthalpy h_* with H_a and h_a substituted for H_δ and h_δ in formula 12.6.19. For a turbulent boundary layer we let (cf. Section 12.7)

$$\frac{u}{U_a} = \left(\frac{y}{\delta_t} \right)^{1/7}, \quad \delta_t = 0.38 x_{\text{eff},t} \text{Re}_{*a}^{-0.2}, \quad \text{Re}_{*a} = \frac{\rho_{*a} U_a x_{\text{eff},t}}{\mu_{*a}} \quad (12.11.3)$$

Then, under the same assumptions, we obtain

$$\psi_{\delta t} = (2\pi)^v r^v f_{\delta t} \mu_{*a}^{1/5} (\rho_{*a} U_a x_{\text{eff},t})^{4/5}, \quad f_{\delta t} = 0.33 \quad (12.11.4)$$

The formulas for ψ_δ are conveniently replaced by the differential equations obtained by taking account of Equation 12.8.11

$$\begin{aligned} \frac{d\psi_{\delta l}^2}{dx} &= (2\pi r_b)^{2v} f_{\delta l}^2 \rho_{*a} \mu_{*a} U_a \\ \frac{d\psi_{\delta t}^{5/4}}{dx} &= (2\pi r_b)^{5v/4} \rho_{*a} \mu_{*a}^{1/4} U_a \end{aligned} \quad (12.11.5)$$

Thus, the generalization of the effective length method to the mass-average parameter method is based on the assumption that the heat flux and friction on a wall q_w and τ_w are determined by the same formulas 12.8.10 to 12.8.14, only with the parameters U_a and H_a substituted for the boundary parameters U_δ and H_δ , and the gas flow rate ψ_δ .

The reasoning behind the method proposed is intuitive and needs testing, which will be performed here with reference to several examples.

1. For the problem of the power-law enthalpy profile $h_n \sim \psi^n$ in the initial section of the boundary layer considered in Section 12.10, the approximate-to-exact heat-flux ratios q_w/q_{w0} (for $h_w = 0$) are given in the table in the same section. Clearly, for $n \leq 2$ the accuracy of the approximate method is rather high, while for $n = 3$ it is fairly satisfactory. At higher n the deformation of the enthalpy profile in the external flow manifests itself, leading to an increase in the enthalpy on the outer edge of the boundary layer and, hence, in the heat flux.
2. In Figure 12.18b (Section 12.9) we presented the heat flux distribution q_w/q_{w0} for the laminar boundary layer on a flat plate downstream of the point $x = x_0$ at which the exact velocity and enthalpy profiles were preassigned. Here, a new internal boundary layer at $x > x_0$ is actually absent; this is simply a test problem. Clearly, curves 1 calculated by the mass-average parameter method are very close to unity,

whereas curve 2 calculated from the external parameters of the internal boundary layer (with the velocity $U^{(0)}$ substituted for U_a in formula 12.11.2 for ψ_δ) gives an appreciably overestimated heat flux up to rather long distances $x/x_0 \approx 5$. In the same figure, we have presented the $f^{(0)} = x_0^{-1/2} \psi_\delta$ curve, the function $f^{(0)}$ being in proportion to the gas flow rate through the internal boundary layer. The gas flow rate through the initial section $x = x_0$ of the external boundary layer is equal to $\psi^{(0)} = x_0^{1/2} f_\delta$, where $f_\delta = 3.3$; therefore, as follows from the behavior of curve 2, the initial section effect decays only when the boundary layer absorbs an about threefold initial gas flow rate.

Let now the plate have different temperatures, T_1 for $x < x_0$ and T_2 for $x > x_0$. Then for a small vicinity of the point x_0 , in the domain of influence of the linearity of the velocity and temperature profiles, at $\text{Pr} = 1$ and $\rho\mu = \text{const}$ the heat flux distribution for $x > x_0$ is determined by the mass-average parameter method from the formula*

$$\begin{aligned} q_w &= aq_{w0}(1 + \bar{x}^{-1/3}\kappa\Theta), \quad \Theta = \frac{h_{w2} - h_{w1}}{H_\delta - h_{w1}}, \quad \bar{x} = \frac{x - x_0}{x_0} \\ a &= (8/9)f_w''f_\delta \approx 0.975, \quad \kappa = 3(4f_w''f_\delta)^{-2/3} \approx 1.12 \end{aligned} \quad (12.11.6)$$

Here, q_{w0} is the heat flux immediately to the left of point x_0 . Clearly, q_w increases without bound as $x \rightarrow x_0$.

This solution almost coincides with the exact solution (presented in the same work) and can be used to interpret the indications of a small, usually copper, calorimeter measuring heat fluxes on the surface of another material. The average heat flux \bar{q}_w to the Δx -long calorimeter is as follows (we let $a = 1$):

$$\bar{q}_w = q_{w0} \left[1 + \frac{3}{2}\kappa \left(\frac{x_0}{\Delta x} \right)^{1/3} \right] \quad (12.11.7)$$

3. In Figure 12.18d we have presented the calculated and measured heat fluxes on a flat plate set along the streamline separating the mixing zone and the ambient gas at rest in the case of a two-dimensional supersonic turbulent jet (simulated by an initial region of the jet issuing from an axisymmetric nozzle; Karpov, 1971). The mass-average parameter method provides good agreement with the experimental data, whereas the calculation using the external parameters of the boundary layer overestimates heat fluxes almost twofold. As for the calculations using the data on the outer boundary of the jet or the separating streamline (curves 3 and 4), these are completely inadequate.
4. In a supersonic or hypersonic flow past a blunt body in the vicinity of the stagnation point the gas velocity increases normal to the body (Figure 7.23 from Section 7.8). Because of this, at a finite thickness of the boundary layer the gas velocity at the outer edge of the boundary layer differs from that on the wall and the corresponding solutions of Sections 12.6 and 12.8 give an error that will be evaluated in the following.

Since in the plane flow the derivative of the velocity with respect to the normal to the wall is zero, we restrict ourselves to axisymmetric flows (see Section 12.13 for

* The formula was obtained in the work of Zemlyanskii and Marinin (1974) who solved also a more general problem including gas injection into the $x < x_0$ region.

details). In this case, in the vicinity of the blunt-body stagnation point in curvilinear coordinates x, y fitted to the body surface, the gas velocity varies in accordance with the law

$$\begin{aligned} U^{(0)} &= cx(1+by) = cx(1+z)^{1/2} = c^{(0)}x \\ c, b &= \text{const}, \quad z = \frac{b\psi}{\pi\rho cx^2} \end{aligned} \quad (12.11.8)$$

In this case, the mass-average velocity is as follows:

$$U_a = c_a x, \quad c_a = c\varphi(z_{\delta a}), \quad \frac{1}{2}\varphi(z) = \frac{(1+z)^{3/2} - 1}{3z} \quad (12.11.9)$$

Compared with Equation 12.11.2 we obtain the boundary values of $z_\delta^{(0)}$ and $z_{\delta a}$

$$z_\delta^{(0)} = \left(\frac{c^{(0)}}{c}\right)^{1/2} \Omega, \quad z_{\delta a} = \left(\frac{c_a}{c}\right)^{1/2} \Omega, \quad \Omega = f_\delta \left(\frac{\mu}{\rho c}\right)^{1/2} b \quad (12.11.10)$$

The quantity c_a is determined from the equation $c_a = c_0\varphi(z_{\delta a})$, while the ratio $q_w/q_w^{(0)} = (c_a/c)^{1/2}$ of the heat fluxes calculated with and without taking vorticity into account is plotted in Figure 12.21 versus Ω for $v = 1$ and $f_\delta = 3.3$ (curves 1) and is fairly close to the exact curve 3 (Kemp, 1958). At the same time, the calculation using the external boundary velocity $U^{(0)}(z_\delta^{(0)})$ (curve 2) appreciably overestimates the heat flux value.

The examples considered are fairly general in order to make the conclusion on a quite satisfactory accuracy of the mass-average parameter method, at least, for estimating the nature of the external nonuniformity and, maybe, other disturbances introduced into the boundary layer through its outer edge. Additional testing of the method for blunt bodies will be performed in Section 12.13.

However, similar averaging methods are completely inadequate to allow for disturbances introduced near the body surface. To elucidate this question, we will consider the

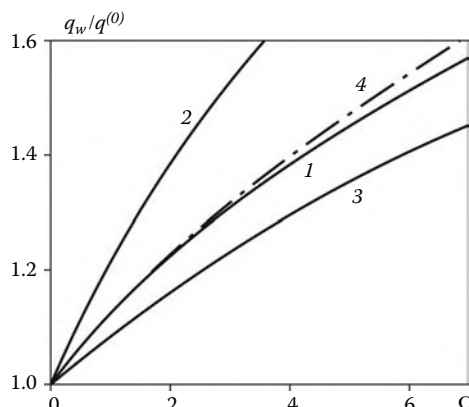


FIGURE 12.21
Vorticity effect on the heat flux at the stagnation point on a body of revolution.

self-similar solution for an incompressible boundary layer on a flat plate with internal heat sources of the form $Q(x, \zeta) = (H_\delta U_\delta/x)Q_1(\zeta)$. This problem possesses a simple solution which will be written down only for a near-pointwise source of heat released in a small vicinity of point ζ_0 at $\text{Pr} = 1$

$$\frac{\Delta q}{q_0} = Q_0 \frac{1 - f'(\zeta_0)}{f''(\zeta_0)}, \quad Q_0 = \int_0^\infty Q_1 d\zeta \quad (12.11.11)$$

Here, Δq is the heat flux increment due to the internal heat release. In this case, we determine the mass-average total gas enthalpy as follows:

$$H_a = H_\delta + \frac{1}{\psi_\delta} \int_0^x \int_0^\delta \rho Q dx dy = H_\delta \left(1 + \frac{2}{f_\delta} Q_0 \right) \quad (12.11.12)$$

For large ζ_0 using the L'Hospital rule and the Blasius equation $2f'' = -ff'''$, from Equation 12.11.11 we obtain $\Delta q/q_0 \approx 2Q_0/f(\zeta_0)$; for $\zeta_0 \approx \zeta_\delta$ and $f \approx f_\delta$ this result coincides with the approximate result $\Delta q/q_0 = 2Q_0/f_\delta$ obtained by the mass-average parameter method with account for 12.11.12, which was asserted previously. At the same time, as $\zeta_0 \rightarrow 0$ the exact value $\Delta q/q_0 \approx Q_0/f_w''$, where $f_w'' = f''(0) = 0.332$, is by a factor of about five greater than the approximate value. In this case, all the heat released goes directly to the wall without heating the gas in the boundary layer and producing any mass-average effect.

12.12 Hypersonic Boundary Layer on Thin Sharp Bodies

The inviscid hypersonic flow past thin sharp bodies was considered in Chapter 8. In what follows, we will generalize the results obtained in that chapter to the flows of viscous and heat-conducting gases, with our attention concentrated on the viscous-inviscid interaction effects discussed in Section 12.9.

In the hypersonic flow past thin sharp bodies, the orders of the flow parameters in an inviscid shock layer* are determined by the relation of Equation 8.2.7 in which the relative boundary layer displacement thickness δ^*/L (L is the length scale) should be added to the relative body thickness θ_0 and the parameter ε should be replaced by

$$\varepsilon = M_\infty^{-1} + \theta_0 + \delta^*/L \ll 1 \quad (12.12.1)$$

Here, the subscript ∞ refers to the freestream conditions. In the shock layer, the longitudinal velocity is equal to the total velocity, $u \approx U \approx U_\infty$, the total enthalpy is $H \approx U_\infty^2/2$, and the Mach number is of the order $M \sim \varepsilon^{-1} \gg 1$, that is, the shock-layer flow is still hypersonic.

At the same time, inside the boundary layer, in accordance with estimates 12.5.10, the enthalpy is of the order $h \sim h_* \sim H_\delta = H_\infty$, where h_* is the characteristic, for example,

* In this section the term *inviscid shock layer* refers to the inviscid flow region between the thin bow shock and the boundary layer.

determining enthalpy in the boundary layer (see 12.6.15). In order to determine other characteristic boundary layer parameters, such as ρ_* and μ_* entering in formulas 12.5.9, 12.6.4, 12.6.5, and so on, we will express them in terms of the freestream parameters ρ_∞ , h_∞ , and μ_∞ via Equation 1.3.11 and the equation of state for a perfect gas

$$\begin{aligned} \rho_*\mu_* &= \rho_\infty\mu_\infty \left(\frac{h_*}{h_\infty} \right)^{-n} \frac{p_\delta}{p_\infty} = \rho_\infty\mu_\infty \left(\frac{H_\infty \bar{h}_*}{h_\infty} \right)^{-n}, \quad \bar{h} = \frac{h}{H_\infty} \\ \frac{p}{\rho h} &= \frac{\gamma - 1}{\gamma}, \quad \frac{\rho_* h_*}{\rho_\infty h_\infty} = \frac{p_\delta}{p_\infty} = \gamma M_\infty^2 \bar{p}_\delta \\ \bar{p} &= \frac{p}{\rho_\infty U_\infty^2}, \quad \frac{H_\infty}{h_\infty} = \frac{\gamma - 1}{2} M_\infty^2 \end{aligned} \quad (12.12.2)$$

Here, $p_\delta \sim \rho_\infty U_\infty^2 \varepsilon^2$ is the pressure at the outer edge of the boundary layer, the parameters on which are referred by the subscript δ , and, therefore, in accordance with 12.5.12 within the layer as well.

In accordance with the results of Section 12.5, the displacement effect is, strictly speaking, determined by the boundary layer displacement thickness δ^* rather than its thickness δ . For an axisymmetric, finite-thickness boundary layer, expression 12.5.15 for δ^* should be generalized. For this purpose, as in the derivation of formula 12.5.15, we equate the gas flow rate through the boundary layer and the rate of the external flow with the parameters ρ_δ and $U_\delta = U_\infty$ between the outer surface of the boundary layer with the radius r_σ and the displacement surface of radius r^* (for a thin body, the radius $r = r_b(x) + y$, where y is the same, normal to the body surface $r = r_b(x)$, coordinate as previously). As a result, we obtain the relation

$$\begin{aligned} \psi_\delta &= (2\pi)^\nu \int_0^\delta \rho u r^\nu dy = \pi^\nu \rho_\delta U_\infty (r_\sigma^{1+\nu} - (r^*)^{1+\nu}) \\ r_\sigma &= r_b + \delta, \quad r^* = r_b + \delta^* \end{aligned} \quad (12.12.3)$$

Since $\psi_\delta \sim \rho_* U_\infty r_\sigma^\nu \delta$, hence follows the estimate

$$\frac{\delta - \delta^*}{\delta} \sim \frac{\rho_*}{\rho_\delta} \sim \bar{h}_\delta \sim \frac{h_\delta}{H_\infty} \sim M_\delta^{-2} \ll 1 \quad (12.12.4)$$

Thus, for a hypersonic boundary layer the thicknesses δ and δ^* almost coincide, since the relative enthalpy \bar{h}_δ is small, together with M_δ^{-2} (these estimates are also illustrated in Figure 12.11).

Hence follow two important conclusions. First, that the outer edge δ of the hypersonic boundary layer is clearly defined, since the term f_δ in 12.6.23, which introduces a certain conventionality in its definition, is relatively small. Second, that the ratio $\psi_\delta/\psi_s \sim \rho_*/\rho_\delta$ of the flow rate ψ_δ to the flow rate ψ_s through a layer of thickness δ but with the shock-layer parameters, is small.

Thus, in the $M_\delta \rightarrow \infty$ limit it can be assumed that the external inviscid flow streams past a certain *effective* body whose shape $r = r_\sigma(x)$ coincides with the edge of the boundary layer, for which the limiting external conditions can be imposed on a clearly defined boundary

$$y = \delta(x) : \quad h_\delta = 0, \quad u = U_\delta = U_\infty \quad (12.12.5)$$

We note that the condition $h_\delta \approx 0$ makes the density at the boundary layer edge ρ_δ indefinite; because of this, the notion of the displacement thickness δ^* determined, for example,

by formulas 12.5.15 or 12.12.3 involving ρ_δ , loses its meaning. However, in the variables ξ , ζ (see 12.6.4), more adequate for a compressible boundary layer, it should be expected that, as $\zeta \rightarrow \infty$, the enthalpy vanishes ($h \rightarrow 0$) and the density increases without bound following an asymptotic exponential law, which ensures the convergence of the integral $\bar{\zeta}$ in 12.6.5 and, therefore, the finite value $y \rightarrow \delta$ when $\zeta \rightarrow \infty$ (an analogous approach was used for solving the Stewartson problem in Section 6.10).

In order to estimate the boundary layer thickness and, moreover, to derive an approximate formula for it, we will take into account that, as shown in Section 8.4, the shock layer flow is determined by the parameter $M_\infty \varepsilon$ and, therefore, also the parameter $\tilde{\delta} = M_\infty \delta / L$, which can conveniently be expressed in terms of the freestream parameters ρ_∞ , and so on. For this purpose, from formula 12.6.5 or 12.6.23, taking 12.12.2 into account, we obtain

$$\begin{aligned}\tilde{\delta} \sim \tilde{\delta}_\xi &= \frac{M_\infty \delta}{\xi} = K_1 \left(\frac{p_\infty}{p_\delta} \right)^{1/2} \chi_\xi, \quad \chi_\xi = \frac{M_\infty^{3-n}}{\sqrt{\text{Re}_{\infty\xi}}} \sim \chi = \frac{M_\infty^{3-n}}{\sqrt{\text{Re}_{\infty L}}} \\ \text{Re}_{\infty\xi} &= \frac{\rho_\infty U_\infty \xi}{\mu_\infty}, \quad \text{Re}_{\infty L} = \frac{\rho_\infty U_\infty L}{\mu_\infty}\end{aligned}\quad (12.12.6)$$

Here, the coefficient K_1 is as follows:

$$K_1 = \left(\frac{\gamma - 1}{2} \right)^{1-n/2} \bar{h}_*^{-n/2} K, \quad \bar{h} = \frac{h}{H_\infty}, \quad K = \bar{h}_\delta \bar{\delta}_* \quad (12.12.7)$$

Here, the coefficient K and the function $\bar{\delta}_*$ are the same as in formula 12.6.22 and obtained from the comparison with the latter. Obviously, the coefficient K has a finite limit as $h_\delta \rightarrow 0$ or $M_\delta \rightarrow \infty$; with account for this limit and using also the expression of Equation 12.6.9 for h_* for estimates we obtain the following formulas for the coefficient K_1 as $M_\delta \rightarrow \infty$

$$\begin{aligned}K_1 &= \left(\frac{\gamma - 1}{2} \right)^{1-n/2} (1.72 \bar{h}_w + 0.664)(0.35 + 0.5 \bar{h}_w)^{-n/2}, \quad \text{Pr} = 1 \\ K_1 &= \left(\frac{\gamma - 1}{2} \right)^{1-n/2} (1.94 \bar{h}_w + 0.58)(0.35 + 0.5 \bar{h}_w)^{-n/2}, \quad \text{Pr} = 0.72\end{aligned}\quad (12.12.8)$$

For \bar{h}_w ranging from 0 to 1, $\gamma = 1.4$, and $n = 0.3$ we have $K_1 = 0.2$ to 0.63 for $\text{Pr} = 1$ and $K_1 = 0.175$ to 0.66 for $\text{Pr} = 0.72$.

Based on the effective length method, we can hope that formula 12.12.8 is reliable for plane ($v = 0$) and, by straining a point, axisymmetric ($v = 1$) flows at $\delta > r_b$. However, at $v = 1$ and $\delta > r_b$ the boundary layer velocity profiles can, as shown in the following, be appreciably different from the Blasius profile upon which the formulas of Equation 12.12.8 are based.

The formulas obtained demonstrate clearly the viscous-inviscid interaction process due to the displacement effect: the thickness δ is dependent on the local pressure p_δ which, in turn, depends on δ . Letting $p_\delta \sim \rho_\infty U_\infty^2 \varepsilon^2$ in 12.12.6 and taking 12.12.1 into account, we obtain a relation between the parameters $\tilde{\delta}$, M_∞ , θ_0 , and χ

$$(1 + M_\infty \theta_0 + \tilde{\delta}) \tilde{\delta} = \bar{K} \chi \quad (12.12.9)$$

where \bar{K} is a coefficient independent of the previous parameters. Using this relation, we will analyze the limiting viscous-inviscid interaction regimes caused by the displacement effect or, in what follows, simply the *interaction effect*.

Weak interaction is realized at $\chi \ll 1$. In this case, the relation of Equation 12.12.9 takes the form $(1 + M_\infty \theta_0) \tilde{\delta} = \bar{K} \chi$; these problems can be solved using linearization of the inviscid problem at the thickness δ^* calculated within the framework of the classical boundary layer model.

By way of illustration, we present the solution for a flat plate ($\theta_0 = 0$) with a sharp leading edge using formula 12.12.8 at $\xi = x$ and formula 2.8.4 of the linear theory for the pressure on a thin wing in a hypersonic ($M_\infty \gg 1$) flow

$$\frac{\Delta p}{p_\infty} = \gamma M_\infty \frac{d\delta}{dx} = \frac{1}{2} \gamma K \chi_x \quad (\chi_x = \chi \text{ for } L = x) \quad (12.12.10)$$

In Figure 12.22 we have presented the experimental pressure ratios p/p_∞ for a thermally insulated plate ($\bar{h}_w \approx 1$) in a hypersonic flow. The figure is taken from Hayes and Probstein (1966); measured along the abscissa axis is the parameter $\bar{\chi} = [(\gamma - 1)/2]^{-n/2} \chi_x = 1.27 \chi_x$ (in our designations). The dependence is near-linear in $\bar{\chi}$ up to $\bar{\chi} \approx 3$ and is on this range in fairly good agreement with formula 12.12.10, $p/p_\infty - 1 - 0.43 \chi_x = 0.32 \bar{\chi}$ (line 1).

Strong interaction is realized when the conditions $\chi \gg 1$ and either $\tilde{\delta} \sim M_\infty \theta_0$ or $\tilde{\delta} \gg M_\infty \theta_0$ are simultaneously fulfilled. In this case, relation 12.12.9 reduces to the formula $(M_\infty \theta_0 + \tilde{\delta}) \tilde{\delta} = \bar{K} \chi$, where $\tilde{\delta} \sim \chi^{1/2} \gg 1$. These conditions mean that the boundary layer introduces strong (in the hypersonic sense) disturbances in the external flow, not smaller in the order of magnitude than those introduced by the body itself.

However, in this case the parameter χ must be bounded from above by the condition

$$\frac{\delta}{L} \sim \frac{1}{M_\infty} \chi^{1/2} \ll 1, \quad \text{Re}_{\infty L}^{1/4} \gg M_\infty^{(1-n)/2} \quad (12.12.11)$$

Otherwise, the problem is beyond the scope of the boundary layer model and should be solved within the framework of the complete Navier–Stokes equations. Thus, for the interaction problems under consideration the conventional limiting regime $M_\infty \rightarrow \infty$ considered in the inviscid theory loses its meaning unless the condition $\text{Re}_{\infty L} \rightarrow \infty$ holds simultaneously.

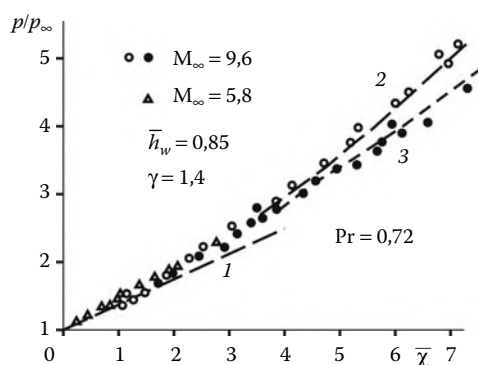


FIGURE 12.22
Displacement effect of the pressure on a thermally insulated flat plate.

A simple example of the strong interaction is realized in the flat-plate flow (Stewartson, 1955). In this case, the boundary layer thickness is determined by the formula of the form:

$$M_\infty \delta = K_2 x \chi_x^{1/2} = K'_2 x^{3/4} \quad (12.12.12)$$

where the coefficients K_2 and K'_2 are determined in the process of the solution of the boundary layer problem. As for the pressure on the boundary of this effective power-law body, it is determined by the self-similar solution of the time-dependent problem of the expansion of a piston in time in accordance with the power law $r_p \sim t^m$ (see the problems discussed in Sections 6.8 and 7.6). Within the framework of the time-dependent analogy (Section 8.2), this solution is applicable to the hypersonic flow past a thin power-law body $r_b \sim x^m$, with the pressure determined, in view of 12.12.12, by the formula

$$\frac{p}{p_\infty} = \gamma A_0 M_\infty^2 \left(\frac{d\delta}{dx} \right)^2 = A'_0 \chi_x = A''_0 x^{-1/2} \quad (12.12.13)$$

The solution presented is a particular case of self-similar solutions for the boundary layer on thin bodies with allowance for the displacement effect (Lunev, 1960). To derive these solutions, we turn to the system of Equations 12.5.5 through 12.5.7 and recall that outside the boundary layer, or in the shock layer, the dissipative terms can be omitted from these equations so that the system takes the same form as for an inviscid shock layer, while in the boundary layer region the transverse momentum Equation 12.5.6 can be omitted. As shown previously, in the hypersonic flow these regions are separated by a clearly defined boundary $\delta \approx \delta^*$, on which the impermeability condition should be imposed on the shock-layer side and the conditions $h = 0$ and $U = U_\infty$ (12.12.5) on the boundary-layer side, with the preassigned pressure distribution $p(x)$ determined by the shape of the effective body having the overall thickness $r_\sigma = r_b + \delta(x)$.

Obviously, in order for the solution as a whole to be self-similar, it must be self-similar in the shock layer; in accordance with the solutions presented in Section 6.8 and the time-dependent analogy of Section 8.2, this is possible only for a power-law effective body $r_\sigma \sim x^m$ and, therefore, when the body itself and the displacement thickness taken separately are also of power-law shape: $r_b \sim x^m$ and $\delta \sim x^m$.

Correspondingly, we will take these quantities, together with the pressure at the boundary layer edge (and, hence, on the body surface), in the form:

$$\begin{aligned} r_b &= b_b x^m, & \delta &= b_\delta x^m, & r_\sigma &= b_\sigma x^m, & b_\sigma &= b_b + b_\delta \\ \bar{p} &= \frac{p}{p_\infty U_\infty^2} = A_v \left(\frac{dr_\sigma}{dx} \right)^2 = m^2 A_v b_\sigma^2 x^{2(m-1)} \end{aligned} \quad (12.12.14)$$

Here, the coefficient b_b is given, while b_δ is sought for; the coefficient A_v is determined from the solution of the inviscid problem.

Thus, in order for the solution to be self-similar as a whole, it is sufficient to derive the conditions of the boundary-layer solution self-similarity. For this purpose, we will change variables in system 12.5.5 and 12.5.7

$$x, y \rightarrow x, \tilde{\eta}, \quad \tilde{\eta}(x, y) = \int_0^y \rho r^v dy \quad (12.12.15)$$

At $v = 0$ the variable $\tilde{\eta}$ coincides with $\bar{\eta}$ in 12.6.1. Performing the procedure analogous to that of Section 12.6 (substituting ur_b for u and ρr^v for ρ in transformations 12.6.3) we can bring this system into the form:

$$\begin{aligned} u \frac{\partial u}{\partial x} + V \frac{\partial u}{\partial \tilde{\eta}} &= -\frac{1}{\rho} \frac{\partial p}{\partial x} + \frac{\partial}{\partial \tilde{\eta}} \left(\rho \mu r^{2v} \frac{\partial u}{\partial \tilde{\eta}} \right) \\ \frac{\partial u}{\partial x} + \frac{\partial V}{\partial \tilde{\eta}} &= 0, \quad V = \rho v r^v + u \frac{\partial \tilde{\eta}}{\partial x} \\ u \frac{\partial h}{\partial x} + V \frac{\partial h}{\partial \tilde{\eta}} &= \frac{u}{\rho} \frac{\partial p}{\partial x} + \frac{\partial}{\partial \tilde{\eta}} \left(\frac{\rho \mu r^{2v}}{\text{Pr}} \frac{\partial h}{\partial \tilde{\eta}} \right) + \rho \mu r^{2v} \left(\frac{\partial u}{\partial \tilde{\eta}} \right)^2 \end{aligned} \quad (12.12.16)$$

For the new conditions we change variables 12.6.4 for the following variables

$$\begin{aligned} \xi &= \frac{1}{\rho_* \mu_* r_\sigma^{2v}} \int_0^x \rho_* \mu_* r_\sigma^{2v} dx = \frac{1}{\rho_* r_\sigma^{2v}} \int_0^x p r_\sigma^{2v} dx = \frac{x}{2m(1+v)-1} \\ \zeta &= \sqrt{\frac{U_\infty}{\rho_* \mu_* r_\sigma^{2v} \xi}} \tilde{\eta} = \sqrt{\frac{\rho_* U_\infty}{\mu_* \xi}} \eta, \quad \eta = \frac{\tilde{\eta}}{\rho_* r_\sigma^v} \end{aligned} \quad (12.12.17)$$

Here, we took $U_\delta = U_\infty$ and, in accordance with 1.3.11 and 12.12.2, $\rho_* \mu_* = C_* p$, $C_* = Ch_*^{-n} = \text{const}$, since for $h_\delta \ll H_\delta = H_\infty$ and under the additional condition that $\bar{h}_w = \text{const}$ (isothermal wall) the quantity \bar{h}_* in 12.6.19 is also constant. In accordance with 12.12.14, the last formula for ξ pertains to a power-law body, the denominator in this formula being always positive due to the constraint $m > 2/(3+v)$ imposed on the existence of such self-similar solutions (Section 6.8).

We will seek the self-similar solution of the problem in the form:

$$u = U_\infty f'(\zeta), \quad h = H_\infty \bar{h}(\zeta) \quad (12.12.18)$$

at the following (with 12.12.5 taken into account) boundary conditions

$$\begin{aligned} \zeta = 0 : \quad f' &= f = 0, \quad \bar{h} = \bar{h}_w = \text{const} \\ \zeta \rightarrow \infty : \quad f' &\rightarrow 1, \quad \bar{h} \rightarrow 0 \end{aligned} \quad (12.12.19)$$

In variables 12.12.17 and functions 12.12.18, by applying the procedure analogous to that used in deriving system 12.6.11 and taking 12.12.14 into account, we can reduce Equation 12.12.16 to a system of ordinary differential equations

$$\begin{aligned} 2(\omega Y f'')' + ff'' &= c_1 \bar{h} \\ 2 \left(\frac{\omega}{\text{Pr}} Y \bar{h}' \right)' + f \bar{h}' + 2\omega Y f''^2 &= c_1 f \bar{h} \\ \omega = \frac{\rho \mu}{\rho_* \mu_*} &= \left(\frac{h}{h_*} \right)^{-n} = \bar{h}_*^{-n} \bar{h}^{-n}, \quad Y = \frac{r^{2v}}{r_\sigma^{2v}}, \quad \bar{h} = \frac{h}{H_\infty} \\ c_1 = -\frac{2\xi}{\rho h U_\infty^2} \frac{dp}{dx} &= \frac{4(\gamma-1)(1-m)}{\gamma[2m(1+v)-1]} \end{aligned} \quad (12.12.20)$$

Taking of the equality $r = r_b + y$ for thin bodies, together with Equations 12.12.2, 12.12.6, and 12.12.7, we can express the radius r in terms of the variable ζ by inverting formulas 12.12.15 and 12.12.17 for the variable $\tilde{\eta}$

$$\begin{aligned} r^{1+\nu} - r_b^{1+\nu} &= (1 + \nu) \sqrt{\frac{\rho_* \mu_* r_\sigma^{2\nu} \xi}{U_\infty}} \int_0^\zeta \frac{d\xi}{\rho} = c_2 r_\sigma^\nu \bar{p}^{-1/2} M_\infty^{1-n} \sqrt{\frac{\mu_\infty x}{\rho_\infty U_\infty}} \bar{J}(\zeta) \\ J &= \int_0^\zeta \bar{h} d\xi, \quad \bar{J} = \frac{J}{J_\delta}, \quad c_2 = \frac{(1 + \nu) K_1}{\sqrt{\gamma [2m(1 + \nu) - 1]}}, \quad \bar{p} = \frac{p}{\rho_\infty U_\infty^2} \end{aligned} \quad (12.12.21)$$

Letting then $r = r_\sigma$ and $J = J_\sigma$ in 12.12.21 we obtain, taking 12.12.14 into account, an equation for the unknown parameter $b_\sigma = b_b + b_\delta$

$$\begin{aligned} M_\infty^2 b_\sigma^{1-\nu} (b_\sigma^{1+\nu} - b_b^{1+\nu}) &= c_3 x^\beta M_\infty^{3-n} \sqrt{\frac{\mu_\infty}{\rho_\infty U_\infty}} \\ c_3 &= \frac{c_2}{mA_v^{1/2}}, \quad \beta = \frac{3}{2} - 2m \end{aligned} \quad (12.12.22)$$

In order for the problem to be self-similar, the right-hand side must be independent of x , which is possible only when the exponent $\beta = 0$ or $m = 3/4$. At the same time, for a limitingly thin boundary layer, that is, when $(M_\infty r_b/x)^2 \gg \chi_x$, we have $b_\tau \approx b_b$ and $Y \approx 1$, so that in this case the solution obtained simply enlarges the class of the self-similar solutions for the classical boundary layer considered previously at a given pressure $p_b \sim x^m$ and an arbitrary m .

Turning back to the problem of the strong interaction on a flat plate, letting $b_b = 0, b_\tau = b_\delta$, and $\nu = 0$ in 12.12.22, we obtain in Equations 12.12.12 and 12.12.13

$$\frac{p}{p_\infty} = A'_0 \chi_x, \quad A'_0 = \frac{9}{16} \gamma c_3 A_0 = \frac{3\gamma^{1/2}}{2\sqrt{2}} A_0^{1/2} K_1 \quad (12.12.23)$$

In accordance with the data given in Section 6.10, for $\gamma = 1.4$ we have $A_0 = 1.43$, $A'_0 = 1.5K_1$, and $p/p_\infty = 0.69\bar{\chi}$, which is in good agreement with the experimental data in Figure 12.22 obtained for a thermally insulated flat plate ($\bar{h}_w = 0.85$) (line 2).*

In general, in addition to Equation 12.12.14 we introduce the notation

$$\begin{aligned} b_b &= \theta_0 L^{1-m}, \quad b_\delta = \bar{b}_\delta \theta_0 L^{1-m} \\ b_\sigma &= \bar{b}_\sigma \theta_0 L^{1-m}, \quad \bar{b}_\sigma = 1 + \bar{b}_\delta \end{aligned} \quad (12.12.24)$$

In this case $m = 1/4$; θ_0 is the relative thickness of the power-law L -long body. Then we reduce Equation 12.12.22 to the form:

$$\bar{b}_\sigma^{1-\nu} (\bar{b}_\sigma^{1+\nu} - 1) = c_3 N, \quad N = \frac{\chi}{M_\infty^2 \theta_0^2} \quad (12.12.25)$$

* Generally speaking, particular significance should not be attached to the agreement of formulas 12.12.10 and 12.12.23 with the experimental data in Figure 12.22 owing to the fact that the value of K_1 is only approximate and there is no complete information on the conditions of the experiment, for example, a possible effect of the plate bluntness that was first found in precisely similar experiments (Hammit and Bogdonoff, 1956). We note that the solutions obtained under other assumptions, namely, $p/p_\infty + 1 = 0.31\bar{\chi} + 0.05\bar{\chi}^2$, coinciding with Equation 12.12.10 at $\bar{\chi} \ll 1$, for weak interaction and $p/p_\infty = 0.514\bar{\chi} + 0.76$ (curve 3 in Figure 12.22) for strong interaction are presented in Hayes and Probstein (1966).

In this case, in the similarity variables 8.4.2 the pressure at the boundary layer edge and, hence, on the body can be written in the form:

$$p' = \frac{p}{\rho U_\infty^2 \theta_0^2} = \frac{9}{16} A_v \bar{b}_\sigma^2 \left(\frac{L}{x} \right)^{1/2} \quad (12.12.26)$$

For $\gamma = 1.4$ the coefficient $A_0 = 1.43$ and $A_1 = 0.9$. Clearly, the parameter p' , as well as other parameters 8.4.2 on the boundary of the effective body $r_\sigma(x)$ and inside the shock layer (except for the parameters γ , n , and \bar{h}_w), are dependent on the interaction parameter N only.

By way of illustration, in Figure 12.23 we have plotted the velocity and enthalpy profiles obtained by the solution of system 12.12.20 for a body of revolution at $\omega = 1$, or $n = 0$, and a very large value of the parameter $N = 100$. In this case, the ratio $r_\sigma/r_b \approx 10 \gg 1$, which makes it possible to model a slender spike with $r_b \approx 0$ in a viscous hypersonic flow. A distinctive feature of these profiles is that the boundary values are rather large ($\zeta_\delta = 12$ to 18) and, as distinct from the conventional boundary layer with $\zeta_\delta \approx 5$, are appreciably dependent on the enthalpy factor \bar{h}_w which is due to the effect of the coefficient Y in Equation 12.12.20.

The result obtained is a particular case of the more general similarity law for the hypersonic viscous flow past thin bodies (Lunev, 1959; Hayes and Probstein, 1966). To derive this law, by analogy with 8.4.1 and 8.4.2 and taking 12.12.1 into account, we introduce the following dimensionless variables and functions:

in the entire flow region

$$\begin{aligned} x &= Lx', & r &= \varepsilon Lr', & r_b &= \varepsilon Lr'_b \\ p &= \rho_\infty U_\infty^2 \varepsilon^2 p', & u &= U_\infty u', & v &= \varepsilon U_\infty v' \\ \varepsilon &= M_\infty^{-1} + \theta_0 + \delta_0/L \ll 1 \end{aligned} \quad (12.12.27)$$

where δ_0 is the characteristic boundary layer thickness determined by formula 12.12.6;

in the inviscid region

$$h = H_\infty \varepsilon^2 h', \quad \rho = \rho_\infty \rho' \quad (12.12.28)$$

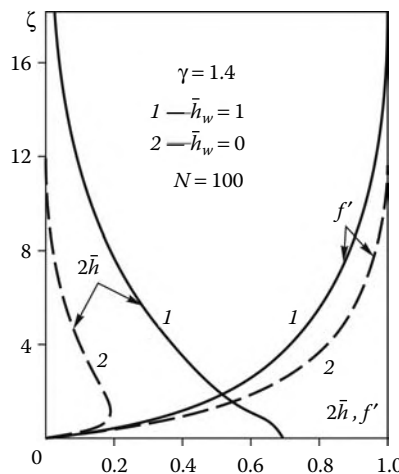


FIGURE 12.23

Velocity and enthalpy profiles in the boundary layer on an $r_b \sim x^{3/4}$ body.

and in the boundary layer

$$h = H_\infty \bar{h}, \quad \rho = \rho_\infty \varepsilon^2 \bar{\rho}, \quad \mu = \mu_\infty M_\infty^{2(1-n)} \bar{\mu}, \quad \bar{h}_w = \bar{h}_w(x') \quad (12.12.29)$$

In accordance with Section 8.4, for bodies of affinely similar shape $r' = r'_\sigma(x')$ the flows in the inviscid regions are similar for the same values of the similarity criteria $M_\infty \varepsilon$ and γ . Therefore, in the subsequent discussion it is sufficient to establish the conditions of the boundary layer flow similarity. In particular, for determining the boundary $r'_\sigma(x')$ we should pass to the dimensionless variables 12.12.27 and 12.12.29 in the first equation of Equation 12.12.21; taking 12.12.2 into account we bring this equation into the form:

$$(r'_\sigma)^{1+\nu} - (r'_b)^{1+\nu} = \frac{1}{\gamma^{1/2}} (1 + \nu) \left(\frac{\gamma - 1}{2} \right)^{1-n/2} \bar{h}_w^{-n/2} (p')^{-1/2} \sqrt{\xi'} N_\varepsilon J_\delta(x') \\ N_\varepsilon = \frac{\chi}{M_\infty^2 \varepsilon^2} = \frac{\theta_0^2}{\varepsilon^2} N, \quad N = \frac{\chi}{M_\infty \theta_0}, \quad N_\varepsilon = \frac{\delta_0}{\varepsilon L}, \quad \xi' = \frac{\xi}{L} \quad (12.12.30)$$

In going over to the same variables, the equations of motion of Equation 12.12.16 involve a single parameter N_ε^2 ahead of the viscous and heat-conducting terms. As for the boundary conditions (12.12.5), for $\zeta \rightarrow \infty$ these conserve their form.

Thus, in the dimensionless form 12.12.27 through 12.12.29 accepted by us the solution of the problem depends, except for the parameters γ and \bar{h}_w and the exponent n in the viscosity law, on two similarity criteria $M_\infty \theta_0$ and χ_L or N_ε (N_0 for $\varepsilon \sim \theta_0$). The rigorous formulation of the similarity law is analogous to that presented in Section 8.4. At $\theta_0 = 0$, for the cases of a flat plate and a slender spike considered previously, only the parameter χ remains of these two; this similarity law is supported by Figure 12.22.

Another example is furnished by the solution of the problem of weak interaction on a sharp slender cone with the semivertex angle θ_0 in a hypersonic flow (Lunev, 1959) at $\gamma = 1.4$ and $\text{Pr} = 1.72$. In this case, the induced pressure $\Delta p = p - p_0$ and the boundary layer thickness are as follows:

$$\frac{\Delta p}{p_c} = \alpha_1 (0.103 + 0.33 \bar{h}_w) N_x, \quad \bar{\delta} = \frac{\delta}{\theta_0 x} = \alpha_2 (0.068 + 0.22 \bar{h}_w) N_x \quad (12.12.31)$$

where the subscript c refers to the flow parameters in the case of zero-thickness boundary layer and $N_x = N$ for $L = x$.

The relative friction and heat-flux increments due to the displacement effect and the transverse curvature are given by the formulas

$$\begin{aligned} \tau &= \tau_c + \Delta \tau, & q &= q_c + \Delta q \\ \Delta \tau &= \Delta \tau_p + \Delta \tau_r, & \Delta q &= \Delta q_p + \Delta q_r \\ \frac{\Delta \tau_p}{\tau_c} &= \alpha_1 [0.044 + 0.15 \bar{h}_w + 0.036 \bar{h}_w^2] N_x \\ \frac{\Delta \tau_r}{\tau_c} &= \alpha_2 [0.025 + 0.113 \bar{h}_w] N_x \\ \frac{\Delta q_p}{q_c} &= \alpha_1 [0.041 + 0.13 \bar{h}_w - 0.038 \bar{h}_w^2] N_x \\ \frac{\Delta q_r}{q_c} &= \alpha_2 [0.03 + 0.12 \bar{h}_w] N_x \end{aligned} \quad (12.12.32)$$

Here, the increments Δq_p and $\Delta \tau_p$ are due to the induced pressure Δp , while Δq_r and $\Delta \tau_r$ are caused by the transverse curvature effect. The coefficients α_1 and α_2 depend only on the parameter $M_\infty \theta_0$; this dependence is presented in Figure 12.24.

Judging from the coefficients of the formulas given previously, in this case the parameter N overestimates considerably the actual relative boundary layer thickness $\bar{\delta}$ and, therefore, the displacement effect as a whole, particularly on a cold wall, that is, for $\bar{h}_w \approx 0$, which is typical of hypersonic flight conditions. The relative pressure increment $\Delta p/p_c$ is generally similar in value to the relative boundary layer thickness $\bar{\delta}$, the terms $\Delta q_r/q_c$ and $\Delta \tau_r/\tau_c$, caused by the transverse curvature effect, are near to $\bar{\delta}/2$, while the terms $\Delta q_p/q_c$ and $\Delta \tau_p/\tau_c$ are near to or smaller than the latter terms.

Obviously, in a certain vicinity of the conical nose, this solution is invalid (this pertains also to the previous problems and, moreover, to the entire boundary layer theory) and has the asymptotics $\Delta p \sim x^{1/2}$, $\Delta q \sim x^{-1}$, and $\Delta \tau \sim x^{-1}$, as $x \rightarrow 0$. However, since the conical surface area is in proportion to x^2 , these functions are integrable.

Finally, strictly speaking, the flow vorticity caused by the induced curvature of the shock must also have an effect on the solution given previously. However, the contribution of vorticity is relatively small, and the corresponding terms are omitted from the solution.

We will now write formulas for the heat flux and friction on the wall in the similarity variables 12.12.27 through 12.12.29 based, for the sake of simplicity, on the general structure of formulas 12.8.5 and 12.6.21. Thus, we obtain

$$\begin{aligned} C_q &= \frac{2q_w}{\rho_\infty U_\infty^3} = \varepsilon^3 N_\varepsilon^2 \varphi_l^{(q)}, & C_\tau &= \frac{2\tau_w}{\rho_\infty U_\infty^2} = \varepsilon^3 N_\varepsilon^2 \varphi_l^{(\tau)} \\ \varphi_l^{(q,\tau)} &= \varphi_l^{(q,\tau)}(x', \chi, M_\infty \theta_0, \bar{h}_w, \text{Pr}, n, \gamma), & x' &= x/L \end{aligned} \quad (12.12.33)$$

Here, $\varphi_l^{(q,\tau)}$ are dimensionless functions determined from the solution of the problem and C_q is the Stanton number 12.6.21 for $H_e = U_\infty^2/2$ and $\bar{h}_w = 0$.

An analogous similarity law can also be formulated for a turbulent boundary layer (Luney, 1962) on the basis of the available empirical dependences on the governing

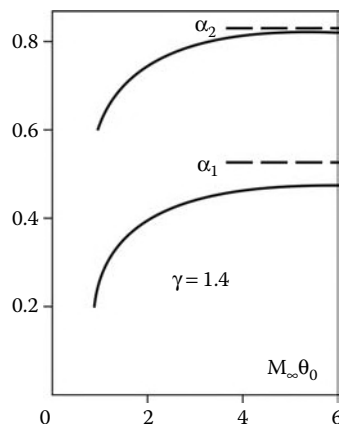


FIGURE 12.24
Weak interaction on a slender cone.

parameters ρ_* and μ_* (see Section 12.7). In this approximation, using transformations 12.12.29, for the boundary layer thickness we obtain

$$\frac{\delta}{\varepsilon L} \sim \frac{1}{\varepsilon} \left(\frac{\mu_*}{\rho_* U L} \right)^{0.2} \sim \frac{M_\infty^{0.4(1-n)}}{\varepsilon^{1.4} \text{Re}_{\infty L}^{0.2}} = N_t = \frac{\chi_t}{(M_\infty \varepsilon)^{1.4}}$$

$$\chi_t = \frac{M_\infty^{(1.8-0.4n)}}{\text{Re}_{\infty L}^{0.2}} \quad (12.12.34)$$

Transforming formula 12.7.1 for the turbulent heat flux in the same fashion and using the Reynolds analogy we obtain

$$C_q = \frac{2q_w}{\rho_\infty U_\infty^3} = \varepsilon^3 N_t \varphi_t^{(q)}, \quad C_f = \frac{2\tau_w}{\rho_\infty U_\infty^3} = \varepsilon^3 N_t \varphi_t^{(\tau)} \quad (12.12.35)$$

Here, the functions $\varphi_t^{(q)}$ and $\varphi_t^{(\tau)}$ are analogous to the functions $\varphi_l^{(q)}$ and $\varphi_l^{(\tau)}$ in Equation 12.12.33.

We note that the similarity criteria χ and N_ε , introduced previously in accordance with the classical, original version of the theory outlined, can be inconvenient in the limiting case $M_\infty \varepsilon \rightarrow \infty$, in which within the framework of inviscid theory the temperature T_∞ turns out to be inessential due to flow stabilization. This forces us to eliminate the coefficient μ_∞ from the relevant parameters replacing it by μ_0 , that is, the viscosity corresponding to the blunt body stagnation enthalpy (and temperature). For this purpose, we should let $\mu = \mu_0 \tilde{\mu}$ and substitute $\tilde{\mu}$ for $\bar{\mu}$ in Equation 12.12.29. Then the new similarity parameter $N_\varepsilon^{(0)}$ introduced instead of N_ε is determined as follows:

$$N_\varepsilon^{(0)} = \frac{1}{\varepsilon^2 \sqrt{\text{Re}_0}}, \quad \frac{\delta_0}{L} = \frac{1}{\varepsilon \sqrt{\text{Re}_0}}, \quad \text{Re}_0 = \frac{\rho_\infty U_\infty L}{\mu_0}$$

$$\mu_0 = \left(\frac{\gamma - 1}{2} \right)^{1-n} M_\infty^{2(1-n)} \mu_\infty \quad (12.12.36)$$

This formula for δ_0 is equivalent to the general formula 12.5.9 $\delta \sim (\mu_* L / \rho_* U_\delta)^{1/2}$; thus, in the boundary layer on a thin body we have $U_\delta \sim U_\infty$, $\mu_* \sim \mu_0$, and $\rho_* \sim p_\delta / H_\infty \sim \varepsilon^2 \rho_\infty$.

In conclusion, we will touch on one more displacement effect that takes into account the end effect mentioned in Section 12.9. We will explain its essence with reference to a simple model example of a thin homogeneous inviscid sublayer on a flat plate immersed in an unbounded supersonic flow with the parameters p_∞ and M_∞ , when $x \rightarrow -\infty$. The gas flow rate across the sublayer is constant, $G = \rho u \delta = \text{const}$, where ρ , u , and M (see Equation 12.12.37) are the density, the velocity, and the Mach number, constant across the sublayer, and δ is the sublayer thickness.

In the presence of stationary disturbances in the $x \rightarrow -\infty$ region, the pressure increment on the sublayer boundary and inside it is determined by formula 2.8.4 of the linear theory; for the sake of simplicity, for $M_\infty \gg 1$ we let

$$\frac{p - p_\infty}{p_\infty} = \gamma M_\infty \frac{d\delta}{dx} = \gamma M_\infty G \frac{d}{dx} \frac{1}{\rho u} = \frac{\kappa \delta}{p_\infty} \frac{dp}{dx}$$

$$\kappa = \frac{M_\infty^2}{M^2} (1 - M^2) \quad (12.12.37)$$

In deriving the expression for the coefficient κ we used formula 2.2.2; at small disturbances, we will let it be constant, as well as the parameter δ which enters in the coefficient of the last equality ($\delta = \delta_\infty$). Then Equation 12.12.37 has a simple solution

$$\frac{\Delta p}{p_\infty} = Ce^{\kappa x/\delta}, \quad C = \text{const} \quad (12.12.38)$$

At $M > 1$ we have $\kappa < 0$, so that a solution bounded as $x \rightarrow -\infty$ can exist only at $C = 0$ and $\Delta p = 0$, that is, the supersonic sublayer located below the supersonic flow is stable against stationary disturbances. However, at $M < 1$, or $\kappa > 0$, there exists an entire family of solutions attenuating when $x \rightarrow -\infty$ with a coefficient C determined from any downstream condition, say, $p = p_*$ at a certain point $x = x_*$; formally, the subsonic sublayer is sensitive to these conditions, however small its thickness may be.

The hypersonic boundary layer including a relatively extended subsonic region can also possess the analogous sensitivity to downstream conditions or, in accordance with the terminology of Section 12.9, the end effects. In Figure 12.25 we have plotted the Mach number profiles in such a boundary layer. Clearly on a thermally insulated wall ($\bar{h}_w \approx 1$) the subsonic flow region occupies a considerable part of the boundary layer thickness with the result that such *subcritical* boundary layer can actually be responsive to downstream conditions, for example, be affected by a body base region with a reduced pressure behind it, $p_d < p_b$.

Of course, the direct transfer of this model result to boundary layer flows is improper in view of the appreciable viscosity effect, particularly, in the wall zone of the boundary layer; nevertheless, these qualitative considerations would stand for the problems of the boundary layer interaction as well. In particular, Neiland showed (1970) that for the linearized problem of strong interaction on a flat plate the corresponding equations admit eigensolutions of the form $C(x/x_*)^\alpha$ with an arbitrary constant that can be determined only from a certain end condition at point $x = x_*$. True, in this case the exponent α is rather

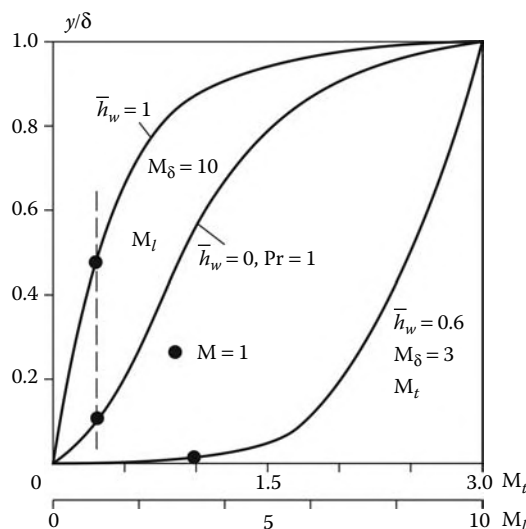


FIGURE 12.25

Mach numbers in laminar (M_l) and turbulent (M_t) boundary layers.

large; thus, we have $\alpha \sim 50$ for $\bar{h}_w \approx 1$ and, moreover, $\alpha \rightarrow \infty$ for $\bar{h}_w \rightarrow 0$, which is due to the shrinking of the subsonic region of the boundary layer, as shown in Figure 12.25. For so great values of the exponent α , the ratio $(x/x_*)^\alpha$ is negligibly small outside the immediate vicinity of point $x = x_*$; actually, this reduces the interaction process to a local end effect and thus does not hamper the use of the self-similar solutions and the similarity laws derived previously to real flows, though, strictly theoretically, the adequacy of these solutions must be checked against the end effect role.

Boundary layers having the properties of supersonic sublayers, in which the upwind propagation of disturbances is only local and the dimensions of separation zones ahead of steps are bounded, are termed *supercritical*. In particular, they usually include supersonic turbulent boundary layers in which supersonic flow region extends almost to the wall, which also follows from Figure 12.25. In more detail, this theory is presented in Neiland (2003).

12.13 Entropy Effect on Bluff and Thin Blunt Bodies

The most distinctive feature of the boundary layer on blunt bodies in a hypersonic flow is that it is developed in a nonuniform external flow with an appreciable entropy gradient across streamlines, though at a constant total enthalpy $H = H_\infty$; this is due to the fact that the bow shock detached from the frontal part of the body is curvilinear. This *vortical viscous-inviscid interaction* or *entropy effect* is the most important among other viscous-inviscid interaction effects listed in Section 12.9 if we restrict ourselves (as it is done in the following) only to *viscous shock layer* and *boundary layer* (in accordance with terminology adopted in Section 12.9) flow regimes realized at fairly high Reynolds numbers. We will consider this effect separately for bluff and thin blunt bodies. As for the flows in *continuous viscous layers* at low Reynolds numbers (see Section 12.9), they will be considered in Section 12.14.

Bluff bodies. We will first estimate the relative boundary layer thickness in the vicinity of stagnation points. For this purpose, within the framework of the effective length method (Section 12.8) we should let, by analogy with Equations 12.8.17 and 12.12.2 and using the same notation, in formula 12.6.5

$$\begin{aligned} \rho_\delta &= \rho_0 = \frac{\rho_\infty}{k_0}, & h_\delta &= H_\delta = H_\infty, & \rho h &= \rho_0 H_\infty \bar{Z} \\ \rho\mu &= \rho_0\mu_0 \left(\frac{h}{H_\infty} \right)^{-n}, & \rho_0\mu_0 &= \rho_\infty\mu_\infty \frac{p'_0}{p_\infty} \left(\frac{h_\infty}{H_\infty} \right)^{-n} = \\ && & \rho_\infty\mu_\infty\gamma \left(\frac{2}{\gamma-1} \right)^n \left(1 - \frac{1}{2}k \right) M_\infty^{2(1-n)} \\ \xi &= \frac{x}{2(1+\nu)}, & U_\delta &= \bar{c}U_\infty \frac{x}{r_0}, & \bar{c} &= \sqrt{2\bar{k}\beta} \frac{r_0}{R_s} \\ \bar{h}_* &= \frac{h_*}{H_\infty} = \frac{1}{2}(1 + \bar{h}_w), & k_0 &= k \left(1 - \frac{1}{2}k \right), & \bar{k} &= k(1-k) \\ k &= \frac{\rho_\infty}{\rho_s} = \frac{\gamma_* - 1}{\gamma_* + 1}, & \bar{Z} &= \frac{Z}{Z_0} \end{aligned} \tag{12.13.1}$$

Here, r_0 is the midsection radius of a bluff body or the nose radius of a thin blunt body, x is the curvilinear coordinate measured along the body surface (see Figure 7.4 of Section 7.1), γ is the adiabatic exponent in the freestream, γ_* is the effective adiabatic exponent behind the shock (see Equation 1.13.8), which does not generally coincide with γ , R_s is the radius of curvature of the shock, ρ_0 , μ_0 , p'_0 , and Z_0 are the inviscid flow parameters at the blunt-body stagnation point, and the function Z is the same as in the equation of state (1.3.8). For a sphere of radius $R = r_0$, in accordance with 12.8.17, we have $\bar{c} = \sqrt{2\bar{k}\bar{\beta}}$, where $\bar{\beta} = 1.17$. If the vorticity effect is taken into account, the coefficient \bar{c} should be replaced by the *mass-average* coefficient \bar{c}_a , as was done in Section 12.11.

In Section 12.6 for the case $\bar{Z} = 1$ we derived formula 12.6.23 for the boundary layer thickness; we will use this formula, with account for 12.13.1, for the stagnation point introducing for our estimates the mean, in the sense of the integral $\bar{\zeta}$ in 12.6.5, value Z_* . Then using Equation 12.6.22 for δ^* we obtain

$$\begin{aligned} \frac{\delta}{r_0} &= \tilde{K}_1 \text{Re}_0^{-1/2} = \tilde{K}_2 M_\infty^{(1-n)} \text{Re}_\infty^{-1/2}, & \text{Re}_\infty &= \frac{\rho_\infty U_\infty r_0}{\mu_\infty}, & \text{Re}_0 &= \frac{\rho_\infty U_\infty r_0}{\mu_0} \\ \tilde{K}_1 &= \frac{\bar{h}_*^{-n/2} k_0^{1/2} \bar{\delta}}{C[2\bar{c}(1+\nu)]^{1/2}}, & \tilde{K}_2 &= \left(\frac{k_0}{\gamma}\right)^{1/2} \left(\frac{2}{\gamma-1}\right)^{n/2} \tilde{K}_1, & C &= \bar{Z}_* \left(\frac{\bar{c}_a}{\bar{c}}\right)^{1/2} \\ \bar{\delta} &= f_\delta + \bar{\delta}_*, & \bar{\delta}_* &= 1.94 \bar{h}_w - 0.21 \quad (\text{Pr} = 0.72, \quad f_\delta = 3.3) \end{aligned} \tag{12.13.2}$$

Here, the coefficient C allows for the gas imperfection and the flow vorticity at the boundary layer edge. In hypersonic flows, in which the condition $k \ll 1$ is fulfilled, the coefficient $\bar{c} \sim k^{1/2}$ and $\delta \sim r_0 k^{1/4} \text{Re}_0^{-1/2}$, while, in accordance with Section 7.3, the inviscid shock layer thickness $\delta_0 \sim kr_0$. The ratio $\delta/\delta_0 \sim (k^{3/2} \text{Re}_0)^{-1/2}$ determines the portion of the boundary layer in the entire thickness of the disturbed region on a bluff body. We note that for $\bar{h}_w \ll 1$ the boundary layer displacement thickness δ^* determined by the same formula 12.13.2 with $\bar{\delta}$ replaced by $\bar{\delta}^*$ is small and can even be negative. By virtue of the equality $\rho_\infty U_\infty = \rho_s U_s$, where ρ_s and U_s are the density and the velocity immediately behind the normal shock, the Reynolds number Re_0 characterizes the viscosity effect in the vicinity of the stagnation point. We note that the ratio $\text{Re}_\infty/\text{Re}_0 = \mu_0/\mu_\infty \sim [(\gamma-1)M_\infty^2]^{1-n} \gg 1$.

In what follows we will take into account that at fairly high Reynolds numbers in the *vortex* (for bluff bodies) and *high-entropy* (for thin blunt bodies, see Sections 9.1 and 9.2) inviscid layers, external in relation to the boundary layer, at a constant pressure in the wall region of a body, the quasiperfect gas (see Section 1.3.9) flow parameters can be presented, on the basis of the general formulas 7.1.4, in the form:

$$\begin{aligned} h^{(0)}(\bar{\psi}, \bar{p}_b) &= h_b(\bar{p}_b)G(\bar{\psi}), & U^{(0)} &= \sqrt{2(H_\infty - h^{(0)})} \\ h_b &= H_\infty \bar{p}^{(\gamma_*-1)/\gamma_*}, & G(\bar{\psi}) &= s^{1/\gamma_*} = [\sin \alpha(\bar{\psi})]^{2/\gamma_*} \\ \gamma_* &= \gamma_*(\bar{\psi}), & \bar{h} &= \frac{h}{H_\infty}, & \bar{p}_b &= \frac{p_b}{p'_0} \\ \bar{\psi} &= \frac{\psi}{\psi_0}, & \psi_0 &= \pi^\nu r_0^{1+\nu} \rho_\infty U_\infty \end{aligned} \tag{12.13.3}$$

Here, h_b and p_b are the enthalpy and the pressure on the body surface, s is the entropy function introduced in Section 7.1, and $\alpha(\bar{\psi})$ is the angle of inclination of the shock at the

point of its intersection with the streamline associated with the given value of the dimensionless function $\bar{\psi}$. As shown in Section 1.5 (Figure 1.13), the effective adiabatic exponent γ_* varies along the streamlines only slightly.

For bluff and blunt bodies in a hypersonic flow the mass-average value method of Section 12.11 is used in a modified form in which, as distinct from formulas 12.11.1, the mass-average enthalpy h_a is expressed in terms of the integral of the function $h^{(0)}$ in 12.13.3, while the mass-average velocity is determined from the Bernoulli integral

$$h_a = h_b G_a(\bar{\psi}), \quad C_a(\bar{\psi}) = \frac{1}{\bar{\psi}} \int_0^{\bar{\psi}} G(\bar{\psi}) d\bar{\psi}$$

$$U_a = \sqrt{2(H - h_a)} = U_\infty \sqrt{1 - G_a \bar{p}_b^{(\gamma_* - 1)/\gamma_*}} \quad (12.13.4)$$

Otherwise, the algorithm of the mass-average value method is not different from that presented in Section 12.11. An example of the functions $G(\bar{\psi})$ and $G_a(\bar{\psi})$ for equilibrium air is presented in Figure 12.26; their comparison indicates a prolonged lagging of the mass-average enthalpy h_a behind the local enthalpy h_δ on the outer edge of the boundary layer at a given flow rate across the latter.

As noted previously, in the vicinity of the blunt-body stagnation point the velocity coefficient \bar{c} in formula 12.8.20 of the effective length method should be replaced by the mass-average value \bar{c}_a , as it was done in Section 12.11 (example 4, see formula 12.11.9 and Figure 12.21). For determining \bar{c}_a , we transform formulas 12.13.3 and 12.13.4 for the velocities U_b on the body surface (for $G = 1$) and $U^{(0)}(\bar{\psi})$ in the vortex layer, as well as for the mass-average velocity $U_a(\bar{\psi})$, to the form:

$$U_b = U_\infty \sqrt{1 - \bar{p}_b^{(\gamma_* - 1)/\gamma_*}} = U_\infty \bar{c} \bar{x}, \quad \bar{x} = \frac{x}{r_0}$$

$$U^{(0)} = U_b \sqrt{1 - \frac{1 - G(\bar{\psi})}{U_b^2}} = U_\infty \bar{c}^{(0)} \bar{x}$$

$$U_a = U_b \sqrt{1 - \frac{1 - G_a(\bar{\psi})}{U_b^2}} = U_\infty \bar{c}_a \bar{x} \quad (12.13.5)$$

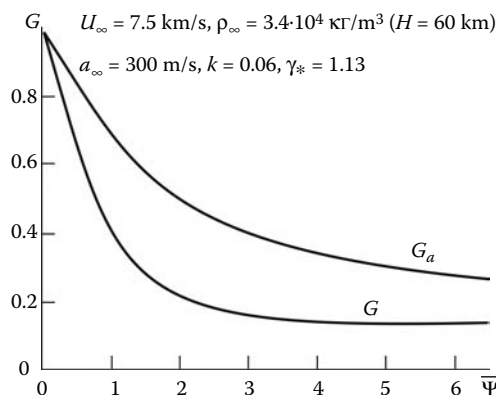


FIGURE 12.26

Functions G and G_a for equilibrium-dissociated air; k and γ_* are the parameters behind the normal shock.

Based on the diagram presented in Figure 7.4 of Section 7.1, in the vicinity of the stagnation point $x \approx 0$, in view of formulas 12.13.3 for $G(\bar{\psi})$ and 12.13.1 for \bar{c} , we obtain the following expansions

$$\begin{aligned} \psi &= \pi^\nu \rho_\infty U_\infty x^{1+\nu}, & \bar{\psi} &= \bar{x}^{1+\nu} \\ 1 - s &= \frac{x_s^2}{R_s^2} = \left(\frac{r_0}{R_s} \right)^2 \bar{\psi}^{2/(1+\nu)}, & 1 - G &= \frac{1}{\gamma_*} \left(\frac{r_0}{R_s} \right)^2 \bar{\psi}^{2/(1+\nu)} \\ 1 - G_a &= g_a \bar{\psi}^{2/(1+\nu)}, & g_a &= \frac{1+\nu}{\gamma_*(3+\nu)} \left(\frac{r_0}{R_s} \right)^2 \end{aligned} \quad (12.13.6)$$

Rewriting Equation 12.11.2 with account for Equation 12.8.15 we determine the boundary function $\bar{\psi}_\delta$ as follows:

$$\begin{aligned} \bar{\psi}_\delta &= \frac{\psi_\delta}{\psi_0} = \alpha_\nu \overline{\text{Re}}^{-1/2} c_a^{1/2} \bar{x}^{1+\nu} \\ \alpha_\nu &= \frac{2^\nu f_\delta}{[2(1+\nu)]^{1/2}}, & \overline{\text{Re}} &= \frac{\rho_\infty^2 U_\infty r_0}{\rho_* \mu_*}, & f_\delta &= 3.3 \end{aligned} \quad (12.13.7)$$

Using Equation 12.13.1 for $\rho_* \mu_*$ we can express the Reynolds number $\overline{\text{Re}}$ as follows:

$$\overline{\text{Re}} = \frac{1}{\gamma} \left(\frac{\gamma - 1}{2} \right)^n \bar{h}_*^n M_\infty^{-2(1-n)} \text{Re}_\infty, \quad \text{Re}_\infty = \frac{\rho_\infty U_\infty r_0}{\mu_\infty} \quad (12.13.8)$$

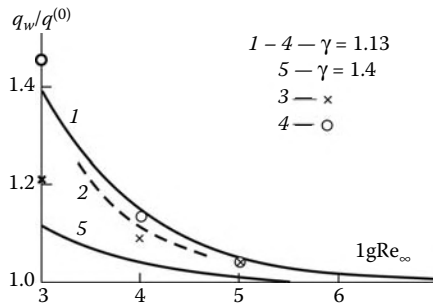
Obviously, for $M_\infty \gg 1$ we have $\overline{\text{Re}} \ll \text{Re}_\infty$.

From formulas 12.13.6 and 12.13.7 it follows that in axisymmetric $\text{Re} \gg 1$ flows the difference $1 - G_a$ is of the order $\overline{\text{Re}}^{-1/2}$, while for plane flows it is of the order $\overline{\text{Re}}^{-1}$, that is, of the higher order than in the whole boundary layer theory, which is due to the equality of the normal velocity derivatives at the wall to zero, $\partial U / \partial y = 0$ (Section 7.8, Figure 7.23). Because of this, we will take into account the vorticity effect on the heat transfer in the vicinity of the blunt-body stagnation point only for $\nu = 1$. In this case, $1 - G_a = 0.5(1 - G)$, so that formulas 12.13.5 for $\bar{c}^{(0)}$ and \bar{c}_a take the form:

$$\begin{aligned} \frac{\bar{c}^{(0)}}{\bar{c}} &= \left[1 + \Omega \left(\frac{\bar{c}^{(0)}}{\bar{c}} \right)^{1/2} \right]^{1/2}, & \frac{\bar{c}_a}{\bar{c}} &= \left[1 + \Omega \left(\frac{\bar{c}_a}{\bar{c}} \right)^{1/2} \right]^{1/2} \\ \Omega &= \frac{f_\delta}{\gamma_* \bar{c}^{3/2}} \left(\frac{r_0}{R_s} \right)^2 \overline{\text{Re}}^{-1/2} \end{aligned} \quad (12.13.9)$$

At the stagnation point the ratio $q_w/q^{(0)}$ of the heat fluxes calculated with (q_w) and without $(q^{(0)})$ allowance for vorticity from the mass-average (U_a) and external ($U^{(0)}$) velocities is equal to $(\bar{c}_a/\bar{c})^{1/2}$ and $(\bar{c}^{(0)}/\bar{c})^{1/2}$, respectively, where the coefficient \bar{c} is determined by formula 12.13.1.

In 12.13.9 the parameter Ω has the same meaning as in formula 12.11.10 obtained by averaging the external velocity $U^{(0)}$ in 12.11.8, while formula 12.13.9 for the ratio $\bar{c}^{(0)}/\bar{c}$ coincides with Equation 12.11.8. The formulas for \bar{c}_a/c , though differing in appearance, lead to near-coincident quantitative results; this follows from Figure 12.21 in which curves 1 and 4 are plotted in accordance with formulas 12.11.9 and 12.13.9 for \bar{c}_a/\bar{c} , respectively. As the Reynolds number increases, the coefficient $(\bar{c}_a/\bar{c})^{1/2}$ has $(\bar{c}_a/\bar{c})^{1/2} - 1 \sim \text{Re}_\infty^{1/2}$ as the asymptotics. The Re_∞ -dependence of the ratio $q_w/q^{(0)}$ is plotted in Figure 12.27 for a sphere

**FIGURE 12.27**

Vorticity effect on the heat flux at the stagnation point on a sphere: 1 and 5, mass-average value method; 2, boundary layer; 3 and 4, exact calculation in accordance with the Navier–Stokes model using the shock-capturing and the shock-fitting technique, respectively.

at $M_\infty = 25$, $\gamma_* = 1.13$ (the conditions of Figure 12.26) and $M_\infty = 20$, $\gamma_* = 1.4$ (the conditions of Figure 12.19 of Section 12.9). Clearly, for $\gamma = 1.4$ the vorticity has almost no effect on the heat flux, though at $\gamma_* = 1.13$ the effect is noticeable.

By way of illustration, in Figure 12.19 for a perfect gas with $\gamma = 1.4$ and in Figure 12.28 for equilibrium air (the conditions of Figure 12.26) we have plotted the flow parameter distributions in the shock layer on a sphere of radius R obtained by Gorshkov (see Section 12.14) by solving the Navier–Stokes equations using both the shock-fitting and the shock-capturing techniques. For $Re_\infty \geq 10^4$ the shock front is fairly thin, while at the axis of symmetry the shock layer thickness is weakly dependent on the Reynolds number and similar in value to the inviscid shock layer thickness equal to $\delta_0 \approx 0.8Rk$ (7.3.2); this is due to the smallness of the displacement thickness δ^* (see 12.13.2) for $M_\delta \approx 0$ and a small value of the enthalpy factor ($\bar{h}_w = 0.05$) typical of hypersonic flows. In this case from formula 12.13.2 it follows that $\delta/\delta_0 \approx 30Re_\infty^{-1/2}$ under the conditions of Figure 12.19 ($k = 1/6$, $M_\infty = 20$) and $\delta/\delta_0 \approx (55/C)Re_\infty^{-1/2}$ under the conditions of Figure 12.26 ($k = 0.06$, $M_\infty = 25$, and $C = 1$ to 0.7 for $Re_\infty = 10^5 - 10^3$), which for $Re_\infty \geq 10^4$ is generally consistent with the behavior of the temperature profiles in Figures 12.19 and 12.28. At the same time, for $Re_\infty = 10^3$ the boundary layer extends right to the slightly broadened shock in the former case and almost merges with the shock, whose thickness is comparable with that of the inviscid shock layer, in the latter case (these flow regimes will be considered in Section 12.14).

The distributions of the relative heat fluxes $q_w(\omega)/q_w(0)$ over the spherical surface under the conditions of Figure 12.28 are qualitatively similar to those plotted in Figure 12.14 of Section 12.8 and form a fairly narrow bundle which is not presented here. In Figure 12.29 we have plotted the profiles of the ratio q_w/q_{w0} for a sphere-cone body under the conditions of Figure 12.28, the cone angle being $\theta = 10^\circ$; here, q_{w0} is the heat flux in the absence of vorticity, that is, in our case, for $Re_\infty = 10^6$. Here, curves 1, 1', 2, and 2' were obtained by the same method, as the data in Figure 12.28, while curves 3, 4, and 5 (for $Re_\infty = 10^4$) were obtained within the framework of the PNSE model by Vlasov (as the data in Figures 12.32 to 12.34), within the framework of the exact boundary layer model,* and using the mass-average method, respectively. Clearly, curves 2 and 3 almost coalesce, curve 2' is

* Murzinov (1966); numerical calculation of the boundary layer subject to conditions 12.10.2 of its matching with an inviscid high-entropy layer.

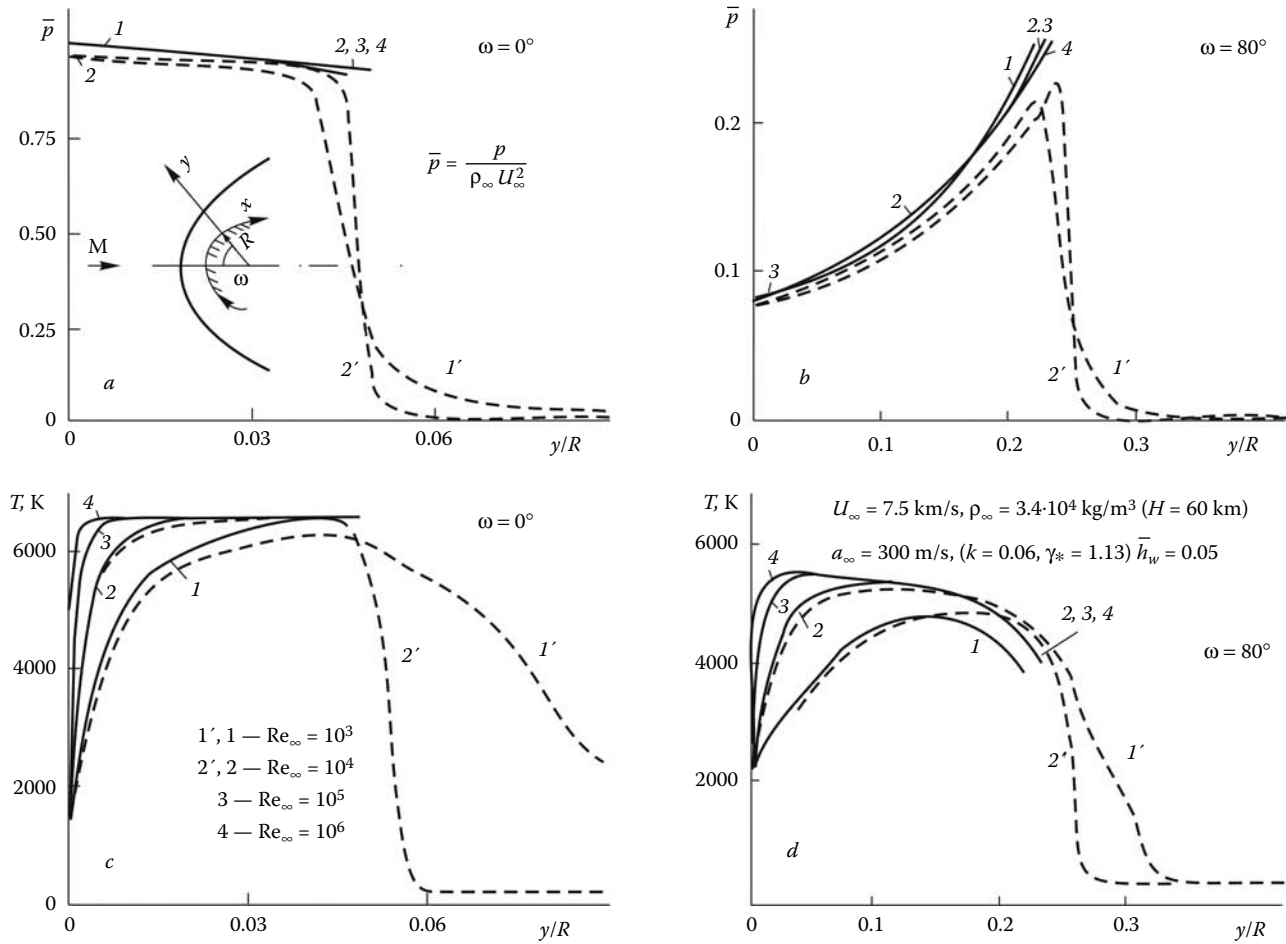


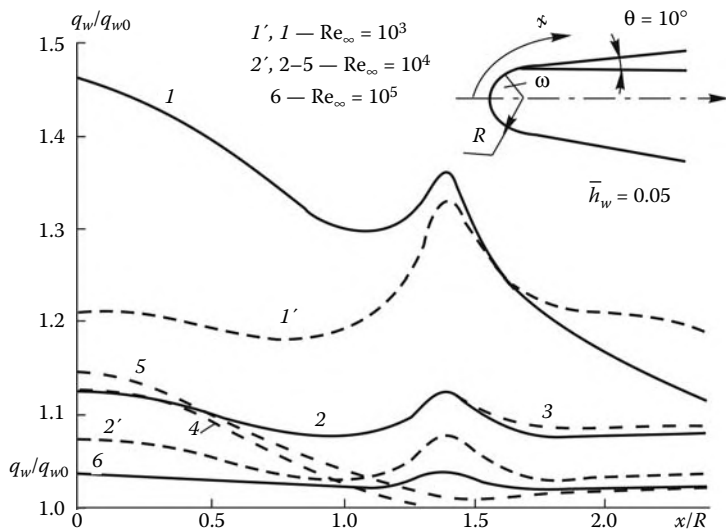
FIGURE 12.28

Pressure and temperature profiles in the shock layer on a sphere in equilibrium-dissociated air flow: (a-d), calculations using the shock-fitting technique and 1' and 2', the shock-capturing technique.

fairly near to them, while curves 4 and 5 are close to each other and to the exact data on the sphere nose. However, in the $\omega > 50^\circ$ region, curves 4 and 5 lie somewhat below the exact curves, which should be attributed to the transverse curvature effect, since in this region the boundary layer thickness is comparable with the body radius r_b (see Figure 12.28). As for the difference between curves 1 and 1', it will be discussed in Section 12.14.

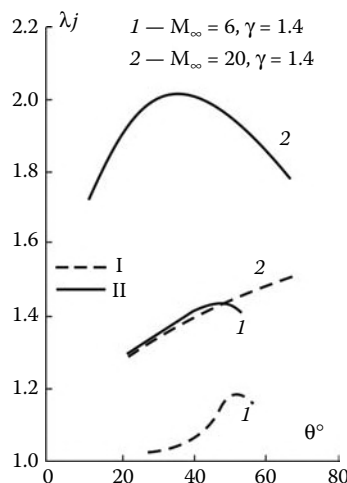
In Figure 12.27 the ratios $q_w/q^{(0)}$ for the stagnation point taken from Figure 12.29 are plotted against Re_∞ ; they form a fairly narrow bundle of curves up to $Re_\infty \geq 5 \cdot 10^3$; however, already for $Re_\infty = 10^3$ curves 1, 2, and 4 provide overestimated data, as compared with the more accurate data 3.

As for the original value of the heat flux $q^{(0)}$ at the blunt-body stagnation point without allowance for the vorticity effect, it is determined by formula 12.8.15, which is in good agreement with the results of the calculations for $Re_\infty \geq 10^4$ presented previously and, in view of the transformations 12.13.1, gives the values $q^{(0)} Re_\infty^{1/2} / \rho_\infty U_\infty^3 \approx 2.5 - 4.5$ for $M_\infty \approx 10 - 25$.

**FIGURE 12.29**

Ratio of the heat fluxes to the sphere-cone body calculated with and without account for vorticity. Curves 1, 2, and 6 relate to the calculations of the Navier-Stokes model using the shock-fitting technique, curves 1' and 2' to the same calculations using the shock-capturing technique, 3 is the PNSE model, 4 is the boundary layer model, and 5 is the mass-average value method.

We are coming now to slightly blunted bodies of the type of cones ($\nu = 1$) and wedges ($\nu = 0$); we will not assume their semi-vertex angle θ to be necessarily small, but it is smaller than the limiting value associated with the shock detachment from the corresponding sharp body. For these bodies we will estimate the greatest possible magnitude of the entropy effect by comparing the heat fluxes on the sharp and slightly blunted bodies within the framework of the classical model of the limitingly thin boundary layer, with the same

**FIGURE 12.30**

Heat flux ratio λ on sharp and blunt cones for the laminar (I) and turbulent (II) boundary layers.

pressure on their lateral surfaces and the same effective length x_{eff} 12.8.13. Then referring the subscripts 1 and 2 to the parameters on the blunt and sharp bodies, we obtain from 12.8.5 the following formulas for the heat flux ratios in the laminar ($\lambda = \lambda_l$) and turbulent ($\lambda = \lambda_t$) cases

$$\begin{aligned}\lambda_l &= \frac{q_{2l}}{q_{1l}} = \left(\frac{h_{*1}}{h_{*2}} \right)^{0.15} \left(\frac{U_2}{U_1} \right)^{0.5} \frac{He_{2l} - h_w}{He_{1l} - h_w} \\ \lambda_t &= \frac{q_{2t}}{q_{1t}} = \left(\frac{h_{*1}}{h_{*2}} \right)^{0.66} \left(\frac{U_2}{U_1} \right)^{0.8} \frac{He_{2t} - h_w}{He_{1t} - h_w}\end{aligned}\quad (12.13.10)$$

Here, as before, an asterisk refers to the relevant boundary layer parameters (see Section 12.6). To obtain the ratios of the corresponding friction parameters, the values of λ should simply be multiplied by the velocity ratio U_2/U_1 .

For cones, the ratios λ_l are presented in Figure 12.30 as functions of the semivertex angle θ . As shown previously, on a blunt body the heat fluxes are always smaller than on the corresponding blunt body; for a laminar boundary layer this entropy effect is small at $\gamma = 1.4$ and $M_\infty = 6$ but it is quite appreciable at $\gamma = 1.2$ and $M_\infty = 20$ (the dissociated air model of Sections 1.3 and 7.1). At the same time, for a turbulent boundary layer the entropy effect is considerably stronger: thus, at $\gamma = 1.4$ the maximum value is $\lambda_t \approx 1.4$, while at $\gamma = 1.2$ the peak $\lambda_t \approx 2.2$ is located in the $\theta \approx 40^\circ$ region.

The behavior of the $\lambda(\theta)$ curves is mainly determined by the velocity ratio U_2/U_1 , both velocities increasing with the angle θ . In fact, in the hypersonic Newtonian approximation of Sections 7.2 and 7.5, which is used here to make estimates, we can let for the cones with $\theta \approx 30^\circ - 60^\circ$

$$\begin{aligned}U_1 &= U_\infty \sqrt{1 - \bar{p}_b^{(\gamma-1)/\gamma}} \approx \sqrt{2k} U_\infty \cos \theta \\ U_2 &\approx U_\infty \cos \theta, \quad \bar{p}_b \approx \sin^2 \theta, \quad k = \frac{\gamma - 1}{\gamma + 1} \ll 1\end{aligned}\quad (12.13.11)$$

Thence we have $U_2/U_1 \approx (2k)^{-1/2} = 3.2 \div 1.7$ for γ ranging from 1.1 to 1.4. The peaks of the λ_t curves at $\theta \approx 40^\circ$ are due to the effect of the factor $(h_{*1}/h_{*2})^{0.66}$ in formula 12.13.10 for λ_t (on the outer edge of the boundary layer the equilibrium enthalpy H_e is only slightly dependent on the Mach number M_δ).

It is important to note that the ratios λ_i characterizing the *maximum entropy effect* are independent of the Reynolds number, which determines only the *length of the absorption* of the vortex or the high-entropy layer by the boundary layer. As the boundary layer, say, on a slightly blunted cone, is absorbed, the heat fluxes and the friction on the body surface vary from q_1 and τ_1 to q_2 and τ_2 .

By way of illustration, in Figure 12.31 we have presented the measured heat fluxes to the 45° cones with spherical noses of different dimensions for the case in which the boundary layer is turbulent; clearly, the heat fluxes are appreciably smaller for the cones with a larger bluntness, that is, a higher entropy on the boundary layer edge (Zemlyanskii, Lunev, and Marinin, 1981). The experimental data are in fairly good agreement with the results of the calculations using the mass-average value method outlined previously. In the same figure we have presented the calculated (using the same method) turbulent heat fluxes to the same cone in a $M_\infty = 20$, $\gamma = 1.2$ flow (solid curve). Here, the dash curve relates to the calculations in which viscosity was not taken into account; it lies considerably below the solid curve.

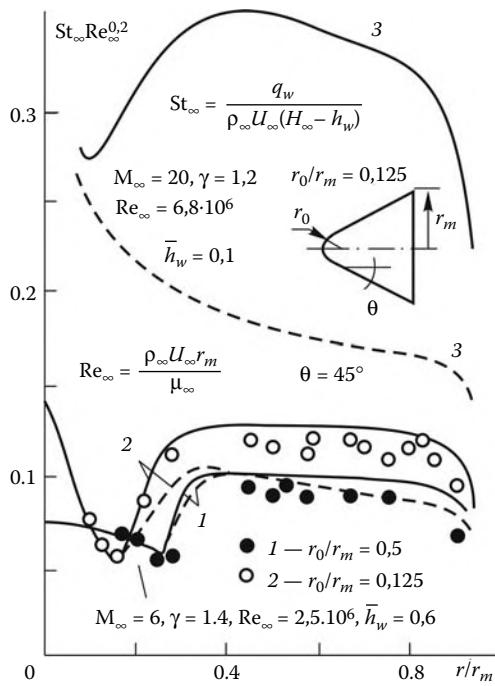
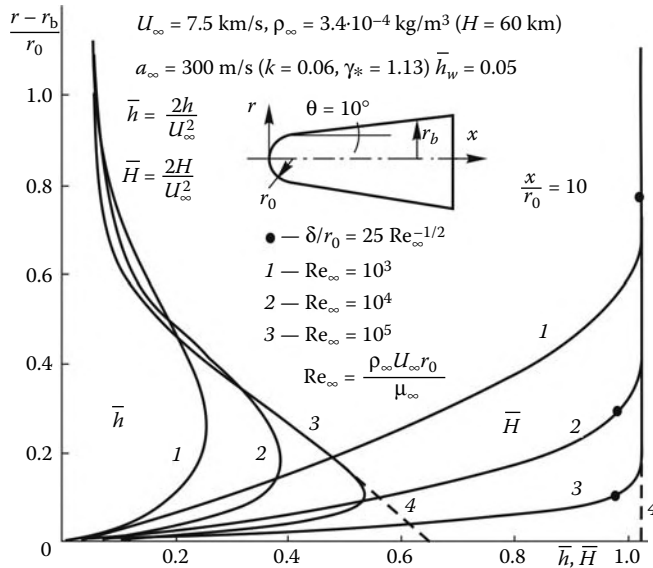


FIGURE 12.31
Experimental (symbols) and calculated (lines) turbulent Stanton numbers.

We will now consider the hypersonic flow past a thin blunt body. In this case, as distinct from the case of sharp bodies discussed in Section 12.12, the interface between the inviscid flow and the boundary layer is not so clearly defined owing to comparatively low Mach numbers in the high-entropy layer ($M \approx 2.5 \div 4$; see Figure 9.2 of Section 9.1). Therefore, in describing these flow regions separately, their interaction should be taken into account using smooth matching of the solutions of type 12.10.1 or 12.10.2.

Generally speaking, the boundary and high-entropy layers on the lateral surfaces of thin blunt bodies in hypersonic flow form an, as it were, single, transversely *isobaric* low-density layer with a small gas flow rate equal to the flow rate $\psi_0 = \pi^v r_0^{1+v} \rho_{\infty} U_{\infty}$ across the high-entropy layer (Sections 9.1 and 9.2) until it is absorbed by the boundary layer with the flow rate ψ_{δ} , that is, for $\psi_{\delta} < \psi_0$, and equal to the flow rate ψ_{δ} in the subsequent region with the same order of magnitude of ψ_{δ} as for thin sharp bodies of Section 12.12. Therefore, in any case, in accordance with the estimates of Sections 9.1, 9.2, and 12.12, we have the conditions $\psi_s \gg \psi_0$ and $\psi_s \gg \psi_{\delta}$, where ψ_s is the gas flow rate across the entire disturbed region between the body and the shock. This means that on thin blunt bodies, as on thin sharp bodies, the main gas flow rate passes through an inviscid shock layer adjoining the shock, with a high density and a low enthalpy (as compared with the stagnation values). The flow in the single isobaric layer can theoretically be described by the boundary layer equations with the same boundary conditions 12.12.5 as for thin sharp bodies.

This flow nature is visible in Figure 12.32 in which the enthalpy profiles are plotted for a cross-section on the lateral surface of a spherically blunted cone in an equilibrium air flow under the conditions of Figures 12.28 and 12.29 for different Reynolds numbers Re_{∞} (the calculations were performed within the framework of the PNSE model). Clearly, even for $Re_{\infty} = 10^3$ near the shock the enthalpy profile is similar to the original inviscid profile.

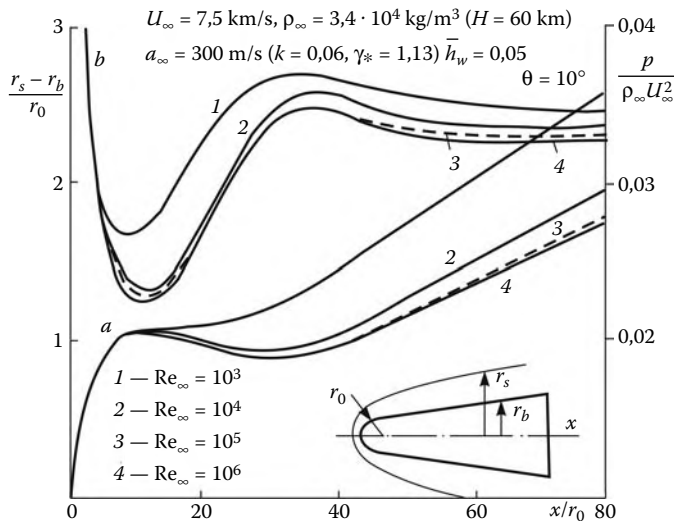
**FIGURE 12.32**

Enthalpy (\bar{h} and \bar{H}) profiles in the shock high-entropy (curves 4) and boundary (1 to 3) layers on a spherically blunted cone in equilibrium-dissociated air flow under the same conditions as in Figures 12.26 and 12.28.

Apart from the entropy effect, the displacement effect on thin blunt bodies and the transverse curvature effect on bodies of revolution can additionally take place. These effects are determined by the relative boundary layer thickness δ/r_b , where $r_b(x)$ is the shape of the lateral surface of the body. The thickness δ is determined by the local pressure and the characteristic enthalpy h_* , which is of the same order as the stagnation enthalpy, as well as by the effective length $\xi = x_{\text{eff}}$ (see Section 12.18) of the boundary layer with account for the contribution of the blunt body nose. Within the framework of the mass-average method of Section 12.11 the parameter δ can be determined by substituting the mass-averaged values for the exact ones in the corresponding formulas (for example, 12.6.23 or 12.11.3) and solving simultaneously Equation 12.11.5. However, at distances well away from the nose, $L \gg r_0$, it should be expected that the order of the boundary layer thickness is the same for the sharp and blunt bodies and can be evaluated using formula 12.12.6, which, under conditions of Figure 12.32 with account for the data of Figure 12.33b for \bar{p} and Figure 12.13b for ξ , gives a quite plausible value of $\delta/r_0 \approx 25 Re_\infty^{-1/2}$.

In Figure 12.33 we have plotted the shock shape and the pressure distribution over the body surface for a spherically blunted cone with $\theta = 10^\circ$ calculated under the conditions of Figure 12.32 and by the same method for different Re_∞ . Clearly, at $Re_\infty \geq 10^4$ the boundary layer effect on the parameters presented in the figure is not too great, so that in this case the boundary layer displacement thickness effect on the general pattern of the flow past thin blunt bodies can be neglected.* It should also be borne in mind that, though at, say, $Re_\infty = 10^4$ the boundary layer fills a considerable part of the entire disturbed layer, the

* An exception to this law is provided by the time-dependent boundary layer (laminar or turbulent) on oscillating bodies, where the displacement can affect their damping characteristics (see Krasil'nikov, Lipnitskii, Pokrovskii, and Shmanenkov, 2002).

**FIGURE 12.33**

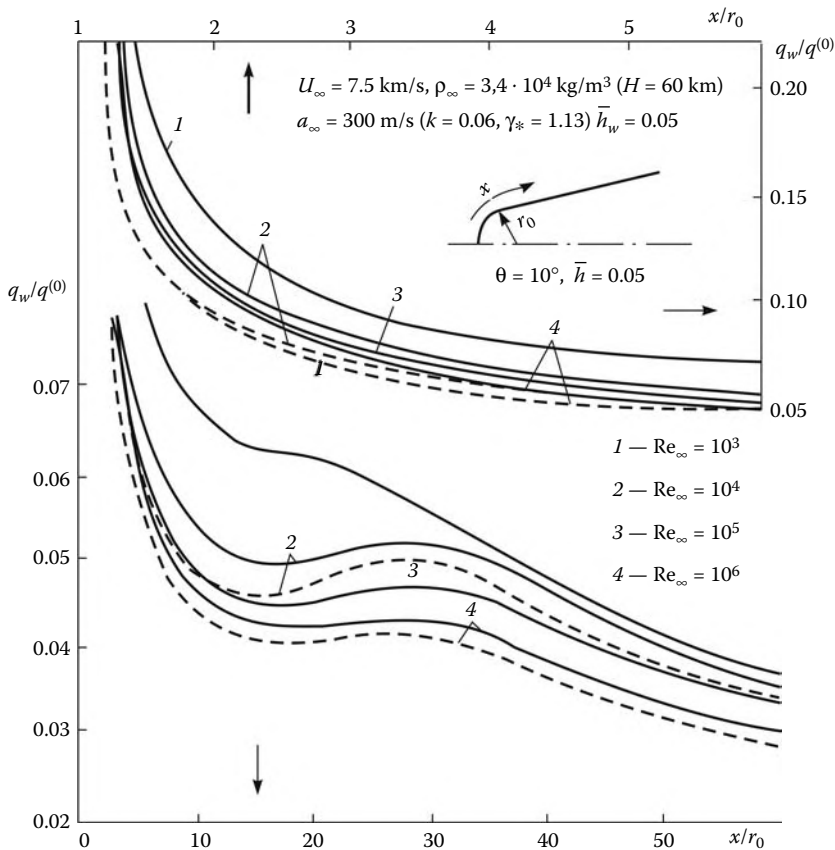
Shock wave stand-off distance (a) and pressure (b) on a cone under the same conditions as in Figures 12.28 and 12.32.

boundary layer displacement thickness is several times smaller than its own thickness due to the smallness of the enthalpy factor inherent in the hypersonic flight conditions (in this case $\bar{h}_w = 0.05$; see, e.g., Figure 12.11 of Section 12.6). At the same time, at $Re_\infty = 10^3$ the boundary layer in Figure 12.32 is appreciably thicker, while in Figure 12.33 the pressure and the shock stand-off distance are considerably greater than the same parameters for $Re_\infty \geq 10^4$.

The heat flux distribution over the same cone under the same conditions as in Figure 12.33, is presented in Figure 12.34 in the form of the ratio $q_w/q^{(0)}$, where $q^{(0)}$ is the heat flux at the stagnation point on a sphere without allowance for vorticity. Clearly, the entropy effect results in an increase of the heat fluxes when Re_∞ decreases, the heat flux maximum $q_w/q_{w0} \approx 1.2$, where q_{w0} is the heat flux in the absence of vorticity, being achieved at $Re_\infty = 10^4$ at a distance $x/r_0 \approx 40$. At the same time, in Figure 12.34 for $Re_\infty = 10^3$ the ratio q_w/q_{w0} amounts to the value of 1.4 to 1.6, which must be attributed to the transverse curvature effect and, moreover, the elevated pressure (see Figure 12.33).

For the sake of comparison, in Figure 12.35 we have also plotted the profiles of the boundary function $\bar{\psi}_\delta$, as well as the external $\bar{U}^{(0)}$ and mass-average \bar{U}_b velocities on the boundary layer edge and the velocity \bar{U}_b on the cone surface. These data should be compared with the behavior of the functions $G(\bar{\psi})$ and $G_a(\bar{\psi})$ in Figure 12.26. As the Reynolds number increases, the zone of the high-entropy layer absorption by the boundary layer extends in accordance with the $\psi_\delta \sim r_b^\nu (x/r_0)^{1/2} Re_\infty^{-1/2} = \text{const}$ law.

In Figure 12.36 the relative heat fluxes q_w/q_{w0} are presented for the same cone at $Re_\infty = 10^4$. The curves, taken from Figure 12.34, are calculated within the framework of the exact boundary-layer model (Murzinov, 1966) and by the mass-average method. As in Figure 12.29, both methods give similar results, though somewhat underestimated on the frontal surface of the cone, as compared with the exact data; this should be attributed to the fact that these methods do not allow for the transverse curvature effect.

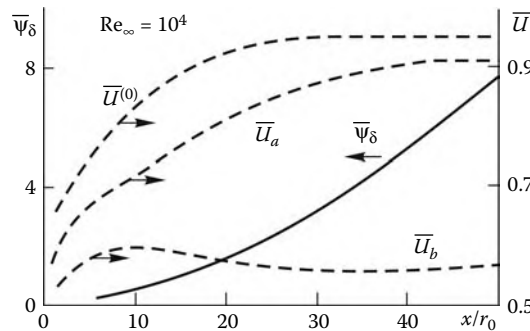
**FIGURE 12.34**

Heat flux distribution over a spherically blunted cone in equilibrium-dissociated air flow: the solid curves relate to the PNSE method and the dashed curves to the mass-average value method.

For a turbulent boundary layer in equilibrium air, the heat flux and friction distributions over the blunt cone surface obtained by the mass-average value method are presented in Figure 12.37. As compared with the laminar boundary layer, the entropy effect is, in accordance with Figure 12.30, more pronounced: the heat flux varies by a factor of 1.5 and the friction by a factor of 2.5. As the Reynolds number decreases, the q_w/q_{w0} ratio increases with simultaneous shrinking of the zone of the high-entropy layer absorption by the boundary layer. The calculations using the external velocity $\bar{U}^{(0)}$ lead to further shrinking of the absorption zone and an increase in the heat flux.

We call attention to the wavy character of the heat flux distributions over blunt cones, which is similar to the behavior of the pressure distribution in Figure 12.33 and, particularly, Figure 12.37 for the turbulent boundary layer.

In Figure 12.38a the experimental distribution of the turbulent heat flux over a slender blunt cone is compared to the calculation performed by the mass-average value method (curve 1) and the turbulent parabolized Navier-Stokes equations (Kovalev, 1997). Curve 2 is obtained within the framework of the algebraic turbulence model (Boldwin and Lomax, 1978) and curve 3 within the framework of the differential $k-\omega$ model (Wilcox, 1994, see Section 12.7). In Figure 12.38b similar experimental data are presented for a blunt double

**FIGURE 12.35**

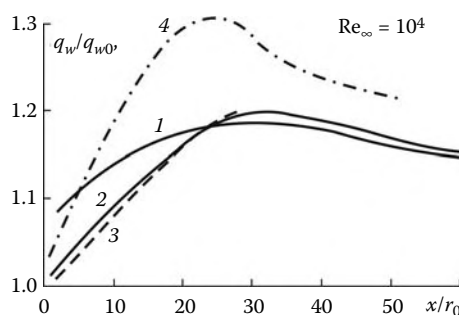
Distributions of the stream function $\bar{\psi}_\delta$, the external velocity $\bar{U}^{(0)}$, and the mass-average velocity \bar{U}_a along the outer edge of the boundary layer on a blunt cone and the velocity \bar{U}_b distribution over the body surface.

cone (Karpov). In both cases, the agreement between the calculated and measured results is quite satisfactory. However, it is important that the use of seemingly more promising, higher-order models, as compared with the mass-average value method, does not generally lead to the higher accuracy of the calculated results. However, here there is no contradiction, since all the turbulence models are tested and adapted against the same set of experiments.

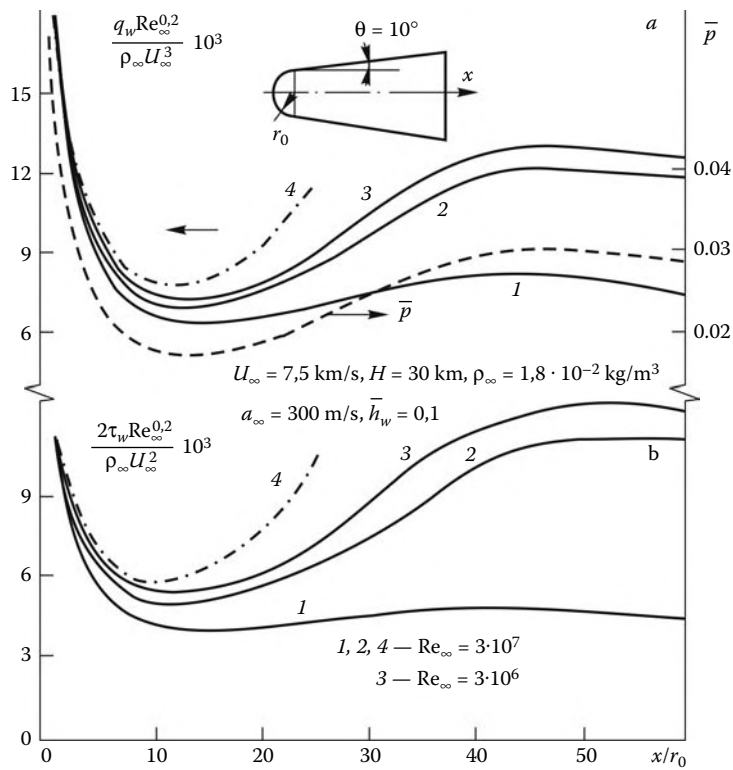
We will now consider briefly the similarity laws for the viscous hypersonic flow past thin blunt bodies (Lunev, 1961, 1962); for inviscid flows such laws were derived in Chapter 9 and for viscous flows past sharp bodies in Section 12.12. Within the framework of the scheme of Section 9.1, which accounts for the body nose effect on the flow as a whole, taking dissipative terms into account requires introducing two new relevant parameters, namely, the overall heat loss Q_0 in the vicinity of the nose and the force X_f acting on the nose, or in the dimensionless form

$$\bar{Q}_0 = \frac{Q_0}{\pi^\nu r_0^{1+\nu} \rho_\infty U_\infty^3}, \quad \bar{X}_f = \frac{X_f}{\pi^\nu r_0^{1+\nu} \rho_\infty U_\infty^2} \quad (12.13.12)$$

However, at fairly high Reynolds numbers these parameters can be neglected as compared with the total flux of the enthalpy $\pi^\nu r_0^{1+\nu} \rho_\infty U_\infty H_\infty$ through the nose vicinity and the nose drag X_0 . Then the set of the similarity criteria incorporates the same criteria as for

**FIGURE 12.36**

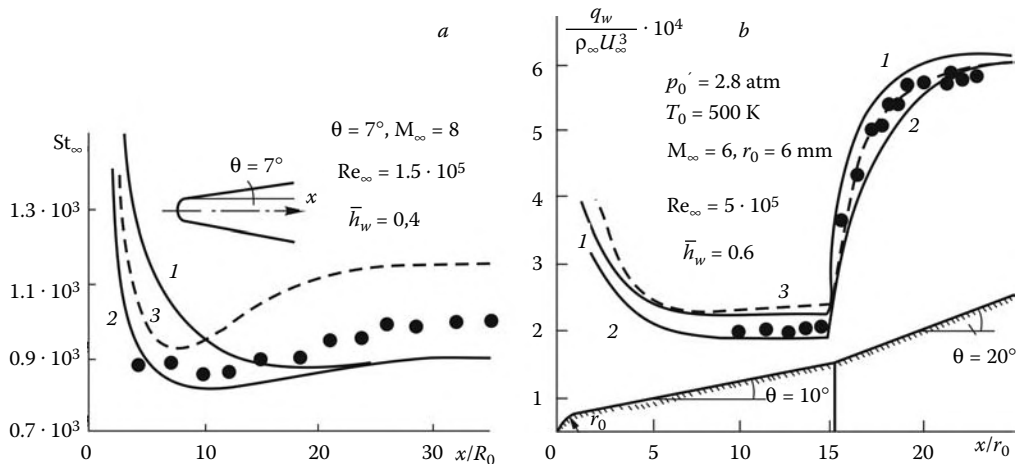
Ratio of the heat fluxes to a blunt cone calculated with and without account for vorticity: 1, exact calculation; 2, mass-average value method (the data of Figure 12.34); 3, boundary layer model; and 4, calculation on the basis of the external parameters.

**FIGURE 12.37**

Turbulent heat flux (a) and friction (b) distributions over a spherically blunted cone: 1, calculation without regard for vorticity; 2 and 3, mass-average value method; and 4, calculation on the basis of the parameters on the outer edge of the boundary layer.

inviscid flows, namely, parameters 9.2.2 or 9.2.8 for bodies with geometrically and affinely similar shapes of the surface, respectively. Then the whole variety of the bluntness shapes is characterized by their drag coefficient c_{x0} .

At the same time, due to the fact that, in view of the smallness of the density in this layer (see Sections 9.1 and 9.2), the pressure is constant across the high-entropy layer on the lateral surface of the body, it can be united with the boundary layer developing within it and described by the single system of Equations 12.5.5 through 12.5.8. For this system, the corresponding initial conditions should be preassigned in an initial section of the lateral surface. Within the framework of the scheme adopted in Sections 9.1 and 9.2, these conditions must involve, first, the entropy distribution $s(\bar{\psi})$ in the high-entropy layer and, second, the momentum (δ^{**}) and energy (Θ) thicknesses determined by formula 12.8.2 and 12.8.3. As shown in Section 9.2, in high-entropy layers the flow similarity is ensured by the semiempirical fact that the function $s(\Psi)$, where $\Psi = 2\bar{\psi}/c_{x0}$, is universal, though the parameters δ^{**} and Θ are, in the general case, dependent on the nose shape, so that the sought similarity law is related with the possibility of neglecting the effect of these parameters. This possibility is demonstrated in Figure 12.13b and c, of Section 12.8 in which the effective length of the boundary layer on a body surface fairly rapidly “forgets” its initial (at $x = 0$) value.

**FIGURE 12.38**

Comparison of the calculated results (curves) with the experimental data (symbols) for blunt cones: mass-average value method (a) and algebraic (b) and differential (c) turbulence models.

In this approximation, for obtaining a complete set of the required similarity criteria, only the criteria χ_l and χ_t obtained in Section 12.12 for the laminar and turbulent boundary layers, respectively (see 12.12.6 and 12.12.34), should be added to the inviscid criteria of Equation 9.2.2 or 9.2.8. In this case, the similarity variables are the same as in 8.4.1 and 8.4.2 of Section 8.4 or in 12.12.27 to 12.12.29 of Section 12.12; as for heat fluxes and friction, the following dimensionless functions of the variable x/L are the same in similar flows: $\tilde{C}_q = 2q_w/\rho_\infty U_\infty^3 \theta_0^3$ and $\tilde{C}_f = 2\tau_w/\rho_\infty U_\infty^2 \theta_0^3$.

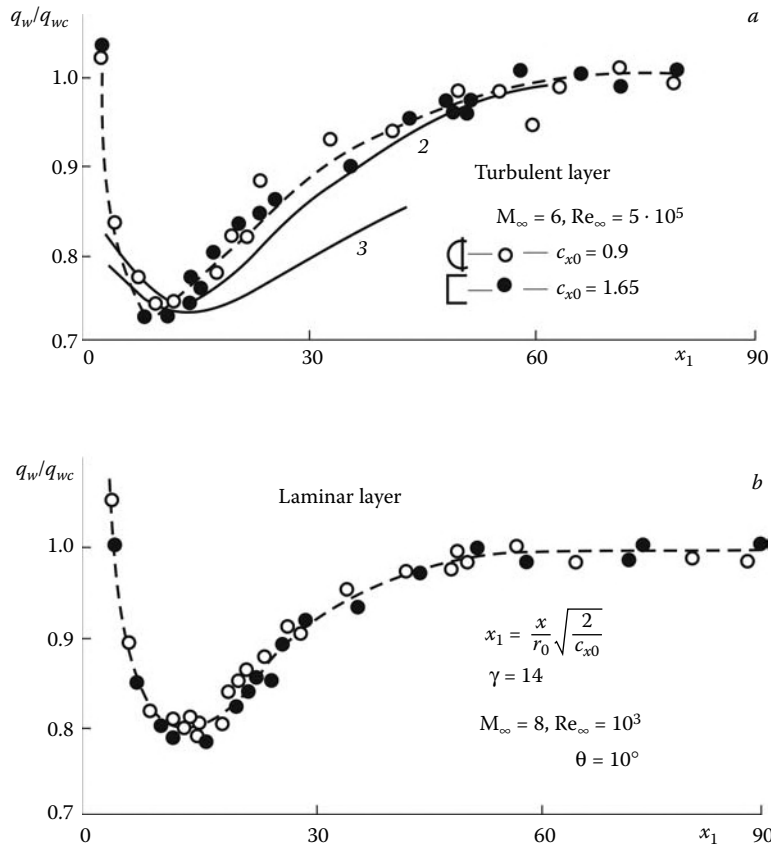
Since blunt cones have no characteristic dimensions, in accordance with Section 9.2, the scale length L should be determined from the condition $\bar{X}_2 = 1$ (see Equation 9.2.8) or $L = (2/c_{x0})^{1/(1+\nu)} \theta_0^{-(3+\nu)/(1+\nu)} r_0$. Then the expressions for the parameters χ_l and χ_t take the form:

$$\begin{aligned} \tilde{\chi} &= M_\infty^{3-n} \left(\frac{c_{x0}}{2} \right)^{\frac{1}{2(1+\nu)}} \theta_0^{(3+\nu)/2(1+\nu)} \text{Re}_\infty^{-1/2}, \quad \text{Re}_\infty = \frac{\rho_\infty U_\infty r_0}{\mu_\infty} \\ \tilde{\chi}_t &= M_\infty^{1.8-0.4n} \left(\frac{c_{x0}}{2} \right)^{\frac{0.2}{1+\nu}} \theta_0^{0.2(3+\nu)/(1+\nu)} \text{Re}_\infty^{-0.2} \end{aligned} \quad (12.13.13)$$

In this case, in accordance with 9.2.8, the parameters $M_\infty \theta_0$ and γ , or, for real gases, the freestream parameters ρ_∞ and U_∞ , are also the similarity criteria.

In Figure 12.39a and b,* for the cones differing only in the nose shape (sphere and flat-ended nose) the measured heat flux distribution is plotted against the similarity variable $x_1 = (2/c_{x0})^{1/2}(x/r_0)$. The ratio q_w/q_{wc} is presented, where q_{wc} is the heat flux on the local sharp cone of the same cross-section. In any case, the experimental points in Figure 12.39 are concentrated in the vicinity of unified curves. The calculations of the turbulent heat flux by the mass-average value method (for a spherically blunted cone) gives a satisfactory accuracy, the entropy effect being appreciable in this case.

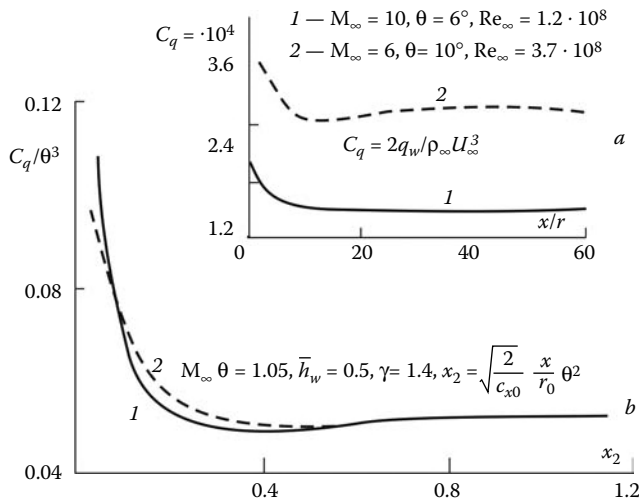
* The data in Figures 12.39 to 12.41 were obtained by Karpov (1968).

**FIGURE 12.39**

Distributions of the relative heat fluxes over blunt cones with spherical and flat-ended noses in the similarity coordinates: the solid curves relate to the calculations with (2) and without (3) account for vorticity; q_{wc} is the heat flux on the sharp cone.

In Figure 12.40 we have presented the results of calculations by the mass-average value method of the turbulent heat fluxes on spherically blunted cones; the cone angles θ are different but the parameters $M_\infty \theta_0$ and $\tilde{\chi}_t$ are the same. The curves are appreciably different when plotted in the original variables, but in the similarity coordinates $\tilde{C}_q(x_2)$, where $x_2 = (2/c_{x0})^{1/2}(x/r_0)\theta^2$, they are very close. Finally, in Figure 12.41 the calculated heat flux ratios q_w/q_{w0} on cones in an equilibrium air flow are plotted against the similarity variable x_2 . In these variables, all the data are grouped near the same universal curve.

In conclusion, we note one more property of high-entropy layers on slender blunt cones, which also bears direct relationship to boundary layers. In Figure 12.42 we have presented the ratio Re/Re_s of the Reynolds numbers based on the local parameters in the disturbed layer (Re) and those directly behind the shock (Re_s). Clearly, on the surface of the blunt cone in a hypersonic flow the Reynolds numbers Re are considerably smaller than those on the sharp cone. However, so great discrepancy in Re does not lead to the corresponding difference in the heat fluxes, which are mainly dependent on the relevant parameters of the boundary layer (ρ_* and others), which, in turn, are determined by the stagnation enthalpy to a higher degree than by the boundary Mach number M_δ . However, this reduction in

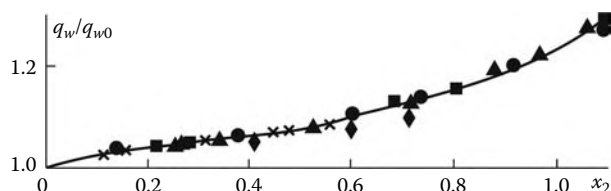
**FIGURE 12.40**

Heat flux distributions over blunt cones in the original (a) and similarity (b) coordinates.

the Reynolds number in the high-entropy layer can appreciably displace downstream the onset of laminar-turbulent transition in the boundary layer or to affect the dimensions of the transition zone.

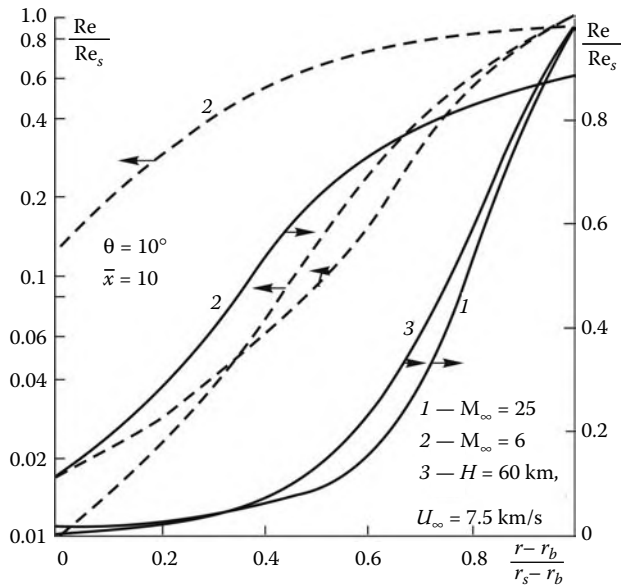
12.14 Flows in Viscous Continuous and Shock Layers

In Section 12.13 the viscous heat-conducting gas flow past bluff and blunt bodies was mainly considered for high and moderate Reynolds numbers, when the boundary layer

**FIGURE 12.41**

Ratio of the turbulent heat fluxes calculated with and without account for vorticity in the similarity coordinates for the parameters given in table:

	$U_\infty, \text{km/s}$	θ_0, deg	Re_∞
●	4	15	$5 \cdot 10^5$
△	7.5	10	$3 \cdot 10^7$
□	6	10	$5 \cdot 10^6$
◊	3	10	$4 \cdot 10^5$
×	6	5	$2 \cdot 10^7$

**FIGURE 12.42**

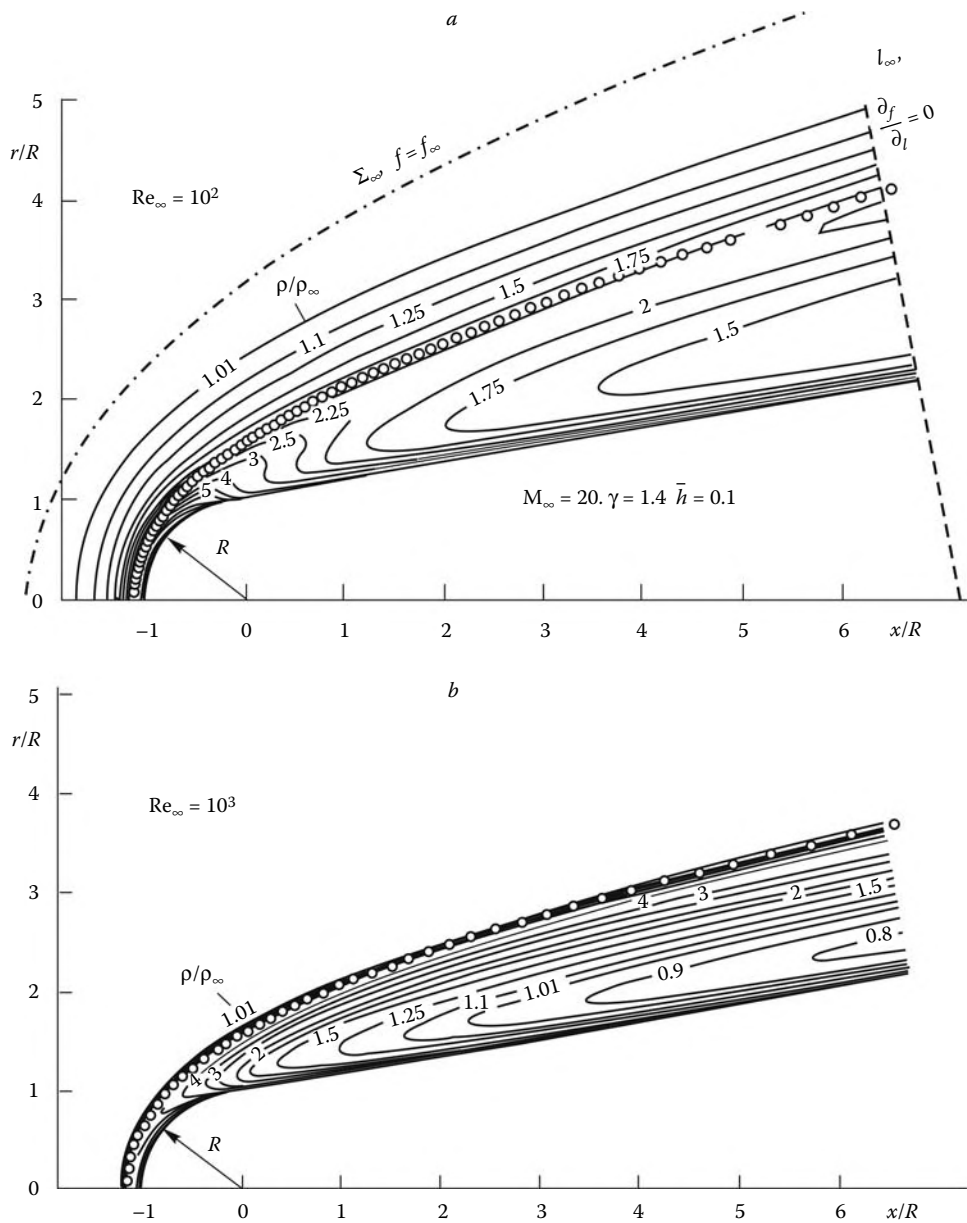
Reynolds number profiles in the shock layer on a blunt cone.

thickness was not greater than that of the disturbed layer though it could be comparable with it. However, as the Reynolds number decreases, the flow nature changes with the formation of a *continuous viscous layer* ahead of the body (see Section 12.9); this is illustrated by the curves for $Re_\infty = 10^2$ in Figure 12.19 and $Re_\infty = 10^3$ in Figure 12.28. In Figures 12.43 and 12.44 we have plotted the *isochores*, or density contours, in the perfect-gas flow past a spherically blunted cone and a sphere (the same conditions and method of calculation as in Figure 12.19). While at $Re_\infty = 10^3$ a high-density near-inviscid flow region still exists between the body and the broadened shock, at $Re_\infty = 10^2$ such a layer no longer exists.

For a blunt cone in Figure 12.45 we have plotted the density profiles across the shock layer, including that for the inviscid flow. Outside the boundary layer the inviscid curve coincides with the curve for $Re_\infty = 10^3$, which indicates the presence of an inviscid shock layer adjoining the shock in this case. However, viscosity smears the shock front, so that the maximum density behind the shock is considerably lower than the inviscid one. At the same time, at $Re_\infty = 10^2$ a continuous viscous layer is formed, that is, the viscosity effect extends over the entire disturbed layer and the maximum density in the broadened shock is lower than the inviscid one by a factor of 2.5.

The pressure distribution over the same body under the same conditions is presented in Figure 12.46 and that over a sphere in Figure 12.47a. As in Figure 12.33, the pressure considerably increases as Re_∞ decreases.

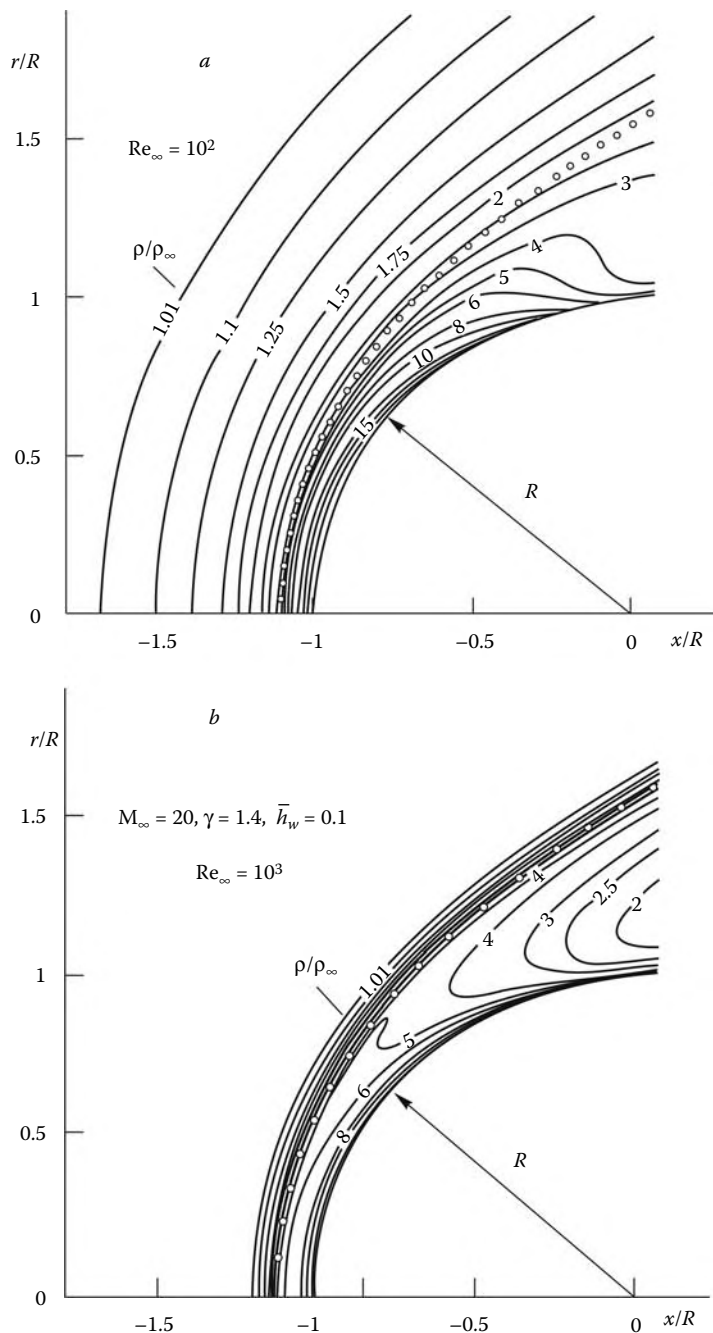
For describing such flows the complete system of Navier–Stokes equations (see Section 12.1) should be invoked, at least, for moderately dense (in the meaning of Sections 1.1 and 1.4) gases, the description of which does not require transition to the Boltzmann equations or equivalent *statistic simulation models* (see Section 11.13). For these flows, far upstream ahead of the body the condition that the flow parameters tend asymptotically to their undisturbed values is imposed; the same condition is preassigned far from the body in the

**FIGURE 12.43**

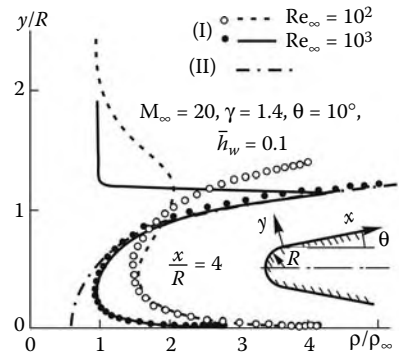
Density contours ($\rho/\rho_\infty = \text{const}$) in the spherically blunted cone flowfield in a perfect gas. Symbols relate to the shock front calculated by the PNSE method.

lateral direction, while in a certain downstream section $l = l_\infty$, where l is the longitudinal coordinate, the soft boundary conditions (see Sections 1.11 and 5.3) are imposed

$$\begin{aligned} \tilde{R} &= \sqrt{x^2 + y^2} \rightarrow \infty, \quad l < l_\infty : \quad f \rightarrow f_\infty \\ f &= u, v, p, \dots, \quad l = l_\infty : \quad \frac{\partial f}{\partial l} = 0 \end{aligned} \quad (12.14.1)$$

**FIGURE 12.44**

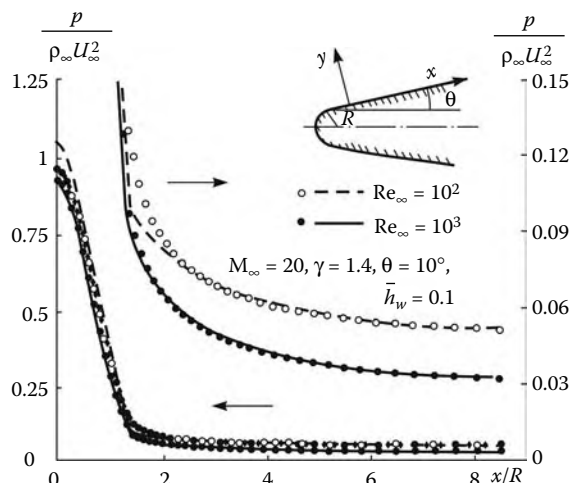
Density contours ($\rho/\rho_\infty = \text{const}$) in the sphere flowfield under the same conditions as in Figure 12.43. Symbols relate to the shock front calculated by the PNSE method.

**FIGURE 12.45**

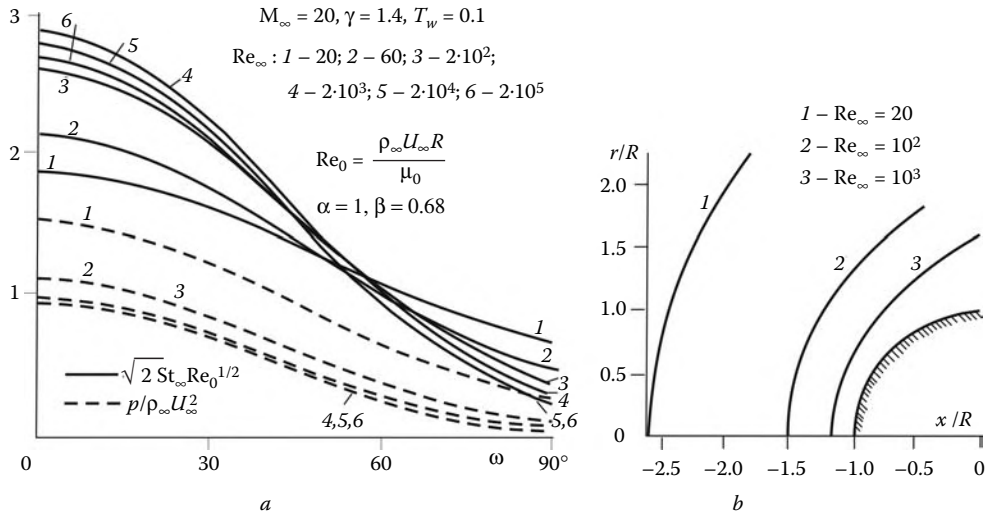
Density profiles in the shock layer on a blunt cone under the same conditions as in Figure 12.43. Curves relate to the calculations using the Navier-Stokes (I) and inviscid (II) models and symbols to the PNSE method.

The corresponding flow diagram is presented in Figure 12.43a; it is similar to that outlined in Section 5.3 (Figure 5.5) with the difference that here a simplified version of condition 5.3.2 in the section $l = l_\infty$ is used. By analogy with the problem of Section 3.2 on the structure of the broadened shock front, it might be expected that the solution approaches the undisturbed flowfield in accordance with a power law, $f - f_\infty \sim e^{-\tilde{R}/r_0}$, so that we can actually transfer the boundary conditions at infinity to a certain surface Σ_∞ at a finite distance from the body; such a surface is conditionally shown in Figure 12.43a.

However, in formulating the boundary conditions on a body surface at Reynolds numbers $Re_\infty \leq 10^2$ the slip and temperature jump effects outlined in Section 12.1 should be taken into account; these effects are described by formulas 12.1.2 and 12.1.4 for the velocity u_g and the temperature T_g at the wall. We will transform these formulas using the well-known formula for the local mean free path $l = \kappa(\mu_g/\rho_g)(\pi \bar{M}/2RT_g)^{1/2}$, where the

**FIGURE 12.46**

Pressure distributions over blunt cones under the same conditions as in Figure 12.43. Curves relate to the Navier-Stokes equations and symbols to the PNSE method.

**FIGURE 12.47**

Heat fluxes and pressure (a) and disturbed layer thicknesses (b, $\rho/\rho_\infty = 1.1$ contours) on a sphere for low Reynolds numbers.

subscript g refers to the parameters at the temperature $T = T_g$ and $\kappa \sim 1$ is a correction coefficient. This formula is derived from Equation 1.4.9 with 11.13.4 taken into account. Since $\mu(\partial u/\partial y) = \tau_w$ and $\lambda(\partial u/\partial y) = q_w + \tau_w u_g \approx q_w$, for a perfect gas the previously mentioned formulas can be presented in the form:

$$\begin{aligned} \bar{u}_g &= \frac{u_g}{U_\infty} = \frac{1}{\bar{p}} A_u \bar{T}_g^{1/2} C_f, & C_f &= \frac{2\tau_w}{\rho_\infty U_\infty^2}, & \bar{T} &= \frac{T}{T_0}, & \bar{p} &= \frac{p}{\rho_\infty U_\infty^2} \\ \bar{T}_g - \bar{T}_w &= \frac{1}{\bar{p}} A_T \bar{T}_g^{1/2} St_\infty, & St_\infty &= \frac{q_w}{\rho_\infty U_\infty c_p (T_0 - T_w)} \end{aligned} \quad (12.14.2)$$

Here, T_0 is the characteristic temperature and A_u and A_T are the following functions of the accommodation coefficients α and β

$$A_u = \frac{(2-\alpha)\kappa}{4\alpha}, \quad A_T = \frac{(2-\beta)\kappa \Pr}{2\beta}, \quad F = \frac{2\mu T_0 R}{U_\infty^2 \bar{M}} \quad (12.14.3)$$

Strictly speaking, the quantities u_g and T_g thus obtained should be referred to the boundary of the Knudsen layer having a thickness of the order of a mean free path, which generates the *Knudsen displacement effect*, which is not taken into account within the framework of the Navier-Stokes model.

The nature of the flow past blunt bodies at small Reynolds numbers is determined by the relative thickness of an isolated shock. Since in the Navier-Stokes approximation the problem of Section 3.2 on the shock structure does not involve a scale length, the thickness Δ_0 of the *high-temperature* subdomain of the shock front can be determined from the condition

$$Re_{0\Delta} = \frac{\rho_\infty U_\infty \Delta_0}{\mu_0} \sim 1, \quad \mu_0 \sim \mu_\infty M_\infty^{2(1-n)} \quad (12.14.4)$$

Here, μ_0 is viscosity corresponding to the stagnation temperature determined from 12.12.1. Thence for the ratios of Δ_0 to the thickness δ of the boundary layer on a blunt

body and to the body dimension r_0 we obtain the following estimates

$$\bar{\Delta}_{0\delta} = \frac{\Delta_0}{\delta} \sim \text{Re}_0^{-1/2} \sim \left(\frac{\mu_0}{\mu_\infty} \right)^{1/2} \text{Re}_\infty^{-1/2}, \quad \bar{\Delta}_0 = \frac{\Delta_0}{r_0} \sim \frac{\mu_0}{\mu_\infty \text{Re}_\infty} \quad (12.14.5)$$

The parameters $\bar{\Delta}_0$ and $\bar{\Delta}_{0\delta}$ are the counterparts of the Knudsen number introduced in Section 12.1 under the particular conditions of the hypersonic flow past bodies and Re_∞ is the Reynolds number based on the freestream parameters: $\text{Re}_\infty = \rho_\infty U_\infty r_0 / \mu_\infty$.

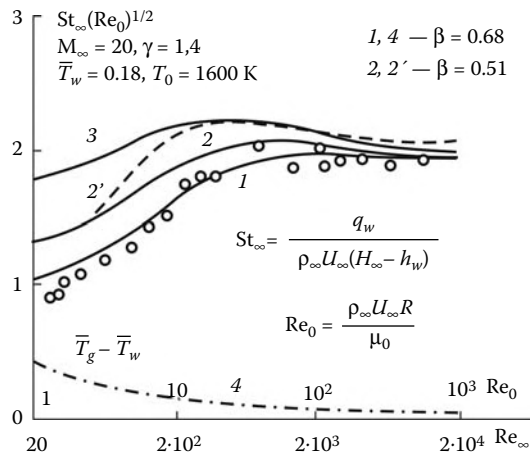
At the same time, the thickness Δ_∞ of the outer part of the shock front with viscosity $\mu \sim \mu_\infty$ or the temperature $T \sim T_\infty$ is of the order $\Delta_\infty / \Delta_0 \sim M_\infty^{2(n-1)} \ll 1$, which is the cause of fairly clearly defined boundaries of the fronts of propagation of high-temperature domains in many figures presented previously (and strictly clearly defined fronts in the $\mu_\infty / \mu_0 \rightarrow \infty$ limit; Sychev, 1961).

Naturally, estimate 12.14.5 is accurate to coefficients of the order of unity and describe only the asymptotic dependence of the parameters $\bar{\Delta}_0$ and $\bar{\Delta}_{0\delta}$ on the Mach and Reynolds numbers, when $M_\infty \rightarrow \infty$ and $\text{Re}_\infty \rightarrow \infty$. As for the actual, *visual* flow pattern, it is also affected by other flow parameters, in particular, the gas density ρ_0 in the disturbed layer or the ratio $\Delta_0 / \delta^{(0)}$, where $\delta^{(0)} \sim r_0 \rho_\infty / \rho_0$ is the disturbed layer thickness. Thus, in Figure 12.28 the ratio $\delta^{(0)} / r_0$ for $\text{Re}_\infty = 10^3$ is considerably smaller than that in Figure 12.19 (Section 12.9) for $\text{Re}_\infty = 10^2$; however, in the former case the value of Δ_0 is also smaller, so that in both cases the flow patterns are qualitatively similar. It should also be noted that there is a difference between an isolated shock and a broadened shock lying on the blunt body in the flow, since in the latter case the shock thickness is affected by gas spreading.

We will note one more effect. Earlier (in Section 12.13) it was shown that, at least, at $\text{Re}_\infty \geq 10^3$ the reduction in the Reynolds number leads to a relative increase in the heat flux $q_w / q^{(0)}$ at the blunt-body stagnation point; here, $q^{(0)} = q_w$ as $\text{Re}_\infty \rightarrow \infty$ (see, e.g., Figures 12.27 and 12.29 and formula 12.13.9). This effect is related with an increasing role of the shock-layer flow vorticity as the boundary layer thickness grows. However, with further decrease in the Reynolds number the inverse process of a decrease in the product $\text{St}_\infty \text{Re}_\infty^{1/2}$, which remains constant as $\text{Re}_\infty \rightarrow \infty$, is observed; here, St_∞ is the Stanton number (see 12.14.2). This follows from Figures 12.47a (calculations) and 12.48 in which the measured values of the heat flux at the stagnation point on a sphere in a perfect gas flow are presented; they indicate a twofold decrease in the product $\text{St}_\infty \text{Re}_\infty^{1/2}$ when Re_∞ decreases from about 10^3 to about 20 (Gusev and Nikol'skii, 1971*).

In order to provide the explanation of this effect, in the same Figure 12.48 we have presented the curves calculated within the framework of the Navier–Stokes equations (Vlasov and Gorshkov, 2001; Figures 12.50 to 12.52 are also taken from that work). Curves 1 and 2 were obtained with allowance for the temperature jump effect at quite plausible parameters $\kappa = 1$, $\beta_1 = 0.68$, and $\beta_2 = 0.51$ (see Kogan, 1966). Clearly, curve 1 is in good agreement with the experimental data; the corresponding curve $T_g / T_0 = \bar{T}_g(\text{Re}_\infty)$ is also plotted in the same figure. At the same time, in Figure 12.48 curve 3 calculated without regard for the temperature jump, is located considerably above curve 1 and the experimental data in the low Reynolds number region. This makes it possible to suppose that the main cause for

* In the original figure the Reynolds number $\text{Re}_0 = \rho_\infty U_\infty r_0 / \mu_0$, where μ_0 is viscosity at the stagnation temperature $T_0 = 1600$ K, was used. In this case, the freestream temperature was $T_\infty \approx 20$ K; since the Sutherland formula 1.3.9 used in the calculations was not checked at so low temperatures, the Reynolds numbers $\text{Re}_\infty \approx 20 \text{Re}_0$ presented here, indicate only the order of magnitude.

**FIGURE 12.48**

Reynolds-number dependence of the heat flux and temperature at the stagnation point on a sphere; curves 1 to 4 relate to the Navier-Stokes model, 2' to the PNSE method, curve 3 is calculated without regard for the temperature jump; symbols are the experimental data.

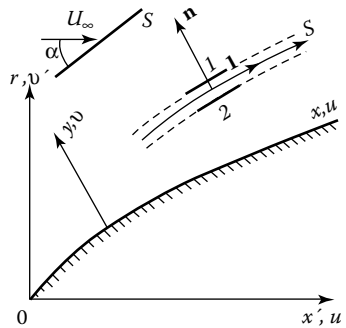
the reduction in the relative heat flux $q_w/q^{(0)}$ with the Reynolds number is the temperature jump effect.

In connection with the data in Figures 12.47 and 12.48 we note that at small Reynolds numbers $Re_{\infty} \approx 20$ the heat flux to the stagnation point and at $Re_{\infty} < 10^2$ also the pressure p'_0 can be greater than seemingly the greatest possible incident energy flux $\rho_{\infty} U_{\infty}^3/2$ and momentum $\rho_{\infty} U_{\infty}^2$. However, here there is no contradiction, since the effect is caused by the ejecting action of stream jetlets in a thickened layer adjoining the axis of symmetry.*

In view of the results presented, there is reason to hope that the heat flux level can reliably be predicted for the Reynolds numbers as low as $Re_{\infty} \approx 20$, though, considering that this suggestion has not been adequately tested, an excessive optimism should scarcely be displayed in this question, the more so that the problem of determining the accommodation coefficients is in no way simple. Moreover, the solution of the analogous problem within the framework of molecular kinetic theory (using statistical simulation; see, e.g., Gupta and Simmond, 1986) indicate that at $Re_{\infty} \approx 20$ the disturbed layer on the sphere is considerably thicker than it is predicted by the Navier-Stokes model.

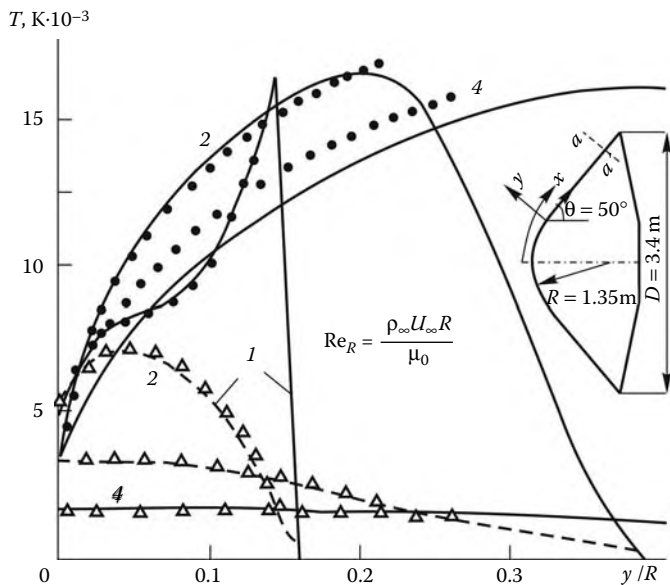
We are now coming to the subsequent issue. For *moderately high* (in the meaning of Section 12.9) Reynolds numbers, that is, for *viscous shock layers*, the model of the parabolized Navier-Stokes equations, called the *PNSE model* in Section 12.9, can be used as intermediate asymptotics between the Navier-Stokes equations and the model of inviscid flow with the classical boundary layer on the wall. The PNSE model is based on the system of Equations 12.5.5 through 12.5.8 (see Section 12.5) written in the body-fitted curvilinear coordinate system x, y with the velocity projections u and v onto these axes and with the right-hand side F_j omitted from Equation 12.5.6, that is, for the *inviscid* form of this equation.

* This effect takes place also at $M_{\infty} \approx 0$, when for $Re_{\infty} \approx 20$ the ratio $2(p'_0 - p_{\infty})/\rho_{\infty} U_{\infty}^2 \approx 1.3$ (see, e.g., Shue, 1975, and Lunev and Selezneva, 2000).

**FIGURE 12.49**

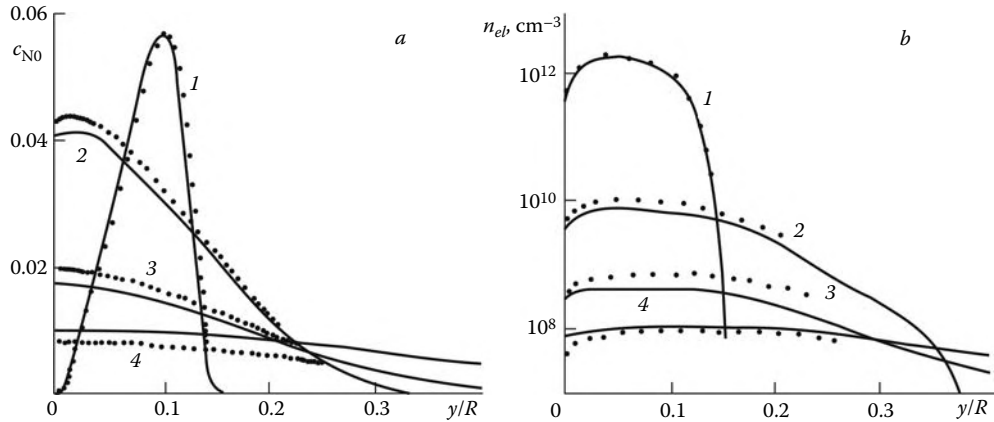
On the derivation of the generalized Hugoniot relations.

Within the framework of this model it is possible to allow for a relatively small, though finite, thickness of the shock wave. In this case, the external boundary conditions are transferred to a conditional midline S of the shock wave using the *generalized Hugoniot relations* represented by Equations 1.7.12 derived in Section 1.7. We will write down these relations

**FIGURE 12.50**

Distribution of the translational (I) and vibrational (II) temperatures in section $a - a'$ of the OREX vehicle for the parameters given in the following table. The vehicle shape is presented at the right of the figure. Curves and symbols relate to the Navier-Stokes and PNSE models, respectively.

	H, km	$\text{Re}_{\infty R}$	$\rho_{\infty}, \text{kg/m}^3$	$U_{\infty}, \text{m/s}$	T_{∞}, K	T_w, K
1	84	7300	$1.095 \cdot 10^{-5}$	7416	189	785
2	96.8	630	$9.36 \cdot 10^{-7}$	7456	190	485
3	101.1	320	$4.83 \cdot 10^{-7}$	7455	197	402
4	105	150	$2.34 \cdot 10^{-7}$	7451	211	332

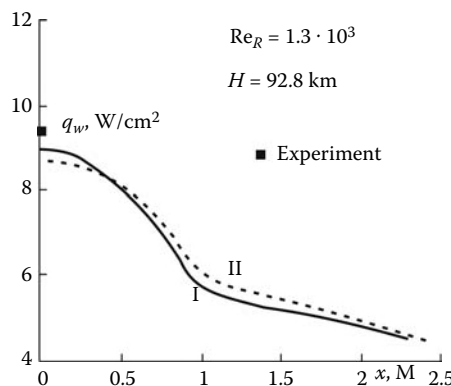
**FIGURE 12.51**

Distributions of NO (1) and electron (2) concentrations in section $a - a'$ of the OREX vehicle under the same conditions as in Figure 12.50.

as applied to our problem. For this purpose, we introduce a local Cartesian coordinate system l, n fitted to the shock front S (Figure 12.49). Here, the direction of the vector \vec{n} of the normal is opposite to that in Figure 1.16d of Section 1.7; therefore, in Equations 1.7.12 the signs of the vectors \vec{n} , $\vec{\tau}_2$, and \mathbf{J}_i must be reverted, which does not change the form of the equations themselves. Assuming the external stream inflowing into the shock to be uniform and the flow adiabatic, we let $\vec{\tau}_1 = \mathbf{J}_1 = \mathbf{q}_m = 0$ in Equation 1.7.12; then the viscous stress vector $\vec{\tau}_2$ is as follows

$$\vec{\tau}_2 = \tau_{nn}\vec{n} + \tau_{nl}\vec{l} \quad (12.14.6)$$

The τ_{nn} and τ_{nl} components of the stress tensor are determined by the sequence of formulas 1.10.10 and 1.8.9 in which the coordinates x and y must be replaced by l and n , respectively. At a small relative thickness of the viscous shock layer the directions of the coordinate lines l, n and the body-fitted curvilinear coordinates x, y are close; within the framework of the PNSE model this makes it possible to drop the derivatives with respect

**FIGURE 12.52**

Heat flux distribution over the OREX vehicle surface under the same conditions as in Figure 12.50: (a), Navier-Stokes equations and (b), PNSE.

to l inside the shock wave. Then denoting by v_l and v_n the components of the velocity $\vec{U} = \vec{l}v_l + \vec{n}v_n$ in the l and n axes we obtain

$$\tau_{nn} = \frac{4}{3}\mu \frac{\partial v_n}{\partial n}, \quad \tau_{nl} = \mu \frac{\partial v_l}{\partial n} \quad (12.14.7)$$

Substituting Equations 12.4.6 and 12.4.7 in Equation 1.7.12 and projecting the momentum equation onto the \vec{n} and \vec{l} axes we obtain the required generalized Hugoniot relations as applied to the PNSE model

$$\begin{aligned} \rho_s v_{ns} &= \rho_\infty v_{n\infty} = m, \quad v_n = -\vec{n} \cdot \vec{U} \\ mv_{ns} + p_s - \frac{4}{3}\mu \left. \frac{\partial v_n}{\partial n} \right|_s &= mv_{n\infty} + p_\infty \\ mv_{ls} - \mu \left. \frac{\partial v_\tau}{\partial n} \right|_s &= mv_{l\infty} \\ mH_s + J_s - \mu v_l \left. \frac{\partial v_l}{\partial n} \right|_s - \frac{4}{3}\mu v_n \left. \frac{\partial v_n}{\partial n} \right|_s &= H_\infty \end{aligned} \quad (12.14.8)$$

Here, subscripts 1 and 2 in formulas 1.7.12 are replaced by ∞ and s . These relations are referred to a certain conditional shock front—the zero-thickness line S in Figure 12.49. In this case, we have $v_{n\infty} = U_\infty \sin \alpha$ and $v_{l\infty} = U_\infty \cos \alpha$, where α is the local angle of attack of the front S . In view of Equation 1.10.14 and the simplifications made previously, in the last Equation 12.14.8 the energy flux J may be presented in the form:

$$J_2 = J_T + J_D, \quad J_T = -\lambda \frac{\partial T}{\partial n} \quad (12.14.9)$$

The term J_D is caused by energy transfer due to diffusion processes in a multicomponent gas and will as yet be unspecified (see Section 13.1). As shown in Section 1.2, in an equilibrium flow, by analogy with 1.2.11 it can be let $J_D = 0$; in this case thermal conductivity λ should be replaced by its effective value λ_{eff} .

Equations 12.5.5 to 12.5.8 with $F_j = 0$ in Equation 12.5.6 are of the overall sixth order so that four relations (12.4.8) and three conditions imposed on the wall (e.g., $u = v = 0$ and $h = h_w$) are sufficient for closing the problem and determining the shock shape S or its equation $r_s = r_s(x)$ provided that—this is important—a Cauchy problem is formulated in a certain initial section $x = x_0$ (this is problematical for blunt bodies; however, we postpone the discussion of this question).

In this connection, we note the fundamental importance of the inviscid form of Equation 12.5.6. In fact, if the term with the second derivative $\partial^2 v / \partial y^2$ is retained in formula 12.5.4 for F_j , then the formal parabolicity of the system of Equations 12.5.5 through 12.5.8 thus obtained is not violated. However, in this case the overall order of the system increases, which makes impossible a unique determination of the position of the front S . In other words, this system requires the same asymptotic closing conditions 12.14.1 as for the complete system of Navier–Stokes equations.

Formally, this problem arises in solving the parabolized Navier–Stokes equations written in the conservation-law form, which are obtained from the complete Equations 1.13.30 by omitting all the derivatives, except for higher-order (second-order) ones with respect to η (or y), in the viscous terms. The general steady-state form of these equations can be written as follows

$$\frac{\partial \bar{F}^*}{\partial \xi} + \frac{\partial \bar{G}^*}{\partial \eta} = 0 \quad (12.14.10)$$

where in the operator \bar{F}^* only inviscid terms are retained and in the operator \bar{G}^* both the inviscid terms and the derivatives with respect to η (or y) in the viscous terms are retained. However, as distinct from Equations 12.5.5 through 12.5.8 written in the simple variables with account for the condition $v \ll u$, the Cartesian components of the velocity u' and v' (Figure 12.49) may be of the same order; therefore, in Equation 12.14.10 in the general case both higher-order derivatives of u' and v' must be retained, with all that this implies. In this case we can abandon the asymptotic conditions 12.14.1 or the introduction of the conditional boundary Σ_∞ at the cost of saving the inviscid supersonic region of the shock layer. Then an additional condition can be derived using a segment of the first-family characteristic between the penultimate point of the preceding computational layer and the shock S in accordance with the algorithm of the problem presented in Figure 4.3d of Section 4.2 (Kovalev, 1997).

The PNSE method gained a wide use due to its economy related with the possibility of the application of marching techniques for calculating two-dimensional and certain classes of three-dimensional flows (as distinct from the complete Navier–Stokes equations) and the feasibility of the simultaneous calculation of the inviscid flow region and the boundary layer as a whole, which is more preferable from the algorithmic standpoint than successive solution of inviscid and boundary-layer problems, including the case of fairly high Reynolds numbers.

It might seem that in the limiting case $Re_\infty \rightarrow \infty$ we could restrict ourselves to the conventional rather than generalized Hugoniot relation at a thin shock. However, this is possible only for equilibrium flows and can lead to inaccuracies in calculating nonequilibrium flows. In fact, in the latter case the shock waves are followed by relaxation zones with fairly high gradients of all the flow parameters, which, in the presence of dissipative terms in the governing equations, generate spurious, nonphysical fluxes of heat, gas components, and so on, thus inevitably violating the conservation laws.* Thus, in calculating nonequilibrium flows by the PNSE method, taking the generalized Hugoniot conditions into account (see also Section 13.2) is necessary at any arbitrary Reynolds numbers.

The limit of the correspondence between the solution based on the PNSE method and the complete Navier–Stokes equations can be established only by comparing the numerical solutions for these two cases. For the sake of illustration, in Figures 12.43 and 12.44 we have plotted the shocks S calculated by the PNSE method. For $Re_\infty = 10^2$ these shocks are deeply immersed in the disturbed layer but for $Re_\infty = 10^3$ the shock S ahead of the blunt cone, as distinct from the case of a sphere, confines the compressed layer formed by the shock front and the inviscid shock layer. At the same time, the density profiles in the wall region of the blunt cone in Figure 12.45, as well as the pressure distributions in Figure 12.46, calculated by both methods are very close to each other for both $Re_\infty = 10^3$ and $Re_\infty = 10^2$.

Additionally, for the full-scale vehicle OREX reentering into the Earth's atmosphere (Inouye, 1995), in Figures 12.50 and 12.51 we have plotted the calculated distributions of certain nonequilibrium flow parameters in section aa' . Clearly, the curves obtained within the framework of the Navier–Stokes and PNSE models are fairly close down to $Re_\infty = 10^2$.

As for the heat fluxes to the body surfaces, in Figure 12.29 of Section 12.13, we compared the heat fluxes to a short blunt cone calculated by both methods at $Re_{\infty 0} = 10^4$ and in Figure 12.52 those for the OREX vehicle at $Re_R \approx 10^3$, the curves pertaining to the same parameters being close to each other in both cases. In Figure 12.48 for the stagnation point

* Zalgin and Lunev (1973), Voronkin and Zalgin (1975).

on a sphere (where the two methods give the largest discrepancy in the qualitative flow pattern; see Figures 12.44 and 12.47) curve 2' obtained by the PNSE method is fairly close to curve 2 calculated under the same conditions down to the Reynolds numbers $\text{Re}_\infty \approx 10^2$, or $\text{Re}_0 = \rho_\infty U_\infty R / \mu_0 \approx 5 \div 10$.

However, using marching techniques to the solution of the parabolized Navier-Stokes equations is related with the same problems, as for the inviscid flows of Section 7.13, in spite of the parabolicity of these equations. First of all, these equations require preassigning initial conditions in a certain section $x = x_0$, or, for bluff bodies, at the axis of symmetry $x = 0$, if there is such a thing. On the axis only the symmetry conditions are known, which do not determine the Cauchy problem. Therefore, as for the inviscid flows of Section 7.7, the limiting form of the equations when $x \rightarrow 0$ must be used in determining the initial conditions for a marching algorithm.

For this purpose, we will use expansions 7.7.14 in powers of xK_s corresponding to the hypersonic approximation. However, distinct from Chapter 7, we will not neglect the terms of the order $k, \delta K$, and δK_s , where k is the disturbed layer thickness, $K = R^{-1}$, and $K_s = R^{-1}$, while R and R_s are the radii of curvature of the body and the shock at the axis of symmetry, supplementing them by the analogous expansion for the enthalpy $h = H_\infty(h_0 + K_s^2 x^2 h_2)$. Then, from Equations 12.5.5 through 12.5.7 with $F_j = 0$ we obtain the following system of ordinary differential equations for the leading terms of these expansions

$$\begin{aligned} \frac{1}{k_0 \text{Re}_s^{(0)}} (\bar{\mu} f'_1)' + \lambda \rho_0 f_0 f'_1 - \frac{1}{H_x} \lambda^2 \rho_0 f_1^2 + \lambda^2 \frac{k_0 \rho_0 f_0 f_1}{H_x K_s R} &= -2k_0 \lambda^2 p_2 \\ \frac{d}{d\zeta} (H_x \rho_0 f_0) &= (H_x \rho_0 f_0)' = \lambda(1 + \nu) \rho_0 f_1, \quad p'_0 = -k_0 \rho_0 f_0 f'_0 \\ \frac{1}{k_0 \text{Re}_s^{(0)}} \left(\frac{\bar{\mu}}{\text{Pr}_{\text{eff}}} h'_0 \right)' + \lambda \rho_0 f_0 h'_0 &= -\lambda k_0^2 \rho_0 f_0^2 f'_0 \frac{U_\infty^2}{H_\infty}, \quad \rho_0 = \rho(p_0, h_0) \end{aligned} \quad (12.14.11)$$

Here, the following notation is introduced

$$\begin{aligned} \zeta &= \frac{y}{\delta}, \quad \lambda = \frac{\delta}{k_0 R_s}, \quad k_0 = \frac{\rho_\infty}{\rho_s^{(0)}}, \quad \text{Pr}_{\text{eff}} = \frac{\mu_0}{c_p \lambda_{\text{eff}}} \\ \rho_0 &= \frac{\rho k_0}{\rho_\infty}, \quad \bar{\mu} = \frac{\mu}{\mu_0}, \quad \text{Re}_s^{(0)} = \frac{\rho_\infty U_\infty R_s}{\mu_0}, \quad H_x = 1 + \frac{y}{R} \end{aligned} \quad (12.14.12)$$

where μ_0 is the gas viscosity at the stagnation parameters, and $\rho_s^{(0)}$ is the gas density behind the normal shock in the inviscid flow. The last equation of the system follows from the equation of state of the gas $\rho = \rho(p, h)$ under the given conditions. For the sake of simplicity, here we have adopted the effective heat-conduction model for an equilibrium gas.

Similarly, for the coefficients of the terms of the order $K_s^2 x^2$ we obtain the following system

$$\begin{aligned} \frac{1}{\lambda \rho_0} p'_2 + \frac{R_s}{H_x R} f_1^2 &= \Phi_p = -k_0 f_0 f'_0 \frac{\rho_2}{\lambda \rho_0} + R_s(K_s - K) \left[\frac{1}{\lambda} (f_0 f_2)' - \frac{2}{H_x} f_1 f_2 \right] \\ \frac{1}{k_0 \text{Re}_s^{(0)}} \left(\frac{\bar{\mu}}{\text{Pr}_{\text{eff}}} h'_2 \right)' + \lambda \rho_0 f_0 h'_2 - \frac{2}{H_x} \lambda^2 \rho_0 f_1 h_2 &= \Phi_h(f_2, p_2) \\ \frac{\rho_\infty}{k_0} \rho_2 &= -\rho_\infty U_\infty^2 \rho_p p_2 + H_\infty \rho_h h_2 \end{aligned} \quad (12.14.13)$$

Being too cumbersome, the expression for the function Φ_h is not written down, since for the following it will suffice to state that the function is dependent on f_2 and p_2 .

Similarly, the expansion of the solution in powers of $K_s x$ should be applied to conditions 12.14.8 at the shock. As in Equation 12.5.6, we will omit the viscous term in the second momentum equation, that is, let $F_j = 0$. Then, for the leading terms of the expansions these equations take the form:

$$\begin{aligned}\zeta = 1 : \quad & \rho_0 f_0 = 1 \\ p_0 + k_0 f_0 &= 1 + (\gamma M_\infty^2)^{-1} \\ f_1 - 1 &= \frac{\mu_0}{\rho_\infty U_\infty \delta} f'_1 = \frac{\bar{\mu}}{\lambda k_0 \text{Re}_s^{(0)}} f'_1 \\ h_0 - 1 &= \frac{\bar{\mu}}{\text{Pr}_{\text{eff}} \lambda k_0 \text{Re}_s^{(0)}} h'_0, \quad \rho_0 = \rho_0(p_0, h_0)\end{aligned}\quad (12.14.14)$$

The boundary conditions for the functions p_2, h_2, f_2 , and ρ_2 are derived from 12.4.8 using the procedure 2.4.11 through 2.4.13 of transferring the boundary conditions from the actual shock $y = y_s(x)$ to the line $\zeta = y/\delta = 1$; by analogy with 7.7.19 their general form is as follows

$$\varphi(y_s) = \varphi_0(y_s) + K_s^2 x^2 \varphi_2(y_s) = \varphi_0(\delta) + \frac{1}{2\delta}(y_s - \delta)\varphi'_0(\delta) + K_s^2 x^2 \varphi_2(\delta) \quad (12.14.15)$$

Here, $\varphi = p, u, v, h$.

Substituting expansions 7.7.14 and 12.14.15 into relations 12.14.8 and taking 7.7.13 into account we obtain a system of linear equations in the boundary values $p_2(1), \rho_2(1), h_2(1)$, and $f_2(1)$; since they are too cumbersome, we will write down only the equation following from the second relation 12.14.8

$$p_2(1) - 1 = k_0 \rho_2 f_0^2 + R_s(K_s - K) \left[\frac{1}{2} \rho_0 f_0 f'_0 - 2\rho_0 \left(f_1 + f_2 - \frac{1}{2} \lambda f'_0 \right) \right] \quad (12.14.16)$$

Let us analyze the problem formulated. The system of Equation 12.14.11 consists of four differential equations for five unknown functions f_0, f_1, p_0, p_2 , and h_0 and the algebraic equation of state for determining the density ρ_0 ; thus, the system is unclosed. Involving three equations in 12.14.13 that incorporate three new functions f_2, ρ_2 , and h_2 does not save the situation that is analogous to that considered in Sections 7.7 through 7.11 for inviscid problems.

However, as in the case of inviscid flows, this is not the only manifestation of the system nonclosure. In fact, system 12.14.11 is of the sixth overall order in the derivatives and requires six conditions for its solvability. For this system, three conditions on the wall ($f_0 = f_1 = 0$ and $h_0 = h_{0w}$ or conditions 12.14.2) and four conditions in 12.14.14 are preassigned. An extra condition serves for determining the unknown parameter $\lambda = \delta/k_0 R_s$, which, in turn, involves two unknown parameters δ and R_s .

The problem formulated for the leading terms of the expansions can be closed only in the hypersonic approximation within the framework of the *thin viscous shock layer* model for moderately blunt (in the meaning of Section 7.1) bodies, for which at $k_0 \ll 1$ the shock layer thickness is $\delta \sim k_0 R_s \approx k_0 R \ll R$. In this case, the right-hand sides can be dropped from the first Equation 12.14.13 and 12.14.16, which leads, as in Section 7.7, to the condition closing the problem

$$R_s = R, \quad f_2 = 0, \quad p'_2 = \lambda \rho_0 f_1^2, \quad p_2(1) = 1 \quad (12.14.17)$$

In the general case the problem of the viscous shock layer on bluff and blunt bodies can be solved within the framework of the PNSE model using the *global iteration method*,* whose concept was outlined in Section 7.13 for inviscid flows and can be almost completely transferred to the problems of the viscous shock layer.

In this case, only one question of fundamental importance requires an additional analysis. Due to the subsonic nature of the flow in the inviscid shock layer on a blunt body, the procedure of artificial parabolization of the governing equations is used in each iteration stage in order that marching techniques could be used; this contradiction is removed in the process of iteration convergence. This procedure can seem to be superfluous for the PNSE system that is originally parabolic; however, this is not the case and it turns out that the parabolicity of this system gives no possibility of applying marching techniques directly to its solution, since the correctness of the formulation of the initial-value problem for such systems is determined by the inviscid part of their operator.

In order to convince ourselves of it, we will study the mathematical properties of these equations; for this purpose, by analogy with Section 2.4, we will first transform the continuum equation introducing the speed of sound into it. Restricting ourselves to equilibrium flows and using relations 1.6.8, we rewrite Equation 2.4.1 in the form:

$$\frac{1}{\rho a^2} \frac{dp}{dt} + \operatorname{div} \vec{U} = \frac{1}{\rho} \left(\frac{\partial \rho}{\partial h} \right)_p q_{\text{eff}}, \quad q_{\text{eff}} = T \frac{ds}{dt} \quad (12.14.18)$$

Here, the term q_{eff} is defined by Equations 1.9.6, 1.10.14, and 12.1.11 and, after the derivatives with respect to the longitudinal x coordinate have been dropped as being of the lower order in the PNSE model, takes the form:

$$q_{\text{eff}} = \mu \left(\frac{\partial u}{\partial y} \right)^2 + \frac{\partial}{\partial y} \left(\lambda \frac{\partial T}{\partial y} \right), \quad \lambda \frac{\partial T}{\partial y} = \frac{\mu}{\Pr} \frac{\partial h}{\partial y} \quad (12.14.19)$$

Though systems 12.5.5 through 12.5.8 thus transformed contains the speed of sound, it is still rather complicated for a mathematical analysis. For this reason, we will restrict ourselves to the simplest example of the linearized problem of a near-stratified gas flow along the x axis. By analogy with Section 2.4, we introduce the small parameters

$$\begin{aligned} u_1 &= U_0 - u \ll U_0, & v &= v_1 \ll U_0 \\ p_1 &= p_0 - p \ll p_0, & h_1 &= h_0 - h \ll h_0 \\ H_1 &= H_0 - H \ll H_0, & \rho_1 &= \rho_0 - \rho \ll \rho_0 \end{aligned} \quad (12.14.20)$$

Here, the parameters with the subscript 0 are constant and relate to the undisturbed flow. Substituting these into Equations 12.5.5 through 12.5.8 and neglecting the quadratic terms, we obtain a system of linear equations in the perturbations and formulate for it an initial-value problem on the infinite line $x = 0$, the correctness of which will be studied in the following. Since our purpose is to demonstrate the ill-posedness of the problem, at least for particular cases, we will assume the gas to be perfect and viscosity constant and let the Prandtl number $\Pr = 1$. Moreover, we will restrict the class of the perturbations introduced

* The method was developed in the works cited in Section 7.13; see also Golovachev (1996) devoted to the problems of viscous shock layers and the algorithms of their numerical solution.

into the flow to the condition $H = \text{const}$, or $H_1 = h_1 + U_0 u_1 = 0$, which, for $\text{Pr} = 1$, does not contradict condition 12.5.8.

Then, after the momentum Equations 12.5.5 and 12.5.6 and the continuity Equation 12.14.18 have been linearized, we obtain the system

$$\begin{aligned} \frac{\partial \bar{u}_1}{\partial x} + j_1 \frac{\partial \bar{p}_1}{\partial x} - \bar{v} \frac{\partial^2 \bar{u}_1}{\partial y^2} &= Q_u, \quad \bar{v} = \frac{\mu_0}{\rho_0 U_0} \\ j_2 \frac{\partial \bar{v}_1}{\partial x} + \frac{\partial \bar{p}_1}{\partial y} &= Q_v \\ M_0^2 \frac{\partial \bar{p}_1}{\partial x} + j_5 \frac{\partial \bar{u}_1}{\partial x} + \frac{\partial \bar{v}_1}{\partial y} + \bar{v}(\gamma - 1)M_0^2 \frac{\partial^2 \bar{u}_1}{\partial y^2} &= Q_p \\ \bar{p}_1 = \frac{p_1}{\rho_0 U_0^2}, \quad \bar{u}_1 = \frac{u_1}{U_0}, \quad \bar{v}_1 = \frac{v_1}{U_0}, \quad M_0^2 = \frac{U_0^2}{a_0^2} \end{aligned} \quad (12.14.21)$$

Here, by analogy with Section 7.13, the coefficients $j_i \leq 1$ are introduced at the same terms as in system 7.7.5 through 7.7.7 in order to elucidate their influence on the mathematical properties of system 12.14.21. The terms of the type $(1 - j_i)\partial/\partial x$ are contained in the right-hand sides Q_i which are determined in the preceding iteration stage and, within the limits of this stage, do not affect the type of this system of equations.

A very simple example of such an initial-value problem is provided by the conditions $u_1 = u_1(y)$ and $v_1 = p_1 = 0$ imposed on the line $x = 0$. Then for small x the solution of the homogeneous system 12.14.21 is represented by the equality $v_1 \approx 0$; then, eliminating $\partial \bar{p}_1/\partial x$ from the first and third equations we obtain the following equation for the function $u_1(x, y)$

$$(M_0^2 - j_1 j_5) \frac{\partial \bar{u}_1}{\partial x} = \bar{v} \gamma M_0^2 \frac{\partial^2 \bar{u}_1}{\partial y^2} \quad (12.14.22)$$

This is the heat conduction equation, for which the initial value problem is well-posed only at positive coefficients. However, at $M_0^2 - j_1 j_5 < 0$ or at $j_1 = j_5 = 1$ for subsonic flows, this problem is ill posed and leads to unbounded growth of initial perturbations as $x > 0$ increases (the negative viscosity effect). For this reason, for $M_0 < 1$ the well-posedness of this problem can be provided only by an appropriate decrease in the coefficients j_1 and j_5 ensuring, as in Section 7.13, the fulfillment of condition $M_0^2 > j_1 j_5$.

Generally speaking, this single example will suffice to demonstrate the ill-posedness of such an initial-value problem; however, we will consider one more class of more general solutions of system 12.14.21 analogous to those used in Section 4.1

$$f_k = C_k e^{\alpha x} e^{i\omega y}, \quad f_k = u_1, v_1, p_1 \quad (12.14.23)$$

Here, ω is a given perturbation frequency along the y axis, α is the unknown *wavenumber* of the problem, and the coefficients C_k are the perturbation amplitudes. After this solution has been substituted into system 12.14.21 with $Q_i = 0$, the system reduces to a system of linear homogeneous equations in the coefficients C_k . In order for the system to have a nontrivial solution, the determinant composed of its coefficients must be zero, which leads to the following characteristic equation for α

$$\begin{aligned} F(\alpha) = A\alpha^3 + B\alpha^2 + C\alpha + D &= 0 \\ A = j_2(M_0^2 - j_1 j_5), \quad B = j_2 \bar{v} \omega^2 M_0^2 [1 + j_1(\gamma - 1)] \\ C = \omega^2, \quad D = \bar{v} \omega^4 \end{aligned} \quad (12.14.24)$$

The simplest case is that in which $j_2 = 0$; it is associated with the single root of Equation 12.14.24, $\alpha = -\bar{v}\omega^2 < 0$, which indicates the well-posedness of the problem formulated. In the general case Equation 12.14.24 has either three real roots or one real root $\alpha = \alpha_1$ and two complex roots $\alpha_{\pm} = \alpha_r \pm i\alpha_i$. For $A < 0$, or $M_0^2 < j_1 j_5$, in the real variable plane the function $F(\alpha) \rightarrow \infty$ when $\alpha \rightarrow -\infty$ and $F(\alpha) \rightarrow -\infty$ when $\alpha \rightarrow \infty$. Since $F(0) = D > 0$, in this case the equation possesses at least one real positive root $\alpha_1 > 0$, which indicates the ill-posedness of the initial-value problem formulated.

Let now $A > 0$; this is fulfilled always for $M_0 > 1$, while for $1 > M_0 > 0$ this can be achieved by an appropriate choice of the coefficients j_1 and j_5 as at hyperbolization of the shock layer equations in Section 7.13. The fact that the single real root is negative is easily proved by analogy with the $A < 0$ case, while for three real roots their negativity follows from the fact that the extrema $F'(\alpha) = 0$ of the function $F(\alpha)$ are, as can easily be shown, located in the $\alpha < 0$ region. Complicating somewhat this reasoning, the fact that the real parts of the complex roots are negative, $\alpha_r < 0$, can also be proved; however, we will omit the demonstration making reference to the *Routh-Hurwitz criterion* (see Chetaev, 1955), which is satisfied by Equation 12.14.24.

Of course, the demonstration of the well-posedness of the initial-value problem for particular problems cannot be transferred automatically to the general case. However, the experience of applying the PNSE method, based on the approaches of parabolization and hyperbolization of inviscid operators for subsonic flows (Section 7.13), has indicated the possibility of transferring these approaches to the PNSE model.

We will now return to the case $j_2 = 0$, which corresponded in Sections 7.7 and 7.13 to the complete parabolization of the inviscid operator of the governing equations and the earlier mentioned thin shock layer model, within the framework of which in the equation for the transverse momentum only the centrifugal, or Busemann, term is retained. Obviously, transition to the PNSE model does not introduce any fundamental changes in the properties of the model described in Section 7.13, which was used in the past for solving the problems of both inviscid and viscous flow past blunt bodies, but at present cannot be recognized as satisfactory owing to its poor accuracy. An exception in this regard is provided only by the problem of the flow in the vicinity of the axis of symmetry in which this model makes it possible to obtain some simple illustrative results.

We note in conclusion that the analysis drawn for three-dimensional inviscid flows in Section 7.13 can also be transferred to the viscous problems with the same restriction that there exist two planes of symmetry of the flow, the corresponding viscous equations for the axis of symmetry being derived by analogy with Equations 7.10.5, 7.10.6, and 12.14.11.

12.15 Problems of a Three-Dimensional Boundary Layer

Here we will briefly consider the basic properties of the boundary layer in a three-dimensional flow. To make our analysis more illustrative, we will draw it mainly within the framework of the approximate effective-length method presented in Section 12.18. For this purpose, we will fit the curvilinear coordinate system of (x_1, x_2, x_3) Section 1.13 to the surface in the flow and replace the coordinate x_2 orthogonal to the wall ($x_2 = y = 0$ at the wall itself) by the normal y to the surface writing in what follows u_2 for v . For a relatively thin boundary layer to which we will restrict ourselves, this coordinate system is close to a tri-orthogonal system (with the same accuracy as the boundary layer equations themselves).

In these variables, the Navier-Stokes equations in the conventional boundary-layer approximation with inviscid operators 7.10.5 (in the same designations and with Equations 1.9.2, 1.9.6, 1.13.1, and 1.14.3 taken into account) takes the form:

$$\begin{aligned} \frac{u_1}{H_1} \frac{\partial u_1}{\partial x_1} + v \frac{\partial u_1}{\partial y} + \frac{u_3}{H_3} \frac{\partial u_1}{\partial x_3} + \frac{u_1 u_3}{R_{1\Gamma}} - \frac{u_3^2}{R_{3\Gamma}} &= -\frac{1}{\rho H_1} \frac{\partial p}{\partial x_1} + \frac{1}{\rho} \frac{\partial}{\partial y} \left(\mu \frac{\partial u_1}{\partial y} \right) \\ \frac{u_1}{H_1} \frac{\partial u_3}{\partial x_3} + v \frac{\partial u_3}{\partial y} + \frac{u_3}{H_3} \frac{\partial u_3}{\partial x_3} + \frac{u_1 u_3}{R_{3\Gamma}} - \frac{u_1^2}{R_{1\Gamma}} &= -\frac{1}{\rho H_3} \frac{\partial p}{\partial x_3} + \frac{1}{\rho} \frac{\partial}{\partial y} \left(\mu \frac{\partial u_3}{\partial y} \right) \\ \frac{\partial}{\partial x_1} (H_2 H_3 \rho u_1) + \frac{\partial}{\partial y} (H_1 H_3 \rho v) + \frac{\partial}{\partial x_3} (H_1 H_2 \rho u_3) &= 0 \\ \frac{u_1}{H_1} \frac{\partial h}{\partial x_1} + v \frac{\partial h}{\partial y} + \frac{u_3}{H_3} \frac{\partial h}{\partial x_3} &= \frac{u_1}{\rho H_1} \frac{\partial p}{\partial x_1} + \frac{u_3}{\rho H_3} \frac{\partial p}{\partial x_3} + \\ \frac{1}{\rho} \frac{\partial}{\partial y} \left(\frac{\mu}{\text{Pr}} \frac{\partial h}{\partial y} \right) + \frac{\mu}{\rho} \left(\frac{\partial u_1}{\partial y} \right)^2 + \frac{\mu}{\rho} \left(\frac{\partial u_3}{\partial y} \right)^2 & \end{aligned} \quad (12.15.1)$$

Here, H_i are the scale factors (in what follows $H_2 = H_y = 1$), while $R_{i\Gamma} = K_{i\Gamma}^{-1}$ are the radii of geodesic curvatures of the coordinate lines (R_{13} and R_{31} in Equation 1.13.23). As for two-dimensional boundary layers, this system is valid for $\delta \ll L, R_{i\Gamma}$, where δ is the boundary layer thickness and L is the longitudinal scale length of the flow.

The boundary conditions for this system are conventional

$$\begin{aligned} y = 0 : \quad u_i = 0, \quad h = h_w \\ y = \delta : \quad u_1 \rightarrow u_{1\delta}, \quad u_3 \rightarrow u_{3\delta}, \quad h \rightarrow h_\delta \end{aligned} \quad (12.15.2)$$

As before, the boundary conditions on the outer edge of the boundary layer are imposed asymptotically, as $y \rightarrow \infty$.

These equations are of parabolic type (cf. Sections 12.3 and 12.5) with the temporal coordinate represented by the streamlines $dx_3/dx_1 = u_3/u_1$, so that when the initial data are specified on a certain surface Σ orthogonal to the surface $x_2 = 0$, the domain of its influence is bounded by streamsurfaces passing through lateral sides of Σ .

This result is especially pictorial in a coordinate system fitted to the inviscid streamlines $x_3 = 0$ on the body surface. In this case, $u_3 = 0$ both on the outer edge of the boundary layer and on the wall; however, under the action of the transverse pressure difference, or the derivative $\partial p/\partial x_3$, a secondary flow with a velocity $u_3 \neq 0$ occurs within the boundary layer. The term with $\partial p/\partial x_3$ in the second equation of Equation 12.5.1 is offset by the centrifugal term $\rho U^2/R_{1\Gamma}$ on the outer edge, where $U = u_1$, and by the viscous term on the right-hand side inside the boundary layer, which leads to the following estimate for u_3

$$\frac{\partial}{\partial y} \left(\mu \frac{\partial u_3}{\partial y} \right) \sim \frac{\mu u_3}{\delta^2} \sim \frac{\partial p}{\partial x_3} \sim \frac{\rho U^2}{R_{1\Gamma}}, \quad \frac{u_3}{U} \sim \frac{L}{R_{1\Gamma}}, \quad \left(\delta \sim \frac{L}{\text{Re}^{1/2}} \right)$$

Thus, for $L \ll R_{1\Gamma}$, that is, when the radius of streamline curvature $R_{1\Gamma}$ is much greater than the streamwise flow scale L (situation typical of fairly elongated bodies), we can neglect the secondary flow at all and let $u_3 = 0$ in system 12.15.1. Then this system takes the form:

$$\begin{aligned} u \frac{\partial u}{\partial l} + v \frac{\partial u}{\partial y} &= -\frac{1}{\rho} \frac{\partial p}{\partial x} + \frac{1}{\rho} \frac{\partial}{\partial y} \left(\mu \frac{\partial u}{\partial y} \right), \quad \frac{\partial}{\partial l} (H_3 \rho u) + \frac{\partial}{\partial y} (H_3 \rho v) = 0 \\ u \frac{\partial H}{\partial l} + v \frac{\partial H}{\partial y} &= \frac{1}{\rho} \frac{\partial}{\partial y} \left(\frac{\mu}{\text{Pr}} \frac{\partial H}{\partial y} \right) + \frac{1}{\rho} \frac{\partial}{\partial y} \left[\mu \left(1 - \frac{1}{\text{Pr}} \right) \frac{\partial u^2}{\partial y} \right] \end{aligned} \quad (12.15.3)$$

Here, we have let $u_1 = u$, $x_1 = l$, and $H_1 = 1$, where l is the length measured along streamlines, and gone over to the total enthalpy.

We note that if an inviscid streamline coincides with a geodesic line of the surface (e.g., within the framework of the Newtonian flow scheme of Section 7.10), then $K_{1\Gamma} = 0$ and system 12.15.3 becomes exact. This system differs from the analogous system for a limitingly thin axisymmetric boundary layer only in that the parameter H_3 is substituted for the body cross-section radius r_b and, on this basis, can be called the *axisymmetric analogy model*, or approximation for the three-dimensional boundary layer. Within the framework of this analogy, the boundary layer develops within streamsurfaces orthogonal to the wall and passing through inviscid streamlines on its outer edge.

In this case, the scale factor H_3 , or the *effective radius* of the equivalent axisymmetric body $H_3 = r_{\text{eff}}$, is determined in terms of the inviscid velocity field on the wall. For this purpose, we apply formula 1.8.13 to unit vector \vec{l}_1 and use relations 1.13.1 and 1.13.24 for an orthogonal coordinate system

$$\begin{aligned} \operatorname{div} \vec{l}_1 &= \lim_{\Delta l_1 \rightarrow 0} \frac{(\Delta l_2 \Delta l_3)_{x_1+\Delta x_1} - (\Delta l_2 \Delta l_3)_{x_1}}{\Delta l_1 \Delta l_2 \Delta l_3} = \\ &= \frac{1}{H_1 H_2} \frac{\partial H_2}{\partial x_1} + \frac{1}{H_1 H_3} \frac{\partial H_3}{\partial x_1} = \frac{1}{H_3} \frac{\partial H_3}{\partial l} \end{aligned} \quad (12.15.4)$$

Here, the latter equation applies to our case $\vec{l}_1 = \vec{l}$ and $H_2 = 1$. In the general case, in arbitrary coordinates on the body surface with their own H_1 and H_2 , by definition of the divergence operator we have

$$\frac{1}{r_{\text{eff}}} \frac{\partial r_{\text{eff}}}{\partial l} = \operatorname{div} \vec{l} = \frac{1}{H_1} \frac{\partial}{\partial x_1} \left(H_3 \frac{u_1}{U} \right) + \frac{1}{H_3} \frac{\partial}{\partial x_3} \left(H_1 \frac{u_3}{U} \right) \quad (12.15.5)$$

The most fruitful consequence of the axisymmetric analogy is the possibility of its application to the calculation of heat transfer by the effective length method* outlined in Section 12.8; for this purpose, in formulas 12.8.11 for x_{eff} the quantity r_{eff} should be substituted for r_b at $v = 1$. In this case, it is not necessary to perform calculations precisely along streamlines; for a given velocity field we can use a differential equation written in an arbitrary coordinate system (x_1, x_3) and obtained by the differentiation of formulas 12.8.11 with respect to l (for $H_e - h_w = \text{const}$)

$$\frac{dx_{\text{eff}}}{dl} = \frac{u_1}{U_\delta H_1} \frac{\partial x_{\text{eff}}}{\partial x_1} + \frac{u_3}{U_\delta H_3} \frac{\partial x_{\text{eff}}}{\partial x_3} = 1 - x_{\text{eff}} \frac{d}{dl} \ln(\rho_* \mu_* U_\delta r_{\text{eff}}^\kappa) \quad (12.15.6)$$

Here and in what follows, $\kappa = 2$ for a laminar and $\kappa = 5/4$ for a turbulent boundary layer. In this case, on a certain initial line L^* an initial distribution of the quantity x_{eff} should be preassigned; the algorithm of its obtaining can be seen from the examples presented in the following.

We will now consider the *three-dimensional stagnation point* with two planes of symmetry and the coordinates x_1, x_3 and the velocity components u_1, u_3 related with them; in this case,

* Vaglio-Laurin (1959), Avduevskii (1962, 1975), Zemlyanskii (1966), and others.

the scale factors are $H_1 = H_3 = 1$. By analogy with Sections 12.6 and 7.10 and in view of Equation 2.11.5 we will seek the solution in the vicinity of the stagnation point in the form:

$$\begin{aligned} u_i &= a_i x_i f'_i(\zeta), \quad \frac{\partial p}{\partial x_i} = \rho_\delta a_i^2 x_i, \quad h = h_w + (h_\delta - h_w) \Theta(\zeta) \\ \rho v &= -V \sqrt{\frac{1}{2} \rho_* \mu_* (a_1 + a_3)}, \quad V = b_1 f_1 + b_3 f_3, \quad i = 1, 3 \\ b_1 &= \frac{a_1}{a_1 + a_3}, \quad b_3 = \frac{a_3}{a_1 + a_3}, \quad \zeta = \sqrt{\frac{2\rho_*(a_1 + a_3)}{\mu_*}} \int_0^y \frac{\rho}{\rho_*} dy \end{aligned} \quad (12.15.7)$$

Then from Equation 12.15.1 we obtain a system of ordinary differential equations

$$2(\omega f''_i)' + V f''_i + b_i \left(\frac{\rho_\delta}{\rho} - f_i^{12} \right) = 0, \quad 2 \left(\frac{\omega}{\Pr} \Theta' \right) + V \Theta' = 0, \quad \omega = \frac{\rho \mu}{\rho_* \mu_*} \quad (12.15.8)$$

At $a_1 = a_3$ we have an axisymmetric problem and, for example, at $a_3 = b_3 = 0$ a plane problem (see Section 12.6). Numerical solutions of this system (see, e.g., Ermak and Neiland, 1964) give an almost linear dependence of the heat flux to the stagnation point on the parameter \bar{a}

$$q_w(\bar{a}) = q_w(1)(0.75 + 0.25\bar{a}), \quad \bar{a} = a_3/a_1 \quad (12.15.9)$$

We will apply the effective length method to this problem within the framework of the axisymmetric analogy. In accordance with Equations 2.11.5 through 2.11.7, in the vicinity of a stagnation point, the inviscid streamline shape, the differential dl along the streamlines, and the total velocity U can be presented in the form:

$$x_3 = \lambda x_1^{\bar{a}}, \quad u_1 dl = U dx_1, \quad U = a_1 \sqrt{x_1^2 + \lambda^2 \bar{a}^2 x_1^{2\bar{a}}} \quad (12.15.10)$$

Here, the parameter λ has its own constant value on each streamline. The effective radius r_{eff} is determined from Equation 12.15.5, which can be written in the form:

$$\frac{d \ln r_{\text{eff}} U}{dl} = \frac{a_1 + a_3}{U}, \quad \frac{d(r_{\text{eff}} U)^2}{dl} = 2(a_1 + a_3) r_{\text{eff}}^2 U \quad (12.15.11)$$

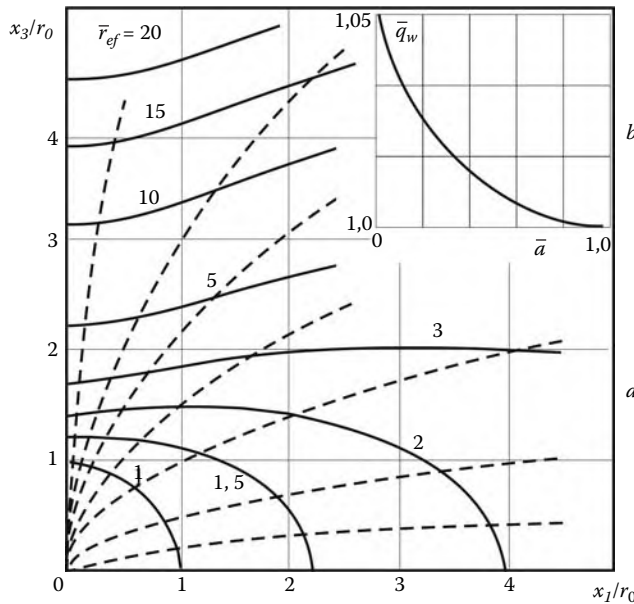
The second form of this equation will be required in what follows; as for the first equation, it has a one-parameter solution

$$r_{\text{eff}} U = \exp \left[(a_1 + a_3) \int \frac{dl}{U(l, \lambda)} \right] = C_0(\lambda) x_1^{1+\bar{a}}, \quad x_1 = x_1(l, \lambda) \quad (12.15.12)$$

Here, $C_0 = C_0(\lambda)$ is an arbitrary constant, which, in accordance with Equation 12.8.11, has no effect on the value of x_{eff} . By way of illustration, in Figure 12.53 we have plotted the streamlines and the ratios $\bar{r}_{\text{eff}} = r_{\text{eff}}/r_0$ with the coefficients C_0 chosen from the condition $\bar{r}_{\text{eff}} = 1$ on the circle of radius r_0 .

To determine the heat fluxes at the stagnation point, we will take into account that the corresponding formula 12.8.10 involves precisely the ratio x_{eff}/U for which, letting $\rho \mu = \text{const}$, from Equation 12.8.11 in view of the second equation for $U, l \rightarrow 0$ we arrive at the following limit

$$\frac{x_{\text{eff}}}{U} = \frac{1}{U^2 r_{\text{eff}}^2} \int_0^l U r_{\text{eff}}^2 dl = \frac{1}{2(a_1 + a_2)} \quad (12.15.13)$$

**FIGURE 12.53**

Streamlines and $f_s = \text{const}$ contours (dashed and solid curves, respectively) in the vicinity of the stagnation point for $a_3 = 0.5a_1$ (a); the exact-to-approximate heat flux ratio \bar{q}_w (b).

This means that at a three-dimensional stagnation point the heat flux is expressed by the same formula 12.8.15, only with the mean velocity coefficient $(a_1 + a_3)/2$ substituted for c . This is confirmed by the plot of the ratio \bar{q}_w of the exact heat flux 12.15.9 to that determined by the previously mentioned way, as presented in Figure 12.53b; clearly, this ratio is near-unity.

12.15.1 Heat Transfer in a Divergent Flow

We will deal, first of all, with spreading lines on the windward plane of symmetry of bodies and wing edges; however, for the sake of generality, we will also consider the flow diverging to both sides of a streamline, for example, a rectilinear one. We will direct the $x = l$ axis with $H_1 = 1$ along this line and the $x_3 = z$ axis with $H_3 = 1$ normal to it on the body surface, the velocity projections onto these axes being $u_1 = u$ and $u_3 = w$. On the x axis we have $u = U$ and $w = 0$; in its vicinity we let $w = cz$. Then, in accordance with 12.15.5, we have

$$\frac{1}{r_{\text{eff}}} \frac{\partial r_{\text{eff}}}{\partial x} = \frac{c}{U}, \quad r_{\text{eff}} = \text{const} \cdot e^J, \quad J = \int \frac{c}{U} dx \quad (12.15.14)$$

Let us present some examples. We will first consider the flow in the vicinity of the windward spreading line on a semi-infinite cylinder (wing edge) in a supersonic flow at an angle of attack $\alpha = \pi/2$. In this case, from Equations 12.15.14 and 12.8.11 it follows that

$$r_{\text{eff}} = \text{const} \cdot e^{cx/U}, \quad x_{\text{eff}} = \frac{1}{\chi} (1 - e^{-\chi x}), \quad \chi = \frac{\kappa c}{U} \quad (12.15.15)$$

For $\chi x \ll 1$ we have $x_{\text{eff}} = x$, as in the case of a sharp plate; however, as χx increases, $x_{\text{eff}} \rightarrow 1/\chi$ following a power law. In this case, on the spreading line the heat flux is determined by formulas 12.8.5, whose limiting (for $\chi x \gg 1$) forms are written

$$\begin{aligned} q_{wl} &= 0.47 \Pr^{-2/3} \sqrt{\rho_* \mu_* c} (H_{el} - h_w) \\ q_{wt} &= 0.031 (\rho_* U_\delta)^{0.6} (\rho_* \mu_* c)^{0.2} (H_{et} - h_w) \\ H_{ei} &= h_\delta + \kappa_i \frac{U_\delta^2}{2}, \quad \kappa_l = \Pr^{1/2}, \quad \kappa_t = 0.89 \end{aligned} \quad (12.15.16)$$

The equilibrium enthalpies H_{ei} are determined by Equations 12.6.17 and 12.7.1, and for given outer flow parameters (U_∞ , ρ_∞ , etc.) are only slightly dependent on the angle of attack α or the sweep angle $\lambda = \pi/2 - \alpha$ of the cylinder and independent of $\kappa_i = 1$.

We will estimate the dependence of the heat fluxes q_{wi} on α or λ from the following considerations. Since the determining enthalpy h_* depends chiefly on the stagnation enthalpy H_δ (see Equation 12.6.19), we can, in accordance with Equation 1.3.11, let $\rho_* \mu_* \sim p \sim \sin^2 \alpha$.

At the same time, in a supersonic stream, the flow in the normal sections of the cylinder (generally speaking of any shape) is equivalent to the flow past the contour of this section with the normal velocity $U_n = U_\infty \sin \alpha$. In this case, in accordance with 12.8.17, we have $c \sim r_0^{-1} \infty \sin \alpha$, where r_0 is the radius of curvature of the cylinder contour. Therefore, for the laminar layer $q_w \sim (\sin \alpha)^{1.5}$. For turbulent heat transfer, letting additionally $\rho_* \sim p/h_* \sim \sin^2 \alpha$ and $U_\delta \sim U_\infty \cos \alpha$, we obtain $q_w \sim (\sin \alpha)^{1.8} (\cos \alpha)^{0.6}$. This function reaches a maximum for $\alpha \approx 60^\circ$ and vanishes as $\alpha \rightarrow \pi/2$, or $U_\delta \rightarrow 0$, as at the stagnation point on the cylinder (see Equation 12.8.19, where x is the distance measured along the contour of the cylinder cross-section). Both dependences of $q_w/q_{w\max}$ (for laminar and turbulent heat transfer) are presented in Figure 12.54.

On a blunt cone with the semivertex angle θ and the nose radius r_0 in a flow at an angle of attack α , for $\varphi \ll 1$ we have

$$\begin{aligned} r_b &= r_0 + x \sin \alpha \\ w = Ug\varphi &= Ug \frac{z}{r_b} = cz, \quad c = \frac{gU}{r_b} \end{aligned} \quad (12.15.17)$$

The parameter g is determined in terms of the azimuthal distribution of the pressure, likewise in Sections 6.6 and 9.8. Then, under the same assumptions on the constancy of the

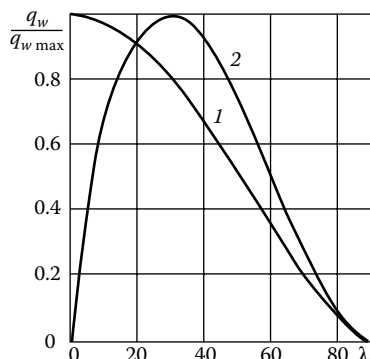


FIGURE 12.54

Dependence of the laminar (a) and turbulent (b) heat fluxes at the cylinder edge on the sweep angle λ .

flow parameters along the windward conical generator, as those made in deriving formulas 12.8.21, from Equation 12.15.14 we obtain

$$r_{\text{eff}} = \text{const} \cdot r_b^{1+\mu}, \quad \mu = \frac{g}{\sin \theta} \quad (12.15.18)$$

Using the previous result and Equation 12.8.11 we can easily derive a formula for x_{eff} generalizing Equation 12.8.21; however, we will omit it restricting ourselves to the result for a sharp (or blunt at $r_b \gg r_0$) cone

$$x_{\text{eff}} = \frac{x}{\kappa(1 + \mu) + 1} \quad (12.15.19)$$

For $\alpha = 0$ we have $\mu = 0$ and $x_{\text{eff}} = x/(\kappa + 1)$, as in Section 12.8.

Obviously, each cone at an angle of attack can be associated with a local cone with the semivertex angle $\theta_l = \theta + \alpha$, if it is the windward generator only that is considered; then, in accordance with Sections 6.6 and 9.5, the main parameters on these cones are similar in value. However, as follows from Equation 12.15.19, the heat fluxes to the original cone at $\mu > 0$ are always greater than those to the local equivalent cone at $\mu = 0$, since $q_w \sim x_{\text{eff}}^{-1/2}$ for laminar and $q_w \sim x_{\text{eff}}^{-0.2}$ for turbulent heat transfer.

We will estimate this spreading effect referring the heat flux q_w on the spreading line of a sharp cone with the semivertex angle θ set at angle of attack α to the heat flux $q_{w,\text{loc}}$ on the local cone with the angle $\theta_l = \theta + \alpha$ set at zero incidence. For high Mach numbers M_∞ the flow parameters (p_δ , ρ_δ , U_δ , etc.) are the same, so that the corresponding ratio of the heat fluxes is as follows:

$$\begin{aligned} \frac{q_w}{q_{w,\text{loc}}} &= \left(\frac{x_{\text{eff}}^{(0)}}{x_{\text{eff}}} \right)^m = \left(\frac{\kappa(1 + \mu) + 1}{\kappa + 1} \right)^m = (1 + K)^m, \quad K = \frac{\kappa \mu}{\kappa + 1} \\ K_l &= \frac{2}{3}\mu, \quad K_t = \frac{5}{9}\mu, \quad m_l = 0.5, \quad m_t = 0.2 \end{aligned} \quad (12.15.20)$$

Hence follows that for laminar heat transfer the spreading effect is considerably larger than in the turbulent case.

For the sake of illustration, we will calculate the parameter g and, hence, μ for a thin cone at a low angle of attack, that is, for $\alpha, \theta \ll 1$. In this case, from Equation 6.6.11 there follows

$$\begin{aligned} \beta M^{-2} &\approx \frac{2}{\bar{\rho}_\delta} \cos \theta \sin(\theta + \alpha) \sin \alpha \approx \frac{2}{\bar{\rho}_\delta} \theta^2 (1 + \bar{\alpha}) \bar{\alpha} \\ \bar{\rho}_\delta &= \rho_\infty / \rho_\delta, \quad \bar{\alpha} = \alpha / \theta \end{aligned} \quad (12.15.21)$$

Here, ρ_δ is the density on the wall in the inviscid flow. Substituting this result in Equation 6.6.14 and taking account of Equation 12.15.18 we obtain

$$\mu = \frac{g}{\sin \theta} = \frac{2\mu_0}{1 + \sqrt{1 + 4\mu_0}} < \mu_0, \quad \mu_0 = \frac{2(1 + \bar{\alpha})\bar{\alpha}}{\bar{\rho}_\delta} \quad (12.15.22)$$

Obviously, in the limit $4\mu_0 \ll 1$, or $\alpha/\rho_0 \ll 1$, we have $\mu \approx \mu_0$. It can be easily seen that μ increases with μ_0 and, therefore, $\bar{\alpha}$.

For small $\mu \ll 1$ (or $\alpha \ll \theta$) from formulas 12.15.20 there follows

$$\frac{q_{wl}}{q_{w,\text{loc}}} = 1 + \frac{1}{3}\mu, \quad \frac{q_{wt}}{q_{w,\text{loc}}} = 1 + \frac{1}{9}\mu, \quad q_{w,\text{loc}} \sim (\theta + \alpha)^2 \quad (12.15.23)$$

At the same time, for $\alpha \ll 1$ the ratios $q_{w,\text{loc}}/q_{wl}$ on the spreading line of the local cone and on the cone at $\alpha = 0$ for the laminar and turbulent heat transfer regimes are, respectively, as follows (the local cone effect)

$$\begin{aligned} \left(\frac{q_{w,\text{loc}}}{q_{w0}} \right)_l &\approx \left(\frac{p_{\text{loc}}}{p_0} \right)^{1/2} \approx 1 + \alpha \quad (q_{w0} \sim \theta^2) \\ \left(\frac{q_{w,\text{loc}}}{q_{w0}} \right)_t &\approx \left(\frac{p_{\text{loc}}}{p_0} \right)^{0.8} \approx (1 + \alpha)^{1.6} \approx 1 + 1.6\alpha \end{aligned} \quad (12.15.24)$$

From the comparison with Equations 12.15.23 and 12.15.22 it follows that for $\rho_\delta > 1$ for laminar heat transfer the local cone effect is stronger than the spreading effect, though both effects are of the same order. At the same time, for turbulent heat transfer the local cone effect is considerably larger than the spreading effect that makes it possible to formulate, at least, in the vicinity of the spreading line, the local cone rule for this heat transfer regime.

On blunt cones at angles of attack, gas spreading on the windward generator reduces the entropy effect described in Section 12.13, since the reduction in heat fluxes due to the entropy layer effect is partially offset by an increase in the coefficient μ in Equation 12.15.19 due to the fact that in the high-entropy layer the density is smaller than on the sharp cone. This inference is supported by Figure 12.55 in which the results of the calculations of Zemlyanskii (1975; generalization of the mass-average value method of Section 12.11 to three-dimensional boundary layers) are compared with the experimental data of Karpov under conditions of Figure 12.39.

In this figure, as in Figure 12.39, the data are presented in the form of the heat flux ratios for blunt and sharp cones for the same cross-sections. For turbulent heat transfer regime the relative position of the curves is similar to that in Figure 12.39b. However, for the laminar regime for the same heat fluxes calculated with and without account for vorticity a region with $q_w/q_{wc} > 1$ is observable, which can be attributed only to the greater spreading effect on the blunt cone, as compared with the sharp cone, and is called the *entropy spreading effect*.

The examples presented previously pertain to spreading lines induced by local pressure peaks. However, heat transfer can also be enhanced in the absence of such peaks, at inertia-driven gas spreading, as mentioned in Sections 4.10, 9.6, and 9.7. Moreover, the most

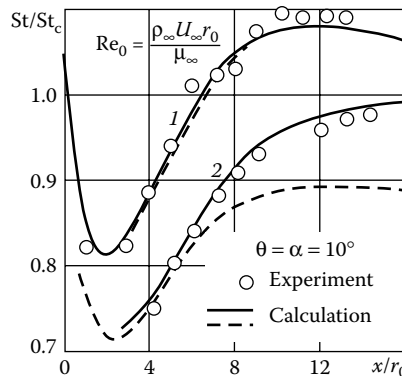


FIGURE 12.55

Ratio of the heat fluxes on blunt and sharp cones: (a), laminar regime, $M_\infty = 8.3$, $Re_0 = 2 \cdot 10^3$, and $\bar{h}_w = 0.1$; (b), turbulent regime, $M_\infty = 6$, $Re_0 = 8.3 \cdot 10^5$, and $\bar{h}_w = 0.6$; the solid and dashed curves relate to the calculations with and without account of vorticity.

canonical example of this spreading is the behavior of streamlines on a sharp cone at $\alpha = 0$. Such spreading also leads to an increase in heat fluxes on a delta wing with a blunt nose (Figure 9.9 of Section 9.7), where at a fairly large distance from the nose the streamlines form a divergent bundle of straight lines and, in complete agreement with the previous results, the heat flux on that plate is by a factor of about $\sqrt{3}$ greater than that on the plate with a sharp nose, as on the sharp cone as compared with a flat plate (Vlasov and R. V. Kovalev, 2005).

In conclusion, we will dwell on a possible influence of streamline convergence (or gas sinkage) on heat transfer. The corresponding effect can be qualitatively simulated by letting $c < 0$ and, therefore, $\mu < 0$ in Equations 12.15.18 and 12.15.19. This leads to an increase in x_{eff} and, therefore, to a reduction of heat fluxes. This qualitative effect is beyond question, since at given external parameters, enhancement or attenuation of heat fluxes is primarily due to a decrease or an increase in the boundary layer thickness, which occurs at gas spreading or sinkage, respectively. However, quantitatively the fact that the effective length method has not been tested for convergent flows does not allow us to recommend it to practical application under these conditions.

13

Viscous Flows of Multicomponent Gases

Previously we outlined the problems of hypersonic viscous flows past bodies regarding the gas as being at equilibrium with the equation of state 12.1.12. Below, proceeding to nonequilibrium flows, we will give a brief outline of the basic elements of the model of dissipative processes, such as viscosity, heat conduction, and diffusion, in a nonequilibrium multicomponent gas based upon the results of molecular-kinetic theory of gases.

13.1 Physical and Chemical Models of Nonequilibrium Dissipative Gas Flows

For a multicomponent gas mixture in nonequilibrium physical and chemical state, the system of the governing equations must be supplemented by physicochemical kinetics equations for the *kinetic variables*, that is, the mass concentrations of individual species c_i of the gas mixture or the energies e_{ik} of their internal degrees of freedom k , cf. Section 10.3. Moreover, certain *dissipative* terms must be introduced in the corresponding equations for inviscid flows derived in Chapter 10 and having the general form 11.1.4; we will consider these terms below.

The *diffusion-kinetics equation* for the mass concentration c_i has the same structure as Equation 1.2.8 written for one-dimensional flows but a more general form:

$$\rho \frac{dc_i}{dt} = \rho \Lambda_i - \operatorname{div} \vec{l}_i \quad (13.1.1)$$

Here, \vec{l}_i is the *diffusion mass flux vector* for species i across a unit *fluid area* (see Sections 1.2 and 1.7), while Λ_i is the source term. The last term on the right-hand side is derived similarly to the term $\operatorname{div} \vec{j}$ in the energy Equation 1.9.6. From the mass conservation law and the definition of the fluid area (see Section 1.4) there follow the conservation conditions

$$\begin{aligned} \sum_i c_i &= 1, & \sum_i \Lambda_i &= 0, & \sum_i \vec{l}_i &= 0 \\ \sum_i x_i &= 1, & x_i &= \frac{\bar{M}}{M} c_i, & \frac{1}{\bar{M}} &= \sum_i \frac{c_i}{M_i} \end{aligned} \quad (13.1.2)$$

We will present some suggestions elucidating the structure of the expressions for the fluxes \vec{l}_i within the framework of the elementary version of kinetic theory of gases used in Section 1.4. For this purpose, we will consider a binary gas mixture with number concentrations n_1 and n_2 , particle masses m_1 and m_2 , mean free molecular paths l_1 and l_2 , and thermal velocities V_{y1} and V_{y2} , letting the pressure and the temperature and, hence, the overall molecular number concentration $n = n_1 + n_2 = p/kT$, be constant. Previously, in Sections 1.2 and 1.4, a fluid surface was defined as a surface confining a constant mass, which was used in Section 10.4 in deriving Equation 13.1.1. If the fluid area ($y = 0$ in

Figures 1.12 or 13.1) is chosen as a surface moving at a mass-average velocity \vec{U} (cf. Equation 1.4.1) under the assumption of the thermal velocity equality $V_{iy}^{(+)} = V_{iy}^{(-)}$ above (+) and below (-) this area at $T^{(+)} = T^{(-)}$ (we will call this area *ideal*), then generally, owing to the difference of diffusivities D_i of different components, a mass transfer will occur through the area; to avoid this mass transfer an *actual* fluid area must move relative to the ideal one at a velocity u_0 and mean molecular velocities across the area $W_{iy}^{(\pm)} = (V_{yi} \pm u_0)$. Then reasoning in the same manner as in deriving the formulas for viscosity coefficients in Section 1.4, we obtain the diffusive mass fluxes of the molecules of the first and second type along the y axis across the $y = 0$ area

$$I_i = -m_i D_i \frac{dn_i}{dy} + m_i n_i u_0, \quad D_i = \frac{1}{2} l_i V_{yi}, \quad i = 1, 2 \quad (13.1.3)$$

We will call diffusivity D_i entering in Equation 13.1.3 *original* (as distinct from other coefficients introduced in the following). By definition of the fluid (actual) area, the condition $I_1 + I_2 = 0$ must be fulfilled on it; this makes it possible to exclude the velocity u_0 from Equation 13.1.3. Then, letting $dn_1 = -dn_2$ and using the relations

$$x_i = \frac{n_i}{n} = \frac{mc_i}{m_i} = \frac{\bar{M}_i}{M} c_i, \quad m = \sum_i m_i x_i, \quad \rho = mn, \quad dx_i = \frac{m^2}{m_1 m_2} dc_i \quad (13.1.4)$$

where m is the mean molecular mass, we obtain the following formula for the diffusive fluxes I_i and the velocity u_0

$$I_i = m_i n_i U_i = -\rho D_{12} \frac{dc_i}{dy}, \quad u_0 = \left(\frac{m}{m_2} D_1 - \frac{m}{m_1} D_2 \right) \frac{dc_1}{dy}, \quad D_{12} = x_2 D_1 + x_1 D_2 \quad (13.1.5)$$

where U_i are the *diffusive velocities* of species i . Obviously, the relative velocity $u_0/V_y \ll 1$, together with $l_i/L \ll 1$, where L is the scale length of the problem; for $m_1 D_1 = m_2 D_2$ we have $u_0 = 0$. The *binary diffusion coefficient* D_{12} determines the *concentration diffusion flux* and, in view of the relations $l_1 \sim n_2^{-1}$ and $l_2 \sim n_1^{-1}$, within the framework of the rigorous

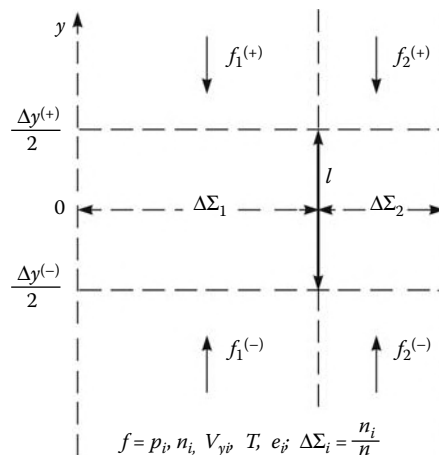


FIGURE 13.1

On the derivation of the formula for diffusion and energy fluxes.

theory is independent of the component concentrations (see Section 13.3). In the general case, in which the temperature and pressure gradients are also present, the formulas for \vec{l}_i must involve the terms containing these gradients by virtue of, at least, the dependences $n(p, T) = p/kT$ and $V_{yi} = V_{yi}(T)$; this leads to the occurrence of the *thermal diffusion* and *barodiffusion* effects.

In the same context we will consider an ionized gas, that is, a triple mixture of a neutral component, or simply *neutrals*, ions, and electrons with concentrations n_1 , $n_{\text{ion}} = n_2$, and n_{el} , respectively. In the absence of a superimposed electric field and an electric current, we will consider the plasma as *quasineutral*, that is, let $n_2 = n_3$ or $x_1 + 2x_2 = 1$. Moreover, as previously, we will assume the quantity $n = n_1 + 2n_2$ to be constant (for $p, T = \text{const}$) and neglect the electron mass, that is, let $c_1 + c_2 = 1$. Then, by analogy with Equation 13.1.4, we arrive at the equations

$$dx_1 = \frac{2m^2}{m_1 m_2} dc_1, \quad dx_2 = \frac{m^2}{m_1 m_2} dc_2, \quad m = m_1 x_1 + m_2 x_2 \quad (13.1.6)$$

The quasineutrality condition does not suggest the complete disappearance of electrostatic polarization fields; taking account for them within the framework of theory of weakly ionized gases leads to the acceleration of the diffusion of ions following the law (Smirnov, 1982; and Raizer, 1989)

$$D_{\text{ion}}^{(a)} = 2\alpha D_{\text{ion}}, \quad \alpha = \frac{1}{2} \left(1 + \frac{T_{\text{el}}}{T} \right) \quad (13.1.7)$$

Here, $D_{\text{ion}} = D_2$ in Equation 13.1.3, $D_{\text{ion}}^{(a)}$ is the ion *ambipolar diffusion* coefficient, and T_{el} is the electron temperature. Obviously, $D_{\text{el}}^{(a)} = D_{\text{ion}}^{(a)}$.

We obtain diffusive fluxes corresponding to binary ambipolar diffusion substituting the coefficient $D_2^{(a)} = D_{\text{ion}}^{(a)}$ for $D_2 = D_{\text{ion}}$ in Equation 13.1.3 and using Equation 13.1.6 rather than Equation 13.1.4

$$I_2 = \vec{l}_2^{\text{ion}} = -\rho D_{12}^{(a)} \frac{dc_2}{dy}, \quad D_{12}^{(a)} = 2(x_2 D_1 + \alpha x_1 D_2) \quad (13.1.8)$$

Clearly, the binary ambipolar diffusion coefficient $D_{12}^{(a)}$ is twice as large (for $\alpha = 1$) as the conventional coefficient with the reservation that the coefficient D_2 for ions can be different from the same coefficient for neutrals due to the difference in their free paths l_2 .

The results obtained here, as well as in Section 1.4 and in what follows for the energy flux \vec{J} , within the framework of such a simplified theory elucidate the qualitative and structural nature of the source terms in the equations and the order of magnitude of their coefficients; however, they cannot naturally claim good accuracy, which can be obtained only within the framework of the rigorous molecular-kinetic theory and plasma physics. We will present the results of this theory without derivation.*

* The presentation of this theory and its results, useful in solving gas dynamic problems, can be found in Hirshfelder, Curtiss, and Bird (1954), Dorrens (1966), Frank-Kamenetskii (1967), Kogan (1967), Bird (1976), Smirnov (1982), Alekseev and Grishin (1985), Tirsikii (1989), and others.

For the mass diffusion fluxes in a multicomponent gas, molecular-kinetic theory gives the *Stephan–Maxwell equations*

$$\sum_j \frac{x_i x_j}{\rho D_{ij}} \left(\frac{\vec{I}_j}{c_j} - \frac{\vec{I}_i}{c_i} \right) = \nabla x_i + (x_i - c_i) \nabla \ln p + k_{Ti} \nabla \ln T \quad (13.1.9)$$

Here, D_{ij} are the *binary multicomponent diffusion coefficients*, generally different from D_{12} in Equation 13.1.5, and k_{Ti} are the *thermal diffusion ratios*.

Obviously, by virtue of the conservation laws 13.1.2, the sum of all similar terms of Equation 13.1.2 over i is zero, which makes it possible to exclude one equation from the system.

System 13.1.9 is written for a mixture of electrically neutral gases, while for a quasineutral weakly ionized mixture of gases it must include terms proportional to the polarization field E in the corresponding equations. As previously, we will demonstrate the situation that arises with reference to the example of a triple mixture (more general study was performed by Tirsikii, 1989). For $x_2 \approx x_3$ the field E is of the order $E \sim x_2 - x_3$ and vanishes as $x_2 - x_3 \rightarrow 0$. In this case, from the equality of the ion and electron fluxes there follows $I_2/c_2 = I_3/c_3$, so that the differences of these ratios disappear from Equation 13.1.9, which, in the absence of barodiffusion and thermal diffusion, take their limiting form

$$\begin{aligned} \frac{x_1 x_2}{\rho D_{12}} \left(\frac{\vec{I}_2}{c_2} - \frac{\vec{I}_1}{c_1} \right) + \frac{x_1 x_3}{\rho D_{13}} \left(\frac{\vec{I}_3}{c_3} - \frac{\vec{I}_1}{c_1} \right) &= \nabla x_1 \\ \frac{x_1 x_2}{\rho D_{12}} \left(\frac{\vec{I}_1}{c_1} - \frac{\vec{I}_2}{c_2} \right) = \nabla x_2, & \quad \frac{x_1 x_3}{\rho D_{13}} \left(\frac{\vec{I}_1}{c_1} - \frac{\vec{I}_3}{c_3} \right) = \nabla x_3 \end{aligned} \quad (13.1.10)$$

From the comparison of two last equations for $x_2 = x_3$ there follows $D_{13} = D_{12}$; then, in view of Equation 13.1.6, the first equation reduces to the equation $\vec{I}_1 = -\rho D_{12} \nabla c_1$, while from the comparison with Equation 13.1.8 it follows that the coefficient D_{12} must be replaced by the ambipolar coefficient $D_{12}^{(a)}$.

System 13.1.9 in the fluxes \vec{I}_i/c_i determines a solution for them only correct to a constant and must be supplemented by the condition $\sum_i \vec{I}_i = 0$ for the fluxes across a fluid area. Then the solution of system 13.1.9 takes the form:

$$\begin{aligned} \vec{I}_i &= \vec{I}_i^{(c)} + \vec{I}_i^{(T)} + \vec{I}_i^{(p)}, & \vec{I}_i^{(c)} &= \sum_k a_{ik} \nabla x_k = -\rho \sum_k \bar{D}_{ik} \nabla c_k \\ \vec{I}_i^{(p)} &= -\rho D_i^{(p)} \nabla \ln p, & \vec{I}_i^{(T)} &= -\rho D_i^{(T)} \nabla \ln T \end{aligned} \quad (13.1.11)$$

Here, the term $\vec{I}_i^{(c)}$ is due to concentration diffusion, $\vec{I}_i^{(T)}$ to thermal diffusion, and $\vec{I}_i^{(p)}$ to barodiffusion; $D_i^{(T)}$ and $D_i^{(p)}$ are the *thermal diffusion* and *barodiffusion coefficients*, respectively. The coefficients \bar{D}_{ij} are called the *unary multicomponent diffusivities*; their relation with the coefficients a_{ij} and the inverse relation follow from the equality $c_i = (\bar{M}_i/\bar{m})x_i$

$$\begin{aligned} \frac{1}{\bar{M}} \nabla x_i &= \frac{1}{\bar{M}_i} \nabla c_i = -\frac{\bar{M}}{\bar{M}_i} c_i \sum_j \frac{1}{\bar{M}_j} \nabla c_j \\ \nabla c_i &= \sum_j \frac{\bar{M}_i \bar{M}_j}{\bar{M}^2} (x_j \nabla x_i - x_i \nabla x_j) \end{aligned} \quad (13.1.12)$$

For a binary gas mixture, from Equation 12.5.2 there follows

$$\vec{I}_i^{(c)} = -\rho D_{12} \nabla c_i, \quad D_i^{(p)} = \rho(x_i - c_i) D_{12} \frac{\bar{M}_1 \bar{M}_2}{\bar{M}^2}$$

$$D_i^{(T)} = \rho D_{12} \frac{\bar{M}_1 \bar{M}_2}{\bar{M}^2} k_{Ti} \quad (13.1.13)$$

Here, the first formula coincides with Equation 13.1.3. Obviously, barodiffusion favors the displacement of lighter components ($x_i > c_i, D_i^{(p)} > 0$) toward the low-pressure region, and vice versa. The barodiffusion effect may be neglected in boundary-layer and near-boundary-layer flows due to the absence of the transverse pressure difference. At the same time, the effect should apparently be taken into account in calculating the shock wave structure. As for thermal diffusion coefficient, within the framework of the problems considered in this book the thermal diffusion effect is usually not taken into account (although maybe without proper substantiation).

We will also mention the *self-diffusion* process with coefficients D_{ii} for mutually diffusible molecules with the same masses m_i and free paths l_i differing, for example, in the excitation degree of one or another degree of freedom. Naturally, in this case using the coefficients D_{ii} instead of the corresponding binary coefficients is only rough approximation to the reality, since the equality of the free molecular paths l_i for, say, vibrationally excited and unexcited molecules could hardly be substantiated. However, in this stage taking this difference into account is hardly possible.

Substituting formula 13.1.11 for $\vec{I}_i^{(c)}$ into the diffusion Equation 13.1.1 is accompanied by the appearance of the second derivatives of the concentrations of all (in the general case) the species on the right-hand sides of these equations, while an alternative approach of using systems 13.1.9 and 13.1.11 in addition to Equation 13.1.1 increases appreciably the overall order of the general system thus obtained. In both cases, we must deal with the systems of equations whose mathematical properties and algorithms of their solution are obviously too complicated even within the framework of the PNSE approximation (see Section 12.14). For this reason, in practice, the simplified *generalized Fick law* is often used

$$\vec{I}_i = -\rho D_{i,\text{eff}} \nabla c_i, \quad D_{i,\text{eff}} = (1 - x_i) \left(\sum_{j \neq i} \frac{x_j}{D_{ij}} \right)^{-1} \quad (13.1.14)$$

with the *effective diffusion coefficient* D_i determined by the *Wilkie formula* in terms of the binary diffusion coefficients D_{ij} ; for the same D_{ij} for all components of the mixture we have $D_{i,\text{eff}} = D_{ij}$.

Formula 13.1.14 reduces the algorithms for the solution of particular problems to the conventional algorithms for the Navier–Stokes equations; however, generally it also leads to the situation in which the mass conservation law 13.1.1, or the equality of the sum of the fluxes \vec{I}_i to zero are not automatically fulfilled.

This can lead to the occurrence of spurious mass, momentum, and energy sources in the equations of motion, which must be eliminated using one or another artificial approach, for example, replacing the fluxes \vec{I}_i determined by formula 13.1.14, by the *corrected* fluxes $\vec{I}_{i,\text{corr}}$

$$\vec{I}_{i,\text{corr}} = \vec{I}_i + c_i \Delta \vec{I}, \quad \Delta \vec{I} = - \sum \vec{I}_i \quad (13.1.15)$$

The fluxes $\vec{I}_{i,\text{corr}}$ satisfy the conservation laws.

We will now touch upon other diffusion-kinetics equations. The equation for the energies of the internal degrees of freedom can be obtained from Equation 10.4.12 for inviscid flow by adding the diffusion term

$$\rho \frac{dc_i e_{ik}^{(k)}}{dt} = \frac{\rho_i (e_{ike}^{(v)} - e_{ik}^{(v)})}{\tau_{ik}} - \operatorname{div} \vec{I}_{ik}^{(i)}, \quad \vec{I}_{ik}^{(i)} = \vec{I}_i e_{ik}^{(v)} \quad (13.1.16)$$

Here, $e_{ik}^{(v)}$ is the energy of internal degree of freedom k of species i per unit mass of the component.

In an ionized gas the diffusion-kinetics equation for the ion concentration $c_i = c_i^{(\text{ion})}$ has the same form 13.1.1 with the structure of the terms $\Lambda_i = \Lambda_i^{(\text{ion})}$ considered in Section 10.12. In approximation 13.1.14 the following formula for the diffusion fluxes $\vec{I}_i^{(\text{ion})}$ of the ions of species i can be used

$$\vec{I}_i^{(\text{ion})} = -\rho D_i^{(a)} \nabla c_i^{(\text{ion})} \quad (13.1.17)$$

The electron concentration is determined in terms of the ion concentrations from Equations 10.5.5 or 10.12.3.

Finally, in inviscid flow the electron temperature T_{el} is determined by Equation 10.12.2; introducing dissipative terms in this equation we obtain an equation for the electron energy e_{el} per unit mass

$$\frac{dc_{\text{el}} e_{\text{el}}}{dt} + \frac{2}{3} c_{\text{el}} e_{\text{el}} \operatorname{div} \vec{U} = \Lambda_{\text{el}} - \operatorname{div} \vec{J}_{\text{el}}, \quad c_{\text{el}} e_{\text{el}} = \frac{3n_{\text{el}} k T}{2\rho} \quad (13.1.18)$$

Here, c_{el} and n_{el} are the mass and number concentrations of electrons, while the generating function Λ_{el} was described in Section 10.12. The electron energy flux \vec{J}_{el} will be determined in the following.

The *energy flux* \vec{J} entering in the energy Equations 1.9.6 and 1.9.10 or 13.1.18 is expressed in the form of the sum

$$\vec{J} = \vec{J}_0 + \vec{J}_D, \quad \vec{J}_D = \sum_i \vec{J}_i h_i \quad (13.1.19)$$

Here, the term \vec{J}_0 is due to the gradients of the internal energies e_i of individual components and the term \vec{J}_D to the diffusion transport of energy. To elucidate their structures, we will use the same approximate model that was used in the derivation of formula 13.1.3.

We will begin with the term \vec{J}_0 restricting ourselves to the case of a single-component gas and turn to Figure 1.12 of Section 1.4 or Figure 13.1 assuming the occurrence of the temperature gradient $\partial T / \partial y$ with respect to the y axis only. Then per unit time the energy fluxes $(1/2)mn^{(+)}V_y^{(+)}e^{(+)}$ and $(1/2)mn^{(-)}V_y^{(-)}e^{(-)}$ arrive to the middle fluid area $y = 0$ from the upper $(\Delta y^{(+)}/2)$ and lower $(\Delta y^{(-)}/2)$ areas. From the fluid area condition it follows that $n^{(+)}V_y^{(+)} = n^{(-)}V_y = nV_y$; hence, in view of the formula $n = p/kT$ we obtain

$$p^{(+)}V_y^{(+)} = nV_y k T^{(+)}, \quad p^{(-)}V_y^{(-)} = nV_y k T^{(-)} \quad (13.1.20)$$

The product $p^{(\pm)}V_y^{(\pm)}/2$ is the work on forcing the gas across the area $\Delta y^{(\pm)}/2$, which should be taken into account in writing the balance of the energy transport across the fluid area $y = 0$ (the factor 1/2 is due to the fact that only a half of the molecules moves in the same direction and, therefore, "penetrates" only a half of the area). Therefore, using the

relation $kT = p/n = mp/\rho$ and comparing with 1.4.9 and 13.1.3 we obtain the following expression for the flux \vec{J}_0

$$-\vec{J}_0 = \frac{1}{2} n m l V_y \frac{\partial}{\partial y} \left(e + \frac{p}{\rho} \right) = \mu \frac{\partial h}{\partial y} = \rho D \frac{\partial h}{\partial y} \quad (13.1.21)$$

In this case, $D = D_{ii}$ is the self-diffusion coefficient. Generalizing, we write the flux \vec{J}_{0i} for a single-component gas i in the form:

$$\vec{J}_{0i} = -\rho D_{ii} \nabla h \quad (13.1.22)$$

In accordance with Section 10.3, the internal energy and the entropy of species i are equal to

$$e_i = e_i^{(0)} + e_i^{(v)} + h_{0i}, \quad e_i^{(0)} = c_{vi}^{(0)} T, \quad e_i^{(v)} = \sum_k e_{ik}^{(v)}, \quad h_i = e_i + p_i / \rho_i \quad (13.1.23)$$

Here, h_{0i} is the energy of formation, $e_i^{(0)}$ is the energy of the external, that is, translational and rotational, degrees of freedom (in accordance with the model adopted in Chapter 10). Therefore, in the case of excited internal degrees of freedom, the term \vec{J}_{0i} can be presented in the form:

$$\begin{aligned} \vec{J}_{0i} &= \vec{J}_{Ti} + \vec{J}_i^{(v)}, & \vec{J}_{Ti} &= -\rho D_{ii} \nabla h_i^{(0)} = -\lambda_i^{(0)} \nabla T, & \vec{J}_i^{(v)} &= \sum_k \vec{J}_{ik}^{(v)} \\ \vec{J}_{ik}^{(v)} &= -\rho D_{ii} \nabla e_{ik}^{(v)}, & \lambda_i^{(0)} &= \rho D_{ii} = \mu c_p^{(0)} \text{Sc}_i^{-1}, & \text{Sc}_i^{-1} &= \frac{\mu_i}{\rho D_{ii}} \end{aligned} \quad (13.1.24)$$

Here, $\lambda_i^{(0)}$ is thermal conductivity with frozen internal degrees of freedom and Sc_i is the *self-diffusion Schmidt number* for species i .

When only a part of the energies is at equilibrium, $e_{ik}^{(v)} = e_{ike}^{(v)}(T)$, using the change $de_{ik}^{(v)} = [de_{ike}^{(v)}/dT]dT$ the corresponding terms \vec{J}_{ik} can be transferred from the sum $\vec{J}_i^{(v)}$ to the term \vec{J}_{Ti} ; then the flux \vec{J}_{0i} is brought to the form:

$$\begin{aligned} \vec{J}_{0i} &= \vec{J}_{Ti}^{(k_e)} + \vec{J}_i^{(v k_e)}, & \vec{J}_{Ti}^{(k_e)} &= -\lambda_i^{(k_e)} \nabla T, & \vec{J}_i^{(v k_e)} &= \sum_{k>k_e} \vec{J}_{ik}^{(v)} \\ \lambda_i^{(k_e)} &= \lambda_i^{(0)} + \rho \sum_i D_{ii} \sum_{k=1}^{k_e} \frac{de_{ike}^{(v)}}{dT} \end{aligned} \quad (13.1.25)$$

Here, k_e is the number of equilibrium internal degrees of freedom of species i , while $\lambda_i^{(k_e)}$ is the corresponding effective thermal conductivity analogous to 1.2.11. When all the internal degrees of freedom are at equilibrium, the coefficient $\lambda_i^{(k_e)}$ depends only on the temperature: $\lambda_i^{(k_e)} = \lambda_{ie}(T)$. In this case we have

$$\vec{J}_{0i} = \vec{J}_{0ie} = -\lambda_{ie} \nabla T \quad (13.1.26)$$

In the same context we will estimate the diffusion flux of energy \vec{J}_D for a binary gas mixture under the assumption that the temperature and the energies $e_i^{(v)}$ of the gas components are constant but there exist diffusive fluxes $I_i = m_i n_i U_i$, where U_i is the diffusion velocity of the mass of species i flowing across a real fluid area (see Equation 13.1.5). In this case,

the work on forcing the gas across a unit area is equal to $p_i U_i$. Then, reasoning in the same fashion as in the derivation of the previous formula of this set, we obtain the following formula for the diffusion transport of energy for species i

$$\vec{J}_{Di} = m_i n_i \vec{U}_i \left(e_i + \frac{p_i}{\rho_i} \right) = \vec{I}_i h_i \quad (13.1.27)$$

Within the framework of the rigorous theory, the term h_i in this formula contains an additional summand, proportional to the thermal diffusion coefficient, which is usually small and is not taken into account in practice (Tirskii, 1989).

We note that an analogy with the derivation of the energy conservation law 1.7.12 for a plane front (Figure 1.16d) is pertinent if the pressure force work is taken into account when deriving formulas 13.1.21 and 13.1.27. For a binary gas mixture, the nature of this model is explained in Figure 13.1 in which the fluxes of species 1 and 2 are schematically separated into two parallel fluxes. We also note that in the reasoning of this level, this effect often is not taken into account, which leads to the formula $\lambda^{(0)} = \mu c_v$ and the Prandtl number $\text{Pr} = \mu c_p / \lambda = c_p / c_v$. As for formula 13.1.24 for $\lambda^{(0)}$, it provides a more likely value $\text{Pr} \approx \text{Sc} \approx 1$ for perfect gases.

Similarly, the term \vec{J}_{el} in Equation 13.1.18 can be determined as follows:

$$\begin{aligned} \vec{J}_{el} &= -\lambda_{el} \nabla T_{el} + \vec{I}_{el} h_{el} \\ \vec{I}_{el} &= \sum_k \frac{m_{el}}{m_k} \vec{I}_k^{(\text{ion})}, \quad h_{el} = \frac{5}{2} \frac{n_{el} k T_{el}}{m_{el}} \end{aligned} \quad (13.1.28)$$

Here, λ_{el} is *electronic thermal conductivity*, m_{el} and m_k are the electron and ion masses, and $\vec{I}_k^{(\text{ion})}$ are diffusion fluxes of ions.

For multicomponent gas mixtures, the final form itself of formula 13.1.27 assumes additivity of law 13.1.19 for the overall flux \vec{J}_D . At the same time, due to the fact that the free paths l_i of particles i are dependent on the entire composition of the gas mixture, the dependence of the overall viscosity μ and thermal conductivity $\lambda^{(0)}$ on the individual quantities μ_i and λ_i is more complicated and nonadditive. The most widespread formula for μ for inert gases following from the rigorous theory is the Wilkie formula, which can be written in the form:

$$\begin{aligned} \mu &= \sum_i x_i \mu_i f_{i\mu}^{-1}, \quad f_{i\mu} = \sum_k x_k \varphi_{ik} \\ \varphi_{ik} &= \frac{\sqrt{2}}{4} \frac{[1 + (\mu_i/\mu_k)^{1/2} (\bar{M}_k/\bar{M}_i)^{1/4}]^2}{(1 + (\bar{M}_i/\bar{M}_k)^{1/2})}, \quad x_i = \frac{\bar{M}_i}{\bar{M}_i} c_i \end{aligned} \quad (13.1.29)$$

In the general case, $\varphi_{ik} \neq 1$, which underlines the nonadditive character of the viscosity (and heat conduction, see the following) laws for gas mixtures. For thermal conductivity $\lambda^{(0)}$ with frozen degrees of freedom (vibrational or electronic) the *Masson–Saxena formula* is known*

* The choice of the coefficients $\alpha_1 \neq 1$ and $\alpha_2 \neq 0$ in the formula for $\lambda^{(0)}$ leads to a certain logical contradiction, since at equal $\lambda_i^{(0)}$ and \bar{M}_i for all the components we obtain that $\lambda^{(0)} \neq \lambda_1^{(0)}$. However, this is the choice of the original work.

$$\begin{aligned}\lambda^{(0)} &= \sum x_i \lambda_i^{(0)} f_{i\lambda}^{-1} \\ f_{i\lambda} &= \frac{\sqrt{2}}{4} \left(\alpha_1 \sum_k x_k \varphi_{ik} - \alpha_2 \right) \\ \alpha_1 &= 1.065, \quad \alpha_2 = 0.065\end{aligned}\tag{13.1.30}$$

Obviously, this formula was originally derived precisely for the energy fluxes under the assumption that there exists a relationship $\vec{J}_{0i} = -\lambda_i^{(0)} \nabla T$, that is, without taking the possible nonequilibrium of internal degrees of freedom into account. Since the same diffusible molecules are the carriers of their translational, rotational, and internal energies, formula 12.15.30 for the overall energy flux \vec{J}_0 is naturally generalized as follows

$$\vec{J}_0 = \sum_i x_i \vec{J}_{0i} f_{i\lambda}^{-1} \tag{13.1.31}$$

Here, the function $f_{i\lambda}$ and the fluxes \vec{J}_{0i} are determined by formula 13.1.25. At total equilibrium of internal degrees of freedom $\lambda_i^{(0)}$ and $\lambda^{(0)}$ in formula 13.1.30 should be replaced, in accordance with 13.1.25, by λ_{ie} and λ_e .

We are now coming to the formulation of the *boundary conditions* for the diffusion-kinetics equations on the body surface. These conditions are conventional for the momentum and energy equations: the conditions $u = v = 0$ are imposed and the wall temperature $t = T_w$ is preassigned if the slip and temperature jump effects may be neglected (see Section 12.1); precisely this will be assumed in what follows.

At the same time, in a nonequilibrium gas the component concentrations c_{iw} on the wall and the gas enthalpy h_w are not known beforehand, since they are appreciably influenced by *heterogeneous processes*, that is, those proceeding directly on the body surface. In particular, in a dissociated binary mixture of atoms and molecules, the gas atoms striking the wall adhere to it due to the *adsorption* process and can further recombine to molecules following separation from the wall or *desorption*. In this case, recombination can proceed due to both direct collision of incident and adsorbed atoms (*Eley–Rideal mechanism*) and the interaction of two adsorbed atoms (*Langmuir–Hinshelwood mechanism*). In both cases a certain role is played by the *population density* or the *surface concentration* θ of adsorbed atoms determined by the rates of adsorption and desorption processes.

Depending on the surrounding conditions, all these processes can proceed in both forward and back direction with their own reaction rates and activation energies, the overall rates of these reactions being written by analogy with the homogeneous reactions of Sections 10.7 and 10.9. Only taking all these factors into account simultaneously determines the *heterogeneous, or catalytic recombination rate*, for atoms.*

The processes are considerably more complicated in a multicomponent gas mixture. The point is that the number of *active adsorption centers* per surface area unit is bounded and their distribution in the atoms of individual components, that is, their surface concentrations θ_i , is dependent on their relative adsorptive properties and other conditions. This leads to the mutual dependence of catalytic recombination rates, for example, for nitrogen and oxygen atoms in air.

* These questions are discussed in detail in Berkut, Doroshenko, Kovtun, and Kudryavtsev (1994) and V. L. Kovalev (2002).

Precisely the previously mentioned effects determine the boundary conditions for the component concentrations on the body surface. Within the framework of the simple molecular-kinetic model used previously these conditions are derived as follows. Let a mass flux $\rho c_i V_{yi}/2$ of species i arrive at the wall per unit time (Figure 12.53); here, V_{yi} is the mass-average thermal velocity of all the particles in the same direction determined by formula 11.13.4 in which $V_{yi} = V_2$. Let also a fraction $\bar{\gamma}_i$ of the incident particles vanish owing to heterogeneous reactions, which must be offset by the corresponding diffusion flux. Then the conservation law for this component on the wall takes the form:

$$-I_i = \rho D_i \frac{\partial c_i}{\partial y} = \rho K_{wi} c_{iw} = \bar{\gamma}_i \sqrt{\frac{RT}{2\pi \bar{M}_i}} \quad (13.1.32)$$

The coefficient K_{wi} is termed the *catalytic reaction rate constant* or, shorter, the *catalyticity constant* of the given gas relative to the given material, while the coefficient $\bar{\gamma}_i$ is the *catalyticicity probability* under the same conditions.

At $\bar{\gamma}_i = 0$, or $K_{wi} = 0$, that is, on an *ideally noncatalytic surface*, from 13.1.32 there follows the condition $\partial c_i / \partial y = 0$. Contrariwise, for $K_{wi} \rightarrow \infty$, or on an *ideally catalytic* surface (this is a mathematical abstraction, since, physically, the quantity K_{wi} is bounded by formula 13.1.32), we obtain that $c_{iw} \rightarrow 0$; at fairly low surface temperatures (say, for $T_w < 2000$ K for air) this value can coincide with the equilibrium value for air $c_{ie}(T_w) \approx 0$. However, in the general case the value of c_{iw} obtained from condition 13.1.32 can be both greater and smaller than the equilibrium value $c_{ie}(T_w)$.

The energies of internal degrees of freedom are also subject to heterogeneous processes, since excited atoms and molecules adsorbed on the wall can leave or, in the general case, acquire a part of their internal energy on the wall on desorption. Moreover, at heterogeneous atom recombination a molecule thus generated and desorbed may be in any energetic state, both vibrational and electronic. By way of illustration, we will write down the corresponding boundary condition of type 13.1.32 for the vibrational energy e_v per unit molecular mass with concentrations of molecules and atoms in the mixture c_m and c_a

$$-I_w^{(v)} = \rho D_{mm} \frac{\partial c_m e}{\partial y} = \rho K_w^{(v)} c_m e_{vw} - \rho \bar{\gamma}_v K_{wa} c_{aw} \quad (13.1.33)$$

Here, the first term is similar to the right-hand side of Equation 13.1.32 and is due to the variation of the vibrational energy at the interaction with the wall at a catalyticity constant $K_w^{(v)}$, while the second term accounts for the vibrational energy possessed at a probability $\bar{\gamma}_v$ by the molecules formed due to atom recombination.

As for the boundary conditions for ions at the surface (wall), usually the condition $c_i^{(\text{ion})} = 0$ is imposed. However, for an electrostatically insulated wall, the more natural condition seems to be that of the absence of the electrical current through the wall, with the complete mutual neutralization of ions and electrons. In this model, the wall is, as it were, an ion sink, so that, by analogy with Equation 13.1.32, for $\bar{\gamma} = 1$ the required boundary condition can, with account for Equation 13.1.8, be presented in the form:

$$I^{(\text{ion})} = -\rho D^{(a)} \frac{\partial c_i^{\text{ion}}}{\partial y} = I_w^{(\text{ion})} = -\rho c^{\text{ion}} K_w^{\text{ion}}, \quad K_w^{\text{ion}} = \sqrt{\frac{RT}{2\pi \bar{M}^{\text{ion}}}} \quad (13.1.34)$$

Actually, this process is more complicated, since due to the fact that in the wall *Debye layer*, whose thickness is negligibly small for the problems under consideration, the thermal

velocities of electrons are greater than those of ions, a potential difference is formed which decelerates electrons and accelerates ions. Taking this factor into account (Raizer, 1989) leads to a formula similar to 13.1.34, only with the electron temperature T_{el} substituted for T on the right-hand side.

The system of equations and boundary conditions written previously for a multicomponent nonequilibrium gas mixture should be closed by a system of equations of state, for example, 11.1.5 and the corresponding system of transport coefficients, which will be presented in Section 13.3.

13.2 Properties of Nonequilibrium Boundary Layers and Viscous Shock Layers

We will study these properties with reference to the example of the boundary layer flow on a flat plate for a binary gas mixture. We will write Equation 13.1.1 in the relaxation form using the simplified diffusion model 13.1.14 and denoting, for the sake of simplicity, $D_{i,\text{eff}}$ by D_i

$$\begin{aligned} \rho \frac{dc_i}{dt} &= \rho \Lambda_i - I_i, & I_i &= -\frac{\partial}{\partial y} \left(\mu_i \text{Sc}_i \frac{\partial c_i}{\partial y} \right) \\ \Lambda_i &= \frac{c_{ei} - c_i}{\tau_i}, & \text{Sc}_i &= \frac{\rho D_i}{\mu_i} \end{aligned} \quad (13.2.1)$$

Here, τ_i , D_i , and Sc_i are the appropriate relaxation time, diffusivity, and the Schmidt number, while $c_{ei}(T)$ is the locally equilibrium value of the concentration c_i of the given component. For Equation 13.2.1, some boundary conditions must be imposed on the outer edge of the boundary layer and the wall; for the time being, we impose the conditions $c_i = c_{i\delta}$ and $c_i = c_{iw}$, respectively.

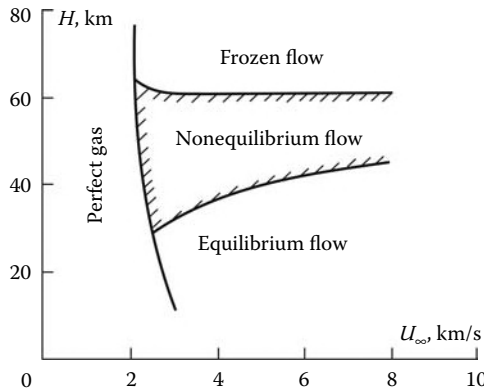
We will consider the *limiting regimes* of the boundary layer flow. Since the Schmidt number is near unity, the diffusion term in Equation 13.2.1 is of the same order as the convective term (this is also true for dissipative terms in any boundary layer equation), that is, of the order $\Delta c_i/t_0$, where $t_0 = U_\delta/L$ is the *gas dynamic time scale*, U_δ is the velocity at the boundary layer edge, L is the streamwise flow scale, and Δc_i is the concentration difference across the boundary layer (e.g., $\Delta c_i = c_{i\delta} - c_{iw}$).

Then, as in the case of inviscid flow considered in Sections 10.4 and 11.3, the flow pattern depends on the parameter t_0/τ . We note that for the boundary layer problems the *Dahmkeller number* $\text{Da} = \tau D/\delta^2$ is often used as the criterion for characteristic flow regimes. Here, δ is the boundary layer thickness and the order of this number is the same as for the ratio of the diffusion term to the source term in Equation 13.2.1.

Thus, depending on the parameter t_0/τ , the following limiting flow regimes can be realized.

13.2.1 Frozen Boundary Layer

Let $t_0/\tau \ll 1$. Then the term Λ_i can be dropped from Equation 13.2.1; however, as distinct from inviscid flows, the concentration c_i is not constant but is determined by the homogeneous Equation 13.2.1 or, in the general case, by Equation 13.1.1 with $\Lambda_i = 0$. This regime is associated with the condition $\text{Da} \gg 1$.

**FIGURE 13.2**

Approximate ranges of the influence of different physical and chemical processes in the boundary layer at the stagnation point on a sphere of $R = 1$ m radius.

13.2.2 Equilibrium Boundary Layer

Let, on the contrary, $t_0/\tau \gg 1$. Then multiplying Equation 13.2.1 by τ we obtain its limiting solution $c_{ie} = c_{ie}(p, T, c_j^*)$, where c_j^* stands for the totality of the concentrations of the mixture components, which, as distinct from inviscid flows, is not known beforehand. The regime is associated with the condition $Da \ll 1$. The ranges, on which different boundary layer regimes are realized at the stagnation point on a sphere of radius $R = 1$ m, are presented in Figure 13.2 for the flight conditions in the Earth's atmosphere.

The quantity c_j^* is rigorously known only for single-component gases. In multi-element gas mixtures a specific element separation effect can occur, namely, the *element separation effect*.^{*} To analyze this effect we transform system 13.1.1 multiplying each of its i equations by its own coefficient d_{ij} , that is, the mass fraction of element j in species i (see 10.5.3) and summing all these equations. In this case all the source terms are offset; in view of 10.5.3, this leads to the following *equation of element diffusion* with element concentrations c_j^* and diffusion fluxes \vec{I}_j^*

$$\rho \frac{dc_j^*}{dt} = -\operatorname{div} \vec{I}_j^*, \quad c_j^* = \sum_i d_{ij} c_i, \quad \vec{I}_j^* = \sum_i d_{ij} \vec{I}_i \quad (13.2.2)$$

On the outer edge of the boundary layer $c_j^* = c_{j\delta}^*$, while on the wall the flux projection onto the normal is $\vec{I}_{j\text{w}}^* = 0$. Further results depend on the model adopted for the fluxes \vec{I}_i . In the case of equal diffusivities, $D_i = D_{12}$ (see Equation 13.1.14), and in the absence of barodiffusion and thermal diffusion we obtain for the boundary layer $I_j^* = -\rho D_i (\partial c_j^*/\partial y)$ and system 13.2.2 becomes homogeneous with a single solution $c_j^* = \text{const}$. In the general case using 13.1.11 we obtain

* See Anfimov, 1963; and Tirkii, 1964, 1989.

$$\begin{aligned}\vec{I}_j^* &= \vec{I}_j^{*(c)} - \rho \bar{D}_j^{*(p)} \nabla \ln p - D_j^{*(T)} \nabla \ln T \\ \vec{I}_j^{*(c)} &= - \sum_i D_{jk}^* \nabla c_k, \quad D_{jk}^* = \sum_k d_{ij} \bar{D}_{ik} \\ D_j^{*(p)} &= \sum_i d_{ij} D_i^{(p)}, \quad D_j^{*(T)} = \sum_i d_{ij} D_i^{(T)}\end{aligned}\quad (13.2.3)$$

Thus, the element fluxes \vec{I}_j^* always accompany the pressure and temperature gradients. At the same time, the fluxes $\vec{I}_j^{*(c)}$ depend on the component concentration gradients and are generally independent only of the element concentrations themselves.

However, in the case of total equilibrium of the system all Equations 13.1.1 degenerate, as in inviscid flow (see Section 11.2) to the equilibrium conditions, so that for all the concentrations we have $c_i = c_{ie}(p, T, c_j^*)$. Then the concentration flux $\vec{I}_j^{*(c)}$ is equal to

$$\begin{aligned}\vec{I}_j^{*(c)} &= -\rho \sum_k \tilde{D}_{jl}^* \nabla c_l^* - \rho \tilde{D}_j^{*(p)} \nabla \ln p - \rho \tilde{D}_j^{*(T)} \nabla \ln T \\ \tilde{D}_{jl}^* &= \sum_k D_{jk}^* \frac{\partial c_{ke}}{\partial c_l^*}, \quad \tilde{D}_j^{*(p)} = p \sum_k D_{jk}^* \frac{\partial c_{ke}}{\partial p}, \quad \tilde{D}_j^{*(T)} = T \sum_k D_{jk}^* \frac{\partial c_{ke}}{\partial T}\end{aligned}\quad (13.2.4)$$

Substituting this result in system 13.1.1 we obtain a system of inhomogeneous (owing to the terms involving the pressure and temperature gradients) equations in c_j^* having a nontrivial solution, which in the general case gives $c_{jw}^* \neq c_{j\delta}^*$, indicating element separation even when the barodiffusion and thermal diffusion effects are not taken into account. However, for equilibrium air this effect is relatively weak (see footnote) and is often neglected for boundary layers due to its slight influence on heat fluxes.

More complicated is the case of partial equilibrium of only a few reactions. For inviscid flows this case was considered in Section 11.2, where it was recommended to exclude the equations that involve the terms governing these reactions from the complete system of kinetic equations, replacing them by the corresponding equilibrium conditions. For viscous flows the situation is appreciably more complicated, since the previously mentioned equilibrium conditions must be supplemented by the system of equations 13.2.2 for the elements.

As for the energy flux \vec{J} at complete equilibrium of the system, letting $c_i = c_{ie}(T, P, c_j^*)$ from Equations 13.1.19 and 13.1.11, by analogy with 13.2.4 we obtain the following formula for the equilibrium energy flux \vec{J}

$$\begin{aligned}-\vec{J} &= \lambda_{\text{eff}} \nabla T + \lambda_p \nabla P - \vec{J}^*, \quad -\vec{J}^* = \rho \sum_i h_i \sum_k D_{ik} \sum_j \frac{\partial c_{ke}}{\partial c_j^*} \nabla c_j^* \\ \lambda_{\text{eff}} &= \lambda_e + \rho \sum_i h_i \left(\sum_k \bar{D}_{ik} \frac{\partial c_{ke}}{\partial T} + \frac{1}{T} D_i^{(T)} \right) \\ \lambda_p &= \rho \sum_i h_i \left(\sum_k \bar{D}_{ik} \frac{\partial c_{ke}}{\partial p} + \frac{1}{p} D_i^{(p)} \right)\end{aligned}\quad (13.2.5)$$

Precisely this effective coefficient λ_{eff} for equilibrium air is presented in Figure 1.11. In the boundary layer and near-boundary-layer flows the term ∇p is small and is not usually taken into account.

We will now consider the *external boundary* conditions for diffusion-kinetics equations. For a classical thin boundary layer in an equilibrium external flow, the equilibrium conditions $c_i = c_{ei}(p, T)$ or $e_i^{(v)} = e_i^{(v)}(T)$ are also imposed on the outer edge. This situation can occur on a blunt body, where the equilibrium state in the boundary layer flow does not follow from the equilibrium state in the shock layer flow.

However, the analogous conditions for the boundary layer in a nonequilibrium flow are obtained from the solution of the inviscid nonequilibrium problem, in the simplest approximation, by solving Equations 11.1.4 and 11.1.5 along a surface streamline with a pressure distribution preassigned along it (the streamline method), the pressure being a much more conservative function (see Sections 9.4 and 11.10) than a possible variety of accompanying nonequilibrium gas states.

In the general case, the boundary layer on blunt and bluff bodies develops within a nonuniform nonequilibrium high-entropy layer. The qualitative nature of the interaction between the two layers is the same as in Sections 12.9 to 12.13, though the quantitative extension of the approximate methods developed in those sections to nonequilibrium flows is fairly difficult (with the exception, maybe, of frozen flows). In the latter case, for moderately high (in the meaning of Section 12.14) Reynolds numbers the solution of this problem is possible within the framework of the parabolized Navier-Stokes equations (PNSE model of Section 12.14). The procedure of the parabolization of equations of type 13.1.1 is not different from that outlined in Section 12.5.

Finally, at low Reynolds numbers the solution of such problems is possible, at least within the framework of the complete Navier-Stokes equations. By the way, a comparative analysis of both models in Section 12.14 (Figures 12.51 and 12.52) was performed for precisely nonequilibrium flows.

Far ahead of the body the conditions $c_i = c_{i\infty}$ are usually preassigned; however, within the framework of the PNSE model, if a conditional shock S is fitted (Figure 12.43 of Section 12.14) and the generalized Hugoniot conditions 12.14.18 are imposed on it, these conditions must be supplemented by analogous conditions for the concentrations

$$\rho_\infty v_n (c_{is} - c_{i\infty}) = -I_{ns} = \rho D_i \left. \frac{\partial c_i}{\partial n} \right|_s \quad (13.2.6)$$

Moreover, the energy flux J_{ns} in the last formula 12.14.8 must be determined from formula 13.1.19. In this case, it is assumed, and this is important, that, in accordance with the model of Sections 10.4 and 11.5, all the reactions are frozen in the outer (with respect to shock S) region of the broadened shock wave. In this case the dissipative fluxes penetrating the shock wave are offset by the counterconvective fluxes of the same components.

We recall that, as shown in Section 12.14, within the framework of the nonequilibrium PNSE model it is admissible to use only the generalized Hugoniot relations 12.14.18 and 13.2.6 even for comparatively thin shocks at high Reynolds numbers, since the use of conventional relations on a thin shock leads to spurious fluxes across it, due to dissipative terms of the equations.

We are now coming to an analysis of the effect of heterogeneous reactions described by formulas 13.1.32 and 13.1.33 on the nonequilibrium boundary layer in general and, in particular, on heat fluxes to the wall; as shown in the following, this effect can be considerable. We will demonstrate it with reference to the example of a frozen boundary layer. In

this case, the result of the solution of Equation 13.2.1 with $\Lambda_i = 0$, together with Equation 13.1.32, can be presented in the form:

$$-I_{iw} = \left(\rho D_i \frac{\partial c_i}{\partial y} \right)_w = \beta_i (c_{i\delta} - c_{iw}) = \rho_w K_{wi} c_{iw} \quad (13.2.7)$$

where β_i is the *mass transfer coefficient*, which is a counterpart of the heat transfer coefficient α formula 12.6.20. To evaluate the coefficient β_i we note that at $Sc = 1$ Equation 13.2.1 coincides with the equation of motion 12.5.5 and at $Sc = Pr = 1$ also with the energy Equation 12.5.8. This leads respectively to integrals analogous to the Crocco integral 12.6.15

$$\frac{c_i - c_{iw}}{c_{i\delta} - c_{iw}} = \frac{u}{U_\delta} = \frac{H - h_w}{H_\delta - h_w} \quad (13.2.8)$$

Clearly in this case $\alpha = \beta$ and, hence, in the general case $\alpha \sim \beta$ (for $Pr \sim Sc \sim 1$). Thus, from 13.2.7 it follows that

$$c_{iw} = c_{i\delta} (1 + z_i)^{-1}, \quad z_i = \rho_w K_{wi} / \beta_i \quad (13.2.9)$$

On the other hand, for the frozen boundary layer the heat flux to the wall can be presented, in view of formulas 12.6.20 and 10.3.6 and in the same designations, in the form:

$$\begin{aligned} q_w &= \alpha (H_e - h_w), & h_w &= \sum_i c_{iw} h_{iw} = c_p^{(0)} T_w + h_{fw} \\ h_{fw} &= e_w^{(v)} + h_{0w}, & e_w^{(v)} &= \sum_i c_{iw} e_{iw}^{(v)}, & h_0 &= \sum_i c_{iw} h_{0i} \end{aligned} \quad (13.2.10)$$

Here, $c_p^{(0)}$ is the frozen specific heat of the gas, $e_i^{(0)}$ are the energies of the internal degrees of freedom, and h_f is the energy of physicochemical transformation of the gas, which is zero in air frozen with respect to its cold state, in particular, in the freestream. Thus, in this case the quantity q_w depends on the species concentrations at the wall and their energies h_f .

For the sake of convenient representation, we will consider a binary mixture of atoms and molecules with concentrations c_a and $c_m = 1 - c_a$; we let for atoms $e_a^{(v)} = 0$ and $h_{0a} = h_{0w}$ and for molecules $h_{0m} = 0$ but $c_m^{(v)} > 0$. In this case, in a frozen boundary layer it is admissible conditionally to divide the molecules into two subgroups, or pseudocomponents (1) and (2). The former arrive from the outer edge of the boundary layer with a concentration $c_m^{(1)} = c_{m\delta}$ and an energy $e_m^{(1)} = e_{m\delta}^{(v)}$, which are conserved up to the wall (catalytic effects for this energy are not taken into account). The latter subgroup of molecules formed at the wall due to heterogeneous analysis has a concentration $c_{mw}^{(2)} = c_{a\delta} - c_{aw}$ and an energy $e_m^{(v)} = e_{mw}^{(2)}$ of vibrational or electronic levels, which can generally be rather large, for example, $e_{mw}^{(2)} \gg e_{m\delta}^{(v)}$. Then rewriting formula 13.2.10 in terms of 13.2.9 and letting $H_e = H_\delta$ yields

$$\begin{aligned} q_w &= q_{we} (1 - \Phi), & q_{we} &= \alpha (H_\delta - h_{ew}) \\ (H_\delta - h_{ew}) \Phi &= h_w - h_{ew}, & h_w &= c_{pw}^{(0)} T_w = h_{fw} \\ h_{fw} &= c_{aw} h_{0a} + c_{m\delta} e_{m\delta}^{(v)} + (c_{a\delta} - c_{aw}) e_{mw}^{(2)} \end{aligned} \quad (13.2.11)$$

The parameter c_{aw} is determined from Equation 13.2.9. For a relatively cold wall, which will be assumed in the following, for $h_{ew}, c_w^{(0)} T_w \ll H_\delta$ the ratio $\Phi \approx h_{fw}/H_0$.

As noted in Section 1.1 (Figure 1.5), in a high-velocity atmospheric flight the ratio $h_{f\delta}/H_\delta$ can amount to 3/4 even on a nonideally catalytic surface; for $K_{wa} \approx 0$ (or $z \approx 0$) we obtain $\Phi \approx h_{f\delta}/H_\delta$, which leads to a fourfold reduction of heat fluxes to the surface. In this case $c_{aw} \approx c_{as}$ and the term with the energy $e_{mv}^{(2)}$ drops out of formula 13.2.11 for h_{fw} . However, also in the general case this term is usually dropped under tacit assumption on the smallness of the mean value of $e_{mv}^{(2)}$ as compared with h_{0a} ; as for the data on the values of the ratio $e_{mv}^{(2)}/h_{0a}$, they are practically absent.

On the contrary, on an ideally catalytic surface, for $K_{wa} \rightarrow \infty$ we have $c_{aw} \ll 1$, while the value of Φ is small and the heat flux to the surface is near to the equilibrium value q_{we} in spite of the fact that the boundary layer is frozen. Moreover, in the equilibrium boundary layer in an equilibrium external flow, on a sufficiently cold wall (at $T_w < 20000$ K for air) the equilibrium values c_{aw} and $e_{me}^{(v)}$ are sufficiently low, so that, in accordance with 13.2.10, the heat flux is independent of the wall material catalyticity.

However, generally speaking, the catalyticity effect on the heat transfer is determined by the parameter $z = \rho K_w/\alpha$ of the order $\rho^{1/2} K_w$, since, in accordance with Section 12.6, $\alpha \sim \rho^{1/2}$. Therefore, for low densities (at high flight altitudes) the surface material can behave as noncatalytic even at a finite value of K_w .

We note also that for $h_w \ll H_\delta$ the value q_{we} differs from the frozen value q_{wf} only in the ratio of the heat transfer coefficients, $q_{we}/q_{wf} \approx \alpha_e/\alpha_f$, which is near unity (see Figures 13.3 and 13.4).

For the sake of illustration, in Figure 13.3 we have plotted the K_w -dependence of the heat flux ratio q_w/q_{we} at the blunt-body stagnation point, where q_w and q_{we} relate to the nonequilibrium and equilibrium boundary layers, with the equal parameters in the air shock layer; the values $K_{wO} = K_{wN} = K_w$ are equal for oxygen and nitrogen atoms. Curve 1 relates to an almost frozen boundary layer and the heat flux associated with it varies fourfold for K_w ranging from 0 to ∞ . At the same time, curve 3 relates to the near-equilibrium boundary layer with the corresponding weak K_w -dependence of the heat flux.

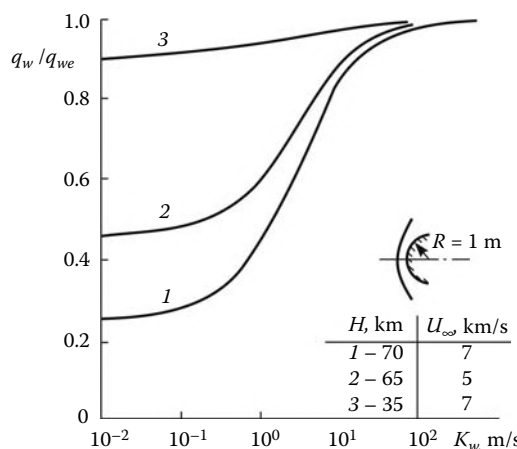
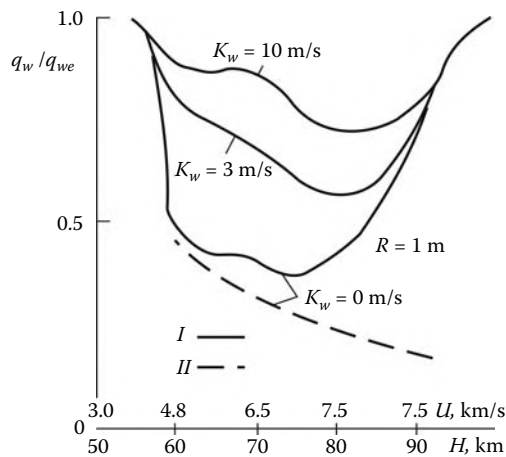


FIGURE 13.3
Catalyticity effect on the heat flux at the stagnation point on a sphere.

**FIGURE 13.4**

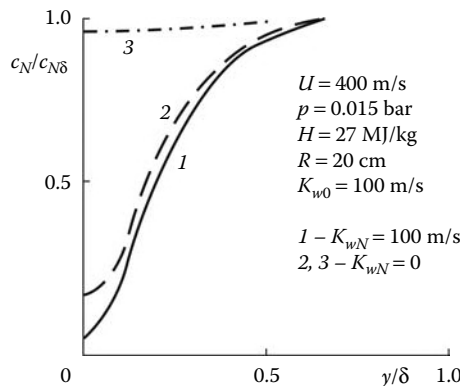
Catalytic effect on the heat flux at the stagnation point on the BOR-4 vehicle: q_w is the heat flux in equilibrium air; I is the viscous shock layer model; and II relates to the boundary layer within the equilibrium shock layer.

Figure 13.4 presents another example, namely, the heat flux at the stagnation point of the BOR-4 vehicle, whose trajectory is plotted along the abscissa axis.* In this figure the ratio q_w/q_{we} is near unity for any K_w both at high altitudes, $H > 90 \text{ km}$, where the flow is completely frozen, and at $H < 55 \text{ km}$, where, on one hand, the flow is near equilibrium and, on the other hand, the energy h_f of physicochemical transformations has reduced with decreasing flight velocity. At intermediate altitudes the heat flux considerably reduces with decreasing K_w . We note that the characteristics of the calculated boundary layer with the equilibrium parameters on its outer edge are considerably different from the exact curves at high H .

From the preceding discussion it follows that in hypersonic flight of vehicles in the terrestrial atmosphere at altitudes $H = 55$ to 90 km , the parameter determining essentially the heat fluxes to the body surface and, hence, the choice of its material, is the material catalyticity. Hence follows the importance of determining the material catalyticity constants K_{wi} .

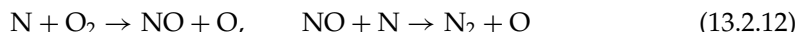
For the time being, these constants can be determined only experimentally, by comparing the heat fluxes to a tested material and a material with a fairly high catalyticity (usually, platinum or copper). The questions of data interpretation, which arise in this case, are far from trivial, since the catalyticity constants (as the reaction rate constants considered earlier in Chapter 10) are constant only by name, though actually, in view of the reasons mentioned in Section 13.1, they are complicated functions of the pressure, temperature, and concentrations of individual components. Moreover, due to the fact that the rates of heterogeneous recombination of individual elements are interrelated, which was noted in the same section, the values of K_{wi} obtained in the experiments with single-element gases cannot, strictly speaking, be used for gas mixtures. We also recall that, as noted previously, the relative role played by the excitation energy $e_{mo}^{(2)}$ in formula 13.2.11 is still unclear.

* Figures 13.4, 13.6, and 13.7 are taken from the work of Voinov, Zalgin, Lunev, and Timoshenko (1994), while the trajectories of BOR-4 and BURAN vehicles are from the work of Lozino-Lozinskii and Timoshenko (1998), where the vehicles themselves are also described.

**FIGURE 13.5**

Distribution of the nitrogen concentration in the boundary layer. Curves 1 and 2 are calculated with and curve 3 without account for exchange reactions; H is the stagnation enthalpy.

The interpretation of the experimental data on the constants K_{wi} can also be complicated by the effect of homogeneous physical and chemical processes that are not always controllable. Thus, even if direct homogeneous recombination of oxygen and nitrogen atoms proceeding in accordance with the schemes $O + O \rightarrow O_2$ and $N + N \rightarrow N_2$ are frozen in the boundary layer, but heterogeneous oxygen recombination proceeds, nitrogen recombination can occur due to the exchange reactions (see Section 10.5) proceeding by the scheme



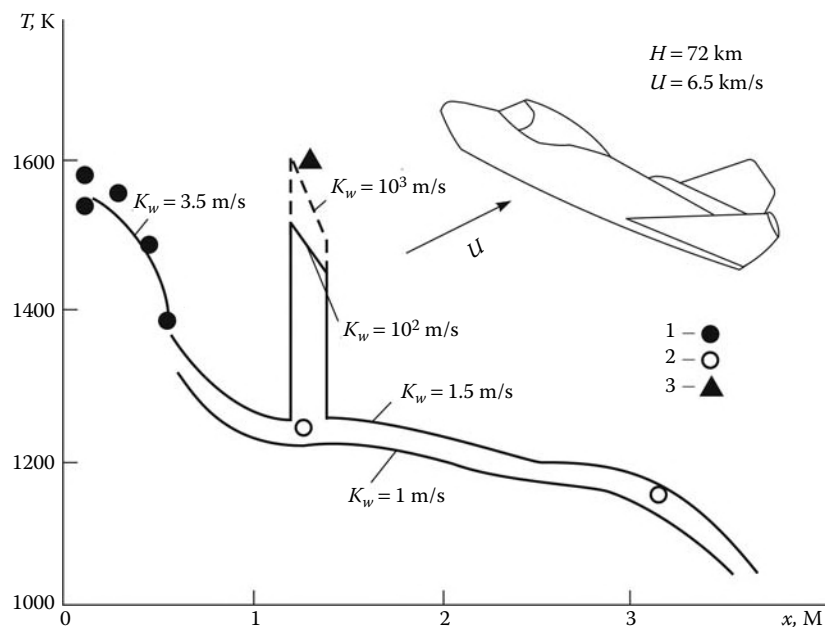
An example in which this situation is realized is shown in Figure 13.6; in this case, nitrogen atoms simply do not reach the surface with fairly high catalytic activity (platinum), and the process is governed only by heterogeneous oxygen recombination and the exchange reaction 13.2.11.

Sometimes such situations can result in certain unexpected effects, such as the *catalytic sublimation* effect of platinum in pure nitrogen.* The effect is due to an excess of the energy released at nitrogen atom recombination ($\varepsilon_N = 9.76$ eV) over the energy of the platinum atom release ($\varepsilon_p = 5.85$ eV). At the same time, this effect is absent from air under the conditions of Figure 13.5, since for oxygen $\varepsilon_0 = 5.1$ eV $< \varepsilon_p$.

For the reasons mentioned previously, for the time being only experimentally determined effective catalytic constants $K_{w,\text{eff}}$ for the mixture as a whole are actually used; they are also used in calculations for all atoms of the mixture. However, even in this approximation, for determining the structure of the formulas for the functions $K_{wi,\text{eff}}$ and their values, the processing of the experimental data obtained over a wide range is needed in combination with *a priori* ideas on the heterogeneous reaction rates (see, e.g., V. L. Kovalev and Suslov, 1995; and Zalugin and Lunev, 1997).

The reliability of the transfer of these data to the full-scale conditions can be ensured only by the benchmark modeling in such relevant parameters as the pressure, the stagnation enthalpy, the nitrogen and oxygen dissociation degree on the boundary layer edge, and the body surface temperature T_w .

* Itin, Zalugin, Lunev, and Perov, 1987; the experiments were conducted in the high-frequency plasma gun of TsNIIMash.

**FIGURE 13.6**

Temperature distribution over the windward generator of the BOR-4 vehicle. Curves relate to calculations and symbols to full-scale experiments; 1, siliconized carbon; 2, heat-shield tile; and 3, platinum.

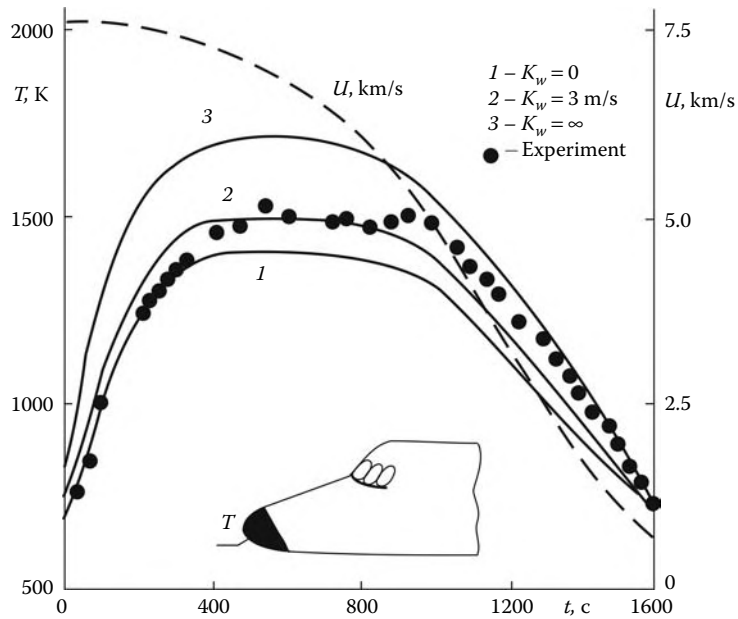
For determining the catalyticity of low-catalytic thermal-protective coatings of BOR-4 and BURAN vehicles it became necessary to simulate the needed conditions in high-frequency plasma guns.* This is supported by the testing of the values of $K_{wi,eff}$ obtained in those experiments (see Figures 13.6 and 13.7 in which the experimental data are compared with the calculated results).

One more example of the comparison between the theory and the experiment is presented in Figure 13.8 in which the data of the full-scale experiment with the OREX vehicle (Figure 12.50) are presented. At the stagnation point the experimental heat fluxes and those calculated at the catalyticity $K_w = 0$ coincide for high altitudes $H > 92$ km. At lower altitudes the discrepancy of the data can be attributed to the finite material catalyticity, which does not play any role at high altitudes in view of the smallness of the parameter $z = \rho K_w / \beta$.

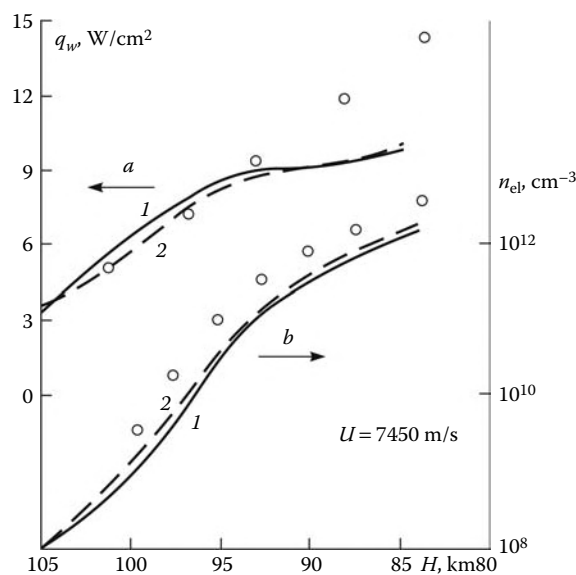
The experimental and calculated electron concentrations (at a certain distance from the body surface in $a-a'$ section in Figure 12.50) are fairly similar in value within the framework of the notions on the satisfactory accuracy adopted for electron concentrations. The point is that the processing of the probe measurement data for these parameters requires invoking a more sophisticated theory than that described in Section 13.1 due to the necessity of taking superimposed electric fields into account.

Unfortunately, for the range of the conditions associated with the high-velocity gas dynamic problems, the techniques for testing these physicochemical and molecular-kinetic models are restricted, from the engineering standpoint, to the possibility of measuring heat

* The studies were conducted in TsNIIMash (Anfimov, Zalgin, Lunev, et al., 1985; and TsAGI (Zhestkov, 1986), and the Institute for Problems in Mechanics (Baronets, Gordeev, Kolesnikov, and Yakushin, 1990).

**FIGURE 13.7**

Temperature at the stagnation point on the BURAN vehicle and its velocity as functions of time t along its entry trajectory.

**FIGURE 13.8**

Dependence of the heat flux (a) and the electron concentration (b) in section $a - a'$ of the OREX vehicle (Figure 12.50) on the flight altitude H . Symbols relate to the experimental data and curves to the calculations within the framework of the Navier-Stokes (1) and PNSE (2) models for $K_w = 0$.

fluxes and, more rarely, electron concentrations in shock layers. At the same time, some assuring examples of the testing of this kind were presented previously.

13.3 Transport Coefficients of Individual Components

In Sections 1.4 and 13.1 we have given a preliminary idea of the transport coefficients in gases and presented the corresponding formulas for gas mixtures in terms of the transport coefficients for individual components. Here we will specify the latter coefficients.

13.3.1 Thermal Conductivities

Generalizing the well-known *Eiken formula* we will write it for the coefficients $\lambda_i^{(k_e)}$ corresponding to partially equilibrium internal degrees of freedom

$$\lambda_i^{(k_e)} = \frac{15}{4} \frac{R\mu_i}{\bar{M}_i} \cdot E, \quad E = 0.115 + 0.354 \frac{c_{pi}^{(k_e)} \bar{M}_i}{R} \quad (13.3.1)$$

Here, $c_{pi}^{(k_e)}$ is the specific heat of species i with k_e equilibrium internal degrees of freedom. In frozen flows the coefficient $E = 1$ for a monatomic gas ($\gamma = 5/3$) and $E = 1.35$ for a diatomic gas. In these two cases the frozen Prandtl numbers are similar in value:

$$\begin{aligned} \text{Pr}_i^{(0)} &= \frac{c_{pi}^{(0)} \mu_i}{\lambda_i^{(0)}} = \frac{4c_{pi}^{(0)} \mu_i}{15RE} = \frac{4\gamma_i}{15(\gamma_i - 1)E} \\ \text{Pr}_i^{(0)} &= \frac{2}{3} \quad \text{for } \gamma_i = \frac{5}{3}, \quad \text{Pr}_i^{(0)} = 0.69 \quad \text{for } \gamma_i = \frac{7}{5} \end{aligned} \quad (13.3.2)$$

In this case the overall thermal conductivity is determined by formula 13.1.30 with $\lambda^{(0)}$ and $\lambda_i^{(0)}$ replaced by $\lambda^{(k_e)}$ and $\lambda_i^{(k_e)}$ or, at total equilibrium of the internal degrees of freedom, by λ_e and λ_{ie} .

13.3.2 Viscosity

In accordance with 1.4.9, viscosities of individual components are of the order $\mu_i \sim \sigma_i^{-2} (m_i kT)^{1/2}$. The rigorous theory gives the following formula for μ_i

$$\mu_i = 2.67 \cdot 10^{-6} \frac{(\bar{M}_i T)^{1/2}}{\sigma_i^2 \Omega^{(2,2)} T^*} \frac{\text{kg}}{\text{m} \cdot \text{s}}, \quad T^* = \frac{kT}{\varepsilon_i} \quad (13.3.3)$$

Here, $\Omega^{(2,2)}$ is the so-called *collision integral* dependent on the *potential* of the interparticle collision; the *effective molecule diameter* σ_i is measured in Angströms ($1\text{\AA} = 10^{-8} \text{ cm}$) and ε_i is the characteristic interaction energy in the *Lennard-Jones potential*, which at present is used in the theory. The term *transport cross-section* of molecular collisions is also used for the area σ_i^2 .

For neutral gases the function $\Omega^{(2,2)}(T^*)$ is presented in Figure 13.9. The values of σ_i and ε_i for the neutral components of air are given in the following table:

Gas	O ₂	O	N ₂	N	NO
$\sigma_i, \text{\AA}$	3.47	3.05	3.80	3.30	3.49
$\varepsilon_i/k, \text{K}$	107	107	71	71	117
$\bar{\mu}_{i1}$	1.51	1.38	1.29	1.21	1.43
$\bar{\mu}_{i2}$	1.68	1.53	1.38	1.29	1.58

Clearly, all $\sigma_i \approx 3 \div 3.8 \text{\AA}$ and $\varepsilon_i/k \approx 70 \div 110 \text{ K}$, that is, these parameters are similar in value for all the atoms and molecules presented in the table.

The data presented are sufficient for calculating the coefficients μ_i ; however, at the same time the usefulness of simple approximate formulas is also doubtless. We will offer two such formulas based on different, though similar, approximations of the collision integral

$$\Omega^{(2,2)} = 1.3(T^*)^{-\kappa_k}, \quad \mu_i = \bar{\mu}_{ik} \bar{T}^{\omega_k} \cdot 10^{-5} \frac{\text{kg}}{\text{m} \cdot \text{s}}, \quad \bar{T} = \frac{T}{200 \text{ K}}$$

$$\kappa_1 = 0.2, \quad \omega_1 = 0.7; \quad \kappa_2 = 0.15, \quad \omega_2 = 0.65 \quad (13.3.4)$$

The approximate curves $\Omega_k^{(2,2)}$ are plotted in Figure 13.9, while the corresponding values of $\bar{\mu}_{ik}$ are given in the table (approximation for $k = 2$ belongs to Anfimov, 1962).

For nondissociated air the first overall value $\bar{\mu}_{\Sigma 1} = 1.3$ obtained with account for 13.1.29 coincides with that in formula 1.3.10 (we note that for a mixture of O and N atoms only we have $\bar{\mu}_{\Sigma 1} \approx 1.2$).

For all the atoms and molecules presented previously viscosities are fairly similar in value (the difference does not exceed 20%).

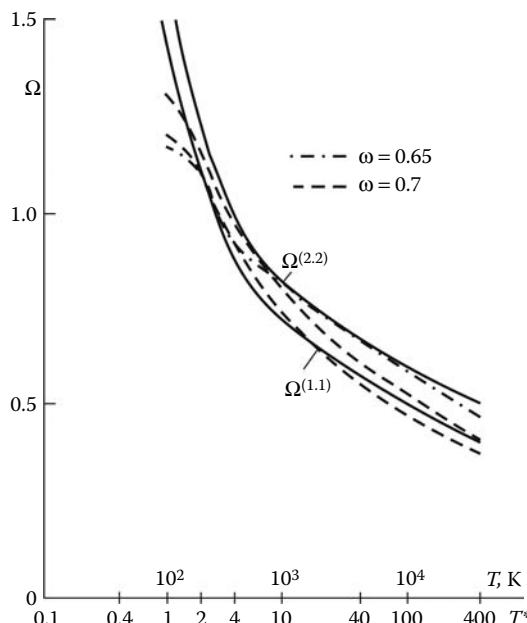


FIGURE 13.9

Exact and approximate temperature dependence of the collision integrals; the T^* scale corresponds to $\varepsilon/k = 100 \text{ K}$.

13.3.3 Diffusivities

We will write the well-known theoretical formula for the binary diffusion coefficients with account for the equation of state $\rho\bar{M} = R\rho T$ as follows

$$\begin{aligned}\rho D_{ij} &= 3.15 \cdot 10^{-6} \frac{\bar{M}T^{1/2}}{\sigma_{ij}^2 \Omega^{(1,1)}(T^*)} \left(\frac{\bar{M}_i + \bar{M}_j}{2\bar{M}_i \bar{M}_j} \right)^{1/2} \frac{\text{kg}}{\text{m} \cdot \text{s}} \\ T^* &= \frac{kT}{\varepsilon_{ij}}, \quad \varepsilon_{ij} = (\varepsilon_i \varepsilon_j)^{1/2}, \quad \sigma_{ij} = \frac{1}{2}(\sigma_i + \sigma_j)\end{aligned}\quad (13.3.5)$$

Precisely in this form these coefficients enter in the diffusion equation. Here, $\Omega^{(1,1)}(T^*)$ is the corresponding collision integral presented in Figure 13.9. This function is satisfactorily approximated by the formula $\Omega^{(1,1)} = 1.2(T^*)^{-0.2}$ (the lower dotted curve in the figure), which will be taken as the starting point. In this case, by analogy with 13.3.4, we will write formula 13.3.5 in the form:

$$\rho D_{ij} = B_{ij} \cdot 10^{-5} \bar{T}^\omega \frac{\text{m}^2}{\text{s}}, \quad \bar{T} = \frac{T}{200 \text{ K}}, \quad B_{ij} = \bar{B}_{ij} \cdot \bar{M} \quad (13.3.6)$$

The coefficients \bar{B}_{ij} are dependent only on the properties of the gases involved in formula 13.3.5. Calculations give similar values of \bar{B}_{ij} for each of the component pairs presented in the table, namely, molecule-molecule (\bar{B}_{mm}), atom-molecule (\bar{B}_{am}), and atom-atom (\bar{B}_{aa}). We will choose the following values

$$\bar{B}_{mm} = 0.06, \quad \bar{B}_{am} = 0.08, \quad \bar{B}_{aa} = 0.105 \quad (13.3.7)$$

Hence follows, in particular, the nearness of the self-diffusion coefficients for molecules (D_{mm}) and atoms (D_{aa}), which, in turn, in view of the nearness of the coefficients $\bar{\mu}_i$ for atoms and molecules in Equation 13.3.4, reflects the exact result following from the comparison of formulas 13.3.4 and 13.3.6, namely, that the self-diffusion Schmidt numbers of all the components are the same and equal to

$$Sc_{ii} = 0.847 \Omega^{(2,2)} / \Omega^{(1,1)}, \quad \Omega^{(k,k)} = \Omega^{(k,k)}(T^*) \quad (13.3.8)$$

with the same argument $T^* = kT/\varepsilon_i$ and are weak functions of the temperature. In the approximation $\Omega^{(k,k)} \sim T^{-0.2}$ adopted previously, the value $Sc_{ii} = 0.78$ is constant.

As for the binary coefficient B_{am} , it ranges from 1.2 to 2.4 when the molar mass \bar{M} varies from about 15 (only atoms) to 30 (only molecules). In this case, the corresponding Schmidt numbers based on the overall viscosity of the mixture vary from $Sc_{am} \approx 1$ in the almost atomic gas to $Sc_{mm} \approx 0.55$ in the almost molecular gas.

The estimates presented previously lie in the foundation of a simple model, in which diffusivities are the same, $D_{ij} = D$, for all the components, where D is determined by the formula

$$\rho D = \mu / Sc, \quad Sc \approx 0.7 \div 0.8 \quad (13.3.9)$$

In this approximation the conservation laws (13.1.2) are automatically fulfilled but, as noted in Section 13.2, the element separation effect is absent.

We note in conclusion that the analysis performed is valid only for neutral particles for which, by the way, all the formulas used previously, including formulas 13.1.29 and 13.1.30, were obtained. With increasing gas ionization degree (at flight velocities $U_\infty > 8 \div 9 \text{ km/s}$) the overall viscosity is appreciably affected by ions and electrons, whose own viscosity is

considerably smaller than that of neutral particles. This is attributable to considerably larger transport cross-sections σ_i^2 for charged particles due to the Coulomb interaction effect and, therefore, considerably smaller free paths of these particles. Even from the Wilkie formula 13.1.29 it follows qualitatively that a strong reduction in the ratio $\mu_k/\bar{M}_k^{1/2}$ for any individual component leads to a reduction in the overall viscosity. These effects provide an explanation for the nonmonotonic character of the temperature dependence of viscosities and thermal conductivities (for $T > 10^4$ K) in Figure 1.11.

However, the study and presentation of these particular questions can be a subject of another book.

14

Elements of Radiating Gas Dynamics

As early as in Section 1.1, we noted that manifestations of radiation effects in high-temperature gas dynamic flows are widely diversified. Thus, under the high-altitude flight conditions at velocities $U_\infty \leq 10$ km/sec the effect of the energy loss for radiation on the main shock layer flow parameters is negligible. However, radiation can turn out to be important from the standpoint of detection of flying objects and in view of its influence on the kinetics of physicochemical processes and electron concentration.

At the same time, at high flight velocities, the energy loss due to radiation and variation of the main thermodynamic parameters in shock layers can be appreciable and, hence, should be taken into account for spacecraft entering in the atmospheres of different planets (thus, the vehicle velocity at the entry into the Jovian atmosphere can be as high as 50 km/sec).

Though the radiative gas dynamics is a wide division of the gas dynamics as a whole, below we will restrict ourselves only to the presentation of its general model and some examples illustrating the previously mentioned effects.*

14.1 Physics of Gas Radiation

The hot gas radiation is due to the capability of excited molecules or atoms to return spontaneously onto a lower excitation level due to the release of an *energy quantum*, or *photoquenching*, for example, at the transition from an n -th electronic level to a lower, m -th level. The reverse *photoexcitation* effect consists in the excitation of these particles due to the absorption of external light quanta. Since the energetic states between excited levels are discrete, the frequency ν_{nm} of the radiated or absorbed quanta, or photons, is strictly determined by the condition $h\nu_{nm} = \varepsilon_n - \varepsilon_m$, where $h = 6.26 \cdot 10^{-34}$ J·sec is the *Planck constant*, while ε_n and ε_m are the level energies. This circumstance generates the well-known line spectrum of atomic gas radiation.

More complicated is the molecular radiation mechanism. Each molecule excited on an n -th electronic level at energy ε_n possesses also its own vibrational mode with the set of energetic levels ε_k . Therefore, the energy that can be absorbed or released by a molecule at transition from the n -th electronic level with the k -th vibrational level to the m -th electronic level with the l -th vibrational level is equal to

$$\begin{aligned}\varepsilon_{ij} &= \varepsilon_i - \varepsilon_j = h\nu_{ij} = h\nu_{nm} + h\nu_{kl} \\ h\nu_{nm} &= \varepsilon_n - \varepsilon_m, \quad h\nu_{kl} = \varepsilon_k - \varepsilon_l = \varepsilon_{kl}\end{aligned}\tag{14.1.1}$$

The n -th and k -th levels taken together will be called level $i = n + k$, while the m -th and l -th levels will be called level $j = m + l$; the transition itself is called the $i - j$ transition.

* For those who wish to read more widely in particular subjects, we recommend Zeldovich and Raizer (1966), Pai (1968), Pilyugin and Tirsikii (1989), Stulov and Mirskii (1995), Surzhikov (2004), and others.

Since for most molecules the energetic distance between neighboring electronic levels is well over that between the vibrational ones ($\varepsilon_{nm} \gg \varepsilon_{kl}$), we have $\nu_{nm} \gg \nu_{kl}$. Moreover, each molecule possesses also a set of quantum levels of rotational energy. Though in the medium model adopted the rotational degrees of freedom of molecules were assumed to be equilibrium excited in the classical fashion at the mean energy $kT/2$ per each rotational mode, the radiation from these complex electronic-vibrational-rotational levels obeys to quantum physics laws. For this reason, the frequency and energy spectra of molecules have the form of bands centered on the basic, or central, lines with the frequencies ν_{nm} .

Transitions of this kind, accompanied by energy radiation from one quantum level to another, are called *bound-bound*. We note that the real spectral lines are slightly smeared and have a finite width $\Delta\nu$ due to a number of effects; we will not dwell upon them. We also emphasize that, though any transitions from one complex level to the other are formally possible, in quantum mechanics there are certain prohibitions against admissible transitions.

Moreover, in an ionized gas, or plasma, a continuous radiation spectrum may also exist; it is due, first, to the *bremssstrahlung*, or *braking radiation*, of electrons whose trajectories are bent in the vicinity of positive ions or neutral particles (*free-free transitions*) and, second, by binary deionization reactions proceeding by the scheme $A^+ + e^- = A + h\Delta\nu$ (*bound-free transitions*). In this case, the excess energy of electrons is released as an energy quantum at a frequency $\Delta\nu$. Taken from the right to the left, this scheme describes the *photoionization* process. However, for the gas flow regimes considered in this book, the probability of such processes is low; precisely for this reason they were not included in the reaction list 10.5.7 of Section 10.5.

To determine the energy loss for radiation we note that in the general case n_i/τ_{ij} spontaneous $i - j$ transitions are taking place per unit time and per unit volume; here, n_i is the concentration of particles A_i with excited level $i = (n + k)$, while τ_{ij} is their *lifetime*. In this case, the energy

$$\rho q_{ij} = \varepsilon_{ij} \frac{n_i}{\tau_{ij}} = h\nu_{ij} \frac{n_i}{\tau_{ij}} \quad (14.1.2)$$

is released per unit time and per unit volume. The total radiation rate q of a unit mass of the gas mixture is determined by summing the partial energies q_{ij} over all the frequencies with allowance for the line broadening and the continuous radiation spectrum. It is the practice to represent the total rate of the energy flux on the frequency range $d\nu$ as $d_\nu q = q_\nu d\nu$, where

$$q_\nu = q_\nu^{(+)} - q_\nu^{(-)}, \quad q_\nu^{(-)} = 4\pi\eta_\nu \quad (14.1.3)$$

Here, *plus* refers to the absorbed and *minus* to the radiated energy and η_ν is the mass coefficient of its own radiation. The term $q_\nu^{(+)}$ will be determined in Section 14.2.

Thus, gas radiation is determined by the presence of electronically or vibrationally excited atoms and molecules, as well as free electrons. At the same time, the energy release from any quantum energy level results in a decrease of the concentration of the corresponding particles, while transitions onto this level from other levels as a result of light energy absorption lead to their increase. Therefore, the processes of the excited particle radiation and relaxation are interrelated and, aside from the energy equation, are governed by the set of the corresponding kinetic equations (to be written in Section 14.4) and the laws of the radiant energy propagation in gas media (Section 14.2).

Thus, in our formulation gas radiation introduces the heat source q in the gas energy equation and the corresponding source terms in the equations for relaxations of internal degrees of freedom. This formulation of the problem is sufficient for the range of problems considered in this book and related with the spacecraft (or meteoroid) entry in the atmosphere or

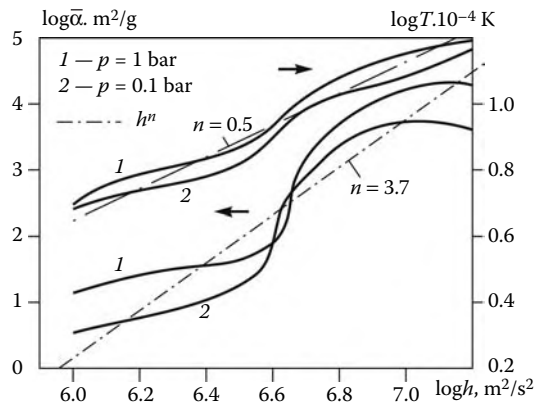


FIGURE 14.1
Absorption coefficient of high-temperature air.

the flows in chambers and nozzles of high-temperature gas dynamic setups. In the general case, at superhigh radiation intensities, the gas flow equations must involve the volume radiant energy (*photon gas energy*), which can be shown to be equal to $e_v = 4\pi I_v/c\rho$, where c is the *speed of light*, and I_v is the *radiation intensity* (cf. Section 14.2), and the *light pressure* (the photon gas momentum) equal to $p_v = \rho e_v/3$. However, in the gas dynamic problems under consideration these terms are unessential, so that the flows of both nonequilibrium and equilibrium radiating gases are governed by the same equations written down previously for inviscid and viscous flows with the corresponding specification of the source terms q or Λ_i .

All the preceding pertains to the general case of the nonequilibrium state of a gas determined by the kinetic equations. In an equilibrium gas all the relative concentrations are functions of the temperature and the pressure. In this case, the energy radiated by a unit mass of the gas is determined by the *Kirchhoff law*

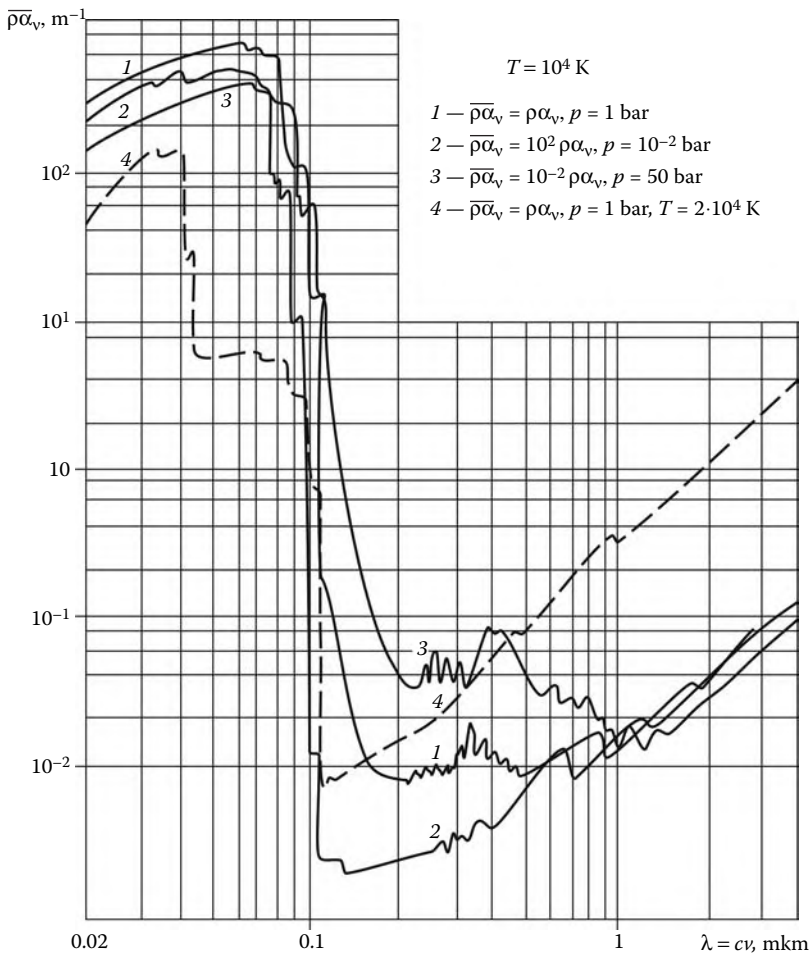
$$q_v^{(-)} = 4\pi\eta_v, \quad \eta_v = \alpha_v B_v, \quad B_v = 2hv^3 c^{-2} (e^{hv/kT} - 1)^{-1} \quad (14.1.4)$$

Here, B_v is the *Planck function* governing the equilibrium frequency distribution of the black body radiation intensity and α_v is the mass absorption coefficient. The total radiation energy is in this case as follows

$$q_v^{(-)} = 4\pi \int_0^\infty \alpha_v B_v dv = \bar{\alpha} B(T), \quad B = \frac{\sigma}{\pi} T^4, \quad \sigma = 5.7 \cdot 10^{-8} \frac{\text{J}}{\text{m}^2 \text{K}^4} \quad (14.1.5)$$

Here, σ is the *Stephan–Boltzmann constant* and $\bar{\alpha}$ is the frequency-average *mean-energy* absorption coefficient. For a black body we have $\alpha_v = \bar{\alpha} = 1$, so that the quantity $\bar{\alpha}$ could also be termed the *grayness coefficient* of the medium. The coefficients α_v and $\bar{\alpha}$ increase rapidly with the temperature, which is due to the accompanying increase in the degree of the atom and molecule excitation and in the electron concentration. For equilibrium air the function $\bar{\alpha}(p, T)$ is presented* in Figure 14.1; it increases with the gas enthalpy and temperature as $\bar{\alpha} \sim h^{3.7} \sim T^{7.4}$, the latter follows from the dependence $T \sim h^{1/2}$ plotted in the

* The function is determined from the data given in Kamenshchikov, Nikolaev, Novikov, and Plastinin (1971).

**FIGURE 14.2**

Dependence of the absorption coefficients of air on the radiation wavelength.

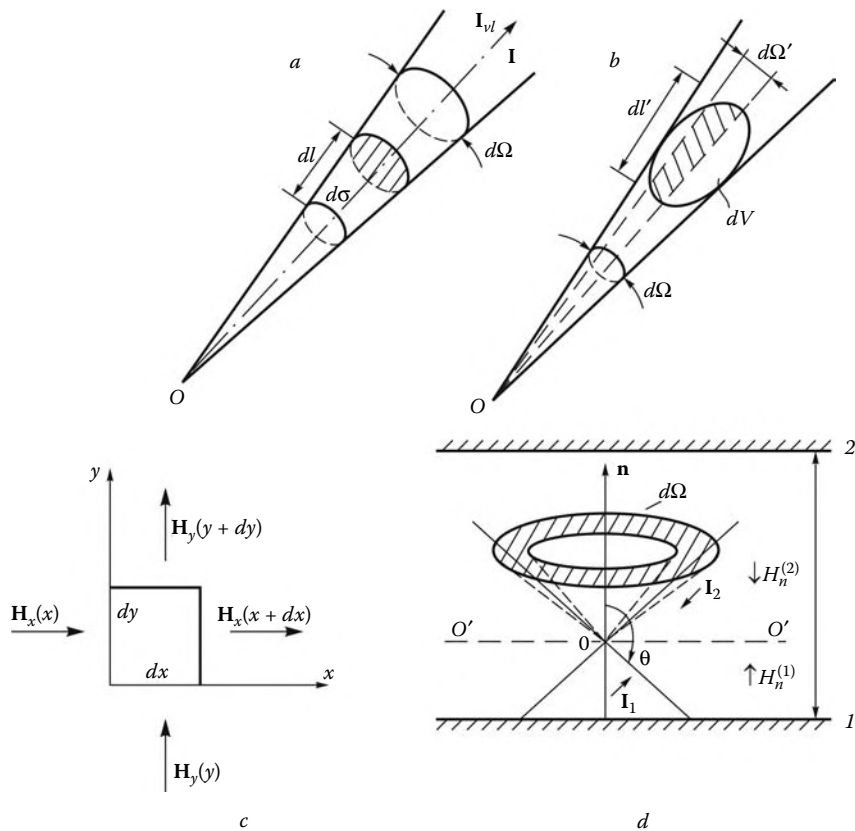
same figure. We will also note appreciable (several orders of magnitude) nonmonotonicity of the dependence of the equilibrium coefficient α_v on the frequency v (Figure 14.2).

However, the equilibrium gas state assumes the absence of the heat flux, that is, the equality between the radiated and absorbed energies ($q_v = 0$).

However, the complete and rigorous equilibrium radiation condition cannot be formulated without taking into account the structure of the radiant field of a medium, which is considered in Section 14.2.

14.2 Radiant Field in Radiating and Absorbing Jets

Let us now consider the radiant energy propagation in gases. Let $d\Omega$ be an element of the solid angle along the direction \vec{l} , as shown in Figure 14.3a. Within this angle the energy flux $\vec{I}_{vl}d\nu d\sigma d\Omega$ is transported along the direction \vec{l} through the cross-section $d\sigma$ in unit time and in the frequency interval from $\nu + d\nu$ to ν . Strictly speaking, the vector \vec{I}_{vl} itself ($\vec{I}_{vl} = I_{vl}\vec{l}$)

**FIGURE 14.3**

On the derivation of the radiant transfer equation.

is the radiation intensity in the direction of the unit vector \vec{l} ; however, in what follows for the sake of brevity we will refer to this term as the scalar I_{vl} . As this beam bundle passes through the volume $dV = d\sigma dl$, the energy transported by it varies over the value

$$\rho q_{vl} dv dV d\Omega = -\frac{\partial}{\partial l} (I_{vl} d\sigma) dv d\Omega dl = -\left(\frac{\partial I_{vl}}{\partial l} + I_{vl} \frac{\partial \ln(d\sigma)}{\partial l} \right) dv dV d\Omega \quad (14.2.1)$$

This variation is due, first, to the energy absorption in the volume dV , which is equal to $\rho \alpha_v I_{vl} dv dV d\Omega$, and, second, to the gas's own radiation $\rho \eta_v dv dV d\Omega$, where, as earlier, the coefficients α_v and η_v are assumed to be isotropic in various \vec{l} directions.

Moreover, in the general case the gas scattering, that is, the energy reradiation from other directions \vec{l}' to the \vec{l} direction, should also be taken into account. However, this effect is appreciable only for dusty gases; for pure gases it is usually very small, so that we will not allow for it.

Further, if l is the distance from the area $d\sigma$ to the vertex O of the angle $d\Omega$, then $d \ln(d\sigma)/dl = 2/l$; therefore, fixing $d\sigma$ and assuming that $d\Omega \rightarrow 0$, we can drop the second

term in the parentheses on the right-hand side of Equation 13.2.1. Then from the energy balance for the volume dV we obtain the *radiant energy transport equation*

$$\frac{\partial I_{vl}}{\partial l} = -\rho q_{vl} = \rho \eta_v - \rho \alpha_v I_{vl} \quad (14.2.2)$$

In the general case of strongly nonstationary processes, the left-hand side must also include the term $c^{-1} \partial I_{vl}/\partial t$. However, in the gas dynamic problems under consideration this term is extremely small (c is the speed of light); therefore, it can be omitted and the radiant field can be assumed to be quasistationary.

The *radiant energy flux* across the area $d\sigma$ with the normal \vec{n} (in section $O' - O'$ in Figure 14.3d) is determined by the integral over all the directions passing through the area

$$H_{vn} = \int_{4\pi} (\vec{I}_{vl} \cdot \vec{n}) d\Omega = H_{vn}^{(2)} + H_{vn}^{(1)}, \quad H_{vn}^{(i)} = \int_{2\pi} I_{vl} (\vec{l} \cdot \vec{n}) d\Omega$$

$$(\vec{l} \cdot \vec{n}) > 0, \quad i = 1, \quad (\vec{l} \cdot \vec{n}) < 0, \quad i = 2 \quad (14.2.3)$$

Here, H_{vn} is the projection of the radiant energy flux \vec{H}_v onto the vector \vec{n} , $H_{vn}^{(2)}$ is the radiant flux incident onto the area from the side of the outward normal or from above, as in Figure 14.3d; and $H_{vn}^{(1)}$ is the similar flux incident from below. We note that each straight line in the space is associated with two oppositely directed rays (the unit vectors \vec{l}_2 and \vec{l}_1 in Figure 14.3d) with different intensities I_{vl} .

We note that in a vacuum $I_{vl} = \text{const}$; however, the energy flux through the area $d\sigma$, being at a distance l from the point light source and illuminated at the solid angle $d\Omega = \Delta\sigma/l^2$, decreases, as l increases: $H_v \sim l^{-2}$.

To derive the formula for the heat flux rate per unit mass of a gas, we will consider an arbitrary volume element dV inscribed in the angle $d\Omega$ (Figure 14.3b) and divide it to narrower tubes $d\Omega'$ of length dl' and volume dV' (one of these tubes is shaded in the figure). The energy variation in the volume dV' is determined by formula 14.2.1, thus making the summation we obtain the same formula for the volume dV . Then integrating Equation 14.2.2 over Ω we derive the required formula concretizing formula 14.1.3

$$q_v = \int_{4\pi} q_{vl} d\Omega = q_v^{(+)} - q_v^{(-)}, \quad q_v^{(-)} = 4\pi \eta_v$$

$$q_v^{(+)} = 4\pi \alpha_v I_v, \quad I_v = \frac{1}{4\pi} \int_{4\pi} I_{vl} d\Omega \quad (14.2.4)$$

Here, I_v is the direction-averaged radiation intensity.

Another equivalent formula for q_v can be obtained by applying the operations described in Section 1.8 to the vector \vec{H}_v , that is, to the radiant energy flux through the volume dV (see Figure 14.3c)

$$q_v = -\frac{1}{\rho} \operatorname{div} \vec{H}_v \quad (14.2.5)$$

Equation 14.2.2 has the solution

$$I_{vl} = I_{vl}^{(0)} e^{-(\xi_v - \xi_{v0})} + \int_{\xi_{v0}}^{\xi_v} \frac{\eta_v}{\alpha_v} e^{-(\xi_v - \xi'_v)} d\xi'_v$$

$$\Delta\xi_v = \xi_v - \xi_{v0} = \int_{l_0}^l \rho\alpha_v dl = (\rho\alpha_v)_a (l - l_0) \quad (14.2.6)$$

Here, l_0 and $I_{vl}^{(0)}$ are some initial quantities, while $(\rho\alpha_v)_a$ is a mean value. Substituting this formula into Equation 14.2.4 we can evaluate the quantity q_v , if the volume distributions of the parameters ρ , η_v , and α_v are known, together with that of the external radiation.

We will now consider in more detail the question about the nature of the radiative interaction of separate parts of the radiating gas volume. We will call the difference $\Delta\xi_v \sim (\rho\alpha_v)_a L_l$ entering into Equation 14.2.6 the *optical thickness* of the given volume of dimension L along the ray \bar{l} . For $\Delta\xi_v \gg 1$ the initial radiation effect decays, so that the corresponding quantity $l_{Rv} = (\rho\alpha_v)_a^{-1}$ can be called the *radiation path* at a frequency v . For a small optical thickness of the gas volume, $l_{Rv} \gg L_l$, the second term in Equation 14.2.6 can be neglected, so that we obtain $I_{vl} \approx I_{vl}^{(0)}$. In this case, the quantity q_v is determined only by local gas parameters, while in the absence of the external radiation $q_v \approx q_v^{(-)}$. We will call such gas volumes with the purely local law of the radiant heat flux *transparent*. We note that we deal with precisely this case when considering the problems of the reentry of bodies with dimensions $L \leq 1$ m at velocities $U_\infty \leq 10$ km/sec.

In the general case, the intensity I_{vl} and the quantity q_v are determined by an integral taken over the entire volume. However, in the limiting case of a very large optical thickness of the volume, or at $L \gg l_{Rv}$, the first term in Equation 14.2.6 can be neglected and the term η_v/α_v can be factored outside the integral sign with the upper limit $\xi'_v = \xi_v$. Then letting $l/R \rightarrow 0$ in limit we obtain an isotropic radiant field

$$q_v = 0, \quad I_{vl} = I_v = \eta_v/\alpha_v \quad (14.2.7)$$

The latter condition follows directly from Equation 14.2.4.

This equality is as yet not identical to the equilibrium condition, since it can also be fulfilled in a nonequilibrium, though optically rather dense gas. However, since in accordance with 14.1.4, $\eta_v/\alpha_v = B_v$ in the equilibrium state, we arrive at the conclusion that in order for the equilibrium in a gas volume to be total, two conditions must be fulfilled

$$I_{vl} = I_v = \eta_v/\alpha_v = B_v \quad (14.2.8)$$

In other words, the total thermodynamic equilibrium of a system is possible only in the limitingly optically dense gas volume in an isotropic radiant field, in which the own gas radiation for any frequency range dv would be offset by the absorption of the radiation of the gas volume as a whole, while the external radiation does not penetrate into this volume.

However, the limiting condition 14.2.7 for optically dense media gives no way for determining the radiant heat flux q_v for media with a small, though finite value of the parameter l_{Rv}/L . To make allowance for this effect under the assumption of the smallness of this parameter, we let under the integral sign in 14.2.6

$$\frac{\eta_v}{\alpha_v} = f(\xi'_v) = f(\xi_v) + \frac{\partial f}{\partial \xi_v} (\xi'_v - \xi_v) \quad (14.2.9)$$

Then, integrating and letting $|\xi_v - \xi_{v0}| \gg 1$ we obtain

$$\begin{aligned} I_{vl} - \frac{\eta_v}{\alpha_v} &= -\frac{\partial}{\partial \xi_v} \left(\frac{\eta_v}{\alpha_v} \right) = -\frac{1}{\rho \alpha_v} \frac{\partial}{\partial l} \left(\frac{\eta_v}{\alpha_v} \right) = \\ &= -\frac{1}{\rho \alpha_v} \left(\vec{l} \cdot \nabla \frac{\eta_v}{\alpha_v} \right) = (\vec{l} \cdot \vec{l}_0) I_{v,\max} \\ I_{v,\max} &= -\frac{1}{\rho \alpha_v} \frac{d}{dl_0} \frac{\eta_v}{\alpha_v} \end{aligned} \quad (14.2.10)$$

Here, the unit vector \vec{l}_0 is directed along the gradient of the function η_v/α_v at the given point. This radiant field is locally axisymmetric, so that the flux of the vector \vec{H}_v across any area parallel to \vec{l}_0 is zero. For an area with the normal $\vec{n} = \vec{l}_0$, substituting 14.2.10 into 14.2.3 and letting, in accordance with Figure 14.3d

$$\begin{aligned} (\vec{l} \cdot \vec{l}_0) &= \cos \theta, \quad d\Omega = 2\pi \sin \theta \, d\theta \\ (\vec{l}_{vl} \cdot \vec{n}) &= I_{v,\max} \cos \theta \end{aligned} \quad (14.2.11)$$

we obtain the following expression for the radiant energy flux

$$H_{vn} = 2\pi I_{v,\max} \int_0^\pi \cos^2 \theta \sin \theta \, d\theta = \frac{4\pi}{3} I_{v,\max} \quad (14.2.12)$$

This formula does not include the isotropic term η_v/α_v (the integral from $(\vec{l} \cdot \vec{n})$ over 4π is zero). Clearly, the flux H_{vn} is of the same sign as the quantity $I_{v,\max}$, that is, the vector \vec{H}_v and the gradient of the function η_v/α_v are opposite in direction. At the same time, we recall that this formula, along with formula 14.2.10, is valid only for a point at a large distance $l \gg l_{Rv}$ from the boundaries of the region (point O in Figure 14.3d), which excludes the influence of the boundaries. In the same approximation, the one-sided radiant energy flux onto a plane (e.g., from above onto plane 1 in Figure 14.3d), is given by the formula

$$H_{vn}^{(2)} - \frac{2\pi}{3} I_{v,\max} = 2\pi \frac{\eta_v}{\alpha_v} \int_0^{\pi/2} \cos \theta \sin \theta \, d\theta = \pi \frac{\eta_v}{\alpha_v} \quad (14.2.13)$$

Substituting Equation 14.2.12 into 14.2.5 we obtain the following formula for the heat flux in an optically thin layer

$$\rho q_v = -\operatorname{div} \vec{H}_v = \operatorname{div} \left(\frac{4\pi}{3\rho\alpha_v} \nabla \frac{\eta_v}{\alpha_v} \right) \quad (14.2.14)$$

If the gas is in thermodynamic equilibrium, then $\eta_v/\alpha_v = B_v(T)$ and the formula 14.2.14 takes the form:

$$\rho q_v = \operatorname{div}(\lambda_{Rv} \nabla T), \quad \lambda_{Rv} = \frac{4\pi}{3\rho\alpha_v} \frac{dB_v}{dT} \quad (14.2.15)$$

Here, λ_{Rv} is the *radiant thermal conductivity* of the gas. For a “gray” gas with a v -independent coefficient $\alpha_v = \bar{\alpha}$, in view of 14.2.8, for the total (with respect to v) value of λ_R we obtain $\lambda_R = 16\sigma T^3 / 3\rho\bar{\alpha}$.

In conclusion, we will derive the general formula for the heat flux for a plane layer of a gas (of thickness δ) in which all the parameters vary only along the normal \vec{n} to the layer

(Figure 14.3d), while the radiation intensity I_{vl} at each point of the layer depends only on the angle θ of the ray \vec{l} deflection from the normal. In this case, passing to the variable $\zeta_v = \xi_v \cos \theta$ in 14.2.6, integrating over Ω with Equation 14.2.11 taken into account, and dividing the integration domain to the upper and lower halves of the layer, we cast formula 14.2.4 to the form:

$$\begin{aligned} q_v &= -4\pi \eta_v + 2\pi \alpha_v (Q_{v1} + Q_{v2}) \\ Q_{v1} &= I_{v1}^{(0)} E_2(\zeta) + \int_0^\zeta \frac{\eta_v}{\alpha_v} E_1(\zeta_v - \zeta') d\zeta' \\ Q_{v2} &= I_{v2}^{(0)} E_2(\zeta_{v\delta} - \zeta_v) + \int_\zeta^{\zeta_\delta} \frac{\eta_v}{\alpha_v} E_1(\zeta'_v - \zeta_v) d\zeta' \\ E_n(x) &= \int_1^\infty e^{-xs} \frac{ds}{s^n}, \quad \zeta_v = \int_0^\eta \rho \alpha_v dn \end{aligned} \quad (14.2.16)$$

Here, the subscripts 1 and 2 refer to the contributions of the rays above and below this layer, respectively, while the intensities $I_{vi}^{(0)}$ of the external radiations incident onto these planes are assumed to be isotropic. In the same approximation and with Equation 14.2.4 taken into account, the one-sided radiant energy flux onto a wall (1 in Figure 14.3d) is equal to

$$\begin{aligned} H_{vn}^{(2)} &= 2\pi \int_{-\pi/2}^0 I_v(\theta) \cos \theta \sin \theta d\theta = \\ &\pi H_{vn}^{(0)} E_3(\zeta_{v\delta}) + 2\pi \int_0^{\zeta_\delta} \frac{\eta_v}{\alpha_v} E_2(\zeta_{v\delta} - \zeta') d\zeta' \end{aligned} \quad (14.2.17)$$

Here, $H_{vn}^{(0)}$ is the flux incident from outside onto boundary 2 of the layer. The functions $E_n(v)$ are presented in Figure 14.4; they are related by the recurrent formulas

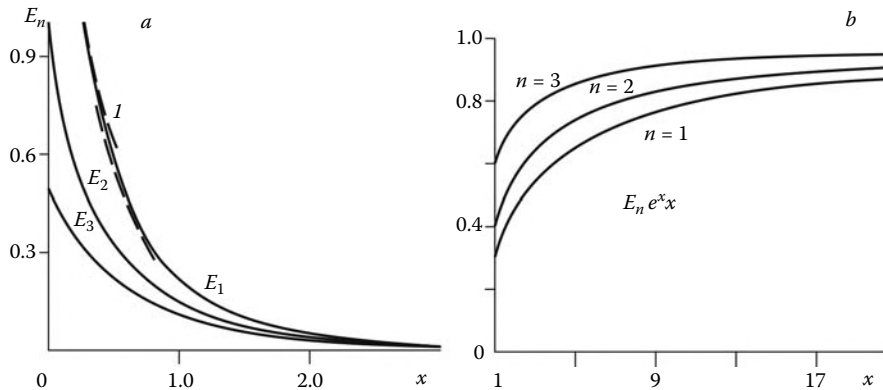
$$\begin{aligned} \frac{dE_{n+1}}{dx} &= -E_n(x), \quad E_0(x) = \frac{e^{-x}}{x} \\ nE_{n+1}(x) &= e^{-x} - xE_n(x) \end{aligned} \quad (14.2.18)$$

At large x all these functions decrease exponentially, $E_n(x) \approx e^{-x}/x$. For $n \geq 2$ we have $E_n(0) = (n-1)^{-1}$; however, the function $E_1(x)$ has a logarithmic singularity, as $x \rightarrow 0$, and can be represented in a power-series form

$$E_1(x) = -C_0 - \ln x - \sum_{k=1}^{\infty} (-1)^k \frac{x^k}{k \cdot k!} \quad (14.2.19)$$

where $C_0 = 0.557$ is the *Euler number*.

In this case, the functions Q_{vi} in 13.2.16 decrease as $x \ln x$. Thus, for the vanishingly small optical thickness of the layer, $\xi_{v\delta} \ll 1$, this layer becomes, as it were, transparent with $q_v = -4\pi \eta_v$, in spite of its unboundedness in one direction. Therefore, in the general case the requirement $\Delta \xi_v \sim (\rho \alpha_v)_a L \ll 1$ for all the diameters of the radiating volume can be excessive from the standpoint of the applicability of the transparency model to this volume.

**FIGURE 14.4**

Functions $E_n(x)$. The dashed curves are sums of series 14.2.19 for $k = 1$ and 2.

14.3 Flows of Intensely Radiating Gases

In this section we will consider the gas radiation effect with reference to equilibrium inviscid flows and defer the description of purely nonequilibrium effects until the next section. Under the previous assumptions the gas radiation effect manifests itself only via the energy Equation 1.9.6, which, in the absence of other heat sources, can be written in the form:

$$\frac{dh}{dt} = \frac{1}{\rho} \frac{dp}{dt} + q_{\text{eff}}, \quad q_{\text{eff}} = q + q_{\tau} - \text{div} \vec{J}$$

$$q = q^{(+)} - q^{(-)}, \quad q^{(+)} = \int_0^\infty q_v^{(+)} dv, \quad q^{(-)} = \int_0^\infty q_v^{(-)} dv \quad (14.3.1)$$

Here, $q^{(+)}$ is the absorbed and $q^{(-)}$ the radiated radiant energy. The quantities $q_v^{(+)}$ and $q_v^{(-)}$ are determined by formulas 14.2.4, and the terms q_{τ} and \vec{J} by formulas 12.1.11 and 13.1.9 (in the following they are omitted).

We will first consider a very simple local law of the radiant heat flux, within the framework of which the quantity q is dependent only on the gas state or coordinates. This law is typical of transparent volumes, in which reabsorption of the energy radiated by this volume is unessential, while the quantity $q_v^{(+)} = 4\pi\alpha_v I_v$ is determined only by the local absorption coefficient α_v and the intensity I_v of the external radiation incident on the volume, the latter being constant along rays. As for the quantity $q_v^{(-)} = 4\pi\alpha_v\eta_v$ (η_v is its own radiation intensity), it is local by definition.

In this case, Equation 14.3.1 remains purely differential, so that taking radiation into account does not change the mathematical properties of the governing equations as described previously.

Otherwise, when $q^{(+)}$ is dependent on radiation of the gas volume as a whole, these equations are *integro-differential*. However, for gas volumes of relatively small optical thickness, the allowance for integral terms entering in q does not usually violate the basic mathematical properties determined by the differential operator of the governing equations (see, e.g., Znamenskii, 1976). A special case is that of optically dense gas volumes described by the

radiant heat conduction model (14.2.14 for q) in which the energy equation is of the second order, as in the case of viscous heat-conducting gases. However, in the aerodynamic and gas dynamic problems the use of this model is restricted due to the fact that the shock layer thickness on a body of standard dimensions is usually not so large.

For equilibrium gas flows in transparent volumes writing formula 14.3.1 for q in terms of 14.2.4 and 14.2.8 yields

$$q^{(+)} = -4\pi\tilde{\alpha}(T)I^{(0)}, \quad q^{(-)} = 4\pi\bar{\alpha}(T)B(T) \quad (14.3.2)$$

Here, $B(T)$ is the black body radiation intensity, $\bar{\alpha}(T)$ is the energy-average absorption coefficient (see 14.1.5), $I^{(0)}$ is the frequency-average external-radiation intensity, and $\tilde{\alpha}$ is the coefficient of its absorption; generally, $\tilde{\alpha} \neq \bar{\alpha}$. In the body flowfield problems the quantity $I^{(0)}$ is usually determined by the body surface radiation at a temperature $T = T_w$. Therefore, it can be assumed that $I^{(0)} \sim B(T_w)$, so that the inequality $q^{(-)} \gg q^{(+)}$ holds when the gas temperature $T \gg T_w$ and $\tilde{\alpha} \sim \bar{\alpha}$.

When q is determined by the local law (Equation 14.3.2), the radiation effect on the gas parameters is usually maximum and can be evaluated as follows. The relative variation of the enthalpy of a gas particle at a velocity U during its stay $t_0 \sim L/U$ in the given volume with the characteristic diameter L , is of the order

$$\Delta h/h \sim \beta = 4\pi\bar{\alpha}BL/Uh \quad (14.3.3)$$

where $\bar{\alpha}$, B , and h stand for the scale parameters of the volume. On the axis of symmetry, behind a normal shock and ahead of a blunt body, we have $h \approx U_\infty^2/2$, $U \sim U_\infty k$, and $L \sim \delta$, where k is the density ratio across the shock and δ is the shock layer thickness. For spherelike bodies of radius R we have $\delta \approx kR$ (cf. Section 7.8); therefore, $L/U \approx R/U_\infty$.

In Figure 14.5 we have plotted the dependence $\beta(U_\infty)$ corresponding to the data of Figure 14.1 and the gas parameters behind the normal shock; it can be seen that for bodies of dimension $R \approx 1$ m the radiation effect on the main thermodynamic gas parameters should be taken into account only at flight velocities $U_\infty \geq 10^4$ m/s.

We will now consider some gas dynamic properties of radiating inviscid gas flows. The most simple cases are those in which the heat influx law is local (for both equilibrium and

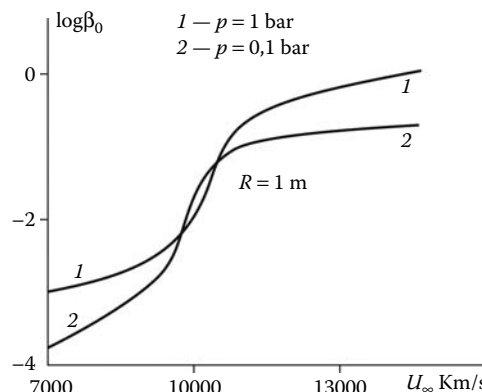


FIGURE 14.5
Relative influence of the radiation on the sphere shock-layer parameters.

nonequilibrium flows); they are realized in optically thin disturbed layers or when the radiation effect on the main flow is slight and can be considered within the framework of the small perturbation method (e.g., the problem of a wedge, Lunev, 1960). In this case, the streamline method outlined in Section 11.10 for nonequilibrium flows can be applied for evaluating the hypersonic flow past bodies with a thin shock layer and the conservative nature of the pressure distribution.

For equilibrium flows under the assumption that the intensity $I^{(0)}$ in Equation 14.3.2 is constant we obtain $q = q(h)$ and solution 7.9.1 is valid with an integral $t = t(h)$. In accordance with formula 11.10.3, for a wedge or a cone we have $Ut = l - l_0$, where $l - l_0$ is the distance measured from the shock along a streamline; together with the equation of state $\rho = \rho(p, h)$, solution 7.9.1 makes it possible, by analogy with Section 11.10, to determine the shock layer flow parameters and to evaluate the layer thickness from formula 11.10.4 and 11.10.5.

For the axis of symmetry of a blunt body, time t is determined by formula 7.9.2 and the subsequent solution of Section 7.9, which should also be obtained together with the solution of Equation 7.9.1 and the equation of state, this joint solution being a simplified counterpart of the corresponding nonequilibrium problem of Section 11.10. In this case, $t \sim -\ln(y/R) \rightarrow \infty$, as the distance to the flow stagnation point $y \rightarrow 0$, the integral $t(h)$ is improper, and the physically meaningful solution must be associated with the condition $q \rightarrow 0$ as $y \rightarrow 0$. In the absence of external radiation ($q^{(+)} = 0$) the nature of the corresponding solution can be elucidated using the approximations of Figure 14.1, $\bar{\alpha} \sim h^n$ and $T \sim h^{1/2}$. Then taking into account that $B(T) \sim T^4$ we can let

$$q = Ch^m, \quad m = n + 2, \quad C = \text{const} \quad (14.3.4)$$

Under the conditions presented in Figure 14.1 we have $n = 3.7$ and $m = 5.7$. In this case solution 7.9.1 has the form:

$$h^{-(m+1)} - h_s^{-(m+1)} = (m+1)Ct \quad (14.3.5)$$

Here, $h = h_s$ and $t = 0$ immediately behind the shock.

Clearly, in this solution $h \rightarrow 0$ as $t \rightarrow \infty$. However, in the presence of external radiation, the condition $q \rightarrow 0$ as $t \rightarrow \infty$ means that the gas temperature approaches a certain limiting value: $T \rightarrow T_R$ or $h \rightarrow h_R$. Then letting in this vicinity $q = a(h - h_R)$, $a = \text{const} > 0$ we obtain the asymptotic solution

$$h - h_R = \text{const} e^{-at} \quad (14.3.6)$$

Thence in the vicinity of the stagnation point, taking 7.9.2 into account and letting the velocity $v = -v_0y/R$, for $y \ll R$ we obtain

$$h - h_R = \text{const}(y/R)^\chi, \quad \chi = R/av_0 \quad (14.3.7)$$

As for nonequilibrium flows, this solution is singular as $y \rightarrow 0$; its behavior in dependence of the parameter χ is qualitatively described by curves in Figure 11.17, in which κ should be replaced by χ .

We will briefly dwell on some features of similar problems with allowance for a finite optical thickness of the shock layer. The fact that this thickness is relatively small, $\delta/L \ll 1$, allows us to use formula 14.2.16 for a plane unbounded layer for evaluating q . This formula can even be simplified in the case in which the optical thickness of the shock layer is relatively small. First, due to the logarithmic singularity of the function $E_1(\zeta)$ when $\zeta \rightarrow 0$, we can factor out the quantity η_v/α_v from the integral sign assigning to this quantity the value

corresponding to the upper limit of the integral. Then integrating by parts with allowance for Equation 14.2.18 and letting the external radiation intensity $I_v^{(0)} = 0$ we obtain ($\zeta = \zeta_v$)

$$q_v = -2\pi\eta_v[E_2(\zeta) + E_2(\zeta_\delta - \zeta)] = -4\pi\eta_vE_2^*(\zeta, \zeta_\delta) \quad (14.3.8)$$

The function $E_2^*(\zeta, \zeta_\delta)$ is plotted in Figure 14.6 for different values of the optical thickness ζ_δ ; its dependence on ζ is appreciably weaker than that of the function $E_2(\zeta)$, which is presented in the same figure for $\zeta_\delta = 1$. Therefore, at small ζ_δ the function E_2^* can be replaced by a constant in making estimates or as a first approximation in an iteration procedure, thus reducing the problem to that considered earlier for a transparent gas (Lunev and Murzinov, 1962).

Energy release in the shock layer on a body results, first, in a decrease in the gas temperature and, hence, in the reduction of radiant fluxes to the body surface; however, this effect can be appreciably weakened owing to internal reabsorption of this energy. An example is presented in Figure 14.7 (a sphere of radius $R = 1$ m at $U_\infty = 14.5$ km/sec). It is significant that curve 2 plotted using the energy-average coefficient $\bar{\alpha}$ (formulas 14.1.5 and 14.3.2) in the functions $E_2(\zeta_v)$, is very similar to curve 1 for a transparent gas. At the same time, curve 3 plotted using the exact spectral distribution of the coefficients α_v in the functions $E_2(\zeta_v)$ lies considerably higher than the two previously mentioned curves. In other words, the coefficient $\bar{\alpha}$, *per se*, does not determine the optical thickness of a radiating layer. In this sense, more significant is the *mean optical coefficient* α_E , which represents a mean value in the sense of the integral

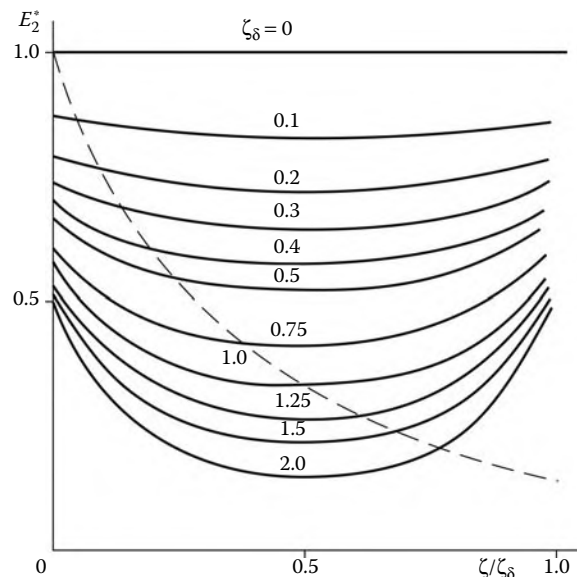
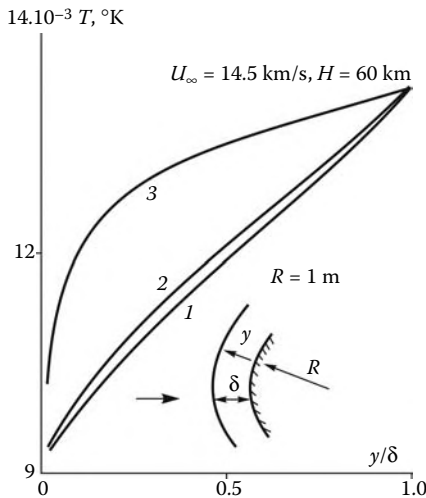


FIGURE 14.6

On the problem of a plane layer of finite optical thickness. The dashed curve is $E_2(\zeta)$.

**FIGURE 14.7**

Temperature distribution along the axis of symmetry in the shock layer on a sphere: 1, without absorption; (2 and 3), with allowance for reabsorption.

$$\bar{\alpha}_{\Sigma} E_2(\alpha_E \rho \delta) = \int_0^{\infty} \alpha_v B_v E_2(\rho \alpha_v \delta) dv \quad (14.3.9)$$

As distinct from $\bar{\alpha}$, this coefficient is dependent not only on the temperature and the pressure, but also on the radiating layer thickness δ . Thus, for the example considered previously, $\alpha_E/\bar{\alpha} \approx 10$, which explains so considerable a discrepancy between curves 2 and 3 in Figure 14.7.

In view of rather strong frequency dependence of the absorption coefficients for gases (Figure 14.2), the same gas layer can be transparent on one frequency range and optically thick on the other. This circumstance almost eliminates the possibility of the *a priori* determination of the coefficient α_E , particularly for inhomogeneous volumes, and makes it difficult to calculate radiative heat fluxes from the general spectral formula of 14.1.5; in view of the properties of the functions $E_n(x)$ this is quite a complicated problem, even for plane gas layers.

In conclusion, we will dwell briefly on viscous radiating gas flows. The example in Figure 14.7 relates to a near-inviscid flow past a body. Due to a fairly large shock-layer pressure ($p = 0.7$ atm) and rather high Reynolds number ($Re \approx 10^6$), the viscosity effect is concentrated in a wall boundary layer, which, as it were, absorbs the singularity arising in the inviscid solution 14.3.5. In matching the boundary-layer and inviscid solutions, the “radiative vorticity” of the latter should be taken into account; it is similar to the *relaxation vorticity* in relaxation sublayers (Section 11.10) in nonequilibrium flows past bodies (Lunev and Rumynskii, 1961).

The problem of solution matching does not arise, for example, when using the viscous shock layer model or the parabolized Navier-Stokes equations (Section 12.5), which are quite applicable for describing fairly thin hypersonic shock layers. The examples and methods of the solution of particular problems of the hypersonic radiating-gas flows, both viscous and inviscid, past bodies can be found in the books cited in the preceding paragraph.

14.4 Flows of Nonequilibrium Radiating Gases

Methodically, taking radiation into account in Equations 11.1.1 through 11.1.5, which govern nonequilibrium gas flows, is related to taking into account not only the heat flux q (*nonadiabaticity effect* considered in Section 14.3) but also some additional nonequilibrium effects, which will be considered here.

In a nonequilibrium radiating gas the concentration of excited particles and electrons is governed by the corresponding kinetic equations, which must allow for energy release. For the sake of illustration, we will consider the model example of a one-component gas containing only ions, electrons, and neutrals, with a single excited electronic level from which both energy release and ionization occur. We write down the corresponding system of equations for molar mass concentrations κ_i , which were used in Equation 11.1.7. Calling the concentrations of excited and unexcited particles κ_1 and κ_2 , respectively, we will generalize Equation 10.4.10 by introducing into it some additional terms, thus obtaining the required relaxation equation

$$\begin{aligned} \frac{d\kappa_2}{dt} &= \Lambda_2 = \frac{\kappa_{2e} - \kappa_2}{\tau_c} + \Lambda_R - \Lambda_3 + \frac{1}{M} \operatorname{div} \vec{I}_2 \\ \Lambda_R &= CI_v \kappa_1 - \kappa_2 / \tau_R, \quad \kappa_i = \frac{c_i}{M} \end{aligned} \quad (14.4.1)$$

Here, τ_c is the collisional relaxation time. The second term in Λ_R is due to excited particle radiation, τ_R being their lifetime, while the first term is caused by photoexcitation of particles due to absorption of the external radiant field energy at intensity I_v and a coefficient C . The diffusive flux I_2 , as the term I_3 below, has the same form as in Section 13.1.

The term Λ_3 in Equation 14.4.1 is due to excited particle ionization proceeding by scheme 10.6.9, $AB = A+B$, where AB is the symbol of excited particles with a concentration κ_3 , while A and B are the symbols of ions and electrons with the same concentration κ_3 . As a result we obtain Equation 11.1.6 governing the ion formation rate, which, in view of Equation 13.1.1, can be brought into the form:

$$\begin{aligned} \frac{d\kappa_3}{dt} &= \frac{1}{\tau_3} \left(\frac{\kappa_{3e}^2}{\kappa_{2e}} - \frac{\kappa_3^2}{\kappa_2} \right) + \frac{1}{M} \operatorname{div} \vec{I}_3 \\ \frac{1}{\tau_3} &= k_r^{\text{eff}} p^2 R T \bar{M}^3 \kappa_M \kappa_2, \quad \left(\frac{\kappa_{3e}^2}{\kappa_{2e}} = \frac{\bar{M}}{p} K_s(T) \right) \end{aligned} \quad (14.4.2)$$

Here, κ_M is the concentration of third particles that take part in the reaction, while k_r^{eff} is the effective (in the meaning of formula 10.9.8) reaction rate.

Let us consider the properties of the solution of the system of equations obtained; we will restrict ourselves to inviscid flows ($I_i = 0$) and, which is most important, to transparent gas layers, in which photoexcitation caused by radiation of the gas volume as a whole can be neglected, so that the first term in the expression for Λ_R can be dropped. Moreover, for the sake of simplicity we assume that the gas ionization degree is so small that the term Λ_3 in Equation 14.4.1 can be neglected. Then this equation becomes independent of Equation 14.4.2 and takes the form:

$$\frac{d\kappa_2}{dt} = \frac{\kappa_{2e} - \kappa_2}{\tau_c} - \frac{\kappa_2}{\tau_R} \quad (14.4.3)$$

We will formulate the following initial-value problem for system 14.4.2 and 14.4.3: $\kappa_2 = \kappa_{20}$ and $\kappa_3 = \kappa_{30}$ at $t = 0$ (e.g., for the gas state immediately behind a shock); as in Section 11.9, time t of the gas particle motion is the argument. Then the point $t = 0$ is followed by a relaxation zone; to evaluate the thickness and the nature of this zone, we take the coefficients of Equation 14.4.3 to be constant, which leads to the solution

$$\begin{aligned}\kappa_2 &= (\alpha\kappa_{2e} - \kappa_{20})e^{-t/\tau_{\text{eff}}} + \alpha\kappa_{2e} \\ \frac{1}{\tau_{\text{eff}}} &= \frac{1}{\tau_c} + \frac{1}{\tau_R}, \quad \alpha = \frac{\tau_R}{\tau_c + \tau_R}\end{aligned}\quad (14.4.4)$$

Clearly, as distinct from the solution 10.4.3, in this case the relaxation zone thickness is determined by precisely the *effective* relaxation time τ_{eff} and decreases with the ratio τ_R/τ_c . Moreover, the limiting, as $t \rightarrow \infty$, value κ_2 is smaller than the equilibrium value and equal to the *quasistationary* (in the meaning of Section 11.2) *value*

$$\kappa_2 = \kappa_2^{(\text{st})} = \alpha\kappa_{2e} = \frac{\tau_R}{\tau_c + \tau_R}\kappa_{2e} \quad (14.4.5)$$

For $\tau_R \gg \tau_c$ we obtain $\alpha \approx 1$ and the standard equilibrium gas state $\kappa_2 \approx \kappa_{2e}$. However, for $\tau_R < \tau_c$ the quantity $\kappa_2^{(\text{st})} < \kappa_{2e}$, that is, the process of excited level depletion is not compensated by the collisional process of particle excitation. Moreover, when $\tau_R/\tau_c \rightarrow 0$ the ratio $\kappa_2^{(\text{st})}/\kappa_{2e}$ vanishes.

We are now coming to the solution of Equation 14.4.2 for the ion or electron concentration. This solution is dependent on the excited particle concentration κ_2 ; for this reason, the electron concentration κ_3 cannot become equal to the equilibrium one ($\kappa_3 = \kappa_{3e}$) if the equality $\kappa_2 = \kappa_{2e}$ is not attained. As for a fairly extended range on which the state of excited particles is quasistationary and described by Equation 14.4.5, there the electron concentration also approaches the quasistationary one, which, in view of Equation 14.4.5, is equal to $\kappa_3 = \kappa_3^{(\text{st})} = \alpha^{1/2}\kappa_{3e}$.

Thus, photoextinction of the excited levels of atoms and molecules can lead to the formation of an extended zone of quasistationary parameters with reduced, as compared with equilibrium values, concentrations of excited particles and, hence, electron concentrations. Moreover, the reduction in excited particle concentrations lead to the reduction of the gas flow intensity in both atomic lines and molecular bands, which follows directly from formula 14.1.2, as well as in the continuous spectrum due to the electron concentration decrease.

These theoretical conclusions are supported by the results of shock-tube experiments; in these tubes the small cross-sectional area ensures the transparency of the working gas plug. In Figure 14.8 we have presented an example of the distribution of the radiation intensity I_v in the atomic oxygen line and the electron concentration n_{el} behind a shock in air. Obviously, after a relatively small relaxation zone, both parameters acquire quasistationary constant values different from locally equilibrium ones (by factors of 40 for I_v and 3 for n_{el} ; see Zalogin, Lunev, and Plastinin, 1980).

In Figure 14.9 the experimental values of n_{el} in quasistationary zones behind shocks produced in air in a shock tube and characterized by velocities $U_\infty = 7 - 12$ km/sec, are compared with the calculated equilibrium values, which for $U_\infty > 9$ km/sec are considerably higher than the experimental data (Gorelov and Kil'dyusheva, 1987). Correspondingly, for $U_\infty < 9$ km/sec the gas temperature T is near equilibrium though it becomes appreciably higher, as the velocity increases, and is close to the equilibrium value obtained at the equilibrium composition, but with zero electron concentration (dashes).

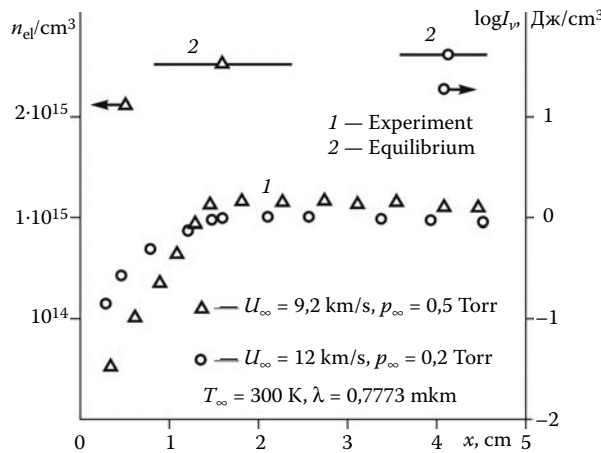


FIGURE 14.8
Electron concentration and radiation intensity behind a shock in air.

From the previous discussion it follows that the calculation of the atom ionization rate constants from the electron concentration behind a shock without making allowance for depletion of the electronic level population due to energy release can result in gross mistakes.

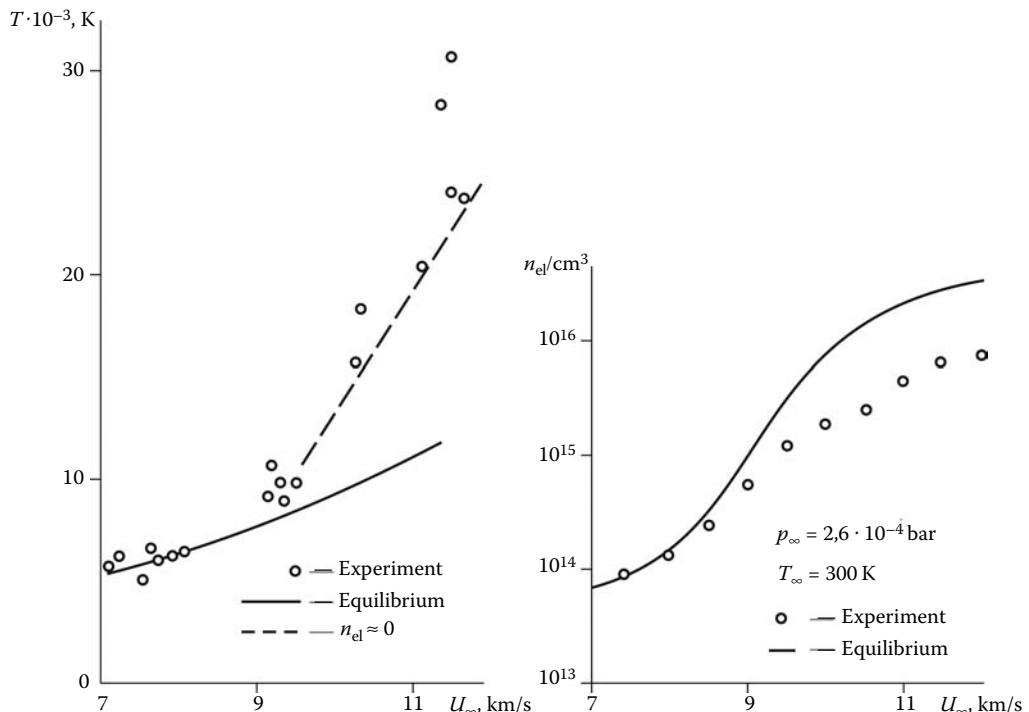


FIGURE 14.9
Temperature and electron concentrations in the quasistationary zone behind a shock.

We note that in all these experiments the appearance of electrons is due to atom ionization by electron impact. Therefore, it should be let $\kappa_M = \kappa_3$ in formula 14.4.2 for τ_3 , while in Equation 14.4.1 we have also $\tau_c \sim \kappa_3^{-1}$. This can enlarge appreciably the zones of relaxation of the processes governed by these equations, as compared with the usual dissociation relaxation zones by analogy with the example presented in Figure 11.6 in Section 11.5.

Naturally, the same effects can manifest themselves in shock layers on bodies in hypersonic atmospheric flight. In this case, the quasistationary radiation regimes are realized in the flight at fairly high altitudes, since the collisional relaxation time τ_c increases when the gas density decreases, while the excited level lifetime τ_R is a physical constant of the process under consideration.

Bibliography*

- Abramovich, G. N., *Applied Gas Dynamics* [in Russian], Nauka, Moscow (1976).
- Akimov, G. A., *Development of Theoretical and Applied Gas Dynamics by Professor Ginzburg's School* [in Russian], State Baltic Technical University, St. Petersburg (2002).
- Alekseev, B. V., and A. M. Grishin, *Physical Gas Dynamics of Reacting Media* [in Russian], Vysshaya Shkola, Moscow (1985).
- Anfimov, N. A., *Izv. Akad. Nauk SSSR, Mekh. Mash.*, No. 1, 25 (1962); No. 5, 117 (1963).
- Anfimov, N. A., V. G. Voronkin, G. N. Zalomin, and V. V. Lunev, in: *Gagarin Scientific Readings on Cosmonautics and Aviation* [in Russian], Nauka, Moscow (1985).
- Antonets, A. V., and A. V. Krasil'nikov, *Fluid Dynamics*, **4**, No. 5, 94 (1969).
- Avduevskii, V. S., in: *Foundations of Heat Transfer in Aircraft, Rocket, and Space Engineering* [in Russian], Mashinostroenie, Moscow (1975).
- Bachmanova, N. S., V. I. Lapygin, and Yu. M. Lipnitskii, *Fluid Dynamics*, **8**, No. 6, 915 (1973).
- Baldwin, B. S., and H. Lomax, *AIAA Paper*, No. 0257 (1978).
- Baranov, V. B., K. V. Krasnobaev, and A. G. Kulikovskii, *Dokl. Akad. Nauk SSSR*, **194**, No. 1, 41 (1970).
- Barenblatt, G. I., *Similarity, Self-Similarity, and Intermediate Asymptotics* [in Russian], Gidrometeoizdat, Leningrad (1982).
- Baronets, P. N., A. N. Gordeev, A. F. Kolesnikov, M. I. Yakushin, et al., in: *Gagarin Scientific Readings on Cosmonautics and Aviation* [in Russian], Nauka, Moscow (1991).
- Bashkin, V. A., *Delta Wings in Hypersonic Flow* [in Russian], Mashinostroenie, Moscow (1984).
- Belotserkovskii, O. M., *Dokl. Akad. Nauk SSSR*, **113**, No. 3, 509 (1957).
- Belotserkovskii, O. M. (ed.), *Supersonic Flow Past Blunt Bodies* [in Russian], USSR Academy of Sciences, Computer Center, Moscow (1966).
- Belotserkovskii, S. M., *Thin Lifting Surfaces in Subsonic Flow* [in Russian], Nauka, Moscow (1965).
- Berkut, V. D., V. M. Doroshenko, V. V. Kovtun, and N. N. Kudryavtsev, *Nonequilibrium Physical and Chemical Processes in Hypersonic Aerodynamics* [in Russian], Energoatomizdat, Moscow (1994).
- Bertram, M., *J. Aeronaut. Sci.*, **23**, No. 9 (1956).
- Bird, G., *Molecular Gas Dynamics*, Clarendon Press, Oxford (1976).
- Blottner, F. G., *J. Computers Fluids*, **20**, No. 3, 295 (1991).
- Bond Jr., J. W., K. W. Watson, and J. A. Welch, *Atomic Theory of Gas Dynamics*, Addison-Wesley, Reading, MA (1965).
- Brode, H., *Phys. Fluids*, **2**, No. 2, 217 (1959).
- Cheng, H., and A. Pallone, *J. Aeronaut. Sci.*, **23**, No. 7 (1956).
- Chernyi, G. G., *Applied Math. Mech.*, **29**, No. 4 (1965).
- Chernyi, G. G., *Gas Dynamics* [in Russian], Nauka, Moscow (1988).

* References to the books by Russian and other non-English-speaking authors are given in accordance with their English translations, if there are any and they are known to the author or the translators. As for the papers from Russian scientific journals cited in this book, most of them were published in the following three journals: *Prikladnaya Matematika i Mekhanika*, *Izvestiya Akademii Nauk, ser. Mekhanika Zhidkosti i Gaza*, and *Zhurnal Prikladnoi Mekhaniki i Tekhnicheskoi Fiziki*. All the three journals are translated into English—the first by Elsevier under the name *Applied Mathematics and Mechanics* and the other two by Springer as *Fluid Dynamics* and *Journal of Applied Mechanics and Technical Physics*. References to the papers published in these journals are given in accordance with the previous translations, while references to the papers from other Russian journals are given in accordance with the original publications.

- Chernyi, G. G., *Introduction to Hypersonic Flow Theory*, Academic Press, New York (1966).
- Chernyi, G. G., in: *Theoretical Mechanics*, No. 9 [in Russian], Oborongiz, Moscow (1952).
- Chernyi, G. G., and S. A. Losev, *Handbook on Physical and Chemical Processes in Gas Dynamics* [in Russian], Moscow University Press, Moscow (1995 [Vol. 1], 2002 [Vol. 2]).
- Chetaev, N. G., *Theory of Stability* [in Russian], Gostekhizdat, Moscow (1955).
- Chue, S., *Progress Aerospace Sci.*, No. 2 (1975).
- Chushkin, P. I., *Appl. Math. Mech.*, **21**, No. 3 (1957).
- Clarke, J. F., and M. McChesney, *Dynamics of Real Gases*, Butterworth, London (1964).
- Cole, J. D., and L. P. Cook, *Transonic Aerodynamics*, North Holland, Amsterdam (1986).
- Davis, R. T., *AIAA J.*, **8**, No. 5, 843 (1970).
- Diesperov, V. N., Yu. V. Lifshits, and O. S. Ryzhov, *Fluid Dynamics*, **9**, No. 5, 717 (1974).
- Donaldson, C. P., R. S. Snedecker, and D. P. Margolis, *J. Fluid Mech.*, **45**, Pt. 3, 477 (1971).
- Dorodnitsyn, A. A., in: *Proceedings of the 3rd All-Union Congress on Mathematics. 1956. Vol. III* [in Russian], USSR Academy of Sciences, Moscow (1958).
- Eckert, E., *Trans. ASME*, No. 6 (1956).
- Edney, B. E., *AIAA J.*, **6**, No. 1, 15 (1968).
- Ermak, Yu. I., and V. Ya. Neiland, *Zh. Vychisl. Mat. Mat. Fiz.*, **4**, No. 5 (1964).
- Fal'kovich, S. V., *Appl. Math. Mech.*, **11**, No. 4 (1947).
- Fal'kovich, S. V., and I. A. Chernov, *Appl. Math. Mech.*, **28**, No. 5 (1964).
- Fay, J. A., and F. R. Riddell, *J. Aeron. Sci.*, **25**, No. 2, 73 (1958).
- Ferrari, C., in: A. Miele (ed.), *Theory of Optimum Aerodynamic Shapes*, Academic Press, New York (1965).
- Ferri, A., *Elements of Aerodynamics of Supersonic Flows*, MacMillan, New York (1949).
- Fletcher, C., *Computational Techniques for Fluid Dynamics*, Springer, Berlin (1988).
- Frank-Kamenetskii, D. A., *Diffusion and Heat Transfer in Chemical Kinetics* [in Russian], Nauka, Moscow (1967).
- Garabedian, P. J., *Physics*, No. 1 (1958).
- Glazkov, Yu. V., G. A. Tirkii, and V. G. Shcherbak, *Mat. Model.*, No. 8 (1990).
- Glushko, G. S., in: *Turbulent Flows* [in Russian], Nauka, Moscow (1970).
- Godunov, S. K., A. V. Zabrodin, M. Ya. Ivanov, A. N. Kraiko, and G. P. Prokopov, *Numerical Solution of Multi-Dimensional Problems of Gas Dynamics* [in Russian], Nauka, Moscow (1976).
- Golovachev, Yu. P., *Numerical Modeling of Viscous Flows in Shock Layers* [in Russian], Fizmatlit, Moscow (1996).
- Gonor, A. L., *Izv. Akad. Nauk SSSR. Mekh. Mash.*, No. 7, 102 (1958); *Dokl. Akad. Nauk SSSR*, **309**, No. 4, 812 (1989).
- Gordiets, B. F., A. M. Osipov, and L. A. Shelepin, *Kinetic Processes in Gases and Molecular Lasers* [in Russian], Nauka, Moscow (1980).
- Gorelov, V. A., and L. A. Kil'dyusheva, *J. Appl. Mech. Techn. Phys.*, **28**, No. 6, 825 (1987).
- Gorshkov, A. B., and V. V. Lunev, *Kosmonavt. Raketotstr.*, No. 10 (1997).
- Grigoryan, S. S., *Appl. Mat. Mech.*, **22**, No. 2 (1958).
- Gubanova, O. I., I. M. Karpman, and V. V. Lunev, *Fluid Dynamics*, **23**, No. 5, 785 (1988).
- Gubanova, O. I., V. V. Lunev, and L. I. Plastinina, *Fluid Dynamics*, **6**, No. 2, 298 (1971).
- Gubanova, O. I., B. A. Zemlyanskii, A. B. Lesin, V. V. Lunev, and A. N. Nikulin, in: *Aerodynamics of Aispace Systems* [in Russian], Central Hydroaerodynamics Institute (TsAGI) (1992).
- Gulyaev, A. N., V. E. Kozlov, and A. N. Sekundov, *Fluid Dynamics*, **28**, No. 4, 485 (1993).
- Gupta, R., and A. Simmonds, *AIAA Paper*, No. 1349 (1986).
- Gurzhienko, G. A., *Tr. TsAGI*, No. 182 (1934).
- Gusev, V. N., and Yu. V. Nikol'skii, *Uch. Zap. TsAGI*, No. 1 (1971).
- Hammitt, A. G., and S. M. Bogdonoff, *Jet Propulsion*, **26**, No. 4, 241 (1956).
- Hansen, C., *NASA Rept.*, No. R-50 (1959).

- Hayes, W. D., *Quart. Appl. Math.*, **5**, No. 1, 105 (1947).
- Hayes, W. D., and R. F. Probstein, *Hypersonic Flow Theory*, Academic Press, New York (1966).
- Hinze, J. O., *Turbulence. An Introduction to Its Mechanisms and Theory*, McGraw Hill, New York (1959).
- Hirschfelder, J. O., C. F. Curtiss, and R. B. Bird, *Molecular Theory of Gases and Liquids*, Wiley, New York (1954).
- Il'yushin, A. A., *Appl. Mat. Mech.*, **20**, No. 6 (1956).
- Inouye, Y., in: *Proc. 2nd European Symposium on Aerothermodynamics for Space Vehicles. ESTEC, Noordwijk, the Netherlands, European Space Agency*, 1995 (1995).
- Itin, P. G., G. N. Zalozin, V. V. Lunev, and S. L. Perov, *Pisma Zh. Tekhn. Fiz.*, **14**, No. 22 (1988).
- Ivanov, V. V., and A. V. Krasil'nikov, *Fluid Dynamics*, **7**, No. 2, 339 (1972).
- Kamenshchikov, V. A., V. M. Nikolaev, L. A. Novikov, and Yu. A. Plastinin, *Radiation Properties of Gases at High Temperatures* [in Russian], Mashinostroenie, Moscow (1971).
- von Kármán, T., *J. Aeronaut. Sci.*, **14**, No. 7, 373 (1947).
- Karpov, V. A., *Fluid Dynamics*, **3**, No. 3, 100 (1968); **6**, No. 6, 1046 (1971); **10**, No. 4, 693 (1975).
- Kemp, N. H., *J. Aeronaut. Sci.*, **25**, No. 8 (1958).
- Kerson Huang, *Statistical Mechanics*, Wiley, New York (1987).
- Kestenboim, Kh. S., G. S. Roslyakov, and L. A. Chudov, *Point Explosion* [in Russian], Nauka, Moscow (1974).
- Khristianovich, S. A., in: *Mechanics of Continuous Media* [in Russian], Nauka, Moscow (1981).
- Khristianovich, S. A., *Tr. TsAGI*, No. 481 (1940).
- Kochin, N. E., I. A. Kibel', and N. V. Roze, *Theoretical Hydromechanics*, Interscience, New York (1964).
- Kogan, M. N., *Inzh. Zh.*, **1**, No. 3 (1961).
- Kogan, M. N., *Rarefied Gas Dynamics*, Plenum Press, New York (1969).
- Kogan, M. N., and N. K. Makashev, *Fluid Dynamics*, **6**, No. 6, 913 (1971).
- Kolmogorov, A. N., *Dokl. Akad. Nauk SSSR*, **30** (1941).
- Kolmogorov, A. N., I. G. Petrovskii, and N. S. Piskunov, *Bull. MGU, Sektsiya A*, **1**, No. 6 (1937).
- Korobeinikov, V. P., *Theory of Point Explosion* [in Russian], Nauka, Moscow (1985).
- Kovalev, R. V., *Kosmonavt. Raketostr.*, No. 11 (1971).
- Kovalev, V. L., *Heterogeneous Catalytic Processes in Aerodynamics* [in Russian], Fizmatlit, Moscow (2002).
- Kovalev, V. L., and O. N. Suslov, *Dokl. Ross. Akad. Nauk*, **345**, No. 4, 483 (1995).
- Kraiko, A. N., *Appl. Math. Mech.*, **38**, No. 3, 6 (1974).
- Kraiko, A. N., and D. E. Pudovikov, *Appl. Math. Mech.*, **61**, No. 5 (1997).
- Kraiko, A. N., and R. A. Tkachenko, *Fluid Dynamics*, **3**, No. 6, 13 (1968).
- Krasil'nikov, A. V., *Fluid Dynamics*, **4**, No. 6, 106 (1969).
- Kuznetsov, N. M., *Thermodynamic Functions and Shock Adiabats of Air at High Temperatures* [in Russian], Mashinostroenie, Moscow (1965).
- Kuznetsov, N. M., *Kinetics of Monomolecular Reactions*, Nauka, Moscow (1982).
- Lam, C. K. G., and K. A. Bremhorst, *J. Fluid Engng.*, **103**, No. 456 (1981).
- Landau, L. D., and E. M. Lifshitz, *Fluid Mechanics*, Pergamon, London (1959).
- Lapin, Yu. V., *Turbulent Boundary Layers in Supersonic Flows* [in Russian], Nauka, Moscow (1982).
- Launder, B. E., and B. I. Sharma, *Lett. Heat Mass Transfer*, **1**, No. 1, 131 (1974).
- Launder, B. E., and D. B. Spalding, *Computer Methods in Applied Mechanics and Engineering*, **3**, No. 269 (1974).
- Lebedev, M. G., and I. D. Sandomirskaya, in: *Numerical Methods and Programming*. No. 34, p. 70 [in Russian], Moscow University Press, Moscow (1981).
- Lees, L., *Jet Propulsion*, **26**, No. 4 (1956).
- Lesin, A. B., and V. V. Lunev, *Fluid Dynamics*, **29**, No. 2, 258 (1994).
- Levin, V. A., and G. G. Chernyi, *Appl. Math. Mech.*, **31**, No. 3 (1967).

- Li, T., and R. Geiger, *J. Aeronaut. Sci.*, **24**, No. 1, 25 (1957).
- Liepmann, H. W., and A. Roshko, *Elements of Gasdynamics*, Wiley, New York (1957).
- Lifshitz, E. M., and P. L. Pitaevskii, *Physical Kinetics* [in Russian], Nauka, Moscow (1979).
- Lighthill, M., in: H. W. Liepmann and A. Roshko, *Elements of Gasdynamics*, Wiley, New York (1957).
- Lighthill, M., *J. Fluid Mech.*, **2**, Pt. 1, 1 (1957).
- Lipnitskii, Yu. M., A. V. Krasil'nikov, V. N. Pokrovskii, and V. N. Shmanenkov, *Time-Dependent Aerodynamics of Ballistic Flight* [in Russian], Fizmatlit, Moscow (2003).
- Loitsianskii, L. G., *Mechanics of Liquids and Gases*, Pergamon, Oxford (1966).
- Lozino-Lozinsky, G. E., and V. P. Timoshenko, in: *Proc. 3rd European Symp. on Aerothermodynamics of Space Vehicles. ESTEC, Hoodwink, the Netherlands, December 1998* (1998).
- Lunev, V. V., *Hypersonic Aerodynamics* [in Russian], Mashinostroenie, Moscow (1975).
- Lunev, V. V., *Izv. Akad. Nauk SSSR. Mekh. Mash.*, No. 4, 13 (1962); *Appl. Math. Mech.*, **23**, Nos. 1 and 6 (1959); **24**, No. 3 (1960); **25**, No. 6 (1961); *J. Appl. Mech. Techn. Phys.*, **1**, No. 2 (1960); **9**, No. 3 (1968); *Fluid Dynamics*, **2**, No. 1, 83 (1967); **6**, No. 6, 958 (1971); **22**, No. 1, 121 (1987); **35**, No. 3, 443 (2000).
- Lunev, V. V., and N. E. Khramov, *Fluid Dynamics*, **5**, No. 3, 444 (1970).
- Lunev, V. V., K. M. Magomedov, and V. G. Pavlov, *Hypersonic Flow Past Blunt Cones with Account for Equilibrium Physical and Chemical Processes* [in Russian], USSR Academy of Sciences, Computer Center, Moscow (1968).
- Lunev, V. V., and I. N. Murzinov, *J. Appl. Mech. Techn. Phys.*, **2**, No. 2 (1961).
- Lunev, V. V., I. N. Murzinov, and O. N. Ostapovich, *Izv. Akad Nauk SSSR. Mekh. Mash.*, No. 3, 121 (1960).
- Lunev, V. V., and V. G. Pavlov, *Fluid Dynamics*, **1**, No. 6, 75 (1966).
- Lunev, V. V., V. G. Pavlov, and S. G. Sinchenko, *Zh. Vychisl. Mat. Mat. Fiz.*, **6**, No. 1 (1966).
- Lunev, V. V., and A. N. Rumynskii, *J. Appl. Mech. Techn. Phys.*, **1**, No. 6 (1960); *Fluid Dynamics*, **1**, No. 5, 20 (1966).
- Lunev, V. V., and S. V. Selezneva, *Kosmonavt. Raketotstr.*, No. 11 (1997), No. 19 (2000).
- Lunev, V. V., and V. A. Semin, *Fluid Dynamics*, **24**, No. 3, 462 (1989).
- Lyubimov, A. N., and V. V. Rusanov, *Gas Flows Past Blunt Bodies* [in Russian], Nauka, Moscow (1970).
- Magomedov, K. M., and A. S. Kholodov, *Grid-Characteristic Numerical Methods* [in Russian], Nauka, Moscow (1988).
- Maikapar, G. I., V. P. Agafonov, V. K. Vertushkin, A. A. Gladkov, and Yu. A. Polyanskii, *Nonequilibrium Physical and Chemical Processes in Aerodynamics* [in Russian], Mashinostroenie, Moscow (1972).
- Marrone, P. V., and C. E. Treanor, *Phys. Fluids*, **6**, No. 9, 1215 (1963).
- Marvin, J. G., and A. R. Sinclair, *AIAA J.*, **5**, No. 11, 1940 (1967).
- Meyerovich, B. E., *Zh. Eksp. Teor. Fiz.*, No. 5 (1971).
- Miele, A. (ed.), *Theory of Optimum Aerodynamic Shapes*, Academic Press, New York (1965).
- von Mises, R., *Mathematical Theory of Compressible Fluid Flow*, McGraw Hill, New York (1953).
- Murzinov, I. N., *Fluid Dynamics*, **1**, No. 2, 131 (1966).
- Napolitano, L., *Arch. Mech. Stosowanej*, No. 2 (1964).
- Neiland, V. Ya., V. V. Bogolepov, G. N. Dudin, and I. I. Lipatov, *Asymptotic Theory of Supersonic Viscous Flows*, Elsevier, Amsterdam (2007).
- Ovsyannikov, L. V., *Lectures on the Foundations of Gas Dynamics* [in Russian], Nauka, Moscow (1982).
- Pilyugin, N. N., and G. A. Tirskii, *Dynamics of Ionized Radiating Gases* [in Russian], Moscow University Press, Moscow (1989).
- Pirumov, U. G., and G. S. Roslyakov, *Gas Flow in Nozzles*, Springer, Berlin (1986).
- Pokrovskii, A. N., and V. N. Shmanenkov, *Fluid Dynamics*, **14**, No. 4, 524 (1979).
- Polyanskii, O. Yu., *Fluid Dynamics*, **1**, No. 4, 20 (1966).

- Predvoditelev, A. S., E. V. Stupochenko, A. S. Pleshanov, E. V. Samuilov, and I. B. Rozhdestvenskii, *Tables of Thermodynamic Functions of Air for Temperatures from 12,000 to 20,000°K and Pressures from 0.001 to 1000 atm* [in Russian], USSR Academy of Science Press, Moscow (1959).
- Probstein, R., M. Adams, and P. Rose, *Jet Propulsion*, No. 1 (1958).
- Raizer, Yu. P., *J. Appl. Mech. Techn. Phys.*, **9**, No. 3, 239 (1968).
- Raizer, Yu. P., *Physics of Gas Discharge* [in Russian], Nauka, Moscow (1987).
- Rakhmatullin, Kh. A., A. Ya. Sagomonyan, A. I. Bunimovich, and I. N. Zverev, *Gas Dynamics* [in Russian], Vysshaya Shkola, Moscow (1965).
- Rose, P. H., and W. I. Stark, *J. Aeronaut. Sci.*, **25**, No. 2, 86 (1958).
- Roslyakov, G. S., A. L. Starykh, and V. N. Uskov, *Fluid Dynamics*, **22**, No. 4, 614 (1987).
- Rouse, C., in: W. G. Chace and H. K. Moore (eds.), *Exploding Wires*, Plenum, New York & Chapman and Hall, London (1959).
- Ryzhov, O. S., *Appl. Math. Mech.*, **35**, No. 6 (1971).
- Ryzhov, O. S., and S. A. Khristianovich, *Appl. Math. Mech.*, **22**, No. 5 (1958).
- Ryzhov, O. S., and E. D. Terent'ev, *Appl. Math. Mech.*, **38**, No. 1 (1974).
- Safarov, R. A., and G. A. Tirkii, in: *Turbulent Flows* [in Russian], Nauka, Moscow (1977).
- Safiullin, R. A., *Fluid Dynamics*, **6**, No. 6, 989 (1971).
- Schlichting, H., *Boundary Layer Theory*, McGraw Hill, New York (1968).
- Sedov, L. I., *Mechanics of Continuous Media*, World Science Publishing Company, Singapore (1997).
- Sedov, L. I., *Similarity and Dimensional Methods*, London (1959).
- Sedov, L. I., *Two-Dimensional Problems in Hydrodynamics and Aerodynamics*, Interscience Publishing Company, New York (1965).
- Selezneva, S. E., *Fluid Dynamics*, **33**, No. 4, 630 (1998).
- Shevelev, Yu. D., *Three-Dimensional Problems of Laminar Boundary Layers* [in Russian], Nauka, Moscow (1977).
- Shih-I Pai, *Radiation Gas Dynamics*, Springer, New York (1966).
- Shmyglevskii, Yu. D., *Analytical Studies in Fluid Dynamics* [in Russian], Editorial URSS, Moscow (1999).
- Sinchenko, S. G., *Zh. Vychisl. Mat. Mat. Fiz.*, **8**, No. 4 (1968).
- Slezkin, N. A., *Dynamics of Viscous Incompressible Fluids* [in Russian], Gostekhizdat, Moscow (1955).
- Smirnov, B. M., *Introduction to Plasma Dynamics* [in Russian], Nauka, Moscow (1982).
- Spalart, P. R., and S. R. Allmaras, *AIAA Paper*, No. 0439 (1992).
- Stewartson, K., *Proc. Cambridge Soc.*, **51**, No. 1, 202 (1955); *J. Aeronaut. Sci.*, **22**, No. 5, 303 (1955).
- Stulov, V. P., V. N. Mirskii, and A. I. Vislyi, *Aerodynamics of Bolides* [in Russian], Fizmatlit, Moscow (1995).
- Surzhikov, S. T., *Optical Properties of Gases and Plasmas* [in Russian], Moscow State Technical University Press, Moscow (2004).
- Sychev, V. V., *Dokl. Akad. Nauk SSSR*, **131**, No. 4, 776 (1960); *Appl. Mat. Mech.*, **24**, No. 2 (1960); **25**, No. 4 (1961); **29**, No. 3 (1965).
- Sychev, V. V., A. I. Ruban, Vic. V. Sychev, and G. L. Korolev, *Asymptotic Theory of Separated Flows*, Cambridge University Press, Cambridge (1998).
- Taylor, G., *Proc. Roy. Soc.*, **21**, No. 8, 1065 (1950).
- Telenin, G. F., *Similarity Laws at High Supersonic Velocities* [in Russian], Oborongiz, Moscow (1956).
- Telenin, G. F., and G. P. Tinyakov, *Dokl. Akad. Nauk SSSR*, **154**, No. 5 (1964).
- Tirkii, G. A., *Dokl. Akad. Nauk SSSR*, **155**, No. 6, 1278 (1964); in: N. N. Pilyugin and G. A. Tirkii (eds.), *Dynamics of Ionized Radiating Gases* [in Russian], Chapter 8, Nauka, Moscow (1982).
- Tsien, H., *J. Math. Phys.*, **25**, No. 3, 247 (1946).
- Vaglio-Laurin, R., *ARS J.*, No. 2 (1959).
- Vaglio-Laurin, R., *J. Fluid Mech.*, **9**, Pt. 1, 81 (1960).
- Vaglio-Laurin, R., and A. Ferri, *J. Aeronaut. Sci.*, **25**, No. 12, 761 (1958).

- Van Dyke, M. D., *Perturbation Methods in Fluid Mechanics*, Academic Press, New York (1964).
- Vasil'evskii, S. A., I. A. Sokolova, and G. A. Tirskii, *J. Appl. Mech. Techn. Phys.*, **25**, No. 4, 510 (1984); **27**, No. 1, 61 (1986).
- Vasil'kov, A. P., and I. N. Murzinov, *Fluid Dynamics*, **8**, No. 3, 428 (1973).
- Vigneron, Y. C., J. V. Rakich, and J. V. Tannehill, *AIAA Paper*, No. 1137 (1978).
- Vlasov, V. I., and A. B. Gorshkov, *Fluid Dynamics*, **36**, No. 5, 812 (2001).
- Vlasov, V. I., and R. V. Kovalev, in: *European Conference for Aerospace Sciences (EUCASS)*, Moscow (2005).
- Vlasov, V. I., and A. P. Kusov, in: *Abstracts of 46th Scientific Conference of Moscow Physico-Technical Institute* [in Russian] (2003).
- Voinov, L. P., G. N. Zalomin, V. V. Lunev, and V. P. Timoshenko, *Kosmonavt. Raketostro.*, No. 2 (1964).
- Vorob'yev, N. F., *Aerodynamics of Lifting Surfaces in Steady Flows* [in Russian], Nauka, Novosibirsk (1985).
- Voronkin, V. G., *Fluid Dynamics*, **5**, No. 1, 147 (1970); **9**, No. 6, 950 (1974).
- Voronkin, V. G., V. V. Lunev, and A. N. Nikulin, *Fluid Dynamics*, **13**, No. 2, 274 (1978).
- Voronkin, V. G., and G. N. Zalomin, *Tr. TsAGI*, No. 1656 (1975).
- Zalomin, G. N., and V. V. Lunev, *Fluid Dynamics*, **8**, No. 5, 832 (1973); **32**, No. 5, 748 (1997).
- Zalomin, G. N., V. V. Lunev, and Yu. A. Plastinin, *Fluid Dynamics*, **15**, No. 1, 85 (1980).
- Zel'dovich, Y. B., in: *Chemical Physics and Fluid Dynamics. Selected Works* [in Russian], Nauka, Moscow (1984).
- Zel'dovich, Y. B., G. I. Barenblatt, V. B. Librovich, and G. M. Makhliladze, *The Mathematical Theory of Combustion and Explosion*, Plenum, New York (1985).
- Zel'dovich, Y. B., and Y. P. Raizer, *Physics of Shock Waves and High Temperature Hydrodynamic Phenomena. Vols. 1 and 2*, Academic Press, San Diego (1967).
- Zemlyanskii, B. A., *Fluid Dynamics*, **1**, No. 4, 47 (1966).
- Zemlyanskii, B. A., O. I. Gubanova, V. V. Lunev, et al., in: *Aerodynamics of Aerospace Systems* [in Russian], Central Hydroaerodynamics Institute (TsAGI) (1992).
- Zemlyanskii, B. A., A. B. Lesin, V. V. Lunev, and G. A. Shmanenkova, *Fluid Dynamics*, **17**, No. 5, 764 (1982).
- Zemlyanskii, B. A., V. V. Lunev, and K. M. Magomedov, *Fluid Dynamics*, **4**, No. 3, 140 (1969).
- Zemlyanskii, B. A., V. V. Lunev, and K. M. Marinin, *Fluid Dynamics*, **16**, No. 2, 199 (1981).
- Zemlyanskii, B. A., and V. P. Marinin, *Fluid Dynamics*, **9**, No. 5, 765 (1974).
- Zemlyanskii, B. A., and G. N. Stepanov, *Fluid Dynamics*, **16**, No. 5, 787 (1981).
- Zhestkov, B. E., in: *Proceedings of the 8th All-Union Conference on Rarefied Gas Dynamics* [in Russian], Moscow Aviation Institute (1986).
- Zhigulev, V. N., *Dokl. Akad. Nauk SSSR*, **144**, No. 6, 1251 (1962).
- Znamenskii, V. V., *Fluid Dynamics*, **11**, No. 2, 266 (1976).

Index

A

Absorbing jets, 706–711
Accelerated motion of bodies, 143–145
Accommodation coefficient of tangential momentum, 564
Acting mass law, 473
Activation energy, 478
Active adsorption centers, 687
Adiabatic entropy, 463
Adiabatic equation, 26
Adiabatic shock, 147
Adiabatic wall enthalpy, 593
Adiabatically isolated system, 24
Aerodynamic characteristics, 140–143, 329–337
Algebraic turbulence models, 599
Ambipolar diffusion coefficient, 681
Angle of attack, 140–141, 397
Anomalous media, waves in, 235–238
Area rule, 333–334
Arrhenius law, 478
Associative ionization, 460
Axis of symmetry
 constant-density flow in vicinity of, blunt body, 349–354
 variable-density flow along, 354–357
Axisymmetric problems, 119

B

Barodiffusion coefficients, 682
Barotropic gases, 87–89
Bernoulli equation, 87, 191, 383, 622
Bernoulli integral, 85, 639
Bicharacteristics, 183
Binary diffusion, 10
Binary diffusion coefficients, 701
Binary reactions, 461
Binary similarity law, 535–536
Blasius function, 619
Blasius profile, 583
Blast
 flows past thin blunt bodies, 405–410
 in heat-conducting gas, 303–305
 in real gases, 301–303
 strong, 294–300
Blast analogy, 407
Bluff bodies, entropy effect on, 637–653

Blunt bodies

axis of symmetry of, constant-density flow
 in vicinity of, 349–354
boundary layer on, 602–612
limitingly, 318
similarity law, 327–329
supersonic flows past, 250–255
three-dimensional vortex layers on, 437–441
Blunt cones
 flows past, 412–421
 local rule, 424
 pressure distributions over, 657
Blunt edges, wings with, 429–434
Blunt noses, wings with, 434–437
Blunt-body stagnation points
 boundary layer at, 595–597
 description of, 539–543
Bodies of revolution at incidence, 421–429
Boltzmann distribution, 468–472, 481
Boltzmann equation, 7, 20, 654
Boundary conditions
 description of, 56–58
 for dissipative viscous gas flows, 563–567
Boundary layer
 at blunt-body stagnation point, 595–597
 in compressible gas, 589–597
 description of, 79
 equations, 577
 equilibrium, 690–699
 frozen, 689
 hypersonic, on thin sharp bodies, 625–637
 internal, 616
 nonequilibrium, 689–699
 in nonuniform flow, 616–625
 on blunt bodies, 602–612
 on flat plate in an incompressible flow, 579–583, 592–595
 three-dimensional, 669–677
Boundary layer displacement thickness, 572, 581

Bound-bound transitions, 704

Bow shocks, 251, 314
Bow wave front, 100
Braking radiation, 704
Bremsstrahlung, 704
BURAN vehicle, 697–698
Busemann formula, 319–326, 337

C

Cartesian coordinate system, 65–66, 82, 131
 Catalytic reaction rate constant, 688
 Catalytic recombination rate, 687
 Catalytic sublimation, 696
 Cauchy problem, 181
 Cauchy-Kovalevskaya theorem, 182, 252
 Cauchy-Riemann equations, 128
 Center of pressure, 142
 Centered expansion wave, 205
 Centrifugal accelerations, 71
 Chaplygin equations, 245–246
 Characteristic boundary layer temperature, 586
 Characteristic surface, 182
 Clapeyron equation of state, 3, 11
 Clausius-Clapeyron formula, 559
 Closed group of equations, 97
 Cold air, 4
 Combustion waves, 525
 Compatibility relations, 186
 Complex potential method, 128
 Compressed shock layer, 313–318
 Compressible gas, boundary layer in, 589–597
 Compression shocks, 149, 156
 Compression waves, 206–208
 Concave walls, 202
 Concentration diffusion flux, 680
 Cone
 at incidence, 284–289
 in incompressible flow, 271–273
 in supersonic flow, 276–280
 Conformal mapping method, 128
 Conical body, flow in the vicinity of the planes
 of symmetry of, 362–368
 Conical equations, 280
 Conical flows, 64, 280–283
 Conical limiting angle of the shock, 276
 Conical polar diagram, 276
 Conical problems, 270
 Conical shocks, 286
 Conical streamlines, 281
 Conoid surfaces, 198
 Conservation-law equations, 71
 Conservative equations, 50
 Constant-density flow, in vicinity of axis of
 symmetry of a blunt body, 349–354
 Continuity equation, 8, 46–47
 Continuous media
 description of, 2
 waves in, 208–209
 Convergence, 134
 Convergence lines, 440
 Coriolis accelerations, 71

Couette flow, 567, 569
 Coulomb forces, 459
 Countermoving shocks, 221
 Counterpressure, 298
 Courant criterion, 190
 Crocco integral, 592, 619
 Curl circulation, 82
 Curl rate, 41–44
 Curved body rule, 394–400
 Curvilinear conoid, 197
 Curvilinear coordinates
 description of, 65
 Navier-Stokes equations in, 72–75
 Curvilinear surface-fitted coordinate system,
 69–70
 Cylindrical system, 67

D

Dahmkeller number, 689
 Dalembert paradox, 137
 Debye layer, 688–689
 Deformation rate, 41–44
 Degenerate modes, 471
 Degenerate shock layers equations, 371–376
 Deionization, 488
 Detailed balancing principle, 466, 469
 Detonation waves, 525
 Differential equations
 description of, 25
 energy equation, 48–51
 mass conservation equation, 8, 46–47
 momentum equation, 47–48
 Differential turbulence models, 600
 Differential vector operators
 curl rate, 41–44
 deformation rate, 41–44
 description of, 39
 particle trajectories, 39–40
 streamlines, 39–40
 vector divergence, 44–46
 Diffusion-kinetics equation, 679
 Discontinuity
 breakdown of, 219–227
 capturing techniques, 248
 weak, 519
 Dissipative gas flows, nonequilibrium, 679–689
 Dissipative heat flux, 585
 Dissipative viscous flows, 563–567
 Dissociation degree, 475
 Dissociation-type reactions, 464
 Dissociative reactions, 461
 Disturbance potential, 136
 Disturbances

- interaction of, with a subsonic region, 262–267
in thin layers, 227–230
- Disturbances propagation
speed of, 503–505
velocity of, 432
- Divergence, 134
- Divergence lines, 440
- Divergent equations, 50
- Divergent flow, heat transfer in, 673–677
- Domain of definiteness, 188
- Dorodnitsyn method, 373
- Dorodnitsyn variable, 355, 589
- Drag coefficients, 139
- Dynamic compatibility, 220
- E**
- Effective drag coefficient, 411
- Effective energy method, 301
- Effective energy of the equivalent explosion, 411
- Effective length method, 604–605, 621
- Eigenvalues, 583
- Eiken formula, 699
- Elastic hard body collisions, 446
- Electron exchange reaction, 461
- Electron temperature, 449, 487–489
- Electronic thermal conductivity, 686
- Element composition conservation conditions, 459
- Element diffusion, 690
- Element separation effect, 586
- Ellipses, 126
- Ellipsoids, 126
- Elliptic equation, 106
- Endothermal waves, 527
- Endothermic reactions, 460
- Energy conservation law, 9–10
- Energy equation, 34–39, 48–51
- Energy equipartition principle, 21
- Energy flux, 684
- Enthalpy, 451
- Entrainment velocity, 152, 529
- Entropy
description of, 24–27, 461–468
effect on bluff and thin blunt bodies, 637–653
- Entropy spreading effect, 676
- Equations in stresses, 50
- Equations of state
description of, 3, 11–18
for gas mixtures, 450–454
- Equilibrium
local-equilibrium thermodynamic subsystem, 449
of chemical reactions, 472–476
of composition of gases, 472–476
quasi-equilibrium process, 458
- Equilibrium adiabatic shock waves, 149
- Equilibrium approximation, 458
- Equilibrium boundary layer, 690–699
- Equilibrium constants, 473
- Equilibrium flows, 6, 494–496
- Equilibrium gas dynamics, 6
- Equilibrium process, 458
- Equilibrium speed of sound, 31, 499
- Equilibrium-frozen cone, 544
- Equilibrium-frozen processes, 496
- Euler equations, 4, 50, 65–72
- Euler formula, 359
- Euler number, 711
- Eulerian coordinates, 40
- Evaporation waves, 558
- Exchange reactions, 460
- Exothermal waves, 527
- Exothermic reactions, 460
- Expansion fans, 102–105
- Expansion waves, 203–206
- Explosion-piston model, 407
- External inviscid solution, 578
- F**
- Ferri point, 288
- Flow(s)
around thin wings, 388–390
conical, 64, 280–283
constant-density, 349–354
dissipative, 563–567, 679–689
divergent, heat transfer in, 673–677
equilibrium, 6, 494–496
frozen, 6, 494
hypersonic. *See* Hypersonic flows
incompressible. *See* Incompressible flows
isentropic, 87, 92–94
jet. *See* Jet flows
limiting. *See* Limiting flows
mixed, 239–242
nonequilibrium supersonic, 545–549
nonuniform, boundary layer in, 616–625
one-dimensional stationary, 90–96
one-dimensional unsteady, 184–191
past blunt cones, 412–421
past bodies, nonequilibrium, 536–549
past sharp bodies with an attached shock, 537
- Poiseuille, 567–569
- self-similar, 64
- shear, 9

subsonic. *See* Subsonic flows
 supersonic. *See* Supersonic flows
 three-dimensional, 196–200
 time-dependent, 394–400
 transonic, 4, 195, 250
 turbulent, 76–78, 597–602
 unsteady, 63–64
 viscous. *See* Viscous flows
 Flows past thin blunt bodies
 blast analogy, 405–410
 general pattern of, 401–404
 similarity law, 405–410
 Forward wave front, 100
 Free interaction region, 264
 Free layer, 337–341
 Free-free transitions, 704
 Friction coefficient, 581
 Froude number, 64
 Frozen adiabatic exponent, 204
 Frozen boundary layer, 689
 Frozen flows, 6, 494
 Frozen shock transition, 455
 Frozen shock wave, 506
 Frozen speed of sound, 499
 Function of molecular distribution, 19

G

Gas(es)
 barotropic, 87–89
 composition of, 458–461
 compressible, boundary layer in, 589–597
 heat-conducting, 303–305
 ideal, 12
 ideally dissociated, 475
 intensely radiating, 712–716
 inviscid perfect, 59–60
 nonequilibrium. *See* Nonequilibrium gases
 normal, 156–162
 perfect. *See* Perfect gases
 quasiperfect, 15
 real, 62–63
 relaxing, 445–446
 total enthalpy of, 37
 viscous. *See* Viscous gases
 Gas dynamic equations
 description of, 51
 integrals of, 85–89
 linear, 96–99
 Gas dynamic model
 of medium, 3
 outline of, 1–7
 Gas dynamics
 formulation of problems, 246–250

one-dimensional flow, 7–10
 similarity and modeling in, 58–65
 Gas mixtures, equations of state for, 450–454
 Gas radiation, 703–706
 Generalized Fick law, 683
 Generalized friction law, 53
 Generalized Hugoniot relations, 661, 663, 692
 Generalized independent kinetic variables, 467
 Generalized local similarity method, 609
 Gibbs distribution, 469
 Gibbs paradox, 453
 Global iteration, 255, 372
 Goursat problem, 188
 Grid-characteristic method, 190
 Gromeka-Lamb equations, 83

H

Hadamard solutions, 184
 Hardening effect, 494, 549–551
 Harmonic oscillator model, 470
 Heat flux distribution, 662
 Heat transfer in divergent flow, 673–677
 Heat-conducting gas, 303–305
 Helmholtz theorem, 41
 High incidence, thin bodies at, 390–394
 High-entropy layer
 description of, 403
 in real gas effects, 410–412
 Hodograph variables, 245
 Hydraulic, 90
 Hydrostatic pressure, 8
 Hyperbolic degeneration, 372
 Hyperbolic equation, 106
 Hypersonic approximation, 279
 Hypersonic boundary layer on thin sharp
 bodies, 625–637
 Hypersonic flow
 jet flowing counter to, 368–371
 nonuniform, past yawed cylinder, 442–444
 past thin sharp bodies, 377–400
 thin shock layer in, 538–539
 Hypersonic shocks, 508–510
 Hypersonic stabilization, 155, 313–318
 Hypersonic time-dependent analogy, 382

I

i - j transition, 703
 Ideal gases, 12
 Ideally dissociated gas, 475
 Incidence
 bodies of revolution at, 421–429
 cone at, 284–289

Incompressible flows
 boundary layer on flat plate in, 579–583, 592–595
 cone in, 271–273
 description of, 123–129, 133–134
 Incompressible fluid model, 4
 Incompressible Navier-Stokes equations, 574–578
 Induced drag, 138
 Inertia-like spreading, 293
 Initial conditions, 55–56
 Integral conservation laws, 383–385
 Integral relation method, 297
 Integro-differential equations, 712
 Intensely radiating gases, 712–716
 Interaction effect, 627
 Intermittance coefficient, 598
 Internal degrees of freedom, 447, 468–472
 Inverse methods, 252
 Inviscid flow models, 78–80
 Inviscid perfect gas, 59–60
 Ionization, 5
 Ionization degree, 475
 Irregular shock interactions, 225–227
 Isentrope, 26–27
 Isentropic flows, 87, 92–94
 Isentropic speed of sound, 499
 Isentropicity, 496–497
 Isochores, 654
 Isothermal speed of sound, 30
 Isothermobaric system, 466

J

Jet flows
 counter to hypersonic flow, 368–371
 description of, 256–260, 318
 hardening effect, 549–551
 Joukowski hypothesis, 121
 Jouquet points, 530

K

Kelvin theorem, 83
 Kinetic theory of gases, 3
 Kirchhoff law, 705
 Knudsen displacement effect, 658
 Knudsen layer, 557, 564
 Knudsen number, 19

L

Lagrange integral, 85, 87
 Lagrangian coordinates, 84–85

Lamé coefficients, 65
 Laminar boundary layer, 611
 Laminar heat flux, 610
 Landau-Teller equation, 481
 Langmuir-Hinshelwood mechanism, 687
 Laval nozzle, 92–94
 Legendre equation, 271
 Lennard-Jones potential, 699
 Lewis number, 16
 Lift coefficients, 139
 Lift-drag ratio, 142, 331
 Limiting angle, 165
 Limiting flows
 isentropicity of, 496–497
 regimes, 454–457, 493–498
 Limiting speeds of sound, 498–503
 Limitingly blunt bodies, 318
 Linear approximations, 174–175
 Linear small-perturbation theory, 97
 Linear strain rate, 43
 Linearization, 98
 Liouville formula, 619
 Local blunt cone rule, 424
 Local similarity method, 604
 Local wedge method, 323
 Local-equilibrium thermodynamic subsystem, 449
 Longitudinal momentum conservation law, 383
 Low-entropy shock layer, 403

M

Mach angle, 105
 Mach cone, 105
 Mach disk, 225, 227
 Mach number, 4, 90–92, 152, 261, 284, 313, 420, 593
 Mach number effect, 413
 Mass accommodation coefficient, 559
 Mass conservation equation, 8, 46–47
 Mass conservation law, 7–8, 33
 Mass transfer coefficient, 693
 Mass-average parameters, for boundary layer
 in nonuniform flow, 621–625
 Maximum entropy effect, 644
 Maxwell scheme, 565
 Maxwellian distribution function, 21–22
 Mean optical coefficient, 715
 Metastable nonequilibrium model, 531
 Mixed flows, 239–242
 Modified explosion analogy, 408
 Modified linear theory, 115
 Modified Newton formula, 321
 Molar mass of a gas mixture, 12

Molar thermodynamic potential, 465
 Molar-mass concentrations, 450
 Molecular kinetic equilibrium, 21–22, 446
 Molecular kinetic theory, 18–24
 Molecular-kinetic approach, 7
 Momentum conservation law, 8–9, 33–34, 383
 Momentum equation, 47–48
 Momentum thickness, 581
 Motion of bodies in heavy fluids, 64
 Moving conservation law, 32
 Multicomponent diffusion coefficients, 682

N

Navier-Stokes equations
 in boundary-layer approximation, 670
 description of, 10, 50, 72–75, 78, 149, 505
 incompressible, parabolization of, 574–578
 parabolization of, 574–578, 583–589
 solutions of, 567–574
 Near-equilibrium flows, 516–525
 Near-equilibrium system of equations, 518
 Negatively defined quadratic form, 467
 Neutrals, 681
 Newton formula, 175–179, 319–326, 342, 395
 Newton friction law, 9, 53
 Newtonian fluids and gases
 description of, 8
 rheological model of, 51–55
 Newtonian pressure distribution, 289
 Nonadiabaticity effect, 717
 Nonequilibrium boundary layers, 689–699
 Nonequilibrium gas(es)
 dynamics of, 6
 short waves in, 512–516
 weak shocks in, 512–516
 Nonequilibrium gas flows
 dissipative, 679–689
 equations of, 491–493
 limiting flow regimes, 493–498
 past bodies, 536–549
 Nonequilibrium radiating gases, 717–720
 Nonequilibrium shock waves, 511–512
 Nonequilibrium supersonic flows, 545–549
 Nonlinear theory, 377–379
 Non-thin shock effect, 614–615
 Nonuniform flow, boundary layer in, 616–625
 Normal curvature vector, 358
 Normal gases, 156–162
 Normalized drag coefficient, 112
 Nozzle flow, 256–260, 549–551
 Nozzle-to-ambient pressure ratio, 257

O

Oblique shocks, 163–170
 Ogive bodies, 108
 One-dimensional stationary flows, 90–96
 One-dimensional unsteady flows, 184–191
 OREX vehicle, 698–699
 Outward derivatives, 181
 Overcompressed detonation wave, 532
 Overexpanded jets, 258
 Overtaking shocks, 221

P

Parabolic degeneration, 196, 372
 Parabolization
 of compressible Navier-Stokes equations, 583–589
 of incompressible Navier-Stokes equations, 574–578
 Paradox of two speeds of sound, 505
 Particle trajectories, 39–40
 Perfect gases
 description of, 3, 6, 59–60
 shock waves in, 151–156
 Phenomenological approach, 7
 Photoexcitation effect, 703
 Photoionization, 704
 Photon gas energy, 705
 Photoquenching, 703
 Piston problems, 173–179, 342–344
 Plane of the angle of attack, 141
 Plane section law, 378, 390, 396
 PNSE model, 660, 664
 Poiseuille flows, 567–569
 Power monomials, 60
 Prandtl equations, 577
 Prandtl formula, 153
 Prandtl numbers, 16, 18
 Prandtl-Meyer waves, 201
 Pressure distributions over blunt cones, 657
 Pressure waves, 285

Q

Quadratic approximations, 174–175
 Quantum levels, 447
 Quasi-equilibrium process, 458
 Quasilinearity, 181
 Quasineutral plasma model, 460
 Quasiperfect gases, 15
 Quasistationary solutions, 497–498, 718

R

Radiant energy transport equation, 708
Radiant field, in radiating and absorbing jets, 706–711
Radiant thermal conductivity, 710
Radiating gases
 intensely, 712–716
 nonequilibrium, 717–720
Radiating jets, 706–711
Rarefaction shocks, 149, 238
Reaction rate constants, 456
Reaction rates, 476–479
Real gas effects, high-entropy layer in, 410–412
Real gases, 62–63
Rear wave front, 100
Recovery coefficient, 593
Reflection coefficient, 213
Refraction coefficient, 213
Relaxation compression wave, 506
Relaxation equations, 454–458
Relaxation of complex systems, 479–482
Relaxation time, 455
Relaxation viscosity, 523–524
Relaxation zones, 505–512, 600
Relaxation-reaction interaction, 482–487
Relaxing gases, 445–446
Relaxing medium model, 446–449
Reverse photoexcitation effect, 703
Reverse reaction rate, 456
Reversible process, 24
Reynolds analogy, 595
Reynolds number, 4, 62, 79, 598, 608, 659, 692
Rheological model, 4, 8, 51–55
Riemann invariants, 200, 207

S

Saddle point, 130
Scale factors, 65
Schmidt number, 16
Second law of thermodynamics, 24–27
Secondary waves, 221
Sedov integral, 296
Self-similar flows, 64
Self-similar problems, 270
Self-similar solutions
 concepts of, 269–270
 definition of, 269
Self-similar time-dependent dissipative flows, 303–306
Self-similarity of the first kind, 65
Semi-boundary-value, 618
Separation point, 339

Shear flow, 9
Shock adiabat, 153, 157, 159
Shock detonation waves, 531
Shock front equation, 231–235
Shock front splitting, 237
Shock layers
 degenerate equations, 371–376
 description of, 175
 flow parameters in, 404
 flows in, 653–669
 low-entropy, 403
 thin three-dimensional, 357–362
Shock polar method, 222–224
Shock shape, 337
Shock tubes, 220
Shock waves
 compression, 149
 equilibrium adiabatic, 149
 expansion fans and, 102–105
 formulation of problems, 147–149
 frozen, 506
 hypersonic stabilization of, 155
 losses across, 170–173
 nonequilibrium, 511–512
 in normal gases, 156–162
 in perfect gases, 151–156
 propagation of, 203
 relaxation zones and, 505–512
 shapes of, 148
 sound waves and, 215–219
 in viscous gas, 149–151
 weak, 207–208
Shocks
 hypersonic, 508–510
 oblique, 163–170
Short waves
 contact discontinuity interaction, 211
 in nonequilibrium gases, 512–516
 in vortex flow, 209–211
Similarity laws, 58–59, 107–109, 327–329, 385–388, 634
 binary, 535–536
Similarity theory, 58, 60–62
Simple waves, 200–203
Singular lines, 129–135
Singular stream surfaces, 135
Slip angle, 141
Sommerfeld atom model, 469
Sonic angle of the cone, 277
Sonic lines, 214
Sound waves
 propagation of, 99–102
 shock waves and, 215–219

Spatial singular lines, 135
 Specific energy, 451
 Speed of disturbances propagation in nonequilibrium gases, 503–505
 Speed of sound, 28–32, 229
 limiting, 498–503
 paradox of two speeds of, 505
 Spherical coordinates, 68, 74
 Spherically blunted cone, 543–545
 Stagnation enthalpy, 86, 164
 Stagnation points
 description of, 129–135
 laminar boundary layer at, 611
 on blunt body, 539–543
 three-dimensional, 671–672
 truncation series method for vicinity of, 344–348
 in viscous flow, 570
 Standard atmosphere, 1
 State-to-state kinetics equations, 480
 Stationary waves in relaxing media, 525–534
 Statistic simulation models, 654
 Statistical modeling theory, 561
 Steady-state adiabatic flows, 86
 Steady-state flows
 past thin bodies, 105–110
 two-dimensional, 191–196
 Steady-state solutions, 267–268
 Stephan-Boltzmann constant, 705
 Stepwise ionization, 487
 Stoichiometric difference, 464
 Stokes theorem, 83
 Strain rates, 42, 52
 Streamlines
 conical, 281
 description of, 39–40, 81, 183, 193
 enthalpy distributions in, 338
 pressure distributions in, 338
 types of, 288
 velocity distributions in, 338
 Stress tensor matrix, 51
 Stripe rule, 389
 Strong blast, 294–300
 Strong discontinuities, 185
 Strouhal number, 63
 Sublimation, 696
 Sublimation waves, 525, 557–561
 Subsonic edge regime, 291
 Subsonic flows
 description of, 4, 249–250
 forces in, 135–140
 past a convex corner, 260–262
 past thin bodies, 117–123

Subsonic jets
 barriers and, interactions between, 259–260
 description of, 259
 Supersonic edge regime, 291
 Supersonic flows
 cone in, 276–280
 description of, 4, 247–249
 nonequilibrium, 545–549
 past blunt bodies, 250–255
 thin bodies in, 110–117
 thin delta wing in, 290–294
 Supersonic jets, 257–259
 Surface singular lines, 135
 Sutherland formula, 62
 Sutherland law, 15
 Sweep angle, 290

T

Temperature accommodation coefficient, 565
 Thermal conductivity, 10
 Thermal diffusion ratios, 682
 Thermal nozzle, 95
 Thermal rarefaction waves, 552–557
 Thermal waves, 532
 Thermal-conductivity coefficient, 594
 Thermodynamic pressure, 8
 Thin blunt bodies
 drag coefficients of, 419
 entropy effect on, 637–653
 flows past. *See* Flows past thin blunt bodies
 Thin bodies
 at high incidence, 390–394
 hypersonic flow past, 377–400
 steady-state flow past, 105–110
 subsonic flow past, 117–123
 in supersonic flow, 110–117
 von Kármán equation for, 243
 Thin layers, disturbances in, 227–230
 Thin sharp bodies, hypersonic boundary layer on, 625–637
 Thin shock layer
 description of, 175–179
 equations, 346
 in hypersonic flow, 538–539
 Thin shock layer method, 374
 Thin three-dimensional shock layers, 357–362
 Thin wings
 delta, supersonic flows in, 290–294
 flow around, 388–390
 Three-dimensional boundary layer, 669–677
 Three-dimensional flows, 196–200
 Three-dimensional stagnation points, 671–672

Three-dimensional vortex layers on blunt bodies, 437–441
Time-dependent analogy, 379–383
Time-dependent flows, 394–400
Tomson theorem, 83
Total enthalpy of gas, 37
Total enthalpy thickness, 603
Trajectory characteristics, 183, 186
Transonic equations, 192, 241–246
Transonic flow stabilization law, 240
Transonic flows, 4, 195, 250
Transonic problems, 273–276
Transport coefficients, 10, 699–702
Tricomi-type equation, 245, 255
Truncated harmonic oscillator model, 470
Truncation series method, for vicinity of stagnation point, 344–348
Turbulence model, 648
Turbulence theory, 597
Turbulent flows, 76–78, 597–602
Turbulent Prandtl number, 599
Turbulent viscosity, 598
Two-dimensional flows, steady-state, 191–196

U

Unsteady flows, 63–64

V

Variable flow-rate nozzle, 95–96
Variable-density flow along axis of symmetry, 354–357
Vector divergence, 44–46
Vector pair, 46
Vector-tensor product, 50
Velocity circulation, 82
Velocity coefficient, 89
Velocity distribution, 338
Velocity potential, 84–85
Velocity projection, 193
Velocity rotor, 42
Vibration-dissociation, 482
Viscosity, 699–700
Viscosity-relaxation analogy, 516–525
Viscous continuous and shock layers, 653–669
Viscous flows
dissipative, 563–567
models of, 78–80
Viscous gases
heat-conducting, 62
shock wave structure in, 149–151
Viscous shock layer, 615, 637

Viscous shock layer equations, 587
Viscous stress, 8, 47–48
Viscous-inviscid interaction
description of, 612
displacement effect, 612
end effects, 613–614
external flow nonuniformity effect, 614
non-thin shock effect, 614–615
transverse curvature effect, 613
von Kármán equation, 241–246, 254, 274
von Neumann condition, 106
von Neumann criterion, 227
Vortex sheet, 138
Vortical viscous-inviscid interaction effect, 637
Vorticity field, 42

W

Wall enthalpy factor, 590
Wave(s)
in anomalous media, 235–238
in continuous media, 208–209
endothalmic, 527
exothermal, 527
shock. *See* Shock waves
sound. *See* Sound waves
stationary, in relaxing media, 525–534
sublimation, 557–561
thermal, 532
thermal rarefaction, 552–557
Wave characteristics, 183, 186, 282
Wave drag, 241
Weak branch, 165
Weak discontinuity, 519
Weak injection of gas, 353
Weak shock wave, 207–208, 216
Weak shocks, in nonequilibrium gases, 512–516
Wedge, in incompressible flow, 133–134
Wedge problems, 173–179
Well-streamlined bodies, 139
Wilkie formula, 683, 702
Windward generator, 367
Wing span, 290
Wings
with blunt edges, 429–434
with blunt noses, 434–437
thin. *See* Thin wings

Y

Yawed cylinder, nonuniform hypersonic flow, 442–444

REAL GAS FLOWS WITH HIGH VELOCITIES

Details the Origin, Structure, and Specific Features of Gas Dynamic Equations

Despite generations of change and recent rapid developments in gas dynamics and hypersonic theory, relevant literature has yet to catch up, so those in the field are generally forced to rely on dated monographs to make educated decisions that reflect present-day science.

Written by preeminent Russian aerospace researcher Vladimir Lunev, *Real Gas Flows with High Velocities* reflects the most current concepts of high-velocity gas dynamics. For those in aviation and aerospace, this is a vital methodical revitalization and reassessment of real gas flows with regard to the physical and gas dynamic effects related to high-velocity flight, and, in particular, the entry of bodies into the atmosphere of Earth and other planets.

Much more than just a manual on gas physics, this book:

- Analyzes fundamental challenges associated with super- and subsonic flight
- Describes the physical properties of gas mixtures and their associated high-temperature processes from the phenomenological standpoint
- Explores use of computational mathematics and equipment to simplify previously unsolvable problems of inviscid and viscous gas dynamics
- Explains why numerical methods remain inferior to analytical methods for creating a conceptual understanding of gas dynamic and other physical problems

Avoiding older, cumbersome approximate methods, this reference outlines the general patterns and features of typical flows and how real gas affects them. Referencing simple, analytically treatable examples, similarity laws, and asymptotic analysis, the author omits superfluous explanations of reasoning. This valuable reference summarizes general theory of super- and subsonic flow and uses practical problems to develop a solid understanding of modern real-gas flows and high-velocity gas dynamics.



CRC Press

Taylor & Francis Group
an **Informa** business

www.crcpress.com

6000 Broken Sound Parkway, NW
Suite 300, Boca Raton, FL 33487
270 Madison Avenue
New York, NY 10016
2 Park Square, Milton Park
Abingdon, Oxon OX14 4RN, UK

K10255

ISBN: 978-1-4398-0465-0

90000



9 781439 804650